

Advances in Science, Technology & Innovation
IEREK Interdisciplinary Series for Sustainable Development

Haroun Chenchouni · Helder I. Chaminé ·
Md Firoz Khan · Broder J. Merkel · Zhihua Zhang ·
Peiyue Li · Amjad Kallel · Nabil Khélifi *Editors*

New Prospects in Environmental Geosciences and Hydrogeosciences

Proceedings of the 2nd Springer Conference
of the Arabian Journal of Geosciences (CAJG-2),
Tunisia 2019

Advances in Science, Technology & Innovation

IEREK Interdisciplinary Series for Sustainable Development

Editorial Board

Anna Laura Pisello, Department of Engineering, University of Perugia, Italy

Dean Hawkes, University of Cambridge, Cambridge, UK

Hocine Bougdah, University for the Creative Arts, Farnham, UK

Federica Rosso, Sapienza University of Rome, Rome, Italy

Hassan Abdalla, University of East London, London, UK

Sofia-Natalia Boemi, Aristotle University of Thessaloniki, Greece

Nabil Mohareb, Faculty of Architecture - Design and Built Environment,
Beirut Arab University, Beirut, Lebanon

Saleh Mesbah Elkaffas, Arab Academy for Science, Technology, Egypt

Emmanuel Bozonnet, University of la Rochelle, La Rochelle, France

Gloria Pignatta, University of Perugia, Italy

Yasser Mahgoub, Qatar University, Qatar

Luciano De Bonis, University of Molise, Italy

Stella Kostopoulou, Regional and Tourism Development, University of Thessaloniki,
Thessaloniki, Greece

Biswajeet Pradhan, Faculty of Engineering and IT, University of Technology Sydney,
Sydney, Australia

Md. Abdul Mannan, Universiti Malaysia Sarawak, Malaysia

Chaham Alalouch, Sultan Qaboos University, Muscat, Oman

Iman O. Gawad, Helwan University, Egypt

Anand Nayyar , Graduate School, Duy Tan University, Da Nang, Vietnam

Series Editor

Mourad Amer, International Experts for Research Enrichment and Knowledge Exchange
(IEREK), Cairo, Egypt

Advances in Science, Technology & Innovation (ASTI) is a series of peer-reviewed books based on important emerging research that redefines the current disciplinary boundaries in science, technology and innovation (STI) in order to develop integrated concepts for sustainable development. It not only discusses the progress made towards securing more resources, allocating smarter solutions, and rebalancing the relationship between nature and people, but also provides in-depth insights from comprehensive research that addresses the **17 sustainable development goals (SDGs)** as set out by the UN for 2030.

The series draws on the best research papers from various IEREK and other international conferences to promote the creation and development of viable solutions for a **sustainable future and a positive societal** transformation with the help of integrated and innovative science-based approaches. Including interdisciplinary contributions, it presents innovative approaches and highlights how they can best support both economic and sustainable development, through better use of data, more effective institutions, and global, local and individual action, for the welfare of all societies.

The series particularly features conceptual and empirical contributions from various interrelated fields of science, technology and innovation, with an emphasis on digital transformation, that focus on providing practical solutions to **ensure food, water and energy security to achieve the SDGs**. It also presents new case studies offering concrete examples of how to resolve sustainable urbanization and environmental issues in different regions of the world.

The series is intended for professionals in research and teaching, consultancies and industry, and government and international organizations. Published in collaboration with IEREK, the Springer ASTI series will acquaint readers with essential new studies in STI for sustainable development.

ASTI series has now been accepted for Scopus (September 2020). All content published in this series will start appearing on the Scopus site in early 2021.

More information about this series at <https://link.springer.com/bookseries/15883>

Haroun Chenchouni · Helder I. Chaminé ·
Md Firoz Khan · Broder J. Merkel ·
Zhihua Zhang · Peiyue Li · Amjad Kallel ·
Nabil Khélifi
Editors

New Prospects in Environmental Geosciences and Hydrogeosciences

Proceedings of the 2nd Springer Conference
of the Arabian Journal of Geosciences
(CAJG-2), Tunisia 2019

Editors

Haroun Chenchouni
Department of Forest Management
Higher National School of Forests
Khenchela, Algeria

Md Firoz Khan
Department of Chemistry
Faculty of Science
University of Malaya
Kuala Lumpur, Malaysia

Zhihua Zhang
Shandong University
Jinan, China

Amjad Kallel
Laboratory of Water, Energy
and Environment (Lab 3E)
National Engineering School
of Sfax (ENIS)
University of Sfax
Sfax, Tunisia

Helder I. Chaminé
Lab of Cartography and Applied Geology
School of Engineering
Instituto Superior de Engenharia do Porto (ISEP)
Polytechnic of Porto
Porto, Portugal

Broder J. Merkel
Department for Geology
TU Bergakademie Freiberg
Freiberg, Sachsen, Germany

Peiyue Li
School of Water and Environment
Chang'an University
Xi'an, China

Nabil Khélifi
Springer, a part of Springer Nature
Heidelberg, Germany

ISSN 2522-8714 ISSN 2522-8722 (electronic)
Advances in Science, Technology & Innovation
IEREK Interdisciplinary Series for Sustainable Development
ISBN 978-3-030-72542-6 ISBN 978-3-030-72543-3 (eBook)
<https://doi.org/10.1007/978-3-030-72543-3>

© The Editor(s) (if applicable) and The Author(s), under exclusive license to Springer Nature
Switzerland AG 2022

This work is subject to copyright. All rights are solely and exclusively licensed by the Publisher, whether the whole or part of the material is concerned, specifically the rights of translation, reprinting, reuse of illustrations, recitation, broadcasting, reproduction on microfilms or in any other physical way, and transmission or information storage and retrieval, electronic adaptation, computer software, or by similar or dissimilar methodology now known or hereafter developed.

The use of general descriptive names, registered names, trademarks, service marks, etc. in this publication does not imply, even in the absence of a specific statement, that such names are exempt from the relevant protective laws and regulations and therefore free for general use.

The publisher, the authors and the editors are safe to assume that the advice and information in this book are believed to be true and accurate at the date of publication. Neither the publisher nor the authors or the editors give a warranty, expressed or implied, with respect to the material contained herein or for any errors or omissions that may have been made. The publisher remains neutral with regard to jurisdictional claims in published maps and institutional affiliations.

This Springer imprint is published by the registered company Springer Nature Switzerland AG
The registered company address is: Gewerbestrasse 11, 6330 Cham, Switzerland

About the 2nd Springer Conference of the Arabian Journal of Geosciences (CAJG-2), Tunisia 2019



The Arabian Journal of Geosciences (AJG) is a Springer journal publishing original articles on the full range of Earth sciences in partnership with the Saudi Society for Geosciences. The journal focuses on, but is not limited to, research themes which have regional significance for the Middle East, the Euro-Mediterranean, Africa, Asia, and some other regions of the world. The journal receives on average 4000 submissions a year and accepts around 1000 papers for publication in its 24 annual issues (acceptance rate around 25%). It benefits from the participation of an editorial team of 100 international associate editors who generously help in evaluating and selecting the best papers.

In 2008, Prof. Abdullah Al-Amri, in close partnership with Springer, founded the Arabian Journal of Geosciences (AJGS). In 2018, the journal celebrated its 10th anniversary. To mark the event, the founder and editor-in-chief of the AJGS organized the 1st Conference of the Arabian Journal of Geosciences (CAJG) in close collaboration with Springer on November 12–15, 2018. The conference was an occasion to endorse the journal's long-held reputation and brought together 450 authors from 70 countries, who work in the wide-ranging fields of Earth sciences. The dynamic four-day conference in a stimulating environment in Hammamet, Tunisia, provided attendees with opportunities to share their latest unpublished findings and learn about the latest geosciences studies. The event also allowed attendees to meet and talk to

the journal's editors and reviewers. Three field trips were organized alongside the conference, and many participants enjoyed the wonders of the geology of Tunisia.

In a continuation of the successful 1st CAJG, the 2019's conference aimed to bring geoscientists from all over the world to present and discuss their most recent findings. The 2nd CAJG was an occasion to publish the newest findings in its proceedings by Springer and a special issue in the AJGS, with a clear mission to drive greater North-South (Europe-Africa) scientific cooperation and to open doors to new and enriching collaborations with geoscientists based on Asia and the Americas. The 2nd CAJG devoted a special session (workshop) to studies focusing on unraveling the undiscovered oil and gas resources in the Mediterranean and North Africa. Many international experts took part in the discussion.

The conference covered all cross-cutting themes of geosciences and focused principally on the following 15 tracks:

- Track 1. Atmospheric sciences, meteorology, climatology, oceanography
- Track 2. Biogeochemistry, geobiology, geoecology, geagronomy
- Track 3. Earthquake seismology and geodesy
- Track 4. Environmental Earth sciences
- Track 5. Exploration and theoretical geophysics, seismic and well logging methods, mathematical geosciences
- Track 6. Geoinformatics and remote sensing
- Track 7. Geochemistry, mineralogy, petrology, volcanology
- Track 8. Geological engineering, geotechnical engineering
- Track 9. Geomorphology, geography, soil science, glaciology, geoarcheology, geoheritage
- Track 10. Hydrology, hydrogeology, hydrochemistry
- Track 11. Marine geosciences, historical geology, paleoceanography, paleoclimatology
- Track 12. Numerical and analytical methods in mining sciences and geomechanics
- Track 13. Petroleum and energy engineering, petroleum geochemistry
- Track 14. Sedimentology, stratigraphy, paleontology, geochronology
- Track 15. Structural geology, tectonics and geodynamics, petroleum geology

The dynamic four-day conference provided more than 400 attendees with opportunities to share their latest unpublished findings and learn the newest geosciences studies. The event also allowed attendees to meet and discuss with the journal's editors and reviewers.

More than 710 short contributing papers to the conference were submitted by authors from more than 74 countries. After a pre-conference peer-reviewed process by more than 500 reviewers, 462 papers were accepted. These papers are published as chapters in the conference proceedings which consists of four edited volumes, each edited by the following group of Arabian Journal of Geosciences (AJGS) editors and other guest editors:

Proceedings Volume 1: New Prospects in Environmental Geosciences and Hydrogeosciences

Haroun Chenchouni: University of Tebessa—Higher National School of Forests, Khenchela, Algeria

Helder I. Chaminé: School of Engineering—ISEP, Polytechnic of Porto, Porto, Portugal

Md Firoz Khan: Department of Chemistry, Faculty of Science, University of Malaya, Kuala Lumpur, Malaysia

Broder J. Merkel: TUBAF, Freiberg, Germany

Zhihua Zhang: Shandong University, Jinan, China

Peiyue Li: School of Water and Environment, Chang'an University, Xi'an, China

Amjad Kallel: Laboratory of Water, Energy and Environment (Lab 3E), Sfax National School of Engineers, University of Sfax, Tunisia

Nabil Khélifi: Springer, a part of Springer Nature, Heidelberg, Germany

Proceedings Volume 2: Advances in Geophysics, Tectonics and Petroleum Geosciences

Mustapha Meghraoui: Institut de Physique du Globe, Université de Strasbourg, Strasbourg, France

Narasimman Sundararajan: Sultan Qaboos University, Muscat, Oman

Santanu Banerjee: Indian Institute of Technology Bombay, Mumbai, India

Klaus-g. Hinzen: University of Cologne, Germany

Mehdi Eshagh: University West, Trollhättan, Sweden

François Roure: IFP—Energies Nouvelles, France, France

Helder I. Chaminé: School of Engineering—ISEP, Polytechnic of Porto, Porto, Portugal

Said Maouche: Center for Research in Astronomy and Astrophysics Geophysics, Algeria

André Michard: Paris-Sud University, France

Abdullah Al-amri: King Saud University, Saudi Arabia

Proceedings Volume 3: Recent Research on Geomorphology, Sedimentology, and Geochemistry

Attila Ciner: Istanbul Technical University, Turkey

Stefan Grab: School of Geography, Archeology and Environmental Studies, University of the Witwatersrand, South Africa

Etienne Jaillard: Université Grenoble Alpes, France

Domenico M. Doronzo: National Institute of Geophysics and Volcanology, Rome, Italy, Spain

André Michard: Paris-Sud University, France

Marina Rabineau: CNRS, Univ Brest, Laboratoire Géosciences Océan, Institut Universitaire Européen de la Mer, France

Helder I. Chaminé: School of Engineering—ISEP, Polytechnic of Porto, Porto, Portugal

Proceedings Volume 4: Research Developments in Geotechnics, Geoinformatics and Remote Sensing

Hesham M. El-askary: Schmid College of Science and Technology at Chapman University, United States

Zeynal Abiddin Erguler: Kutahya Dumlupinar Universitesi, Kutahya, Turkey

Murat Karakus: School of Civil, Environmental and Mining Engineering, the University of Adelaide, Australia

Helder I. Chaminé: School of Engineering—ISEP, Polytechnic of Porto, Porto, Portugal

About the Conference Steering Committee

General Chair



Abdullah Al-Amri
Founder and Editor-in-Chief
Arabian Journal of Geosciences
King Saud University, Saudi Arabia

Conference Supervisor



Nabil Khélifi
Senior Publishing Editor, MENA program
Journal Publishing Manager
Arabian Journal of Geosciences
Springer, a part of Springer Nature, Germany

Advisory Co-chair



Walter D. Mooney
Guest of Editorial Board
Arabian Journal of Geosciences
United States Geological Survey Western Region, USA

Advisory Co-chair

Dorrik Stow
Guest of Editorial Board
Arabian Journal of Geosciences
Heriot-Watt University, Edinburgh, Scotland

Scientific Committee Co-chair

François Roure
Chief Editor—Track 15
Arabian Journal of Geosciences
IFP—Energies Nouvelles, France

Scientific Committee Co-chair

Biswajeet Pradhan
Chief Editor—Track 6
Arabian Journal of Geosciences
University of Technology Sydney, Australia

Local Organizing Co-chair



Mohamed Soussi
Former Associate Editor
Arabian Journal of Geosciences
Tunis El Manar University, Tunis, Tunisia

Local Organizing Co-chair



Samir Bouaziz
Former Associate Editor
Arabian Journal of Geosciences
University of Sfax, Sfax, Tunisia

Publications Co-chair



Beatriz Bádenas
Chief Editor—Track 14
Arabian Journal of Geosciences
University of Zaragoza, Zaragoza, Spain

Publications Co-chair

Marina Rabineau
Chief Editor—Track 11
Arabian Journal of Geosciences
University of Brest, Brest, France

Program Co-chair

Amjad Kallel
Chief Editor—Track 4
Arabian Journal of Geosciences
ENIS, University of Sfax, Tunisia

Program Co-chair

Sami Khomsî
Former Associate Editor
Arabian Journal of Geosciences
King Abdulaziz University, Jeddah, Saudi Arabia

Proceedings Editorial Manager



Mourad Amer
Editor of Springer/IEREK ASTI Series
Guest of Editorial Board of AJGS
IEREK, Alexandria, Egypt

Communication Chair



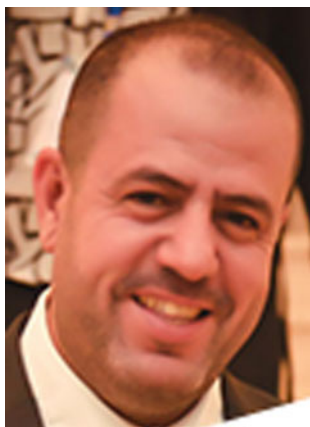
Zakaria Hamimi
Associate Editor
Arabian Journal of Geosciences
Benha University, Benha, Egypt

Public Relations Chair



Faïez Gargouri
Director of the Higher Institute of Computer Science
and Multimedia
President of the AIG
University of Sfax, Tunisia

Conference Manager



Mohamed Sahbi Moalla
Journal Coordinator
Arabian Journal of Geosciences
ISET, University of Sfax, Tunisia

Preface

The Earth system, particularly biosphere, is a complex system formed on the surface of planet Earth by the association of environments with unique physicochemical characteristics: oceans, atmosphere, upper layers of the lithosphere, with which all living things are connected. The biosphere is characterized by a state of dynamic equilibrium resulting from extremely complex interactions between the biological and physicochemical processes specific to the systems in which life thrives, viz., the atmosphere, lithosphere, and hydrosphere. Although human beings do belong to the biosphere, they occupy a specific niche as a unique sphere, the anthroposphere, grounded in the lithosphere. Man plays a key role in the functioning of other systems by using natural resources. Human societies have indeed considerably modified the ecosystems and its relations with other systems by adopting an entirely different model of insertion within the spheres and use of resources. Inappropriate human practices and activities such as different forms of pollutions generated from industrial activities and urban areas, habitat disturbances and urbanization, deforestation combined with adverse natural drivers such as climate variability and change are the main causes of disturbances in biogeochemical processes, land degradation, ecosystem destruction and water scarcity, and other natural disasters and hazards. Currently, it is possible to shape a correct management of natural resources and contributing with balanced solutions to the development and design with nature in a geoethical way.

This volume gives a general overview of current research, focusing on geoenvironmental issues and challenges in model regions in Asia, Europe, and America, with a focus on the Middle East and Mediterranean region and surrounding areas. This proceedings volume is based on the accepted papers for either oral/poster presentations or selected for online publication during the 2nd Springer Conference of the Arabian Journal of Geosciences (CAJG-2), Tunisia, 2019. The book offers a broad range of recent studies that discuss the latest advances in geoenvironmental and hydrogeosciences from diverse backgrounds including climate change, geocology, biogeochemistry, water resources management, and environmental monitoring and assessment. It shares insights of experienced scientists from, but not limited to, research institutes worldwide, focused on the Mediterranean and Middle East regions on how the understanding of ecological, climatological, oceanic and hydrological processes is the key for improving practices in environment management, including the eco-responsibility, scientific integrity, social and ethical dimensions.

The main themes covered in this volume include four topics of AJGS (T1, T2, T4, T10): (i) Global Environmental Change (T1): Atmosphere, Ocean, and Land Surface; (ii) Biogeochemistry, Geobiology, Geocology, Geoagronomy (T2), with emphasis on: Biogeochemical Investigations, Geobiology and Geomicrobiology, Geocology and Phytoecology, and Recent Advances in Geoagronomy; (iii) Environmental Earth Sciences (T4) covering Pollution Monitoring and Assessment, Geoenvironmental Hazards, and Environmental Remediation; (iv) Hydrology, Hydrogeology, Hydrochemistry, Water Resources (T10) underlining: Hydrology, Land Use and Climatology, Hydrogeology and Hydrochemistry, and Water Resources Management.

The high diversity of topics and new results published in this volume contributes to the understanding of environmental impacts and the state of Earth environmental systems is improved because maximizes reader's insights into emerging environmental issues and challenges related to biogeosciences and hydrogeosciences. It will be of interest to scientists, engineers, practitioners, and policymakers in the field of environmental sciences including climatology, oceanography, ecology, biogeochemistry, environmental management, hydrology, hydrogeology, and geosciences in general. The book will also be great value to students and environment-related professionals for further investigations on the state of Earth systems.

Khenchela, Algeria
Porto, Portugal
Kuala Lumpur, Malaysia
Freiberg, Germany
Jinan, China
Xi'an, China
Sfax, Tunisia
Heidelberg, Germany
July 2020

Haroun Chenchouni
Helder I. Chaminé
Md Firoz Khan
Broder J. Merkel
Zhihua Zhang
Peiyue Li
Amjad Kallel
Nabil Khélifi

Contents

Global Environmental Change (T1): Atmosphere

Climate Networks	3
Zhihua Zhang	
Assessment of Temperature Trends in Different Bioclimatic Zones of India	7
Amit Dhorde, Amitesh Gupta, and Anargha Dhorde	
Statistical Analysis of Wind to Assess Climate Change (Central Italy)	11
Matteo Gentilucci, Marwan Ghanem, and Maurizio Barbieri	
Impact of Estimated Wind Speed on Temperature-Based on ET_0 Methods	15
Slavisa Trajkovic and Milan Gocic	

Global Environmental Change (T1): Ocean

The Remote Response of Northern Hemisphere Atmosphere Circulation to ENSO in a Changing Climate	21
Daria Gushchina and Maria Kolennikova	
Inter-Annual Variability of Mediterranean Evaporation and Its Drivers During Summer	25
Igor Zveryaev and Abdel Hannachi	
Low Frequency Sea-Level Oscillations in Algiers Harbour (Algeria)	29
Chawki Zerrouki and Yacine Hemdane	
Modeling Interactions Among the West Atlantic Hurricanes Through Empirical Recurrence Rates Ratio Inspired Hidden Markov Chains	33
Moinak Bhaduri	
Performance Evaluation of a New Source Term Package ST6 of Wavewatch III in Catalan Coasts (Spain)	37
Nasser Kessali, Mohamed Bouhamadouche, and Yacine Hemdane	
Enhanced Methane Emission from Arctic Seas in Winter: Satellite Data	41
Leonid Yurganov, Frank Muller-Karger, and Ira Leifer	

Global Environmental Change (T1): Land Surface

Seasonal Heat Fluxes of Land Surface Models, NOAA and MOSAIC Within NLDAS-2 Over USA During the Period of 1979–2018	47
Muhammed Eltahan, Mohammed Magooda, Karim Moharm, Ahmed El-Hennawi, and Sabah Alahmadi	
Ecological Security Assessment of Qinghai Province in China Based on a Pressure-State-Response Model	51
Wang Fangping, Yao Buqing, Guo Jing, Ma Li, and Zhou Huakun	

Detecting and Monitoring Dust Storm and Studying the Effect of Temperature and Relative Humidity Parameters Using Remote Sensing	57
Behnaz Ghaderi and Zahra Azizi	
Granulometric, Mineralogical, and HYSPLIT Analysis of Siliciclastic Sediments Derived from Sahara	61
Alex Kovács, György Varga, Nadia Gammoudi, and János Kovács	
Solar Power Plant Site Selection and Thermodynamic Analysis	65
Rafika Maali and Tahar Khir	
Biogeochemistry, Geobiology, Geoecology, Geoagronomy (T2): Biogeochemical Investigations	
Blue Carbon Sinks on Polar Seabeds and Their Feedbacks on Climate Change	71
David Keith Alan Barnes	
Climatic Conditions as Factors Influencing the Formation of High-Moor Peat Organic Part	75
Alexander Orlov, Ivan Zubov, Valeria Tatarintseva, Tamara Sokolova, Victoria Pechtereva, and Svetlana Zabelina	
Coastal Deltas of Big Rivers as Synergetic Transformation Elements of the Earth System—(An Example of the Don River Delta)	79
Sergey Venevsky, Sergey Berdnikov, Vera Sorokina, Valerii Kulygin, Aleksey Kleshchenkov, Igor Sheverdyayev, Olga Arkhipova, Lyudmila Dashkevich, Victoria Gerasyuk, Karine Mesropyan, Pavel Ukrainsky, and Natalia Yaitskaya	
Investigation of the Impacts of the Saponite-Containing Waste on Wetland Ecosystems	83
Svetlana Selyanina, Tamara Ponomareva, Elena Churakova, and Olga Yarygina	
Evaluation of the Impact of Diamond Mining on the Radioecological State of the Arctic Zone Ecosystems (Example of Arkhangelsk Region, Russia)	87
Evgeny Yakovlev, Alexander Malov, and Svetlana Selyanina	
Biogeochemistry, Geobiology, Geoecology, Geoagronomy (T2): Geobiology and Geomicrobiology	
Scientific and Methodological Foundations of Biogeology	95
Georgii Rudko	
Natural and Resource Potential of Officinal Plants Flora of Ciscaucasia (Russian Federation)	99
Nadezhda B. Leonova, Inessa M. Miklyaeva, and Svetlana M. Malkhazova	
Properties of Plant Growth Promoting Rhizobacteria Isolated from Rhizospheric Soil of <i>Citrulus colocynthis</i> (Cucurbitaceae) in northeastern Algeria	103
Ahmed Dekak, Hichem Slama, Maroua Chergui, and Mohamed Nacer Mekahlia	
Microbiological Consortium of Thermokarst Lake and Its Significance in the Biodegradation of Petroleum Hydrocarbons	107
Irina Ivanova and Nina Nalivayko	
Use of Biosurfactants in Bioremediation of Petroleum-Contaminated Soil	111
Rihab Belgacem, Olfa Ben Said, Ezzeddine Mahmoudi, and Hamouda Beyrem	

Bio-cementation of Lateritic Soil Using Microbial-Induced Calcium Carbonate Precipitation Techniques for Use as Road and Embankment Materials	115
Kolawole Junwolo Osinubi, Adrian Oshioneme Eberemu, Thomas Stephen Ijimdiya, and Paul Yohanna	
Sewage Sludge Compost Disposal on a Chernozem Soil: Impacts on Bacterial Activity and Nutrient Contents	121
Andrea Farsang, Izabella Babcsányi, Zsuzsanna Ladányi, Katalin Perei, Attila Bodor, Katalin Tímea Csányi, and Károly Barta	
Ecological Significance of Selected Marine Bryozoans from Bay of Bengal, East Coast of India	125
K. Tabita Symphonia	
Biogeochemistry, Geobiology, Geocology, Geoagronomy (T2): Phytoecological Studies	
Pre- and Post-reclamation Land-Use Change and Its Ecological Effects: A Case Study of Pan'an Lake, Xuzhou, East China	129
Zhiqiang Wang, Long Li, Ting Zhang, Longqian Chen, Ruiyang Liu, and Ziqi Yu	
Effects of Sand Encroachment on Vegetation Diversity in the Sahara Desert	133
M'hammed Bouallala, Lyès Bradai, and Haroun Chenchouni	
Functional Diversity of Alpine Meadow Under Simulated Warming and Grazing	139
Zhonghua Zhang, Li Ma, Bingrong Zhou, and Huakun Zhou	
Meta-Analysis of the Response of Plant and Soil to Alpine Meadow Degradation	143
Yandi She, Dangjun Wang, Qian Zhang, and Huakua Zhou	
Temporal Changes in Carbon and Nitrogen Concentrations in the Rhizosphere Soil of Two Plant Species	147
Irina Shtangeeva, Eric Visser, and Paul van der Ven	
Effect of Edaphic Factors on Essential Oil Production in Wild Plants Growing Under Semiarid Mediterranean Conditions	151
Souad Mehalaine and Haroun Chenchouni	
Geographical Mapping of <i>Salvadora oleoides</i> in Northwestern India	157
Maneesh S. Bhandari, Rama Kant, Rajeev Shankwar, Rajendra K. Meena, Sandeep Maikuri, Santan Barthwal, and Shailesh Pandey	
Biogeochemistry, Geobiology, Geocology, Geoagronomy (T2): Recent Advances in Geoagronomy	
Improving Date Palm Morphology and Yield Production of <i>Deglet Nour</i> Dates by the Application of Organic and/or Mineral Amendment	165
Nissaf Karbout, Roland Bol, Rawan Mlih, Mohamed Moussa, Nadhem Brahim, and Habib Bousnina	
Impact of Subsurface Drip Irrigation on Water Distribution, Photosynthetic Production and Crop Yield in Olive Orchard in Southern Tunisia	169
Abderrahman Sghaier, Dalenda Boujnah, Mohamed Ouessar, Rayda Ben Ayed, and Kamel Naggaz	

Heavy Metal Content of <i>Mentha piperita</i> Samples Irrigated with Wastewater and Appraisal of Human Health Risk	173
Ilker Ugulu, Zafar Iqbal Khan, Sidrah Rehman, Kafeel Ahmad, and Yunus Dogan	
Yields and Nutritive Value of Triticale Grown on Sludge-Amended Soil	177
Rajia Kchaou, Rim Baccar, Jalel Bouzid, and Saloua Rejeb	
Impact of Species and Nitrogen Addition on Plant Litter Decomposition in Sheepgrass Meadow in Northeast China	181
Xiaolei Kong, Qiang Zhang, Guili Di, Ruifen Zhu, and Jishan Chen	
Trace Elements Deficiency in Dairy Cows in the Biogeochemical Province of the Republic of Belarus and Biological Effects of Its Correction	185
Vladimir Safonov and Anton Chernitskiy	
Environmental Earth Sciences (T4): Pollution Monitoring and Assessment	
Heavy and Trace Elements Distribution in Plants and Soils of Urban and Rural Areas of Egypt: A Comparison	191
Wael Badawy, Yasmin Sarhan, Octavian Dului, Marina Frontasyeva, Hussein El-Samman, Abdel Azim Hussein, and Wafaa Arafa	
Trace Metal Contamination in Sediment Core of El Mellah Lagoon (El Kala, Algeria)	195
Houria Athmani, Mostefa Boulahdid, Noura Bouchahm, and Nadia Hocini	
Environmental Quality Assessment in the Kuwait Bay (Kuwait): An Integrated Approach	199
Eqbal Al-Enezi, Fabrizio Frontalini, Shaker Al-Hazeem, and Talal Dashti	
Geostatistical Study of Landfill Contaminated Topsoil and Impacts of Urban Waste on Its Immediate Environment (Gafsa, South-West Tunisia)	203
Feyda Srarfi, Mohamed Salah Hamdi, Raouen Rachdi, and Najet Slim Shimi	
Rational Scheme of Chemical Analysis of Urban Soils for Ecological Monitoring	207
Elena V. Shabanova, Irina E. Vasil'eva, Byambasuren Tsagaan, Ochirbat Ganbaatar, Khuukhenkhuu Byambaa, and Marina Y. Khomutova	
The Spatial Distribution of Copper and Zinc in Vineyard Soils (in Tokaj, Hungary) as Impacted by Soil Erosion	211
Izabella Babcsányi, Nhung Thi Ha Pham, István Fekete, and Andrea Farsang	
Geo-accumulation Indexes of Trace Elements in Sediments from Uranium Environments (Central Portugal)	215
Margarida Antunes, Rui Teixeira, Teresa Valente, and António Santos	
Content of Natural Hydrocarbons in Arctic and Subarctic Soils	219
Evgeny Lodygin	
Polycyclic Aromatic Hydrocarbons in Hummocky Peatlands in the Southern Tundra Zone	223
Dmitriy Gabov, Evgeniya Yakovleva, and Roman Vasilevich	
Heavy Metals (Pb, Zn, Cd) and Metalloids (Sb, As) in Carbonated Soils Contaminated by Mine Tailings (North Tunisia)	227
Yosra Achour, Radhia Souissi, Haifa Tlil, Mikael Motelica Heino, and Foued Souissi	

Organohalogenated Micropollutants: Polybrominated Diphenyl Ether (PBDE) Contamination Gradient of the Seine River in France	231
Khawla Tlili, Pierre Labadie, Marie-Jeanne Teil, Fabrice Alliot, Catherine Bourges, Annie Desportes, and Marc Chevreuil	
Impact of the Gypsiferous Formations of Djebel Djebissa on the Salinity of the Water: Plain of Tebessa Northeast Algeria	235
Lassaad Ghrieb and Ammar Maoui	
Seasonal Evaluation of Heavy Metals Speciation in Municipal Landfill Leachate Using ‘WATEQ4F’	239
Lathamani Ramachandra and Suresha Sidduraiah	
Assessment of Particulate Pollutant Exposure of Residents Around an Opencast Coal Mine	243
Aditya Patra, Vaibhav Rengede, and Ravish Dubey	
Assessment of Risk from Atmospheric Air Pollution and Traffic Load Intensity in the City of Kazan (Republic of Tatarstan)	247
Natalya Stepanova, Alisa Ilyasova, Naila Yusupova, Lily Khairullina, Suryana Fomina, and Rustem Saifullin	
Effects of Outdoor Air Pollution on Human Health in Kenitra, Morocco	251
Rachida El Morabet, Said Mouak, Roohul Abad Khan, Abderrahmane Adoui El Ouadrhiri, and Mohamed Aneflouss	
Contamination Levels and Health Risks of Heavy Metals in Street Dusts from Ulaanbaatar, Mongolia	255
Sonomdagva Chonokhuu, Chultem Batbold, and Khongor Gankhuyag	
Comparative Study of Different Multi-target Regression Approaches Performances for Air Pollutants Forecasting	259
Sahar Masmoudi, Haytham Elghazel, Dalila Taieb, and Amjad Kallel	
Magnetic Properties of Road Dust Using Environmental Magnetism Settings in Greater Hyderabad Municipal Corporation (GHMC), Telangana State, India	263
R. Sudarshan, B. Madhusudan Rao, B. Nagaraju, S. K. Patil, and K. Lohith Kumar	
Environmental Earth Sciences (T4): Geo-environmental Hazards	
Assessing the Vulnerability of Soil Losses by Mapping: Case of the Watershed of Oued Chemorah Northeast Algeria	273
Nabil Kabouche, Faiza Balla, and Kamel Khanchoul	
Risk Assessment of Coastal Erosion Hazard of Ngazidja Island in Comoros Archipelago	277
Avouca Mahamoud, Nadjim Ahmed Mohamed, Gzam Maher, and Mabrouk Montacer	
Effect of Salt Accompany with Sodium Chloride on Soil Loss by Wind Erosion in the Dried Bed of Uremia Lake	281
Abbas Ahmadi, Shahin Oustan, and Nazanin Gholampour	
Identifying Vulnerable Lands Using the Duration-Frequency of Mediterranean Exceptional Rainfall Events in Semiarid Watersheds	285
Khaoula Khemiri and Sihem Jebari	

Inland Water Resources Depletion Under CO₂ Accusation	289
Miah Muhammad Adel	
Assessment of Adolescent Health Risk Caused by Chemicals' Entry with Soil	293
Emilia Valeeva, Ismagilova Gulgena, Ziyatdinova Alfia, and Yusupov Neylya	
Assessing Preparedness-Insufficiency Spatial Patterns and Geostatistics to Build-Back-Better: An Application in Malinao Albay, Philippines	295
Ana Marie R. Abante	
Emerging and Re-emerging Natural Focal Diseases in Russia: A Medico-Geographical Study	303
Svetlana M. Malkhazova, Polina V. Pestina, and Anna I. Prasolova	
Environmental Earth Sciences (T4): Environmental Remediation	
Removal of Iron from Groundwater onto Raw Clay (Ka-II)	309
Sana Ghrab, Zied Marzougui, Leila Chaari, Mohamed Damak, Abdelhamid Elaissari, and Boubaker Elleuch	
Investigation of Flocculation Activity of Cactus <i>Opuntia ficus-indica</i> juice in Phosphate Clay Treatment	313
Raouen Rachdi, Feyda Srarfi, Mohamed Salah Hamdi, and Najet Slim Shimi	
Enhancing the Chromium Removal Capacity of Banana Peel Wastes by Acid Treatment	317
Haili Chen, Zhouyang Huang, Jiahong Wu, and Chirangano Mangwandi	
Removal of Nickel from Aqueous Solution and Industrial Effluent by Iron Oxide	321
Nesrine Boujelben, Zaineb Bakari, Nesrine Turki, and Boubaker Elleuch	
Chemically Treated Seagrass Fibers as Biosorbent for Crude Oil Removal	325
Senda Ben Jmaa and Amjad Kallel	
Soil Salinization: A Severe Environmental Hazard and Electrokinetic Treatment as One of the Innovative Technologies for Its Mitigation	329
Mohammed Mustapha Bessaim, Aicha Bessaim, and Hanifi Missoum	
Contaminants Transfers Through Composite Liners Exhibiting Aged GCLs: A Numerical Prediction	333
Hajer Bannour, Farouk Ben Abdelghani, and Nathalie Touze	
Physicochemical Adsorption Properties of Heavy Metals by Different Clay Combinations in the Context of Phosphogypsum Storage	337
Kawther Ben Moussa, Saifeddine Eturki, Philip Tack, Rinehart Van Poucke, Samuel Budet, Johan De Grave, Mohamed Moussa, and Mohamed Ouessar	
The New Approach to γ-Spectrometry Based on Electron-Positron Pair Selection for Solution of Various Geochemical Problems	341
Vsevolod Volodin, Anna Travkina, and Yuri Sapozhnikov	
Rimsulfuron Herbicide: Study of the Interaction and Distribution Between Soil and <i>Zea mays</i> L., 1753 (Model Experiments)	345
Lydia Bondareva, Valerii Rakitskii, and Nataliia Fedorova	
Olive Mill Waste Water Contaminated Soil: Toxicological Effects and Treatment with Gypsum	349
Salsabil Trigui, Amjad Kallel, Emilia Fernández Ondoño, and F. J. Martín Peinado	

Use of Diatomaceous Earth and Lime for the Remediation of Olive Mill Waste Contaminated Soils	353
Salsabil Trigui and Amjad Kallel	
Durability and Leaching Behavior of Mine Tailings After Inerting Geomaterials in Tunisia	357
Rania Hbaieb, Marilyne Soubrand, Emmanuel Joussein, Sonia Lazaar, and Mounir Medhioub	
Physicochemical Characterization of Diatomite from Ouled Djilali-Mostaganem Region of Algeria	361
Amal Touina, Safia Chernai, Bouaheur Mansour, and Boualem Hamdi	
Prioritizing Drainage Rehabilitation in Kasavanahalli Village, Bengaluru (India) Using AHP	365
Shivika Saxena, Aakash, G. Ajith Kumar, B. S. Bharath Raj, and Syed Isaac Peeran	
Comparison Between Two Samples Granulates Differences of Thermal Activated Biochar from Date Palm Fiber	369
Djehad Bentarfa, Mohamed Lamine Sekirifa, Youcef Touil, and Mahfoud Hadj-Mahammed	
Study of Rheological Behavior of “Gafsa” Clay	373
Safa Mkaouar, Walid Maherzi, Patrick Pizette, and Mourad Benzina	
Thermal Energy Use in Hammam Righa spa, Algeria	377
Salima Ouali, Mohammed Moundji Hadjiat, Khaled Imessad, Khelifa Salhi, and Abdelkader Ait-Ouali	
Hydrology, Hydrogeology, Hydrochemistry, Water Resources (T10): Hydrology, Land Use and Climatology—Rainfall and Evaporation	
Statistical Prediction of Sri Lankan Rainfall from October to December	383
Pabodini Karunapala	
Spatiotemporal Rainfall Variations: Case Study of Wadi Koutine Watershed (South Tunisia)	387
Mongi Ben Zaied, Mohamed Ouessar, and Messaoud Guied	
Rainwater Quality in Some Urban and Rural Sites of Cameroon (Central Africa)	391
Aicha Foupouagnigni, Andrew Ako, Jude Mengnjo, Gloria Eneke, Josephine Ndjama, Bertil Nlend, George Nkeng, and Takeshi Ohba	
Probabilistic Analysis Using Physically Based and Hydrogeological Models for Rainfall-Induced Shallow Landslide Susceptibility (Northern of Morocco) . . .	395
Hassane Rahali and Houda Loukili	
Assessment of Climate Variability and Its Impact on the Environment and Water Resources in the Mount Cameroon Area	401
Andrew Ako Ako, Monjoa Monono Zita, and Enoch Jeanot Fongoh	
Mapping and Assessment of Evapotranspiration Over an Oasis in Arid Ecosystem Using Remote Sensing and Biophysical Modeling	405
Khalid Turk, Faisal Zeineldin, and Abdullah S. Aljughaiman	
Interception Loss from the Sprinkler-Irrigated Coffee Plantation	409
Pandu Narayana and K. Varija	

Hydrology, Hydrogeology, Hydrochemistry, Water Resources (T10):	
Hydrology, Land Use and Climatology—Runoff and Catchment Studies	
Predicting Vertical Distribution of Sediment Concentrations in Uniform Open Channel Flows	415
Abdelali Terfous, Mira Sabat, and Abdellah Ghenaim	
Contribution to the Study of Flood Risks in the North West of Algeria (Case of Oued Khemis in Tlemcen)	419
Sarra Bouraoui and Abderrahmane Medjerab	
Risk Assessment of Flash Floods in Eastern Egyptian Desert	423
Ahmed Mohamed Helmi, Omar Zohny, and Ashraf El Mustafa	
Flood Hazards Mapping in Arid Region by Integrating Hydrologic and Hydraulic Modeling: Case Study of Wadi Qows, Jeddah, Saudi Arabia	429
Kuswanto Marko, Amro Elfeki, Nassir Alamri, and Hatem Ewea	
What About the Erosion in the Coastal Algiers Watershed (Algeria)?	433
Abdelhadi Ammari and Boualem Remini	
Climate Change and Its Impact on Runoff and Sediment Yield (Case Study: Dez River Dam, Iran)	439
Mohammad Reza Eini, Kourosh Mohammadi, Reza Najib, Saman Javadi, and Golmar Golmohammadi	
Investigation of Hydrological Variability in Medjerda Watershed (NW Tunisia)	443
Hamida Cherni, Imen Turki, Zeineddine Nouaceur, Nicolas Icoq, Walid Oueslati, Mohsen Ben Alaya, Valérie Mesnages, and Radhia Souissi	
Water Quality Variation Along the Tigris River	447
Ali Chabuk, Nadhir Al-Ansari, Ali Almaliki, Jan Laue, and Hussain M. Hussain	
Physicochemical Quality of Surface Water in the Jijel Region (Northeast Algeria)	451
Abdelmalek Drouiche, Faouzi Zahi, Taha Hocine Debieche, Hocine Sakta, and Souhil Mahdid	
Hydrology, Hydrogeology, Hydrochemistry, Water Resources (T10):	
Hydrology, Land Use and Climatology—Hydraulic Modeling	
Pairing GIS and Distributed Hydrological Models Using MATLAB	457
Sleimane Hariri, Sylvain Weill, Jens Gustedt, and Isabelle Charpentier	
Use of Hydrological Modeling as a Tool for Climate Model Evaluation at Oued el Abid Catchment [Tunisia]	461
Khalil Djebbi and Hamouda Dakhlaoui	
Hydraulic Modeling with HEC-RAS 2D in the Urban Area of Casimcea (Romania) Catchment	465
Constantin Cerneaga, Gabriel Dobrica, and Carmen Maftei	
Sensitivity Analysis of the SAFSAF River Catchment Model Using Two Objective Functions	469
Fares Laouacheria, Leila Djellit, Said Kechida, Moncef Chabi, and Faiza Balla	

Optimized Agricultural Scenarios of Proposed Kalabagh Dam Under Conjunctive Operation of Tarbela and Kalabagh Reservoirs Using Agro-Economic Model	473
Muhammad Sanaullah, Abdur Rehman, Muhammad Kamran, Ejaz Ahmed Abbasi, Muhammad Qasim Mahmood, and Muhammad Imran	
Hydrology, Hydrogeology, Hydrochemistry, Water Resources (T10): Hydrology, Land Use and Climatology—Surface Water Management	
Pressure Change Control to Avoid Pipes Burst Disaster: An Exploratory Study	481
Wahiba Mokrane	
A Review on the Reuse of Treated Wastewater in Algeria: Scenario and Sustainability Issues	485
Sabri Dairi, Dounia Mrad, Ali Bouamrane, Yassine Djebbar, and Habib Abida	
Infiltration Boxes as a Part of Urban Storm-Water Management. A Case Study: Port of Pancevo, Serbia	489
Denisa Djordjevic, Mladen Milanovic, Dragan Milicevic, and Zeljka Ostojic	
Application of Different LID Technologies for the Drainage of Urban Areas: A Case Study—Pek Settlement, Serbia	493
Slavisa Trajkovic, Dragan Milicevic, Mladen Milanovic, and Milan Gocic	
An Overview of Vadose Zone Characterization for the Assessment of the Impact of Burial on Groundwater in South-Western Nigeria	497
Charles A. Oyelami, Olabanji A. Ojo, Mutiu A. Fakunle, Oluwole E. Ajayi, and Uche E. Tochukwu	
Water Quality Indicators in River Basins—A Portuguese Case Study (Northern Portugal)	501
Margarida Antunes, Ana Brás, and Paula Marinho	
Hydrology, Hydrogeology, Hydrochemistry, Water Resources (T10): Hydrogeology and Hydrochemistry—Hydrodynamics Aspects	
Transient Drain Spacing Equations for Different Initial Water Table Conditions	507
Ammar Yousfi and Mohammed Mechergui	
Geoelectrical Studies for Groundwater Exploration in Fractured Rock Terrane (Ambaji Basin, India)	511
Rudra Mohan Pradhan, Ramesh Deshmukh, Enamundram Chandrasekhar, Guru Balamurugan, and Tapas Kumar Biswal	
Hydrodynamic Functioning of Rhythmic Springs—Case of the M'chaki Spring (Jijel, NE Algeria)	515
Taha-Hocine Debieche, Azzedine Bouzenoune, Faouzi Zahi, Abdelmalek Drouiche, Souhil Mahdid, Youcef Rouikha, Boualem Mayache, Amal Chine, Asma Gherib, and Fatima Aidli	
Hydrology, Hydrogeology, Hydrochemistry, Water Resources (T10): Hydrogeology and Hydrochemistry—Chemical and Quality Aspects	
Assessment and Mapping of the Pollution Risk of Springs Water: The Case Study of Taher Region (Jijel, Northeast Algeria)	521
Amal Chine, Taha-Hocine Debieche, and Boualem Mayache	

Seasonal Variation of Water Quality/Jericho Spring Group (Palestine)	525
Amer Marei, Saed Khayat, and Husam Uteir	
Estimating Natural Backgrounds and Threshold Values of Hydrochemical Parameters in a Desert Area (India)	529
Abdur Rahman, Kamal Tiwari, and Nepal Mondal	
Influence of Water-Rock Interaction on the Fluoride Contamination of Groundwaters from Bhokar, (Nanded District, Maharashtra, India)	533
Dipak Panaskar, Vasant Wagh, and Ranjeet Pawar	
Signatures of Dryas Groundwater in Stratified Aquifers of Kuwait-Paleoclimatic Significance	537
Chidambaram Sabarathinam and Tariq Rashid	
The Role of Hydraulic Turnover Time in the Assessment of Water Quality in Portuguese Aquifer Systems	543
Lisa Martins, Alcino Oliveira, Luís Sanches Fernandes, and Fernando Pacheco	
Hydrogeological and Hydrochemical Characterization of Mejel Bel Abbas Aquifer (West-Central Tunisia)	547
Mouez Gouasmia, Abdelkader Mhamdi, Ferid Dhahri, and Mohamed Soussi	
Spatial Distribution of Nitrate Level in a Deep Aquifer Located in an Agricultural Region (North Tunisia)	551
Nizar Troudi, Fadoua Hamzaoui-Azaza, Ourania Tzoraki, and Mounira Zammouri	
Evaluation of Groundwater Quality in Rural Part of Central India with Special Emphasis on Fluoride Concentration	557
Rajshree Yenkie, Deepak Malpe, Deepali Marghade, Dhananjay Meshram, and Biswajit Hazarika	
Groundwater Arsenic and Iron Contamination in the Gangetic Plains of India: Safe Drinking Water Option on Quaternary Stratigraphy	561
Babar Ali Shah	
Hydrochemical Characteristics and Assessment of the Impact of Mining Activities on Groundwater Quality in Enyigba-Ameri, Southeastern Nigeria	565
Olufemi Victor Omonona, Amobi Chigozie Ekwe, and George-Best Azuoko	
Groundwater Hydrochemistry in a Coalmine and Source Analyses of Major Ions (Qingdong Coalmine, China)	569
Kai Chen, Linhua Sun, and Jiying Xu	
Chemical and Organic Contamination Degree of Waters in the Lacustrine Complex of El Kala (Northeastern Algeria)	575
Badreddine Saadali, El Fadel Derradji, Hicham Zerrouki, Nabil Bougherira, Sofia Bahroun, and Abdelkader Khiari	
Identification of Groundwater Quality and Hydrogeochemical Processes in the Shallow Aquifer of El-Oued (Algerian Sahara)	579
Boualem Bouselsal and Kamel Zouari	

Stable Isotope Evidences on Mechanisms and Sources of Groundwater Recharge in Quaternary Aquifers of Kelantan, Malaysia	585
Mohammad Muqtada Ali Khan, Kishan Raj, Aweng A./L. Eh Rak, Hafzan Eva Mansor, Roslanzairi Mostapa, Kamarudin Samuding, and Zameer Ahmad Shah	
Identification of Contamination Sources Through the Application of Nitrogen, Oxygen and Deuterium Isotopes in Estarreja Shallow Aquifer, Aveiro (Portugal)	589
Ana Carolina Pires Marques, Maria do Rosário Carvalho, and Eduardo Anselmo Ferreira da Silva	
Hydrogeological Conceptual Modelling of Geothermal Waters in Urganlı, Western Anatolia, Turkey	593
Nevzat Özgür and Seher Büyüksahin	
Hydrogeological Modeling of Geothermal Waters in Balçova, İzmir, Turkey	597
Nevzat Özgür and Mine Alacalı	
Assessment of Seawater Intrusion in a Coastline City Using GIS (Tripoli Lebanon)	601
Marianne Saba, Amal Iaaly, and Najib Gerges	
Hydrology, Hydrogeology, Hydrochemistry, Water Resources (T10): Water Resources Management	
Groundwater Resource Management in the Hard Rock Terrain of Upper Ponnaiyar Watershed Using Remote Sensing and GIS	609
Arunachalam Subramaniam, Parameswari Kaliyaperumal, and Sakthivel Rathinagiri	
Innovative Conveyancing System Techniques Implemented by Saudi Geological Survey to Ensure Minimum Hydrogeological Impact on Wadi Ibrahim Groundwater Aquifer	619
Ahmed El-Hames, Samer Shouman, Abdulaziz Al-Solami, and Bandar Tunisi	
A Sustainable Water Resources Management Plan for the Kurdistan Region, Iraq	623
Serwan M. J. Baban and Ghazi F. Haji	
Aquifers Depletion and Asymmetry Access to Groundwater: A Study Across Farmers' Classes in Tunisia	629
Hacib El Amami, Sondes Fkiri, and Jean Robert Kompany	
Hydrogeological Features of Geothermal Waters and Travertine Deposits in Pamukkale, Western Anatolia, Turkey	633
Nevzat Özgür and Emre Uzun	

About the Editors



Dr. Haroun Chenchouni is an associate professor and research scientist (Ecologist) at the Higher National School of Forests (Khenchela, Algeria). He is a former associate professor at the University of Tebessa (Algeria). He holds a M.Sc. (Magister) in Dryland Ecology from the University of Ouargla (Algeria) and a doctorate degree in Ecology and Environment from the University of Batna. He graduated as an engineer in Plant Ecology and Forest Ecosystems from the Department of Biological Sciences (University of Batna, Algeria). His research interests are fairly broad; he uses statistical modeling approaches to understand how natural environments, mainly climatic and edaphic factors, and anthropogenic perturbations influence biological interactions, shape trends in population dynamics, and influence community diversity. He uses various biological models to investigate biological interactions and community ecology of arid and semiarid ecosystems of North Africa. At various universities in Algeria, he teaches forest ecology, biostatistics, and ecological modeling. He has published more than 100 peer-reviewed publications and internationally recognized research papers. He is also involved in national and international research projects. In 2017, he joined the *Arabian Journal of Geosciences* (AJGS) as an associate editor. Then in 2019, he was assigned as a chief editor of Topic 2 (biogeochemistry, geobiology, geoecology, geoagronomy) to handle submissions dealing with various fields of biogeosciences, geoecology, climate change, plant and soil science, agricultural and forest environment, and environmental sciences.



Helder I. Chaminé is a skilled geologist and professor of Engineering Geosciences at School of Engineering (ISEP) of the Polytechnic of Porto, with over 29 years' experience in multidisciplinary geosciences research, consultancy, and practice. He studied geological engineering and geology (B.Sc., 1990) at the Universities of Aveiro and Porto (Portugal), respectively. He received his Ph.D. in geology at the University of Porto in 2000 and spent his postdoctoral research in applied geosciences at the University of Aveiro (2001–2003). In 2011, he received his Habilitation (D.Sc.) in geosciences from Aveiro University. Before joining academy, he worked over a decade in international projects for mining, geotechnics and groundwater industry and/or academia related to geodynamics and regional geology, hard-rock hydrogeology and water resources, engineering geosciences and applied geomorphology, rock engineering and georesources. His research interests span over fundamental to applied fields: GIS mapping techniques for applied geology, structural geology and regional geology, engineering geosciences and rock engineering, slope geotechnics, mining geology and hydrogeomechanics, hard-rock hydrogeology, exploration hydrogeology, urban groundwater and hydromineral resources. He has interests on mining geoheritage, history of cartography, military geosciences and higher-education dissemination, skills and core values. Presently, he is the head of the Laboratory of Cartography and Applied Geology (LABCARGA | ISEP), senior researcher at Center GeoBioTec | U. Aveiro and Center IDL | U. Lisbon, as well as belongs to the executive board of the M.Sc.+B.Sc. Geotechnical and Geoenvironmental Engineering (OE+EUR-ACE Label) and the Department of Geotechnical Engineering (ISEP). Currently, he belongs to the board of the Portuguese Geotechnical Society (SPG) and IAH—Portuguese Chapter. He was a board member of the APGeom—Portuguese Association of Geomorphologists (2009–2013). He was a consultant and or responsible over 70 projects of rock engineering, applied geology, hydrogeomechanics, slope geotechnics, mining geology, exploration hydrogeology, hard-rock hydrogeology, water resources, urban groundwater and applied mapping (Mozambique, Portugal, and Spain). He has been co-authored over 200 publications in indexed journals, conference proceedings/full papers, book chapters, technical, and professional papers. He co-edited over 13 special volumes, as well as is presently evolved in editing themed issues for three international journals (Geotechnical Research ICE, Springer Nature Applied Sciences, Water MDPI). He has a wide activity as a referee for several international journals. He served as an invited expert evaluator of Bologna Geoscience program for DGES (Portugal) and Scientific Projects Evaluation for NCST, 2017–2019 (Kazakhstan) and NRF | RISA, 2019 (South Africa), as well as a coordinator of “Geology on Summer/Ciência Viva” program at ISEP, since 2005, for geosciences dissemination. He has been also active with teaching and supervising of many Ph.D., M.Sc., and undergraduate

students. He has been on the editorial board, among others, of *Arabian Journal of Geosciences* (SSG+Springer), *Hydrogeology Journal* (IAH+Springer), *Euro-Mediterranean Journal for Environmental Integration* (Springer), *Springer Nature Applied Sciences* (Springer), *Mediterranean Geoscience Reviews* (Springer), *Geotechnical Research* (ICE), *Geosciences* (MDPI), *Revista Geotecnia* (Portugal), and *Geología Aplicada a la Ingeniería y al Ambiente* (Argentina). He integrates as a moderator or session chair in several conferences, workshops and meetings. Currently, is a co-chair of the International Conference “Geoethics and Groundwater Management” (IAH +IAPG, Porto, May 2020) and in organizing/scientific committee of the 3rd International Workshop on Natural Hazards—NATHAZ’21 (Terceira Island, Azores, May 2021).



Dr. Md Firoz Khan is a senior lecturer in the Department of Chemistry, University of Malaya, Malaysia. He received his Ph.D. degree from the National University of Yokohama, Japan, in 2010 as a Monbukagakusho scholar (Japanese Government Scholarship). He received his M.Sc. degree in Air Pollution from the University of Birmingham, UK, and his bachelor’s degree in chemistry from the University of Dhaka, Bangladesh in 2005 and 1994, respectively. He also received a M.Sc. degree in Chemistry from the University of Dhaka, Bangladesh, in 1995. During his academic career, he worked as a postdoctoral research at the University of Tokyo, Japan, from 2010–2011. Then, he joined the Center for Tropical Climate Change System at the Universiti Kebangsaan Malaysia, as a senior lecturer and attained the position till November 2018. He has been serving as an associate editor to two Web of Science indexed journals, *Elementa: Science of the Anthropocene* and *Arabian Journal of Geosciences* (Springer). His research interests cover a wide variety of topics in analytical chemistry, air pollution, source apportionment, and human health impact of the emerging pollutants. He is an author of more than 80 high impact peer-reviewed journal papers and book chapters. Currently, he leads a research group focusing on air pollution with a number of students at undergraduate, postgraduate, and Ph.D. level.



Broder J. Merkel born: 1949 in Münster (Germany); widowed, three children; 1978: Diploma (master) in Geology/Hydrogeology (TU München); 26.9.1983: Dissertation (Ph.D.) Dr. rer.nat. as Hydrogeologist (TU München); 15.4.1992: Habilitation (Dr. habil) Christian-Albrechts Universität Kiel; 1993–2015: Full Professor for Hydrogeology at Technische Universität Bergakademie Freiberg (TUBAF); 1994–2015: Member of faculty council; 1995–2014: Head of the Geology Department; 1996–2002: Head of a DFG-Graduiertenkolleg; 1996–2000 and 2010–2015: Dean of study course geoecology; 2012–2015: Dean of study course Groundwater Management (Master); 2002–2006: Dean of the Faculty Geoscience, Geotechnics, and Mining; 2012–2014: DFG liaison officer of TUBAF; 2014–2017: Vice rector of TUBAF; Head of the Scientific Diving Center of TUBAF; Editor of the open access journal *Freiberg Online Geoscience* (FOG); Associate Editor of *Environmental Earth Sciences*; Chief Editor of *Arabian Journal of Geoscience*; Teaching: hydrogeology, hydrochemistry, chemical thermodynamics, reactive transport modeling and related subjects (geostatistics, GIS, and remote sensing); Teaching scientific work under water as scuba diver; Field work in Bolivia, China, Chile, Czech Republic, Iraq, Iran, Israel, Italy, Jordan, Hungary, Mexico, Mozambique, Namibia, Palestine, Russia, Spain, USA; Organization of seven International Conferences Uranium Mining and Hydrogeology; Organizing 15 international workshops around the world; >150 peer-reviewed publications, H-Index 24, contributions to more than 15 books; two patents.



Zhihua Zhang is a Taishan distinguished professor and a director of climate modeling laboratory at Shandong University, China. His research interests include mechanisms of climate change, big data mining, carbon emissions, climate policy, and sustainability. He has published five first-authored books and about 50 first-authored papers. He is a chief editor, associate editor, or editorial board member in many global known journals on *climate change*, *meteorology*, and *environmental science*.



Dr. Peiyue Li is a full professor in hydrogeology and environmental science at Chang'an University, one of the national key universities in China, and is the vice dean of the School of Water and Environment at this university. He obtained his Ph.D. from Chang'an University. His research interests include hydrogeology, hydrogeochemistry, and groundwater modeling. He is a member of International Association of Hydrogeologists (IAH), International Mine Water Association (IMWA) and Geological Society of China (GSC) and an associate editor of *Exposure and Health*, *Mine Water and the Environment*, and *Human and Ecological Risk Assessment*. He has been awarded over ten national and provincial awards by Chinese governments and organizations for recognizing his outstanding achievements in geosciences. He was awarded the Ten Thousand Talent program and the Changjiang Scholar program in 2018. He has been principal investigator (PI) for more than 20 research projects supported by the National Natural Science Foundation of China (NSFC), Ministry of Science and Technology of China (MSTC), and other national and provincial governments. He is now working in the field ranging from groundwater quality evolution in a changing environment to permeability variation of porous media.



Dr. Amjad Kallel is currently an associate professor of Environmental Geology in the Sfax National School of Engineers at the University of Sfax, Tunisia. He holds a B. Eng. in Georesources and Environment (1998) from the University of Sfax (Tunisia) and a M.Sc. degree and a Ph.D. degree in Georesources and Environment (2004) from Hokkaido University (Japan). He joined Venture Business Laboratory (VBL) at Akita University, Japan (2005–2006), as a researcher focusing on refining and recycling technologies for the recovery of rare elements from natural and secondary sources. On his return to Tunisia, he worked at the University of Gabes from 2006 to 2011, where he contributed to the elaboration of teaching programs at the Higher Institute of Water Sciences and Technologies of Gabes. Since 2011, he has joined the Sfax National School of Engineers. There, he has also been involved in various research projects related to environmental geology and environmental geotechnics. He has co-organized many prestigious workshops, seminars, and international conferences. In 2016, He joined the *Arabian Journal of Geosciences* (Springer) and the *Euro-Mediterranean Journal for Environmental Integration* (Springer) as a chief editor and managing editor, respectively.



Dr. Nabil Khélifi undertook fellowships at the System for Analysis, Research and Training (START) in 2005 and the German Academic Exchange Service (DAAD), as part of his Ph.D. studies in Marine Geosciences at the University of Kiel in Germany (2006–2010). After his Ph.D., he received a research grant from the German Science Foundation (DFG) to conduct research projects at the GEOMAR Ocean Research Center in Kiel, Germany, on oceanography and climate reconstructions in the North Atlantic and the Mediterranean (2010–2013). His research findings have been presented at many conferences and published in esteemed journals. He co-organized workshops on the Pliocene climate in Bordeaux, France (2009) and Bristol, UK (2013), funded by the European Science Foundation (ESF). In late 2013, he received the Swiss Government Excellence Scholarship (SGES). In 2014, he joined Springer in Heidelberg, Germany, as an Editor, was promoted to Senior Editor in 2017 responsible for developing their publishing program in the MENA region. He is active in educational seminars for authors, reviewers, and editors to help improve publication output and quality. He is a visiting lecturer at King Saud University, KSA, where he gives M.Sc. lectures on scientific presentations and publishing techniques, as well as career development workshops. He has launched two Springer conferences (more details at www.emcei.net and www.cajg.org). In 2016, he was awarded the Africa Green Future Leadership Award for his promotion of publications from Africa. In 2020, he received the Saudi Society for Geosciences Award for successful management of the *Arabian Journal of Geosciences*.

Global Environmental Change (T1): Atmosphere



Climate Networks

Zhihua Zhang

Abstract

The climate system is a complex, multidimensional multiscale nonlinear system in which different physical processes act on different temporal and spatial scales. The climate networks use the theory of known complex networks to analyse climate system and enable novel insights into trends, patterns and mechanisms of global climate change over a wide range of spatio-temporal scales. Any change in climate system can be detected easily by various network measures (e.g., degree distribution, diameter, clustering and cut sets). In this article, we will briefly review the latest advances on climate networks.

Keywords

Climate change • Climate networks • Network measurements • Teleconnection

1 Introduction

The climate system is composed of individual parts linked together in some way. The application of the complex network in modeling global and regional climate system opens a brand-new approach for studies on patterns, teleconnections and internal mechanisms of climate system (Zhang and Li 2019). The nodes in climate network are generally chosen

as geographical sites. Each node always carries one or several measured climate states/variables that change with time. Pearson correlation coefficient at various lag between measured climate states/variables on any pair of nodes is used to quantify the degree of statistical interdependence between nodes (Akram 2016). If Pearson correlation coefficient is larger than a given threshold, then the corresponding pair of nodes is considered as connected, i.e., there exists an edge between nodes. In some cases, Pearson correlation coefficients are also used as the weight of edges. By this way, the strong connections and teleconnections of climate states/variables among geographical sites are well captured by their edges and their weights on the climate network (Zhang and Li 2019).

2 Climate Network Measurements

A climate network consists of a set of nodes and edges. The topology of climate network can reveal important and novel features of the climate system which it represents. Any change in the climate system can be easily detected by various network measures (Zhang and Li 2019).

2.1 Degree Distribution

In a climate network with N nodes v_1, v_2, \dots, v_N and M edges, if there exists an edge between nodes v_i and v_j , then v_i and v_j are said to be adjacent. Denote by k_i the number of adjacent nodes of the node v_i , then k_i is called the degree of the vertex v_i . The degree sequence k_1, k_2, \dots, k_N of nodes v_1, v_2, \dots, v_N can measure the basic property of climate network. Super nodes are nodes with significantly large degree. Denote by N_k the number of nodes with degree k . Then $p_k = N_k/N$ ($k = 0, 1, 2, \dots$) are called the degree distribution of climate network.

Z. Zhang (✉)
Climate Modeling Laboratory, School of Mathematics,
Shandong University, Jinan, China
e-mail: zhangzhihua@sdu.edu.cn

Z. Zhang
MOE Key Laboratory of Environment Change and Natural
Disaster, Beijing Normal University, Beijing, China

2.2 Path, Distance and Diameter

A path in a climate network is a sequence of nodes $v_i = v_{i0}, v_{i1}, \dots, v_{il} = v_j$, where any consecutive pair of nodes v_{ik} and v_{ik+1} is connected by an edge. The distance between nodes v_i and v_j is the number of edges in the shortest path between v_i and v_j . The diameter of the climate network is the maximal value of distance between any two nodes in the network. In some cases, the diameter is also defined by the average value of the distance between any two nodes in the network.

2.3 Clustering

The cluster structure of climate networks provides rich information about the overall composition of the network and identifies closely related regions. Assume that a node v_i has k_i adjacent nodes. The total number of possible edges among k_i adjacent nodes is $k_i(k_i - 1)/2$. If the number of actually existing edges among these adjacent nodes is E_i , then the clustering coefficient of the node v_i is $C_i = 2E_i/k_i(k_i - 1)$. The clustering coefficient of the whole climate network is the average of C_i 's over all the nodes.

2.4 Cut Sets and Communities

Two paths connecting a pair of nodes are edge-independent if they share no edges. Two paths are node-independent if they share no node other than the starting and the ending nodes. If two paths are node-independent, then they are also edge-independent; conversely, it is not true. The number of independent paths between a pair of nodes is called the connectivity of nodes. A node cut set is a set of nodes whose removal or non-functioning will disconnect a given pair of nodes. An edge cut set is a set of edges whose removal will disconnect a pair of nodes. Communities are groups of densely connected nodes with only a few connections between groups.

3 Results

The climate network framework has been successfully applied in the analysis of various climatological data. Results from climate networks have been found consistent with well-known climate phenomena and have also provided new insight into internal mechanisms of global and regional climate change (Tirabassi and Masoller 2013).

3.1 Patterns and Teleconnections

Climate networks generated by different climate parameters can be used to explain major climate teleconnections and shifts (Steinhaeuser et al. 2010). Tsonis and Roebber (2004) studied the NCEP/NCAR reanalysis 500 hPa data set with 2664 grid points which will be viewed as the nodes of the climate network. The edge between any pair of nodes exists if the corresponding Pearson correlation coefficient of climatic data on these two nodes is larger than 0.5. After the analysis of the degree distribution of climate network, Tsonis and Roebber (2004) found that the supernodes in North America and the Northeast Pacific Ocean coincide with the well-known Pacific-North America Pattern, and the super nodes over the southern tip of South America, Antarctica, and the South Indian Ocean coincide with some features of the Pacific-South America pattern. Tsonis et al. (2006) revealed further that climate networks have more long-range connections and less small-range connections under global warming. It means that more teleconnections occur. Gong et al. (2011) showed that these long-range connections greatly shorten the distance between any pair of nodes in climate networks, leading to the rapid transfer of local fluctuation information over the whole climate network and then stabilize the climate system, at the same time, due to a smaller mean path length and a larger mean clustering coefficient, this kind of climate network possesses typical small-world features. By analyzing 500 hPa height network, the surface pressure network and surface temperature network, Tsonis et al. (2011) revealed that effective communities in these climate networks can be traced to known dynamical properties of climate, e.g., North Atlantic Oscillation, Rossby waves, Pacific Decadal Oscillation.

3.2 El Niño

El Niño, a massive burst of heat exchange between the ocean and the atmosphere in the Pacific Ocean, is regularly tracked by measurements of sea surface temperatures and pressure differences Gozolchiani et al. (2008). Gozolchiani and Harlin (2011) constructed a climate network by using 1957–2001 global surface air temperature from ERA40 gridded datasets. By the analysis of degree distributions of 14 nodes located in the eastern equatorial of El Niño Basin, Gozolchiani and Harlin (2011) revealed that when El Niño events began, the El Niño basin partially lost its influence on its surroundings, and after three months, this influence was restored while the basin lost all dependence to its surroundings and became autonomous. Martin et al. (2013)

showed that during El Niño periods the connectivity in the climate network is higher than that during normal periods. Meng et al. (2018) introduced a forecasting index based on edge weights of climate network to accurately and simultaneously forecast both the onset and magnitude of El Niño.

3.3 North Atlantic Oscillation

The North Atlantic Oscillation (NAO) is the most dominant mode of variability of the surface atmospheric circulation in the Atlantic which reflects a large-scale seesaw in atmospheric mass between the subtropical high and the polar low. NAO has a significant effect on winter climate/weather in Europe and North Asia. Guez et al. (2012) constructed a regional climate network based on NCEP/NCAR reanalysis of air temperature, and found that the NAO variations influence the number of edges in the climate network, in details, the number of strong links in the network increases during times of positive NAO indexes, and decreases during times of negative NAO indexes. Guez et al. (2013) further revealed that NAO might interact with very far locations from the North Atlantic basin, in the Southern Pacific Ocean.

4 Discussion and Conclusions

The climate system is a complex, multidimensional multi-scale nonlinear system in which different physical processes act on different temporal and spatial scales. The climate network is becoming a powerful tool to reveal climate patterns and internal mechanisms, quantify uncertainties of climate parameters, analyse strength and range of teleconnections and examine structure sensitivity of the climate system. Super nodes in climate networks can reveal and re-discover key climate patterns and related dynamical properties. Change of degree distributions in climate networks can reflect impacts known as climate events (e.g.,

El Niño) on different regions and demonstrate how the climate system responds to these events. Until now, the method of climate network is only marginally explored and is expected to have a big development in the near future.

References

- Akram, M.: Integrated development and climate network: climate and development. *IOP Conf. Ser. Earth Environ. Sci.* **6** (2016)
- Gong, Z., Wang, X., Zhi, R., Feng, A.: Circulation system complex networks and teleconnections. *Chin. Phys. B* **20**, 079201(2011)
- Gozolchiani A., Harlin, S.: Emergence of El Niño as an autonomous component in the climate network. *Phys. Rev. Lett.* **107**, 148501 (2011)
- Gozolchiani, A., Yamasaki, K., Gazit, O., Havlin, S.: Pattern of climate network blinking links follows El Niño events. *Europhys. Lett.* **83**, 28005 (2008)
- Guez, O., Gozolchiani, A., Berezin, Y., Brenner, S., Havlin, S.: Climate network structure evolves with North Atlantic Oscillation phases. *Europhys. Lett.* **98**, 38006 (2012)
- Guez, O., Gozolchiani, A., Berezin, Y., Wang, Y., Havlin, S.: Global climate network evolves with North Atlantic Oscillation phases: coupling to Southern Pacific Ocean. *Europhys. Lett.* **103**, 68006 (2013)
- Martin, E.A., Paczuski, M., Davidsen, J.: Interpretation of link fluctuations in climate networks during El Niño periods. *Europhys. Lett.* **102**, 48003 (2013)
- Meng, J., Fan, J., Ashkenazy, Y., Bunde A., Havlin, S.: Forecasting the magnitude and onset of El Niño based on climate network. *New J. Phys.* **20**, 043036 (2018)
- Steinhaeuser, K., Chawla, N.V., Ganguly, A.R.: An exploration of climate data using complex networks. *ACM SIGKDD Explor.* **12** (1), 25–32 (2010)
- Tirabassi, G., Masoller, C.: On the effects of lag-times in networks constructed from similarities of monthly fluctuations of climate fields. *Europhys. Lett.* **102**, 59003 (2013)
- Tsonis, A.A., Roebber, P.J.: The architecture of the climate network. *Phys. A* **333**, 497–504 (2004)
- Tsonis, A.A., Swanson, K.L., Roebber, P.J.: What do networks have to do with climate? *Bull. Am. Meteorol. Soc.* **87**, 585–595 (2006)
- Tsonis, A.A., Wang, G., Swanson, K.L.: Community structure and dynamics in climate networks. *Clim. Dyn.* **37**, 933–940 (2011)
- Zhang, Z., Li, J.: *Big Data Mining for Climate Change*. Elsevier (2019)



Assessment of Temperature Trends in Different Bioclimatic Zones of India

Amit Dhorde, Amitesh Gupta, and Anargha Dhorde

Abstract

Trends in maximum, minimum and mean temperatures in seven bioclimatic zones have been studied at seasonal and annual scales with the help of data from 57 stations all over India for the period from 1901 to 2015. Linear regression model is used to determine the rate of change of temperature and student t-test is applied for significance testing. Results are cross-checked with those obtained with the Mann-Kandall test. The study reveals that in all zones maximum temperature is increasing at higher rates than minimum temperature except the sub-humid moist zone and typic arid zone during the summer season. The investigation also reveals that the increasing trend in maximum temperature is higher in moist areas than in arid areas, while the increasing trend in minimum temperature is greater in arid areas than in moist areas.

Keywords

Maximum temperature • Minimum temperature • Bioclimatic zones • Linear regression • India

1 Introduction

IPCC (2014) has stated that global temperature has increased by 0.89 °C over the period 1901–2012. Furthermore, it has been projected that the global mean surface temperature may

A. Dhorde (✉)
Department of Geography, Savitribai Phule Pune University,
Pune, 411007, India

A. Gupta
Indian Institute of Remote Sensing, ISRO, Dehradun, 248001,
India

A. Dhorde
Department of Geography, Nowrosjee Wadia College (Affiliated
to Savitribai Phule Pune University), Pune, 411001, India

increase by 0.3–1.7 °C by 2100. In these changing circumstances, many studies were carried out in India. Jain and Kumar (2005), Arora et al. (2005), Kothawale et al. (2010), Pal and Al-Tabba (2010), and Kothawale et al. (2016) found that trends of TMAX, TMIN, TM showed significant warming over most parts of the country. Paul et al. (2015) studied temperature trends over agro-climatic zones in India and found that arid and semi-arid temperate zones witnessed increasing temperature all over India while humid and semi-arid tropics experienced increasing temperature trend during most of the months in the year. Singh et al. (2007) reclassified bioclimatic zones for North-East India considering temperature and humidity as one of the most important factors. A study by Kothawale and Kumar (2005) found that the accelerating warming trend of annual TM after 1971 was more than four times than the warming trend of annual TM before 1971. Similarly, a study carried out by Srivastava et al. (2017) showed that the annual TM increased by 0.17 °C/decade during 1981–2010 while it was only 0.06 °C/decade during 1901–2010. Hence, it is very clear that there is a remarkable shift of change in temperature trend in the decade of 1971–80. Therefore, in the present study, trend analysis was carried out for the entire period (i.e. 1901–2015) and also for two different time periods (i.e. 1901–75 and 1976–2015), so as to understand the behavior of temperature trends during these two phases as well as for the entire period. The temperature series has been divided into two periods based on the findings by Kothawale and Kumar (2005) and Srivastava et al. (2017).

2 Study Area, Data and Methods

The study area is covered by well distributed 57 stations all over India. All 57 stations are located in 7 different bio-climatic zones such as per humid, humid, sub humid moist, sub humid dry, semi-arid moist, semi-arid dry and typic arid. These bioclimatic zones have been adopted from

Mandal et al. (1999). For each station, monthly TMAX, TMIN and TM data were used to construct seasonal and annual series, based on criteria of seasons: Summer (March, April, May), Monsoon (June, July, August, September), Post-Monsoon (October, November) and Winter (December, January).

For computation of long term temperature trend, linear regression method was used. The significance of the trends was evaluated by Student's t test and cross checked by the Mann_Kendall test. The results from linear regression and Mann-Kandall test were tested at 95% confidence level. The same technique is applied for the analysis of two periods (i.e. 1901–75 and 1976–2015).

3 Results and Discussion

The trend analysis for TMAX and TMIN at seasonal and annual scale for the period of 1901–2015 indicates that except the summer season, trends during all other seasons and at an annual scale revealed that the decadal rate of TMAX is maximum in humid zone followed by the per humid zone, while the decadal rate of TMIN is highest in typical arid zone during all the seasons and at an annual scale too (Table 1). The scenario changes as the analysis for 1901–1975 period shows that semi humid areas registered the highest rate of increase in TM; whereas for the 1975–2015 period, typical arid zones experienced the highest rate of increase in TM at annual and seasonal scales.

The obtained results suggest that there must be an inconceivable change in the pattern of temperature distribution around 1975 as arid areas started experiencing a sudden and continuous increase of temperature than that of the other areas after 1975. In case of TMAX, the humid and semi humid moist areas recorded a maximum increase before 1975, but after 1975 the typical arid zone experienced higher increasing rate than other areas except during monsoon and post-monsoon seasons when per humid and humid areas witnessed higher increasing rate than the other zones. It implies that the decrease in cloud cover, especially over moist areas, allows the ground to be warmer during day time, hence playing a key role in the distribution of TMAX. Interestingly, during pre-1975 period, sub humid areas were experiencing the highest rate of increase in TMIN, but typical arid areas started to warm with the highest rate during post 1975 period. It indicates that, in spite of the decrease in cloud cover over the whole country, the moisture availability had increased in arid areas over the time, hence the depth of the cloud must be showing tendency to be lesser over long-term. It also indicates that the wind flow pattern in different isobaric level might have been changing since the 70s as the moisture carried by the wind towards the arid areas from the moist areas results in a decrease in condensation process for the formation of clouds in humid areas, although it is not very sure that arid areas are getting more rainfall or not because of the increasing moisture availability only, but it helps the arid region to be warmer during night-time. Not only that the decreasing trend of wind speed

Table 1 Decadal trends in TMAX and TMIN observed over different bioclimatic zones

Bioclimatic zones	Annual		Summer		Winter	
	TMAX	TMIN	TMAX	TMIN	TMAX	TMIN
Per humid	0.097*	0.006	0.077*	0.001	0.122*	0.006
Humid	0.11*	0.023*	0.105*	0.004	0.147*	0.05*
Sub-humid dry	0.055*	0.036*	0.046*	0.035*	0.065*	0.054*
Sub-humid moist	0.039*	0.045*	-0.0026	0.061**	0.034*	0.067*
Semi-arid dry	0.03*	0.005	0.035*	0.006	0.03*	-0.003
Semi-arid moist	0.045*	0.02*	0.057*	0.021*	0.03*	0.019*
Typic arid	0.095*	0.086*	0.109*	0.112**	0.117*	0.105*
Bioclimatic zones	Monsoon		Post-monsoon			
	TMAX	TMIN	TMAX	TMIN		
Per humid	0.082*	0.012	0.122*	0.006		
Humid	0.084*	0.0006	0.118*	0.056*		
Sub-humid dry	0.044*	0.012	0.076*	0.063*		
Sub-humid moist	0.056*	-0.004	0.1*	0.086*		
Semi-arid dry	0.023*	0.01	0.033*	0.01		
Semi-arid moist	0.042*	0.004	0.049*	0.039*		
Typic arid	0.069*	0.029*	0.091*	0.137*		

*Values are significant at 0.05 level (95% confidence)

as noticed by Padmakumari et al. (2013) also helped to increase the night time temperatures in the areas which are far away from the coast, because, lesser wind speed is not able to push the air near ground surface away in a particular area. Hence, the places like arid zones in India which are far from the coast must be experiencing the warmer stagnant air during night time.

This study supports findings by other researchers, such as Oldenborgh et al. (2017) who reported increasing humidity over Northwestern India. The increase in humidity will lead to an increase in TMIN rather than an increase in TMAX in typical arid and semi-arid dry areas. Conclusion by Jaswal (2010), Jaswal et al. (2017) about the decrease in amounts of annual cloud cover as well as the decreasing trend of cloud cover in summer season in northeastern India by Roy and Balling (2005) are well supported by the findings of the present study.

4 Conclusions

The present study aims to detect trends in temperature over the major Indian cities with special reference to their location in the bioclimatic zones of India. Trend analysis for the entire period (1901–2015) revealed that, except for the Summer's TMAX and Monsoon's TMIN of sub-humid moist bioclimatic zone, all the trends during all seasons for all zones were positive. Annual TMAX has increased with the highest rate, which is of 0.11 °C/decade. This rate remains above 0.1 °C/decade during all seasons except Monsoon. But, post 1975 except for sub-humid dry zone; all the other zones witnessed a rise in TMAX with rates above 0.1 °C/decade. During summer season it is observed that the rates in TM in all zones prior to 1975 were between 0 and 0.1 °C/decade, but after 1975 the rates have remained above 0.1 °C/decade. In fact they are much higher (more than 0.4 °C/decade) in the typical arid zone. The rapid increase of temperature after 1975 gives a hint that there is a substantial scope left for further research on climatic variations over India. The climate change in terms of change in temperature trend is found to be sounder in arid areas; hence other climatological phenomena are required to be investigated to understand the process of change such as warming with a high alarming rate, is expected in the near future.

References

- Arora, M., Goel, N.K., Singh, P.: Evaluation of temperature trends over India. *J. Hydrol. Sci.* **50**, 81–93 (2005)
- IPCC: Climate Change 2014: synthesis report. Contribution of Working Groups I, II and III to the Fifth Assessment Report of the Intergovernmental Panel on Climate Change [Core Writing Team, Pachauri, R.K., Meyer, L.A. (eds.)]. IPCC, Geneva, Switzerland, p. 151 (2014)
- Jain, S.K., Kumar, V.: Trend analysis of rainfall and temperature data for India. *Curr. Sci.* **1**, 102–105 (2005)
- Jaswal, A.K., Kore, P.A., Singh, V.: Variability and trends in low cloud cover over India during 1961–2010. *Mausam* **68**, 235–252 (2017)
- Jaswal, A.K.: Changes in total cloud cover over India based upon 1961–2007 surface observations. *Mausam* **61**, 455–468 (2010)
- Kothawale, D.R., Kumar, K.R.: On the recent changes in surface temperature trends over India. *Geophys. Res. Lett.* **32**, L18714 (2005). <https://doi.org/10.1029/2005GL023528>
- Kothawale, D.R., Munot, A.A., Kumar, K.K.: Surface air temperature variability over India during 1901–2007, and its association with ENSO. *Clim. Res.* **42**, 89–104 (2010)
- Kothawale, D.R., Deshpande, N.R., Kolli, R.K.: Long term temperature trends at major, medium, small cities and hill stations in India during the period 1901–2013. *Am. J. Clim. Chan.* **5**, 383–398 (2016)
- Mandal, C., Mandal, D.K., Srinivas, C.V., Sehgal, J., Velayutham, M. S.: Soil-climatic database for crop planning in India. National Bureau of Soil Survey and Land Use Planning, Nagpur, Technical Bulletin, NBSS Publ. No. 53, 994, p. 15 (1999)
- Oldenborgh, J.V., Philip, S., Sarah, K., Weele, M.V., Uhe, P., Otto, F., Singh, R., Pai, I., Rao, K.A.: Extreme heat in India and anthropogenic climate change. *Nat. Hazards Earth Syst. Sci. Discussions* 1–23. <https://doi.org/10.5194/nhess-2017-107> (2017)
- Padmakumari, B., Jaswal, A.K., Goswami, B.N.: Decrease in evaporation over the Indian monsoon region: implication on regional hydrological cycle. *Clim. Chan.* (2013). <https://doi.org/10.1007/s10584-013-0957-3>
- Pal, I., Al-Tabbaa, A.: Long-term changes and variability of monthly extreme temperatures in India. *Theor. Appl. Clim.* **100**, 45–56 (2010)
- Paul, R.K., BIRTHAL, P.S., Paul, A.K., Gurung, B.: Temperature trend in different agro-climatic zones in India. *Mausam* **66**, 841–846 (2015)
- Roy, S.S., Balling, R.C., Jr.: Analysis of trends in maximum and minimum temperature, diurnal temperature range, and cloud cover over India. *Geophys. Res. Lett.* **32**, L12702 (2005). <https://doi.org/10.1029/2004GL022201>
- Singh, M.K., Mahapatra, S., Atreya, S.K.: Development of bio-climatic zones in north-east India. *Energ. Build.* **39**, 1250–1257 (2007). <https://doi.org/10.1016/j.enbuild.2007.01.015>
- Srivastava, A.K., Kothawale, D.R., Rajeevan, M.N.: Variability and long-term changes in surface air temperatures over the Indian subcontinent. In: Rajeevan, M.N., Nayak, S. (eds) *Observed Climate Variability and Change Over the Indian Region*. Springer Geology, pp. 17–35. https://doi.org/10.1007/978-981-10-2531-0_2 (2017)



Statistical Analysis of Wind to Assess Climate Change (Central Italy)

Matteo Gentilucci, Marwan Ghanem, and Maurizio Barbieri

Abstract

Knowledge of weather dynamics is very important, because it controls the climate. These processes are known both globally and in smaller areas. However, there is not always a statistical assessment of the possible changes that may occur in the atmosphere over the years. In order to evaluate from a climatic point of view the atmospheric dynamics that have occurred over the years, one of the most interesting tools used is wind analysis. This study aims to use anemometric data to assess changes in atmospheric dynamics, also investigating possible relations with precipitation. The prevailing wind directions, wind speed and precipitation were related in order to obtain a schematization of the dynamics occurred in micro areas. This has resulted in interesting reports that have shown a more pronounced change in the last 10 years.

Keywords

Wind • Precipitation • Atmospheric dynamics • Climate change

1 Introduction

Building a model of atmospheric circulation is a very complex and expensive operation, which requires great precision. The atmosphere is composed of gases that tend to put themselves in a situation of balance of energy,

M. Gentilucci (✉)
University of Camerino, 62032 Camerino, Italy
e-mail: matteo.gentilucci@unicam.it

M. Ghanem
Birzeit University, Ramallah, Palestine

M. Barbieri
Sapienza University of Rome, 3029 Rome, Italy

redistributing solar energy. This generates the displacement of air masses, which in turn is responsible for atmospheric phenomena that occur at macro and micro scales. To summarize such a situation is very difficult, although some parameters such as the wind are explanatory of the dynamics that have insisted on certain areas. This research aims to statistically analyze, on a daily basis, the prevailing wind direction and wind speed and find possible correlations with precipitation. This study represents a pilot project that has been developed for the weather station of Macerata, with the intention of extending the methodology to the entire Marche region, which is an area of about 9700 km², located on the Adriatic side of central Italy. There are many studies that have used wind in relation to precipitation to explain it or find a strong relationship with it (Johansson and Chen 2016). None, however, has ever put the wind at the center of the discussion by assessing the atmospheric dynamics of this variable in relation to the changes over the years. Other studies have evaluated the impact of wind gusts and extreme precipitation events on different areas of the Mediterranean (Raveh-Rubin and Wernli 2015).

2 Methods

For this study, daily data on wind direction, wind speed and precipitation were collected for the Macerata weather station from 1989 to 2019. The data were obtained through the Experimental Geophysical Observatory of Macerata that has previously validated the data. The validation is initially instantaneous in order to verify if data are within acceptable range limits, then the data are compared with other nearby anemometric stations to assess their reliability. The anemometer is located on the crest of a hill and has a height of 20 m. Daily data were processed by evaluating the prevailing wind direction for each day, placing them in a rose of 16 directions, one distant from the other 22°30'. In addition, the average daily wind speeds and the average gust speeds

were evaluated. The search for a relationship with the rain has required, in the same way as the wind, of daily rainfall data. The rainfall data have been further validated following the methodologies outlined by the WMO (World Meteorological Organization) and put into practice by other studies (Gentilucci et al. 2018). Initially, general statistics were carried out for the entire period under investigation from 1989 to 2019, both annually and monthly, in order to investigate 30 years period. Subsequently, the period was divided into 10-year intervals with the aim of assessing any climate change that had occurred (1989–1999; 1999–2009; 2009–2019).

3 Results

In the last 30 years, there is a clear prevalence in percentage of winds from NNW (19.2%) and NW (15.3%), followed by winds from SE (10.2%) and SSE (8.7%). Also, over the period of 30 years. The average speed has been investigated in relation to the prevailing daily direction to understand if there is a relationship between a wind in a given direction and the average speed of the same. The highest average speeds were reached by the winds from SW, WSW, W and NNW, all between 4.12 and 4.16 m/s. The analysis of the prevailing directions in relation to the average of the daily gusts is much more significant. In fact, there are 3 directions SW, WSW, W that have an average gust velocity higher than 13 m/s; while in this case the NNW is not the fourth direction and it has an average of 10.7 m/s. As regards to the relationship with the rains, we can observe that the rainiest

winds for this area in the last 30 years have come from the NE (5.4 mm) and NNE (4.3 mm); while the least amount of rainfall is corresponding with the wind direction from SSE (1.2 mm) and SE (1.2 mm). Climate change has been assessed at ten-yearly intervals, initially taking into account the percentage value assumed by the prevailing wind direction.

The prevailing wind has changed in the last decade, in fact if until 2009 it was the NNW wind, from 2009 it became the NW wind (Fig. 1).

From Fig. 2, it can be seen that there is a significant increase in average rainfall with winds from NNE, ENE and NNW, with a clear decrease in rainfall from southern winds; although the analysis of distribution through a fourth-order polynomial does not reveal huge differences in distributions. Finally, the variation in wind speed between the 3 periods was also evaluated; and in this case, the period 1999–2009 showed an average speed 14–16% higher than the other two intervals.

4 Discussion

The prevailing winds for this region in the past 30 years are those from the north-west and those from the south-east, although on the Adriatic coast the prevailing winds are indicated by other studies such as bora (NNE) and sirocco (SE) (Pomaro et al. 2017). This analysis highlights the climate changes in a single weather station in terms of wind. In fact, during the last 10 years, there has been a decrease in winds from NNW direction and an increase in those from

Fig. 1 Wind rose for the prevailing wind directions in Macerata for the entire period 1989–2019 and for the ten-yearly interval (1989–1999; 1999–2009; 2009–2019)

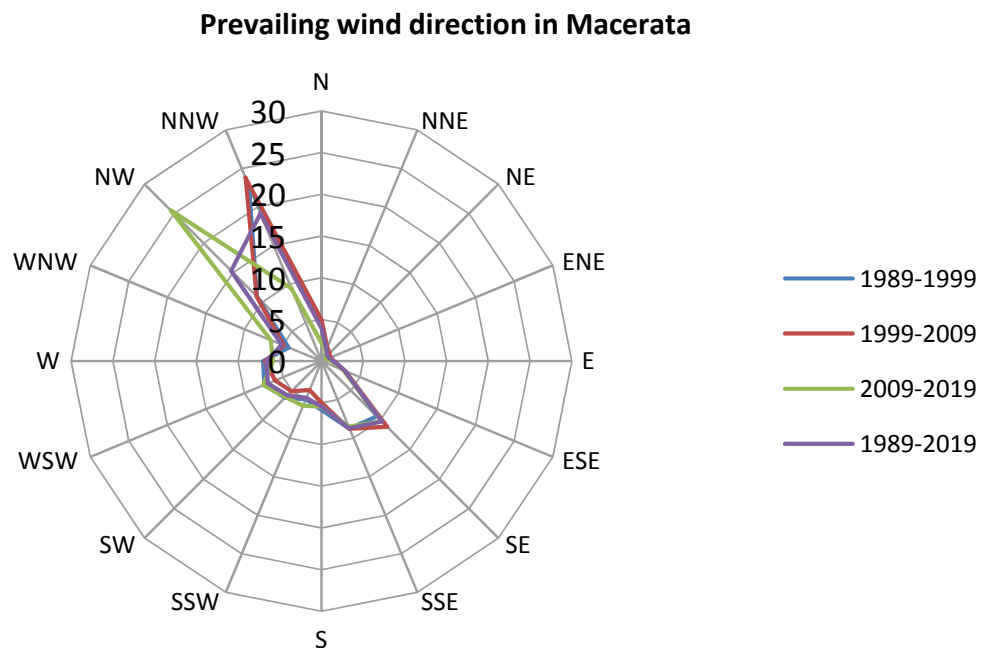
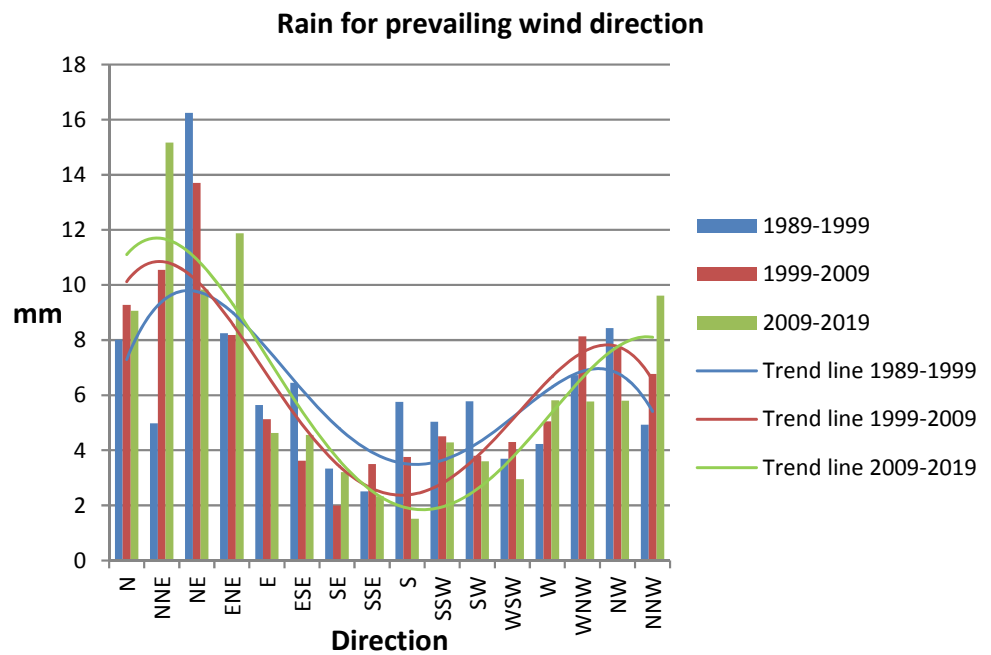


Fig. 2 Percentage of rain per prevailing wind direction for each decade (1989–1999; 1999–2009; 2009–2019), 4th order polynomial trend line for all intervals



NW direction. In addition, the percentage of rain per prevailing wind has changed; the rainfall concomitant with the winds from NNE, ENE and NNW has increased, while the winds from NE have decreased. As far as the wind speed average is concerned, the trend of the last decade shows a decreasing trend. Other works testify to a growing trend from the mid-1970s in Italy until at least the end of the 1990s (Pirazzoli and Tomasin 2003). This trend is in line with the present study until 2009, when the trend becomes decreasing.

5 Conclusions

The survey of winds is not very common in this part of Italy. However a mapping of the anemometric conditions of a region is a prerequisite for full knowledge of the climate and climate change of a region. This study could provide important developments in many fields both by analyzing

the variation of atmospheric dynamics, but also for the exploitation and profitability of wind energy.

References

- Gentilucci, M., Barbieri, M., Burt, P., D'Aprile, F.: Preliminary data validation and reconstruction of temperature and precipitation in Central Italy. *Geosciences* **8**(6), 202 (2018)
- Johansson, B., Chen, D.: The influence of wind and topography on precipitation distribution in Sweden: statistical analysis and modelling. *Int. J. Climatol.* **23**(12), 1523–1535 (2016)
- Pirazzoli, P.A., Tomasin, A.: Recent near-surface wind changes in the central Mediterranean and Adriatic areas. *Int. J. Climatol.* **23**(8), 963–973 (2003)
- Pomaro, A., Cavaleri, L., Lionello, P.: Climatology and trends of the Adriatic Sea wind waves: analysis of a 37-year long instrumental data set. *Int. J. Climatol.* **37**(12), 4237–4250 (2017)
- Raveh-Rubin, S., Wernli, H.: Large-scale wind and precipitation extremes in the Mediterranean: a climatological analysis for 1979–2012. *Q. J. Royal Meteorol. Soc.* **141**(691), 2404–2417 (2015)



Impact of Estimated Wind Speed on Temperature-Based on ET_0 Methods

Slavisa Trajkovic and Milan Gocic

Abstract

Many data are used to estimate reference evapotranspiration (ET_0). Wind speed is usually the least available parameter required for ET_0 estimation. The objective of this study is to evaluate the impact of estimated wind speed on temperature-based ET_0 methods. Data from three Serbian stations (Southeast Europe) are used in this research. Five temperature-based approaches using three different estimated wind speed values were compared to the standard Penman–Monteith (PM) method. Temperature-based PM equation with local average wind speed (U_{2l}) gives accurate ET_0 estimates at each location. If the regional average wind speed ($U_{2r} = 1.3 \text{ m s}^{-1}$) is used at windless locations, the ET_0 estimates are less precise. The general average wind speed value ($U_{2g} = 2.0 \text{ m s}^{-1}$) should be used with caution especially at windless locations. Overall results strongly support using of the PM method even if limited data are available.

Keywords

Evapotranspiration • Temperature • Wind speed • Penman–Monteith

1 Introduction

Evapotranspiration (ET) is one of the key factors in the hydrological cycle (Ermolaeva et al. 2019). The reference evapotranspiration (ET_0) is the ET from reference crop surface. Knowledge of ET_0 is of great significance for hydrology, agriculture, irrigation and climate change studies (Hussein 2018). The United Nations Food and Agricultural

Organization (FAO) recommends the Penman–Monteith (PM) method for the ET_0 estimation (Allen et al. 1998). This method uses many weather data (wind speed, humidity, temperature and solar radiation) (Allen et al. 1998; Quej et al. 2019). However, it is difficult to obtain all necessary input data. In such circumstances, simplified methods are used for ET_0 estimation (Trajkovic et al. 2019; Trajkovic and Kolakovic 2010). Wind speed is usually the least available meteorological parameter required for the ET_0 estimation. This parameter is not observed at many locations and may need to estimate wind speed when temperature-based equations are used. The main objective of this study is to evaluate the impact of estimated wind speed on temperature-based ET_0 methods.

2 Materials and Methods

Full meteorological data sets from three stations (Nis, Novi Sad and Sombor) in Serbia (Southeast Europe) during the period of 1980–2010 are used in this study. Unfortunately, the data between 2010 and 2018 were not available to the authors. The annual average temperature (T) ranged between 11.5 and 12.4 °C. The average wind speed (U_2) varied between 0.9 and 1.9 m s^{-1} . The average ET_0 estimates varied between 2.2 and 2.4 mm day^{-1} . According to the aridity index, all stations are humid. The annual precipitation sums are unevenly distributed over months.

The temperature-based (TB) PM equation used in this paper is (Allen et al. 1998):

$$ET_0(T) = \frac{0.408 \cdot \Delta \cdot R_n(T) + \gamma \frac{900}{T+273} U_{2e} \cdot (e_s - e_a(T))}{\Delta + \gamma(1 + 0.34 \cdot U_{2e})} \quad (1)$$

where $ET_0(T)$ = temperature-based ET_0 (mm day^{-1}), Δ = slope of the saturation vapor pressure function ($\text{kPa } ^\circ\text{C}^{-1}$), γ = psychrometric constant ($\text{kPa } ^\circ\text{C}^{-1}$), $R_n(T)$ = temperature-based net radiation ($\text{MJ m}^{-2} \text{ day}^{-1}$), G : soil heat flux

S. Trajkovic (✉) · M. Gocic
Faculty of Civil Engineering and Architecture, University of Nis,
18000 Nis, Serbia
e-mail: slavisa@gaf.ni.ac.rs

density ($\text{MJ m}^{-2} \text{day}^{-1}$), T = mean air temperature ($^{\circ}\text{C}$), e_s = saturation vapor pressure (kPa), $e_a(T)$ = temperature-based actual vapor pressure (kPa) and U_{2e} = estimated average 24 h wind speed at 2 m height (m s^{-1}).

Alternative procedures for estimating the missing weather data were introduced by Allen et al. (1998). If humidity data (e_a) and radiation data (R_n) are not available, the minimum temperature should be used for the estimation of actual vapor pressure ($e_a(T)$) and radiation ($R_n(T)$). If wind speed is lacking, then the average wind speed can be used. In this study, three values of wind speed were applied. The "local" values of wind speed (U_{2l}) were calculated as the average wind speed for each location. These values are: 0.9 m s^{-1} for Nis, 1.9 m s^{-1} for Novi Sad, and 1.6 m s^{-1} for Sombor. The "regional" value (U_{2r}) of 1.3 m s^{-1} was obtained from Trajkovic and Kolakovic (2010) as the average wind speed in Serbia and the "global" value (U_{2g}) of 2.0 m s^{-1} was suggested by Allen et al. (1998) as the average wind speed worldwide. Three TB PM equations were used in this study: $\text{PM}_{ig}(T, R_n(T), e_a(T), U_{2g})$, $\text{PM}_{ir}(T, R_n(T), e_a(T), U_{2r})$ and $\text{PM}_{il}(T, R_n(T), e_a(T), U_{2l})$. The temperature-based Hargreaves (HR) (Hargreaves 1994) and Thornthwaite (TH) (Thornthwaite 1948) equations were also used in this study. The Root-Mean-Square Error (RMSE), Nash–Sutcliffe Efficiency coefficient model (NSE), ratio of temperature-based estimates (ET) to PM estimates (ET/PM) and coefficient of determination (R^2) were used as statistical parameters.

3 Results and Discussion

The three temperature-based PM approaches, Hargreaves and Thornthwaite equations were compared to the PM equation. The values of statistical indicators are shown in Table 1.

The PM_{il} approach with U_{2l} gave excellent matching with the Penman–Monteith (PM) for all locations with the smallest RMSE values at windless Nis and windy Sombor. The RMSE values for this approach did not vary significantly (from 0.23 to 0.24 mm day^{-1}). The PM_{ir} approach

with U_{2r} had excellent agreement with the PM estimates for windy locations such as Novi Sad and Sombor. The RMSE values varied from 0.19 to 0.35 mm day^{-1} . The PM_{ig} with U_{2g} was reasonably good at locations with a local average wind speed near to 2 m s^{-1} such as Novi Sad and Sombor. This approach was very poor in estimating ET_0 at Nis. This result was expected because of small average wind speed at Nis ($U_{2l} = 0.9 \text{ m s}^{-1}$).

The Hargreaves method (HR) was poor in estimating ET_0 . The RMSE values for this approach ranged from 0.42 to 0.79 mm day^{-1} . The Hargreaves was the lowest ranking method at Nis and the second lowest at Novi Sad and Sombor. The values of statistical indicators for this method were increased by decreasing the wind speed.

The Thornthwaite method (TH) found to be poor in ET_0 estimation independent from wind speed. The RMSE values for this approach varied from 0.51 to 0.60 mm day^{-1} . The Thornthwaite was the lowest ranking approach at Novi Sad and Sombor and the second lowest at Nis.

The PM_{ig} and HR approaches highly overestimated annual PM ET_0 sum at all locations except PM_{ig} for Novi Sad. The TH approach underestimated PM ET_0 between 8 and 17%. All approaches gave very similar coefficient of determination (0.98 – 0.99) except TH which R^2 varied from 0.92 to 0.96 .

A plot of $\text{PM}_{il} \text{ET}_0$ vs. PM ET_0 values for all three locations is presented at Fig. 1. A large number of points close to the 1:1 line demonstrate excellent agreement between estimates. The average overestimation was 5%.

4 Conclusions

In this study, three temperature-based PM approaches, Hargreaves and Thornthwaite methods were compared to the PM method using data from three humid locations with different wind speed values. If wind speed is not measured, using temperature-based Penman–Monteith equation with local average wind speed (U_{2l}) gives accurate estimates at each location. If the regional wind speed value ($U_{2r} = 1.3$

Table 1 Statistical indicators for three Serbian sites

Method	Nis ($U_{2l} = 0.9 \text{ ms}^{-1}$)			Novi Sad ($U_{2l} = 1.9 \text{ ms}^{-1}$)			Sombor ($U_{2l} = 1.6 \text{ ms}^{-1}$)		
	RMSE	NSE	ET/PM	RMSE	NSE	ET/PM	RMSE	NSE	ET/PM
PM_{ig}	0.57	0.78	1.22	0.25	0.96	1.05	0.32	0.93	1.11
PM_{ir}	0.35	0.92	1.12	0.24	0.96	0.97	0.19	0.98	1.02
PM_{il}	0.23	0.96	1.05	0.24	0.96	1.04	0.24	0.96	1.06
HR	0.79	0.58	1.29	0.42	0.89	1.12	0.52	0.83	1.17
TH	0.51	0.83	0.92	0.60	0.77	0.83	0.58	0.78	0.85

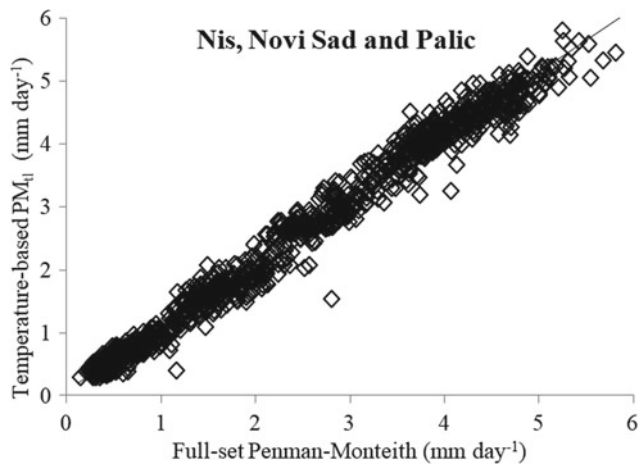


Fig. 1 Temperature-based PM (PM_{t_l}) versus PM ET_0 values

$m\ s^{-1}$) is used at windless location (Nis), the estimates are less precise with higher RMSE. The general average wind speed value ($U_{2g} = 2.0\ m\ s^{-1}$) should be used with caution, especially at windless locations. Low reliability of the Hargreaves method additionally decreases by decreasing the wind speed. Wind speed does not affect already low reliability of the Thornthwaite method. The RMSE values for all temperature-based PM estimates were found to be lower than the corresponding RMSE values of Hargreaves and Thornthwaite equations with the exception of PM_{t_g} at non-windy Nis. This fact strongly supports using the Penman–Monteith method even if limited data are available.

Acknowledgements The presented research is a part of the project of Serbian Academy of Sciences and Arts Branch in Nis (O-15-18), also funded by the Ministry of Education, Science and Technological Development of the Republic of Serbia (TR37003).

References

- Allen, R.G., Pereira, L.S., Raes, D., Smith, M.: Crop evapotranspiration. Guidelines for Computing Crop Water Requirements. FAO Irrigation and Drainage Paper 56 (1998)
- Ermolaeva, O., Zeyliger, A., Muzilev, E., Startseva, Z.: Warm season trends of ET_a : a case study of Near-North Caspian low lands. In: Chamine et al. (eds.) *Advances in Sustainable and Environmental Hydrology, Hydrogeology, Hydrochemistry and Water Resources*, *Advances in Science, Technology and Innovation*, pp. 41–44. Springer Nature (2019)
- Hargreaves, G.H.: Defining and using reference evapotranspiration. *J. Irrig. Drain. Eng.* **120**(6), 1132–1139 (1994)
- Hussein, M.M.A.: Evaluation of Alexandria Eastern Harbor evaporation estimate methods. *Arab. J. Geosci.* **11**(24), 768 (2018)
- Quej, V.H., Almorox, J., Arnaldo, A.J., Moratiel, M.: Evaluation of temperature-based methods for the estimation of reference evapotranspiration in the Yucatán Peninsula, Mexico. *J. Hydrol. Eng.* **24**(2), 05018029 (2019)
- Thornthwaite, C.W.: An approach toward a rational classification of climate. *Geogr. Rev.* **38**(1), 55–94 (1948)
- Trajkovic, S., Kolakovic, S.: Comparison of simplified pan-based equations for estimating reference evapotranspiration. *J. Irr. Drain. Eng.* **136**(2), 137–140 (2010)
- Trajkovic, S., Gocic, M., Pongracz, R., Bartoly, J.: Adjustment of thornthwaite equation for estimating evapotranspiration in Vojvodina. *Theoret. Appl. Climatol.* (2019). <https://doi.org/10.1007/s00704-019-02873-1>

Global Environmental Change (T1): Ocean



The Remote Response of Northern Hemisphere Atmosphere Circulation to ENSO in a Changing Climate

Daria Gushchina and Maria Kolennikova

Abstract

The response of atmosphere circulation in the Northern Hemisphere to the ENSO forcing is revisited in the light of ENSO modifications over the last decades and the possible changes in future climate. It is argued that the planetary circulation response to ENSO differs in dependence on El Niño types: the Eastern Pacific (EP) event is associated with the Rossby wave propagating poleward and is confined to the Pacific region, while the Central Pacific (CP) event induces the circulation pattern at planetary scale similar to the negative phase of Arctic Oscillation (AO). The different response in temperature anomalies is further documented. In the warmer climate the difference between the CP and EP associated circulation patterns vanishes with predominance of AO-like circulation.

Keywords

El Niño Southern Oscillation (ENSO) • Tropics-mid latitude interaction • Temperature anomalies

1 Introduction

Weather and climate variability in extra-tropical regions is influenced by the tropical forcing. The main mode of tropical variability at the interannual timescale is the El Niño Southern Oscillation (ENSO). The ocean warming associated to the El Niño results in a release of large amounts of heat and moisture into the atmosphere; the anomalous heat and moisture are then transferred to the mid-to-high latitudes via atmospheric teleconnections. Understanding the mid

latitude response to ENSO is important for seasonal climate prediction.

The previous investigations suggested that the heat source located in the equatorial Pacific induces the long Rossby wave propagating poleward, that results in pressure anomalies over the Pacific and North America known as a Pacific North American pattern—PNA (Trenberth et al. 1998). However, the recently documented diversity of the El Niño phenomenon that refers to the existence of two types of events: the central Pacific (CP) and the Eastern Pacific (EP) Niño (Capotondi and coauthors 2015) implies the change of teleconnection patterns. Moreover, the shift of sea surface temperature (SST) maximum toward the central Pacific, characterized by the well-developed deep convection, favors the heat and moisture release to the atmosphere strengthening the atmospheric response. The atmospheric response to the two types of El Niño has been mentioned in several studies (Weng et al. 2009; Zheleznova and Gushchina 2016) but they mostly focused on regional peculiarities. Here we revisit the response of Northern Hemisphere planetary scale atmosphere circulation to ENSO forcing taking into account the changes in ENSO properties over the last decades and the possible changes under the global warming.

2 Data and Methods

The monthly geopotential at 1000 and 500 hPa (H1000 and H500) and near surface air temperature were obtained from the NCEP–NCAR reanalysis for the period 1950–2017. The Hadley Centre Global Sea Ice and Sea Surface Temperature (HadISST) archive is used to derive monthly SST anomalies.

The two ENSO indices introduced by Takahashi et al. (2011) are used. They account for the variability associated to the EP El Niño and the CP El Niño events respectively (here after E and C indexes) and are defined based on the

D. Gushchina (✉) · M. Kolennikova
Faculty of Geography, Moscow State University, Leninskie gory
1, Moscow, 119991, Russia

first two EOF modes of SST data from HadISST over the tropical Pacific (120°E – 90°W ; 11°S – 11°N).

The Arctic oscillation (AO) was defined as the first EOF mode of the monthly 1000 (500) hPa geopotential height anomalies poleward of 20°N .

We analyzed the 23 climate models of Coupled Model Inter-comparison Project phase5 (CMIP5), which demonstrated the skill in simulating the two types of El Niño (Matveeva et al. 2018). For the analysis of future climate 6 amongst them (CCSM4, CESM1-BGC, CMCC-CESM, CMCC-CM, CMCC-CMS, FIO-ESM) were chosen based on the quality of simulation of AO structure and regression of the geopotential field onto the ENSO indexes in the CMIP5 experiment “Historical”.

3 Results

To examine the circulation patterns associated to the two types of ENSO, the regression of H1000 against the E and C indexes were calculated (Fig. 1). The regression for C-index is characterized by positive anomalies over the Arctic and a decrease in the surface pressure over the extratropical Pacific and Atlantic (Fig. 1a), that is similar to the circulation pattern associated to a negative phase of Arctic Oscillation (Fig. 1c). The regressed H1000 onto the E-index (Fig. 1b) evidences the wave structure and is reminiscent of PNA

pattern (Fig. 1d). The significance test shows that the centers of anomalies are significant at 90% confidence level. The similar results with even more pronounced annular (wave) structure for the CP (EP) event were obtained for H500.

The difference in extratropical circulation response to the different El Niño types may be associated to the shift of SST anomalies during CP events to the region of enhanced convective forcing that implies stronger and more spatially spread teleconnection patterns.

The different circulation response results in different temperature anomalies in mid-to-high latitudes of Northern Hemisphere with positive anomalies located over Eurasia and America and negative anomalies confined to the polar region during a EP event. The temperature response to an CP event has opposite sign over the most part of Northern Hemisphere with positive/negative maximums centered over Western/Eastern Arctic and is similar to the temperature anomalies associated to the negative AO phase (Fig. 2).

To evaluate the modification of planetary circulation response to ENSO in warmer climate, the regression of geopotential height at 500 hPa onto E and C indexes were calculated from the data of RCP8.5 experiment for 6 CMIP5 models (see Sect. 2). The main difference with modern climate is observed for EP events: the circulation response has no more wave structure but is similar to the AO-like circulation, i.e. to the circulation response to CP events.

Fig. 1 Regression of geopotential anomalies at 1000 hPa onto **a** C, **b** E. index; **c** negative phase of Arctic Oscillation; **d** positive phase of PNA. Credits CMMAP. The thick solid line is zero value

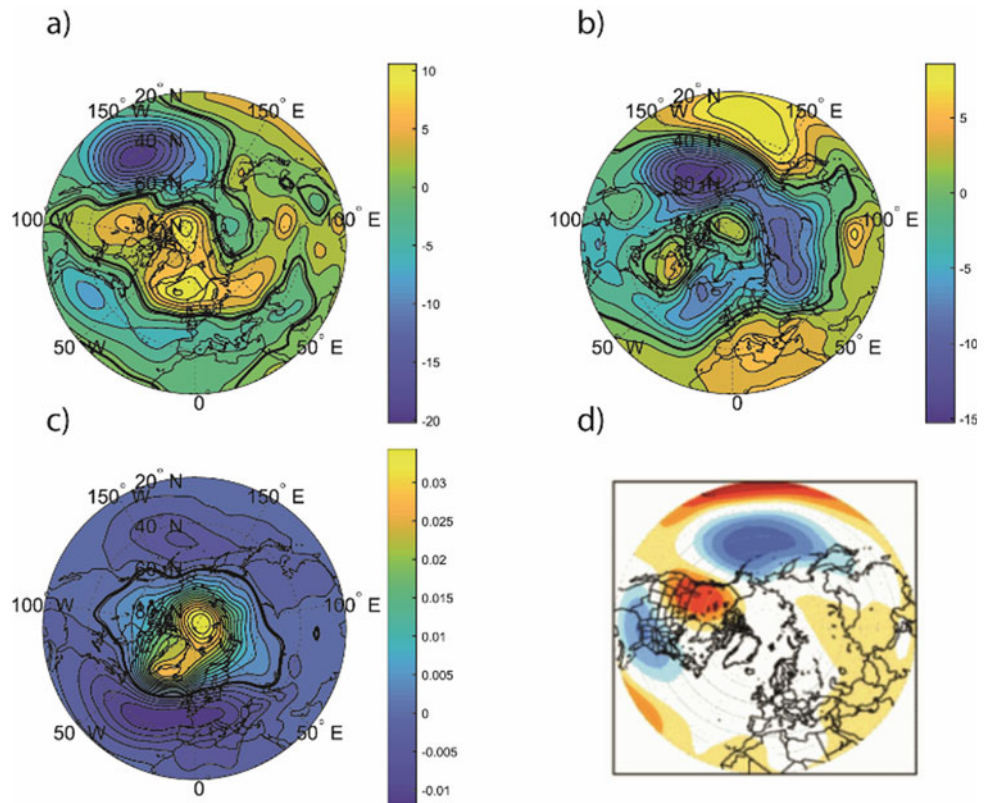
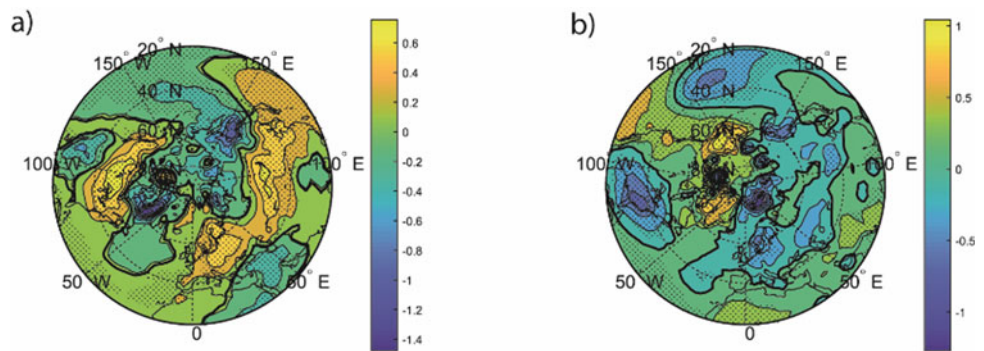


Fig. 2 Regression of near surface air temperature anomalies onto **a** E, **b** C index. The thick solid line is zero value



Noteworthy, the circulation response to CP events does not change significantly with global warming.

4 Discussion

The modification of ENSO associated circulation pattern over the Northern Hemisphere in the future climate is likely to follow the westward shift of the center of action of the EP El Niño; which, combined to the warming SST trend, has the potential to impact the ENSO teleconnection. As was demonstrated in Sect. 3, the SST anomalies localized in the central Pacific induce the atmosphere response similar to the AO negative phase structure (Fig. 1a, c).

5 Conclusions

The planetary circulation response to the ENSO differs in dependence on El Niño types: the EP event is associated with the Rossby wave propagating poleward and is confined to the Pacific region, while the CP event induces the negative AO-like circulation pattern and has a planetary scale.

In the warmer climate, the difference between the CP and EP's associated circulation patterns vanishes with predominance of AO-like circulation. This results from westward shift of SST maximum during the EP El Niño. The Arctic Oscillation was shown to affect the temperature and precipitation over a large area of Northern Hemisphere. Therefore, the ENSO remote response in future warmer

climate may manifest in larger spread weather anomalies in the Northern Hemisphere even the intensity of ENSO diminishes with global warming.

Acknowledgements D. Gushchina and M. Kolennikova acknowledge support from Russian Scientific foundation (RFS), project 19-17-00198

References

- Capotondi, A., et al.: Understanding ENSO diversity. *Bull. Am. Meteorol. Soc.* **96**, 921–938 (2015). <https://doi.org/10.1175/BAMS-D-13-00117.1>
- Matveeva, T., Gushchina, D., Dewitte, B.: The seasonal relationship between intraseasonal tropical variability and ENSO in CMIP5. *Geosci. Model Dev.* **11**, 2373–2392 (2018). <https://doi.org/10.5194/gmd-11-2373-2018>
- Takahashi, K., Montecinos, A., Goubanova, K., Dewitte, B.: ENSO regimes: reinterpreting the canonical and Modoki El Niño. *Geophys. Res. Lett.* **38** (2011). <https://doi.org/10.1029/2011GL047364>
- Trenberth, K.E., Branstator, W.B., Karoly, D., Kumar, A., Lau, N.-C., Ropelewski, C.: Progress during TOGA in understanding and modeling global teleconnections associated with tropical sea surface temperatures. *J. Geophys. Res.* **103**(C7), 14291–14324 (1998). <https://doi.org/10.1029/97jc01444>
- Weng, H., Behera, S.K., Yamagata, T.: Anomalous winter climate conditions in the Pacific rim during recent El Niño Modoki and El Niño events. *Clim. Dyn.* **32**, 663–674 (2009). <https://doi.org/10.1007/s00382-008-0394-6>
- Zheleznova, I.V., Gushchina, D.Y.: Circulation anomalies in the atmospheric centers of action during the Eastern Pacific and Central Pacific El Niño. *Russ. Meteorol. Hydrol.* **41**(11–12), 760–769 (2016). <https://doi.org/10.3103/s1068373916110030>



Inter-Annual Variability of Mediterranean Evaporation and Its Drivers During Summer

Igor Zveryaev and Abdel Hannachi

Abstract

Monthly evaporation data for 1958–2015 from the Woods Hole Oceanographic Institution dataset are used to investigate inter-annual variability of Mediterranean evaporation and its links to regional climate during the extended (June–September) summer season. An EOF (Empirical Orthogonal Functions) analysis performed on the monthly means (i.e., separately for June, July, August and September time series) revealed two leading modes of evaporation variability, characterized by the monopole (EOF-1) and zonal dipole (EOF-2) patterns. These modes explain together more than 50% of the total variability of Mediterranean evaporation. It is shown that the EOF-1 reflects interdecadal changes characterized by below normal evaporation during the period 1970–2000, and above normal evaporation before and after that period. The EOF-2 reflects inter-annual and decadal scale variations of Mediterranean evaporation. Analysis of correlations between the leading PCs (principal components) of evaporation and indexes of large-scale teleconnections suggests moderate, but statistically significant links between Mediterranean evaporation and the North Atlantic Oscillation, Scandinavian teleconnection, East Atlantic teleconnection, Atlantic Multi-decadal Oscillation and the Asian monsoon. It is revealed that the dynamic impact on the North Atlantic Oscillation on evaporation weakens toward the end of the summer season, whereas thermodynamic impact from the Asian monsoon increases.

Keywords

Mediterranean evaporation • Summer season • Inter-annual variability • EOF analysis

1 Introduction

Climate change can significantly impact the hydrological cycle of the Mediterranean region. Recent studies show that significant changes in the regional hydrological cycle are already underway. It is shown that during recent decades, Mediterranean evaporation has increased, whereas regional precipitation has decreased (Allan and Zveryaev 2011). Together, these two tendencies resulted in significant increases in the loss of fresh water from the Mediterranean Sea into the atmosphere. Moreover, recent model simulations suggest an acceleration of the increase in fresh water deficit in the current century (Mariotti et al. 2008). Therefore, deeper understanding of the regional hydrological cycle and its variability and changes could lead to a better adaptation and mitigation strategy in the Mediterranean region.

Among the key elements of hydrological cycle, evaporation is the largest component in the Mediterranean fresh water budget, whereas precipitation is only about half the evaporation (Mariotti et al. 1674). Thus, the understanding of inter-annual variability of Mediterranean evaporation is crucial for the proper assessment of changes in the regional hydrological cycle.

2 Materials and Methods

In this study we used evaporation data from the Woods Hole Oceanographic Institution OAFflux data set (Yu and Weller 2007). The OAFflux data set provides evaporation data on a $1^\circ \times 1^\circ$ latitude–longitude grid over the global oceans for 1958–2015. We also used sea surface temperature, air

I. Zveryaev (✉)
Shirshov Institute of Oceanology, RAS, Moscow, Russia
e-mail: igorz@sail.msk.ru

A. Hannachi
Department of Meteorology, Stockholm University,
Stockholm, Sweden

temperature, specific humidity and wind speed data from this data set.

We used indexes of the major teleconnection patterns that have been documented and described in Barnston and Livezey (1987). The teleconnection patterns used here to examine links to Mediterranean evaporation include, in addition to the North Atlantic Oscillation (NAO), the East Atlantic (EA), East Atlantic–West Russia (EAWR) and the Scandinavian (SCA) patterns. To examine links between Mediterranean evaporation and South Asian monsoon, we used well-known monsoon indexes (Webster and Yang 1992; Parthasarathy et al. 1995), particularly the Webster and Yang index (WYI).

To investigate the spatial–temporal structure of inter-annual variability of the monthly summer Mediterranean evaporation, we apply Empirical Orthogonal Function (EOF) analysis (Wilks 1995; Hannachi et al. 2007). Conventional correlation analysis has been applied to study the links to teleconnection patterns and the key climate variables. According to the Student’s t-test (Bendat and Piersol 1966), the minimum significant correlation coefficients between the time series analyzed are 0.26 for the 95% significance level. Since the significance level of the correlation coefficient might be reduced if the time series are influenced by autocorrelation, the potential impact of autocorrelation on the estimation of significance of correlation coefficients has been examined. Significant autocorrelations have not been found in the analyzed time series.

3 Results and Discussion

3.1 Leading EOF Modes of Mediterranean Evaporation

We performed an EOF analysis of the monthly mean evaporation for extended summer (JJAS) season. Given that the leading two modes, in each month, explain more than 50% of total variability of evaporation (Table 1), we have limited our analysis to the first two EOFs. As an example, we show the spatial patterns of these modes of evaporation and associated time series of principal components (PCs) for July in Figs. 1 and 2.

Table 1 Fractions (in %) of the total Mediterranean evaporation variability explained by the leading EOFs

	June	July	August	September
EOF-1	45.98	48.19	44.10	43.93
EOF-2	13.91	19.90	17.01	21.97
EOF-3	8.70	9.07	9.25	7.18
EOF-4	5.13	3.66	5.39	4.96
EOF-5	3.95	2.71	3.33	4.02

The first EOF explains from 43.93% (in September) to 48.19% (in July) of the total variance of Mediterranean evaporation. In all considered months the spatial pattern of this mode (Fig. 1) reflects coherent variations of evaporation over the entire Mediterranean basin. In all months, respective PCs of this mode (Fig. 2) demonstrate a clear inter-decadal changes with prevailing below normal evaporation from the early 1970s to the late 1990s, and above normal evaporation before and after that period, implying that this mode is associated with Atlantic multi-decadal Oscillation (Enfield et al. 2001). These results are generally consistent with previous analyses of seasonal mean global and Mediterranean evaporation (Yu 2007; Zveryaev and Hannachi 2012).

Contribution of the second EOF mode to the total variance of Mediterranean evaporation varies from 13.91% (in June) to 21.97% (in September). The spatial patterns of this mode are characterized by an east–west dipole (Fig. 1) with opposite variations of evaporation in the eastern and western parts of the Mediterranean Sea. Despite the similarity between the spatial patterns, the associated PCs (Fig. 2) show quite a different inter-annual variability during different summer months.

3.2 Links to Regional Climate

To investigate the links to regional atmospheric circulation, we computed correlations between the leading PCs of evaporation and indexes of known regional teleconnections (Barnston and Livezey 1987) as well as indexes of Asian summer monsoon (Webster and Yang 1992; Parthasarathy et al. 1995).

Obtained correlations imply moderate (but statistically significant) impacts from Asian monsoon (in September), SNAO (in June), SCA, EA and AMO. These impacts vary significantly during summer (Table 2). Moreover, in the same month, Mediterranean evaporation might be impacted by the different climate signals which can potentially offset each other. Different signals may also impact different parts of the Mediterranean Sea. Thus, to assess more regional (i.e., sub-basin) impacts of teleconnections on Mediterranean evaporation, we further estimated for each month direct

Fig. 1 Spatial patterns of the first and second EOFs of July evaporation. Values are $^{\circ}\text{C}\cdot 10$

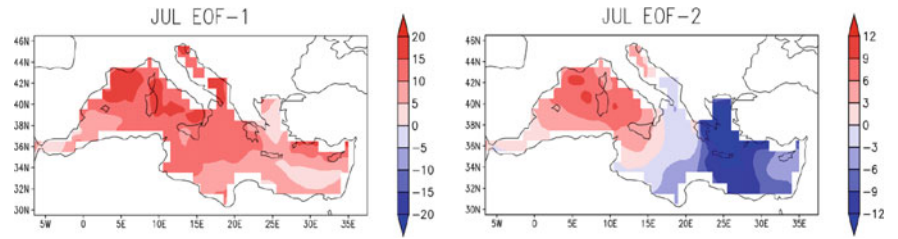


Fig. 2 Principal components of the first and second EOFs of July's evaporation

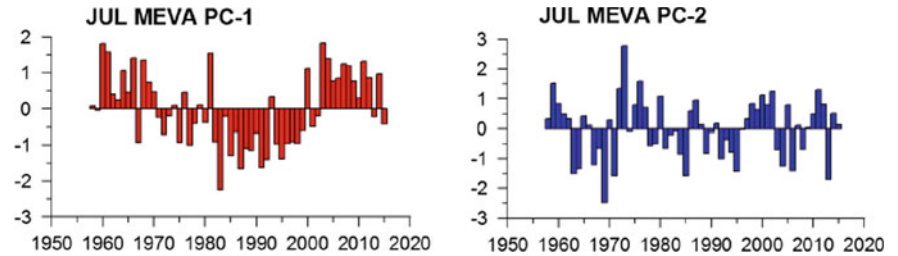


Table 2 Correlations between the leading PCs of Mediterranean evaporation and indexes of regional teleconnections. Statistically significant correlations are shown in bold

	June		July		August		September	
	PC-1	PC-2	PC-1	PC-2	PC-1	PC-2	PC-1	PC-2
SNAO	0.237	-0.26	-0.226	-0.196	-0.253	0.001	0.034	-0.248
SCA	-0.221	0.172	0.166	0.39	0.33	0.027	0.216	0.211
EA	0.235	-0.045	0.186	-0.040	-0.119	0.050	0.029	-0.35
AMO	0.229	0.072	0.205	0.056	0.32	0.004	0.31	-0.056
WYI	0.062	-0.172	-0.095	-0.134	-0.223	0.053	0.38	-0.217

correlations between indexes of teleconnections and evaporation in each grid point (not shown). This analysis revealed increasing (decreasing) role of the Asian monsoon (SNAO) toward the end of the summer season and differing nature (dynamic/thermodynamic) of the impacts of these two climate signals on Mediterranean evaporation. The relative roles of atmospheric dynamics and thermodynamics were assessed through the analysis of links to the near surface wind speed and specific humidity. Note, regional correlations are essentially larger (up to 0.8) than those presented in Table 2.

4 Conclusions

The major conclusions of the present study can be formulated as follows:

- The leading EOF mode of Mediterranean evaporation characterized by the monopole basin-scale pattern reflects inter-decadal changes associated with the AMO. These inter-decadal changes and links to the AMO are best pronounced during the late summer (i.e., in August - September).

- The second EOF characterized by the zonal dipole pattern reflects inter-annual variability of evaporation. Contrasting to the first EOF, this variability varies significantly during the summer season, reflecting changing impacts from different climate signals (e.g., NAO, SCA, Asian monsoon).
- It is shown that the NAO impacts the Mediterranean evaporation variability mostly in early summer (June) and this impact decreases during the summer season. Opposite tendency is found for the Asian monsoon whose impact on the evaporation is stronger in September (i.e., during mature phase of the monsoon).
- We also found differing nature of the impacts from the NAO and the Asian monsoon. While the NAO impact on Mediterranean evaporation is dynamic (i.e., through the regional wind changes), the impact from the Asian monsoon is mostly thermodynamic (i.e., through the changes of atmospheric humidity near sea surface).

Acknowledgements This research was supported by the Russian Ministry of Science and Higher Education (agreement № 075-15-2019-1490 (05.616.21.0112), project ID RFMEFI61619X0112).

References

- Allan, R.P., Zveryaev, I.I.: Variability in the summer season hydrological cycle over the Atlantic–Europe Region 1979–2007. *Int. J. Climatol.* **31**, 337–348 (2011)
- Barnston, A.G., Livezey, R.E.: Classification, seasonality and persistence of low-frequency atmospheric circulation patterns. *Mon. Weather Rev.* **115**, 1083–1126 (1987)
- Bendat, J.S., Piersol, A.G.: *Measurement and Analysis of Random Data*, p. 390. Wiley, New York (1966)
- Enfield, D.B., Mestas-Núñez, A.M., Trimble, P.J.: The Atlantic multidecadal oscillation and its relation to rainy autumn and river flows in the continental US. *Geophys. Res. Lett.* **28**, 2077–2080 (2001)
- Hannachi, A., Jolliffe, I.T., Stephenson, D.B.: Empirical orthogonal functions and related techniques in atmospheric science: a review. *Int. J. Climatol.* **27**, 1119–1152 (2007)
- Mariotti, A., Struglia, M.V., Zeng, N., et al.: The hydrological cycle in the Mediterranean region and implications for the water budget of the Mediterranean Sea. *J. Clim.* **15**, 1674–1690 (2002)
- Mariotti, A., Zeng, N., Yoon, J.-H., et al.: Mediterranean water cycle changes: transition to drier 21st century conditions in observations and CMIP3 simulations. *Environ. Res. Lett.* **3**. <https://doi.org/10.1088/1748-9326/3/4/044001> (2008)
- Parthasarathy, B., Munot, A.A., Kothawale, D.R.: All India monthly and seasonal rainfall series: 1871–1993. *Theor. Appl. Climatol.* **49**, 217–224 (1995)
- Webster, P.J., Yang, S.: Monsoon and ENSO: selectively interactive systems. *Quart. J. Roy. Meteor. Soc.* **118**, 877–926 (1992)
- Wilks, D.S.: *Statistical Methods in the Atmospheric Sciences*, p. 467. Academic Press (1995)
- Yu, L.: Global variations in oceanic evaporation (1958–2005): the role of the changing wind speed. *J. Clim.* **20**, 5376–5390 (2007)
- Yu, L., Weller, R.A.: Objectively analyzed air-sea heat fluxes for the global ice-free oceans (1981–2005). *Bull. Am. Meteorol. Soc.* **88**, 527–539 (2007)
- Zveryaev, I.I., Hannachi, A.A.: Interannual variability of Mediterranean evaporation and its relation to regional climate. *Clim. Dyn.* (2012). <https://doi.org/10.1007/s00382-011-1218-7>



Low Frequency Sea-Level Oscillations in Algiers Harbour (Algeria)

Chawki Zerrouki and Yacine Hemdane

Abstract

The sea-level disturbances caused by meteorological event of June and July 2002 at Algiers Harbour is examined by spectral analysis applied to the original signal measured tide gauge with a frequency sampling of 0.003 Hz. The global sea-level signal is filtered using cutoff frequencies of bandpass filter to extract the meteorological oscillations induced by storm. Results of the spectral analysis show the existence of the periods of 16, 20 and 30 min that correspond to the frequent range of tsunamis, meteotsunamis and seiches. The absence of a seismic event and the atmospheric disturbance observed during this event suggest that these signals are related to the seiches phenomena that are very frequent in the Bay of Algiers. On the other hand, it is important to notice that the frequency sampling of 0.003 Hz is relatively low because it does not allow the detection of infragravity waves and wind waves/swells. Indeed, these signals could be important and could help to better understand meteotsunamis and harbor oscillations.

Keywords

Sea-level • Spectral analysis • Frequency sampling • Meteotsunamis • Seiches • Algiers Bay

1 Introduction

It has been considered for a long time that the microtidal coasts are less exposed to coastal flooding than the coasts with high tide range. However, the low tide could, in some cases, increase the occurrence of some coastal risks. In the macrotidal ($TR > 4$) range, the wave energy can be reduced by the large intertidal area. In addition, in some places of coastal world where the tidal range is not significant as microtidal coasts (< 2 m), other forces can disturb hugely the sea level which may generate low frequency oscillations and cause significant damage on the coast. These long waves are described as atmospherically generated tsunami and the term “meteorological tsunami” (“meteotsunami”) is then employed (Nomitsu 1935; Defant 1961; Rabinovich and Monserrat 1996, 1998; de Jong et al. 2004; Rabinovich 2009). These low frequency oscillations are also called seiches and harbors oscillations when they enter a harbor basin. These long waves are regularly observed in different areas in the world like in The Balearic Islands (Rabinovich and Monserrat 1996, 1998) the Adriatic sea (Šepić et al. 2009) and Algeria (Hemdane et al. 2017).

In this paper, sea-level disturbances induced in Algiers Harbour during the meteorological event of June and July 2002 are analyzed. The objective of this work is to improve our understanding of seiches and harbor oscillations and then contribute to reduce the risk of coastal flooding. The other objective of this paper is to emphasize the importance of the sampling rate of tide gauge to detect all potential signals (sea-level oscillations) that can be observed in the sea-level.

Our conference paper of CAJG2019, untitled “The study of low-frequency sea-level oscillations. Case of Algiers harbour (Algeria)”, has been improved and published online as an article in the Arabian Journal of Geosciences (Special Issue CAJG2019), with the same title, figures, and almost the same content. Our article DOI is the following: <https://doi.org/10.1007/s12517-021-06921-x>

C. Zerrouki (✉) · Y. Hemdane
Laboratoire Géo-Environnement, Faculté des Sciences de la Terre,
Géographie et Aménagement du Territoire, Université des
Sciences et de la Technologie Houari Boumediene, BP 32 El-alia,
Bab ezzouar, Algiers, Algeria
e-mail: czerrouki@usthb.dz

2 Methods

Sea-level disturbances induced in Algiers Harbour during the meteorological event of June and July 2002 were kindly obtained by the (*Office National de Signalisation Maritime, ONSM*).

Sea-level signal used in this study is obtained by tide gauge with the sampling frequency of 0.003 Hz (every 300 s). Firstly, all sea-level data is checked by visual verification to eliminate possible general noises. In order to observe the different energies characterizing our signal, spectral analysis of sea-level data is applied using the Power Spectral Density (PSD). The PSD used in this study was estimated by Fourier analysis using the Welch's method (Welch 1967). This method improves the statistical stability of the spectral estimate which is widely used in the low frequency sea-level oscillations study. Once the spectral energies are known, the signal is then filtered through a Butterworth filter to extract the different waves included in the overall signal. The cutoff frequencies of bandpass filter used in this study are $frequency_1$ (f_1) and $frequency_2$ (f_2) with $f_1 < f_2$. These cutoff frequencies are 0.000069 Hz (f_1) and 0.0033 Hz (f_2) with taking into account the Nyquist sampling criteria.

All these analysis were done using GNU Octave free software (www.octave.org). GNU Octave provides capabilities for the numerical solution of linear and nonlinear problems and for performing other numerical experiments (Eaton 2012).

Finally, we examined the period of a fundamental mode of the bay of Algiers using the following Merian's formula (Rabinovich 2009; Šepić et al. 2009):

$$T_0 = 2220 \cdot \left[2L / (g \cdot h)^{1/2} \right] \quad (1)$$

where, L is the length of the bay of Algiers (15,000 m), g is the gravitational acceleration and h is the water depth at the entrance of the bay (about 80 m).

3 Results and Discussion

Results show that low frequency waves with very low heights (less than 10 cm) exist even during the absence of meteorological event (Fig. 1). The same situation is observed in several signals measured during events of low atmospheric disturbance where these low frequency oscillations have very small heights (less than 10 cm). However, the results show that the sea level signal measured between June and July 2002 shows a considerable disturbance in the signal (Fig. 2). Indeed, this signal shows the presence of low frequency oscillations exceeding heights of 60 cm. It is important to emphasize the flooding potential of these oscillations and the damage they can cause in the harbor. Moreover, the spectral analysis shows that these waves belong to the frequency range of meteotsunamis and seiches. In addition, the results show that these low (or medium) frequency waves are characterized by a peak frequency corresponding to the 20 min period (Fig. 3).

On the other hand, the application of Eq. 1 shows that the fundamental mode is about 40 min. However, the periods observed in the signal are smaller (16, 20 and 30 min). This difference between the fundamental mode and measured frequencies is observed by Šepić et al. (2009). The high frequency observed could be related to the wind and waves occurred during this meteorological event. It is important to notice that the data used in this work are obtained with frequency sampling of 0.003 Hz. Then, the infragravity

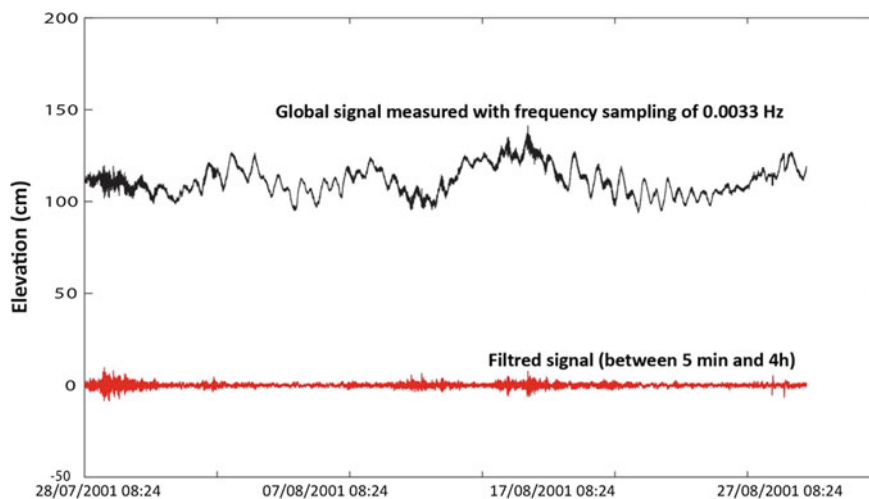


Fig. 1 Sea level and seiches observed at Algiers harbor during low disturbances event (August 2001)

Fig. 2 Sea level observed at Algiers harbor during the meteorological events of June and July 2002

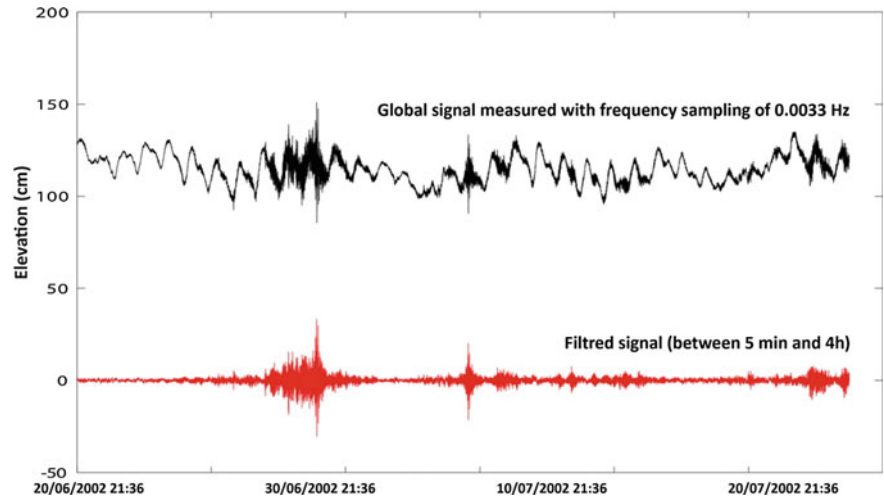
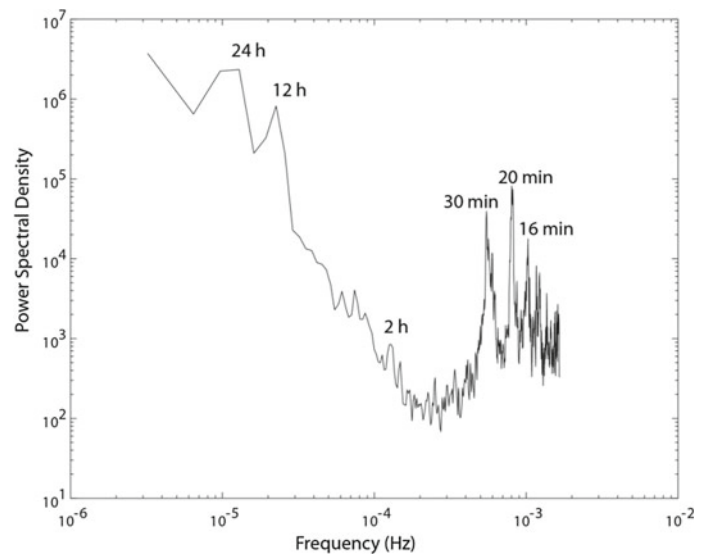


Fig. 3 Spectral analysis of the sea level signal observed at Algiers harbor during the meteorological events of June and July 2002



waves and the waves were not detected by the tide gauge. Indeed, it is important to increase the frequency sampling to obtain all high frequencies signals. Therefore, waves and infragravity waves could be recorded to better understand meteotsunamis and seiches.

4 Conclusion

The analysis of sea-level measured by tide gauges at Algiers Harbour during the meteorological events of June and July 2002 allowed highlighting the existence of low frequency oscillations at the bay of Algiers. These signals are observed at the frequency range of meteotsunamis and seiches (and tsunamis) and they exceed the heights of 60 cm. The spectral analysis applied for this signal shows the periods of 16, 20 and 30 min. This work shows that low frequency waves exist

even during the low agitation periods. However, they become more important during atmospheric disturbances and pose a risk to the coastal population and coastal infrastructures. It is important to emphasize that the data used in this work are obtained with frequency sampling of 0.003 Hz. Therefore, the infragravity waves and the waves were not detected by the tide gauge. Then, this work also allowed to highlight the importance of increasing the frequency sampling (of the tide gauge) to better understand meteotsunamis and seiches.

References

Candella, R.N.: Meteorologically induced strong Seiches observed at Arraial Do Cabo, RJ, Brazil. *Phys. Chem. Earth Parts A/B/C* **34**(17–18), 989–997 (2009)
 Defant, A.: *Physical Oceanography*, vol. 2. Pergamon Press, Oxford, UK (1961)

- de Jong, M.P.C., Battjes, J.A.: Low-frequency sea waves generated by atmospheric convection cells. *J. Geophys. Res. Oceans* **109**(C01), 011 (2004). <https://doi.org/10.1029/2003JC001931>
- Eaton, J.W.: GNU octave and reproducible research. *J. Process Control* **22**(8), 1433–1438 (2012). <https://doi.org/10.1016/j.jprocont.2012.04.006>
- Hemdane, Y., Bouhamadouche, M., Atroune, F., Meghraoui, M.: Very low cost high frequency tide gauge: the rotary tide gauge—Tsunamis, meteotsunamis/seiches, harbor oscillations, waves/swell and tide observations. In: Final meeting 6–8 April 2017—Mallorca, Balears. Assessment, Strategy and Risk Reduction for Tsunamis in Europe (2017)
- Nomitsu, T.: A theory of tsunamis and Seiches produced by wind and barometric gradient. *Memoirs Coll. Sci. Kyoto Imperial Univ. A* **18** (4), 201–214 (1935)
- Rabinovich, A.B., Monserrat, S.: Meteorological tsunamis near the Balearic and Kuril Islands: descriptive and statistical analysis. *Nat. Hazards* **13**(1), 55–90 (1996)
- Rabinovich, A.B., Monserrat, S.: Generation of meteorological tsunamis (large amplitude seiches) near the Balearic and Kuril Islands. *Nat. Hazards* **18**(1), 27–55 (1998)
- Rabinovich, A.B.: Seiches and harbor oscillations. In: Kim, Y.C. (ed.) *Handbook of coastal and ocean engineering*, pp. 193–236. World Scientific Publ, Singapore (2009)
- Šepić, J., Vilibić, I., Belušić, D.: Source of the 2007 IST meteotsunami (Adriatic Sea). *J. Geophys. Res.* **114**, C03016 (2009)
- Thomson, R.E., Rabinovich, A.B., Krassovski, M.V.: Double jeopardy: concurrent arrival of the 2004 Sumatra tsunami and storm-generated waves on the Atlantic coast of the United States and Canada. *Geophys. Res. Lett.* **34**, L15607 (2007)
- Welch, P.: The use of fast fourier transform for the estimation of power spectra: a method based on time averaging over short, modified periodograms. *IEEE Trans. Audio Electroacoust.* **15**, 70–73 (1967)



Modeling Interactions Among the West Atlantic Hurricanes Through Empirical Recurrence Rates Ratio Inspired Hidden Markov Chains

Moinak Bhaduri

Abstract

Hurricanes of varied intensities strike the east coast of the United States with unrelenting regularity. Despite the implementation of myriad sophisticated techniques, estimating the number of strikes within a given period and predicting the next remains daunting. Through classifying hurricanes into categories based on their strengths, this work promotes a statistic termed Empirical Recurrence Rates Ratio (ERRR) and describes the way it may be treated as a hidden Markov chain generating the strike time series for one of the hurricane types. It proposes a new hidden Markov modeling technology where the unobserved state transition probability matrix in the likelihood of the established Poisson based model is replaced by the transition probabilities of a discretized ERRR. Comparisons with established competitors demonstrate how predictions improve dramatically without paying a hefty price in terms of model complexity. The described methods are general enough to be extended to other ocean basins or other meteorological/geological hazards, especially those with meager occurrence probabilities.

Keywords

Empirical recurrence rates and ratios • Hidden Markov chain • Change-point detection • West Atlantic hurricanes • Forecasts for rare events

1 Introduction

In view of their damage-inflicting capabilities, hurricanes and tropical cyclones constitute the most unnerving of natural hazards. Bhaduri and Ho (2018) demonstrate how the amount

of research into the modeling and prediction of these calamities continues to swell by the day with varying degrees of success and we point interested readers to its necessity and the current literature review to this previous work of ours. The questions this work tries to answer quantitatively are both ancient—can one come up with storm forecasts better than the ones available? And—do hurricanes of different strengths (defined shortly) bear some kind of relationship among each other with regards to their striking patterns?

Categorization, thus, becomes imperative. We adopt the National Oceanic and Atmospheric Administration (NOAA)'s established classification, shown in Table 1 below, based on maximum wind speeds (MSWs).

We have chosen to work exclusively on the West Atlantic basin, bordering the east coast of the United States. This is motivated both by geographical relevance and the fact that this stretch of water mass remains one of the most restless. Publicly available data are collected from the NOAA webpage maintained at <https://coast.noaa.gov/hurricanes/?redirect=301ocm> over the period 1923–2013. Our conversation with NOAA experts led us to choose this time stretch since records prior to this are based primarily on eyewitness accounts and thus, they lack reliability. We have collected 32 H5, 84 H4, 87 H3, 93 H2, 150 H1, 271 tropical, and 24 subtropical storms. The date a storm/hurricane originates is taken as its occurrence date.

2 Methodology

In the context of rare event modeling zero-inflated time series with (like hurricane strikes) or without (like earthquakes) seasonal patterns, we have introduced the statistics Empirical Recurrence Rates (ERR) and Empirical Recurrence Rates Ratio (ERRR) through a series of papers: Tan et al. (2014), Ho and Bhaduri (2015), Ho et al. (2016), Ho and Bhaduri (2017), Bhaduri and Zhan (2018), and Bhaduri

M. Bhaduri (✉)
Department of Mathematical Sciences, Bentley University,
Waltham, MA 02452, USA
e-mail: mbhaduri@bentley.edu

Table 1 NOAA hurricane classification based on maximum wind speeds attained

Category	MSW (kts)
Hurricane 5	>135
Hurricane 4	114–135
Hurricane 3	96–113
Hurricane 2	83–95
Hurricane 1	64–82
Trop/subtrop	34–63

and Ho (2018). Formally, given a time series $\{X_t\}_{t=1,2,3,\dots}$, the ERR at a time t is defined as:

$$Z_t = \frac{\sum_{k=1}^t X_k}{t} \quad (1)$$

While corresponding to two (possibly related) time series $\{X_t\}_{t=1,2,3,\dots}$ and $\{Y_t\}_{t=1,2,3,\dots}$, the ERRR (the ratio of two ERRs) at a time t is given by:

$$R_{X,Y;t} = \frac{\sum_{k=1}^t X_k}{\sum_{k=1}^t X_k + \sum_{k=1}^t Y_k} \quad (2)$$

As evidenced in the papers mentioned above, both these functions have excellent smoothing and clustering capabilities. But for the purpose of the present work, we collect two observations: first, being statistics, these fractions are always computable given the generating time series and second, the ERRR curve (plotted as a function of time t) will exhibit a wave-like periodic pattern if and only if the building series X and Y are inversely related (i.e., large values on one is accompanied by small values on the other).

As our next tool, we need to briefly introduce the idea of Poisson-based Hidden Markov Modeling (P-HMM). Zucchini and MacDonald (2009) is an excellent resource. Integral to the model is an *unobserved* parameter process $\{C_t\}_{t=1,2,3,\dots}$ satisfying the familiar one-step Markovian property and a state-dependent observable time series $\{X_t\}_{t=1,2,3,\dots}$ such that given the current C_t , knowledge of X_t is free of the past. When the state dependent probability law is the Poisson, we have the P-HMM. Closed form expressions for the forecast distributions (at horizon h) and the one-out conditionals can be found in Zucchini and MacDonald (2009), but we will explain these again in the following section in the context of our specific analyses. Tools are available to estimate the unobserved parameter chain $\{C_t\}_{t=1,2,3,\dots}$. The key result this work establishes is that the ERRR series, sufficiently discretized, works as an observed version of this chain, leading to our proposal, the ERRR-HMM, generating better forecasts. This is achieved by replacing the transition probability matrix involved in the P-HMM likelihood by the transition probabilities of the discretized ERRR.

3 Results

For the sake of computational ease, we have merged H3, H4, and H5 hurricanes to form the strong category, H₂ and H₁ to form the weak category and the rest to form the tropical class. The resulting ERRR graphs for the $\binom{3}{2} = 3$ interactions are shown in the left panel of Fig. 1 below. We have subsequently isolated the strong–weak interaction (left panel of Fig. 2) and through a minimum AIC criteria, partitioned it according to

$$c(t) = \begin{cases} 1, & r_t \in [0, 0.45) \\ 2, & r_t \in [0.45, 1] \end{cases} \quad (3)$$

to generate the underlying states for our ERRR-HMM, to be described in Sect. 3.2.

3.1 Change-Point Identification

The three ERRR interaction combinations show considerable oscillations, indicating inverse dependence. This seems to confirm Emanuel (2003, 2006)’s views that in recent times, possibly due to causes like global warming, it gets increasingly difficult to start a strong hurricane, but in case it gets started somehow, it has the potential to get deadly.

Another striking observation is that the three curves seem to intersect at around $t = 45$. In terms of actual time, this translates to $1923 + 45 = 1968$. Due to man-made and often preventable causes, earth’s temperature started rising around that point. A closer look at the Strong–Weak interaction curve (central panel, Fig. 1) reveals several peaks and troughs (needed to induce a wave-like pattern). By construction of the ERRR, a peak can be taken as the time the Y series (weak hurricanes in this case) is getting more frequent and a valley as the time the X series (strong hurricanes here) is getting more active. Unless one employs advanced likelihood based inference, such insights cannot be concluded from the raw time series of the two processes (graphed as the right panel in Fig. 2). The ERRR, thus, can provide a quick visual alternative to detecting change-points.

3.2 ERRR Based HMC Modeling

We extracted the one-out conditional probability distributions from both the established P-HMM and our proposal, the ERRR-HMM for varying choices of the time point t . The results have been graphed on the left panel of Fig. 2. The horizontal axis on each subgraph on this panel represents the number of hurricanes (i.e., the observation space x) while

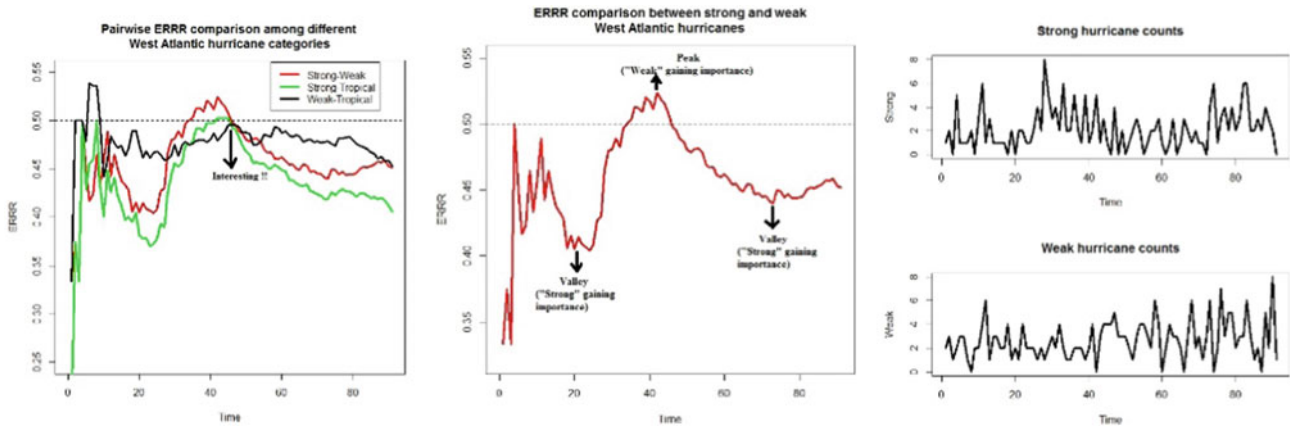


Fig. 1 ERRR curves for three possible interactions

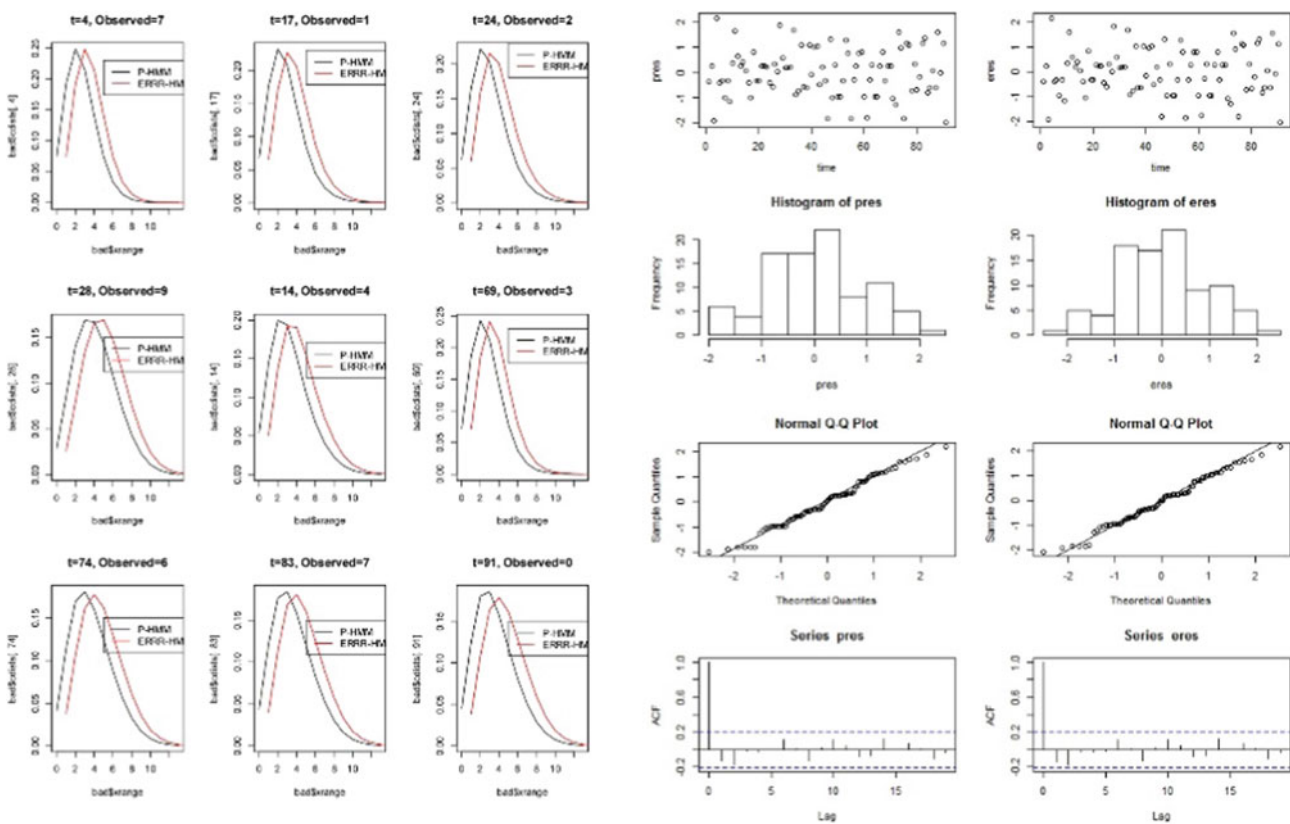


Fig. 2 Comparison between P-HMM and ERRR-HMM with respect to one-out conditional densities (left panel) and residual analyses (right panel, showing white noise residuals)

the vertical axis represents the probability of observing that many at the specified time point assuming the availability of the remaining history. The actual observed number is also recorded on the top for ready reference. The central panel of the last row (corresponding to time point $t = 83$) for instance, tells us that at that time, the actual number of observed hurricanes was 7, and our model (shown by the red line) makes

this more plausible in terms of an elevated probability, than its competitor. It is interesting to note that our proposal performs better in modeling large count values at instances such as $t = 28, 14, 74, 83$, etc. (but not, for instance, $t = 91$, when there was no hurricanes)—and those are precisely the years that inflicted great damages, and hence merit accurate forecasting. Finally, we extract the forecast probability distributions for both models and record them in Table 2.

Table 2 Comparison between the probability distributions generated by the two competing methods on the observation space

x	P-HMM			ERRR-HMM		
	$h = 1$	$h = 2$	$h = 3$	$h = 1$	$h = 2$	$h = 3$
0	0.059	0.058	0.058	0.050	0.047	0.046
1	0.156	0.154	0.153	0.134	0.129	0.126
2	0.211	0.210	0.209	0.190	0.184	0.181
3	0.199	0.198	0.198	0.190	0.187	0.186
4	0.150	0.150	0.151	0.155	0.156	0.157
...
9	0.009	0.009	0.010	0.013	0.014	0.015

Thus, the probability of observing one hurricane ($x = 1$) next year (horizon $h = 1$) is 0.156 from the P-HMM framework and 0.134 from ours. It is comforting to note that the new ERRR based model follows a decreasing probability trend (with increasing x) similar to the established P-HMM. Thus, the possibility of observing nine hurricanes, for instance, remains remote even through our proposal compared to observing one.

4 Discussion and Conclusions

Owing to strange technicalities (such as zero inflation) and data peculiarities (such as seasonality), modeling rare events has baffled scientists across different fields. Handling strong hurricane occurrences (both through providing forecasts and unearthing strike patterns) is one instance where the need for better techniques is now felt stronger than ever before. The present work achieves the following:

- (i) It promotes the use of smoothing statistics Empirical Recurrence Rates and Empirical Recurrence Rates Ratio in the context of relationship modeling between hurricane types—we found an inverse dependence between strong and weak hurricane frequencies, evidenced through the ERRR's oscillatory property.
- (ii) It demonstrates how ERRR can be viewed as a change-detection tool that signals whether strong or weak hurricanes are getting significantly more prevalent, through providing easily calculable peaks and valleys. This provides a welcome alternative to likelihood-based change-point inferences whose mathematical technicalities might prove forbidding to applied scientists.
- (iii) It proposes a new ERRR based hidden Markov modeling technology where the unobserved state transition probability matrix in the likelihood of the established Poisson based hidden Markov model is replaced by the

transition probabilities of a discretized ERRR. We found that in addition to providing logical results (such as witnessing a large number of hurricanes is less likely than a small number), the new technique forecasts large hurricane counts more accurately than the established P-HMM. Pragmatically too, this scenario needs to be estimated quite accurately.

The same ERRR tool can, thus, be exploited both in identifying change-points and furnishing forecasts. In addition, its discretized version can be taken as an observed snapshot of the underlying state space, which remains hidden in the traditional P-HMM framework. Due to space constraints, we have refrained from elaborating a few technicalities such as the reasoning behind two states in (3) or using 0.45 as the threshold. We intend to provide details in an enlarged version of this work. Finally, the modeling was conducted on the statistical software R. We would be happy to share codes with interested researchers.

References

- Bhaduri, M., Ho, C.: On a temporal investigation of hurricane strength and frequency. *J. Environ. Model. Assess.* (2018)
- Bhaduri, M., Zhan, J.: Using empirical recurrence rates ratio for time series data similarity. *IEEE ACCESS* **6**, 30855–30864 (2018)
- Ho, C., Bhaduri, M.: A quantitative insight into the dependence dynamics of the Kilauea and Mauna Loa Volcanoes, Hawaii. *Math. Geosci.* **49**(7), 893–911 (2017)
- Ho, C., Zhong, G., Cui, F., Bhaduri, M.: Modeling interaction between bank failure and size. *J. Finan. Bank Manag.* **4**(1), 15–33 (2016)
- Ho, C., Bhaduri, M.: On a novel approach to forecast sparse rare events: applications to Parkfield earthquake prediction. *Nat. Hazards* **78**(1), 669–679 (2015)
- Tan, S., Bhaduri, M., Ho, C.: A statistical model for long term forecasts of strong dust sand storms. *J. Geosci. Environ. Prot.* **2**, 16–26 (2014)
- Zucchini, W., MacDonald, I.L.: *Hidden Markov Models for time series.* CRC Press (2009)



Performance Evaluation of a New Source Term Package ST6 of Wavewatch III in Catalan Coasts (Spain)

Nasser Kessali, Mohamed Bouhamadouche, and Yacine Hemdane

Abstract

In the present study, we analysed the performance of the wave model, Wavewatch III[®], forced by the ECMWF wind dataset in the Mediterranean Sea. The simulation results have been compared to the coastal buoy measurements of Tarragona (Catalan coast, Spain) using statistical indicators such as bias and root mean square error (RMSE) at a single point. A performance evaluation of the growth-dissipation source term packages ST4 and ST6 respectively were carried out, taking into account of the nearshore parametrization physics such as the depth breaking, non-linear interactions (TRIAD), reflexion, and bottom friction. In this Approach, we used two grids with different resolutions, treated as two individual wave model grids with low resolution which provide boundary conditions for the high resolution grid. This is the traditional technique of one-way nesting (ww3_shel) implemented in WW3 wind wave model to give consistent results across grid scales and provide a tool to locally increase the spatial resolution of wave models. A comparison of the simulations with the measurements for a period of six months (January–June 2017), using single point statistical indicators, shows that for all wave heights, mean wave periods and wave directions, ST4 provides better results than ST6 in these comparisons with measurements.

Keywords

ECMWF • Source term • ww3_shel • One-way • TRIAD • ST6

1 Introduction

Today the demand for information on sea states has considerably increased and become crucial for the various economic activities and social actors such as fishing, coast guards, search and rescue operations (SAR), from where the accuracy of the wave parameters provided by the models is very important. For this reason, we tested the new ST6 physics introduced in the WW3 wave model to evaluate its performance and to quantify its strengths in order to develop a reliable forecasting system of wave parameters.

2 Materials and Methods

We used the WAVEWATCHIII[®] © 2009–2016 National Weather Service (NWS), National Oceanic and Atmospheric Administration (NOAA) version 5.16, WW3 is the third-generation wind-wave modelling framework WAVEWATCHIII[®], code management of this system is undertaken by the National Center for Environment Prediction (NCEP), WW3 is one of the effective tools for global and regional scale wave modelling studies and has been implemented in different parts of the world for studying the wave spectral evolution, air-sea interactions and non-linear wave-wave interactions in deep water (Tolman 2011, 2014; Deanna and Tolman 2008), from version 3.14, some source term options for extremely shallow water (surf zone) have been included, as well as wetting and drying of grid points. In this study, we have set up the model for traditional one-way nesting (ww3_shel), where model grids are run as separate models consecutively, starting with the models with the lowest spatial resolution to provide boundary conditions to the nested grid. This approach is developed in WW3 to estimate wave parameters in coastal areas, taken into account physical processes occurring in shallow water such as non-linear resonant wave-wave interactions, depth induced breaking and bottom friction, for more details refer to the user manual

N. Kessali (✉) · M. Bouhamadouche · Y. Hemdane
USTHB University, BP 32 Bab Ezzouar, 16111 Algiers, Algeria
e-mail: nkessali@usthb.dz

N. Kessali
National Office of Meteorology, BP 153 Dar El Beida,
16011 Algiers, Algeria

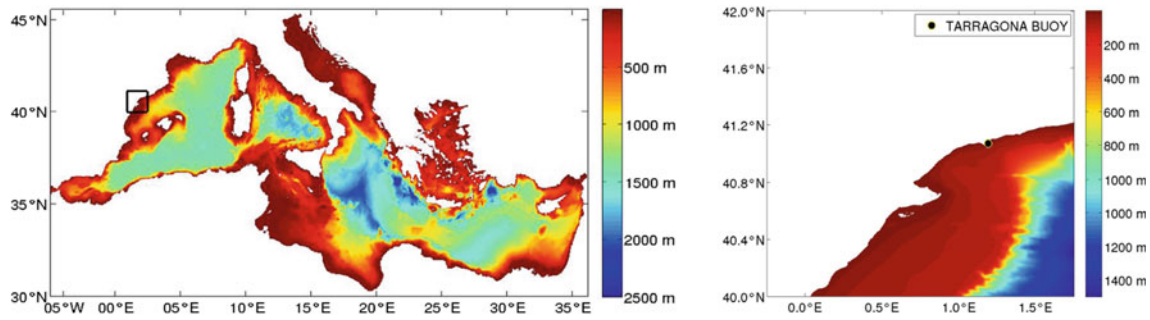


Fig. 1 Model domain and bathymetry for WW3 coarse grid (left side). The small domain around Tarragona shows the model domain for WW3 nested grid. Location of buoy (right side)

and system documentation the WAVEWATCH III Development Group. 2016 (ww3 5.16).

Two model grids were used for the present study. The coarse grid ranges from 30 to 46° N and from 6° W to 36.30° E in 142×54 equidistant grids with a resolution of 0.3° (Fig. 1), this area includes all the basin of Mediterranean Sea is almost completely closed which allowed us to neglect boundary conditions at this scale.

The fine grid used in WW3 has a domain from 40 to 42° N and 0.25° W to 1.75° E in 201×201 equidistant grids with a resolution of 0.01° , nesting of these models enables to simulate the waves near the south Catalan coast (Tarragona).

Bathymetry from The 1-arc minute resolution bathymetry data ETOPO1 (Amante and Eakins 2009) available from the National Geophysical Data Center (NGDC) was used in WW3 coarse model simulations, while Global Multi-Resolution Topography (GMRT) from Marine Geoscience Data System (MGDS) was used in WW3 fine model simulations to take care of the variations in bathymetry in near-shore areas, the nested domain encompasses the coastal area of Tarragona.

The wind forcing employed in the simulations was provided by 10 m wind fields that were obtained from ERA5 dataset at ECMWF (European Centre for Medium-Range Weather Forecasts) with a temporal resolution of 3 h and spatial resolution of 0.3° for the WW3 coarse model (Fig. 1), whereas ECMWF-IFS wind with a temporal resolution of 6 h and spatial resolution of 0.1° was used for the WW3 fine grid (Fig. 1). Wave frequencies were discretized from 0.04 to 0.69 Hz over 25 bins on a logarithmic scale; 24 bins of 15° each taken for direction.

3 Results

Figure 2 represents the comparison between observed (black line) and model-simulated (red line) wave parameters at shallow water. We observe that the peaks of H_s are better simulated by ST4 physic than by ST6 during the simulation period, and from March to April ST6 underestimates

strongly the H_s , whereas ST4 is in good agreement with measured data for the same period. H_s is showing variations similar to the observed values for ST4, but with more deviations ($SI = 0.24$) than ST6 ($SI = 0.21$) (Figs. 3 and 4).

4 Discussion

To evaluate nested model's performance, we have compared model-simulated wave parameters with a single point buoy observations in the nearshore (~ 15 m water depth). The results show that for different wave classes, ST4 physics underestimate the H_s of 23.9% and overestimate the wave mean period (T_{m02}) of 2.5%, whereas an underestimation of wave height (H_s) and T_{m02} of 51.41% and 17.86% respectively for the ST6 physic (Table 1). During January 2017, the maximum observed value was 3.52 m, the maximum model-simulated with ST4 was 3.15 m whereas the maximum obtained with ST6 was 2.82 m (Fig. 2). However, for the category of occurrence of low waves ($0.5 < H_s < 1.25$ m), the observations belonging to this category are 487 values and the model-simulations for ST4 physic represents 54.62%, whereas model-simulations represents 23% for ST6. For the middle waves ($1.25 < H_s \leq 2.5$ m), 77 values were observed in this category, model-simulations for ST4 represents 93.5% with an accuracy of 41% ($RE = 0.41$), and model-simulations for ST6 represents 40.26% with an accuracy of 13% ($RE = 0.13$) (Table 2).

5 Conclusions

Using different source term packages, ST4 and ST6 in WW3 wave model, simulations of wave parameters during Jan to Jun 2017 were carried out. Validation was performed with observations from Tarragona buoy (~ 15 m depth water). The results obtained using ST4 physics are better than ST6 physics in high sea state (peaks), middle, and low sea state. Also for wave mean period and wave directions, ST4 physics has a considerable advantage. For the future work, the forcing of

Table 1 Statistics for significant wave height, mean wave period and direction from WW3 nested grid using ST4 and ST6 physics in WW3 compared to measurements from the buoy at shallow water location during January–May 2017

Statistical parameter	ST4 physics			ST6 physics		
	Hs	Tm02	Dir	Hs	Tm02	Dir
BIAS	-0.14	0.10	-19.34	-0.31	-0.70	12.36
RMSE	0.27	0.88	43.52	0.38	1.05	48.13
RE (Relative Error)	0.46	0.19	0.24	0.67	0.22	0.23
R (corr. coefficient)	0.85	0.69	0.48	0.85	0.67	0.38
SI (scatter index)	0.24	0.31	0.17	0.21	0.29	0.21

Fig. 2 Comparison of measured and simulated significant wave height (H_s) from WW3 nested grid at a shallow water point (left side) during January–May 2017 and scatter plot for the same (right side) using ST4 and ST6 physics respectively

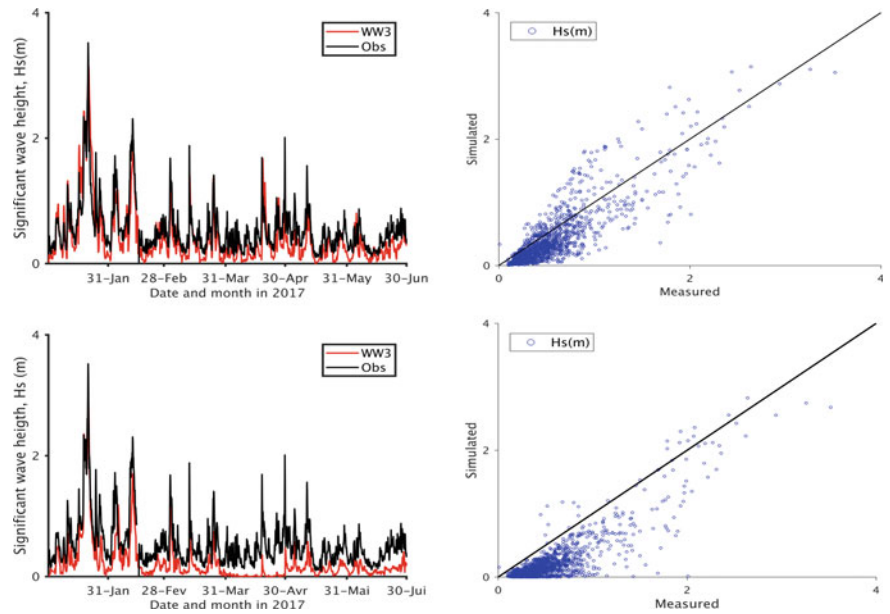
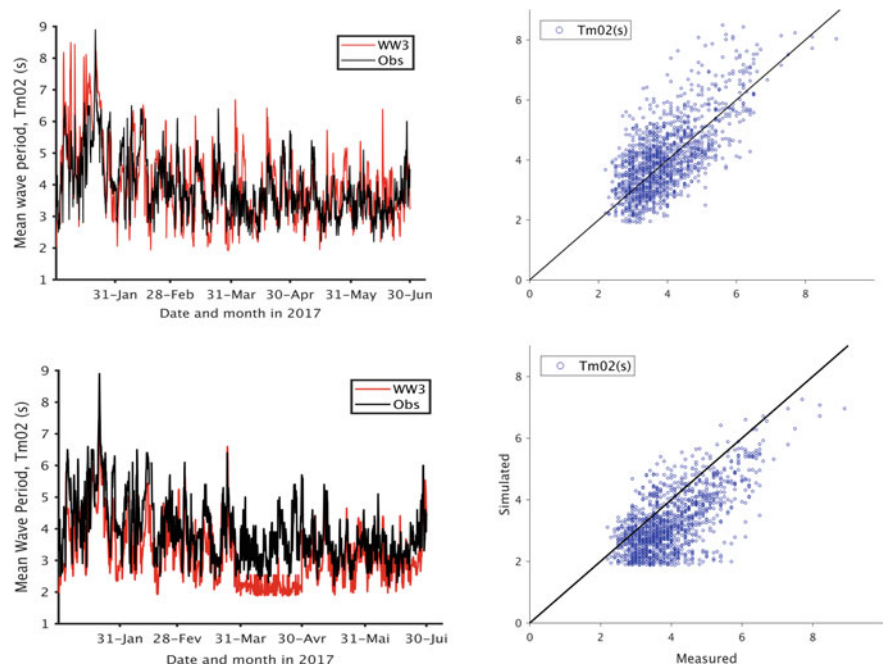


Fig. 3 Comparison of measured and simulated mean wave period (T_{m02}) from WW3 nested grid at a shallow water point (left side) during January–May 2017 and scatter plot for the same (right side) for different physics ST4 and ST6 respectively



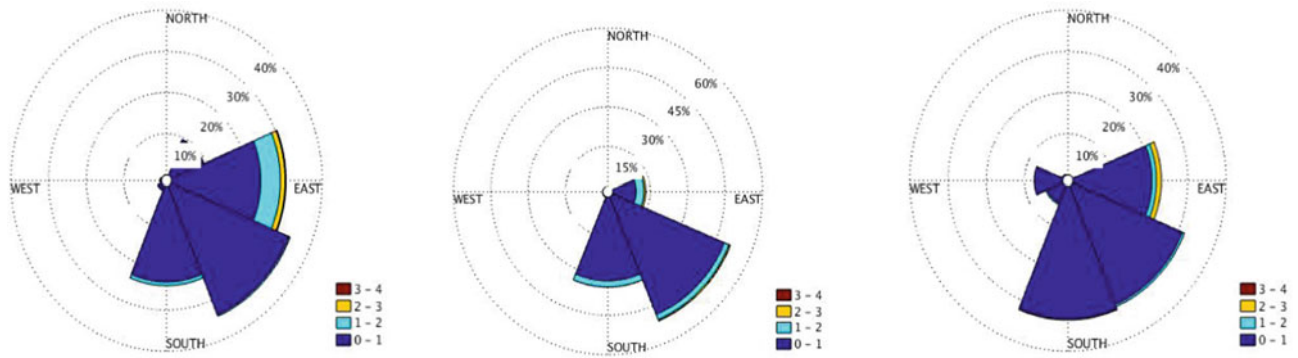


Fig. 4 Wave rose diagram comparing the observed (middle) and simulated (Dir.) for ST4 physics (left side) and for ST6 (right side) at the shallow water point (41.07° N, 1.19° E)

Table 2 Validation results for three sea state simulation-model H_s with observation at shallow water location from Jan to Jun 2017

Sea state	ST4 physics in WW3				ST6 physics in WW3			
	Statistical parameter							
	Bias	RMSE	RE	R	Bias	RMSE	RE	R
Low waves	-0.08	0.31	0.27	0.47	-0.35	0.47	0.35	0.39
Middle waves	0.28	0.52	0.41	0.54	-0.16	0.34	0.13	0.52
Great waves	0.29	0.54	0.20	0.60	-0.29	0.48	0.13	0.19

currents and water levels will be taken into account in the wave model WW3. The measured data shows that 98% of the time waves were from the sector between east and south, whereas the model results show that 88% of the time they were from the same sector using ST4 and 82% using ST6.

References

Amante, C., Eakins, B.W.: ETOPO1 1 Arc-minute global relief model

The WAVEWATCH III[®] Development Group (WW3DG): User manual and system documentation of WAVEWATCH III[®] version 5.16. Tech. Note 329, NOAA/NWS/NCEP/MMAB, College Park, MD, USA, p. 326 (2016)

Tolman, H.L.: A mosaic approach to wind wave modeling. *Ocean Modell.* **25**, 35–47 (2008)

Tolman, H.L.: On the impact of nonlinear interaction parameterizations in practical wave models. In: 12th International Workshop on Wave Hindcasting and Forecasting and 3rd Coastal Hazards Symposium. Paper 115, p. 10 (2011)

Tolman, H. L.: WAVEWATCH III[®] development best practices. Tech. Note 286, Ver., NOAA/NWS/NCEP/MMAB, p. 23 (2014)



Enhanced Methane Emission from Arctic Seas in Winter: Satellite Data

Leonid Yurganov, Frank Muller-Karger, and Ira Leifer

Abstract

Seven operational Thermal Infrared (TIR) spectrometers launched at sun-synchronous polar orbits supply huge amounts of information about Arctic methane (CH₄) year-round, day and night. TIR data are unique for estimating methane emissions from a warming Arctic, both terrestrial and marine. This report is based on publicly available methane concentrations retrieved by NOAA and NASA from spectra of TIR radiation delivered by EU IASI and US AIRS sounders. Data were filtered for high thermal contrast in the troposphere. Validation versus aircraft measurements at three US continental sites reveal a reduced, but still significant, sensitivity to methane anomalies in the troposphere below 4 km of altitude. The focus area is the Barents and Kara Seas (BKS). BKS is impacted with warm Atlantic water and is mostly free of sea ice. It is a shelf area with vast deposits of oil and natural gas (~90% methane), as well as methane hydrates and submarine permafrost. Although in summer AIRS and IASI observe no significant difference in methane between BKS and N. Atlantic, a strong monthly positive methane anomaly of up to 30 ppb occurs during late autumn–winter. We propose that this difference is explained by stable thermal ocean stratification in summer and its fall/winter breakdown, which enhances methane emissions from BKS due to a deeper winter mixing. This was confirmed by a good correlation of methane anomaly with the Mixed Layer Depth annual cycle.

Keywords

Satellite data • Methane emission • Arctic

1 Introduction

Thermal Infrared (TIR) satellite day/night observations are extremely useful for characterization of Arctic methane, especially over the sea, due to their continuous and wide-spread data record.

The seasonal summer pycnocline prevents the turbulent diffusion of methane, with concentrations near the seafloor may be extremely high (Gentz et al. 2013). The summer Mixed Layer Depth (MLD) is very shallow, ~50 m or less (see below and (Kara et al. 2002)). Gentz et al. (2013) has studied dissolved methane concentrations in the West of Prins Karls Forland (Svalbard) in August 2010 and found that dissolved plumes of methane are trapped by the pycnocline above the sea floor preventing the vertical transport. The most comprehensive methane measurements at the seafloor and in the atmosphere in the region were collected to the West of Svalbard in June–July, 2014, by Myhre et al. (2016). They have also found that summer methane release from seabed sediments substantially increases methane concentrations above the seafloor with a sharp decrease above the pycnocline. Yurganov et al. (2016) concluded that seasonal increase in methane has been observed by satellites since late October–early November. They explained this effect by the beginning of vertical convection in the ocean, caused by the cooling of the surface layers and the simultaneous increase in the temperature of the underlying water layers. Bottom layers saturated with methane are brought to the surface. Here, we found that methane anomaly correlates with the MLD variation. Therefore, an increase of emissions in winter, predicted by Gentz et al. (2013), agrees with the remote sensing data.

L. Yurganov (✉)
University of Maryland Baltimore County (ret), Baltimore, MD,
USA

F. Muller-Karger
University of Southern Florida, St. Petersburg, FL, USA

I. Leifer
Bubbleology Research International, Inc, Solvang, CA, USA

2 Materials and Methods

The nadir cross-track scanning diffraction grating spectrometer AIRS/Aqua was launched in May 2002. Version 6 of the retrieval algorithm and data (AIRX3STD.006 and AIRX3STM.006) are available from the NASA GSFC since 2002: <https://disc.gsfc.nasa.gov/datasets/>.

The IASI/MetOp-A is a cross-track-scanning interferometer that measures spectra of outgoing long wave radiation with an apodized resolution of 0.5 cm^{-1} at the ν_4 methane band near $7.65\text{ }\mu\text{m}$ wavelength. The MetOp-A satellite operated by EUMETSAT was launched in 2006. Like AIRS, IASI has a 2200 km swath with a scan angle of $\pm 48.3^\circ$. The IASI retrieval algorithm NUCAPS was built at NOAA/NESDIS to emulate the AIRS Version 5 code and has been put into operation at NOAA's CLASS site since 2008 (Maddy et al. 2009). Level 2 data for 2×2 matrices of 4 circular, 12-km diameter pixels are available from <https://www.avl.class.noaa.gov/saa/products/>.

Both satellites have sun-synchronous polar orbits a geometry that favors a better coverage of the polar regions. Aqua crosses the equator at approximately 01:30 and 13:30 local time, MetOp-A does it at 09:30 and 21:30 local time. Retrieval algorithms for these two instruments are not identical, but similar. Pixel matrices combined with microwave radiometer field of view allowed retrieval of methane profiles for cloud-free and partially clouded conditions. A significantly higher spectral resolution of IASI (0.5 cm^{-1}) compared to that of AIRS (1.5 cm^{-1}) is a reason for giving preference to IASI data. Data over the North Atlantic and the Barents Kara Seas (BKS) with sufficiently high vertical Thermal Contrast (ThC) were analyzed. ThC is defined as the temperature difference between the surface (SST, Surface Skin Temperature) and 4-km altitude; a criterion $\text{ThC} > 10^\circ\text{C}$ was suggested by Yurganov et al. (2016).

3 Results and Discussion

Monthly mean BKS maps for two seasons (Fig. 1a–d) show similar patterns for both instruments. Seasonal variation of Lower Troposphere (LT), 0–4 km, methane over our focus area measured by IASI was analyzed for selected boxes, designated from 1 to 7 along the path from Iceland to Kara Sea (Fig. 1e). IASI (Fig. 1d) found increased methane along coasts of Norway, Novaya Zemlya, and Svalbard. These local enhancements need further evaluation and comparison with in situ data to avoid misinterpretation.

The annual cycle amplitudes for selected boxes (Fig. 1e) increases from box 1 ($\sim 25\text{ ppb}$) to box 7 ($\sim 55\text{ ppb}$), i.e., a factor of 2. In situ, NOAA flask measurements at the Svalbard (ZEP, Zeppelin, Ny-Alesund, 78.9° N , 11.9° E , 474 m

above sea level, asl) observatory and similar data for the Iceland NOAA site (ICE, Storhofdi, Vestmannaeyjar, 63.4° N , 20.3° W , 118 m asl) are shown for reference after offsetting surface data by -18 ppb for comparison. The cycle amplitude of surface methane in Svalbard is $\sim 30\%$ higher than in Iceland.

Box 8 was chosen for an area to the SW of Svalbard (Fig. 1b). This area is at the edge of the continental shelf and is known for numerous seeps from the seafloor detected from ships. We calculated the methane seasonal anomalies as differences between data for box 8 and combined boxes 1 and 2, then we compared them with in situ anomalies (Fig. 1f): Both curves have two maxima, in November–December and in March, but amplitudes of seasonal cycles were different; that may be explained by different techniques; remote and local. Also, a $\sim 350\text{ m}$ difference in elevations of surface measurement sites may matter for the Arctic conditions.

Patches of increased methane in winter may be explained by a breakdown of the thermal stratification of the seawater over methane sources. To test this hypothesis, we extracted MLD for a box 8 located to the SW from Svalbard (Fig. 1f, blue curve) from a global circulation model (Wunsch et al. 2009). The shape of the MLD cycle is similar to the shape of methane anomaly for the same location. Note, a mixing depth of $\sim 400\text{ m}$ is sufficient to transport methane from the bottom layer to the surface.

A strong correlation between methane anomaly and MLD for both instruments also is observed for the total period of measurements (Fig. 2).

A significant flux of methane to the atmosphere requires two conditions: (1) There should be methane sources in the seawater and/or at the seafloor; (2) there should be an effective transport of methane to the surface seawater layer. Significant emission of methane from the seafloor to deep water layers around Svalbard has been documented in multiple studies (Gentz et al. 2013; Myhre et al. 2016; Mau et al. 2017). Transport by turbulent diffusion and convection is possible only in winter, after the pycnocline breaks down. It is noteworthy that the pycnocline is not a barrier for bubbles, bubble-mediated methane transport should be effective year-round. Negligible methane anomaly in summer evidences for a secondary role of ebullition (bubbling) in direct methane transport to air.

To our best knowledge, direct measurements of methane flux in winter have not been published so far. Remote sensing data on methane in the lower troposphere over the winter Arctic Ocean not only confirms a significant winter methane flux, but also gives an idea on areas where these emissions occur, as well as their annual cycle. Specifically, for BKS, maximum emissions are observed in November–December–January with a secondary maximum in March.

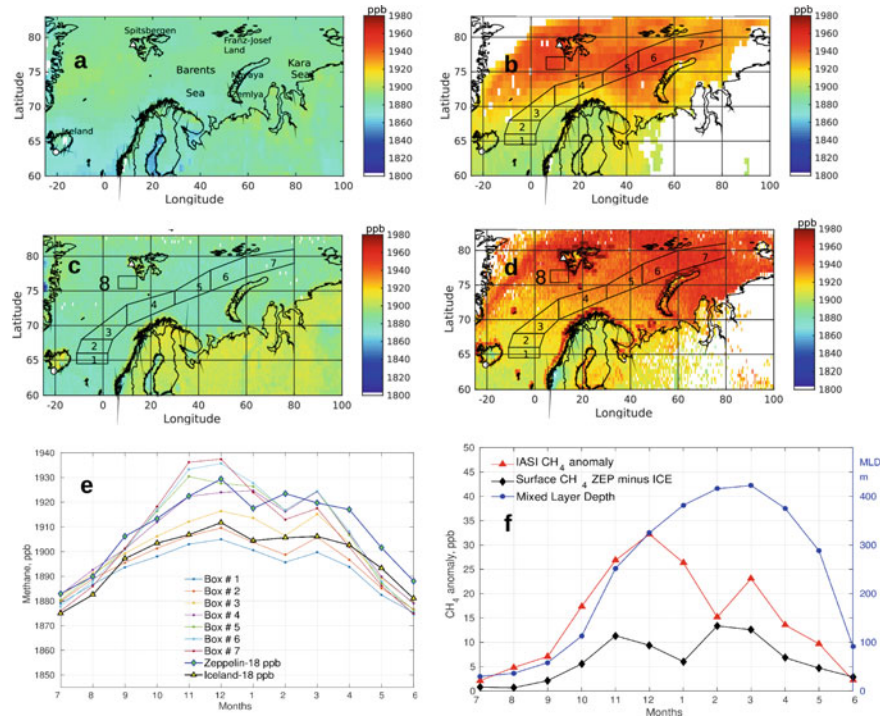


Fig. 1 a and b: Mean LT methane concentrations measured by AIRS for 2013–2015 in June and December, respectively; c and d: mean LT methane concentrations were measured by IASI for 2014–2018 in June and December, respectively. Locations of surface stations ICE and ZEP are shown by a circle and a triangle, respectively. e Monthly mean LT concentrations measured by IASI and averaged over 2014–2018 for

boxes shown on the maps above. Surface concentrations have been lowered downwards by 18 ppb for comparison. f Red line is a difference between concentrations for the box 8 and combined boxes 1–2. Black line is the difference between surface methane at ZEP and ICE. Blue line is for the seawater MLD for box 8. All three lines are 2014–2016 averages

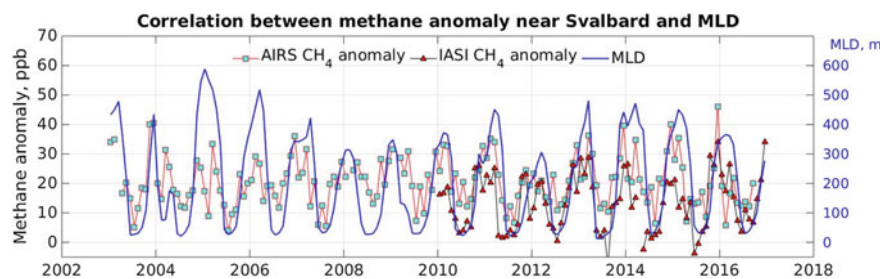


Fig. 2 Monthly mean LT AIRS and IASI methane anomalies for Box 8 referred to combined Boxes 1 and 2 compared with smoothed daily MLD for Box 8

Other areas of significant methane emissions include Baffin Bay, seas of the East Siberia continental shelf (Yurganov et al. 2016) and the Sea of Okhotsk (Yurganov and Leifer 2016). Seasonal cycles are slightly different for different areas and are assumed to depend on the seasonality of seawater mixing. e. g., for an area to the Southwest of Svalbard, the observed methane cycle correlates with a cycle of MLD. Yurganov et al. (2016) estimated the annual methane emissions from the Arctic Ocean in 2010–2014 as $\sim 2/3$ of land emission to the North from 60° N that is equivalent to $\sim 1/3$ of land emission to the North from 50° N. The Arctic land emission from 60° N is estimated in the range of 20–30 Tg

CH₄ per year (AMAP Assessment 2015). Thus, the current marine contribution may be in the range of 15–20 Tg/yr, i.e., 3–4% of the global emissions. This flux may increase with increasing temperature and must be carefully monitored.

4 Conclusions

Satellite measurements of CH₄ concentration in the lower 4 km of the troposphere reveal a significant, up to 30 ppb, monthly anomaly maximized in November–December–

January over vast areas of BKS, as well as a part of the Greenland Sea. This CH₄ is transported to the sea surface layer mostly by turbulent diffusion and/or convection. Ebullition (bubbling) is assumed to be a secondary way for transport of methane into the troposphere. Marine emission should be taken into account in models simulating and predicting regional and global climatic changes.

References

- AMAP Assessment 2015: Methane as an Arctic climate forcer. Arctic Monitoring and Assessment Programme (AMAP), Oslo, Norway. vii +, p, 116. Available at <http://www.amap.no/documents/doc/AMAP-Assessment-2015-Black-carbon-and-ozone-as-Arctic-climate-forcers/1299>
- Gentz, T., Damm, E., von Deimling, J., et al.: A water column study of methane around gas flares located at the West Spitsbergen continental margin. *Cont. Shelf Res.* **72**, 107–118 (2013)
- Kara, A.B., Rochford, P.A., Hurlburt, H.E.: Mixed layer depth variability over the global Ocean. *J. Geophys. Res.* **108**(C3) (2002)
- Maddy, E., Barnet, C., Gambacorta, A.: A computationally efficient retrieval algorithm for hyperspectral sounders incorporating a priori information. *IEEE Geosci. Rem. Sens. Lett.* **6**, 802–806 (2009)
- Mau, S., Römer, M., Torres, M.E.: Widespread methane seepage along the continental margin off Svalbard from Bjørnøya to Kongsfjorden. *Sci. Rep.* **7**, 42997 (2017)
- Myhre, C.L., Ferré, B., Platt, S.M., et al.: Extensive release of methane from Arctic seabed west of Svalbard during summer 2014 does not influence the atmosphere. *Geophys. Res. Lett.* **43**, 4624–4631 (2016)
- Wunsch, C., Heimbach, P., Ponte, R., et al.: The global general circulation of the Ocean estimated by the ECCO-consortium. *Oceanography* **22**, 88–103 (2009)
- Yurganov, L., Leifer, I.: Abnormal concentrations of atmospheric methane over the Sea of Okhotsk during 2015/2016 winter. *Curr. Prob. Rem. Sens. Earth Space* **13**(3), 231–234 (2016). <https://doi.org/10.21046/2070-7401-2016-13-3-231-234>
- Yurganov, L., Leifer, I., Myhre, L.C.: Seasonal and interannual variability of atmospheric methane over Arctic Ocean from satellite data. *Curr. Prob. Rem. Sens. Earth Space* **13**(2), 107–119 (2016). <https://doi.org/10.21046/2070-7401-2016-13-2-107-119>

Global Environmental Change (T1): Land Surface



Seasonal Heat Fluxes of Land Surface Models, NOAA and MOSAIC Within NLDAS-2 Over USA During the Period of 1979–2018

Muhammed Eltahan, Mohammed Magooda, Karim Moharm, Ahmed El-Hennawi, and Sabah Alahmadi

Abstract

Estimation of the different types of heat fluxes at earth's surface is critical in energy budget calculation and climate change impacts. 40 years (1979–2018) seasonal spatial and temporal analysis of heat flux from the American Land Data Assimilation System, phase 2 (NLDAS-2) over the United States of America (USA) is presented. Two types of heat fluxes are investigated: Sensible heat flux and latent heat flux. Sensitivity of NLDAS-2 to the two integrated different land surface models (LSMs); NOAA, MOSAIC are shown in terms of the calculated three types of heat fluxes. The spatial maps' analysis revealed that the estimated sensible and latent heat fluxes from both models have different distribution, while the temporal analysis revealed that NLDAS with NOAA estimate higher sensible heat flux and lower latent heat flux than NLDAS coupled with MOSIAC.

Keywords

Heat Flux • NOAA Land Surface Model • MOSAIC Land Surface Model • NLDAS • North America

1 Introduction

Heat fluxes with its different types (latent, sensible and ground) are very critical and effective in the earth's energy budget studies (Xia 2012; Xia et al. 2013). The importance of heat flux estimations rose after its vital role in shaping the boundary layer that controls both weather and climate (Berbery et al. 1999). Many previous studies were conducted to investigate, compare and validate between different land surface models in terms of heat fluxes' estimation (Berbery et al. 1999; Berg et al. 2003; Cosgrove et al. 2003; Hinkelman et al. 2009). This work is conducted to evaluate the recent and long-term performances of both land surface models over the USA.

2 Methods and Data

In this paper, two types of heat fluxes (latent and sensible) are presented from earth's numerical integrated model North American Land Data Assimilation System (NLDAS). Both two types of heat fluxes are calculated based on two different land surface models (MOSAIC and NOAA). Spatial resolution for the used data set is 0.125° .

2.1 NLDAS-2System

NASA Land data assimilation system (NLDAS) is a framework constructed in order to build high quality spatiotemporal products for land surface models (datasets). NLDAS system uses forcing datasets from daily

M. Eltahan (✉) · M. Magooda
Aerospace Engineering Department, Cairo University,
Cairo, 12613, Egypt
e-mail: m.eltahan@fz-juelich.de

K. Moharm
Electrical Engineering Department, Alexandria University,
Alexandria, Egypt

A. El-Hennawi
Department of Mechanical Engineering, Ain Shams University,
Cairo, 11517, Egypt

A. El-Hennawi
Mechanical Engineering Department, Technische Hochschule
Luebeck, Luebeck, Germany

S. Alahmadi
National Satellite Technology Center, Space and Aeronautics
Research Institute, King Abdulaziz City for Science
and Technology, Riyadh, 11442, Saudi Arabia

meteorological parameters to drive the selected land surface model. This system is running now near real time (around 4-day lag). The output of this framework mainly is surface fluxes and soil moisture.

2.2 MOSAIC Land Surface Model

During the development of NASA's global climate model, the MOSAIC land model was developed as the land model (Koster and Suarez 1996; Koster et al. 2000) by different initiates.

2.3 NOAH Land Surface Model

During the development of NOAA NCEP meso-scale Eta model, the NOAH land component had been developed (Ek et al. 2003; Betts et al. 1997). NOAH Land surface model is considering the main land model in many weather and climate

models. This model has four soil layers with different thicknesses: 10, 30, 60 and 100 cm. The first three layers form the root zone in non-forested regions, the fourth layer contains forested regions. The simulation capability of this model is the parameterization of the soil's freeze–thaw process and its effect on the heating and cooling process of the soil.

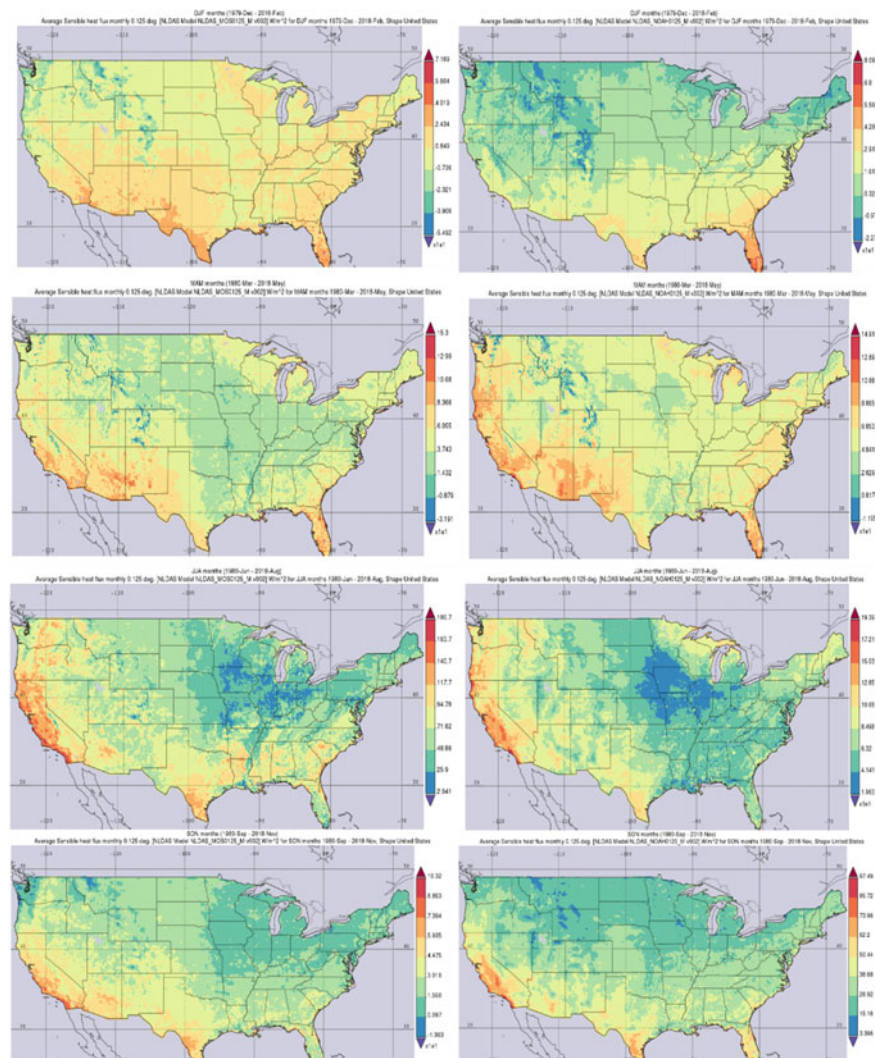
3 Results and Discussion

In this section, Seasonal two types of heat fluxes (sensible and latent) based on different land surface models are presented for a period of 40 years (1979–2018) with a spatial resolution of 0.125° .

3.1 Spatial Sensible Heat Flux

Spatial sensible heat flux is when energy is transferred from the earth's surface to the atmosphere by both

Fig. 1 Seasonal Spatial maps of sensible heat flux from both MOSIAC and NOAH within NLDAS-2(1979–2018)



conduction and convection. The amount of transmitted heat per unit area per unit time can be defined as sensible heat flux. In Fig. 1, the spatial and temporal sensible heat flux is presented. From the spatial maps, MOSIAC is underestimating sensible heat flux compared to the NOAA model in some areas.

3.2 Spatial Latent Heat Flux

Spatial latent heat flux is the flux of heat that moves from earth’s surfaces to the atmosphere and is associated with surface water’s evaporation. Latent heat flux impacts the earth’s surface energy budget directly. Seasonal spatial

average of 40 years is shown in Fig. 2. This figure reveals that latent heat flux from MOSIAC model has higher spatial values than NOAA.

3.3 Temporal Latent and Sensible Heat Fluxes

Analysis of seasonal time series for both latent and sensible heat fluxes are presented in Fig. 3. For all seasons, the average of seasonal sensible heat fluxes in case of NLDAS coupled with NOAA is higher than NLDAS coupled with MOSIAC. On the other hand, NLDAS coupled with MOSIAC provides higher statistical averages for all seasons with respect to NLDAS coupled with NOAA.

Fig. 2 Seasonal spatial maps of latent heat flux from both MOSIAC and NOAA within NLDAS-2 (1979–2018)

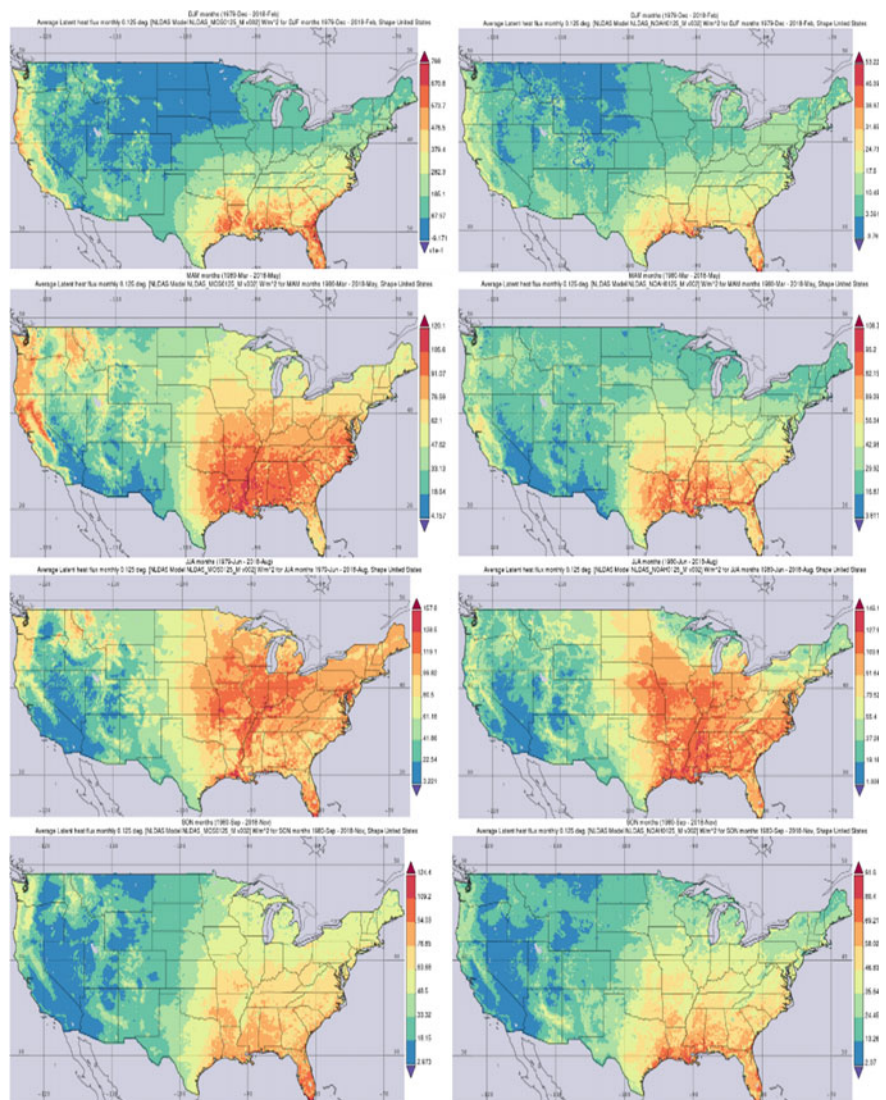
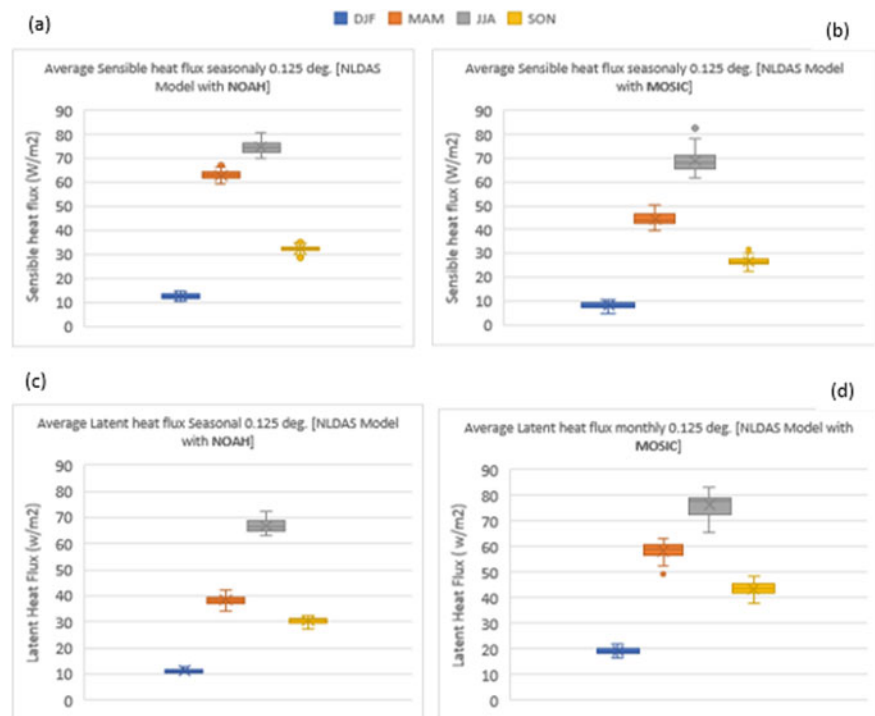


Fig. 3 Box plot for seasonal time series (1979–2018) over the USA
a Sensible heat flux NLDAS + NOAH, **b** Sensible heat flux NLDAS + MOSIAC, **c** Latent heat flux NLDAS + NOAH, **d** Latent heat flux NLDAS + MOSIAC



4 Conclusions

In this paper, we present the average spatial distribution of both Sensible and latent heat fluxes over the USA for a period of 40 years (1979–2018) from two different land surface models within NASA land data assimilation system, phase-2 (NLDAS-2). It is concluded that NLDAS model coupled with NOAH gives estimation for average seasonal sensible heat flux higher than NLDAS model coupled with MOSIAC. On the other hand, the estimation of average seasonal latent heat flux from NLDAS model coupled with MOSIAC is higher than NLDAS model coupled with NOAH. Future work will include more statistical analysis from both models and a comparison with numerical standalone community land model (CLM).

References

Berbery, E.H., Mitchell, K.E., Benjamin, S., Smirnova, T., Ritchie, H., Hogue, R., Radeva, E.: Assessment of land-surface energy budgets from regional and global models. *J. Geophys. Res.* **104**, 19329–19348 (1999). <https://doi.org/10.1029/1999JD900128>

Berg, A.A., Famiglietti, J.S., Walker, J.P., Houser, P.R.: Impact of bias correction to reanalysis products on simulations of North American soil moisture and hydrological fluxes. *J. Geophys. Res.* **108**(D16), 4490 (2003). <https://doi.org/10.1029/2002JD003334>

Betts, A.K., Chen, F., Mitchell, K.E., Janjić, Z.I.: Assessment of the land surface and boundary layer models in two operational versions of the NCEP eta model using FIFE data. *Mon. Wea. Rev.* **125**, 2896–2916 (1997). [https://doi.org/10.1175/1520-0493\(1997\)125%3c2896:AOTLSA%3e2.0.CO;2](https://doi.org/10.1175/1520-0493(1997)125%3c2896:AOTLSA%3e2.0.CO;2)

Cosgrove, B.A., et al.: Real-time and retrospective forcing in the North American Land Data Assimilation System (NLDAS) project. *J. Geophys. Res.* **108**(D22), 8842 (2003). <https://doi.org/10.1029/2002JD003118>

Ek, M.B., Mitchell, K.E., Lin, Y., Rogers, E., Grunmann, P., Koren, V., Gayno, G., Tarpley, J.D.: Implementation of Noah land surface model advances in the National Centers for Environmental Prediction operational mesoscale Eta model. *J. Geophys. Res.* **108**(D22), 8851 (2003). <https://doi.org/10.1029/2002JD003296>

Hinkelman, L.M., Stackhouse, P.W., Wielicki, B.A., Zhang, T., Wilson, S.R.: Surface insolation trends from satellite and ground measurements: comparisons and challenges. *J. Geophys. Res.* **114**, D00D20 (2009). <https://doi.org/10.1029/2008JD011004>

Koster, R.D., Suarez, M.J.: The influence of land surface moisture retention on precipitation statistics. *J. Clim.* **9**(10), 2551–2567 (1996). JSTOR, www.jstor.org/stable/26201452

Koster, R.D., Suarez, M.J., Ducharme, A., Stieglitz, M., Kumar, P.: A catchment-based approach to modeling land surface processes in a general circulation model: 1. Model structure. *J. Geophys. Res.* **105**, 24809–24822 (2000). <https://doi.org/10.1029/2000JD900327>

Xia, Y., et al.: Continental-scale water and energy flux analysis and validation for the North American Land Data Assimilation System project phase 2 (NLDAS-2): 1. Intercomparison and application of model products. *J. Geophys. Res.* **117**, D03109 (2012). <https://doi.org/10.1029/2011JD016048>

Xia, Y., et al.: Validation of Noah-simulated soil temperature in the North American Land data assimilation system phase 2. *J. Appl. Meteorol. Climatol.* **52**, 455–471 (2013). <https://doi.org/10.1175/JAMC-D-12-033.1>



Ecological Security Assessment of Qinghai Province in China Based on a Pressure-State-Response Model

Wang Fangping, Yao Buqing, Guo Jing, Ma Li, and Zhou Huakun

Abstract

A Pressure-State-Response (PSR) model framework was used to construct an ecological security assessment index system and to evaluate the degree of ecological security for Qinghai Province in China from 1996 to 2015. Our results indicate that the degree of ecological security has increased between the years 1996 and 2015. During this time period the eco-environmental pressures in this region have been mitigated to some extent. From 1996 to 2011, the degree of ecological security was in a state of extreme warning and the regional ecological system was very insecure. From 2012 to 2015, the degree of security was in a state of serious warning and the regional ecological system was insecure. Pressure indexes increased from 0.068 in 1996 to 0.197 in 2015, accompanied by continuously increasing eco-environmental pressures. The state index during this period has also generally increased. On the whole, the response index from 1996 to 2015 showed an upward trend. During the economic development of the Qinghai Province, long-term consumption of the environment and the resources has made

it difficult to significantly improve the eco-environmental condition of this region over a short-term period. The findings from our investigation provide references for future regional ecological environment administration and decision-making.

Keywords

Ecological security • Pressure-State-Response (PSR) model • Qinghai Province

1 Introduction

Social and technological progress has led to unprecedented changes to the global environment which has resulted in a number of environmental and ecological issues. Ecological security is a significant part of national security (Huang et al. 2010). Research on the assessment and administration of ecological security has become important for geonomy, science of resources, the environment and ecology.

Recently, ecological security assessments have become the main field of ecological security research. Regional ecological security assessments can provide a scientific basis for regional ecological environmental administration and decision-making (Alcamo et al. 2001). Commonly-used models in ecological security assessments include the “Ecological Footprint” concept and the “Pressure-State-Response” (PSR) model and so on (Guelfo et al. 2018; Rak and Pietrucha-Urbanik 2019). The PSR model is commonly used to determine assessment index systems (Huang et al. 2017). The PSR model classifies and organizes environmental indexes from the perspective of the interactions between the human system and the environmental system, and it is highly systematic (Wang and Pang 2012).

Qinghai Province, situated in the east of the Tibetan Plateau, is the source area of the Yangtze River, the Yellow River and the Lantsang River (being termed the Three-River

W. Fangping

College of Ecological and Environmental Engineering,
State Key Laboratory of Plateau Ecology and Agriculture,
Qinghai University, Xining, 810016, China

Y. Buqing (✉) · G. Jing · M. Li · Z. Huakun (✉)
The Key Laboratory of Restoration Ecology in Cold Region
of Qinghai Province, Northwest Plateau Institute of Biology,
Chinese Academy of Sciences, Xining, 810008, China
e-mail: bqyao@nwipb.cas.cn

Z. Huakun
e-mail: hkzhou@nwipb.cas.cn

G. Jing · M. Li · Z. Huakun
University of Chinese Academy of Sciences,
Beijing, 100049, China

G. Jing
Qinghai Academy of Social Sciences, Xining, 810000, China

M. Li
Grassland Station of Qinghai Province, Xining, 810008, China

Sources). However, as well as having an irreplaceable strategic position in national ecological security, its ecological environment is extremely vulnerable (Zhou et al. 2016).

2 Materials and Methods

2.1 Location of Qinghai Province and Data Sources

Qinghai Province is situated on the Tibetan Plateau of western China (89°20′–103°05′ East and 31°40′–39°15′ North). The acreage of the area is 7.22×10^5 km², accounting for 1/13 of China's total acreage. The average altitude of the province is greater than 3000 m, and its climate is a typical plateau continental climate, characterized by being dry, windy and cold with low oxygen levels.

Data used in this investigation was obtained from the Statistical Yearbook of Qinghai Province, and the Environmental Quality Report of Qinghai Province from 1996 to 2015, amongst other sources.

2.2 Research Methods

2.2.1 Assessment Model, the Assessing Index System and Index Quantization and Weight

In accordance with the index system framework of the PSR Model, and the construction principle of hierarchy analysis, the ecological security assessment index system was divided into three layers. Different indexes have different effects on the degree of ecological security. At present, the methods of determining index weights can be divided into two methods: Subjective weighting method and objective weighting method. Each method has its advantages and disadvantages. In order to avoid its disadvantages, subjective and objective weighting methods have been combined in different ways to determine the weights of assessing the indexes (Xu et al. 2010). In this investigation we used the Analytical Hierarchy Process (AHP) and the Entropy Method to determine the index weight.

2.2.2 Calculation of the Degree of Ecological Security

For this investigation, we adopted the regional Ecological Security Degree composite index ESI (Liang et al. 2010; Bai and Tang 2010), which is expressed as:

$$ESI_p = \sum_{j=1}^m Y_{ij} W_j \quad (1)$$

$$ESI = \sum_{p=1}^k W_p ESI_p \quad (2)$$

where ESI is the degree of ecological security of each sub-system ($p = 1, 2, 3$); ESI_p is the total ecological security degree; Y_{ij} is the standardized value of the j th index; W_j is the weight of the j th index; and the value range of is $[0, 1]$; W_p is the weight index of the Criterion Layer. The greater the value of the ESI, the higher the ecological security.

3 Results and Discussion

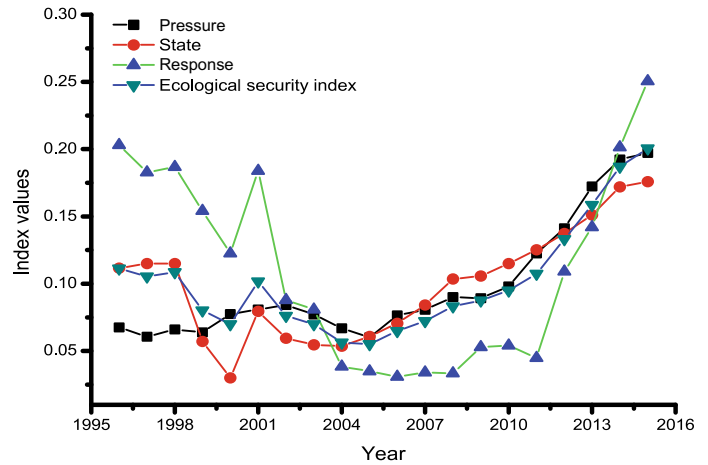
From 1996 to 2015, the degree of ecological security for Qinghai Province has increased from 0.111 (1996) to 0.201 (2015) (Fig. 1). However, the overall index value was low. From 1999 to 2011, the degree of ecological security was in a state of extreme warning, and the regional ecological system was extremely insecure. These results were due to the economic structure of Qinghai Province being based on agriculture. The economic aggregate was small and its economic development lagged behind.

Results showed that the systematic pressure index of Qinghai Province had an increasing trend, going from 0.068 (1996) to 0.197 (2015) (Fig. 1). These results reflect those identified by Wei et al. (2007) for this province from 1985 to 2003, indicating that the eco-environmental pressure has been continuously increasing in this region. Systematic state results can be seen that although there was a general trend of increase (Fig. 1), indicating that, with economic development and technological progress, people's lives constantly improved, accompanied by an increase in the rate of resource utilization and the continuous improvement of social infrastructure. Systematic response index showed an increase between 1996 and 2015 (Fig. 1), indicating that, for a long time, eco-environmental protection was not undertaken in Qinghai Province and the investment in environmental pollution governance was not sufficient, resulting in a serious aggravation of the eco-environment.

So based on the PSR model framework, Qinghai Province has made progress in the construction of the ecological province and its eco-environmental situation has been improved to some extent. However, the general trend in this area has been known as consuming land and environmental resources, and a minor focus has been paid to eco-environmental protection. Therefore, the eco-environmental situation of this province will not improve on the short-term, and the task of long-term eco-environmental protection will be difficult.

Data collection needs to be further improved. GIS, spatial technology and information management technology can be

Fig. 1 The degree of ecological security of Qinghai province from 1996 to 2015



used to realize data collection, which will further enhance the credibility of the evaluation results. Due to the limitation of technical means, this paper is used to consult the local yearbook and consult the management department to obtain index values. Due to the lack of data for many indexes, it was difficult to obtain the exact functional relationship among ecological state, pressure and response indexes, which still requires further studies.

Acknowledgements This study was supported by the Qinghai Innovation Platform Construction Project (2017-ZJ-Y20, 2017-S-1-04) and the National Social Science Foundation of China (16CJY012).

The Appendix 1

See Table 1.

Table 1 Ecological security assessing index system of Qinghai Province

Criterion layer	Index layer	AHP weight	Entropy method weight	Combination weight
Pressure (0.436)	Per Capita GDP (RMB) (C ₁)	0.073	0.050	0.026
	Natural Increase Rate of Population (%) (C ₂)	0.085	0.021	0.013
	Proportion of the Third Industry (%) (C ₃)	0.084	0.017	0.010
	Urbanization Rate (%) (C ₄)	0.083	0.084	0.051
	Industry Distribution Density (Yuan/ sq.km.) (C ₅)	0.054	0.053	0.021
	Economy Density (10 thousand/ sq.km.) (C ₆)	0.065	0.050	0.024
	Population Density (Person/ sq.km.) (C ₇)	0.068	0.036	0.018
	Road Net Density (km/ 10 thousand square.km.) (C ₈)	0.056	0.042	0.017
	Intensity of Applying Chemical Fertilizer (kg/ha.) (C ₉)	0.073	0.022	0.012
	Intensity of Using Pesticide (kg/ha.) (C ₁₀)	0.091	0.035	0.024
	Discharge of Industry Effluent (10 thousand ton) (C ₁₁)	0.103	0.033	0.025
	Per Capita Agricultural Acreage (mu) (C ₁₂)	0.070	0.030	0.016
	Raising Ratio of Independent Population (%) (C ₁₃)	0.073	0.016	0.009
State (0.357)	Per Capita Grain Yield (kg/person) (C ₁₄)	0.165	0.083	0.100
	Engel Coefficient (%) (C ₁₅)	0.131	0.016	0.015
	Unit GDP Energy Consumption (ton standard coal/10 thousand yuan) (C ₁₆)	0.205	0.014	0.021
	Number of Medical Personnel per 10 thousand Persons (person) (C ₁₇)	0.136	0.059	0.059
	Number of College Students per 10 thousand Persons (person) (C ₁₈)	0.161	0.032	0.038
	Per Capita Public Green Land Acreage (sq.m.) (C ₁₉)	0.129	0.030	0.028
	Per Capita Road Acreage (sq.m.) (C ₂₀)	0.073	0.011	0.006

(continued)

Table 1 (continued)

Criterion layer	Index layer	AHP weight	Entropy method weight	Combination weight
Response (0.207)	Proportion of Natural Protection Area to Regional Acreage (%) (C ₂₁)	0.280	0.072	0.148
	Proportion of Investment in Environment Pollution and Governance to GDP (%) (C ₂₂)	0.309	0.092	0.208
	Forestation Acreage in Those Years (10 thousand ha.) (C ₂₃)	0.182	0.045	0.060
	Proportion of R&D Expenditure above County Level to GDP (%) (C ₂₄)	0.170	0.034	0.043
	Agricultural Machinery Power (10 thousand kw.) (C ₂₅)	0.058	0.024	0.010

The Appendix 2

See Table 2.

Table 2 Classification of the degree of ecological security

Ecological security level	Ecological security degree	Description of warning situation	Index characteristics
Extremely Insecure	[0, 0.15)	Extreme Warning	The relationship between regional people and land is seriously imbalanced; the ecological system is destroyed; the ecological system structure is incomplete with the loss of basic functions; the restoration and reconstruction of ecological system are difficult to realize; natural disasters are normalized; and the development and survival of the population is seriously threatened
Insecure	[0.15, 0.4)	Serious warning	The relationship between regional people and land is imbalanced to an extent; the regional ecological system is destroyed; and the ecological system structure is incomplete with the loss of some functions. It is relatively difficult to restore the ecological system and its restoration will take a long time. The ecological environment has an obvious negative effect on the development of society and the economy. Natural disasters frequently occur
Comparatively Insecure	[0.4, 0.5)	High Degree Warning	The relationship between regional people and land is under threat and the ecological system is seriously damaged. There is a relatively significant effect on system functions and it is difficult to restore and reconstruct the ecological system. The ecological environment also has negative effects on the development of society and the economy. Natural disasters occur frequently
Critically secured	[0.5, 0.6)	Mid-degree Warning	The relationship between regional people and land is confronted with certain threats, and the ecological system is damaged. There is a certain effect on the system functions but they can be adjusted by themselves. There is also an obvious interruption to outside surroundings. The ecological environment has a certain negative effect on the development of society and the economy. Natural disasters occur infrequently
Comparatively secured	[0.6, 0.85)	Slight-degree warning	The relationship between regional people and land is comparatively harmonious and the ecological system is slightly damaged. Furthermore, system functions are complete and in normal operation; the ecological system has a strong ability to restore itself. The ecological system has a slight detrimental effect on the development of society and the economy. There are a few natural disasters
Secured	[0.85, 1]	No warning	The relationship between regional people and land is harmonious, and the ecological system has minor damage. The ecological system is secure with complete and good functions, with normal adjustment functions. The ecological environment is helpful to the development of society and the economy. Ecological problems are inconspicuous

References

- Alcamo, J., Endejan, M.B., Kaspar, F., et al.: The GLASS model: a strategy for quantifying global environmental security. *Environ. Sci. Pol.* **4**(4), 1–12 (2001)
- Bai, X.R., Tang, J.C.: Ecological security assessment of Tianjin by PSR model. *Procedia Environ. Sci.* **2**, 881–887 (2010)
- Guelfo, J.L., Marlow, T., Klein, D.M., et al.: Evaluation and management strategies for per-and polyfluoroalkyl substances (PFASs) in drinking water aquifers: perspectives from impacted US Northeast communities. *Environ. Health Persp.* **126**(6), 065001 (2018)
- Huang, B.Q., Liu, Q., Hu, Z.P., et al.: A review on ecological security assessment. *Resour. Environ. Yangtze Basin* **25**(s2), 74–78 (2010)
- Huang, H., Chen, B., Ma, Z., et al.: Assessing the ecological security of the estuary in view of the ecological services—a case study of the Xiamen Estuary. *Ocean Coast. Manag.* **137**, 12–23 (2017)
- Liang, P., Du, L.M., Yue, G.J.: Ecological security assessment of Beijing based on PSR model. *Procedia Environ. Sci.* **2**, 832–841 (2010)
- Rak, J.R., Pietrucha-Urbanik, K.: An approach to determine risk indices for drinking water—study investigation. *Sustainability* **11**(11), 3189 (2019)
- Wang, L., Pang, Y.S.: A review of regional ecological security evaluation. *Appl. Mech. Mate. Trans. Tech. Publ.* **178**, 337–344 (2012)
- Wei, L.H., Zhao, X.G., Gao, L.F.: Preliminary research of ecological safety based on ecological footprint in Qinghai Province. *Bull. Soil Water Conserv.* **27**(1), 155–158 (2007)
- Xu, H., Qiu, T., Zhao, J.S.: Synchronized method for construction a fuzzy judgement matrix and checking its matrix consistency. *J. Tsinghua Univ. Sci. Technol.* **50**(6), 913–916 (2010)
- Zhou, H.K., Yao, B.Q., Yu, L., et al.: Degraded Succession and Ecological Restoration of Alpine Grassland in the Three River Source Region of China. Science Press, Beijing (2016)



Detecting and Monitoring Dust Storm and Studying the Effect of Temperature and Relative Humidity Parameters Using Remote Sensing

Behnaz Ghaderi and Zahra Azizi

Abstract

Iran is in dry and semi-dry belt. It has always been exposed to storm dust. Recently, dust storms in the southwest of Iran have been abundantly reported and have had a great impact on a variety of sectors, including health, agriculture, transportation, tourism and industry. This paper was designed with the aim of assessing and monitoring dust by using climate, temperature, humidity and remote sensing data from 2010 to 2017. After receiving MOD021KM product images from the days of the dust storm, two methods of visual interpretation of the images with different colour combinations and use of visibility methods—such as dust indicators—were to identify and monitor the source of dust. With extraction of stormy days, the studied area was subdivided by drowning storms with interpolation methods. Using statistical algorithms, the effect of weather data on temperature, relative humidity, precipitation, visibility <1000 m, air pressure at synoptic station, wind direction, and wind speed with dust indexes was evaluated. So, with the determination of R^2 , the highest and lowest correlations of the BTM, TDI, NDDI indices were determined with meteorological parameters. As a result, external dust is considered as coming from neighbouring countries to the south-western and western parts of Iran.

Keywords

Dust storm detection • Climate data • Satellite image MODIS • Statistical algorithm • Correlation

1 Introduction

Dust is a phenomenon in arid and semi-arid areas due to high wind speeds on the unpolluted soil surface and prone to erosion (Khoshhal et al. 2016). Dust storms increase the esterification trend (Hao and Qu 2007), one of the most important environmental problems, which increases in the west and south of the country in the spring and summer seasons (Baaghdeh and Ahmadi 2014). Every year, it causes many losses in various sectors such as health, agriculture, transportation, tourism and industry. Finally, it is one of the most important contaminating sources in the world. Remote sensing and Geographic Information Systems (GISs) are a powerful tool for detecting and monitoring dust storms and for analysing data (Safari et al. 2017; Vafaeinezhad et al. 2009). Research on dust storm is of great interest because it can help to find methods to prevent and/or counteract its negative effects. This study was designed with the aim of assessing and monitoring dust by using temperature, humidity and remote sensing.

2 Materials and Methods

The study area is the southwest of Iran, the Khuzestan Province. The latitude and longitude of the study area are 47° 50' E and 30° 33' N, respectively, and is considered the centre of Iranian oil and gas production. Khuzestan is the fifth most populous city in Iran. Ahvaz is the capital of Khuzestan Province. Khuzestan Province has two climates: semi-desert and warm steep. Vegetation is affected by two important climatic factors, namely relative humidity and temperature. It is divided into three categories, including forests and trees, natural plants and pastures. Usually, the area has a rangeland. In this research, 20 synoptic stations, temperature, and humidity parameters were prepared and meteorological data with visibility of <1000 m was used in the station.

B. Ghaderi · Z. Azizi (✉)
Department of Remote Sensing and GIS, Faculty of Natural Resources and Environment, Islamic Azad University, Science and Research Branch, 1477893855 Tehran, Iran
e-mail: zazizi@srbiau.ac.ir

Satellite images from the MODIS sensor, MOD021KM, were produced on USGS and NASAs dusting days. Then the necessary corrections were made on the images. The image data Terra/MODIS were acquired on 21 July 2010, 17 June 2012, 2 September 2015, 22 June 2017, at 07:30 am. Two methods for detecting dust storms can be used. Use true colour combinations and dust storm index. In the visual method, dust and soil are created as a cloud in the image. Therefore, in MODIS images, the colour combination of bands (3-4-1) shows us the true colour combination (Karimi et al. 2012). In this research, BTM, NDDI, TDI dust storm index was used. Bands in the BTM index indicate the brightness temperature difference. Therefore, we use the algorithm of combining brightness temperature difference of dust between the wavelengths of 8.5 μm (MODIS band-29) and 11 μm (MODIS band-31) with negative values of bands-31 and 32 brightness temperature differences (Taghavi et al. 2013). Based on the so-called normalised difference dust index (NDDI), it is proposed to detect dust storms from cloud and non-sandy ground (Qu 2006). However, it does not give good results over sandy ground such as the Sahara Desert because the reflectance of strong dust storms and clouds are similar in band 3. The index TDI or thermal infrared dust index was performed and compared with the R, G, B. This indicator is suitable for dust and shows the pixels of dust in a separate way.

2.1 Dust Storm Zoning

By extraction of dusty days in the studied years, interpolation methods have been used for the zoning. The zone shows

that there are a lot of dusts at many stations in Khuzestan, and that southern parts of the Khuzestan province have more dust storms. Therefore, dust storms occur in June, July, August and early autumn, due to the high temperature and humidity.

2.2 Correlation of Temperature and Humidity Parameters with the Dust Index

In this section, the correlation and the relationship between the dust index with the parameters of temperature and humidity are shown. The value of R^2 was the lowest correlation between the BTM, TDI and NDDI drought indexes with temperature, humidity and temperature parameters.

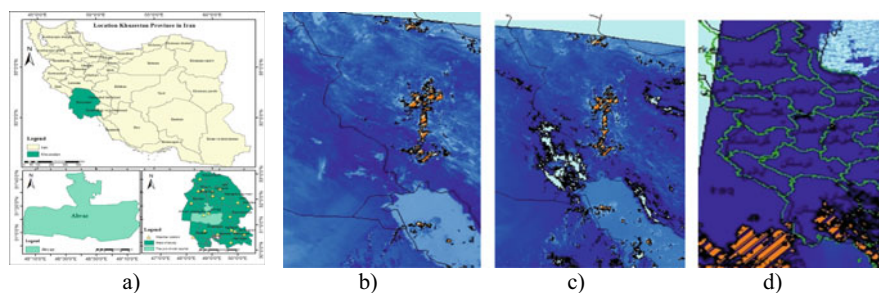
3 Results

Two methods for detecting dust storms were used. True colour combinations and the dust storm index. To define the dust areas, we used (BT8.5-BT11)—(BT11-BT12) values larger than the obtained threshold and (BT11-BT12) smaller than zero (Taghavi et al. 2013). And the BTM results are appropriate to identify the dust areas. The NDDI index for the dust phenomenon is >0 , and for the cloud and water <0 , the output index is usually weak. Thereafter, the TDI Index, which is not defined by the threshold research for TDI. In this study, we compared the RGB image. The results of RMSE and R^2 show the correlation and the relationship between temperature and humidity with dust (Table 1). Zoning shows that there are many dust days in most

Table 1 Review the result from the regression model

Regression	P value	R^2	RMSE
BTM-Temperature	0.000	0.2	31.96034
NDDI-temperature	0.000	0.7	1.32988
TDI-temperature	0.000	0.69	1.126526
BTM-humidity	0.000	0.19	32.67588
NDDI-humidity	0.000	0.9	1.33

Fig. 1 a Study area, b BTM, Index, June/17/2012, c TDI Index, June/17/2012, d NDDI, September/02/2015



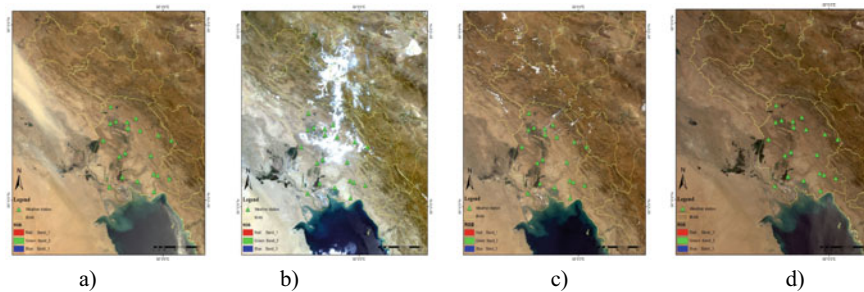


Fig. 2 Original images event, **a** July/21/2010, **b** June/17/2012, **c** September/02/2015, **d** June/22/2017

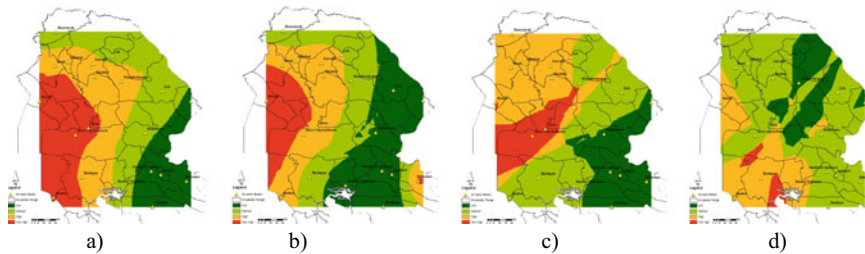


Fig. 3 Dust storm interpolation map, **a** July/21/2010, **b** June/17/2012, **c** September/02/2015, **d** June/22/2017

Khuzestan stations and the southern parts of Khuzestan Province have more dust storms.

4 Discussion

Many studies have been conducted on the detection and monitoring of dust storms in the world, including previous studies: Sabah et al., in their research “*dust and dust storms in Kuwait*” Ground-based and satellite observations of aerosol optical depth (AOD) using Aeronet and MODIS sensor images for the period 2007–2012 were made and correlated the relationship between the data. Among the findings was the fact large particles of aerosol were higher in spring and in summer (Sabbah et al. 2018). In another study (*Estimating the Effective Dust Particle Size from Satellite*), Albodi et al. estimated the pulse particle size from satellite observations in 2018 and measured the size of the red and infrared bands that Meteosat made (Albadi et al. 2018). The results indicated that the TDI index, along with BTM, was the best in identifying and monitoring dust storms and that the pixel dust storm shows up in the cloud. With linear regression on the parameters of humidity and temperature and the index of the dust, we reached the results that the dust was not related to temperature and humidity. Therefore, foreign dust comes from neighbouring countries to the south-western and western parts of Iran. Dust days occurred during the warmest and driest months (Figs. 1, 2, 3 and Table 1).

References

- Albadi, H., John, B., Bruce, D., Wedding, B.: Estimating effective dust particle size from satellite observations. *Rem. Sens. Appl. Soc. Environ.* **11**, 186–197 (2018)
- Baaghdeh, M., Ahmadi, H.: Dust and detector analysis of the changes in the west and southwest of Iran. *J. Rescue* **6** (2014)
- Hao, X., Qu, J.: Saharrah dust storm detection using moderate resolution imaging spectroradiometer thermal infrared bands. *J. Appl. Rem. Sens.* **1** (2007)
- Khosshal dastjerdi, J., Mousavi, H., Kashki, A.: Analysis of Ilam dust storm. *Geogr. Environ. Plann. J.* **2**, 99–110 (2016)
- Karimi, K., Taheri, H., Hafezi Moghaddas, N., Habibi Nokhandan, M.: Identifying and classifying the dust lands in the middle east using the combination of MODIS sensing reflective and infrared thermal characteristics. *J. Iran. Eng. Soc. Geol.* **5**(1 & 2), 93 (2012)
- Qu, J.J.: Asian dust storm monitoring combining Terra and Aqua MODIS SRB measurements. *IEEE Geosci. Rem. Sens. Lett.* **3**, 484–486 (2006)
- Sabbah, I., Leon, J., Sorribas, M., Guinot, B., Carmen Cordoba-Jabonero, C., Souza, A., Sharifi, F.: Dust and dust storms over Kuwait: ground-based and satellite observations. *J. Atmosph. Solar-Terrestrial Phys.* **179**, 105–113 (2018)
- Safari, A., Sohrabi, H., Powell, S., Shataee, S.: A comparative assessment of multi-temporal Landsat 8 and machine learning algorithms for estimating aboveground carbon stock in coppice oak forests. *Int. J. Rem. Sens.* **38**(22), 6407–6432 (2017). <https://doi.org/10.1080/01431161.2017.1356488>
- Taghavi, F., Olad, E., Safarad, T., Irannejad, P.: Detection and monitoring of dust storms in western Iran using remote sensing methods. *J. Phys. Earth Space* **39**(3), 96–83 (2013)
- Vafaeinezhad, A., Alesheikh, A., Roshannejad, A., Shad, R.: A new approach for modeling spatio-temporal events in an earthquake rescue scenario. *J. Appl. Sci.* **9**(3), 513–520 (2009)



Granulometric, Mineralogical, and HYSPLIT Analysis of Siliciclastic Sediments Derived from Sahara

Alex Kovács, György Varga, Nadia Gammoudi, and János Kovács

Abstract

Wind-blown (or aeolian) dust emissions of arid/semi-arid areas contribute about 1–3 billion tons to the global atmospheric mineral dust load. The Sahara Desert is responsible for more than 50% of the global dust emissions, as well as the dust storms, which reach Europe. This research focuses on two such dust events which occurred in January and April 2018 and aims to identify the possible source areas of those dust storms using geological methods and HYSPLIT application. The intensity of the discussed dust events can be explained by the unusual stationary behavior of major pressure systems and blocking mechanisms.

Keywords

Siliciclastics • Sediments • Laser diffraction • X-ray powder diffraction • Automated static image analysis • Scanning electron microscopy • Sahara

1 Introduction

Several hundred tons of wind-blown dust material are lifted into the atmosphere and are transported every year from Saharan dust source areas, Arabia, the Arabian Gulf, and Iraq toward Europe with important climatic and other environmental effects even on distant areas (Varga et al. 2016; Al-Hemoud et al. 2018; Al-Dousari et al. 2016,2017; Al-Awadhi et al. 2014; Al-Dousari 2005; Ahmed et al. 2016). According to the systematic observations of modern

Saharan dust events, it can be stated that dust deflated from North African source areas is a significant constituent of the atmosphere of the Carpathian Basin and that Saharan dust deposition events are identifiable several times in a year (Varga et al. 2016). Dust episodes are connected to distinct meteorological situations, which are also the determining factors of the different kinds of depositional mechanisms (Varga et al. 2013). North African desert dust has been identified on 130 occasions in the atmosphere of the Central European Carpathian Basin between 1979 and 2012, primarily based on data from NASA's Total Ozone Mapping Spectrometer (TOMS) and Aerosol Index (AI) measurements from the Ozone Monitoring Instrument (OMI). SDEs in the Carpathian Basin typically occur in spring, with a secondary maximum in summer; about three quarters of the identified episodes occur between March and August (Varga et al. 2013). In this study, air mass transport routes and possible source areas of two unusual Saharan dust events are discussed. An explanation for the peculiar nature of these dusty episodes in the Carpathian Basin is also offered. One specific objective of this study was to analyze in detail the content, physical and textural properties, mineralogy, and composition—including individual particles—of the clay fraction ($\phi < 2 \mu\text{m}$). This is typically a major fraction in desert dust. It is considered responsible for most of the scattering of sunlight, includes most of the bioavailable iron, and due to its long atmospheric residence time, is the one that can affect most distant locations.

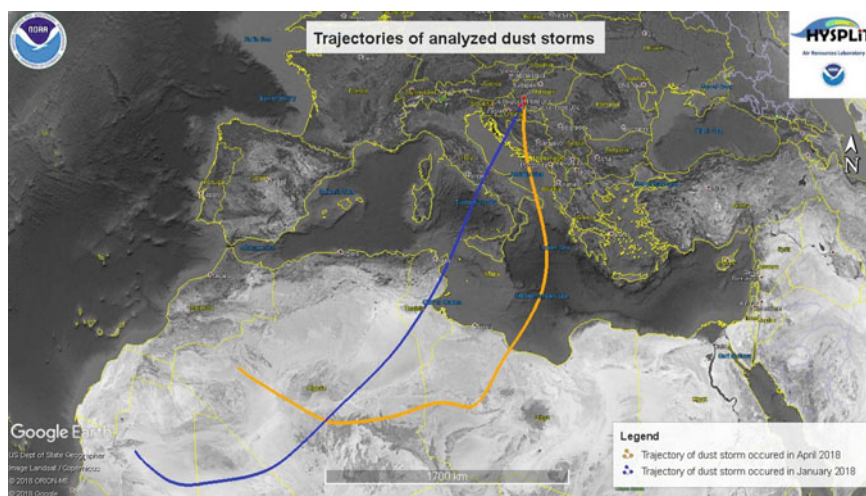
2 Materials and Methods

Sediment samples were collected from Morocco and Tunisia (as possible sources of sediments) and from Hungary (2018 dust events) and analyzed with the following measurements: laser diffraction, X-ray powder diffraction, automated static image analysis, and scanning electron microscopy (SEM). Similarities were expected in the results of desert-originated

A. Kovács · N. Gammoudi · J. Kovács (✉)
Department of Geology and Meteorology, University of Pécs,
7624 Pécs, Hungary
e-mail: jones@gamma.ttk.pte.hu

G. Varga
Geographical Institute, Research Centre of Astronomy
and Earth Sciences, 1112 Budapest, Hungary

Fig. 1 Different trajectories occurred in January and April 2018



samples and samples collected in Hungary. This is how the possible source area was going to be determined. In order to identify the typical dust transportation routes and possible source areas, the backward trajectories were plotted using the NOAA HYSPLIT model (Draxler and Rolph 2012).

3 Results and Discussion

According to particle size distribution results, an active dust emission is taking place at the location of investigated desert samples, and the samples collected in Hungary can be the particles out-blown from the source areas. The evaluated mineralogical results show that every sample contains quartz and phyllosilicates. SEM micrographs and image analyses results assume that the samples collected in Hungary are from the same source area. Using HYSPLIT application, trajectories of two analyzed dust events reveal that one desert sample, as a possible source is excluded and that the two trajectories cross each other at a junction point above North Africa (depression area between the Hoggar Mts. and Tadmait). This point can be the sought possible source location (see Fig. 1). The results in this study are in line with those found by Blott et al. (2004) and Ahmed et al. (2016).

4 Conclusions

The investigated events were connected to a steep pressure gradient between a western low-pressure system and a southeastern blocking high; the exact location of these pressure centers could be slightly varied. Synoptic meteorological conditions during the Central European dust episodes created enhanced meridionally, leading to warm incursions in southeastern and Eastern Europe, while the western parts of the continent suffered from unseasonably cold weather.

This period has been identified as the major interval of high dust loading of the atmosphere over the Sahara, due to the activity of dust source areas as emitters of wind-blown mineral particles. The intensity of the discussed dust events can be explained by the unusual stationary behavior of major pressure systems and blocking mechanisms.

Acknowledgements Support of the National Research, Development and Innovation Office NKFIH KH130337 and K120213 is gratefully acknowledged.

References

- Ahmed, M., Al-Dousari, N., Al-Dousari, A.: The role of dominant perennial native plant species in controlling the mobile sand encroachment and fallen dust problem in Kuwait. *Arab. J. Geosci.* **9**, 134 (2016)
- Al-Awadhi, J.M., Al-Dousari, A.M., Khalaf, F.I.: Influence of land degradation on the local rate of dust fallout in Kuwait. *Atmosph. Clim. Sci.* **4**, 403–437 (2014)
- Al-Dousari, A.M.: Causes and indicators of land degradation in northwestern part of Kuwait. *Arab. Gulf J. Sci. Res.* **23**(2), 69–79 (2005)
- Al-Dousari, A.M., Aba, A., Al-Awadhi, S., Ahmed, M., Al-Dousari, N.: Temporal and spatial assessment of pollen, radionuclides, minerals and trace elements in posited dust within Kuwait. *Arab. J. Geosci.* **9**, 95 (2016)
- Al-Dousari, A., Doronzo, D., Ahmed, M.: Types, indications and impact evaluation of sand and dust storms trajectories in the Arabian Gulf. *Sustainability* **9**, 1526 (2017)
- Al-Hemoud, A., Al-Dousari, A., Al-Shatti, A., Al-Khayat, A., Behbehani, W., Malak, M.: Health impact assessment associated with exposure to PM10 and dust storms in Kuwait. *Atmosphere* **9**, 6 (2018)
- Blott, S.J., Al-Dousari, A.M., Pye, K., Saye, S.E.: Three-dimensional characterization of sand grain shape and surface texture using a nitrogen gas adsorption technique. *J. Sediment. Res.* **74**, 156–159 (2004)
- Draxler, R.R., Rolph, G.D.: HYSPLIT (Hybrid Single-Particle Lagrangian Integrated Trajectory) Model Access via NOAA ARL READY Website. NOAA Air Resources Laboratory, Silver Spring,

- MD (2012). <http://ready.arl.noaa.gov/HYSPLIT.php>. Last accessed 2019/03/20
- Varga, G., Cserhádi, C., Kovács, J., Szeberényi, J., Bradák, B.: Unusual Saharan dust events in the Carpathian Basin (Central Europe) in 2013 and early 2014. *Weather* **69**, 309–313 (2014)
- Varga, G., Cserhádi, C., Kovács, J., Szalai, Z.: Saharan dust deposition in the Carpathian Basin and its possible effects on interglacial soil formation. *Aeolian Res.* **22**, 1–12 (2016)



Solar Power Plant Site Selection and Thermodynamic Analysis

Rafika Maali and Tahar Khir

Abstract

This study focuses on a thermal power plant design working according to an Organic Rankine Cycle using solar energy. A study will be conducted on the potential of the solar deposit in southern Tunisia. The results proved that Kebili is a suitable site to install the thermal power plant. A thermodynamic analysis of a solar power plant is conducted to simulate the cycle performances during the 15th day of January. The maximum net power was obtained at noon because the increase in solar radiation improved the net power. A calculation code was performed using equation engineering solver (EES) software to simulate the developed model.

Keywords

Solar energy • Renewable energy • Southern Tunisia • Organic Rankine Cycle • Thermal power plant

1 Introduction

Since 2000, Tunisia has been facing a depletion of natural sources and the global energy demands are highly dependent on fossil fuels which have led to harmful environmental problems. Consequently, the promotion of renewable energy sources increased in recent years (Olivier et al. 2017). Many researchers proved that solar energy is a promising solution to produce electricity from safe technology (Rajesh et al. 2016). On the other hand, the establishment of solar energy units in desert regions should take into consideration important environmental challenges, which include solar radiation, humidity, fallen dust, and mud and carbonates in

the dust (Al-Dousari et al. 2019). Tunisia is one of the countries which have high solar potential. Indeed, the solar radiation is about 1800 kWh/m²/year in the north of Tunisia and it is about 2800 kWh/m²/year in the south (Balghouthi et al. 2016). In the last decades, solar energy has received great interest due to its advantages. On the other hand, the literature proved that the Organic Rankine Cycle (ORC) is one of the most appropriate technologies to produce electricity from solar energy (Remi et al. 2017). To choose the localization of the thermal power plant, the solar potential of the targeted site must be investigated. In this work, Gabes, Tozeur, and Kebili are the selected sites to optimize the placement of the thermal power plant. The main objectives are selecting the site of the thermal power plant location and then simulating the cycle performances during two representative days in winter and in summer.

2 Methods

2.1 System Description

The system is a solar power plant working according to an Organic Rankine Cycle (ORC). The solar energy was used to generate the working fluid steam as shown in Fig. 1. The solar direct flux is determined by Chelbi et al. (2015)

$$R_{dir} = R_{out} \tau^M \sin \alpha \quad (1)$$

R_{out} is the solar flux present in the atmosphere. And it is given by:

$$R_{out} = Sc \left(1 + 0.034 \cos \left(360 \frac{j}{365} \right) \right) \quad (2)$$

where the solar inclination α is determined as follow:

$$\sin \alpha = \sin \varphi \sin \delta + \cos \varphi \cos \delta \cos \eta \quad (3)$$

R. Maali (✉) · T. Khir
Research Laboratory of Applied Thermodynamics, University of
Gabes, 6029 Gabes, Tunisia

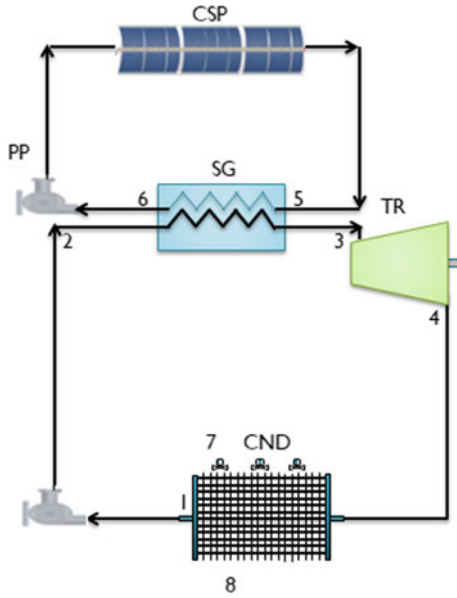


Fig. 1 Solar Power Plant diagram flow

where τ , η , ϕ , δ , j , and Sc are the transmissivity coefficient, the hour angle, the place latitude, the place declination, the day number, and the solar constant, respectively.

The net power of the solar power plant is the generated power through the turbine subtracted by the consumption of the pump.

$$\dot{W}_{\text{net}} = \dot{W}_{\text{TR}} - \sum \dot{W}_{\text{PP}} \quad (4)$$

The thermal efficiency of the solar power plant is determined as follows:

$$\eta_{\text{th}} = \frac{\dot{W}_{\text{net}}}{\dot{Q}_{\text{in}}} \quad (5)$$

3 Results and Discussion

3.1 Site Comparison

The solar power plant will be located in southern Tunisia. This study concentrates on three sites: Gabes (33° 55' N, 10° 6' E), Tozeur (33° 55' N, 8° 08' E), and Kebili (33° 42' N, 8° 57' E).

Figure 2 shows that, in January, Gabes has the least average hourly solar radiation of about 339 W/m². This

result is validated by Chelbi's results (Remi et al. 2017) with an error of 6%. Then comes Tozeur with a value of about 370 W/m². It also shows that Kebili has the highest average hourly solar radiation of 384 W/m². The same figure shows that in June Kebili had the highest average hourly solar radiation. Accordingly, the simulation of the solar power plant will take into account the solar radiation of Kebili.

3.2 Solar Power Plant Output

Figures 3 and 4 represent the evolution of the net power generated by the solar power plant (red) and the thermal efficiency (blue). The thermal power plant worked on the Kebili site during 9 h on 15 January, and during 14 h on 15 June.

4 Discussion

The net power increases with the time to reach a maximum of about 977.5 kW on a winter day and 2409 kW on a summer day, then, it decreases. The figures also show that the thermal has a maximum of about 15.97 and 13.88% on a winter day and a summer day, respectively. These results agree with the investigations of Otong Nurhilal et al. (Nurhilal et al. 2016). This is can be explained by solar radiation evolution since it reaches the maximum value at noon. On the other hand, the amount of heat consumed through the steam generator increases which makes the thermal efficiency constant.

5 Conclusions

A thermodynamic analysis of a solar power plant was conducted. The main objectives are to select the site of the thermal power plant location and then simulate the cycle performances during the 15th day of January and the 15th day of June.

The major results obtained are as follows:

- Kebili is a suitable site to localize the thermal power plant.
- The maximum net power was obtained at noon.
- The increase in solar radiation improved the net power.

Fig. 2 Average Hourly Solar Radiation (AHSR) in southern Tunisia in January and June

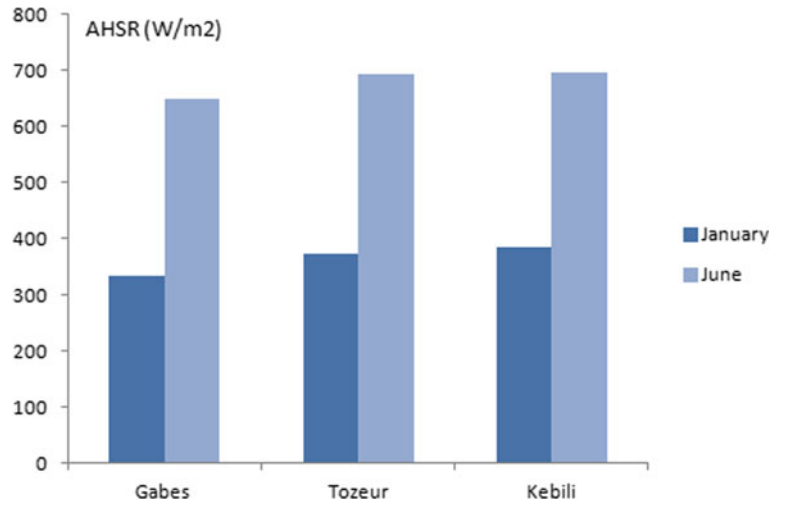


Fig. 3 The solar power plant in January

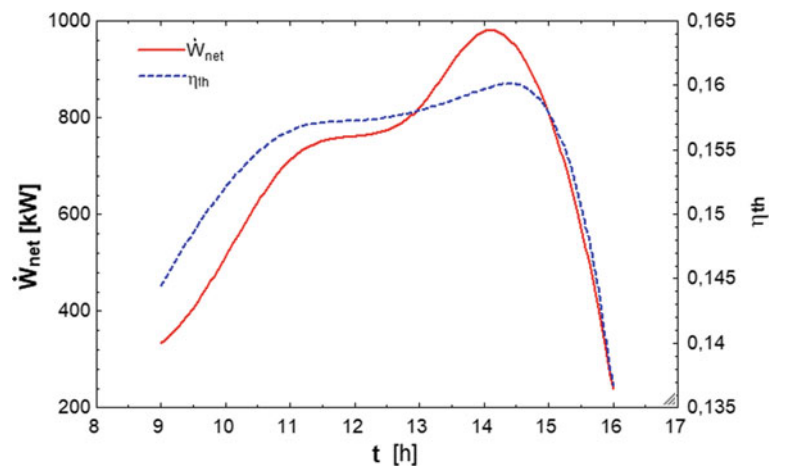
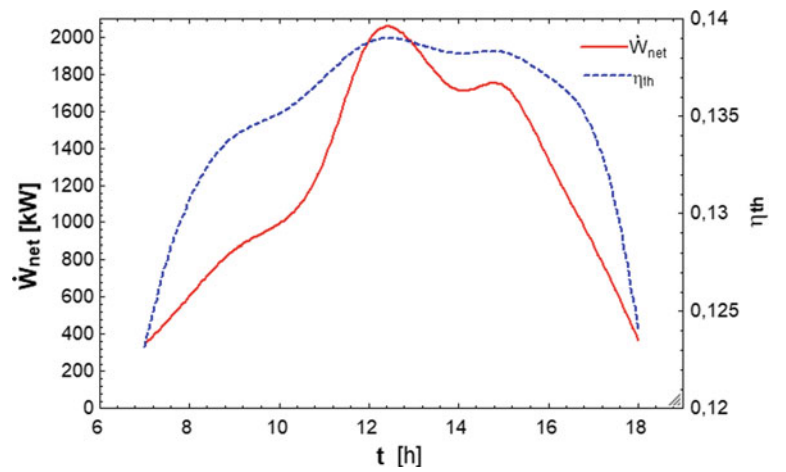


Fig. 4 The solar power plant in June



References

- Al-Dousari, A., Al-Nassar, W., Al-Hemoud, A., Alsaleh, A., Ramadan, A., Al-Dousari, N., Ahmed, M.: Solar and wind energy: challenges and solutions in desert regions. *Energy* **176**, 184–194 (2019). <https://doi.org/10.1016/j.energy.2019.03.180>
- Chelbi, M., Gagnon, Y., Waewsak, J.: Solar radiation mapping using sunshine duration-based models and interpolation techniques: application to Tunisia. *Energ. Convers. Manag.* **101**, 203–215 (2015). <https://doi.org/10.1016/j.enconman.2015.04.052>
- Moncef Balghouthi, N., Trabelsi, S.E., Amara M.B., Ali, A.B.H., Guizani, A.: Potential of concentrating solar power (CSP) technology in Tunisia and the possibility of interconnection with Europe. *Renew. Sustain. Energ. Rev.* **56**, 1227–1248 (2016). <https://doi.org/10.1016/j.rser.2015.12.052>
- Nurhilal, O., Mulyana, C., Suhendi, N., Sapdiana, D.: The simulation of organic rankine cycle power plant with n-pentane working fluid. In: Conference Proceedings, vol. 1712, p. 040003 (2016). <https://doi.org/10.1063/1.4941880>
- Olivier, J., et al.: Trends in global CO₂ and total greenhouse gas emissions: 2017 report. PBL Netherlands Environmental Assessment Agency, The Hague (2017). http://www.pbl.nl/sites/default/files/cms/publicaties/pbl-2017-trends-in-global-co2-and-total-greenhouse-gas-emissions-2017-report_2674.pdf. Accessed 10 July 2018
- Rajesh, K., Bhuvanesh, A., Kannan, S., Thangaraj, C.: Least cost generation expansion planning with solar power plant using differential evolution algorithm. *Renew. Energ.* **85**, 677–686 (2016). <https://doi.org/10.1016/j.renene.2015.07.026>
- Remi, D., Olivier, D., Remi, D., Sylvain, Q., Vincent, L.: Modelling of organic Rankine cycle power systems in off-design conditions: An experimentally-validated comparative study. *Energy* **123**, 710–727 (2017). <https://doi.org/10.1016/j.energy.2017.01.130>

**Biogeochemistry, Geobiology, Geoecology,
Geoagronomy (T2): Biogeochemical Investigations**



Blue Carbon Sinks on Polar Seabeds and Their Feedbacks on Climate Change

David Keith Alan Barnes

Abstract

Blue carbon held in polar organisms has been little considered in terms of global carbon sinks and impacts on climate change. Although the magnitude of sinks is small compared with elsewhere, they are amongst the biggest negative feedbacks on climate. As polar seas lose seasonal sea ice, ice shelves and glaciers retreat, new and longer phytoplankton blooms are occurring. This in turn supports the growing and extensive, long-lived, benthic biomass which is effective at storing and ultimately sequestering carbon. By far, the biggest impact per area is ice shelf collapse—a new giant iceberg may generate a million tons of blue carbon. However, losses of seasonal sea ice occurs over a far bigger area across the Arctic and West Antarctic shelves and thus is more important feedback. Blue carbon gains from glacier retreat are likely to be highly productive and efficient hotspots but ultimately occupy only small areas relative to a total shelf space. Small increases in temperature, as has happened to date, seem likely to increase polar blue carbon gains but big (2 °C) changes, ocean acidification and plastic pollution are all considerable threats to polar blue carbon natural capital.

Keywords

Blue carbon • Natural capital • Ecosystem services • Climate change • Benthic ecology • Polar ecosystems • Antarctic benthos

1 Introduction

The major organismal sinks of blue carbon storage are the coastal primary production habitats of mangrove swamps, kelp forests, salt marshes and seagrass beds. Apart from kelp, these are not found at high polar latitudes, and even kelp is restricted to ice shelf free coast. However, most carbon entering the biological cycle is captured by phytoplankton (micro-algae), most of which is recycled through respiration and the microbial loop (on death). A small proportion is eaten by animals and some sinks direct to the seabed and becomes buried and directly sequestered (see Fig. 1). Phytoplankton eaten by primary consumers (polar animals) also recycle some carbon through respiration whilst alive and breakdown by microbes when dead. Less than 1% of the original capture is estimated to be sequestered (Barnes 2017), but that still amounts to a ton of carbon per km² per year (on continental shelves). Polar ectotherms typically process meals and grow slowly and only have a very seasonal supply of primary production so it is unsurprising that such a value is globally low. This carbon sink is still very important for several reasons. Firstly, polar continental shelves are big. They are a 1000 km wide in places, and even the shelf around the Antarctic Peninsula is 800,000 km². Secondly, they are little disturbed (by humans or natural impacts) so sequestration chances of benthic carbon are high. Thirdly, they are one of the only, and biggest, sinks that is increasing in response to climate; i.e. they are a negative (mitigating) feedback. Carbon held in forests, swamps, salt marshes and dissolved in oceans dwarves that are held by polar animals. However, forests, swamps and marshes all decrease with rapid warming, so they are positive (exacerbating) feedbacks on climate change.

The negative feedback of polar carbon sequestration is driven by marine ice loss over continental shelves. This mainly takes three forms: ice shelf loss, seasonal sea ice loss and glacier retreat. The current work evaluated these three types of polar carbon sink.

D. K. A. Barnes (✉)
British Antarctic Survey, NERC, Cambridge, CB3 0ET, UK
e-mail: dkab@bas.ac.uk

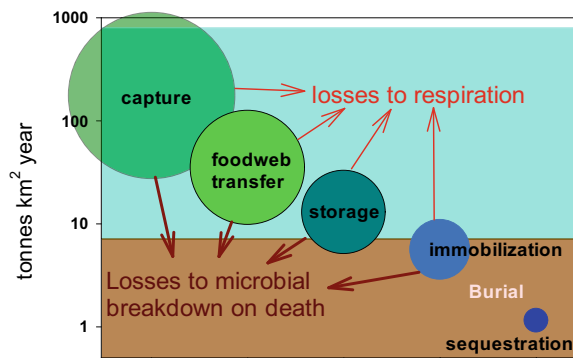
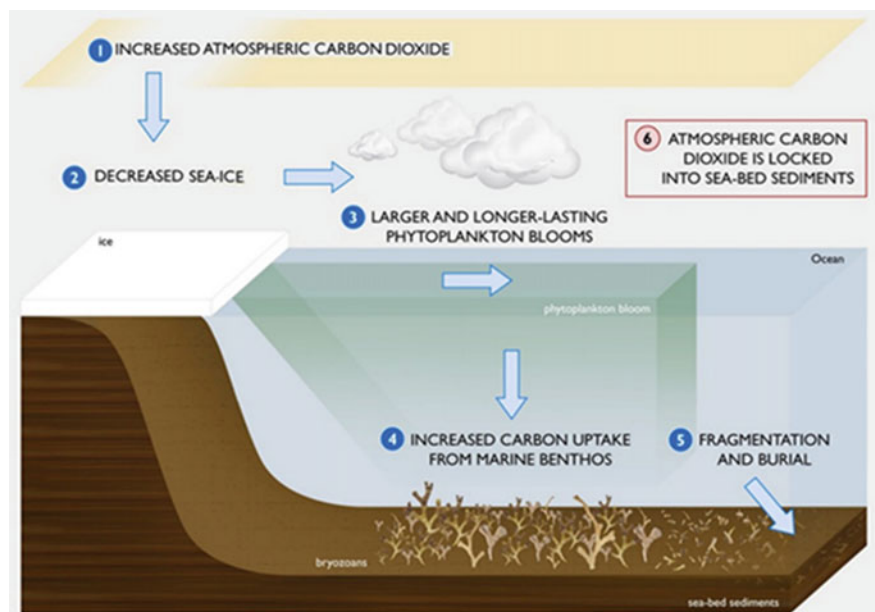


Fig. 1 Schematic of carbon mass from capture to sequestration in polar oceans. The size of the circles is scaled to mass at each step (redrawn from Barnes (2017))

2 Measuring Benthic Blue Carbon

The seabed is the key site of stored carbon burial and thus representing a true sequestration. Stored carbon standing stock can be measured by a variety of methods, which include accurate imaging of the seabed, from which density of functional groups or taxa can be derived from analysis. Matching specimens can be captured from tows of Agassiz trawls, which can be dried, weighed and ashed to obtain organic and skeletal masses. There is the literature of carbon content of mass by taxon but it can also be gained directly by carbon hydrogen nitrogen (CHN) analysis. The numbers of each organism by area (from images) can be multiplied by their carbon mass to derive total carbon per area. Finally, these values can be groundtruthed by collecting sediment

Fig. 2 Less marine ice in space and time allows more light to enter the water column, driving longer phytoplankton blooms and longer mealtimes for benthos



area/volume in box cores and multicore and process these to evaluate organic and inorganic carbon profiles, from surface to ~30 cm.

3 Major Polar Blue Carbon Feedbacks

3.1 Seasonal Sea Ice Loss Influences

Seasonal sea ice losses have been largest over Arctic continental shelves but there is more blue carbon response data from West Antarctic shelves. Even the 2.3% of the shelf in the shallow water, there holds 11 million tons and increments this at 0.27 million a year. However, there are considerable under ice algal masses that are reduced with seasonal sea ice losses and icebergs (which would otherwise be 'locked in' frozen sea surface) are free to scour the seabed. Thus, most of the gains in shallow water are negated by similarly big losses. In deeper water (100+ m) beyond regular iceberg scour depths, the longer phytoplankton blooms, driven by sea ice losses, result in more benthic blue carbon (Fig. 2). Different seas clearly perform at very different rates (Amundsen low, Scotia high) and are also changing at different rates. The shelf around the West Antarctic Peninsula generates ~5 million tons carbon per year of which about a third is sequestered. In terms of feedback on climate, this has doubled over the last 25 years, which is ~2.3% increase per year. Current work such as the Changing Arctic Ocean programme should reveal blue carbon storage and sequestration levels for the Barents Sea, but initial observations are that standing stock values may be high.

3.2 Ice Shelf Disintegration Influences

Ice shelf loss is very different from sea ice loss because there is effectively no in situ production beforehand, and it is from a distinct location. Phytoplankton blooms generated are thus brand new as are the seabed carbon sinks, which seem to progress much faster than normal benthic growth (Filinger et al. 2013). Disintegration of ice shelves (e.g. Larsen A, B & C) generates giant icebergs, and these in their own right fertilize new phytoplankton blooms as they melt (Duprat et al. 2016) but also destroy existing seabed carbon stocks when they scour (Barnes et al. 2018). The breakup of ice shelves is not gradual like seasonal sea ice losses, so there may be little or no blue carbon gain some years but a huge amount once in a decade. A single 5000 km² iceberg may generate 1 million tons of blue carbon (Barnes et al. 2018) and its seabed collisions recycle 4000 tons of blue carbon per year.

As with seasonal sea ice losses, there are albedo changes to be taken into consideration (open water absorbs more heat than ice). Ice shelves also buttress ice sheets so their loss can result in increased seaward flow and thus ultimately sea level rise.

3.3 Glacier Retreat and Emerging Fjord Influences

Nearly 90% of the glaciers along the Antarctic Peninsula are in retreat and the retreat rates are increasing. A NERC-CONICYT project 'ICEBERGS' is currently trying to establish how glacier ice loss translates to blue carbon change, both in the water column, through seabed processes. It seems likely that the small area of fjords emerging will be locally important hotspots of sequestration but small in the wider carbon sink budget.

4 Discussion

How big are polar continental shelf biological carbon sinks? Around Antarctica this may be 30–60 million tons in terms of storage on the seabed along with periodic boosts of a million tons with every giant iceberg calved. However, these are not big storage sinks compared with tropical forests. Their increase with marine ice loss, however, represents the biggest negative feedback on climate change measured to date. Southern Ocean temperature change has been biologically minor so far and a 1 °C increase may increase blue carbon storage further (even with capture change) (Ashton et al. 2017). Higher temperature rises, ocean acidification and microplastic pollution of foodwebs represent threats to polar blue carbon ecosystem services and their powerful negative feedback.

References

- Ashton, G., et al.: Warming by IC drives species and assemblage level responses in Antarctica's marine shallows. *Curr. Biol.* **27**, 2698–2705 (2017). <https://doi.org/10.1016/j.cub.2017.07.048>
- Barnes, D.K.A.: Polar zoobenthos carbon storage increases with sea ice losses, because across-shelf gains from longer algal blooms outweigh ice scour mortality in the shallows. *Glob. Change Biol.* **23**, 5083–5091 (2017). <https://doi.org/10.1111/gcb.13772>
- Barnes, D.K.A., et al.: Icebergs, sea ice, blue carbon and Antarctic climate feedbacks. *Philos.Trans. Royal Soc. London A* **376**, 20170176 (2018). <https://doi.org/10.1098/rsta.2017.0176>
- Duprat, L.P.A.M., et al.: Enhanced Southern Ocean marine productivity due to fertilization by giant icebergs. *Nat. Geosci.* **9**, 219–221 (2016). <https://doi.org/10.1038/ngeo2633>
- Filinger, L., et al.: Rapid glass sponge expansion after climate induced Antarctic ice shelf collapse. *Curr. Biol.* **23**, 1330–1334 (2013). <https://doi.org/10.1016/j.cub.2013.05.051>



Climatic Conditions as Factors Influencing the Formation of High-Moor Peat Organic Part

Alexander Orlov, Ivan Zubov, Valeria Tatarintseva, Tamara Sokolova, Victoria Pechtereva, and Svetlana Zabelina

Abstract

In this paper, the authors identified a number of characteristic features of the transformation of peat organic matter in the conditions of the North. In particular, it has been established that the subarctic zone is characterized by a decrease of humification depth and the predominance of fulvate type of humus formation. This is caused by the presence of particular climatic influences and, in particular, frost deposits, as a factor having a significant effect on the formation of the structure and group chemical composition of peat. The influence of the bitumen component on the process of humification of the organic part during peat accumulation has been revealed. It is primarily due to the inhibition of the formation of polyconjugation structures which are the main structure-forming humic substances.

Keywords

High-moor peat • Organic matter • Organic component composition • Humification • Geoclimatic conditions

1 Introduction

Peat as one of the main components of wetland ecosystems is actively involved in the global carbon cycle and serves as a geobarrier (Bambalov 1984). In addition, it is a renewable source of energy and raw material for the production of various natural organic substances. In recent years, a complex chemical processing to obtain a number of valuable

products and new materials is considered more promising. As a result, the number of studies on peat chemistry has noticeably increased (Bambalov 1984; Tomson and Nau-mova 2009).

Biogeochemical transformation of organic compounds in the process of peat accumulation in cold climate proceeds slowly. This is due to a significant change in chemical and microbiological regimes in cold climate conditions and, accordingly, humification mechanisms. This leads to the formation of specific properties of peat deposits. However, these aspects are poorly studied, and on this issue, there are only a few publications in recent years (Parfenova et al. 2016).

The goal of the study was to establish a comparative analysis of the stratigraphic features and group chemical composition of peat deposits organic part in different climatic zones. This will deepen the understanding of the influence of climatic conditions on the peat accumulation process and the formation of the organic matter composition.

2 Materials and Methods

Five representative layers of averaged moss peat samples were taken as an object of study. The selection was carried out on the territory of the Arkhangelsk Region, Western Siberia, and Belarus. The study sites are similar to hydrological conditions, botanical composition, and degree of decomposition.

The obtained samples of the natural material were pre-dried to an air-dry state and sieved on a 2 mm sieve. Images of temporary water preparations were taken with an Axio Scope A1 Zeiss microscope complete with a Canon G10 digital camera.

The group composition of peat samples was evaluated by sequential disassembly using various solvents (Metodika et al. 2017). The initial sample was consistently processed by diethyl ether (in the Soxhlet apparatus), 0.1 n. sodium hydroxide solution to isolate bitumens and humus biopolymers,

A. Orlov · I. Zubov · V. Tatarintseva (✉) · S. Zabelina
FCIARctic N. Laverov Federal Center for Integrated Arctic
Research, Arkhangelsk, Russia

T. Sokolova · V. Pechtereva
Institute for Nature Management, Belarussian Academy
of Sciences, Minsk, Belarus

respectively. The electron spin resonance (ESR) spectra of analyzed samples were recorded simultaneously with a reference sample based on MgO powder containing trace impurities of Mn^{2+} and Cr^{3+} ions developed at the Institute for Nature Management of the National Academy of Sciences of Belarus. This allowed us to increase the accuracy of determining the parameters of the ESR signal and control the level of microwave power in the working cavity of the device (Lishtvan et al. 2018).

3 Results

Composition of organic matter groups in the low-decomposed high-moor peat for subarctic maritime climate, temperate continental climate, temperate continental climate, temperate continental climate, and continental climate is shown in Table 1. The distribution of organic components of peat formed in the subarctic climate zone for different depths (0–2.15 m) are represented in Table 2.

4 Discussion

The formation of peat deposits is a long process that takes hundreds and thousands of years (Bambalov 1984). The conditions in which peat is located are constantly changing. Currently, the hydrothermal hypothesis of the formation of peat deposits is the most popular. According to this hypothesis deposit can be divided into the upper peat layer and the lower conservation layer. Their boundary is the level of groundwater fluctuation and aeration zone. It should be

noted that for the peat deposits of the subarctic zone an intermediate layer can be distinguished, boundaries of which are the groundwater level and the depth of freezing of the peat deposits (Lishtvan et al. 2018).

The chemical composition and structure of peat are formed in the upper biologically active layer. Climatic factors play a key role in this process (temperature and precipitation, which determine the biologically active period and the oxidative regime of the peat-forming layer) (Tomson and Naumova 2009).

Component peat composition data are presented in Table 1. For samples with the same *R* content of fulvic acid and non-hydrolyzable residue increase as a result of the increase in latitude. This can be explained by both the specificities of the biosynthesis of the original peat-forming plants and by the features of biogeochemical transformation. The lower degree of biodegradation of the peat from the subarctic region has been established with a microscope.

The chemical composition of peat organic part even in a genetically homogeneous deposit varies considerably with the depth of its occurrence (Table 2). The nonlinearity of the redistribution of groups of substances in the composition of peat organic part with a depth of occurrence is apparently due to the simultaneous occurrence of multidirectional destruction and condensation oxidative processes (humification and mineralization). During the biogeochemical transformation, both of the quantitative content and qualitative composition of bitumen change. The contribution of humic acids to the total content of HA increases along with the depth of the deposit. However, this trend covers only the peat layer and the zone of freezing, where the transition from aerobic to anaerobic conditions occurs

Table 1 Group composition of low-decomposed high-moor peat

RR, %	A, %	Content, % of organic matter						
		ES	HFA	FA/HA	WSS	EHS	HHS	LK
<i>Subarctic maritime climate (Arkhangelsk Region)</i>								
5–10	0.8	4.7	14.3	3.5	0.4	39.3	22.1	19.7
<i>Temperate continental climate (Arkhangelsk Region)</i>								
10–15	1.8	5.2	33.4	–	–	–	–	–
<i>Temperate continental climate (Central Russia)</i>								
10–15	–	0.9	30.9	0.7	16.9	31.7	8.4	20.8
5–10	–	1.0	12.3	2.3	2.6	8.3	33.6	15.5
<i>Temperate continental climate, transitional to the southern (Belarus)</i>								
10–15	–	4.6	35.4	1.0	7.3	42.8	8.8	6.2
5–10	–	1.6	13.8	–	7.4	45.5	26.0	5.7
<i>Continental climate (Western Siberia)</i>								
5–10	1.6	4.2	30.9	1.3	4.0	46.8	7.6	6.5

Note: RR—the degree of decomposition, A—ash content, ES—extractive substances, HFA—humic acids, HA—humic acids; FA—fulvic acids; WSS—water-soluble substances, EHS—easily hydrolyzable substances, HHS—hardly hydrolyzable substances, LK—lignin Klason.

Table 2 Distribution of components of peat formed in the subarctic climate zone

Depth, cm	A, %	Content, % of organic matter						
		ES	HFA	FA/HA	WSS	EHS	HHS	LK
0–5	3.15	0.94	19.65	9.32	10.33	49.69	11.50	18.22
5–25	3.41	2.38	20.20	13.27	6.93	44.07	11.27	22.08
25–75	2.32	1.49	13.74	12.55	1.19	54.90	14.53	15.34
75–125	1.01	2.19	15.85	12.86	2.99	47.77	10.07	24.12
165–215	1.04	2.74	22.28	17.99	4.29	45.05	12.84	17.09

Note A—ash content, ES—extractive substances, HFA—humic acids, HA—humic acids; FA—fulvic acids; WSS—water-soluble substances, EHS—easily hydrolyzable substances, HHS—hardly hydrolyzable substances, LK—lignin Klasson

(Tomson and Naumova 2009). Apparently, the process of oxidative condensation of phenolic compounds, which are part of the fulvic acid fraction and can act as a material for the synthesis of humic acids, most effectively takes place in the presence of oxygen. Humus formation in the upper layer of the deposit probably occurs by the condensation mechanism. Symbate change in the content of HFA and ES with depth manifested quite clearly. It can be assumed that it is due to the formation of the intermolecular polyconjugation system in the first case and quasi-polarization in the second. This imparting resistance to the degradation of molecular structures, on the one hand, and contributing to the condensation process, on the other.

The ESR spectroscopy data confirm ideas about the significant influence of climatic features on the degradation processes of the original peat-forming plants. The specificity of bitumen composition, formed in the conditions of the European North of the Russian Federation, explains the special effect of their impact on biogeotransformation. The contribution of bitumens to the process of peat formation is apparently due to their high enveloping ability. It complicates the intermolecular interaction of aromatic fragments and prevents the formation of polyconjugation systems, which are one of the main structural elements of humic substances.

5 Conclusions

The most important distinctive feature of high-moor peat formed in the conditions of the subarctic marine climate is a low index of humification and a rather pronounced predominance of fulvate type of humus formation. This is caused by the presence of particular climatic influences and, in particular, permafrost deposits, as a factor having a

significant effect on the formation of the structure and group chemical composition of peat. In this case, the oxidation regimes and kinetics of the humification process of plant residues in the upper and lower layers of the deposit may differ significantly.

The screening role of bitumen during the formation of intermolecular aggregates of aromatic components of peat was revealed. This effect makes a significant contribution to the humification of plant residues during peat accumulation and is primarily caused by inhibition of the formation of the polyconjugation structures, which are the main structural factor of humic substances.

Acknowledgements The study was carried out with the financial support of the RFBR project no. 18-05-70087.

References

- Bambalov, N.N.: Balans organicheskogo veshchestva torfyanyh pochv i metody ego izucheniya / N. N. Bambalov. – Minsk: Nauka i tekhnika, 1984. – 175s (1984)
- Lishtvan, I.I., Sokolova, T.V., Sosnovskaya, N.E., Orlov, A.S., Selyanina, S.B., Trufanova, M.V., Yarygina, O.N.: Formation of the organic matter of high-moor peat under conditions of the European North of Russia. *Solid Fuel Chem.* **52**(4), 211–216 (2018)
- Metodika izmerenij gruppovogo himicheskogo sostava torfa gravimetrichestkim metodom: svidetel'stvo ob attestacii № 88-16365-009-RA.RU.310657-2017. – Arhangel'sk (2017)
- Parfenova, L.N., Selyanina, S.B., Trufanova, M.V., Bogolitsyn, K.G., Orlov, A.S., Volkova, N.N., Ponomareva, T.I., Sokolova, T.V.: Influence of climatic and hydrological factors on structure and composition of peat from northern wetland territories with low anthropogenic impact. *Sci. Total Environ.* **551–552**, 108–115 (2016)
- Tomson, A.E., Naumova, G.V.: Torf i produkty ego pererabotki Minsk: Bel. Nauka (2009)



Coastal Deltas of Big Rivers as Synergetic Transformation Elements of the Earth System—(An Example of the Don River Delta)

Sergey Venevsky, Sergey Berdnikov, Vera Sorokina, Valerii Kulygin, Aleksey Kleshchenkov, Igor Sheverdyayev, Olga Arkhipova, Lyudmila Dashkevich, Victoria Gerasyuk, Karine Mesropyan, Pavel Ukrainsky, and Natalia Yaitskaya

Abstract

We discussed in this study the beginning of a new research initiative “Coastal deltas of big rivers as synergetic transformation elements of the Earth System” which the Southern Scientific Centre of the Russian Academy of Sciences is going to run on the case of the Don River delta. We suggested elaborating Delta Functional Types and quantifying these units according to the collected data. We compared energy and water management at the Don River with 100 major deltas of the world and concluded that our case study area is “coastal semi-arid with a relatively low energy and high-water management”.

Keywords

Coastal delta • Earth System • Climate change

1 Introduction

Deltas of big rivers (with basins over 50,000 km²) are playing a key role in transforming matter and energy fluxes in continuum land–ocean, and the fluxes are interacting

with each other in a synergetic way. Thus, deltas of big rivers, which represent regions with diverse landscapes and ecosystems, belonging to the biosphere, hydrosphere and atmosphere, are important synergetic transforming elements of the Earth System. Besides their functions as biogeochemical (e.g. hydrological, carbon and nitrogen cycle) and energetic (e.g. wave and gravitational energy) transformers, deltas are providing geomorphological ecological and economic services (Chenchouni and Si Bachir 2010). These geomorphological, ecological and economic services can be used to define deltas sustainability (Day 2016) by estimating some integrative variables like accretion against sea-level rise (geomorphological sustainability), NPP of wetlands (ecological sustainability) and the delta total economic monetary value (economic sustainability). From the thermodynamic prospective, deltas are open systems for which permanent flows of matter and energy are necessary to sustain their functions in the Earth System and ecological, economic and geomorphological services. Thus, the status of a river basin, influenced by climate change and anthropogenic activities (e.g. water uptake, reservoir’s construction) and the status of the adjacent ocean shelf (also highly influenced by climate change), will determine the deltas future structure and dynamics. Deltas are highly dynamic systems operating at different temporal scales, mainly determined by hierarchy of pulse inputs of energy and matter like daily tides, frontal wind passages, storms and associated storm surges and river floods. All pulse events in deltas are affected both by human activities and climate change, as well. Therefore, we can find both similarities and differences between different deltas of the world in relation to their climate zonation and anthropogenic pressure. From the view of Earth System Sciences, the major question regarding deltas is how to describe in qualitative and quantitative ways the functions of coastal deltas of big rivers and their geomorphological, ecological and economic services?

S. Venevsky (✉) · S. Berdnikov · V. Sorokina · V. Kulygin · A. Kleshchenkov · I. Sheverdyayev · O. Arkhipova · L. Dashkevich · V. Gerasyuk · K. Mesropyan · N. Yaitskaya
Southern Scientific Centre of the Russian Academy of Sciences, Chekhova 41, Rostov-on-Don, Russia
e-mail: veneovsky@tsinghua.edu.cn

S. Venevsky
Tsinghua University, Haidian, Beijing, China

P. Ukrainsky
Belgorod National Research University, Pobedy 85,
Belgorod, Russia

2 Materials and Methods

The Southern Scientific Centre of the Russian Academy of Sciences has just launched the research initiative “Coastal deltas of big rivers as synergetic transformation elements of the Earth System” addressing the major questions of this abstract.

We started from the structure of dynamic global vegetation models where each unit of vegetation is defined as plant functional type (PFT) determined by certain quantitative constraints. As an analogy, we suggested using Delta Functional Types (DFT) as a subset of all Coastal Functional Types and take as an initial classification of deltas suggested by Day et al. (2016). We, however, proposed adding an additional qualitative attribute “water management”, to Koppen climatic classification and “energy management”. As an “energy management” attribute, “water management” attribute can be either “high” or “low”. Our suggested classification aimed to be an intermediate complexity, being a trade-off between classifications based on mainly hydrological and geomorphic attributes as in Tagliapietra et al. (2009) and classifications based on functional traits of coastal deltas as in Levin et al. (2001). The intermediate complexity classification of coastal deltas fits the general approaches of Earth System Sciences and allows further inclusion in Earth System models.

For quantification of definition of Delta Functional Type, we took the Don River delta as a case study. The Don River is the eleventh largest river in Europe by discharge and the third by drainage area for tributaries of the Azov-Black Sea. The Don River delta is the most important agricultural, industrial and fishing conservation area in South Russia. It is nowadays strongly affected by climate change and anthropogenic pressure.

3 Results

3.1 Definition of Delta Functional Type for the Don River

The Don River delta is situated in a semi-arid climate Koppen zone. We compared energy management and water management at the Don River to 100 major deltas of the world (<http://www.geol.lsu.edu/wdd/publications/hcbk04/deltadata&images.pdf>) and concluded that our case study area is “coastal semi-arid with relatively low energy and high-water management”. High-water management was explained by the low-flow period in the region and the use of large Tsymlyansk Reservoir (2,700 km²).

3.2 Don River Delta Mapping

We started the creation of a GIS for the Don River delta (see Fig. 1). This delta contains natural land cover types like wetlands important for birds’ conservation (including charismatic local Russian Red Book ibis), riparian vegetation and grasslands, meaning that anthropogenic agricultural and urban areas, roads, industrial enterprises and fishery harbours may affect the delta.

3.3 Collection of Databases for the Don River Delta

The Southern Scientific Centre of RAS collected significant amount of data based on permanent field observations and historical records. A simplified version of the metadata is presented in Table 1. This database was used for quantitative

Fig. 1 Don River delta map with major land-use types

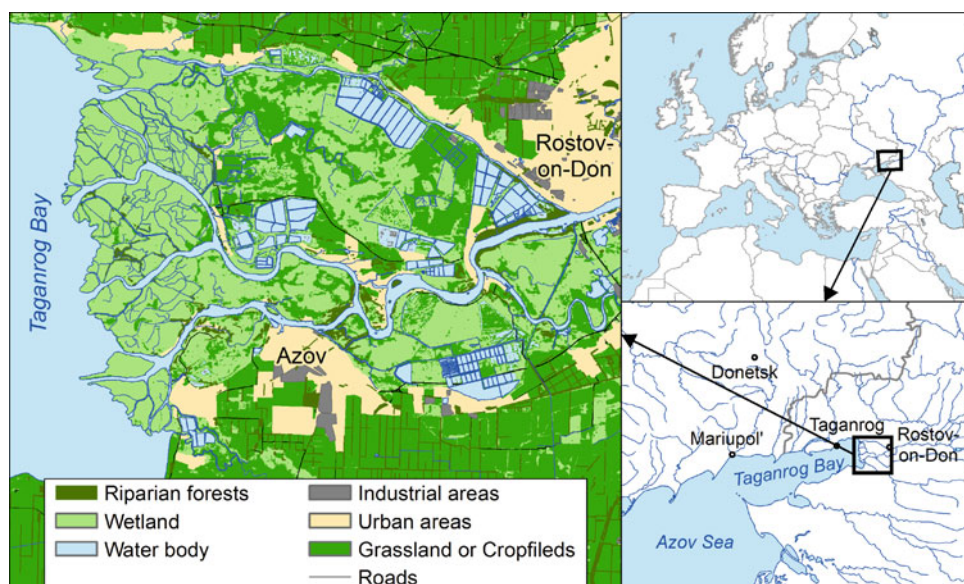


Table 1 Simplified metadata on the *Don River* delta (Mikhailov 2014, 2008, 1997)

Type of data	From	To	Periodicity
Weather parameters	2004	2018	Once every 10 min
Water level	2007	2018	Once every 10 min
River discharge	2002	2018	By day
Sediment load	1936	2016	By month
Water temperature	2004	2018	Once every 10 min
Mineralization	2004	2018	Once every 10 min
Chemistry	2006	2018	By month
Carbon in water	2006	2018	By month
Chlorophyll a	2008	2018	By month
Biology (zooplankton, benthos)	2005	2018	By season
Water use	2000	2018	By year

estimation of sustainability and function variables for the *Don River* delta.

4 Discussion

Our approach in defining the Delta Functional Type as a subset of Coastal Functional types in the Earth System is quite novel and needs discussion with terrestrial and marine ecosystems researchers for further refining and quantification of these broad-scale ecosystems. For example, deltas classification in the Russian hydrological science is based mainly on river typology and coastal shelf geomorphological typology. So, according to Mikhailov (1997) the *Don River* delta is classified as “No tide with abundant channels and shallow shelf”. We may argue, however, that a broader classification definition, accounting not only for geomorphological features, but also for climatic and anthropogenic pressure features is necessary for purposes of general Earth System analysis.

5 Conclusion

The dataset acquired on the *Don River* delta is enough for the definition of “coastal semi-arid with relatively low energy and high-water management” Delta Functional Type. It is also possible to make a long-term and short-term integrated assessment of the *Don River* function within the Earth System and geomorphological, ecological and economic sustainability of this River delta.

Acknowledgements The work was funded by the State Assignment research of the SSC RAS for 2019, project No. 01201363188 and by the National Natural Science Foundation of China (31570475).

References

- Chenchouni, H., Si Bachir, A.: Zones humides et biodiversités—Classification et typologie des zones humides du Bas-Sahara algérien et caractérisation de la biocénose du Lac Ayata (Vallée d’Oued Righ). Sarrebruck, Germany: Editions Universitaires Européennes (2010). ISBN-13: 978-613-1-55662-3
- Day, J.W., et al.: Approaches to defining deltaic sustainability in the 21st century. *Estuarine, Coastal Shelf Sci.* **183**, 275–291 (2016). <https://doi.org/10.1016/j.ecss.2016.06.018>
- Levin, L.A., et al.: The function of marine critical transition zones and the importance of sediment biodiversity. *Ecosystems* **4**(5), 430–451 (2001). <https://doi.org/10.1007/s10021-001-0021-4>
- Matishov, G., Matishov, D., Gargopa, Yu., Dashkevich, L., Berdnikov, S., Kulygin, V., Archipova, O., Chikin, A., Shabas, I., Baranova, O., Smolyar, I. Climatic Atlas of the Sea of Azov 2008. In: Matishov, G., Levitus, S. (eds.), NOAA Atlas NESDIS , U.S. Government Printing Office, Washington, D.C. 148pp. CD-ROM (2008)
- Matishov, G.G., Berdnikov, S.V., Zhichkin, A.P., Dzhenyuk, S.L., Smolyar, I.V., Kulygin, V.V., Yaitskaya, N.A., Povazhniy, V.V., Sheverdyayev, I.V., Kumpan, S.V., Tretyakova, I.A., Tsygankova, A. E., D'yakov, N.N., Fomin, V.V., Klochkov, D.N., Shatohin B. M., Plotnikov, V.V., Vakulskaya, N.M., Luchin, V.A., Kruts, A.A.: Atlas of Climatic Changes in Nine Large Marine Ecosystems of the Northern Hemisphere (1827–2013). In: Matishov, G.G., Sherman, K., Levitus, S. (Eds.), NOAA Atlas NESDIS **78**, 131pp (2014) <https://doi.org/10.7289/V5Q52MK5>
- Mikhailov, V.N.: Hydrological processes in river deltas, p. 176. GEOS, Moscow (1997). (in Russian)
- Tagliapietra, D., et al.: A review of terms and definitions to categorise estuaries, lagoons and associated environments. *Marine Freshwater Res.* **60**(6), 497–509 (2009). <https://doi.org/10.1071/MF08088>



Investigation of the Impacts of the Saponite-Containing Waste on Wetland Ecosystems

Svetlana Selyanina, Tamara Ponomareva, Elena Churakova, and Olga Yarygina

Abstract

The monitoring of the industrial impact is usually carried out in the immediate vicinity of the enterprises. Exposure may spread to remote areas and has a prolonged effect. This research work aimed at investigating the natural complexes of the Zolotitsa River (Arkhangelsk region, Russia) outside the official zone of influence of the diamond-mining enterprise. The study of the diversity of aquatic vascular plants of the river lower course in 2018 showed that the number of species increased from 14 to 16, in comparison with earlier observations. The *Elodea canadensis* Michx. was identified here for the first time and forms large thickets in some areas. Previously, its resettlement was hindered by the poverty of the waters in mineral elements. Laboratory modeling of saponite-containing water suspension entering both directly into the watercourse and through the filtration fields demonstrates the deoxidizing effect of saponite and the limited buffering capacity of peat. At the same time, the formation of intermolecular mineral associates with humic substances contributes to the transfer of saponite particles down to the lower reaches of the Zolotitsa River, their accumulation in bottom sediments, as well as the prolonged nature of mineral substances desorption. This provides the most favorable conditions for the new species settlement in the river. The obtained data are important for understanding the changes taking place and also for planning remediation activities.

Keywords

High-moor peat • Saponite • Invasive species • Wetland ecosystems

S. Selyanina (✉) · T. Ponomareva · E. Churakova · O. Yarygina
N. Laverov Federal Center for Integrated, Arctic Research Russian Academy of Science (FCI Arctic RAS), 163000 Arkhangelsk, Russia
e-mail: gumin@fciarctic.com

1 Introduction

The kimberlite region of the Arkhangelsk diamondiferous province (ADP) is located in the zone of heavily swamped tundra forests. The ecological balance of this zone is very unstable. The commercial mining of diamonds is carried out here using the opencut mining method. One of the distinctive features of the kimberlite rocks of this area is the high content of saponite in the extracted ore. Production of “Severalmaz” enterprise is certified and recognized as environmentally friendly. In the impact area, directly at the borders of the industrial estate, regular environmental monitoring is conducted. Nevertheless, the consequences of diamond mining in an open pit way in the upper reaches of the Zolotitsa River give cause for concern. The river is spawning for salmons and other fish species. In this regard, the study of changes in the state of natural complexes near the subsoil use areas is relevant to prevent irreversible changes, as well as for an artificial recovery of territories. This study aimed to identify changes in the state of the natural complexes of the Zolotitsa River outside the official zone of impact of the diamond mining enterprise.

2 Materials and Methods

Studies were conducted on the north of the mainland part of the Arkhangelsk Region, within the large geological structure—the Belomorsko-Kuloi Plateau. The mining and processing plant is located in the upper reaches of the Zolotitsa River.

One of the objects of the study was true aquatic vascular plants. As shown in literary sources, the species composition of aquatic vascular plants, especially fully submerged, rooting, or attached to the bottom of water bodies, can be used to evaluate the ecological condition of the water bodies (Poikane et al. 2018).

Floristic studies consisted in compiling a preliminary list of species of hydrophytes for this area based on data on the specific flora Zolotitsa (Shmidt 2005) and in collecting of field materials in the lower reaches of the Zolotitsa River in 2018, at the maximum distance from the quarry and processing.

The flora samples were collected by the route method to identify modern species diversity. Herbarium samples were determined using standard guidelines (Maevskiy 2014).

The laboratory modeling experiment was performed on the entry of a saponite-containing suspension into a watercourse, both directly and through filtration (oligotrophic bogs). Resistance to sedimentation of an aqueous suspension of saponite was evaluated by the change in the optical density, measured by using a UV spectrophotometer, during the settling (Khodakov and Yudkin 1980). The ratio of saponite-containing suspension: bog water varied from 1:250 to 1:2000.

In the second stage, the bog water with the addition of saponite at the concentration of 0.1 was passed through the peat layer. The pH value and electrical conductivity were monitored in the filtrate for 5 days.

3 Results

The changes in the composition of true aquatic vascular plants were recorded during the investigation of the natural systems of the river in comparison with materials on the flora of the study area, obtained by previous researchers in 1969–1970 (Dobrovolskaya 1971). Overall, 16 species of true aquatic vascular plants have been identified in 2018. Of these, the *Elodea canadensis* Michx. (Hydrocharitaceae) is of great interest. It forms in some parts of the riverbed large thickets even though it is uncharacteristic for this area.

The results of the first laboratory experiment (Table 1) demonstrate the dependence of the indicators on optical density and active acidity of bog water on the addition of saponite-containing suspension. In the course of this experiment, the period of upholding of the system was five days.

During the second laboratory experiment, simulating the flow of water through the filtration fields, the pH value of

bog water with the addition of saponite was 7.4 ± 0.05 , and the electrical conductivity due to total salinity was 87.6–88.7 $\mu\text{S}/\text{cm}$. In the filtrate, collected 4 h after the start of the model experiment, the pH value decreased to 3.7–3.9 units, the electrical conductivity also decreased to 44.6–57.7 $\mu\text{S}/\text{cm}$, and after 5 days, pH and electrical conductivity changed to 4.1–4.3 units and 20.4–23.9 $\mu\text{S}/\text{cm}$, respectively.

4 Discussion

The species that were recorded in 2018 for the first time, on the contrary, are more often found in waterbodies with relatively high mineralization and hardness of the water. In 2018, *E. canadensis* was discovered first in the lower reaches of the Zolotitsa. This invasive species is able to displace aboriginal plants from their characteristic growing areas. According to the latest floristic report (Shmidt 2005), the *E. canadensis* was noted only in the southern part of the Belomorsko-Kuloi plateau. Its resettlement, apparently, was hampered by the low content of mineral elements in the waters. The Zolotitsa River Waters have a relatively high mineralization, but during the period of snowmelt or heavy precipitation, it decreases significantly; the waters become slightly acidic. The settlements in the lower course are mostly sandy. This is not optimal for *E. canadensis*.

Saponite forms a stable fine-dispersed suspension in the aquatic environment. The oligotrophic bogs of the Zolotitsa River catchment are used as natural filters that prevent the entry of the saponite into watercourses. At the same time, the buffering capacity of peat in relation to saponite is studied poorly.

During the adsorption of saponite, one can expect an increase in the density, a change in the water–air regime and alkalization of the peat deposits and, accordingly, the removal of organic matter into the watercourses. The entry of saponite into the natural waters increases their turbidity and, presumably, mineralization. Accordingly, it can influence the species diversity of aquatic plants, including contributing to the dispersal of alien species.

The mechanism of interaction of a suspension of saponite with peat and bog water is somewhat different. Peat provides clarification of the suspension due to the mechanical

Table 1 Characteristics of model solutions on the 5th day of the experiment

The ratio of the suspension of saponite/bog water	Active acidity (pH)	Optical density at 465 nm (D, y.e)	Optical density at 665 nm (D, y.e)	Springer coefficient, (E4/E6)
1/250	4.82	0.626	0.179	3.50
1/500	4.33	0.526	0.151	3.48
1/2000	3.86	0.390	0.111	3.51
The bog water	3.56	0.276	0.095	2.91

retention of saponite particles. This is confirmed by an increase in the pH value during filtration through a peat layer. As the sorption capacity of peat is exhausted, the gradient of indicators decreases and stabilizes at the level of 2–6%, and by the end of the model experiment, no cleaning effect is observed.

It can be stated that the buffering capacity of peat is relatively high with respect to saponite, while the organic matter of the bog waters prevents sedimentation, ensuring the transit of mineral particles. The formation of intermolecular associates with humic substances can be attributed to the transfer of saponite particles over long distances from the enterprise, down to the lower reaches of the Zolotitsa River, their accumulation in sediments, as well as the prolonged nature of the desorption of mineral substances. Under such conditions, one can expect an increase in the role of *E. canadensis* in the formation of communities of aquatic plants in the Zolotitsa River and a decrease in the role of the native species.

5 Conclusions

The development of deposits causes changes in a number of factors affecting the structure, properties, and vegetative processes of ecosystems located in the immediate vicinity and quite distant from the diamond-mining areas. The findings of the *E. canadensis* in the lower reaches of the

Zolotitsa River mean they reached the northernmost of the European part of Russia. It indicates the entry of saponite into watercourses. The laboratory modeling showed that high-moor peat has high buffering capacity with respect to saponite, but at the same time the organic matter of the bog waters prevents sedimentation of mineral particles, ensuring their transmission. Within this framework, it appears that the buffer capacity of the peatlands in the catchment area can be characterized by the distribution of the macrophyte.

Acknowledgements The study was carried out with the financial support of the RFBR in the framework of project No. 18-05-60151 (Arctic).

References

- Dobrovolskaya, T.G.: Materials for the analysis of the flora of the vicinity of the village Zolotica of the Primorsky district Arkhangelsk region. Leningrad (1971)
- Khodakov, G.S., Yudkin, Yu.P.: Sedimentation Analysis of Highly Dispersed Systems. Nauka, Moscow (1980)
- Maevskiy, P.F.: Flora of the Middle Zone of the European Part of Russia, 11th edn. KMK, Moscow (2014)
- Poikane, S., Portielje, R., Denys, L., Elferts, D., Kelly, M., Kolada, A., van den Berg, M.S.: Macrophyte assessment in European lakes: Diverse approaches but convergent views of “good” ecological status. *Ecol. Ind.* **94**, 185–197 (2018). <https://doi.org/10.1016/j.ecolind.2018.06.056>
- Shmidt, V.M.: Flora of Arkhangelsk Region. St. Petersburg (2005)



Evaluation of the Impact of Diamond Mining on the Radioecological State of the Arctic Zone Ecosystems (Example of Arkhangelsk Region, Russia)

Evgeny Yakovlev, Alexander Malov, and Svetlana Selyanina

Abstract

The paper was devoted to the study of the activity of natural and technogenic radionuclides in the environment components around the Lomonosov diamond deposit. This is the only large diamond mining and beneficiation complex in Europe. Samples of river sediments and surface waters were taken from the Zolotitsa River and its tributaries in the area of the diamond deposit. Samples of kimberlites and rocks were selected to assess the radioactivity parameters of the rocks extracted from the quarries. Radionuclide activity in bottom sediments and rocks was measured using low-background semiconductor gamma spectrometry with HPGe high-purity germanium detector, and isotopes ^{234}U and ^{238}U in bottom sediments while the waters were studied using alpha spectrometry. The influence of mining and beneficiation complex on the increase in radionuclides activity in bottom sediments of Zolotitsa River was found. The parameters of radiation safety of bottom sediments were calculated regarding the human health of the personnel of the mining and beneficiation complex and the mining camp. The values of radiation parameters were found to be, on average, below the global average, and therefore, radiation parameters do not pose a significant hazard to the personnel and public. Several patterns of radionuclide accumulation have been found depending on the physicochemical parameters of river sediments. These patterns are due to the technogenic influence of the mining and beneficiation complex.

Keywords

Radionuclides • Sediments • Water quality • Hazard parameters • Diamond deposits

1 Introduction

Radioecological studies of river sediments were conducted in the area of the Lomonosov diamond deposit located in the Arkhangelsk region. This area is part of the Arctic zone of Russia. The Lomonosov diamond deposit is the largest deposit with commercially exploitable reserves in Europe (Verzhak et al. 1987). The Zolotitsa River is the main river flowing around the deposit (Bednaruk 2008). The Zolotitsa River has a special conservation status; it is the largest spawning ground for the Atlantic salmon in the White Sea basin (Kalyuzhin 2003). Villagers use the waters of the Zolotitsa for drinking and human consumption. The only man-made object that can pollute the aquatic ecosystem of the Zolotitsa River is the mining and beneficiation complex of Lomonosov diamond deposit (Fig. 1).

Currently, the deposit is under active development involving the extraction of large volumes of ore, including a full enrichment cycle, various measures to ensure the functioning of the mining and processing industry (the construction of dumps and tailings, water decrease, cleaning water used for washing of the concentration plant, and the construction of filtration fields) (Soldatova 2016). Therefore, a radioecological study in this area is extremely important.

2 Materials and Methods

Samples of bottom sediments and water were taken from the Zolotitsa River and all its tributaries in the area of the Lomonosov diamond deposit. Rocks were taken from the quarries of the Arkhangelskaya and Karpinsky-1 pipes. Bottom sediments from the Zolotitsa and its tributaries were selected using a Petersen hand sampler. After sampling, the bottom sediment samples were oven-dried at a temperature of 105 °C to an air-dry state. The granulometric composition of the bottom sediments was determined using a vibrating screening machine. In the river sediments samples, the

E. Yakovlev (✉) · A. Malov · S. Selyanina
N. Laverov Federal Centre for Integrated Arctic Research,
163000 Arkhangelsk, Russia
e-mail: evgeny.yakovlev@fciactic.ru

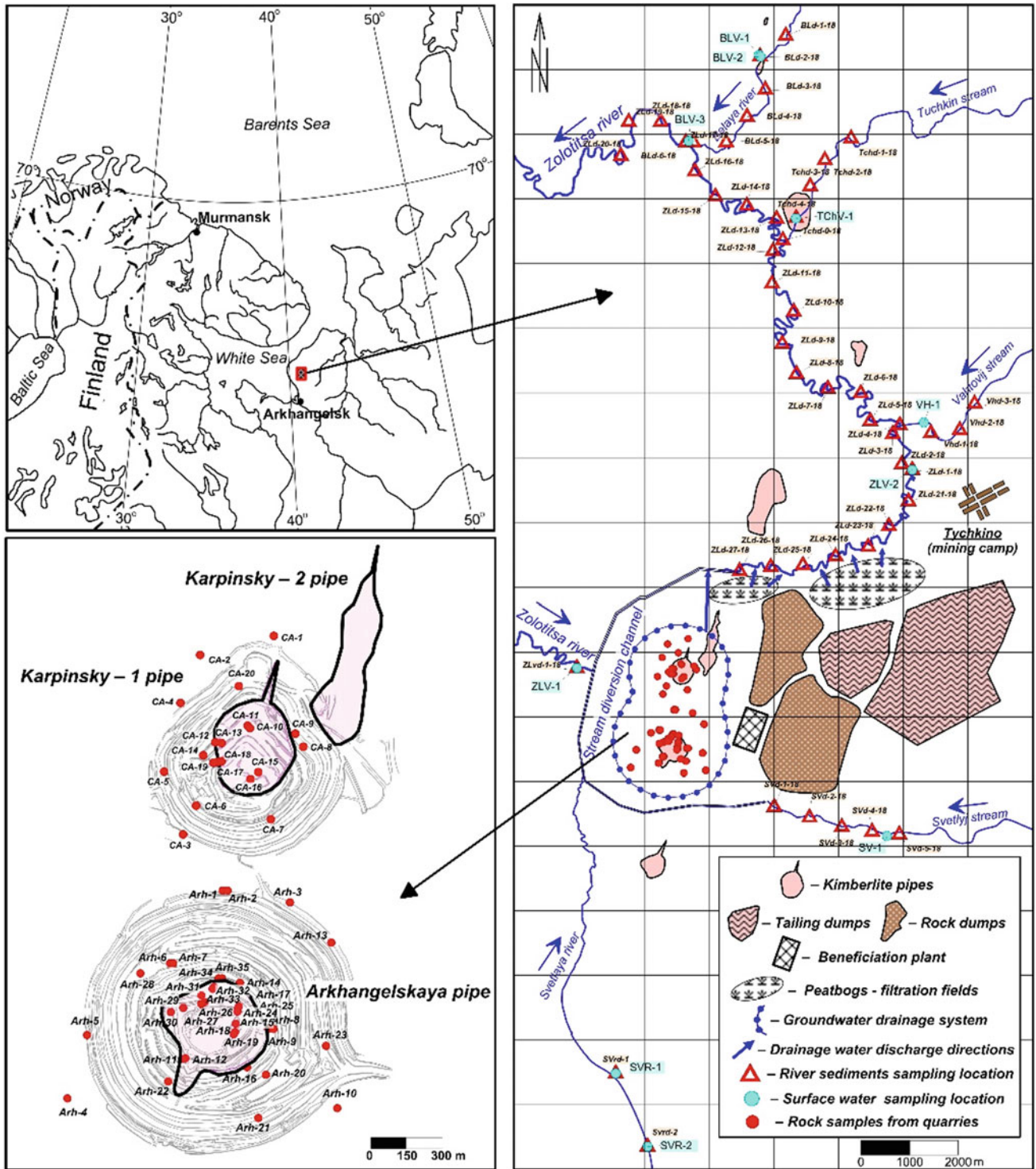


Fig. 1 Location of the studied area and sampling points

physicochemical parameters were determined, such as the content of organic matter, water-soluble salts, carbonates (CO_3^{2-}), and the pH of the aqueous extract. For the measured activities of ^{226}Ra , ^{232}Th , and ^{40}K , radiation safety

parameters were calculated, such as radium equivalent (R_{eq}), external hazard index (H_{ex}), and gamma-ray absorbed dose rate (D_R) (Ibrahim 1999; UNSCEAR 2000; Al-Hamarneh and Awadallah 2009; Rafique et al. 2014).

3 Results

The results of the study of the concentration of radionuclides in the river sediments, ores, and rocks in the area of the Lomonosov diamond deposit are shown in Table 1.

The average radionuclides concentrations in river sediments decrease in the order $^{40}\text{K} > ^{232}\text{Th} > ^{226}\text{Ra} > ^{137}\text{Cs}$. The average activities of ^{137}Cs , ^{226}Ra , ^{232}Th , and ^{40}K radionuclides as a whole for the studied river sediments are 5.4, 9.0, 11.2, 318.8 $\text{Bq}\cdot\text{kg}^{-1}$, respectively. According to UNSCEAR (2000), the activity values of the natural radionuclides in river sediments are below the world average.

The enclosing rocks V_2 extracted from quarries and stored in rock dumps contain, on average, almost twice as much ^{226}Ra and three times more ^{232}Th than Zolotitsa River sediments. The concentration of ^{226}Ra in the overlying Quaternary Q and Carbon C_2 deposits are comparable to the activity of radium in river sediments; however, their content in ^{232}Th is twice as large. Kimberlites are also somewhat enriched in ^{226}Ra and ^{232}Th , relative to river sediments, but are depleted in ^{40}K . For other types of rocks, the average contents of ^{40}K is at the same level $\sim 300 \text{ Bq}\cdot\text{kg}^{-1}$.

4 Discussion

Among the physicochemical parameters, which may mainly affect the accumulation of radionuclides, the content of organic matter, carbonates (CO_3^{2-}), water-soluble salts, and pH were considered. The influence of mining and beneficiation complex on the increase in radionuclides activity in the bottom sediments of Zolotitsa River was found (Table 2). The maximum average values of physicochemical

parameters and radionuclides are observed in the site of Zolotitsa River where drainage water is being unloaded into the riverbed from peatbog-filtration fields (Fig. 2).

The discharge of saline drainage water in this area, containing significant amounts of clay particles, leads to an increase in the share of the clay component, carbonates, water-soluble salts, and natural radionuclides in the bottom sediments. The filtration of drainage waters through the swamp massif also leads to an increase in the mass fraction of organic matter in the bottom sediments, the source of which is organic peat compounds. An increase in organic peat matter, which in turn, leads to an increase in the activity of technogenic ^{137}Cs in the bottom sediments since organic complexes of peat deposits fix global fallout radionuclides (Rosern et al. 2009). In other areas of the Zolotitsa riverbed, elevated values of the clay component, the content of organic matter, carbonates, and water-soluble salts are localized in the tributary estuaries.

The radiation hazard parameters of the bottom sediments and rocks from quarries were calculated. The average absorbed dose rate of gamma radiation D_R of river sediments were $24.4 \text{ nGy}\cdot\text{h}^{-1}$. Radium equivalent R_{aeq} for bottom sediments averages $47.3 \text{ Bq}\cdot\text{kg}^{-1}$. R_{aeq} and D_R are slightly higher for rocks from quarries than for those in the bottom sediments. The maximum average values of R_{aeq} and D_R are characteristic of sandy-clay Vendian deposits of the Padun suite (V_2) and are $87.2 \text{ Bq}\cdot\text{kg}^{-1}$ and $41.5 \text{ nGy}\cdot\text{h}^{-1}$, respectively. The calculated external hazard index H_{ex} for the river sediments and rocks extracted from quarries does not exceed 1. This indicates that the dose rate is at a level below the permissible value of $1 \text{ mSv}\cdot\text{y}^{-1}$ (International Commission on radiological protection 1993). The total alpha activity in water does not exceed the established values of $0.2 \text{ Bq}\cdot\text{L}^{-1}$ for drinking water (NRB 99/2009).

Table 1 Average concentration values of radionuclides and radiation hazard parameters in the studied quarry rocks and river sediments

Type of sediment	Number of Samples	^{137}Cs ($\text{Bq}\cdot\text{kg}^{-1}$)	^{226}Ra ($\text{Bq}\cdot\text{kg}^{-1}$)	^{232}Th ($\text{Bq}\cdot\text{kg}^{-1}$)	^{40}K ($\text{Bq}\cdot\text{kg}^{-1}$)	R_{aeq} ($\text{Bq}\cdot\text{kg}^{-1}$)	Dose rate ($\text{nGy}\cdot\text{h}^{-1}$)	H_{ex}
Overlying rocks, Q and C_2^*	10	–	9.2	21.0	318.0	61.5	30.3	0.17
Enclosing rocks, V_2^*	27	–	18.2	32.7	317.5	87.2	41.5	0.24
Kimberlites, D_3 - C_2^*	18	–	13.6	19.1	230.3	57.1	27.5	0.16
River sediments	49	5.4	9.0	11.2	318.8	47.3	24.4	0.13

*Q—Quaternary fluvio-glacial, glacial, lacustrine, marsh and alluvial sediments (sand, loam, pebble, sandy loam),

* C_2 —Middle Carboniferous sediments (sandstones, limestones, and dolomitic limestones),

* V_2 —Upper Vendian sediments (siltstones, argillites, and sandstones),

* D_3 - C_2 —Kimberlites of Upper Devonian–Middle Carboniferous age.

Table 2 Correlation matrix from the studied parameters of the Zolotitsa River sediments

	100 μ	45 μ	<45 μ	$^{234}\text{U}/^{238}\text{U}$	U	^{137}Cs	^{226}Ra	^{232}Th	^{40}K	Organic matter	CO_3^{2-}	pH	Soluble salts
100 μ	1.00												
45 μ	0.45	1.00											
<45 μ	0.44	0.92	1.00										
$^{234}\text{U}/^{238}\text{U}$	0.07	0.13	0.22	1.00									
U	0.18	0.81	0.62	-0.08	1.00								
^{137}Cs	0.46	0.75	0.89	0.21	0.45	1.00							
^{226}Ra	0.25	0.82	0.71	-0.08	0.78	0.51	1.00						
^{232}Th	0.20	0.79	0.64	-0.11	0.84	0.47	0.95	1.00					
^{40}K	0.34	0.69	0.45	-0.21	0.80	0.29	0.85	0.91	1.00				
Organic matter	0.32	0.75	0.76	0.00	0.48	0.74	0.61	0.52	0.41	1.00			
CO_3^{2-}	0.33	0.95	0.86	0.14	0.83	0.68	0.87	0.84	0.72	0.74	1.00		
pH	0.13	0.40	0.17	-0.16	0.63	0.02	0.44	0.54	0.59	0.04	0.42	1.00	
Soluble salts	0.39	0.80	0.89	0.15	0.43	0.85	0.67	0.57	0.36	0.84	0.80	0.04	1.00

Bold face values are significant correlations at the 0.01 level

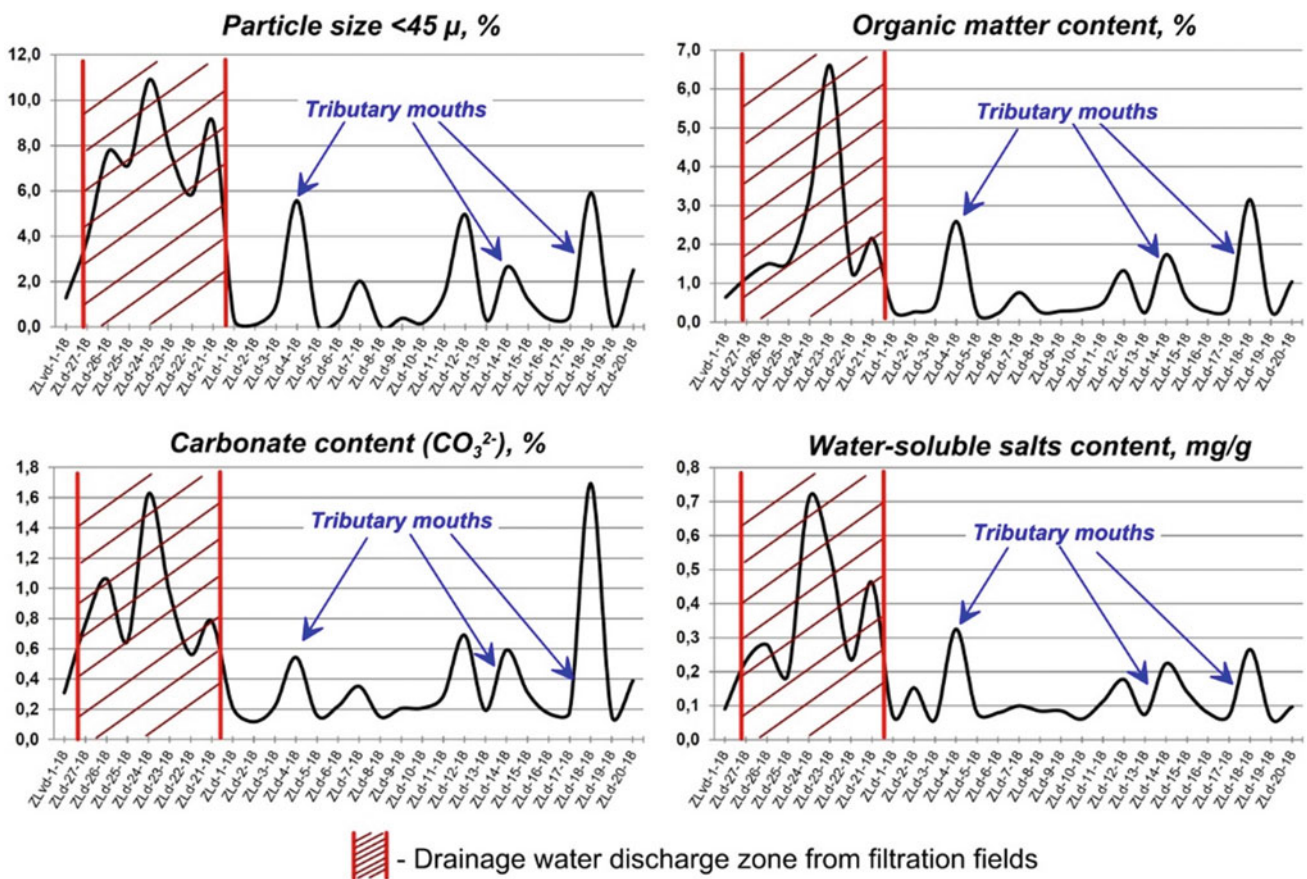


Fig. 2 Changes in the content of the fine fraction < 45 μ , organic matter, carbonates, and water-soluble salts in the bottom sediments of the Zolotitsa River

5 Conclusions

The impact of the development of the Lomonosov diamond deposit on the change in the radioecological state of the bottom sediments was evaluated. Unloading of mineralized drainage waters into the Zolotitsa riverbed leads to an increase in the proportion of clay components, carbonates, water-soluble salts, and activity of radionuclides in the river sediments. Filtration of drainage waters through the swamp massif also leads to an increase in the mass fraction of organic matter in the bottom sediments, the source of which is organic peat compounds. This, in turn, leads to an increase in the activity of anthropogenic ^{137}Cs in the bottom sediments.

The values of the radiation hazard parameters are, on average, at a level below the world average and do not represent a significant danger to the mining complex personnel and the population of the mining camp. However, in the future, with the increasing ore production, deepening of quarries, increasing pumping volumes, and drainage waters salinity, and with an even greater decrease in the sorption capacity of peatbog-filtration fields, we can expect an increase in radioactivity in the bottom sediments of the Zolotitsa River.

Acknowledgments This work was supported by the Russian Ministry of Education and Science (project no. № AAAA-A19-119011890018-3), the UB RAS (project no. 18-5-5-26), the Russian Foundation for Basic Research (projects no. 19-55-04001_Bel_mol_a; 18-05-60151_Arctic; no. 18-05-01041_A).

References

- Al-Hamarneh, I.F., Awadallah, M.I.: Soil radioactivity levels and radiation hazard assessment in the highlands of northern Jordan. *Radiat. Meas.* **44**(1), 102–110 (2009)
- Bednaruk, S.E.: Hydrographic Zoning of the Territory of the Russian Federation. NIA-Priroda, Moscow (2008)
- Ibrahim, N.: Natural activities of ^{238}U , ^{232}Th and ^{40}K in building materials. *J. Environ. Radioact.* **43**(3), 255–258 (1999)
- International Commission on radiological protection: Protection against radon-222 at home and at work, ICRP Publication 65. *Ann. ICRP* **23**(2), 1–45 (1993)
- Kalyuzhin, S.M.: Atlantic Salmon of the White Sea: Problems of Reproduction and Exploitation. PetroPress, Petrozavodsk (2003)
- NRB—99/2009. Radiation Safety Standards. Moscow (2009)
- Rafique, M., Khan, A.R., Jabbar, A., et al.: Evaluation of radiation dose due to naturally occurring radionuclides in rock samples of different origins collected from Azad Kashmir. *Russ. Geol. Geoph.* **55** (9), 1103–1112 (2014). <https://doi.org/10.1016/j.rgg.2014.08.005>
- Rosem, K., Vinichuk, Johanson K.J.: ^{137}Cs in a raised bog in central Sweden. *J. Environ. Radioactivity* **100**, 534–539 (2009)
- Soldatova, O.A.: Assessment of the Impact of Drainage Water Discharge from the Development of the Lomonosov Diamond Deposit on the Zolotitsa River. RGGMU, Saint Petersburg (2016)
- UNSCEAR, 2000. Sources and Effects of Ionizing Radiation. United Nations, Report to the General Assembly with Annexes, New York (2000)
- Verzhak, V.V., Medvedev, V.A., Verichev, E.M.: Report on the Results of the Exploration of Kimberlite Pipes on the Territory of Lomonosov Diamond Deposit in 1983–1987. Arkhangelskgeologiya, Arkhangelsk (1987)

**Biogeochemistry, Geobiology, Geoecology,
Geoagronomy (T2): Geobiology and
Geomicrobiology**



Scientific and Methodological Foundations of Biogeology

Georgii Rudko

Abstract

The biogeological history of the Earth as a process of continuous transformation and adaptation from the primary forms of life and until its current state has been considered in the present article. The basic scenarios of human and biosphere development within the technogene have been defined. The results of studies helped to identify the biogeological conditions of the life on Earth. The article researches scenarios of technogene development as well as the role of human under the conditions of intensive biosphere transformation due to the anthropogenic activities.

Keywords

Biosphere • Biota • Geodynamics • Geological environment • Environmental safety • Environmental disaster • Technogene

1 Introduction

One of the main tasks of modern theoretical geology is to create a global geodynamic model of the evolution of the Earth and to predict its further development. In order to understand how life arose on Earth, it is important to establish and consider what the environment has been like throughout its geological history.

The development of the biosphere and the geological environment of the Earth is closely interconnected. In the XXI century, this led to the establishment of the new interdisciplinary science—biogeology.

G. Rudko (✉)
State Commission of Ukraine On Mineral Resources, 18/7
Kutuzova Str, Kyiv, 01133, Ukraine
e-mail: rudko@dkz.gov.ua

Biogeology is a branch of science which studies global, regional, and local ecosystems in the context of the evolution of the Earth's geological environment. Changes in spatial and temporal scales studied within the framework of biogeology make it a key discipline to clarify the issues of the development of our planet in the past, present, and future. Understanding of evolutionary changes plays a decisive role in the interpretation of socially important issues of the future. The purpose of the study was the biogeological history of the Earth as a model of life development in the galaxy and on the planets of the solar system (Rudko and Bala 2014).

In light of major global issues facing humanity today, great interest is drawn to such questions as, whether life is possible or exists on other planets besides Earth. Therefore, it is important to study in detail all the processes that took place on our planet in the course of its evolution, especially the impact of living organisms.

2 Materials and Methods

The structure of biogeological research is rather complicated and requires careful scientific development. The main research areas can be considered cognition of the life essence, clarification of the conditions and mechanisms of the origin of life on Earth, initial and biosecurity roles of geological structures, study of life of the past geological epochs, changes in biological diversity, mechanisms and laws of biological evolution, biogeological co-evolution, search for life in space, problems of biological contamination of outer space, cognition and periodization of geological history, establishment of parameters of the environmental state and their changes in geological history, study of the role of organisms and biogenic material in the formation of geospheres, study of the role of organisms in migration and concentration of matter, formation of mineral deposits, etc (Chenchouni et al. 2019).

The dominance of the uniformity (modern is the way to the past) position in the study of the history of the Earth's

development by geologists ended with the development of new methods for the research of organic remains contained in the Archean and Proterozoic rocks, as well as remains of microscopic cell structures. One of the most amazing paleontological discoveries of recent decades is the registration of traces of life even in the most ancient earth crust. Consequently, the appearance of protolife on Earth was almost instantaneous, the evolution from organic compounds to living cells occurred in a very short time, at the very beginning of the history of the Earth. It is now suggested that life on Earth exists as long as our planet itself.

An opportunity arose to analyze the causes of “significant extinction” of organisms in the past and the conditions of the appearance of new forms of life in a completely new way.

3 Results

One of the most amazing and not fully explored properties of evolution of life on Earth is its overall progressive direction, movement from simple to complex. Today one of the most discussed theories of the origin of life on Earth is the theory of panspermia, in other words, the cosmic origin of the primary living matter, according to which life could have arisen one or several times in different periods, in different parts of the galaxy or universe. The germs of life scattered in space (e.g., spores of microorganisms) were transported from one celestial body to another by meteorites or under light pressure. The presence of the organic compounds and fossilized primitive organisms in meteorites is the evidence of that (Roazanov 1996; Wickramasinghe et al. 2013). Nowadays forms of life, starting with single-celled organisms—prokaryotes—are indicators of the age of entire formation complexes.

Life developed synchronically with the geological development of the planet. According to some assumptions at the beginning of the Proterozoic, there was a single continent of Megagea, which was surrounded by a single ocean. The primary atmosphere, by its composition, was close to meteorite and volcanic gases. It consisted of CH₄, CO, CO₂, H₃BO₃, NH₃, H₂S, HCl, HF, and a small amount of inert gases.

4 Discussion

The oldest unicellular organisms (Cyanobacteria) have an age of about 3.5 billion years, which gives grounds for considering the early Precambrian as the existence of a special world formed by prokaryotic (non-nuclear) organisms—bacteria and cyanobacteria, their domination lasted for 1.5–2 billion years. Microorganisms became more and more numerous and diverse. The more oxygen was

accumulated in the atmosphere, the more preconditions for prokaryotes extinction were created.

The transition of the renewable atmosphere to the oxidizing was observed at the beginning of the Proterozoic, as it is shown through changes in the chemical composition of the rocks. During this period, deposits of banded iron ores (so-called jaspilites) were recorded, in which the oxidized iron alternated with the non-oxidized one. Another important consequence of the activities of prokaryotes is the accumulation of organic matter deposits.

The formation of the oxidizing atmosphere was the impetus for the rapid development of eukaryotic organisms, whose energy is based on the process of breathing. Obviously, the eukaryotic form of life is closely connected with the aerobic environment prepared by the prokaryotes (Roazanov and Fedonkin 1994).

The last phase of the Proterozoic, which lasted for about 100 million years (vend), demonstrated an explosion of multicellular diversity. A new stage in the development of the organic world is the massive appearance of different external and internal multicellular skeletons. Since then, Phanerozoic was dated—the “era of explicit life,” as the preservation of skeletal remains in the earth's layers allows us to reproduce in a more detailed way the course of biological evolution. The formation of the conscious existence of living organisms is associated with the appearance of a human being from the genus *Homo* and society, which approximately coincides with the boundary of the Neogene and Quaternary chronostratigraphic scale systems.

Technogene is the modern stage of geological history, characterized by intense human activity and the intensification of its influence on the geological environment; it began in the Holocene and will continue until humanity exists. It is characterized by a rapid increase of technogenic transformation of the geological environment under the influence of man.

Today, there are the following scenarios of human and biosphere development as a result of technogene:

- way of technogene intensification, overpopulation of the planet, and struggle for resources with everybody;
- way of civilized colonization of space and the development of its resources;
- way of regulation of the Earth's population in accordance with the resources of the biosphere.

5 Conclusions

Humanity already consumes way too many natural resources than one can remove from the biosphere without harming its biochemical cycles and without disturbing the process of

renewal. In other words, humanity, since the twentieth century, has lived at the expense of its descendants. Moreover, it has put the biosphere and accordingly itself as an integral part of the biosphere on the edge of complete degradation. The rapid growth of the population on Earth, rapid acceleration of the use of natural resources put new challenges in front of mankind, which consist in the development of outer space, search for life on the neighboring planets, and their future development.

Consideration of the hypothetical possibility of life on other planets from the point of view of most scholars is fully justified, and the theory of life on other planets has the right to exist. On the contrary to popular belief that scientists consider the general theoretical preconditions for the suitability of planets for the development of life, today the leading researchers in this field have the opportunity to conduct specific studies of non-Earth objects, to analyze the conditions on planets close to Earth.

For example, Venus, which at the beginning of space exploration was considered to be the main and ideal candidate for the title of Cradle of extraterrestrial life, is unequivocally recognized as unsuitable for life due to high temperatures and atmospheric pressure on its surface, which are almost 100 times higher than the indicators on Earth, presence of an intense greenhouse effect, etc. However, there are some recent hypotheses that suggest the existence of microbes on Venus, life activity of which is based on a completely different chemical mechanism of metabolism than of those on Earth. Nevertheless, the existence of some complex or more intelligent form of life on Venus is impossible. Almost the same conclusion has been made about Mars, main characteristics of which are similar to those of Earth, but due to the almost complete absence of

atmosphere, low atmospheric pressure (almost 200 times lower than on Earth) red planet, according to scientists, is permanently deprived of water in the liquid state. Under such conditions, the development of multicellular organisms is impossible, but scientists do not exclude the possible existence of bacteria on Mars, including those brought by meteorites.

The study and improvement of our knowledge of the major biostratigraphic stages in the history of Earth's development should allow us to consider and understand the mechanisms of development of other planets of the solar system, to answer the following questions: was it possible for living organisms to appear on these celestial bodies, how can we influence the development of human-friendly conditions on the surface of these and other planets?

References

- Chenchouni, H., Errami, E., Rocha, F., Sabato, L.: Exploring the Nexus of Geocology, Geography, Geoarcheology and Geotourism.: Advances and Applications for Sustainable Development in Environmental Sciences and Agroforestry Research. Springer, Cham (2019). <https://doi.org/10.1007/978-3-030-01683-8>
- RozaNov, AYu.: The history of the formation of skeletal faunas. *Sorosovskiy Educ. Magaz.* **12**, 62–68 (1996)
- RozaNov, A.Yu., Fedonkin, M.A.: The Problem of the Primary Biotope of Eukaryotes. Ecosystem Rearrangements and Evolution of the Biosphere. Nedra, Moscow (1994)
- Rudko, G.I., Bala, G.R.: Basic biostratigraphic stages of Earth's history. Technogene scripts. Bukrek, Kyiv (2014)
- Wickramasinghe, N.C., Wallis J., Wallis, D.H, et al.: Fossil diatoms in a new carbonaceous meteorite. *J. Cosmol.* **21**(37), 9560–9571 (2013)



Natural and Resource Potential of Official Plants Flora of Ciscaucasia (Russian Federation)

Nadezhda B. Leonova, Inessa M. Miklyaeva,
and Svetlana M. Malkhazova

Abstract

The study of natural and resource potential of official plants of Ciscaucasia, i.e., plants permitted for medical use by the Ministry of Health care of Russia, has been implemented using the database developed by authors of the Medical-Geographical Atlas of Russia “Healing Springs and Plants.” Ciscaucasia flora of official plants consist of 153 species from 126 genera and 54 families. Most of official species grow in forest and shrub communities; some other species are cultivated in plantations. By natural features, Ciscaucasia may be divided into three parts: Western and Central with favorable conditions for plants, and the Eastern part with less suitable climatic conditions. Therefore, the regional specificities of official plants distribution result in 150 species in Western and Central parts and only 67 species in the Eastern part. Official plants have various pharmacological properties: antiseptic, anti-inflammatory, cardiotonic, hemostatic, hypotensive, expectorant, and many others due to high concentrations of active substances. Official plants are used for the treatment of 14 principal classes of diseases (according to International Statistical Classification of Diseases (ICD-10)). The most frequent use is for curing diseases of the digestive system, of the circulatory system, and of the respiratory system. Large-scale stocking of medicinal raw materials results in reducing wild-growing plants populations. These processes are dangerous because the areas with nature protection status are scanty, all the while 13 official species are included into the Red Data Book of Russia and another 12 species—into regional Red Data books.

Keywords

Taxonomic diversity • Regional specifics • Active substances • Diseases classes • Rational use

1 Introduction

Contemporary medicinal industry widely uses plant raw materials for manufacturing of drugs; however, the study of official (from the Latin *officina*—drugstore) plants, their ecology and geography, perspectives for rational use still remains urgent. Regional features of natural and resource potential of official plants are determined by geographical specifics, degree of pharmacological knowledge about flora, and empirical experience of the indigenous people with using plants for treatment of different diseases. The list of official plants as sources of pharmacologically active substances, allowed for medical use by the Ministry of Healthcare of Russia, is included into the State Pharmacopeia and the State Register for Medicines (Pharmacognosy 2010). The plants from the southern regions of Russia are of high value for pharmaceutical industry because of the high concentrations of biologically active substances accumulated in warm and dry climatic conditions in comparison with analogous species from northern regions. Thus, the research of official plants of Ciscaucasia as important raw material base for the pharmaceutical industry has scientific and applied significance. The purpose of this study was the characterization of natural and resource potential of official plants of Ciscaucasia. The main research tasks included: detection of taxonomic, ecological and geographical diversity of official plant flora; characterization of pharmacological properties and the uses of the plants for illnesses treatment according to International Statistical Classification of Diseases (ICD-10); discussion of contemporary measures for conservation of official plant populations.

N. B. Leonova (✉) · I. M. Miklyaeva · S. M. Malkhazova
Faculty of Geography, Lomonosov Moscow State University,
Moscow, Russia

2 Materials and Methods

The study is based on materials from the database (software registration certificate N 2018621769) generalizing actual cartographic and scientific publications data as well as Internet sources on medicinal plants of Russia. The database was compiled by authors during the work on the Medical–Geographical Atlas of Russia «Healing Waters and Plants» (Medical–Geographical Atlas of Russia 2019). The collected data were included in an information retrieval system based on the Web-GIS technology on the Web site www.biomap.ru (Informational retrieval system, Database of the healing springs and plants 2019). Relational table is compiled in MS Excel. The attributes are presented in 42 columns (taxonomic nomenclature, range, biological features, chemical composition, pharmacological properties, indications for use in the illnesses treatment, contraindications for the use, nature conservation status, and so on). A total of 239 lines contain wild growing and cultivated in open ground officinal plant species, included into the State Register of Pharmacopoeia and permitted for medical use by the RF Ministry of Health Care. Disease classes are used according to the International Classification ICD-10, developed by the World Health Organization. The Latin names of species are given in accordance with International Nomenclature (The Plantlist 2019). During the study, we selected the plant species, growing within Ciscaucasia using column “geographical distribution.” Then, these plants list was analyzed as: (1) taxonomic affiliation; (2) living forms; (3) distribution in different parts of territory; (4) cultivation in fields; (5) use for illnesses treatment. The study territory is situated within the following geographical coordinates: in the North 47°05′ N, in the South—44° 22′ N; in the West—37° 35′ E; in the East—47° 22′ E. Some of the used data was collected from the National Atlas of Russia (2008) for physical geographic conditions.

3 Results and Discussion

Ciscaucasia area is limited by the Azov Sea coast and Kerch Strait to the west, Kumo-Manych Depression to the north, Caspian Sea to the east, and northern foothill of the Greater Caucasus to the south. The specificities of the physical geographical conditions divide this area into three parts: Western, Central, and Eastern. Natural features of the Western and Central parts are rather similar: it is a moderately continental steppe climate (with average July temperature between +21 and +24 °C, and January between –2 and –5 °C). The average annual precipitation reaches 450–600 mm in Kuban-Priazov lowland, 350–400 mm in Taman peninsula. Within Central Caucasus, the average annual

precipitation reaches 600–800 mm. The relief is characterized as both plain and also hilly and low mountains. In the Western and Central Caucasus, there are such fertile soils as carbonate chernozems, residual-carbonate chernozems, and dark brown and brown soils. Within Eastern Caucasus, the desert-steppe continental climate is typical. The July temperature is between +25 and +26 °C, in January between –5 and –7 °C, and the average annual precipitation reaches 350 mm in the west and 200–300 mm in the east part of the region; thus, prolonged droughts are possible. The plain relief prevails here with eolian forms in the south; soils are light brown. Nature diversity determines high botanical diversity. Ciscaucasia flora consists of 2353 vascular plants, and about 400 species are used in traditional medicine (Ivanov 1998).

3.1 Flora of Officinal Plants of Ciscaucasia

The flora of officinal plants consists of 153 species from 126 genera and 54 families. This number is 63% of all Russian officinal plants and 6% of Ciscaucasia flora of vascular plants. The predominating families are the following: Asteraceae (22 species), Orchidaceae (12), Rosaceae (10), and Apiaceae (10). Wild-growing officinal plants represent 72% of total population. Most of these species (48 species) grow in forests and shrubs in river valleys, hills, and low mountain slopes. Steppe and meadow habitats contain only 18 species each because of considerable arable areas in the plain part region. There are 43 cultivated species in fields and plantations. In total, there are 150 species of officinal plants in the Western and the Central parts of Ciscaucasia. Toward the east, the diversity of officinal plants decreases down to 67 species, as the climate continentality increases.

3.2 Pharmacological Properties and Use of Officinal Plants

The pharmacological properties and use of officinal plants depend on the composition of the active substances (Zouaoui et al. 2020). The concentrations of active substances in officinal plants are determined by natural conditions of Ciscaucasia to a great extent. More than 17% of all species contain high concentrations of alkaloids (e.g., *Atropa belladonna* L., *Colchicum speciosum* Steven); 16% of species contain essential oils (*Verbascum densiflorum* Bertol., *Digitalis purpurea* L.); 15% species – mucus (*Althaea officinalis* L., *Orchis ustulata* L. et al.), many plants contain bio-effective agents (*Sambucus nigra* L., *Echinacea purpurea* (L.) Moench), phenol compounds (*Astragalus falcatus* Lam., *Ammi visnaga* (L.) Lam.), and so on. Plants containing

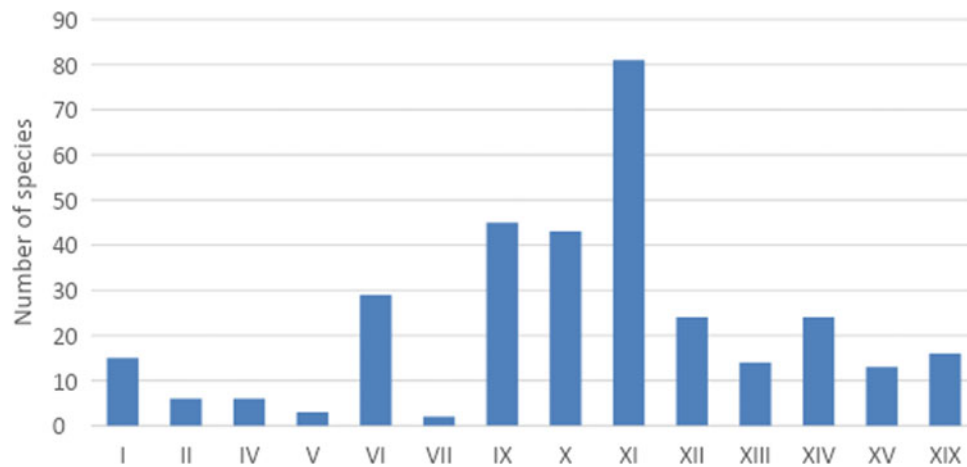


Fig. 1 Distribution of official plants' number in classes of diseases (ICD-10): I—certain infectious and parasitic diseases; II—neoplasms; IV—endocrine, nutritional, and metabolic diseases; V—mental and behavioral disorders; VI—diseases of the nervous system; IX—diseases of the circulatory system; X—diseases of the respiratory

system; XI—diseases of the digestive system; XII—diseases of the skin and subcutaneous tissue; XIII—diseases of the musculoskeletal system and connective tissue; XIV—diseases of the genitourinary system; XV—pregnancy, childbirth, and the puerperium; XIX—injury, poisoning, and certain other consequences of external causes

alkaloids have cardiogenic, hemostatic, expectorant, and other pharmacological properties; mucus provides a coating and antidotal effect; flavonoids possess anastaltic germicidal properties and so on.

Official plants of Ciscaucasia are used for treatment of 14 principal classes of diseases (according to International Statistical Classification of Diseases ICD-10) (International Statistical Classification of Diseases and Related Health Problems 10th Revision (ICD-10) 2019). More than 80 species are used to treat diseases of the digestive system (XI); 45 species are used for treatment of diseases of the circulatory system (IX), and 42 species are used to treat diseases of respiratory system (X) (Fig. 1).

Experimental plant stations and collection test sites in botanical gardens carried out the tasks of researching pharmacological properties of medicinal plants, selecting new varieties and looking for plants with perspective for introduction. There are nine botanical gardens with medicinal plants collections in Ciscaucasia affiliated with state universities and academies in Vladikavkaz, Krasnodar, Maykop, Makhachkala (2 gardens), Nalchik, Pyatigorsk (2 gardens), and Stavropol.

3.3 Cultivation of Official Plants

There are some phyto farms in Krasnodar and Stavropol Territories (the Western and the Central Ciscaucasia), where 62 official species are cultivated in fields. There are 19

aboriginal species among them, wild growing in natural vegetation communities, such as *Cichorium intybus* L. and *Silybum marianum* (L.) Gaertn. Nine official species are widespread agricultural crops: *Allium cepa* L., *Cucurbita pepo* L., *Zea mays* L., etc. Favorable natural climatic and soil conditions of Ciscaucasia permit to cultivate 34 official plant species which have been introduced from subtropical and tropical regions: for example, *Solanum laciniatum* Aiton from Australia, *Ocimum gratissimum* L., *Ricinus communis* L. from Africa, *Datura innoxia* Mill.; *Echinacea purpurea* (L.) Moench from Northern and Southern America, *Macleaya microcarpa* (Maxim.) Fedde from South-Eastern Asia. Most of the introduced species are from the Mediterranean region such as *Calendula officinalis* L. and *Melissa officinalis* L.

3.4 Rational Use of Official Plants

The rational use of official plants is connected to protection measures development, study, and conservation of their valuable gene pool (Mehalaine and Chenchouni 2021). Natural populations of *Althaea officinalis* L., *Artemisia taurica* Willd., *Melissa officinalis* L., and many other plants are disturbed by their stocking, so it is reasonable to cultivate those in fields. The especially protected natural areas are absent in Ciscaucasia indeed. The single measure of official plants protection is to include them into the Red Data books. Nowadays, 13 official plant species are included in the Red

Data Book of the Russian Federation. Some other 12 officinal species are included into the regional Red Data Books (Krasnodar and Stavropolsky Territories).

4 Conclusion

The Ciscaucasia officinal flora has a significant natural resource potential, which can be used as a source of medicinal raw materials for the pharmaceutical industry at present and in the future. However, it is necessary to reorient the obtainment of officinal plants stock to cultivation in fields, and to introduce the nature conservation regime within the area of wild-growing officinal plants habitats.

References

- Informational retrieval system (Database of the healing springs and plants). <https://www.biomap.ru/>. Last accessed 21 May 2019
- International Statistical Classification of Diseases and Related Health Problems 10th Revision (ICD-10). <https://icd.who.int/>. Last accessed 25 May 2019
- Ivanov, A.L.: Ciscaucasia Flora and Its Genesis. Stavropol State University Publishing House, Stavropol (1998)
- National Atlas of Russia. Publishing House "Astrel". Moscow (2008)
- Medical–Geographical Atlas of Russia «Healing Waters and Plants». Moscow State University, Geographical Faculty. Moscow (2019)
- Mehalaine, S., Chenchouni, H.: New insights for the production of medicinal plant materials: ex vitro and in vitro propagation of valuable *Lamiaceae* species from northern Africa. *Curr. Plant Biol.* **27C**, 100216 (2021). <https://doi.org/10.1016/j.cpb.2021.100216>
- Pharmacognosy. Medicinal Raw Materials of Plant and Animal Origin. Spetslit, Sankt-Petersburg (2010)
- The Plantlist: A working list of all plant species. <http://www.theplantlist.org/>. Last accessed 12 May 2019
- Zouaoui, N., Chenchouni, H., Bouguerra, A., Massouras, T., Barkat, M.: Characterization of volatile organic compounds from six aromatic and medicinal plant species growing wild in North African drylands. *NFS J.* **18**, 19–28 (2020). <https://doi.org/10.1016/j.nfs.2019.12.001>



Properties of Plant Growth Promoting Rhizobacteria Isolated from Rhizospheric Soil of *Citrullus colocynthis* (Cucurbitaceae) in northeastern Algeria

Ahmed Dekak, Hichem Slama, Maroua Chergui, and Mohamed Nacer Mekahlia

Abstract

The use of plant growth promoting rhizobacteria (PGPR) can enhance agricultural practices toward a sustainable and more environmental-friendly perspective. Thirty seven isolates were collected from four samples of *Citrullus colocynthis* rhizospheric soil, in severe aridity conditions in northeastern Algeria (Bir El-Ater) area, and used to isolate and identify these PGPR trait bacteria, evaluating their efficiency in producing phytohormone Indol 3-Acetic Acid (IAA), solubilizing Phosphate (SP) and Potassium (SK) which will help to understand their mechanisms of action and select strains of interest. This work allowed us to note a diversity of microorganisms, translated by the results of various tests studied, in particular, the production of IAA which is a common feature of these PGPR, twelve strains capable of SP, eighteen strains able to SK and finally five strains of interest that showed significant PGP, which are likely to be involved in programs of agricultural productivity improvement. Further molecular characterization of bacterial isolates from *C. colocynthis* using conventional methods should be performed for further examination of diversity.

Keywords

Citrullus colocynthis • Rhizosphere • PGPR • Phytohormone • Solubilization of minerals

1 Introduction

Agricultural productivity must increase significantly in the coming years to cope with rising global population growth and environmental change and obtain higher crop yields.

A. Dekak (✉) · H. Slama · M. Chergui · M. N. Mekahlia
Laarbi Tebessi University, 12000 Tebessa, Algeria
e-mail: ahmed.dekak@univ-tebessa.dz

Farmers are dependent on chemical fertilizers, which, in addition to being expensive, deplete non-renewable energy resources and cause risks to humans, animals and the environment (FAO 2015). Exploring the soil microbial diversity for PGPR, which in combination with PGP activities and well adapted to the particular soil environment has become a real necessity (Yadav et al. 2010; Chenchouni et al. 2020).

Sustainable development strategies envisaged that plant growth promoting bacteria (PGPR) will begin to replace chemicals in agriculture as the production of biofertilizers containing bacteria isolated from plant rhizosphere have considerable importance as they are more tolerant of extreme abiotic conditions, such as temperature, salinity and drought. They also improve productivity by facilitating the uptake of nutrients by plants without displaying any danger to the environment and humans (Vessey 2003).

The search for bacterial forms, among other PGPR, from endemic and spontaneous plants belonging to the flowering species of Algeria, growing under extreme environmental conditions, has become a quality choice, since the number of scientific works remains very limited in this field area (Dekak et al. 2020).

Our work aimed to isolate bacteria from the rhizospheric soil of *C. colocynthis*, commonly called colocynth, because it presents good medicinal properties. The plant withstands extreme environmental conditions such as severe droughts of desert regions and it is a source of vital biomass.

2 Materials and Methods

The sampling zone is located at Bir El-Ater region (Tebessa, northeastern Algeria) that belongs to the eastern end of the Saharan Atlas range and constitutes the natural geographical boundary between the Constantine highlands and the Saharan area (Benchebira and Boumansoura 2016). The climate of the region is hot arid with the dry period lasting all the year round (Fatmi et al. 2020).

Rhizospheric soil samples were collected at four different sites in February 2019. Site 1 (34.76° N, 8.07° E, altitude = 866 m a.s.l.), site 2 and site 3 located on both banks of Oued El Kebir (34.55° N, 8.06° E, altitude = 582 m a.s.l.), and site 4 located on the bank of Oued El Fride (34.46° N, 7.99° E, altitude = 490 m a.s.l.).

Soil chemical characteristics were analysed to determine contents of Sodium (Na), Potassium (K) and Calcium (Ca) using atomic absorption spectrophotometer (Diallo et al. 2015). Hydrogen potential (pH), electrical conductivity (EC) were also measured. Three replicates were carried out from different sites.

One series of dilutions (10^{-1} to 10^{-6}) was prepared for each sample by taking 1 g of soil and placing it in 9 mL of sterile distilled water. We opted to work with dilutions ranging from 10^{-3} to 10^{-6} , seeded on the surface, 100 μ L of each dilution were taken and then spread in petri dishes containing King A and King B media.

Macroscopic examination of cultures was the first examination performed from isolation after incubation according to the appearance of well isolated colonies that were sub-cultured onto National Botanical Research Institute's Phosphate growth medium (NBRIP) broth [$\text{MgCl}_2 \cdot 6\text{H}_2\text{O}$ (5 g L^{-1}), $\text{MgSO}_4 \cdot \text{H}_2\text{O}$ (0.25 g L^{-1}), KCl (0.2 g L^{-1}), $(\text{NH}_4)_2\text{SO}_4$ (0.1 g L^{-1}), $\text{Ca}_3(\text{PO}_4)_2$ (5 g L^{-1}), glucose (10 g L^{-1}) and pH = 7.0] and incubated at 30 °C for 72 h before undergoing the different tests (Nautiyal et al. 1999).

Thirty seven potential isolates of pure bacterial cultures were selected to undergo the various tests of minerals solubilization and (IAA) phytohormon production.

Phosphate solubilization was carried out by digging four wells (repetitions) with an ounce of platinum on the surface of each petri dish containing the NBRIP Agar medium (NBRIP broth supplemented with 15 g Agar L^{-1}), then 10 μ L of the bacterial inoculum is deposited in each well, and these dishes were incubated at 28 °C for 72 h.

The solubilization capacity is determined from the existence of a transparent halo which corresponds to the lysis zone around the bacterial colony. (Abiala et al. 2015; Gonzalez et al. 2019). The calculation of phosphate solubilization index (P.S.I.) was carried out according to the formula developed by Kumar and Narula (1999):

P.S.I. = Diameter of the halo around the spot/Diameter of the colony

Qualitative screening of Potassium solubilization was conducted on Aleksandrow medium (5 g glucose, 0.005 g $\text{MgSO}_4 \cdot 7\text{H}_2\text{O}$, 0.1 g Fe-Cl_3 , 2.0 g Ca-CO_3 , 3.0 g Mica (2.0 g in original media), 2.0 g calcium phosphate and 15 g agar L^{-1}) 10 μ L of each bacterial inoculum per replicate (four replicates) was transferred to the petri dishes and incubated at 30 °C for a period of seven days, and the

formation of clear zones proved a solubilization of Potassium (Meena et al. 2014). The calculation of the Potassium solubilization index (K.S.I.) was performed according to Holt et al. (1994).

K.S.I. = Diameter of the halo around the spot/Diameter of the colony

For the determination of Indol 3-Acetic Acid (IAA) production, the isolates were inoculated into a nutrient broth (Peptone 5 g L^{-1} , Beef extract 3 g L^{-1} , pH = 7) with 500 μ g mL^{-1} of tryptophan. These cultures were incubated at 28 °C with constant shaking of 150 rpm for 4 days and centrifuged at 13,400 rpm for 10 min. The supernatant was mixed with the Salkowski reagent (Fe-Cl_3 (0.5 M) 5 mL, H_2SO_4 150 mL, SDW 250 mL) at a ratio of 2:1, the whole (supernatant plus Salkowski reagent) was incubated in total darkness for 75 min at room temperature, and then read in spectrophotometer at 525 nm (Gonzalez et al. 2019). The concentration of IAA in each sample was calculated based on a standard curve.

Statistical analyses of the obtained results were conducted by Mintab16 software to perform analysis of variance and multiple comparisons between averages. Principal components analysis was achieved with XLstat version 2014.

3 Results

Soils chemical analysis showed that sites III and VI are rich in Na and Ca, compared to the first two sites, we also observed that the four soils are rich in K, especially the 2nd soil, given the agricultural specificity of the region which can be amended by fertilizers. According to Bocoum (2004), the four soils were neutral with a pH ranging between (6.96 ± 0.08) to (7.30 ± 0.19) and non-saline with an electrical conductivity ranging between (146.90 ± 11.85 $\mu\text{S cm}^{-1}$) and (220 ± 10.82 $\mu\text{S cm}^{-1}$).

Plates from 10^{-3} to 10^{-6} dilutions allowed us to isolate thirty seven clear colonies (Isolates) based on their macroscopic appearance: color, shape and texture. A great diversity of colonies was found in the two used media (King A and King B), which are known to allow the differentiation between bacterial species, by highlighting the production of specific pigments.

The statistical analysis revealed a highly significant difference, between the eighteen isolates (p -value < 0.001) that were able to solubilize K from Aleksandrow medium, grouped into 4 different groups by the Tukey test at a level of significance $\alpha = 5\%$ and the twelve isolates which are able to solubilize P presented highly significant difference (p -value < 0.001) divided by Tukey test on six different groups.

The qualitative test marked by the color change of the culture medium after the addition of Salkowski's reagent to pinkish or brown indicated a clear production of IAA by thirty-six isolates out of the thirty seven strains tested, indicating that the isolate E3B2 could not transaminate tryptophan into IAA. The statistical analysis revealed a very highly significant difference between isolates for IAA production pooled by the Tukey test at $\alpha = 5\%$ significance level in twenty-six different groups.

Moreover, the proportional distribution of isolates according to studied PGP traits allowed detecting the presence of twelve isolates (32%) producing only IAA, six isolates (16%) solubilize the P and produce IAA, thirteen isolates (35%) solubilize K and produce IAA, five isolates (14%) produce IAA and solubilize P and K, and a single isolate is (3%) able to solubilizing only by Potassium.

The pattern observed in the biplot projection of isolates in the principal component analysis (Fig. 1), divided all the tested bacteria into four distinct groups. It is noteworthy mentioning that the 4th group hold bacteria with PGP traits (E1B4, E2B1, E3B4, E3B1 and E3A1).

4 Discussion

This study allowed us to discuss some questions about the resistance of the studied plant species to the extreme environmental conditions that exist in the studied

distribution area, highlighting the relationship between microorganism and plant to deal with the stressful development conditions.

Our results are in conformity with previous studies which have estimated that phosphate-solubilizing microorganisms constitute about 20–40% of microorganism populations that can be isolated from the rhizosphere (Chabot et al. 1993).

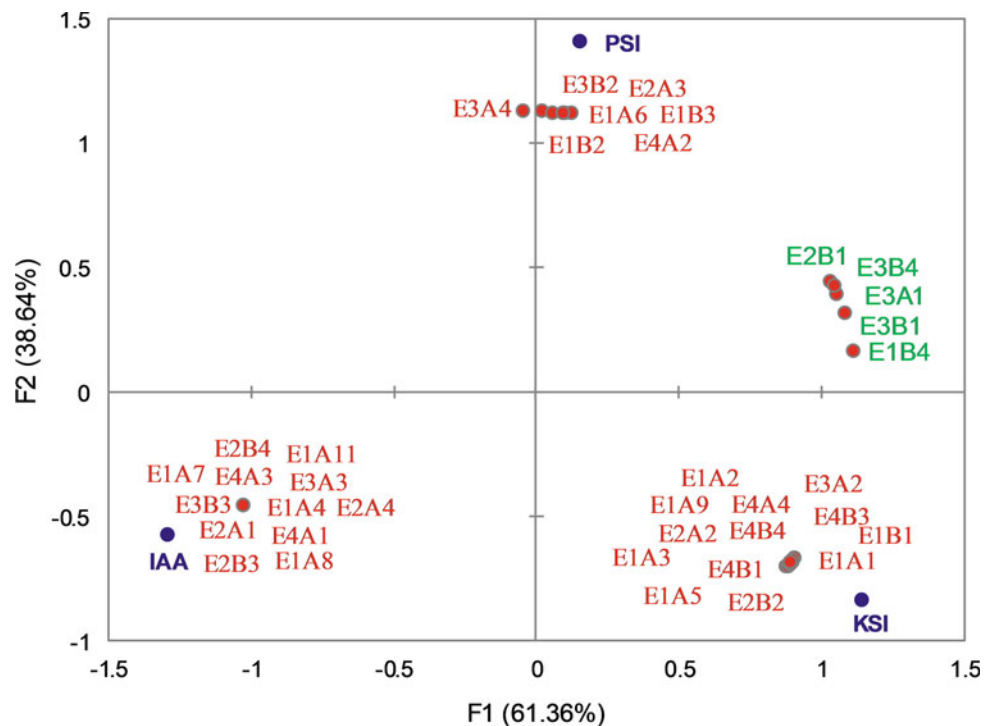
The results of Potassium solubilization confirm previous research (Meena et al. 2014) that demonstrated the presence of a variety of bacteria in the soil capable of solubilizing different insoluble forms of Potassium by producing organic and inorganic acids (Etesami et al. 2017).

The strain yielded IAA in a wide range of pH (5–9), giving its maximum IAA production at pH = 8. High IAA concentration was also observed in the presence of 0.5% and 1% NaCl IAA producing bacterial isolate in the field, as a result, the possibility of using it as alternative valuable biofertilizer (Yousef 2018).

5 Conclusion

The isolation of PGPR from the rhizosphere of *C. colocythis* allowed us to select certain bacteria characterized by interesting PGPR traits. The majority of isolated bacteria is able to produce IAA, although the production rate varied considerably from one isolate to another. It has been possible

Fig. 1 Biplot projection pattern of isolates (in red) in the principal component analysis. Isolates characterized with the three PGP traits studied are marked in green. (K.S.I.: Potassium solubilization index, P.S.I.: Phosphate solubilization index, and IAA: Indol 3-Acetic Acid)



to identify five strains with agronomic interest, capable of producing IAA and solubilizing K and P. These strains can be incorporated into programs for improving yields of crops with large consumption by introducing them as biofertilizers to facilitate the absorption of minerals and reduce the need for chemical fertilizers. Further molecular characterization of bacterial isolates from rhizosphere of *C. colocynthis* using conventional methods should be performed for further examination of PGPR diversity.

References

- Abiala, M.A., Odebode, C., Hsu, S.F., Blackwood, C.B.: Phytobeneficial properties of bacteria isolated from the rhizosphere of maize in southwestern Nigerian soils. *Appl. Environ. Microbiol.* **81**(14), 4736–4743 (2015). <https://doi.org/10.1128/aem.00570-15>
- Benchebira, A., Boumansoura, L.: Etude géostatistique d'un projet minier: cas du gisement de phosphate à Bled El-Hedba (W. Tébessa). Master dissertation, Univ. Bejaia, Algeria (2016)
- Bocoum, M.: Méthodes d'analyses des sols. Doc de travail. Institut National de Pédologie, pp. 1–55, Dakar – Senegal (2004)
- Chabot, R., Antoun, H., Cescas, M.P.: Stimulation in the growth of corn and romaine lettuce by microorganisms dissolving inorganic phosphorus. *Can. J. Microbiol.* **39**, 941–947 (1993). <https://doi.org/10.1139/m93-142>
- Chenchouni, H., Mekahlia, M.N., Beddiar, A.: Effect of inoculation with native and commercial arbuscular mycorrhizal fungi on growth and mycorrhizal colonization of olive (*Olea europaea* L.). *Sci. Hortic.* **261**, 108969 (2020). <https://doi.org/10.1016/j.scienta.2019.108969>
- Dekak, A., Menasria, T., Benhizia, Y., Chenchouni, H.: Endophytic passenger bacteria associated with *Genista cinerea* nodules growing in North African drylands. *Rhizosphere* **14**, 100205 (2020). <https://doi.org/10.1016/j.rhisph.2020.100205>
- Diallo, M.D., Ngamb, T., Tine, A.K., Guisse, M., Ndiaye, O., Saleh, M. M., Diallo, A., Diop, A., Guisse, A.: Caractérisation agropédologique des sols de Mboltime dans la zone des Niayes (Sénégal). *Agr. Afr.* **27**(1), 57–67 (2015)
- Etesami, H., Emami, S., Alikhani, H.A.: Potassium solubilizing bacteria (KSB): mechanisms, promotion of plant growth, and future prospects—a review. *J. Soil Sci. Plant Nutr.* **17**(4), 897–911 (2017). <https://doi.org/10.4067/S0718-95162017000400005>
- FAO: World fertilizer trends and outlook to 2018. Food and Agriculture Organization of the United Nations. Rome, Italy, www.fao.org/3/a-i4324e.pdf (2015)
- Fatmi, H., Mâalem, S., Harsa, B., Dekak, A., Chenchouni, H.: Pollen morphological variability correlates with a large-scale gradient of aridity. *Web Ecol.* **20**, 19–32 (2020). <https://doi.org/10.5194/we-20-19-2020>
- Gonzalez, A.H., Morales Londono, D., Pille da Silva, E., et al.: *Bradyrhizobium* and *Pseudomonas* strains obtained from coal-mining areas nodulate and promote the growth of *Calopogonium muconoides* plants used in the reclamation of degraded areas. *J. Appl. Microbiol.* **126**(2), 523–533 (2019). <https://doi.org/10.1111/jam.14117>
- Holt, J.G., Krieg, N.R., Sneath, P.H., Staley, J.T., Williams, S.T.: *Bergey's manual of determinative bacteriology*. 9th. William & Wilkins, Baltimor (1994)
- Kumar, V., Narula, N.: Solubilization of inorganic phosphates and growth emergence of wheat as affected by *Azotobacter chroococcum* mutants. *Biol. Fertil. Soils* **28**(3), 301–305 (1999). <https://doi.org/10.1007/s003740050497>
- Meena, V.S., Maurya, B.R., Verma, J.P.: Does a rhizospheric microorganism enhance K⁺ availability in agricultural soils? *Microbiol. Res.* **169**(5–6), 337–347 (2014). <https://doi.org/10.1016/j.micres.2013.09.003>
- Nautiyal, C.S.: An efficient microbiological growth medium for screening phosphate solubilizing microorganisms. *FEMS Microbiol. Lett.* **170**(1), 265–270 (1999). <https://doi.org/10.1111/j.1574-6968.1999.tb13383.x>
- Vessey, J.K.: Plant growth promoting rhizobacteria as biofertilizers. *Plant Soil* **255**, 571–586 (2003). <https://doi.org/10.1023/a:1026037216893>
- Yadav, J., Verma, J.P., Tiwari, K.N.: Effect of plant growth promoting rhizobacteria on seed germination and plant growth chickpea (*Cicer arietinum* L.) under *in vitro* conditions. *Biol. Forum* **2**(2), 15–18 (2010)
- Yousef, N.M.: Capability of plant growth-promoting rhizobacteria (PGPR) for producing indole acetic acid (IAA) under extreme conditions. *Eur. J. Biol. Res.* **8**(4), 174–182 (2018). <https://doi.org/10.5281/zenodo.1412796>



Microbiological Consortium of Thermokarst Lake and Its Significance in the Biodegradation of Petroleum Hydrocarbons

Irina Ivanova and Nina Nalivayko

Abstract

The intensive development of the oil and gas industry in the northern regions of Russia contributes to a sharp increase in the anthropogenic load on the natural ecosystems of the Arctic. The microflora of thermokarst lake is mainly represented by psychrophilic saprophytes, oligotrophs, ammonifying, and denitrifying bacteria. In the Arctic regions, the processes of biodegradation of hydrocarbons, with the participation of native hydrocarbon-oxidizing microflora, do not have time to fully develop, and the universal biologics used in the petroleum industry have low efficiency at low temperatures. In connection with the indicated problem, the aim of the present study was to investigate the ability of indigenous microorganisms of the Arctic natural waters to degrade oil. The analysis of the obtained experimental data showed that microorganisms which were cultivated under low temperature conditions (5 °C) did not show growth nor did they degrade the oil. It is shown that the oil degradation process starts at 10 °C and above, and that the maximum biodegradation intensity is observed in the first 15 days.

Keywords

Microbiological consortium • Biodegradation • Petroleum hydrocarbons • Oil pollution • Arctic

1 Introduction

Intensive economic exploitation of the Arctic part of the European North of Russia entails a sharp increase in the anthropogenic load on the vulnerable ecosystems of the Far North. In connection with the development of the oil and gas industry in the Arctic regions, one of the most important environmental problems arising today is not only the pollution of soils, but also water systems with petroleum hydrocarbons. Petroleum hydrocarbons are toxic, and many of them are known to be carcinogens and neurotoxic organic pollutants and can have huge consequences for biotic and abiotic components of ecosystems (Bacosa et al. 2010; Bacosa and Inoue 2015).

Microorganisms are the main agents in the process of self-purification of water bodies. The purpose of this study was to evaluate the enzymatic activity of natural (native) microflora in the oil processes in the degradation leading to the complete mineralization of organic pollutants (petroleum hydrocarbons) into carbon dioxide, water, inorganic compounds, and cellular protein or the conversion of complex organic pollutants into other simpler organic compounds.

2 Materials and Methods

Since the beginning of 2015 on the territory of the Bolshzemelskaya tundra (BZT) staff of the Federal Center for Integrated Arctic Research RAS (FCIARctic RAS) and Tomsk branch of the Institute of Petroleum Geology and Geophysics, SB RAS has carried out field studies including hydrogeochemical and microbiological sampling of natural waters. Thus, in 2015, one of the key research areas 40 km from Naryan-Mar has been developed in order to conduct observations of the ecosystem stay of thermokarst lakes (Fig. 1).

The BZT belongs to the Timan-Pechora oil and gas province, on the territory of which there is an active

I. Ivanova (✉)

Tomsk Branch of the Trofimuk Institute of Petroleum Geology and Geophysics of Siberian Branch of Russian Academy of Sciences, 634055 Tomsk, Russia

N. Nalivayko

National Research Tomsk Polytechnic University, 634050 Tomsk, Russia

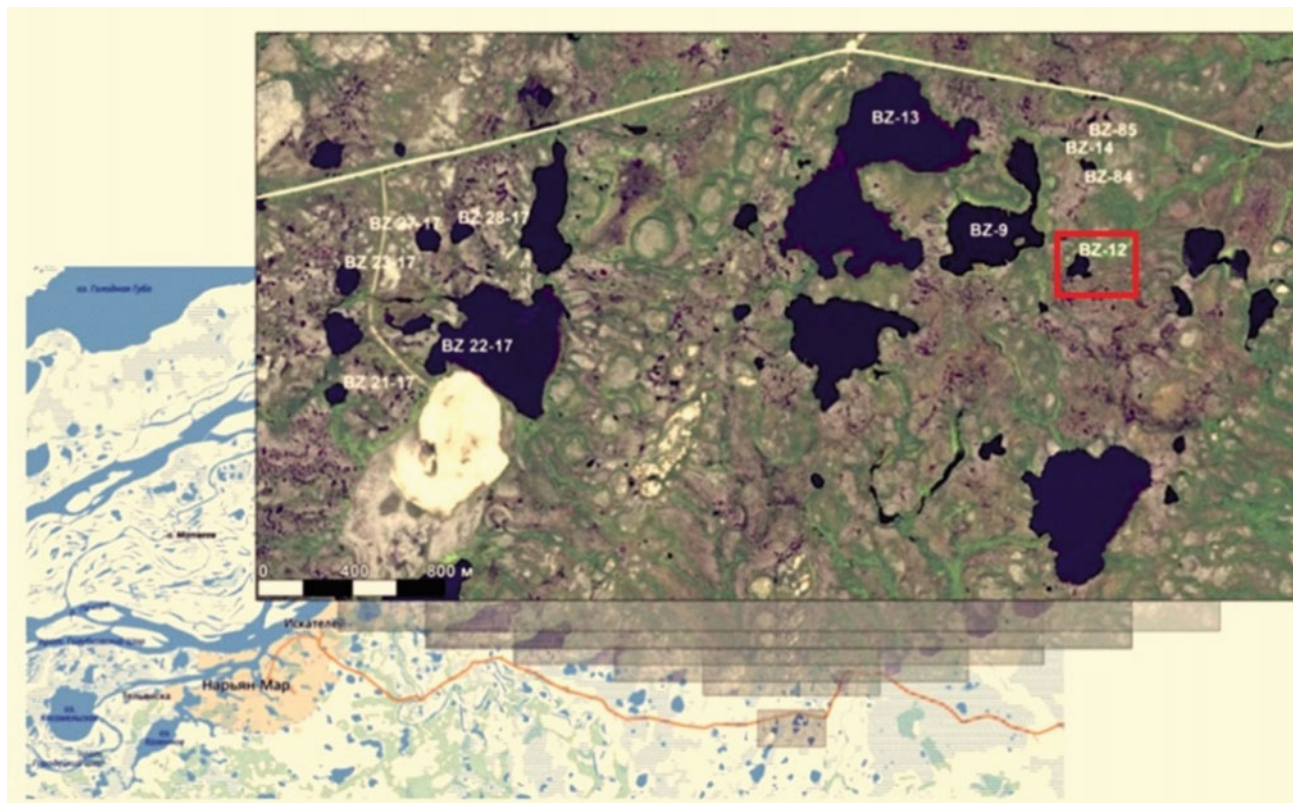


Fig. 1 Scheme of sampling plot near Naryn-Mar, Bolshezemelskaya tundra

production of hydrocarbons. It is worth noting that the largest in the Nenets Autonomous District, the Kharyaginskoe oil field, which has been developed for over 45 years, is located 120 km southeast of the plot.

The most sensitive indicators of changes in the chemical and ecological conditions of aquatic ecosystems are microorganisms, the number and species diversity which characterizes the processes occurring in the study object, that is, the ecological state of the ecosystem. So, for a detailed research of the water microbiological composition, a typical thermokarst lake BZ-12 at an early stage of development was chosen (Pokrovsky et al. 2011) in 2016 in the study area (Fig. 1). The research of the qualitative and quantitative composition of microbial communities of water was carried out according to conventional techniques (Gerhardt et al. 1981).

3 Results

The microflora of the lake is mainly represented by psychrophilic saprophytes, oligotrophs, and ammonifying and denitrifying bacteria (Table 1). It is noted that the saprophytes and ammonifying bacteria count of the surface layer is much higher. The value of the oligotrophic index indicates intensively occurring processes of destruction of organic

substance in the waters. The water area of the lake contains a significant amount of oil-degrading bacteria, but they are mostly represented by very small colonies. In the bottom layer, the number of these bacteria is much lower than in the surface layer. The identified oil-degrading bacteria in the surface layer of water are able to grow in oil vapors, but they are unable to oxidize pentane, benzene, and toluene. At the same time, intensively oxidizing decane bacteria were identified in the lake. All these facts indicate the presence of oil pollution in the lake.

It is known that microorganisms form a natural mechanism of self-purification of the environment and, above all, water from oil pollution. The issue of the effectiveness of this mechanism at low temperatures in the Arctic is not clear enough. Only experiments would enable the study of the ability of Arctic hydrocarbon-oxidizing microorganisms to utilize oil and its derivatives.

To carry out this work, hydrocarbon-oxidizing microorganisms were obtained from natural habitat by the method of auto-selection. A total of 150 mL of sterile nutrient medium (composition of nutrient medium (g/L): $(\text{NH}_4)_2\text{PO}_4$ —10.0; K_2HPO_4 —8.0; MgSO_4 —0.7; trace elements (mg/L): $\text{FeSO}_4 \cdot 7\text{H}_2\text{O}$ —12.5; $\text{MnSO}_4 \cdot 5\text{H}_2\text{O}$ —12.5; $\text{ZnSO}_4 \cdot 7\text{H}_2\text{O}$ —12.5; $\text{CuSO}_4 \cdot 5\text{H}_2\text{O}$ —3.0; and crude oil) were placed in 500-mL flasks. The flasks were covered with cotton-gauze

Table 1 Microflora of thermokarst lake at different layers, cells/mL

Physiological groups of bacteria	BZ-12 (surface layer)	BZ-12 (bottom layer)
Psychrophilic saprophytes	6950	2580
Oligotrophs	1020	6600
Ammonifying	1000	100
Denitrifying	100	1000
Oil degrading	17700	920
Oligotrophic index	0.6	6.0

plugs and sterilized in an autoclave. After that, 100 mL of lake water was added. One flask was not inoculated for control. Cultivation was carried out at room temperature under aeration and stirring conditions. At the beginning of the experiment, visual observations were made by the state of the liquid and oil in the experimental and control flasks and recording all changes. The duration of the experiment was about six months. The objective was to determine the total number of oil-oxidizing bacteria and saprophytes.

4 Discussion

The first visual signs of the influence of the microflora on oil appeared a week later—the solution in the experimental flasks acquired a weak color and turbidity. Visual signs of changes in the film of oil appeared after 30 days. In the experimental flask, the oil began to be dense, and the oil in the control flask, as well as the solution, remained unchanged. After 3 months, the density of saprophytic and oil-oxidizing bacteria in the experimental flask with was 10^{12} cells/mL. In bacterial landscapes of saprophytic bacteria, rounded colonies of medium size cream color prevailed. In non-inoculated culture flask the microbial growth, no growth was observed, and the change in oil was also not

visually observed. At the final stage, the oil in the experimental flasks was very dense, asphalt-like substance. The microbial suspension from the experimental flask with lake water was later used as inoculum culture to study its destructive properties of oil and its fractions. For this purpose, several test experiments were performed at a temperature of 5, 20, and 37 °C. During 15, 30, and 40 days, the density of microbes was 10^9 cells/mL. Experiments were performed in flat-bottom 150-mL flasks, and Nizhnevartovsk oil was used as a pollutant.

The resulting biomass was determined by filtering through a blue ribbon paper filter. The residual content of oil and hydrocarbon was determined by a gravimetric method. The analysis of the obtaining experimental data showed the following. When cultivating microorganisms in a laboratory refrigerator at 5 °C, oil and hydrocarbon are not degraded. The degradation of oil and hydrocarbon was observed with increasing temperature to 10 °C. It was determined that the process of oil decomposition starts at 10 °C and higher, and the maximum intensity of biodegradation is observed in the first 15 days (Table 2).

The ability of bacteria to degrade petroleum hydrocarbons at low temperature is affected by environmental factors and the phylotype of developed and dominant bacteria (Liu et al. 2017).

Table 2 Ability of Arctic hydrocarbon-oxidizing microorganisms to utilize oil

Conditions			Experimental flask		Control flask	
T (°C)	t (days)	Initial mass of oil (g)	Mass of the remained oil (g)	% of utilize oil	Mass of the remained oil (g)	% of utilize oil
5	15	2	2	0	2	0
5	30	2	2	0	2	0
5	40	2	2	0		
20	15	2	0.94	53	2	0
20	30	2	0.80	60	1.93	3
20	40	2	0.47	77		
37	15	2	0.67	68	1.86	7
37	30	2	0.95	52	1.69	15
37	40	2	1.10	45		

5 Conclusions

The intensive development of the oil and gas industry in the northern regions of Russia contributes to a sharp increase in the anthropogenic load on the natural ecosystems of the Arctic. In the Arctic regions, the processes of biodegradation of hydrocarbons, with the participation of native hydrocarbon-oxidizing microflora, do not have time to fully develop at low temperatures. Therefore, in order to preserve the natural potential of the Arctic regions, it is necessary to develop new environmentally friendly ways to combat oil pollution, which can be based on the study of native microflora of natural waters and their ability to self-purification.

In connection with the indicated problem, the aim was to study the ability indigenous microorganisms of the Arctic natural waters to degrade oil. To carry out this work, we used the cultures of hydrocarbon-oxidizing microorganisms obtained by auto-selection from the water of the thermokarst lake (BZ-12). The analysis of the obtained experimental data obtained showed that microorganisms which cultivated under low temperature conditions (5 °C), the growth of the number of microorganisms, and accordingly, the destruction of hydrocarbons does not occur. It is shown, that the process of oil decomposition starts at 10 °C and above, and the

maximum intensity of biodegradation is observed in the first 15 days.

Acknowledgements The research was supported by the Russian foundation for basic research, project no. 19-05-00290, and by the grant of President of Russian Federation MK-160.2020.5.

References

- Bacosa, H.P., Inoue, C.: Polycyclic aromatic hydrocarbons (PAHs) biodegradation potential and diversity of microbial consortia enriched from tsunami sediments in Miyagi, Japan. *J. Hazard. Mater.* **283**, 689–697 (2015)
- Bacosa, H., Suto, K., Inoue, C.: Preferential degradation of aromatic hydrocarbons in kerosene by a microbial consortium. *Int. Biodegrad. Biodegrad.* **64**, 702–710 (2010)
- Gerhardt, Ph., Murray, R., Costilow, R., Nester, Eu., Wood, W., Krieg, N., Phillips, G.: *Manual of Methods for General Bacteriology*. American Society for Microbiology, Washington (1981)
- Liu, J, Bacosa, H.P., Liu, Z.: Potential environmental factors affecting oil-degrading bacterial populations in deep and surface waters of the northern Gulf of Mexico. *Front Microbiol* **7**, 2131 (2017)
- Pokrovsky, O.S., Shirokova, L.S., Kirpotin, S.N., Audry, S., Viers, J., Dupré, B.: Effect of permafrost thawing on the organic carbon and metal speciation in thermokarst lakes of western Siberia. *Biogeosciences* **8**, 565–583 (2011)



Use of Biosurfactants in Bioremediation of Petroleum-Contaminated Soil

Rihab Belgacem, Olfa Ben Said, Ezzeddine Mahmoudi, and Hamouda Beyrem

Abstract

The objective of this research was to use biosurfactant-producing bacteria in bioremediation of oil-contaminated soil. Two approaches were studied. Biostimulation with the addition of crude biosurfactants extracted from *Rhodococcus fascians*, strain already isolated from hydrocarbon contaminated soils, and bioaugmentation with the addition of bacterial cells suspensions of the same strain. The bacterial quantification results revealed significant microbial abundance in both treatments. The results of soil hydrocarbon analysis revealed an efficiency of hydrocarbons elimination in both treatments (>30%). Metals analysis showed significant results of metals removal using both treatments (>75% for chromium). The ecotoxicity test showed an important decrease of oil-contaminated soil toxicity using the two treatments (>55%). Both approaches used showed an efficient elimination of hydrocarbons and metals and represented an environmentally friendly technology.

Keywords

Biosurfactants • Bioremediation • Hydrocarbons • Metals • Petroleum • Bacterial cells

1 Introduction

The decontamination of polluted soils has become an urgent need today, especially in the presence of petroleum activities, such as oil extraction, transporting, storage processing in oil landfill, which lead to environmental pollution risks (Belhouchet et al. 2019; Ben Said et al. 2019).

R. Belgacem (✉) · O. Ben Said · E. Mahmoudi · H. Beyrem
Environment Biomonitoring Laboratory LBE, Faculty of Sciences of Bizerte (FSB), University of Carthage, 7021 Zarzouna, Bizerte, Tunisia

Bioremediation applications were known as a cost-effective clean-up technology to treat petroleum-polluted soils and sediments (Ebadi et al. 2017). In recent years, researchers have focused on biosurfactants application in bioremediation as ecological alternative technologies for the removal of these contaminants (Pradeep et al. 2012). Biosurfactants are amphiphilic molecules produced by microorganisms to help them to use hydrocarbons as carbon source, either by making the hydrocarbon accessible by releasing biosurfactant into the environment or by changing its cell surface so that the contaminant can be absorbed (Ben Said et al. 2015). Moreover, they are ecofriendly biomolecules, due to their unique properties like low toxicity and emulsification (Pradeep et al. 2012). Our purpose was to use biosurfactant-producing bacteria in bioremediation of hydrocarbons contaminated-soils of the STIR refining company using two approaches, biostimulation with crude biosurfactant of *Rhodococcus fascians* and bioaugmentation with addition of bacterial cells of the same strain.

2 Materials and Methods

2.1 Biosurfactant-Producing Bacterial Strain

Rhodococcus fascians strain used in this study was obtained from the strain collection of our Environment Biomonitoring Laboratory LBE LR 01 ES 14. The bacterial strain is already isolated from oil-contaminated soil of STIR refinery. *Rhodococcus fascians* selection was based on its ability to degrade hydrocarbons and resist to metals as well as its biosurfactant production potential.

2.2 Bioremediation Trials

The studied soil was sampled in oil landfills of STIR refining company. Three types of mesocosms were set up in

triplicates, one control and two treatments. Each mesocosm contained 400 g of soil. All mesocosms were incubated in room temperature for 41 days (Ben Said et al. 2015). During the experimental period, the soil was mixed weekly until the end, and the soil water evaporation was adjusted by the addition of sterile distilled water. The hydrocarbons contaminated soil was bioaugmented in the first test with 4% of bacterial cells and biostimulated in the second test with 4% of biosurfactants (Pradeep et al. 2012).

2.2.1 Quantification of Oil-Degrading Bacteria

Microorganisms counting were estimated using the “Most Probable Number” (MPN) method (Quadros et al. 2016). The growth medium was mineral salt medium (MSM) supplemented with 0.2 μL of crude oil and 0.1 μL aliquot resazurin was added to each tube. A serial dilution was performed from a suspension of 1 g of soil in 9 mL physiological water, and each tube was inoculated with 10^{-3} – 10^{-5} serial dilutions. The tubes were incubated at 30 °C for 7 days (Ebadi et al. 2017).

2.2.2 Monitoring of Total Petroleum Hydrocarbons (TPH) and Metal Analyses

The TPHs analysis was performed, after their extraction, by Gas Chromatography coupled to a Flame Ionization Detector (GC-FID Model no Agilent 78908B) (Pradeep et al. 2012). The metal analysis was performed, after calcination and extraction, by Inductively Coupled Plasma—Atomic Emission Spectroscopy (ICP-AES Model no iCAP 6300) (Ben Said et al. 2019).

2.2.3 Germination Test

Soil phytotoxicity was assessed using a corn seeds germination test (*Zea mays* L.). Seeds were placed in sterile Petri dishes containing oil-contaminated soil and then placed in an incubator at 25 ± 1 °C in dark, for 7 days. The germination rate (G) was presented as follows (Ebadi et al. 2017).

$$G\% = \frac{\text{number of sprouted seeds}}{\text{total number of seeds sown}} \times 100$$

3 Results

3.1 Abundance of Oil-Degrading Bacteria in Oil-Contaminated Soil

After 41 days of incubation, the results revealed a significant abundance of oil-degrading bacteria in both treatments. Thus, for the treatment with bacterial suspensions, the abundance reached was from $1.6 \times 10^3 \pm 0.2 \times 10^3$ bacteria/g of soil up to $4.8 \times 10^5 \pm 0$ bacteria/g of soil.

In the case of addition of biosurfactants, the abundance reached from $1.6 \times 10^3 \pm 0.2 \times 10^3$ bacteria/g of soil up to $7.2 \times 10^5 \pm 3.6 \times 10^5$ bacteria/g of soil (Fig. 1).

3.2 Total Petroleum Hydrocarbons TPHs Biodegradation in Oil-Contaminated Soil

The treatment with bacterial suspensions of *R. fascians* showed a TPH degradation percentage of $32.25 \pm 9.15\%$. While the treatment with biosurfactants indicated $37.38 \pm 58.52\%$.

3.3 Metal Removal in Oil-Contaminated Soil

Both treatments showed a high percentage of metal removal (>70%) from oil-contaminated soil mainly for copper (87.14%) and chromium (86.08%) using bacterial cells and nickel (75.71%) and zinc (73.42%) using crude biosurfactants.

3.4 Germination Test

The treatment using crude biosurfactant favored the germination of about $60 \pm 10\%$ of the seeds, while the germination percentage recorded in the treatment using bacterial suspensions was about $55 \pm 10\%$.

4 Discussion

After 41 days of mesocosms incubation, we observed a significant increase in abundance of oil-degrading bacteria in both used treatments. The bacterial abundance was higher in the bioaugmentation treatment than in untreated contaminated soil (control), indicating that the bioaugmentation increased the initial bacterial abundance presented in the oil-contaminated soil. The TPH analysis revealed an

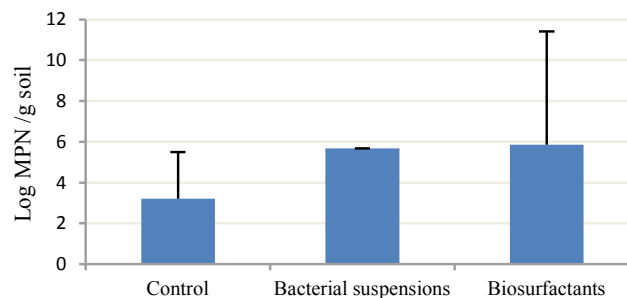


Fig. 1 Abundance of oil-degrading bacteria in oil-contaminated soil with different treatments

efficiency of TPHs elimination in the two treatments. Many studies reported similar results of TPH removal from the soil (Quadros et al. 2016). Both treatments, effectively, reduced metal contents in soil. The percentage of reduction, using bacterial suspensions cells of *R. fascians* strains, reached more than 80%, mainly for copper and chromium. Also using biosurfactants, the percentage of reduction exceeded 70% for nickel and zinc. In a previous study, Ben Said et al. (2019) reported similar results of reducing metals in bioremediation treatment of oil-contaminated soil. The germination test showed an important decrease of oil-contaminated soil toxicity using the two treatments. Both treatments improve soil quality by supporting plant growth.

5 Conclusion

The two approaches used for bioremediation treatment in oil-contaminated soil showed a significant effect on increasing the abundance of oil-degrading bacteria, the decreasing of TPH and metal content and the improvement of soil quality. This biological treatment represents an environmentally friendly technology. Further studies will be needed to improve the efficiency of the bioremediation techniques as well as to investigate the potential of biosurfactants with other approaches.

References

- Belhouchet, N., Hamdi, B., Chenchouni, H., Bessekhoud, Y.: Photocatalytic degradation of tetracycline antibiotic using new calcite/titania nanocomposites. *J. Photochem. Photobiol. A: Chem* **372**, 196–205 (2019). <https://doi.org/10.1016/j.jphotochem.2018.12.016>
- Ben Said, O., Louati, H., Soltani, A., Preud'homme, H., Cravo-Laureau, C., Got, P., Prin-gault, O., Aissa, P., Duran, R.: Changes of benthic bacteria and meiofauna assemblages during bio-treatments of anthracene-contaminated sediments from Bizerta lagoon (Tunisia). *Environ. Sci. Pollut. Res.* **22**(20), 15319–15331 (2015). <https://doi.org/10.1007/s11356-015-4105-7>
- Ben Said, O., Belgacem, R., Ben Gaffar, B., Beyrem, H., Kahn, J.R.: Remediation treatments and economic assessment of oil residual sludge from the bottom of tunisian refinery crude oil storage tanks. In: *Recent Advances in Geo-Environmental Engineering, Geomechanics and Geotechnics, and Geohazards*, pp. 81–83. Springer, Cham (2019). https://doi.org/10.1007/978-3-030-01665-4_19
- De Quadros, P.D., Cerqueira, V.S., Cazarolli, J.C., Maria do Carmo, R. P., Camargo, F.A., Giongo, A., Bento, F.M.: Oily sludge stimulates microbial activity and changes microbial structure in a landfarming soil. *Int. Biodeterioration Biodegradation* **115**, 90–101 (2016). <https://doi.org/10.1016/j.ibiod.2016.07.018>
- Ebadi, A., Sima, N.A.K., Olamaee, M., Hashemi, M., Nasrabadi, R.G.: Effective biore-mediation of a petroleum-polluted saline soil by a surfactant-producing *Pseudomonas aeruginosa* consortium. *J. Adv. Res.* **8**(6), 627–633 (2017)
- Pradeep, N.V., Anupama, S., Anitha, G., Renukamma, A.S., Afreen, S. S.: Bio-remediation of oil contaminated soil using biosurfactant produced by *Pseudomonas aeruginosa*. *J. Res. Biol.* **2**(4), 281–286 (2012)



Bio-cementation of Lateritic Soil Using Microbial-Induced Calcium Carbonate Precipitation Techniques for Use as Road and Embankment Materials

Kolawole Junwolo Osinubi, Adrian Oshioneme Eberemu, Thomas Stephen Ijimdiya, and Paul Yohanna

Abstract

This study evaluated the potential of *Bacillus coagulans*—induced calcite precipitate on the geotechnical properties of lateritic soil classified as A–4(2) class in the American Association of State Highway and Transportation Officials (AASHTO) system and SC in the Unified Soil Classification System (USCS), respectively. Tests carried out included calcium carbonate content (CCC), unconfined compressive strength (UCS) and microanalysis. Soil specimens were prepared with 0, 1.5×10^8 , 6.0×10^8 , 1.2×10^9 , 1.8×10^9 and 2.4×10^9 cells/mL *B. coagulans* suspension density at 1/3 pore volume before compaction with West African Standard (WAS) energy. Cementitious reagent containing 3 g of Nutrient broth, 20 g of urea, 10 g of NH_4Cl , 2.12 g of NaHCO_3 and 2.8 g CaCl_2 per litre of distilled water was injected into the soil after compaction by gravity until saturation was achieved. Results showed that CCC increased from 3.6 to 3.9% for 0/mL and 2.4×10^9 cell/mL, respectively. The UCS values increased with the increase in *B. coagulans* suspension density. Values of 300.82, 598.02, 674.08, 688.98, 786.02 and 789.47 kN/m² were recorded for 0, 1.5×10^8 , 6×10^8 , 1.2×10^9 , 1.8×10^9 and 2.4×10^9 cells/mL of *B. coagulans* suspension density, respectively. It is recommended that lateritic soil be treated with optimally 2.4×10^9 cells/mL *B. coagulans* suspension density/mL for use in geotechnical

engineering applications such as low trafficked roads and small embankments.

Keywords

Bacillus coagulans • Calcium carbonate content • Lateritic soil • Unconfined compressive strength

1 Introduction

Microbial-induced calcite precipitate (MICP) is a relatively new technique that uses bacterial activity in the improvement of the physical characteristics of soil. This technique uses biochemical processes in the soil to increase the engineering performance of soils (i.e., strength and hydraulic conductivity). The technique involves a cementation process that bonds natural subsurface soils by the hydrolysis of urea (ureolysis) to induce calcite precipitation at particle–particle contact in the soil environment (Dejong et al. 2006). The MICP studies the application of microbial techniques to geological materials that are predominantly used in engineering; it is a method that is under a much broader category in science referred to as biomineralization. This is a desirable technique for soil improvement because the entire process is environmentally sustainable.

Mitchell and Santamarina (2005) reported on the relative abundance of microbes in the soil, which favours their suitability for use as a sustainable and eco-friendly mechanism for soil improvement. MICP effectively precipitates calcite in the soil, through the process of urea hydrolysis; this process improves the strength and stiffness and decreases the hydraulic conductivity of the soil (Nemati and Voordouw, 2003; Harkes et al. 2010; van Paassen et al. 2010; Choi et al. 2016; Chi et al. 2017). Weaver et al. (2011) established that native microorganisms could be applied to facilitate calcite precipitation of satisfactory amount to alter soil properties. The results of the experiments to date have

K. J. Osinubi · T. S. Ijimdiya
Department of Civil Engineering, Ahmadu Bello University,
Zaria, Kaduna State, Nigeria

A. O. Eberemu (✉)
Department of Civil Engineering and African Centre of Excellence
On New Pedagogies in Engineering Education (ACENPEE),
Ahmadu Bello University, Zaria, Nigeria

P. Yohanna
Department of Civil Engineering, University of Jos, Jos, Nigeria

shown that bio mineralization is a promising approach in improving the engineering performance of soils.

Some lateritic soils are suitable for use in bio-cementation due to their large pore throat sizes which allows free movement of the microbes within the soil to enhance its bio-cementation and bio-clogging. Osinubi et al. 2017, 2018 established that lateritic soil could be effectively improved using the MICP techniques due to the ability of the microbes to move freely through the soil pore throat to induce calcite formation. This is in agreement with the report of Rebata-Landa (2007) and Wei-Soon et al. (2012) that large quantity of silt and clay soils have significant impact on the capability of native microbes to freely move within the soil. This study aimed at assessing the potential of soil microbes (*Bacillus coagulans*) on the geotechnical properties of compacted lateritic soil for geotechnical engineering applications.

2 Materials and Methods

2.1 Materials

2.1.1 Soil Sample

Lateritic soil used for this research was obtained from Abagana, Anambra State, Nigeria.

2.1.2 Microorganism

Bacillus coagulans, a urease positive bacteria was used in this research. *B. coagulans* were isolated from the soil. A rod shaped and spore forming bacteria.

2.1.3 Cementation Reagent

Cementation reagent used for the research is made up of 3 g of Nutrient broth, 20 g of urea, 10 g of NH_4Cl , 2.12 g of NaHCO_3 and 2.8 g CaCl_2 per litre of distilled water as recommended by Stocks-Fischer et al. (1999).

2.1.4 Bacteria Solution

The bacteria solution used for inoculation of *B. coagulans* suspension contained 3 g of Nutrient broth and 20 g of urea per litre of distilled water.

2.2 Methods

2.2.1 Isolation of the Bacterium Specie

The isolation of the microbes from the soil was carried out by means of serial dilution. The isolates were stored at 4 °C in nutrient medium proceeding to classification and characterization.

2.2.2 The Culture Medium and Growth Conditions

The method used was in agreement with that defined by Stocks-Fischer et al. (1999).

2.2.3 Mass of Calcium Carbonate Measurements

The sample used for calcium carbonate content (CCC) measurement was treated before compaction with *B. coagulans* suspension at one-third (1/3) pore volume (as recommended by Rowshanbakhta et al. 2016) in stepped suspension densities of 0, 1.5×10^8 , 6×10^8 , 1.2×10^9 , 1.8×10^9 and 2.4×10^9 cells/mL, respectively. Cementitious reagent was injected into the soil after compaction by gravity until saturation was achieved. Compacted specimens in the mould were used for each stepped suspension densities. The samples were then allowed to air dry at laboratory temperature of 25 ± 2 °C before tests were carried out. The measurement procedure used is in accordance with that proposed by Mortensen et al. (2011) and Choi et al. (2017) called the acid wash method. This washing method was able to remove all soluble calcium from the soil particles. Then, all solid particles remaining on the sieve were oven-dried and weighed. The weight difference between the original soil sample (A) and post washing sample (B) was the mass of calcium carbonate. The CCC was calculated as

$$CCC = 100 - \frac{B}{A} \times 100 \quad (1)$$

2.2.4 Unconfined Compressive Strength

The unconfined compressive strength (UCS) tests were performed on the soil in accordance with BS 1377; 1990 part (7). Soil samples were treated before compaction with *B. coagulans* suspension at one-third (1/3) pore volume (as recommended by Rowshanbakhta et al. 2016) in stepped suspension densities. Soil samples were prepared at optimum moisture content (OMC) compacted using West African Standard (WAS) Compaction Energy. Cementitious reagent was injected into the soil (Three cycles of injection) after compaction by gravity. The samples were then cured. After curing, the samples were positioned in a load frame machine driven strain controlled at 0.01% /min until failure occurred.

3 Results and Discussion

3.1 Index Properties

Summary of the properties of the natural soil is shown in Table 1.

Table 1 Properties of natural lateritic soil

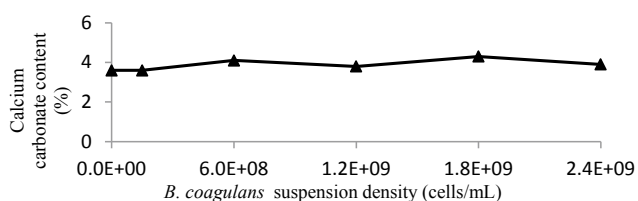
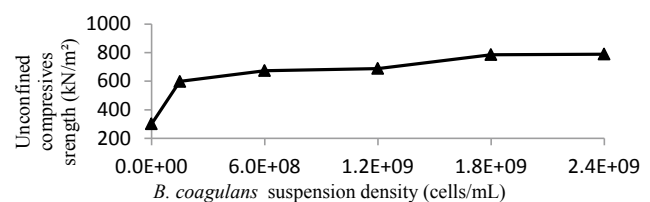
Property	Quantity
Percentage passing BS No. 200 sieve	35.4
Natural moisture content (%)	11.3
Liquid limit (%)	37.5
Plastic limit (%)	19.3
Plasticity index (%)	18.2
Specific gravity	2.62
AASHTO classification	A-4(2)
USCS	SC
Maximum dry density (Mg/m ³)	1.86
Optimum moisture content (%)	14.5
Colour	Reddish brown

3.2 Calcium Carbonate Content

One of the guiding principles for soil improvement using the microbial improvement technique is the formation of soil binding material called calcium carbonate which stiffens the soil and improves its workability. The variation in calcium carbonate content with *B. coagulans* suspension density is shown in Fig. 1. Calcium carbonate content formed within the soil matrix amplified with an increase in the population of the microbes from 0 cell/mL up to 2.4×10^9 cell/mL. Calcium carbonate content values marginally increased from 3.6 to 3.9%. This increase may be associated with the increase in the amount of urease enzymes produced by *B. coagulans*. As the population of *B. coagulans* increased, it is presumed that more urease enzymes are released by the microbes leading to the rise in the formation of the calcium carbonate. Chi et al. (2017) and Osinubi et al. (2018) in their research, they reported that increased bacteria density resulted in greater enzyme activities because the surface of the microbes served as a nucleation site to induce calcite precipitation within the soil.

3.3 Unconfined Compressive Strength

The unconfined compressive strength (UCS) of lateritic soil with *B. coagulans* suspension density/mL is shown in Fig. 2.

**Fig. 1** Calcium carbonate content measurement with *B. coagulans* suspension density**Fig. 2** Unconfined compressive strength with *Bacillus coagulans* suspension density

UCS values increased with the increase in *B. coagulans* suspension density. Values of 300.82, 598.02, 674.08, 688.98, 786.02 and 789.47 kN/m² were recorded for 0, 1.5×10^8 , 6×10^8 , 1.2×10^9 , 1.8×10^9 and 2.4×10^9 cells/mL of *B. coagulans* suspension density, respectively. The increase in UCS value could be attributed to the increased *B. coagulans* cells that facilitated the precipitation of higher quantities of calcium carbonate from the hydrolysis of urea (Abo-El-Enein et al. 2012). As *B. coagulans* suspension density/mL increased higher quantity of calcite was formed that bridged the soil particles by clogging pore spaces through bio-cementation within the soil structure. Similar findings were reported by Abo-El-Enein et al. (2012), Tsukamoto et al. (2013), Cheng et al. (2014) and Rowshanbakhta et al. (2016). Biogas generation, extracellular polymeric substances formation and gelatinous biofilms secreted by microorganisms may be responsible for strength increase (Dejong et al. 2010, 2013; Osinubi et al. 2018).

3.4 Microanalysis

The micrographs (at 200 μ m scale and zoomed to 370 \times) of the microscopic examination using scanning electron microscope (SEM) of specimens of natural lateritic soil and soil treated with *B. coagulans* suspension density/mL are shown in Figs. 3 and 4, respectively. It is observed that the

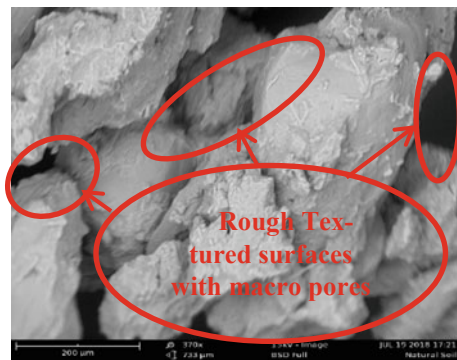


Fig. 3 Micrograph of natural lateritic soil

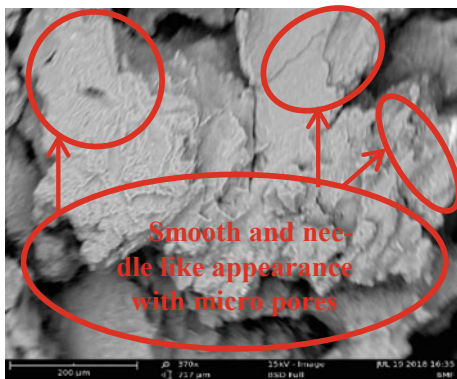


Fig. 4 Micrograph of lateritic soil optimally treated with 2.4×10^9 /mL *B. coagulans* suspension density

natural soil has a rough textured appearances with black patches of openings or macropores within the soil matrix. In the case samples treated with *B. coagulans*, smooth and needle like surface appearance with micropores were observed (see Fig. 4). The smooth appearance could be associated with the formed calcite that blocked the micropores within the soil matrix or may be due to other geochemical processes (biogas generation, extracellular polymeric substances formation and gelatinous biofilms secreted by microorganisms may be responsible for such morphology (Dejong et al. 2010, 2013; Osinubi et al. 2018).

4 Conclusion

The natural soil specimens were prepared with $0, 1.5 \times 10^8, 6.0 \times 10^8, 1.2 \times 10^9, 1.8 \times 10^9$ and 2.4×10^9 cells/mL *B. coagulans* suspension density/mL at 1/3 pore volume before compaction with West African Standard (WAS) energy. Cementitious reagent was injected into the soil after compaction by gravity until saturation was achieved. Results show that CCC and UCS values increased with the increase in *B. coagulans* suspension density. Although the obtained

result for optimal blend falls below 1710 kN/m^2 , recommended by the literature for road construction, it is recommended that lateritic soil treated with optimally 2.4×10^9 cells/mL *B. coagulans* suspension densities be used in geotechnical engineering applications such as low trafficked roads and small embankments. Further studies should consider microanalysis of the treated specimen at different energy levels.

References

- Abo-El-Enin, S.A., Ali, A.H., Talkhan, F.N, Abdel-Gawwad, H.A.: Utilization of microbial induced calcite precipitation for sand consolidation and mortar crack remediation. *J. Housing Build. Natl. Res. Cente*, **8**, 185–192 (2012)
- BS 1377: Method of Testing Soils for Civil Engineering Purpose. British Standard Institute, BSI, London (1990)
- Cheng, L., Shahin, M.A., Cord-Ruwisch, R., Addis, M., Hartanto, T., Elms, C.: Soil stabilisation by microbial induced calcium carbonate precipitation: investigation of some important physical and environmental aspects. In: 7th International Congress on Environmental Geotechnics, Australia (2014)
- Chi, L., De, Y., Shihui, L., Tuanjie, Z., Siriguleng B., Yu, G., Lin, L.: Improvement of geomechanical properties of bio-remediated aeolian sand. *Geomicrobiology J.* (2017). <https://doi.org/10.1080/01490451.2017.1338798>
- Choi, S.G., Wang, K., Chu, J.: Properties of biocemented, fiber reinforced sand. *J. Const. Build. Mater.* **120**, 623–629 (2016)
- Choi, S.G., Park, S.S., Wu, S., Chu, J.: Methods for calcium carbonate content measurement of biocemented soils. *J. Mater. Civ. Eng. Tech. Note* **29**(11), 06017015 (2017)
- DeJong, J.T. et al.: Biogeochemical processes and geotechnical applications: progress opportunities and challenges. *Geotechnique* **63**(4), 287–301 (2013). <https://doi.org/10.1680/geot.SIP13.P.017>
- DeJong, J.T., Fritzsche, M.B., Nusslein, K.: Microbial induced cementation to control sand response to undrained shear. *ASCE J. Geotech. Geoenviron. Eng.* **132**(11), 1381–1392 (2006)
- DeJong, J.T., Mortensen, M.B., Martinez, B.C., Nelson, D.C.: Biomediated soil improvement. *Ecolog. Eng.* **36**(2), 197–210 (2010)
- Harkes, M.P., van Paassen, L.A., Booster, J.L., Whiffin, V.S., van Loosdrecht, M.C.: Fixation and distribution of bacterial activity in sand to induce carbonate precipitation for ground reinforcement. *Ecolog. Eng.* **36**, 112–117 (2010)
- Mitchell, J.K., Santamarina, J.C.: Biological considerations in geotechnical engineering. *J. Geotech. Geoenviron. Eng.* **131**(10), 1222–1233 (2005)
- Mortensen, B.M., Haber, M.J., DeJong, J.T., Caslake, L.F., Nelson, D. C.: Effects of environmental factors on microbial induced calcium carbonate precipitation. *J. Appl. Microbiol.* (2011). <https://doi.org/10.1111/j.1365-2672.2011.05065.x>
- Nemati, M., Voordouw, G.: Modification of porous media permeability, using calcium carbonate produced enzymatically *in situ*. *Enzyme Microb. Technol.* **33**, 635–642 (2003)
- Ng, W.-S., Lee, M.-L., Hii, S.-L.: An overview of the factors affecting microbial-induced calcite precipitation and its potential application in soil improvement. *World Acad. Sci. Eng. Technol.* **6**, 683–689 (2012)
- Osinubi, K.J., Eberemu, A.O., Ijimdiya, S.T., Yakubu, S.E., Sani, J.E.: Potential use of *B. pumilus* in microbial induced calcite precipitation improvement of lateritic soil. In: Proceedings of the 2nd Symposium on Coupled Phenomena in Environmental Geotechnics

- (CPEG2), Leeds, United Kingdom, 6–8 Sept. Session: Clean-ups, Paper #64, pp. 1–6 (2017)
- Osinubi, K.J., Yohanna, P., Eberemu, A.O., Ijimdiya, T.S.: Evaluation of hydraulic conductivity of lateritic soil treated with *Bacillus coagulans* for use in waste containment applications. In: Proceedings of the 8th International Congress on Environmental Geotechnics (ICEG 2018), 28th October–1st November, Hangzhou, China, pp. 401–409 (2019). https://doi.org/10.1007/978-981-13-2227-3_50
- Rebata-Landa, V.: Microbial Activity in Sediments: Effects on Soil Behaviour. Georgia Institution of Technology, PhD thesis (2007)
- Rowshanbakhta, K., Khomehchiana, M., Sajedib, R.H., Nikudela, M. R.: effect of injected bacterial suspension volume and relative density on carbonate precipitation resulting from microbial treatment. *J. Ecol. Eng.* **89**, 49–55 (2016)
- Stocks-Fischer, S., Galinat, J.K., Bang, S.S.: Microbiological precipitation of CaCO₃. *Soil Biol. Biochem.* **31**(11), 1563–1571 (1999)
- Tsukamoto, M., Inagaki, T., Sasaki, Y., Oda, K.: Influence of relative density on microbial carbonate precipitation and mechanical properties of sand. In: Proceedings of the 18th International Conference on Soil Mechanics and Geotechnical Engineering, Paris (2013)
- Van Paassen, L.A., Ghose, R., van der Linden, T.J.M., van der Star, W. R.L., van Loosdrecht, M.C.M.: Quantifying biomediated ground improvement by ureolysis: large-scale biogROUT experiment. *ASCE J. Geotech. Geoenviron. Eng.* **136**(12), 21–1728 (2010)
- Weaver, T., Burbank, M., Lewis, R., Lewis, A., Crawford, R., Williams, B.: Bio-induced calcite, iron, and manganese precipitation for geotechnical engineering applications. In: Proceeding GeoFrontiers 2011: Advances in Geotechnical Engineering, Dallas, TX, ASCE Geotechnical Special Publication vol. 211, pp. 3975–3983 (2011)



Sewage Sludge Compost Disposal on a Chernozem Soil: Impacts on Bacterial Activity and Nutrient Contents

Andrea Farsang, Izabella Babcsányi, Zsuzsanna Ladányi, Katalin Perei, Attila Bodor, Katalin Tímea Csányi, and Károly Barta

Abstract

Sewage sludge contains organic matter, micro- and macronutrients which are potentially useful for agricultural usage. However, it can be harmful when containing undesirable amounts of organic pollutants, heavy metals, or pathogens. Our study focused on examining the changes in the extractable nutrient and humus contents of Chernozem soils and the alteration of the soil biological activity as a consequence of municipal sewage sludge spreading. Sampling campaigns were achieved in 2018 near Újkígyós (SE-Hungary) during which composite samples (0–30 cm and 30–60 cm) were collected and also upper soil (0–50 cm) and subsoil (50–80 cm) samples for assessing biological parameters, considered to be aerobic and anaerobic soil layers, respectively. Soils were analyzed for the basic pedological parameters (pH, organic matter, etc.) and nutrient concentrations (K_2O , P_2O_5 , N-forms, and humus) following standard extraction procedures. The soil biological activity has been assessed by counting colony forming units (CFU) and enzyme activity measurements. The results of the nutrient analyses show significantly increased soil-bound K_2O , P_2O_5 , and $NO_2^- + NO_3^-$ contents linked to the sewage sludge treatment. However, the humus content did not vary significantly compared to the control site. The microbiological analysis showed that the sewage sludge disposal

tends to increase the aerobic CFUs, but not that of the anaerobic microbes. The average catalase enzyme activity in both aerobic and anaerobic samples and the average dehydrogenase activity only in the aerobic layers show a slight, however, insignificant increase in the compost-amended soils.

Keywords

Sewage sludge disposal • Soil protection • Soil nutrient content • Soil enzymatic activity

1 Introduction

The main by-product of waste water treatment plant, sewage sludge, is rich in organic and inorganic nutrients; hence, it can be applied on agricultural land as an alternative to mineral fertilizers. Land application of sewage sludge is an increasingly popular means of the reuse of sewage sludge as it allows for recycling of valuable components such as organic matter, N, P, and other nutrients (Boudjabi and Chenchouni 2021). Understanding the impacts of sewage sludge treatments is essential in the correct management of agricultural land. Indeed, sewage sludge amendment to the soil modifies the soil's physico-chemical and biological properties, such as plant-available macro/micronutrient contents and organic matter content. Besides amending the soil with plant nutrients and organic matter, sewage sludge application can significantly increase the amount of microbial biomass in the soil and can also increase the soil enzyme activities (Banerjee et al. 1997). Dehydrogenase (DHA) and catalase (CAT) enzyme activities can be used to decipher the impacts of the sewage sludge treatments on the soil biological activity (Lakhdar et al. 2010). The aim of the present study was to investigate the impact of municipal sewage sludge compost disposal on the nutrient status and the biological activity in a Chernozem soil.

A. Farsang (✉) · I. Babcsányi · Z. Ladányi · K. T. Csányi · K. Barta

Department of Physical Geography and Geoinformatics, University of Szeged, Egyetem utca 2-6, 6722 Szeged, Hungary
e-mail: farsang@geo.u-szeged.hu

K. Perei · A. Bodor
Department of Biotechnology, University of Szeged, Középfásor, 6726 Szeged, Hungary

A. Farsang · K. Perei
Institute of Environmental Science and Technology, University of Szeged, Tisza L. krt 132, 6720 Szeged, Hungary

2 Materials and Methods

The study area is located near Újkígyós, in Southeastern Hungary (Ladányi et al. 2018). The study area is a 5.6 ha arable land, where municipal sewage compost has been regularly disposed since 2013 between October and November (2.5 m³/ha/year). The rate of compost application was calculated based on the nutrients (N, P, K) content of the compost and the nutrient requirements of cultivated plants. The soil sampling was carried out in March 2018. Composite samples were collected from the upper soil (0–30 cm) and subsoil (30–60 cm) from six sites of 2500 m² within the study area (four sites were affected by sewage disposal and two control sites). In order to assess soil biological parameters (heterotrophic bacterial counts, DHA, and CAT activities), the soil samples were also collected from the upper soil (0–50 cm) and subsoil (50–80 cm) considered to be aerobic and anaerobic soil layers, respectively. The pH (in H₂O) and humus content of soils were measured according to standard procedures. The macronutrients P₂O₅ and K₂O were extracted using ammonium-lactate, while the nitrogen forms (NO₂⁻ + NO₃⁻ - N) were extracted with KCl-solution. The nutrient content was then determined by FIA spectrometer.

Modified colony forming unit (CFU) method of Wu et al. (2017) was used to enumerate viable heterotrophic bacteria both in aerobic and anaerobic layers of sewage-treated and control soils. Homogenized soil samples (5–5 g) were suspended in 10 mL of physiological saline solution and shaken for 30 min. Serial dilutions of each suspension were pipetted onto nutritionally rich Luria Bertani (LB) agar plates (Sambrook et al. 1989). Individual colonies were counted after 3 days of incubation at 25 °C. Activities of CAT and DHA in soils were determined according to the procedure described by Wolińska et al. (2016). The results were presented as µg of produced triphenylformazan (TPF) per dry soil weight.

The nonparametric Mann Whitney U test was applied for comparing data between the amended and the control soils ($p < 0.05$) using the SPSS software (IBM SPSS Statistics, Version 24).

3 Results and Discussion

3.1 Nutrients and Humus Contents of Soils Impacted by Sewage Sludge Compost Disposal

The soils were characterized by a slightly alkaline pH (7.0–8.1), a little-to-medium humus content (1.53–2.55%), a low carbonate content (0.14–3.56%), and a sandy loam texture.

The available nutrient contents showed increased values in the compost-amended sites compared to control areas (Fig. 1). The statistically higher plant available N, P, and K nutrients can be explained by the slow decomposition of the composts and the continuous supply of nutrients to the soil through the conversion of macronutrients (N, P, S, etc.) into inorganic (and mostly plant available) forms by microorganisms (Diacono et al. 2011). However, the humus content did not show statistically significant differences in the investigated soils between the amended and the control sites (Fig. 1). It has been previously found during a long-term (50-year long) arable field experiment in Hungary with Chernozem and Cambisols that repeated applications of animal manure increased the soil organic carbon pool by 10 to 30% depending on the manure doses (Sleutel et al. 2006). The lower compost dose (in terms of organic matter input) and the shorter period of compost application likely explain the lack of a significant increase in the soil humus content of the amended soils near Újkígyós.

3.2 The Modifications of Soil Biology Due to the Compost Amendment

The modification of bioavailable nutrient contents of agricultural soils can induce notable changes in the soil microbiology. The mean aerobic CFU was 8.25 ± 4.19 million per g in the amended soil, while 4.48 ± 2.57 million per g were enumerated in the control soil (Table 1). Although higher average aerobic CFUs characterized the sludge-treated soils, statistically no significant difference was observed between the treated and the control soils. The anaerobic microorganisms were assessed in terms of nitrate-, sulfate-, and iron-reducing forms. Overall, the iron-reducing bacteria were the most abundant and averaged 1.91 ± 0.69 million CFU per g in the compost-amended and 5.79 ± 1.56 million CFU per g in the control soils (Table 1). Both the average CAT and the DHA activities seem to be slightly increased in the compost-amended soils, however, without any statistical significance (Table 1). Indeed, previous studies have shown that both sewage sludge applications and irrigation with municipal wastewater have stimulating effects on the soil biological activity with increased DHA, CAT, as well as other enzymatic activities measured in the treated soils (Brzezinska et al. 2001; Lakhdar et al. 2010; Ladányi et al. 2018). Here, the lack of a DHA activity increase in the anaerobic soil and the decrease in the anaerobic CFUs in the treated soils may be explained by the introduction of some toxic metabolites (such as sulfides) or potentially toxic heavy metal pollutants present in the sewage sludge compost (Chen et al. 2008; Ladányi et al. 2018).

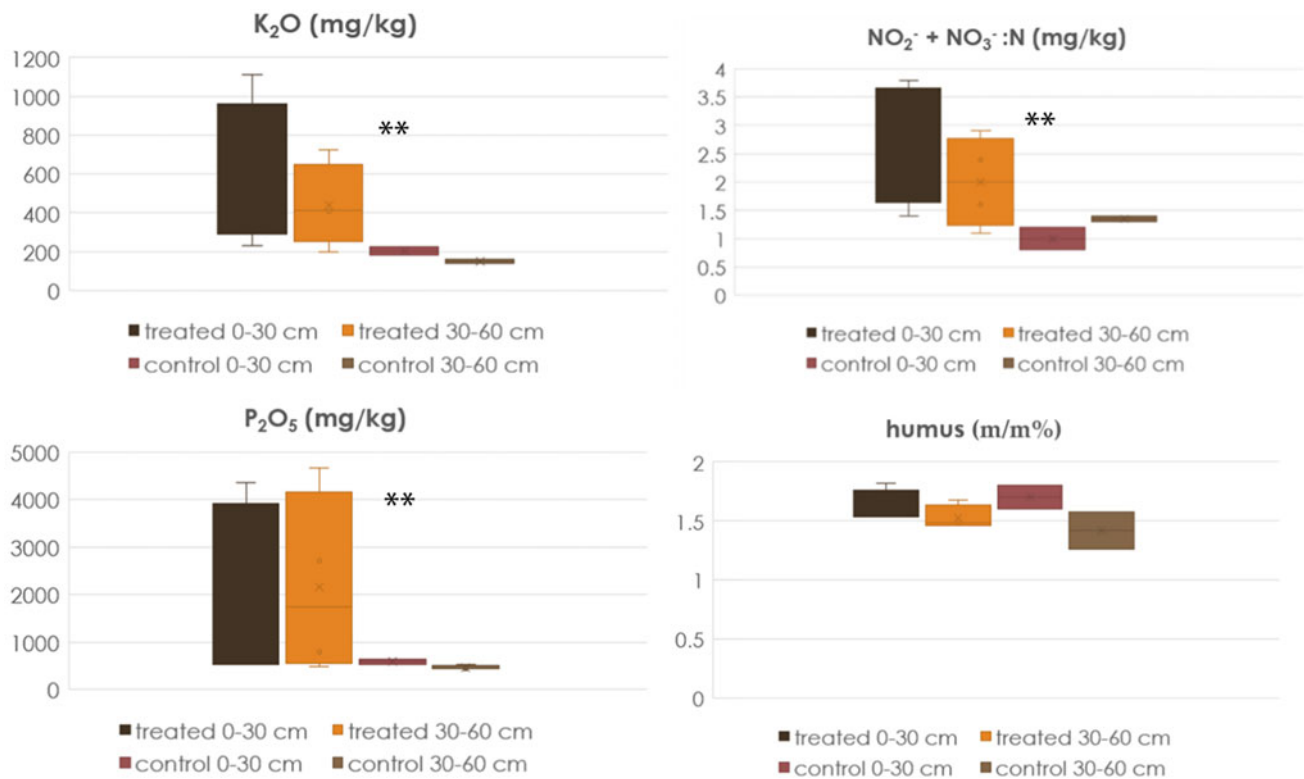


Fig. 1 Extractable nutrient (K_2O , $NO_2^- + NO_3^- - N$, P_2O_5) contents and the humus contents in the compost-amended and the control soils. **: indicates significant difference between the compost-amended and the control sites ($p \leq 0.05$)

Table 1 Mean \pm SE of the CFU counting, the catalase (CAT), and dehydrogenase (DHA) activities in the sewage sludge-treated and the control soils in aerobic and anaerobic soil layers

		CFU (million per g)		DHA (μ g TPF/g/24 h)		CAT(μ mol H ₂ O /g/min)	
		Compost-amended	Control	Compost-amended	Control	Compost-amended	Control
Aerobic		8.25 \pm 4.19	4.48 \pm 2.57	33.76 \pm 4.60	21.48 \pm 13.39	12.88 \pm 1.07	12.43 \pm 0.33
Anaerobic	Nitrate-red	1.08 \pm 0.44	6.69 \pm 0.09	14.27 \pm 1.24	18.96 \pm 2.92	12.47 \pm 0.83	11.57 \pm 0.44
	Sulfate-red	0.04 \pm 0.01	1.98 \pm 0.52				
	Iron-red	1.91 \pm 0.69	5.79 \pm 1.56				

4 Conclusions

Organic amendments, such as municipal sewage sludge composts, influence soil characteristics by the modification of biological, chemical, and physical attributes. Here, we showed that the sewage sludge compost application on Chernozem soils improved the soil properties, by adding slowly decomposing organic matter abundant in plant macronutrients (N, K, P). Although the anaerobic microorganisms and the DHA enzyme activity in the anaerobic soil layers did not increase in the compost-amended soils, aerobic microorganisms (CFUs) and CAT activity tended to be higher in the treated soils compared to the non-amended

(control) site, however not significantly. These results suggest that the soil biological activity is only moderately affected by the compost applications.

Acknowledgements The research was funded by the 'Thematic Network for the Sustainable Use of Re-sources—RING2017' project (program code: EFOP-3.6.2-16-201700010).

References

Banerjee, M.R., Burton, D.L., Depoe, S.: Impact of sewage sludge application on soil biological characteristics. *Agr. Ecosyst. Environ.* **66**, 241–249 (1997). [https://doi.org/10.1016/S0167-8809\(97\)00129-1](https://doi.org/10.1016/S0167-8809(97)00129-1)

- Boudjabi, S., Chenchouni, H.: On the sustainability of land applications of sewage sludge: how to apply the sewage biosolid in order to improve soil fertility and increase crop yield? *Chemosphere*, **282**, 131122 (2021). <https://doi.org/10.1016/j.chemosphere.2021.131122>
- Brzezinska, M., Stepniewska, Z., Stepniewski, W.: Dehydrogenase and catalase activity of soil irrigated with municipal wastewater. *Pol. J. Environ. Stud.* **10**(5), 307–311 (2001)
- Chen, Y., Cheng, J.J., Creamer, K.S.: Inhibition of anaerobic digestion process: a review. *Biores. Technol.* **99**, 4044–4064 (2008). <https://doi.org/10.1016/j.biortech.2007.01.057>
- Diacono, M., Montemurro, F. : Lichtfouse E., et al. (eds), *Sustainable Agriculture Vol. 2*, Springer, New York, (2011).
- Ladányi, Zs., Farsang, A., Gulácsi, A., Kovács, F.: The impact of extreme weather conditions and municipal sewage disposal on vegetation using sentinel images In: SE Hungary. Proceedings of the International Symposium on Analytical and Environmental Problems, **24**, 325–329 (2018)
- Lakhdar, A., Scelza, R., Scotti, R., Rao, M.A., Jedidi, N., Gianfreda, L., Abdelly, C.: The effect of compost and sewage sludge on soil biologic activities in salt affected soils. *Revista De La Ciencia Del Suelo y Nutrición Vegetal* **10**(1), 40–47 (2010)
- Sambrook, J., Maniatis, T., Fritsch, E.F.: *Molecular Cloning: A Laboratory Manual*. Cold Spring Harbor Laboratory Press, Cold Spring Harbor, New York (1989)
- Sleutel, S., De Neve, S., Németh, T., Tóth, T., Hofman, G.: Effect of manure and fertilizer application on the distribution of organic carbon in different soil fractions in long-term field experiments. *Eur. J. Agron.* **25**, 280–288 (2006). <https://doi.org/10.1016/j.eja.2006.06.005>
- Wolińska, A., Kuźniar, A., Szafranek-Nakonieczna, A., Jastrzębska, N., Roguska, E., Stepniewska, Z.: Biological activity of autochthonic bacterial community in oil-contaminated soil. *Water Air Soil Pollut.* **227**(5), 130 (2016). <https://doi.org/10.1007/s11270-016-2825-z>
- Wu, M., Ye, X., Chen, K., Li, W., Yuan, J., Jiang, X.: Bacterial community shift and hydrocarbon transformation during bioremediation of short-term petroleum-contaminated soil. *Environ. Pollut.* **223**, 657–664 (2017). <https://doi.org/10.1016/j.envpol.2017.01.079>



Ecological Significance of Selected Marine Bryozoans from Bay of Bengal, East Coast of India

K. Tabita Symphonia

Abstract

The ecological record of bryozoans from the continental shelf–slope region of the southwestern Bay of Bengal is very sparse, prompting this investigation. Forty-five sea-floor sediment samples were collected along eight transects during the cruise—*R/V Sagar Paschimi* from the offshore region between Chennai and Cuddalore in the southwestern Bay of Bengal. The distribution of bryozoans was assessed based upon fragments of bryozoan colonies and their skeletal masses from these samples, which were collected at depths ranging from 10 to 350 m. The goal was to determine the relationship between environmental parameters measured from the study area and the abundances of various bryozoan morphotypes. The results revealed eight morphotypes of bryozoans, the most abundant being Cheilostomatida. The distribution of bryozoan fragments appeared to respond to changes in depth-related factors such as nature of substrate, turbulence and rate of sedimentation.

Keywords

Marine bryozoans • Shelf-slope sediments • Distribution • Chennai–Cuddalore • Bay of Bengal

1 Introduction

Bryozoans are sessile, primarily marine organisms encountered throughout most marine environments, and a few species are even found in freshwaters (Cook 1981; Gordon 1999). Their abundance in the marine realm is largely controlled by the availability of favorable substrate in addition to the changes in the physicochemical parameters of the oceanic waters. Several studies across the globe have shown

that growth forms of bryozoan colonies are related to depths, hydrodynamic energy conditions, acidification of oceanic waters, different types of substrate, rate of sedimentation, etc. (Moissette et al. 2007; Rodolfo-Metalpa et al. 2010). Thus, morphotypes of fossil bryozoans are important in interpreting paleo-environmental conditions.

2 Materials and Methods

Forty-five surface sediment samples were collected from the study area at various depths (<10–350 m) along eight transects using Van Veen grab sampler. At each station, temperature, depth and salinity were measured using a Sea-Bird SBE-25 CTD. The samples were carefully preserved on board for further processing in the laboratory. A representative fraction of each sample was used for textural analyses and for picking and counting of bryozoans. For grain size analysis, the samples were pretreated with H₂O₂ to remove organic matter, and sodium hexametaphosphate was used as a dispersing agent to deflocculate the sediments. The sieving technique was used for samples with abundant coarser (>63 μm) fraction and pipette method for samples with sufficient (<63 μm) fraction. Depending upon the gravel, sand and mud content measured in each homogenized subsample, textural class was assigned. (Reineck and Siefert 1980; Pejrup 1988; Flemming 2000). The selected bryozoan specimens were cleaned with distilled water, dried and mounted on aluminum stubs. They were examined using SEM Hitachi S-3400 N after splutter coating with carbon. The micrographs thus obtained were used to identify the bryozoan morphotypes.

3 Results

The present study revealed the presence of eight bryozoan morphotypes used as environmental indicators. The most abundant forms were Cheilostomatida bryozoans constituting 80–90% of the total bryozoan assemblage. A very few

K. Tabita Symphonia (✉)
Eritrea Institute of Technology, Asmara, Eritrea

Cyclotomatida forms were also recovered. Environmental factors such as temperature, salinity and pH varied minimally between the sample sites. Lunulitiform bryozoans such as *Cupuladria cf. guineensis* and *C. indica* were found on the sandy bottom in inner-shelf settings (below 30 m water depth). A few encrusting bryozoans such as *Parasmittina spp.* and *Mucropetraleilla sp.* were found in all depths encrusted on molluscan shells, including gastropods.

4 Discussion

The grain size analysis revealed that the shelf region in the southern part of the Bay of Bengal is covered by sediments ranging from coarse to fine sands and silt (Selvaraj et al. 2004) and the sedimentation rate is relatively less than in the northern Bay (Symphonia and Nathan 2018). Based upon the numerical abundance of bryozoan species belonging to different morphotypes, the nature of the available substrate associated with different depths has a pronounced effect on the colonial forms of bryozoans found in the Chennai–Cuddalore shelf. The most common morphotypes, such as Cellariiform, Lunulitiform, Setoselliniform and Membrani-poriform, indicate that their growth patterns are influenced by the high-energy, turbulent conditions in the inner shelf and calm environments in the middle and outer-shelf regions, respectively (Cook 1981). Moreover, the slight variations in temperature, salinity and pH in this region do not appear to influence the distribution of habitat-forming bryozoans.

5 Conclusions

The presence of predominantly erect, flexible bryozoans in the inner-shelf sediments confirms the low sedimentation rates, relatively high-energy environments and the sandy

substrates availability. Encrusting bryozoans such as *Parasmittina spp.* were found in almost all the depths. Overall, the distribution of bryozoan fragments indicates the large-scale sediment transport and strong current activity in the near shelf setting and less dynamic conditions in the middle and outer-shelf region influence distribution of bryozoans in the southwestern Bay of Bengal.


References

- Cook, L.P.: The potential of minute colonies in the analysis of deep-sea sediments. *Cah. Biol. Mar.* **12**, 89–106 (1981)
- Flemming, B.W.: A revised textural classification of gravel-free muddy sediments on the basis of ternary diagrams. *Cont. Shelf Res.* **20**, 1125–1137 (2000)
- Gordon, D.P.: Bryozoan diversity in New Zealand and Australia. In: Ponder W., Luney D. (eds.) *The other 99%: The conservation and biodiversity of invertebrates*. Transactions of the Royal Zoological Society of New South Wales, Mosman (1999)
- Moissette, P., Dulai, A., Escarguel, G., Kázmer, M., Müller, Pal and Martin, S.J-P.: Mosaic of environments recorded by bryozoan faunas from the Middle Miocene of Hungary. *Palaeogeography, Palaeoclimatology, Palaeoecology*, **252**, 530–556 (2007)
- Pejrup, M.: The triangular diagram used for classification of estuarine sediments: a new approach. In: de Boer, P.L., van Gelder, A., Nio, S.D. (eds.) *Tide-influenced sedimentary environments and facies*. Reidel, Dordrecht (1988)
- Reineck, H.E., Siefert, W.: Faktoren der Schlickbildung im Sahlenburger Watt und Neuwerker Watt. *Die Kuste* **35**, 26–51 (1980)
- Rodolfo-Metalpa, R., Lombardi, C., Cocito, S., Hall-Spencer, J.M., Gambi, M.C.: Effects of ocean acidification and high temperatures on the bryozoan *Myriapora truncata* at natural CO₂ vents. *Mar. Ecol.* **31**, 447–456 (2010)
- Selvaraj, K., Ram Mohan, V., Szefer, P.: Evaluation of metal contamination in coastal sediments of the Bay of Bengal, India: geochemical and statistical approaches. *Mar. Pollut. Bull.* **49**(3), 174–185 (2004)
- Symphonia, T., Nathan, S.D.: Geochemistry and distribution of sediments in the East Indian shelf, SW Bay of Bengal: Implications on weathering, transport and depositional environment. *J. Earth Syst. Sci.* **127**, 1–18 (2018). <https://doi.org/10.1007/s12040-018-0999-z>

**Biogeochemistry, Geobiology, Geoecology,
Geoagronomy (T2): Phytoecological Studies**



Pre- and Post-reclamation Land-Use Change and Its Ecological Effects: A Case Study of Pan'an Lake, Xuzhou, East China

Zhiqiang Wang, Long Li , Ting Zhang, Longqian Chen, Ruiyang Liu, and Ziqi Yu

Abstract

Human-induced land-use change has a profound impact on the eco-environment, and a good example is Pan'an Lake in the east Chinese city of Xuzhou where massive land reclamation was conducted over the past years. This study characterized the pre- and post-reclamation land-use change by the transfer matrix method and the resulting evolution of ecosystem services value (ESV) by the equivalent value method. Results show clear changes in both land use and the ESV during different stages. During the 2005–2010 period, coal mining caused much land subsidence and loss of arable land, thus a significantly reduced ESV. During the 2010–2015 period, because of land reclamation projects, land-use pattern changed drastically. The newly reclaimed arable land has made up for the loss of arable land, and the ESV increased considerably. During the 2015–2018 period, increasing arable land appeared and the long-term benefits of land reclamation gradually became prominent. This study revealed that the self-regulation of the ecosystem and human protection greatly contribute to the increasing ESV.

Keywords

Land reclamation • Land use • Ecosystem services value • Pan'an Lake • Xuzhou

1 Introduction

Land use has always been a hot topic because it is not only a complex process but it may also exert a variety of effects on the eco-environment. Human activity is a dominant factor in land-use change in populated and industrialized regions, such as mining areas. Land may be exploited for mining initially and then reclaimed afterward—the consequent effects of such land-use change on the ecosystem are profound (Arar and Chenchouni 2012; Gaglio et al. 2017). In China, a growing number of coal mines are being closed and previously destroyed land is being restored through land reclamation projects. Much of the land is converted into usable land such as arable land, grassland, and water bodies. It is, therefore, important to assess whether such projects are beneficial to the eco-environment. In this study, we examined land-use change and estimated the value of ecosystems services (ESV) before and after land reclamation. The objective of this study was to provide an understanding of how human-induced land-use change impacts the eco-environment.

2 Data and Method

We selected Pan'an Lake, located in the east Chinese city of Xuzhou, as the study area (Fig. 1). This area was affected by land subsidence in a coal mine and has now become a national wetland park (known as Pan'an Lake National Wetland Park). The timeline detailing the transformation of Pan'an Lake is shown in Table 1.

Image data used for mapping land use were downloaded from Google Earth. The spatial resolution of these data was 0.3 m, allowing manual vectorization at high accuracy. They were all imaged in the winters of 2005, 2010, 2015, and 2018. As such, seasonal variability is thus minimized, and more importantly, land-use maps before and after land reclamation could be produced.

Z. Wang · L. Li (✉) · T. Zhang · L. Chen · R. Liu · Z. Yu
School of Public Policy & Management, China University
of Mining and Technology, Xuzhou, 221116, China
e-mail: long.li@cumt.edu.cn

L. Li
Department of Geography and Earth System Science,
Vrije Universiteit Brussel, 1050 Brussels, Belgium

Fig. 1 Geographical location of the study area

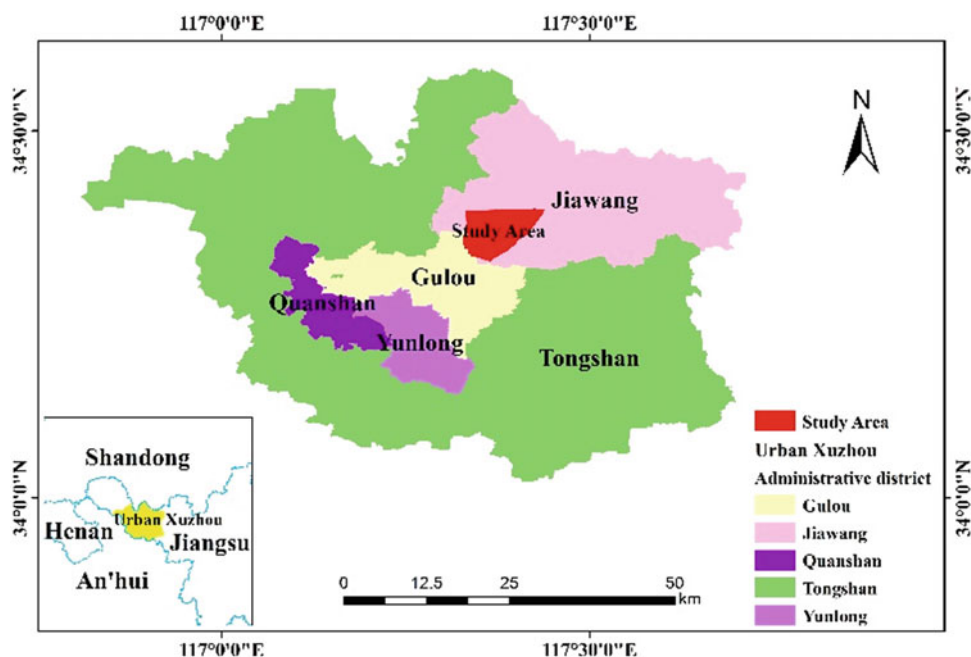


Table 1 Timeline of Pan'an Lake

Time	Event
December 2005	Land subsidence in a coalmine
February 2010	The work on restoring destroyed land began
December 2011	The wetland park landscape planning was approved
April 2012	The work on constructing the wetland park began
October 2012	The wetland park opened
Fall 2013	The work on extending the wetland park began
May 2014	The extended area of the wetland park started to operate
December 2015	The work was almost completed

As above-mentioned land-use maps of the study area were created (Fig. 2) through manually vectorizing the multitemporal Google Earth data. In total, eight different land-use types were considered (see legend in Fig. 2). Use of transfer matrices (not presented due to limited space) was made to analyze the land-use change over time (Zhu and Li 2003).

We assessed the service values (ESV) by revising the method of equivalence factor per unit area (Zhang et al. 2010; Xie et al. 2015), and then calculating the land use-specific ESV and overall ESV before and after land reclamation.

3 Results

After producing land-use transfer matrices based on the land-use maps, we plotted the land-use change over the 2005–2018 period (Table 2). It is clear that arable land was the main land-use type, first decreasing and then increasing.

The wetlands area continued to increase by 1575.35% over the 13 years, particularly after land reclamation.

The ESV of Pan'an Lake for each period is given in Fig. 3. The overall ESV increased by 43.71% in 13 years, particularly after land reclamation. This reveals the short- and long-term ecological effect of land reclamation on the eco-environment.

4 Discussion

During the 2005–2010 period (i.e., before land reclamation), due to the collapse of coal mining and the large reduction of arable land, the overall ESV of the study area decreased drastically. During the 2010–2015 period, land reclamation projects contributed to the change in land-use pattern. As the area of the reclaimed arable land made up for the reduction of arable land and the reclaimed wetland and unused land increased, the ESV increased significantly. During the 2015–2018 (i.e., after land reclamation),

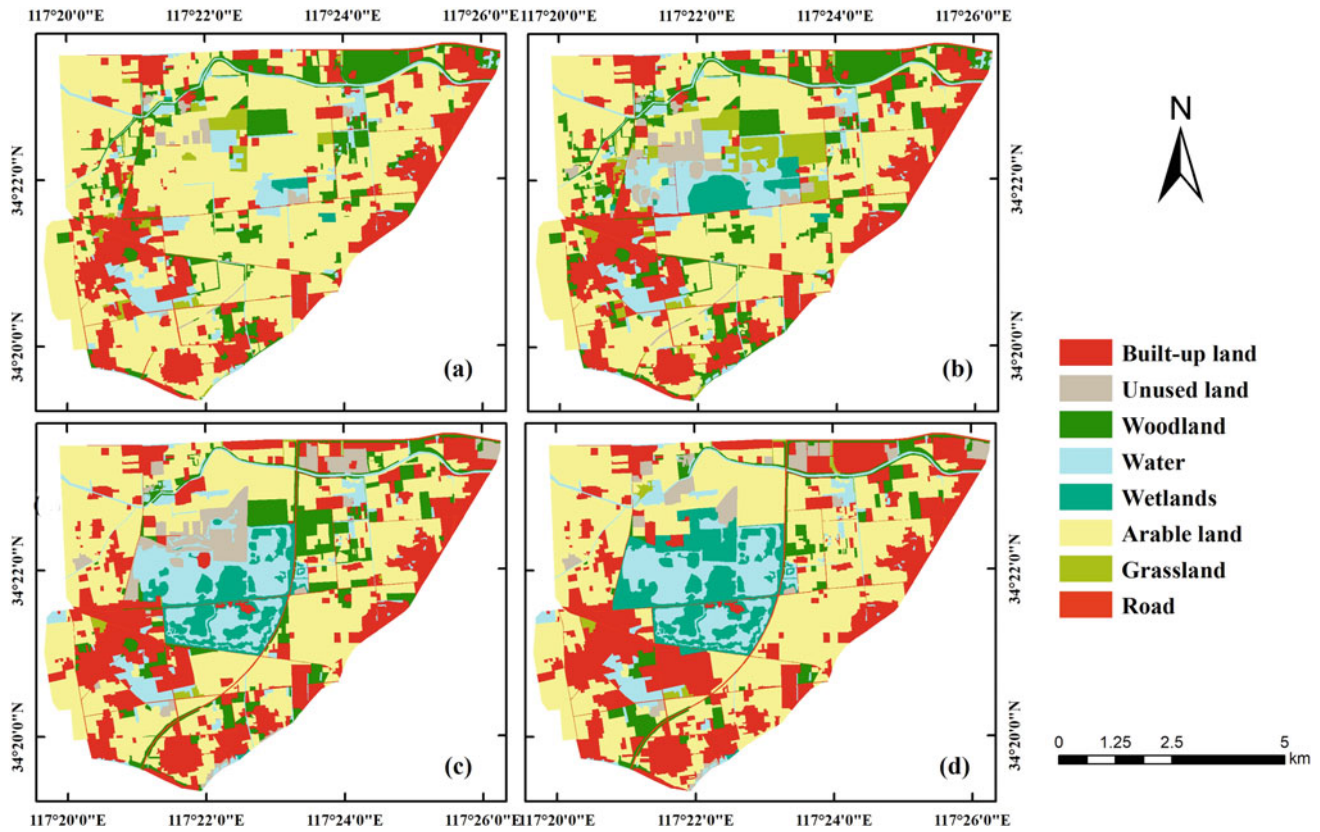


Fig. 2 Land-use maps in **a** 2005; **b** 2010; **c** 2015; and **d** 2018

Table 2 Land-use change over the 2005–2018 period

Time	Area (hectare)				Long-term rate of change (%)			
	2005	2010	2015	2018	2005–2010	2010–2015	2015–2018	2005–2018
Grassland	109.69	245.40	22.42	32.46	+123.72%	−90.87%	+ 44.79%	−70.41%
Road	67.57	69.66	94.36	91.28	+3.09%	+ 35.46%	−3.26%	+ 35.09%
Arable land	3064.58	2388.41	2218.46	2329.70	−22.06%	−7.12%	+5.01%	−23.98%
Built-up land	1068.11	1123.68	1245.32	1336.02	+5.20%	+10.82%	+7.28%	+25.08%
Woodland	568.98	658.79	487.23	269.76	+15.78%	−26.04%	−44.63%	−52.59%
Wetlands	28.60	145.13	300.42	479.21	+407.39%	+106.99%	+59.52%	+1575.35%
Water	378.34	535.77	664.93	638.02	+41.61%	+24.11%	−4.05%	+68.64%
Unused land	62.82	181.87	315.58	172.25	+189.49%	+73.52%	−45.42%	+174.18%

because of the land reclamation long-term benefits, some unused land gradually changed into arable land, and the ESV increased greatly.

5 Conclusions

While coal mining caused much land subsidence and loss of arable land, the ESV was obviously reduced, and the land reclamation changed the pattern of land use by

providing new arable land and wetland, which increased the ESV significantly. From our field verification, Pan'an Lake is a successful case in China. For coal-mining subsidence, therefore, there is no doubt that land reclamation has considerable influence on the ecosystem, and the long-term benefits of land reclamation are gradually becoming prominent. The government could reclaim subsidence-affected mining land into wetland or arable land in the future, which will benefit the eco-environment.

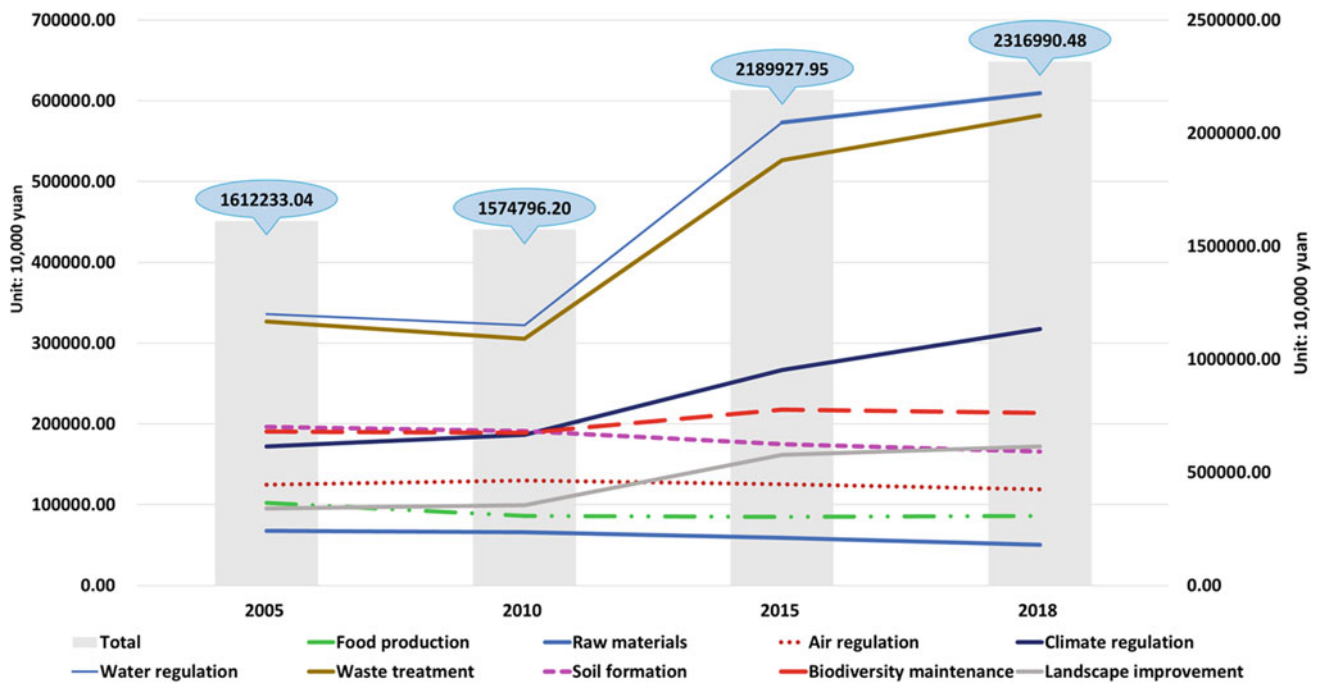


Fig. 3 ESV change over the 2005–2018 period (currency: CNY)

References

- Arar, A., Chenchouni, H.: How could geomatics promote our knowledge for environmental management in Eastern Algeria?. *J. Environ. Sci. Technol.* **5**(5), 291–305 (2012). <https://doi.org/10.3923/jest.2012.291.305>
- Gaglio, M., et al.: Land Use Change Effects on Ecosystem Services of River Deltas and Coastal Wetlands: A Case Study in Volano–Mesola–Goro in Po River Delta (Italy). *Wetlands Ecol. Manag.* **25**, 67–86 (2017). <https://doi.org/10.1007/s11273-016-9503-1>
- Xie, G.D., et al.: The value of ecosystem services in China. *Res. Sci.* **37** (09), 1740–1746 (2015)
- Zhang, B.A., Li, W.H., Xie, G.D.: Ecosystem services research in china: progress and perspective. *Ecol. Econ.* **69**(7), 1389–1395 (2010). <https://doi.org/10.1016/j.ecolecon.2010.03.009>
- Zhu, H.Y., Li, X.B.: Discussion on the index method of regional land use change. *Acta Geogr. Sin.* **57**(5), 643–650 (2003)



Effects of Sand Encroachment on Vegetation Diversity in the Sahara Desert

M'hammed Bouallala[✉], Lyès Bradai, and Haroun Chenchouni[✉]

Abstract

This study aimed at investigating the effect of sand encroachment on plant biodiversity of desert pavements, called 'Reg' at the region of El-Guerrara in Ghardaia (Sahara Desert of Algeria). A total of 15 floristic surveys were performed in three sites representing desert pavements 'Reg' with different levels of sand encroachment (low, medium, high), with five replicates. In each sample-plot (100 m²), the number of individuals 'density' of every plant species identified was determined. Plant community of desert pavements included 19 plant species classified into 18 genera and 13 families, with Asteraceae and Poaceae the most important families. The species *Anabasis articulata* characterized low sand encroachment desert totaling eleven species, whereas *Thymelaea microphylla* and *Genista saharae* are the characteristic species of deserts with moderate (14 species) and high (10 species) level of sand encroachment, respectively. The highest values of species richness and biodiversity were recorded in sites with moderate sand encroachment.

M. Bouallala (✉)
Laboratoire Ressources Naturelles Sahariennes,
Faculty of Sciences and Technology, University of Ahmed Draia,
01000 Adrar, Algeria
e-mail: alim39hammed@yahoo.fr

L. Bradai
Laboratoire Bio-ressources Sahariennes: Préservation et
Valorisation, Faculty of Natural and Life Sciences,
University of Kasdi Merbah, 30000 Ouargla, Algeria

H. Chenchouni (✉)
Department of Natural and Life Sciences, Faculty of Exact
Sciences and Natural and Life Sciences, University of Tebessa,
12002 Tebessa, Algeria
e-mail: chenchouni@gmail.com

H. Chenchouni
Laboratory of Natural Resources and Management of Sensitive
Environments 'RNAMS', University of Oum-El-Bouaghi,
04000 Oum-El-Bouaghi, Algeria

H. Chenchouni
Higher National School of Forests, 40000 Khenchela, Algeria

Conversely, lower values of these ecological parameters were obtained in Reg with high sand encroachment. Desert pavements with low sand encroachment levels were characterized with the highest values of species abundances. High sand encroachment intensity of desert habitats favors the degradation of vegetation cover and triggers biodiversity erosion.

Keywords

Desert pavements • Hot arid rangelands • Plant diversity • Land degradation • Sand encroachment • Sahara

1 Introduction

The Sahara is the largest desert worldwide but also the most expressive and typical for its extreme aridity. This ecoregion is characterized by prolonged periods of drought and special flora with remarkable adaptations (Ozenda 1991). Several landscapes exist in the Sahara, among which the desert pavement also called 'Reg' is the most widespread. According to Parsons and Abrahams (2009), a desert pavement is a flat desert surface covered with closely packed, interlocking angular or rounded rock fragments of pebble and cobble size. The flora of the Saharan habitats has been studied by Chehma (2005) and Bouallala (2013) to assess the carrying capacity of camel rangelands. However, sand encroachment and land degradation of these rangelands represent a serious challenge to ensure the sustainability of the ecosystem functioning. Sand encroachment is the consequence of a complex phenomenon resulting from multiple causes and manifests in different ways; including sand tearing, Aeolian transportation, deposit and accumulation to build different forms of dunes (FAO 2014). Like natural factors, anthropogenic perturbations contribute to aggravate the consequences of sand encroachment in hot deserts. Land

degradation of rangelands is observed in the form of biodiversity loss of plants with multiple uses (medicinal, food, forage, energy, industrial, etc.), knowing that hundreds of hectares of land are lost each year due to climate change and droughts and/or poor land management practices such as overgrazing and the transformation of natural vegetation

into agricultural lands (Neffar et al. 2013, 2018; Kouba et al. 2021; Merdas et al. 2021). Within this context, the current survey studied the effect of sand encroachment on the vegetation of desert pavements at El-Guerrara (Ghardaia, Algeria) through the evaluation and comparison of plant biodiversity between different levels of sand encroachment.

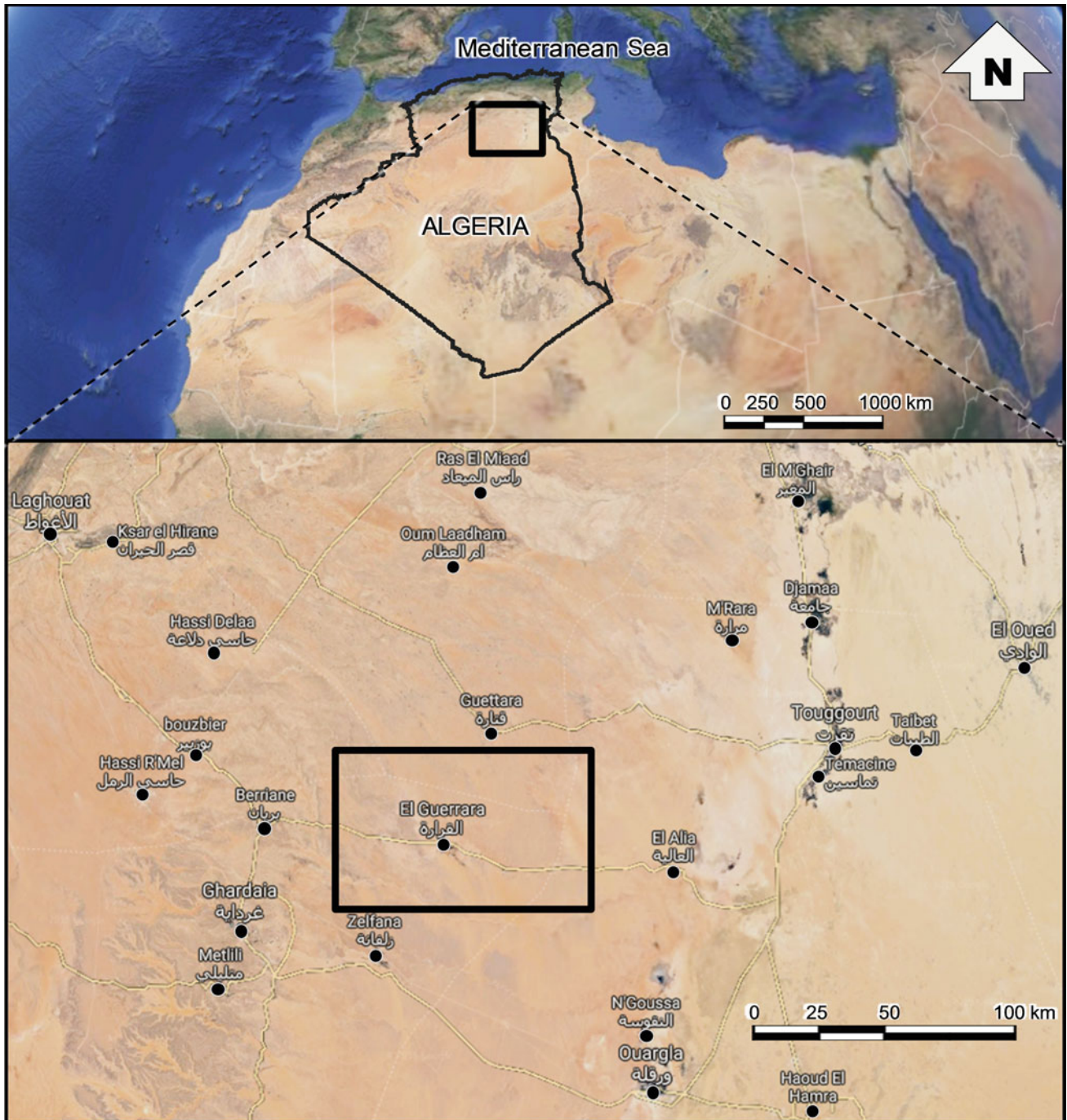


Fig. 1 Map displaying location of the study area at the region of El-Guerrara near the Wilaya 'Province' of Ghardaia in the Sahara Desert of Algeria

2 Materials and Methods

2.1 Study Area

The region of El-Guerrara is located 115 km northeast of the Wilaya ‘Province’ of Ghardaia (Sahara Desert of Algeria) (Fig. 1). The climate of this region is hyper-arid (De Martonne aridity index = 1), where the dry season lasts all the year. The annual rainfall totals 40 mm with precipitation deficit of 1639 mm/year. The coldest month is January (min temperature = 4.4 ± 3.2 °C) and the warmest month is July (max temperature = 42.7 ± 4.6 °C) (Guemmaz et al. 2019). The main agricultural activity in this Saharan region is date palm cultivation (Mihi et al. 2019a) and recently other vegetables in the understory of date palm oasis.

2.2 Plant Data Collection and Analysis

Spontaneous wild plants were sampled within three desert pavements ‘Reg,’ representing different levels of sand encroachment (low, medium, and high) at El-Guerrara. The sampling took place during the period of optimal vegetation development (February–April) of 2015, with five replicates per site. In each sample-plot, the number of individuals

‘density’ of each plant species identified was determined in an area of 100 m² (10 m × 10 m) (Chehema 2005; Bouallala 2013). Species identification followed Quézel and Santa (1962, 1963).

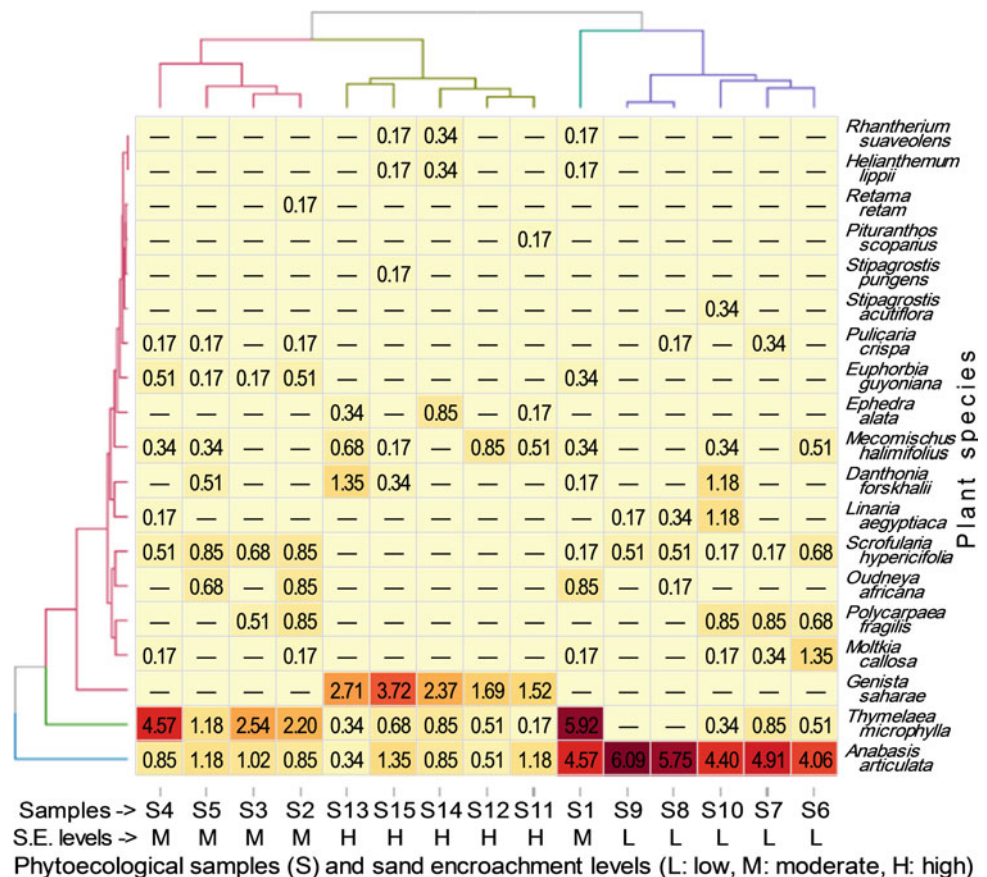
The sample-based data served for computing some alpha-biodiversity estimates (Azizi et al. 2021; Bradai et al. 2015): (i) total number of individuals (*N*) of all species abundances (*n_i*) pooled, (ii) species richness (*S*), (iii) Shannon diversity index (*H*), $H = -\sum((n_i/N) \times \log_2(n_i/N))$. *H* values are the highest when species of the community have the same relative abundance (RA), and (iv) and maximum of Shannon diversity (*H_{max}*), where $H_{max} = \log_2(S)$. The variation in values of *N*, *S*, *H* and *H_{max}* between site sand encroachment levels was tested using non-parametric one-way Kruskal–Wallis test (Chenchouni 2014). Beta-biodiversity was compared between these desert pavements using a Venn diagram.

3 Results

3.1 Flora Composition and Phytocological Groups

The flora of the desert pavements ‘Reg’ invaded with sand in the region of El-Guerrara included 19 plant species classified

Fig. 2 Heatmap with two-way clustering analysis of plant communities sampled in desert pavements of the region of El-Guerrara in the Algerian Sahara Desert. Clustering was performed using absolute species abundances, whereas figures associated to color intensity and displayed in the plot are relative abundances in percent



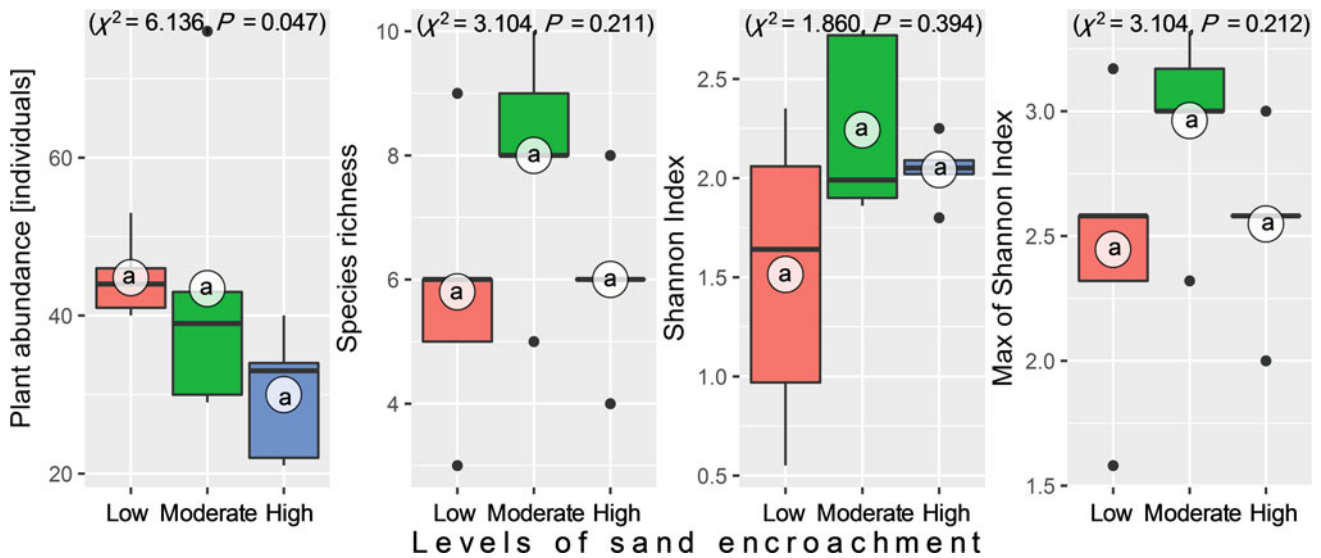


Fig. 3 Variation of plant diversity parameters for different levels of sand encroachment in desert pavements of the region of El-Guerrara, Sahara Desert of Algeria. Small letters associated to white circles (averages) represent results of Tukey post hoc tests. Black circles are outliers

into 18 genera and 13 families, where the most important were Asteraceae and Poaceae. The double clustering analysis associated to heat map plot showed that this flora consisted of three distinct phytoecological groups, which were linked to the three levels of sand encroachment (Fig. 2): (i) the first group included samples of moderate sand encroachment that were characterized by the high relative abundances 'RA' of *Thymelaea microphylla*, (ii) the second group included high sand encroachment samples, which were characterized by the high RA of *Genista saharae*, and (iii) the third group included low sand encroachment samples and one sample with moderate level, which all have *Anabasis articulata* as the characteristic species (RA ranged between 4.1 and 6.1%).

3.2 Plant Diversity Patterns

Species abundances decreased significantly with the increase of sand encroachment intensity in the habitat (Kruskal–Wallis test: $\chi^2 = 6.136, P = 0.047$). Desert pavements with low level of sand encroachment averaged 44.8 ± 5.17 individuals/100² (range: 40–53), whereas plant density observed in sites with moderate and high sand encroachment averaged 43.4 ± 19.17 individuals (range: 29–76) and 30 ± 8.22 individuals (range: 21–40), respectively (Fig. 3). Species richness, Shannon index, and maximum diversity did not vary between the studied sites (Kruskal–Wallis test: $P > 0.05$). Values of these parameters were slightly higher in desert pavement with moderate sand encroachment ($S = 8 \pm 1.87$ species, $H = 2.24 \pm 0.45$) compared to sites with high ($S = 6 \pm 1.41$ species, $H = 2.04 \pm 0.16$) and low

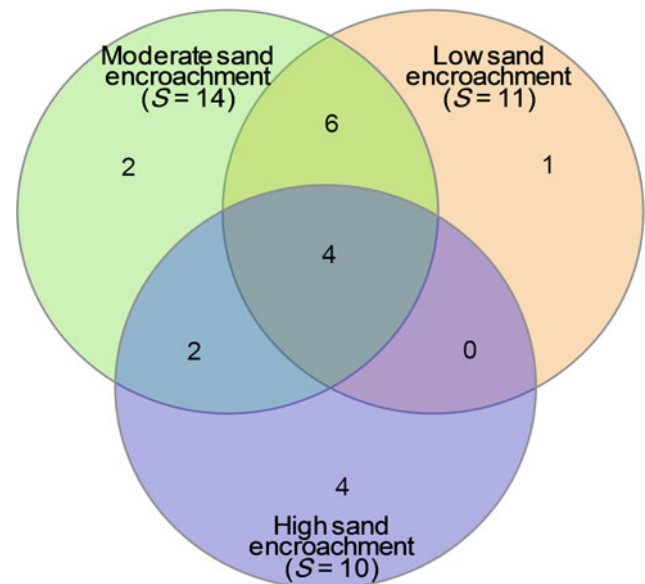


Fig. 4 Three-set Venn diagram displaying plant species richness (S) recorded for different levels of sand encroachment in desert pavements of the region of El-Guerrara, Wilaya of Ghardaia, Sahara Desert of Algeria

levels, which recorded the lowest values ($S = 5.8 \pm 2.17$ species, $H = 1.51 \pm 0.75$).

3.3 Species Richness Partitioning

Desert pavements with moderate sand encroachment recorded numerous species ($S = 14$), whereas sites with high level of sand encroachment recorded the lowest

species richness ($S = 10$). Similarity, the analysis among sites showed the existence of generalist species (i.e., common for all Reg) viz. *Anabasis articulata*, *Mecomis-chus halimifolius*, *Danthonia forskhalii*, and *Thymelaea microphylla*. The Venn diagram revealed that desert pavements with moderate sand encroachment have six and two species exclusively common with sites of low and high sand encroachment, respectively. No common species were observed exclusively between these sites (low and high levels) (Fig. 4). Desert pavements with low sand encroachment level had only one exclusive species (*Stipagrostis acutiflora*), while two (*Euphorbia guyoniana* and *Retama retam*) and four (*Ephedra alata*, *Genista saharae*, *Pituranthos scoparius*, and *Stipagrostis pungens*) plant species were observed solely in sites with moderate and high sand encroachment, respectively.

4 Discussion

Our findings showed the dominance of plant species belonging to Asteraceae and Poaceae in desert pavements invaded with sands. This taxonomic pattern was reported in other Saharan habitats, including the Reg, of Algeria (Chehma 2005; Chenchouni 2012; Bouallala 2013; Bradai et al. 2015). Although desert pavements stretch over vast areas, they have low biodiversity and high homogeneity of landscape and sparse vegetation. However, low levels of sand encroachment can increase plant species richness and diversity of the Reg, as observed in sites with moderate sand encroachment. However, high species abundances were recorded in low level of sand encroachment. This can be explained by the positive effect of sand encroachment at low level, i.e., superficial and thin sand encroachment does not have a negative effect that can induce significant degradation of the specialized vegetation established on the desert pavements and Saharan rangelands. Indeed, desert pavements with high level of sand encroachment recorded the lowest values of species abundance and diversity. When sand encroachment is important, several species cannot tolerate these new conditions, resulting in the decrease of the overall vegetation cover of rangelands as a consequence of the decrease in the number of individuals of dominant species (Abd El-Ghani et al. 2017). Dune accumulations resulting from Aeolian movements of the loose part of the soil constitute a permanent threat for the vegetation of hot deserts and rangelands (Mihi et al. 2019b). Sand dune is an environment that provides difficult planting, growth, and survival conditions for most plant species, except for psammophytes and stress-tolerant species (Ferchichi 1996).

5 Conclusion

The level and intensity of sand encroachment in hot desert habitats influence vegetation cover, species richness and community diversity. High sand encroachment levels in the Saharan regions can trigger long-lasting and severe land degradation resulting in the loss of plant and animal biodiversity. The degradation of native vegetation fixing loess habitats of the Saharan regions causes accumulations of sand on different types of desert rangelands. High risk of plant biodiversity loss in the fragile Saharan ecosystems is positively linked to the magnitude and intensity of sand encroachment. Under such conditions, restoration and rehabilitation of degraded lands through operations of planting and dune fixation operations are necessary.

References

- Abd El-Ghani, M.M.A., Huerta-Martínez, F.M., Hongyan, L., Qureshi, R.: Plant Responses to Hyperarid Desert Environments. Springer, Cham (2017). <https://doi.org/10.1007/978-3-319-59135-3>
- Azizi, M., Chenchouni, H., Belarouci, M.E.H., Bradai, L., Bouallala, M.: Diversity of psammophyte communities on sand dunes of the Sahara Desert. J. King Saud Univ. Sci. **33** (8), 101656 (2021). <https://doi.org/10.1016/j.jksus.2021.101656>
- Bouallala, M.: Etude floristique et nutritive spatio-temporelle des parcours camelins du Sahara Occidental Algérien: Cas des régions de Béchar et Tindouf. PhD thesis, Univ. Ouargla, Algeria (2013)
- Bradai, L., Bouallala, M., Bouziane, N.F., Zaoui, S., Neffar, S., Chenchouni, H.: An appraisal of eremophyte diversity and plant traits in a rocky desert of the Sahara. Folia Geobot. **50**, 239–252 (2015). <https://doi.org/10.1007/s12224-015-9218-8>
- Chehma, A.: Etude floristique et nutritive spatio-temporelle des parcours camelins du Sahara septentrional algérien. Cas des régions de Ouargla et Ghardaia. Doctoral thesis, Univ. Annaba, Algeria (2005)
- Chenchouni, H.: Diversité floristique d'un lac du Bas—Sahara algérien. Flora diversity of a lake at Algerian Low-Sahara. Acta Bot. Malacitana **37**, 33–44 (2012). <https://doi.org/10.24310/abm.v37i0.2664>
- Chenchouni, H.: Diet of the little owl (*Athene noctua*) during the pre-reproductive period in a semi-arid Mediterranean region. Zool. Ecol. **24**, 314–323 (2014). <https://doi.org/10.1080/21658005.2014.965919>
- FAO: Manuel de formation à la lutte contre la désertification, la fixation des dunes et la gestion des boisements en Mauritanie. 2nd Edition, FAO, MEDD, APEFE, Nouakchott (2014)
- Ferchichi, A.: Essai de fixation biologique des dunes en Tunisie présaharienne. In: Proceedings du Séminaire la lutte contre l'ensablement et la stabilisation des dunes. Médenine, Tunisia. Printed by ISESCO, Rabat, Morocco, pp. 165–174 (1996)
- Guemmaz, F., Neffar, S., Chenchouni, H.: Physicochemical and bacteriological quality of surface water resources receiving common wastewater effluents in drylands of Algeria. In: Negm, A., Bouderbala, A., Chenchouni, H., Barcelo, D. (eds). Water Resources in Algeria: Part II: Water Quality, Treatment, Protection and Development. Springer, Cham (2019). https://doi.org/10.1007/698_2019_400

- Kouba, Y., Merdes, S., Mostephaoui, T., Saadali, B., Chenchouni, H.: Plant community composition and structure under short-term grazing exclusion in steppic arid rangelands. *Ecol. Indic.* **120**, 106910 (2021). <https://doi.org/10.1016/j.ecolind.2020.106910>
- Merdas, S., Kouba, Y., Mostephaoui, T., Farhi, Y., Chenchouni, H.: Livestock grazing-induced large-scale biotic homogenization in arid Mediterranean steppe rangelands. *Land Degrad. Dev.* **32**(17), 5099–5107 (2021). <https://doi.org/10.1002/ldr.4095>
- Mihi, A., Nacer, T., Chenchouni, H.: Monitoring dynamics of date palm plantations from 1984 to 2013 Using Landsat Time-Series in Sahara Desert Oases of Algeria. In: El-Askary, H.M. et al. (eds.) *Advances in Remote Sensing and Geo Informatics Applications*. pp. 225–228. Springer, Netherlands (2019a). https://doi.org/10.1007/978-3-030-01440-7_52
- Mihi, A., Tarai, N., Chenchouni, H.: Can palm date plantations and oasisification be used as a proxy to fight sustainably against desertification and sand encroachment in hot drylands? *Ecol. Indic.* **105**, 365–375 (2019b). <https://doi.org/10.1016/j.ecolind.2017.11.027>
- Neffar, S., Chenchouni, H., Beddiar, A., Redjel, N.: Rehabilitation of degraded rangeland in drylands by Prickly pear (*Opuntia ficus-indica* L.) plantations: effect on soil and spontaneous vegetation. *Ecologia Balkanica* **5**(2), 63–83 (2013)
- Neffar, S., Menasria, T., Chenchouni, H.: Diversity and functional traits of spontaneous plant species in Algerian rangelands rehabilitated with prickly pear (*Opuntia ficus-indica* L.) plantations. *Turk. J. Bot.* **42**(4), 448–461 (2018). <https://doi.org/10.3906/bot-1801-39>
- Ozenda, P.: *Flora and Vegetation of the Sahara*. CNRS, Paris (1991)
- Parsons, A.J., Abrahams, A.D. (eds.): *Geomorphology of Desert Environments*. Springer, Dordrecht (2009). <https://doi.org/10.1007/978-1-4020-5719-9>
- Quézel, P., Santa, S.: *Nouvelle flore de l'Algérie et des régions désertiques méridionales*, vol. 1. CNRS, Paris (1962)
- Quézel, P., Santa, S.: *Nouvelle flore de l'Algérie et des régions désertiques méridionales*, vol. 2. CNRS, Paris (1963)



Functional Diversity of Alpine Meadow Under Simulated Warming and Grazing

Zhonghua Zhang, Li Ma, Bingrong Zhou, and Huakun Zhou

Abstract

The response of biodiversity and biological function under global change has been a hot spot of ecological research in recent years. We selected seven dominant species on a 6 years multi-gradient warming and simulated grazing interaction experimental platform in the alpine meadow of Qinghai-Tibet Plateau to determine the changes in functional diversity under warming and grazing. The results showed that the increase of temperature and its interaction with grazing significantly reduced functional richness and functional separation, whereas functional evenness did not change substantially; mild grazing had no significant effect on all functional diversity indices. There are interactions between functional traits, and the study of multiple traits included more information and more attention should be paid to this issue in future research.

Keywords

Qinghai-Tibet plateau • Functional diversity • Open top chamber • Simulated grazing • Alpine meadow

1 Introduction

The increasing impact of climate change and man-made activities on ecosystems have changed the structure and function of terrestrial ecosystems (Xu et al. 2018), and then affected biodiversity and ecosystem functions and their relationship. This trend is likely to be more intense in the future (Bellard et al. 2012). As the cornerstone of terrestrial ecosystems, plants are more affected. Plant functionality is closely related to the environment, plants, and ecosystems. On the other hand, it also reflects the response and adaptation of plants to environmental changes (Sun et al. 2017). The study of single trait may ignore some information, while functional diversity takes into account the species diversity and the multi-dimensionality of plant traits and will more accurately predict changes in ecosystem function and process than species diversity or plant traits (Lei et al. 2016; Kouba et al. 2021; Merdas et al. 2021). It is also a key driver of ecological processes, ecosystem resilience to environmental change, provides better solutions and explanations for the exploration of community structures and functions under global change (Legendre et al. 2010). As one of the most sensitive regions of global change, the interaction between climate change, fragile ecosystems, and human activities in Qinghai-Tibet Plateau and its response to climate change in this region or the world are of great importance in the field of ecological research.

2 Materials and Methods

This experimental research site is situated in the High Cold Meadow Ecosystem Positioning Station in Haibei, Qinghai Province, China. We used the Open Top Chamber (OTC, defined by the International Tundra Experiment) to simulate temperature increase. The OTC was established in 2012. The chamber set four specifications (A, B, C, and D) to simulate different temperature increase gradients; undisturbed

Z. Zhang · L. Ma · H. Zhou (✉)

Key Laboratory of Cold Regions Restoration Ecology, Qinghai Province, Northwest Institute of Plateau Biology, Chinese Academy of Sciences, Xining, 810008, China
e-mail: hkzhou@nwipb.cas.cn

B. Zhou

Qinghai Institute of Meteorological Science, Xining, 810001, China

Z. Zhang · L. Ma

University of Chinese Academy of Sciences, Beijing, 100049, China

meadows near OTC were randomly selected as control (CK), each treatment and control set 10 repetitions, with 5 replicates (repetitions 1, 3, 5, 7, 9). And mowing hay 50–70% of plot to simulated grazing when not regreened. The preliminary results showed that the effect of OTC was significant and proved a gradient change.

Data were collected in 2017–2018. The dominant species of *Kobresia humilis*, *Poa annua*, *Elymus nutans*, *Gentiana straminea*, *Saussurea pulchra*, *Medicago ruthenica*, and *Oxytropis ochrocephala* were selected as the measurement objects. And selective indicators we included biomass of individual species, plant height, leaf N content, specific leaf area, leaf thickness, leaf dry matter quality, plant phenology, and leaf chlorophyll relative content.

Three functional indicators were used to illustrate the functional diversity of plant communities: functional richness (Fric), functional evenness (Feve), and functional divergence (Fdiv). For a detailed description of these three functional indicators, see Mason et al. (2005).

Functional diversity was calculated using the FD-package package (Laliberté et al. 2014) in R (Version-3.5.2). The normality and variance homogeneity (Levene's test) were then tested at R (Version-3.5.2). Data that do not conform to normal distribution used the SPSS 24.0 as normal conversion (Rank cases). The variance analysis was used to test the difference of functional trait index between different species and different treatments. The LSD (least-significant difference) method was used to test the significance at the 95% confidence level.

3 Results

Functional richness and functional divergence were significantly affected by the increasing temperature (Table 1), while grazing did not significantly modify any functional diversity index, which may be due to the slight effects of simulated grazing in our experiment on plants. The interaction of increased temperature and grazing significantly changed the functional richness and functional divergence and had a small effect on the functional evenness.

The functional richness is very small, which may be one of the reasons of the vulnerability of the Qinghai-Tibet Plateau ecosystem. Functional evenness increases with the increasing temperature, while the functional divergence exhibits a hump curve change (Fig. 1).

By calculating the functional diversity of individual traits, we found that only the functional diversity of relative chlorophyll content, functional diversity of phenology, and functional diversity of leaf ammonium nitrogen were significantly different under warming. The functional diversity of other traits was not significantly different under warming, grazing, and their interaction. It is inconsistent with the results of the functional diversity index for the calculation of multiple traits, so there are trade-offs between multiple traits, which proves that we should pay more attention to the study of comprehensive traits.

The functional diversity of leaf thickness, single leaf mass, plant height, leaf N content (nitrate nitrogen, nitrite nitrogen, and ammonium nitrogen) increased slightly, and the functional diversity of other traits did not obviously

Table 1 ANOVA of functional diversity and its three components

Source of variance	Fric		Feve		Fdiv	
	<i>F</i>	<i>p</i>	<i>F</i>	<i>p</i>	<i>F</i>	<i>p</i>
W	26.046	0.000*	1.171	0.338	7.803	0.000*
G	0.029	0.865	0.093	0.762	2.463	0.124
W × G	29.296	0.000*	0.047	0.996	6.015	0.001*

*, $p < 0.05$. Fric: functional richness; Feve: functional evenness; Fdiv: functional divergence. W: warming; G: grazing. × : interaction

Table 2 ANOVA of functional diversity of single traits

Source of variance	FD _{LDM}	FD _{SLA}	FD _{LT}	FD _{RC}	FD _{SB}	FD _H	FD _P	FD _{nitrateN}	FD _{nitriteN}	FD _{aN}
	<i>p</i>	<i>p</i>	<i>p</i>	<i>p</i>	<i>p</i>	<i>p</i>	<i>p</i>	<i>p</i>	<i>p</i>	<i>p</i>
W	0.253	0.629	0.237	0.017*	0.125	0.161	0.013*	0.052	0.184	0.001*
G	0.431	0.082	0.119	0.734	0.729	0.885	0.184	0.091	0.476	0.202
W × G	0.162	0.998	0.624	0.154	0.230	0.819	0.140	0.799	0.472	0.149

*, $p < 0.05$. where FD_{LDM}, FD_{SLA}, FD_{LT}, FD_{RC}, FD_{SB}, FD_H, FD_P, FD_{nitrateN}, FD_{nitriteN}, FD_{aN} are functional diversity of leaf dry matter, specific leaf area, leaf thickness, leaf relative chlorophyll content, biomass of individual species, plant height, plant phenology, leaf nitrate nitrogen, leaf nitrite nitrogen, leaf ammonium nitrogen, respectively. W: warming; G: grazing; × : interaction

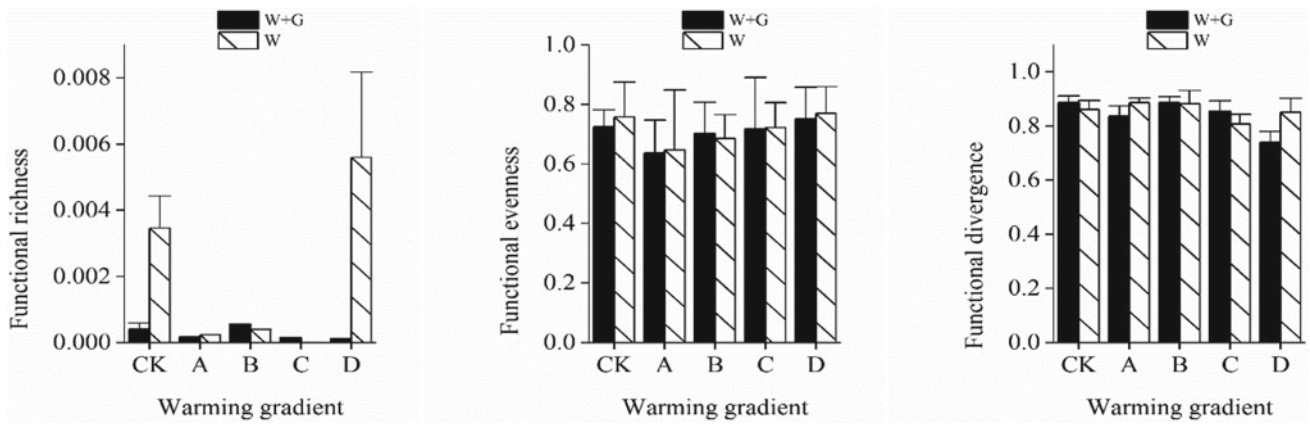


Fig. 1 Changes of functional diversity (CK: Control; A, B, C, D: Warming gradient from small to large; W + G: Warming and grazing; W: Warming)

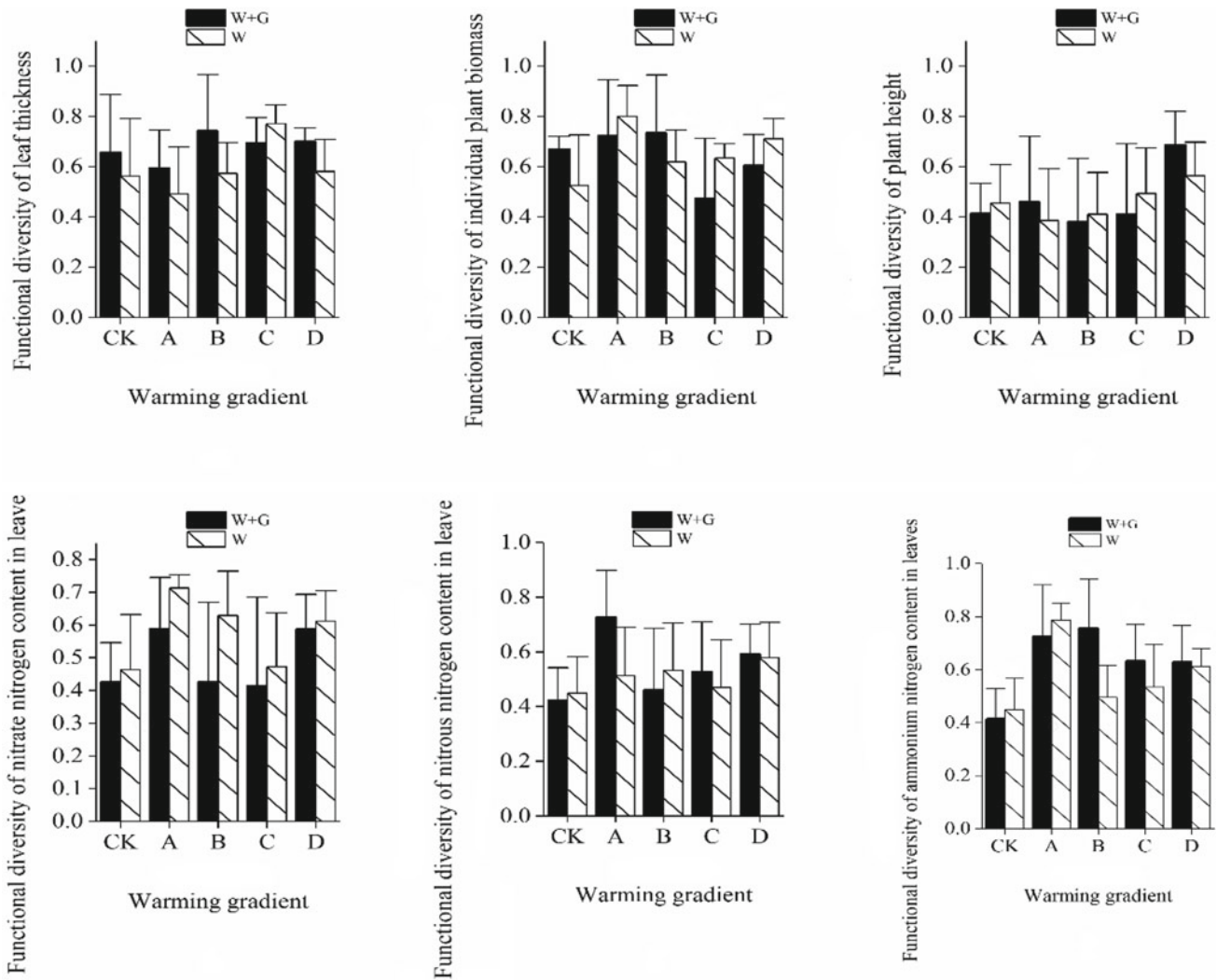


Fig. 2 Changes in functional diversity of single traits (CK: Control; A, B, C, D: Warming gradient from small to large; W + G: Warming and grazing; W: Warming)

change. Grazing did not significantly affect the functional diversity of individual traits, but it reduced the effect of warming on the functional diversity of single traits (Fig. 2).

4 Conclusion

The increase in temperature and its interaction with grazing significantly reduced the functional richness and functional divergence, and the functional evenness of the community did not change significantly; mild grazing had no significant effect on all functional diversity indices. There is a trade-off between plant traits, and multiple trait studies can show more ecosystem information.

Acknowledgements The study was financially supported by the National Key Research and Development Program of China (2016YFC0501901), National Natural Science Foundation of China (31672475), Natural Science Foundation of Qinghai Province of China (2019-ZJ-908, 2016-NK-A7-BA-02), Scientific Research and Promotion of the Second Phase Project of Ecological Protection and Construction of the Three Rivers Sources in Qinghai (2017-S-1).

References

- Bellard, C., Bertelsmeier, C., Leadley, P., et al.: Impacts of climate change on the future of biodiversity. *Ecol. Lett.* **15**(4), 365–377 (2012). <https://doi.org/10.1111/j.1461-0248.2011.01736.x>
- Kouba, Y., Merdes, S., Mostephaoui, T., Saadali, B., Chenchouni, H.: Plant community composition and structure under short-term grazing exclusion in steppe arid rangelands. *Ecol. Indic.* **120**, 106910 (2021). <https://doi.org/10.1016/j.ecolind.2020.106910>
- Laliberté, E., Legendre, P., Shipley, B., et al.: Package ‘FD’ [EB/OL]. (2014) [2019–06–20]. <ftp://137.208.57.37/pub/R/web/packages/FD/FD.pdf>
- Legendre, E., Legendre, P.: A distance-based framework for measuring functional diversity from multiple traits. *Ecology* **91**(1), 299–305 (2010). <https://doi.org/10.1890/08-2244.1>
- Lei, L.J., Kong, D.L., Li, X.M., et al.: Plant functional traits, functional diversity, and ecosystem functioning: current knowledge and perspectives. *Biodiversity Sci.* **24**(8), 922–931 (2016). <https://doi.org/10.17520/biods.2015295>
- Mason, N.W., Mouillot, D., Lee, W.G., et al.: Functional richness, functional evenness and functional divergence: the primary components of functional diversity. *Ecology* **1**, 112–118 (2005). <https://doi.org/10.1111/j.0030-1299.2005.13886.x>
- Merdes, S., Kouba, Y., Mostephaoui, T., Farhi, Y., Chenchouni, H.: Livestock grazing-induced large-scale biotic homogenization in arid Mediterranean steppe rangelands. *Land Degrad. Dev.* **32**(17), 5099–5107 (2021). <https://doi.org/10.1002/ldr.4095>
- Sun, M., Tian, K., Zhang, Y., et al.: Research on leaf functional traits and their environmental adaptation. *Plant Sci. J.* **35**(6), 940–949 (2017)
- Xu, Z.W., Li, M.H., Niklaus, Z.E., et al.: Plant functional diversity modulates global environmental change effects on grassland productivity. *J. Ecology* **106**(5), 1941–1951 (2018). <https://doi.org/10.1111/1365-2745.12951>



Meta-Analysis of the Response of Plant and Soil to Alpine Meadow Degradation

Yandi She, Dangjun Wang, Qian Zhang, and Huakua Zhou

Abstract

In this study, 145 data on alpine meadow plants and soils under different degradation gradients in different locations in the Qinghai-Tibet Plateau were selected for meta-analysis. With the worsening of degradation, plant biomass, height, coverage and species diversity is reduced, and the total nitrogen and phosphorus as well as the available nitrogen and phosphorus of soil nutrients are also reduced, but the bulk density and pH are increased. Based on the quantitative analysis results, the four degraded stages of the alpine meadow were compared, and the results would help to elucidate the alpine meadow degradation process and provide useful data for the restoration of these damaged meadows.

Keywords

Meta-analysis • Alpine meadow • Degree of degradation • Plant characteristics • Soil characteristics • Qinghai-Tibet plateau

Y. She · D. Wang · Q. Zhang · H. Zhou (✉)
Key Laboratory of Cold Regions Restoration Ecology,
Qinghai Province, Northwest Institute of Plateau Biology,
Chinese Academy of Sciences, Xining, 810008, China
e-mail: hkzhou@nwipb.cas.cn

D. Wang
Key Laboratory of Aquatic Botany and Watershed Ecology,
Wuhan Botanical Garden, Chinese Academy of Sciences,
Wuhan, 430074, China

Y. She · D. Wang · Q. Zhang
University of Chinese Academy of Sciences,
Beijing, 100049, China

1 Introduction

In recent years, meadow degradation caused by natural and human factors has become one of the key issues in the study of the Qinghai-Tibet Plateau. The grass resources over-consumption and the meadow ecosystem weakening have jeopardized the sustainable development of the plateau itself and its ecological environment. Therefore, analyzing the causes and effects of alpine meadows degradation is important for their treatment and restoration. Meta-analysis is widely used in the field of ecology (Tian et al. 2014; Jia 2009; Guo et al. 2009). This study used the meta-analysis to increase quantitative indicators on the basis of evaluation, reveal the characteristic changes and main driving factors of the different degradation stages of the alpine meadow, and determine the relationship between plant characteristics and soil quality, providing theoretical and scientific basis for meadow protection and management.

2 Materials and Methods

2.1 Data Sources and Processing

China national knowledge infrastructure and Web of Science used the following search terms: “different degradation gradients,” “alpine meadow” and “Qinghai-Tibetan plateau” and conducted literature search. The data for charts and graphs in the literature need to be extracted using Get Data Digitizer 2.24 software. Designed in Excel 2010 to match the data collection table format used in the integration analysis, the average and standard deviation of plant community and soil characteristics in different degradation gradients of non-degraded, lightly, moderately, highly and severely degraded meadows were all included. This study collected data on plant characteristics (biomass, coverage, height and species diversity) and soil characteristics (total nitrogen, total phosphorus, available nitrogen, available

phosphorus, bulk density and pH). In order to reduce the bias in the publication of meta-integrated analysis, the following requirements are necessary: (1) do not include macro-evaluation and overview articles; standard deviation or standard error (SD or SE) (Wei et al. 2018), the degree of degradation includes the non-degraded, lightly, moderately, highly and severely degraded gradients (NDG, LDG, MDG, HDG and SDG, respectively). (2) The sample time and number of experiment repetitions. (3) The processing group in the experiment should be basically the same as the test conditions of the control group. (4) In the description of plant community characteristics and soil properties of the indicator units must be consistent, and may also include the conversion of the consistent situation. (5) The scale of the meadow with different Degradation level shall meet certain standards (Lu 2015).

2.2 Meta-Analysis and Calculation Results

We used Meta Win 2.1 for consolidation analysis, then calculated the effect values, and plotted and related analysis using Sigma Plot 12.5 and Origin Pro 9.1. Since a large number of consolidation analyses were done by statistical software and the process is not visible, the main calculation parameters used in Meta-analysis are listed here as follows:

K: number of original studies; n: number of repetitions in the design of the original research experiment; SE: standard error; SD: standard deviation.

3 Results

The response of plant and soil in different degradation gradients of alpine meadows was expressed by their response ratio (RR) frequency distribution, and the values

between brackets in the figure were the percentage changes in the degradation variable relative to the un-degraded meadow, with the number next to each point being the sample size.

3.1 Plant Response to Meadow Degradation

The above ground biomass showed a downward trend with the degree of degradation. LDG, MDG, HDG and SDG decreased by 27.18%, 45.15%, 61.42% and 63.98%, respectively, compared to NDG, and the difference was statistically significant ($P < 0.05$). The below ground biomass showed a downward trend. LDG, MDG, HDG and SDG decreased by 19.37%, 27.34%, 63.06% and 79.12%, respectively, compared to NDG, and the difference was statistically significant ($P < 0.05$).

Among the plant characteristics of different degraded stages in alpine meadows, plant coverage, height, species uniformity, species richness and the Shannon Wiener Index are shown in Table 1 (Fig. 1).

3.2 Soil Response to Meadow Degradation

The changes of soil available nitrogen in different gradients of degradation of meadow: LDG, MDG, HDG and SDG decreased by 7.94%, 28.40%, 35.87% and 31.09%, respectively, compared to NDG, and the difference was statistically significant. The change of soil available phosphorus in different gradients of meadow degradation: MDG, HDG and SDG decreased by 8.69%, 28.01% and 20.21%, respectively, compared to NDG, and LDG increased by 1.58%.

The soil characteristics of different degraded stages of alpine meadow: the response of soil total nitrogen, total phosphorus, soil moisture, organic matter, bulk density and pH are shown in Table 2.

Table 1 The degree of response of plant characteristics to NDG to degradation gradients

Degradation gradient	VC		VH		J		R		H	
	<i>m</i> (%)	<i>n</i>	<i>m</i> (%)	<i>n</i>	<i>m</i> (%)	<i>n</i>	<i>m</i> (%)	<i>n</i>	<i>m</i> (%)	<i>n</i>
LDG	-12.62	78	-25.92	32	7.46	37	-5.49	39	3.21	41
MDG	-32.13	85	-47.59	31	-1.25	38	-12.54	46	-1.25	46
HDG	-53.25	77	-62.53	31	-1.62	38	-38.56	39	-12.03	44
SDG	-67.38	33	-70.59	15	-5.38	11	-61.04	9	-36.26	13
Total	-36.67	273	-48.30	109	1.00	124	-20.81%	133	-7.05	144

VC: vegetation coverage; VH: vegetation height; J: Species Evenness Index; R: Species Richness Index; H: Shannon Wiener Index; *m* represents the degree of response of plant characteristics to NDG under different degradation gradients; *n* represents the number of data sets, i.e., sample size of plant features in different degradation gradients in the data collected.

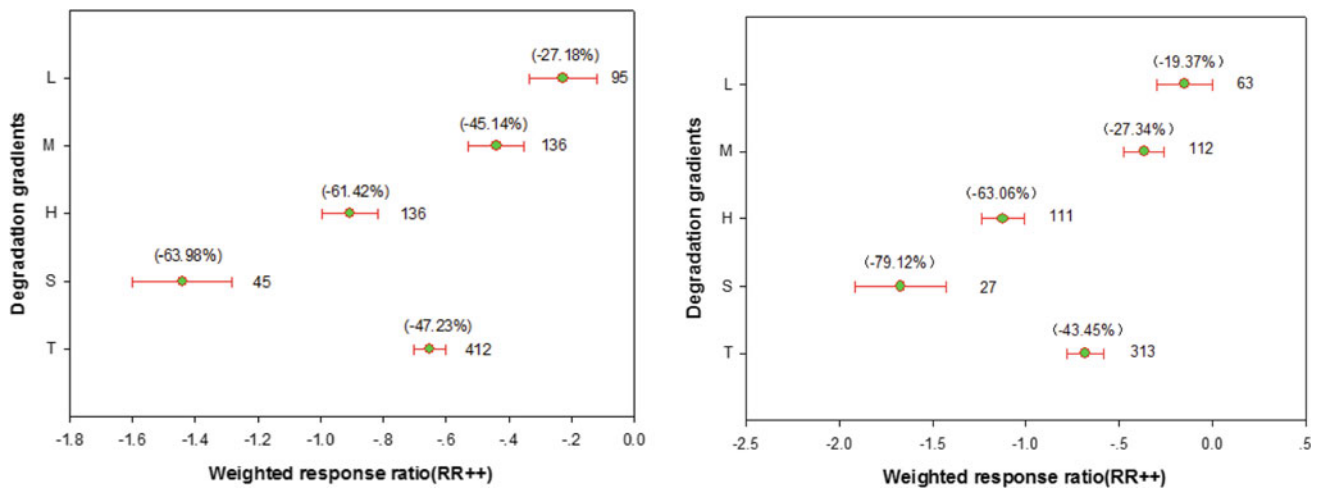


Fig. 1 Response of above- and below-ground biomass to degradation gradients (L—Light; M—Moderate, H—High, S—Severe, T—Total)

Table 2 The response degree of soil characteristics to NDG to degradation gradients

Degradation gradient	TN		TP		SM		SOM		BD		pH	
	m (%)	n	m (%)	n	m (%)	n	m (%)	n	m (%)	n	m (%)	n
LDG	-22.09	80	-10.28	39	-25.57	55	-17.76	53	12.12	46	6.17	40
MDG	-36.35	76	-31.97	36	-36.60	64	-25.62	75	18.10	89	4.84	41
HDG	-43.88	78	-30.40	48	-50.36	57	-52.97	71	32.09	65	11.85	41
SDG	-63.25	32	-44.34	17	-52.74	28	-76.46	29	47.50	25	19.09	18
Total	-37.97	266	-28.79	140	-39.95	204	-36.12	228	24.06	225	9.15	140

TN Total Nitrogen; TP Total Phosphorus; SM Soil Moisture; SOM Soil Organic Matter; BD Bulk Density

4 Discussion

In the mild degradation stage of alpine meadows, climate change or grazing factors cause changes in plant coverage and biomass. Vegetation coverage and biomass decline during periods of mild and severe degradation. With the worsening of the degradation degree, a series of processes, such as the transformation of the soil texture from cold and wet to warm and dry, leading to the decomposition and mineralization of organic matter, are gradually strengthened. Comprehensive data analysis shows the trend of coverage and biomass during the degradation of alpine meadows: from mild to extreme, it has been declining, but due to serious vegetation degradation, the decline trend is slow. The organic matter is drastically reduced and the soil is warm. Drying tends to slow down the decomposition of organic matter and gradually reduce plant processes. At the same time, soil nutrient change becomes the dominant process at

this stage, and the vegetation coverage is very low (Boudjabi and Chenchouni 2022). Under the natural process, the content of organic matter and minerals in the soil drops sharply. During the extreme degradation of alpine meadows on the Tibetan Plateau, soil nutrient loss increases the rate of vegetation degradation, which will make the recovery process of degraded meadows very difficult. These processes are likely to be a feedback mechanism that will accelerate the degradation of alpine meadow ecosystems (Lu 2015).

5 Conclusion

Using the meta-analysis method, we conducted a comprehensive analysis of a large number of observational data on plant and soil characteristics of alpine meadows in different degraded stages of the Qinghai-Tibet Plateau. The results showed that the main deduction at the early stage of degradation was the decrease of plant coverage, followed by

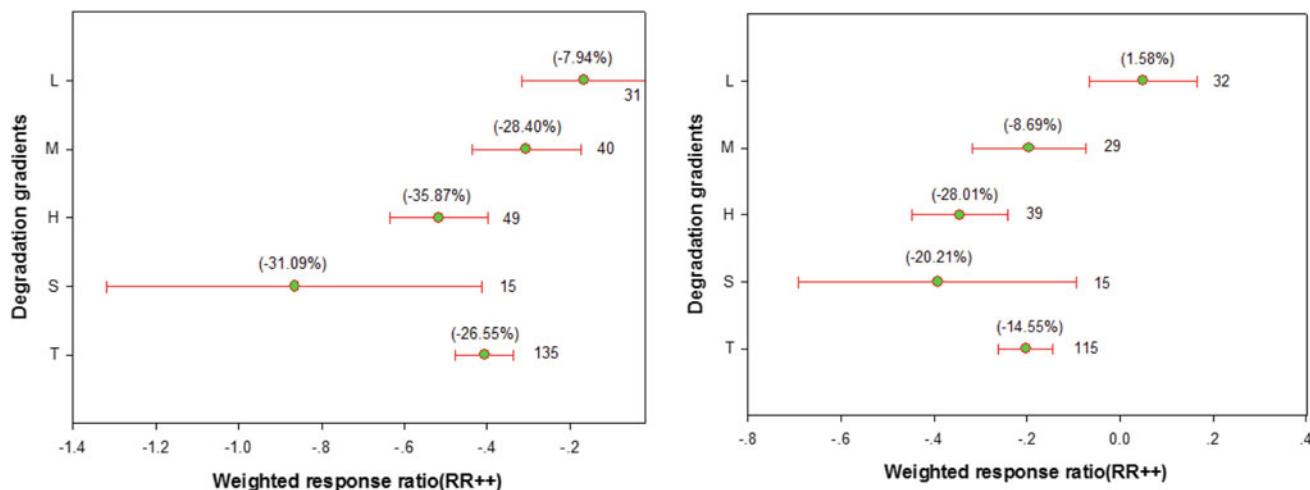


Fig. 2 Response of soil available nitrogen and available phosphorus to degradation gradients (L—Light; M—Moderate, H—High, S—Severe, T—Total)

the decrease of biomass. In the late stage of degradation, soil nutrient change became the dominant process. The plant characteristics changed, and the soil characteristics are also changed. The decline of vegetation coverage indicated that the meadow began to degenerate, and the loss of soil nutrients aggravated the process of meadow degradation. The research results will help our understanding of the degradation process and mechanism of alpine meadows. The understanding of scientific guidance will help for the implementation of restoration measures.

Acknowledgements The study was financially supported by the National Key Research and Development Program of China (2016YFC0501901), National Natural Science Foundation of China (31672475), Natural Science Foundation of Qinghai Province of China (2019-ZJ-908, 2016-NK-A7-BA-02), Qinghai innovation platform construction project (2017-ZJ-Y20, and the Science and Technology Service Network Initiative Project of Chinese Academy of Sciences (KFJ-STZ-ZDTP-036), Scientific Research and Promotion of the Second Phase Project of Ecological Protection and Construction of the Three Rivers Sources in Qinghai (2017-S-1).

References

- Boudjabi, S., Chenchouni, H.: Soil fertility indicators and soil stoichiometry in semi-arid steppe rangelands. *Catena* **210**(3), 105910 (2022)
- Guo, M., Li, X.: Meta-analysis and its application in the research of ecological environment. *J. Desert. Res.* **29**, 911–919 (2009)
- Hu, L.U., Tuo, Y.A.O., Jianhong, L.I., et al.: Study on microbial characteristics and correlation of different degraded meadow vegetations and soils in alpine regions. *Acta Pratacultura Sinica Sinica* **24**(05), 34–43 (2015)
- Jia, Y.: *Integrated Analysis of Soil Use Impacts in Purple Soil Areas*. Hebei Normal University (2009)
- Lu, H.: *Study on Soil Microbial Characteristics of Different Degraded Meadows in Qilian Mountains*. Gansu Agricultural University (2015)
- Tian, K., Zhao, Y.C., Xu, X.H., et al.: Variation characteristics of soil organic carbon in dryland of China under different fertilizations-A meta-analysis based on localization test data. *China J. Ecol.* **34**, 3735–3743 (2014)
- Wei, W.D., Liu, Y.H., Ma, H.: Meta-analysis of soil organic carbon content in degraded meadows of alpine meadows. *Environ. Sci. Manag.* **43**, 53–58 (2018)



Temporal Changes in Carbon and Nitrogen Concentrations in the Rhizosphere Soil of Two Plant Species

Irina Shtangeeva, Eric Visser, and Paul van der Ven

Abstract

The aim of the current research was to assess the impact of root exudates of widely distributed natural plant species, a monocot (couch grass) and a dicot (dandelion), on the total amount of carbon (C) and nitrogen (N) in the rhizosphere soils of these plants when they are grown separately or in close proximity to each other. A field trial was carried out to study the short-term variations in the concentrations of C and N in the soil resulting from the activity of exudates produced by the plant roots and soil contamination by RbCl. During daytime, the total amount of C and N in the rhizosphere soil of both plant species was found to be constantly decreasing, from 7.0% to 4.5% (C) and from 0.3% to 0.2% (N). Probably, plant growth in the soil contaminated by RbCl and possible additional effect of organic compounds produced by roots of couch grass and dandelion caused the decrease in C concentration in the rhizosphere soil, while changes in the soil N concentrations were insignificant.

Keywords

Carbon • Nitrogen • Rhizosphere Soil • Couch Grass • Dandelion • RbCl

1 Introduction

Soil organic matter is a key component of terrestrial ecosystems. Any variation in its abundance and composition has an essential effect on various processes that occur within these systems (Batjes 1996). Carbon (C) and nitrogen (N) are the most important elements in soil organic matter.

I. Shtangeeva (✉)

St. Petersburg University, St. Petersburg, 199034, Russia

E. Visser · P. van der Ven

Radboud University, 6525 AJ Nijmegen, The Netherlands

Monitoring the dynamics of these components in the rhizosphere soil can help to assess the ability of the soil to store and recycle these nutrients (Boudjabi and Chenchouni 2022).

The aim of the research was to study the impact of root exudates of two plant species, a monocot and a dicot, on the total amount of C and N in the rhizosphere soils of these plants when they were grown separately or in close proximity to each other. The other aim was to assess how RbCl-contaminated soil may affect the amount of C and N in the rhizosphere soil. Rubidium (Rb) is a chemical analogue of potassium (K), an essential plant nutrient. Plants can take up Rb (which is highly mobile and is mainly transferred to the aboveground part of the plant) instead of K. The increase in Rb in the soil may cause certain toxic effects for both plants and soil microbiota, which may lead to a decrease in the plant growth and exudation activity.

2 Methods

A field trial was performed in May 2019 in a park in St. Petersburg, Russia. The soil samples were collected from the rhizosphere zone of two plant species (couch grass, *Elymus repens*, and dandelion, *Taraxacum officinale*). The age of the plants was ~3 weeks. The soil was collected three times during a day from two plots located close to each other. The area of each plot was 2 m². One of the plots served as control; another plot was spiked with RbCl (75 mg/L, 1 L of solution per 1 m²) 24 h before sampling was started. Soil was taken from roots of couch grass and dandelion that grew separately or together (in close vicinity to each other). To collect rhizosphere soil samples, we used the protocol of Luster et al. (2009). After sampling, soil was air-dried to constant weight. The concentrations of C and N in the soil samples were determined by Vario Micro Cube (Elementar). For analysis, we used two replicates of the soil samples. For the data analysis, STATISTICA for Windows 6.0 Software package (StatSoft, Tulsa, OK, USA) was applied.

3 Results and Discussion

During the day, the total amount of C and N in the rhizosphere soil of both plant species grown separately and together decreased gradually, with the highest values achieved in the morning and the lowest in the evening (Fig. 1). This was probably caused by short-term variations in the release of root exudates. The release of C and N into the rhizosphere depends on many factors, including light intensity, temperature, nutritional status of plants, etc.

Under control conditions (in a non-contaminated soil), relationships between root exudates of couch grass and dandelion resulted in the decrease in the C concentration in the rhizosphere soil of the plant species. When the plants were very close to each other, the concentration of C in the soil taken from roots of both plants decreased by ~10% compared to the C concentration in the rhizosphere soil of the plants growing separately (Table 1). This means that the roots of couch grass and dandelion likely produced allelochemicals that negatively affected the amount of rhizosphere C. It is also possible that plants growing together and separately could

host different rhizosphere microorganisms. This in turn could affect root activity and/or C turnover leading to different concentrations of C and N in the rhizosphere soil.

A similar decrease in C concentration in the rhizosphere soil of the plants was observed when the soil was spiked with RbCl. The impact of soil contamination was less marked in the case when dandelion and couch grass were grown together. On the other hand, soil contamination with RbCl and the interactions of root exudates of the two plant species did not lead to major changes in the concentrations of N in the rhizosphere. We have currently no firm explanation of the observed phenomenon, and follow-up experiments might be needed.

There are significant differences between monocots and dicots in the nature and quantity of root exudates (Zagal 1994). Moreover, the organic compounds released by roots of different plant species have an essential effect on the microbial activity in the rhizosphere. Plant species differ in their ability to attract root-associated microorganisms (Clairmont et al. 2019). Therefore, it would be expected to observe certain differences in C and N concentrations in the

Fig. 1 Variations of C and N concentrations in the rhizosphere soil of couch grass and dandelion during a day

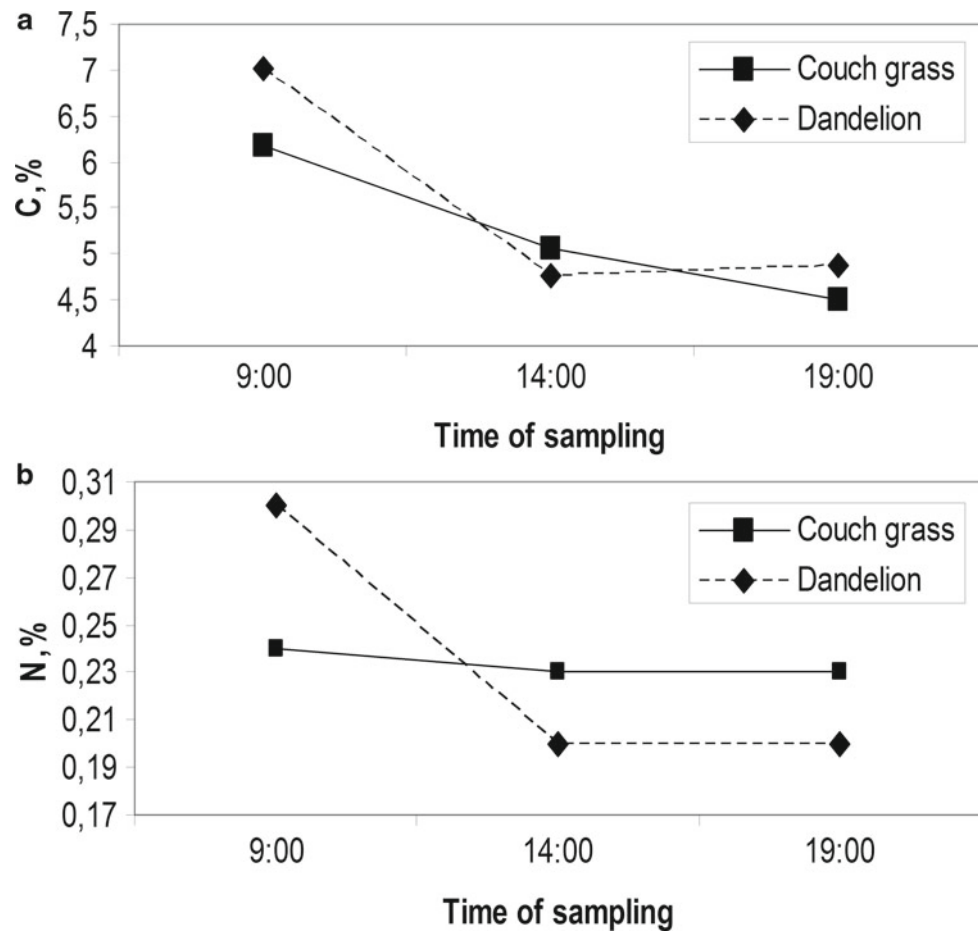


Table 1 Mean concentrations of C and N in the soil taken from roots of couch grass and dandelion when the plants grow far from each other (1) or in close proximity to each other (2) in non-contaminated soil (control) and in the soil spiked with RbCl

	Couch grass		Dandelion	
	1	2	1	2
C (%)				
Control	5.25 ± 0.85 ^{a,b}	4.55 ± 0.89	5.55 ± 1.26 ^{a,b}	4.32 ± 0.56
RbCl	3.98 ± 0.51	4.23 ± 0.17	4.12 ± 0.07	4.12 ± 0.28
N (%)				
Control	0.23 ± 0.06	0.23 ± 0.02	0.23 ± 0.01	0.22 ± 0.02
RbCl	0.21 ± 0.02	0.23 ± 0.01	0.24 ± 0.01	0.24 ± 0.03

^aDifferences between the rhizosphere soils of the plants grown separately and close to each other were statistically significant ($P < 0.05$). ^bDifferences between control and treated with RbCl soils were statistically significant ($P < 0.05$)

rhizosphere soils of two different plant species (couch grass belongs to monocots and dandelion to dicots). However, the differences were less marked than anticipated.

4 Conclusions

During the daytime, the total amount of C and N in the rhizosphere soil of couch grass and dandelion decreased gradually. It may be due to the fact that the allelopathic activity of the root exudates of the two plants and/or the activity of different microorganisms hosted by the two plant species may have resulted in this decrease in C concentration in the rhizosphere soil of both plants. The contamination of the soil by RbCl also negatively affected the C concentration in the rhizosphere soil of couch grass and dandelion. The variations in the soil N concentrations, however, were not as strong as the changes in the C concentrations.

References

- Batjes, N.H.: Total carbon and nitrogen in the soils of the world. *Eur. J. Soil Sci.* **47**, 151–163 (1996). <https://doi.org/10.1111/j.1365-2389.1996.tb01386.x>
- Boudjabi, S., Chenchouni, H.: Soil fertility indicators and soil stoichiometry in semi-arid steppe rangelands. *Catena*, **210**(3), 105910 (2022). <https://doi.org/10.1016/j.catena.2021.105910>
- Clairmont, L.K., Stevens, K.J., Slawson, R.M.: Site-specific differences in microbial community structure and function within the rhizosphere and rhizoplane of wetland plants is plant species dependent. *Rhizosphere* **9**, 56–68 (2019). <https://doi.org/10.1016/j.rhisph.2018.11.006>
- Luster, J., Göttlein, A., Nowack, B., Sarret, G.: Sampling, defining, characterising and modelling the rhizosphere—the soils science toolbox. *Plant Soil* **321**, 457–482 (2009)
- Zagal, E.: Carbon distribution and nitrogen partitioning in a soil-plant system with barley (*Hordeum vulgare* L.), ryegrass (*Lolium perenne*) and rape (*Brassica napus* L.) grown in a ¹⁴C₂-atmosphere. *Plant Soil* **166**, 63–74 (1994). <https://doi.org/10.1007/bf02185482>



Effect of Edaphic Factors on Essential Oil Production in Wild Plants Growing Under Semiarid Mediterranean Conditions

Souad Mehalaine¹ and Haroun Chenchouni²

Abstract

In this study, we investigated the effect of soil chemical composition on essential oil content in two plant species collected from the semiarid region of Algeria: *Rosmarinus officinalis* L. and *Thymus algeriensis* Boiss and Reut. The results indicated that the yield of essential oils showed significant differences ($P < 0.001$) during the years of the study: *Rosmarinus officinalis* recorded the best yield during the year 2010 ($1.00 \pm 0.18\%$) and *Thymus algeriensis* during the year 2013 ($1.08 \pm 0.02\%$). The chemical composition of the soil significantly affected the content of the essential oils in both plants ($P < 0.001$ and $P < 0.05$): the pH, total CaCO_3 (CCE), active CaCO_3 (ACCE), and N:P ratio positively influenced the oil concentration in *Rosmarinus officinalis*, whereas salinity and total nitrogen (N) showed a negative effect. In *Thymus algeriensis*, essential oil yield was positively correlated with pH, salinity and N:P ratio and negatively correlated with total CaCO_3 (CCE), active CaCO_3 (ACCE) and organic carbon.

Keywords

Rosmarinus officinalis • *Thymus algeriensis* • Essential oils • Edaphic effects • Soil C:N:P stoichiometry

1 Introduction

Rosmarinus officinalis L. and *Thymus algeriensis* Boiss and Reut. are two native plant species very common in Algeria (Quezel and Santa 1963; Zouaoui et al. 2020). Both plants are highly appreciated in Algerian popular medicine because of their very important therapeutic properties, in addition to their multiple uses in pharmaceutical and agri-food sectors. In fact, this appreciation and use are related to their synthesis of essential oils. Essential oils as all the secondary metabolites possess crucial biological and ecological activities (Msaada et al. 2009). Several studies have reported the effect of the environment on secondary metabolism in general, and the amount of essential oils and their chemical composition, in particular, in different plant species. Factors that affect the performance and chemical composition of essential oils are: season and growing region (Perry et al. 1999; Msaada et al. 2009; Hassani et al. 2017). Many studies have investigated the effect of the climate and soil on the production of essential oils in different plant species (Razmjoo et al. 2008; Singh et al. 2016; Hassani et al. 2017; Mehalaine and Chenchouni 2019, 2020, 2021). Most of the research on the action of climatic and soil factors on secondary metabolism of plants was carried out under well-defined controlled conditions, but in our previous study we evaluated the effect of semiarid climate on the accumulation of essential oils (EOs) in *Rosmarinus officinalis* and *Thymus algeriensis* in situ (Mehalaine and Chenchouni 2019). The present study is the continuation of our previous work in order to test the effect of edaphic factors on the variation of essential oils yield in the same species to obtain crucial information on the behavior and the mode of adaptation of these species in semiarid climate conditions.

S. Mehalaine (✉) · H. Chenchouni
Department of Natural and Life Sciences, Faculty of Exact Sciences and Natural and Life Sciences, Larbi Tebessi University, 12002 Tebessa, Algeria
e-mail: souad.mehalaine@univ-tebessa.dz

H. Chenchouni
Laboratory of Natural Resources and Management of Sensitive Environments 'RNAMS', Larbi Ben M'hidi University, 04000 Oum-El-Bouaghi, Algeria

2 Materials and Methods

2.1 Plant Material and Extraction of Essential Oils

The plant material used for extracting the essential oils from *R. officinalis* and *T. algeriensis*, was the young stems, leaves and flowers. The plant collection was carried out during the full bloom stage of the two species in Ain Beida region (latitude: 35°47'47"N, longitude: 7°23'34"E, elevation: 891 m a. s.l.). After removing the woody parts, the samples were cut into small pieces of 5–10 mm and dried in the open air and dark until the constancy of their dry weight. For each plant, 80 g of vegetable dry matter were used for the distillation of essential oils in a Clevenger apparatus for two hours. The yield of the isolated essences was estimated in relation to the weight of the plant dry matter and calculated as a percentage.

2.2 Soil Chemical Analysis

Soil samples were collected randomly at a depth of 30 cm from the study station during the February, which coincides with the full vegetative stage of both plant species for chemical analyses. The samples were sorted, crushed and sieved through a 2-mm sieve. The dominant reference soil group (RSG) in the study area is the haplic calcisol (Boudjabi and Chenchouni 2022).

The physicochemical analysis of the soil was performed according to the standard methods of the soil analysis (Baize 2000; Bonneau et al. 2003; Mathieu and Pieltain 2003). The parameters analyzed were: pH, electrical conductivity 'EC', total Calcium Carbonate Equivalent 'CCE', active Calcium Carbonate Equivalent 'ACCE', organic carbon 'C' and level of organic matter (OM), assimilable phosphorus 'P', and total nitrogen 'N'. Based on C, N, and P contents, soil stoichiometric relationships, namely C:N, C:P, and N:P ratios, were determined (Mehalaine and Chenchouni 2020).

2.3 Data Management and Statistical Analysis

The variation of essential oil yields during the study years were statistically analyzed using a generalized linear model (GLM) with Gaussian distribution error and identity link. The interaction of both factors "Year × Species" was included in the model. In addition, multiple comparisons of means via Tukey's post hoc test were conducted over the study years separately for each species. In addition, the variation of each soil parameter between years was tested using GLM. Collinearity was tested between the chemical properties of the soil. Pearson correlation tests were built as a correlation matrix. The multicollinearity was checked for the

edaphic variables (Fig. 1) which involved only eight edaphic variables (pH, salinity, CCE, ACCE, carbon, nitrogen, C:N, N:P) out of twelve as predictable variables for modeling the variation of essential oil yields. Then, the effects of pH, salinity, CCE, ACCE, carbon, nitrogen, C:N, N:P on the variation of EO amounts of each species were tested using a GLM with Gaussian distribution error and identity link. The statistical analyses were carried out using the R software (R Core Team 2019).

3 Results

3.1 Pedological Characterization

The performances of the studied pedological parameters differ significantly ($P < 0.001$ and $P < 0.05$) between the years with the exception of C:P. The obtained values indicated that the soil has an alkaline pH between 7.85 and 8.12 with an average of 7.96 ± 0.08 . The soil is slightly saline with salinity values that vary between 103.00 mg/L and 233.03 mg/L and moderately limestone, the percentage of CCE changes between 3.18% and 17.50% with an average of $8.52 \pm 3.82\%$. The assimilable phosphorus (P_2O_5) content is low, between 74.43 ppm and 208.99 ppm. However, the soil showed significant percentages of organic matter (OM) (2.64% to 14.28%) with an average of $5.99 \pm 2.75\%$ (Table 1).

3.2 Interrelationship Between Edaphic Parameters

The correlation matrix (collinearity test) between soil parameters made it possible to distinguish 122 significant correlations ($P < 0.05$) out of 132 existing ones. The most important correlations ($P \leq 0.001$) were recorded between the parameters: electrical conductivity (EC) with salinity ($r = 1$); organic matter (OM) with organic carbon ($r = 1$); phosphorus with all the parameters with the exception of CCE; and finally the C:N ratio with all the parameters ($P < 0.001$) except pH and CCE (Fig. 1).

3.3 Yearly Variation of Essential Oils Yield

The yield of essential oils in both species showed very highly significant differences ($P < 0.001$) during the five study years. *Rosmarinus officinalis* recorded levels of essential oils between $0.46 \pm 0.02\%$ during the year 2014 and $1.00 \pm 0.18\%$ during the year 2010. The oil concentrations marked in *T. algeriensis* were between $0.47 \pm 0.03\%$ in the year 2010 and $1.08 \pm 0.02\%$ in the year 2013 (Table 2).

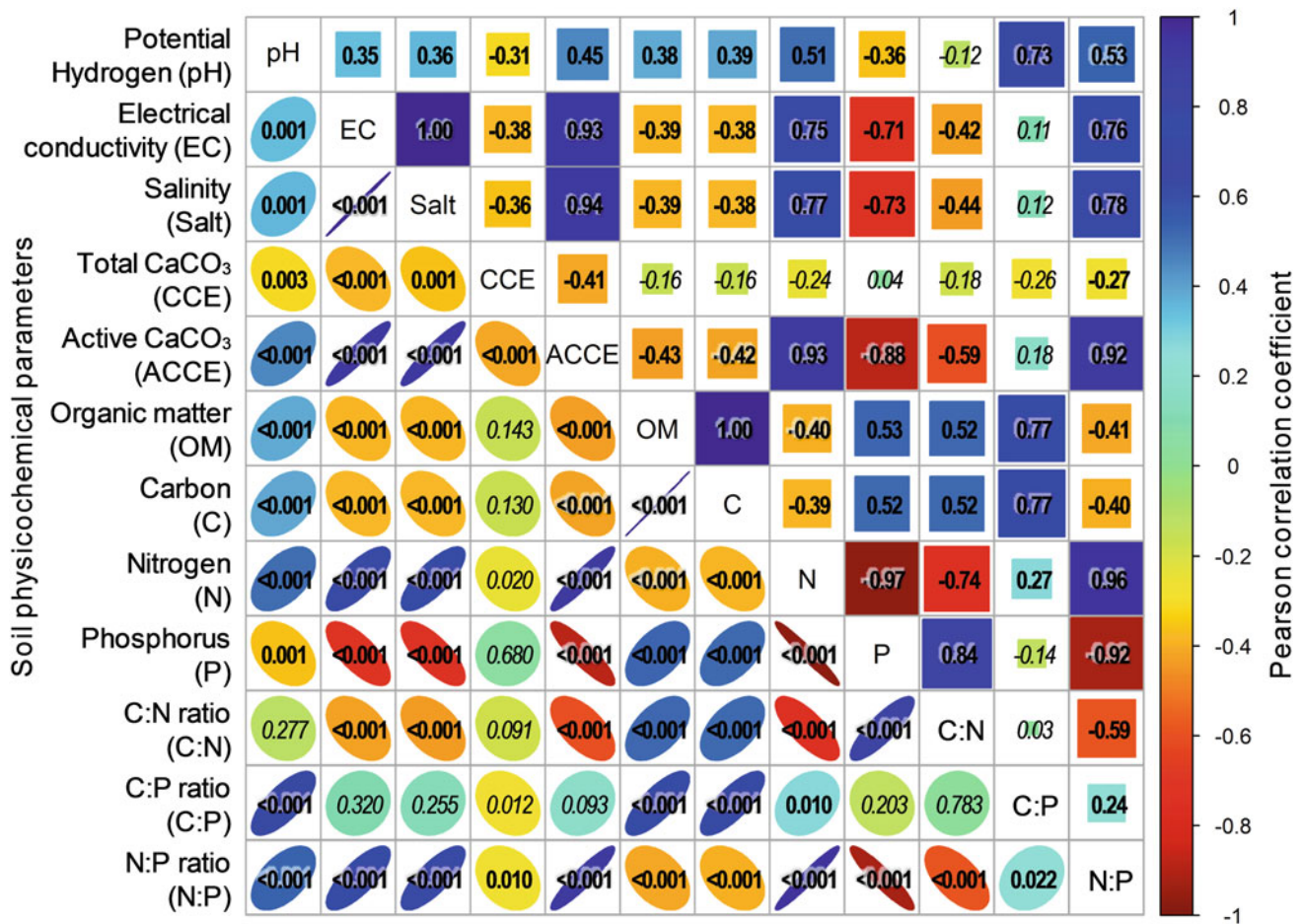


Fig. 1 Correlation matrix applied for soil variables of the region of Ain Beida, Province of Oum-El-Bouaghi (northeastern Algeria). Values of Pearson correlation tests are given within pie charts as the correlation

coefficient, coloration and pie-chart size (above diagonal) and *P*-value (under diagonal)

3.4 Effects of Soil Proprieties on Specific Essential Oils Production

The GLM showed that the chemical properties of the soil: pH, total CaCO₃ (CCE), active CaCO₃ (ACCE), N:P positively affected the yield of essential oils in *R. officinalis* (*P* < 0.001 and *P* < 0.05). Salinity and total nitrogen had negative effects (*P* < 0.001) while C:N showed no significant effect. In *T. algeriensis*, pH, salinity and N:P positively influenced the essential oil content (*P* < 0.001). In contrast, total CaCO₃, active CaCO₃ and organic carbon negatively affected the concentrations of essential oil (*P* < 0.001) (Table 3).

4 Discussion

The two species *R. officinalis* and *T. algeriensis* showed significant variations in the quantities of essential oils according to the years of collection. This is due to the effect

of climatic factors. In our previous study, we found that precipitation, wind speed, hygrometry, air humidity and aridity significantly affect the yield of essential oils in both species (Mehalaine and Chenchouni 2019, 2021).

The obtained results showed that the increase of salinity and nitrogen caused a decrease in the oil content in *R. officinalis*. However, the increase of salinity and the ratio N:P leads to an increase of essential oil yield in *T. algeriensis*. This is in accordance with studies reported previously. According to Hassani et al. (2017), the electrical conductivity negatively affected the number of chemical compounds in the essential oil of *Heracleum persicum*, and this parameter may positively or negatively affect the oil chemical composition, and the phosphorus content positively affected the yield of essential oil in this species. In addition, the concentration of certain oil chemical molecules increases if the soil is rich in salts and contains a low level of nitrogen. Salinity reduced the essential oil amount in *Matricaria chamomile* (Razmjoo et al. 2008). On the other hand, Jeshni et al. (2017)

Table 1 Descriptive statistics of soil parameters collected in sites of *Rosmarinus officinalis* and *Thymus algeriensis* growing in semiarid lands of Algeria. *F* and *P* statistics are results of *Type-II* tests derived from GLM testing the variation among years

Soil variables	Descriptive statistics										<i>Type-II F</i> -tests		
	Mean	SD	SE(m)	IQR	CV	0%	25%	50%	75%	100%	<i>F</i>	<i>P</i>	Sig
pH	7.96	0.08	0.01	0.15	0.01	7.85	7.88	7.93	8.03	8.12	117.80	<0.001	***
EC ($\mu\text{s}/\text{cm}$)	345.06	58.33	6.15	67.37	0.17	193.00	310.00	349.83	377.37	429.33	38.44	<0.001	***
Salinity (mg/L)	186.38	32.70	3.45	40.70	0.18	103.00	165.00	192.04	205.70	233.03	39.94	<0.001	***
CCE (%)	8.52	3.82	0.40	4.29	0.45	3.18	6.36	7.49	10.65	17.50	10.11	0.002	**
ACCE (%)	7.86	2.50	0.26	2.93	0.32	3.00	6.50	8.10	9.43	12.10	67.37	<0.001	***
OM (%)	5.99	2.75	0.29	2.54	0.46	2.64	4.32	5.58	6.86	14.28	6.06	0.016	*
Carbon (%)	3.51	1.59	0.17	1.43	0.45	1.53	2.56	3.28	3.99	8.30	5.71	0.019	*
Nitrogen (mg/100 g soil)	39.66	18.45	1.94	20.53	0.47	5.60	30.80	41.53	51.33	70.93	65.36	<0.001	***
Phosphorus (ppm)	126.85	34.06	3.59	41.96	0.27	74.43	105.86	121.58	147.82	208.99	44.13	<0.001	***
C:N ratio	16.98	23.75	2.50	12.84	1.40	3.41	4.97	7.38	17.81	33.21	10.90	0.001	**
C:P ratio	28.00	9.33	0.98	5.45	0.33	10.70	25.37	28.44	30.82	33.55	2.37	0.128	NS
N:P ratio	3.76	2.60	0.27	2.70	0.69	0.27	2.15	3.42	4.85	9.53	86.97	<0.001	***

Table 2 Descriptive statistics of essential oil concentrations in *Rosmarinus officinalis* and *Thymus algeriensis* growing wild in semiarid lands of Algeria

Years	Mean	SD	SE(m)	IQR	CV	0%	25%	50%	75%	100%	Tukey
<i>Rosmarinus officinalis</i>											
2010	1.00	0.18	0.11	0.18	0.18	0.83	0.91	0.99	1.09	1.19	A
2011	0.64	0.01	0.01	0.01	0.01	0.63	0.64	0.64	0.64	0.65	B
2012	0.93	0.05	0.03	0.05	0.06	0.90	0.90	0.90	0.95	0.99	A
2013	0.88	0.00	0.00	0.00	0.00	0.88	0.88	0.88	0.88	0.88	A
2014	0.46	0.02	0.01	0.02	0.05	0.44	0.45	0.45	0.47	0.49	B
Overall	0.78	0.22	0.06	0.27	0.28	0.44	0.64	0.88	0.90	1.19	
<i>Thymus algeriensis</i>											
2010	0.47	0.03	0.02	0.03	0.07	0.44	0.46	0.47	0.49	0.50	C
2011	0.59	0.07	0.04	0.07	0.11	0.52	0.57	0.61	0.63	0.65	B
2012	0.68	0.02	0.01	0.02	0.03	0.65	0.67	0.69	0.69	0.70	B
2013	1.08	0.02	0.01	0.02	0.02	1.06	1.07	1.08	1.09	1.10	A
2014	0.49	0.02	0.01	0.02	0.03	0.47	0.49	0.50	0.50	0.51	C
Overall	0.66	0.23	0.06	0.19	0.35	0.44	0.50	0.61	0.69	1.10	

reported that the application of optimal doses of mineral elements such as phosphorus improved the yield of essential oils in *Matricaria recutita*. According to Lantemona et al. (2013), the genetic factor and environmental variation can affect the chemical compounds of essential oils. Besides, environmental stresses, such as climate aridity, heat and soil salinity, influence the expression of genes, production of enzymes and the synthesis of chemical molecules constituting the essential oils and other secondary metabolites (Senoussi et al. 2021).

5 Conclusion

In this study, we examined the impact of some soil chemical properties on the production of essential oils in *R. officinalis* and *T. algeriensis* collected from the semiarid zone of Algeria. Both plants responded differently to the studied edaphic factors. The obtained results can provide crucial information on the nutrient needs of the two plants but it is still necessary to test the effect of the soil chemical

Table 3 GLM testing the effects of soil proprieties on the production of essential oils in *Rosmarinus officinalis* and *Thymus algeriensis* growing wild in semiarid lands of Algeria

Parameters	Estimate	SE	t-value	P	Sig
<i>Rosmarinus officinalis</i>					
(Intercept)	-18.225	2.883	-6.321	<0.001	***
pH	2.615	0.378	6.925	<0.001	***
Salinity	-0.026	0.007	-3.987	<0.001	***
CCE	0.040	0.016	2.545	0.015	*
ACCE	0.672	0.171	3.939	<0.001	***
Nitrogen	-0.074	0.012	-6.327	<0.001	***
N:P ratio	1.201	0.496	2.422	0.020	*
C:N ratio	-0.487	0.276	-1.762	0.086	NS
<i>Thymus algeriensis</i>					
(Intercept)	-7.430	1.133	-6.560	<0.001	***
pH	1.121	0.146	7.659	<0.001	***
Salinity	0.011	0.001	14.077	<0.001	***
CCE	-0.027	0.002	-11.805	<0.001	***
ACCE	-0.358	0.018	-19.594	<0.001	***
Carbon	-0.062	0.007	-8.410	<0.001	***
N:P ratio	1.015	0.098	10.316	<0.001	***

SE: standard error, P: P-value, Sig.: statistical significance, ***: $P < 0.001$, *: $P \leq 0.05$, NS: $P > 0.05$.

parameters on both plants under controlled conditions in order to confirm the findings.

References

- Baize, D.: Guide des analyses en pédologie. 2ème édition, Paris (2000)
- Bonneau, M., Lévy, G., Montpied, P.: Evaluation de la pertinence des deux méthodes d'analyse du phosphore dans les sols forestiers. Rev. For. Fr. **55**, 57–64 (2003)
- Boudjabi, S., Chenchouni, H.: Soil fertility indicators and soil stoichiometry in semi-arid steppe rangelands. CATENA **210**(3), 105910 (2022). <https://doi.org/10.1016/j.catena.2021.105910>
- Hasani, R., Mehregan, I., Larjani, K., Nejadstari, T., Scalone, R.: Survey of the impacts of soil and climatic variations on the production of essential oils in *Heracleum persicum*. Biodiversitas **18**(1), 365–377 (2017). <https://doi.org/10.13057/biodiv/d180148>
- Jeshni, M.G., Mousavinik, M., Khammari, I., Rahimi, M.: The changes of yield and essential oil components of German Chamomile (*Matricaria recutita* L.) under application of phosphorus and zinc fertilizers and drought stress conditions. J. Saudi Soc. Agric. Sci. **16**, 60–65 (2017). <https://doi.org/10.1016/j.jssas.2015.02.003>
- Lantemona, H., Abadi, A.L., Rachmansyah, A., Pontoh, J.: Impact of altitude and seasons to volume, brix content, and chemical composition of aren sap in North Sulawesi. IOSR J. Environ. Sci. Toxicol. Food Technol. **4**(2), 42–48 (2013)
- Mathieu, C., Pieltain, F.: Analyse chimique des sols. Edition Lavoisier, France (2003)
- Msaada, K., Ben Taarit, M., Hosni, K., Hammami, M., Marzouk, B.: Regional and maturational effects on essential oils yields and composition of coriander (*Coriandrum sativum* L.) fruits. Sci. Hortic. **122**, 116–124 (2009). <https://doi.org/10.1016/j.scienta.2009.04.008>
- Mehalaine, S., Chenchouni, H.: Effect of climatic factors on essential oil accumulation in two Lamiaceae species from Algerian semiarid lands. In: Chenchouni, H., et al. (eds.), Exploring the nexus of Geoecology, Geography, Geoarcheology and Geotourism, pp. 57–60. Springer, Cham (2019). https://doi.org/10.1007/978-3-030-01683-8_12
- Mehalaine, S., Chenchouni, H.: Plants of the same place do not have the same metabolic pace: soil properties affect differently essential oil yields of plants growing wild in semiarid Mediterranean lands. Arab. J. Geosci. **13**(23), 1263 (2020). <https://doi.org/10.1007/s12517-020-06219-4>
- Mehalaine, S., Chenchouni, H.: Quantifying how climatic factors influence essential oil yield in wild-growing plants. Arab. J. Geosci. **14**(13), 1257 (2021). <https://doi.org/10.1007/s12517-021-07582-6>
- Perry, N.B., Anderson, R.E., Brennan, N.J., Douglas, M.H., Heaney, A. J., McGimpsey, J.A., Smallfield, B.M.: Essential oils from dalmatian sage (*Salvia officinalis* L.): variations among individuals, plant parts, seasons, and sites. J. Agric. Food Chem **47**, 2048–2054 (1999). <https://doi.org/10.1021/jf981170m>
- Quezel, P., Santa, S.: Nouvelle Flore de l'Algérie et des Régions Désertiques Méridionales. Tome 2. Edition CNRS, Paris (1963)
- Razmjoo, K., Heydarzadeh, P., Sabzalian, M.R.: Effect of salinity and drought stresses on growth parameters and essential oil content of *Matricaria chamomile*. Int. J. Agric. Biol. **10**, 451–454 (2008)
- R Core Team: R: A language and environment for statistical computing. R Foundation for Statistical Computing, Vienna, Austria. (2019). <https://www.R-project.org/>
- Senoussi, A., Schadt, I., Hioun, S., Chenchouni, H., Saoudi, Z., Aissaoui Zitoun Hamama, O., Zidoune, M.N., Carpino, S., Rapisarda, T.: Botanical composition and aroma compounds of semi-arid

- pastures in Algeria. *Grass Forage Sci.* **76**(2), 282–299 (2021). <https://doi.org/10.1111/gfs.12510>
- Singh, M., Masroor, M., Naeem, K.M.: Effect of nitrogen on growth, nutrient assimilation, essential oil content, yield and quality attributes in *Zingiber officinale* Rosc. *J. Saudi Soc. Agric. Sci.* **15**, 171–178 (2016). <https://doi.org/10.1016/j.jssas.2014.11.002>
- Zouaoui, N., Chenchouni, H., Bouguerra, A., Massouras, T., Barkat, M.: Characterization of volatile organic compounds from six aromatic and medicinal plant species growing wild in North African drylands. *NFS J.* **18**, 19–28 (2020). <https://doi.org/10.1016/j.nfs.2019.12.001>



Geographical Mapping of *Salvadora oleoides* in Northwestern India

Maneesh S. Bhandari, Rama Kant, Rajeev Shankhwar, Rajendra K. Meena, Sandeep Maikuri, Santan Barthwal, and Shailesh Pandey

Abstract

Salvadora oleoides, belongs to the family Salvadoraceae, is an ecologically important species of Indian Arid Regions (IAR). It grows well in heavy and non-saline soil, and dry to marshy semiarid region. In spite of its great adaptability, the species is depleting at a high rate and therefore, needs population assessment. In present study, the distribution range of *S. oleoides* in northwestern India was determined through extensive ground surveys conducted during 2016–2018 in the states of Punjab, Haryana, Rajasthan and Gujarat. The distribution map was prepared using geo-coordinates and LANDSAT-8 satellite imagery data. A total geographical area (1558.72 ha.) of *S. oleoides* was calculated, where 1107.49 ha, 278.79 ha and 172.44 ha were found to be open, moderately dense and scattered, respectively. The present study would be useful to the forest departments, scientists and researchers for future *in situ* and *ex situ* conservation. This approach can be best utilized to model its potential distribution and future prediction mapping.

Keywords

Salvadora oleoides • LANDSAT-8 • Geo-coordinates • Distribution map

1 Introduction

The Indian forests ranges from the evergreen tropical rain forest in Andaman and Nicobar Islands, and the Western Ghats, to dry alpine scrubs of the Himalayas. The area between the two extremes is dominated by semi-evergreen rain forests, deciduous monsoon forests, thorn forests and subtropical pine forests (Ashutosh et al. 2010). The western part of India is occupied by arid, semiarid and desert regions, where desert occupies one-seventh of the total land area. The desert biome plays a key role in species evolution and adaptation. Topographically, the arid zone, which is distinctly marked with sand, rocks and steep slopes, is a storehouse of important tree species including *Prosopis spicigera*, *Salvadora persica*, *S. oleoides*, *Capparis aphylla* and *Tamarix articulata*. Among these, *S. oleoides* is an ecologically important tree species of arid zone (Saini and Yadav 2013). This species grows well in dry, saline and sand dunes of deserts to heavy soils, non-saline to highly saline soils (Singh et al. 1996). The habitat of *S. oleoides* (Salvadoraceae) in dry regions, marshy semiarid regions, water-logged areas, swamps, thorn shrubs, desert flood plains and grassy savannah, relates to its wider adaptability (Zodape and Indusekhar 1997; Ahmad 2007; Hardikar et al. 2011). The species is known to tolerate very dry environment having mean rainfall lesser than 200 mm (Singh et al. 1996; Bhandari 1978). However, the actual geographical distribution mapping through ground truthing, Remote Sensing and Geographical Information System (RS&GIS) of this species have not been conducted yet. Therefore, the present study aimed to generate the distribution map of *S. oleoides* in northwestern India using RS&GIS technology, and suggest suitable conservation measures.

M. S. Bhandari (✉) · R. Kant · R. Shankhwar · R. K. Meena · S. Maikuri · S. Barthwal

Division of Genetics and Tree Improvement, Forest Research Institute, Dehradun, Uttarakhand 248195, India

S. Pandey

Division of Forest Protection, Forest Research Institute, Dehradun, Uttarakhand 248006, India

2 Materials and Methods

The status map of Forest Survey of India, Dehradun, and the data from the working plan of state forest departments of northwestern India were reviewed to obtain the distribution status of the species. In addition, data related to biodiversity and distribution were also gathered from the documents available in National Forest Library Information Centre (NFLIC), Forest Research Institute, Dehradun, and as reported earlier (Malik et al. 2010).

Four Indian states, viz., Punjab, Haryana, Rajasthan and Gujarat were surveyed during the period 2016–2018. The geo-spatial parameters were recorded with GARMIN-650 model handheld Global Positioning System (GPS) device for scattered trees, whereas 30 representative sample units (plot size 6 m x 6 m) were recorded in community forest areas. The area demarcation tool (in GARMIN-650 model device) was used to demarcate *S. oleoides* tree patches in polygons. In the geo-informatics laboratory at FRI, Dehradun, point and polygons were used for marking the location of individual trees as well as to demarcate the population patches over the satellite image. To refine the boundary of *S. oleoides* population patches, geo-coordinates were converted into Keyhole Markup Language (KML) and used in the Google Earth for visible interpretation (Shankhwar et al. 2019). Further, using Google Earth imagery, *S. oleoides* population was classified into three density classes: scattered, open and the moderately dense type. Finally, the district-wise density classes were calculated.

2.1 Satellite Data

LANDSAT-8 Operational Land Imager (OLI) satellite imagery of four northwestern states (Haryana, Gujarat, Punjab and Rajasthan) was downloaded from United States Geological Survey (USGS) website during April 2017. Metadata of satellite imagery contains UTM (Universal Transverse Mercator) map projection with WGS-84 (World Geodetic System) datum of time zones 42 and 43, respectively. LANDSAT-8 having 7 optical spectral bands with 30 m spatial resolution with three bands (visible green: 0.525–0.600 μm , visible red: 0.630–0.680 μm and near-infrared: 0.845–0.885 μm) was used to compose False Color Composite (FCC) images. To enhance the FCC image spatial resolution for better image interpretation, eighth band (15 m spatial resolution) was merged with FCC image in ERDAS imagine Digital Image Processing (DIP) software.

3 Results

3.1 Geographical Mapping of *S. oleoides* Population

The distribution, area (in ha), percent dominance and the population density of *S. oleoides* in various districts of Haryana, Rajasthan, Gujarat and Punjab are presented in Table 1. LANDSAT-8 mosaic image of all the four states showed distribution in different geographical regions of northwestern India (Fig. 1). Maximum tree population was found to be scattered in all the four states, followed by open type and moderately dense forest. In total, 1558.72 ha area was recorded under *S. oleoides*, out of which 1107.49 ha, 278.79 ha and 172.44 ha areas were detected as open, moderately dense and scattered, respectively. District-wise, the highest forest area of 1058.73 ha was recorded in Rajasthan, followed by Haryana (399.17 ha), Gujarat (68.35 ha) and Punjab (32.47 ha). Two hundred thirty-eight scattered trees on highways, district major roads (DMR), village and connecting roads, canals, villages, community lands, etc., were also recorded. The highest distribution was observed in Jhunjhunu (864 ha, open forest) of Rajasthan, followed by Bhiwani (113.77 ha, open forest; 91.0 ha, moderate forest) of Haryana, and Jaisalmer (0.25 ha, open forest; 139.67 ha, scattered) of Rajasthan. The species was found to be highly dominating in the village areas of southern and southwestern districts of Haryana and Punjab. Most of the trees were found in community forest area, village panchayat land and sparsely distributed under the areas of the state forest departments. The individual trees were located near National Highways, State Highways and connecting roads between villages.

In Punjab, 7 sites were surveyed and the geo-spatial parameters were recorded. The maximum area of 13.2 ha (Dera Baba Dhyani Das in Mansa), followed by 9.35 ha (Bir Sikhawala in Faridkot), was recorded as open forest and moderately dense forest, respectively. The minimum area of 0.31 ha (Gurudwara Tibbisahib), followed by 1.28 ha (Sattal Khara Gurudwara), was under open forest in Muktsar. In the state Haryana, the minimum area of 0.65 ha (Dhandlan, Jhajjar, Nazia Khera, Sirsa) was recorded as open forest, followed by 2.58 ha area of moderately dense forest in Matanhail, Jhajjar and 3.37 ha open forest in Kairu, Bhiwani. In moderately dense forest areas of Haryana, the maximum area of 56.8 ha (Nandha Reserve Forest, Rewari), followed by 52.5 ha (Khudana Gram Panchayat, Nimbi, Mahendragarh) and 51.8 ha (Balali, Bhiwani), was recorded.

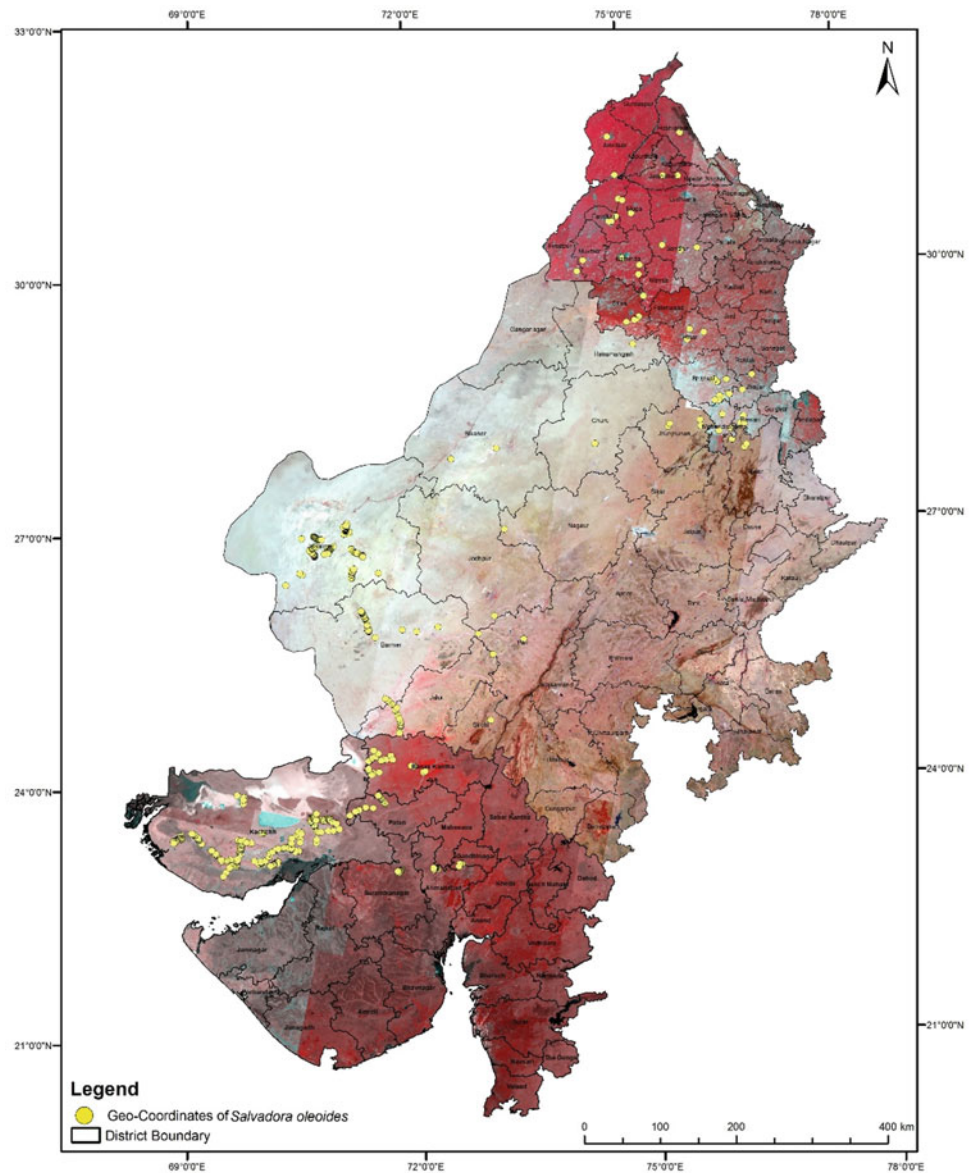
Table 1 Distribution of *Salvadora oleoides* in northwestern India

Sl. No	States	Districts	Area (in ha), dominance (%), population density (trees/ha)			
			Moderate	Open	Scattered trees (Nos.)	Total area
1	Punjab	Faridkot	9.35, 90, 111.11	–	A*	9.35
2		Mansa	–	16.79, 95, 66.67	A	16.79
3		Muktsar	–	1.59, 97, 55.57	P (1 + 1*)	1.59
4		Bhatinda	–	4.74, 98, 55.57	A	4.74
5		Amritsar [#]	–	–	P (1)	–
6		Jalandhar [#]	–	–	P (1)	–
7		Firozpur [#]	–	–	P (1)	–
8		Sangraur [#]	–	–	P (1)	–
9		Moga [#]	–	–	P (1)	–
10		Hoshiarpur [#]	–	–	P (1)	–
		Total	9.35	23.12	P (8)	32.47
1	Haryana	Rewari	82.60, 98, 133.32	15.90, 95, 33.33	P (7)*	98.5
2		Jhajjar	2.58, 98, 77.78	0.65, 96, 11.11	P	3.23
3		Bhiwani	91.0, 98, 88.89	113.77, 95, 33.33	P (3)*	204.77
4		Sirsa	9.37, 95, 33.33	0.65, 98, 22.22	P (2)	10.02
5		Mahendragarh	52.50, 95, 155.54	16.43, 90, 22.22	P (2 + 10*)	68.93
6		Hisar	–	13.72, 96, 144.43	A	13.72
		Total	238.05	161.12	P (24)	399.17
1	Rajasthan	Jhunjhunu	–	864.00, 92, 199.98	P (4)*	864.00
2		Hanumangarh	–	–	P (1)	–
3		Jodhpur	0.540, 97, 88.89	–	0.132, 95, 11.11, P (8 + 2*)	0.672
4		Jalore	0.258, 95, 88.89	0.58, 98, 22.22	P (17)	0.838
5		Barmer	–	20.66, 94, 33.33	32.64, 90, 11.11; P (21)	53.30
6		Pali	–	–	P (3 + 4*)	–
7		Jaisalmer	–	0.25, 98, 22.22	139.67, 70, 22.22, P (47 + 9*)	139.92
8		Bikaner*	–	–	P (7)	–
9		Churu*	–	–	P (3)	–
10		Sirohi*	–	–	P (1)	–
11		Alwar*	–	–	P (6)	–
		Total	0.798	885.49	172.44, A (133)	1058.73
1	Gujarat	Bhuj (Kachchh)	21.18, 98, 55.56	20.80, 96, 22.22	P (53)	41.98
2		Patan	1.27, 96, 44.44	3.51, 98, 11.11	P (2)	4.78
3		Banaskantha	8.14, 98, 55.56	–	P (17)	8.14
4		Ahmedabad	–	12.13, 98, 11.11	–	12.13
5		Surendranagar	–	1.32, 90, 22.22	–	1.32
6		Bharauch*	–	–	P (1)	–
		Total	30.59	37.76	P (73)	68.35
Grand Total			278.79	1107.49	172.44, P (238)	1558.72

Note: 1. The points indicated by # and * were selected from Bast and Kaur (2017) and Malik et al. (2010)

2. P = Tree Present; A = Tree Absent.

Fig. 1 LANDSAT 8 showed geographical distribution of *S. oleoides* in northwestern India



In Rajasthan, a total of 106 sites and scattered trees were surveyed. The maximum area of 864 ha was recorded as open forest in Bhuna-Ke-Jaal, Jhunjhunu. This was followed by Jaisalmer (0.25 ha, open; 139.67 ha, scattered) and Barmer (20.66 ha, open; 32.64 ha, scattered), respectively. The minimum area was recorded in Jodhpur (0.540 ha, moderate; 0.132 ha, scattered) and Jalore (0.258 ha, moderate; 0.58 ha, open), respectively. In Gujarat, data pertaining to 145 sites and scattered trees were recorded, where only 0.15% trees were under moderately dense, 34.93% belong to open forest and 0.50% were sparsely distributed. The maximum moderately dense forest area of 6.86 ha was recorded in Charda village, Banaskantha, which was followed by 3.42 ha in Loriya village and 2.10 ha in Bhimasar village, Kachchh, Bhuj, respectively. In the open forests, the

maximum area was recorded as 6.43 ha (Ahmedabad), followed by 3.28 ha (Kakdbit village) and 3.10 ha (Sumrasar) of Kachchh, Bhuj.

4 Discussion

Various anthropogenic activities, physiological, ecological and genetic causes, invasion of exotic species and poor scientific knowledge have significantly contributed to the declining population of *S. oleoides*. Consequently, the moderate dense forest has gradually converted into open type. In all the states, *S. oleoides* is categorized into open, moderately dense and scattered trees. The map prepared herein gives the detailed distribution of species across its

geographical range. Assessment of forest genetic resources is a key for any conservation programme. In spite of its high ecological value, limited efforts have been made regarding its conservation, which requires immediate attention. The preservation of evolutionary perspective of the species by maintaining genetic diversity is one of the major goals in species conservation. Therefore, restoration programmes, such as cryogene bank, *ex situ* and *in situ* conservation would play a significant role in sustainable germplasm management (Bissati et al. 2020; Mehalaine and Chenchouni 2021). Furthermore, sacred groves may play a key role in the conservation and protection of plant species having religious as well as medicinal value (Yadav et al. 2010). The high genetic diversity maintained within populations indicates an appropriate sampling design for *ex situ* safeguarding to capture and ensure the long-term viability of this species.

5 Conclusion

The important aspects of genetic conservation of *S. oleoides* include the status of geographical distribution and the knowledge of ecological adaptation. The population showed homogeneity of diversity indices and bore a greater capacity to oppose the natural loss of variability by genetic drift. The species revealed irregular and erratic flowering, fruit bearing, low seed viability and susceptible to fungal attack, thus, macropropagation of this species would play a vital role in large-scale afforestation and restoration programmes in the arid zones. For the administrative setup and policy decision makers of the country, the corridors for grazing needs to be decided and critically examined with scientific impetus in the open forest and revenue land.

The sites are of immense importance to forest officials, scientists and academician for future planning, management and research. The distribution map would be helpful in predicting new sites of potential distribution through an appropriate modelling approach.

Acknowledgements The financial support by the Ministry of Environment, Forest and Climate change (MoEF & CC), Government of India, New Delhi, is gratefully acknowledged. The corresponding author is highly obliged for travel support to attend the 2nd—Springer Conference of the Arabian Journal of Geosciences (CAJG), 25–28 November, 2019 at Sousse, Tunisia by the Uttarakhand State

Council for Science & Technology (UCOST), Dehradun, India, vide reference No. UCS&T/TRAVEL-10/19-20/17190/1, dated 10/12/2019. Authors are also thankful to the four anonymous reviewers for critically examining the manuscript.

References

- Ahmad, F.: GIS, GPS and remote sensing application to investigate agricultural potential in Cholistan. *Sociedade Natureza Uberlandia* **19**, 55–64 (2007)
- Ashutosh, S., Pandey, D., Kaur, T., Bajpai, R.K.: Knowledge-based remote sensing and GIS approach for forest type mapping in Kathua district, Jammu and Kashmir. *Tropical Ecol.* **51**, 21–29 (2010)
- Bast, F., Kaur, N.: Nuclear and plastid DNA sequence-based molecular phylogeography of *Salvadora oleoides* (Salvadoraceae) in Punjab, India reveals allopatric speciation in anthropogenic islands due to agricultural expansion. *J. Phylogenetics Evol. Biol.* **5**(180), 1–7 (2017)
- Bhandari, M.M.: *Flora of Indian Desert*, Scientific Publisher, Jodhpur, p. 471 (1978)
- Bissati, S., Boudjenah, S., Morisset, C., Chenchouni, H.: Does pre-culture in sugar-rich media affect carbohydrate content and post-thawing recovery rate of cryopreserved potato (*Solanum phureja*) shoot tips?. *J. King Saud Univ. Sci.* **32**(3), 1917–1924 (2020). <https://doi.org/10.1016/j.jksus.2020.01.045>
- Hardikar, S.A., Panchal, N.S., Pandey, A.N.: Growth, water status and nutrient accumulation of seedlings of *Salvadora oleoides* (Decne.) in response to soil salinity. *Tropical Ecol.* **2**(3), 253–264 (2011)
- Malik, S.K., Chaudhury, R., Dhariwal, O.P., Bhandari, D.C.: *Salvadora* Species (Pilu and Miswak). In: *Genetic Resources of Tropical Underutilized Fruits in India*. NBPGR, New Delhi, pp. 125–128, 168 (2010)
- Mehalaine, S., Chenchouni, H.: New insights for the production of medicinal plant materials: *ex vitro* and *in vitro* propagation of valuable Lamiaceae species from northern Africa. *Curr. Plant Biol.* **27C**, 100216 (2021). <https://doi.org/10.1016/j.cpb.2021.100216>
- Saini, S., Yadav, J.P.: Genetic variation in natural population of *Salvadora oleoides*: an important medicinal plant that need conservation. *Asian J. Plant Sci. Res.* **3**(5), 20–27 (2013)
- Shankhwar, R., Bhandari, M.S., Meena, R.K., Sekhar, C., Pandey, V. V., Saxena, J., Kant, R., Barthwal, S., Naithani, H.B., Pandey, S., Pandey, S., Ginwal, H.S.: Potential eco-distribution mapping of *Myrica esculenta* in Northwestern Himalayas. *Ecol. Eng.* **128** (2019), 98–111 (2019)
- Singh, M.N., Mishra, A.K., Bhatnagar, S.P.: *In vitro* production of plants from cotyledon explants of *Cucumis melo* L. and their successful transfer to field. *Phytomorph* **46**, 395–402 (1996)
- Yadav, S., Yadav, J.P., Arya, V., Panghal, M.: Sacred groves in conservation of plant biodiversity in Mahendergarh district of Haryana. *Indian J. Traditional Knowl.* **9**, 693–700 (2010)
- Zodape, S.T., Indusekhar, V.K.: *Salvadora persica*: a boon to wasteland development. *J. Sci. Ind. Res.* **56**, 657–661 (1997)

**Biogeochemistry, Geobiology, Geoecology,
Geoagronomy (T2): Recent Advances in
Geoagronomy**



Improving Date Palm Morphology and Yield Production of *Deglet Nour* Dates by the Application of Organic and/or Mineral Amendment

Nissaf Karbout, Roland Bol, Rawan Mlih, Mohamed Moussa, Nadhem Brahim, and Habib Bousnina

Abstract

A field study was carried out during the years 2014, 2015 and 2016 on 30-year-old Deglet Nour cultivar trees growing in sandy soil in oasis of Fatnassa (Tunisia). Organic fertilizer originated from farm manure (F) and mineral amendment bentonite (B) were applied into sandy soils (S). Farm manure was applied either singly (SF) or in combination with bentonite (SBF) in order to study their influence on the date yield, morphology and NPK contents of date palm trees. The results revealed that applying organic manure singly or in combination with bentonite did increase palm yield as compared with the untreated soil (U). In general, the morphology of date palm trees was improved after the amendment addition. Higher production and amelioration were obtained by the application of organic manure in combination with bentonite (SBF) compared with organic manure fertilization apart.

Keywords

Soil amendment • Deglet Nour • Date palm • Organic fertilizer • Bentonite

1 Introduction

Date palm (*Phoenix dactylifera* L.) is one of the oldest fruit trees in the world. It is known as “tree of life” because of its resilience, need for limited water inputs, long-term productivity and multiple uses (Marzouk and Kassem 2011). In Tunisia, the date palm crop covers an area of 42,000 ha producing annually 241,000 metric tons of dates. Dates contribute significantly to the economic development of the desert areas in southern Tunisia and have an important social impact, providing a livelihood for nearly 50,000 oasis citizens. Tunisia is the world's leading export value of date crops and the world leading producer of “Deglet Nour” variety (Mbage et al. 2011). Most of the date palms produced in Tunisia are grown in sandy soils. This type of soils lacks for fertility. The use of chemical fertilizer is thus necessary for supplying the nutrient requirements as N, P and K. However, the continuous use of chemical fertilization leads to the deterioration of soil characteristics and fertility, as well as the probability of accumulation of heavy metals in plant tissues which contributes to the deterioration of fruit nutritional value and edible quality (Hannachi et al. 2015). The second source of nutrients is organic manure which is derived from animal or plant sources. Manure contains the macro- and micro-mineral elements and provides key nutrients for crop growth (Fronning et al. 2008; Oustani et al. 2015). Manure has several other beneficial effects on soil properties. It was found to improve the structural stability and decrease the bulk density of the soil. It improves moisture retention, water infiltration rate and the hydraulic conductivity of soil. On the long term, the use of organic manure enhances the crop growth and yield (Gregory et al. 2016). On the other hand, the use of mineral amendment has positive effects on soil structure, water retention and bulk density. Bentonite, specifically, has a great effects when applied to sandy soils as it improves soil health through amelioration of soil physical characteristics which in turn results in better yield of the crop (Zhou et al. 2019).

N. Karbout (✉) · M. Moussa
Institute of Arid Regions, Djorf km 22, Mednine, Tunisia

N. Karbout · H. Bousnina
National Institute of Agronomic of de Tunisia, 43 Street Charles
Nicolle 1082, Tunis, Tunisia

R. Bol · R. Mlih
Institute of Bio- and Geosciences, Agrosphere (IBG-3),
Forschungszentrum Jülich GmbH, Jülich, Germany

N. Brahim
Faculty of Sciences of Tunis, University of Tunis El Manar, 2092
El Manar II, Tunis, Tunisia

However, studies on the use of organic manure in combination with bentonite and their effects on the morphological characteristics of date palm and the yield are lacking. The present study was undertaken to investigate the effect of farm manure (F) and bentonite (B) on the morphology, fruit quality and nutritional value of Deglet Nour date palm.

2 Materials and Methods

A fully randomized, experimental block design was implemented in Fatnassa oasis for three years. The design contains nine plots (3 treatments \times 3 replicates) of the same dimension (3 m \times 3 m). These treatment plots were: (i) untreated soil plots (U), (ii) farm manure with local sand (SF), (iii) Farm manure (F) with bentonite (B) and local sand (S). The manure was applied at a rate of 27 kg per plot, equivalent to 30 t/ha, the sand was applied at a height of 20 cm which is equal to 180 kg per plot, while the bentonite was applied at a rate of 8 t/ha. Chemical characteristics are shown in Table 1. Date palms of Deglet Nour variety with similar vigor, height, and age (30 years old) were selected and subjected to the normal cultural practices applied for different treatments; we have three replicates (1 replicate = 2 palm trees) per treatment (i.e. 2 \times 3 \times 3 = 18 palm trees).

3 Results

3.1 Effect of Organic/mineral Amendment on Morphological Characteristics of the Date Palm

In the first year after the introduction of the various amendments (2014), the circumference, the number of palms per palm tree and the length of the palms of the palm did not change ($p > 0.05$) among all treatments. In the second and

third year (2015, 2016) after the implementation of the various amendments, the circumference of the palms of the amended plots improved in comparison with the control plots. The differences were more pronounced in the third year. The recorded values were 226 ± 0.64 cm for SBF, and 192 ± 0.98 cm for SF while 172 ± 0.55 cm for the control treatment. The number and length of date palms increased significantly ($p < 0.05$) in the amended plots compared to the control treatment (Table 2).

3.2 Amendment Effects on Leaf NPK Composition and Total Production Yield

The effect of the amendments on NPK contents in date palm leaf was not significant until the second season after the soil was amended. The N contents recorded during the third season were 160 ± 0.9 mg kg⁻¹ and 220 ± 0.6 mg kg⁻¹ for SF and SBF, respectively. The P contents were 16 mg kg⁻¹ and 17 mg kg⁻¹ for, SF and SBF, respectively, against 10 mg kg⁻¹ for the control soil. The K contents were 120 mg kg⁻¹ and 200 mg kg⁻¹ for SF and SBF, respectively, against 10 mg kg⁻¹ for the control soil. The maximum production of dates increased to 79.15 ± 5.2 kg date/palm for soil amended with SBF (Fig. 1).

4 Discussion

In the first year of application of the various amendments, an insignificant change was observed in date palm morphology, NPK composition and dates production in general in all treatments. This can be explained by the distraction of the roots following the renewal of the substrate and the plowing activity for the upper layers of the soil, which induced the palm tree to regenerate its root system (Ibrahim et al. 2013). In the years 2015 and 2016, a significant improvement was

Table 1 Physical and chemical characteristics of the materials used in the amendment

Treatment	Untreated soil (U)	Farm manure (F)	Bentonite (B)
pH	8.07 \pm 0.02	6.05 \pm 0.2	7.9 \pm 0.02
EC (dS m ⁻¹)	2.61 \pm 0.01	11.87 \pm 0.3	8.3 \pm 0.01
Gypsum (%)	72.5 \pm 0.9	nm ^a	nm
Phosphorus (mg kg ⁻¹)	0.34 \pm 0.03	3.99 \pm 0.2	3.4 \pm 0.03
potassium (mg kg ⁻¹)	175 \pm 2.6	1230 \pm 0.2	46,76 \pm 2.6
C (%)	<0.05	47.05 \pm 2.3	nm
N (%)	<0.05	19.5 \pm 3.6	0.22 \pm 0.05
Permeability (cm h ⁻¹)	67.4 \pm 2.3	nm	nm
Porosity	0.48 \pm 0.01	nm	nm
Bulk density (g cm ⁻³)	1.37 \pm 0.04	nm	nm

^anm denotes not measured

Table 2 Effect of organic amendments farm manure (F) with and without the addition of bentonite (B) on the morphological characteristics of the date palms

Treatments	Circumference (cm)			Number of palms/palm tree			Length of palm tree (cm)		
	2014	2015	2016	2014	2015	2016	2014	2015	2016
U	172 ± 0.25 ^a	172 ± 0.55 ^c	172 ± 1.2 ^b	40 ^a	40 ^b	42 ^d	32 ± 0.1 ^a	33 ± 0.2 ^b	29 ± 0.1 ^a
SF	189 ± 0.96 ^a	190 ± 0.88 ^a	192 ± 0.98 ^a	45 ^a	50 ^a	54 ^a	37 ± 0.2 ^a	60 ± 0.5 ^a	59 ± 0.3 ^c
SBF	180 ± 0.84 ^a	195 ± 0.52 ^b	226 ± 0.64 ^a	41 ^a	54 ^b	60 ^b	34 ± 0.5 ^a	65 ± 0.2 ^a	69 ± 0.8 ^c

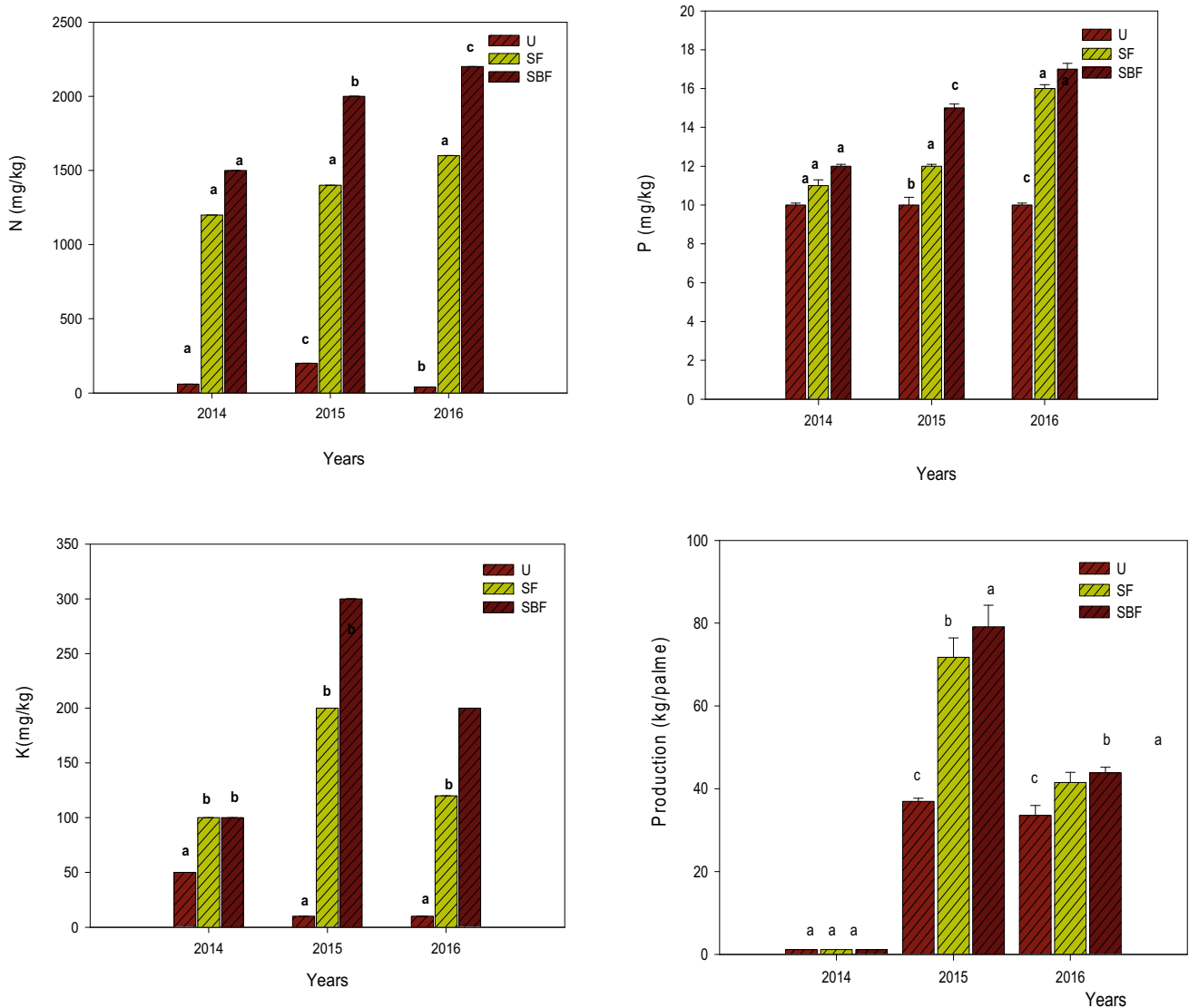


Fig. 1 Amendment effects on leaf NPK composition and total production yield

observed in the morphology and crop yield production in SF and SBF treatment plots; the effects were more pronounced in SBF compared to SF. The above results support the importance of bentonite combined with the organic matter

for overall improvement of the soil physical and chemical properties and thereafter date palm morphological characteristics and dates yield (Shawky et Yousif 1990; Abou Sayed-Ahmed et al. 2005; Mbaga et al. 2011).

5 Conclusion

The use of organic fertilizers (manure) integrated with bentonite clay can sustainably improve sandy soils fertility in oasis agrosystem and thus enhance the yield of date palm crop.

References

- Abou Sayed-Ahmed, T.A., Abdalla, K.M., EL-Makhtoum, F.B., Aly, M.A.: Influence of some fertilization treatments on yield and fruit quality of amry date palms grown in sandy soil. *Zagazig J. Agric.* **32**(9), 1475–149 (2005)
- Fronning, B.E., Thelen, K.D., Min, D.H.: Use of manure, compost, and cover crops to supplant crop residue carbon in corn stover removed cropping systems. *Agron. J.* (2008). <https://doi.org/10.2134/agronj2008.0052>
- Gregory, A.S., Dungait, J.A.J., Watts, C.W., Bol, R., Dixon, E.R., White, R.P., Whitmore, A.P.: Long-term management changes topsoil and subsoil organic carbon and nitrogen dynamics in a temperate agricultural system. *Eur. J. Soil Sci.* (2016). <https://doi.org/10.1111/ejss.12359>
- Hannachi, N., Cocco, S., Fornasier, F., Agnelli, A., Brecciaroli, G., Massaccesi, L., Weindorf, D., Corti, G.: Effects of cultivation on chemical and biochemical properties of dryland soils from Southern Tunisia. *Agr. Ecosyst. Environ.* **199**, 249–260 (2015). <https://doi.org/10.1016/j.agee.2014.09.009>
- Ibrahim, M.M., El-Beshbeshy, R.T., Kamh, N.R., Abou-Amer, A.I.: Effect of NPK and biofertilizer on date palm trees grown in Siwa Oasis, Egypt. *Soil Use Manage.* **29**, 315–321 (2013)
- Marzouk, H.A., Kassem, H.A.: Improving fruit quality, nutritional value and yield of Zaghoul dates by the application of organic and/or mineral fertilizers. *Sci. Hortic.* **3**(127), 249–254 (2011)
- Mbaga, M., Al-Shabibi, M.S.R., Boughanmi, H., Zekri, S.M.: A comparative study of dates export supply chain performance: the case of Oman and Tunisia. *Benchmarking: Int. J.* **18**, 386–408 (2011)
- Oustani, M., Halilat, M. T., Chenchouni, H.: Effect of poultry manure on the yield and nutrients uptake of potato under saline conditions of arid regions. *Emir. J. Food Agric.* **27**(1), 106–120 (2015). <https://doi.org/10.9755/ejfa.v27i1.17971>
- Shawky, I., Yousif, M., El-Gazzar, A.: Effect of nitrogen fertilization on ‘Sewy’ datepalm. In: *Inter. Conf. Date Palm*. Assiut University, 9–11 (1990)
- Zhou, L., Monreal, C.M., Xu., Shengtao, McLaughlin, N.B., Zhang, H., Hao, G., Liu, J.: Effect of bentonite-humic acid application on the improvement of soil structure and maize yield in a sandy soil of a semi-arid region. *Geoderma* **338**, 269–280 (2019). <https://doi.org/10.1016/J.GEODERMA.2018.12.014>



Impact of Subsurface Drip Irrigation on Water Distribution, Photosynthetic Production and Crop Yield in Olive Orchard in Southern Tunisia

Abderrahman Sghaier, Dalenda Boujnah, Mohamed Ouessar, Rayda Ben Ayed, and Kamel Naggaz

Abstract

A two-year study was conducted to evaluate the physiological and biological effects of the introduction of an SDI system on adult olive tree in a 58-year-old olive (*Olea europaea* L. cv. Zarrazi) orchard located at Bir-lahmar, Tataouine, Tunisia. Irrigation was applied every three days at 3 am, by an automatic subsurface drip irrigation system with four (3.8 L h⁻¹) dripper per tree buried at a depth of 0.6 m. The water salinity was 1.5 g L⁻¹. Net photosynthetic production and soil water content were monitored regularly during the experiment. Soil characteristics were analyzed at the beginning of the experiment. Olive production and olive-oil production were measured at the end every year. Irrigated trees reached more than 60% higher photosynthesis production than rainfed ones. In the second year only, irrigated trees produced olives. The wetting pattern showed that most of irrigation water was delivered to the deep soil layer. As well, the system appeared efficient in distributing the water horizontally.

Keywords

Subsurface drip irrigation • *Olea europaea* • Arid-land • Wetting pattern • Tree physiology

A. Sghaier (✉)

Faculty of Sciences of Gabes, University of Gabes, 6072 Gabes, Tunisia

A. Sghaier · M. Ouessar · K. Naggaz

Institut des Régions Arides (IRA), 4119 Médenine, Tunisia

D. Boujnah

Laboratoire d'Amélioration de la Productivité de l'Olivier et de la Qualité des Produits, Institut de l'olivier, Unité Spécialisée de Sousse, Rue Ibn Khaldoun, B.P. 14, 4061 Sousse, Tunisia

R. Ben Ayed

Laboratory of Molecular and Cellular Screening Processes, Center of Biotechnology of Sfax, Address: B.P 1177, 3018 Sfax, Tunisia

1 Introduction

In southern Tunisia, most olive orchards (*Olea europaea* L.) are rainfed. Moreover, future projections of climate change show an even more dramatic situation characterized by an increase in temperature and a decrease in precipitation (Sonwa et al. 2017). Thus, a proper management of irrigation is crucial to achieve maximum water efficiency. Subsurface drip irrigation (SDI) is one of the most promising systems in terms of water use efficiency. This system supplies water directly to the root zone via buried drippers (Greenland et al. 2018).

However, the SDI introduction has been tested on either young or already irrigated crops. The SDI installation in fully grown non-irrigated trees may face the well-developed and expended root system, that can reach 50 m in length (Soda et al. 2017). Besides, the fine roots, which are crucial for water absorption, are usually deep in soil and well spread. A problem that is absent in irrigated olives when the root system is reshaped to settle around the dripper (Deng et al. 2017).

The authors set out to understand the physiological and biological effects of the introduction of an SDI system on a fully grown olive tree. The authors specifically investigated the influence of a simple and easy to install SDI system on net photosynthesis production and yield on mature cv. Zarrazi olive trees also study the wetting pattern of the underground dripper in the presence of a lime crust.

2 Materials and Methods

The experiment was conducted between Mars 2016 and February 2018 in a 58-year-old olive (*Olea europaea* L. cv. Zarrazi) orchard located at Bir-lahmar, Tataouine, Tunisia (33°11'37.9"N, 10°29'32.7"E, 142 m altitude).

Soil moisture measurement: The volumetric water content of the soil (θ_v) was monitored using a time domain

reflectometry TDR IPH. The photosynthesis was measured using an LCI-SD portable photosynthesis system equipped with a broad leaf chamber (Analytical Development Company Ltd., England) using sunlight as a source of light and external air as a source of CO₂.

A soil profile was dug at a depth of 120 cm to study the soil characteristics in the orchard. At a depth of 40 cm, a lime crust of between 15 and 25 cm in thickness was observed. The gravimetric method was used to determine the soil texture. The field capacity (0.33 bar, pF 2.5) and the permanent wilting point (15 bar, pF 4.2) were determined by the membrane method.

3 Results

3.1 Climatic Data

Weather data were provided by the national institute of meteorology-Tunisia from their station in Bir-lahmar. The data of daily evolution of maximum daily temperature (MDT) and daily precipitation (P) were analyzed. The maximum daily temperature (MDT) ranges between 3.4 °C during the month of January and 46.8 °C during the month of June, which holds the highest monthly average temperature. During 2017, precipitation exceeded the annual average for the region. According to Fig. 1, rainfalls were scattered on numerous small rainy events.

3.2 Soil Characteristics

Soil texture characteristics, field capacity (FC) and permanent wilting point (WP) are shown in Table 1. For the depth

0.2 m, the soil was sandy. However, it was classified as sandy-loam for depths ranging from 0.6 m to 1 m. The deepest sample (1.2 m) was sandy-clay-loam. Field capacity ranged from 15.08% to 22.43%. While permanent wilting point showed more variability (5.53–16.73%). Both parameters were typical for the region.

3.3 Water Distribution

Measurement points E1 and E2 showed higher soil water content at depths near the dripper. Furthermore, measurements taken above the lime crust were the lowest. This indicates that irrigation water did not rise to the surface. In addition, the system delivered the irrigation water at depths safe from evaporation.

3.4 Photosynthesis

From Fig. 1, it is clear that the trend of net photosynthetic production in irrigated trees is not following the changes in rainfall. Hence, the photosynthetic production in irrigated olives do not depend on precipitation. This indicates that irrigation was indeed beneficial and effective for olive trees despite the well-developed and spread root system typical in olive trees in this region.

4 Discussion

In 2017, the irrigated trees produced 47.25 kg/tree which is above the national average for the south of Tunisia (33 kg/tree) (OLIVÆ 2018). The rainfed trees did not

Fig. 1 Changes in the photosynthesis production for irrigated (Irr) and rainfed (Rfed) olive orchards in southern Tunisia

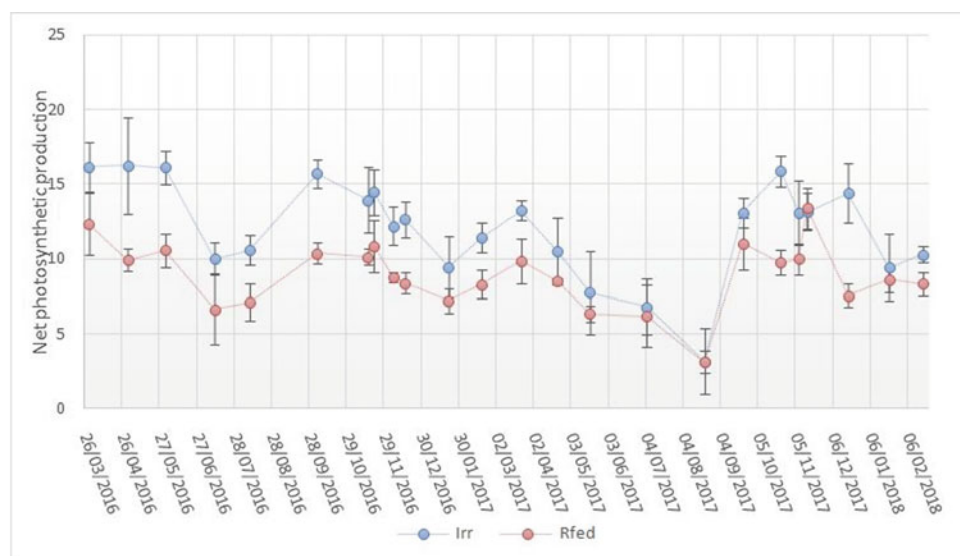


Table 1 Soil characteristics for different depths (up to 1.2 m)

Soil depth, cm	% Sand	% Silt	% Clay	% OM	% FC	% WP
20	93	0	8.5	0.34	15.08	5.53
60	77.9	8.7	8.5	0.138	20.29	11.97
80	76	8	11.75	0.966	22.43	16.73
100	70.5	9	15	0.483	26.92	19.23
120	66	12	20.5	0.138	19.03	15.40

produce in 2017. This is considered normal since the alternation for rainfed trees can be reached 3–5 years depending on the climatic condition (Fleskens et al. 2005). Moreover, water productivity showed better results than other traditional drip irrigation techniques (Correa-Tedesco et al. 2010). This shows that irrigation was not only successful in improving the physiological aspects, but it was advantageous in significantly improving the yield.

5 Conclusions

The present work shows the physiological and biological effects of the introduction of an SDI system on an adult olive tree. The subsurface drip irrigation successfully delivered most of the irrigation water to the deep soil layer avoiding the top layer. Further, the system appeared efficient in distributing the water horizontally. These improvements showed a clear impact on photosynthesis production and olive production, which means that the use of the SDI on adult olives is effective. Consequently, the SDI can be considered as an efficient and effective solution to shift rainfed olive orchard to irrigation.

References

- Correa-Tedesco, G., Rousseaux, M.C., Searles, P.S.: Plant growth and yield responses in olive (*Olea europaea*) to different irrigation levels in an arid region of Argentina. *Agric. Water Manag.* **97**(11), 1829–1837 (2010)
- Deng, S., Yin, Q., Zhang, S., Shi, K., Jia, Z., Ma, L.: Drip Irrigation affects the morphology and distribution of olive roots. *Hort. Sci.* **52** (9), 1298–1306 (2017)
- Fleskens, L., Stroosnijder, L., Ouassar, M., De Graaff, J.: Evaluation of the on-site impact of water harvesting in Southern Tunisia. *J. Arid Environ.* **62**(4), 613–630 (2005)
- Greenland, S.J., Dalrymple, J., Levin, E., O'Mahony, B.: Improving agricultural water sustainability: strategies for effective farm water management and encouraging the uptake of drip irrigation. In: *The Goals of Sustainable Development*. Springer, Berlin, pp. 111–123 (2018)
- OLIVÆ: The Tunisian olive sector. *Olivæ (Official Journal of the International Olive Council)* (124), 1–38 (2018)
- Soda, N., Ephrath, J.E., Dag, A., Beiersdorf, I., Presnov, E., Yermiyahu, U., Ben-Gal, A.: Root growth dynamics of olive (*Olea europaea* L.) affected by irrigation induced salinity. *Plant Soil* **411** (1–2), 305–318 (2017)
- Sonwa, D.J., Dieye, A., El Mzouri, E.-H., Majule, A., Mugabe, F.T., Omolo, N., Brooks, N., et al.: Drivers of climate risk in African agriculture. *Climate Dev.* **9**(5), 383–398 (2017)



Heavy Metal Content of *Mentha piperita* Samples Irrigated with Wastewater and Appraisal of Human Health Risk

Ilker Ugulu, Zafar Iqbal Khan, Sidrah Rehman, Kafeel Ahmad, and Yunus Dogan

Abstract

The aim of the present research was to determine the trace metal accumulations in water, soil and *Mentha piperita* samples irrigated with three different water regimes. The analysis was conducted by AAS. Metal concentrations in water samples ranged from 0.84 to 1.67, 0.42 to 0.72, 0.45 to 0.85, 2.51 to 9.99, 1.21 to 1.92, 1.82 to 9.98 and 0.64 to 0.91 mg/kg for Cd, Cr, Cu, Fe, Ni, Zn and Mn, respectively. Concentrations in soil samples were determined as 0.79, 0.166, 0.218, 10.01, 0.46, 1.34 and 0.34 mg/kg for Cd, Cr, Cu, Fe, Ni, Zn and Mn, respectively. Accumulations in *M. piperita* samples ranged from 0.48 to 1.06, 0.11 to 0.35, 0.15 to 0.29, 1.43 to 8.39, 0.39 to 0.54, 2.1 to 3.05 and 0.42 to 0.47 mg/kg, respectively. The metal accumulation in plant samples was lower than the permissible limits except for Cd.

Keywords

Trace metal • Vegetable • Wastewater • Health risk

1 Introduction

Unnecessary deposition of heavy metals in soil due to wastewater irrigation not only causes soil pollution, but also disturbs the safety and nutritional value of food (Ahmad et al. 2019; Bouaroudj et al. 2019; Khan et al. 2018a,b,

2019a,b). Uptake of heavy metals occurs in vegetables and accumulates in their different eatable and inedible parts (Khan et al. 2018c; Ahmad et al. 2018; Rak and Pietrucha-Urbanik 2019; Nadeem et al. 2019; Dogan and Ugulu 2013; Dogan et al. 2014a,b); the quantity of these toxic compounds is so high that it causes health problems in human beings (Dogan et al. 2013; Durkan et al. 2011; Erkol and Ugulu 2014; Ugulu 2012,2015a,b,c; Ugulu et al. 2009a, b, 2012,2016; Ugulu and Baslar 2010; Unver et al. 2015; Yorek et al. 2016; Khan et al. 2018d).

The present study was performed to determine the accumulation and translocation of trace metals in water, soil and vegetables, and also health risk index by *M. piperita* irrigated with sugar mill water.

2 Materials and Methods

This study was conducted in Khushab, Punjab, Pakistan. Seeds of *M. piperita* were grown at the end of October 2016 in 60 small plastic pots. Ten seeds of vegetable were sown in each plastic pot. One liter of the water samples was applied in experimental pots for irrigation purpose. Different treatments used for this experiment were: T-I: groundwater irrigation (GWI), T-II: canal water irrigation (CWI) and T-III: mill water irrigation (MWI). Vegetable leaves were harvested at the end of April 2017. The samples were dried and ground in a domestic grinder. Fine powder of vegetable samples was kept in the oven for three days at 75 °C and digested. The analysis was conducted by AAS (Shimadzu model AA-6300). Health risk index (HRI) is defined as ratio of daily intake of metals in food crops to the oral reference dose (Khan et al. 2018d).

$HRI = \text{Daily intake of metals} / \text{oral reference dose}$.

An HRI < 1 for any metal in vegetable means that the consumer population faces serious health risks. However, HRI > 1 does indicate a considerable health risk to the organisms consuming these vegetables.

I. Ugulu (✉)

Usak University, Usak, Turkey

Z. I. Khan · S. Rehman · K. Ahmad

University of Sargodha, Sargodha, Pakistan

Y. Dogan

Dokuz Eylul University, Izmir, Turkey

3 Results and Discussion

Trace metal concentrations in water samples ranged from 0.84 to 1.67, 0.42 to 0.72, 0.45 to 0.85, 2.51 to 9.99, 1.21 to 1.92, 1.82 to 9.98 and 0.64 to 0.91 mg/L for Cd, Cr, Cu, Fe, Ni, Zn and Mn, respectively. Among three treatments, the mean values of Fe and Zn were higher than other metal accumulations for all treatments (Fig. 1).

Maximum permissible limits (MPL) of the Cd, Cr, Cu, Fe, Ni, Zn and Mn in water were reported as 0.01, 0.5, 0.2, 5, 0.2, 2 and 0.2 mg/L, respectively, by USEPA (Khan et al. 2018d). Except for Mn, the heavy metal accumulation values in the present study were higher than these permissible maximum limits in water. According to these results, it can be mentioned that there is a water pollution in the study area.

Trace metal concentrations in soil samples were determined as 0.79, 0.166, 0.218, 10.01, 0.46, 1.34 and 0.34 mg/kg for Cd, Cr, Cu, Fe, Ni, Zn and Mn, respectively. Among three treatments, the mean concentrations of Fe, Zn and Mn were higher than other metal accumulations for all treatments (Fig. 2).

The MPL of the Cd, Cr, Cu, Fe, Ni, Zn and Mn accumulation in soil were reported as 3, 100, 50, 21,000, 50, 200 and 2000 mg/kg by USEPA (Khan et al. 2018d). All metal concentrations in the present research remained below these limits.

Trace metal accumulations in *M. piperita* samples gathered from where soil samples were taken are as follows: The

contents of Cd, Cr, Cu, Fe, Ni, Zn and Mn ranged from 0.48 to 1.06, 0.11 to 0.35, 0.15 to 0.29, 1.43 to 8.39, 0.39 to 0.54, 2.1 to 3.05 and 0.42 to 0.47 mg/kg, respectively. Among three treatments, the mean concentrations of Fe and Zn were higher than the other metals (Fig. 3).

The MPL of the Cd, Cr, Cu, Fe, Ni, Zn and Mn accumulation in plants were reported as 0.1, 5, 73, 425, 67, 100 and 500 mg/kg, respectively, by WHO (Khan et al. 2018b). The metal accumulation in *M. piperita* samples was lower than the permissible limits except for Cd. In the present study, all HRI values were less than 1 except for Cd (Table 1). If Cd is continuously deposited in human body through food, it causes fatal diseases of kidneys and many other tissues. High Cd values may be due to its usage in industrial parts (Belabed et al. 2017).

4 Conclusions

Environmental pollution by trace metals released from industrial effluent is one of the major challenging issues in many countries. In this framework, Cd, Cr, Cu, Fe, Ni, Zn and Mn accumulation in *M. piperita* samples irrigated with sugar mill water was investigated in this study. The metal accumulation in plant samples was lower than the permissible limits except for Cd. On the other hand, the recorded health risk index values were lower than 1 except for Cd.

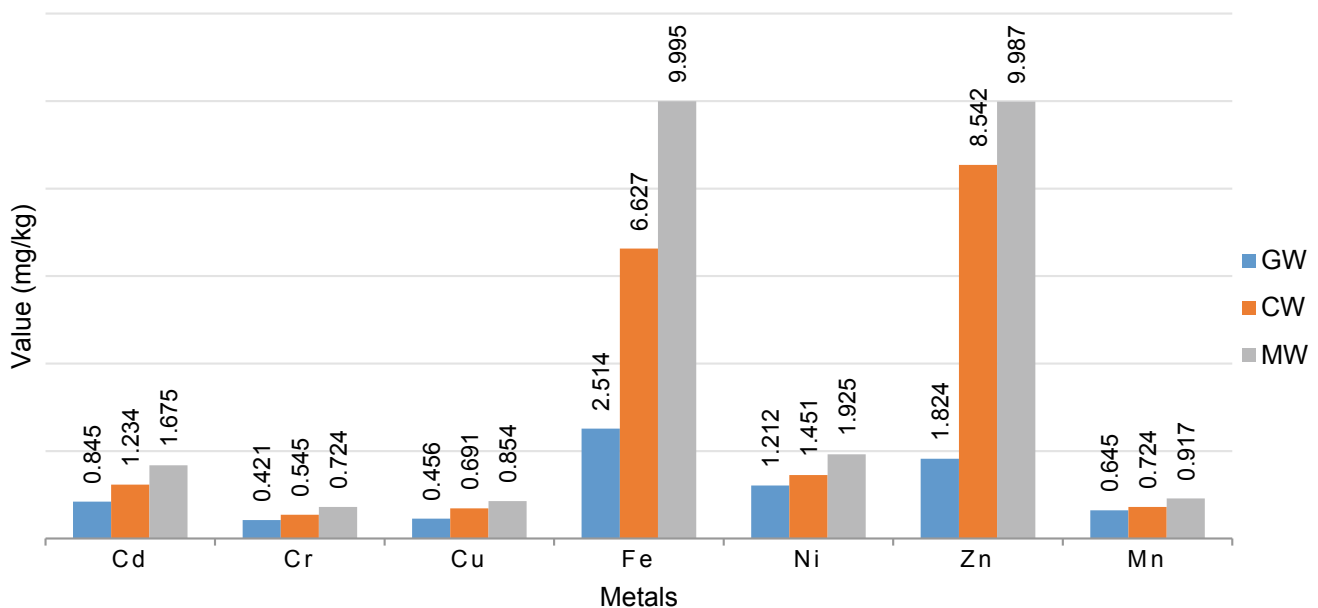


Fig. 1 Trace metal concentrations in irrigation water

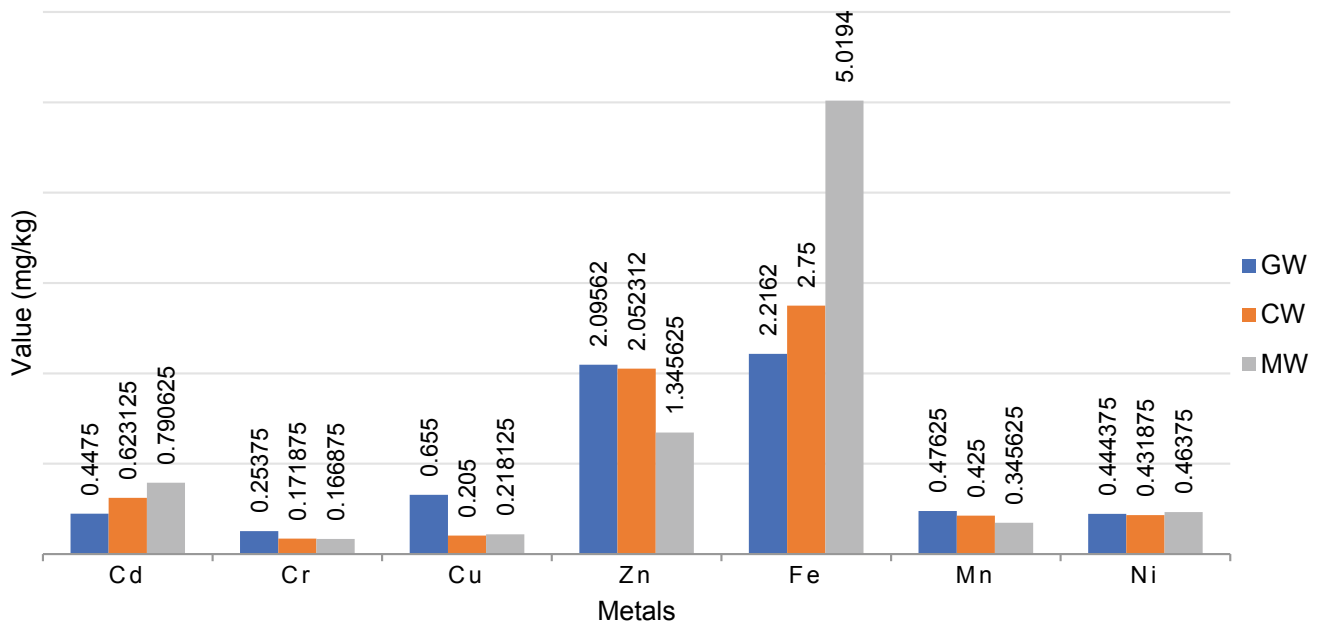


Fig. 2 Trace metal concentrations in soil

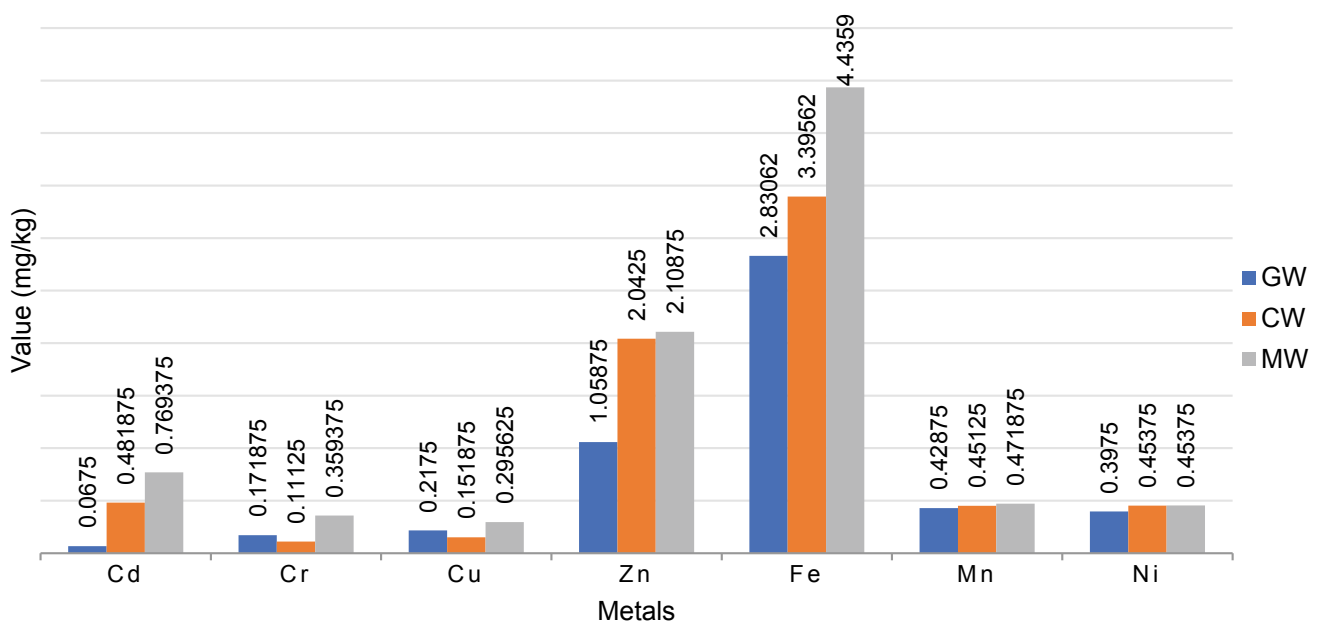


Fig. 3 Trace metal concentrations in vegetable

Table 1 Health risk index for *M. piperita*

Irrigation	Metal						
	Cd	Cr	Cu	Fe	Ni	Zn	Mn
I	6.138	0.000	0.031	0.039	0.114	0.058	0.060
II	2.770	0.000	0.021	0.068	0.130	0.048	0.063
III	4.423	0.001	0.042	0.011	0.130	0.040	0.066

References

- Ahmad, K., Nawaz, K., Khan, Z.I., et al.: Effect of diverse regimes of irrigation on metals accumulation in wheat crop: an assessment-dire need of the day. *Fresenius Environ. Bull.* **27**(2), 846–855 (2018)
- Ahmad, K., Wajid, K., Khan, Z.I., Ugulu, I., Memoona, H., et al.: Evaluation of potential toxic metals accumulation in wheat irrigated with wastewater. *Bull. Environ. Contam. Toxicol.* **102**, 822–828 (2019)
- Belabed, B.E., Meddour, A., Samraoui, B., Chenchouni, H.: Modeling seasonal and spatial contamination of surface waters and upper sediments with trace metal elements across industrialized urban areas of the Seybouse watershed in North Africa. *Environ. Monit. Assess.* **189**(6), 265 (2017)
- Bouaroudj, S., Menad, A., Bounamous, A., Ali-Khodja, H., Gherib, A., Weigel, D.E., Chenchouni, H.: Assessment of water quality at the largest dam in Algeria (Beni Haroun Dam) and effects of irrigation on soil characteristics of agricultural lands. *Chemosphere* **219**, 76–88 (2019)
- Dogan, Y., Ugulu, I.: Medicinal plants used for gastrointestinal disorders in some districts of Izmir Province, Turkey. *Stud. Ethno-Med.* **7**, 149–162 (2013)
- Dogan, Y., Ugulu, I., Durkan, N.: Wild edible plants sold in the local markets of Izmir. *Pak. J. Bot.* **45**(S1), 177–184 (2013)
- Dogan, Y., Baslar, S., Ugulu, I.: A study on detecting heavy metal accumulation through biomonitoring: content of trace elements in plants at Mount Kazdagi in Turkey. *Appl. Ecol. Environ. Res.* **12**(3), 627–636 (2014a)
- Dogan, Y., Unver, M.C., Ugulu, I., Calis, M., Durkan, N.: Heavy metal accumulation in the bark and leaves of *Juglans regia* planted in Artvin City, Turkey. *Biotechnol. Biotechnol. Equip.* **28**(4), 643–649 (2014b)
- Durkan, N., Ugulu, I., Unver, M.C., Dogan, Y., Baslar, S.: Concentrations of trace elements aluminum, boron, cobalt and tin in various wild edible mushroom species from Buyuk Menderes River Basin of Turkey by ICP-OES. *Trace Elem. Electrolytes* **28**(4), 242–248 (2011)
- Erkol, S., Ugulu, I.: Examining biology teacher candidates' scientific process skill levels and comparing these levels in terms of various variables. *Proc. Soc. Behav. Sci.* **116**, 4742–4747 (2014)
- Khan, Z.I., Ugulu, I., Ahmad, K., et al.: Assessment of trace metal and metalloid accumulation and human health risk from vegetables consumption through spinach and coriander specimens irrigated with wastewater. *Bull. Environ. Contam. Toxicol.* **101**, 787–795 (2018a)
- Khan, Z.I., Ugulu, I., Sahira, S., et al.: Determination of toxic metals in fruits of *Abelmoschus esculentus* grown in contaminated soils with different irrigation sources by spectroscopic method. *Int. J. Environ. Res.* **12**, 503–511 (2018b)
- Khan, Z.I., Ugulu, I., Umar, S., et al.: Potential toxic metal accumulation in soil, forage and blood plasma of buffaloes sampled from Jhang, Pakistan. *Bull. Environ. Contam. Toxicol.* **101**, 235–242 (2018c)
- Khan, Z.I., Ahmad, K., Safdar, H., et al.: Manganese bioaccumulation and translocation of in forages grown in soil irrigated with city effluent: an evaluation on health risk. *Res. J. Pharm., Biol. Chem. Sci.* **9**(5), 759–770 (2018d)
- Khan, Z.I., Safdar, H., Ahmad, K., et al.: Health risk assessment through determining bioaccumulation of iron in forages grown in soil irrigated with city effluent. *Environ. Sci. Pollut. Res.* **26**, 14277–14286 (2019a)
- Khan, Z.I., Arshad, N., Ahmad, K., et al.: Toxicological potential of cobalt in forage for ruminants grown in polluted soil: a health risk assessment from trace metal pollution for livestock. *Environ. Sci. Pollut. Res.* **26**, 15381–15389 (2019b)
- Nadeem, M., Qureshi, T.M., Ugulu, I., et al.: Mineral, vitamin and phenolic contents and sugar profiles of some prominent date palm (*Phoenix dactylifera*) varieties of Pakistan. *Pak. J. Bot.* **51**(1), 171–178 (2019)
- Rak, J.R., Pietrucha-Urbanik, K.: An approach to determine risk indices for drinking water—study investigation. *Sustainability* **11**, 3189 (2019)
- Ugulu, I.: Fidelity level and knowledge of medicinal plants used to make therapeutic Turkish baths. *Stud. Ethno-Med.* **6**(1), 1–9 (2012)
- Ugulu, I.: Determination of heavy metal accumulation in plant samples by spectrometric techniques in Turkey. *Appl. Spectrosc. Rev.* **50**(2), 113–151 (2015a)
- Ugulu, I.: A quantitative investigation on recycling attitudes of gifted/talented students. *Biotechnol. Biotechnol. Equip.* **29**, 20–26 (2015b)
- Ugulu, I.: Development and validation of an instrument for assessing attitudes of high school students about recycling. *Environ. Educ. Res.* **21**(6), 916–942 (2015c)
- Ugulu, I., Baslar, S.: The determination and fidelity level of medicinal plants used to make traditional Turkish salves. *J. Altern. Complement. Med.* **16**(3), 313–322 (2010)
- Ugulu, I., Baslar, S., Yorek, N., Dogan, Y.: The investigation and quantitative ethnobotanical evaluation of medicinal plants used around Izmir province, Turkey. *J. Med. Plants Res.* **3**(5), 345–367 (2009a)
- Ugulu, I., Baslar, S., Dogan, Y., Aydin, H.: The determination of colour intensity of *Rubia tinctorum* and *Chrozophora tinctoria* distributed in Western Anatolia. *Biotechnol. Biotechnol. Equip.* **23**(SE), 410–413 (2009)
- Ugulu, I., Dogan, Y., Baslar, S., Varol, O.: Biomonitoring of trace element accumulation in plants growing at Murat Mountain. *Int. J. Environ. Sci. Technol.* **9**, 527–534 (2012)
- Ugulu, I., Unver, M.C., Dogan, Y.: Determination and comparison of heavy metal accumulation level of *Ficus carica* bark and leaf samples in Artvin, Turkey. *Oxidation Commun.* **39**(1), 765–775 (2016)
- Unver, M.C., Ugulu, I., Durkan, N., Baslar, S., Dogan, Y.: Heavy metal contents of *Malva sylvestris* sold as edible greens in the local markets of Izmir. *Ekoloji* **24**(96), 13–25 (2015)
- Yorek, N., Ugulu, I., Aydin, H.: Using self-organizing neural network map combined with ward's clustering algorithm for visualization of students' cognitive structural models about aliveness concept. *Computational Intelligence and Neuroscience ID 2476256*, 1–14 (2016)



Yields and Nutritive Value of Triticale Grown on Sludge-Amended Soil

Rajja Kchaou, Rim Baccar, Jalel Bouzid, and Saloua Rejeb

Abstract

The agricultural use of sewage sludge (SS) has increased worldwide, but few studies have been conducted in Tunisia, especially with forage crops. The aim of this research study was to estimate the impact of sewage sludge on the growth, yield and nutritional quality of triticale “*X Triticosecale* Wittmack” crop used as a diet of the milking Sicilo-Sarde ewes. Treatments were a zero-N- control (C), 6 t ha⁻¹ of (SS) equivalent to 92 kg N ha⁻¹ and 100 kg N ha⁻¹ of mineral fertilizer (MF). The results showed an increase in dry matter production with SS application, by an average value of 62% at heading stage, when compared to control. Heavy metal contents in different parts of triticale did not vary in the presence of SS, remaining approximately similar to those recorded in C and MF treatments. Results indicated that sewage sludge could be used as a fertilizer nitrogen source for triticale, without risks associated with toxic heavy metals.

Keywords

Triticale • Crop production • Nutritional quality • Sewage sludge • Organic fertilization • Soil fertility

1 Introduction

Soil fertility greatly affects forage production which often requires significant inputs of N fertilizer. A wide range of organic amendments, i.e., green waste compost, manure and other organic wastes, were tested in order to minimize the use of commercial fertilizers, achieve economic interest and avoid soil quality depletion (Alvarengaa et al. 2015). Sewage sludge, organic solid residue resulting from water treatment, may be used as an excellent substitute for inorganic fertilizers (Boudjabi and Chenchouni 2021). Due to its richness in nitrogen and phosphorus, it could be used as a soil conditioner and inexpensive source of essential plant nutrients within agriculture to improve forage production and nutritive value (Kchaou et al. 2018; Boudjabi et al. 2015, 2019).

Therefore, the current study aimed to evaluate the short-term fertilizing effect of sewage sludge application on production and nutritional quality of triticale used as a diet of the milking Sicilo-Sarde, in comparison with a classic fertilization, the ammonium nitrate, and with a control.

2 Materials and Methods

Field experiment was carried out at the experimental station of the Regional Field Crops Research Center of Beja, Lafareg (North West of Tunisia). The soil at the experimental site presented a clay-loam texture and had 7.53 pH, 18.63% moisture, 2.2% organic matter and 11.67% CaCO₃ content. Urban sewage sludge was collected at Beja wastewater treatment plant (WWTP) from sludge drying beds and analyzed. Its heavy metal contents and microbiological characteristics (fecal Coliform and nematode eggs) were below the limit values established by the Tunisian regulations (NT, 106.20) (2002).

Three treatments were applied with 4 replications: a control, a treatment fertilized with 100 kg N ha⁻¹ applied as

R. Kchaou (✉)
Regional Field Crop Research Center, BP 350, 9000 Beja, Tunisia

R. Baccar · J. Bouzid
Laboratory of Environmental Engineering and Eco Technology,
University of Sfax-Tunisia, ENIS, BP 1173-3038, Sfax, Tunisia

S. Rejeb
National Research Institute of Rural Engineering,
Water and Forest, BP 10, 2080, Ariana, Tunisia

ammonium nitrate (33%) and 6 t ha⁻¹ of SS applied 15 days before sowing, by mixing it with the 5–10 cm top soil layer. Before sowing, the cultivation area was plowed, harrowed and divided into four blocks (each of 50 m × 10 m), separated by a 2 m alley.

To follow the effect of sewage sludge on triticale plants, two harvests were conducted at tillering and heading stages. Growth parameters were analyzed with respect to shoot length, and biomass production. All plant samples were ground and analyzed. All analyses were carried out in accordance with standard methods. Total N content of plants was following the Kjeldhal digestion method. Heavy metal contents were determined by spectrophotometer.

Collected data in this study were analyzed and examined statistically using analysis of variance (ANOVA) with SPSS 20.0 for Windows. Means of four samples were compared by the Duncan Test at the 5% level of significance.

3 Results

The data recorded on shoot dry matter production variations within different treatments (SS, MF, and Control) are presented in Fig. 1. Data analysis showed that dry matter production appeared to be slightly affected by MF treatment as compared to unamended soil (control).

In contrast, this parameter showed positive response under SS application for the two stages, with an increase of 62% at heading stage compared to the control (Fig. 1).

The data recorded on heavy metal concentrations of triticale shoot parts are presented in Table 1.

It was revealed that all the heavy metal contents at heading stage were usually lower than those recorded at tillering stage. On the whole, the concentrations of all heavy metals in different parts of triticale did not vary in the presence of SS, remaining similar to those recorded in control for both development stages (Table 1). Only Cu Mn

and Ni stem contents increased significantly in the presence of SS at heading stage, but remained lower than those recorded with MF.

4 Discussion

The positive contribution of sewage sludge on crop yields was mainly reported in (Kchaou et al. 2017, 2018; Boudjabi et al. 2015, 2019). Yagmur et al. (2017) demonstrated increases in yield components and straw yields of triticale upon sewage sludge application and reported that 30 t ha⁻¹ of sewage sludge was more beneficial compared to control and inorganic fertilizer. It was observed that sewage sludge, applied at three rates (3, 6 and 9 t ha⁻¹) enhanced soil fertility and crop yield in sorghum compared to control soil (Kchaou et al. 2010). Such increments in plant biomass shown in the presence of sewage sludge can be attributed to the short-term input of plant-available nutrients, particularly N (Kchaou et al. 2017), and stimulates microbial activity contributing to a long-term maintenance of nutrients and organic matter pools.

Heavy metal contents in different parts of triticale did not vary in the presence of SS, remaining approximately similar to those recorded in C and MF treatments. The results of our study corroborated those of other investigations. In fact, it was found that sewage sludge applied at different rates did not increase heavy metal (Al, Cd, Cr, Ni, Pb and Cu) concentrations in triticale straw (Yagmur et al. 2017). In addition, they proved that straw material obtained after 30 t ha⁻¹ of SS application may be recommended for animal feeding operations without heavy metal risk. It was showed that heavy metal concentrations in wheat hay after continuous application of sewage sludge at recommended plant-available nitrogen rates were similar to those with inorganic nitrogen fertilization (Day et al. 1988). Significant heavy metal crop uptake can only occur from land application of excessive amounts of sewage sludge or its application to strongly acidic soils. Indeed, it was reported that sewage sludge, when applied to alkaline soil, precipitates heavy metals with low concentrations (Usman et al. 2012).

5 Conclusions

The data obtained from this study highlight the suitability of using SS for enhancing forage production, at least in the short term. Thus, land application of such material, obtained at little or no cost, in forage production systems is an environmentally and economically sound waste management alternative, since it can be used, as a good substitute for synthetic N fertilizer. However, such use requires a complete analysis of heavy metal contents in soil and sheep milk to

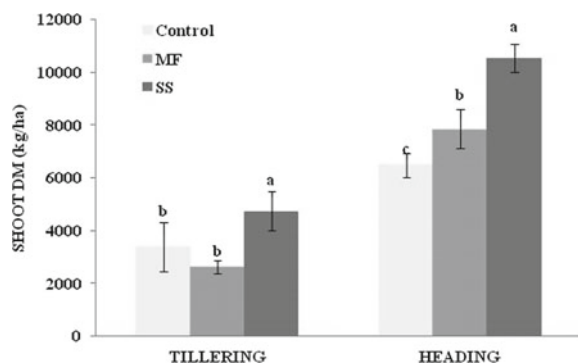


Fig. 1 Shoot dry matter (DM) of triticale at tillering and heading stages in each treatment. Different letters show significant difference within treatments in each stage at $p < 0.05$

Table 1 Heavy metal concentrations of triticale shoot parts (stem (S) and ears (E)) at tillering (T) and heading (H) stages in each treatment (Tr)

Tr	Stage	Pb		Mn		Co		Cd		Cu		Ni	
		µg/g DM											
		S	E	S	E	S	E	S	E	S	E	S	E
C	T	14.6 ab	–	134.1 a	–	8.99 a	–	1.11 a	–	11.21 a	–	29.87 a	–
	H	3.1 a	2.69 a	10.2 b	19.4 b	1.78 a	1.24 a	0.36 a	0.57 a	1.07 b	1.86 c	3.99 b	4.96 ab
MF	T	18.7 a	–	141.2 a	–	10.29 a	–	1.05 a	–	10.39 a	–	31.44 a	–
	H	2.8 a	1.88 a	13.8 a	26.8 a	1.76 a	1.15 a	0.55 a	0.37 a	2.36 a	3.26 a	4.61 a	5.5 a
SS	T	12.7 b	–	137.6 a	–	10.79 a	–	1.1 a	–	10.95 a	–	31.51 a	–
	H	3.6 a	2.56 a	13.4 a	19.4 b	1.80 a	1.44 a	0.47 a	0.32 b	2.01 a	2.44 b	4.87 a	4.56 b

(a, b, c) and (a, b, c) indicate significance differences in Pb, Mn, Co, Cd, Cu and Ni contents at tillering and heading stages, respectively.

guarantee its utilization without harmful effects on soil–plant–animal system. In addition, more continuous long-term experiments are needed to improve the understanding of the effect of different sewage sludge rates on soil fertility and crop yield to contribute to the development of sustainable agricultural practices.

References

- Alvarengaa, P., Mourinhaa, C., Fartoa, M., Santosa, T., Palmaa, P., Sengod, J., Moraisd, M.C., Cunha-Quedab, C.: Sewage sludge, compost and other representative organic wastes as agricultural soil amendments: Benefits versus limiting factors. *Waste Manage.* **40**, 44–52 (2015)
- Boudjabi, S., Chenchouni, H.: On the sustainability of land applications of sewage sludge: how to apply the sewage biosolid in order to improve soil fertility and increase crop yield? *Chemosphere* **282**, 131122 (2021)
- Boudjabi, S., Kribaa, M., Chenchouni, H.: Growth, physiology and yield of durum wheat (*Triticum durum*) treated with sewage sludge under water stress conditions. *EXCLI J.* **14**, 320–334 (2015)
- Boudjabi, S., Kribaa, M., Chenchouni, H.: Sewage sludge fertilization alleviates drought stress and improves physiological adaptation and yield performances in Durum Wheat (*Triticum durum*): a double-edged sword. *J. King Saud Univ. Sci.* **31**, 336–344 (2019)
- Day, A.D., Ottman, M.J., Taylor, B.B., Pepper, I.L., Swingle, R.S.: Liquid sludge as fertilizer for wheat. *Biocycle* **29**, 60–61 (1988)
- Kchaou, R., Khelil, M.N., Gharbi, F., Rejeb, S., Henchi, B., Hernandez, T., Destain, J.P.: Isotopic evaluations of dynamic and plant uptake of N in soil amended with ¹⁵N-labelled sewage sludge. *Pol. J. Environ. Stud.* **19**(2), 363–370 (2010)
- Kchaou, R., Khelil, M.N., Gharbi, F., Rejeb, S., Henchi, B., Destain, J. P.: Direct and residual effect of sewage sludge in a sudangrass-barley cropping system. In: Ouessar et al., (eds.), *Water and Land Security in Drylands*, chapter 11. Springer International Publishing AG, pp. 111–117 (2017)
- Kchaou, R., Baccar, R., Bouzid, J., Rejeb, S.: Agricultural use of sewage sludge under sub-humid Mediterranean conditions: effect on growth, yield, and metal content of a forage plant. *Arab. J. Geosci.* **11**, 746–752 (2018)
- Usman, K., Khan, S., Ghulam, S., Khan, M.U., Khan, N., Khan, M.A., Khalil, S.K.: Sewage sludge: an important biological resource for sustainable agriculture and its environmental implications. *Am. J. Plant Sci.* **3**, 1708–1721 (2012)
- Yagmur, M., Arpalı, D., Gulser, F.: The effects of sewage sludge treatment on triticale straw yield and its chemical contents in rainfed condition. *J. Animal Plant Sci.* **27**(3), 971–977 (2017)



Impact of Species and Nitrogen Addition on Plant Litter Decomposition in Sheepgrass Meadow in Northeast China

Xiaolei Kong, Qiang Zhang, Guili Di, Ruifen Zhu, and Jishan Chen

Abstract

Plant litter has a great potential to maintain meadow soil fertility. However, it remains unclear whether plant litter with higher N concentration would decompose faster than that with lower N, and that increase in soil nutrient availability would stimulate litter decomposition. Hence, we examined the differences in decomposition rate of litter of *Arundinella hirta*, *Carex duriuscula* and *Leymus chinensis* and nutrient availability in soils from four different N-fertilization rate treatments in a Sheepgrass (*L. chinensis* Tzvel) dominated Meadow in Northeast China. The decomposition rate was estimated by measuring the CO₂ emission during incubation. Significant interspecific differences among the treatments were found. Moreover, litter decomposition rates positively correlated with the litter N concentration in the initial stage of the incubation; then it negatively correlated with litter N and P concentrations in the late stage, while responses of litter decomposition to soil nutrient availability differed among species. Our results suggest that species type is likely the main determinant of litter decomposition, while soil nutrient availability under nutrient enrichment could affect the decomposition with consequences on C and nutrient cycling in Sheepgrass Meadow.

Keywords

Plant litter • Nitrogen Addition • Litter Decomposition

1 Introduction

Plant litter supplies nutrients and organic matter to soil via decomposition and thus can maintain soil fertility. Litter decomposition, releasing nutrients for plant and microbial uptake as well as the CO₂ emissions into the atmosphere (Austin and Vivanco 2006), has attracted considerable attention in recent decades. Litter decomposition is controlled by many biotic and abiotic factors, including chemical composition of litter or litter quality (Aerts and de Caluwe 1997b), environmental conditions, such as soil properties and climate, and decomposer communities (Aerts 1997; Araujo et al. 2012). Species types have long been suggested as one of the controlling factors affecting the litter decomposition rate, with considerable variations in decomposition rates of leaf litters among species. Overall, a large body of previous studies concentrated on the identification of general chemical predictors of litter decomposition and suggested that the decomposition rate is substantially controlled by litter properties (Aerts and de Caluwe 1997b). For example, N concentration, C/N ratio, P and lignin contents of litter were considered as a good predictor of litter decomposition rate. Some studies suggested N as the predictor in the initial stage of the decomposition, while lignin determines the late stages. However, studies on the interactive effects of soil nutrient availability and litter quality on litter decomposition remain limited (Aerts and de Caluwe 1997a, b).

Therefore, it is essential to explore N deposition on litter decomposition dynamics for an exhaustive understanding of the C cycle (Aerts et al. 2003, 2006). Here, we postulated that both N addition and species type would have strong effects on litter decomposition of single species. Specifically, N addition should promote decomposition of single-species litter, higher N concentrated litter would decompose faster than that with lower N, and increases in soil nutrient availability would stimulate litter decomposition. We hypothesized that plant litter with higher N concentration would

X. Kong · Q. Zhang · G. Di · R. Zhu · J. Chen (✉)
Institute of Pratacultural Science, Heilongjiang Academy of
Agricultural Science, Harbin, 150086, Heilongjiang, China
e-mail: cyszps@163.com

decompose faster than that with lower N concentration, which would increase soil nutrient availability and stimulate litter decomposition.

2 Materials and Methods

2.1 Site Description

The field experiment was carried out at the Forage Research Station located at Lanxi County, Heilongjiang Academy of Agricultural Sciences (HAAS).

2.2 Experimental Design and Sampling

The study consists of a field experiment and indoor incubation. The field experiment design involves four N-addition treatments in four replicates: CK (no N addition as control); LD (low addition, $1.49 \text{ g N m}^{-2} \text{ y}^{-1}$); MD (medium addition, $2.99 \text{ g N m}^{-2} \text{ y}^{-1}$); HD (high addition, $5.99 \text{ g N m}^{-2} \text{ y}^{-1}$), and the area of each block was $10 \times 10 \text{ m}$ with a 2 m buffer between the plots ($5 \times 5 \text{ m}$).

To test the interspecific differences and fertilization effects on litter decomposition, we collected the litter of the selected three dominant species (*Arundinella hirta* (C₄ grass), *Carex duriuscula* (perennial forb), and *Leymus chinensis* (C₃ grass)) in the no fertilization and later N-treated plots. Prior the implementation of the treatments in late 2010, these three species were collected from the unfertilized plots as senescent litters were used for the incubation experiment.

2.3 Laboratory Incubation and Analyses

Indoor incubation began in 2012. Plant decomposition rate was determined as described by Angers and Recous (1997). Thus, we used a laboratory incubation experiment to investigate the litter decomposition patterns of three plant species from the Songnen grassland. The plant litter decomposition rate (from 0.017 day^{-1} to 0.068 day^{-1}) was determined by measuring the CO₂ emission during decomposition.

2.4 Kinetic Model and Statistical Analyses

Decomposition kinetics was fitted with a single exponential model. All analyses were conducted using SPSS 17.0 (SPSS Inc., Chicago, USA).

3 Results

The results on the effect of N addition on litter decomposition showed that the rates of the latter differed significantly ($P < 0.001$) among the three species in each incubation period. N additions significantly influenced the decomposition rate in all incubation periods, except between 21 and 30 days. In addition, there were significant interactions between the species and N fertilization on the rate of litter decomposition (Table 1).

For all the three species, the first-order decomposition rate constant (k) varied from 0.017 day^{-1} for *A. hirta* under N-fertilized soils to 0.068 day^{-1} for *C. duriuscula* under HD fertilized soils. Among the four species, *A. hirta* had the lowest decomposition rate in all the fertilized soils (Table 4). In addition, for all the three species, the first-order decomposition rate constant (k) in N-treated soils increased with increasing nitrogen. The cumulative amount of CO₂-C evolved from *C. duriuscula* litter was generally the highest while the lowest was from *A. hirta* under litter all treatments by the models. Species types had a significant effect on litter decomposition for single species and litter decomposition decreased in the order: *C. duriuscula* > *L. chinensis* > *A. hirta*.

In the first five days of incubation, the litter decomposition rate showed positive and negative relationships with the initial litter TN concentration ($r = 0.687$, $P < 0.01$), and C/N ratio ($r = -0.625$, $P < 0.01$, Table 2), respectively. Similarly, at days 6–10, the litter decomposition rate positively and negatively correlated with the initial litter TN concentration ($r = 0.536$, $P < 0.05$), and C/N ratio ($r = -0.510$, $P < 0.05$), respectively. The decomposition rate had no relationship with TN, TP, C/N, N/P and C/P ratio at days 11–15 and 16–20, and with TN and C/P at 21–25, respectively. During the late stage of the incubation (at days 26–30), however, the litter decomposition rate had negative and positive relationship with the initial litter TN concentration ($r = -0.642$, $P < 0.01$), and C/N ratio ($r = 0.782$, $P < 0.01$), respectively. Moreover, the litter decomposition rate was negatively correlated with initial litter TP concentration ($r = -0.761$, $P < 0.01$), and positively correlated with C/P ratio ($r = 0.769$, $P < 0.01$, Table 2).

4 Discussion

The results of previous studies suggest that nitrogen inputs from litter decomposition contribute to meeting N requirement of decomposers in the initial stage of decomposition and produce a stimulating effect on the decomposition. However, the rate of litter decomposition showed a negative relationship with the initial litter TN and TP concentrations

Table 1 Two-way ANOVA of the effect of species (S) and Nitrogen (N) addition on litter decomposition in each incubation stage

Variables	Incubation days					
	1–5	6–10	11–15	16–20	21–25	26–30
Species (S)	<0.001	<0.001	<0.001	<0.001	<0.001	<0.001
Nitrogen (N)	<0.001	<0.001	<0.001	<0.001	0.376	0.054
S × N	<0.001	<0.001	<0.001	0.169	0.461	0.039

Table 2 Pearson correlation coefficients between initial litter quality parameters and litter decomposition rate

Incubation days	TN	TP	C/N	C/P	N/P
1–5	0.687**	0.266	−0.625**	−0.326	0.522
6–10	0.536*	0.258	−0.510*	−0.342	0.671
11–15	0.294	0.034	0.138	−0.025	−0.181
16–20	−0.006	−0.423	−0.276	−0.010	0.036
21–25	−0.369	−0.554*	0.466*	0.467	1.002**
26–30	−0.642**	−0.761**	0.782**	0.769**	0.983**

Asterisks indicate degree of significance (*P < 0.05; **P < 0.01).

in the late stage, which suggests that litter P concentration could also influence decomposition processes (Aerts and de Caluwe 1997a, b). Hence, our results found that the first-order decomposition rate constant (k) under N-treated soils were higher than those under unfertilized soils for all the species, and the relationships between cumulative CO₂–C evolution and soil property parameters showed that responses of cumulative CO₂–C evolution to increased soil nutrient availability differed among species. Previous studies have found that N addition results in increased N availability across different ecosystems, such as grasslands (Aerts et al. 2003), peatlands (Aerts et al. 2006) and forests, and that nutrient enrichment usually alters botanical composition and productivity of plant community. Our results corroborate the previous reports that N addition led to dramatic changes in vegetation composition and species diversity, and that N and P fertilizations significantly changed the soil physico-chemical and microbial properties. In our study, it is noteworthy that the cumulative amount of CO₂–C evolved from *L. chinensis* litter during 30-day incubation in the unfertilized treatment (590.6 mg g^{−1}) was larger than the amount of C that the *L. chinensis* litter contain (446.3 mg g^{−1}). This phenomenon could be explained by the priming effect of added litter.

5 Conclusion

There were significant differences in litter decomposition rate of the three species included in this experiment. In addition, N addition changed species composition, and importantly, legumes disappeared under medium and high N addition. Also, the relationship between cumulative CO₂–C evolution and soil property parameters differed among

species. Our results suggest that species type is likely the main determinant of litter decomposition, and soil nutrient availability under nutrient enrichment could affect litter decomposition and consequently C and nutrient cycling in Sheepgrass Meadow Steppe.

Acknowledgements This project was financially supported by National key research and development plan (2016YFC0500607-2). We thank our colleagues of the Institute of Pratacultural Science for their support and assistance on the field data collection, and three anonymous reviewers for revising and improving the manuscript.

References

- Aerts, R., de Caluwe, H.: Initial litter respiration as indicator for long-term leaf litter decomposition of *Carex* species. *Oikos* **80**, 353–361 (1997a)
- Aerts, R., de Caluwe, H.: Nutritional and plant mediated controls on leaf litter decomposition of *Carex* species. *Ecology* **78**, 244–260 (1997b)
- Aerts, R.: Climate, leaf litter chemistry and leaf litter decomposition in terrestrial ecosystems: a triangular relationship. *Oikos* **79**(3), 439–449 (1997)
- Aerts, R., de Caluwe, H., Beltman, B.: Plant community mediated vs. nutritional controls on litter decomposition rates in grasslands. *Ecology* **84**, 3198–3208 (2003)
- Aerts R., Van logtestijn, R.S.P., Karlsson, P.S.: Nitrogen supply differentially affects litter decomposition rates and nitrogen dynamics of sub-arctic bog species. *Oecologia* **146**(4), 652–658 (2006)
- Angers, D.A., Recous, S.: Decomposition of wheat straw and rye residues as affected by particle size. *Plant Soil* **189**(2), 197–203 (1997). <https://doi.org/10.1023/A:1004207219678>
- Araujo, P.I., Yahdjian, L., Austin, A.T.: Do soil organisms affect aboveground litter decomposition in the semiarid Patagonian steppe, Argentina?. *Oecologia* **168**(1), 221–230 (2012)
- Austin, A.T., Vivanco, L. Plant litter decomposition in a semi-arid ecosystem controlled by photodegradation. *Nature* **442**(7102), 555–558 (2006)



Trace Elements Deficiency in Dairy Cows in the Biogeochemical Province of the Republic of Belarus and Biological Effects of Its Correction

Vladimir Safonov and Anton Chernitskiy

Abstract

Trace elements low content in soils and fodder plants leads to their deficiency in farm animals, which could cause diseases and a decrease in productivity thereof. The purpose of this paper was to study selenium, zinc, manganese, cobalt and copper content in fodder plants, diet and hair of dairy cows in the biogeochemical province of the Republic of Belarus in connection with their dairy productivity and reproductive characteristics. Two groups of cows were formed with $n = 30$ each: the control group got the basic diet only, while the experimental group was injected with “Antimiopatik” intramuscularly three times, 60, 40 and 20 days before the intended calving in a single dose of 10 mL, containing selenium 8.0 mg, manganese 4.0 mg, copper 1.0 mg, cobalt 0.2 mg, zinc 2.0 mg. Trace elements content in plants, dietary items and cow hair samples were determined by inductively coupled plasma mass spectrometry. Median samples were compared by nonparametric Wilcoxon test. Selenium, zinc, cobalt, copper low levels were found in fodder plants and cow diet. Selenium, manganese and cobalt content in hair of the experimental group cows injected with “Antimiopatik” was by 113.3%, 133.2% and 87.5% higher ($P < 0.001$) than with those of the control group, but remained below the physiological interval. It should be mentioned that even partial replenishment of these trace elements deficiency with cows by injecting “Antimiopatik” significantly improved their reproductive function, raised milk yields and fat content, and reduced the postpartum endometritis and mastitis disease incidence.

Keywords

Biogeochemistry • Trace elements • Fodder plants • Dairy cows

1 Introduction

Soils of the Republic of Belarus are enriched with silica and depleted in alumina, iron, magnesium, calcium, potassium, sodium and sulfur. Most trace elements are also contained in insignificant amounts in soils and plants of this landscape and geochemical zone, and therefore, its territory belongs to a biogeochemical province (Kovalsky 1974; Beus et al. 1976). Selenium, zinc, manganese, cobalt and copper low content in plants that form the cattle diet basis determines the use of supplementary feedings and premixes containing these trace elements in the dairy cattle practices (Goff 2018; Miroshnikov et al. 2019). An alternative method is the use of prolonged injectable preparations containing trace elements that are missing from the cattle diet. One of these preparations widely used at the Republic of Belarus dairy farms is “Antimiopatik” (Kuchinsky et al. 2015). 1 mL of the “Antimiopatik” preparation contains selenium in 0.8 mg, manganese in 0.4 mg, copper in 0.1 mg, cobalt in 0.02 mg, zinc in 0.2 mg, vitamin E in 40 mg and vitamin A in 30,000 IU (Kuchinsky et al. 2015).

The purpose of this paper was to study selenium, zinc, manganese, cobalt and copper in fodder plants, diet and hair of dairy cows receiving both basic diet and additional “Antimiopatik” preparation injections in the biogeochemical province of the Republic of Belarus, as well as their relationship with the dairy productivity and reproductive characteristics of cows, such as milk yield during 305 days of lactation, fat content in milk, duration of the period from calving to first insemination, inter-calving period, service period, cases of retained placenta, postpartum endometritis and mastitis.

V. Safonov (✉)

Vernadsky Institute of Geochemistry and Analytical Chemistry of the Russian Academy of Sciences, 119991 Moscow, Russia

A. Chernitskiy

All-Russian Veterinary Research Institute of Pathology, Pharmacology and Therapy, 394087 Voronezh, Russia

2 Materials and Methods

The study was conducted in Glusky district of Mogilev region of the Republic of Belarus. Two groups of Holstein breed cows (*Bos taurus taurus*) were selected, $n = 30$ in each. Control group (CG) of animals received only the basic diet, which included 9 kg of hay (*Phleum pratense*), 30 kg of haylage (*Trifolium pratense*), 5 kg of rye grain (*Secale cereale*) and 25 kg of corn silage (*Zea mays*) per day. Cows in the experimental group (EG), in addition to the basic diet, were injected intramuscularly with the “Antimiopatik” preparation three times in 60, 40 and 20 days before the intended calving with a single dose of 10 mL. In order to conduct the study, fodder plants samples (with $n = 10$ of each species) included in the diet were selected by the V. Kovalsky method (Kovalsky 1974); and hair samples were obtained from the tail brush of cows immediately after calving (Samokhin 2003). Selenium, zinc, manganese, cobalt and copper content in the samples were determined using the inductively coupled plasma mass spectrometry method (Nexion 300D, Perkin Elmer, USA). Milk yield during 305 days of lactation, fat content in milk, duration of the period from calving to first insemination, inter-calving period, service period, cases of retained placenta, postpartum endometritis and mastitis were taken into account with the cows. All data were expressed as mean \pm standard deviation (SD) and median. The validity of differences between groups of cows was determined by comparing the medians using the nonparametric Wilcoxon test in the IBM SPSS Statistics 20.0 (IBM Corp., USA). The null hypothesis was rejected at $P < 0.05$.

3 Results

The content of trace elements in fodder plants and the diet of cows are presented in Table 1. The cow diet was deficient in selenium, zinc, cobalt and copper, while the manganese content was within the normal range (Samokhin 2003; Juknevičius and Sabienė 2007; Goff 2018).

Trace elements content in hair samples of cows is shown in Table 2. Selenium, manganese and cobalt low content in hair of cows pertaining to both groups was found, which indicates a deficiency of these trace elements in the cows (Zamana 2006; Miroshnikov et al. 2019). Zinc and copper content in the hair of cows was at the lower boundary of the physiological interval (Zamana 2006). Selenium, manganese, cobalt and zinc content in the EG cows hair was by 113.3% ($P < 0.001$), 133.2% ($P < 0.001$), 87.5% ($P < 0.001$) and 5.8% ($P < 0.05$) higher, respectively, than with the CG cows. In regard to the hair content of copper in

cows, no statistically significant differences were found between EG and CG.

In the EG, three cases of retained placenta were recorded, while in CG, 12 cases were recorded. In the EG, acute postpartum endometritis was recorded in two cows (6.7%), mastitis ($\geq 300,000$ somatic cell counts) in three cows (10.0%), while in the CG, acute postpartum endometritis was in nine cows (30.0%) and mastitis was in eight cows (26.7%), respectively. The period from calving to the first insemination in experimental animals averaged 63.3 ± 3.70 days, while in animals from the CG, it averaged 79.6 ± 4.45 days, which was 16.3 days ($P < 0.01$) less. Service period in the EG averaged 79.0 ± 3.15 days, while in the CG, it averaged 92.2 ± 3.92 days, which was 13.2 days ($P < 0.05$) less. The duration of the inter-calving period in the EG was 355.1 ± 3.40 days, compared to CG with 384.7 ± 5.11 days, which was 29.6 days ($P < 0.05$) more. Milk yield for the 305 days lactation period with the EG cows was 7565 ± 781 kg and fat in milk was $3.93 \pm 0.13\%$, while with the CG cows, these indicators were 5514 ± 485 kg and $3.50 \pm 0.18\%$, which was by 37.3% and 12.3% ($P < 0.001$) higher, respectively.

4 Discussion

Our study results identified the selenium and cobalt deficiency in the food (trophic) chain caused by the biogeochemical characteristics of the region (Kovalsky 1974; Beus et al. 1976; Kuchinsky et al. 2015). Despite the deficiency of zinc and copper in fodder plants and cow diet, these elements content in the dairy cows was found at the lower boundary of the physiological interval (Zamana 2006). Manganese content in plants and cow diet was optimal (Samokhin 2003; Juknevičius and Sabienė 2007; Goff 2018). Manganese deficiency in the cows was probably associated with distortion in its absorption from plants (Goff 2018). Selenium, manganese and cobalt content in the hair of EG cows that were injected with “Antimiopatik” was by 113.3% ($P < 0.001$), 133.2% ($P < 0.001$) and 87.5% ($P < 0.001$) higher than with the hair of CG cows, but remained lower than the physiological interval (Zamana 2006; Miroshnikov et al. 2019). The antioxidant defense system imbalance in cows, resulted from selenium and manganese deficiency, causes multiple metabolic disorders, cellular biomembranes damage and the development of various pathologies in organs (Samokhin 2003; Spears and Weiss 2008; Safonov 2018). In cattle, deficiency in these trace elements could have negative economic impacts, such as decreased fertility, retention of the placenta, increased incidence of mastitis and metritis (Samokhin 2003; Wilde

Table 1 Trace elements content in fodder plants and the diet of cows (Mean \pm SD, $\mu\text{g/g}$ of dry matter)

Dietary item	Selenium	Zinc	Manganese	Cobalt	Copper
<i>Phleum pratense</i> (grass), $n = 10$	0.05 \pm 0.018	23.0 \pm 4.8	79.3 \pm 17.6	0.03 \pm 0.01	4.4 \pm 1.3
<i>Trifolium pratense</i> (grass), $n = 10$	0.01 \pm 0.003	28.9 \pm 7.3	84.4 \pm 5.1	0.13 \pm 0.03	5.4 \pm 0.8
<i>Secale cereale</i> (grain), $n = 10$	0.02 \pm 0.004	23.4 \pm 1.9	24.6 \pm 4.3	0.01 \pm 0.002	3.1 \pm 0.5
<i>Zea mays</i> (grain), $n = 10$	0.03 \pm 0.009	21.5 \pm 3.6	50.1 \pm 9.2	0.01 \pm 0.002	2.6 \pm 0.4
Daily diet, $n = 10$	0.03 \pm 0.008	23.9 \pm 4.2	66.1 \pm 8.9	0.04 \pm 0.01	3.9 \pm 0.08
Diet norms (Goff 2018; Samokhin 2003)	0.08–0.30	30.0–60.0	25.0–70.0	0.2–1.0	5.0–12.0

Table 2 Trace elements content in the hair of cows ($\mu\text{g/g}$ of dry matter)

Element	Control group ($n = 30$)		Experimental group ($n = 30$)		Physiological interval (Zamana 2006)
	Mean \pm SD	Median	Mean \pm SD	Median	
Selenium	0.083 \pm 0.020	0.090	0.177 \pm 0.069	0.130	0.6–0.8
Zinc	98.8 \pm 3.6	99.0	104.5 \pm 6.9	104.0	100–130
Manganese	3.49 \pm 0.81	3.18	8.14 \pm 2.61	6.67	10–20
Cobalt	0.008 \pm 0.001	0.008	0.015 \pm 0.005	0.015	0.02–0.05
Copper	6.80 \pm 1.49	7.51	7.80 \pm 0.73	7.62	7–15

2006; Spears and Weiss 2008; Shabunin et al. 2017; Safonov 2018). It should be mentioned that even partial replenishment of these trace elements deficiency in cows significantly improved their reproductive function, raised milk yield and fat content, and even reduced the postpartum endometritis and mastitis disease incidence. The current results open possible ways to increase the efficiency of dairy cattle breeding in biogeochemical provinces.

5 Conclusion

Trace element deficiencies replenishment in fodder plants and in diet by injecting cows with the “Antimiopatik” preparation led to raising selenium, manganese and cobalt content in their organism, improved the reproductive function thereof, raised milk yield and fat content, and reduced the postpartum endometritis and mastitis disease incidence. Future work should be aimed at studying the economic effects of the trace elements deficiency correction with dairy cows.

References

Beus, A., Grabovskaya, L., Tikhonova, N.: Geochemistry of the environment, 1st edn. Nedra, Moscow (1976)

Goff, J.: Invited review: Mineral absorption mechanisms, mineral interactions that affect acid–base and antioxidant status, and diet considerations to improve mineral status. *J. Dairy Sci.* **101**(4), 2763–2813 (2018)

Juknevičius, S., Sabienė, N.: The content of mineral elements in some grasses and legumes. *Ekologija* **53**(1), 44–52 (2007)

Kovalsky, V.: Geochemical ecology, 1st edn. Nauka, Moscow (1974)

Kuchinsky, M., Bezborodkin, A., Azizbekyan, S., Belkevich, I., Kuchinskaya, S., Nikolayenko, S., Fedotov, D.: Guidelines for the use in animals of new drugs based on microelements and vitamins (Antianemin, Antianemin-forte, Neovetselen, Nanoselen, Antimiopatik, Antimiopatik-2), 1st edn. Ministry of Agriculture and Food of the Republic of Belarus, Minsk (2015)

Miroshnikov, S., Zavyalov, O., Frolov, A., Slepsov, I., Sirazetdinov, F., Poberukhin, M.: The content of toxic elements in hair of dairy cows as an indicator of productivity and elemental status of animals. In: *Environmental Science and Pollution Research*, pp 1–11 (2019)

Safonov, V.: Biological role of selenium and correction effects of its content in the organism of animals. *Geochem. Int.* **56**(10), 1046–1050 (2018)

Samokhin, V.: Prevention of microelement metabolic disorders in animals, 2nd edn. Voronezh State University, Voronezh (2003)

Shabunin, S., Nezhdanov, A., Mikhalev, V., Lozovaya, E., Chernitskiy, A.: Dilelementosis as a risk factor of embryo loss in lactating cows. *Turkish J. Vet. Anim. Sci.* **41**(4), 453–459 (2017)

Spears, J., Weiss, W.: Role of antioxidants and trace elements in health and immunity of transition dairy cows. *Vet. J.* **176**(1), 70–76 (2008)

Wilde, D.: Influence of macro and micro minerals in the peri-parturient period on fertility in dairy cattle. *Anim. Reprod. Sci.* **96**(3–4), 240–249 (2006)

Zamana, S.: Determination of chemical element composition of the hair cover in cattle. *Sel'skokhozyaistvennaya Biologiya* **4**, 121–125 (2006)

**Environmental Earth Sciences (T4):
Pollution Monitoring and Assessment**



Heavy and Trace Elements Distribution in Plants and Soils of Urban and Rural Areas of Egypt: A Comparison

Wael Badawy¹, Yasmin Sarhan, Octavian Dului², Marina Frontasyeva, Hussein El-Samman, Abdel Azim Hussein, and Wafaa Arafa

Abstract

For a comprehensive description of the biomonitoring and geochemistry of trace elements in two different regions of Egypt (urban Cairo and rural Menoufia), Instrumental Neutron Activation Analysis was used to determine the concentration of 40 elements in 30 samples of soil and 32 elements in an equal number of samples of *Eucalyptus globulus* Labill and *Ficus Benjamina* L. 1767 leaves collected during 2018 Spring. Concordantly, literature data, Na, Al, Cl, Ca, Sc, Ti, V, Cr, Fe, Co, Ni, As, Se, Br, Sr, Sb, La, Sm, Tb, Hf, Ta, Th, and U showed significant concentrations mg/kg in both soil and plant leaves. Moreover, despite a high-density population, heavy traffic, and urban pollution, the Cairo samples showed significantly reduced values comparing with the corresponding values from Menoufia, most probably related to the uncontrolled industrial and domestic waste disposal outside Cairo. Besides, the study shows *F. Benjamina* responsiveness to heavy and trace elements to be higher

than those of *E. globulus*, which could be recommended *F. Benjamina* plantation to retain in a more significant measure the urban pollutants.

Keywords

Plant biomonitoring • Air and soil pollution • Neutron activation analysis • Trace element

1 Introduction

Plants, either vascular or non-vascular, due to their foliar system showed a remarkable capacity to retain a variety of polluting agents transported by atmospheric circulation and deposited on leaves or another aerial part. Although in this regard, mosses and lichens, due to the lack of root system, showed the highest capacity to retain airborne material, there is a multitude of the vascular plant of which leaves, together with root system could retain pollutants, resulting from industry as well as domestic activities (Norouzi et al. 2015; Baldantoni and Alfani 2016). Unfortunately, mosses, which proved to be the best biomonitor plant, need certain well-defined environmental conditions to grow and develop such as a minimum level of air humidity or the quasi-absence of direct insolation that makes their use to be restrained to some geographic areas, mainly at medium and high latitude. For this reason, in locality situated in a dry climate, for the biomonitoring could be used and vascular plant, provided they are well acclimatized to local conditions (Norouzi et al. 2015). The present biomonitoring study, regarding the city of Cairo urban area and neighboring settlements such as Menoufia, was focused on two vascular plants: *Eucalyptus globulus* Labill. and *Ficus benjamina* L. 1767, well disseminated in both locations. Moreover, soil-sampling sites from the two places were tested for major and trace elements.

W. Badawy (✉)

Radiation Protection & Civil Defense Department, Egyptian Atomic Energy Authority (EAEA), Nuclear Research Center, Abu Zaabal, 13759, Egypt
e-mail: wael@jinr.ru

W. Badawy · O. Dului · M. Frontasyeva
Joint Institute for Nuclear Research, Frank Laboratory of Neutron Physics, 6, Joliot Curie str, 141980 Dubna, Russian Federation

Y. Sarhan · H. El-Samman · A. A. Hussein
Faculty of Science, Department of Physics, Menoufia University, Shibin El-koom, Egypt

O. Dului
Faculty of Physics, Department of Atomic and Nuclear Physics, University of Bucharest, 405, Atomistilor str., 077125 Magurele, Romania

W. Arafa
Faculty of Women, Department of Physics, Ain Shams University, Cairo, Egypt

2 Materials and Methods

Two locations in the Cairo municipal area and in Menoufia have been selected. In the case of Cairo, one location was in the central area and the other one on the city outskirts. In all locations, during 2018 Spring, we have collected 30 leaves of *F. Benjamina* and *E. globulus* as well as an equal number of samples of adjacent soil.

After collection, all leaves were cleaned, washed with distilled water, air-dried at constant weight, ground and homogenized, and, finally, resulting in 30 different samples. A similar procedure was followed in the case of soil specimens. Then, all samples were sent to Frank Laboratory of Neutron Physics—Joint Institute for Nuclear Research in Dubna, Russian Federation for further Epithermal Neutron Activation Analysis (ENAA). The concentrations of 32 and 40 major and trace elements were determined in the leaves and soils samples, respectively. For a better characterization of the distribution of all elements mentioned above in leaves and soil, the single pollution index (*SPI*) was calculated. *SPI* is defined as the ratio between the concentrations of the considered elements in leaves and soil and a reference system considered unaffected by the human activity such as reference

plant (RP) (Markert et al. 2015) for tree leaves and the upper continental crust (UCC) (Rudnick et al. 2014) for soil.

For a number of n elements considered as anthropogenic contaminants—V, Cr, Mn, Co, Ni, Zn As and Sb, the *SPI*s were further used to calculate for each sampling point the pollution load index (*PLI*) (Tomlinson et al. 1980) following the equation:

$$PLI = \sqrt[n]{\prod_{i=1}^n SPI_i} \quad (1)$$

The final results concerning the spatial distribution of *PLI* was represented by means of esri® ArcGIS™ 10.5 software.

3 Results and Discussions

The results concerning the *SPI* distribution of 40 elements in leaves and soil are illustrated through Fig. 1 box-plots. In the case of leaves, Fig. 1a, b prove the existence of significant differences between the *E. globulus* and *F. Benjamina* as different taxa, but within the same taxa, Cairo values were lower than the Menoufia ones.

Fig. 1 Three box-plots illustrating the distribution of the *SPI* in leaves of *F. benjamina* (a), *E. globulus* (b) as well as in the adjacent soil (c) of Cairo and Menoufia

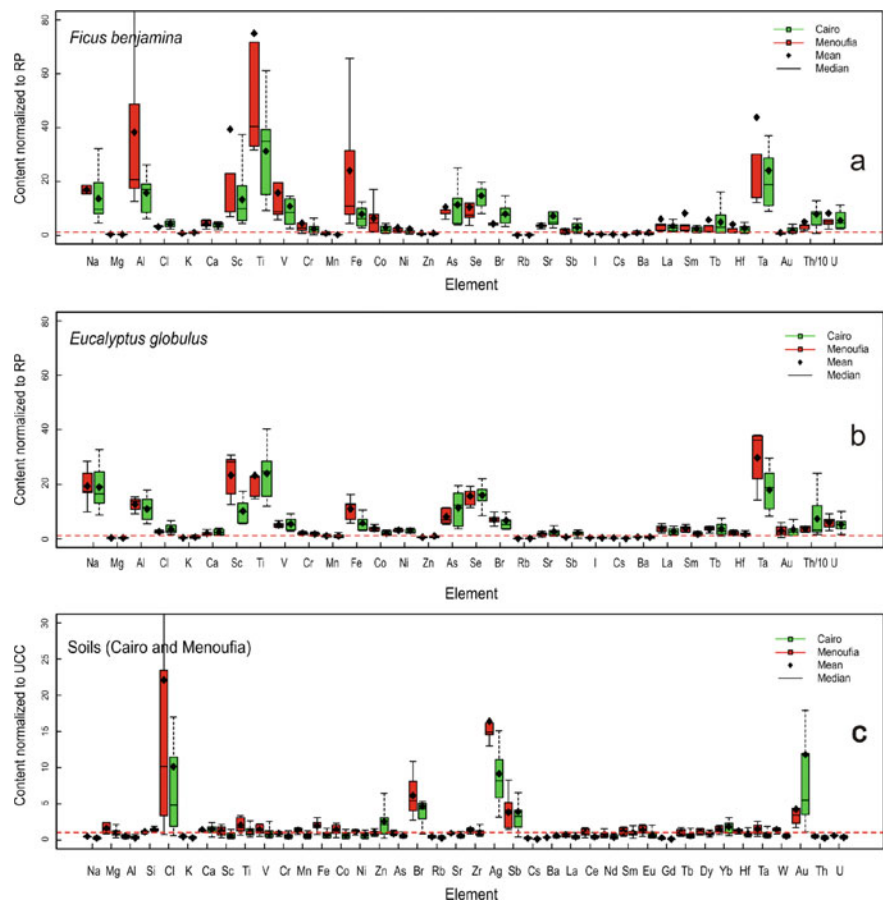
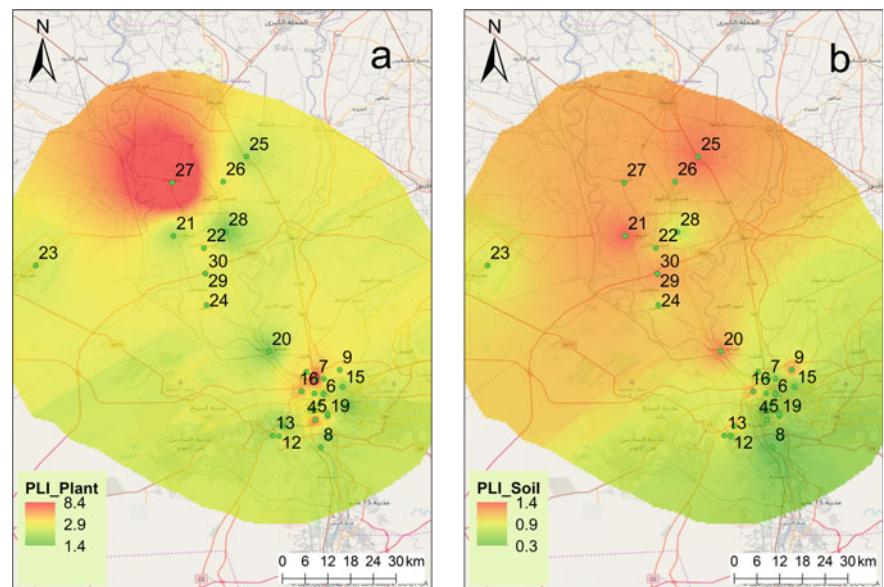


Fig. 2 Spatial distribution of tree leaves (a) and soil (b) *PLI* on the investigated areas



The same peculiarity was also evidenced in case of soil (Fig. 1c) and could be explained, in our opinion, by the fact that Menoufia locality, although situated at about 70 km of Cairo has a significantly higher population density. This population density significantly increases the anthropogenic activities.

The final results concerning the spatial distributions of *PLI* for Cairo and Menoufia (Fig. 2) for both soils and tree leaves show with clarity that Menoufia, significantly more affected by anthropogenic contamination than Cairo. The corresponding *PLI* showing higher values in case of tree leaves than in case of soil (Fig. 2). This finding could be due to a higher density of population as well as the uncontrolled industrial and domestic waste disposal.

4 Conclusions

The distribution of 40 elements in soils and 32 in 30 leaves samples of two different tree species, collected from Great Cairo and Menoufia Governorate was determined by Epithermal Neutron Activation Analysis and interpreted employing single pollution and pollution loading indices *SPI* and *PLI*, respectively. The *PLI* distribution function calculated on the concentration of V, Cr, Mn, Co, Ni, Zn As, and Sb in tree leaves as well as in adjacent soil samples

evidenced, as ArcGIS maps showed, a significant degree of anthropogenic contamination, higher in Menoufia Governorate than in the Cairo Metropolitan Area. This finding most probably reflects a higher population density as well as improper management of both domestic and industrial wastes in the investigated area of Menoufia Governorate.

Moreover, our results showed that, in the absence of bryophyte plants, tree leaves could be successfully used for the biomonitoring of anthropogenic contamination.

References

- Baldantoni, D., Alfani, A.: Usefulness of different vascular plant species for passive biomonitoring of Mediterranean rivers. *Environ. Sci. Pol. Res.* **23**, 13907–13917 (2016)
- Markert, B., Fränze S., Wünschmann, S.: Chemical evolution. In: *The Biological System of the Elements*. Springer, Heidelberg, p. 78 (2015)
- Norouzi, S., Khademi, H., Faz Cano, A., et al.: Using plane tree leaves for biomonitoring of dust borne heavy metals: a case study from Isfahan, Central Iran. *Ecol. Indic.* **57**, 64–73 (2015)
- Rudnick, R.L., Gao, S.: Composition of the continental crust. In: Holland, H.D., Turekian, K.K. (eds.) *Treatise on Geochemistry*, pp. 1–51. Elsevier, Oxford (2014)
- Tomlinson, D.L., Wilson, J.G., Harris, C.R., et al.: Problems in the assessment of heavy-metals in the estuaries and the formation of the pollution index. *Helgol. Mar. Res.* **33**, 566–575 (1980)



Trace Metal Contamination in Sediment Core of El Mellah Lagoon (El Kala, Algeria)

Houria Athmani, Mostefa Boulahdid, Noura Bouchahm, and Nadia Hocini

Abstract

This work focuses on the assessment of metal contamination of sediments in El Mellah lagoon. The results are as follows: (a) identification of the chemical composition by XRF of particular samples and confirmation by DRX of major elements and especially SiO₂ which dominates the entire chemical composition of the core; (b) the content of organic material; the results show an enrichment of organic material in the deep core layers and a distribution of heterogeneous carbonate contents along the core; (c) trace metals' contents per AAS also indicate a heterogeneous distribution along with the core of the contents (Mn, Fe, Cu, Zn) and the others (Ag, Cd, Co, Cr, Ni, Pb and Sc) have a homogeneous distribution; and (d) the factor of enrichment EF and correlation between metals. The results show a moderate to significant enrichment of the first centimeters of the metal elements. The positive correlations were observed for the metal pairs: Cu–Pb, Cr–Ag, Mn–Ag, Mn–Cr and Mn–Zn.

Keywords

Sediment core • CaCO₃ • XRF • Organic matter • Trace metals • Enrichment factor • Water pollution

1 Introduction

Lagoon environments are defined as shallow ecosystems, connected to the sea by one or more restricted admission (Pinot 1998). The mixing of marine and continental waters makes these bodies of water unique systems with great biological and socioeconomic interest (Benmarce 2012). The El Mellah lagoon, the only coastal lagoon on the Algerian coast, is classified as a priority conservation area (Grimes 2002) and protected by the Ramsar Convention. Today, it is the receptacle of domestic sewage from nearby houses. This wastewater is charged with different types of organic and inorganic chemical contaminants. Trace metal contamination of these aquatic ecosystems remains an increasingly severe environmental problem (Issabayeva et al. 2008). This work focuses on the quantification of the geochemical background of trace metals (Mn, Zn, Ag, Pb, Sc, Cr, Fe, Co, Ni, Cu, Cd) and the assessment of the level of concentration in sediments by these trace metals as a result of anthropogenic influence in the context of ongoing monitoring of coastal environment.

2 Materials and Methods

El Mellah lagoon is located in the extreme northeast of Algeria, precisely at 36°53' N and 08°20' E between Rosa and Roux Capes near the Algerian–Tunisian borders. It has an area of about 837 ha and a maximum depth of 6 m (Morgan 1982). The sampling of one sediment core was made during a companion carried out on May 18, 2009, in the lagoon near the mouth of the lake with the Mediterranean; the length of the core was about 32 cm. The core was cut to thicknesses of 0.5, 1 and 2 cm, lyophilized, ground and sieved to 2 mm. The samples underwent several techniques to analysis: the determination of clay minerals by XRD, the determination of significant elements by XRF (Bouzonville et al. 2008), quantification of calcium carbonate by Bernard calcimeter according to the NF X 31-105,

H. Athmani (✉)
University Mohamed Khider, Biskra, Algeria

M. Boulahdid
ENSSMAL, Algiers, Algeria

N. Bouchahm
CRSTRA, Biskra, Algeria

N. Hocini
CRNA, Algiers, Algeria

and the determination of trace metals by SAA. The digestion was done in Teflon tubes. We added to the sediment HNO_3 69% and HCl 37%, and we allowed them to act in the cold. Then, hydrofluoric acid was added on a hot plate. After digestion, it was preceded to the analysis of metal elements. The combustion allowed direct measurement of the organic matter in the sediment (Wang et al. 2011)—the calculation of the inter-metal correlation. The enrichment factor (EF) has been proposed for standardization and discrimination of anthropogenic inputs of natural sources, and thus, defined the degree of contamination. In general, a conservative element representative of the clay fraction, such as Al or Sc, was used. Scandium (Sc) was chosen as the stationary reference element for making this calculation:

$$EF = ([M]/[Sc])_s / ([M]/[Sc])_{RM}$$

where EF is the enrichment factor; [M] the studied metal concentration; [Sc] scandium concentration; s sample; and RM reference materials.

The enrichment factors can be grouped into five classes (Tessier et al. 2011): $EF < 2$: no or low enrichment; $2 < EF < 5$ moderate enrichment; $5 < EF < 20$: significant enrichment; $20 < EF < 40$: strong enrichment.

3 Results and Discussion

3.1 Chemical Composition by XRF, XRD, Carbonate and Organic Matter

The chemical composition of the sediments by XRF and XRD was: $\text{SiO}_2 \approx 42\%$; oxides (Fe_2O_3 , MgO , K_2O and Na_2O) reached 14.5%, 20%, 2% and 13.2%, respectively, which showed that the sediment was rich in oxides; CaO levels were deficient $\leq 2\%$; the contents of $\text{SO}_3 \approx 8.3\%$; sulfur was an essential element in the mobility of trace metals by oxidation–reduction; and the contents of Al_2O_3

ranged between 10 and 12%, which indicated the significant presence of clays in the core.

The results indicated that the sedimentary core was rich in organic matter with an average of $16.2 \pm 5.10\%$. The nature of this study area was characterized by the richness of aquatic species in addition to significant fishing activity. The distribution of carbonate contents was heterogeneous along with the core ($4.02 \pm 2.30\%$). The values of CaCO_3 were higher than CaO values, indicating that CaO was in other forms than calcite. The sampling point was near a shellfish farm (mussels and clams), which can be considered as a significant source of carbonates.

3.2 Distribution of Trace Metals in the Sediment

The Mn distribution was identical to zinc distribution (Fig. 1). The highest values were observed at the surface layers of the core: $\text{Mn} = 461.23 \mu\text{g g}^{-1}$ and $\text{Zn} = 216.43 \mu\text{g g}^{-1}$. The vertical profiles of the Cd and Zn showed a strong similarity between both, because Cd is generally associated with zinc as impurities (Robbe 1981).

3.3 Enrichment Factor (EF) and Correlations Inter-Metals

According to the calculated EF of the elements, Co, Cu, Ni, Fe and Ag did not exceed two, which makes it felt in the range of natural variability. For other trace metals, there was a slight contamination ($0.86 < EF (\text{Pb}) < 2.34$; $0.66 < EF (\text{Mn}) < 4.79$; $0.65 < EF (\text{Cd}) < 3.94$ and $0.66 < EF (\text{Cr}) < 2.51$), except for the elements Zn ($0.84 < EF (\text{Zn}) < 5.39$), so the habitat was contaminated with Zn. After the 14 cm depth, the values were below the detection limits for all the analyzed elements. The correlation values (Table 1) between metals revealed, for the ten trace metals analyzed, high

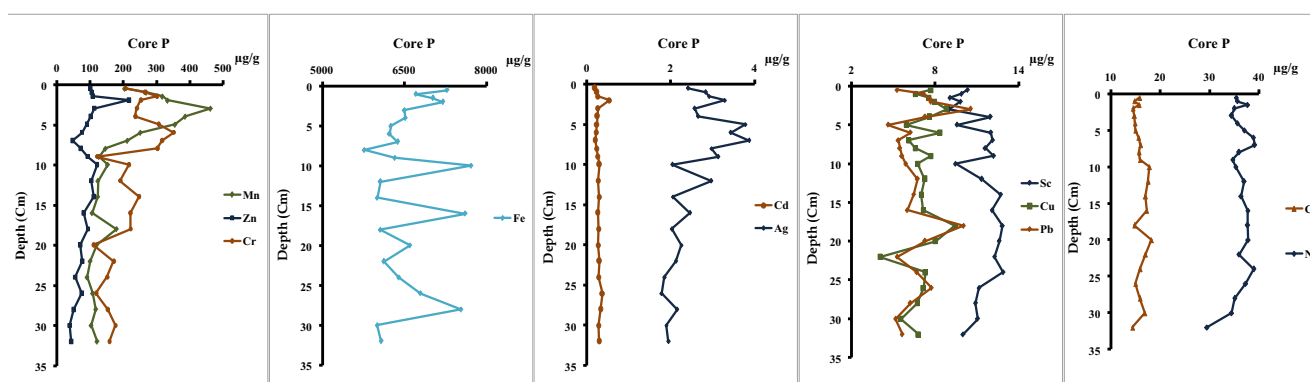


Fig. 1 Vertical profiles of trace metals in the sedimentary core of El Mellah lagoon

Table 1 Matrix of correlations between metals in the sediment core of El Mellah lagoon

	Mn	Zn	Ag	Pb	Sc	Cr	Fe	Co	Ni	Cu	Cd
Mn	1										
Zn	0.51	1									
Ag	0.53	0.27	1								
Pb	0.42	0.37	-0.20	1							
Sc	-0.56	-0.37	-0.18	-0.09	1						
Cr	0.58	0.25	0.69	-0.03	-0.25	1					
Fe	0.08	0.33	-0.10	0.04	-0.39	-0.10	1				
Co	-0.56	-0.19	-0.22	-0.34	0.35	-0.27	0.12	1			
Ni	-0.02	-0.04	0.28	0.09	0.45	0.31	0.03	0.29	1		
Cu	0.33	0.35	0.02	0.72	0.01	0.04	0.13	-0.28	0.13	1	
Cd	0.04	0.35	0.31	0.32	0.10	0.04	-0.20	0.13	0.31	0.36	1

Significance correlations ($p < 0.05$) are indicated in bold

positive correlations for the metal pairs: Cu–Pb, Cr–Ag, Mn–Ag, Mn–Cr and Mn–Zn, which would mean that these elements evolve in the same direction of the variations of the concentrations in the core. The non-significant correlations between pairs of metallic elements such as Ni–Pb, Cu–Cr and Cd–Pb imply that these metals did not come from the same natural and/or anthropogenic sources and do not have the same affinities and the same chemical and geochemical behaviors in the natural environment (Ouali et al. 2018).

4 Conclusions

The mineralogical composition is relatively similar along with the core; it has been identified by XRF and Bernard calcimeter where silica, oxide, dominates followed by low carbonate contents. The contents of SiO₂ and Al₂O₃ indicate the presence of clays which allow the fixation of trace metals. The core sediments are rich in organic matter. The degradation of organic matter is followed by different sequences of redox metallic elements in the sediments. The profiles of trace metals' core contents obtained by SAA and EF results show moderate to significant enrichment of the first centimeters. Vertical profiles of trace metal contents and EF results show moderate to significant enrichment of the first centimeters. This significant enrichment toward the top of the core would indicate the existence of a recent metallic contribution probably coming from the intensive agricultural activities which mainly use the elements such as zinc and manganese like amendment to increase the yield, without excluding, of course, the rejections and road traffic that contribute to the enrichment of lead, cadmium, copper and chromium. The positive functional correlations observed for the pairs of metals: Mn–Zn, Cu–Pb, Cr–Ag, Mn–Ag and

Mn–Cr, confirm these results—this would mean that these elements evolve in the same direction of the variations of the concentrations in the core and can prevent the same sources.

References

- Benmarce, S.: Potentialités aquacoles de la lagune Mellah à travers la connaissance du chaînon de la macrofaune benthique. Magister Dissertation, Univ. Annaba, Algeria (2012)
- Bouzonville, A., Colin, A., Durin, L., Gruffat, V., et Chassagnac, T.: Analyse rapide des métaux et autres minéraux dans des milieux solides pollués (déchets, sols) à l'aide de méthodes non destructives de terrain par fluorescence X. Rapport Final RECORD, p. 44 2008:
- Grimes, S.: Espaces marins d'Algérie d'intérêt écologique. In Atlas de l'Environnement de l'Algérie: espace côtier. In : Symbiose-Burlington ressources Edition, 51–51 (2002)
- Issabayeva, G., Aroua, M., Sulaiman, N.: Continuous adsorption of lead ions in a column packed with palm shell activated carbon. *J. Hazard. Mater.* **155**(1–2), 109–113 (2008)
- Ouali, N., Belabed, B.E., Chenchouni, H.: Modelling environment contamination with heavy metals in flathead grey mullet *Mugil cephalus* and upper sediments from north African coasts of the Mediterranean Sea. *Sci. Total Environ.* **639**, 156–174 (2018)
- Morgan, N.C.: An ecological survey of standing water in North west Africa II. Site descriptions for Tunisia and Algeria. In: *Biological Conservation*, pp. 24–83–113 (1982)
- Pinot, J.P.: La gestion du littoral. Institut océanographique, Paris, 2 vol, 759p (1998)
- Robbe, D.: Pollution métallique du milieu naturel. Guide méthodologique de leur étude à partir des sédiments. Rapport bibliographique. Rapport de recherche LPC N°1 04. Laboratoire central des Ponts et Chaussées. 88 pp (1981)
- Tessier, E., Garnier, C., Mullot, J., Lenoble, V., Arnaud, M., Raynaud, M., Mounier, S.: Study of the spatial and historical distribution of sediment inorganic contamination in the Toulon Bay (France) *Mar. Pollut. Bull.* **2011**(7), 22 (2011)
- Wang, Q., Li, Y., Wang, Y.: Optimizing the weight loss-on-ignition methodology to quantify organic and carbonate carbon of sediments from diverse sources. *Environ. Monit. Assess.* **174**, 241–257 (2011)



Environmental Quality Assessment in the Kuwait Bay (Kuwait): An Integrated Approach

Eqbal Al-Enezi, Fabrizio Frontalini, Shaker Al-Hazeem, and Talal Dashti

Abstract

The increased urbanization and developmental activities in Kuwait and the consequent effluent discharges into marine environments have resulted in changes in the water and sediment quality of coastal and marine ecosystems. These areas, like the Kuwait Bay, have been negatively affected by the discharges of hydrocarbon, heavy metals and other organic compounds impacting marine ecosystems and the biota living therein. The Kuwait Bay is among the most critical marine and productive ecosystems along the Kuwaiti coast. In light of it, this baseline investigation aims to document by the integration of physicochemical data on water, sediment geochemistry both organic and inorganic and preliminary data of benthic foraminiferal assemblages, the environmental conditions within the Kuwait Bay that will be used for the implementation of future biomonitoring programs.

Keywords

Environmental quality • Pollution • Integrated approach • Sediment • Kuwait Bay

1 Introduction

Rapid urban development and industrialization have been directly promoting the widespread contamination of coastal areas (Ouali et al. 2018). These areas, like Kuwait, have been negatively affected by the discharges of hydrocarbon,

heavy metals and other organic compounds that have resulted in a decline of the water and sediment quality. These contaminants have also adversely impacted marine ecosystems and the biota living therein (Sheppard et al. 2010). The Kuwait Bay and Khor Al-Sabiyah are among the most critical marine and productive ecosystems along the Kuwaiti coast and have supplied 40–50% of the country's food demand (Al-Mutairi et al. 2014). During the last few decades, the marine environmental quality of the Kuwait Bay has been threatened and affected by industrial activities, power and desalination plants, and effluent discharges from Shatt Al-Arab. The total petroleum hydrocarbons (TPHs), trace elements (i.e., Cu, Cd, Hg), and sewage contamination are among the most common contaminant in the Kuwait Bay (Saeed et al. 2015; Nicolaus et al. 2017). In this context, the definition of the natural variability in no-stressed environments and the comparison with polluted ones in the Kuwait Bay will provide a basis for the recognition of areas of concern and implement future biomonitoring, conservation, management and restoration programs. In particular, biological monitoring, through bioindicators like benthic foraminifera, has enabled the detection of unforeseen impacts and is more directly related to the “ecological health” of an ecosystem than are chemical data. The increasing importance of bioindicators is also encouraged within, for instance, the European Union Water Framework Directive (WFD 2000/60/EC), Marine Strategy Framework Directive (MSFD 2008/56/EC) and HELCOM (Baltic Marine Environment Commission, HELSINKI COMMISSION). The integrations of physicochemical data of water, sediment characteristics and bioindicators allowed us to define the baseline condition for the Kuwait Bay. In light of these data, we documented the environmental conditions within the Kuwait Bay that will be used for the implementation of future biomonitoring programs by integrating physicochemical data on water, sediment geochemistry both organic and inorganic and preliminary data of benthic foraminiferal assemblages.

E. Al-Enezi (✉) · S. Al-Hazeem · T. Dashti
Environment and Life Sciences Research Center, Kuwait Institute
for Scientific Research, P.O. Box 24885, 13109 Safat, Kuwait
e-mail: enezi@kisir.edu.kw

F. Frontalini
Dipartimento di Scienze Pure e Applicate (DiSPeA), Università
degli Studi di Urbino, Urbino, Italy

2 Materials and Methods

Physico-chemical parameters such as temperature, salinity/conductivity, pH and Eh were measured along the water column at each site. A total of 45 stations were collected within the Kuwait Bay. Sampling stations cover areas such as Sulaibikhat Bay, known points of effluent input like Al Ghazali, Salmiya, Al Bedaa, Al Messela and Shatt Al-Arab Delta that are known to be highly contaminated. Samples were collected in three replicates for geochemical and foraminiferal analyses and kept apart to capture the environmental variability of the system. These sub-samples were cool-preserved and transported to the KISR laboratory for, a) organic matter qualification and quantification, b) total petroleum hydrocarbon (TPH) analyses (ROPME 2010). Samples for foraminiferal morphological analyses were treated with a Rose Bengal solution that allowed us to distinguish living and non-living specimens at the time of collection and processed using the standard micropaleontological technique. A further aliquot was used for foraminiferal metabarcoding (Fig. 1).

3 Results and Discussion

The sampling stations ranged from 1 to 15 m water depth. The water salinity varied between 40 and 44, the pH fluctuated between 6 and 8, whereas the DO between 1 mg/L and 13 mg/L. The nutrients in the water (i.e., NO₂, NO₃, NH₄, PO₄, SiO₂ and TSS) were also measured to constrain the water quality. The ranges of each parameter were 0.01 to 0.1 mg/L for NO₂, 0–0.01 mg/L for NO₃, 0.8–1.9 mg/L for PO₄, 0.3–0.9 mg/L for SiO₂ and 10–70 mg/L for TSS. The TPH varied between 0.13 and 1.86 µg/mL. A total of sixty-five benthic foraminiferal taxa were identified in the preliminary analyses of the living assemblages. Following WoRMS (201), five orders of benthic foraminifera were found, and these include Lituolida, Textulariida, Miliolida,

Lagenida and Rotaliida. The dominant species belonging to the genera *Quinqueloculina*, *Spiroloculina*, *Asterorotalia*, *Ammonia* and *Elphidium*.

Based on the preliminary and available data, several areas within the Sulaibikhat Bay are impacted by relatively high values of TOC, TPH and trace elements due to the occurrence of several activities (Al-Enezi and Frontalini 2015, Alenezi et al. 2018). The concentrations of trace elements were found to be above background levels and those reported for the USEPA's sediment guidelines. In this area, benthic foraminifera show relatively lower values of diversity compared to other more open areas.

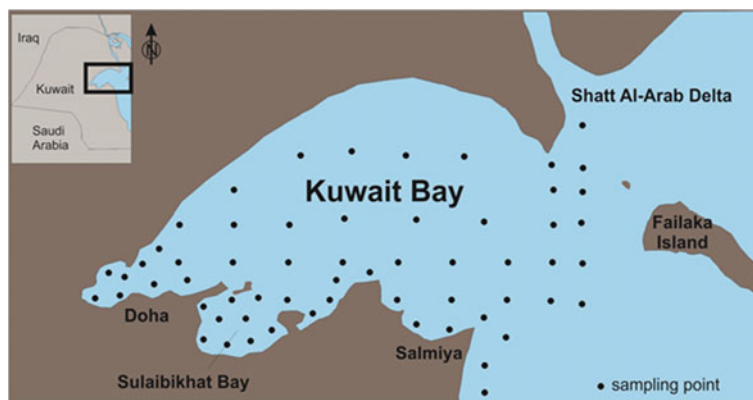
4 Conclusion

This preliminary study attempted to evaluate the level of pollution in the Kuwait Bay by using a multidisciplinary approach that integrated water parameters and nutrients, sediment characteristics and geochemistry as well as benthic foraminifera. The available data allowed us to define some areas within the Sulaibikhat Bay and Shatt Al-Arab that have revealed relatively high concentrations of pollutants and a reduced foraminiferal assemblage. The complete analyses of all available samples coupled with the foraminiferal (eDNA) metabarcoding will permit to document the benthic foraminiferal diversity, distribution and assemblages' composition, to mark particularly contaminated areas and to ultimately determine the environmental quality within the Kuwait Bay that will be employed for the implementation of future biomonitoring.

References

- Al-Enezi, E., Frontalini, F.: Benthic foraminifera and environmental quality: the case study of Sulaibikhat Bay (Kuwait). *Arab. J. Geosci.* **8**(3), 8527–8538 (2015). <https://doi.org/10.1007/s12517-015-1812-9>

Fig. 1 Location map of the sampling stations (solid black circles)



- Al-Mutairi, N., Abahussain, A., Al-Battay, A.: Environmental assessment of water quality in Kuwait Bay. *Int. J. Environ. Sci. Dev.* **5**, 527–532 (2014)
- Eqbal Al-Enezi, Al-Ghadban, A.N., Al-Refai, I., Pieretti, N., Frontalini, F.: Living benthic foraminifera around the unique Umm al Maradim Island. *Kuwait J. Sci.* **46**(2), 59–66 (2018)
- Nicolausa, E.E.M., Wright, S.R., Barry, J., Bolam, T.P.C., Ghareeb, K., Ghaloom, M., Al-Kanderi, N., Harley, B.F.M., Le Quesne, W.J.F., Devlin, M.J., Lyons, B.P.: Spatial and temporal analysis of the risks posed by total petroleum hydrocarbon and trace element contaminants in coastal waters of Kuwait. *Mar. Pollut. Bull.* **120**, 422–427 (2017). <https://doi.org/10.1016/j.marpolbul.2017.04.031>
- Ouali, N., Belabed, B.E., Chenchouni, H.: Modelling environment contamination with heavy metals in flathead grey mullet *Mugil cephalus* and upper sediments from north African coasts of the Mediterranean Sea. *Sci. Total Environ.* **639**, 156–174 (2018). <https://doi.org/10.1016/j.scitotenv.2018.04.377>
- ROPME: Manual of Oceanographic Observations and Pollutant Analyses Methods (MOOPAM). In: 4th, Kuwait: Regional Organization for the Protection of the Marine Environment (ROPME) (2010)
- Saeed, T., Al-Shimmari, F., Al-Mutairi, A., Abdullah, H.: Spatial assessment of the sewage contamination of Kuwait's marine areas. *Mar. Pollut. Bull.* **94**, 307–317 (2015)
- Sheppard, C., Al-Husiani, M., Al-Jamali, F., et al.: The Gulf: a young sea in decline. *Mar. Pollut. Bull.* **60**, 13–38 (2010). <https://doi.org/10.1016/j.marpolbul.2009.10.017>



Geostatistical Study of Landfill Contaminated Topsoil and Impacts of Urban Waste on Its Immediate Environment (Gafsa, South-West Tunisia)

Feyda Srarfi, Mohamed Salah Hamdi, Raouen Rachdi, and Najet Slim Shimi

Abstract

Inadequate waste management coupled with increasing urban expansion, industrial developments produces significant alterations in the physical environment and increases trace metallic element concentration in soil. In this study, spatial concentrations of Chromium (Cr), Copper (Cu), Nickel (Ni), Zinc (Zn) and Cadmium (Cd) in 16 sampling sites from the Gafsa landfill were investigated using a Kriging interpolation and multivariate statistical analysis. Their respective concentrations are 3.96, 0.42, 63.80, 79.75 and 6.01 mg kg⁻¹. The spatial distribution of trace element factor coordinates shows higher values in the eastern part of the study area, with important loadings on Zn (-0.881) and Cu (-0.922). However, the areas of higher Ni (0.753) and Cr (0.786) contents were mainly distributed in the south and the southwest of landfill. They were indicating that both intrinsic and extrinsic factors controlled these trace elements. These results can be considered as baseline information for other soil quality monitoring studies in Gafsa city.

Keywords

Topsoil • Heavy metals • Multivariate statistic • Kriging • Gafsa

1 Introduction

The occurrence of various heavy metals such as Cr, Cd, Ni, Zn, and Cu in solid waste dumpsites was reported in various researches (Jafari et al. 2016; Abegunde et al. 2018).

F. Srarfi (✉) · M. S. Hamdi · N. S. Shimi
Faculty of Sciences Tunis, Laboratory 3G, University El Manar
Tunis, Tunis, Tunisia

R. Rachdi
Laboratory 3G, University El Manar Tunis, Tunis, Tunisia

Environmental impact of these practices can usually result from the run-off of the toxic compounds into surface water and groundwater (Osakwe et al. 2012), which eventually lead to water pollution because of percolation of leachate. Besides, the incineration of municipal solid waste contributes significantly to the presence of heavy metals in urban area aerosols. Quantities and different chemical forms of the heavy metals are emitted from the incineration municipal waste piles (Jafari et al. 2016; Chenchouni et al. 2019). Therefore, this study attempted to quantify the changes in the properties of soil under municipal waste dumping by investigating the spatial distribution of trace metallic elements and their factor coordinate.

2 Materials and Methods

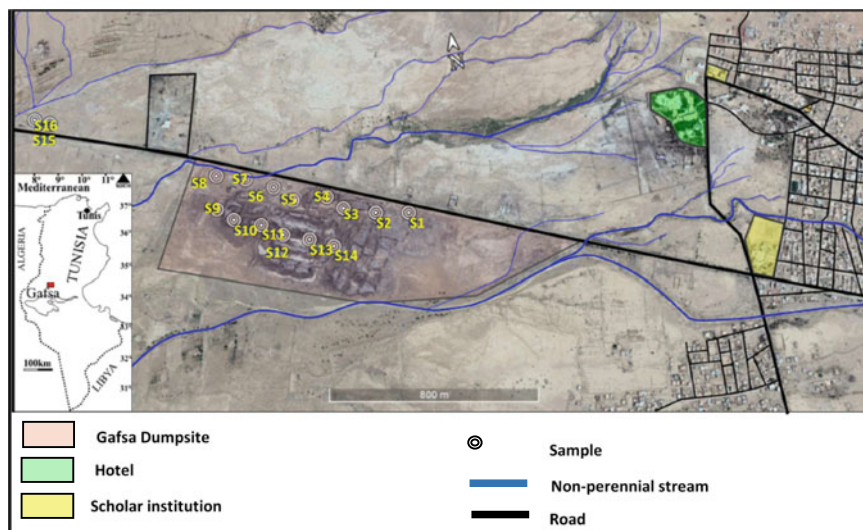
2.1 Samples Collection and Chemical Analysis

A total of 16 samples of topsoil (0–10 cm) from sampling sites were collected at intervals of almost 50 m (Fig. 1). For each sampling site, 100 g samples were collected using a polyethylene shovel and then placed in a polyethylene bag (Adagunodo et al. 2018). Samples were placed in Teflon tubes and digested with HCl, HNO₃, HF, and HClO₄ (Li et al. 2018). Then the solutions were diluted with 2% (v/v) HNO₃, and analysed for Cu, Zn, Cr, Cd and Ni by an atomic absorption spectrophotometer (AAS, AAnalyst-800, Perkin-Elmer).

2.2 Evaluation of Statistical Parameters and Multivariate Statistical Analysis

The multivariate statistical analysis (PCA) is a useful tool to provide information about the relationship between five different chemical metals (Cd, Cr, Ni, Zn and Cu), to determine which elements share probably the same origin,

Fig. 1 Location of the study area and the sampling sites in the landfill of Gafsa, Tunisia



and to identify the geological processes that govern their distribution. Moreover, PCA is a technique used to reduce the available data, which intends to explain most of the data variability with few independent variables (Morenikeji et al. 2017; Fathi et al. 2018). The multivariate analysis was conducted utilizing the software STATISTICA.

2.3 Ordinary Kriging Interpolation

The ordinary Kriging (OK) method was applied by several authors, to map the spatial distribution of pollutants (Chen et al. 2015; Kim et al. 2017). In this study, it is used as an interpolation method based on the SURFER software.

3 Results

3.1 Principal Components Analysis (PCA) of Metallic Elements Contents in Gafsa Soil Dumpsite

Three significant factors represent 89.66% of the total variance. The first factor F1 accounts for 61% of the total variability and involves high positive loadings of Cr (0.786) and Ni (0.753) and high negative loadings with Cu (−0.922) and Zn (−0.881). This factor represents anthropogenic activity of the waste deposits, atmospheric deposition from industrial sources and road traffic (Mohamed et al. 2014).

The second factor F2 represents 18% of the total variance. It comprises high negative loadings of Cd (−0.799) and less significant values for the other elements. It seems to be influenced by background contents rich in Cd and can be suggested that this factor is affected by lithogenic and phosphate rocks (Mello et al. 2018).

The third factor accounts for 10.34% of the total variance and has little loadings of all metals (Table 1).

The correlations between the metal elements show two types of geochemical associations: Cu–Zn and Ni–Cr. The cadmium element appears to be quite distinct from other metals.

3.2 Kriging of Metallic Elements Factor Coordinate in Gafsa Soil and Landfill

The exponential nature of the fitted semi-variogram may indicate that at the site, the analysed metals had a gradual transition or that several patterns interfered (Sulieman and AlGarni 2019).

The contribution of Cu (Fig. 2a) is considerable in the northeast and the east of the discharge land. The coordinate factor values of Cu increased from west to the east and S1 were relatively higher than the other sites. Comparable to Cu, the spatial distribution of Zn in soil showed an increased gradient from west to east.

4 Discussion

The urban area is the most prejudiced, suggesting that the concentrations of metallic elements vary strongly, and this may be due to the influence of extrinsic factors, such as anthropogenic activities and atmospheric deposition. The distribution of heavy metals in atmospheric dust along significant roads in Gafsa city is essential for surrounding soil enrichment of Zn and Cu. Abegunde et al. (2018) found that dusty samples holding trace metallic elements such Zn and Cu from significant roads in Ekiti State in Nigeria have received varying inputs of contaminants from vehicles

Table 1 Factor coordinate of heavy metals in the topsoil of Gafsa landfill

Element	Factor 1	Factor 2	Factor 3
Cu	-0.922	-0.03	0.283
Zn	-0.881	-0.113	0.389
Cd	-0.506	-0.799	-0.321
Ni	0.753	-0.369	0.373
Cr	0.786	-0.324	0.204

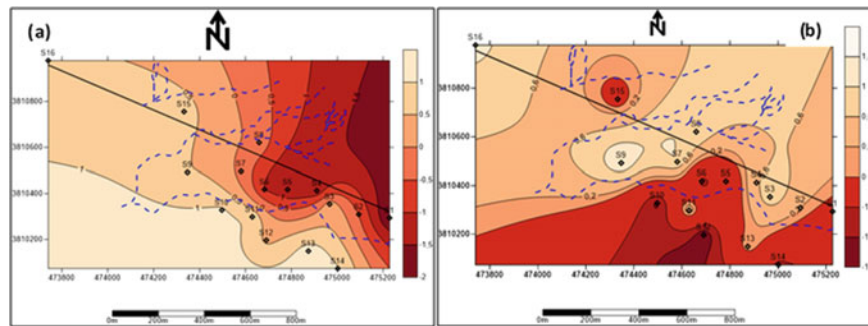


Fig. 2 Spatial distribution of factor coordinate in the topsoil of Gafsa landfill, **a** factor 1 (Cu, Zn, Cr and Ni); **b** factor 2 (Cd). For Ni, the sampling sites S9, S10, S13 and S14 were of relatively higher Ni contamination. The higher Ni content was mainly distributed in the south and the southwest of dumpsite (Fig. 2a). The localities of relatively higher Cr were principally located in the southwest of the

landfill, which was similar to the pollution distribution of Ni. The spatial distribution pattern for Cd in Gafsa landfill soil was not in a discernible regularity (Fig. 2b). The contents of Cd in sampling sites were above the standard limit of three mgkg^{-1} (MEC 2011). Spatially, the Cd contamination in S1, S5, S6, S10, S12, S14 and S15 shows relatively higher values than the other sites

emission and waste incineration. So, higher values of Zn and Cu in Gafsa soil were expected since the samples were obtained from the roadside with dense traffic rate. Alonge-Emmanuel et al. (2018) in the Plateau State in Nigeria found similar results. Chromium in contaminated sites can originate from a wide variety of anthropogenic sources such as municipal waste and atmospheric deposition from industrial sources (Mohamed et al. 2014). The primary supplies of Cr and Ni in the municipal waste dumps include nickel-cadmium batteries and PVC stabilizer (Grag 2017). Cd was identified as a hazardous element when compared with standards values—indicating that this trace element was controlled by both intrinsic items (e.g. geochemical background and natural phosphate parent materials) and extrinsic factors (e.g. waste deposits, and atmosphere deposits from garbage incineration and phosphate industry).

5 Conclusion

In this study, Kriging method was applied to investigate the spatial interpolation of factor coordinate of Zn (-0.881), Cu (-0.922), Cd (-0.506), Cr (0.786) and Ni (0.753) using the measured data from 16 samples in the topsoil of the open landfill in Gafsa city. The correlations between the metal

elements show two types of geochemical associations: Cu-Zn and Ni-Cr. The cadmium element appears to be quite distinct from other metals. This could indicate a natural phosphate origin. The urban area is the most prejudiced, suggesting that the concentrations of metallic elements vary strongly. These results indicated that metallic elements in this study were controlled by both intrinsic factors (e.g. geochemical background) and extrinsic factors (e.g. waste deposits, and atmosphere deposits from garbage incineration, traffic road and phosphate industry). The significance of this work resides in providing baseline information for further soil quality monitoring studies, especially for landfill selection in an urban area.

References

- Abegunde, S.M., Bola, D.E., Idowu, A.O.: Assessment of Heavy Metals Distribution and Contamination in Atmospheric Dust from Major Roads in Ado-Ekiti Ekiti State Using Pollution Indices. *Int. J. New Technol. Res.* **4**(4), 34–40 (2018)
- Adagunodo, T.A., Sunmonu, L.A., Emetere, M.E.: Heavy metals data in soils for agricultural activities. *Data Brief* **18**, 1847–1855 (2018). <https://doi.org/10.1016/j.dib.2018.04.115>
- Ali, S.M., Pervaiz, A., Afzal, B., Hamid, N., Azra, Y.: Open dumping of municipal solid waste and its hazardous impacts on soil and vegetation diversity at waste dumping sites of Islamabad city.

- J. King Saud Univ. Sci. **26**, 59–65 (2014). <https://doi.org/10.1016/j.jksus.2013.08.003>
- Alonge, E., Dada, E.B., Ajewole, S.S.: Determination of heavy metals in soil of high traffic road in Jos, Plateau State, Nigeria. *J. Adv. Res. Agri. Sci. Tech.* **1**(3), 5–7 (2018)
- Chen, C., Hu, K., Li, H., Yun, A., Li, B.: Three-dimensional mapping of soil organic carbon by combining kriging method with profile depth function. *PLoS ONE* **10**(6), 1–15 (2015). <https://doi.org/10.1371/journal.pone.0129038>
- Chenchouni, H., Errami, E., Rocha, F., Sabato, L.: Exploring the nexus of geoecology, geography, geoarcheology and geotourism: advances and applications for sustainable development in environmental sciences and agroforestry research. Springer, Cham (2019). <https://doi.org/10.1007/978-3-030-01683-8>
- Fathi, E.Z.R., Mahmoodi, A., Zare-Bidaki, R.: Water quality evaluation using water quality index and multivariate methods, Beheshtabad River, Iran. *Appl. Water Sci.* **8**(210), 209–215 (2018)
- Garg, Sh.: Bioremediation of agricultural, municipal, and industrial wastes, Chapter 15. In: *Handbook of Research on Inventive Bioremediation Techniques*, published by IGI Global, pp. 341–363 (2017)
- Jafari, K., Moghaddas, N.H., Bajestani, A.M., Ghazi, A.: Investigation of heavy metals contaminant in downstream landfilling site of ardebil municipal waste. *J. Environ. Stud.* **42**(3), 487–504 (2016)
- Kim, S.M., Choi, Y., Yi, H., Park, H.D.: Geostatistical prediction of heavy metal concentrations in stream sediments considering the stream networks. *Environ. Earth Sci.* **76**(72), 1–18 (2017)
- Li, F., Cai, Y., Zhang, J.: Spatial characteristics health risk assessment and sustainable management of heavy metals and metalloids in soils from Central China. *Sustainability* **10**, 91 (2018). <https://doi.org/10.3390/su10010091>
- Mahurpawar, M.: Effects of heavy metals on human health. *Int. J. Res. Soc. Issues Environ. Problems*, 1–7 (2015)
- Mello, F.M., Essid, B., Mesquita, G.N.C., Teodoro, M.E., Araujo, P.T., Gallice, F.: Background and reference values for the cadmium contents of Brazilian soils compared. *Rom. J. Mineral Deposits* **91** (1–2), 91–96 (2018)
- Ministry of the Environment of Canada M.E.C: Soil, ground water and sediment standards for use under Part XV.1 of the Environmental Protection Act. Ontario, 40p (2011)
- Mohamed, R., Taieb, D., Ben Brahim, A.: Chemical and mineralogy characteristics of dust collected near the phosphate mining basin of Gafsa (South-Western of Tunisia). *J. Environ. Anal. Toxicol.* (4)234 (2014)
- Morenikeji, W., Umaru, E., Pai, H., Jiya, S., Idowu, O., Adeleye, B.M.: Spatial analysis of housing quality in Nigeria. *Int. J. Sustain. Built Environ.* **6**, 309–316 (2017)
- Osakwe, S.A., Akpoveta, O.V., Okoh, B.E., Ize-Iyamu, O.K.: Chemical forms of heavy metals in soils around municipal waste dumpsites in Asaba Metropolis Delta State, Nigeria. *Chem. Speciation Bioavailability* **24**(1), 23–38 (2012)
- Sulieman, M.M., AlGarni, A.M.: Soil organic carbon mapping and prediction based on depth intervals using kriging technique: a case of study in alluvial soil from Sudan. *Eurasian J. Soil Sci.* **8**(1) (2019)



Rational Scheme of Chemical Analysis of Urban Soils for Ecological Monitoring

Elena V. Shabanova, Irina E. Vasil'eva, Byambasuren Tsagaan, Ochirbat Ganbaatar, Khuukhenkhuu Byambaa, and Marina Y. Khomutova

Abstract

The ecological monitoring of soils requires a set of modern analytical methods that is being often expensive. Sometimes, analytical methods provide customers with the same analytical information. Therefore, in order to assess the environmental state of the soil cover, a few chemical analysis methods are united into rational schemes, and then, they are used in analytical studies. In this work, on the example of Ulaanbaatar city (Mongolia), a rational scheme of chemical analysis of urban soils is compiled using the informativity criterion of analytical methods. In this scheme, the total contents of 33 elements and concentrations of mobile species of 30 elements, extracted by an ammonium acetate buffer, were determined by rapid multi-element methods. The rational scheme of chemical analysis contains the methods of d.c. and a.c. arc discharge atomic emission spectrometry; flame atomic emission spectrometry; and X-ray fluorescence analysis. Analytical data obtained using a rational scheme provided an amount of the information required for visualizing the spatial distribution of total concentrations of elements and their mobile species within Ulaanbaatar city via geostatistical modeling methods.

Keywords

Ecological monitoring • Urban Soils • Analytical Methods • Informativity

1 Introduction

The growth of the urban population changes fragile natural ecosystems and leads to an increase in areas with polluted soils, thus violating natural processes of soil self-remediation. A distinguishing characteristic of urban soils is the spatial distribution of their composition and properties. Therefore, environmental monitoring is mainly focused on assessing the ratios of the total contents of toxic and biophilic elements and their mobile species in urban soils (Kasimov et al. 2011).

A complete soil characterization requires the application of a set of modern analytical methods that are rather expensive (Pansu and Gautheyrou 2006; Kabata-Pendias 2011). In some cases, analytical methods provide customers with the same analytical information, despite their laboriousness and high cost, thus confirming the economic unprofitability of their simultaneous use. Therefore, in order to assess the environmental state of the soil cover, a few chemical analysis methods are united into rational schemes, and then, they are used in analytical studies (Kuz'min 1996; Proidakova and Vasil'eva 2010). It is essential that at minimum financial and time costs, such rational schemes should provide enough complete and reliable information regarding total concentrations of elements and their mobile species at or below the local background values and maximum permissible concentrations (MPC) in order to provide appropriate recommendations for soil protection measures.

It is well known that for the coordination of qualitative and quantitative interests in complex systems, it is not sufficient to have a “universal scalarization” whose role is played by the money. For standardization and comparison of analytical processes, Kaiser (1970,1973) suggested using the concepts of quantitative limits of determination, as well as the informativeness of analytical methods (P_{inf})

$$P_{inf} = \sum_{u:i} \log_2 \left(\frac{(C_{upper} - C_{lower})\sqrt{n}}{2t\sigma_{iu}} \right) \quad (1)$$

E. V. Shabanova (✉) · I. E. Vasil'eva · M. Y. Khomutova
A.P. Vinogradov Institute of Geochemistry, Siberian Branch,
Russian Academy of Sciences, 1A Favorsky str., Irkutsk, 664033,
Russia
e-mail: shev@igc.irk.ru

B. Tsagaan · O. Ganbaatar · K. Byambaa
Institute of Physics and Technology; Mongolian Academy of
Sciences, Peace Ave 54b, Ulaanbaatar, 13330, Mongolia

where C_{upper} and C_{lower} —upper and lower limits of determined contents of u element at a certain constant mean value of the absolute standard deviation (σ_i , %); t —Student's test; n —number of parallel measures. This is an objective test for selecting a particular method from a variety of options and inclusion of this method in a rational scheme.

The present study aims to develop a rational analysis scheme of urban soils for environmental monitoring on the example Ulaanbaatar city (Mongolia).

2 Materials and Methods

In 2010–2012, we collected 325 soil samples from different residential, ger, industrial and protected zones of Ulaanbaatar city (see Fig. 1). The city lies at an elevation of about 1300–1500 m above the sea level in north central Mongolia, in an intermountain basin, drained by the Tuul River, at the foot of Bogd Khan Uul Mountain and Khentei Ridge. The geochemical regional background is the foot of Bogd Khan Uul Mountain.

The total contents of 33 elements (Si, Al, Mg, Ca, Fe, Ti, Mn, Ba, Sr, Na, K, Li, Rb, B, P, Ni, Co, V, Cr, Mo, Sn, Pb, Cu, Zn, Ag, Bi, Cd, Sb, As, Ge, Tl, F, S) were determined in the samples. For these investigations, we used the methods of d.c. and a.c. arc discharge atomic emission spectrometry (arc AES) via evaporation of powder samples (1) from the carbon electrode channel and (2) injection-spilling (Vasil'eva and Shabanova 2012) for defining the contents of 15 and 21 elements, respectively; flame atomic emission spectrometry (FAES) (Shabanova et al. 2018), for defining the contents of

four elements; X-Ray fluorescence analysis (XRF) (Guni-cheva 2012), for determining the contents of 12 elements; atomic absorption spectrometry with flame and electrothermal atomization (AAS) (Proidakova and Vasil'eva 2010) for defining the contents of 14 elements. The sample preparation for FAES and AAS analyses was done in open systems and in autoclaves under various reaction mixtures (HNO_3 , HF, HCl, HClO_4).

The concentrations of mobile species of 30 elements (Si, Al, Mg, Ca, Fe, Ti, Mn, P, Ba, Sr, B, Ni, Co, V, Cr, Mo, Sn, Pb, Cu, Zn, Ag, Bi, Cd, S, Sb, As, Na, K, Li, Rb) were determined. For this analysis, we employed the methods of inductively coupled plasma atomic emission spectrometry (ICP-AES, 26 elements), FAES (4 elements) and AAS (14 elements). The ammonium acetate buffer (pH 4.8) was used to extract mobile species from soil samples.

3 Results

Our data showed wide variations of chemical elements in the analyzed soil samples and ammonium acetate extracts from those samples. The detection limits of elements by different methods had the threshold limits below the regional background and MPC. The background and polluted soils analyzed by different methods demonstrated similar concentration values and a similar analytical error. The reliability of the obtained analytical information was confirmed by high correlation coefficients (0.85–0.99) between the results of the same samples analyzed by different methods with dissimilar physicochemical principles; as well

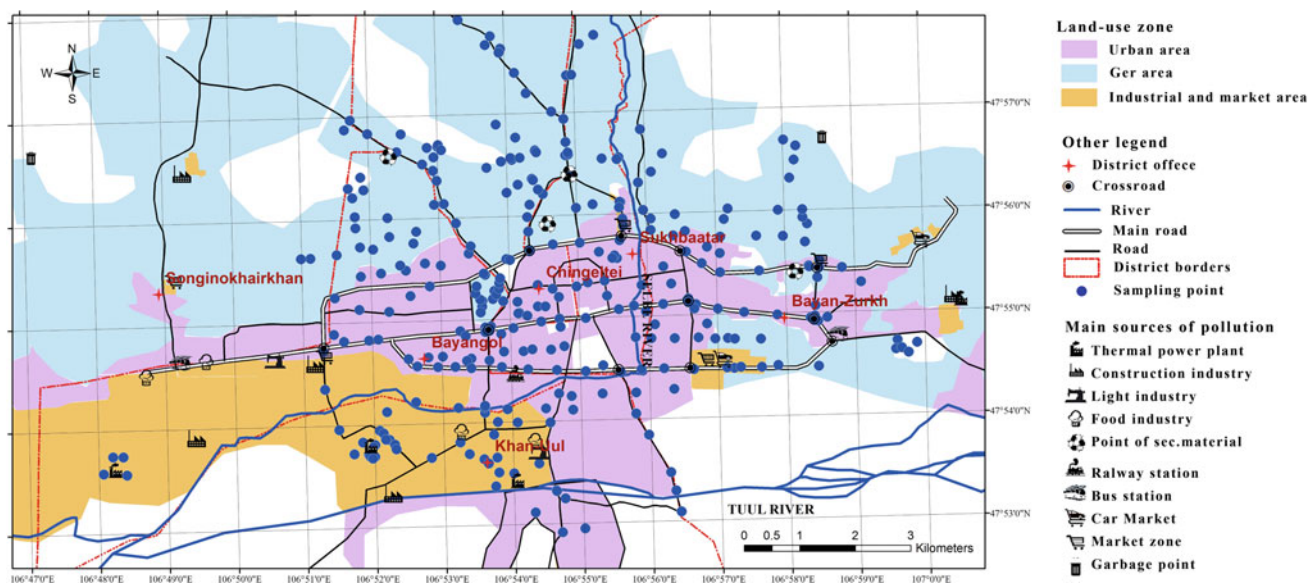


Fig. 1 Scheme of soil sampling with the characterization of different Ulaanbaatar districts, north central Mongolia

as inter-method control via Russian and International certified reference materials of soils.

4 Discussion

The analytical methods providing the same data are grouped into four rational schemes: the first two schemes are employed to determine the total contents of elements ('XRF-AAS' and 'XRF-arc AES' with P_{inf} 306 and 462 accordingly); and the other two—to determine the concentrations of their mobile species ('ICP-AES-FAES' and 'AAS-FAES' with P_{inf} 356 and 200 accordingly). The detection limits of these methods are lower than the regional background values of analytes. The scheme, which includes 'XRF-AAS,' is less informative as compared with the scheme 'XRF-arc AES.' Therefore, the scheme based on 'XRF-arc AES' and combined with the data on mobile species analyzed by ICP-AES is regarded as rational.

Correlations between total element concentrations and their mobile species in different soil classes are individual. Total manganese concentrations in different types of urban soils do not exceed the regional background. However, contents of manganese mobile species in soils of industrial and ger zones are generally 1.2–2.5 times higher than the regional background.

Analytical data obtained using a rational scheme provided an amount of the information required for visualizing the spatial distribution of total concentrations of elements and their mobile species within Ulaanbaatar city via geostatistical modeling methods (Byambasuren et al. 2018).

5 Conclusion

During the environmental monitoring of urban soils, the proposed rational scheme of chemical analysis was used to analyze total concentrations of major and trace elements via

express multi-element methods (XRF and arc AES). Those procedures provided excellent reliability for determination of 33 elements without any chemical sample preparations. The ICP-AES is recommended to be included in the rational scheme for obtaining concentrations of mobile species of 26 elements, extracted by an ammonium acetate buffer.

References

- Byambasuren, T., Shabanova, E.V., Korolkov, A.T., Vasilyeva, I.E., Ochirbat, G., Khuukhenkhuu, B.: Distribution of trace elements in soils of Ulaanbaatar. *Bull. Irkutsk State Univ. Ser. Earth Sci.* **26**(4), 31–45 (2018) (in Russian)
- Gunicheva, T.: Application of nondestructive X-Ray fluorescence method (XRF) in soils, friable and marine sediments and ecological materials. In: Panagiotaras, D. (ed.) *Geochemistry—Earth's System Processes*. InTech, pp. 371–388 (2012)
- Kabata-Pendias, A.: *Trace Elements in Soils and Plants*. 4th edn. Taylor and Francis Group, LLC (2011)
- Kaiser, H.: Quantitation in elemental analysis. *Anal. Chem.* **42** (February and April), 24A–41A; 26A–59A (1970)
- Kaiser, H.: Guiding concepts relating to trace analysis. *Pure Appl. Chem.* **34**(1), 35–62 (1973)
- Kasimov, N.S., Kosheleva, N.E., Sorokina, O.I., Bazha, S.N., Gunin, P. D. Enkh-Amgalan, S.: Ecological-geochemical state of soils in Ulaanbaatar (Mongolia). *Eurasian Soil Sci.* **44**(7), 709–721 (2011)
- Kuz'min, N.M.: On the construction of analytical schemes. *J. Anal. Chem.* **51**(3), 242–249 (1996)
- Pansu, M., Gautheyrou, J.: *Handbook of Soil Analysis. Mineralogical, Organic and Inorganic Methods*. Springer, Berlin (2006)
- Proidakova, O.A., Vasil'eva, I.E.: Method to improve schemes of sample preparation and atomic-absorption analysis of geochemical samples. *Inorg. Mater.* **46**(14), 1503–1512 (2010)
- Shabanova, E.V., Zak, A.A., Vasil'eva, I.E.: Preparation of geological samples to the simultaneous determination of five alkali elements by flame atomic emission spectrometry. *J. Anal. Chem.* **73**(9), 671–679 (2018)
- Vasil'eva, I.E., Shabanova, E.V.: Arc atomic-emission analysis in geochemical research. *Industrial laboratory. Diagnostics Mater.* **78** (1-II), 14–24 (2012) (in Russian)



The Spatial Distribution of Copper and Zinc in Vineyard Soils (in Tokaj, Hungary) as Impacted by Soil Erosion

Izabella Babcsányi, Nhung Thi Ha Pham, István Fekete, and Andrea Farsang

Abstract

Copper and zinc are essential micronutrients for plant growth; however, the long-term use of Cu fungicides and Zn-containing fertilizers can lead to their accumulation in the topsoils of vineyards. It has become evidential that European vineyards can display elevated levels of Cu and to a lesser extent Zn in their topsoils. The fate of the presumably high soil-bound Cu and Zn in vineyards needs further investigations insofar as soil erosion can significantly affect their distribution in soils. Our study conducted in March 2019 focused on evaluating Cu and Zn enrichment in the topsoil layers in a study vineyard plot (1.8 ha) located in the historic winegrowing region of Tokaj (Hungary). The experimental plot was divided into six sampling zones in order to study the spatial distribution of Cu and Zn in the sloping vineyard plot. Composite soil samples and borehole samples have been collected from the sampling zones. Our preliminary results show a significant Cu and also a slight Zn enrichment in the topsoil (0–20 cm, Cu 36.0 ± 6.3 mg/kg, Zn 44.2 ± 2.9 mg/kg), compared to a local forested site and the deepest sampled layers (180–200 cm, Cu 13.3 ± 0.8 mg/kg, Zn 36.7 ± 2.3 mg/kg) considered as the local geochemical background. Additionally, we evidenced that soil erosion significantly affects the topsoil Cu concentrations, as higher Cu concentrations have been found downslope, where the eroded sediments accumulate, compared to the erosion bases upstream. Our results imply that the downstream transport of Cu (and also Zn) can result in the formation of hot spots within vineyards.

Keywords

Sediment • Soil erosion • Transport • Heavy metal • Fungicide

1 Introduction

Copper-based fungicides have been applied in European vineyards since the end of the nineteenth century to combat fungal diseases. The long-term use of Cu pesticides resulted in the accumulation of Cu in vineyard topsoils (Komárek et al. 2010). Cu is a micronutrient, essential for living organisms, but can present ecotoxicological concerns at higher concentrations (Komárek et al. 2010). On the other hand, when assessing the sustainability of viticulture, it is essential to consider the availability of micronutrients for adequate plant growth. Zinc is a delicate micronutrient, because Zn deficiency often presents problems in vineyards, especially in alkaline and sandy soils, while in the case of long-term Zn applications in agriculture (in manures, sewage sludge, pesticides, fertilizers), Zn toxicity may occur (Alloway 2008). Soil erosion caused by the overland flow of rainwater is the main problem in sloping vineyards and results in the relocation (i.e., downstream transport) of Cu- and Zn-bearing soil particles (Farsang et al. 2012). Cu and Zn are generally enriched compared to the average topsoil in eroded sediments transported by runoff (Farsang et al. 2012). Here, we assessed the spatial distribution of Cu and Zn in a sloping vineyard plot in the Tokaj winegrowing region (Hungary) in a context of ongoing soil erosion.

2 Materials and Methods

The 1.8 ha study vineyard plot is situated in northeast Hungary on the Tokaj Big Hill (at Tokaj) (Fig. 1). Organic viticulture is practised on the studied vineyards implying that

I. Babcsányi (✉) · N. T. H. Pham · I. Fekete · A. Farsang
Department of Physical Geography and Geoinformatics,
University of Szeged, Egyetem utca 2-6, 6722 Szeged, Hungary
e-mail: babcsani@geo.u-szeged.hu

Cu-based fungicides are extensively used. The mean slope of the experimental plot is of 8° . Twelve composite soil samples were collected in March 2019 from 0–10 cm to 10–20 cm soil depths at 5 points (from the middle of the grapevine inter-rows) from six equally divided sampling zones ($\sim 1300 \text{ m}^2$) (Fig. 1). The sampling zones have been assigned in order to investigate erosion bases (BH1-3), transitional areas (BH4-5) and accumulation zones (BH6). The distance between the presumed erosion bases and accumulation zones is of $\sim 160 \text{ m}$.

Additionally, soil samples from boreholes and composite soil samples (0–10 cm, 10–20 cm) from a local forested site (control soils) have been collected to assess the impact of Cu- and Zn-containing pesticides' and fertilizers' use on the soil-bound Cu and Zn concentrations. The deepest sampled soil layers were considered as the local geochemical background (180–200 cm). The soils are chernozem soils, developed on loess and characterized by a silt loam texture (Novák et al. 2014). The climate is temperate continental, characterized by warm summers and cold winters and a mean annual temperature of 8.5°C at the summit and almost 10°C at the base of the hill (Novák et al. 2014). The mean annual precipitation is 617 mm (Tokaj) (Novák et al. 2014) with frequent heavy rainfalls during summer, causing significant erosion events on soils.

The pH (in KCl) (MSZ-08-0206/2:1978) ($\pm 3\%$) and organic matter content (MSZ-21470/52-83) ($\pm 15\%$) of soils were measured according to standard procedures. Before total element analyses, samples were dried in the laboratory at 105°C for 24 h and powdered ($<100 \mu\text{m}$) in an agate ball mill following removal of larger organic debris and foreign

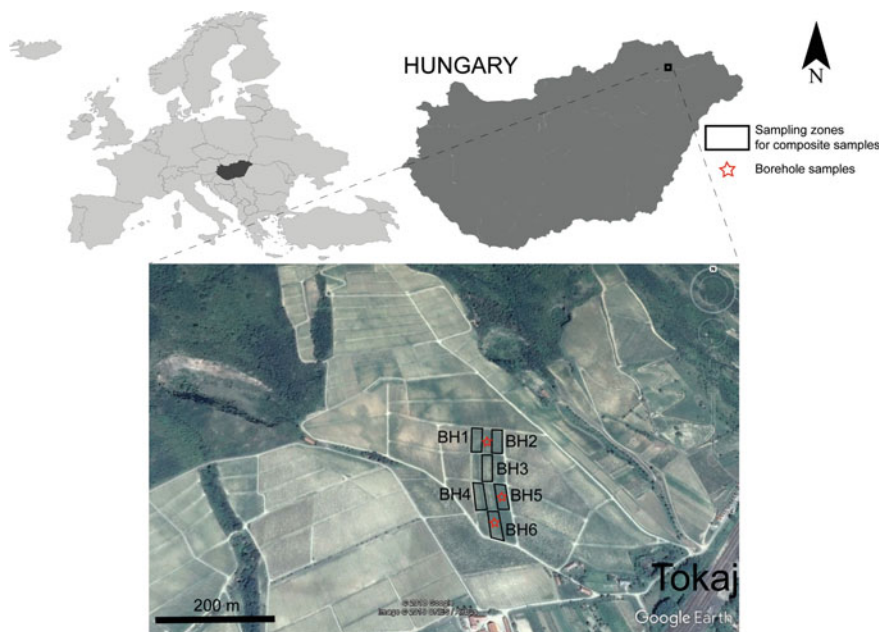
material. Powdered soil samples (0.5 g) were digested in aqua regia (hydrochloric acid:nitric acid = 3:1) in closed vessels in a microwave oven (Anton Paar Multiwave 3000) before Cu and Zn analysis with an inductively coupled plasma optical emission spectrometer (ICP-OES) (PerkinElmer ICP-OES Optima 7000 DV) (with a precision of $\pm 5\%$ and a limit of detection for Cu and Zn of 1 mg/kg).

The nonparametric Mann–Whitney U test was applied for comparing Cu and Zn concentration data in the studied soils ($p < 0.05$) using the SPSS software (IBM SPSS Statistics, version 24).

3 Results and Discussion

The studied soils are characterized by a slightly alkaline pH ranging from 7.85 to 8.64. The organic matter content averages $1.38 \pm 0.33\%$ in the topsoil, while in the deeper soil layers, it is of $0.66 \pm 0.32\%$. Metal analyses revealed that topsoil (0–20 cm) Cu and Zn concentrations are $36.0 \pm 6.3 \text{ mg/kg}$ and $44.2 \pm 2.9 \text{ mg/kg}$, respectively, compared to the deepest sampled layers (180–200 cm) and the local forested soil that bears an average of 13.3 ± 0.8 and $17.2 \pm 0.3 \text{ mg/kg}$ Cu and 36.7 ± 2.3 and $41.0 \pm 2.7 \text{ mg/kg}$ Zn, respectively. These results corroborate previous studies insofar as the long-term and extensive use of Cu- and Zn-containing pesticides and fertilizers causes Cu and to a smaller extent, Zn accumulation in the surface layers of vineyard soils. However, the detected Cu and Zn concentrations are still under the contamination limit according to the Hungarian standards (6/2009. [IV. 14.]

Fig. 1 Study vineyard plot at the Tokaj Big Hill (Tokaj, northeast Hungary) displaying the sampling zones for collecting composite soil samples and borehole sampling points



KvVM-EüM-FVM) (Duplay et al. 2014). The spatial redistribution of the accumulated Cu and Zn in the surficial soil layers due to soil erosion processes has rarely been evidenced.

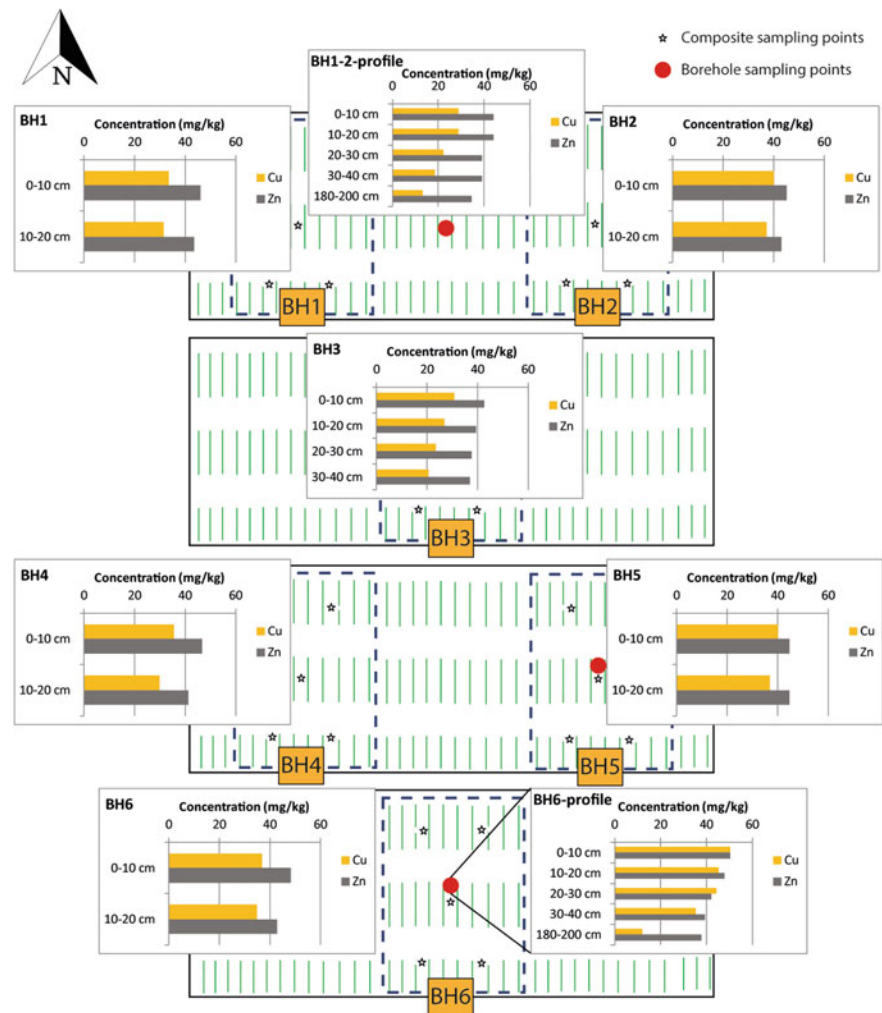
Figure 2 shows the measured soil-bound Cu and Zn concentrations. Cu and Zn concentrations display 32.2 ± 4.5 mg/kg and 43.5 ± 2.0 mg/kg in the uppermost sampling zones (BH1-3) and increase to 41.8 ± 7.8 mg/kg Cu and 47.3 ± 3.2 mg/kg Zn at the accumulation base (BH6) (Fig. 2). In the transitional areas of BH4-5, Cu and Zn concentrations are of 35.7 ± 4.3 mg/kg and 44.3 ± 2.2 mg/kg, respectively. The difference in the Cu concentrations between the erosion base and the accumulation zone is statistically significant, while in the case of Zn, no significant difference can be observed. This downstream increase in the topsoil Cu concentrations shows that the sediment transport during erosion results in the redistribution of Cu in vineyard

soils. Indeed, a previous study has shown that the sediments transported by runoff downstream in sloping vineyards are enriched in Cu (Farsang et al. 2012).

4 Conclusions

Both Cu and Zn are enriched in the surface soil layers in the studied vineyards (Tokaj, Hungary) compared to the deepest sampled layers and the local forested surface soils, probably due to Cu-based fungicide treatments of grapevines and the application of Zn-containing fertilizers. The accumulated Cu is redistributed in the topsoil due to soil erosion processes, as higher Cu concentrations have been observed in the topsoils downstream compared to upslope areas. However, the bioavailability of the redistributed Cu and Zn needs further investigations.

Fig. 2 Cu and Zn concentrations of composite soil samples (0–10 cm and 10–20 cm) and soil depth profiles (boreholes) from the different sampling zones of the experimental vineyard plot at the Tokaj Big Hill



Acknowledgements Izabella Babcsányi expresses her gratitude towards the Hungarian Academy of Sciences for the Premium Post-doctoral Fellowship.

References

- Alloway, B.J.: Zinc in Soils and Crop Nutrition, 2nd edn. IZA and IFA, Brussels, Belgium and Paris (2008)
- Duplay, J., Semhi, K., Errais, E., Imfeld, G., Babcsányi, I., Perrone, T.: Copper, zinc, lead and cadmium bioavailability and retention in vineyard soils (Rouffach, France): the impact of cultural practices. *Geoderma* **230–231**, 318–328 (2014)
- Farsang, A., Kitka, G., Barta, K., Puskás, I.: Estimating element transport rates on sloping agricultural land at catchment scale (Velence Mts., NW Hungary). *Carpathian J. Earth Environ. Sci.* **7** (4), 15–26 (2012)
- Komárek, M., Cadova, E., Chrastny, V., Bordas, F., Bollinger, J.-C.: Contamination of vineyard soils with fungicides: a review of environmental and toxicological aspects. *Environ. Int.* **36**(1), 138–151 (2010)
- Novák, T.J., Incze, J., Spohn, M., Glina, B., Giani, L.: Soil and vegetation transformation in abandoned vineyards of the Tokaj Nagy-Hill, Hungary. *CATENA* **123**, 88–98 (2014)



Geo-accumulation Indexes of Trace Elements in Sediments from Uranium Environments (Central Portugal)

Margarida Antunes, Rui Teixeira, Teresa Valente, and António Santos

Abstract

Stream sediments are usually used as a tool for contamination evaluation. The studied area is an abandoned uranium mine located in Central Portugal, in a not steep area, with altitudes ranging from 360 to 380 m. Geoaccumulation index and contamination factor have been used in the assessment of the degree of contamination of stream sediments with toxic metals. The stream sediments are heavily-to-extremely contaminated in U and Th and moderately-to-heavily contaminated in As and W. The contamination factor is moderate for Al, Cu and Pb, considerably contaminated for As and W, and very highly contaminated for U and Th. The degree of contamination is very high. The contamination of stream sediments is mainly related to the erosion and leaching of the mine dumps located in the study area. Furthermore, the contaminant concentrations tend to decrease downstream of the source, due to hydrodynamic and chemical processes in fluvial systems affected by the mine drainage.

Keywords

U-mines • Stream sediments • Contamination indexes • Portugal • Nanomineralogy

1 Introduction

Minerals are the central repositories of the chemical elements in Earth's crust and are the primary sources of elements that impact global and local ecosystems. These elements are released from minerals mainly through anthropogenic activities, such as mining activities (Brown and Calas 2011), which contributes to approximately 46% of the total anthropogenic flux of uranium to the environment (Sen and Peucker-Ehrenbrink 2012). The composition of natural aquatic environments is mainly controlled by the interactions between mineral surfaces and surface water. A fundamental understanding of these interface processes requires molecular-scale information about minerals, especially those in the nanoscale domain. Colloids and nanominerals, often iron-rich, are shared hosts of toxic elements in mining systems.

Consequently, they play critical roles in fate and transport of toxic elements, mainly due to strong reactivity (Brown and Calas 2011; Valente et al. 2015). Toxic metals may be transferred from mining areas to nearby stream sediments, soils and waters by surface runoff and atmospheric deposition. Abandoned mines are one of the most important sources of contamination (Siegel 2002; Neiva et al. 2014; Antunes et al. 2018). Stream sediments, and particularly their nanomineralogy, are recognized to act as a sink or reservoir for toxic metals and are usually used as a tool for contamination assessment (Valente et al. 2015; Cui and Xin 2011).

The present study aims to analyze the spatial variation in the contents of the stream sediments trace element in a uranium mine-affected system. The obtained results will allow assessing the potential toxic contamination and environmental risks associated with an abandoned U-mine, which may contribute to technical, economical and environmentally sustainable remediation processes.

M. Antunes (✉) · T. Valente
ICT, University of Minho, Campus de Gualtar, 4710-057 Braga,
Portugal
e-mail: imantunes@dct.uminho.pt

R. Teixeira
CEMUC, UTAD, Quinta de Prados, 5000-801 Vila Real, Portugal

A. Santos
Department of Earth Sciences, GEOBIOTEC, Rua Silvio Lima,
3030-790 Coimbra, Portugal

2 Material and Methods

The study area is an abandoned uranium mine (Picoto mine) located at Central Iberian Zone of the Iberian Massif (ZCI), Central Portugal (Fig. 1). This sector contains granitic batholiths that intruded, during the last ductile deformation phase of the Variscan orogeny, a Precambrian to Cambrian phyllites and metagraywackes. The mine area is in a soft slope area, with altitudes ranging from 360 to 380 m, and is cut by a stream, with a dominant NE-SW flow direction. Stream sediments were collected upstream (SD8A, SD8B) and downstream (SD1, SD5, SD6, SD8, SD10) the mine influence area, and Al, Fe, As, Cr, Cu, Mn, Pb, Sr, Th, U, W, and Zn contents were determined by an ICP-OES (Horiba Jobin Yvon JY 2000 2).

There are several international evaluation methods for potentially toxic elements in sediments (Håkanson 1980; Wenyi et al. 1997; Verca and Dolenc 2005). Geoaccumulation index and contamination factor were used for the assessment of mining contamination of the stream sediments in the influence area of the old uranium mine area. Geoaccumulation index (Igeo) is defined as $I_{geo} = \log_2[C_n/(1.5 B_n)]$, with C_n = chemical element concentration and B_n = background level (Müller 1979). Background values for trace elements were defined using median data from a low-density geochemical survey of Portuguese stream

sediments (Ferreira 2000; Ferreira et al. 2001). Contamination factor ($C_f = M_s/M_b$) results from the ratio between a metal content (M_s) and the corresponding background value (M_b). The degree of contamination ($C_d = \sum C_f$) is the sum of the contamination factor for each element (Håkanson 1980).

3 Results and Discussion

Stream sediments collected downstream receive the direct drainage from the mine area and contain higher As (49.70 mg/kg), W (3.29 mg/kg), U (32.90 mg/kg) and Th (97.38 mg/kg) contents than stream sediments located upstream (As: 47.65 mg/kg; W: 2.75 mg/kg; U: 27.34 mg/kg; Th: 95.50 mg/kg). Inside the mine influence area, all the stream sediments are heavily contaminated in Th and moderately–heavily to heavily–extremely contaminated in U (Igeo = 4–5). Some of them are moderately–heavily contaminated in W and also moderately–heavily contaminated in As (Igeo = 3–2). Contamination factor (C_f) and the degree of contamination (C_d) are presented in Table 1. The stream sediments from this area show a low contamination factor for Fe, Cr, Mn, Sr and Zn, a moderate contamination factor for Al, Cu and Pb ($1 \leq C_f < 3$), a considerable contamination factor for As and W ($3 \leq C_f < 6$) and a very

Fig. 1 Location of stream sediments samples (▲) in the Picoto mine area

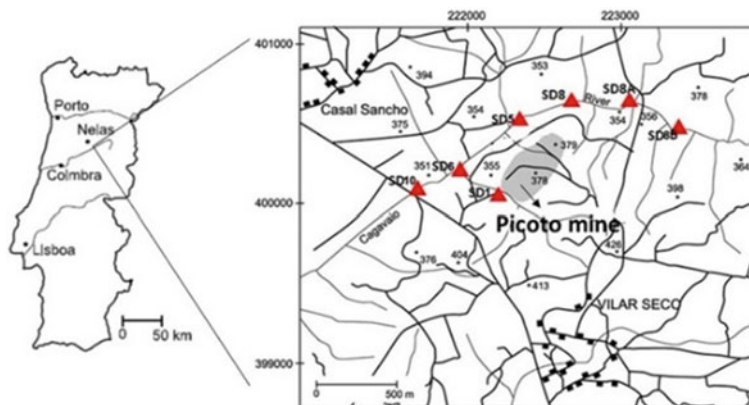


Table 1 Contamination factor and degree of contamination for stream sediments

Contamination factor ^a C_f												
Al	Fe	As	Cr	Cu	Mn	Pb	Sr	Th	U	W	Zn	^b C_d
1.1	0.6	5.5	0.1	1.0	0.6	1.0	0.7	17.9	16.0	5.2	0.9	50.6

^a C_f —Calculated average content for each heavy metal; ^b C_d —degree of contamination. Classes of contamination factor: $C_f < 1$ —low; $1 \leq C_f < 3$ —moderate; $3 \leq C_f < 6$ —considerable; $C_f \geq 6$ —very high. Degree of contamination: $C_d < 8$ —low; $8 \leq C_d < 16$ —moderate; $16 \leq C_d < 32$ —considerable; $C_d \geq 32$ —very high

high contamination factor in Th and U ($C_f \geq 6$). The degree of contamination is very high ($C_d = 50.6$).

The stream sediments receiving the influence of the mining area contain higher trace element contents than background sediments (upstream sediments). Therefore, abandoned uranium mine and associated dumps and tailings are responsible for the contamination. Stream sediments contamination tends to decrease downstream the abandoned uranium mine, which is mainly associated with hydrodynamic and chemical processes in fluvial systems affected by the mine drainage. In the study area, the low size fraction, probably composed by newly formed nanominerals (e.g., iron-rich phases), should retain high contents of contaminants (Valente et al. 2019).

4 Conclusions

Contamination of stream sediments is mainly associated with erosion, mineral weathering and leaching of the mine dumps from the mine area. Furthermore, concentrations tend to decrease downstream of the source, due to hydrodynamic and chemical interactions that typically occur in systems affected by mine drainage. One of these processes may be sorption on the surface of ochre nanoparticles, as previously reported for U and Th in another mine system in the region (Valente et al. 2019). The obtained results reinforce the evidence of environmental and human health risks associated with old abandoned uranium mine areas and emphasize the need for adequate remediation measures. The environmental characterization in terms of trace elements dispersion provides analytical, theoretical and modeling tools that may help the development of further mitigation/remediation projects. Developing a better understanding of sediments properties is a significant challenge for such an achievement. For example, nanogeoscience data such as nanomineralogy of the sediments could be critical for modeling environmental implications. Furthermore, reactivity, stability and surface behavior of the nanoparticles (naturally present in the system or synthesized) are critical properties for their potential application in remediation processes.

Acknowledgements This work was co-funded by the European Regional Development Fund (EU), COMPETE 2020—project ICT (UID/GEO/04683/2013) with reference POCI-01-0145-FEDER-007690 and project Nano-MINENV 029259.

References

- Antunes, I.M.H.R., Neiva, A.M.R., Albuquerque, M.T.D., Carvalho, P. C.S., Santos, A.C.T., Cunha, P.P.: Potential toxic elements in stream sediments, soils and waters in an abandoned radium mine (Central Portugal). *Environ. Geochem. Health* **40**, 521–542 (2018)
- Brown, G.E., Jr., Calas, G.: Environmental mineralogy—understanding element behavior in ecosystems. *C. R. Geosci.* **343**, 90–112 (2011)
- Cui, Y., Xin, D.: Soil heavy metal and wheat phytotoxicity in the vicinity of an abandoned lead–zinc mine in Shangyu City, Eastern China. *Environ. Earth Sci.* **62**, 257–264 (2011)
- Ferreira, A.M.P.J.: Dados geoquímicos de base de sedimentos fluviais de amostragem de baixa densidade de Portugal Continental: Estudo de factores de variação regional. Unpublished PhD thesis, Univ. Aveiro, Portugal (2000)
- Ferreira, A., Inácio, M.M., Morgado, P., Batista, M.J., Ferreira, L., Pereira, V., Pinto, M.S.: Low-density geochemical mapping in Portugal. *Appl. Geochem.* **16**, 1323–1331 (2001)
- Håkanson, L.: An ecological risk index for aquatic pollution control—a sedimentological approach. *Water Res.* **14**(8), 975–1001 (1980)
- Müller, S.N.: Den sediment des Rheins-Veränderungen seit. *Unschau* **79**, 778–783 (1979)
- Neiva, A.M.R., Carvalho, P.C.S., Antunes, I.M.H.R., Silva, M.M.V.G., Santos, A.C.T., Cabral Pinto, M.M.S., Cunha, P.P.: Contaminated water, stream sediments and soils close to the abandoned Pinhal do Souto uranium mine, Central Portugal. *J. Geochem. Exploration* **136**, 102–117 (2014)
- Sen, I.S., Peucker-Ehrenbrink, S.: Anthropogenic disturbance of element cycles at the earth's surface. *Environ. Sci. Technol.* **46** (16), 8601–8609 (2012)
- Siegel, F.R.: *Environmental Geochemistry of Potentially Toxic Metals*. Springer, Berlin, p. 218 (2002)
- Valente, T., Gomes, P., Sequeira Braga, M.A., Dionisio A., Pamplona, J., Grande, J.A.: Iron and arsenic-rich nanoprecipitates associated to clay minerals in sulfide-rich waste dumps. *Catena* **131**, 1–13 (2015)
- Valente, T., Antunes, I.M.H.R., Sequeira Braga, M.A., Neiva, A., Santos, A., Moreno, F.: Mobility control of uranium and other potentially toxic elements in mine waters by ochre-precipitates. In: *Proceedings of IMWA'19*, Perm, Russia (2019)
- Verca, P., Dolenc, T.: Geochemical estimation of copper contamination in the Healing Mud from Makirina Bay, Central Adriatic. *Environ. Int.* **31**(1), 53–61 (2005)
- Wenyl, H., Fengru, H., Jingsheng, C.: Comparative study of assessment method for river particulate heavy metal pollution. *Sci. Geogr. Sin.* **17**(1), 81–86 (1997)



Content of Natural Hydrocarbons in Arctic and Subarctic Soils

Evgeny Lodygin

Abstract

The assessment of the natural background of the hydrocarbon (HC) content in soils is an urgent task, the solution of which will allow us to objectively determine soil pollution and promptly introduce restrictions on industrial technologies of oil production, transportation and refining. The purpose of this work is to assess the background content, to establish patterns of accumulation of HCs in the arctic and subarctic soils, taking into account the landscape–geochemical characteristics of the territories. The concentration of HCs in soil samples was determined based on the values of the fluorescence intensity of the hexane extract. It has been established that the accumulation and distribution of HCs in the soil cover depend on several factors: the relief of the territory and the nature of the soil formation, the particle size distribution of the soil-forming rocks and the content of soil organic matter. The maximum HC content was detected in the soils of accumulative landscapes and the minimum in soils of eluvial territories. Differentiation of HCs over genetic horizons is more flagrant in soils formed on loams and less on sandy rocks. We created a database and a map for the distribution of the natural HCs in the soils of Komi Republic.

Keywords

Background • Monitoring • GIS technologies • Komi Republic • Soil contamination

1 Introduction

In the Komi Republic, large oil fields are intensively exploited. The growth of hydrocarbon (HC) production complicates the ecological situation in this region (extreme northern and northern taiga) significantly. Soil contamination with oil is a particular type of pollution that leads to a profound change in all the essential characteristics of the soil—its morphological, chemical, physical and biological properties (Beznosikov and Lodygin 2014; Jiang et al. 2016). At present, data on the background content of HCs in northern soils are limited, and, as a rule, contradictory, many of them are not linked sufficiently to the variability of HC content in soils (Abakumov et al. 2014). Therefore, the assessment of the natural background of the HC content in soils is an urgent task, the solution of which will allow us to objectively determine soil pollution and promptly introduce restrictions on industrial technologies of oil production, transportation and refining. Soils in extreme climatic conditions of the north have a low cation exchange capacity and poor self-purification, which leads to systematic control over their pollution by HCs (Gomez and Sartaj 2014). The purpose of this work is to assess the background content, to establish patterns of accumulation of HCs in the arctic and subarctic soils, taking into account the landscape–geochemical characteristics of the territories.

2 Materials and Methods

The objects of the study were background soils of the Komi Republic. Soil samples were sampled from organogenic and mineral soil horizons from various types of Retisols, Histosols, Fluvisols, Podzols, Stagnosols, Umbrisols and Spodosols. The concentration of hydrocarbons in soil samples was determined from the values of the fluorescence intensity of the hexane extract, measured on a Fluorat-02-03 M liquid analyser (Lumex, Russia). The technique is based on the

E. Lodygin (✉)
Institute of Biology of Komi Scientific Centre, Ural Branch of the
Russian Academy of Sciences, 167982 Syktyvkar, Russia
e-mail: lodygin@ib.komisc.ru

extraction of oil from a soil sample with chloroform, evaporation of the extract, dissolving the dry extract in hexane and cleaning the resulting solution on a column of aluminium oxide (PND F 16.1: 2.21-98).

In light of the analytical results, a database on the content of HCs in the organic (litter) horizons of the soils was developed using GIS technologies (ArcView GIS 3.2a).

3 Results

The studied regions were significantly extended in the meridional direction and experience changes in the climate from the south to the north, and, hence, the drainage became weaker, and moisture content of semi-hydromorphic and hydromorphic pedogenesis got enhanced. The soil-forming rocks in the regions studied were clayey and loamy deposits, sands and loamy sands or binary deposits (morainic loams overlain by sands and loamy sands), which gave place to glaciofluvial sands near the rivers. The pedogenesis in the mountain region mainly developed on the loamy eluvium and eluvo-deluvium (colluvium) of acid crystalline rocks. Data on the background content of HCs in the organic (litter) horizons of the soils in the Komi Republic are displayed in Fig. 1. It was established that the accumulation and distribution of HCs in the soil cover depended on several factors: the particle-size composition of the parent rocks, the relief of the area and the type of pedogenesis.

4 Discussion

The analysis of the entire data set showed that the distribution of HCs in the soils has a positive asymmetry. Positive asymmetry usually indicates that most variations in the weight portion of the HCs correspond to values lower than the arithmetic mean. We found that the background variations of the HCs in the organic horizons are similar to the different Retisols at a significance level of 0.5. This similarity is related to the association of parent rocks, the particle-size composition of the soils on the mantle loams and the typical features governing the HC migration in the landscape.

The same distribution of HCs in the forest floor horizons was noted for the soils developed on old alluvial and glaciofluvial sandy deposits and poorly drained watershed ridges and glaciofluvial terraces covered by sandy deposits. However, the entire content of HCs in Podzols is lower than that in the soils developed on loamy soil-forming rocks. The rocky soils (Umbrisols and Spodosols) are characterized by negative asymmetry values (A from -0.75 to -0.29) and an insignificant accumulation of HCs, which is consistent with data obtained by other researchers (Liu et al. 2017).

The determined contents of HCs in the soils under study allowed revealing their accumulation in the organic (forest floor) horizons. These horizons serve as a geochemical barrier for the migration of HCs within the profile. The differentiation of the HCs among the genetic horizons is more pronounced in the soils developed on loams (Retisols) and less pronounced in the soils on sandy parent rocks (Podzols). The profile accumulation of the HCs in the Podzols is significantly lower than in the Retisols. The comparison of the downward migration of the HCs in the Podzols and the Retisols shows that they are more uniformly distributed along the profile. Moreover, it demonstrates that they are leached from the Podzolic horizon of the Podzols while an accumulation of HCs in the A0 and A2B horizons and a decrease of their content in the A2, B and BC horizons occur in the Retisols.

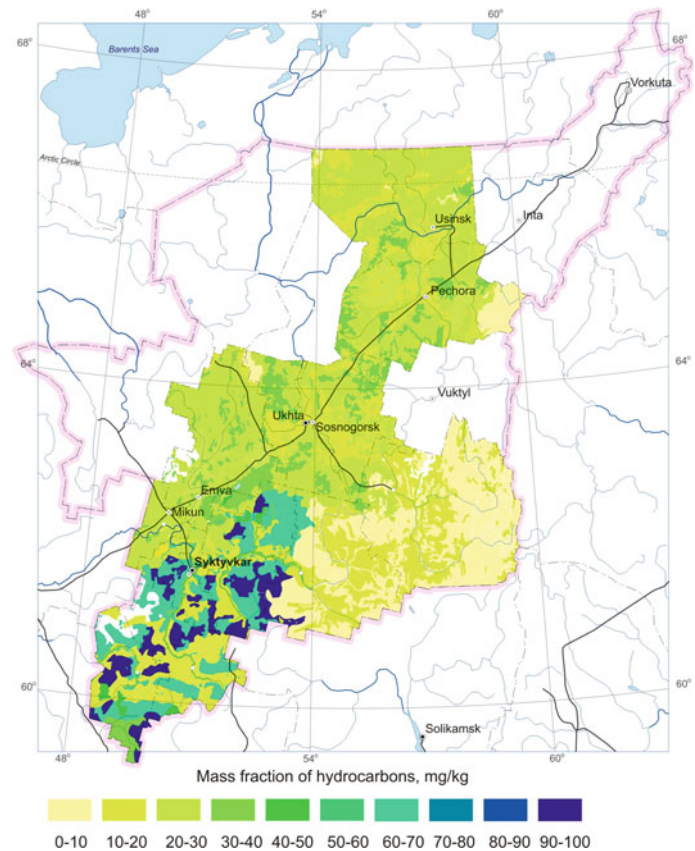
The background concentrations of the HCs vary among the soils in the different landscape elements. Increased content of HCs characterizes the Retisols. These soils occupy accumulative and eluvial-accumulative landscapes. The natural accumulation of HCs during pedogenesis occurs under conditions of periodic anaerobiosis and slow decomposition of plant residues. The accumulation of HCs in the Retisols can also be related to the active lateral inflow from the surrounding landscapes (Beznosikov and Lodygin 2014). In the organic horizons of the Retisols developed on mantle loams, the content of HCs varies in the range from 26 ± 4 to 32 ± 6 mg/kg.

In the litters of the Podzols developed on the different-aged terraces of rivers with old alluvial mainly fine quartz sands, the average content of HCs is 12.7 ± 2 mg/kg; in the Retisols on poorly drained plain watershed ridges and glaciofluvial terraces covered by sandy deposits, the content varies in the range from 13 ± 3 to 22 ± 4 mg/kg. It should be noted that an increase in the HC accumulation was found in the Retisols of the mountain landscapes compared to the Stagnosols.

5 Conclusions

Data obtained on the concentrations of natural hydrocarbons in various background soils of European North-West of Russia with taking into account the landscape-geochemical peculiarities of the region give a possibility for the first time to estimate the pollution level for natural and anthropogenically affected soils. It was established that soils of eluvial positions are less enriched by hydrocarbons in comparison with soils of accumulative territories. Differentiation of hydrocarbons content within the soil horizons was more pronounced in the soil formed on clay textured parent materials than in sandy ones. Data obtained could be used as

Fig. 1 Background contents of hydrocarbons in soils of Komi Republic



background data for further investigation and environmental impact assessment.

Acknowledgements The reported study was funded by Federal budget (Institute of Biology KomiSC UrB RAS).

References

- Abakumov, E.V., Lodygin, E.D., Gabov, D.A., Krylenkov, V.A.: Polycyclic aromatic hydrocarbons content in Antarctica soils as exemplified by the Russian polar stations. *Gigiena i Sanitariya* **93**, 31–35 (2014)
- Beznosikov, V.A., Lodygin, E.D.: Hydrocarbons in the background soils of the southern- and middle- taiga subzones of the Komi Republic. *Eurasian Soil Sci.* **47**, 682–686 (2014)
- Gomez, F., Sartaj, M.: Optimization of field scale biopiles for bioremediation of petroleum hydrocarbon contaminated soil at low temperature conditions by response surface methodology (RSM). *Biodeterior. Biodegrad.* **89**, 103–109 (2014)
- Jiang, Y., Brassington, K.J., Prpich, G., Paton, G.I., Semple, K.T., Pollard, S.J.T., Coulon, F.: Insights into the biodegradation of weathered hydrocarbons in contaminated soils by bioaugmentation and nutrient stimulation. *Chemosphere* **161**, 300–307 (2016)
- Liu, Y., Wu, Y., Xia, Y., Lei, T., Tian, C., Hou, X.: Aliphatic and polycyclic aromatic hydrocarbons (PAHs) in soils of the northwest Qinling Mountains: patterns, potential risk and an appraisal of the PAH ratios to infer their source. *J. Environ. Sci. Health* **52**(4), 320–332 (2017)
- PND F 16.1: 2.21-98. Quantitative chemical analysis of soils. The method of measuring the mass fraction of petroleum products in soil and soil samples by fluorimetric method on a Fluorat-02 liquid analyzer. Moscow, Lumex-Marketing LLC, 212. 25 p



Polycyclic Aromatic Hydrocarbons in Hummocky Peatlands in the Southern Tundra Zone

Dmitriy Gabov, Evgeniya Yakovleva, and Roman Vasilevich

Abstract

The quantitative and qualitative compositions of polycyclic aromatic hydrocarbons (PAHs) were determined, and the vertical stratification of PAHs was characterized along with profiles in hummocky peatlands of southern tundra zone. Benzo[ghi]perylene, naphthalene, pyrene, fluorene, phenanthrene, benzo[b]fluoranthene and benzo[a]pyrene are the most abundant PAHs in peatlands. In seasonally thawed layers, the total PAH content is characterized by low concentrations. On the border of permafrost and seasonally thawed layers 30 (42)–50 cm of Cryic Histosols and in the seasonally thawed layers 18–30 cm of Cryic Histosols (Turbic) in the tundra there is a significant increase in highly condensed 5–6-ring polyarenes: benz[ghi]perylene and benzo[a]pyrene to 688–1300 mg/kg and 2–4-ring polyarenes: naphthalene and pyrene to 485–4382 mg/kg. The relationships between individual PAHs and the botanical composition of peat are traced—an increase in the mass fraction of polyarenes with an increase in the proportion of specific plant residues (grass-tree and moss-shrub). Therefore, it is possible to use PAH ratios as markers of plant residues in soil organic matter during different periods of the Holocene.

Keywords

Polycyclic aromatic hydrocarbons • Tundra • Peatlands • Markers

1 Introduction

Peat deposits of wetlands consisting of weakly humified plant residues are the largest pool of organic carbon in the biosphere, reacting to changes in the composition of the atmosphere, climate, and vegetation. The peat deposits of permafrost regions in the northern hemisphere comprise 1024 Pg of organic carbon (to a depth of 3 m) (Tarnocai et al. 2009). The accumulation of various PAHs in peat deposits can be related to the biogeochemical transformation of initial biogenic material during the decomposition of organic matter (Pastukhov et al. 2017), synthesis in organisms and organomineral systems (Johnson et al. 2004), and geochemical background (Gennadiev et al. 2016). The investigation of PAH transformation in peatlands provides a means to reconstruct past environmental conditions, evaluate the character of PAH accumulation and transformation in the cryogenic zone, and estimate the response of permafrost to climate warming (Ortiz et al. 2004).

This study aims to determine the characteristics of the qualitative and quantitative composition of PAHs, their distribution along with a profile in a hummocky peatland of southern tundra of Northeastern European Russia, and the character of PAH accumulation and transformation in the cryogenic zone and search for markers of peat-forming plant communities and climate changes at high latitudes.

2 Objects and Methods

The region of our study is located in the southern tundra zone (basin of the Padimey-Ty-Vis and Korotaiha rivers) of the Komi Republic, in the area of continuous permafrost. The objects of our study are Cryic Histosols (site 2017–1), Cryic Histosols (Turbic) (site 2017–2) and Fibric Floatic Histosols (site 2017–3), located close to one another. Samples of peat layers were taken with a step of 5 cm to a depth of 30–40 cm and then every 10–20 cm. Samples of peat soil

D. Gabov (✉) · E. Yakovleva · R. Vasilevich
Institute of Biology of Komi Science Centre, Ural Branch of the
Russian Academy of Sciences, Syktyvkar, Komi Republic
167982, Russia
e-mail: gabov@ib.komisc.ru

were collected in August of 2017 using an ice core sampler of the original design (5 cm in diameter): a total of 21 samples from site 2017–1, 20 samples from site 2017–2, 14 samples from site 2017–3. All peat samples were frozen and transported to the laboratory for analysis.

For the complete extraction of PAHs from soils, the ASE—350 system of accelerated solvent extraction (Dionex Corporation, USA) was used. A 1 g sample of peat was placed in an extraction cell and extracted three times with a mixture of methylene chloride/acetone (1:1) at a temperature of 100 °C. Then, the extracts were concentrated using a Kuderna–Danish apparatus at 70 °C, and the solvent was replaced with hexane. The resulting sample concentrate with a volume of 3 cm³ was purified from organic impurities by the method of column chromatography, using aluminum oxide of the II degree of activity according to Brockmann. 30 cm³ of a mixture of hexane/methylene chloride (4:1) was used as eluent. The eluate was concentrated using a Kuderna–Danish apparatus at a temperature in a thermostat of 85 °C to a volume of 5 cm³, and then 3 cm³ of acetonitrile was added and evaporated at a temperature of 90 °C until complete removal of hexane. Reverse-phase HPLC determined the contents of PAHs in peat samples with a spectrofluorimeter detector using an attested procedure of quantitative chemical analysis (PND F 16.1:2.2:2.3:3.62–09) at the Khromatografiya Open Analytical Center of the

Institute of Biology, Komi Research Center, Ural Branch, Russian Academy of Sciences.

3 Results

The total PAHs content varies considerably in the peat profiles within 45–3900 mg/kg (site 2017–1), 115–5700 mg/kg (site 2017–2) and 37–890 mg/kg (site 2017–3) (see Fig. 1). The maximum(s) of PAH contents in the tundra peatland horizons are associated with benz[ghi]perylene, benz[a]pyrene, benz[b]fluoranthene (5–6-ring PAHs), and naphthalene, phenanthrene, pyrene (2–4-ring PAHs).

4 Discussion

Naphthalene, phenanthrene, fluorene, pyrene account for the most considerable mass fraction in the sum of 2–4-ring PAHs (also, for fluoranthene in 2017–3). A high proportion of mosses (*Polytrichum*, *Dicranum*, *Pohlia*, *Sphagnum*) and shrubs (*Salix*, *Betula nana*) determine the content of 2–4-ring PAHs in the thawed horizons of tuberous peatlands of the tundra zone (0–30 (40) cm), which is 210–490 mg/kg. In 2017–3, the concentration of PAHs is 200–490 mg/kg. The concentration of 2–4-ring PAHs in the permafrost and transitional horizons of the peatlands increases in

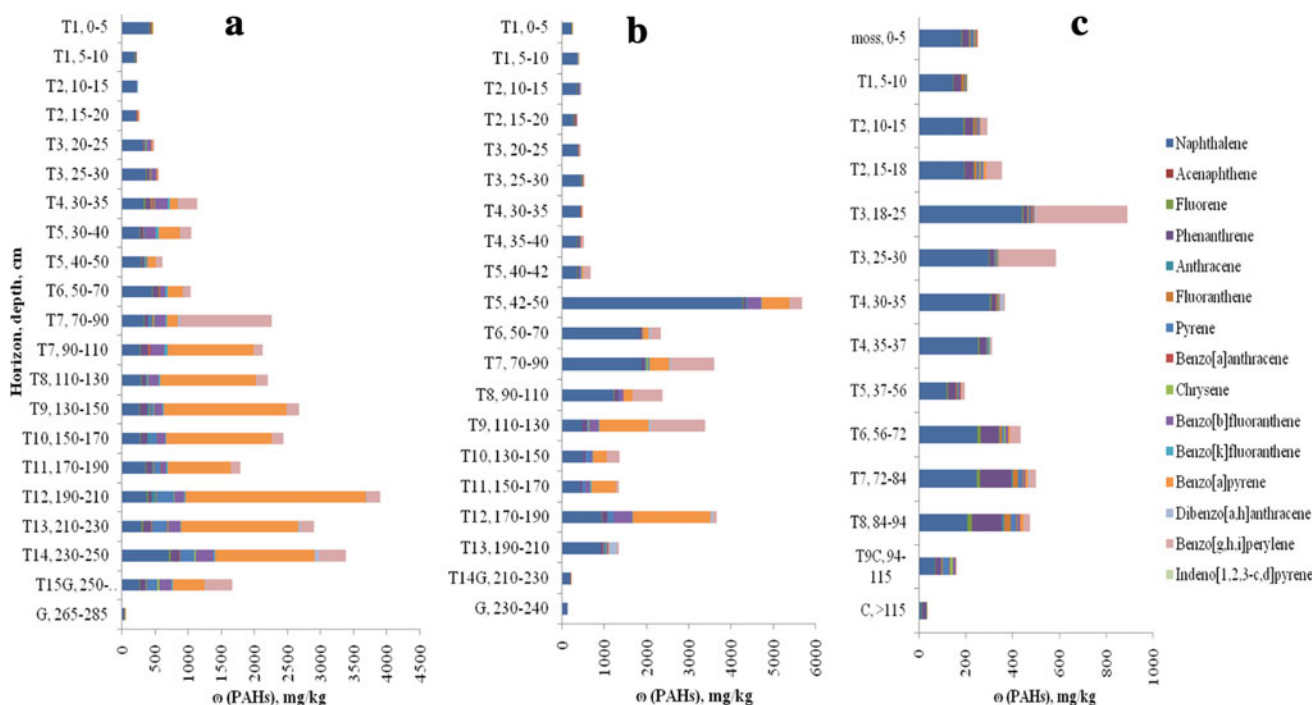


Fig. 1 The distribution of the PAHs in the hummocky peatland of southern tundra: Cryic Histosols (a), Cryic Histosols (Turbic) (b), Fibric Floatic Histosols (c)

comparison with the seasonally thawed layers; the permafrost remains high in moss (*Sphagnum*) with a simultaneous increase in grass and tree residues. In site 2017-1 observed maximum of 2-4-ring PAHs in permafrost horizons 50-90 and 190-265 cm, in site 2017-2—in the horizons 50-110 and 170-210 cm, in site 2017-3—in the horizons of 56-94 cm. Additionally, on the border of the seasonally thawed layer and permafrost (42-50 cm) of the soil Cryic Histosols (Turbic), dynamic processes of defrosting/freezing lead to the release of significant quantities of naphthalene, whose content reaches 4300 mg/kg.

The fraction of 5-6-ring PAHs in seasonally thawed layers of peat bogs of the tundra zone (0-30 (40) cm) is more susceptible to various chemical modifications to other groups of organic compounds: their mass fraction is 0-110 mg/kg the prevalence of benzo[ghi]perylene and benzo[b]fluoranthene. Due to excessive moisture in the bog horse soil, the accumulation of 5-6-ring PAHs occurs in seasonally thawed layers of 18-30 cm to 400 mg/kg. In Cryic Histosols maximum of 5-6-ring PAHs are observed in permafrost horizons of 70-170 and 190-250 cm; in Cryic Histosols (Turbic)—in horizons of 70-130 and 170-190 cm. In the composition of 5-6-ring PAHs, except for benzo[ghi]perylene (1300-1400 mg/kg in extreme values), benz[b]fluoranthene (270-420 mg/kg) and benz[a]pyrene (1800-2700 mg/kg). In the permafrost layers 56-94 cm of Fibric Floatic Histosols, there is a slight increase in 5-6-ring PAHs to 65 mg/kg.

5 Conclusions

In seasonally thawed layers, the total PAH content is characterized by low concentrations. On the border of permafrost and seasonally thawed layers 30(42)-50 cm of Cryic Histosols and in the seasonally thawed layers 18-30 cm of Cryic Histosols (Turbic) in the tundra there is a significant

increase in highly condensed 5-6-ring polyarenes: benz[ghi]perylene and benzo[a]pyrene. Possible additional markers in Fibric Floatic Histosols are 2-4-ring polyarenes: naphthalene and pyrene. Peat permafrost horizons ~70-250 cm of Cryic Histosols, ~50-190 cm of Cryic Histosols (Turbic) and 56-94 cm of Fibric Floatic Histosols are also characterized by an increase in the mass fraction of PAHs. The relationships between individual PAHs and the botanical composition of peat are traced—an increase in the mass fraction of polyarenes with an increase in the proportion of specific plant residues, both grass and tree, and moss-shrub. Therefore, it is possible to use PAH ratios as markers of plant residues in soil organic matter during different periods of the Holocene.

Acknowledgements The reported study was funded by the Federal budget (Institute of Biology KomiSC UrB RAS).

References

- Tarnocai, C., Canadell, J., Schuur, E., Kuhry, P., Mazhitova, G., Zimov, S.: Soil organic carbon pools in the northern circumpolar permafrost region. *Global Biogeochem. Cycles* **23**(2), 1-11 (2009)
- Pastukhov, A.V., Kaverin, D.A., Gabov, D.N.: Polycyclic aromatic hydrocarbons in cryogenic peat plateaus of northeastern Europe. *Eurasian Soil Sc.* **50**(7), 805-813 (2017)
- Johnson, D.L., Maguire, K.L., Anderson, D.R., McGrath, S.P.: Enhanced dissipation of chrysene in planted soil: the impact of a rhizobial inoculum. *Soil Biol. Biochem.* **36**(1), 33-38 (2004)
- Gennadiev, A.N., Pikovskii, Y.I., Kovach, R.G., Koshovskii, T.S., Khlynina, N.I.: Hydrocarbon status of soils under different ages of oil contamination. *Eurasian Soil Sc.* **49**(5), 529-537 (2016)
- Ortiz, J.E., Torres, T., Delgado, A., Julià, R., Lucini, M., Llamas, F.J., Reyes, E., Soler, V., Valle, M.: The palaeoenvironmental and palaeohydrological evolution of Padul Peat Bog (Granada, Spain) over one million years, from elemental, isotopic and molecular organic geochemical proxies. *Org. Geochem.* **35**, 1243-1260 (2004). <https://doi.org/10.1016/j.orggeochem.2004.05.013>



Heavy Metals (Pb, Zn, Cd) and Metalloids (Sb, As) in Carbonated Soils Contaminated by Mine Tailings (North Tunisia)

Yosra Achour, Radhia Souissi, Haifa Tlil, Mikael Motelica Heino, and Foued Souissi

Abstract

Mining and smelting of metal ores activities have increased the dispersion of potential toxic elements (PTE) such as As, Cd, Pb, Sb, Zn and Pb, metal(loid)s in agricultural soils. These elements can be absorbed into the food chain, causing severe threats to human health. This study explores the mobility of these contaminants in agricultural soils developed on carbonated source rocks in the vicinity of two former mining sites in North Tunisia (Jebel Hallouf-Sidi Bouaouane and Jebel Ressas). Besides, it aims to assess the potential hazards of these contaminants on soil eco-dynamics and human health. Calcite and quartz are the abundant mineralogical fraction of these soils. Minor amounts of carbonates (cerussite), sulphates (Gypsum), silicates (hemimorphite), sulphides (sphalerite: (ZnS), pyrite: (FeS₂)), as well as clay minerals, are also present in these soils. Pb, concentrations can reach 22,925 mg/kg; 17,350 mg/kg; 10,321 mg/kg in the soils of Jebel Ressas (JR), Sidi Bouaouane (B) and Jebel Hallouf (JH), respectively. Zn contents reached 69,567 mg/kg; 8,620 mg/kg; 7,951 mg/kg in these soils, respectively. Cd concentrations were much lower than Pb and Zn and did not exceed 20 mg/kg in Jebel Ressas soils and 64 mg/kg in the area

of Sidi Bouaouane. The highest concentrations of metalloids are recorded for Sidi Bouaouane samples, approaching 669 mg/kg for As and 145 mg/kg for Sb.

Keywords

Carbonated soil • Mine tailings • Soil contamination • Mineralogy • Mobility • Potential toxic elements • North Tunisia

1 Introduction

In Northern Tunisia, the majority of the Pb–Zn mining industries have been active during the last century. The exploitation and treatment of metal sulphides have led to the accumulation of considerable quantities of waste rocks and mine (flotation, gravimetry) tailings, which have been stored in dumps, thus promoting the dispersion of potentially toxic metal(loid)s in the nearby environment such as Pb, Zn, Cd, As and Sb. As a result, several studies have been devoted to the determination of the mineralogical and geochemical characteristics of soils and mine tailings in Northern Tunisia (Souissi et al. 2008; Chakroun et al. 2009; Ghorbel et al. 2010, Souissi et al. 2013, 2015; Daldoul et al. 2015). As these potential toxic elements (PTE) can be transported from the mine site to the various compartments of the environment (air, water and soil), via the numerous physicochemical transport mechanisms (water, air and human activity), they pose a threat to the surrounding soils and the nearby plants and animals and even humans via the food chain (Reeves and Brook 1983; Cooke et al. 1990). The originality of this work was to study the mobility of these PTEs in the rhizospheric soils developed on carbonated bedrocks near abandoned mining sites.

Y. Achour (✉) · R. Souissi · H. Tlil · F. Souissi
Laboratoire des Matériaux Utiles, Institut National de Recherche et d'Analyse Physico-chimique, Pôle Technologique, 2020 Sidi Thabet, Tunis, Tunisia
e-mail: yosra.achour@cnrs-orleans.fr

Y. Achour · M. M. Heino
UMR-CNRS 7327 Campus Géosciences, CNRS/ISTO Institut des Sciences de la Terre d'Orléans, 1A rue de la Férellerie, 41071 Orléans, France
e-mail: mikael.motelica@univ-orleans.fr

Y. Achour · F. Souissi
Faculté des Sciences de Tunis, Université Tunis El Manar, 2092 Tunis, Tunisia

2 Materials and Methods

For this work, samples of rhizosphere soils influenced by the associated micro-organisms and the roots of cultivated or spontaneous species were taken around the tailings dumps (Fig. 1) at Jebel Hallouf (rhizosphere of *Thymus capitatus*), Sidi Bouaouane (rhizosphere of *Daucus gingidium*) and Jebel Ressas (rhizosphere of *Daucus gingidium*). Control samples (T) were taken from uncontaminated areas.

In total, five samples were subjected to a textural, mineralogical and geochemical study.

Particle size analysis was carried out using dispersion and flocculation reagents (Lamotte soil texture unit code 1067). Soil pH was measured on the raw soil sample (soil/solution (H₂O) ratio 1/2.5) (NF X 31–117 protocol).

The measurement of soil conductivity (soil/solution ratio 1/2.5) was similarly determined by a multi-3410 conductivity meter.

The estimation of the carbonate content in soil samples was performed using Bernard Calcimeter.

The cation exchange capacity (CEC) was determined by sodium acetate method (Van Bladel et al. 1975).

The mineralogical identification of the minerals in the studied soils was carried out by X-ray diffraction (XRD) on powders of rhizospheric soils.

Chemical analysis, of trace elements, was conducted by Horiba Jobin Yvon-type ICP-AES after mineralization (0.25 g of soil) using a mixture of concentrated acid [HF (3 mL), HCl (1 mL), HNO₃ (7 mL)] and hydrogen peroxide (2 mL H₂O₂). Samples were mineralized at a temperature between 70 and 90 °C for one day until complete evaporation of the acids. Subsequently, the dry residue is taken up with 3 mL of nitric acid (69%) to solubilize while heating slightly. A reference material (SRM 2710) was mineralized and analysed under the same conditions of the soil samples.

Estimation of the proportions of mobile PTEs or ‘bioavailable’ in the rhizosphere that can be absorbed by the plant can be carried out via their extraction with a mixture of low molecular weight organic acids (LMWOAs): acetic acid, lactic acid, citric acid, malic acid and formic acid (4: 2: 1: 1:

1 with a pH = 2.8), developed by Shan et al. (2003) and modified by Feng et al. (2005).

3 Results and discussion

3.1 Grain-size Distribution and Physicochemical Parameters

The sandy fraction dominated soil samples. The values of the electrical conductivity (EC) varied between a minimum value of about 217 μS/cm observed for the soil of Jebel Hallouf and a maximum value of about 500 μS/cm observed for that of Sidi Bouaouane. The CaCO₃ concentrations of all soil samples were high, which were concordant with the carbonated nature of the bedrocks (Table 1).

CEC values were variable from one sector to another: 57.87 Meq/100 g, 127.53 Meq/100 g and 424.18 meq/100 g, respectively.

3.2 Mineralogical Analysis

X-ray diffractograms of soil samples revealed that calcite and quartz were always present, making more abundant mineralogical fraction. The presence of calcite reflected the general carbonated context of the study area.

Other minerals were present as minor phases, such as cerussite (PbCO₃) at Jebel Hallouf and Sidi Bouaouane and Hemimorphite (Zn₄Si₂O₇(OH)₂•(H₂O)) at Jebel Ressas, along with clay minerals (especially kaolinite), were present in these soils.

3.3 Chemical Characterization

The concentrations of PTEs in soils of all localities were so high that they exceeded several times the local geochemical background.

The highest concentrations were recorded for Zn and Pb, (up to 6.95% and 2.29%, respectively, at Jebel Ressas).

Fig. 1 Location map of the study areas

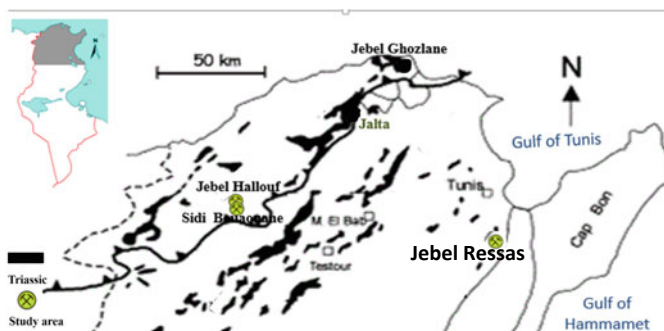


Table 1 Values of pH, electrical conductivity and calcium carbonate, and [PTEs] contents in soil samples

Samples	Electrical conductivity ($\mu\text{S}/\text{cm}$)	pH	% CaCO_3 (average)	[As] (mg/kg)	[Sb] (mg/kg)	[Pb] (mg/kg)	[Zn] (mg/kg)	[Cd] (mg/kg)
JHD	217.2	8.31	75.64	669	103	10,321	7951	55
SB (control)	237.5	7.84	39.74	44	Nd	391	418	7
SB	499	7.78	46.15	683	145	17,350	8620	64
JRS	416.5	8.26	70.51	167	2	22,925	69,567	340
JRS (control)	344	7.96	21.79	3	Nd	1383	4629	20
Reference material SRM2710	Standard			626	38.4	5532	6952	21.8
	Measured			648	53	4905	6521	19

nd: not detected

Table 2 Concentrations of PTEs in soil extracted by organic acids (LMWOAs)

Samples	As ($\mu\text{g}/\text{L}$)	Sb ($\mu\text{g}/\text{L}$)	Pb ($\mu\text{g}/\text{L}$)	Zn ($\mu\text{g}/\text{L}$)	Cd ($\mu\text{g}/\text{L}$)	pH	Conductivity $\mu\text{s}/\text{cm}$
SB	410	650	9470	233,560	420	656	2430
JH	12	80	11,690	5,250,540	370	7.05	1966
JR	30	0	15,110	1,281,830	3130	6.80	886
WHO	10 $\mu\text{g}/\text{L}$	20 $\mu\text{g}/\text{L}$	10 $\mu\text{g}/\text{L}$	3000 $\mu\text{g}/\text{L}$	< 3 $\mu\text{g}/\text{L}$		

Although As was more concentrated than Sb, reaching 600 mg/kg in the area of Jebel Hallouf (Table 1).

3.4 Mobility of PTEs

The presence of metals in the soil extracted depends on the pH and chemical composition of the solution (Ettler et al. 2007). The pH values of the leachates extracted by LMWOAs (6.56–7.05) were higher than those of reagents before extraction (2.8), which proves the buffering of acidity by carbonates excessively present in the soil samples.

The Pb, Zn and Cd contents in the leachates were quite high and exceeded their corresponding limits in surface water, according to the WHO standard, (2006). In all cases, Zn was the most concentrated metal component (233,560 $\mu\text{g}/\text{L}$ at Sidi Bouaouane (SB), 525,540 $\mu\text{g}/\text{L}$ at Jebel Hallouf (JH) and 1,281,830 $\mu\text{g}/\text{L}$ at Jebel Ressas), while quantities released in Pb ranged between 9000 and 15,100 $\mu\text{g}/\text{L}$ and the Cd between 370 and 300 $\mu\text{g}/\text{L}$.

On the other hand, although As and Sb were absent in the leachates of Jebel Ressas (JR) samples, their concentrations exceeded the WHO limits for the samples of Jebel Hallouf (JH: 120 and 80 $\mu\text{g}/\text{L}$, respectively) and Sidi Bouaouane (SB: 410 and 650 $\mu\text{g}/\text{L}$, respectively).

The water-soluble concentrations followed the following order: Zn > Pb > Cd. This order was similar to that observed for the total concentrations in soil samples.

The amount of As extracted by this reagent (LMWOAs) in the rhizosphere of SB and JH samples was considered

quite important because this fraction can be considered as the bioavailable As content in soils (Fayiga et al. 2007), and therefore easily assimilated by plants (Table 2).

4 Conclusion

The high carbonates content in the studied soils is an obvious potential to maintain their environmental neutralization, resulting in neutral to slightly alkaline pH values ranging from 7.78 to 8.31. Zn and Pb heavily contaminate the soils surrounding the Pb–Zn mines in Northern Tunisia, Cd, As and Sb remobilized by transport factors (wind and water) in the form of metal-bearing particles from the tailings. The mineralogical phases carrying these metals are especially hemimorphite, hydrozincite and cerussite. The evaluation of the mobility of the PTEs by the leaching test with organic acids LMWOAs showed solubilization of certain mineral phases (carbonates) which caused an increase in the pH of the starting solution (2.8) to neutral/slightly alkaline values.

References

- Chakroun, H.K., Souissi, F., Bouchardon, J., Souissi, R., Moutte, J., Abdeljaoued, S.: Etude de la mobilité et de la spéciation de Pb-Zn-Cd-Cu-Sb dans les sols d'un site minier abandonné du Nord-Ouest de la Tunisie. *Revue Méditerranéenne de l'Environnement* 3(2009), 567–580 (2009)
- Cooke, A., Andrewss, M., Johnsonm, S.: Lead zinc, cadmium and fluoride in small mammals from contaminated grassland established on fluorspar tailings. *Water Air Soil Pollut.* 51(1–2), 43–54 (1990)

- Daldoul, G., Souissi, R., Souissi, F., Jemmali, N., Chakroun, H.K.: Assessment and mobility of heavy metals in carbonated soils contaminated by old mine tailings in North Tunisia. *J. African Earth Sci.* **110**, 150–159 (2015)
- Ettler, V., Mihaljevic, M., Sebek, O., Grygar, T.: Assessment of single extractions for the determination of mobile forms of metals in highly polluted soils and sediments—analytical and thermodynamic approaches. *Anal. Chim. Acta.* **602**, 131–140 (2007)
- Fayiga, A.O., Ma, L.Q., Zhou, Q.: Effects of plant arsenic uptake and heavy metals on arsenic distribution in an arsenic-contaminated soil. *Environ. Pollut.* **147**(3), 737–742 (2007)
- Feng, M.H., Shan, X.Q., Zhang, Z., Wen, B.: Comparison of a rhizosphere-based method with other one-step extraction methods for assessing the bioavailability of soil metals to wheat. *Chemosphere* **59**, 939–949 (2005)
- Ghorbel, M., Marguerite, M., Courjault-Rade, P., Destrigneville, C., Parseval, P., Souissi, R., Souissi, F., Ben Mammou, A., Abdeljaouad, S.: Health risk assessment for human exposure by direct ingestion of Pb, Cd, Zn bearing dust in the former miners' village of Jebel Ressas (NE Tunisia). *Eur. J. Mineral.* **22**, 639–649 (2010)
- Reeves, D., Brook, R.: Hyperaccumulation of lead and zinc by two metallophytes from mining areas of central Europe. *Environ. Pollut. Ser. Ecol. Biol.* **31**, 277–285 (1983)
- Shan, X.Q., Wang, Z., Wang, W., Zhang, S., Wen, B.: Labile rhizosphere soil solution fraction for prediction of bioavailability of heavy metals and rare earth elements to plants. *Anal. Bioanal. Chem.* **375**, 400–407 (2003)
- Souissi, F., Souissi, R., Bouchardon, J., Moutte, J., Marguerite, M., Chakroun, H.K., Othmani, M., Ghorbel, M.: Mineralogical and geochemical characterization of mine tailing and the effect of Pb, Zn, Cd and Cu mobility on the quality of soils and stream sediments in northern Tunisia. *Congrès International, Gestion des Déchets Solides & Développement Durable*, du 27 au 30 Mars. Hammamet- Tunisie (2008)
- Souissi, R., Souissi, F., Chakroun, H.K., Bouchardon, J.: Mineralogical and geochemical characterization of mine tailings and Pb, Zn, and Cd mobility in a carbonate setting (Northern Tunisia). *Mine Water Environ.* **32**, 16–27 (2013). <https://doi.org/10.1007/s10230-012-0208-2>
- Souissi, R., Souissi, F., Ghorbel, M., Munoz, M., Courjault-Radé P.: Mobility of Pb, Zn, and Cd in a soil developed on a carbonated bedrock in semi—arid climate and contaminated by Pb—Zn tailing, Jebel Ressas (NE Tunisia). *Environ. Earth. Sci.* **73**, 3501–3512 (2015). <https://doi.org/10.1007/s12665-014-3634-6>
- Van Bladel, R., Frankart, R., Gheyi, H.R.: A comparison of three methods of determining the cation exchange capacity of calcareous soils. *Geoderma* **13**, 289–298 (1975)



Organohalogenated Micropollutants: Polybrominated Diphenyl Ether (PBDE) Contamination Gradient of the Seine River in France

Khawla Tlili, Pierre Labadie, Marie-Jeanne Teil, Fabrice Alliot, Catherine Bourges, Annie Desportes, and Marc Chevreuil

Abstract

The Spatio-temporal variability of the Seine River contamination by organic micropollutants such as Polybrominated diphenyl ethers (PBDEs) was investigated in three sites downstream and upstream of Paris between February and November 2010. The mean concentrations of Σ tri-hepta BDE observed at Marnay-Sur-Seine (upstream Paris) are 2.7 times lower than those measured at Bougival-Sur-Seine (downstream Paris), while this ratio is equal to 1.8 for BDE-209. Besides, close concentrations are observed at both downstream sites. The concentration gradient was also observed for PBDE concentrations in sediments collected with particle traps. The PBDE temporal evolution was related to particulate organic matter content which is controlled by river flow variations between February to November. The variation in fluxes of these pollutants seems to result from a regular contribution (case of Bougival and Triel-Sur-Seine) and of a diffuse contribution, case of Marnay-Sur-Seine.

Keywords

PBDEs • Fluxes • Seine River • Upstream • Downstream

1 Introduction

Polybrominated diphenyl ethers (PBDEs) have been widely used in the past decades in many industrial applications. PBDEs are used as additives to prevent fire and constitute a significant class of brominated fire retardants (BFRs). Historically, three major commercial formulation PBDEs have been produced: Penta-BDE, octa-BDE, and deca-BDE. The latter is the only one still allowed in the European Union (EU) after the other formulations were phased out (BSEF 2019). These pollutants, qualified as ubiquitous, have been detected in biotic and abiotic compartments, among others, in river water samples (Carroll et al. 2008). PBDEs have been identified as endocrine disruptors in vivo and in vitro (Darnerud et al. 2001). Surface waters are often considered as an essential compartment for the transport of organic and inorganic micropollutants, especially in urban areas, which are significant emissions areas of anthropogenic pollutants (Lee et al. 2004; Braekevelt et al. 2003). Organic pollutant transport by surface waters is controlled by the hydrological cycle and sorption onto suspended particles matter (SPM) and may also be partly controlled by water characteristics (pH, dissolved organic carbon (DOC), the concentration of essential cations). The aim here is to study the Spatio-temporal variability of the Seine water contamination by organic micropollutants such as PBDEs. PBDE levels were investigated in Seine River under different hydrological conditions (high flows in autumn/winter and lower flows in the spring/summer). The choice of the three sites on the upstream or the downstream of the Paris agglomeration allows apprehending the impact of the Parisian urbanization on the quality of aquatic receiving environments. According to Tlili et al. (2011), the Seine basin (approximately 78,650 km²) is heavily impacted by anthropogenic activities; indeed this river receives vast amounts of urban stormwater overflows and wastewater treatment plant (WWTP) effluents.

K. Tlili (✉)

Faculty of Sciences of Bizerte, 7021 Jarzouna, Tunisia
e-mail: khawla.TLILI@fsb.u-carthage.tn

P. Labadie

UMR 5805 EPOC, Equipe LPTC, 33405 Talence, France

M.-J. Teil · F. Alliot · C. Bourges · A. Desportes · M. Chevreuil
Laboratoire Hydrologie et Environnement EPHE, UMR 7619
Sisyphé, Université Pierre Et Marie Curie, Paris Cedex 05, 75252
Paris, France

2 Materials and Methods

A monthly monitoring of PBDE concentrations was performed on three stations (Fig. 1), representatives of environments under different anthropogenic pressures, upstream (Marnay-Sur-Seine) and downstream of the Paris agglomeration (Bougival and Triel-sur-Seine).

Between February and November 2010, water samples were taken from these three stations. In addition, stainless steel particle traps (height: 25 cm, \emptyset : 15 cm) were also installed at each station, sampling is carried out one time for a period of three months. SPM, DOC, and all samples (water and sediments) were processed as described in Labadie et al. (2010). Statistical differences were evaluated by Mann-Whitney test (XLSTAT PRO software; Copyright holder CC-BY-SA-3.0, Addinsoft, Paris, France).

3 Results

3.1 Hydrological Conditions

The Seine's hydrological cycle is characterized by high flows in autumn/winter and lower flows in the spring/summer. On the Triel-Sur-Seine site located downstream from the confluence of the Yonne, Marne, and Oise, the high water flows (February, March, October, and November) are the highest (from 300 to 600 m³ s⁻¹, (DIREN)). For the period from mid-April to the beginning of September, flows were about 200 m³ s⁻¹ (DIREN), which have been observed. The lowest ones are noted for June and July campaigns (90–110 m³ s⁻¹ (DIREN) at Bougival and 160–190 m³ s⁻¹ (DIREN) at Triel-Sur-Seine).

DOC analyzes were also performed for each campaign. Mean concentrations were estimated at 2.1 ± 0.2 mg L⁻¹ for Marnay, 2.9 ± 0.4 mg L⁻¹ for Bougival and 3.5 ± 0.3 mg L⁻¹ for Triel-Sur-Seine.

3.2 Spatio-temporal Variation of Contamination Levels

Figure 2 illustrates the concentrations of Σ tri-hepta PBDEs and BDE-209 (ng L⁻¹) for the sites of Marnay-Sur-Seine, Bougival and Triel sur-Seine.

The comparison of the concentrations between the upstream (Marnay-Sur-Seine) and downstream (Bougival and Triel-Sur-Seine) sites show a marked concentration gradient. The mean Σ tri-hepta PBDE concentrations observed at Marnay-Sur-Seine are 2.7 times lower than those measured at Bougival-Sur-Seine, while this ratio is equal to 1.8 for BDE-209.

The temporal trend of PBDE concentrations in the water and sediments of the Seine River may be due to the temporal flow variation of the Seine (increases in the winter period and decreases in the summer period) which induces the SPM variation and consequently the PBDE intake associated with these particles. This result confirms our previous findings (Tlili et al. 2011).

The concentration gradient was also observed for PBDE concentrations in sediments collected with particle traps (Fig. 3). In Bougival, the PBDE content is 181 ng g⁻¹ organic carbon (OC) for Σ tri-hepta PBDEs and 1741 ng g⁻¹ OC for BDE-209. These levels are 5 times higher than those determined at Triel (Σ tri-hepta PBDEs: 34 ng g⁻¹ OC and BDE-209: 381 ng g⁻¹ OC) and 16 times higher than

Fig. 1 Sampling sites on the Seine River

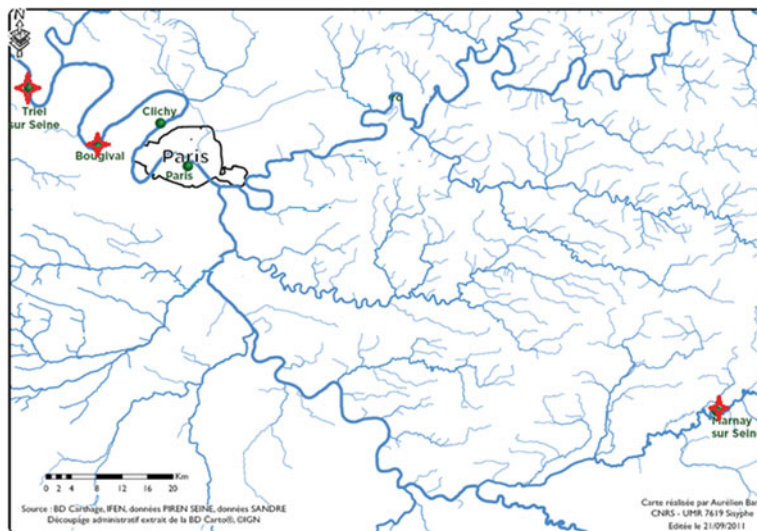


Fig. 2 Spatio-temporal evolution of the PBDE concentration in the raw water of the Seine River, ND: not determined, PBDE concentrations at Marnay in May and November are equal to zero

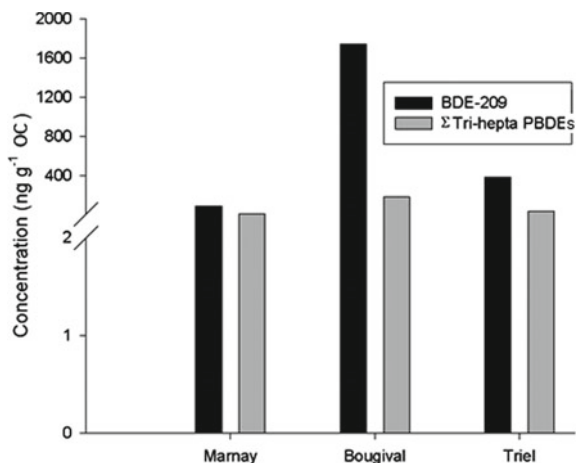
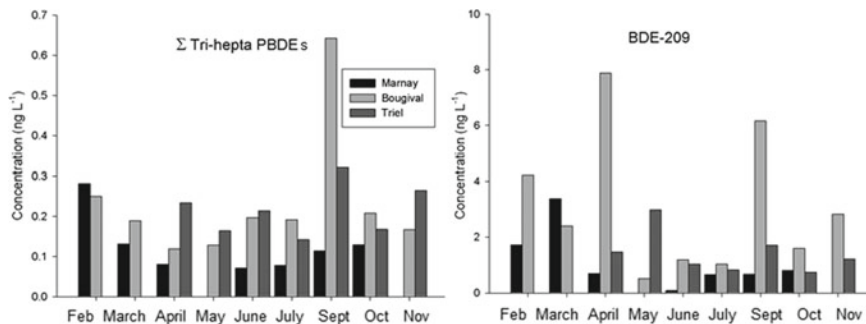


Fig. 3 Spatial variation of PBDE contents in sediments collected using particle traps

those observed in Marnay-Sur-Seine (Σ tri-hepta PBDEs: $11 \text{ ng g}^{-1} \text{ OC}$ and BDE-209: $89 \text{ ng g}^{-1} \text{ OC}$).

4 Discussion

Statistically, the difference between PBDE concentrations in upstream and downstream sites, both for the Σ tri-hepta PBDEs and the BDE-209, is not significant ($p > 0.05$, Mann–Whitney). This result is probably due to the limited number of samples ($n = 9$). Besides, the importance of the concentrations observed in Bougival-Sur-Seine compared to those of Triel-Sur-Seine may result from PBDE inputs associated with several local sources near to the Bougival station, including the port of Gennevilliers, the urban runoff at the Clichy and Briche, and the WWTP Seine Center. Significant concentrations were observed for all PBDEs in the samples from the two downstream stations in September 2010. Such a result is probably related to the contributions associated with urban runoff (Clichy and Briche). The study of temporal variability and dynamics of PBDEs according to

water conditions (high flows in autumn/winter and lower flows in the spring/summer) shows a different behavior compared to the observations made in the center of Paris in a previous study (Tlili et al. 2011).

5 Conclusion

This work enabled us to confirm the presence of PBDEs in the surface waters of the Seine, both in areas under heavy anthropogenic pressure and in reference areas. The Spatio-temporal monitoring of PBDE contamination reveals a significant impact of the Paris agglomeration on measured concentrations, with a strong upstream/downstream gradient. PBDEs are nevertheless detected at the reference station at low levels. The upstream zone appears relatively contaminated, considering the anthropic pressure to which it seems to be subject.

References

- BSEF Bromine Science and Environmental Forum. <http://www.bsef.com>. Last Accessed 14 June 2019
- Braekvelt, E., Tittlemier, S.A., Tomy, G.T.: Direct measurement of octanol-water partition coefficients of some environmentally relevant brominated diphenyl ether congeners. *Chemosphere* **51**, 563 (2003)
- Carroll, J., Savinov, V., Savinova, T., Dahle, S., McCrea, R., Muir, D. C.G.: PCBs, PBDEs and pesticides released to the Arctic Ocean by the Russian Rivers Ob and Yenisei. *Environ. Sci. Technol.* **42**, 69–74 (2008)
- Darnerud, P.O., Eriksen, G.S., Jóhannesson, T., Larsen, P.B., Viluksela, M.: Polybrominated diphenyl ethers: occurrence, dietary exposure, and toxicology. *Environ. Health Perspect.* **109**, 49–68 (2001)
- DIREN: Directions Régionales de l'Environnement. <http://www.ile-de-france.ecologie.gouv.fr/>
- Lee, R.G.M., Thomas, G.O., Jones, K.C.: PBDEs in the atmosphere of three locations in Western Europe. *Environ. Sci. Technol.* **38**, 699–706 (2004)
- Labadie, P., Tlili, K., Alliot, F., Bourges, C., Desportes, A., Chevreuil, M.: Development of analytical procedures for trace-level

- determination of polybrominated diphenyl ethers and tetrabromobisphenol A in river water and sediment. *Anal. Bioanal. Chem.* **396**, 865–875 (2010)
- Tlili, K., Labadie, P., Alliot, F., Bourges, C., Desportes, A., Chevreuil, M.: Influence of Hydrological Parameters on Organohalogenated Micropollutant (Polybrominated Diphenyl Ethers and Polychlorinated Biphenyls) Behaviour in the Seine (France). *Arch. Environ. Contam. Toxicol.* **62**, 570–578 (2011)



Impact of the Gypsiferous Formations of Djebel Djebissa on the Salinity of the Water: Plain of Tebessa Northeast Algeria

Lassaad Ghrieb and Ammar Maoui

Abstract

The semi-arid plain of Tebessa is located in the far northeastern Algeria. Its geology is characterized by Maestrichtian, Turonian and Eocene limestones which border the plain of North as the South. The alluvial formations composed of plio-quaternary sediments respond to all of the plains. The water quality in this region is impacted by the heterogeneity of the geological formations, the chemical facies different in space and time. Deterioration of water quality in the study area decreases the further it gets from gypsiferous formations. The influence of gypsiferous formations on water chemistry is explained by a $\text{Sr}_2^+/\text{Ca}_2^+$ ratio $> 3\text{‰}$ for 78% of the samples.

Keywords

Hydrogeochemistry • Semi-arid lands • Aquifer groundwater quality • Tebessa • Algeria

1 Introduction

The problem of free water resources does not only arise in terms of the quantity available but also the quality of these water is beginning to pose serious problems (Rouabhia et al. 2008). We are now faced with the need to use, manage and protect water sustainably and to ensure that it balances needs and uses because it is the foundation of all life on Earth (Kowalski and Hamimed 2000). Aridity affects a large part of Algeria, with the persistence of drought surface water becomes scarce, groundwater is reduced, and their qualities

deteriorate with the increase of salinity (Negm et al. 2020a, 2020b). This study concerns a semi-arid area at the extreme East of Algeria, which is affected by the lack and degradation of the quality of its groundwater.

2 Geological Overview of the Region

The Tébessa region is part of the Northeastern Auresian structure (Aures Nememcha) of the Atlas Saharian (Kowalski and Hamimed 2000). It consists mainly of the following formations:

- A Triassic diapiric formation dislocating underlying formations in Jebel Djebissa
- Carbonated formations represented by necessary limestone-marl layers and Cretaceous to Tertiary marls. We can observe some of these formations at the level of the borders of the plain of Tébessa (Fig. 1). Significant MioPlio-Quaternary alluvial deposits are non-conforming with the underlying formations and form the filling of the depression, currently the plain. This formation is observable, notably at the foot of the hilly reliefs.

The climatological study of the Tebessa region shows that the climate is typically semi-arid and continental (cold winter and hot summer) (Fatmi et al. 2020). The average annual temperature is 15.53 °C. Precipitation is the first important factor in the water cycle, its distribution in time and space determines the shape of the flows and the contributions to the aquifers.

3 Material and Methods

The elemental chemical analyzes were carried out at the Annaba Earth Sciences Laboratory, at the laboratory of the study and research center applied to the development of

L. Ghrieb (✉)
University 8 May 1945, P.O. Box: 401, Guelma, Algeria

A. Maoui
Laboratory Civil Engineering and Hydraulic, University 8 May 1945, P.O. Box: 401, Guelma, Algeria

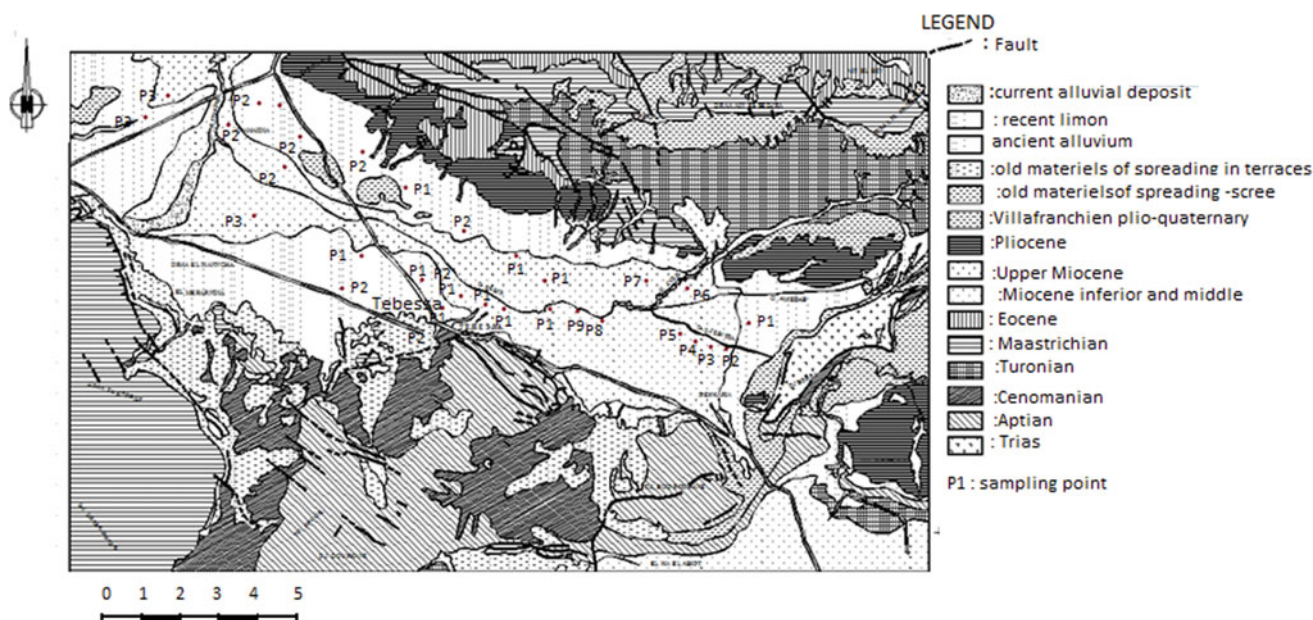


Fig. 1 Geology of the study area

Ferphos, HYDROSID, DRA, at the laboratory of the University of Lille. University of Franche Comte Besancon in France. The samples are filtered beforehand and stored at a temperature of 4 °C.

The applied methods are: the atomic absorption spectrometry for analysis of Ca^{2+} , Mg^{2+} , Na^+ , K^+ , and Sr^{2+} , the titrimetric determination for HCO_3^- , and the colorimetric assays for Cl^- , and SO_4^{2-} . The physical parameters such as pH, and electrical conductivity (undergo transformations once the water has been cut from their initial interaction medium) have been measured in situ (Rouabhia et al. 2008). The same measurement conditions were respected for all campaigns (same equipment and same measurement protocol).

The samples were taken during the sampling campaigns, corresponding to the periods of high and low water, on about thirty domestic wells (Fig. 2) whose average depth is less than 50 m. In this study, we are limited in the area of Djebissa with the existing eight wells.

4 Results and Discussion

The conducted study showed that evaporitic formations influence the chemistry of water. To support our hypothesis, the variation of strontium indicate the evaporitic origin of salinity. The threshold values of $\text{Sr}^{2+}/\text{Ca}^{2+}$ ratio were applied to the results obtained in the study of the region (Fehdi et al. 2009).

The Triassic Gypsifera crops out at Djebel Djebissa, Piezometric mapping (Rouabhia et al. 2008) has shown the flow from this Jebel to the plain, suggesting a relationship

between the geology of the area and salinity. Two control wells were used to highlight the flow relationship: the first which is located a few meters from the Triassic and the second which is quite distant. The obtained results are illustrated in Fig. 3.

Graphs of $\text{Sr}^{2+}/\text{Ca}^{2+}$ ratio of wells 1 and 8 show very high values, more significant than 3‰, indicating an influence of the evaporitic formations, which suggests that Djebel Djebissa (diapir), directly influences the salinity of the waters. The results of $\text{Sr}^{2+}/\text{Ca}^{2+}$ ratios give two main indications: the first shows almost a narrow influence of the evaporitic formations on mineralization and concerns the water table of the Bekkaria-Tebessa system. In this part, the Triassic formations are located upstream of the system and feed it directly. In other regions, the absence of this direct relationship is noticed. The water before reaching the aquifer infiltrates through different formations that influence the chemical composition of the water, thus explaining the heterogeneities of their quality (Fehdi et al. 2009).

5 Conclusion

The $\text{Sr}^{2+}/\text{Ca}^{2+}$ ratio gave important values, confirming the impact of evaporite formations on the water quality of wells and rivers. The curb-forming flows in the center of the plain as well as the dominance of bicarbonates in the sector of Chabro, concur the supply of the water table and the streams from the limestone formations of the Maastrichtian. Algeria loses significant quantities of water due to the salinity generated by the rock water interaction, following the leaching

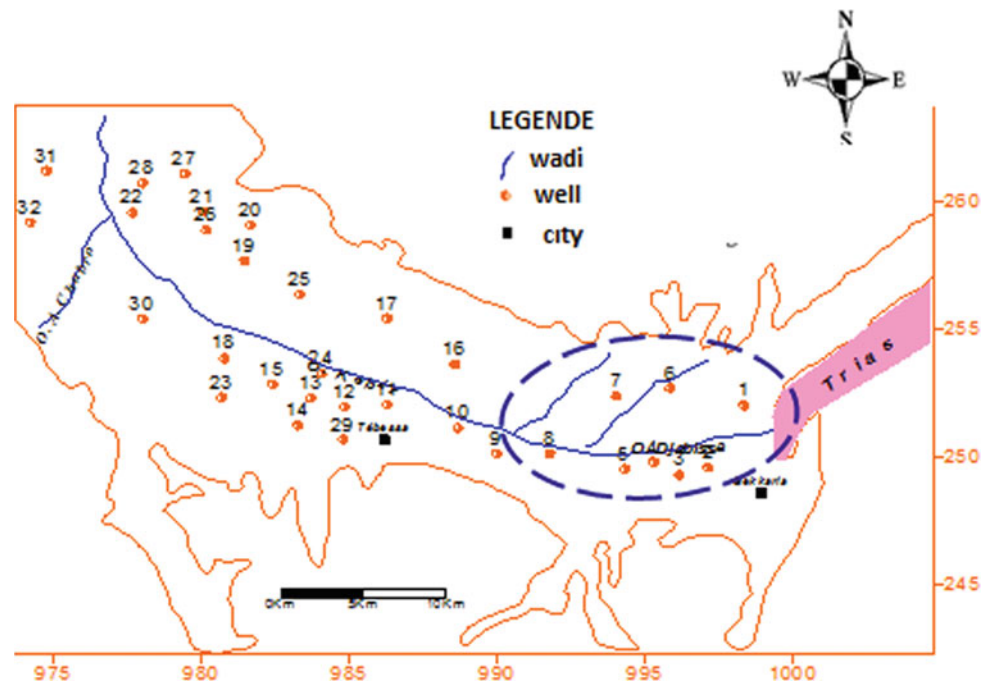


Fig. 2 Position of analyzed wells compared to Djebel Djebissa

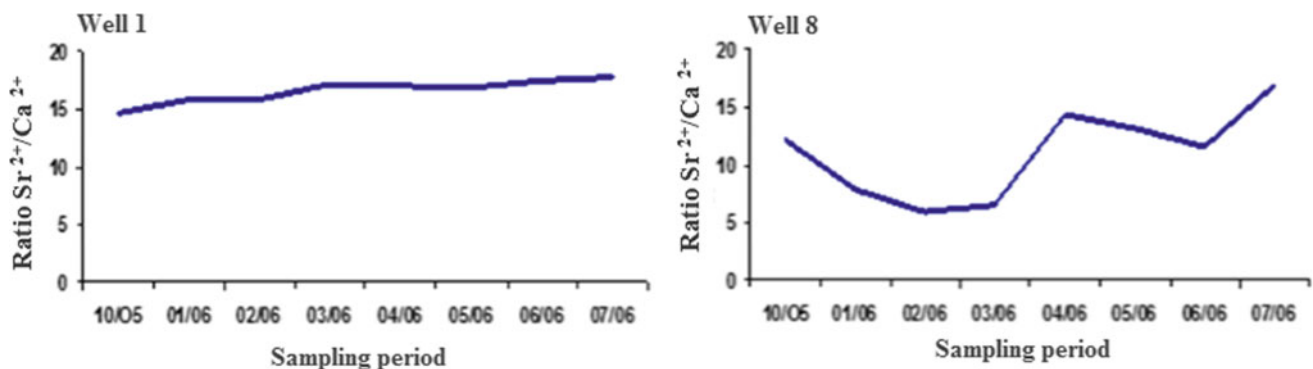


Fig. 3 $\text{Sr}^{2+}/\text{Ca}^{2+}$ ratio changes at the extreme wells (P1 & P8) 2006

of geological formations, which have an undesirable effect on the quality of this resource. Treatment processes to reduce the salinity of this water can allow its use in agriculture and mining industry in the region.

References

- Fatmi, H., Mâalem, S., Harsa, B., Dekak, A., Chenchouni, H.: Pollen morphological variability correlates with a large-scale gradient of aridity. *Web Ecology*, 20, 19–32 (2020). <https://doi.org/10.5194/we-20-19-2020>
- Fehdi, C., Rouabhia, A., Baali, F., Boudoukha: A the hydrogeochemical characterization of Morsott-El Aouinet aquifer, Northeastern Algeria. *Environ. Geol.* **58**, 1611–1620 (2009). <https://doi.org/10.1007/s00254-008-1667-4>
- Kowalski W.M., Hamimed, M.: Polyphase Diapirism or Albian Salt Glacier? Dilemma of the triassic material of the Algerian-Tunisian borders. *Bulletin of the Geological Service of Algeria*. 11(1), 29–60 (2000). (12 fig)
- Negm, A., Bouderbala, A., Chenchouni, H., Barcelo, D. (Eds): *Water Resources in Algeria - Part I: Assessment of Surface and Groundwater. The Handbook of Environmental Chemistry Series.* Springer Nature Switzerland (2020a). <http://doi.org/10.1007/978-3-030-57895-4>
- Negm, A., Bouderbala, A., Chenchouni, H., Barcelo, D. (Eds): *Water Resources in Algeria - Part II: Water Quality, Treatment, Protection and Development. The Handbook of Environmental Chemistry Series.* Springer Nature Switzerland (2020b). <https://doi.org/10.1007/978-3-030-57887-9>
- Rouabhia, A., Baali, F., Fehdi, C., Kherici, N., Djabri, L.: Hydrochemical and isotopic investigation of a sandstone aquifer groundwater in a semi-arid region, El Ma El Abiod, Algeria. *Environ Geol.* **57**, 1699–1705 (2008). <https://doi.org/10.1007/s00254-008-1451-5>



Seasonal Evaluation of Heavy Metals Speciation in Municipal Landfill Leachate Using ‘WATEQ4F’

Lathamani Ramachandra and Suresha Sidduraiah

Abstract

Municipal solid waste landfills leachate can cause significantly adverse impacts on the environment and human health. The most commonly reported danger is the contamination of groundwater and soil by leachate produced from these landfills. Leachate samples were collected in pre- and post-monsoon season using Lysimeter and were analyzed for heavy metals (Fe, As, Hg, Cd, Pb, Cr, Ni and Zn) using AAS. A geochemical model (*WATEQ4F*) was used to study speciation of heavy metals in leachate samples. In pre-monsoon, samples witnessed only four heavy metals, whereas in post-monsoon all heavy metals were present due to dilution process. Most of the metals speciated to chloride and carbonate complexes indicating leaching of landfill effluents due to variations in pH. NaCl deicing salt can potentially affect the transport and speciation of heavy metals (e.g., Cd, Cu, Pb, and Zn) in waters through several physico-chemical processes, including dispersion of metal-bearing colloidal particles, desorption and partitioning into the dissolved phase and increase aqueous solubility through the formation of aqueous chloro-complexes. The concentration of these components increases under favorable conditions close to a landfill and may lead to serious toxic risk to groundwater and soil.

Keywords

Municipal solid waste • Landfills • Leachate • Atomic absorption spectroscopy • *WATEQ4F* • Groundwater

1 Introduction

From the last few years, both developed and developing nations are facing challenge in management of solid waste. Especially in developing countries, unscientific solid waste management is causing more threat to precious natural resources. Series of reactions in solid waste results in leachate production. Leachate, liquid waste if not processed, has the capability to alter groundwater and soil characteristics in landfills (Kanmani and Gandhimathi 2013; Moturi et al. 2004). In the present study, leachate samples were analyzed for heavy metals in different seasons and chemical speciation was studied to understand the possible dilutions of chemicals.

2 Materials and Methods

Totally six landfill leachate samples three each (L1, L2 and L3) in pre-monsoon and post-monsoon season were collected from solid waste dumping site using a Lysimeter (Phillip and Kane 2010). Heavy metals concentration like, iron (Fe), copper (Cu), arsenic (As), mercury (Hg), cadmium (Cd), lead (Pb), total chromium (Cr), nickel (Ni), and zinc (Zn) were analyzed by acid digestion method using atomic absorption Spectrophotometer (GBC Avanta, Version 1.3 Model). ‘*WATEQ4F*’ 2.63 version (2004), a geochemical model, was used to analyze speciation of heavy metals in leachate samples.

3 Results

In pre-monsoon leachate samples (Table 1), only Fe, Cd, Pb, Ni, and Zn were present, but in post-monsoon samples (Table 2), all the heavy metals were present, which may be due to the dilution process taking place during the monsoon.

L. Ramachandra (✉)
Vidyavardhaka First Grade College, University of Mysore,
Mysuru, 560001, India

S. Sidduraiah
Yuvarajas College, University of Mysore, Mysuru, 560005, India

Table 1 Chemical composition of heavy metals in pre-monsoon leachate samples (mg/L)

Sample ID	Fe	Cd	Pb	Ni	Zn
L1	98.9	0.02	0	1.43	1.71
L2	76.9	0.02	0.05	0.78	1.13
L3	12.4	0.02	1.22	0.4	1.8

Table 2 Chemical composition of heavy metals in post-monsoon leachate samples (mg/L)

Sample ID	Fe	Cu	As	Hg	Cd	Pb	Cr	Ni	Zn
L1	80.91	48.12	1.44	5.09	0.18	11.58	0.86	1.59	627.2
L2	60.03	1.94	1.68	20.1	0.001	44.56	3.9	2.5	576
L3	10.44	10.8	0.43	1.61	0.2	3.44	0.56	2.8	676.8

In **PRM**, Fe is the dominant heavy metal followed by Zn, Ni, and Pb in that order. In **POM**, Zn is the dominant heavy metal followed by Fe, Cu, Pb, Hg, Ni, As, Cr, and Cd. Different kinds of wastes are responsible for the presence of heavy metals in the landfills. Sources such as electronic waste, painting waste, and used batteries increase heavy metals content in landfills (Adeolu et al. 2011).

3.1 Heavy Metals Speciation

In **PRM**, Cd is speciated to CdCl^1 , CdCl_2^0 , CdCl_3^0 , $\text{Cd}(\text{CO}_3)^0$, $\text{Cd}(\text{CO}_3)_2$, CdHCO_3^1 , CdOHCl^0 , CdSO_4^0 , and $\text{Cd}(\text{SO}_4)_2$. Fe is speciated to FeCl^1 , FeCO_3^0 , FeHCO_3^1 , FeHPO_4^0 , FeH_2PO_4 , and $\text{Fe}(\text{SO}_4)^0$. Ni is speciated to NiCl^1 , NiCO_3^0 , $\text{Ni}(\text{CO}_3)_2^{-2}$, NiHCO_3^1 , and NiOH^1 . Pb is speciated to PbCO_3^0 , $\text{Pb}(\text{CO}_3)_2^{-2}$, and PbHCO_3^1 . Zn is speciated to ZnCO_3^0 , $\text{Zn}(\text{CO}_3)_2^{-2}$, and ZnHCO_3^1 (Table 3).

In **POM**, Cd is speciated to CdCl , CdCl_2 , CdCl_3 , CdCO_3 , $\text{Cd}(\text{CO}_3)_2$, CdHCO_3 , CdOHCl , and CdSO_4 . Cu is speciated to CuCl_2^{-1} , CuCl_3^{-2} , CuCO_3^0 , $\text{Cu}(\text{CO}_3)_2$, and $\text{Cu}(\text{OH})_2^0$. Fe is speciated to FeCl^1 , FeCO_3^0 , FeHCO_3^1 , FeHPO_4^0 , $\text{Fe}(\text{OH})^1$, $\text{Fe}(\text{SO}_4)^0$, $\text{Fe}(\text{OH})_3^0$, and $\text{Fe}(\text{OH})_4^{-1}$. Ni is speciated to NiCO_3^0 , $\text{Ni}(\text{CO}_3)_2^{-2}$, NiHCO_3^1 , and NiOH^1 . Pb is speciated to PbCO_3^0 , $\text{Pb}(\text{CO}_3)_2^{-2}$, and PbHCO_3^1 . Zn is speciated to ZnCO_3^0 , $\text{Zn}(\text{CO}_3)_2^{-2}$, and ZnHCO_3^1 (Table 3).

4 Discussion

The fate and transport of heavy metals in landfill leachate depend upon their variable complexing abilities, the relative concentrations of other constituents, and the environmental conditions, particularly the acid value.

The high level of Fe indicates the dumping of steel scrap in the landfill. This explains the brown dark color of the leachate which is a product of oxidation of ferrous to ferric form and the formation of ferric hydroxide colloids and complexes with

humic acid (Kanmani and Gandhimathi 2013). The level of Pb in the leachate indicates the disposal of Pb batteries; Pb-based paints, plastics, and pipes in the site (Moturi et al. 2004). Moreover, the detection of Ni in excess can be attributed to the disposal of batteries at the site. Cu may be from paints, blades, bottle caps, insecticides, pharmaceuticals, and cosmetics (Kanmani and Gandhimathi 2013). The presence of Zn can be attributed to the disposal of batteries, fluorescent lamps (Kanmani and Gandhimathi 2013), food wastes, and burning tires at the site (Adeolu et al. 2011).

Most of the metals speciated to chloride and carbonate complexes indicate leaching of landfill effluents which has occurred due to variations in pH. NaCl deicing salt can potentially affect the transport and speciation of heavy metals (e.g. Cd, Cu, Pb, and Zn) in waters through several physico-chemical processes, including dispersion of metal-bearing colloidal particles, desorption and partitioning into the dissolved phase, and increase aqueous solubility through the formation of aqueous chloro-complexes (Amrhein et al. 1992; Warren and Zimmerman 1994; Backstrom et al. 2004). Metal chloride complexation is a mechanism by which effects desorption and subsequent partitioning of trace metals into the dissolved phase (Backstrom et al. 2004, 2003; Doner 1978). This may be initiated by chloride-induced desorption of trace metals (Warren and Zimmerman 1994).

5 Conclusion

The leachate is generally a strongly reducing liquid formed under methanogenic conditions and on coming into contact with aquifer materials has the ability to reduce sorbed heavy metals in the aquifer matrix. The most important reactions are the reduction of Fe and Mn to more soluble species. Hence, the concentration of these components increases under favorable conditions close to a landfill and may lead to serious toxic risk to groundwater and soil.

Table 3 Average values of heavy metal speciation in leachate samples (ppm)

PRE-MONSOON				POST-MONSOON			
Species	L1	L2	L3	Species	L1	L2	L3
Cd	0.00128	0.00047	0.00105	Cd	0.01100	0.00004	0.00634
CdCl ₁	0.00944	0.00852	0.01100	CdCl ¹	0.05300	0.00035	0.05400
CdCl ₂ ⁰	0.00339	0.00597	0.00580	CdCl ₂ ¹	0.01800	0.00021	0.02800
CdCl ₃ ⁰	0.00045	0.00155	0.00116	CdCl ₃ ¹	0.00198	0.00004	0.00493
Cd(CO ₃) ⁰	0.00010	0.00039	0.00027	Cd(CO ₃) ⁰	0.00575	0.00003	0.00558
Cd(CO ₃) ₂	0.00026	0.00630	0.00275	Cd(CO ₃) ⁰	0.16000	0.00083	0.23000
CdHCO ₃ ¹	0.01300	0.00763	0.00776	CdHCO ₃ ¹	0.05100	0.00018	0.02200
CdOHCl ⁰	0.00003	0.00016	0.00014	CdOHCl ⁰	0.00230	0.00002	0.00525
CdSO ₄ ⁰	0.00038	0.00033	0.00003	CdSO ₄ ¹	0.00090	0.00000	0.00077
Cd(SO ₄) ₂	0.00002	0.00003	0.00000	CuCl ₂ ⁻¹	70.95600	2.39700	14.17000
Fe	4.07800	1.49200	0.57900	CuCl ₃ ⁻¹	35.79800	2.09000	10.41500
FeCl ¹	0.53900	0.49100	0.10500	Cu	0.00005	0.00000	0.00000
FeCO ₃ ⁰	13.33900	50.91600	6.16300	CuCO ₃ ⁰	0.23400	0.00294	0.02900
FeHCO ₃ ¹	182.10500	104.97500	18.34300	Cu(CO ₃) ₂	2.85600	0.04300	0.52000
FeHPO ₄ ¹	0.41300	0.26800	0.06200	Cu(OH) ₂ ⁰	0.01000	0.00000	0.00440
FeH ₂ PO ₄	0.12900	0.02700	0.00422	Fe	3.74700	2.48500	0.40500
Fe(SO ₄) ⁰	1.08700	0.96000	0.01400	FeCl ¹	0.34100	0.42300	0.06200
Ni	0.00138	0.00002	0.00005	FeCO ₃ ⁰	82.31300	68.09600	14.55900
NiCl ¹	0.00033	0.20600	0.00000	FeHCO ₃ ¹	77.31700	50.57500	5.99200
NiCO ₃ ⁰	1.36300	2.05400	0.15800	FeHPO ₄ ¹	0.56100	0.29700	0.05700
Ni(CO ₃) ₂ ⁻²	2.13800	0.00190	0.97200	Fe(OH) ¹	0.07100	0.06300	0.01900
NiHCO ₃ ¹	0.08300	0.00190	0.00210	Fe(SO ₄) ⁰	0.27200	0.11700	0.04200
NiOH ¹	0.00193	0.01100	0.00939	Fe(OH) ₃ ¹	0.08400	0.12100	0.12100
PbCO ₃ ⁰	0.00000	0.00607	0.22500	Fe(OH) ₄ ⁻¹	0.01800	0.03400	0.06200
Pb(CO ₃) ₂ ⁻²	0.00000	0.07100	1.63300	Ni	0.00004	0.00004	0.00003
PbHCO ₃ ¹	0.00000	0.00014	0.00732	NiCO ₃ ⁰	0.26000	0.34600	0.31700
Zn	0.00810	0.00010	0.00081	Ni(CO ₃) ₂ ⁻²	4.44000	7.05500	8.03800
ZnCO ₃ ⁰	0.20400	0.02600	0.06600	NiHCO ₃ ¹	0.00109	0.00115	0.00058
Zn(CO ₃) ₂ ⁻²	3.86300	3.14400	4.93800	NiOH ¹	0.02500	0.03200	0.05700
ZnHCO ₃ ¹	0.421	0.008145	0.03	Pb	0.00009	0.00023	0.00001
				PbCO ₃ ⁰	0.85700	2.77700	0.17500
				Pb(CO ₃) ₂ ⁻²	17.20100	66.63200	5.21300
				PbHCO ₃ ¹	0.00879	0.02300	0.00079
				Zn	0.05100	0.03100	0.02300
				ZnCO ₃ ⁰	8.54500	6.55100	6.23600
				Zn(CO ₃) ₂ ⁻²	176.0001	161.15700	190.58200
				ZnHCO ₃ ¹	1.21400	0.73600	0.38800

References

- Adeolu, A.O., Ada, O.V., Gbenga, A.A., Adebayo, O.A.: Assessment of groundwater contamination by leachate near amunicipal solid waste landfill. *Afr. J. Environ. Sci. Technol.* **5**(11), 933–940 (2011)
- Amrhein, C., Strong, J.E., Mosher, P.A.: Effect of deicing salts on metal and organic matter mobilization in roadside soils. *Environ. Sci. Technol.* **26**, 703–709 (1992)
- Backstrom, M., Nilsson, U., HaKansson, K., Allard, B., Karlsson, S.: Speciation of heavy metals in road runoff and roadside total deposition. *Water Air Soil Pollut.* **147**, 343–366 (2003)
- Backstrom, M., Karlsson, S., Backman, L., Folkesson, L., Lind, B.: Mobilization of heavy metals by deicing salts in a roadside environment. *Water Res.* **38**, 720–732 (2004)
- Doner, H.E.: Chloride as a factor in mobilities of Ni(II), Cu(II), and Cd (II) in soil. *Soil Sci. Soc. Am. J.* **42**, 882–885 (1978)
- Kanmani, S., Gandhimathi, R.: Assessment of heavy metal contamination in soil due to leachate migration from an open dumping site. *Appl. Water Sci.* **3**, 193–205 (2013)
- Moturi, M.C.Z., Rawat, M., Subramanian, V.: Distribution and fractionation of heavy metals in solid waste from selected sites in the industrial belt of Delhi India. *Environ. Monit. Assess.* **95**, 183–199 (2004)
- Phillip, M.A., & Kane, M.O.: Lysimeter Field Performance: Design and Installation Factors for Representative Cover Systems Evaluations. 2nd International Soil Sensing Technology Conference, the Soil Physics Technical Committee Annual Meeting, and the ASA Sensor-based Water Management Community (2010)
- Warren, L.A., Zimmerman, A.P.: The influence of temperature and NaCl on cadmium, copper, and zinc partitioning among suspended particulate and dissolved phases in an Urban River. *Water Res.* **28**, 1921–1931 (1994)



Assessment of Particulate Pollutant Exposure of Residents Around an Opencast Coal Mine

Aditya Patra, Vaibhav Rengede, and Ravish Dubey

Abstract

This study aims to investigate the spatiotemporal variations of PM_{10} , $PM_{2.5}$ and PM_1 concentrations at residential sites located in the vicinity of an opencast coal project. PM concentrations and meteorological parameters such as wind speed, wind direction, relative humidity and temperature were collected at five locations. Mean concentrations varied in the following range: PM_{10} : 93.15–369.12 $\mu\text{g m}^{-3}$, $PM_{2.5}$: 38.54–178.83 $\mu\text{g m}^{-3}$ and PM_1 : 32.84–151.09 $\mu\text{g m}^{-3}$. Proportion of coarse fractions ($PM_{2.5-10}$) and fine fractions ($PM_{1-2.5}$ and PM_1) in ambient air varied in the range 48–65% and 15–58%, respectively. The role of meteorology on PM concentration was assessed using correlation analysis. Linear correlations were established among the PM concentrations using least square regression analysis. In addition to emissions contributed by mining activities, road dust raised by vehicular movement, biomass and coal burning in villages also contributed significantly to the PM level in the locality.

Keywords

Opencast coal project • PM_{10} • $PM_{2.5}$ • PM_1 • Exposure • Air pollution

1 Introduction

The generation of huge quantities of particulate matter (PM) during opencast mining activities is a subject of immense concern for human health (Pandey et al. 2014;

A. Patra (✉) · V. Rengede
Department of Mining Engineering, Indian Institute of Technology Kharagpur, Kharagpur, India
e-mail: akpatra@mining.iitkgp.ac.in

R. Dubey
School of Environmental Science and Engineering, Indian Institute of Technology Kharagpur, Kharagpur, India

Gautam et al. 2015). Past studies showed that PM from different mining operations contributed to significant adverse effects on human health in the form of black lung, asthma, cardio-vascular diseases and lung cancer (Aneja et al. 2012). Earlier studies on PM emission from mining operations can be grouped into three categories: (1) Estimation of PM generation from different surface mining operations, (2) Evaluation of in-pit dispersion of particulate matter and (3) Assessment of the PM status in mining locality. Studies in mining locality involved assessment of PM level around the mines (Pandey et al. 2014; Aneja et al. 2012). This paper presents the findings of a study aiming to answer the following problems: (a) Quantification of PM level around the mine; (b) Size distribution (PM_{10} , $PM_{2.5}$ and PM_1) of the particles; (c) Association of meteorological parameters with the PM level in air and (iv) Contribution of sources other than the mining.

2 Materials and Methods

The study was carried out at five residential sites around Bharatpur opencast coal project of Mahanadi Coalfields Limited, located in the eastern part of India. The sites are located on the periphery of the mine at a distance varying from 500 m to 1.5 km. Station 1 and Station 2 are located close to residential area. Station 3 and Station 4 are located on the upwind side of mine. Station 5 is located near the mine store office and through which a road passes (Fig. 1). Particulate matter concentrations were measured using portable aerosol spectrometer (GRIMM 1.108). The aerosol spectrometer records the particle concentration in 15 sizes (range: 0.3–15 μm). It has been used in the past to measure PM concentrations in the air (Gautam et al. 2015). Sampling was carried out daily for 6–8 h. A portable weather station (WatchDog 2000) recorded meteorological parameters.



Fig. 1 Study area and sampling locations. Source Google Earth

3 Results

3.1 Temporal and Spatial Variability of PM Concentrations

The average concentrations varied in the following range: PM_{10} : 93.15–369.12 $\mu\text{g m}^{-3}$, $PM_{2.5}$: 38.54–178.83 $\mu\text{g m}^{-3}$ and PM_1 : 32.84–151.09 $\mu\text{g m}^{-3}$ (Fig. 2a). Therefore, the peak average PM_{10} concentration was 1.65–3.69 times the limit values set by National Ambient Air Quality Standards (NAAQS) of India (CPCB) (100 $\mu\text{g m}^{-3}$; 24 h average). Average $PM_{2.5}$ concentration was 1.29–2.98 times above the limit values set by NAAQS (India) (60 $\mu\text{g m}^{-3}$, 24-h average). In spite of Station 5 being located in the upwind side of the mine, the average PM_{10} concentration was highest in this site ($>350 \mu\text{g m}^{-3}$). Figure 2b shows that the share of PM_{10} to the total pollution level at station 5 was the highest (65%) among all stations. When the wind direction was from the mine, PM_{10} concentrations were dominant (3–3.5 times of $PM_{2.5}$ and PM_1). Mining operations which predominantly

generate coarse particles contributed to this. When wind direction was towards the mine, we observed PM_{10} concentration was ~ 1.5 times of the fine fractions. In this case, mining was not the dominant source. Household and commercial burning of coal in the villages for cooking and boiling water for bathing, which generates more fine than coarse fractions, were the sources. In the third case, the PM concentrations were the lowest (Fig. 3).

3.2 Correlation and Regression

Significant positive correlations ($p < 0.05$) were obtained between $PM_{2.5}$ and PM_{10} ($R = 0.76$), PM_1 and PM_{10} ($R = 0.72$), PM_1 and $PM_{2.5}$ ($R = 1$) and also between pollutants and meteorological parameters. With increase in wind speed and decrease in barometric pressure as well as relative humidity, the air pollutant concentrations decrease faster due to better dispersion (Tiwari et al. 2012). Predictive models for different sized particles were obtained by applying linear regression models (Table 1).

4 Discussion

Resuspension of road dust from the movement of heavy duty vehicles was a major cause of the high concentration at Station 5. Higher PM levels at Stations 1 and 2 in comparison to Stations 3 and 4 are due to local burning of coal and biomass in the villages for household purposes. A high coefficient of determination between PM_1 and $PM_{2.5}$ concentrations suggests that both the particles are quasi-equally affected by the meteorological parameters. For the cases when the wind is flowing from the mine to the surrounds, the high R^2 value indicates mining as a major source in the locality. The R^2 values for $PM_{2.5}$ vs. PM_{10} , PM_1 vs. PM_{10} and PM_1 vs. $PM_{2.5}$ obtained in our study are in the same range with those from

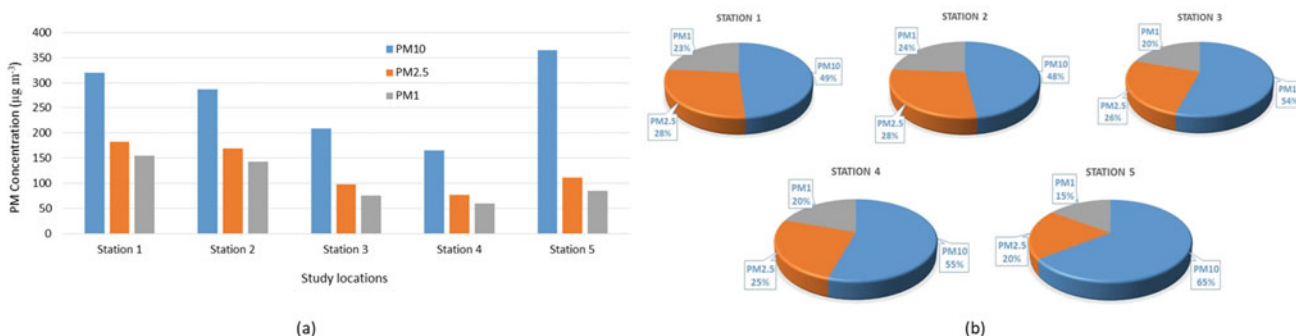


Fig. 2 a Average PM concentration; b Particle size contribution

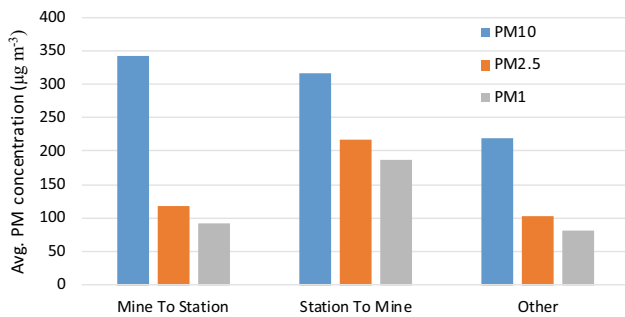


Fig. 3 PM concentration according to wind directions

Table 1 Linear relationship between PM₁₀ and meteorological parameters (P: barometric pressure, RH: relative humidity, WS: wind speed)

Description	Predictive equations	R ²
Mine to village	PM ₁₀ = -23,755 + 31.86 P + 1.157 RH + 0.10 WS	0.1
Village to mine	PM ₁₀ = -16,848 + 22.42 P + 4.426 RH - 36.42 WS	0.29
Mine to village	PM _{2.5} = -14,376 + 19.166 P + 0.7004 RH - 0.967 WS	0.49
Village to mine	PM _{2.5} = -16,967 + 22.48 P + 3.956 RH - 26.75 WS	0.30
Mine to village	PM ₁ = -12,914 + 17.198 P + 0.6259 RH - 0.652 WS	0.56
Village to mine	PM ₁ = -16,166 + 21.40 P + 3.674 RH - 24.02 WS	0.29

other studies (Srimuruganandam and Nagendra 2010; Gupta et al. 2006). The regression model could explain up to 56% of the PM concentration measured in terms of meteorological variables.

5 Conclusion

Residents around the Bharatpur opencast coal project are exposed to respirable particles. While the PM level was much higher when the wind direction was from the mine towards the villages, the study revealed that even in case of wind direction towards the mine, the PM level is high. In addition to emissions from coal production process, resuspension of dust from paved and unpaved roads, open burning of coal and biomass by the residents were contributing to the poor air quality.

References

- Aneja, V.P., Isherwood, A., Morgan, P.: Characterization of particulate matter (PM₁₀) related to surface coal mining operations in Appalachia. *Atmos. Environ.* **54**, 496–501 (2012)
- Gautam, S., Kumar, P., Patra, A.K.: Occupational exposure to particulate opencast mines. *Air Qual. Atmos. Health* **9**, 143–158 (2015)
- Gupta, A., Nag, S., Mukhopadhyay, U.: Characterisation of PM₁₀, PM_{2.5} and benzene soluble organic fraction of particulate matter in an urban area of Kolkata, India. *Environ. Monit. Assess.* **115**(1–3), 205–222 (2006)
- Pandey, B., Agrawal, M., Singh, S.: Assessment of air pollution around coal mining area: emphasizing on spatial distributions, seasonal variations and heavy metals, using cluster and principal component analysis. *Atmos. Pollut. Res.* **5**, 79–86 (2014)
- Srimuruganandam, B. and Nagendra, S. M. S.: Analysis and interpretation of particulate matter (PM₁₀, PM_{2.5}, and PM₁) emissions from the heterogeneous traffic near an urban roadway. *Atmos. Pollut. Res.* **1**(3), 184–194 (2010)
- Tiwari, S., Chate, D., Srivastava, M., Safai, P., Srivastava, A., Bisht, D., Padmanabhamurty, B.: Statistical evaluation of PM₁₀ and distribution of PM₁, PM_{2.5}, and PM₁₀ in ambient air due to extreme reworks episodes (Deepawali festivals) in megacity Delhi. *Nat. Hazard.* **61**(2), 521–531 (2012)



Assessment of Risk from Atmospheric Air Pollution and Traffic Load Intensity in the City of Kazan (Republic of Tatarstan)

Natalya Stepanova, Alisa Ilyasova, Naila Yusupova, Lily Khairullina, Suryana Fomina, and Rustem Saifullin

Abstract

The growth of the vehicles' number in the cities, the proximity of mobile sources to residential areas, poor road maintenance and emission toxicity exacerbate the problem of the atmospheric air quality in the cities. Assessment of exposure to solid particles, PM₁₀ and PM_{2.5} in the four districts was carried out based on average annual concentrations performed by "The Center of Hygiene and Epidemiology in the Republic of Tatarstan" and the Municipal Institution "Automated traffic control system" (MUE ATCS) from 2010 to 2017. High risk of causing non-carcinogenic effects on the population of the city of Kazan and the districts under study was associated with total exposure to suspended particulate matters, the contribution of which to the hazard index (HI) made 42.5% in the city of Kazan, 52.7% in the Vakhitovsky district and 59.9% in the Sovetsky district. The results showed the necessity of shifting the time of the atmospheric air status control at the Air Pollution Observation Station (APOS) by 1 h, which can result in the compliance with the sampling time to a maximum traffic flow. The assessment of epidemiological risk for the population health in the city's microdistricts was carried out for the first time.

Keywords

Atmospheric air • Vehicles • Monitoring • Public health risk

1 Introduction

The availability of urban area development prevents rapid pollutants' from dissipating in the air and thus could exacerbate the situation. The architectural features of large cities negatively affect the dispersion of pollutants, and also contribute to a significant increase in emissions of harmful substances into the air by increasing the operating time of a car engine at traffic lights and at street crossings. The growth of the vehicles' number in the cities, the proximity of mobile sources to residential areas, poor road maintenance and emission toxicity exacerbate the problem of the atmospheric air quality, despite the decrease of industrial emissions (Guerreiro et al. 2014; Keuken et al. 2012). Numerous epidemiological studies indicate adverse health effects from exposure to atmospheric air pollution (Tafeeva et al. 2015; World Health Organization 2016). The issues of external quality control and regulation of the state of the atmospheric air are becoming relevant. This leaves it vital that risk reduction procedures be pursued, and decision-support tools devised, based on analyses and risk assessments.

2 Materials and Methods

Assessment of exposure to the pollutants coming from vehicles emissions in four districts of the city of Kazan was carried out based on the results of retrospective studies of average annual concentrations at the Air Pollution Observation Stations (APOS) between 2010 and 2017. Sampling is carried out during 20 min 4 times a day at intervals of 6 h: 01:00 a.m., 07:00 a.m., 01:00 p.m. and 07:00 p.m. with subsequent analysis. The assessment of epidemiological risk for the population health in the city's microdistricts was carried out for the first time. The assigned areas corresponded geographically to the location of APOS: APOS-3 in the Vakhitovsky district; APOS-8 in the Sovetsky district; APOS-11 in the Novo-Savinovsky district and APOS-15 in

N. Stepanova (✉) · A. Ilyasova · S. Fomina · R. Saifullin
Kazan Federal University (KFU), Kazan, Russian Federation

N. Yusupova · L. Khairullina
FGBOU DPO of the Russian Medical Academy of Postgraduate Continuing Education of the Ministry of Health of the Russian Federation, Kazan State Medical Academy, Kazan, Russian Federation

the Gorki. Information on the traffic intensity in the city of Kazan was additionally completed with the data from the MUE ATCS, the principal activity of which is the road traffic safety with computer use (Voytenkov 2012). The calculation of the traffic intensity was performed during air sampling at the APOS. The risk assessment of the development of non-carcinogenic effects from pollutants contained in the air was carried out according to the total hazard index (HI) in line with Guidelines R 2.1.10.1920–04 (Rakhmanin et al. 2004).

3 Results

The analysis of laboratory studies of the atmospheric air in the city of Kazan showed that 7–13 pollutants were controlled at the APOS. Most of them (nitrogen dioxide, sulphur dioxide, carbon oxide, suspended particulates and formaldehyde) are on the list of priority substances contained in the atmospheric air of the cities of the Russian Federation and the inventory list of toxic substances' emission of the U.S. EPA. For the period under study, the contribution of the automobile transport to atmospheric pollution in Kazan remained high and contributed 69.4%–73.8% of the total gross emissions. Average annual concentrations of suspended particulate matters PM_{10} exceeded the MAC at the APOS -3, APOS-11 and APOS-15 by a factor of 2.0–2.45, and in $PM_{2.5}$ —by a factor of 1.54 and 2.1, correspondingly. APOS-8 was identified as a control one in the content of PM_{10} and $PM_{2.5}$ fractions, the level of which was within the limits of regulations.

We assessed the health risk for the population of the city of Kazan in the specified districts due to the atmospheric air pollution. The value of the total hazard index (HI) of the chemicals coming with exhaust gases from vehicles in the districts under study made 13.7; 14.51; 14.09; 11.8, and that correspond to high risk. High risk of developing non-carcinogenic effects for the population of the districts under study was associated with total exposure TSP, the contribution of which to HI made 42.5% in the Sovetsky, 52.7% in the Vakhitovsky, 56.9% in the Gorki and 58.9% in the Novo-Savinovsky districts.

The calculation of the traffic intensity was performed during air sampling at the APOS. At APOS-3, the periods with maximum traffic were registered in the morning from 08:20 a.m. to 08:40 a.m. (8% of all maximums within a year), and in the evening between 06:00–06:20 p.m. (10%) and between 05:00 p.m. and 05:20 p.m. (14%). The air sampling time agrees with neither maximum of the traffic flow, and this fact results in a discrepancy in the morning—52% of the total maximum traffic, and in the evening—24%. At APOS- 8, the traffic intensity increases after 07:00 a.m., and the difference between 07:00 a.m.–07:20 a.m. and 07:20

a.m.–07:40 a.m. makes 23%, and between the last one and 08:40 a.m.–09:00 a.m.—37%. At APOS-11 and APOS-15, the periods with maximum traffic were registered in the morning from 07:00 a.m. to 09:00 a.m., and in the evening from 04:40–06:00 p.m. (Table 1).

According to the level of the traffic mitigation, the districts under study are arranged as follows; the crossroads at the APOS-11, APOS-15, APOS-8 and APOS-3. Correlation analysis was carried out according to the Spearman criterion ($p < 0.05$). The correlation dependencies between the traffic intensity and the pollutants' concentration (the suspended solids $r = 0.15$ – 0.30 , carbon oxide $r = 0.17$ – 0.23 , nitrogen dioxide $r = 0.18$ – 0.51 and phenol $r = 0.16$ – 0.25) were revealed.

4 Discussion

Epidemiological and toxicological data show that a mass of PM ($PM_{2.5}$, PM_{10}) contains fractions of varying types and degrees of the health impact. Our results corroborate the existing evidence of the fact that atmospheric air pollution is a significant environmental risk factor for the population health (Keuken et al. 2012; Zhang et al. 2011). High risks of developing non-carcinogenic effects for the population of the city of Kazan and the districts under study were associated with total exposure to suspended particulate matters. Meanwhile, in scientific literature, clear emphasis is placed on the opinion that quantitative methods of analysis and risk assessment form the basis of safety management as part of critical infrastructure (Rak and Pietrucha-Urbanik 2019). This is especially of concern in urban areas, where large numbers of people live near substantial road traffic emissions.

5 Conclusions

Currently, the existing monitoring system in the area of the main traffic arteries in the city of Kazan makes it impossible to correctly assess the vehicles' impact on the atmospheric air quality. The critical result of our study is taking into account of supplementary data on the traffic flow intensity in districts of the city, which enabled us to differentiate the long-term effects of the atmospheric air pollution with vehicles on the population health. The results of the analysis showed the necessity of shifting the time of the atmospheric air status control at the APOS by 1 h, which can result in compliance with the sampling time to a peak of traffic flow. The use of ATCS data will allow decreasing the traffic-light creep up to 30% in peak periods and reducing the air environment pollution with exhaust gases. The necessity of determining the risk reduction efficiency with the account of economic factors will provide the basis for future studies.

Table 1 Maximums of vehicle passage at time of day intervals (the number of vehicles)

Time interval	APOS-3	APOS-8	APOS-11	APOS-15
01:00–01:20	577	1094	1132	1134
02:00–02:20	409	739	747	850
07:00–09:00	1934–2948	5556–7616	10,260–11,966	10,298–11,966
13:00–13:20	2838	7729	8859	8293
14:00–14:20	2867	7760	8979	8107
16:40–18:00	2550–2749	7800–8526	9243–12,321	9062–10,006
18:00–18:20	2931	9024	12,101	9873
18:20–20:20	2474–2093	8101–6029	11,736–7390	9616–7202

The risk reduction can influence on the level of the project of modernization of the system for the atmospheric air pollution control and preventive measures. The most effective decisions as regarding the risk reduction should be implemented.

Acknowledgements This work was funded by the subsidy allocated to Kazan Federal University for the state assignment in the sphere of scientific activities 19.9777.2017/8.9.

References

- Guerreiro, C.B., Foltescu, V., Leeuw, F.: Air quality status and trends in Europe. *Atmos. Environ* **98**, 376–384 (2014)
- Keuken, M.P., Jonkers, S., Zandveld, P., Voogt, M., Elshout van den. S.: Elemental carbon as an indicator for evaluating the impact of traffic measures on air quality and health. *Atmos. Environ.* **61**, 1–8 (2012)
- Tafeeva, E.A., Ivanov, A.V., Titova, A.A., Akhmetzyanova, I.F.: Air pollutions as a risk factor for the population health in Kazan city. *Gig Sanit.* **94**(3), 37–40 (2015)
- World Health Organization.: Health risk assessment of air pollution—general principles (2016). http://www.euro.who.int/__data/assets/pdf_file/0006/298482/Health-risk-assessment-air-pollution-General-principles-en.pdf?ua=1
- Voytenkov, E.A.: Historical and legal experience of road traffic and implementation of automated control systems for provision of its safety. *Transp. Law* **1**, 28–30 (2012)
- Rak, J., Pietrucha-Urbanik, K.: An approach to determine risk indices for drinking water—study investigation. *Sustain. Basel* **11**(11), 3189 (2019)
- Rakhmanin, J. A. et al.: Guidelines for health risk assessment for the population on exposure to chemical substances polluting the environment R 2.1.10.1920–04. In: Federal Center of the State Committee for Sanitary and Epidemiological Control, Moscow (2004)
- Zhang, P., Dong, G., Sun, B., Zhang, L., Chen, X., Ma, N. et al.: Long-term exposure to ambient air pollution and mortality due to cardiovascular disease and cerebrovascular disease in Shenyang (China). *PLoS ON* **6**(6), e20827 (2011)



Effects of Outdoor Air Pollution on Human Health in Kenitra, Morocco

Rachida El Morabet, Said Mouak, Roohul Abad Khan, Abderrahmane Adoui El Ouadrhiri, and Mohamed Aneflouss

Abstract

Outdoor air pollution is a severe environmental threat. The study focuses on the urban air quality of Kenitra city in Morocco and its effect on human health. The air quality was evaluated for particulate matter, tropospheric ozone, carbon monoxide, sulfur oxides, nitrogen oxides, and lead. The air pollutant data was obtained for the year 2014 daily. Spatial distribution of air pollutants was obtained using ArcGIS tool to determine the impact on human health. The health data collection comprised of survey investigations and archives of the regional hospital “Al Idrissi.” A correlation between the polluted areas and the incidence of disease was observed.

Keywords

Air pollution • Particulate matter • Carbon monoxide • Spatial distribution • Human health

1 Introduction

The air quality deterioration worldwide is mainly attributed to modern industrialization and economic development (Morsy et al. 2021). In Kenitra city, the industrial sector has experienced remarkable development, particularly in the chemical

and para-chemical industry, the agri-food industry, the textile industry, and the leather industry. In parallel, road traffic and urbanization are developing (Fig. 1). This evolution renders its urban population highly prone to the impacts of air pollution. Hence, this study focused on Kenitra city (Fig. 1a).

2 Methodology

Air pollution data was provided by mobile air quality monitoring unit, which has an automatic suspended particulate sampler, which is programmable to evaluate their ambient air concentrations, allowing take a daily sample of dust. This unit has the latest equipment to measure pollutants instantly and is supported by reliable measurements of various air pollutants, namely the sulfur dioxide analyzer (SO_2), the nitrogen oxide analyzer (NO_x), carbon monoxide (CO) analyzer, ozone analyzer (O_3), and dust analyzer (PM_{10}). The air quality monitoring site location was organized to cover industrial zone and high traffic areas in Kenitra. The ArcGIS tool was employed using interpolation technique in order to obtain the spatial distribution of air pollutants. Data collection comprised of archives of regional hospital “Al Idrissi” (4652 files; Inventory of admissions records from 1 January 2014 to 31 December 2014).

3 Results

3.1 Outdoor Air Pollutants

The average measured values of the primary pollutants were lower than those recommended by the World Health Organization regulations. However, measured average values of (PM_{10}) were higher than the limit value of air quality standards. This exceedance is attributed to industrial emissions (Fig. 2).

R. El Morabet (✉) · S. Mouak · M. Aneflouss
Department of Geography, LADES, FLSH-M, Hassan II
University of Casablanca, B.P. 546, Mohammedia, Morocco

R. A. Khan
Department of Civil Engineering, King Khalid University, Abha,
Kingdom of Saudi Arabia

A. A. El Ouadrhiri
Department of Mathematics and Computer Science, LR2I, FSAC,
Hassan II University of Casablanca, B.P. 5366, Maarif,
Casablanca, Morocco

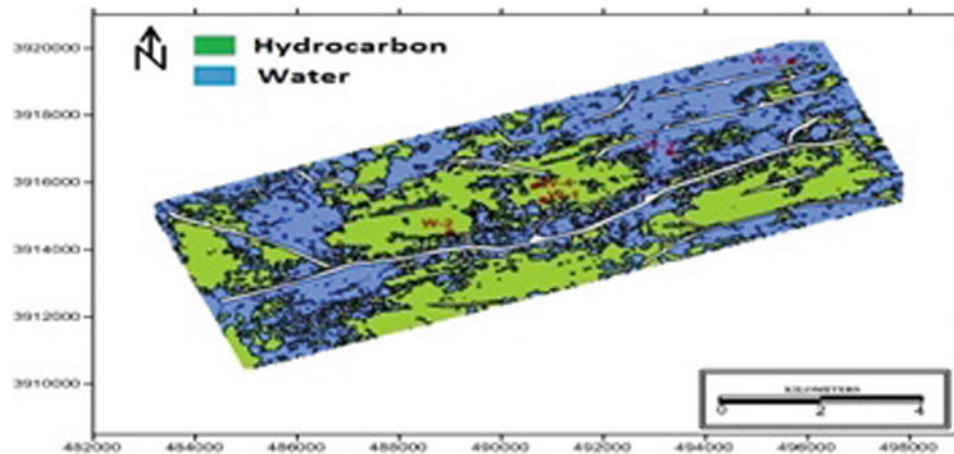


Fig. 1 Study area: Kenitra

3.2 Health Hazards

It can be deduced from the analysis of the data (Fig. 3) obtained from the archives of “Al Idrissi” hospital that there was a correlation between the incidence of cardiovascular and respiratory diseases and the rate of atmospheric pollution.

4 Discussion

Air pollution is closely linked to industrial activity and road traffic, but the distribution of pollutants in Kenitra clearly shows that air pollution can have high concentrations far from its origin, as is the case for PM. Wind and other geographical factors play a significant role in spreading of air pollution. The long atmospheric lifetime further enhances the dispersion of pollutants in more extensive areas (Fig. 1).

The spatial distribution of pollutants is correlated with a high number of health cases reported to El Idrissi hospital in 2014, highly polluted zone correlating with a high percentage of respiratory diseases (El Morabet et al. 2018). Air pollution and human health are in direct correlation. High pollution will have a higher impact on human health. People exposed to a polluted environment are more likely to suffer from heart attacks and respiratory diseases (El Morabet 2018).

5 Conclusion

Kenitra city in Morocco was studied for the relation between air quality and human health. The high number of health cases correlated with polluted areas infers that public human health is affected by air pollution. The study is a continuation of the work previously published (El Morabet et al. 2018) on

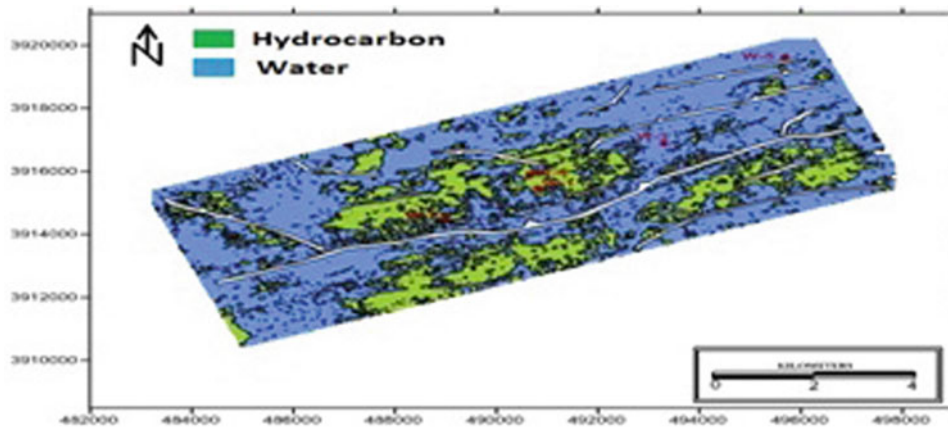


Fig. 2 Pollutants in Kenitra

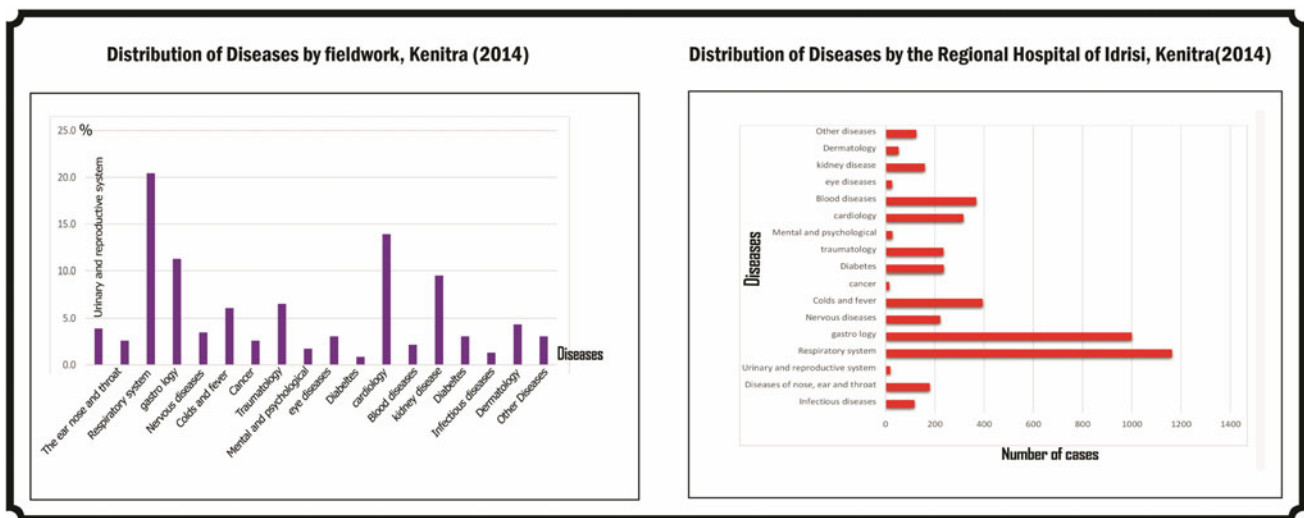


Fig. 3 Diseases in study area

the spatial distribution of Kenitra diseases. However, depth studies are required to determine the combined and collective effect of air pollutants on human health.

References

El Morabet, R., Aneflouss, M., Mouak, S.: Air pollution effects on health in Kenitra. In: Kallel, A., Ksibi, M., Ben Dhia, H., Khélifi, N.

(eds.) EMCEI 2017, pp. 1971–1973. Springer, Cham (2018). https://doi.org/10.1007/978-3-319-70548-4_570
 El Morabet, R.: Effects of outdoor air pollution on human health. In: Reference module in earth systems and environmental sciences. Elsevier Publication (2018). <https://doi.org/10.1016/B978-0-12-409548-9.11012-7>
 Morsy, E., Habebullah, T.M., Othman, A.: Assessing the air quality of megacities during the COVID-19 pandemic lockdown: a case study from Makkah City, Saudi Arabia. Arab. J. Geosci. **14**(7), 548 (2021). <https://doi.org/10.1007/s12517-021-06898-7>



Contamination Levels and Health Risks of Heavy Metals in Street Dusts from Ulaanbaatar, Mongolia

Sonomdagva Chonokhuu, Chultem Batbold, and Khongor Gankhuyag

Abstract

The objective of this research was to study the concentration of heavy metals in street dust, Ulaanbaatar city. We carried out the calculation using geo-accumulation index and non-cancer health risk assessment. Totally, 22 sites were chosen, and samples were collected from the impervious surface above 2–3 m from the land surface by randomly. The results revealed that average I_{geo} of As, Ni, and Pb were unpolluted, whereas Cr, Cu, and Zn presented moderately polluted. In terms of health risk assessment, HI values of children were higher than adults and HQing, typically, roled as the primary contributor for HI value. As and Cr indicated the result that close to the safe level.

Keywords

Contamination level • Dust • Health risk assessment • Ulaanbaatar

1 Introduction

Solid particles that accumulate on outdoor, impervious materials in urban environments are collectively referred to as “street dust,” and it has become among the most significant concerns in the management of urban environment (Harrison 1979; Hopke et al. 1980; Han and Posmentier 2006). Two primary sources of street dust are previously suspended particles (atmospheric aerosol) and displaced urban soil (Hopke et al. Feb. 1980; Schwar et al. Jan. 1988).

Street dust frequently interacts with the atmosphere due to mediums through suspension and deposition of dust particles (Moreno et al. 2013). Therefore, heavy metal elements in street dust are known to quickly enter the human body through ingestion, inhalation, and dermal contact (Cook et al. 2005). This paper presents the main findings of a study carried out in Ulaanbaatar (capital city of Mongolia), during the dry months of January 2019 with two purposes: to determine the various concentration of street dust and assess pollution level in a total 22 sites, and to evaluate, using risk assessment strategies, the potential adverse health effects of the exposure of citizens in Ulaanbaatar to street dust.

2 Materials and Methods

A total of 22 samples of street dust were collected under stable weather conditions in the cold and dry season during January 2019 in Ulaanbaatar. Approximately, 20–50 g of the dust from each random sampling site, accumulated on impervious surfaces between 2 and 3 m (house roof and other surfaces), were collected in through sweeping with plastic brushes and using dust pans.

2.1 Pollution Assessment Methods

The geo-accumulation index (I_{geo}) was used in this study to assess heavy metal contamination in urban soils by comparing current and background concentrations of study area (Muller 1969). Geo-accumulation index is expressed as follows (Ji et al. 2008):

$$I_{geo} = \log_2 \left(\frac{C_n}{1.5B_n} \right) \quad (1)$$

where C_n is the concentration of an element in dust; B_n is the background value of soil. The constant 1.5 allows us to analyze natural fluctuations in the content of a given

S. Chonokhuu (✉) · C. Batbold · K. Gankhuyag
Department of Environment and Forest Engineering, School of Engineering and Applied Science, NUM, Ulaanbaatar, Mongolia
e-mail: sonomdagva@seas.num.edu.mn

substance in the environment and to detect very small anthropogenic influences (Ji et al. 2008). The extracted value can be classified as: (1) $I_{geo} \leq 0$, unpolluted; (2) $0 < I_{geo} < 1$, unpolluted to moderately polluted; (3) $1 < I_{geo} < 2$, moderately polluted; and (4) $2 < I_{geo} < 3$, moderately to heavily polluted, (6) $3 < I_{geo} < 4$, heavily polluted, (7) $4 < I_{geo} < 5$, heavily to extremely polluted, and $5 < I_{geo}$, extremely polluted.

2.2 Health Risk Assessment

The risk assessment model developed by the USEPA was used to evaluate the health risks posed by heavy metals in urban soil. The average daily dose of a pollutant via ingestion, dermal contact, and inhalation as exposure pathways can be estimated using Eqs. (2), (3) and (4):

$$ADD_{ing} = \frac{c * R_{ing} * CF * ED}{BW * AT} \quad (2)$$

$$ADD_{inh} = \frac{c * R_{inh} * EF * ED}{PEF * BW * AT} \quad (3)$$

$$ADD_{derm} = \frac{c * SA * CF * SL * ABS * ED}{BW * AT} \quad (4)$$

where ADD_{ing} is daily exposure amount of metals through ingestion (mg/kg/day); ADD_{inh} is daily exposure amount of metals through inhalation (mg/kg/day); ADD_{derm} is daily exposure amount of metals through inhalation (mg/kg/day).

After the ADD, the three exposure pathways are calculated, a Hazard Quotient (HQ) based on non-carcinogenic toxic risk can then be calculated. When $HQ \leq 1$, it indicates no adverse health effects (USPA 1986). The HQs can be added and generate a Hazard Index (HI) to estimate the risk of mix metal contaminants. If the value of $HI \leq 1$, it is believed that there is no significant risk of non-carcinogenic effects.

3 Results

Below, the I_{geo} value (Fig. 1) and non-cancer health risk assessment with an upper confidence level of 95% (Table 1) is illustrated by the analysis of six heavy metal elements. I_{geo} value is widely used to assess the heavy metal contamination comparing present and background concentration of elements in soils (Ji et al. 2008). In addition, non-cancer health risk was calculated through three main exposure pathways (ingestion, inhalation, and dermal contact) (US EPA 1993).

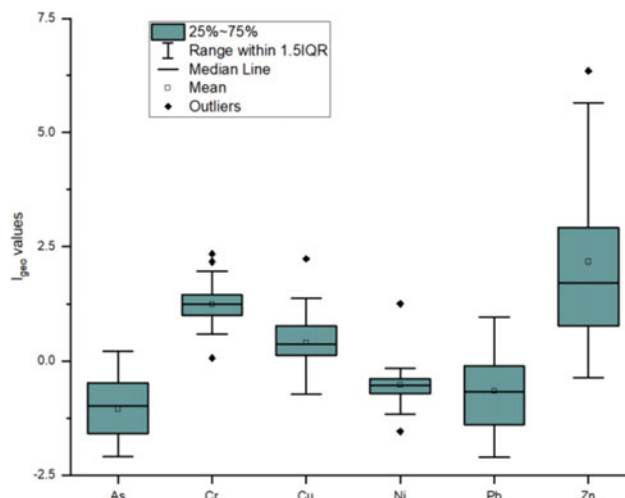


Fig. 1 Boxplots of the I_{geo} values for the six heavy metal elements in street dust of Ulaanbaatar city

3.1 Geo-Accumulation Index

As shown in Fig. 1, Cr, Cu, and Zn are relatively high pollution level, especially Zn which reached the extremely polluted in its high value and have wide range fluctuation. On the other hand, pollution of As, Ni, and Pb are indicated as “moderately polluted” according to the pollution assessment with the highest value.

3.2 Non-cancer Health Risk Assessment

In Table 1, in terms of non-cancer health risk, a total of HQ values or HI indicate that there are no significant risks for both children and adults within all studied heavy elements in this study. However, As and Cr ($2E-03$ and $8E-04$, respectively) for children are close to a safe level. HQ_{ing} values account for between 58 and 99% of HI except for HQ of Cr ingestion (adult and child, 16 and 53%, respectively).

4 Discussion

In order to assess the pollution level, we determined the background value of this area; some elements such as Zn, Cr, and Cu present high pollution level. Therefore, sampling sites, where pollution level relatively high, should be studied further. Similarly, health risk assessment also is evaluated, and its estimation is based on concentration. Each element has symbolic value considering their own properties. For urban dust and soil, the heavy metals mostly originate from anthropogenic sources (Ji et al. 2008). For example, Pb, Zn, and Cu largely come from traffic pollution, whereas Cr is associated with atmospheric deposition (USPA 1986).

Table 1 Non-carcinogenic health risk assessment from heavy metal elements in street dust of Ulaanbaatar city

C (95% UCL–mg/kg)		HQ ingestion		HQ inhalation		HQ dermal		HI	
		Adult	Child	Adult	Child	Adult	Child	Adult	Child
As	13	2E–04	2E–03	5E–06	8E–06	1E–05	1E–04	2E–04	2E–03
Cr	57	4E–05	4E–04	2E–04	4E–04	3E–05	8E–06	3E–04	8E–04
Cu	65	6E–06	6E–05	2E–07	3E–07	7E–07	2E–07	7E–06	6E–05
Ni	20	4E–06	4E–05	1E–07	2E–07	3E–06	7E–07	7E–06	4E–05
Pb	55	6E–05	6E–04	2E–06	3E–06	1E–05	4E–06	8E–05	6E–04
Zn	3252	4E–05	4E–04	1E–06	2E–06	7E–06	2E–06	5E–05	4E–04

5 Conclusions

Heavy metal health risk and pollution level were assessed in this study. As a result, the high-level concentration of Zn and Cr, which are probably originated from coal combustion, was occurred at some sites. However, arsenic (2E-03) was a higher health risk than that of other elements depending on each element's characteristic of health impact. There are several studies conducted with atmospheric particulate mass concentration, while its chemical characteristic has been studied insufficiently in Mongolia. Hence, the result will be valuable for present and prospective studies.

References

- Cook, A.G., Weinstein, P., Centeno, J.A.: Health effects of natural dust. *Biol. Trace Elem. Res.* **103**(1), 1–15 (2005)
- Harrison, R.M.: Toxic metals in street and household dusts. *Sci. Total Environ.* **11**, 89–97 (1979)
- Hopke, P.K., Lamb, R.E., Natusch, D.F.S.: Multielemental characterisation of urban roadway dust. *Environ. Sci. Technol.* **14**, 164–172 (1980)
- Han, Y., Posmentier, E.S.: Multivariate analysis of heavy metal contamination in urban dusts of Xi'an, Central China. *Sci. Total Environ.* **355**, 176–186 (2006)
- Hopke, P.K., Lamb, R.E., Natusch, D.F.S.: Multielemental characterization of urban roadway dust. *Environ. Sci. Technol.* **14**(2), 164–172 (1980)
- Ji, Y., Feng, Y., Wu, J., Zhu, T., Duan, C.: Using geoaccumulation index to study source profiles of soil dust in China. *J. Environ. Sci.* **20**(5), 571–578 (2008)
- Moreno, T., et al.: Daily and hourly sourcing of metallic and mineral dust in urban air contaminated by traffic and coal-burning emissions. *Atmos. Environ.* **68**, 33–44 (2013)
- Muller, G.: Index of geo-accumulation in sediments of the Rhine River. *Geo. J.* **2**, 108–118 (1969)
- Schwar, M.J., Moorcroft, J.S., Laxen, D.P., Armorgie, C.: Baseline metal-in-dust concentrations in Greater London. *Sci. Total Environ.* **68**, 25–43 (1988)
- U.S.E.P.A., Superfund Public Health Evaluation Manual (1986)
- US EPA (United States Environmental Protection Agency). Reference dose (RfD): Description and Use in Health Risk Assessments; US Environmental Protection Agency: Washington, DC, USA (1993)



Comparative Study of Different Multi-target Regression Approaches Performances for Air Pollutants Forecasting

Sahar Masmoudi, Haytham Elghazel, Dalila Taieb, and Amjad Kallel

Abstract

Air pollution is one of the most harmful phenomena in the current context. In this regard, forecasting of air quality helps the appropriate authorities to air pollution management with an adequate measure. Recently, machine learning algorithms have been widely used as a tool to predict the concentration of variables based on available databases. This study evaluates the performance of three multi-target regression approaches in tandem with different data mining techniques, namely random forest, decision tree, k-nearest neighbours and support vector regression, to forecast concentration of multiple air pollutants (simultaneously) in Kairouan Governorate (Tunisia). The obtained results show that ensemble regressor chain (ERC) coupled with random forest ensures better performance in terms of error (aRRMSE = 0.442) compared with other algorithms.

Keywords

Air pollution • Data mining • Multi-target regression • Forecast

1 Introduction

In the last decades, human activities and climatic changes led to major environmental problems, especially air pollution. As a precaution, air quality forecast remains an

obligation to take effective control measures and to ensure an early warning against air pollutants. Several pieces of research are interested in air pollution forecasts in which different approaches are adopted, such as numeric models and statistic models. Indeed, numerical modelling requires a description of pollutant source, emission inventories and complete knowledge of physicochemical processes. For these reasons, statistical approaches are the most appropriate and they are successfully employed for air pollution forecasting (Gómez-losada 2018; Roy et al. 2018). Recently, the emergence of data mining methods (artificial neural network, random forest, classification and regression tree, etc.) has justified the application of statistical approaches for environmental modelling, including air pollution forecasting.

To the best of our knowledge, while multi-target regression (MTR) is recently attracting the interest of several authors in different fields such as ecological and medicine fields (Kocev et al. 2009; Tuia et al. 2011), this study is among the first applications of MTR for air quality forecasting. Indeed, this study aims to evaluate the performance of four regression-based models, namely random forest, decision tree, k-nearest neighbours and support vector regression with different approaches of MTR (single target, regressor chain and ensemble regressor chain) for predicting—simultaneously—multiple air pollutant concentrations based on available database of air measurements in Kairouan Governorate, Tunisia. In this study, it was assumed that the correlation among pollutant can improve the forecasting performance results.

2 Data and Methods

The data set used in this paper was provided by the national network for monitoring air quality (RNSQA/ANPE, Tunisia). The data were collected from the monitoring station of the Kairouan region in 2010 and contain hourly air pollutant concentrations (NO_2 , NO_x , NO , O_3 , $\text{PM}_{2.5}$) and related meteorological variables.

S. Masmoudi (✉) · A. Kallel
Laboratory of Water, Energy and Environment, Sfax National
School of Engineering, University of Sfax, Sfax, Tunisia

H. Elghazel
LIRIS, UMR 5205, University of Lyon 1, Villeurbanne, France

D. Taieb
National Agency for Environment Protection, ANPE, Sfax,
Tunisia

Different regression-based models (Table 1) were used in this study coupled with the MTR approaches.

MTR methods aim to predict multiple continuous targets simultaneously and to consider not only the relationships between features but also target variables (Borchani et al. 2015). The basic approach in MTR, denoted by single target (ST), is to decompose regression problem in m independent models; each one predicts the single target. Then, Xioufis (Spyromitros-xioufis et al. 2016) proposed regressor chain (RC) which is based on chaining single-target models. The RC selects a random chain of target variables and builds a separate regression model. To predict each target, the value of previous target is included as features following the order of the chain (Fig. 1). In order to avoid the sensitivity of the selected order of RC, Xioufis (Spyromitros-xioufis et al. 2016) proposed ensemble regressor chain (ERC) approach which is a set of L regressor chain models with different random chains building on a bootstrap sample of the training set and the final predictions come from the mean of the L estimates for each target.

The experiments are carried out in Python 3.6.0 using scikit-learn library.

The performance of the created models is evaluated with the following statistical parameters:

- The coefficient of determination, R^2 .
- The average relative root mean squared error, aRRMSE (Eq. 1).

$$\text{aRRMSE} = \frac{1}{m} \sum_{j=1}^m \sqrt{\frac{\sum_{l=1}^{N_{(\text{test})}} (y_j^{(l)} - \hat{y}_j^{(l)})^2}{\sum_{l=1}^{N_{(\text{train})}} (y_j^{(l)} - \bar{y}_j^{(l)})^2}} \quad (1)$$

where \hat{y}_j is the predicted output of each target variable, \bar{y}_j is the mean value of target variable y_j over training set and m is the number of target variables.

The model was built up as shown in Fig. 2 in which we present the main steps taken for air quality forecasting.

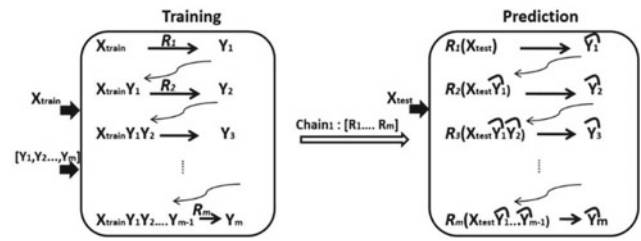


Fig. 1 Graphical illustration of regressor chain (RC)

3 Results

The results of the error aRRMSE are expressed as a boxplot for each MTR approach and for the four regression-based algorithms. The results depicted in Fig. 3 illustrate the performance of ERC to forecast air pollutant concentrations regardless of the data mining algorithms used. It was found that RF achieved higher accuracies to forecast air pollutant concentration with a value of aRRMSE less than 0.5 for the three MTR approaches. The results confirm that the ensemblist approach is robust and ensures better performance. However, the lowest performances are consistently obtained with the decision tree (DTR) algorithm.

We selected the ERC approach to demonstrate the quality of the prediction of each pollutant for the different data mining algorithms (Fig. 4). The coefficient of determination results for each pollutant (Fig. 4a) endorses the findings mentioned above and proves that RF is the most highly representative model. Figure 4b shows an example of the scatter plot of the best-predicted pollutant (O_3) for RF. We notice significant comparability between measured and predicted ozone concentrations with an $R^2 = 0.83$.

4 Discussion

The RF algorithm proves that the ensemblist approach is robust and ensures better performance on air quality prediction. In agreement with previous studies

Table 1 Description of data mining models

Regression-based algorithms	Description	Parameters
Random forest (RF)	Ensemble of decision tree combined together for the final prediction	Ntree
Decision tree (DTR)	The prediction is based on learning simple decision rules inferred from the data features	max_depth
k-Nearest neighbour (k-NN)	The prediction is based on a similarity measure (distance functions)	k: Number of neighbours
Support vector regression (SVR)	The model based on the principle of structural risk minimisation and identifying the optimal separating hyperplane between the classes	C: penalty γ :Gaussian kernel ϵ :Error

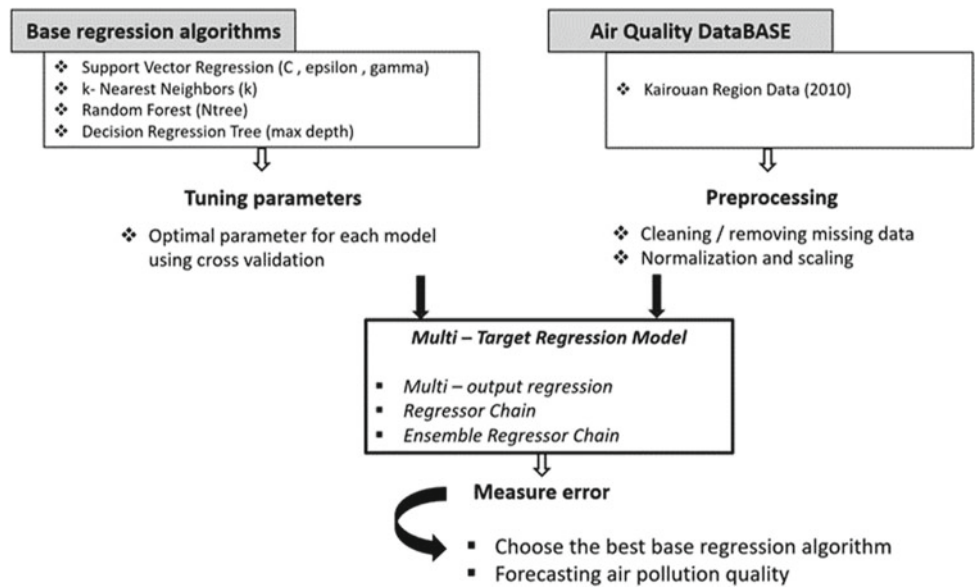


Fig. 2 Schematic representation of the methodology

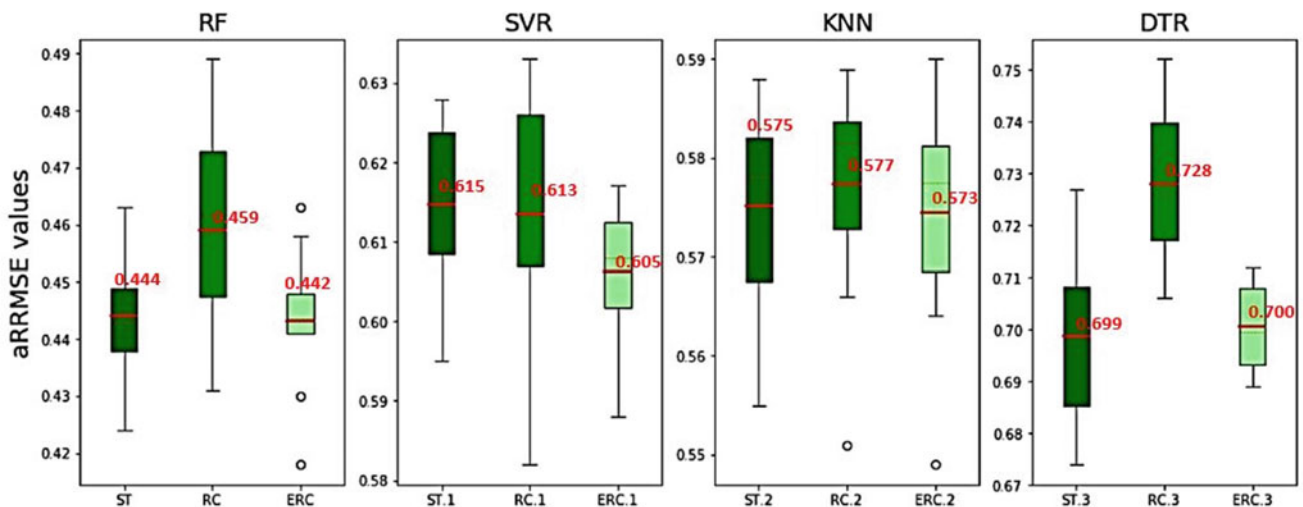


Fig. 3 Boxplots for aRRMSE for different regression-based models

(Spyromitros-xioufis et al. 2016; Moyano et al. 2017; Melki et al. 2017; Masmoudi et al. 2020), the ERC approach proved to be a powerful ensemble method for multi-target regression inferring low to high aRRMSE values. The exploitation of the possible correlations among pollutants produces better results and increases the model’s potential performance, which explains the results obtained by the ERC approach and confirms our assumptions.

5 Conclusion

This study has explored the utility of MTR approaches for simultaneous forecasting of air quality. We compare ST, RC and ERC with different regression-based algorithms. The evaluation of the forecasting algorithms indicates the superiority of the ERC approach, especially when combined with

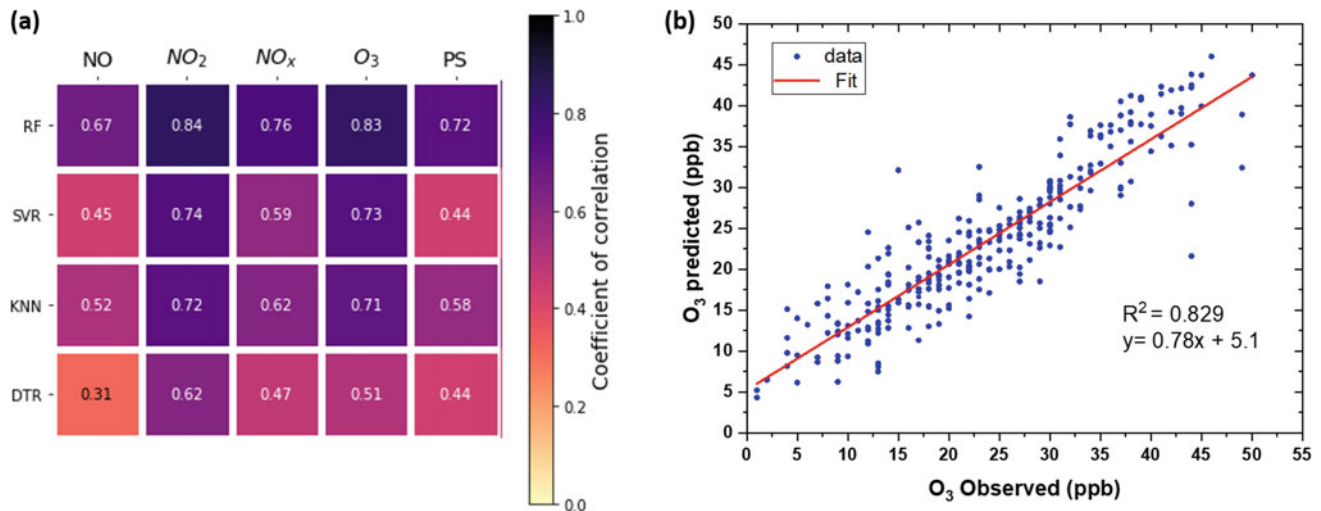


Fig. 4 **a** A heatmap showing the accuracy of each pollutant of ERC approach for different regression-based algorithms and **b** plots of the observed versus predicted ozone concentration

random forest to achieve best results. These findings would be consolidated in the creation of feature ranking method to select the most relevant features for air quality forecasting.

References

- Gómez-losada, Á.: Forecasting ozone threshold exceedances in urban background areas using supervised classification and easy-access information. *Atmos. Pollut. Res.* **9**(6), 1052–1061 (2018). <https://doi.org/10.1016/j.apr.2018.04.002>
- Roy, S.S., Pratyush, C., Barna, C.: Predicting Ozone Layer concentration using multivariate adaptive regression splines, random forest and classification and regression tree. *Soft Comput. Appl.* 140–152 (2018)
- Kocev, D., Džeroski, S., White, M.D., Newell, G.R., Griffioen, P.: Using single- and multi-target regression trees and ensembles to model a compound index of vegetation condition. *Ecol. Model. J.* **220**(8), 1159–1168 (2009)
- Tuia, D., Verrelst, J., Alonso, L., Pérez-cruz, F., Member, S.: Multioutput support vector regression for remote sensing biophysical parameter estimation. *IEEE Geosci. Remote Sens. Lett.* **2014** (2011)
- Borchani, H., Varando, G., Bielza, C., Monte, B.: A survey on multi-output regression, pp. 1–27 (2015)
- Spyromitros-xioufis, E., Tsoumakas, G., Groves, W., Vlahavas, I.: Multi-target regression via input space expansion. *Mach. Learn.* **104** (1), 55–98 (2016)
- Moyano, J.M., Gibaja, E.L., Ventura, S.: An evolutionary algorithm for optimizing the target ordering in ensemble of Regressor chains, pp. 2015–2021 (2017)
- Masmoudi, S., Elghazel, H., Taieb, D., Yazar, O., Kallel, A.: A machine-learning framework for predicting multiple air pollutants' concentrations via multi-target regression and feature selection. *Sci Total Environ.* **715**, 136991 (2020). <https://doi.org/10.1016/j.scitotenv.2020.136991>
- Melki, G., Cano, A., Ventura, S.: Multi-Target Support Vector Regression Via Correlation Regressor Chains. *Inf. Sci. (ny)* **415–416**(11), 53–69 (2017)



Magnetic Properties of Road Dust Using Environmental Magnetism Settings in Greater Hyderabad Municipal Corporation (GHMC), Telangana State, India

R. Sudarshan, B. Madhusudan Rao, B. Nagaraju, S. K. Patil, and K. Lohith Kumar

Abstract

Hyderabad, the capital city of Telangana State, India, in which Greater Hyderabad Municipal Corporation (GHMC), is the extended municipal limits of Hyderabad. Presently, GHMC (India) is experiencing fast urbanization characterized by population growth, infrastructural development, industrialization, and motorization, leading to environmental degradation, causing human health at risk. Globally, environmental degradation causes great concern in the recent past due to many factors like industrial and vehicular traffic in major metropolitan cities. Presently, magnetic measurements and extensive metal analysis are used as proxies to illustrate environmental changes in the GHMC (India) area. In this study, 476 dust samples are collected along the 11 significant roads of GHMC (India) in the summer season of the year 2014 (SD-14), and magnetic measurements like susceptibility (χ), ARM susceptibility (χ_{ARM}), saturation isothermal remanent magnetization (SIRM), SOFT [$\{(SIRM-IRM-20mT)/2\}/mass$] are evaluated in the laboratory. The results reveal the concentration of the ferrimagnetic minerals, due to the variety of the anthropogenic activities. These ferrimagnetic minerals in dust samples contain heavy metals whose concentration significantly increased due to heavy traffic congestion and industrialization. In the process, the results contain the

most significant property of magnetic minerals with magnetite and hematite in different grain sizes and domain that are studied using King plot and Dearing plot of the dust samples, respectively.

Keywords

Environmental magnetism • Urbanization • Traffic • Road dust

1 Introduction

Environmental magnetism is the study of magnetism as it relates to the effects of climate, sediment transport, pollution, and other environmental influences on magnetic minerals. It makes use of techniques from rock magnetism and magnetic mineralogy. The magnetic properties of minerals are used as proxies for environmental change in applications such as paleoclimate, paleoceanography, studies of the provenance of sediments, pollution, and archaeology. The problem of urban soil contamination is drawing the attention of city administrators and gaining more importance in solving air pollution. The problem of urban soil contamination with heavy metals is due to rapid industrialization and urbanization.

Further, the presence of intensive human activities in urban areas has increased the problem of heavy metal contamination in urban soil (Sun et al. 2010). In soil, the total ferrimagnetic component may include secondary minerals such as magnetite and maghemite derived through the chemical and bacterial processes and contaminating polluting dust containing magnetic spherules (Thompson and Oldfield 1986). The composition and quantity of magnetic minerals of road dust are indicators of pollution of the environment, resulting in the toxicity (Alloway and Ayres 1997; Nriagu 1988). Globally, environmental degradation causes great concern in the past due to many factors,

R. Sudarshan · B. M. Rao (✉) · B. Nagaraju
Centre of Exploration Geophysics, Osmania University,
Telangana State, Hyderabad, India

S. K. Patil
K.S.Krishnan Geomagnetic Research Laboratory (KSKGRL)
Allahabad, Allahabad, India

K. Lohith Kumar
National Geophysical Research Institute (NGRI),
Hyderabad, India

including industrial and vehicle traffic, particularly in major metropolitan cities. As a consequence, mapping such areas and addressing appropriate remedial measures are necessary.

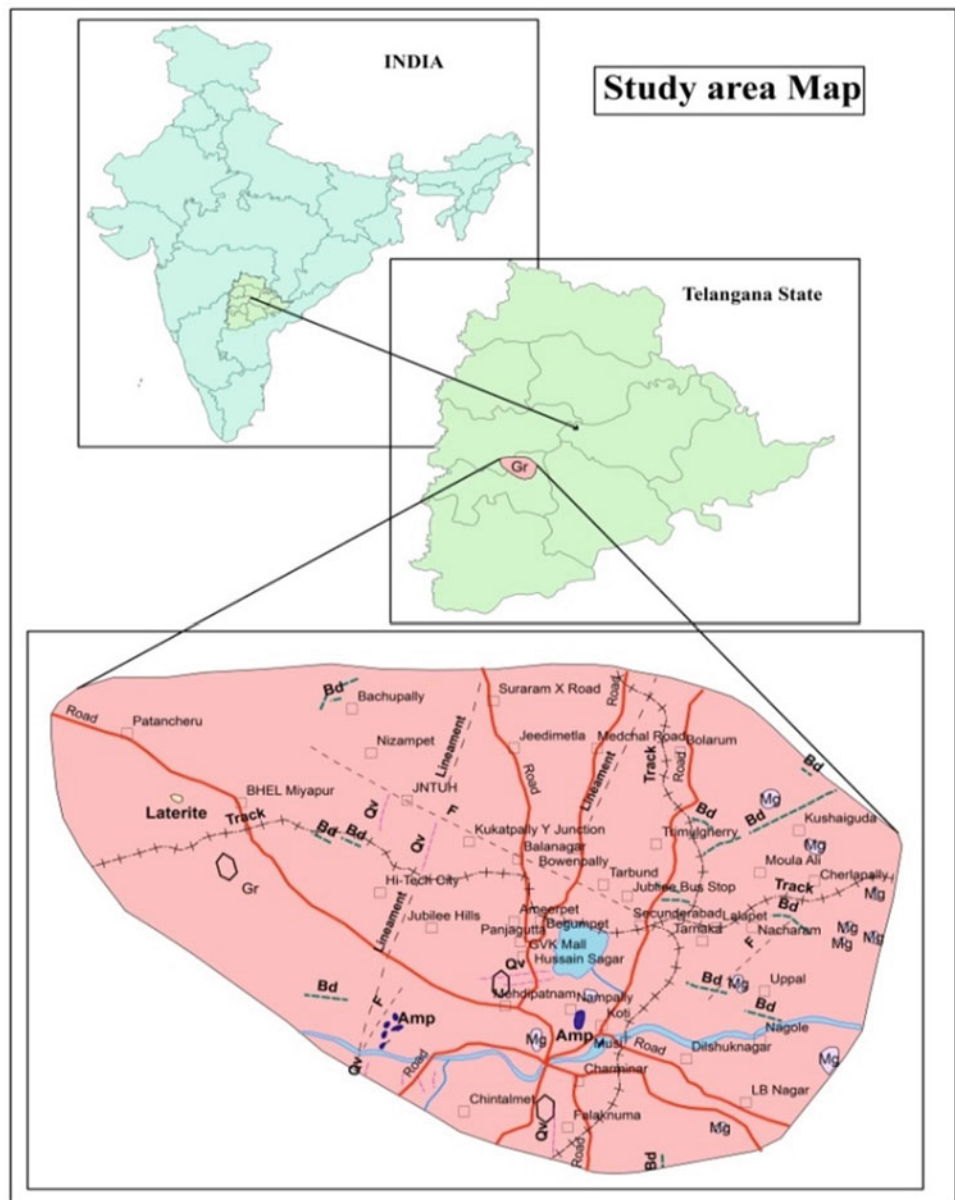
Presently, GHMC (India) is witnessing fast urbanization characterized by rapid urban sprawl, population growth, infrastructural construction, industrialization, and motorization, which is leading to environmental degradation. Thus, it has become necessary to study the pollution caused by road dust that has increased phenomenally since the recent past, placing human health at risk. Thus, the main objectives of this study are pollution distribution, concentration, identification of heavy metals with grain size and domains in the road dust samples that are studied in the entire GHMC (India) area of Hyderabad using magnetic rock techniques.

2 Study Area

The study area is confined in latitude and longitude of 17.3850° N, 78.4867° E. The modern Hyderabad is spread over an area of 650 km^2 (250 sq mi), making it one of the largest metros in India. The predominant topography of the city is sloping rocky terrain of grey and pink granites. Some locations with higher altitude are scattered throughout, giving rise to the appearance of several small hillocks (Fig. 1).

The area is covered mainly by granites of Archaean age, which are highly weathered and fractured, a large number of outcrops are available to map structures and fractures present in the area—the number of intrusive like dolerite dykes. Pegmatite veins and Quartz reef/veins are common in the

Fig. 1 Location map of study area



area. The Hyderabad is the capital city of Telangana State, and it has several roads, scattered all over the city to meet the transportation needs of the population. Out of these, the major roads, which pass through important junctions, are connected to industrial, academic, scientific laboratories, etc. These roads, due to heavy traffic, generate considerable air pollution in the city affecting human health. Hyderabad city produces around 4500 tonnes of solid waste daily, which is transported from the waste collection points to the dumpsite in Jawaharnagar. Rapid urbanization and increased economic activity have also led to increased industrial waste, air, noise, and water pollution, which is monitored and regulated by the Telangana Pollution Control Board (TPCB).

Hyderabad has conferred the software training capital of India and rightly so, by attracting software professionals from within the country and across the world. Thus, the city has steady growth, including environment effect of the tertiary sector in Telangana State. Several roads of Hyderabad

city are spread all over, as the city being capital to Telangana State. Out of these roads, there are 11 major roads, which pass through the essential junctions and are connected to the majority of GHMC (India) area. A total of 476 dust samples are collected along these significant roads called profiles (P1-P11), during March-2014 to May-2014 summer season (SD-14) which pass through major traffic hotspots of road and industrial areas (Fig. 2). The details of the profiles and their connecting roads are presented in Table 1.

3 Laboratory Analysis

There is a perception that pollution is a significant problem in the urban and industrial areas of GHMC (India) area; hence, the samples data on industrial and heavy traffic region are considered. Nevertheless, it is not simple to obtain estimates of industrial emissions and effluent. Thus, to study the

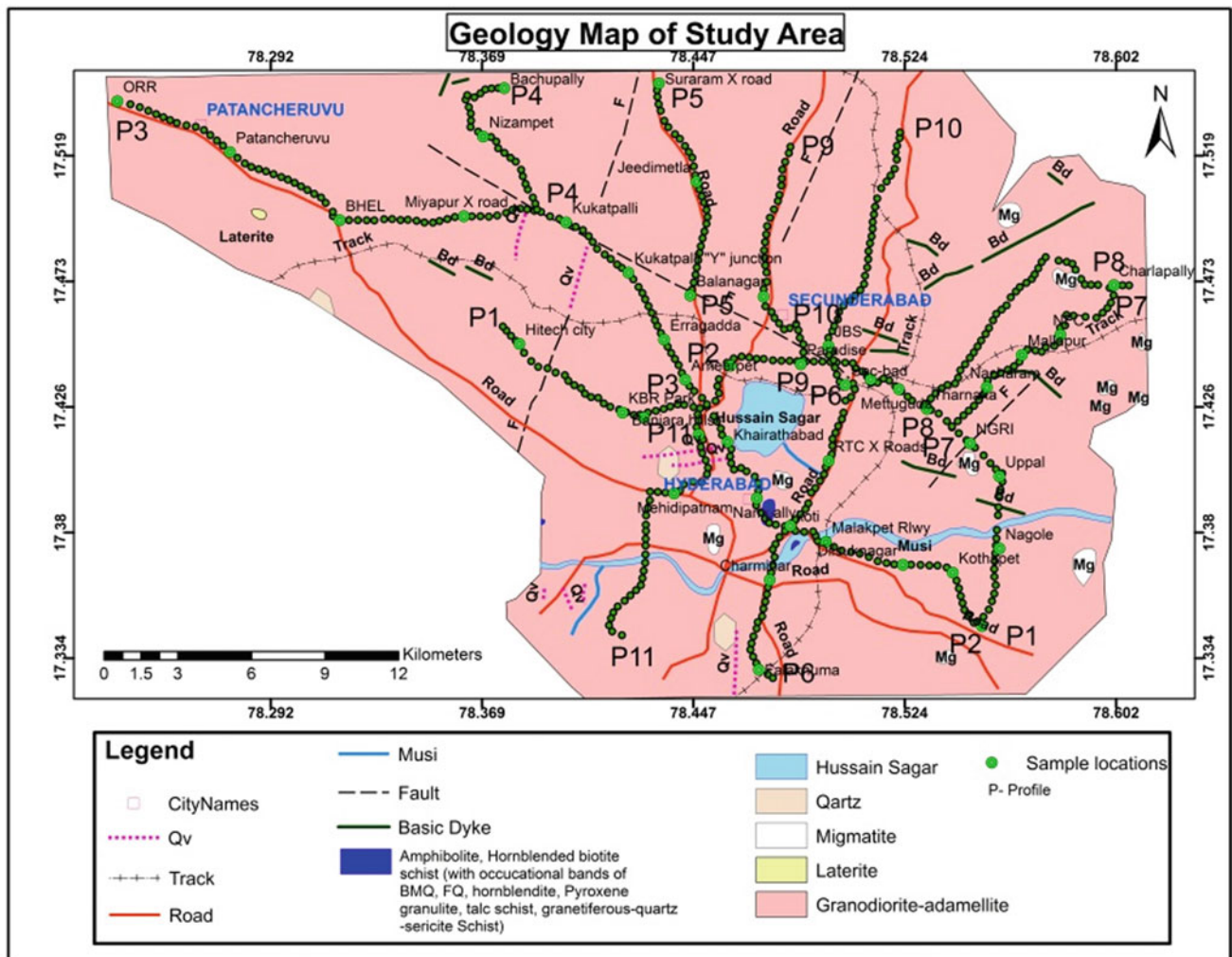


Fig. 2 Sample location map with profile numbers

Table 1 Particulars of profiles

Profile. No	Location of area	
	From	To
P1	LB Nagar	Shilparamam
P2	LB Nagar	Ameerpet
P3	Ameerpet	Patancheru
P4	Miyapur × road	Bachupally
P5	Balanagar	Suraram × road
P6	Jubilee Bus Station	Chandrayangutta
P7	Habsiguda	Cherlapally
P8	Tarnaka	Moula-Ali
P9	Jubilee bus station	Bolarum
P10	Paradise bus stop	Bachupally
P11	Panjagutta	Chintalmet

pollution along the major roads with traffic which pass through important junctions are connected to industrial, academic, scientific labs are considered. The road dust samples of the summer season (SD-14) during February 2014–May 2014 are acquired in a good weather condition with dry deposition on the roads.

As the site locations were distributed in different possible locations of the GHMC (India) area, it took more time for sample collection in the SD-14. The 476 samples have been collected on the road using a small paintbrush with dustpan and a plastic packer. On each pickup, sample at regular interval of 0.25 km distance is collected. The sample weight between 100 and 150 g is measured by using of ‘Anamed’ weighing mission (Model-Z 2000DR, max: 200/2000 g, min: 0.1 g). The samples have been collected in a new plastic zip cover and adequately labelled for later packing. These samples have been wrapped in thin polythene films and packed firmly in pre-weighed standard non-magnetic (styrene) cubic sample holders of 10 cc volume.

The collected dust samples have been analysed with magnetic rock methods to evaluate susceptibility (χ), anhysteretic remanent magnetization (ARM), and isothermal remanent magnetization (IRM). Magnetic susceptibility (χ) of road dust samples has been determined using the Bartington Instrument. Further, the dust sample containing a mineral composition of 1gr samples has been studied using a dual-frequency (470 and 4700 Hz) Bartington Instrument’s MS2 sensor and frequency-dependent magnetic susceptibility ($\chi_{fd}\%$) implement. The ARM is studied by a DC bias field, superimposed over peak alternating (decaying) field of 100 mT using the Molspin Alternating Field Demagnetizer. The IRM acquisition and its backfield demagnetization curves have been measured with the pulse magnetizer, where the applied field has been progressively increased up to 1 T at room temperature (Sudarshan et al. 2018).

4 Results and Discussion

To substantiate, this study, the authors have carried out magnetic measurements using mineral magnetism techniques (Li et al. 2010) off-road dust sample collected from the GHMC (India) area. The magnetic parameters like magnetic susceptibility (χ), ARM (χ_{ARM} susceptibility), saturation isothermal remanent magnetization (SIRM), $SOFT[\{(SIRM-IRM-20mT)/2\}/mass]$ are along 11 profiles, and P1–P11 are evaluated. Each road profile reflects the concentration and their variation in magnetic minerals in the dust samples, while $\chi_{fd}\%$, χ_{ARM}/χ , $\chi_{ARM}/SIRM$, $SIRM/\chi$, $S-300mT$ (backward remanence) are related to the grain size and the type the magnetic minerals in the dust samples. The range of ARM/SIRM and χ_{ARM}/χ is also well discussed to explain diversity and similarity of road dust in the study area. Magnetic susceptibility (χ_{lf}) varies from 102.55×10^{-8} to $1926.83 \times 10^{-8} m^3 kg^{-1}$ (average $587.37 \times 10^{-8} m^3 kg^{-1}$) and the SOFT from 4.77×10^{-5} to $4050.48 \times 10^{-5} Am^2 kg^{-1}$ (average $641.96 \times 10^{-5} Am^2 kg^{-1}$), indicating the different types and concentrations of magnetic material in the study area. These parameters show the diversity and similarity of road dust in GHMC (India).

4.1 Spatio-temporal Variations in Magnetic Minerals

Further, the author attempted to explain the spatial distribution of dust and their effects along with the profile through statistical and contour mapping approach. The variation in these parameters like χ , SIRM and χ_{ARM} is evaluated and contoured using Geosoft software (Oasis mantaje 9.1) and presented in Fig. 3a–c, respectively. The result clearly shows

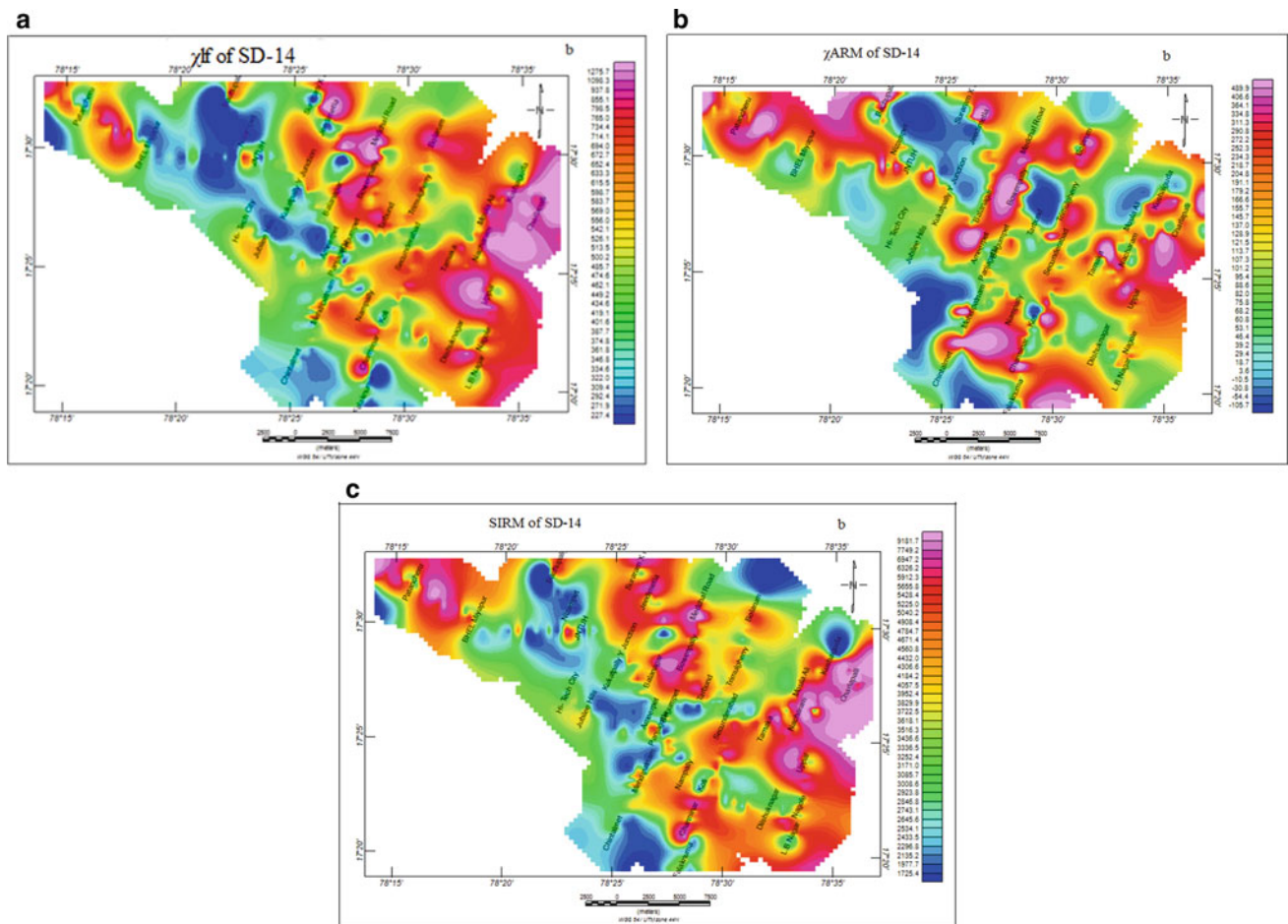


Fig. 3 a Spatial distribution plot of the magnetic susceptibility (χ_f) parameter covering the entire GHMC study area for SD-14. b Spatial distribution plot of Anhyseretic remanent magnetization (χ_{ARM})

parameter covering the entire GHMC study area for SD-14. c Spatial distribution plot of saturated isothermal remanent magnetization (SIRM) parameter covering the entire GHMC study area for SD-14

that variation is different along with each profile. The magnetic susceptibility (χ) varies in the GHMC (India) area. The maximum value of χ along the P1–P11 ($1926.83 \times 10^{-8} \text{ m}^3 \text{ kg}^{-1}$) and the minimum value along the P1–P11 ($102.55 \times 10^{-8} \text{ m}^3 \text{ kg}^{-1}$) show the variation details (Fig. 3a). Similarly, the SIRM maximum and minimum values along the P1–P11 are (Fig. 3b) ($15,149.49 \times 10^{-5} \text{ Am}^2 \text{ kg}^{-1}$, $680.18 \times 10^{-5} \text{ Am}^2 \text{ kg}^{-1}$), and χ_{ARM} maximum and minimum values along the P1–P11 are (Fig. 3c) ($1529.88 \times 10^{-8} \text{ m}^3 \text{ kg}^{-1}$, $6.10 \times 10^{-8} \text{ m}^3 \text{ kg}^{-1}$) that shows the level of variation in these parameters.

Figure 3a shows susceptibility (χ) for SD-14 at various locations covering the entire region, wherein pink-coloured peaks show higher concentration only in individual pockets of areas like Nacharam, charlaally, Uppal, L.B.Nagar, Charminar, Bowenpally, Bolaram, Jeedimetla, kushaiguda, whereas orange coloured peak shows medium level of concentration only in individual pockets of areas like Tarnaka, Secunderabad, Dilshuknagar, Nagole, Nampally, Moula-Ali, Trimulgherry, Patancheru, unlike other areas

Falaknuma, Chintalmet, BHEL Miyapur, JNTUH, Nizampet, Bachupally, Kukatpally where the susceptibility variation due to dust is lower to minimum concentration indicated with green to blue colour.

Figure 3b shows various locations during the SD-14 season in the study area. From the figure, the high concentration pink peaks are almost in the entire area of GHMC, i.e. North, South, East, and West. These areas are Nacharam, Charlapally, Uppal, Kushaiguda, Charminar, Bolaram, Bowenpally, Ameerpet, Patancheru, Bachupally, Mehadipatnam, whereas orange coloured peaks are the medium spread of χ_{ARM} parameter only in limited pockets like Eastern, Northern, Southern sides of the study area. These areas are near Tarnaka, Secunderabad, Nagole, Nizampet, Nampally, Balanagar, Kukatpally. In other study areas like Falaknuma, Koti, L.B. Nagar, Dilshuknagar, Moula-Ali, Tarband, Suraram x road, JNTUH, Hi-Tech city, Jubilee Hills, Chintalmet and other areas of GHMC (India), χ_{ARM} spread due to dust pollution in this season are lower to a minimum which is indicated with green to blue coloured peaks.

Figure 3c shows the SIRM spread at various locations of the study area in the SD-14 season. From the figure, high concentration of SIRM in the study areas is indicated with pink coloured portion. These areas are Nacharam, Charlapally, Uppal, Charminar, Balanagar, Medchal Road, Jeedimetla, Patancheru, whereas orange coloured peaks are the medium spread of SIRM, only in certain areas like L.B. Nagar, Nagole, Dilshuknagar, Secunderabad, Tarnaka, Nampally, Tarband, Trimulgherry, JNTUH. The green to blue coloured spread in the map explains lower to the minimum level of SIRM in the study area. These areas are Falaknuma, Chintalmet, Jubilee Hills, Hi-Tech city, Kukatpally, Nizampet, Bachupally, Ameerpet, Mehadipatnam.

5 Types of Magnetic Mineral

In order to investigate the magnetic minerals present in road dust of GHMC (India) study area, the backfield demagnetization curves have been drawn between backfield demagnetization (B/mT) and S-Ratio (IRM/SIRM). The S-Ratio is obtained by dividing the “backward” remanence by the SIRM. The main objective of the S-ratio is to provide a measure of the relative amounts of high-coercitivity (hard) to low-coercitivity (soft) remanence. This concept provides a fair estimate of the relative importance of antiferromagnetic (hard hematite) versus ferrimagnetic (soft magnetite). Thus, utilizing this concept of back field demagnetization, the road dust samples of summer season profiles P1–P11, acquisition of IRM curves results are presented in Fig. 4, respectively.

Figure 4 shows the backfield demagnetization curve of acquisition of IRM for SD-14 season pertaining to the particular profile samples, namely P₁ 75, P₂ 6, P₃ 67, P₄ 23, P₅ 13, P₆ 12, P₇ 16, P₈ 29, P₉ 28, P₁₀ 22, P₁₁ 23 (total of 11 samples from 11 profiles), as these samples are of higher density. All other samples (IRM/SIRM) density values are lower, hence not included in the curve.

Further, from the above curves of Fig. 4, it is observed that there are differences in the curves obtained from the dust samples. The curves of the summer season samples of profiles show a rapid rise below of 100 mT and reaching 80% SIRM at a magnetic field of 100 mT, and reaching near saturation of remanence at 300 mT, the S_{-300 mT} was also beyond 80%, indicating that magnetically soft mineral in the dominant magnetic mineral. The overall scenario of entire GHMC (India) road dust particles is with more magnetically soft and less hard components are present.

Further, to establish the magnetic mineral type of entire road dust particles of three seasons in the study area of GHMC (India) unlike selected samples, the correlation between SIRM and χ and liner correlation between SOFT and SIRM plots are drawn and presented in Fig. 5 for SD-14. These relation plots explain and indicate that the magnetic

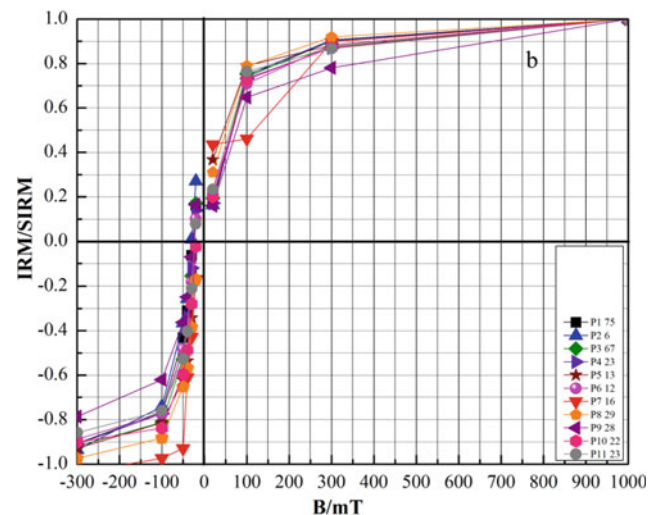


Fig. 4 IRM acquisition curves of typical road dust samples SD-14

properties of the study area dust samples are dominated by ferrimagnetic minerals (Oldfield 1991). We found that the areas with more magnetically soft component had dense crowd flow, and the area with less magnetically soft component had more traffic, building materials, constructions, and industrial belt. Scattered particles in Fig. 5 are more antiferromagnetic minerals and show the hard component like hematite. Thus, these curves and plots explain that different human activity could directly influence the type of magnetic minerals (Li et al. 2010). Thus, the road dust samples in these regions of study area contain more magnetite (soft) and less hematite (hard) magnetic minerals. The distributions of dust particles are almost linear.

6 Grain Size of Magnetic Minerals

In the process of the present study, the evaluated parameters of road dust reflect the characteristics of magnetic material with different grain sizes and, hence, domain range. To explain this, we utilize the concept of King plot (King et al. 1982) and Dearing's plot (Dearing et al. 1997). In continuation, the King plot graph is plotted to utilize the data of $\chi_{fd}\%$ and χ_{ARM} of three seasons and is presented in Fig. 6. The results show that summer season of dust samples is of three different ranges of grain sizes viz. $< 0.1 \mu\text{m}$, $0.1\text{--}1 \mu\text{m}$, and $1\text{--}5 \mu\text{m}$. However, several particles grain size is from $1.0 \mu\text{m}$ and $0.1\text{--}1 \mu\text{m}$ and are less scattered than the $1\text{--}5 \mu\text{m}$ grain size particles.

Further, the Dearing plot graph is plotted utilizing the data of ARM/SIRM and $\chi_{fd}\%$ of summer season and presented in Fig. 7. The results show that most of the magnetic domains are a combination of pseudo-single domain (PSD) and multi-domain (MD). These two domains are

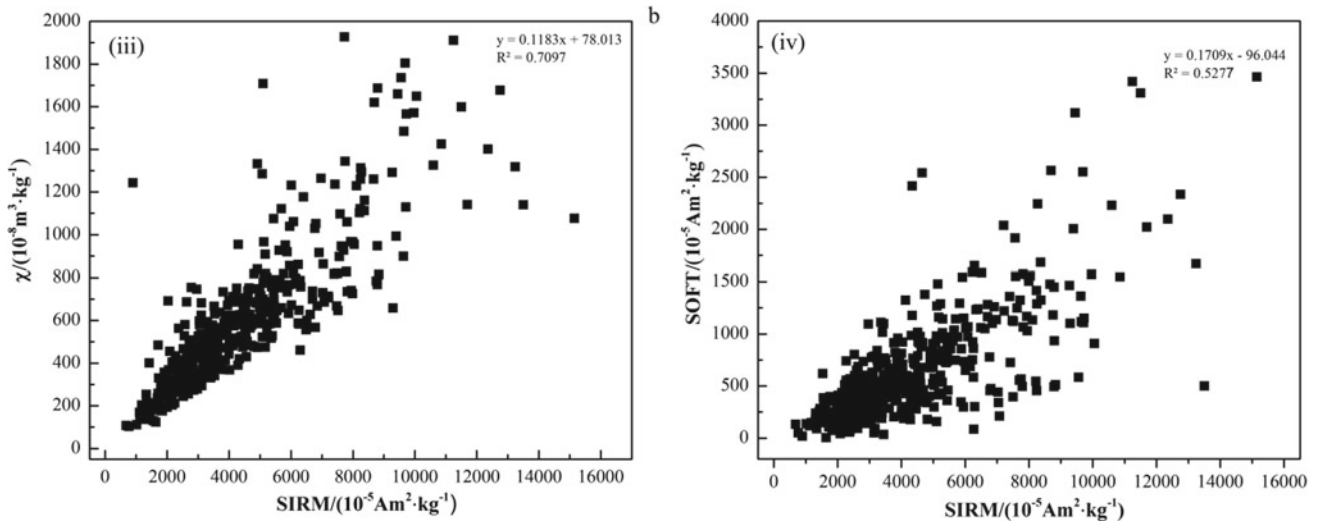


Fig. 5 Bi-plots are showing for summer seasons of different magnetic parameters in road dust samples (iii) correlation between χ and SIRM; (iv) correlation between SOFT and SIRM

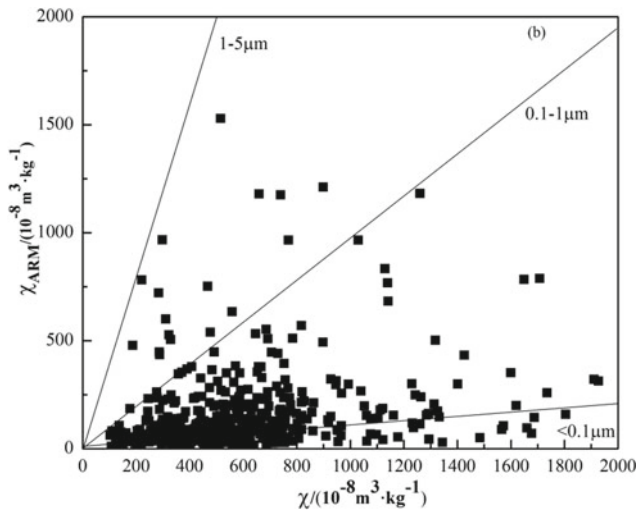


Fig. 6 King plot exhibiting a correlation between χ_{ARM} and χ for the SD-14

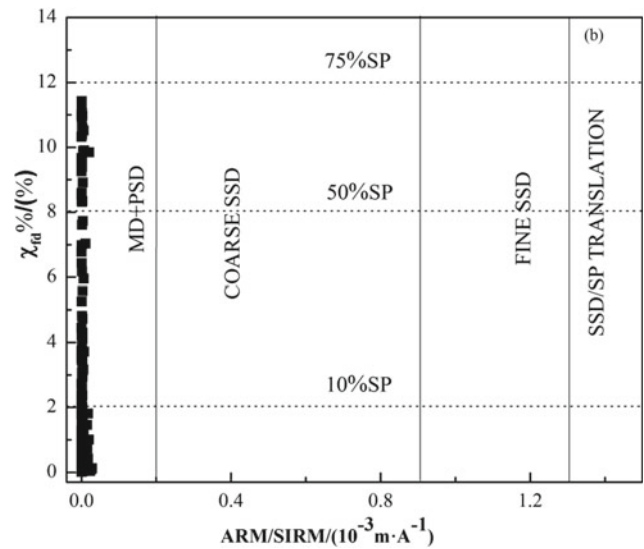


Fig. 7 Dearing plot exhibiting a correlation between $\chi_{fd}\%$ and ARM/SIRM for SD-14

concentrated at lower values of ARM/SIRM and $\chi_{fd}\%$ values. However, the lower values of $\chi_{fd}\%$ could also indicate the low concentrations of superparamagnetic (SP) particles in the dust samples (Dearing et al. 1997).

7 Conclusions

From the above explanation, the concept of types of magnetic minerals, in this study, infers the characteristics mineralogy of pure magnetite (Fe_3O_4) of anthropogenic origin, maghemite ($\gamma-Fe_2O_3$) of pedogenic origin and titanomagnetites

($Fe_{3-x}Ti_xO_4$) as to detrital origin anticipating the topsoils and sediments. Further, these are admixtures of above with dominant and detectable characteristics of MD-PSD magnetite from road dust confirming its anthropogenic origin in samples. It addresses the issue of detecting the magnetic characterization over the ferrimagnetically rich substrate in the urban industrial domains.

There is noticeable evidence of a continuous increase in the concentration of pollutants in the road dust samples due to the consistent increase in the anthropogenic loading. This is demonstrated by the concentration-dependent rock mag-

netic parameters (clf, cARM, and SIRM) along with the profiles.

The grain size of dust samples shows a variety of domain size from SD, PSD to MD with the dominance of SD, whereas the dust shows characteristics domain size of MD-PSD range with its distribution controlled by atmospheric conditions during the summer season.

Types of magnetic minerals are examined by the IRM acquisition curves of typical road dust which reveals that the dust samples contain magnetite and hematite, wherein the percentage of values of their minerals are variable.

The mineral magnetic bi-plots explain magnetic concentration and grain size variations.

The grain size of dust particles is studied using King and Dearing plots. From these, the King plot of the study reveals the size of grain contained in the dust; they are $< 0.1 \mu\text{m}$, $0.1\text{--}1 \mu\text{m}$, and $1\text{--}5 \mu\text{m}$. Dearing plot is the domain range of the grains in the dust samples that are MD + PSD.

Acknowledgements We are grateful to CSIR-UGC for providing funds to do the research. We also acknowledge to Indian Institute of Geomagnetism Laboratory (IIG) Mumbai and Dr. K.S. Krishnan Geomagnetic Research Laboratory (KSKGRL), Allahabad and Centre of Exploration Geophysics, OU, Hyderabad for providing laboratory facilities to the research work.

References

- Alloway, B., Ayres, D.C.: Chemical Principles of Environmental Pollution. CRC Press (1997)
- Dearing, J.A., Bird, P.M., Dann, R.J.L.: Secondary ferromagnetic minerals in Welsh soils: a comparison of mineral magnetic detection methods and implications for mineral formation. *Geophys. J. Int.* **130**, 727–736 (1997)
- King, J., Banerjee, S.K., Marvin, J.: A comparison of different magnetic methods for determining the relative grain-size of magnetite in natural materials—some results from lake-sediments. *Earth Planet. Sci. Lett.* **59**(2), 404–419 (1982)
- Li, P., Qiang, X.-K., Xu, X.-W., Li, X.-B., Sun, Y.-F.: Magnetic properties of street dust: a case in Xi'an city, Shaanxi province, China. *Chin. J. Geophys.* **53**(1), 113–120 (2010)
- Nriagu, J.O.: Production and uses of chromium. *Chromium Nat. Hum. Environ.* **20**, 81–104 (1988)
- Oldfield, F.: Environmental magnetism a personal perspective. *Quatern. Sci. Rev.* **10**(1), 73–85 (1991)
- Sudarshan, R., Madhusudan Rao, B., Nagaraju, B., Patil, S.K., Lohith Kumar, K.: Assessment of urban pollution from heavy metals concentration in road dust in Greater Hyderabad Municipal Corporation (GHMC), Telangana State, India. *J. India Geophys. Union* **22**(4), 436–443 (2018)
- Sun, Y., Zhou, Q., Xie, X., Liu, R.: Spatial, sources, and risk assessment of heavy metal contamination of urban soils in typical regions of Shenyang China. *J. Hazard. Mater.* **174**(1), 455–462 (2010)
- Thompson, R., Oldfield, F.: Environmental magnetism. Allen and Unwin, London (1986)

**Environmental Earth Sciences (T4):
Geo-environmental Hazards**



Assessing the Vulnerability of Soil Losses by Mapping: Case of the Watershed of Oued Chemorah Northeast Algeria

Nabil Kabouche, Faiza Balla, and Kamel Khanchoul

Abstract

The approach used in mapping water erosion at the catchment of Chemorah Wadi in Banta (Algeria) involves an analysis of the main factors of water erosion, namely the climatic map, the lithological map, the slopes, and the land cover. The resulting maps were integrated into a geographic information system (GIS). Observations in the field validated a particular map. Four classes of vulnerability to erosion were distinguished: areas with low vulnerability (0–3 T/ha/year) for an area (52%); areas with moderate vulnerability (3–7 T/ha/year) for an area (25%) and highly vulnerable (7–12 T/ha/year) for an area (15%); and very highly vulnerable (>12 T/ha/year) for an area (8%).

Keywords

Hydro-sedimentary • Chemorah Wadi • Water erosion • GIS • Vulnerability

1 Introduction

Many phenomena threaten our environment, among which water erosion. This phenomenon is one of the most dramatic consequences of the hydro-sedimentary flows which are measured in tons of material per year transported on the terrestrial surface (Arar and Chenchouni 2014). In the

N. Kabouche (✉)
Faculty Science of Matter, Laboratory LEMPAU,
University El-Hadj Lakhdar, Batna 1, Batna, Algeria
e-mail: nabil.kabouche@univ-batna.dz

F. Balla
Faculty of Technology, Laboratory LEMPAU,
University Mostefa Ben Boulaïd, Batna 2, Batna, Algeria

K. Khanchoul
Department of Geology, Faculty of Earth Sciences,
University Badji Mokhtar, Annaba, Algeria

absence of specific degradation data, it was wise to use other methods to show erosion at the catchment Chemorah Wadi in the Banta region.

The Catchment of Chemorah Wadi is located in Northeast Algeria. It is characterized by an area of 755 km² composed of strong reliefs of high slope lithological compositions and vegetation cover promoting the erosive phenomenon (Fig. 1).

2 Materials and Models

In this study, remote sensing and Geographic Information Systems (GIS) are used to assess and map water erosion. The material used in this study is:

Documents:

- Shuttle Radar Topography Mission (SRTM) image with a resolution of 30 m available on the website: <http://srtm.csi.cgiar.org/SELECTION/inputCoord.asp>.
- Land use map 1/100000.
- Lithological map: 1/100000.
- Digital soil maps of the world (DSMW), available on the website: <http://www.fao.org/geonetwork/srv/en/metadata.showid=14116>.
- Landsat 5 ETM + satellite image of 18/05/2006 with a resolution of 30 m.
- Precipitation recorded between 1985 and 2012.

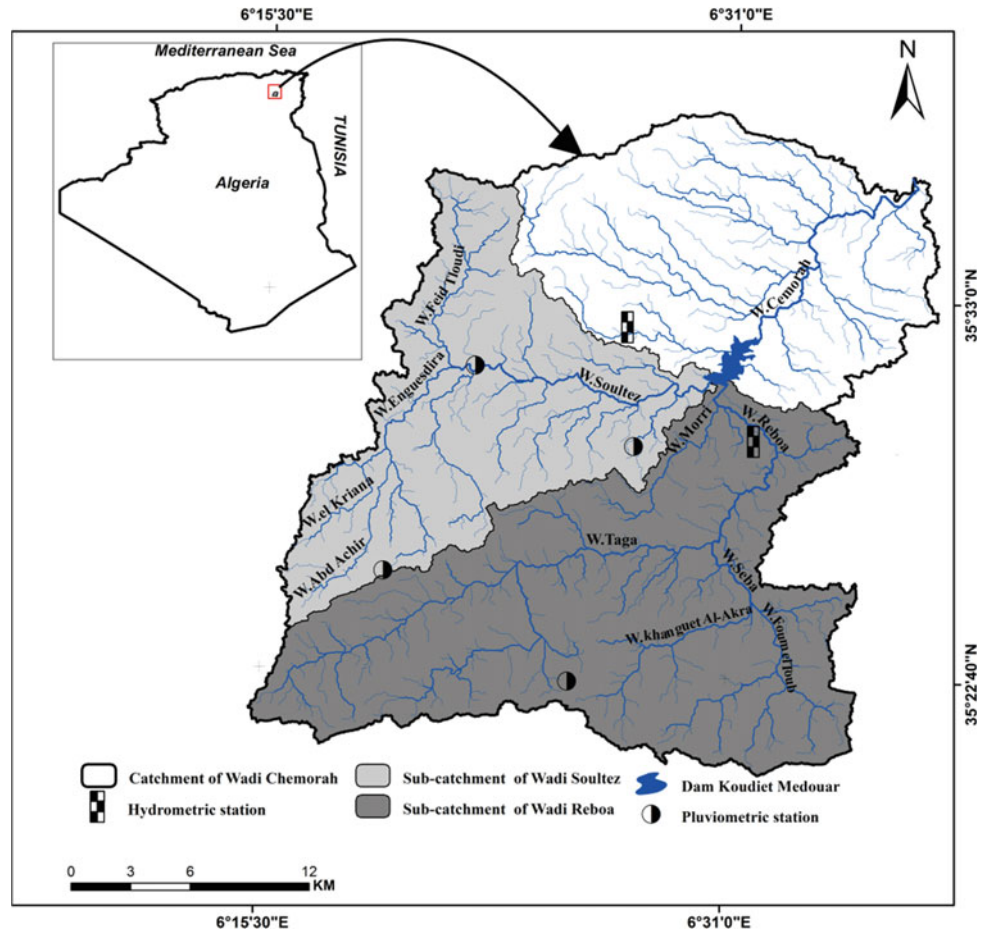
Software:

- Arcgis version 10.2.2.
- Version of the global mapper.

Model

It is an empirical model that brings together the factors that affect precipitation erosion, soil properties, soil characteristics, soil protection by vegetation cover and conservation

Fig. 1 Presentation of the study area catchment of Chemorah Wadi



practices. The empirical model in question is given by the equation of Wischmeier and Smith (1978) revised, and which is written in the following form:

$$A = R \cdot K \cdot LS \cdot C \cdot P$$

- A Expresses the long-term average annual land loss in tonnes/ha/year
- R Corresponds to the rain and runoff factor mm/ha
- K Represents the soil erodibility factor in tonnes/ha
- LS This is the length and slope factor of the slope
- C Corresponds to the crop factor (vegetation) and management factor

The flowchart above (Fig. 2) summarizes all the steps taken to quantify the average annual loss of soil and to assess the vulnerability of soil toward water erosion throughout the catchment of Chemorah Wadi.

3 Results

In recent years, the revised universal soil loss equation RUSLE (Renard et al. 1997; Wischmeier and Smith 1978) has been widely applied by hydrologist to predict the risk of erosion in Africa (Adediji et al. 2010; Benkadja et al. 2015; Bougerra et al. 2017).

In this paper, the evaluation of soil losses by water erosion was obtained by the superposition of thematic maps of the factors of the empirical formula (RUSLE) with their databases using ARCGIS 10.1 and the application of the universal equation according to all the factors that typically influence the erosive phenomenon were estimated. The intersection of these factors in raster mode under GIS has allowed us establishing a soil losses map throughout the catchment of Chemorah Wadi (Fig. 3).

Fig. 2 Presentation of the adopted methodology

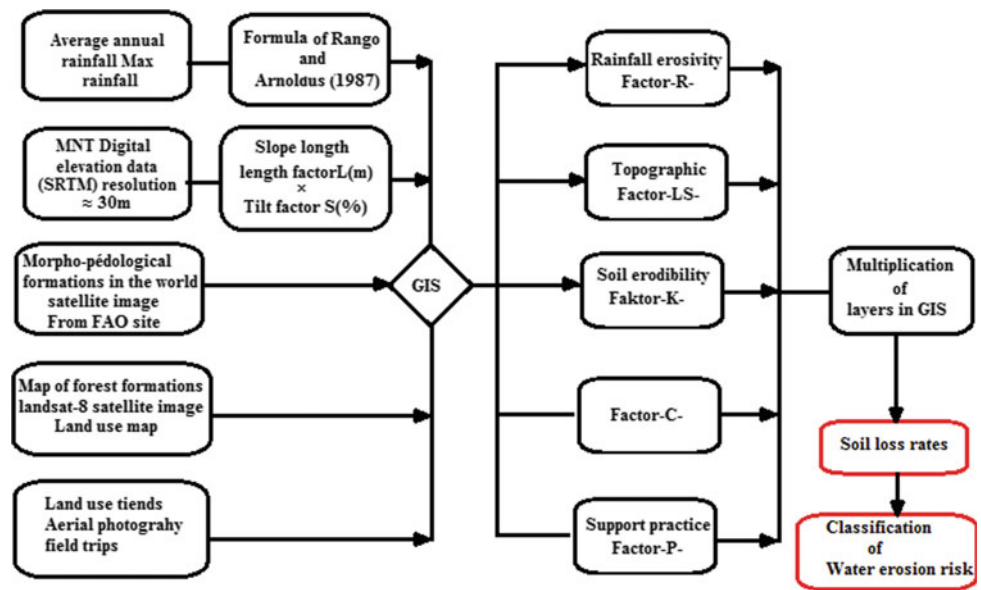
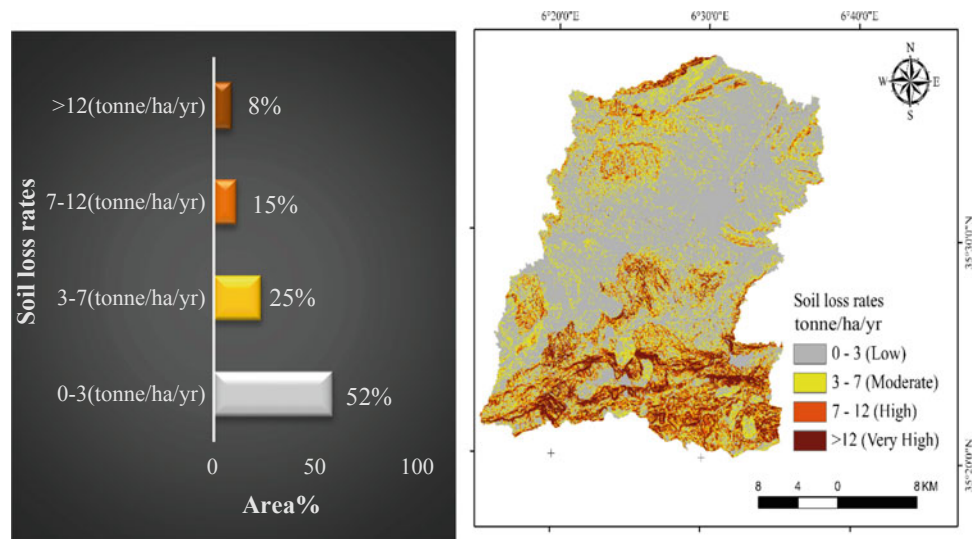


Fig. 3 Soil loss rates (tonnes/ha/year) and erosion risk map in the Catchment of Chemorah Wadi



A long bibliography testifies to the recurrence of the phenomenon of water erosion, as an example, we can cite:

- The rich syntheses of Vita-Finzi (1969) which confirmed that the activity of erosion is intense in the Mediterranean basins.
- According to the Ministry of Agriculture and Rural Development, 50 million hectares of threatened by water erosion, which represents more than 20% of the country’s total surface area which is about 238 million hectares (Mostephaoui et al. 2013).
- The threatened areas are divided into 14 million hectares in mountainous areas 32 million hectares in steppe areas and 4.1 million hectares of forests (Mostephaoui et al. 2013).

- 20 large dams will be highly threatened by the total filling of the reservoir (Remini and Hallouche 2004).

4 Discussion

The average soil losses by water erosion, for all the homogeneous units, are validated by field observations. Four classes of vulnerability to erosion were distinguished: areas with low vulnerability (52%); moderate vulnerability areas (25%), and highly vulnerable areas (15%), and very highly vulnerable areas (8%). The model RUSLE presents a ligature of the results and translates a strong impact of the erosive effect primarily at the level of the Wadi Reboa.

Water erosion risk was assessed and mapped based on the analysis of the main factors involved in of water erosion, namely the maps of climate, lithology, slopes, and land cover. Similar approach was used in this region including adjacent montane areas (Arar and Chenchouni 2012, 2014)

5 Conclusions

It can, therefore, be concluded that for the Catchment of Chemorah wadi, the degree of slope and the erodibility of soils especially in cultivated areas are the factors erosion control and that the interdependence of these factors is a very variable erosion in space.

From all these results can be concluded that most of the sediment production at the Koudiet-Medeour dam comes from the sub-basin of the Wadi Reboa, which requires erosion at the level of the latter and which over time (after 159 years) presents a threat of siltation accelerated reducing the water storage capacity of the dam. Thus, the management provisions mainly at the sub-watershed level of the Wadi Reboa must be taken into account.

Moreover, this first cartographic study is a tool to help the decisionmakers for the attribution of the zones of cultures and the sites that can shelter socioeconomic infrastructures.

References

- Adediji, A., Tukur, A.M., Adepoju, K.A.: Assessment of revised universal soil loss equation (RUSLE) in Katsina area, Katsina state of Nigeria using remote sensing (RS) and geographic information system (GIS). *Iranica J. Energy Environ.* **1**(3), 255–264 (2010)
- Arar, A., Chenchouni, H.: How could geomatics promote our knowledge for environmental management in Eastern Algeria? *J. Environ. Sci. Technol.* **5**(5), 291–305 (2012)
- Arar, A., Chenchouni, H.: A “simple” geomatics-based approach for assessing water erosion hazard at montane areas. *Arab. J. Geosci.* **7**(1), 1–12 (2014)
- Benkadja, R., Boussag, F. and Benkadja, A.: Identification et évaluation du risque d'érosion sur le bassin versant du K'sob (Est Algérien). *Bull. Eng. Geol. Environ.* **74**(1), 91–102 (2015)
- Bouguerra, H., Bouanani, A., Khanchoul, K., Derdous, O., Tachi, S.E.: Mapping erosion prone areas in the Bouhamdane watershed (Algeria) using the revised universal soil loss equation through GIS. *J. Water Land Dev.* **32**(1), 13–23 (2017)
- Mostephaoui, T., Merdas, S., Sakaa, B., Hanafi, M.T., Benazzouz, M. T.: Cartographie des risques d'érosion hydrique par l'application de l'équation universelle de pertes en sol à l'aide d'un système d'information géographique dans le bassin versant d'el Hamel (Boussaada). *Algérie. Journal Algérien des Régions Arides; N° Spécial* 131–147 (2013)
- Remini, B., Hallouche, W.: Le dragage des barrages. Quelques exemples algériens. *Revue Internationale la Houille Blanche* **3**, 95–100 (2004)
- Renard, K.G., Foster, G.R., Weesies, G.A., Mccool, D.K., Yoder, D.C.: Predicting soil erosion by water—a guide to conservation planning with the Revised Universal Soil Loss Equation (RUSLE). United States Department of Agriculture, Agricultural Research Service (USDA-ARS) Handbook No. 703 (1997)
- Vita-Finzi, C.: The mediterranean valleys. Geological changes in historical times, Cambridge Univ. Press, 140 p (1969)
- Wischmeier, W.H., Smith, D.D.: Predicting rainfall erosion losses: a guide to conservation planning (No. 537). Department of Agriculture, Science and Education Administration (1978)



Risk Assessment of Coastal Erosion Hazard of Ngazidja Island in Comoros Archipelago

Avouca Mahamoud, Nadjim Ahmed Mohamed, Gzam Maher, and Mabrouk Montacer

Abstract

This study aims to prove the importance of shoreline mapping and quantification of coastal erosion indicators in the risk classification of Ngazidja Island. The survey involves inventory, tracking, and sizing processes in nine areas. The results display a shoreline represented by 68% of vegetation limit and 20% of the dam. The risk classification of coastal erosion indicates a moderate risk of 56% at the investigated coasts. The coasts of *IKoni* and *Mbachile*, respectively, with 66% and 93% of spatial distributions of dams present a high risk. These proportions refer to the urbanized areas where the dam is omnipresent. In a climate change context, it is fundamental and urgent to discern the contribution of each pressure to reach the integrated management of this environment.

Keywords

Erosion indicator • Shoreline mapping • Coastal erosion • Assessment risk • Ngazidja Island

1 Introduction

The term risk differs widely, depending on the kind of hazard and the exposed stakes. It is the probability or likelihood of the occurrence of hazardous events or trends

A. Mahamoud (✉) · M. Montacer
Laboratory of Geosystems, Georesources and Geoenvironments (U3G), Department of Earth, Sciences, Faculty of Sciences of Gabes, University of Gabes, 6072 Zrig Gabes, Tunisia

N. A. Mohamed
Faculty of Sciences and Technology, University of Comoros, Corniche Road, 2585 Moroni, Comoros

G. Maher
UR Applied Hydro-Sciences, Higher Institute of Water Sciences and Technics, University of Gabes, 6072 Zrig Gabes, Tunisia

multiplied by the impacts in case these events or trends occur (IPCC 2014). In the context of climate change, a sea-level rise rate of 4 mm/year has been foreseen by 2050 (IPCC 2001) in the subregion (the southwest of Indian ocean). This future hazard will effectively accelerate the coastal retreat. Indeed, about 10% of the population will be displaced at a sea-level rise of 20 cm according to the Ministry of Rural Development, Fishery, Arts and crafts, and Environment predictions (2006). The coastal erosion is further increased by various anthropic actions (Sinane 2013) such as extraction of coastal materials (sand, coral, gravel) and dams poorly erected. According to the same Ministry, about 90% of beaches have been eroded for the past 20 years. Researchers resorted to many methods to assess the risk related to these pressures like those used by de Gouveia Souza and Suguio (2003) and Cherian et al. (2012) in Sao Paulo and Tamilnadu coast (India), respectively.

Through this paper, we explore the use of shoreline mapping and quantification of coastal erosion indicators as elements of risk classification of Ngazidja Island. The survey involves inventory, tracking, and sizing processes in nine localities (Fig. 1) the most receptive of which are at about 16 km.

2 Materials and Methods

The vegetation limit (Faye 2010) is suggested as the primary shoreline indicator. Cliff, structure protection tops (Priest 1999; Boak and Turner 2005), and high water level (Hanslow 2007) are retained for cartography reasons. The shoreline is mapped using recent aerial photographs with high resolution (1 m).

The field survey consists of investigation, identification, tracking, stocktaking, sizing, and geo-referencing. The choice of erosion indicators is based on their dimensionality and durability. Thus, four (4) types have been identified: cliff, protection structure, vegetation degradation, and

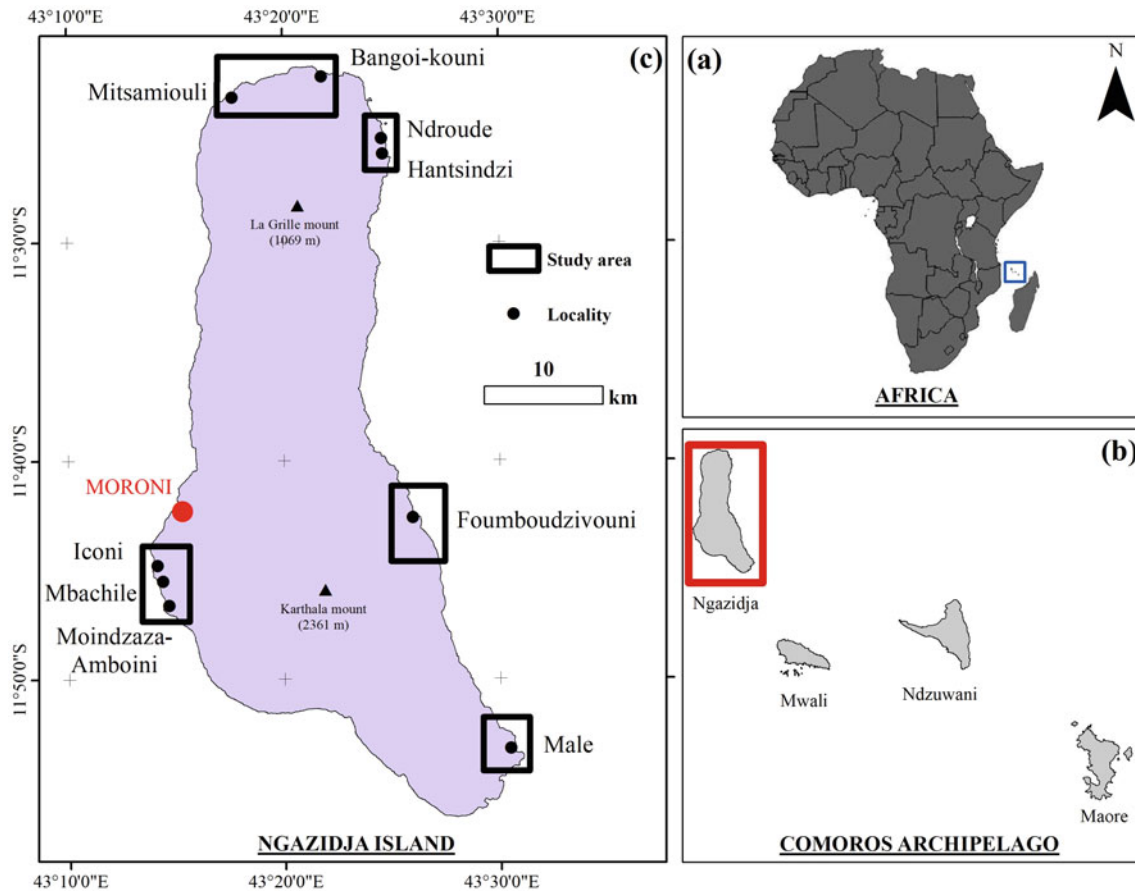


Fig. 1 Map of study area **a** Location of Comoros archipelago, **b** Comoros archipelago, and **c** Ngazidja Island

historical relic (de Gouveia Souza and Suguio 2003; Bernatchez et al. 2011). The location of these indicators is first carried out by GPS. They are also located by measuring the distance between them and the present shoreline by a decameter. The vegetation degradation is deduced by the height of the outcrop of the roots.

Two criteria have been used to determine the risk classification: (i) number of coastal erosion indicators types and (ii) spatial distribution of indicators (Cherian et al. 2012). The second criterion concerns only cliff and protection structures. The distribution (%) has been obtained by the total length of indicators concerning shoreline length. Five risk degrees, very high risk, high risk, moderate risk, low risk, and very low risk, have been defined (Table 1).

3 Results

3.1 Shoreline Mapping

The vegetation limit with 68% is the most highly presented shoreline indicator (Table 2). The dam covers 20% of the

study areas. Cliffs, high water level, and rocks fill occupy 6%, 5%, and 1%, respectively.

3.2 Coastal Erosion Indicators

The coast of *Mitsamiouli* includes most of the dams (7), but the most extended shelter are the coasts of *IKoni* (1253 m), *Mbachile* (850 m), and *Bangoi-kouni* (328 m). These structures can increase the risk of coastal inundation like in *Bangoi-kouni* in August 2015 and 2018. They (these structures) hinder the return of water during 5 h, and about 1.2 ha are inundated with a maximum height of 91 cm.

The rockfill is less frequent and often more modest. It is in *Fouboudzivouni* where its dimensions are critical with 84.8 m of length, 1.70 m of average height, and 2.60 m of average thickness.

The cliff exceeds 400 m in length with 5 m of average height in the south of the beach of *Mbachile*. It is formed by three primary strata: coarse sandstone full of olivine grains on the bottom, fine-grained siltstone, and silt on the top. On the upper beach of *Ndroude*, the cliff is particularly

Table 1 Coastal erosion risk classification matrix. Modified from de Gouveia Souza and Suguio (2003)

Number of coastal erosion indicators types	Spatial distribution along the shoreline			
	> 60%	41–60%	21–40%	≤ 20%
4	Very high risk	Very high risk	High risk	High risk
3	Very high risk	High risk	Moderate risk	Moderate risk
2	High risk	Moderate risk	Moderate risk	Low risk
1	Moderate risk	Moderate risk	Low risk	Low risk
0	Very low risk			

Table 2 Spatial distribution of shoreline indicators

Study areas	Length of shoreline (m)	Spatial distribution				
		Vegetation limit (%)	Top of cliff (%)	Top of dam (%)	Top of rock fill (%)	High water level (%)
Bangoi-Kouni	1119	71	0	29	0	0
Mitsamiouli	2296	68	0	21	0	11
ICONI	1889	13	0	66	0	21
MBACHile	1338	6	30	64	0	0
Moindzaza-Amboini	1639	97	0	0	0	3
Male	2787	92	8	0	0	0
Foumboudzivouni	842	75	5	0	10	10
Hantsindzi	2129	89	0	8	3	0
Ndroude	1565	82	15	0	3	0

constituted by grave silt, but in the east of the coast of *Male*, a stratum of argillaceous silt surmounts volcanic slags. It extends on 324.50 and 232 m, respectively, with 2 m in average height in these areas. The most iterative plants are *Cocos nucifera*, *Terminalia catappa*, and *Guetterda speciosa*.

Historical relics including mosques, houses, cemeteries, and pier are currently located on the present shoreline. The mosques are present on the shore of *Bangoi-kouni* (SHI-WUDA), *Male* (MBUZINI and NDRERENI), and

Foumboudzivouni (WEGNA MAHATUBU and NEMANI). Older cemeteries have located in *Male*, *Hantsindzi*, *Foumboudzivouni*, and *Bangoi-kouni*.

3.3 Risk Classification

The results of risk classification display 56% for moderate risk, 22% for high risk, and 22% for low risk. No shore shows a very high risk (Table 3). The majority reveal a

Table 3 Risk classification of study areas

Study area	Coastal erosion indicators				Spatial distribution (%)	Risk classification
	Cliff	Protection structure	Vegetation degradation	Historical relic		
Bangoi-Kouni		X		X	29	Moderate
Mitsamiouli		X	X	X	21	Moderate
ICONI		X			66	High
Mbachile	X	X			93	High
Moindzaza-Amboini		X			0	Low
Male	X		X	X	8	Moderate
Foumboudzivouni	X	X		X	15	Moderate
Hantsindzi		X		X	11	Low
Ndroude	X	X	X		18	Moderate

moderate risk and their distributions oscillate between 8 and 29%. The shores of *Moindzaza-Amboini* and *Hantsindzi* are the only ones to show a low risk.

4 Discussion

The shoreline mapping showed many similarities with the Global Climate Change Alliance program study in Ngazidja (Courboules 2018) even if we used many shoreline indicators. The vegetation limit has allowed displaying the human actions to the detriment of coastal flora (Maximy 1968). The protection structures, degradation of coastal vegetation, and the current situation of historical relics on or about some meters of the shoreline would be some responses of sea-level rise like shown by regional studies (Zinke et al. 2003).

5 Conclusion

The shoreline mapping has permitted to underline the essential artificial fixing of the shoreline. On 16 km of shoreline length sampled, 20% were fixed by the dam. The quantification of coastal erosion indicators exhibits a considerable frequency of cliffs and dams. The other indicators present a limited number of some areas. The risk classification displays moderate risks for the nine investigated coastal areas. Only the coasts of *Mbachile* and *IKoni* present a high risk which is relative to the quasi-diking of these coasts.

References

- Bernatchez, P., Fraser, C., Lefavre, D., Dugas, S.: Integrating anthropogenic factors, geomorphological indicators and local knowledge in the analysis of coastal flooding and erosion hazards. *Ocean Coast. Manag.* **54**(8), 621–632 (2011). <https://doi.org/10.1016/j.ocecoaman.2011.06.001>
- Boak, E.H., Ian, L.T.: Shoreline definition and detection: a review. *J. Coastal Res.* **21**(4), 688–703 (2005). <https://doi.org/10.2112/03-0071.1>
- Cherian, A., Chandrasekar, N., Gujar, A.R., Rajamanickam, G.V.: Coastal Erosion Assessment along the Southern Tamilnadu Coast, India (2012). <http://drs.nio.org/drs/handle/2264/7596>
- Courboules, J.: Carte Des Classes Côtières à La Grande-Comore, 1:10 000. Programme AMCC En Union Des Comores, EU-AGRER-Direction Générale de l'Environnement et de Forêts (2018)
- de Maximy, R.: Archipel Des Comores: Étude Géographique (1968)
- de Gouveia Souza, C.R., Suguio, K.: The coastal erosion risk zoning and the São Paulo state plan for coastal management. *J. Coastal Res.* **35**, 530–547 (2003). <https://www.jstor.org/stable/40928805>
- Faye, I.: Dynamique du trait de côte sur les littoraux sableux de la Mauritanie à la Guinée-Bissau (Afrique de l'Ouest): Approches régionale et locale par photo-interprétation, traitement d'images et analyse de cartes anciennes. Phdthesis, Université de Bretagne occidentale—Brest (2010). <https://tel.archives-ouvertes.fr/tel-00472200/document>
- Hanslow, D.J.: Beach erosion trend measurement: a comparison of trend indicators. *J. Coastal Res.* **SI50**, 588–593 (2007)
- IPCC.: Assessments of Impacts and Adaptations to Climate Change (AIACC/START/TWAS), AIACC Research Project—Indian Ocean, April 9 2002 (2001)
- IPCC.: Annex II: Glossary [Mach, K.J., Planton, S., von Stechow, C. (eds.)]. In: Climate Change 2014: Synthesis Report. Contribution of Working Groups I, II and III to the Fifth Assessment Report of the Intergovernmental Panel on Climate Change [Core Writing Team, Pachauri, R.K., Meyer, L.A. (eds.)]. IPCC, Geneva, Switzerland, pp. 117–130 (2014)
- Ministry of Rural Development, Fishery, Arts and crafts, and Environment: Programme d'action Nationale d'adaptation Aux Changements Climatiques (PANA), 92 p (2006)
- Priest, G.R.: Coastal Shoreline Change Study Northern and Central Lincoln County, Oregon. *J. Coastal Res.* **SI28**, 140–157 (1999)
- Sinane, K.M.: Les Littoraux Des Comores, Dynamique d'un Système Anthropisé : Le Cas de l'île d'Anjouan. Thesis, La Réunion (2013). <http://www.theses.fr/2013LARE0027>
- Zinke, J., Reijmer, J.J.G., Thomassin, B.A., Dullo, W.C., Grootes, P.M., Erlenkeuser, H.: Postglacial flooding history of Mayotte lagoon (Comoro Archipelago, Southwest Indian Ocean). *Marine Geol.* **194** (3), 181–96 (2003). [https://doi.org/10.1016/S0025-3227\(02\)00705-3](https://doi.org/10.1016/S0025-3227(02)00705-3)



Effect of Salt Accompany with Sodium Chloride on Soil Loss by Wind Erosion in the Dried Bed of Uremia Lake

Abbas Ahmadi, Shahin Oustan, and Nazanin Gholampour

Abstract

The present study investigates the effect of sodium sulfate and magnesium chloride salts along with sodium chloride on the resistance of salt crusts against soil erosion. A soil sample from the previous bed of Uremia Lake was collected, and concentrations of sodium and magnesium ions from that sample were determined. Then, the concentration of each ion in the soil sample was increased twofold and threefold by adding sodium sulfate and magnesium chloride salts solutions. Two types of crust treatment were prepared: crusted and crustless soil. The experiment was conducted in a completely randomized design with two crusts treatments and five salt concentration treatments. Treatments were: N0: control treatment (no salt added), N1: twofold increasing initial sodium sulfate values treatment, N2: threefold increasing initial sodium sulfate values treatment, M1: twofold increasing initial magnesium chloride values treatment, and M2: threefold increasing initial magnesium chloride values treatment. Salt solutions were used in two forms: (1). spraying salts on the surface of soil samples without mixing of soil and (2). spraying salts on the soil surface and swirling of soil with a spatula. So, after drying of samples, there were two types of soil samples: crusted and crustless samples. After that, all samples were placed into the wind tunnel, and soil loss from each treatment was measured. The highest soil loss was observed in soil samples treated with sodium sulfate and the lowest in magnesium chloride treatments.

Keywords

Magnesium chloride • Sodium chloride • Surface crust • Wind erosion

1 Introduction

Dried bed of Uremia Lake has become one of the dust emission sources in the last few years due to prolonged drought and mismanagement of water resources in this area (Ahmadi 2013). The Ca^{2+} and Na^{+} are the dominant cations (Gaury et al. 2018; Kumar et al. 2019a), and SO_4^{2-} and HCO_3^{-} are dominant anions in lakes water (Kumar et al. 2019b). In inland salt lakes, the concentrations of Ca^{2+} , Mg^{2+} , Na^{+} , K^{+} , and HCO_3^{-} varied during the season, due to changing temperature, rainfall pattern, and human activities (Aliat et al. 2016; Chenchouni 2017). Salt crust is one of the natural coatings, which is developed on the soil surface and prevents soil from wind erosion and production of dust storms (Nield et al. 2016). The present experiment aims to investigate the effect of sodium sulfate and magnesium chloride salts along with sodium chloride on the resistance of salt crusts against soil erosion.

2 Materials and Methods

A soil sample was provided from 0 to 5 cm of the previous bed of Uremia Lake. Significant characteristics of this soil are high salinity ($\text{ECe} = 99 \text{ dS/m}$ in saturation paste extract), high sodium content, and loam texture class. The study was conducted in a completely randomized design and under two conditions: crusted and crustless soil with five salt treatments in three replications. Salt treatments were: controlled (N0: no salt added), N1: twofold increasing initial sodium sulfate concentration, N2: threefold increasing initial sodium sulfate concentration, M1: twofold increasing initial magnesium chloride concentration, and M2: threefold increasing initial magnesium chloride concentration. Before the experimental setup, the initial concentrations of sodium and magnesium ions from the soil sample were determined. Then, the

A. Ahmadi (✉) · S. Oustan · N. Gholampour
University of Tabriz, Tabriz, East Azerbaijan Province, Iran
e-mail: A_ahmadi@tabrizu.ac.ir

sodium sulfate and magnesium chloride were dissolved in distilled water individually and sprayed on the surface of soils until reaching the FC-equivalent humidity condition. Salt solutions were used in two forms: (1). spraying on the surface of soil samples without mixing of soil and (2) spraying on the soil surface and swirling of soil with a spatula. So, two types of crust treatments were prepared (crusted and crustless soil). After drying the soil moisture contents (depending on the soil texture, it took about one month to dry the moisture content completely), the trays were placed inside of a wind tunnel for 10 min under 16 m/s wind speed, and total soil loss in each tray was determined. Analysis of variance between treatments and the comparison of means of the treatments were analyzed using MSTATC software.

3 Results and Discussion

Table 1 shows analysis of variance of salt treatments results. Results showed that salt treatments and affected soil losses.

Figure 1 shows that in crustless condition there are no significant differences between salt added treatments and control treatment, but soil loss in N1 and N2 treatments were significantly higher than M1 and M2 treatments.

Figure 2 shows soil loss values from crusted soil samples. Results showed that increasing sodium sulfate caused to increase of soil loss, so that N1 and N2 treatments had more soil loss values in comparing control treatment, but magnesium chloride caused the decrease of soil loss significantly. Therefore, M1 and M2 treatments had less soil loss values.

4 Conclusion

Increasing sodium sulfate concentration boosts soil loss, whereas increasing magnesium chloride decreases soil loss in extra saline soil of the Uremia Lake dried bed.

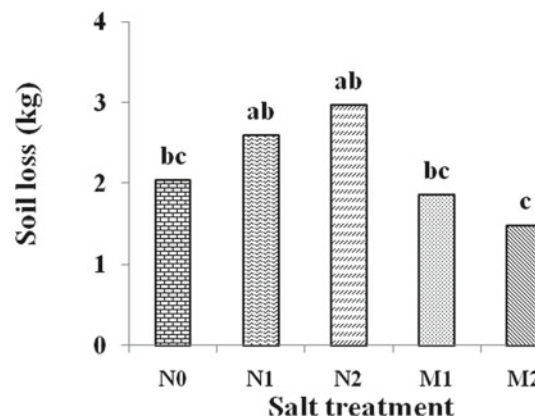


Fig. 1 Soil loss from each salt treatment in crustless soil condition (N0: no salt add, N1 and N2: twofold and threefold increasing initial sodium sulfate concentration, respectively, and M1 and M2: twofold and threefold increasing initial magnesium chloride concentration, respectively)

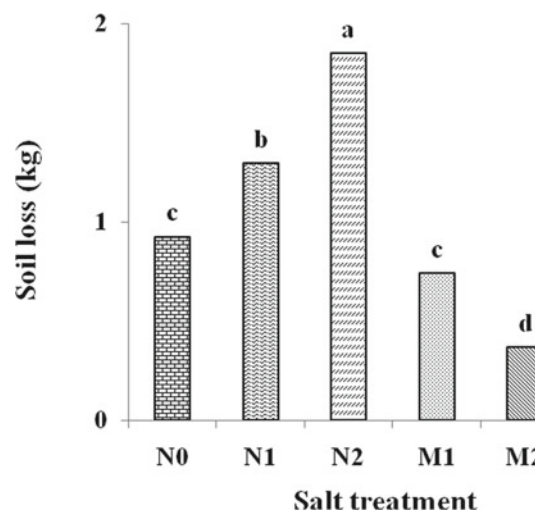


Fig. 2 Soil loss from each salt treatment in crusted soil condition (N0: no salt add, N1 and N2: twofold and threefold increasing initial sodium sulfate concentration, respectively, and M1 and M2: twofold and threefold increasing initial magnesium chloride concentration, respectively)

Table 1 ANOVA table of soil loss from salt treatments

Source	Df	Mean squares (MS)	
		Soil loss (in crustless treatment)	Soil loss (in crusted treatment)
Salt treatments	4	13.6*	12.4*
Error	10	2.133	0.533
CV (%)	–	18.57	19.56

* significant at the P -value = 0.01

References

- Ahmadi, A.: Uremia lake drying, reasons and its consequences. In: 1st International Conference on Environmental Crisis and its Solutions, Kish, Iran, (2013)
- Aliat, T., Kaabeche, M., Khomri, H., Nouri, L., Neffar, S., Chenchouni, H.: A pedological characterisation of some inland wetlands and Ramsar sites in Algeria. *Land Degrad. Dev.* **27**(3), 693–705 (2016). <https://doi.org/10.1002/ldr.2467>
- Chenchouni, H.: Edaphic factors controlling the distribution of inland halophytes in an ephemeral salt lake “Sabkha ecosystem” at North African semi-arid lands. *Sci. Total Environ.* **575**, 660–671 (2017). <https://doi.org/10.1016/j.scitotenv.2016.09.071>
- Gaury, P.K., Meena, N.K., Mahajan, A.K.: Hydrochemistry and water quality of Rewalsar Lake of Lesser Himalaya, Himachal Pradesh, India. *Environ. Monit. Assess.* **190**(2), 84 (2018). <https://doi.org/10.1007/s10661-017-6451-z>
- Kumar, P., Mahajan, A.K., Meena, N.K.: Evaluation of trophic status and its limiting factors in the Renuka Lake of Lesser Himalaya, India. *Environ. Monit. Assess.* **191**(2), 105 (2019a). <https://doi.org/10.1007/s10661-019-7247-0>
- Kumar, P., Meena, N.K., Mahajan, A.K.: Major ion chemistry, catchment weathering and water quality of Renuka Lake, north-west Himalaya, India. *Environ. Earth Sci.* **78**(10), 319 (2019b). <https://doi.org/10.1007/s12665-019-8315-z>
- Nield, J.M., Neuman, C.M., O'Brien, P., Bryant, R.G., Wiggs, G.F.: Evaporative sodium salt crust development and its wind tunnel derived transport dynamics under variable climatic conditions. *Aeol. Res.* **23**, 51–62 (2016). <https://doi.org/10.1016/j.aeolia.2016.09.003>



Identifying Vulnerable Lands Using the Duration-Frequency of Mediterranean Exceptional Rainfall Events in Semiarid Watersheds

Khaoula Khemiri and Sihem Jebari

Abstract

Rainfall in Tunisia is characterized by spatiotemporal variability. It presents a high severity, extension and intensity generate water erosion. The main objective of this paper is to assess water erosion risk under a modeling approach, from storm events of a particular design frequency and duration, in order to identify sensitive land, to develop means to control this phenomenon, and to protect the environment and plan for sustainable use of the country's heritage resources. Thematic layers were integrated into the GIS environment by using the modified universal soil loss equation. The Merguellil watershed was divided into three sub-watersheds, and soil erosion was calculated using the model and compared to observed data. For the simulated events, results reproduced well the observed degradation induced by the erosion processes. The highest rate of soil erosion is found in the northern part of the Merguellil watershed, and we can, therefore, conclude that the areas of more excellent sediment production are related to high volumes of runoff. The watershed displays two kinds of erosion: sheet erosion (flow over the area) and linear erosion (channel formation due to water concentration). Besides, the study showed that Skhira and Haffouz sub-watersheds had the highest rate of specific erosion. In conclusion, these two sub-watersheds require a priority of soil conservation planning to protect the agricultural heritage and El Houarreb dam downstream against siltation.

Keywords

Water erosion • Storm events • MUSLE • Sub-watersheds

1 Introduction

In semiarid countries and Mediterranean regions, soil erosion, due to rain and runoff, is a widespread phenomenon causing land- and water-quality degradation (Arar and Chenchouni 2014). The potential risk of soil erosion in Tunisia is severer than that in other Mediterranean countries (Smetanová et al. 2019). Nonetheless, about 3 million hectares of agricultural lands are threatened by erosion with 50% severely affected, which causes dams and hydraulic infrastructure siltation. To protect the natural resources, the Tunisian government launched, since the 1960s, three successive and complementary strategies in the framework of the Water (Chevrillon et al. 2017), and encourages research projects to assess and predict soil loss in order to consider not only the agricultural heritage as resources to exploit but as common goods to keep. In this context, erosion modeling has become a necessary decision-making tool for the hydrologists in order to be able to conserve agricultural heritage (Negm et al. 2020). Despite the considerable number of erosion models, Universal Soil Loss Equation: USLE (Wischmeier and Smith 1978), its revised version RUSLE (Renard et al. 1994), and its modified version 'MUSLE' (Williams 1975), are widely used over the world (Sadeghi et al. 2014), and especially in Tunisia. Coupled with a Geographic Information System (GIS), it allows quantifying water erosion spatially at the watershed scale (Djoukbal et al. 2019). Also, the integration of the thematic layers in GIS allows defining the impact of each factor in the soil losses process, in terms of quantity and quality, and to prioritize vulnerable areas. The present study aims to seek an analytic and synthetic approach to assess soil erosion risk in

K. Khemiri (✉) · S. Jebari
National Research Institute for Rural Engineering,
Water and Forestry, Tunis, Tunisia

K. Khemiri
National Engineering School of Tunis, Tunis, Tunisia

the Merguellil watershed, located in the center of Tunisia, which is characterized by a semiarid climate, with short duration torrential rainfall (Hajji et al. 2017). The choice for modeling is based on a model that can simulate water erosion on a storm event scale interfaced with the GIS in order to evaluate the phenomenon spatiotemporally.

2 Materials and Methods

Site of study

The Merguellil watershed is located in Central Tunisia, between the parallels 39°60'N 7°55'E and 39°78'N 8°35'E, covered 1183 km². The watershed elevation ranges from 200 to 1200 m, with an average of 500 m (Fig. 1b), divided into three sub-watersheds (Fig. 1a), namely: Skhira (194 km²), Haffouz (480 km²), and El Houarreb (509 km²). The intermittent hydrographic network of Merguellil river starts at an altitude of 950 m (Fig. 1a), supplying El Haouareb reservoir. It was built in 1989. Merguellil watershed is typical of semiarid environments, with a rainfall which is low, 265 mm

in the plain and 515 mm in the upstream, and it is characterized by intense event, especially in spring and autumn, causing river flooding.

Model description

The MUSLE model (1) (Williams 1975) is a modified version of the USLE model (Wischmeier and Smith 1965). This model replaced the rainfall factor (R) with instantaneous peak flows and total runoff factor to predict soil erosion (Djoukbal et al. 2019).

$$Y = \alpha(Q \cdot q_p)^\beta K.L.S.C.P \quad (1)$$

where Q is volume of runoff in m³, q_p is peak flow rate in m³ s⁻¹ and K , L , S , C and P are, soil erodibility, slope length, slope steepness, crop management and soil erosion control practice factors, respectively. Similar to the USLE model, and α and β are location coefficients. For the areas where the equation was developed, α and β were 11.8 and 0.56, respectively.

The present study was, therefore conducted to calibrate the MUSLE model and estimate the specific erosion in the

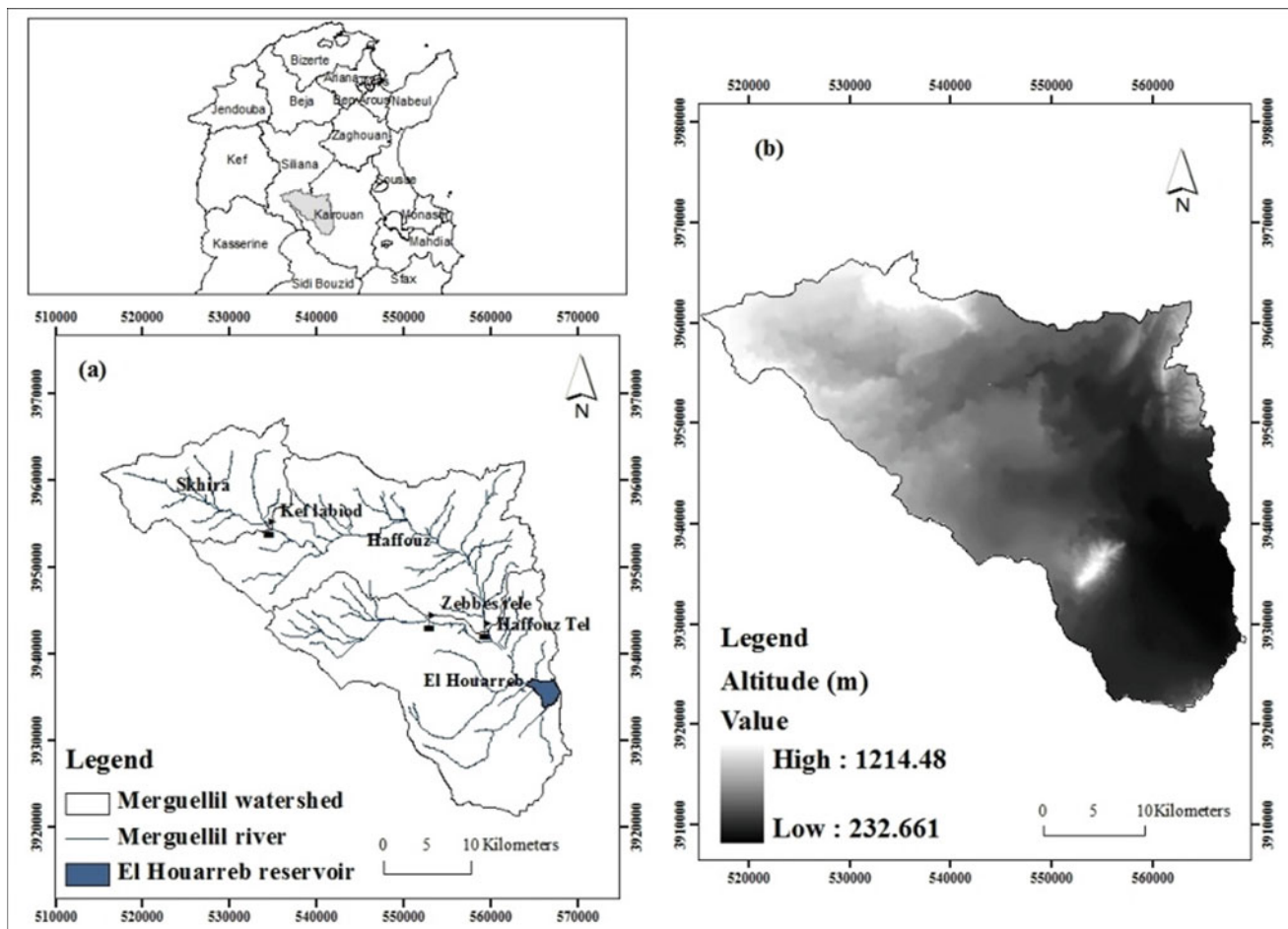


Fig. 1 Location and digital elevation model of the Merguellil watershed: **a** Location, **b** DEM

Merguellil sub-watersheds. The model was calibrated, by optimizing the two MUSLE coefficients, using the raw best data observed during storm events (suspended sediment data, the volume of runoff, and peak flow rate) at the Haffouz and Skhira Kef Labiodh flow-gauge Telepheric stations.

The database used in this work composed of: The LS factor was calculated from the digital elevation model. It was generated from contour lines provided by the significant state maps (1/50000) (DG/ACTA 2000) with contour intervals of 10 m, with a spatial resolution of 30 m. The storm events data are collected from the Haffouz, Zebbes and Skhira flow-gauge Telepheric stations over the observation period of eleven years (2003–2014). The C factor was obtained from land-use map. It is extracted from Landsat 7 ETM + C1 Level-1 (for the date May 05, 2003) from the USGS Earth Explorer. The K factor was generated from soil map, provided by the agricultural map developed in 2000, field visits allowed the update. The P factor was obtained

from the water and soil conservation works, from an agricultural map, and updated from Google Earth (for the date May 05, 2003).

3 Results and Discussion

The soil erosion rate, during the observation period, was the result of the MUSLE model factors combination, including the volume of runoff and peak flow during storm events. The MUSLE coefficients related to Merguellil sub-watershed were determined as well as the soil erodibility factor (K), the topographic factor (LS), the crop management factor (C), and the conservation support practice factor (P). These layers made it possible to know the soil erosion rate and spatial distribution all over our studied area. The outputs from the model were used to get the soil erosion (t/ha/yr) values. The results were then grouped into four classes (Fig. 2).

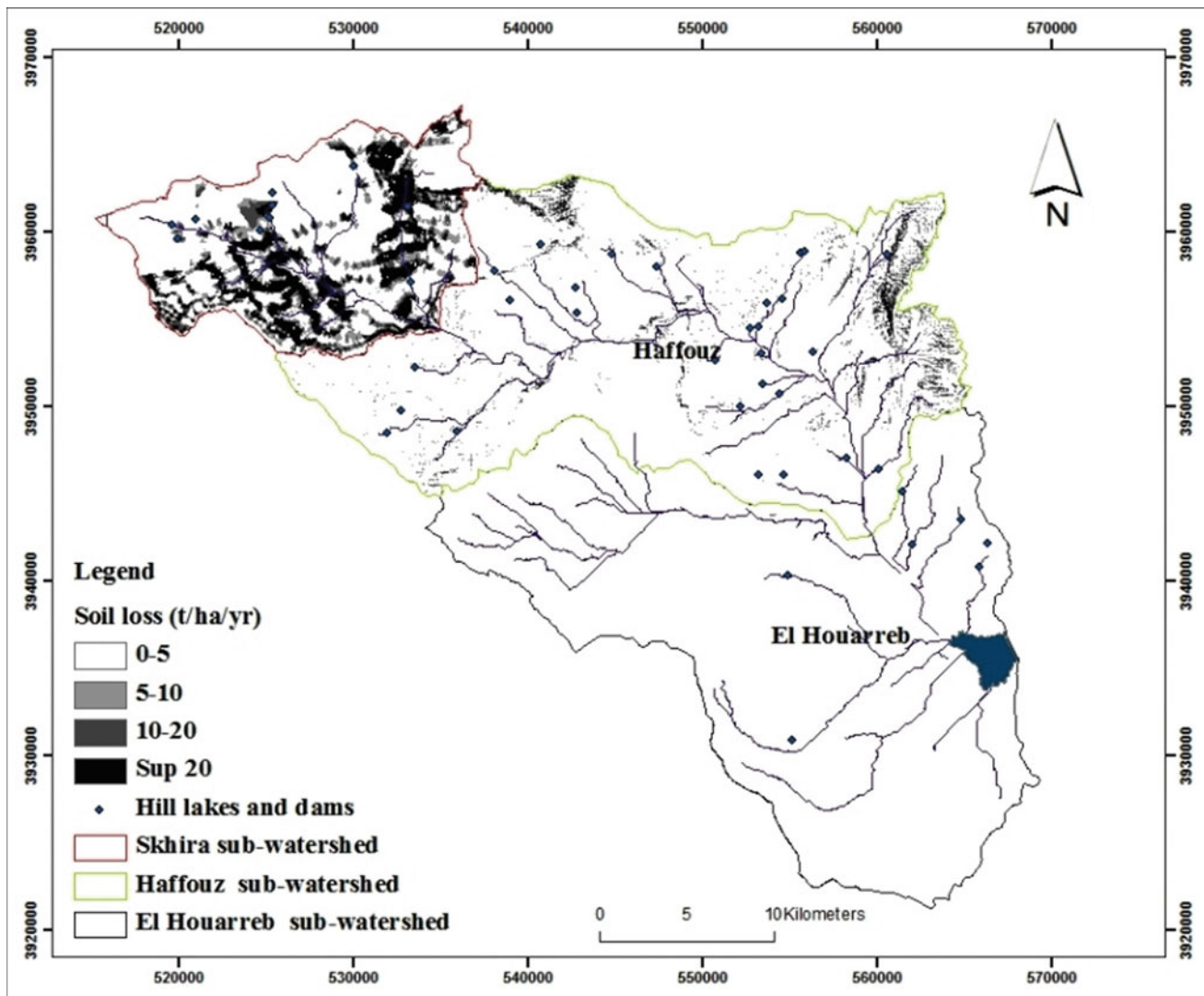


Fig. 2 Soil erosion map in the Merguellil watershed

Significant areas are affected by soil loss less than 5 t/ha/yr covering 80% of areas, followed by the moderate soil loss rate ranging from 5 to 10 t/ha/yr in 4% of areas. The high soil loss for the 10 to 20 t/ha/yr interval is covering 3% of the studied areas. Very high rates are displaying soil loss more than 20 t/ha/yr damage 13% of the areas. The most affected part by the erosion processes is shown in the northwestern part of the Merguellil watershed and specifically at Skhira, referring to Fig. 2. This sub-catchment is located in the foothills of the existing mountainous. It is characterized by moderately strong elevation levels and sparse vegetation cover. The high soil loss rate displayed in the northeastern part of Haffouz sub-watershed is considered a vulnerable zone with poorly developed soils. It is a deep but very erodible alluvial and calci-magnetic soils with cereal crops and rangeland use.

Results also showed that the spatial distribution of soil loss classes indicate that areas of greater sediment production are related to high volumes of runoff. The latter had impacts on the soil loss rates. The validation of the results was ensured via field trips and Google Earth (for the date May 05, 2014). The used model reproduced well the observed degradation induced by the erosion processes. The watershed displays two kinds of erosion: sheet erosion (flow over the area) and linear erosion (channel formation due to water concentration).

4 Conclusions

The main focus of this study is to assess soil loss rates spatially via the MUSLE model. The findings are interesting since observed processes were reproduced by the used modeling tool. The highest rate of soil erosion is found in the northern part of the Merguellil watershed. It covers a small area of the watershed. This explains the severity of soil degradation in the Merguellil watershed due to the high elevation, slope and topography factors. The MUSLE results expressed that specific erosion was directly affected by storm events and topographic factors. Results can be useful by a manager to select the most vulnerable zones and to adopt a suitable solution to conserve water and soil resources, especially in the arid and semiarid watershed.

Acknowledgements The authors are grateful for the helpful funding from the European Union Horizon 2020 program, under Faster project (grant agreement N°[810812]).

References

- Arar, A., Chenchouli, H.: A “simple” geomatics-based approach for assessing water erosion hazard at montane areas. *Arab. J. Geosci.* **7** (1), 1–12 (2014). <https://doi.org/10.1007/s12517-012-0782-4>
- Chevriillon, A., Ben Haha, N., Burte, J. : Vers une territorialisation des politiques rurales en Tunisie: l'exemple des politiques de conservation des eaux et des sols. In : Caron, P., Valette, E., Wassenaar, T., Coppens d'Eeckenbrugge, G., Papazian, V. (eds.) *Des territoires vivants pour transformer le monde*. Versailles, Quae, pp. 172–178 (2017)
- DG/ACTA: (Direction Générale de l'Aménagement et de la Conservation des Terres Agricoles), 2000, 2002. *Etude de protection du barrage El Houareb*. Ministère de l'Agriculture et des Ressources Hydrauliques (2000)
- Djoukbal, O., Hasbaia, M., Benselama, O., Mazour, M.: Comparison of the erosion prediction models from USLE, MUSLE and RUSLE in a Mediterranean watershed, case of Wadi Gazouana (N-W of Algeria). *Model. Earth Syst. Environ.* **5**, 725–743 (2019). <https://doi.org/10.1007/s40808-018-0562-6>
- Hajji, O., Abidi, S., Hermassi, T., Mekni, I.: Evaluation of water erosion risk in Tunisian Semi Arid Area. *Springer Water*, pp. 215–249 (2017). https://doi.org/10.1007/978-3-319-51856-5_13
- Negm, A., Bouderbala, A., Chenchouli, H., Barcelo, D.: *Water Resources in Algeria - Part I: Assessment of Surface and Groundwater*. Cham, Springer (2020). <http://doi.org/10.1007/978-3-030-57895-4>
- Renard, K.G., Foster, G.R., Weesies, G.A., McCool, D.K.: *Predicting soil erosion by water - a guide to conservation planning with the revised universal soil loss equation (RUSLE)*, Agriculture Handbook 703, US Govt. Printing Office (1994)
- Sadeghi, S.H.R., Gholami, L., Khaledi Darvishan, A., Saeidi, I.P.: A review of the application of the MUSLE model worldwide. *Hydrol. Sci. J.* **59**(2), 365–375 (2014). <https://doi.org/10.1080/02626667.2013.866239>
- Smetanová, A., Follain, S., David, M., Ciampalini, R., Raclot, D., Crabit, A., Le Bissonnais, Y.: Landscaping compromises for land degradation neutrality: the case of soil erosion in a Mediterranean agricultural landscape. *J. Environ. Manage.* **235**, 282–292 (2019). <https://doi.org/10.1016/j.jenvman.2019.01.063>
- Williams, J.R.: Sediment-yield prediction with universal equation using runoff energy factor. In: *Present and prospective technology for predicting sediment yield and sources*. ARS.S-40, US Gov. Print. Office, Washington, DC, pp. 244–252 (1975)
- Wischnmeier, W.H., Smith, D.: *Predicting rainfall erosion losses: guide to conservation planning*. USDA, Agriculture Handbook 537. U.S. Government Printing Office, Washington, DC (1978)



Inland Water Resources Depletion Under CO₂ Accusation

Miah Muhammad Adel

Abstract

Extreme summertime heating and wintertime cooling are characteristics of the lack of heat-absorbing and storing water bodies. Upstream water piracy yielded the downstream Aral Basin disaster making its summer warmer and winter colder than before. CO₂ did not play a role there. The lower Ganges basin has been turned into another Aral Sea basin due to the diversion of the Ganges's course by the Farakka Barrage and constructions of dams and barrages upon other Indo-Bangladesh transboundary rivers by India. Estimation of heat absorption and retention by water bodies in the Gangetic Bangladesh shows that the land has been subjected to about ten times more summer heating and winter cooling in the water piracy period. India even threatened her western neighbor Pakistan cutting off water supply voiding the six-decade-old Indus Treaty. Another upstream country's building of dams is going to make more Aral Sea basins in the lower Brahmaputra and the Mekong basins. Several other examples may be brought for other international river basins. Climatologists are very vocal on the CO₂ emission but are silent on the inland water resources depletion. Their inaction on the issue let the upstream riparian countries leverage their water resources depriving the downstream countries' water needs and thus support water resources depletion. The water-deprived downstream becomes a victim of a domino effect. Let climatologists' inaction be not supportive of regional unsustainability and ecosystem destruction.

Keywords

Extreme climate • CO₂ • Ganges basin • Aral Sea basin • Upstream water piracy • Farakka Barrage • Indus Treaty • Brahmaputra basin • Mekong basin • Climatologists • Domino effect

1 Introduction

For earning quickly economic self-sufficiency, some upstream countries are exploiting water resources (<https://www.icsin.org/uploads/2015/07/30/6ff173636ce87ec3825e98fb4a0891ec.pdf>) pirating downstream ecosystem's elixir triggering a domino effect in the downstream. Obvious downstream consequences include surface water resources depletion, riverbeds silting, rivers' increased incapacity to accommodate and discharge sudden water onrush released from the upstream, devastating flood occurrences, heat reservoirs losses, extreme climate generation, saline water front's inland advances, enhanced dependence on groundwater, groundwater table's deep sinking, groundwater contamination, arsenicosis breakouts, family ties breakups, social instability creations, breeding and raising grounds of fishes and other aquatic species and amphibians destructions, increased malnutrition, waterborne and environmental diseases outbreaks, soil organic matter losses, agricultural practice changes, inland navigable routes eradication, livelihood losses, biodiversity losses, increased lightning frequencies and fatalities, religious observances, and pastimes obstructions (Adel 2001). Out of those effects, the article focuses on the generation of extreme climate. Climatologists are more concerned with the global production of CO₂ and do not address the impact of the depletion of inland surface water resources on climate change. Brown (1991) shows the generation of extreme climate among other effects in the Aral Sea basin due to water diversion by the former Soviet Union from the Amu Darya and Sir Darya.

M. M. Adel (✉)
University of Arkansas at Pine Bluff, Pine Bluff, AR 71601, USA
e-mail: adelm@uapb.edu

Water bodies absorb and store heat in summer to reduce their intensity and release it in winter to control temperature drop. The article shows the heat loss in the downstream Ganges due to its water piracy by the Farakka Barrage at the upstream.

2 Settings

The lower Ganges basin (Fig. 1) is like an open laboratory to test what effects can happen if a riverine water-abundant land is turned waterless. Upstream India has built dams and barrages on more than 50% of almost sixty transboundary rivers between India and Bangladesh, on top of building water diversion constructions on the primary, secondary, tertiary, and quaternary tributaries of the main rivers (Adel 2015, 2018). The study is focused on the Ganges basin since the Ganges shapes the lifestyle of the one-third population of Bangladesh. India has been pirating the Ganges water (Fig. 2) for more than four decades—sometimes unilaterally and sometimes under the pretext of following a namesake fragile water sharing treaty in the middle of marathon number of meetings (Adel 2013, 2015). Climate data about the Ganges basin in Bangladesh were analyzed to find any climatic changes in the wake of the upstream water piracy by the Farakka Barrage upon the Ganges (# 6 in Fig. 1). The piracy reduced the Ganges' discharge through its lower basin by more than 75% from a pre-piracy average value of $1932 \text{ m}^3 \text{ s}^{-1}$, depleting water availability in flood plains, ponds, canals, and ditches, and dropping the groundwater table by about 25 times more than the pre-piracy period dry season. It took about five years beyond the water piracy starting in 1975 to unfold the environmental impacts that set 1982 as the baseline year (Fig. 3).

3 Results

Since the 1980s, the northwestern and the southwestern parts of tropical Bangladesh located in the downstream Ganges basin have been having summer temperature above $42.78 \text{ }^\circ\text{C}$ and winter temperature as low as $2.78 \text{ }^\circ\text{C}$. In the post-baseline era during the piracy period: (1) heating degree days (HDDs) (cumulative sum of the daily difference between the average temperature and the threshold temperature of $30 \text{ }^\circ\text{C}$ for March through November) and cooling degree days (CDDs) (cumulative sum of the daily difference between the average temperature and the threshold temperature of $15 \text{ }^\circ\text{C}$ from mid-November, December, January, and February) were, respectively, 1.33 and 1.44 times more than their counterparts during the pre-baseline era; (2) the summertime and wintertime average temperatures were, respectively,

$1 \text{ }^\circ\text{C}$ more and $0.5 \text{ }^\circ\text{C}$ less than the corresponding values during the pre-baseline era; (3) the mode $32 \text{ }^\circ\text{C}$ of summertime maximum temperatures was $1 \text{ }^\circ\text{C}$ higher and occurred 414 times more, and the mode $25 \text{ }^\circ\text{C}$ of wintertime temperature was $1 \text{ }^\circ\text{C}$ less and occurred 17 times less than the corresponding quantities during the pre-baseline era; (4) the average value of maximum relative humidity has increased by more than 2% and that of minimum relative humidity has dropped by the same amount; (5) the mode 95% and 70% of maximum and minimum relative humidity values have occurred 1322 times and 84 times more, respectively, than their pre-baseline counterparts; and (6) the frequency for 100 mm or more rainfall and the monthly average rainfalls have dropped by about 50 and 30%, respectively (Adel 2002). Summertime maximum temperature, HDDs, and CDDs are negatively, and minimum wintertime temperature is positively correlated with the decline of the Ganges's discharge. The approximate heat loss (Table 1) in the environment was calculated from the seasonal and annual water sources absorption and retention.

The entire Ganges basin has lost, at least ten times, the heat used to store in the water-abundant days (Adel et al. 2014). Water bodies absorb and store heat in summer for release in winter to stop summertime warming and wintertime cooling. About 45% evaporation of the massively extracted groundwater by Bangladesh to make up for the surface water shortage goes to merely increase the relative humidity without causing rainfall. Summertime lingering high temperature and high humidity cause the severity of summer weather.

4 Discussion

The issue was raised in the American Meteorological Society's Climate Studies Diversity Project Workshop in Silver Springs, MD (https://drive.google.com/drive/u/1/folders/1xTdAnDqlyn_dcMdDqID2TdC12UQv3-Sf). Niepold (2018), from the NOAA Climate Program Office, admitted the truth of the matter. However, due to many factors, AMS was unable to address all the aspects—the Nobel Laureate. Alley (2018) from Penn State University did not support it. He stressed that energy availability could solve the problem. Alley did not know that India rot surplus in northwest Punjab's storage the production, processing, and storing of which needed the costly commodity energy that India excels in (Choke Point: India initiative, an exploration into the water-energy-food confrontations in the world's second most populous country on April 2, 2014 by the Circle of Blue and the Wilson Center (China Environment Forum Choke Point: India—A Wilson Center-Circle of Blue Joint Initiative, April 02, 2014/9:00 am–11:00 am).

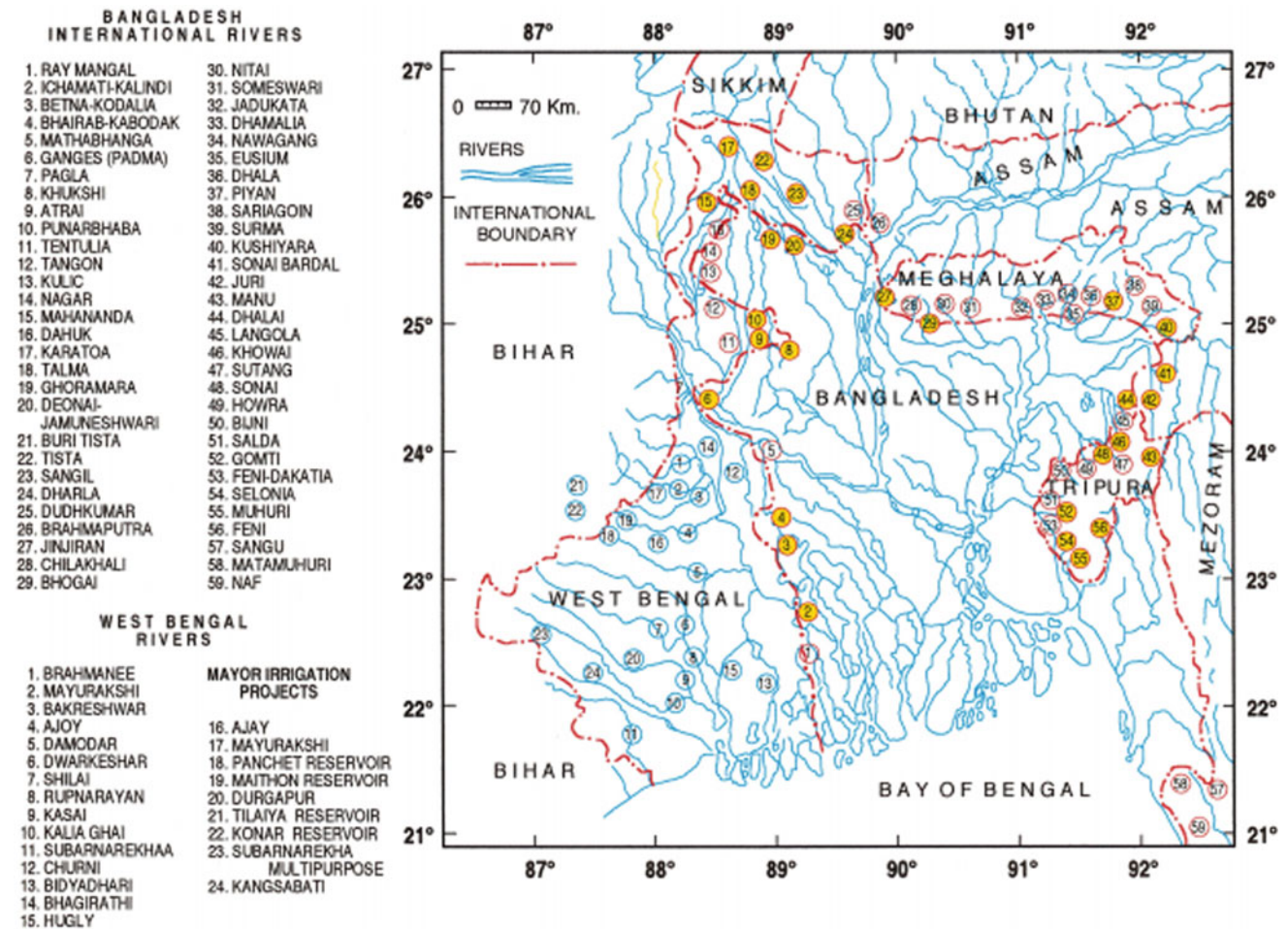


Fig. 1 Bangladesh, the dam-locked delta. Left side top shows the names of rivers. Water piracy goes upon, at least, the yellow-spotted rivers on the map. Left side bottom has the list of West Bengal rivers and the dams and reservoirs on the tributaries of the Hooghly River (Adel 2001).

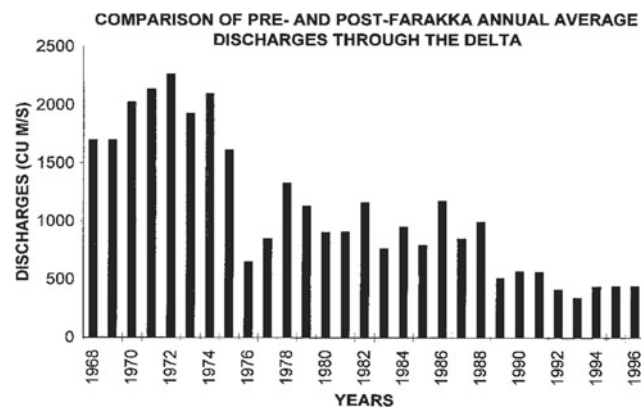


Fig. 2 Ganges’s decreased flow (Hebblethwaite 1997)



Fig. 3 Dried-up miles-wide Ganges (Donald Katz (<http://donnybangla.blogspot.com>))

Table 1 Pre- and ongoing-piracy periods minimum heat retention estimates

Source	Pre-piracy period		Ongoing-piracy period	
	Water	Heat	Water	Heat
	(Sq km)	(kJ)	(Sq km)	(kJ)
Village surface water bodies	2.70E-2	4.44E10	6.75E-3	1.11E10
Least surrounding flood plain	1.51	2.48E13	3.8E-1	6.23E11
Entire Ganges basin surface water	786	1.29E15	197	3.24E14
Entire Ganges basin flood plain	44,043	7.24E16	11,011	1.81F16

Nevertheless, the upstream country wants to subjugate the downstream country using water weapon (Adel 2013). She uses dams to block water flow in the dry season and opens the dams when she cannot accommodate excess water in the rainy season. India's Grand River Networking plan is to subjugate Bangladesh and Pakistan. Also, the drying of the Aral Sea was due to earning excellence in cotton production.

5 Conclusion

Inland surface water resources are a significant factor to avoid climate change. Climatologists should be as vocal on the exploitation of water resources as they are on CO₂ emission to maintain a livable environment for the inhabitants of this planet. If they can be vocal on CO₂ emission by the industrialized nations, there should not have any reason not to raise voice against the indiscriminate water exploitation, the elixir of this living planet. India should take lesson from her father of the nation Mahatma Gandhi's statement that the world has enough resources to meet everybody's need but to no one's greed. CO₂ emission causes global warming, but the H₂O exploitation causes the dual effects of warming as well as cooling. A balanced amount of H₂O can protect the environment from extreme heating and cooling.

References

- Adel, M.M.: Effect on water resources from upstream water diversion in the Ganges basin. *J. Environ. Qual.* **30**(2), 356–368 (2001)
- Adel M.M.: Man-made climatic changes in the Ganges basin. *Int. J. Climatol.* **22**(8), 993–1016, Banner (2002). <https://doi.org/10.1002/joc.732>
- Adel, M.M.: Upstream water piracy, the strongest weapon of cornering a downstream nation. *Environ. Ecol. Res.* **1**(3), 85–128 (2013). <https://doi.org/10.13189/eer.2013.010301>
- Adel, M.M.: Farakka Barrage Vol 1: the symbol of bluffing, blackmailing, bullying, and cornering downstream for upstream water piracy. Lap Lambert, Germany (2015)
- Adel, M.M.: Hegemonic attitude blocks fair sharing of transboundary water issue. *Environ Anal Eco Stud.* **1**(2), (2018). EAES.000509.2018. 21 <https://doi.org/10.31031/EAES.2018.01.000509>
- Adel, M.M., Hossain, M.R., Hossain, S.F.: Climatic severity victims of upstream water piracy strongly evidencing inland water depletion-caused global warming vis-a vis cooling. *Am. J. Environ Sci.* **10**(2), 171–298 (2014). <https://doi.org/10.3844/ajessp.2014.171.198>
- Alley, R.: An Optimistic View of Energy, Environment, and Our Future. Speech Delivered at the 6th Course Implementation Workshop, Silver Spring, MD; 29 July-3 August (2018)
- Brown, L.R.: The Aral Sea: Going, Going *WorldWatch* 4 (Jan/Feb), pp. 24–35 (1991)
- Hebblethwaite.: An undergrad thesis on the impact of the Farakka Barrage, University of New Castle upon Tyne, UK (1997)
- Niebold, F.: In: Building Effective Societal Response to Climate Change: Education, Speech Delivered at the 6th Course Implementation Workshop, Silver Spring, MD, 29 July-3 August (2018)



Assessment of Adolescent Health Risk Caused by Chemicals' Entry with Soil

Emilia Valeeva, Ismagilova Gulgena, Ziyatdinova Alfia, and Yusupov Neylya

Abstract

The main target organs and critical systems of exposure are identified; the priority contaminants and chemicals entering with soil and making a significant contribution to the total value of non-carcinogenic risk are specified. The Kirovsky and the Privolzhsky districts are the most contaminated districts concerning the value of total quotients (Z_c), and this fact can be explained by the concentration of industrial enterprises in these zones of the city. The priority pollutants of the urban soils are oil products, nitrates, cadmium sulfate and zinc. The dermal route is the most significant among all studied ways of the chemicals' entry. Higher distribution of the hazard quotient values for the adolescent health was revealed for the kidneys, the respiratory system, the blood and the hormones.

Keywords

Soil • Priority pollutants • Non-Carcinogenic risk • Health • Adolescents

1 Introduction

Health risk assessment is a method and basis to predict possible consequences of the chemical pollutant effects and make decisions to protect the vulnerable populations, upon which many International Environmental Organizations like WHO, FAO/WHO, the UN Commission, the European Union, WTO rely. Determining priorities in this field can facilitate the reduction of the burden of noncommunicable

E. Valeeva (✉) · I. Gulgena · Z. Alfia
FGAOU VPO “Kazan (Volga Region) Federal University”
Institute of Fundamental Medicine and Biology, Kazan, Russia
e-mail: val_med@mail.ru

Y. Neylya
FSBEI DPO Russian Medical Academy Continuous Professional
Education, Kazan, Russia

diseases of the adult and child population and increase of the population life expectancy (Tsybikova et al. 2015; Zastenskaya et al. 2013). National priorities should be determined based on a regional assessment of the health-related aspects of chemical safety, in particular, emerging issues on the quality control of environmental objects. We aim to assess the non-carcinogenic health risk of adolescents in the city of Kazan for the subsequent substantiation of recommendations for its reduction.

2 Methods or Materials

We analyzed the data obtained during the period of 2004–2018 in the course of carrying out of socio-hygienic monitoring and performed based on FSFHI “Center for Hygiene and Epidemiology in RT”. Soil samples were taken per GOST 17.4.3.01, “Methodological recommendations for conducting field and laboratory studies of soils and plants in the control of environmental pollution by metals” and “Temporary guidelines for monitoring soil pollution” using the “envelope” method, from points of “the elementary” site from a depth of 10 cm. The selection of sampling points was determined by the location of the street transport network of residential areas, enterprises and the correspondence to the sampling points. The selected soil sample was ground in a large porcelain mortar and sieved through a nylon sieve with a hole diameter of 1 mm. Non-sifted lumps of soil were ground and sieved again. Samples for analysis were taken from the soil sample obtained. The content of HM in the soil was determined by atomic absorption analysis based on RD 52.18.191–89 following MU “Methodology for measuring the mass fraction of acid-soluble forms of metal (copper, lead, zinc, nickel, cadmium) in soil samples by atomic absorption analysis”. The soil samples were taken on the territories of increased risk of impact on the population health—the residential areas, children's pre-school, school and medical institutions.

Results

High value of cadmium was identified only in the Sovetsky district (33.9). Zinc was revealed in all districts of the city, but the indices were insignificant: the Kirovsky (6.1), the Sovetsky, the Privolzhsky districts (3.2), and the Vakhitovsky district of the city (2.1) completed the list. The Kirovsky and the Privolzhsky districts were the most contaminated districts with respect to the value of total quotients (Zc), and this fact can be explained by concentration of industrial enterprises in these zones of the city. Comparative analysis of no-carcinogenic risk assessment among adolescents by different ways of entry showed that oil products made the most significant contribution to the risk, primarily with skin exposure.

Total weighted average of chemicals in the soils on the territory of the city of Kazan was distributed as follows. Initially, the oil products ranked first (the Vakhitovsky, the Sovetsky, the Kirovsky, the Privolzhsky districts—distribution in descending order). Nitrates ranked second (the Sovetsky, the Vakhitovsky, the Kirovsky, the Privolzhsky districts—in descending order), while sulfates ranked third (the Vakhitovsky (29.64), the Kirovsky (15.38), the Sovetsky and the Privolzhsky districts (7.19 and 4.49)) correspondingly.

Higher distribution of the hazard quotient values for the adolescent health was revealed for the kidneys, the respiratory system, the blood and the hormones. The risk of kidney diseases was identified in adolescents (0.025142–0.032787), of the Kirovsky and the Sovetsky districts correspondingly, at the level of the 95-th percentile of the hazard quotient. Hormones ranked second in the values of the risk of non-carcinogenic effects with high indices in the Privolzhsky and the Vakhitovsky districts (0.000157–0.000154). The risk for the blood diseases ranked third in general toxic effects of chemicals, high indices being observed in the Vakhitovsky district (0.000179–0.000302).

3 Discussion

With the inhalation route of exposure, the high value of cadmium was detected only in the Soviet district (33.9). Zinc was detected in all areas of the city, but the indicators were insignificant: The Kirovsky (6.1), the Sovetsky, the Volga (3.2) and Vakhitovsky district of the city (2.1) supplement the list. We determined by carried out research that the average total amount of chemicals did not exceed the

established hygienic normatives. The detectable concentrations of oil products can become the cause of a change in physical and chemical characteristics of the soil, result in dysfunction of its self-purification processes, increase of the pollutants' stability in the soil deteriorating the ecologo-hygienic state of the soil on the whole (Aydinov et al. 2017; Bekshin et al. 2017). The non-carcinogenic health risk for adolescents in the districts of the city of Kazan with the cutaneous route of exposure was: the Privolzhsky/Volga (0.00003), the Kirovsky (0.00004), the Sovetsky, (0.00006), and the Vakhitovsky (0.00006) districts. An excess of the reference dose is observed for the cadmium element in all areas, but the largest in the Vakhitovsky and the Sovetsky districts.

4 Conclusion

The priority pollutants of urban soils are oil products, nitrates, cadmium and zinc. The total non-carcinogenic risk was higher in the Kirovsky and the Vakhitovsky districts of the city, and the dermal path was the most significant among the chemical penetration pathways. The distribution of risk factors for adolescent health along the path of inhalation was determined for the following critical target organs: kidneys, hormones, blood and respiratory systems.

Acknowledgements This work was funded by the subsidy allocated to Kazan Federal University for the state assignment in the sphere of scientific activities 19.9777.2017/8.9.

References

- Aydinov, G.T., Marchenko, B.I., Deryabkina, L.A., Sinelnikova, Y.A.: Chemical pollution of the soil of the city of Taganrog as a risk factor for public health. *Analysis of Health Risk* **1**, 13–20 (2017)
- Bekshin, Zh.M., Turmukhambetova, A.A., Uzbekov, V.A., Belonog, A.A., Mamyrbayev, A.A., Perepichko N.Z.: Soil as a source of environmental risks. Problems of rationing and monitoring the level of soil contamination with chemicals. *Med. Ecol.* **3**(76), 42–47 (2017)
- Tsybikova, E., Shantanova, L., Tsybikov, E.: The influence of urbanization on the physical development of Buryat children. *Proceed. Joint Sci. Educ. Conf.* 76–77 (2015)
- Zastenskaya, I., Braubach, M., Héroux, M.E., Korol, N., Paunovic, E.: The potential of the member States of the European region of WHO in the field of prevention of negative effects of chemicals on public health and measures to strengthen it. *Hygiene Sanitation* **2013**(5), 11–15 (2013)



Assessing Preparedness-Insufficiency Spatial Patterns and Geostatistics to Build-Back-Better: An Application in Malinao Albay, Philippines

Ana Marie R. Abante

Abstract

This paper introduces a method to assess the six elements of risk: hazard; vulnerability; exposure; preparedness; coping capacity; and competency variables, wherein spatial patterns and geostatistical data created is logical to changing intervention needs and corrective-measures to get prepared. The technique in looking at correlated spatial patterns derived from the risk location quotients that are continuously distributed 2 km apart represented by points is seen a better way to start building-back-better, compared with the conventional way of reading a geohazard map with cartographic symbols and legends. With the IDW tool in ArcGIS and applying the Abante disaster risk estimate equation, preparedness-insufficiency was quantified and classified. The interpolation ascertains the risk location quotients for the entire Malinao is 119.04 risk location quotients (11,904% risk) for them become resilient. The study discloses that they remained unprepared and far from recovering from the past calamities and disasters. The risk will keep swelling as hazard events happen again and again, placing cities and municipalities in Albay inept at recovering from natural calamities and disasters fully. The practical implication of quantifying 'preparedness-insufficiency' and finding the 'state of balance' is that it reveals the critical factor to become practically prepared for tomorrow by doing our best today.

Keywords

Preparedness • Building-back-better • Risk location quotient • Preparedness-insufficiency • Disaster risk evaluation

1 Introduction

The UNISDR defines the build-back-better which refers to the use of the recovery, rehabilitation and reconstruction phases after a disaster to increase the resilience of nations and communities through integrating disaster risk reduction measures into the restoration of physical infrastructure and societal systems, and into the revitalization of livelihoods, economies and the environment. This paper presents a 'preparedness-insufficiency' model; it is described as an inefficiency in arriving at the border between receptiveness and responsiveness, in which prevention is the first level of receptiveness (Abante 2019). The borderline encompasses: states of alertness; states of emergency; states of calamity; disaster phase; and post-disaster phases. On 25 July 2011, a flash flood traversed unexpectedly swept away rice land, houses and tree branches by the flood as some cars and personal belongings washed away by floodwater. Malinao was submerged when Typhoon "Juaning" (International Code: Nock-ten) dumped about 500 mm of rain in 15 h, resulting in a flash flood as high as three metres. Although the entire Province of Albay truly prepared in which evacuation practices escaping disaster risk is already institutionalized, TD Juaning left one casualty in Malinao though the cause of death is the snake bite not by drowning. Fortunately, the flood event occurs at daytime if not, it can quickly kill more person as they may get hit by the debris or submerged. On 28 December 2016, Typhoon 'Nina' (international name: Nock-Ten) again triggered floods and levelled houses in Malinao, Albay, in which exposed residents fled to safer ground before the storm hit and were forced to spend Christmas in school classrooms that were temporarily converted into evacuation shelters. Based on the report of the Albay Public Safety and Emergency Management Office (APSEMO) Report, there are 50 families or 250 persons in Malinao evacuees.

A. M. R. Abante (✉)
Bicol University, 4500 Legazpi City, Philippines
e-mail: anamarie.abante@bicol-u.edu.ph

1.1 Preparedness Overview

Capability in this work comprises the three elements: Preparedness, coping capacity and competency; preparedness is paired with multiple hazard, coping capacity is paired with vulnerability, and competency is paired with exposure. Preparedness is a capability element (also a risk element inversely related to multiple hazards) which refers to pre-disaster actions undertaken within the context of DRRM to avert or minimize loss of life and properties (Abante 2019; Apostolakis 2004; Scott and Janikas 2010; Getis and Ord 2010). In contrast, the remaining impacts after preventive and mitigating measures imply preparedness-insufficiency. Thus, a negative impacts hint that a risk reduction action did not foresee (unmanaged or emergency response are not in placed) the effect on extreme situations which can put obstacles to recover (Abante 2019; Scott and Janikas 2010). Similarly, the preparedness-insufficiency can be marked between receptive and responsive disaster risk reduction actions of local government units. Competency is another a capability element (also a risk element inversely related to the vulnerability) which refers to local government actions addressing or reducing the underlying causes of vulnerability tweak unemployment or skills development-related strategies to boost employability through pieces of training in search, rescue and retrieval operations (Abante 2019; Apostolakis 2004). Coping capacity is the third capability element (also a risk element inversely related to exposure) which refers to the location (x, y) with a degree to which risk is likely or residents near to such locations are hazard-prone areas at different magnitudes. Thus, it also describes the ability of people, organizations and local government units using available skills and resources, critical infrastructures and so forth to withstand the adverse effects of natural calamities and disasters (Abante 2019; Apostolakis 2004). The capacity to cope requires continuing awareness, resources and proper management, both in regular times as well as during disasters or adverse conditions (Abante 2019; Apostolakis 2004).

Figure 1 exhibits a tangled web analogy pairing the circumspectal stages and DRRM cycle. The tangled spider web signifies the multiple hazard events recurrences in which green arrow (denotes receptive DRR) and red arrow (denoted responsive DRR) in a continuing sequence with five circumspection stages (Abante 2019; Apostolakis 2004). The receptiveness is divided into three stages: state of alertness; state of emergency and state of calamity (Abante 2019; Apostolakis 2004). Anything goes beyond the disaster phase is a piece of receptiveness. Receptiveness is divided into two phases: the disaster phase and post-disaster phase (Abante 2019; Apostolakis 2004). The state line connecting the state of alertness and disaster phase is called the border between receptiveness and responsiveness (Abante 2019;

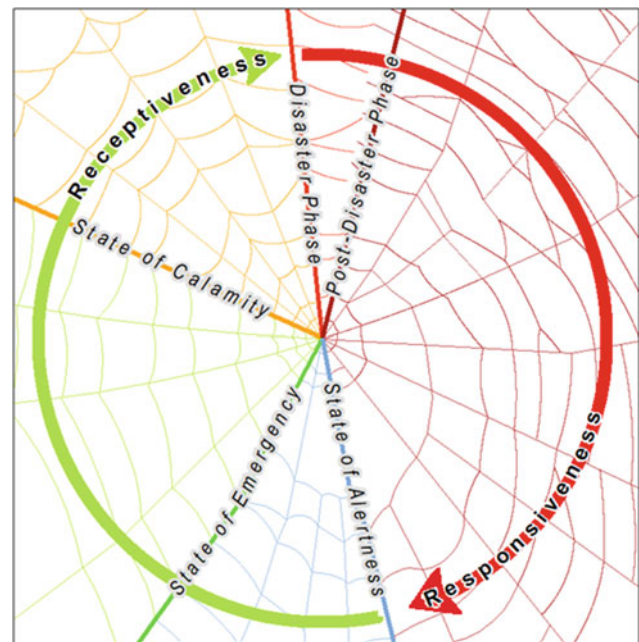


Fig. 1 Circumspectal-DRRM paired cycle (Abante 2019)

Apostolakis 2004; Getis and Ord 2010). It is in that state line where preparedness-insufficiency can take off (Abante 2019). As it is a cyclic process, the risk from previous calamities and disasters' remainders accumulates and freezes local government units to recover from underdevelopment fully (Abante 2019; Apostolakis 2004).

1.2 Preparedness Benchmarking

Being prepared would mean disaster risk is prevented and mitigated where people are in safe and comfortable places. Thus, exposure has been eliminated or reduced to near zero (Abante 2019). Responsive DRR in this work is described as an outcome of an effective emergency response plan to take care of public safety (Abante 2019; Apostolakis 2004). Mainstreaming it into development plans in a perfect city or municipality (the LGUs desire would like to happen), although they realize that resiliency may not seem likely to happen in the absence of seamless receptive local resiliency action plans and responsive emergency management and public safety plans (Apostolakis 2004). It can narrow the gap in preparedness. Figure 1 reveals the border between receptive and responsive DRR where preparedness-insufficiency leans (Abante 2019). Accordingly, Fig. 2 exhibits DRE* Matrix as a starting point to assess where preparedness-insufficiency (Abante 2019; Apostolakis 2004). The preparedness-insufficiency benchmark in this study attempt to provide a basis for the five circumspectal stages: state of alertness; state of emergency; state of calamity; disaster phase

Fig. 2 Disaster risk estimates (DRE*) matrix

DISASTER RISK ESTIMATES (DRE)		CIRCUMSPECTIAL STAGES						
		Responsive DRR		Receptive DRR				
		Post Disaster Phase	Disaster Phase	State of Calamity	State of Emergency	State of Alertness		
DRRM STAGES	Receptive	Prevention	Unsuitable LU	125 & above	64	27	8	1.0 (Bal.)
	Receptive	Mitigation	Unsafe	15.63	8	3.36	1.0 (Bal.)	0.13
	DRR	Preparedness	Uncomfortable	4.63	2.37	1.0 (Bal.)	0.3	0.04
	DRR	Emergency Response & Public Safety	Insensitive Actions/Spatial Plans	1.95	1.0 (Bal.)	0.42	0.13	0.02
	DRR	Recovery	Repetitive Evacuation Exercises	1.0 (Bal.)	0.51	0.22	0.08	0.01
	DRR							

and post-disaster phase (Abante 2019; Apostolakis 2004). The intersection of the two borderlines which enclose both the ‘state of calamity’ and ‘preparedness stage’ as shown in Fig. 2 reveals the same central point as the web centre where the silk winds out in increasing spirals (symbolizing recurrences of natural hazards) as shown in Fig. 1 (Abante 2019). By connecting DRE = 1.0, it creates a borderline separating all DRE values > 1.0 from DRE values < 1.0. Grouping all values < 1.0 hint at bending the borderline, allowing us to connect the ‘state of alertness’ with ‘recovery phase’ (Abante 2019; Apostolakis 2004). This approach corroborates that the web centre analogy point towards the ‘state of balance’. Likewise, authentic preparedness starts from DRE = 1.0 and below. Inversely, preparedness-insufficiency is quantified DRE > 1.0. The DRE: 5/5 would mean a 1.0 Location Quotients (LQ) suggests an immediate re-development or an urgent action to resettle people living in unsafe sites;

4/4 LQ implies an urgent information model to properly and timely respond to relocate people to safer sites with pre-positioned food, medicines and emergency response resources, safe and secured incident command centres and so forth;

3/3 LQ hints at the needs for safe and accessible evacuation routes, safer and sufficient evacuation abiding the zero-casualty strategy of Albay;

2/2 LQ entails DRE models to initiate mainstreaming DRR into comprehensive land use development and investment plans;

1/1 LQ would mean balanced physical developments and flexible spaces (Abante 2019; Apostolakis 2004).

1.3 Disaster Risk Assessment Modelling

In the case of the local government unit of Malinao, this study considers evaluating the land use allocations concerning the compound needs to reduce disaster risks (Abante 2019;

Apostolakis 2004; Scott and Janikas 2010; Getis and Ord 2010). In Malinao, the LGU desire to prevent if not reduce undesired effects of climate-related changes such as stronger typhoons carrying more rainwater transporting lahar, sand, soils from Mayon Volcano, Mt. Masaraga and Mr Malinao triggers Quinali ‘B’ riverbank erosions. It overflows submerging the alluvial flats utilized mostly for rice production in Malinao (Abante 2019; Apostolakis 2004). Mitigation is critical to Malinaons as altogether utilizing the downstream or flood plain areas for agricultural use mixed with dwelling and other socioeconomic land uses (Abante 2019). The improvements of irrigation canals and flood control structures also provide farm-to-market roads and serve as escape routes to the three evacuation centres as the case of Malinao (Abante 2019; Apostolakis 2004; Getis and Ord 2010). Subsequently, the stage of receptiveness is a hinge on the preparedness of the study area emphasizing the need for a safe, comfortable and accessible evacuation centres to ensure the zero-casualty strategy of the Malinaons or Albayanos (Abante 2019; Apostolakis 2004; Scott and Janikas 2010). In this stage, local resiliency action plan where the responsibilities and accountabilities on a share reduction environment among the disaster reduction managers in Albay is in place (Abante 2019; Apostolakis 2004; Scott and Janikas 2010). Also, the stage of responsiveness constitutes the disaster phase as well as the post-disaster phase, wherein the disaster phase deals with emergency response phase placing the public safe from any negative impact of a disaster (Abante 2019; Apostolakis 2004; Scott and Janikas 2010; Getis and Ord 2010). Considering the DREs and RLQs were already estimated, this paper extends the discussion on preparedness variable correlated with the prevention, mitigation, preparedness, response, recovery, responsiveness and receptiveness (Abante 2019; Apostolakis 2004). Both the DRE and RLQ follow the same mathematical equation derived from the $R = \frac{\text{Hazards} \times \text{Vulnerability} \times \text{Exposure}}{\text{Capability}}$, wherein the

capability has also three elements: preparedness, coping capacity and competency, and the mathematical equation is written as:

$$\begin{aligned} \text{Abante } DRE &\approx \text{Risk Location Quotient} \\ &= \frac{\text{Hazards}(H) \text{ Vulnerability } (V)}{\text{Preparedness Coping Capacity}} \\ &\quad \times \frac{\text{Exposure } (E)}{\text{Competency to Escape}} \end{aligned} \quad (1)$$

By applying the principles on geostatistical analysis, the points distributed 2 km apart interpolates the RLQ numerical values (pre-processed elements of risk per point) to create interpolation explicitly determines the risk elements assumptions are close to one another (Abante 2019; Apostolakis 2004). The maximum is, and minimum values range from 125 to 0.01 (see Fig. 2.) interpolated surface can only occur at sample points (see Fig. 4.). RLQ surface pattern relies on both geostatistical and mathematical methods to find where is the border of the state of balance (the edge of safe from risky space) at $RLQ = 1.0$ (Abante 2019; Apostolakis 2004). This paper aims to uncover the 'state of balance' to determine where to start building-back better (responsive) thenceforth becoming resilient (receptive). Specifically, this paper attempts to the look at 'preparedness-insufficiency' as inefficiency in arriving at the border between receptive and responsive quantitative disaster risk assessment and management (Abante 2019).

2 Methods

The search radius to interpolate the RLQs to estimate risk or resilient surface work on evenly spaced location (Abante and Abante 2018). Continuous point features hold geostatistical data from analysed and weighted spatial features of risk elements: multiple hazards; landscape condition; land utilization; income classification of the municipality and exposure through map overlays (Abante 2019; Apostolakis 2004). IDW in ArcGIS takes care of the influence points continuously distributed 2 km apart will predict the risk location quotients (Abante 2019; Apostolakis 2004; Getis and Ord 2010; Daep 2011; Demelletes 2017; Abante and Abante 2018). The IDW tool interpolated the RLQs derived from the valued six elements of risk through the Abante DRE* or RLQ Eq. (1) mention above (Abante 2019; Apostolakis 2004). The target outputs are RLQ models, these are: Household level; Barangay or Village/Community Level; and municipal level were reviewed to extend the discussions towards understanding preparedness-insufficiency, thence visualizing receptive and responsive DRR in the study area (Abante 2019).

2.1 Household Preparedness Assessment

We selected sample households for the following reasons: (i) households consistently vulnerable to the physical characteristics and land condition situated in alluvial flat area and basin of the Mayon Volcano, Mount Masaraga and Mount Malinao Watershed streams all flowing to Quinali 'B' River and contained within an absolute space called Hazard Zone, in which these households were directly affected by 2011 and 2016 flooding resulting to living in makeshift light materials or rebuilding their homes better (Abante 2019). It went through GIS overlay analyses to check their specific locations to verify if they are situated in a flood hazard zone or not (Abante 2019). Mobile GPS was used to collect and tagged geographic locations (x, y). Unique identification numbers and codes were assigned to sequential control questionnaires and field data about families' capability in terms of HH members coping capacity, competency and preparedness (Abante 2019). Using the same DRE*equation, the RLQ at household level was derived (Abante 2019; Apostolakis 2004).

Barangay Balza Preparedness Assessment

Flood occurrences brought by Quinali 'B' River overflow during heavy rains of several hours specifically in 'Balza, Malinao Albay' (Apostolakis 2004). Informants confirmed their flood experiences where river overflows and riverbank erosion submerged or destroyed their houses in 2011 and 2016, thus non-conformity of houses built per approved land use and zoning ordinance likely to repetitively damaged every time flood control structures failed to hold the water in Quinali 'B' River. (Apostolakis 2004). Similarly, the same DRE*equation was used to interpolate the RLQ at the barangay level (Abante 2019; Apostolakis 2004). The disaster risk assessment modelling in this case of 'Balza' demonstrate the conformity of household locations within the safe or not per approved land use and zoning ordinance (Abante 2019; Apostolakis 2004).

2.2 Malinao Preparedness Assessment

In May 2017, the Project NOAH 5, 25- and 100-Year Flood Forecasts published recently by Department of Science and Technology, the result after matching and examining HZ analysed in 2009 by the method of overlaying the three-flood return period, implies disaster risk (Apostolakis 2004). The survey divulges that residents of Purok 1, Balza and Malinao Albay depending on their perceptions on the warning of the local disaster risk reduction management office, they refused to leave their homes or skip to be evacuated in the temporary evacuation centres in which they were assigned to stay until

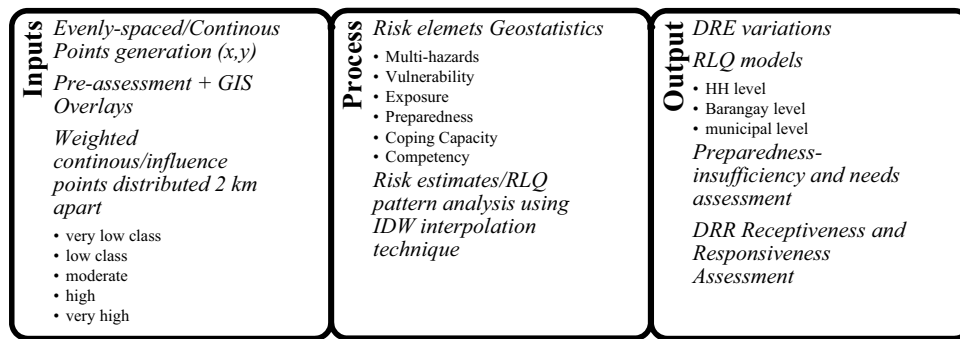


Fig. 3 DRR receptive and responsive assessment process flow

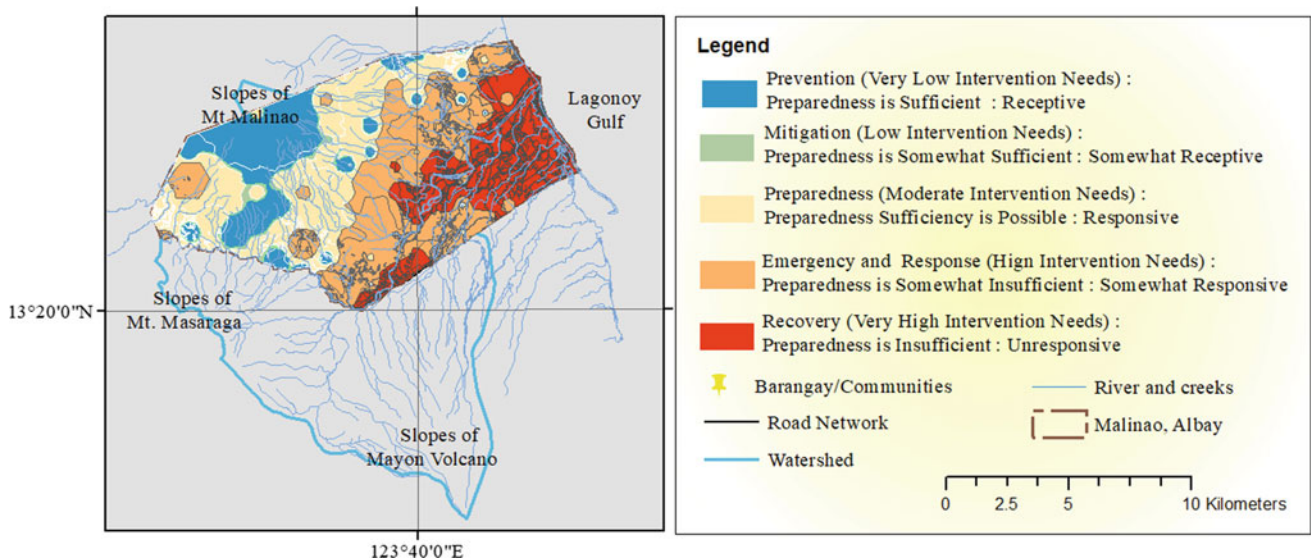


Fig. 4 Preparedness-insufficiency surface map

it is declared safe to return their home (Apostolakis 2004). As an alternative for the case of Purok 1, they evacuated in the two-storey residential houses located adjacent to an exposed school compound within the vicinity of same Purok (Apostolakis 2004). Although the three two-storey residential houses were built back better than the previous condition, still the residents experiencing regular flooding though floor levels were already raised a bit (Apostolakis 2004). Despite this congenital condition and exposure to flood risks, these two-storey residential houses served as a temporary space to stay escaping flood risks only at its lowest level, (Apostolakis 2004) although samples may be authentic municipal-wide considering most of the settlements are situated in an alluvial flat or flood-prone suitable for planting rice (Apostolakis 2004). In the case of the Municipality of Malinao, at least one-third of the entire municipality is forest and reserved for energy purposes (Abante 2019; Apostolakis 2004). Few makeshift houses are utilized for non-forest

products livelihood and eco-tourism purposes. (Apostolakis 2004) The approach was to design continuous points (x, y) distributed equally 2 km apart to pin the six elements of risk and to reject disparity: multi-hazards; vulnerability; exposure; preparedness; coping capacity and competency (Abante 2019; Apostolakis 2004). Again, the same DRE*equation was used to interpolate the RLQ at a municipal level (Abante 2019; Apostolakis 2004).

3 Results

3.1 RLQ-Based Preparedness-Insufficiency Surface Map

The preparedness-insufficiency surface map is the output after interpolating valued data derived from the six elements of risks (Abante 2019; Apostolakis 2004; Daep 2011;

Demelletes 2017; Abante and Abante 2018). The pattern discloses the DRRM complex needs, as shown in Table 1. The RLQ would serve as a multiplicative factor to monitor and evaluate risk reduction efforts to bring down the 119.04 RLQ circling in Malinao DRRM (Abante 2019; Apostolakis 2004; Daep 2011; Demelletes 2017; Abante and Abante 2018). The DRE surface map set aside the swaying intervention needs that may influence the gap in DRRM (Abante 2019; Apostolakis 2004; Daep 2011; Demelletes 2017; Abante and Abante 2018).

3.2 Preparedness-Insufficiency Geostatistics (Malinao, 2018)

The findings of this study clearly show that the method used to disclose the 119.04 RLQ that fall within $64 \geq$ but < 125 risk range hinting at a high to very high disaster risk rendering which could predict catastrophically, environmentally damaging risks, and economic activity disruption during extreme events (Abante 2019; Apostolakis 2004). It is at this stage that mitigation is obligatory in all aspects of development (Abante 2019; Apostolakis 2004). It is a must to protect the environmentally critical areas which suggest relocating people sited in a no-dwelling-zone (Abante 2019; Apostolakis 2004; Scott and Janikas 2010). Table 1 discloses the preparedness-insufficiency per land use and hectare of risk reduction needs in Malinao. The 119.04 RLQ imply that Malinao is at the state of disaster is always

imminent or susceptible economic activity disruption during extreme weather events (Abante 2019; Apostolakis 2004).

4 Discussion

Hint development is in harmony with the environment while keeping the people safe and comfortable in a balanced physical space (Abante 2019; Apostolakis 2004; Scott and Janikas 2010; Getis and Ord 2010). But in the case of Malinao, it needs to try to reduce if not eliminate the 119.04 RLQ or 11,904% to become a resilient municipality with an RLQ equal to 1.0. The 1.0 RLQ denotes resiliency in which a thin borderline between receptiveness and responsiveness reckon preparedness sufficiency (Abante 2019; Apostolakis 2004). In contrast, once the line starts to thicken or to form a gap, it lessens the level of preparedness, thus take down resiliency (Abante 2019). DRE and RLQ geostatistical data and raster surface model are essential in assessing preparedness-insufficiency to reduce risk, including its residuals taken in a continuing sequence of DRRM cycle (Abante 2019; Apostolakis 2004). It is undeniably logical to changing intervention needs and corrective-measures in harmony with development and vulnerable landscape of the municipality (Abante 2019). The DRR complex needs may be understood as the absence of local resiliency action plans in harmony with land use plans and zoning blocking the full recovery towards the development of Malinao (Abante 2019; Apostolakis 2004). It can be DRRM challenges to

Table 1 Preparedness-insufficiency level (Malinao 2018)

Level	Preparedness assessment result	Land use per Barangays	Exposed areas in hectare	DRRM complex needs
5	Insufficient	Economic activities such as commerce and industries located in 7 Barangays of Malinao	1.96	Full recovery
		Residential areas in 19 Barangays of Malinao	103.02	Relocation to suitable, safe, comfortable, accessible sites
4–5	Somewhat insufficient to Insufficient	Social facilities such as schools, religious sites, recreational areas, parks, cemetery and protective services located in 7 Barangays of Malinao	7.83	Emergency, response and recovery
		Institutional Use distributed in the municipalities	1	Emergency, response and recovery
4	Somewhat insufficient	Residential areas across 13 Barangays of Malinao	37.43	Allocation of suitable, safe, comfortable, accessible housing / residential areas
2–5	Somewhat sufficient to insufficient	Utilities connecting all barangays by land and communication facilities and other infrastructures	87.11	Mainstreaming DRRM into Spatial and development plan
1–3	Somewhat sufficient to sufficient	Residential in Burabod and Estancia. 2 out 3 temporary evacuation shelters are in these 2 barangays	1.44	Protection and Land reservation

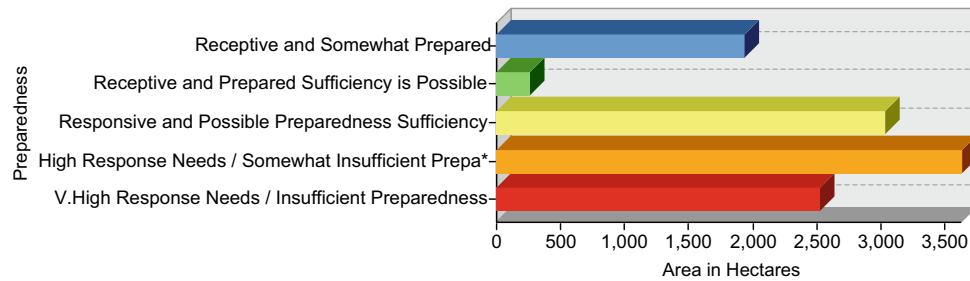


Fig. 5 Responsive and receptive DRR graph (Malinao 2018)



Fig. 6 Responsive and receptive DRR concept model, (Abante 2019)

acquire geospatial data or skills to create geoinformation models to assess and visualize their preparedness, capability and coping capacity to reset vision and missions in achieving the SDGs. The Philippine government directive to set aside the 5% of the local DRRM fund from the local budget, which this cannot offset the 11,904% DRR need. The resulting 119.04 RLQ in Malinao, it hints the multiplicative factor for intervention to make Malinao resilient municipality. Figure 5 shows the Malinao's level of preparedness in graph form (Abante 2019).

Although zero-casualty is a responsive risk reduction strategy (practised in the study area), real preparedness remains unattainable without receptively relocating those who are highly at risk. The result practically implies that preparedness is only valid when risk is estimated at less than one. However, in some cases, preparedness-insufficiency may be accurate but acceptable. Figure 6. Divulge the baseline denoting the bearable residual risks signify that 'state of balance' rely on the geostatistics of the six elements of risk. As extreme multiple hazard events may recur more dangerous, the 'state of balance' and bearable residual risks will relatively change. This 'state of balance' as shown in Fig. 3 is logical to the lines connecting the 'State of Alertness' and 'Disaster Phase' as shown in Fig. 1, at the same time logical to the line connecting the RLQs equal to 1.0 (Abante 2019; Apostolakis 2004).

5 Conclusions

Receptive and responsive risk reduction is both equally essential to keep the physical balance in assessing and managing risk reduction. The risk will keep escalating as hazard events happen again and again, placing cities and municipalities inept at recovering from natural calamities and disasters fully. Risk reduction is logical to 'preparedness-insufficiency', as the 'state of balance' demarcates bearable from intolerable risk. The 'state of balance' serves as the baseline where to pivot risk reduction responsively thenceforth receptively is the critical factor to become prepared for tomorrow by doing our best today.

References

- Abante, A.M.R.: Understanding preparedness insufficiency in the context of DRRM: a case study in Malinao, Albay, Philippines. In: *Recent Advances in Geo-Environmental Engineering, Geomechanics and Geotechnics, and Geohazards* (pp. 497–501). Springer, Cham (2019)
- Abante, A.M.R., Abante, C.G.R.: Sensitive land use planning, Malinao, Albay, Philippines. In: *IOP Conference Series: Earth and Environmental Science* (Vol. 123, No. 1, p. 012001). IOP Publishing (2018)
- Apostolakis, G.E.: How useful is quantitative risk assessment?. *Risk Anal.* **24**(3), 515–520 (2004)
- Daep, C.D.: Bicol University Graduate School Unpublished Dissertation entitled "The Implementation of the Disaster Risk Reduction Management Program in the Province of Albay" (2011)
- Demelletes, R.D. Jr.: Bicol University Graduate School Unpublished Dissertation entitled "Responsiveness of Department of Environment and Natural Resource–National Capital Region in Attaining the Environmental Security". Bicol University Library, Legazpi City Philippines (2017)
- Getis, A., Ord, J.K.: The analysis of spatial association by use of distance statistics. In: *Perspectives on Spatial Data Analysis* (pp. 127–145). Springer, Berlin, Heidelberg (2010)
- Scott, L.M., Janikas, M.V.: Spatial statistics in ArcGIS. In: *Handbook of Applied Spatial Analysis* (pp. 27–41). Springer, Berlin, Heidelberg (2010)



Emerging and Re-emerging Natural Focal Diseases in Russia: A Medico-Geographical Study

Svetlana M. Malkhazova, Polina V. Pestina, and Anna I. Prasolova

Abstract

In Russia, as in other countries, the problem of natural focal emerging (re-emerging) diseases (EIDs) became more acute by the end of the twentieth century. The variability of manifestations of emerging (re-emerging) natural focal diseases that exist on the territory of Russia (tick-borne encephalitis, Lyme borreliosis, hemorrhagic fever with renal syndrome, Crimean-Congo hemorrhagic fever, West Nile fever, Astrakhan spotted fever, leptospirosis, tularemia) is reflected in the modified disease classification and in a series of medico-geographical maps showing current nosoareas and disease risk assessment. The task of converting statistical data series for the transition from administrative divisions to geographically determined mapping units (biomes) was accomplished through the use of original geoinformatics technologies of spatial analysis.

Keywords

Emerging diseases • Classification • Mapping • Disease risk assessment

1 Introduction

In recent decades, the problem of emerging infectious diseases (EIDs) has been identified as one of the significant threats to humanity, given the effects of globalization (Morens and Fauci 2013). In Russia, as in many other countries, this problem became more acute at the end of the twentieth century (Malkhazova et al. 2016). The research focused on EIDs in Russia started from the late twentieth century, after the Crimean-Congo hemorrhagic fever

(CCHF) range began to expand toward neighbouring regions. At the same time, in the southern part of European Russia new epidemic activity of West Nile fever (WNF) was recorded (Malkhazova et al. 2019). Additionally, the foci of some somewhat familiar diseases have become more active, e.g. tick-borne encephalitis (TBE), Lyme borreliosis, hemorrhagic fever with renal syndrome (HFRS), leptospirosis and tularemia. Therefore, such diseases are also qualified as EIDs. The most important representatives of this group are natural focal diseases. The geography of such diseases is highly influenced by natural factors because their hosts and vectors are essential elements of landscapes (Atlas and of Russia 2017). Currently, medico-geographical research of the distribution of EIDs is a matter of top priority. This study aims at the identification of the most acute emerging natural focal diseases present in Russia and the elaboration of approaches to their geographical research.

2 Materials and Methods

A literature review was conducted to examine existing classifications of the entire variety of nosoforms and to identify factors affecting their distribution. Basing on this analysis, we selected eight relevant nosoforms belonging to EIDs with high levels of epidemic activity in recent years: Lyme borreliosis; TBE; HFRS; tularemia; leptospirosis; CCHF; WNF and ASF. A working classification was built in which four groups of diseases were distinguished based on the character of their geographical distribution. A series of maps of the current spread of the model infections across Russia was developed based on the federal agency Rospotrebnadzor's statistics. The authors tested the mapping methodology as they prepared numerous maps of the morbidity of natural focal diseases in Russia (Malkhazova et al. 2014). We used administrative divisions (federal subjects) as map units. The maps reflected morbidity rates for 1997–2015, calculated as the mean annual number of cases per

S. M. Malkhazova · P. V. Pestina (✉) · A. I. Prasolova
Lomonosov Moscow State University, Moscow, Russia
e-mail: polina.pst@yandex.ru

100,000 persons. A more detailed assessment of the risks was confined to European Russia. The task of converting statistical data series for the transition from administrative divisions to geographically determined mapping units was accomplished through the use of geoinformation technologies of spatial analysis (Lurie 2016). In order to achieve the goal, the overlapping (intersection) operation for the borders of the federal subjects and the boundaries of biomes drawn in line with the Russian Biomes Map was performed (Ogureeva and Kotova 2016). Based on the values obtained, an aggregate map of risk assessment for biomes was developed, within which a qualitative background shows the level of risk and the bar graphs reflect the risk of each particular infection.

3 Results

As previously noted, there is a significant number of nosoforms related to EIDs which need to be classified due to a wide variety of pathogens as well as differences in the ecology of agents and vectors, mechanisms of transmission, the severity of the disease, etc. Therefore, we built a working classification in which four groups of diseases were distinguished based on the character of their geographical distribution. Below are some examples of diseases representing each group.

Newly emerging or newly identified diseases. Astrakhan spotted fever (ASF) is an acute infectious natural focal disease caused by *Rickettsia conorii* subsp. *caspiensis* and transmitted by the ixodic tick *Rhipicephalus pumilio*. In Russia, it is registered in two regions. This disease is a classic example of a completely new infection. Official registration of ASF cases in Russia began in 2013. During 2013–2015 a total of 1,199 cases of ASF in humans were detected. Morbidity rate indicators increase from year to year. This phenomenon is associated with both the tick's high environmental plasticity and the expansion of the range of vectors that occurred as a result of intensive economic use of the territory.

Diseases with their areal limits static while changes in internal structure and dynamics occurring. Lyme borreliosis is a group of natural focal infections caused by spirochaetes of the genus *Borrelia* and transmitted by ixodic ticks. Currently, it is the most common vector-borne disease transmitted by ticks in Russia, Europe and the USA (Atlas and of Russia 2017). The nosoform is registered in 74 federal subjects with the most significant number of cases concentrated in 15 regions. Tick-borne encephalitis (TBE) is a congenital focal disease caused by a polytypic virus transmitted by ixodic ticks, primarily *Ixodes persulcatus* and *I. ricinus*. The central part of TBE global area falls within Russian territory. The relative stabilization of

morbidity indicators characterizes the modern epidemiological situation after rapid growth observed in the 1990s. At present TBE is registered in 63 federal subjects. Lyme borreliosis and TBE can be classified as EIDs since in the recent decades their morbidity rates increased as well as the number of biotopes where the infection is possible chiefly owing to ticks' infiltration into urban spaces such as parks and squares. In other words, the territories of the foci and their internal structure are changing.

Diseases spreading through expansion of their nosoareals to new territories. Crimean-Congo hemorrhagic fever (CCHF) is a severe natural focal acute human viral infection transmitted by several species of ixodic ticks. An insignificant portion of its nosoareal is on the territory of Russia. The primary vector is *Hyalomma marginatum* which prefers territories with low humidity and good warm supply. Outbreaks of CCHF occur rarely, and its incidence is sporadic, but it is characterized by periodic upsurges, the causes of which are as yet unclear. CCHF foci are situated in the southern parts of European Russia. Besides activation of the local foci, some time ago the disease expanded. West Nile fever (WNF) is an arbovirus natural focal disease, the main hosts of which are birds and its vectors are different species of mosquitoes. The cases of WNF in the Russia are registered since 1999. The area of the disease has expanded even more in 2011–2012. It was registered already in 21 federal subjects (Adishcheva et al. 2016).

Diseases that periodically give epidemic outbreaks against the background of a relatively stable mean morbidity rates. The most relevant representatives of this group in Russia are such severe infections as tularemia and leptospirosis. Tularemia is a particularly dangerous infection caused by the highly pathogenic bacterium *Francisella tularensis*. Despite a wide distribution, the mean annual (1997–2015) morbidity rate for tularemia in Russia is fair. However, several large outbreaks of this infection have occurred in Russia over the past 15 years affecting a significant number of people. More than 300 cases of tularemia were registered in Central Russia in 2005. An even more massive outbreak occurred in Khanty-Mansiysk Autonomous District in the centre of Western Siberia, in 2013 with 1,005 cases registered. Leptospirosis is also manifest in outbreaks. Their pathogens are transmitted mainly by water via numerous species of moisture-loving rodents as well as farm animals and dogs. The leptospiroses nosoareal in Russia covers 74 federal subjects. Notwithstanding the modest morbidity levels, the outbreaks occur from time to time. The largest ones were registered on the Black Sea coast of the Caucasus in 1997 with nearly 1,500 cases, and in the central part of the Russian Plain in 2004 with 700 cases.

A comprehensive analysis of the human infection risks related to the major natural focal diseases in European

Russia. The aggregate risk of morbidity associated with the complex of the nosofoms mentioned above in Russia is not very significant. Its highest rates are confined to the central regions of European Russia, the Urals and the Volga region, which are naturally related to forest biomes as well as to the southern steppe regions of the interflaves between the Volga and the Don and the foothills of the North Caucasus. It should be noted that the set of actual infections and their epidemics in these two regions are different, and the risk of infection with certain diseases in some areas is quite high. From the epidemic manifestation of natural focal infections, the riskiest are the territories of the Lower Volga. The distinctive feature of the current spread of EIDs in Russia is an increase in the share of the urban population among infected individuals. Urbanization is generally seen as one of the main drivers of emergence and expansion of such infections, and Russia seems to be no exception to this rule.

4 Conclusions

Based on the above analysis, we can assume that various emerging and re-emerging infections are present in the territory of the Russian Federation. The variability of their manifestations is reflected in the modified classification proposed by authors. One of the most commonly cited reasons for EIDs proliferation in Russia is increased human contact with the natural foci of diseases. Summer cottage development (including garden plots belonging to urban residents where they spend the summer months, which is a widespread activity in Russia), enthusiasm for active

recreation associated with wildlife visits, and the settlement of new biotopes by vectors (such as urban parks), cause an increase in the morbidity of natural focal infections.

Funding The paper was prepared within the framework of the Russian Foundation for Basic Research (project N 18-05-60,037).

References

- Adishcheva, O.S., Malkhazova, S.M., Orlov, D.S.: The spread of West Nile fever in Russia. *Vestnik MSU. Seriya 5. Geografiya* **4**, 48–55 (2016) [in Russian]
- Malkhazova, S.M., Mironova, V.A., Pestina, P.V., Orlov, D.S.: Emerging and re-emerging infections in Russia: a medico-geographical aspect. *Vestnik MSU. Seriya 5. Geografiya* **4**, 24–32 (2016) [in Russian]
- Malkhazova, S.M., Mironova, V.A., Shartova, N.V., Orlov, D.S.: Mapping Russia's natural focal diseases: history and contemporary approaches. Springer (2019)
- Malkhazova, S.M., Mironova, V.A., Kotova, T.V., Shartova, N.V., Orlov, D.S.: Natural-endemic diseases: mapping experience for Russia. *Int. J. Health Geograph.* **13**, 21 (2014)
- Medico-geographical Atlas of Russia “Natural Focal Diseases”: In: Malkhazova, S.M. (ed.) 2nd revised edn. Moscow, Faculty of Geography, Lomonosov Moscow State University (2017) [in Russian]
- Morens, D.M., Fauci, A.S.: Emerging infectious diseases: threats to human health and global stability. *PLoS Pathog* **9**(7), (2013)
- Lurie, I.K.: Geoinformatic mapping. In: *Methods of Geoinformatics and Image Visual Processing*. Moscow, Knizhnyj dom Universitet (2016) [in Russian]
- Ogureeva, G.N., Kotova, T.V.: Map “Biomes of Russia”: a new approach to the study of biodiversity. *Modern Science. Int. Sci. J. Strateg. Stud. Institut. LLC* **6**, 155–160 (2016)

**Environmental Earth Sciences (T4):
Environmental Remediation**



Removal of Iron from Groundwater onto Raw Clay (Ka-II)

Sana Ghrab, Zied Marzougui, Leila Chaari, Mohamed Damak, Abdelhamid Elaissari, and Boubaker Elleuch

Abstract

This paper aims to investigate the role of Tunisian clay in the removal of iron ions from groundwater located in Mahdia region (Tunisia) since high concentrations are detected in the water. The adsorption experiment is performed using the batch study. With this optimal condition, the adsorption capacity of iron ions is 7.86 mg/g. Kinetic and isotherm adsorption studies were investigated to determine the adsorption mechanism. The results showed that the pseudo-second-order kinetic model and the Freundlich isotherm fit the experimental data. Based on these results, we concluded that the clay is an effective and low-cost material of iron ions removal from groundwater.

Keywords

Clay • Groundwater • Iron • Adsorption

1 Introduction

Iron is considered to be a common element of groundwater. Natural sources are connected mainly to mineral rocks and volcanic activities. Contrariwise, the use of chemical

S. Ghrab (✉)
National Engineering School of Sfax, Laboratory
Water-Environment and Energy (LR3E), Sfax University,
LR99ES35 1173-3038 Sfax, Tunisia

Z. Marzougui · L. Chaari · M. Damak · B. Elleuch
Laboratory of Environmental Engineering and Ecotechnology.
(GEET) LR16ES19, Sfax University, National Engineering
School of Sfax, 1173-3038 Sfax, Tunisia

Z. Marzougui · A. Elaissari
University of Lyon, 69622 Lyon, France

A. Elaissari
Lyon 1 University, Villeurbanne, France

A. Elaissari
LAGEP, CNRS, CPE, UMR 5007 F-69622 Villeurbanne, France

insecticide in agriculture and industries contributes to the presence of iron in surface water systems then transferred in groundwater (Brunt et al. 2004; Belabed et al. 2017). In this study, the groundwater of Mahdia Malloulouche, used for the development of tropical aquatic species, present very high concentration of iron (3.5 mg/L). That presents a major technical problem. Therefore, it is necessary to adjust the concentration of Fe, in groundwater less than 0.3 mg/L. This study aimed to reduce the iron concentration by adsorption on raw clay.

2 Results

2.1 Characterization of Raw Clay

The clay Kaolinite–Illite (Ka-II) was obtained from Jebel Abderahman, located in Nabeul, Tunisia. The mineralogical analysis of Paly was carried out by XRD (Philips X'Pert Diffractometer) on the powder of total rock and the oriented aggregates; normal (N) was treated with ethylene glycol (T) and heated at 500 °C for 2 h (H). The XRD spectrum presents oriented aggregates (Ghrab et al. 2014). Diffractograms are reported in Fig. 1. They allow determining the mineralogical composition of the (Ka-II). The raw clay sample is mostly constituted by illite (45%), kaolinite (51%) and smectite (4%) as minerals clay, associated with quartz (19%), calcite (3%) and feldspath (2%).

2.2 Adsorption of Iron

To establish excellent results, before the study of adsorption, the parameters of this experience are optimized. The parameter optimization studies of the adsorption of iron ions from groundwater using the sample clay (Ka-II) are shown in (Fig. 2). Later, the conditions of the study of the adsorption isotherm are established as follows: time = 60 min, pH = 5, weight = 0.1 g, temperature = 25 °C ± 2.

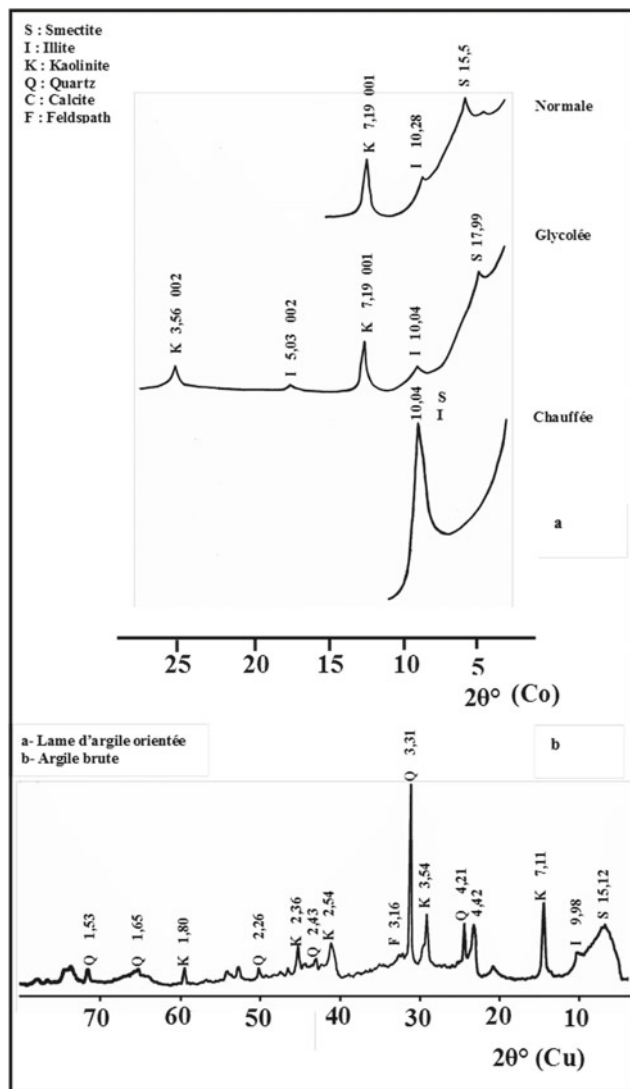


Fig. 1 Diffractograms of raw kaolinite-illite (Ka-II)

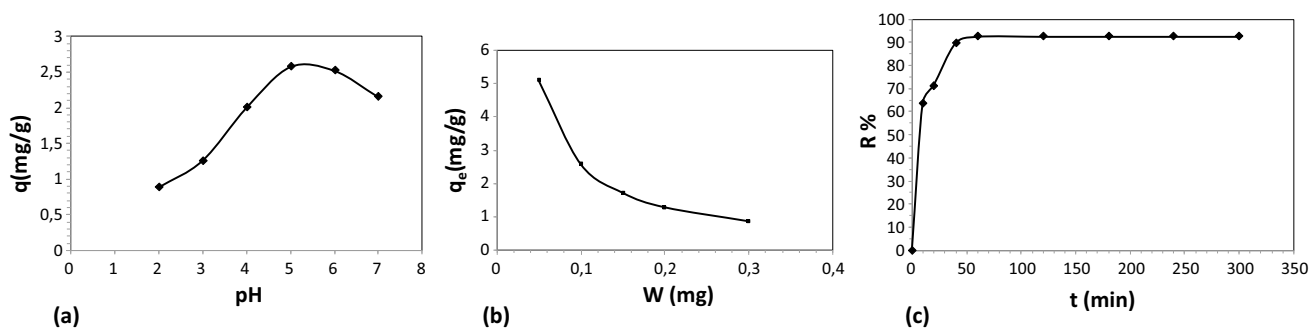


Fig. 2 Adsorption parameter optimization a pH effect, b weight effect, c time effect

Figure 3 presents the curve of iron adsorption isotherm on (Ka-II). It was found that the adsorption capacity decreased with the saturation of surface adsorbent iron (Ghrab et al. 2018).

3 Discussion

The results of the optimization parameter study proved that with the increased adsorbent doses, the adsorption capacity of adsorbate decreased. Increasing the mass of (Ka-II) in bath with a fixed concentration and fixed volume of adsorbate groundwater would increase the number of available adsorption sites and caused a reduction in the adsorption capacity. The adsorption of iron ions is highly pH-dependent. The iron ions adsorption capacity steeply increased with increasing pH from 2 to 5 and then decreased with increasing pH from 5 to 7. The results of adsorption studies, carried out as a function of contact time, for iron ions suggested the adsorption of iron ions by the (Ka-II) adsorbent progress in two steps: a relatively quick phase, followed by a slow increase until the equilibrium was reached. The necessary time to reach the equilibrium was about 60 min. After optimization parameter, the application of the isotherms model showed that the adsorption of iron onto (Ka-II) follows Freundlich isotherm model and the maximum adsorption capacity of (Ka-II) was mentioned to 7.86 mg/g, with a correlation factor $R^2 = 99\%$.

4 Conclusion

In this study, the clay (Ka-II) showed rapid adsorption for iron ions from groundwater and equilibrium was achieved in 60 min. The optimal weight of (Ka-II) is 0.1 g with a

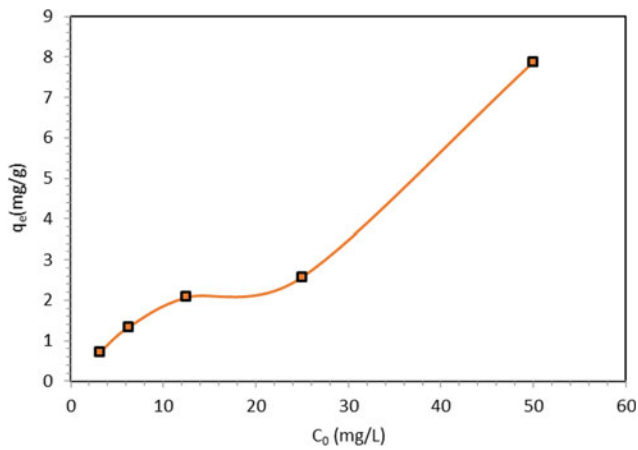


Fig. 3 Isotherm adsorption of iron from groundwater onto (Ka-II).

maximum of adsorption capacity equal to 7.86 mg/g. According to the obtained results, the (Ka-II) could be investigated as an efficient and low-cost material for excess iron removal from groundwater.

References

- Belabed, B.E, Meddour, A., Samraoui, B., Chenchouni, H.: Modeling seasonal and spatial contamination of surface waters and upper sediments with trace metal elements across industrialized urban areas of the Seybouse watershed in North Africa. *Environ. Monit. Assess.* **189**(6), 265 (2017). <https://doi.org/10.1007/s10661-017-5968-5>
- Brunt, R., Vasak, L., Griffioen, J.: IGRAC: International Groundwater Resources Assessment Centre (2004)
- Ghrab, S., Boujelben, N., Medhioub, M., Jamoussi, F.: Chromium and nickel removal from industrial wastewater using Tunisian clay. *Desali Water Treat* **52**, 2253–2260 (2014). <https://doi.org/10.1080/19443994.2013.805165>
- Ghrab, S., Mefteh, S., Medhioub, M., Benzina, M.: Adsorption of nickel(II) and chromium(III) from aqueous phases on raw smectite: kinetic and thermodynamic studies. *Arab. J. Geo.* **11**, 440 (2018). <https://doi.org/10.1007/s12517-018-3749-2>



Investigation of Flocculation Activity of Cactus *Opuntia ficus-indica* juice in Phosphate Clay Treatment

Raouen Rachdi, Feyda Srarfi, Mohamed Salah Hamdi, and Najet Slim Shimi

Abstract

Recently, Cactus *Opuntia ficus-indica* (OFI) has been increasingly regarded as the best available biomaterial used in different domains (cosmetics, medicinal and food industries) owing to its high efficiency as well as its low initial and operating cost. This study aims to investigate the ability of this material as a natural flocculant in the treatment of industrial wastewater (phosphate clay) through the coagulation/flocculation process. The settling velocity on the one hand and the analysis of clear water and dry sludge, on the other hand, allow us to compare the cactus-based flocculant effectiveness with that of chemical flocculant, anionic polyacrylamide nature. The effects of factors such as the dosage, pH and the condition of agitation were also studied. Obtained results indicated significant results regarding the volume of clear water content (supernatant) and several parameters (P_2O_5 , CaO, MgO, Cd, Corg, SiO_2) for the dry sludge. The performance of the cactus as flocculant juice was compelling.

Keywords

Phosphate clay • Cactus • Flocculation • Mining industry • pH

1 Introduction

In the coagulation/flocculation process, the use of chemical products is not deemed suitable due to environmental and economic considerations. Its application is associated with a lack of biodegradability and dispersion of metal residue in

clear water that has recuperated and concentrated slurry (Farooq et al. 2010). It is therefore desirable to reduce the use of these chemicals and encourage the use of product-based plants. They are widely used due to its remarkable ability to flocculate efficiently with the advantages of biodegradability and environmental friendly (Theodoro et al. 2013; Joseane et al. 2013; Muralimohan et al. 2014). Several plants are being used as coagulants/flocculants. The thrust of this work is to replace the use of chemical flocculant with a new natural biodegradable flocculant based on cactus, a plant which is locally produced, is non-toxic and gives the same performance as flocculation.

2 Materials and Methods

2.1 Phosphate Clay Preparation

All tests were carried out on phosphate clay prepared in the laboratory. The procedure of clay preparation conformed to that described in the phosphate laundries following these steps: mechanical preparation, sampling by quarters, settling and high and low cuts.

2.2 Preparation of Bioflocculant Solution

We collected the pads of OFI from the region of El-Sned (in Gafsa in the south-west of Tunisia). The cladodes were collected and transported to the laboratory when they are cleaned. Then, they are cut into small pieces, and they were ground with a grinder. The liquid extract obtained is filtered using a gauze compress. We obtained a viscous liquid with green colour, with a range of pH of 3–4, which is miscible with water. For this study, the initial pH in the cactus juice was adjusted to the desired value with NaOH. A cladodes juice was prepared fresh for each experiment.

R. Rachdi
Laboratory 3G, University El Manar Tunis, Tunis, Tunisia

F. Srarfi (✉) · M. S. Hamdi · N. S. Shimi
Faculty of Sciences, Laboratory 3G, University El Manar, Tunis, Tunisia

2.3 Experimental Protocol

To determine the optimum dose of the biomaterial, we carried out a series of tests while varying each time the added volumes of this bioproduct in a litre of phosphate clay.

2.4 Analytical Methods

Multiple analyses ($P_2O_5\%$, $CaO\%$, $MgO\%$, Cd (ppm), Corg % and $SiO_2\%$) were done on the dried sludge recovered after settling. All the analytical work was done according to an internal protocol at the Chemical Analysis Laboratory (CAL) of the Research Center (RC) in the Gafsa Phosphate Company (GPC). The efficiency of this treatment was, also, evaluated based on the volume of clear water recovered.

3 Results

3.1 Determination of the Optimal Dosage of Organic Flocculant

To determine the optimum dosage of organic flocculant concentrate, we performed several tests while varying in each case the added volume of the bioproduct in a litre of phosphate clay concentration of 60 g/L. For this experiment, we used FCJ with pH equal to 10. We varied the volumes of the bioproduct of 60–120 mL in one litre of phosphate clay. Table 1 presents the results obtained.

From this table, it is noted that at a dosage of 80 mL of FCJ volumes of the highest clear water are obtained. They are 340 mL after 60-s settling, 550 mL after 180 mL seconds of sedimentation and 690 mL after 900 s. It is important to note that with the optimal dosage of chemical flocculant the volume of clear water recovered is 660 at 900 s.

Table 1 Water volume change versus time and dosage of bioflocculant

Time (s)	60 mL	80 mL	100 mL	120 mL
0	0	0	0	0
60	240	340	330	220
120	390	490	480	390
180	470	550	550	490
240	510	580	580	530
300	530	610	600	570
360	550	630	620	590
420	570	640	630	600
480	580	650	650	620
540	590	650	660	630
600	600	660	670	640
900	640	690	700	670

3.2 Characteristics of Dry Sludge

Table 2 shows the characteristics of dry phosphate sludge obtained from raw phosphate clay as a blank (control), treated phosphate clay by CF and phosphate clay treated by the FCJ after 900 s. The obtained results were engaging.

According to Table 2, P_2O_5 , CaO, MgO and Cd contents in sample treated by CF showed a decrease per the control. The percentage of reduction achieved was, respectively, 3.10, 2.75, 27.45 and 5.36%. The concentrations for SiO_2 showed an increase per the control. The rate of increase is, respectively, 4.52%.

Compared to the sludge left over from natural decantation of phosphate clay (control), analysis of the clay of phosphate treated with cactus (FCJ) showed a decrease in the contents of P_2O_5 (4.61%), CaO (2.79%) Cd (4.98%) and SiO_2 (0.10%). In the total amount of sludge, the increase of organic C and MgO concentrations is probably due to a bigger mass of natural flocculation sludge produced and a greater quantity of organic matter.

4 Discussion

The high settling rate obtained by the use of bioflocculant-based cactus is mainly related to the size of the flocs formed. Under the influence of gravity, these larger flocs fall faster. Cactus performs as a faster flocculant thanks to its ability to form larger flocs than the chemical flocculant (Young 2006; Yin et al. 2007; Vijayaraghavan et al. 2011).

According to Table 2, we see that the difference between the results obtained by the use of FCJ and CF concerning the levels of some parameters (P_2O_5 , CaO, Cd, SiO_2) is slightly significant. Taking this minor difference in the treatment performance for the chemical and flocculant-based juice, this solution was deemed efficient in terms of flocculant use.

Table 2 Characteristics of phosphate sludge recovered from control, CF and FCJ

Parameters	Control	CF	FCJ
P ₂ O ₅ %	11.27 ± 0.05	10.92 ± 0.11	10.75 ± 0.09
CaO %	23.94 ± 0.03	23.28 ± 0.33	23.27 ± 0.22
MgO %	0.51 ± 0.05	0.37 ± 0.16	0.56 ± 0.01
Cd ppm	87 ± 1.00	82.33 ± 2.51	82.66 ± 1.52
Corg %	1.01 ± 0.03	1.05 ± 0.04	1.89 ± 0.03
SiO ₂ %	28.52 ± 0.14	29.81 ± 0.17	28.49 ± 0.19

Control: dry raw sludge of phosphate clay; **CF:** dry sludge obtained after treatment of phosphate clay with chemical flocculant; **FCJ:** dry sludge obtained after treatment of phosphate clay with fresh cladodes juice. Values correspond to the mean of 3 measurements ± standard deviation (SD)

5 Conclusion

Experimental results conducted for Cactus *Opuntia ficus-indica* encourage its use for industrial wastewater treatment purpose. The use of this plant is appealing because it is less toxic, and it offers a more economical alternative in terms of treatment of industrial water.

References

- Farooq, U., Kozinski, J.A., Khan, M.A., Athar, M.: Biosorption of heavy metal ions using wheat based biosorbents-a review of the recent literature. *Bioresour. Technol.* **101**, 5043–5053 (2010)
- Muralimohan. N., Palanisamy, T., Vimaladevi, M.N.: Experimental study on removal efficiency of blended coagulants in textile wastewater treatment. *Int. J. Res. Eng. Technol.* **2**(2), 15–20 (2014)
- Theodoro, J.D.P., Lenz, G.F., Zara, R.F., Coagulants, R.B.: Natural polymers: perspectives for the treatment of water. *Plastic Polym. Technol.* **2**(3), 55–62 (2013)
- Theodoro, P.J.D., Lenz, G.F., Zara, R.F., Rosangela, B.: Coagulants and natural polymers: perspectives for the treatment of water. *Plastic Polym. Technol.* **2**(3), 55–62 (2013)
- Vijayaraghavan, G., Sivakumar, T., Vimal Kumar, A.: Application of plant based coagulants for waste water treatment. *Int. J. Adv. Eng. Res. Stud.* **1**(1), 88–92 (2011)
- Yin, C.Y., Suhaimi, A.T., Lim, Y.P., Mohd, S.N.I., Siti, N.A.A., Mahyuddin, A.M.M.: Turbidity removal from surface water and landfill leachate using cactus *Opuntia*. *J. Institut. Eng. Malaysia* **68** (1), 61–64 (2007)
- Young, K.A.: The Mucilage of *Opuntia ficus-indica*: a natural, sustainable, and viable water treatment technology for use in rural Mexico for reducing turbidity and arsenic contamination in drinking water. MSc thesis, University of South Florida, Tampa, USA (2006)



Enhancing the Chromium Removal Capacity of Banana Peel Wastes by Acid Treatment

Haili Chen, Zhouyang Huang, Jiahong Wu,
and Chirangano Mangwandi

Abstract

Banana peels activated by two different methods (acid modified, ABP; acid and paraformaldehyde modified, ABP-C) were used as adsorbents for Chromium (VI) removal, and both kinds of treated banana peels showed high removal efficiency. Preliminary adsorption experiments revealed that the capacity of the untreated banana peels (BP) was 90 mg/g. After modification, the adsorption capacity of the banana peels increased to around 163 mg/g, which is higher than the values reported in the literature. The Freundlich model could fit the adsorption data better on the ABP, while the Langmuir model was much better for Cr⁶⁺ adsorption on the ABP-C.

Keywords

Banana peel waste • Modification • Chromium (VI) • Adsorption

1 Introduction

Heavy metal pollution is a kind of accumulated chronic pollution and the most dangerous potential hazard in water pollution at present. Among all the treatments, biosorption has a broad application prospect in the removal of heavy metals in water, due to its extensive sources of raw materials, low cost, large adsorption capacity, fast adsorption speed, good selectivity and other characteristics (Nilanjana and Vimala 2008). Banana is one of the important tropical and subtropical fruits, and the total output of banana increased by more than 4 times in the past 30 years (FAO 2019; 2019). Banana cultivation produces massive tonnes of waste per

hectare in a single growing season, therefore, how to deal with such a large amount of waste becomes an urgent problem.

So far, the utilizations of banana peels have been studied by many researchers which included composting, ethanol production, anaerobic digestion and so forth (Mohapatra et al. 2010). Among these utilizations, using banana peel wastes as adsorbents for wastewater treatment has attracted widespread attention. Anwar et al. (2010) used the raw banana peels for Pb²⁺ and Cd²⁺ removal. In addition, the removal of Pb²⁺, Cu²⁺, Ni²⁺ and Zn²⁺ from wastewater using the raw banana peels was also investigated by Ashraf et al. (2011). Furthermore, raw banana peel was determined as adsorbent for the selective removal of Cr⁶⁺ from industrial wastewater and the Langmuir adsorption capacity was around 132 mg/g (Memon et al. 2009). Most of these studies were based on the raw banana peels and other heavy metals, only a few studies were based on the chemical treated banana peels to work as adsorbents for Cr⁶⁺ (Ali and Saeed 2013). Therefore, the main objective of this study was to evaluate the performance of the chemically modified banana peel waste as an adsorbent for the removal of Cr⁶⁺ from wastewater.

2 Materials and Methods

2.1 Banana Peels

The fresh banana peels (BP) are sliced into small pieces, washed thoroughly in distilled water at least five times and dried in the oven (Binder FD240, German) at 65 °C for 24 h. The dried banana peels were then crushed into powder and stored in suitable containers until the next treatment. 10 g dried fresh banana powder were put into a 200 ml conical flask with 100 ml H₂SO₄ (50%). The conical flask was then placed in a water bath maintained at 50 °C. After continuously stirring for 24 h, the solids were filtered and washed

H. Chen · Z. Huang · J. Wu · C. Mangwandi (✉)
School of Chemistry and Chemical Engineering, Queen's
University Belfast, David Kier Building, Stranmillis Road,
Belfast, BT9 5GA, UK
e-mail: c.mangwandi@qub.ac.uk

with distilled water to a neutral pH, followed by drying in fume cupboard for 72 h. The resultant product was designed as acid modified banana peels (ABP). 10 g dried fresh banana powder was put into a 200 ml conical flask, 100 ml H_2SO_4 (75%) was then added, followed by 3.6 g paraformaldehyde powder. The conical flask was placed in a water bath maintained at 50 °C. After continuously stirring for 5 h, the solids were filtered and washed with distilled water to a neutral pH, followed by drying in fume cupboard for 72 h. The resultant product was named as acid and paraformaldehyde modified banana peels (ABP-C). The ABP-C would contain the methanol functional group.

2.2 Adsorption Experiments and Analysis Methods

0.02 g treated banana peels were added to 20 ml Cr^{6+} solutions with different concentrations (20 ~ 200 ppm) for three days at room temperature. To measure the absorbance of the Cr^{6+} solution, UV Spectrometer (UV-mini 1240, Shimadzu, Japan) was used. Different concentrations of Cr^{6+} solutions were used in testing adsorption capacity of the generated banana peel samples. The Q_e was calculated using Eq. 1.

$$Q_e = \frac{(C_0 - C_e)V}{M} \quad (1)$$

In Eq. (1) Q_e is equilibrium concentration of adsorbate in solid phase, C_e is equilibrium concentration of adsorbate in liquid phase, M is mass of adsorbent used and V is volume of synthetic wastewater solution used.

2.3 Adsorption Isotherm Models

The five adsorption isotherm models used in this study were the Langmuir (2), the Freundlich (3), the Sips (4), the Redlich -Peterson (5) and Temkin (6) shown as below:

$$q_e = \frac{q_{max}K_L C_e}{1 + K_L C_e} \quad (2)$$

$$q_e = K_F C_e^{1/n} \quad (3)$$

$$q_e = \frac{q_{max}b_s C_e^m}{1 + b_s C_e^m} \quad (4)$$

$$q_e = \frac{q_{max}B_{pb}C_e}{1 + B_{pb}C_e^\beta} \quad (5)$$

$$q_e = B \ln(A \cdot C_e) \quad (6)$$

In Eqs. (2) to (6) where q_e is the adsorption capacity at equilibrium (mg/g); q_{max} (mg/g) is the maximum amount of heavy metal adsorbed by the banana peels; K_L (L/mg) and K_F ($[mg \cdot g^{-1}]/[mg \cdot L^{-1}]^{1/n}$) are the Langmuir constant related to the interaction bonding energies and the Freundlich affinity coefficient, respectively; C_e (mg/L) is the equilibrium concentration of the heavy metal solution; b_s is the Sips isotherm affinity constant (L/mg); B_{pb} is the Redlich-Peterson isotherm constant (L/mg); β is exponent that lies between 0 and 1; A is equilibrium binding constant (L/g); B is the constant related to heat of the adsorption (J/mol).

3 Results

3.1 Characterization of Adsorbent

The FTIR analysis done on the samples of the treated banana peels before and after the biosorption of Cr^{6+} is shown in Fig. 1. The broad bands around 3400 cm^{-1} detected in both biomaterials can be attributed to $-OH$ and $-NH$ stretching vibrations of hydroxyl groups while peaks assigned to alkyl- $C-H$ stretching are observed around 2900 cm^{-1} .

3.2 Adsorption Results of Treated Banana Peels

The adsorption isotherms of Cr^{6+} adsorbed by ABP and ABP-C are shown in Fig. 2a and b respectively. The non-linear regression was used to fit the experimental data to different adsorption isotherm models and the results are

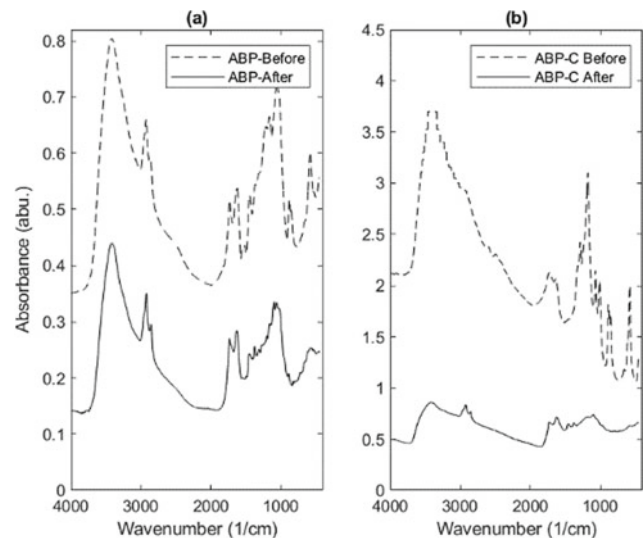
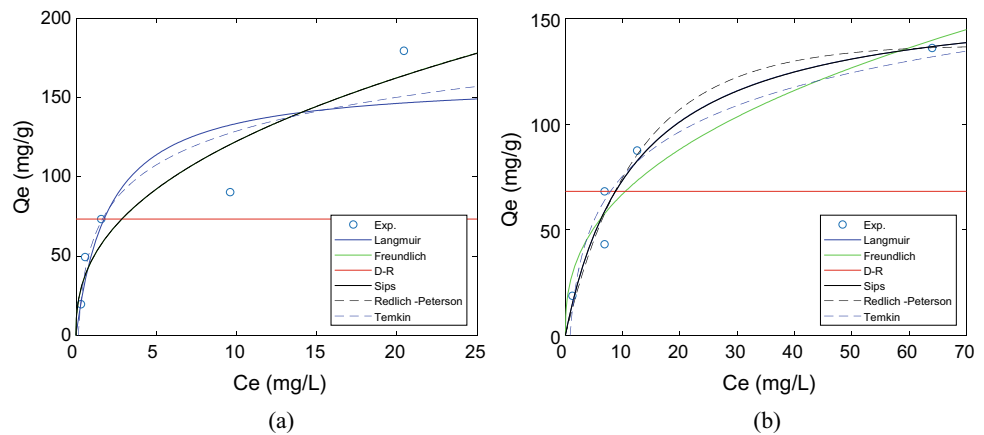


Fig. 1 FTIR spectra of adsorbent materials before and after adsorption

Fig. 2 The adsorption isotherms of Cr⁶⁺ adsorbed by **a** ABP **b** ABP-C



shown in Table 1. It can be noticed from the data presented in Table 1 that there is no significant difference in the adsorption capacities of ABP and ABP-C adsorbents.

4 Discussion

As shown in Fig. 2a and b, the adsorption amount of Cr⁶⁺ by the ABP and ABP-C increased with the increasing concentrations of Cr⁶⁺ solution. From Table 1, Freundlich model was found to fit the adsorption data slightly better considering the *R*² value (0.8513) when the ABP was used as the adsorbent, whereas, it was found that the Langmuir model was much better for Cr⁶⁺ adsorption on the ABP-C with the *R*² value 0.9383. Based on the preliminary experiments, the BP had a Langmuir adsorption capacity around 90 mg/g, and the adsorption capacity increased to over 160 mg/g after modification. Therefore, it can be concluded that the adsorption capacity of banana peel could be enhanced by acid modification. Besides, it was observed that the adsorption capacity of the ABP (161.7 mg/g) and the ABP-C (162.5 mg/g) was quite similar, indicating that the

paraformaldehyde powder did not have a significant effect on the adsorption capacities of the banana peels. The comparison of the adsorption capacities of Cr⁶⁺ adsorbed onto different bio-adsorbents reported by the other researchers are shown in Table 2. The results suggest that the modified banana peels have a high adsorption capacity for Cr⁶⁺; therefore, they could be used as low-cost bio-adsorbents for treatment of Cr⁶⁺ contaminated wastewater. From the FT-IR results, it was found that -OH, -C = O' and -COO- were the main functional groups in all the BP, ABP and ABP-C. Therefore, the differences in the adsorption capacities might be related to the quantities of these functional groups.

5 Conclusions

The results obtained here showed that banana peel could be a useful resource for the production of low-cost adsorbent materials for Cr⁶⁺ removal. The adsorption capacity of banana peel could be increased by acid modification, and adding the paraformaldehyde powder did not have a significant effect on their adsorption capacities. The removal

Table 1 Summary of the parameters of the isotherm models obtained from non-Linear regression

	Langmuir		Freundlich		Sips		Redlich-Peterson		Temkin	
ABP	<i>R</i> ²	0.7153	<i>R</i> ²	0.8513	<i>R</i> ²	0.7769	<i>R</i> ²	0.7770	<i>R</i> ²	0.7905
	<i>K_L</i>	0.5	<i>K_F</i>	47.7	<i>b_s</i>	0.0	<i>B_{pb}</i>	150,804.5	<i>A</i>	6.6
	<i>q_{max}</i>	161.7	<i>n</i>	0.4	<i>m</i>	0.4	<i>β</i>	0.6	<i>B</i>	30.8
					<i>q_{max}</i>	88,256.1	<i>q_m</i>	47.7		
ABP-C	<i>R</i> ²	0.9383	<i>R</i> ²	0.8927	<i>R</i> ²	0.9075	<i>R</i> ²	0.9098	<i>R</i> ²	0.9089
	<i>b</i>	0.1	<i>K_F</i>	26.9	<i>b_s</i>	0.1	<i>B_{pb}</i>	0.0	<i>A</i>	1.2
	<i>q_{max}</i>	162.5	<i>n</i>	0.4	<i>m</i>	1.0	<i>β</i>	1.2	<i>B</i>	30.4
					<i>q_{max}</i>	163.1	<i>q_m</i>	379.1		

Table 2 Adsorption capacities from Langmuir model of Cr⁶⁺ adsorption on different bio-sorbents

Material	Pollutant	Q _{max} (mg/g)	References
Tea factory waste	Cr(VI)	54	Malkoc and Nuhoglu (2007)
Modified masau	Cr(VI)	94.32	Albadarin et al. (2017)
Acid and alkali teated banna peel	Cr(VI)	4.15	Ali and Saed (2013)
Bael fruit shell	Cr(VI)	17.27	Anandkumar and Mandal (2009)
Rice straw	Cr(III)	3.15	Gao et al. (2008)
Modified seaweed	Cr(VI)	58	Yang and Chen (2008)
Acid modifield banana peels	Cr(VI)	162	Current work

capacity of the modified banana peels developed here (around 163 mg/g) is higher than some other bio-sorbent materials reported in the literature. The current work carried out in our lab focuses on using different methods like alkali and metal salt solutions to treat banana peels, then the adsorption studies will also be carried out using these treated banana peels. Our future work will focus on the evaluation of these materials on the treatment of wastewater contaminated with other heavy metals.

References

- Albadarin, A.B., et al.: Single, simultaneous and consecutive biosorption of Cr(VI) and orange II onto chemically modified masau stones. *J. Environ. Manage.* **204**, 365–374 (2017)
- Ali, A., Saeed, K.: Decontamination of Cr(VI) and Mn(II) from aqueous media by untreated and chemically treated banana peel: a comparative study. *Desalin. Water Treat.* **53**, 3586–3591 (2013)
- Anandkumar, J., Mandal, B.: Removal of Cr(VI) from aqueous solution using Bael fruit (*Aegle marmelos correa*) shell as an adsorbent. *J. Hazard. Mater.* **168**, 633–640 (2009)
- Anwar, J., Shafique, U., Waheed-uz-Zaman, Salman, M., Dar, A., Anwar, S.: Removal of Pb(II) and Cd(II) from water by adsorption on peels of banana. *Bioresource Technol.* **101**, 1752–1755 (2010)
- Ashraf, M.A., Wajid, A., Mahmood, K., Jamil Maah, M., Yusoff, I.: Low cost biosorbent banana peel (*Musa sapientum*) for the removal of heavy metals. *Sci. Res. Essays* **6**(19), 4055–4064 (2011)
- FAO: Banana statistical compendium (2019). http://www.fao.org/fileadmin/templates/est/COMM_MARKETS_MONITORING/Bananas/Documents/web_Banana_statistical_review_2017.pdf. Last Accessed 13 June 2019
- FAO: Chapter 1 overview of world banana production and trade (2019). <http://www.fao.org/3/y5102e/y5102e04.htm>. Last Accessed 13 June 2019
- Gao, H., Liu, Y., Zeng, G., Xu, W., Li, T., Xia, W.: Characterization of Cr(VI) removal from aqueous solutions by a surplus agricultural waste - rice straw. *J. Hazard. Mater.* **150**, 446–452 (2008)
- Malkoc, E., Nuhoglu, Y.: Potential of tea factory waste for chromium (VI) removal from aqueous solutions: thermodynamic and kinetic studies. *Sep. Purif. Technol.* **54**, 291–298 (2007)
- Memon, J.R., Memon, S.Q., Bhangar, M.I., El-Turki, A., Hallam, K.R., Allen, G.C.: Banana peel: a green and economical sorbent for the selective removal of Cr(VI) from industrial wastewater. *Colloids Surf. B* **70**, 232–237 (2009)
- Mohapatra, D., Mishra, S., Sutar, N.: Banana and its by-product utilisation: an overview. *J. Sci. Ind. Res.* **69**, 323–329 (2010)
- Nilanjana, D., Vimala, R.: Biosorption of heavy metals—an overview. *Indian J. Biotechnol.* **7**, 159–169 (2008)
- Yang, L., Chen, J.P.: Biosorption of hexavalent chromium onto raw and chemically modified *Sargassum* sp. *Biores. Technol.* **99**, 297–307 (2008)



Removal of Nickel from Aqueous Solution and Industrial Effluent by Iron Oxide

Nesrine Boujelben, Zaineb Bakari, Nesrine Turki, and Boubaker Elleuch

Abstract

The increase of world population and industrial activities require water treatment. Recovery of heavy metal present in industrial effluent into natural material is one of the most widely used solutions. Ion metal such as nickel is classified as a highly toxic element and considered a severe environmental contaminant. Therefore, its removal, separation and enrichment in aqueous solutions play an essential role in the environmental remediation of wastewater. The implementation of such a process on an industrial scale requires the use of adsorbents readily available inexpensive. Iron oxide answers very well to these two requirements. The optimal values of contact time, temperature, pH and the initial substrate concentration were determined in this study. The adsorption was strongly dependent on the pH of the medium with enhanced adsorption as the pH values of 7.9. The maximum uptake capacity of Nickel ion was 30 mg/g grafted resin at 20 °C, at an initial pH value of 7.9. When Freundlich and Langmuir isotherms were tested, the latter had a better fit with the experimental data.

Keywords

Heavy metal • Iron oxide • Adsorption • Isotherm • Nickel

1 Introduction

In recent years, the heavy metals exhibition in the environment has set off concerns around the world, resulting in the use of an array of techniques and treatment processes (Shen et al. 2009). Among the processes used to eliminate them from waters, we can cite the adsorption. In this work, we

have studied the recovery of Nickel from aqueous solution by iron oxide. Several parameters have been investigated such as the pH agitation time and initial concentration? This work aimed to study the influence of a new method using adsorption by iron oxide to determine the maximum amount of metal adsorbed by this support.

2 Materials and Methods

The iron oxide sample used in this work was collected from the Djerissa iron mine in the north of Tunisia (Kef city). The specific surface area of iron oxide was determined using the standard Brunnauer, Emmett, and Teller (BET-N₂) method. The metal adsorption by iron oxide is widely studied: the classical method consisted of mixing a volume of metal solution with a mass iron oxide and then made series of agitation-centrifugation; the supernatant was analyzed by atomic absorption method to determine the concentration adsorbed by iron. The effect of pH was studied at different pH values: 2, 4, 6, 7, 7.9, 8.8 and 10. The suspensions were stirred for two hours. The solution pH was adjusted to 5 with 1 M HNO₃ and 1 M NaOH after which the suspensions were stirred for different time intervals. Adsorption isotherm studies were affected by using a solution containing various nickel ion concentrations (25, 50, 75, 100 mg/L). The initial pH was maintained at 7.9, and the suspensions were stirred for two hours.

3 Results

The BET-N₂ showed that the specific surface area of iron oxide was 70 m²/g.

The isotherm of adsorption was examined. Several parameters such as pH agitation time and initial concentration were studied in order to assess optimal operating conditions. During the adsorption process, Nickel ions uptake

N. Boujelben · Z. Bakari (✉) · N. Turki · B. Elleuch
University of Sfax, 3029 Sfax, Tunisia

shows an increase with time contact until equilibrium. The effect of contact time on the removal of nickel ions was studied for an initial concentration of 140 mg/L.

The kinetic equilibrium obtained at the end of two hours (Fig. 1).

To obtain the optimal value of pH, tests were carried out with 300 rpm rotation speed during two hours at 25 °C.

The study of pH effect on Nickel removal was almost around 7.9 (Fig. 2).

The effect of temperature on the removal of nickel was shown in the Fig. 3.

The data processing showed that the adsorption of Nickel into iron oxide fitted well to the Langmuir model as shown at Fig. 3.

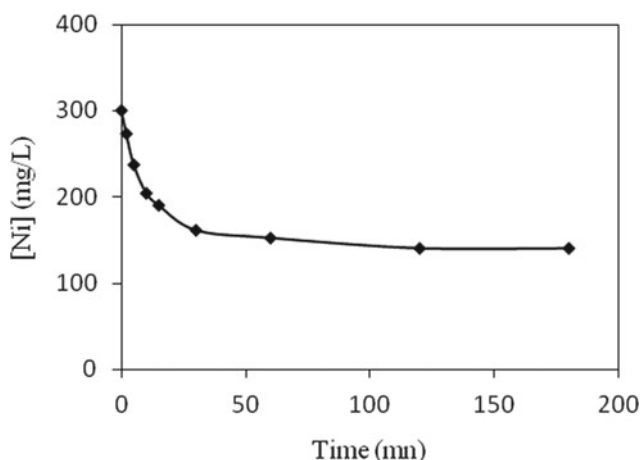


Fig. 1 Kinetic study for nickel ion adsorption on iron oxide

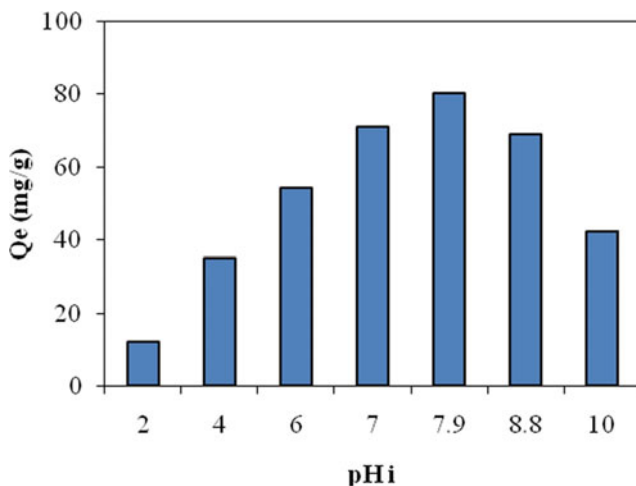


Fig. 2 Effect of pH on the removal of Ni(II) on iron oxide

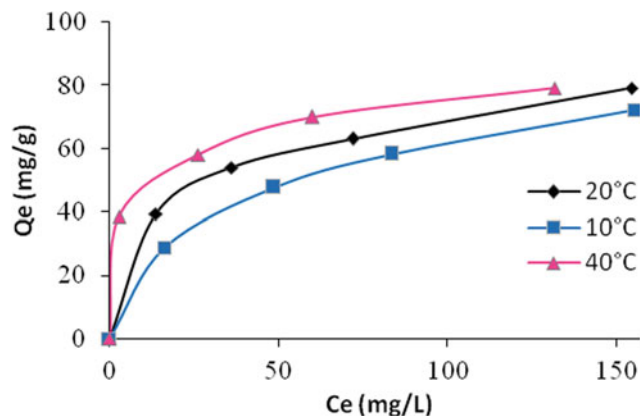


Fig. 3 Ni(II) adsorption isotherm on iron oxide at different temperatures

4 Discussion

The adsorption of nickel by iron oxide at various pH is presented in Fig. 2. We studied the effect of the aqueous solution pH on the removal of nickel by altering the pH between 2 and 10. The pH lower than 7 were unfavourable for the removal of nickel, which could be related to the competition between the cationic ions and the excess of H^+ ions for binding sites (Attallah et al. 2016). As seen in Fig. 3, the nickel adsorption capacity at lower pH was lower than at higher pH, which could be due to the charge of the iron oxide surface. As can be seen, the obtained isotherm is Langmuir type or L-type (Giles et al. 1974).

The adsorption data were modelled using both Freundlich and Langmuir classical adsorption isotherms, suggesting coverage ion onto the substrate surface. The corresponding parameters of the models and the correlation coefficients are reported in Table 1.

Table 1 Freundlich and Langmuir constants for Ni (II) adsorption on iron oxide at 20 °C

Freundlich		
K_f	$1/n$	R^2
14	0.78	0.994
Langmuir		
Q_0	B (L/mg)	R^2
62.5	0.031	0.995

5 Conclusions

The result shows high retention of Ni^{2+} exceeding 53.33% for an initial concentration of 30 mg/L at 20 °C, pH = 7.9 and contact-time of two hours. The lowest performance of adsorption was registered when the test was realized with an acidic medium, while the best results were obtained by adsorbing nickel in an alkaline medium (pH = 7.9). The kinetic equilibrium was obtained at the end of two hours. The adsorption capacity was 80 mg/g of flowing Langmuir isotherms, and the optimum pH was 7.9. This study demonstrated the efficiency of the removal process of nickel ions using the iron oxide as support. Results also indicated the optimal parameters of the adsorption process, which facilitate its implementation in a real plan, namely to purify wastewater from heavy metal ions.

References

- Attallah, O.A., Al-Ghobashy, M.A., Nebsen, M., Salem, M.Y.: Removal of cationic and anionic dyes from aqueous solution with magnetite/pectin and magnetite/ silica/pectin hybrid nanocomposites: kinetic, isotherm and mechanism analysis. *RSC Adv.* **6**, 11461–11480 (2016)
- Giles, C.H., Smith, D., Huitson, A.: A general treatment and classification of the solute adsorption isotherm. I. Theoretical. *Colloid Interf. Sci.* **47**, 755–765 (1974)
- Shen, Y.F., Tang, J., Nie Z.H., Wang, Y.D., Ren, Y., Zuo, L.: Preparation and application of magnetic Fe_3O_4 nanoparticles for wastewater purification. *Separ. Purif. Technol.* **68**, 312–319 (2009)



Chemically Treated Seagrass Fibers as Biosorbent for Crude Oil Removal

Senda Ben Jmaa and Amjad Kallel

Abstract

Oil spills have caused significant environmental and ecological problems. Effective decontamination and cleanups are necessary after the spill to remediate the environment and for human health protection. In the current work, low-cost biomaterial (seagrass) was tested for the removal of crude oil from seawater. Experiments were performed to investigate the oil and water sorption capacity for raw as well as for chemically treated fibers. The sorption capacity tests were conducted in batch for two systems: dry system (pure oil or pure water) and oil–water system. The raw fibers and the milled fibers were found to adsorb/absorb more quantity of water than crude oil due to their hydrophilicity character. However, chemically treated fibers were more hydrophobic than the raw material, where ZnCl_2 and H_3PO_4 solutions at 0.5 M have shown the best enhancement of the sorption capacity. The present study revealed that the tested biosorbent offers an excellent low-cost and eco-friendly alternative for crude removal from seawater. However, further investigation to optimize the process conditions and kinetics would be of great interest.

Keywords

Oil spills • Plant fibers • Oil sorption capacity • Chemical treatment

1 Introduction

The rate of oil production, of different types, is still increasing over years. The environment, however, has borne the brunt of oil exploration and transportation for several decades resulting in oil spills responsible for the contamination of coastal waters and land. Spills may be due to the release of oil from crude oil tankers, offshore platforms, drilling rigs and spills of refined petroleum (Keshawy et al. 2013). The cleanup of oil spill can be carried out by mechanical/physical recovery (booms, skimmers and sorbents), chemical treatments, bio-remediation and burning (Ben Jmaa & Kallel 2019). Sorption is one of the common methods for oil spill cleanup (Olawale and Saidu 2015). Organic sorbents, such as those from agricultural wastes, are candidate materials for oil sorption because they are relatively cheap and easily accessible (Asadpour et al. 2013). Plant derivatives are considered as polymer composites consisting mainly of cellulose, hemicellulose and lignin. These constituents are responsible for the hydrophilicity of the materials. Thus, to have an efficient hydrophobic material for oil sorption, a chemical treatment is necessary (Nwadiogbu et al. 2016).

The aim of this work was to investigate on the effect of chemical treatment on the oil sorption capacity of seagrass raw fibers using different solvents.

2 Materials and Methods

Seagrass fibers were collected from Chaffar Beach (Tunisia) as solid waste. The fibers were manually separated, washed thoroughly with distilled water to remove salts and impurities and then dried in an oven at 40 °C for 74 h (Fig. 1-a). The resulting material was crushed in a Willy mill and sieved into particles with different sizes ranging from 0.063 mm to 2 mm. The raw and sieved fibers were chemically treated with various reagents at 0.5 M to prepare other

S. Ben Jmaa · A. Kallel (✉)
Laboratory of Water, Energy and Environment (3E), Sfax National
School of Engineering, University of Sfax, Sfax, Tunisia
e-mail: amjad.kallel@enis.tn

S. Ben Jmaa
e-mail: sendabenjmaa@hotmail.fr

variants after being over nightly soaked in zinc chloride (ZnCl_2) and phosphoric acid (H_3PO_4) solutions (Fig. 1b), among others. Each sample was then rinsed with deionized water and dried in at 105°C . All samples were stored in labeled containers until use. Oil sorption capacity of the fibers was measured in dry system (pure oil or pure water) and in oil–water layers system (Fig. 1c).

3 Results and Discussion

After its collection and preparation, the seagrass fibers were assessed for their oil sorption capacity (OSC) using different sorbent weights and at different reaction times. The dry system (pure oil or pure water) results revealed that a weight of 0.1 g and 5 min were the best conditions with an OSC value of 5.35 g/g , while in the oil/water system, 0.05 g and 30 min were fixed as the optimized weight sorbent and contact time, respectively, based on preliminary tests (data not shown). For the stirring speed, a low agitation rate (100 rpm) was enough to keep the fibers in the surface layer, when used in a mixed oil/water medium. Moreover, the oil concentration was fixed at 0.03 g/ml . Under these conditions, OSC was estimated at 16.81 g/g .

Despite their interesting OSC in both systems (dry and oil–water layer), the tested fibers were found to adsorb/absorb much more quantity of water, confirming their hydrophilic

nature. To tackle this issue, a physical treatment was performed by crushing raw fibers, and thereafter, several fractions were collected according to their particle size diameters. Each fraction was separately tested for its oil and water sorption capacities. The experiments revealed that $0.5\text{--}1\text{ mm}$ particle size milled fibers had the best results, but they have shown similar water sorption capacity to intact raw fibers (Fig. 2). In fact, the oil sorption capacity was significantly increased from 5.26 to 13.35 g/g , while that of water was evaluated at 15.37 g/g (vs. 14.95 g/g for the raw fibers). Therefore, the chemical treatment was found to be required, and the fraction $0.5\text{ mm--}1\text{ mm}$ was selected for the next analysis.

To this end, different reagents (NaOH , NaCl , H_3PO_4 , KOH , HCl , HNO_3 , ZnCl_2 , H_2O_2 , CH_3COOH) were tested at 0.5 M for their ability to improve fibers hydrophobicity. The results depicted in Fig. 3a reveal that ZnCl_2 and H_3PO_4 gave similar OSC results in the dry system, whereas the lowest water sorption was recorded with ZnCl_2 (8.47 g/g). Concerning the oil–water system, the best enhancement results were obtained with ZnCl_2 (22.93 g/g) followed by H_3PO_4 (19.79 g/g) and HCl (19.32 g/g) as shown in Fig. 3b. Interestingly, the treatment with ZnCl_2 had a beneficial effect on reducing the water sorption down to 0.07 g/g . Relying on the reached findings of the present study, the chemical treatment modified the hydrophilic/hydrophobic ratio of the seagrass fibers resulting in excellent crude oil removal efficiency.

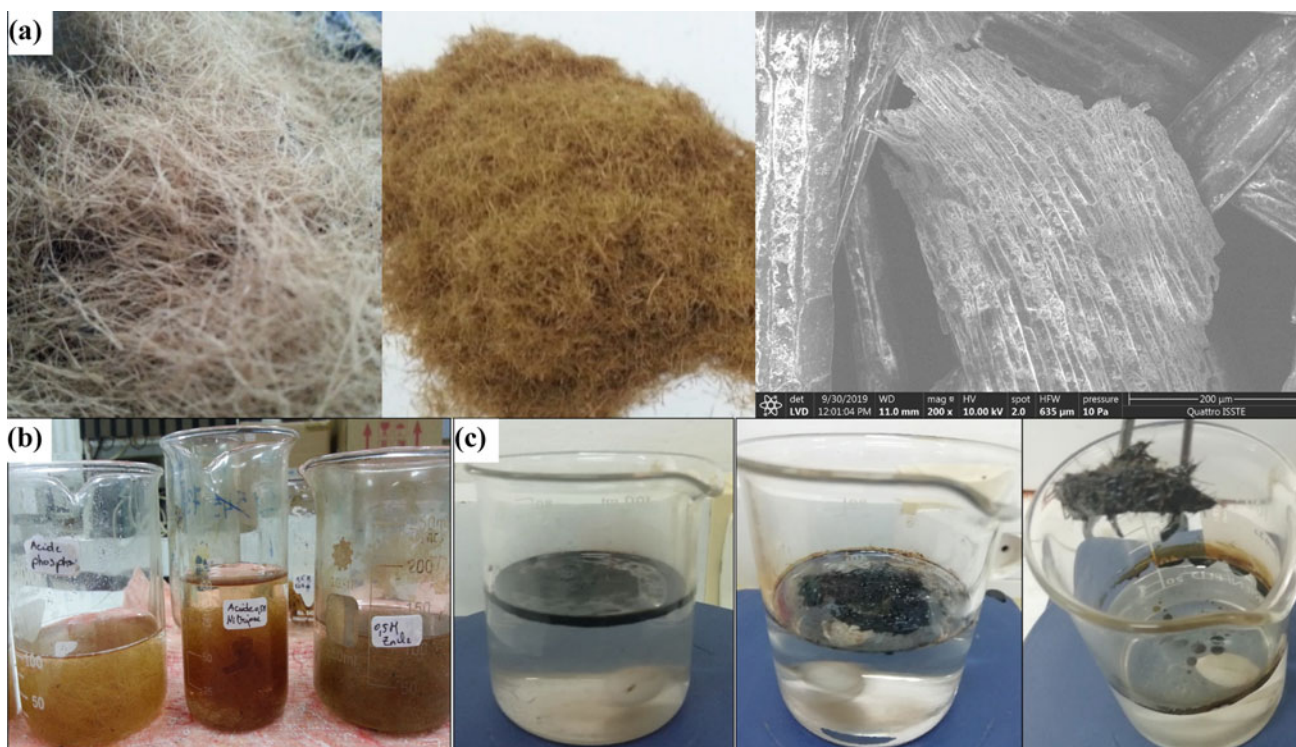


Fig. 1 Seagrass fibers **a** raw and milled; **b** chemically treated and **c** in oil–water system

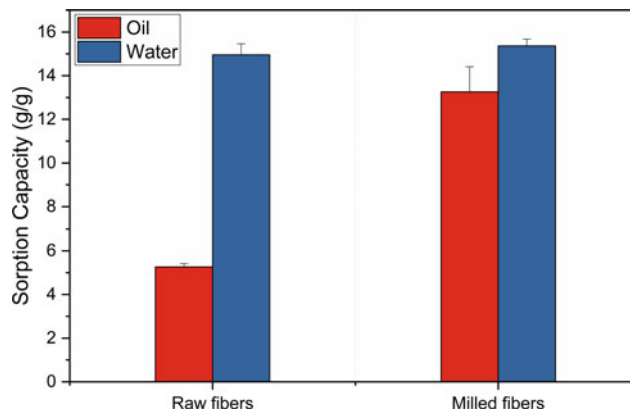


Fig. 2 Oil and water sorption capacities of raw and milled fibers in dry system

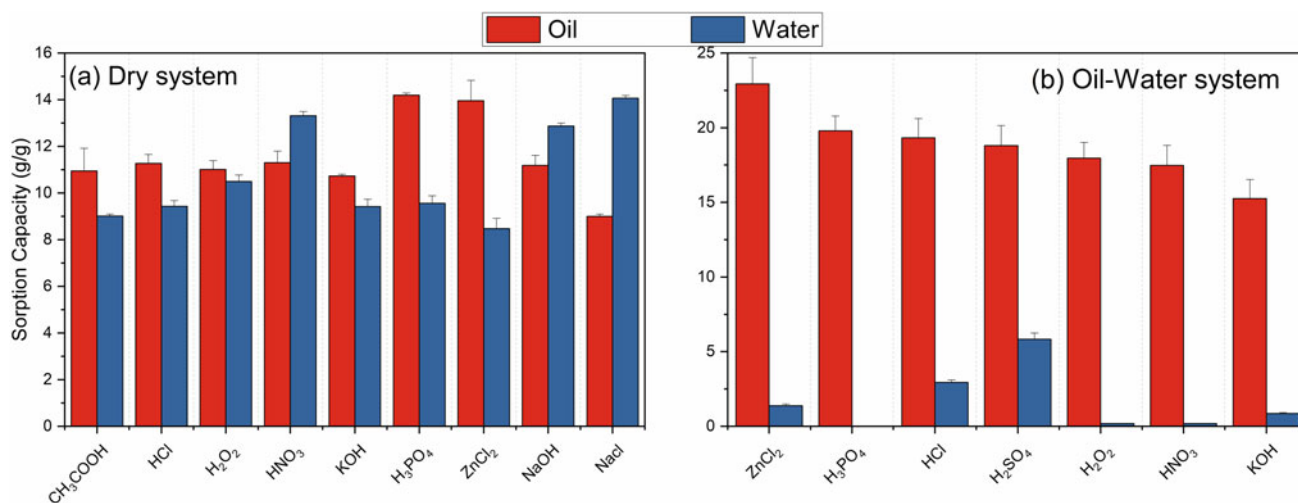


Fig. 3 Effect of different chemical reagents on oil sorption capacity **a** in dry system and **b** in oil–water system

The treated seagrass seems to be a promising biosorbent for oil cleanup, compared to various natural sorbents studied by Annunciado et al. (2005), such as sisal (6.4 g/g), leaves residues (2.7 g/g), saw dust (6.4 g/g), coir fibers (5.4 g/g) and sponge gourd (4.6 g/g).

best OSC results. The present study revealed, therefore, that, besides its low-cost and eco-friendly properties, the tested biosorbent has an excellent crude oil removal capacity in seawater. Further studies still need to be done in order to optimize the oil sorption conditions and dynamics.

4 Conclusions

The removal of crude oil from seawater using seagrass as biosorbent was investigated in this work. The optimum conditions for the best OSC were 0.05 g of weight sorbent, a 30 min reaction time, low-speed stirring and 30 g of oil per L of seawater. The raw fibers and the milled fibers were found to adsorb/absorb more quantity of water than crude oil due to their hydrophilicity character. However, chemically treated fibers were more hydrophobic than the raw material, where ZnCl₂ and H₃PO₄ solutions at 0.5 M have shown the

References

- Annunciado, T.R., Sydenstricker, T.H.D., Amico, S.C.: Experimental investigation of various vegetable fibers as sorbent materials for oil spills. *Mar. Pollut. Bull.* **50**(11), 1340–1346 (2005)
- Asadpour, R., Bin, S.N., Tuan, Z.Z., Jusoh, H., Riahi, A., Uka, O.K.: Application of sorbent materials in oil spill management: a review. *Caspian J. Appl. Sci. Res.* **2**, 46–58 (2013)
- Ben Jmaa, S., Kallel, A.: Assessment of performance of *Posidonia oceanica* (L.) as biosorbent for crude oil-spill cleanup in seawater. *BioMed Res. Int.* **2019**, Article ID 6029654, 9 (2019)
- Keshawy, M., Abd, E.-M., Abdul-Raheim, A.-R.M., Kabel, K.I., El-Hamouly, S.H.: Synthesis and characterization of oil sorbent

- based on hydroxypropyl cellulose acrylate. *Egypt. J. Pet.* **22**, 539–548 (2013)
- Nwadiogbu, J.O., Ajiwe, V.I.E., Okoye, P.A.C.: Removal of crude oil from aqueous medium by sorption on hydrophobic corn cobs: equilibrium and kinetic studies. *J. Taibah Univer. Sci.* **10**, 56–63 (2016)
- Olawale, A.S., Saidu, B.B.: Study of oil sorption capacities of some agricultural wastes. *J. Fuels Energy Environ.* **1**, 1–12 (2015)



Soil Salinization: A Severe Environmental Hazard and Electrokinetic Treatment as One of the Innovative Technologies for Its Mitigation

Mohammed Mustapha Bessaim, Aicha Bessaim, and Hanifi Missoum

Abstract

Recently, soil salinity has become one of the most hazardous environmental issues, affecting thus the ecosystem biodiversity, yield crop, human health as well as urban and rural facilities. Moreover, this threat is increasing day by day at alarming rates, causing losses of billion dollars annually, which affects the country's economic and social prosperity drastically at different levels. Recently, the soil salinity has increased at high levels, mostly in arid and semi-arid regions. These areas are known for their harsh climate, characterized by high temperatures, lack of rainfall and high evapotranspiration, which reduce the leachability of salts and increases their concentrations within the porous medium. On the other hand, the Man-made activities may aggravate the salinity risk via irrigation of cultivated area with salt-rich water. A wide range of conventional adaptations and reclamation strategies has been deployed to mitigate this threat, including soil substitution, cultivation of halophytic plants and chemical amendment. However, such techniques are long-drawn, less productive and cost-intensive. In this regard, the use of a novel, sustainable and cost-effective technology has become a must. Electrokinetic treatment (EKT) can remediate salt-affected soils, due to the application of an electrical field, which effectively removes and eliminates noxious salts from the solid matrix at any depth and under various soil conditions.

Keywords

Soil Salinity • Arid and Semi-arid regions • Mitigation • Remediation • Electrokinetic

1 Introduction

Recently, soil salinity has become an environmental issue of worldwide significance, namely in arid and semi-arid areas. This threat is causing drastic losses of emerging resources, ecosystem imbalance, crop yield, human health, as well as the socio-cultural and general welfare (Daliakopoulos et al. 2016). Nearly 800 million hectares of areas in more than 100 countries around the globe are affected by soil salinity (Srivastava 2020). According to the United Nations Environment Program, half of the cropland and 20% of agricultural regions worldwide are stressed by salts (Srivastava 2020). In North Africa and the Arabian Peninsula, the salinity risk is expected to worsen the situation and to constitute a real menace for the socio-economical situation. In Algeria, salt-affected soils vary in extent from 10 to 15%. Furthermore, the salinity is devastating 93% of the cultivated lands in Egypt and about 54% in Saudi Arabia, while 33.6% of the soils are salinized in the United Arab Emirates (Abdalla 2015). High levels of salts within the soil medium induce several harmful effects on plant and crop yield, including reducing water availability, osmotic adjustment and nutrient uptake (Khanamani et al. 2017). Furthermore, excessive concentration of salts may affect human health, causing several diseases such as methemoglobinemia (blue baby syndrome), birth malformations, infant mortality epidemiological gastric cancer (Choi et al. 2012). In term of constructions, high accumulation of salts may damage buildings, roads, bridges and steel structures. Moreover, excessive concentration of salts deteriorates the soil properties, causing surface crusting, permeability deterioration,

M. M. Bessaim (✉) · H. Missoum
Architecture and Civil Engineering Department, Abdelhamid Ibn
Badis University of Mostaganem, Mostaganem, Algeria

M. M. Bessaim · H. Missoum
Construction, Transport and Protection of Environment
Laboratory (LCTPE), Mostaganem, Algeria

A. Bessaim
Civil Engineering Department, Mustapha Stambouli University
of Mascara, Mascara, Algeria

erosion, waterlogging and a net decrease in soil bearing capacity (Jayasekera 2015).

A wide array of methodologies against soil salinity has been applied to cope with this peril, namely controlled irrigation, soil substitution, chemical amendment and bio-remediation. However, these techniques are expensive and mostly ineffective, namely when dealing with cohesive-soft saline/sodic soils. The electrokinetic treatment (EKT) can be an innovative, eco-friendly and low-cost technique that can fill those deficiencies (Bessaim et al. 2019). The principles of this process involve the application of an electrical field through inserted electrodes within the saline soil. Harmful salts will be dissolved, transported and removed via a set of complex processes, known as electrolysis, electro-migration and electro-osmosis (Cho et al. 2010). The combined effect of these mechanisms alters the chemistry of the soil matrix significantly, changing hence the physicochemical characteristics of the saline/sodic soil. This study aims to provide valuable knowledge about the EKT as a tool for mitigation of salinity risk around the world and especially in arid and semi-arid regions.

2 Electrokinetic Treatment as An Innovative Strategy for Remediation of Saline Soils

Electrokinetic treatment (EK) is one of the most modern methods for removing contaminants as well as salts (Bessaim et al. 2019). The removal of these chemicals is based

on the application of an electrical field via two inserted electrodes into the saline soil, as shown in Fig. 1.

The passage of current causes salts mobilization and removal, due to electrolysis, electro-migration and electro-osmosis (Bessaim et al. 2019). The electrolysis reactions result in the generation of hydrogen (H^+) and hydroxide ions (OH^-), creating an acidic and basic front at the anode and cathode, respectively. The low pH in the anode allows desorption and solubilization of chemical compounds, enhancing thereby their removal (Cameselle 2015). The electro-migration cause salts migration toward the electrodes of opposite charge, facilitating their extraction at the electrodes. On the other hand, the induced water flow during electro-osmosis serves to clean up the soil. Results.

The experimental tests were carried out on Sodic-Saline soils, sampled from the northern-west part of Algeria. The EKT feasibility and effectiveness are summarized in Table 1. As previously shown, the author's previous results (Bessaim et al. 2019) report the targeted salts have been successfully eliminated during EKT, with a removal rate of 93, 63 and 15% for magnesium, chloride and sulfate ions, respectively. Magnesium ions show the highest removal efficiency compared to other ions. Such behaviour is related to the fact that cations are transported via the combination of electro-migration and EOF mechanisms, while the anions will be transported only by electro-migration. The obtained outcomes show that EKT can successfully mitigate salinity hazard and removal of noxious salts.

Fig. 1 Electrokinetic remediation of saline/sodic soils

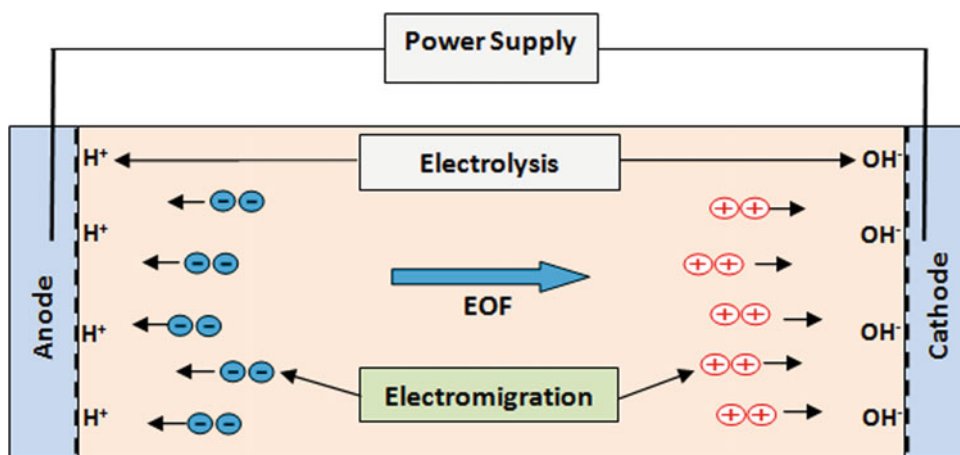


Table 1 Effectiveness of EKT on remediation of saline soil

Technology	Treatment time (h)	Targeted salts	Removal efficiency (%)	Reference
EKT	120	Magnesium (Mg^{2+})	93	Bessaim et al. (2019)
		Chloride (Cl^-)	63	
		Sulfate (SO_4^{2-})	15	

3 Conclusions

Given the different aspects noted above, we can draw the following conclusions:

- The electrokinetic treatment is an innovative, effective and low-cost technology for the remediation of salt-affected soils
- Previously obtained results show that in a short period (120 h), with a removal rate of 93, 63 and 15% for magnesium, chloride and sulfate ions, respectively.
- The obtained outcomes show that this technique can put a term to the proliferation of the soil salinity in arid regions worldwide.
- When dealing with salt-affected soils, the EKT may be the most sustainable alternative for remediation of saline and sodic soils ex-situ and in-situ.

References

- Abdalla, M.A.: Regional assessment of soil changes in the Near East and North Africa. In: Status of the World's Soil Resources (SWSR)-Main Report, FAO and ITPS. Food and Agriculture Organization of the United Nations and Intergovernmental Technical Panel on Soils, Rome, Italy, pp. 399–441. (2015)
- Bessaim, M.M., Missoum, H., Bendani, K., Bekkouche, M.S.: Mitigation of salinity hazard from low permeable soil by electrochemical treatment: a laboratory based investigation. In: Recent Advances in Geo-Environmental Engineering, Geomechanics and Geotechnics, and Geohazards (pp. 93–95). Springer, Cham (2019)
- Cameselle, C.: Enhancement of electro-osmotic flow during the electrokinetic treatment of a contaminated soil. *Electrochim. Acta* **181**, 31–38 (2015). <https://doi.org/10.1016/j.electacta.2015.02.191>
- Cho, J.M., Park, S.Y., Baek, K.: Electrokinetic restoration of saline agricultural lands. *J. Appl. Electrochem.* **40**(6), 1085–1093 (2010)
- Choi, J.H., Lee, Y.J., Lee, H.G., Ha, T.H., Bae, J.H.: Removal characteristics of salts of greenhouse in field test by in situ electrokinetic process. *Electrochim. Acta* **86**, 63–71 (2012)
- Daliakopoulos, I.N., Tsanis, I.K., Koutroulis, A., Kourgialas, N.N., Varouchakis, A.E., Karatzas, G.P., Ritsema, C.J.: The threat of soil salinity: a European scale review. *Sci. Total Environ.* **573**, 727–739 (2016)
- Jayasekera, S.: Electrokinetics to modify strength characteristics of soft clayey soils: a laboratory based investigation. *Electrochim. Acta* **181**, 39–47 (2015)
- Khanamani, A., Fathizad, H., Karimi, H., Shojaei, S.: Assessing desertification by using soil indices. *Arab J Geosci.* **10**, 287 (2017)
- Srivastava, N.: Reclamation of saline and sodic soil through phytoremediation. In: Environmental Concerns and Sustainable Development (pp. 279–306). Springer, Singapore (2020)

Abdalla, M.A.: Regional assessment of soil changes in the Near East and North Africa. In: Status of the World's Soil Resources



Contaminants Transfers Through Composite Liners Exhibiting Aged GCLs: A Numerical Prediction

Hajer Bannour, Farouk Ben Abdelghani, and Nathalie Touze

Abstract

This study presents numerical simulations of contaminants transport through a composite geomembrane geosynthetic clay liner (GMB-GCL) linings system. Organic contaminants have been studied (TCE, P-cresol). GCLs properties are considered after cation exchange and wet-dry cycles to take into account the alteration of the GCL by their environment. Results are compared with contaminant transfers through composite liners involving virgin GCLs to study the durability of these aged GCLs. Typical published values for the diffusion coefficient for both virgin and aged GCL used in this study are shown to give good predictions of contaminants migration and effluent concentration with time. Indeed, obtained relative concentrations evolutions with time agree well with the theoretical break-through curve. Indeed, Simulated contaminant concentrations through GCLs showed that alteration by the environment of GCLs seems not to affect significantly the diffusion of organic contaminant examined in this study.

Keywords

Geosynthetics • Composite liners • Diffusion • Hydro-geosphere

1 Introduction

Composite liners used at the base of modern landfills often contain a high-density polyethylene (HDPE) geomembrane (GMB) over a geosynthetic clay liner (GCL). This GMB-GCL association is intended to minimize the leakage

and transport of contaminants from the landfill to the surrounding environment (i.e., surface and groundwater). Despite special attention regarding manufacturing, transportation, handling, storage and installation, defects in the GMB seem to be unavoidable (Needham et al. 2004; Peggs 2015). They represent preferential flow paths for leachate migration which could reach and pollute the surrounding soil and groundwater. Defects in the GMBs when present could enhance contaminants transport and hence the pollution of the surrounding environment.

1.1 Diffusion of Organic Contaminants Through GCLs

Besides gaseous emissions, and that of methane and trace gases caused by the degradation of organic waste, leachate production from landfills raises the main potential long-term environmental threat (Kjeldsen et al. 2002). The presence of organic contaminants in leachate from municipal solid-waste landfills has been demonstrated in several countries (Rosin-Paumier et al. 2011). A total of 592 different organic and inorganic compounds were identified (Praagh et al. 2011). Quantifying the transfer to the surrounding environment of organic pollutants from compounds emerging from leachate is thus of primary importance. The significant substances identified may be categorized into the following groups (in descending order of several detections): phenolic compounds, aromatic hydrocarbons, heterocyclic substances, carboxylic acids, phthalates, anilines, aliphatic acids, phenoxy acids organo-phosphorous substances, terpenoids, and triazines. The theory related to contaminant diffusion through composite liners and primarily through GCLs has been previously described and detailed by Touze-Foltz et al. (2016).

H. Bannour (✉) · F. Ben Abdelghani
University of Sousse, 4003 Sousse, Tunisia

N. Touze
INRAE Antony, 92160 Antony, France

1.2 Aged GCLs After Cation Exchange and Wet-Dry Cycles

GCLs can be subject to cation exchange and physical dehydration due to moisture or temperature gradients across the entire barrier (Bannour et al. 2015; Benson 2013). Wet-dry cycles, especially in arid regions, can damage GCLs, by causing desiccation with cracks leading to preferential flow paths even after the GCL rehydrates (Lin and Benson 2000). In fact, after some cycles, desiccation cracks do not close up when the GCL rehydrates as the GCL has lost its swelling ability (Touze-Foltz et al. 2010). This leads to substantial increases in the hydraulic conductivity of GCLs, by as much as 4 to 5 orders of magnitude as compared to virgin GCLs (Bannour et al. 2015). It thus seems essential to predict contaminant transfers through composite liners that will arise from the appearance of defects in the GMB. It is also essential to take into account the alteration of GCLs by their environment in order to evaluate the potential impact of the contaminants on the environment, especially on soil liners and groundwater. (Rosin-Paumier et al. 2011; Mendes et al. 2013, 2014) studied the diffusion of organic components (phenolic and VOCs: aromatic hydrocarbons) into virgin and aged specimens. Their main results showed an increase in the diffusion coefficient in GCLs of these components due to cation exchange compared with virgin GCLs.

This study aims to conduct diffusion of organic compounds (phenolic: p-cresol and a VOCs: Trichloroethylene, TCE) transport through GMB-GCL composite liners using the HydroGeosphere code (Therrien et al. 1996). The main idea of the simulation method was to reproduce contaminant transport (advective transport due to a hydraulic gradient coupled to diffusive transport due to concentration gradient). The hydraulic gradient comes from the hydraulic head above a defect in the GMB, and diffusive gradient comes from the existence of contaminants concentrations through the composite liner. To consider the alteration of the GCL by their environment, the properties used are for GCLs after cation exchange and wet-dry cycles. Obtained results are compared with composite liners involving virgin GCLs to study their durability.

2 General Features of Composite Liners

2.1 General Features and Porous Media Characteristics

The studied 2D axisymmetric model is shown in Fig. 1. It consists of a composite liner formed by a damaged GMB stacked on a 0.01-m-thick GCL overlying a 0.045-m-thick compacted clay liner (CCL). This scheme is consistent with the composite liners used in experiments involving transmissivity cells (Touze-Foltz. 2002). The interface between the GM and the GCL was modelled as a thin layer 0.001 m thick, and the hydraulic conductivity was adjusted to give the required transmissivity (Touze-Foltz et al. 2016). The features of the porous media are shown in Table 1.

2.2 Initial and Boundary Conditions

A free-drainage boundary condition was used for the bottom boundary, and a no-flow boundary condition was used for the GMB. The GMB is presenting a 4 mm diameter hole. The hole was modelled as a 0.3 m hydraulic head boundary condition. An initial concentration C_0 (Dirichlet or first type) boundary condition was imposed at nodes of the hole to simulate contaminant diffusion. This simulated initial

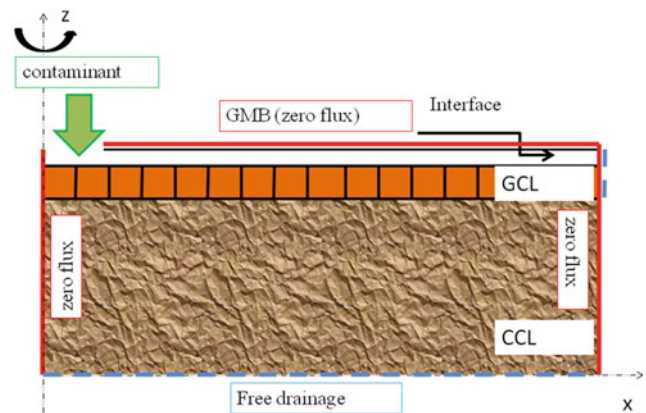


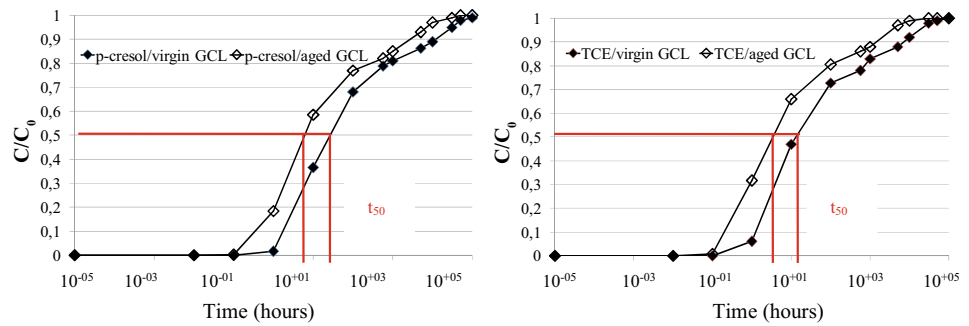
Fig. 1 Feature GMB-GCL composite liners

Table 1 Parameters of porous media

Material	Hydraulic conductivity K_{sat} ($m \cdot s^{-1}$)	Porosity n	Effective diffusion coefficient for TCE (m^2/s)	Effective diffusion coefficient for p-cresol (m^2/s)
Virgin GCL*	2.56×10^{-11}	0.74	3.9×10^{-10}	5.0×10^{-11}
Aged GCL*	5.55×10^{-6}	0.74	7.0×10^{-10}	1.0×10^{-10}

* needle punched containing sodium bentonite

Fig. 2 Contaminant migration with time into GCLs for respectively P-cresol and TCE



condition has been already adopted and confirmed by previous results existing in the literature for inorganic contaminant (Rowe and Abdelatty 2012). The initial concentration is imposed null elsewhere in the model. The intact GMB, side boundaries and axis of symmetry were zero flux boundary conditions. A no-flow boundary condition was also imposed on the left and right boundaries of the model.

3 Results

Figure 2 shows the obtained results of contaminant concentrations with the HydroGeosphere code (Therrien et al. 1996). Curves in Fig. 2 represent relative concentrations C/C_0 with time at the base of the GCLs. It can be seen that C/C_0 ratio values range between 0 and 1, which are the two imposed conditions. Also, contaminant curves reproduce the theoretical evolution of contaminant transport. It could be noticed that, for both studied contaminants, the migration kinetic is approximately the same for virgin and aged GCLs and the entire migration of TCE and P cresol happened after 105 h for virgin and aged GCLs. To examine the relative difference of contaminants transfers through a virgin and aged GCLs we could determine t_{50} which is defined as the time for $C/C_0 = 0.5$ to reach 0.5, corresponding to the position of the advection front and thus to contaminant transport by advection. T_{50} here approximately equals 10 h for both contaminants through aged GCLs and is about 20 h for virgin GCLs.

4 Discussion

These results could be explained by the fact that for aged GCLs contaminants could reach the same concentration ($C/C_0 = 0.5$) at an earlier time. Hence, the breakthrough curve position of advective front is at 10 h. These results showed that the alteration by the environment of GCLs seems not to affect the diffusion of contaminant examined in this study. These assumptions remain to be confirmed for other GCLs and other pollutants.

5 Conclusion

The diffusion of organic contaminants (phenolic: P-cresol and VOC: TCE) through GCLs was modelled. GCLs were considered virgin and experiencing cation exchange and wet-dry cycles in order to study the effect of aged GCLs on contaminant diffusion. GCLs were associated with a GMB exhibiting a hole overlain a CCL layer. Results conducted with the HydroGeosphere code highlight the fact that contaminant concentrations reproduce the classic theoretical curve for contaminant transport by hydrodynamic dispersion. Obtained results also show that alteration by the environment of GCLs seems not to affect the diffusion of examined organic contaminants significantly.

References

- Bannour, H., Barral, C., Touze-Foltz, N.: Altered geosynthetic clay liners: Effect on the hydraulic performance of composite liners. *Europ. J. Environ. Civil Eng.* **19**(9), 1176–1176 (2015)
- Benson, C.H.: Impact of subgrade water content on cation exchange and hydraulic conductivity of geosynthetic clay liners in composite barriers. In: *Coupled Phenomena in Environmental Geotechnics*. pp. 79–84 (2013)
- Kjeldsen, P., Barlaz, M.A., Rooker, A.P., Baun, A., Ledin, A., Christensen, T.H.: Present and long-term composition of MSW landfill leachate: a review. *Crit. Rev. Environ. Sci. Technol.* **32**(4), 297–336 (2002)
- Lin, L.C., Benson, C.H.: Effect of wet-dry cycling on swelling and hydraulic conductivity of GCLs. *Geotech. Geoenviron. Eng.* **126**(1) (2000)
- Mendes, M.J.A., Touze-Foltz, N., Gardoni, M., Ahari, M., Mazeas, L.: Quantification of the diffusion of phenolic compounds in a virgin GCL and in a GCL after contact with a synthetic leachate. *Geotext. Geomembr.* **38**, 16–25 (2013)
- Mendes, M.J.A., Touze-Foltz, N., Gardoni, M., Mazeas, L.: Quantification of diffusion of bisphenol A in a GCL after contact with a synthetic leachate. In: *10th International Conference on Geosynthetics*, Berlin, September 21–25, pp. 8. (2014)
- Needham, A., Gallagher, E., Peggs, I., Howe, G., Norris, J.: *Likely medium to long-term generation of defects in geomembranes*. Bristol: Environment Agency (2004)
- Peggs, I.D.: Abnormal performance characteristics of HDPE geomembranes at sub-zero temperatures. In: *Paper presented at the Geosynthetics 2015*, Portland, Oregon (2005)

- Rosin-Paumier, S., Touze-Foltz, N., Mazeas, L., Guenne, A.: Quantification of volatile organic compounds diffusion for virgin geosynthetic clay liners and for a GCL after contact with a synthetic leachate. *J. Geotech. Geoenviron. Eng.* **137**(11), 1039–1046 (2011)
- Rowe, R.K., Abdelatty, K.: Modeling contaminant transport through composite liner with a hole in the geomembrane. *Can. Geotech. J.* **49**(7), 773–781 (2012)
- Therrien, R., Sudicky, E.A.: Three dimensional analysis of variably saturated flow and solute transport in discretely fractured porous media. *J. Contam. Hydrol* **23**, 1–44 (1996)
- Touze-Foltz, N.: Evaluation of the hydraulic transmissivity in soil liner-geomembrane interfaces. In: *Proceedings of the Seventh International Conference on Geosynthetics*, Nice, France. Swets and Zeitlinger, Lisse, Netherlands vol. 2 (pp. 799–802). (2002)
- Touze-Foltz, N., Croissant, D., Rosin-Paumier, S., Pirrion, T., Ouvry, J. F.: Performance of a GCL in a landfill cover after six years in service. In: *Paper presented at the 3rd International Symposium on Geosynthetic Clay Liners*, Würzburg, Germany (2010)
- Touze-Foltz, N., Bannour, H., Barral, C., Stoltz, G.: A review of the performance of geosynthetics for environmental protection. *Geotext. Geomembr.* **44**, 656–672 (2016)
- Van Praagh, M., Torneman, N., Johansson, M., Ingelstedt Frendberg, L.E., Heander, E., Johansson, A.: Emerging organic contaminants in leachate: a review and risk assessment. In: *Proceedings Sardinia 2011, Thirteenth International Waste Management and Landfill Symposium S. Margherita di Pula, Cagliari, Italy; 3e7 October 2011*. CISA Publisher, Italy, pp. 8. (2011)



Physicochemical Adsorption Properties of Heavy Metals by Different Clay Combinations in the Context of Phosphogypsum Storage

Kawther Ben Moussa, Saifeddine Eturki, Philip Tack, Rinehart Van Poucke, Samuel Budet, Johan De Grave, Mohamed Moussa, and Mohamed Ouessar

Abstract

The storage of phosphogypsum waste has become an essential issue for the environment. The regulations require the presence of a safety barrier with an optimal seal to avoid contamination of the subsoil and the water table. Clays, having low permeability and a high capacity to retain pollutants (heavy metals), are therefore frequently used as a passive safety barrier at the base of a waste heap. However, these clays must ensure the durability of these barriers in contact with the leaching solutions and particularly with the metallic pollutants it contains. This work consists of simulating in the laboratory the infiltration of metal pollutant solutions of phosphogypsum waste onto specific clays, to analyse the interaction mechanisms and thus to predict the hydraulic behaviour and physicochemical of these clays. For this study, we use three types of clays from the Gabes region. Mineralogical characterization shows that clays Romana and Haidoudi are smectitic favouring the adsorption phenomenon. Characterization of phosphogypsum waste shows the high concentration of this latter in heavy metals such as Cd and Cr.

Keywords

Phosphogypsum • Heavy metals • Clay • Adsorption • Storage

K. Ben Moussa (✉) · S. Eturki · M. Moussa · M. Ouessar
Laboratory of Eremology and Combating Desertification, Institute of Arid Regions of Medennine, Djorf Road Km 22.5, Medennine, Tunisia

P. Tack · R. Van Poucke · S. Budet
Faculty of Bioscience Engineering, Department of Green Chemistry and Technology, Ghent University, Ghent, Belgium

J. De Grave
Faculty of Sciences Department of Geology, Ghent University, Ghent, Belgium

1 Introduction

This work deals with current problematic issues of the environment–health interactions in the context of phosphogypsum storage. The phosphate-processing industry occupies an essential place in the Tunisian economy. The waste of this phosphate production is a big problem. These wastes discharged into the sea are rich in heavy metals which are dangerous for the health of man and the remains of living beings when they are present in the environment with high concentrations (Fakayode 2005). Thus, the accumulation of heavy metals in the marine environment has devastating effects on the ecological balance of the aquatic environment (Mondat 2010).

The management of Tunisian phosphogypsum firstly involves an improvement of the current storage conditions respecting at best the environment. For instance, clays have been the subject of various studies for various applications such as adsorption. Clays are known for their adsorption capacity, their vast surface area and their abundance in nature. This work aims to find a solution for the storage of phosphogypsum on a continental scale in Tunisia by the establishment of a clay layer to ensure proper sealing.

2 Materials and Methods

The three clay samples were characterized by XRD, and the records of the XRD charts have been made using a Phillips X pert-pro X-ray diffractometer and X-ray fluorescence analysis. The principle of this method consists in bombarding the material to be analysed by an X-ray beam, which leads to secondary emission of X-rays: we obtained a spectrum of X-rays emitted which presents the characteristic peaks of the different elements existing in the sample. Spectrum analysis can be done in two ways: dispersive wavelength analysis and dispersive energy analysis. The position of the peaks informs about the nature of the element

(qualitative analysis), whereas its intensity makes it possible to quantify the content of each element.

Cationic exchange capacity (CEC) of the sample was determined using the ammonium acetate method (Reeuwijk 1992). Specific surface area (SBET) was determined using the blue stain of methylene. The chemical compositions of the clay samples and phosphogypsum were obtained by inductively coupled plasma atomic emission (ICP-AES) and mass spectrometry (ICP-MS). The samples were dried and underwent an acid attack. This method was carried out following (Baccour et al. 2008) methodology. Small column study was conducted to monitor the capacity of a metal adsorbed clay sample in phosphogypsum waste.

3 Results

3.1 X-ray diffraction of clays

The results of all the minerals estimated through X-ray diffraction are shown in Fig. 1. The nature of the impurities was determined by studying the crude samples; quartz is the dominant impurity (101 reflections), for the clays sample with a small amount of feldspar. The following mineralogical components were identified in the purified fraction: the presence of kaolinite (ICDD reference pattern: 00–001-0527) with reflections at 7.14 and 3.57 Å, which disappear after heating at 500 °C. The mineralogical composition is the same in all cases, mainly including kaolinite, quartz, calcite and feldspar.

There is no smectite in Hmaymet clays, which does not favour the use of this clay in the context of metal adsorption.

3.2 Chemical composition

Chemical compositions of the phosphogypsum and the concentrations of heavy metals were measured by

inductively coupled plasma atomic (ICP-AES). The results in Fig. 2 show that the concentrations of the heavy metals in mg/kg (ppm) found in the phosphogypsum of Gabes are high for some elements (Cd, Cr and U) in comparison with other releases of phosphogypsum in the world or comparing with the grades given for a typical soil.

Column processing

4 Discussion

We see that the composition in heavy metals varies a lot in depending on the origin of the phosphate ore. This composition also depends on the industrial process for manufacturing phosphoric acid (Arman and Seals 1990).

The process of adsorption has become one of the preferred methods for removal of toxic contaminants from water as it is beneficial, economical, versatile and straightforward (Tran et al. 1999). In our case, we relied on the use of three types of clay to investigate their ability to absorb the accumulated heavy metals in the phosphogypsum rejection of the gab region with columns tests. It is found that the metal concentration decreases after each test until the contents are equal to 0. This shows the excellent capacity of these clays Haidoudi and Romana, in particular, in the context of adsorbing metals.

5 Conclusion

The results show that the clays of Haidoudi and Romana are smectitic, which characterizes swelling clay. These two clays are better than Hmaymet clay for the adsorption of concentrated metals in the phosphogypsum waste. The chemical analysis of phosphogypsum shows that the richness of this waste in heavy metals against the study of radioactivity

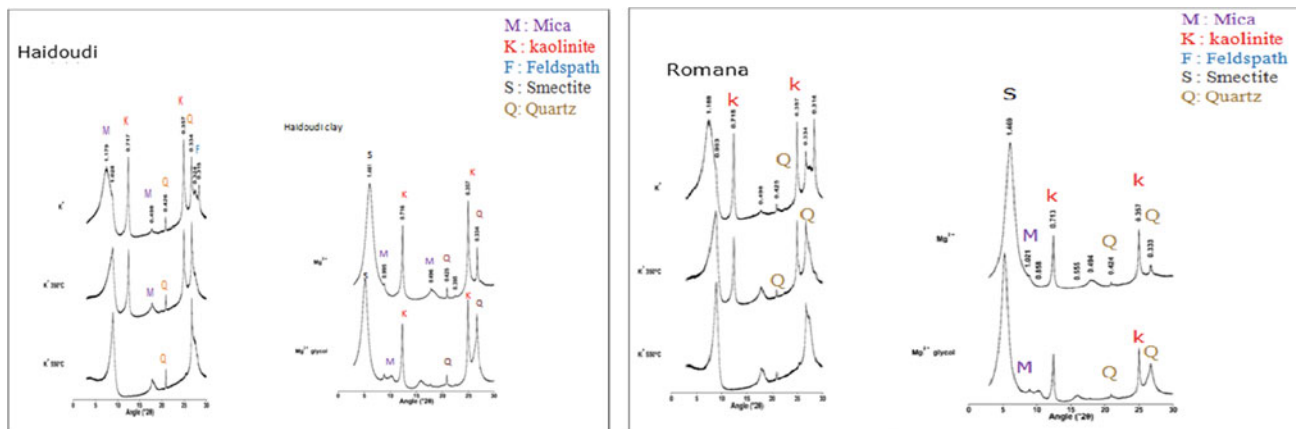
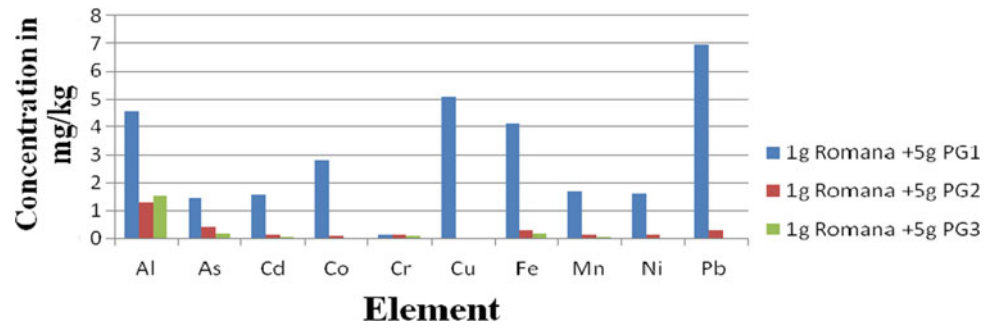


Fig. 1 XRD patterns of the clay fraction of Haidoudi and Romana clay. Unprocessed sample; treated by ethylene glycol and heated at 500 °C

Fig. 2 Metals in a column filled at the base with 1 g of Romana clay topped with 5 g of phosphogypsum and leached 3 times



shows that it is not radioactive, and the measured values are low compared with other releases of phosphogypsum in other countries.

References

- Arman, A., Seals, R.K.: A preliminary assesment of utilization alternatives for phosphogypsum. In: Proceedings of the Third International Symposium on Phosphogypsum, Orlando. Publication FIPR n° 01-060-083, volume II), pp. 562-575. (1990)
- Baccour, H., Medhioub, M., Jamoussi, F., Mhiri, T., Daoud, A.: Mineralogical evaluation and industrial applications of the Triassic clay deposits. Southern Tunisia. *Mater. Charact.* **59**(11), 1613-1622 (2008)
- Fakayode, S.O.: Impact assessment of industrial effluent on water quality of the receiving Alaro River in Ibadan, Nigeria. *AJEAM-RAGEE* **10**, 1-13 (2005)
- Mondat, K. et al.: Assessment and health risks of bioaccumulation of heavy metals in fish species of the Togolese lagoon system. vol. 14 (2010)
- Tran, H.H., Roddick, F.A., O'donnell, J.A.: Comparison of chromatography and desiccant silica gels for the adsorption of metal ion-I . adsorption and kinetics. *Water Res.* **33**(13), 2992-3000 (1999)
- Van Reeuwijk, L.P.: Procedures for soil analysis. In: International Soil Reference and Information Centre, Wageningen, vol 91 (1992)



The New Approach to γ -Spectrometry Based on Electron–Positron Pair Selection for Solution of Various Geochemical Problems

Vsevolod Volodin, Anna Travkina, and Yuri Sapozhnikov

Abstract

New scintillation detector based on electron–positron pair generation event selection for γ -spectrometry was developed and studied. Due to the increase of efficiency with γ -quanta energy, it can be used for spectrometry of short-decay nuclides with high-decay energy.

Keywords

Scintillation • Gamma spectrometry • Radiochemistry • Electron–positron pair • Ternary coincidence circuit • Monte Carlo method

1 Introduction

The detector of γ -rays based on the registration of electron–positron pairs generated by γ -quanta is proposed. The efficiency of this process and hence the efficiency of gamma-ray photon detection in this device are increased with energy. The efficiency of registration of high-energy γ -rays by the pair detector is investigated theoretically using Monte Carlo method. Despite the lower efficiency than in direct mode, pair detector is provided better peak-to-background ratio. Further efficiency increase is possible with using multicrystal pair detector scheme.

V. Volodin · A. Travkina (✉)

Vernadsky Institute of Geochemistry and Analytical Chemistry of Russian Academy of Sciences, Kosygina st. 19, Moscow, 119991, Russia

Y. Sapozhnikov

Lomonosov Moscow State University, Moscow 1, GSP-1, 119991 Moscow, Russia

2 The Experimental Setup

The proposed detector (Fig. 1) in the simplest version consists of three scintillation crystals of plate shape, arranged in a stack. Each crystal is equipped with own photoelectronic multiplier and light insulated from neighboring crystals. The functions of central and side crystals in the stack are different. At the production of an electron–positron pair in the central crystal and positron annihilation, two gamma rays with an energy of 511 keV, moving in opposite directions, are simultaneously absorbed within side crystals, causing simultaneous scintillations in all three crystals, similarly described in Avigone and Khalil (1981). The selection of such events with almost complete suppression of scintillations that are not associated with the generation of electron–positron pairs is carried out using a triple coincidence circuit. In a more complex version, the number of plates is arbitrary (more than 3), and pair generation event is selected as a coincident scintillations in at least three channels. An additional reduction in the number of random coincidences is achieved by discriminating the signals of the side channels by the energy of 511 keV.

The model of a pair spectrometer in the simplest three-channel configuration with three CsI(Tl) crystals 50 mm in diameter and 15 mm thick equipped with MicroFC60035 SiPM photodetectors was assembled.

3 Results

The γ -spectra from $^{232}\text{ThO}_2$ sample, which was used as model source of high-energy gamma rays, were recorded using described setup in two modes: with central crystal directly connected to multichannel analyzer (MCA) without any selection (direct mode) and with coincidence event selection with full-functioned setup (pair mode) (Fig. 2).

In direct mode, there is a complex curve, which is a sum of series of low-energy full absorption peaks, overlapping to

Fig. 1 Construction of pair detector described in our work

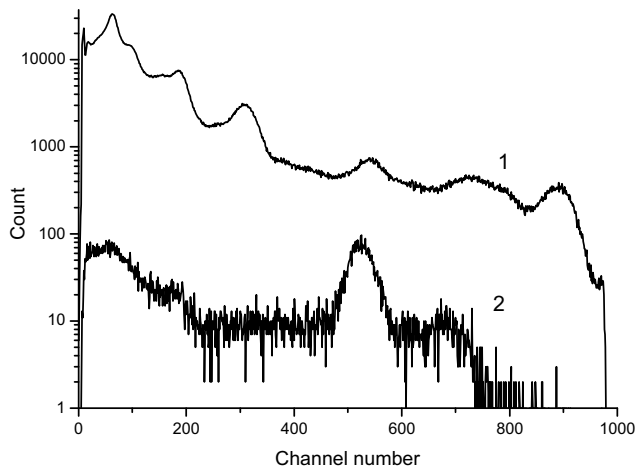
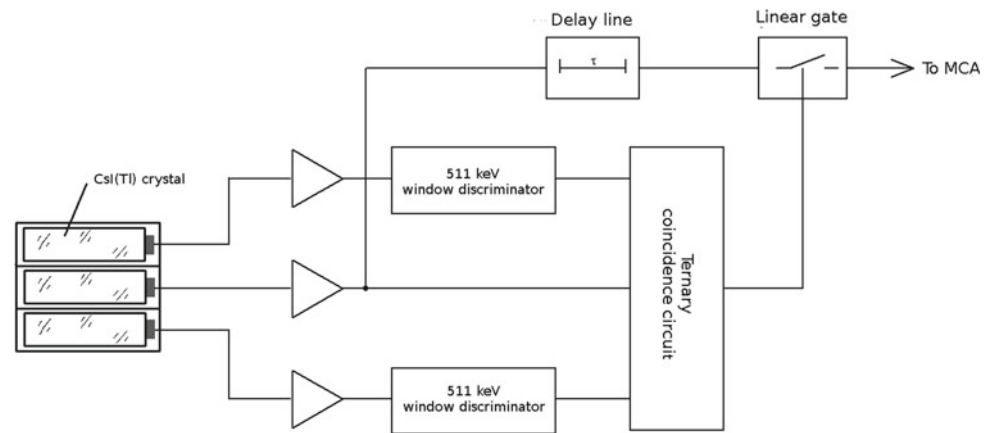


Fig. 2. ^{232}Th γ -emission spectra, recorded from central crystal directly connected to MCA (1) and after coincidence event selection (2). The double escape peak is near 500th channel

Compton distribution and peaks of single and double escape from 2.6 MeV ^{208}Tl γ -rays. The ^{208}Tl full absorption peak is expressed poorly due to the low efficiency of high-energy γ -photon registration.

In pair mode, there is only the ^{208}Tl peak of double escape on weak continuous background, connected with accidental coincidences. The low-energy peaks and Compton plateau are strongly suppressed, and signal-background ratio of double escape peak of ^{208}Tl is increased significantly.

The pair detector was simulated using the Monte Carlo method for the quantum energy of 2.6 MeV. The results of the calculation for cylindrical crystals (CsI, $D = 50$ mm, the thickness of the side crystals fixed $H_s = 15$ mm, the thickness of the central crystal H_c varies in the range of 1–30 mm) are shown in graph in Fig. 3.

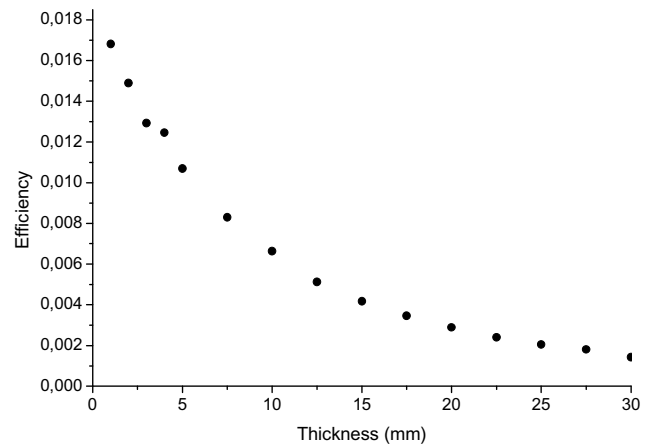


Fig. 3 Monte Carlo calculated dependence of pair registration efficiency with thickness of central crystal

4 Discussion

Gamma ray spectrometric analysis of fresh irradiated nuclear fuel and fresh radioactive emergency emissions is complicated by the high load of the detector due to the low-energy part of the spectrum. The information content is low when using scintillation detectors due to insufficient energy resolution. At the same time, the efficiency of registration in high-energy region decreases rapidly, reducing the information content of the high-energy part of the spectrum, in which the characteristic peaks of short-decay fission products are located.

The described scintillation detector due to insensitivity to low-energy γ -radiation, the relative high efficiency of high-energy γ -ray registration and simple response function of pair spectrometer is deemed suitable for such applications. In addition to the aforementioned solution of the problem of

gamma spectrometric measurements associated with high detector load, the developed model of the pair spectrometer can be performed in the submerged version (Thornton et al. 2013), and due to the effective registration of high energy, gamma radiation can be adapted to solve a number of geochemical problems. The nuclides with short decay and high energy of γ -radiation energy are formed by the decay of radon-220 and radon-222, which delivered from tectonically instable or other disturbed structures of earth crust. Thus, using our device allows us to study anomalies of radioactivity of the seabed, arising, especially, in areas of hydrocarbon deposits (in terms of registration of high-energy decay products of ^{220}Rn (^{208}Tl) (Sartini et al. 2011)). In addition, the device described in this work can be used for monitoring emergency radiation situations in the marine environment, allowing the detection the short-decay technogenic radio-nuclides with high-decay energies.

The efficiency of pair registration lowers with the central crystal thickness due to absorption of annihilation photons in the central crystal. But very thin central crystal excessively reduces the sensitive area of the detector. Optimal thickness of central crystal is estimated at 12–15 mm. Further efficiency rise can be achieved in detector with more than three crystals, which can be made thinner without any area reduction due to the high number of “central” crystals.

5 Conclusion

Through this work, we confirmed the applicability of our hypothesis. In pair mode, spurious peaks and Compton continuum are strongly suppressed, and spectrometer response function has the form of single peak. Thus, despite lower efficiency, pair spectrometer is provided better peak-to-background ratio. Further efficiency increase is possible with using multicrystal pair detector scheme.

Acknowledgements The research results were obtained in the framework of the state assignment (topic No. 0137–2019–0010).

References

- Avigone, F.T., Khalil, A.E.: Cross-section for the production of electron-positron pairs by 1064 MeV photons of germanium. *Phys. Rev. A* **24**(6), 2920–2924 (1981)
- Sartini, L., Simeone, F., Pani, P. et al.: *Nucl. Instrum. Meth. In Phys. Res., Ser. A* 626–627, S145–S147 (2011)
- Thornton, B., Oshnishi, S., Ura, T., et al.: Continuous measurement of radionuclides distribution of Fukushima using a towed sea-bed gamma ray spectrometer. *Deep-Seas Res. I* **79**, 10–19 (2013)



Rimsulfuron Herbicide: Study of the Interaction and Distribution Between Soil and *Zea mays* L., 1753 (Model Experiments)

Lydia Bondareva, Valerii Rakitskii, and Nataliia Fedorova

Abstract

The purpose of this study is to identify the effect of the herbicide (rimsulfuron) on plants in modeling experiments and its distribution between the soil and the common crop—*Zea mays* L., 1753. The herbicide substance used was pre-labeled ^{14}C . When the system contained corn, most of the radiocarbon is accumulated in the leaves ($\sim 41\%$), while in the system without plants, the isotope was in the soil. The absorbed ^{14}C substance was present only on the surface or in the upper layer of the epidermis of the leaf blade, but despite this, the physiology corn leaves did not undergo significant changes. The amount of radiocarbon in the soil is uneven; the highest content was found in the layer from 5 to 7 cm in the system with corn ~ 50 Bq. Using a linear model of absorption kinetics based on R^2 , it was evident that the adsorption of rimsulfuron corresponded to a second-order equation, the use of nonlinear analysis, R^2 increased from 0.67 to 0.99.

Keywords

Herbicide • Radiocarbon • Interaction • Distribution • Soil

1 Introduction

Both the effectiveness of the herbicides and the significance of the adverse effects (agricultural or environmental) are largely dependent on the physicochemical properties and behavior of the herbicides in the soil system (primarily in arable land). This behavior depends on the properties of the active

ingredients, the composition of the herbicide, the method of its use, as well as the characteristics of the soil and climatic conditions (Wolejko et al. 2020). Rimsulfuron is the common ISO terminology for 1-(4, 6-dimethoxypyrimidin-2-yl)-3-(3-ethylsulfonyl-2-pyridinyl)sulfonyl urea (IUPAC). Rimsulfuron is absorbed through the leaves and acts as an effective inhibitor of the growth of roots and shoots of plants, blocking the enzyme of acetolactate synthase (Isaacs et al. 2002). We suggest that an experimental study of the behavior of rimsulfuron in a full range of soil, as well as climatic conditions, would solve a huge problem; first, the effectiveness of the pesticides of this class and migration in the environment with subsequent release to groundwater. Even though the herbicide in question is not stable and decomposes into metabolites as a result of environmental exposure, the resulting metabolites are more resistant and more toxic to living organisms (Radivojević et al. 2011). In this regard, the purpose of this study was to identify the level of impact of the rimsulfuron herbicide on crops—*Zea mays* L., 1753 in model experiments in a confined space—microcosm, in the soil-plant system.

2 Materials and Methods

The experiments were carried out with a labeled preparation ^{14}C -rimsulfuron to track the possible distribution of the substance in the soil layers, as well as in different parts of plants and aerosols of microcosms. The microcosms consisted of polyvinyl chloride tubes with a height of 35 cm and a diameter of 15 cm. A nylon screen was installed at the bottom to prevent soil loss, but it allowed water to enter from the dishes underneath. At the bottom of the microcosm, there was a layer of sand under the thickness of the soil.

L. Bondareva (✉) · V. Rakitskii · N. Fedorova
Federal Scientific Center Named after F.F. Erisman, Semashko
street, 2, Mytischki, Moscow Region, Russia

2.1 Soil and Plants

The soil was classified as sod-podzolic with a sandy-clay texture, taken from the secondary forest of the Moscow region. After debris removal, the soil was taken from the top 20 cm layer, dried at room temperature, and sieved through a 2 mm sieve. The soil was treated with complex fertilizers (30 g per each system) in each microcosm and adjusted to pH 5.0–5.5. The experiment used two-week seedlings of corn—*Zea mays*. This type of culture was chosen from a practical point of view. In the Russian Federation, corn is widespread and is used to feed cattle.

2.2 Herbicide

In this experiment, a solution of a labeled rimsulfuron with one-tenth of the recommended consumption rate of 250 g ha⁻¹ was used, which corresponded to 2.50 µg cm⁻². Labeled radioactive agent ¹⁴C-rimsulfuron was added to the initial solution, the former being previously dissolved in methanol. To completely dissolve the reagent, the solution was placed in an ultrasonic bath and exposed for 1 min. Each microcosm was sprayed with the resulting mixture (either plants or soil were treated, in the absence of plants). The treatment was carried out carefully to minimize the amount of mixture falling on the walls of the system. The introduced reactivity for each microcosm was ~95 kBq.

3 Results and Discussion

Table 1 presents preliminary data on the distribution of radioactivity among the components of model systems.

This table represents the distribution of radioactivity by components of model microcosm systems.

The existing research does not pay enough attention to the modern, organized description and standardization in research procedures and the methodology for using radioisotopes in the study of absorption and translocation of herbicides by plants and soils. This paper is an endeavor to fill this gap.

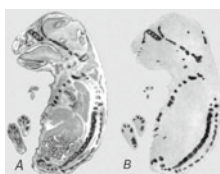
The presented results show that in the system with corn, most of the radioactivity is observed in the leaves (~41%), while in the system without corn, it is observed mainly in the soil, which is associated with the experimental conditions. The physiology of corn leaves has not undergone significant visible changes (O'sullivan et al. 1998). The results obtained using autoradiography showed that the main accumulated content of ¹⁴C is only on the surface and in the upper layer of the epidermis of the leaf blade (Fig. 1).

Studies on the distribution of radiocarbon in the soil revealed that the distribution of the isotope, and consequently, the preparation and/or yoke of metabolites is uneven in both the system with plants and without them (Fig. 2). The most significant herbicide content was in the 5–7 cm layer.

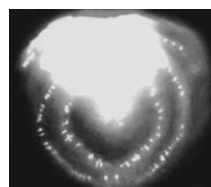
Table 1 Distribution of radioactivity over the components of the experimental systems

№	System	Content ¹⁴ C, kBq (% of the introduced amount)				
		Soil (all samples)	Rhizosphere	Stems (all samples)	Leaves (all samples)	The tube for ¹⁴ C-CO ₂ capture
1	<i>Zea mays</i>	27.1 (28.0)	19.5 (20.5)	6.1 (6.4)	38.8 (41.0)	3.5 (3.6)
2	Soil	94.5 (99.5)	-	-	-	0.5 (0.5)

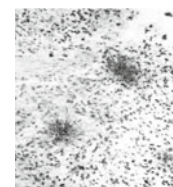
Fig. 1 Distribution of ¹⁴C in the corn leaves



Cross-section of the corn leaf: a) x5000 magnification, б) x500 magnification



The corn leaf, top view



Accumulation of ¹⁴C by the intracellular space of the corn leaf.

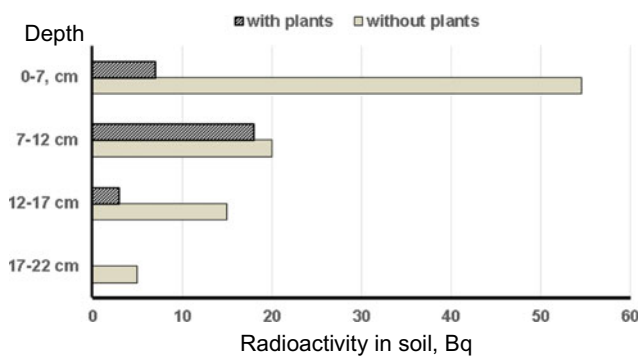


Fig. 2 Distribution ^{14}C radioactivity in different microcosm soil layers. Microcosms without plants and with *Zea mays* L., 1753

3.1 Mathematical Models of Herbicide Sorption Kinetics

While using a linear model of kinetics, based on R^2 , it was evident the adsorption of herbicide followed second order system. However, expending nonlinear analysis, R^2 of pseudo first order (PFO) increase from 0.67 to 0.99. Using a nonlinear approach to analyze the kinetics of herbicide adsorption, the best fit of PFO increased drastically to an average of 0.90. The fitting of $R^2 \geq 0.9$ was statistically proper and can be used to make conclusions. Most error functions have been based on R^2 —this has forced researchers to conclude that both PFO and pseudo-second order (PSO) explained the adsorption of the herbicide. However, further analysis using different error functions can help solve the puzzle.

3.2 Mathematical Models of Herbicide Sorption Kinetics

While using a linear model of kinetics, based on R^2 , it was evident the adsorption of herbicide followed second order system. However, expending nonlinear analysis, R^2 of

pseudo first order (PFO) increase from 0.67 to 0.99. Using a nonlinear approach to analyze the kinetics of herbicide adsorption, the best fit of PFO increased drastically to an average of 0.90. The fitting of $R^2 \geq 0.9$ was statistically proper and can be used to make conclusions. Most error functions have been based on R^2 —this has forced researchers to conclude that both PFO and pseudo-second order (PSO) explained the adsorption of the herbicide. However, further analysis using different error functions can help solve the puzzle.

4 Conclusion

Thus, most of the labeled substance is on the outer layer of corn leaves. The herbicide is unevenly distributed in the soil profile of the microcosm, and the distribution kinetics obeys a nonlinear dependence with correlation coefficients ≥ 0.9 .

Acknowledgements This work was made possible thanks to the financial support of the fundamental investigation of Federal Service for Surveillance on Consumer Rights Protection and Wellbeing

References

- Isaacs, M., Wilson, H., Toler, J.: Rimsulfuron plus Thifensulfuron-methyl combinations with selected postemergence broadleaf herbicides in corn (*Zea mays*). *Weed Technol.* **16**(3), 664–668 (2002). [https://doi.org/10.1614/0890-037X\(2002\)016\[0664:RPTMCW\]2.0.CO;2](https://doi.org/10.1614/0890-037X(2002)016[0664:RPTMCW]2.0.CO;2)
- O'sullivan, J., Thomas, R.J., Bouw, W.J.: Tolerance of sweet corn (*Zea mays*) cultivars to rimsulfuron. *Weed Technol.* **12**(2), 258–261 (1998). <https://doi.org/10.1017/S0890037x00043785>
- Radivojević, L., Šantrić, L., Gajić-Umiļjendić, J.: Rimsulfuron in soil: effects on microbiological properties under varying soilconditions. *Pesticidi i fitomedicina* **26**(2), 135–140 (2011)
- Wolejko, E., Jabłońska-Trypuć, A., Wydro, U., Butarewicz, A., Łozowicka, B.: Soil biological activity as an indicator of soilpollution with pesticides—a review. *Appl Soil Ecol.* **147**, 103356 (2020). <https://doi.org/10.1016/j.apsoil.2019.09.006>



Olive Mill Waste Water Contaminated Soil: Toxicological Effects and Treatment with Gypsum

Salsabil Trigui, Amjad Kallel, Emilia Fernández Ondoño, and F. J. Martín Peinado

Abstract

Olive mill waste water (OMWW) represents a major threat to the environment due to its high levels of polyphenols. The aim of this study was to investigate the toxicological effect of OMWW contaminated soil on a bio-indicator namely *Eisenia andrei* using the reproduction test approach. Soil from OMWW evaporation ponds and artificially contaminated soil were tested. The samples collected from the evaporation ponds were found to be extremely toxic to earthworms leading to their total mortality. However, earthworms exposed to artificially contaminated soil using OMWW at a ratio of 16% survived nonetheless their reproduction cycle was disturbed by a decrease of the juvenile number. Furthermore, gypsum was added into the contaminated soil and its efficiency on the depletion of the toxic effect of OMWW was assessed. It was found that gypsum could be effective for the remediation of the contaminated soil as the juvenile number increased even with OMWW at a ratio of 50% w:w.

Keywords

Olive mill wastewater • Contamination • Toxicity bioassay • Earthworms • Gypsum

1 Introduction

In the Mediterranean countries, olive oil is produced during the harvest season in huge quantities. Tunisia is among the largest olive oil producers in the world (ONH 2016).

S. Trigui (✉) · A. Kallel
Laboratory 3E (Water, Energy, Environment), National School of Engineering of Sfax, University of Sfax, Sfax, Tunisia
e-mail: amjad.kallel@enis.tn

E. F. Ondoño · F. J. Martín Peinado
Department of Soil Science and Agricultural Chemistry,
University of Granada, Campus Fuentenueva, Granada, Spain

Nevertheless, this oleoindustry leads to the generation of large amounts of waste known as olive mill waste water (OMWW). Evaporation ponds is one of the simplest and most economical methods to manage this quantity of waste. Such an uncontrolled disposal presents a major problem of contamination that affects soil and groundwater (S'habou et al. 2009). In fact, it has an effect on acidity, available nutrients and soil hydrophobicity. Polyphenols, for instance, seem to be responsible for the antimicrobial and phytotoxic effect of OMWW and are the most limiting factor against the spread of this waste on soils (Borja et al. 2006). The toxic effect of OMWW on soil microorganisms was studied by Kavadias et al. (2010) demonstrating that it is due to high polyphenols levels.

Nowadays several studies have evaluated the effect on the reproduction or on biomarkers responses in soil invertebrates such as earthworms exposed to organic contaminants (Velki and Hackenberger 2013), but few studies are available about the toxicity of OMWW to earthworms, although this is the main disposal target compartment (Campani et al. 2017). Earthworms are highly adaptable and have a large reproductive capacity. They also present a high tolerance and resistance to organic pollutants (Hickman 2008).

The aim of the present study was to evaluate the OMWW toxicological effect on a soil bioindicator; the earthworm *Eisenia andrei*, and then to evaluate the efficiency of using gypsum as an additive in an attempt of chemical remediation of OMWW contaminated soils using the same approach of reproduction test.

2 Materials and Methods

2.1 Soil Sampling and Analysis

OMWW samples were collected from the evaporation ponds (OMWW discharge pond) in the region of Agareb, located at 20 km in the West of Sfax, Tunisia (34°43' N, 10°26' E).

The soil samples were collected from three evaporation ponds and were mixed and homogenized to have a representative sample. The control soil was collected 50 m away from the evaporation basin.

Before analysis, the soil samples were air dried at room temperature and passed through a 2-mm sieve. This fraction was used to characterize the main soil properties and for the toxicity bioassay. According to official methods of analysis, particle-size distribution was analyzed in the fine-earth fraction by sieving (sand) and using the Robinson pipette method (silt and clay) after the removal of organic matter. The pH and conductivity were potentiometrically measured in a 1:2.5, 1:5 soil–water ratio. The water holding capacity (WHC, 33 kPa) was determined with the method of Richards (1965). The concentration of phenolic compounds in the soil was determined in water extract, the concentration of total phenols in the sample was determined colorimetrically using the Folin–Ciocalteu reactive. The absorbance was measured at 725 nm. The results were expressed in mg/Kg of gallic acid (Box 1983). The main soil properties are presented in Table 1.

2.2 Toxicity Bioassay

Two types of soils were used; a contaminated soil (from the evaporation basin) mixed with distilled water to reach 60% of WHC, and an artificially contaminated one mixed with OMWW. A control level was also included using distilled water. After that, gypsum was added in different percentages (0, 20, 30 and 50% w:w). All the experiments were performed in triplicate.

For the toxicity test; earthworms (*Eisenia andrei*) were obtained from a laboratory culture at the Department of Edaphology and Agriculture Chemistry, Granada Sciences faculty. The tests used adult earthworms with a well-developed clitellum (Fig. 1a). The earthworms tests followed the Organisation for Economic Cooperation and Development (OECD) guideline 207 (OECD 1984), including 28-day exposure of adult animals followed by another 28-day incubation of cocoons to enable the assessment of juvenile production. Using containers with approximately 50 g of soil moistened to 60% of water holding capacity and mixed with horse manure, 5 earthworm adults were added after being gently cleaned and weighed (Fig. 1b). The containers were incubated at 20 °C and their

weights were monitored weekly for maintaining soil moisture content and required food conditions. After 4 weeks, the surviving earthworms were removed (Fig. 1c). Soils containing cocoons were returned to the respective containers and incubated for another 28 days. After this period, the number of juveniles was determined by placing the containers in a water bath at 60 °C, forcing the juveniles to emerge to the surface, where they were counted (Fig. 1d).

3 Results and Discussion

For the experiments achieved with contaminated soil from the evaporation basin, all the earthworms (mixed with or without gypsum) died in less than 5 days. This is probably due to the high level of concentration of polyphenols in the soil.

For the second part of the experiment achieved with artificially-contaminated soil; the experiment was achieved up the end of the 8 weeks. As a result, all the earthworms were still alive and their weight was approximately the same. This result is in agreement with the results of Campani et al. (2017) who found that the use of 12.5% and 25% of OMWW did not show any mortality compared to our experiment where the percentage of OMWW used was 16%.

Although the number and weight of the surviving earthworms was not an efficient parameter, the number of juveniles was a very efficient one. The mean numbers of juveniles are depicted in Fig. 2. The results indicate that the use of OMWW with a proportion of 16% w:w decreases the number of juveniles to 15 juv compared to distilled water (25 juv). This result seems to be logical because of the toxic effect of polyphenols.

Studying the effect of gypsum on OMWW contaminated soil; we found that the more the gypsum percentage is important, the higher the number of juveniles is, (18, 20 and 35 juv respectively to 20, 30 and 50% of gypsum). This result is not the same for the control soil where gypsum has no effect on the number of juveniles. We also noticed that the treatment with 50% Gyp gives better results than the control soil which is not contaminated. This can be explained by the hypothesis that the gypsum can improve the contaminated soil conditions by playing the role of a buffer agent and decreasing the toxic effect of phenols present in the OMWW.

Table 1 Main texture and properties of control and contaminated soil

Soil sample	Sand (%)	Silt (%)	Clay (%)	pH	WHC (%)
Control	76.129	6.946	16.190	8.56	12.32
Contaminated	55.487	15.80	28.712	7.61	18.79

Fig. 1 Steps of the earthworms test: **a** preparation of adult earthworms, **b** preparation of soil containers, **c** removal of earthworms after 28 days, **d** count of juveniles

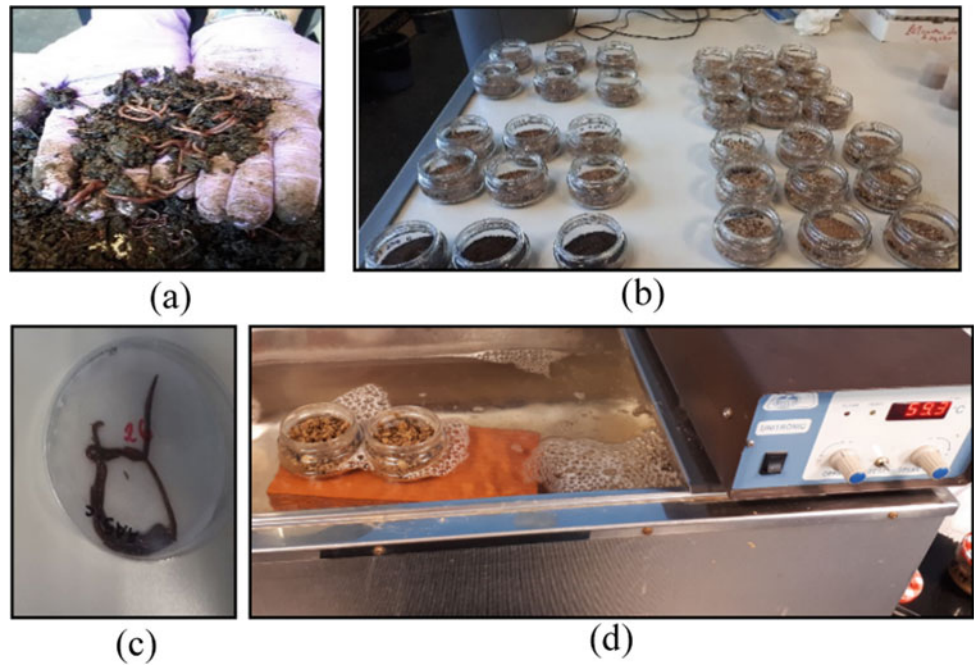
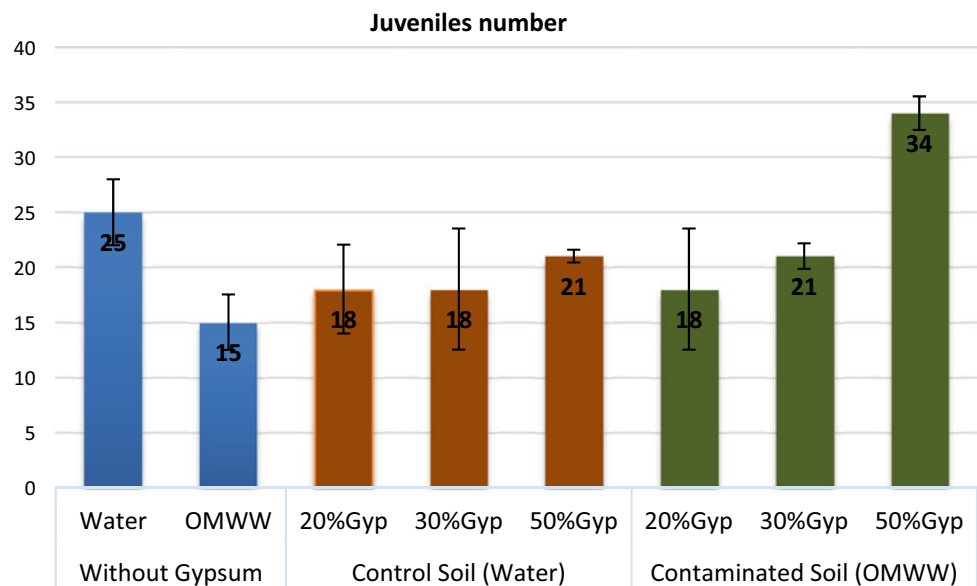


Fig. 2 Number of juveniles (mean \pm standard deviation)



4 Conclusions

The bio-indicator approach using the reproduction test of earthworms was applied to investigate the toxicity effect of OMWW in soil. The results of this study show that the contaminated soil in the evaporation basins is very toxic to earthworms due to the high polyphenols level. The OMWW

has a negative effect on soil invertebrates even at small quantities (up to 16% w:w). Nonetheless, it does not lead to the mortality of earthworms but disturbs their reproduction cycle. The use of gypsum as an attempt to remediate the contaminated soil can be effective for OMWW content up to 50% w:w. Further investigations, using other OMWW proportions, would be of great interest to confirm and support the achieved results.

References

- Borja, R., Sanchez, E., Raposso, F., Rincon, B., Jimenez, A.M., Martin, A.: A study of the natural biodegradation of two- phase olive mill solid waste during its storage in an evaporation pond. *Waste Manage.* **26**, 477–486 (2006)
- Box, J.D.: Investigation of the Folin-Ciocalteu phenol reagent for the determination of the polyphenolic substances in natural waters. *Water Res.* **17**, 249–261 (1983)
- Campani, T., et al.: Assessment of toxicological Effects of raw and bioremediated olive mill waste in the earthworm *Eisenia fetida*: a biomarker approach for sustainable agriculture. *Appl. Soil. Ecology* **119**(May):18–25. Retrieved <http://dx.doi.org/10.1016/j.apsoil.2017.05.016>
- Hickman, Z.A., Reid, B.J.: Earthworm assisted bioremediation of organic contaminants. *Environ. Int.* **34**, 1072–1081 (2008)
- Kavvadias, V., Doula, M.K., Kommitsas, K., Liakopoulou, N.: Disposal of olive oil mill wastes in evaporation ponds: effects on soil properties. *J. Hazard. Mater.* **182**, 144–155 (2010)
- OECD (Organization for Economic Cooperation and Development): Guideline for testing of chemicals. earthworm, acute toxicity tests, p. 207, (1984)
- Office national de l'huile (ONH): (2016) <http://www.onh.com.tn/index.php/fr/2016-05-23-14-44-46/la-production>
- Richards, L.A.: Physical condition of water in soil. In: Black, C. Aed. *Methods of soil analysis*. pp. 128–137. Madison, Wisconsin, Am. Soc. Agron (1965)
- S'habou, R., Zairi, M., Kallel, A. et al.: Assessing the effect of an olive mill wastewater evaporation pond in Sousse, Tunisia. *Environ. Geol.* **58**, 679 (2009)
- Velki, M., Hackenberger, B.K.: Biomarker responses in earthworm *Eisenia andrei* exposed to pirimiphos- methyl and deltamethrin using different toxicity tests. *Chemosphere* **90**, 1216–1226 (2013). <https://doi.org/10.1016/j.chemosphere.2012.09.051>



Use of Diatomaceous Earth and Lime for the Remediation of Olive Mill Waste Contaminated Soils

Salsabil Trigui and Amjad Kallel

Abstract

Contaminated soil with olive mill wastewater (OMWW) was subject to a remediation treatment in the purpose of finding the most suitable and cost-effective procedure to revive such a degraded area. We conducted batch experiments in order to investigate the efficiency of natural diatomaceous earth (DE) and lime on limiting environmental degradation caused by the uncontrolled disposal OMWW. We added both additives at various ratios (0, 7.5, 15 and 30%w/w) to contaminated soil samples, which were collected from an evaporation basin located in the region of Agareb, Sfax, Tunisia. pH, Conductivity, water-soluble polyphenols, and COD were measured in leachates after treating the soil samples with additives. We perceived that water-soluble polyphenols and COD drop substantially with an increase in DE percentage. Besides, the use of lime as an additive was not practical for the reduction of COD compared to the control. However, it was a useful additive in the reduction of polyphenols with a reduction of up to 70%.

Keywords

Olive mill wastewater • Diatomaceous earth • Lime • Soil • Remediation • Polyphenols

1 Introduction

The olive oil production industry is an indispensable activity in the Mediterranean area. Unfortunately, for these countries, the disposal of olive mill wastewater (OMWW) is consid-

ered a major environmental problem due to its effect on water and soil degradation (S'habou et al. 2009). Multiple pieces of research have been mainly focusing on the OMWW treatment or its application in lands for agricultural purposes (Kapellakis et al. 2015). In contrast, the remediation of contaminated soils by such byproduct still requires intensive investigations and concern, especially for highly contaminated soil such as old evaporation basin. Over the last decades, remediation techniques for contaminated soils by various pollutants have been well developed. One of the most cost-effective treatments methods is the use of additives. Additives were used, especially for the stabilization of metals and organic contaminants (Muñoz-Olivas et al. 2007; Cao et al. 2018). In a previous study, Doula et al. (2012) investigated the use of clinoptilolite as a soil additive to protect OMWW contaminated soil. In the present study, OMWW contaminated soils are subject to a remediation treatment by the use of diatomaceous earth (DE) and lime as additives. We added different doses of these additives to assess their efficiency on the immobilization of the pollutants to breakdown the dispersion risk.

2 Materials and Methods

OMWW contaminated soil samples were collected from the OMWW evaporation ponds in the region of Agareb, located at 20 km in the West of Sfax, Tunisia (34°43'North, 10°41'East). Soil samples were collected from three ponds and were mixed and homogenized to have a representative sample. Before analysis, soil samples were air-dried at room temperature and passed through a 2-mm sieve. Batch experiments were conducted with varying soil-additives mixtures (0, 7.5, 15 and 30%). Two additives were used for soil treatment; diatomaceous earth (DE) and lime. The EN12457 leaching test (Santi et al. 2008) was followed for evaluation purposes as detailed in Fig. 1.

S. Trigui (✉) · A. Kallel
Laboratory of Water, Energy and Environment, Sfax National,
School of Engineering, University of Sfax, Sfax, Tunisia

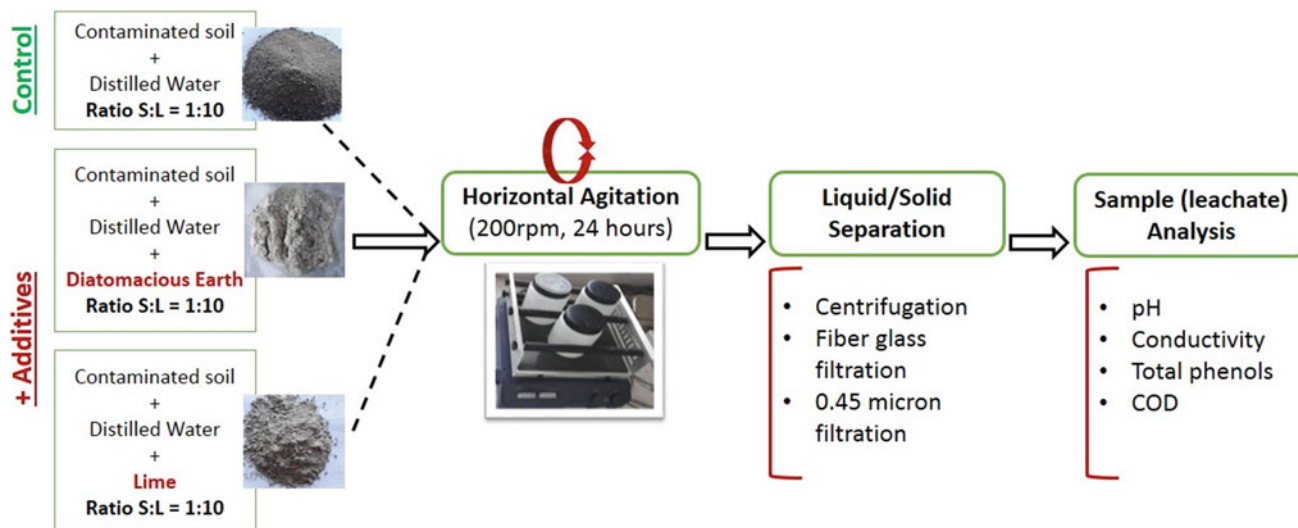


Fig. 1 Batch leaching procedure

3 Results

3.1 Effect on pH and Conductivity

As shown in Table 1, we noticed that DE caused a slight decrease in pH from 9.56 (in control) to 8.85 (30% additive). Whereas, when we used lime as an additive, it always indicated a basic pH around 12.5 with a slight variation between the different doses due to the high alkalinity of lime.

Regarding the conductivity, it was observed that both additives caused a remarkable increase mainly for the dose of 30% leading to two-folds higher values compared to control soil.

3.2 Effect on Polyphenols and COD

The use of DE with different doses caused a notable decrease of phenols content (Fig. 2). A reduction of 66% of total phenols was induced by the addition of 30% of this additive. For the dose of 7.5% of DE, the reduction was not substantial with less than 17%. The most effective reduction was induced by the addition of 30% of lime which indicated a significant reduction of polyphenols up to 73% using a dose

of 30% although the difference between the 15 and 30% doses remains insignificant.

COD can give an idea of the pollutant load present in our soil. A dose of 30% of DE induced a decrease in COD of 75% compared to control. A drop of about 46% was recorded for the COD between the initial value and that of 30% of lime. However, for both additives, there is no significant difference between the two doses, 7.5 and 15%.

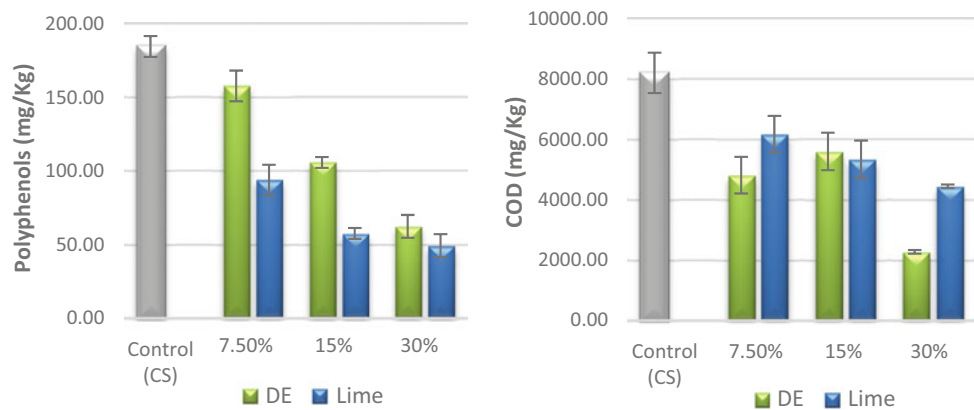
4 Discussion

Our treatment is based on the use of two different additives; As for the additive DE, the pH values remained around 8.5, but for the lime, it is around 12. Such an alkaline pH would be in favour of immobilizing several metals, but at the same time, it is not considered a conductive condition because it leads to a corrosive environment. The treatment efficiency is given mostly by the DE since the pH of a non-contaminated soil was around 8. Concerning the decrease of water-soluble phenols, it should be related to the adsorption of phenols to the additives (Muñoz-Olivas et al. 2007; Cao et al. 2018). The maximum reduction was around 70%, and this value is essential compared to other studies which found a maximum of phenols reduction equal to 50% using zeolites (Doula

Table 1 pH and electrical conductivity variation according to the different doses of additives (DE and Lime in %)

Mixes/additives	pH (-)		Conductivity (mS/cm)	
	DE	Lime	DE	Lime
0% (Control, CS)	9.56	9.56	3.10	3.10
7.5% Additive	9.39	12.37	4.12	4.2
15% Additive	9.06	12.91	5.06	5.07
30% Additive	8.85	12.74	6.67	6.1

Fig. 2 Variation of polyphenols and COD with the different doses of additives (additives DE and Lime in %)



et al. 2012) and 30% using bentonite (Santi et al. 2008). The COD represented a significant pollutant load in the CS which is decreased until 75% using a dose of 30% of DE, compared to the use of bentonite by Santi et al. who found a reduction of only 30% of COD (Santi et al. 2008).

5 Conclusions

The current study dealt with the treatment of olive-waste contaminated soil by adding different doses of DE and lime. The presence of both additives seems to significantly improve the soil's parameters, as far as the organic components and the polyphenols are concerned. The use of DE and lime resulted in a significant reduction of COD. Moreover, it led to a reduction in the retention of excess quantities of polyphenols. Besides, DE at a dose of 30% seems to be more effective than lime, especially that the alkalinity of soil was slightly reduced. It is worth mentioning that more experiments will allow a more accurate evaluation of the properties of soils treated with DE and lime by measuring heavy metals and mineral fraction leaching. Furthermore, the investigation on the effects of these additives on the soil physical/mechanical parameters would be of great interest.

References

- Cao, X., et al.: Effects of a natural sepiolite bearing material and lime on the immobilization and persistence of cadmium in a contaminated acid agricultural soil. *Environ. Sci. Pollut. Res.* **25**(22), 22075–22084 (2018)
- Doula, M.K., Elaiopoulos, K., Kavvadias, V.A., Mavraganis, V.: Use of clinoptilolite to improve and protect soil quality from the disposal of olive oil mills wastes. *J. Hazard. Mater.* **207–208**, 103–110 (2012)
- Kapellakis, I., Tzanakakis, V.A., Angelakis, A.N.: Land application-based olive mill wastewater management. *Water* **7**(2), 362–376 (2015)
- Muñoz-Olivas, R., Bouaid, A., Liva, M., Fernández-herando, P., Luis, J., Cámara, C.: New perspectives for the application of diatomaceous earth to the remediation of polluted waters and soils. *Rev. CENIC Ciencias Quim.* **38**(2), 283–287 (2007)
- Santi, C.A., Cortes, S., D'Acqui, L.P., Sparvoli, E., Pushparaj, B.: Reduction of organic pollutants in Olive Mill Wastewater by using different mineral substrates as adsorbents. *Bioresour. Technol.* **99**(6), 1945–1951 (2008)
- S'habou, R., Zairi, M., Kallel, A., Aydi, A., Ben Dhia, H.: Assessing the effect of an olive mill wastewater evaporation pond in sousse, Tunisia. *Environ. Geol.* **58**(3), 679–686 (2009)



Durability and Leaching Behavior of Mine Tailings After Inerting Geomaterials in Tunisia

Rania Hbaieb, Marilyne Soubrand, Emmanuel Joussein, Sonia Lazaar, and Mounir Medhioub

Abstract

Mining activities are responsible for the increase of pollutants (i.e., metallic elements) in the environment. Mining wastes are highly contaminated by metallic elements which can induce environmental and sanitary risks. For better waste management, valorization appears to be significant especially when it comes to geopolymers since construction sites heavily use these materials at the large scale. In this context, the aim of this study is (i) to synthesize geopolymers from mining waste using silicate solution and (ii) to evaluate speciation and leaching behavior of metallic elements in raw material and new material after geopolymerization. Results demonstrate that metals bearing phases are dissolved during alkaline treatment and redistributed in the geopolymer matrix. Leaching tests evidenced the possibility to stabilize metals into geopolymer matrix. According to this, a new valorization way of mining wastes (alkaline activation) is proposed based on creating new geomaterials which can be used without risks and with low cost.

Keywords

Mining waste • Mineralogy • Heavy metals • Speciation • Alkaline activation

1 Introduction

The northern part of Tunisia, especially the watershed of Medjerda, is the country's most important mining region marked by massive exploitation of metallic reservoirs, such as lead (Pb), zinc (Zn), iron (Fe), and cadmium (Cd).

R. Hbaieb (✉) · M. Soubrand · E. Joussein · S. Lazaar
Université de Limoges, GRESE, Limoges, France

S. Lazaar · M. Medhioub
Faculté des Sciences, EGECU, Université de Sfax, Sfax, Tunisia

This study focuses on an old mining site called Fej Lahdoum (FL) in northwestern Tunisia which has been abandoned since 2004. Mining activity there generates large quantities of waste (an area of 10 ha with a volume of 0.39 Mt) which are stored in the forms of dumps without real management. This waste is localized near the mining site, which is an exclusively agricultural zone. Under the climatic conditions of the area (water or/and wind erosions), the mining waste could be a potential source of release of metals that could be moved in the different compartments of the environment.

Mining activities are the primary anthropogenic source of metal (loids) in the environment. These industrial wastes contain inorganic pollutants that represent the secondary sources of pollution for water, soil, and the atmosphere (Belabed et al. 2017). According to this, these wastes can induce health-related consequences through direct particle ingestion or inhalation or food chain impacts (Uzu et al. 2011, 2012; Pascaud et al. 2015).

This study aims to find an efficient way to valorize the waste by creating new geomaterials from the activation of an aluminosilicate source using an alkaline solution at room temperature (Davidovits 2008). This new material may offer a particular advantage in such a harsh environment since it is marked by excellent mechanical properties, good chemical resistance, low shrinkage, and has an environmentally friendly nature with limiting metals mobility and long-term durability. Whatever the waste treatment, the aim is to minimize the leaching of contaminants and their toxicity.

2 Materials and Methods

Various representative samples of tailings (T) were sampled at different levels, going from the top (H1) to the bottom (H5) (H1, H2, H3, H4, H5) in order to evaluate the potential environmental risks of these tailings (Fig. 1).



Fig. 1 Location of the mining waste of Fej Lahdoun old mining site

Speciation has been determined by BCR (the Community Bureau of Reference) sequential extraction and mineralogical characterization using XRD and FTIR analyses. Leaching experiments have been conducted according to the EN12457-2.

The waste-based material was then synthesized with various mixtures using sodium silicate solution mixed with NaOH pellets in substitution of metakaolin supplied by Imerys and waste. XRD and FTIR then characterized synthesized materials. The environmental risk was evaluated based on the high decrease of metallic element speciation and leaching behavior after geopolymerization.

3 Results

- Mine tailings had high heavy metals concentrations of 20,300, 2650, and 50 mg/kg for Zn, Pb, and Cd, respectively. From XRD, the waste of Fej Lahdoun was composed by calcite, dolomite, quartz, gypsum, galena,

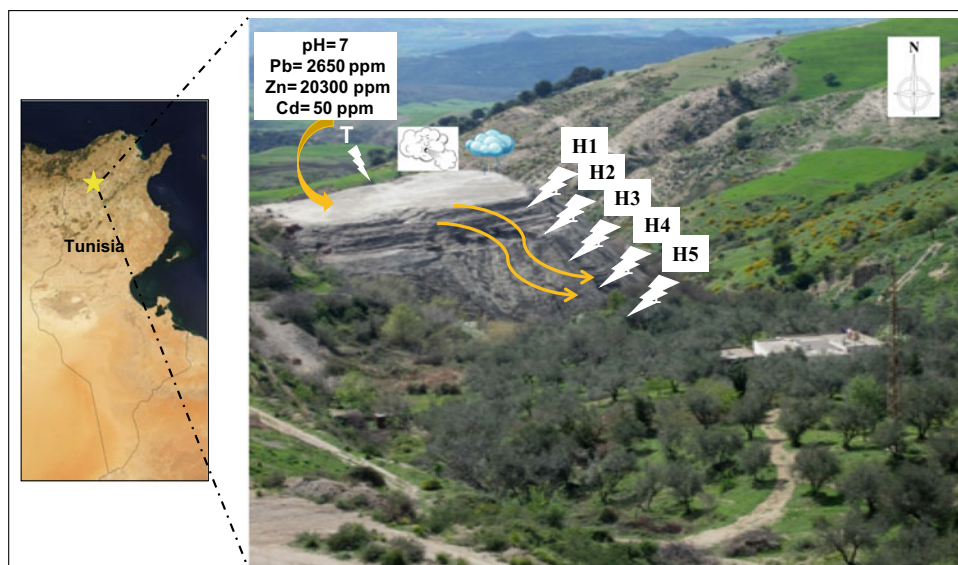
sphalerite, kaolinite, and cerussite following the chemical properties.

- Assessment of the degree of contamination (Igeo) of the waste showed severe pollution with Zn and Cd ($I_{geo} > 5$) and severe to extremely severe pollution for Pb ($3 < I_{geo} < 5$) (Fig. 2) (Müller et al. 1979; Sougo et al. 2014).

Speciation with BCR experiments was conducted in the way to determine the partitioning of these three elements. The distribution of Pb, Zn, and Cd into the various fractions is F exchangeable >>> F oxidable > F residual > F reductible, so a large part of metals can be mobilized, because the equivalent fraction corresponds to the easily soluble metal fraction (Pascaud et al. 2014). According to the European standard for landfilling, ultimate waste classifies mining waste in different categories according to concentrations of leached contaminants. Leaching tests have shown that mining waste of Fej Lahdoun is considered as non-hazardous waste for Cd and Zn and as inert waste for Pb. Finally, these results clearly show that potential environmental risk is quite a threat (Fig. 6).

In an attempt to inert and to reuse this waste, we used the alkaline activation of waste deposits as the reactive compound with different substitutions. Results pointed out that the alkaline-based geomaterials can highly incorporate the waste. In accordance with the literature, synthesized samples (with 10%, 25%, and 50% of waste) are quite consolidated. The increase of the metakaolin substitution by mining waste decreases the mechanical properties up to 50%. After 50%, the mechanical properties are not realized since the materials are not consolidated due to the limitation of Al and Si (reactive elements) used in the geopolymer network (Pascaud 2015) (Fig. 3).

Fig. 2 Lgeo of waste



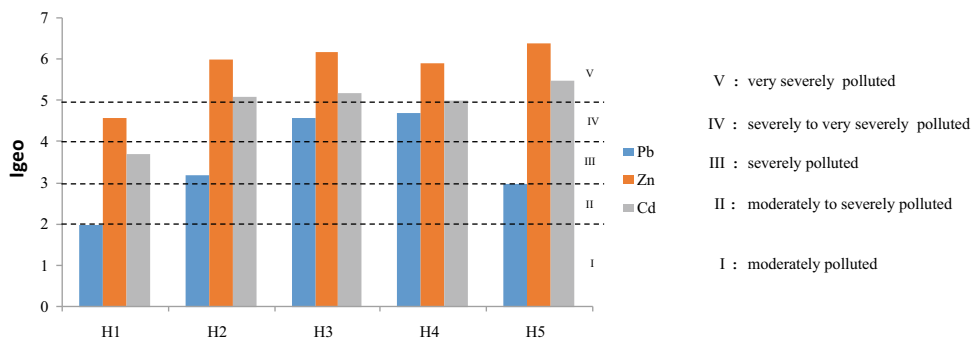


Fig. 3 Example of new synthesized materials

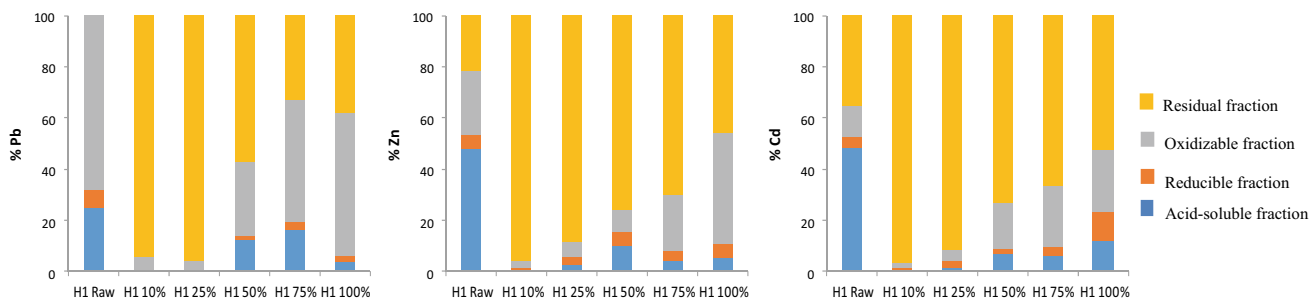


Fig. 4 XRD and FTIR of waste without and with treatment

Moreover, DRX and FTIR investigations evidenced the redistribution of metals into the matrix (Fig. 4).

This experiment is under the BCR experiments showing that the primary pollutants are in the residual fraction (most stable fraction) after alkaline activation (up to 95%) (Fig. 5). This result corroborates the DRX observations which show the presence of quartz particles playing the role of a binder.

The leaching behavior from the EN12457-2 confirms the fact that the environmental risks are quite reduced (Fig. 6).

4 Conclusion

Mineralogical and geochemical approaches coupled with leaching and BCR experiments were applied on Fej Lahdoun, an old mining waste in northwestern Tunisia. Results show that wastes in this area present an environmental risk due to the presence of contaminants such as Pb, Zn, and Cd. Valorization was used based on different mixtures by

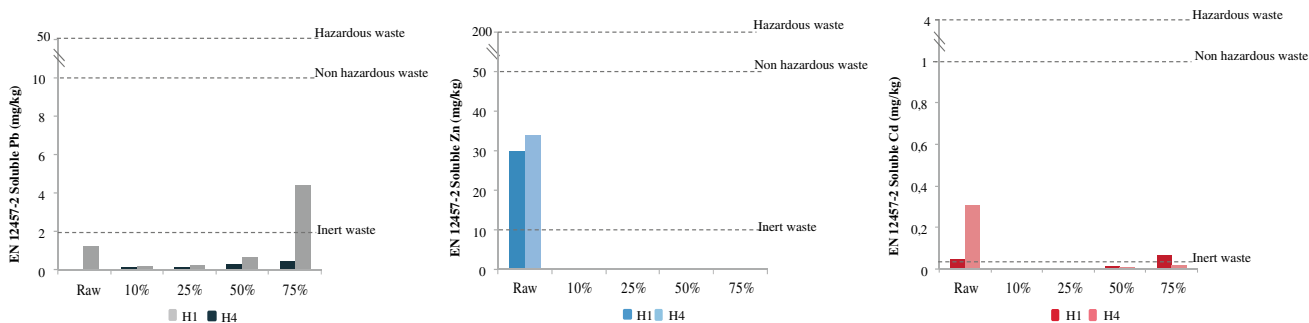
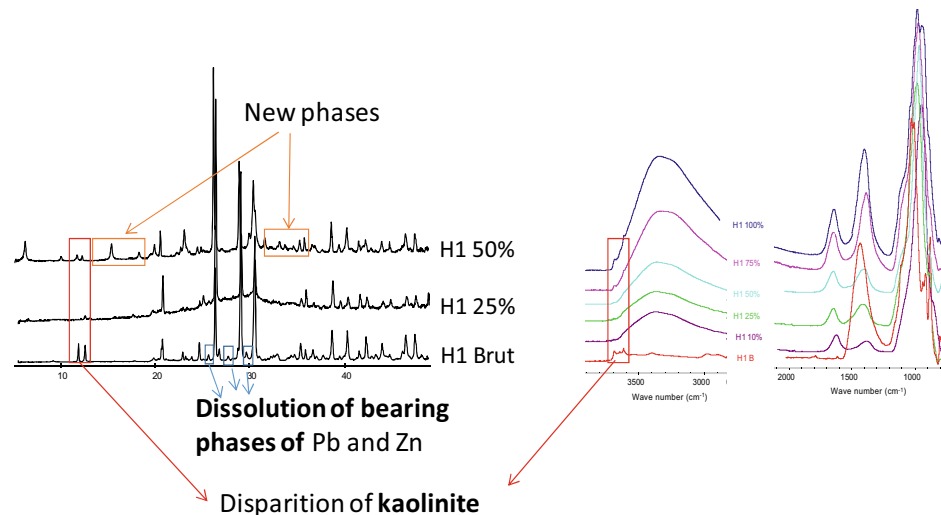


Fig. 5 Chemical speciation by BCR of waste without and with treatment

Fig. 6 Leaching tests of waste without and with treatment



substituting metakaolin, silicate source, and waste before testing. Results evidence that the geopolymeric matrix can provide an ideal binder for the immobilization of toxic contaminants because of its low permeability, resistance to acid attack, and durability in certain situations where traditional Portland cements experience problems (Zhang et al. 2008; Rao and Liu 2015, Pascaud 2015). More investigations into this valorization method should be conducted to increase its potential.

Acknowledgements The authors thank the PHC Utique programs Geasmines in Tunisia for the financial support

References

- Belabed, B.E., Meddour, A., Samraoui, B., Chenchouni, H.: Modeling seasonal and spatial contamination of surface waters and upper sediments with trace metal elements across industrialized urban areas of the Seybouse watershed in North Africa. *Environ. Monit. Assess.* **189**(6), 265 (2017). <https://doi.org/10.1007/s10661-017-5968-5>
- Sougo, C.A., Mireille, A.E., Colette, A.A., Sylvain, M., Kouamé, A., Blanc, G.: Caractérisation des Indices de Pollution (Igeo, Pli, Tec et Pec) d'un environnement Estuarien à Forte Pression Anthropique: la Baie de Biétry (Cote d'Ivoire, Golf de Guinée). *Int. J. Adv. Inf. Sci. Technol.* **3**(12), 135–139 (2014). <https://doi.org/10.15693/ijast/2014.v3i12.135-139>
- Davidovits, J.: *Geopolymer Chemistry and Applications* Institut Géopolymère, 2nd edn. Geopolymer Institute, Saint-Quentin, France (2008)
- Muller, G.: Heavy metals in the sediment of the rhine—changes seity. *Umschau in Wissenschaft Und Technik* **79**, 778–783 (1979)
- Pascaud, G.: *Étude des processus pédogénétique de technosols miniers: de l'analogie naturel a la stratégie de remédiation*. PhD thesis, Univ. Limoges, France (2015)
- Pascaud, P., Leveque, T., Soubrand, M., Boussen, S., Joussein, E., Dumat, C.: Environmental and health risk assessment of Pb, Zn, As and Sb in soccer field soils and sediments from mine tailings: solid speciation and bioaccessibility. *Environ. Sci. Pollut Res.* **21**, 4254–4264 (2014). <https://doi.org/10.1007/s11356-013-2297-2>
- Rao, F., Liu, Q.: Geopolymerization and its potential application in mine tailings consolidation: a review. *Miner Process Extr. Metall Rev.* **36**, 399–409 (2015). <https://doi.org/10.1080/08827508.2015.1055625>
- Uzu, G., Sauvain, J.-J., Baeza-Squiban, A., et al.: In vitro assessment of the pulmonary toxicity and gastric availability of lead-rich particles from a lead recycling plant. *Environ. Sci. Technol.* **45**, 7888–7895 (2011). <https://doi.org/10.1021/es200374c>
- Uzu, G., Sobanska, S., Sarret, G., et al.: Characterization of lead-recycling facility emissions at various workplaces: Major insights for sanitary risks assessment. *J. Hazard Mater.* **186**, 1018–1027 (2012). <https://doi.org/10.1016/j.jhazmat.2010.11.086>
- Zhang, J., Provis, J.L., Feng, D., Van Deventer, J.S.J.: Geopolymers for immobilization of Cr⁶⁺, Cd²⁺, and Pb²⁺. *J. Hazard. Mater.* **157**, 587–598 (2008). <https://doi.org/10.1016/j.jhazmat.2008.01.053>



Physicochemical Characterization of Diatomite from Ouled Djilali-Mostaganem Region of Algeria

Amal Touina, Safia Chernai, Bouaheur Mansour, and Boualem Hamdi

Abstract

Raw diatomite samples from Ouled Djilali-Mostaganem (Lower Chélif basin, Algeria northwestern) are investigated. Four varieties of diatomite are distinguished based on the macroscopic features, color, and fracturing effects. Several characteristics of natural diatomites such as X-ray diffraction (XRD), X-ray fluorescence spectrometry (XRF), Fourier transform infrared spectroscopy (FTIR), and Brunauer, Emmett, and Teller technic (BET) (surface area, pore volumes), scanning electron microscopy (SEM), and chemical and physicochemical analysis were studied. The results of mineralogical studies, chemical, and environmental analysis which have been carried out on various samples are tabulated. From the results of these findings, possible application areas have been suggested. The material of this deposit should also be suitable as adsorbent, filler, and filter.

Keywords

Diatomite • Properties • Characterization • Applications

1 Introduction

Diatomite, otherwise known as diatomaceous earth or silica-rock, is composed of the fossilized diatoms skeletal remains. The frustules of this unicellular organism are mainly composed of silica dioxide (SiO_2 , $n\text{H}_2\text{O}$) (Elden et al. 2010), and CaCO_3 as main impurities besides others (Hamdi 2010; Meradi 2015). Due to its physical and

chemical properties (porosity, high absorption capacity), the diatomite have different applications in sustainable development and environment: purification of drinking water; filtration agent; pesticide absorption; manufacture of antibiotics. This work aims to explore the characteristics of the diatomites from Ouled Djilali-Mostaganem deposits. XRD, XRF, and IR spectra of the diatomites were recorded; several parameters of the diatomites such as chemical composition, surface area, and pore volumes were determined. Furthermore, other chemical and physicochemical properties were studied.

2 Materials and Methods

Four varieties of natural samples of diatomite were distinguished based on the macroscopic features, color, and fracturing effects (Table 1). After the dry step (at 105 °C overnight) and the crushing of the material, the designated natural diatomite of granulometry of 60–100 μm was selected to be analyzed with several techniques described in this papers. In this study, samples of diatomite were obtained from the locations of Ouled Djilali in Mostaganem (Lower Chélif basin, Algeria northwestern) (Fig. 1) in order to determine the mineral composition, surface area, porosity, surface, and composition chemical of samples using several experimental techniques (Belhouchet et al. 2019): XRD, XRF, FTIR, BET, and SEM. Four samples were taken from each geological layer. These samples are named ‘OD’ in reference to Ouled Djilali.

3 Results

3.1 Geochemical Composition by XRF

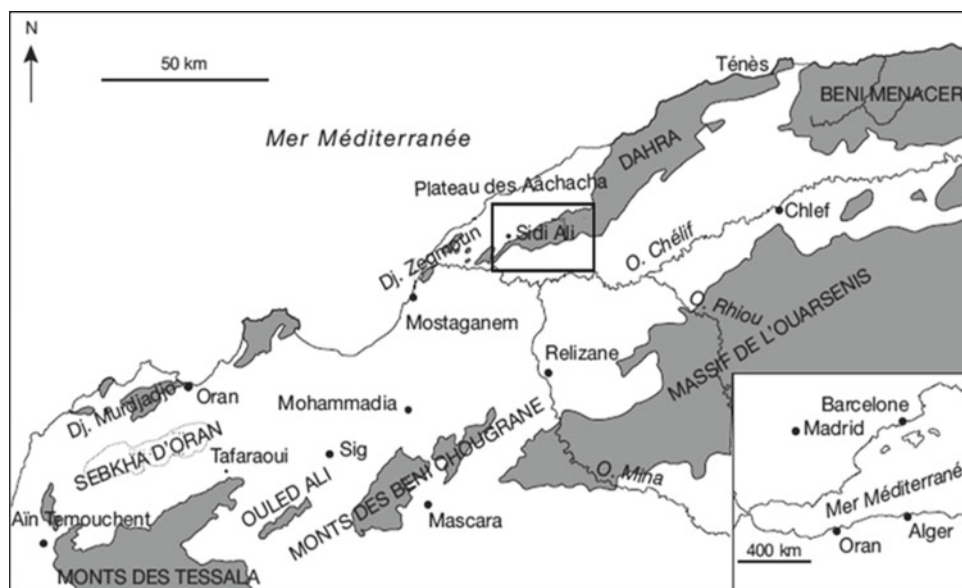
The geochemical composition of the natural diatomite samples determined by XRF is presented on Table 2.

A. Touina · S. Chernai (✉) · B. Hamdi
LCVRM ENSSMAL. BP19, 16320 Dely Ibrahim, Alger, Algeria
e-mail: shamdi.01sh@gmail.fr

B. Mansour
L.P.S.P. Département de Science de la Terre, FSTU, Université d’Oran, Oran, Algeria

Table 1 Macroscopic description of natural diatomite

Sample	Nature	Color	Features and fracturing effects
OD03	Diatomite	Whitish	Laminated, light, pulverous
OD04	Diatomite+	Whitish	++ laminated, light, pulverous
OD05	Marlydiatomite	Beige	Indurate, Massive
OD08	Marlydiatomite	Beige	++ laminated, pulverous

Fig. 1 Deposit localization of diatomite in Ouled Djilali-Mostaganem**Table 2** Geochemical composition of the natural diatomite samples

Samples	SiO ₂ %	CaO %	Impurities %	Loss %
OD03	61.52	13.81	8.53	15.85
OD04	58.9	15.16	7.89	17.2
OD05	32.84	25.94	13.48	27.53
OD08	49.49	21.71	6.87	20.69

Samples typically consist of silica (SiO₂) and significant amounts of CaCO₃ along with other minor constituents.

intense peaks are those of calcite, peaks of dolomite, peaks of illite, and of kaolinite are also observed (Table 3).

3.2 Mineralogy Phases by XRD

Typical for all samples is the presence of amorphous phase in the range between 19 and 32 °C 2 Theta. The halo is more pronounced for the OD04 and OD08 samples. A high content of the crystal phase was also registered. The most

3.3 Fourier Transform Infrared Spectroscopy (FTIR)

The IR spectra of the diatomite samples are shown in Fig. 2. There are no significant differences between the positions of the basic characteristic bands.

Table 3 Mineralogy phase (%) for diatomite samples

Samples	Calcite	Dolomite	Quartz	Pyrite	Illite	Chlorite	Kaolinite	Albite
OD03	47.54	6.66	7.03	0	19.26	0	13.82	5.69
OD04	33.96	24.4	4.66	0.15	18.34	2.33	13.78	2.36
OD05	55.72	8.69	6.61	0	20.25	1.81	4.78	2.13
OD08	49.10	7.16	5.76	0	17.79	0	14.26	5.93

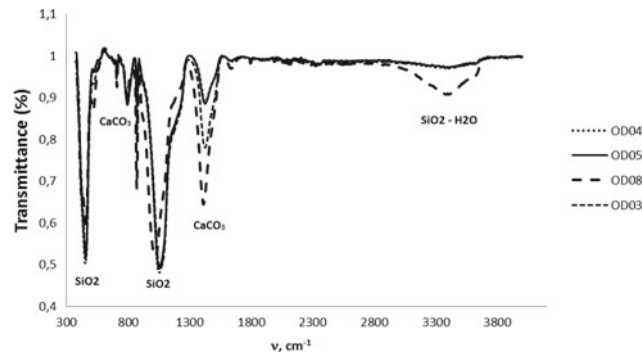


Fig. 2 IR spectra of the diatomite samples

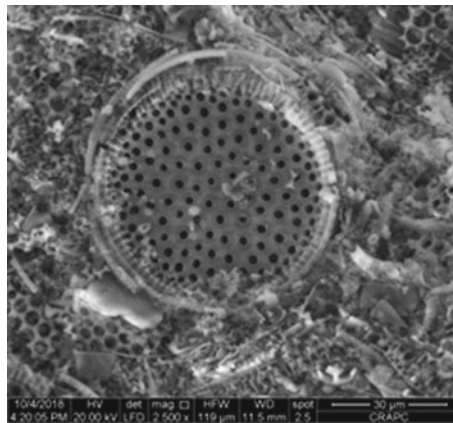


Fig. 3 SEM images of natural diatomite sample OD03

3.4 SEM Microscopy

The observation by scanning electron microscopy showed that diatomite samples were very rich in diatoms (centric and pennate diatoms). Each frustule of diatoms contains areolas due to its high porosity. The size and the disposition of areolas vary with the species. It can be inferred that diatomite has a large void volume (Fig. 3).

3.5 Physicochemical Properties

Physicochemical properties of natural diatomite samples are summarized in Table 4.

Table 4 Physicochemical properties of natural diatomite samples

Samples	S _{BET} (m ² /g)	pH	da(*) g/cm ³	H (%)	Ads H ₂ O (%)	Ads Oils (%)	Chloride (%)
OD03	58.8	8.01	0.48	97.20	37.82	63.85	0.209
OD04	45.2	7.99	0.42	96.60	45.45	62.77	0.105
OD05	69.9	7.82	0.64	90.46	15.89	98.31	2.144
OD08	47.9	8.14	0.49	96.35	32.33	62.88	0.248

(*) da: bulk density

4 Conclusion

The chemical composition of the diatomite samples from the Ouled Djilali-Mostaganem deposits is slightly different (the content of SiO₂ and impurities). They have a relatively low surface area and high sorption capacities for oils and water. Hence, it may be concluded that the diatomite from Ouled Djilali-Mostaganem deposits may be successfully used as low-cost sorbents. The material of this deposit should also be suitable as adsorbent, filler, and filter.

References

- Belhouchet, N., Hamdi, B., Chenchouni, H., Bessekhoud, Y.: Photocatalytic degradation of tetracycline antibiotic using new calcite/titania nanocomposites. *J. Photochem. Photobiol. A: Chem.* **372**, 196–205 (2019). <https://doi.org/10.1016/j.jphotochem.2018.12.016>
- Elden, H., Galal Morsy Mohamed Bakr, G.H.: Diatomite: Its characterization, modifications and applications. *Asian J. Mater. Sci.* **2**(3), 121–136 (2010)
- Hamdi, B.: Study of the possibility to use of diatomaceous earth in the thermal insulation. In: EFEEA'10 International Symposium on Environment Friendly Energies in Electrical Applications, Ghardaïa, Algeria, 6p, (2010)
- Meradi, H.: Characterization by thermal analysis of natural kieselguhr and sand for industrial application. *Energy Procedia* **74**, 1282–1288 (2015)



Prioritizing Drainage Rehabilitation in Kasavanahalli Village, Bengaluru (India) Using AHP

Shivika Saxena, Aakash, G. Ajith Kumar, B. S. Bharath Raj, and Syed Isaac Peeran

Abstract

The use of AHP as a potential decision-making tool in water resource management is presented for Kasavanahalli, Bengaluru. Criteria are set in a hierarchical structure, and the alternatives are selected for rehabilitation by ranking at all levels using the eigenvector method. A sensitivity analysis is conducted at the end of each comparison for consistency check of the final decisions. The selected drains as per analysis are consistent. Hopefully, this method will present itself as an efficient decision-making tool to be used by Bruhat Bengaluru Mahanagara Palike (an administrative body responsible for civic amenities and infrastructure of the Greater Bangalore metropolitan area) to remediate numerous water woes in the selected region and is extended to further parts of the city.

Keywords

AHP • MCDA • Drainage • Water logging • IWRM

1 Introduction

Tremendous population growth and urbanization in Bengaluru is leading to changes in land use and land cover and thus inducing a significant increase in runoff coefficients. A decrease in the recharge efficiency of land surfaces to the groundwater storage increases the stream flows during and after significant rainfall events (Tarigan et al. 2018). Any change in management institutions and in demography which follows rapid urbanization, makes collective remedial action challenging (Seema et al. 2015). In rapidly urbanized cities of India, peri-urbanization management is a rapid and ever-growing challenge where the increasing need for

support infrastructure (resulting in reduced use and maintenance of drainage) is to be balanced with social needs and preventing ecosystem loss (Vanitha and Nagaraju 2015). If drainage capacity decreases due to poor management, it results in flooding and waterlogging even after a small rainfall event. It is beneficial to use multi-criteria decision analysis (MCDA) for integrated water resource management. Due to limited budget, frequent maintenance of city drainages is difficult but essential, especially in heavy rains of Bengaluru. As a solution, drains can be prioritized to address the direst situation to prevent any disruption of day-to-day activities. MCDA helps in creating a priority and finds out hidden causal factors for a given problem. One of the most reliable and robust methods of MCDA is the analytical hierarchy process (AHP), developed by Saaty.

2 Methodology

Based on the judgment of the decision-maker, the AHP aims at quantifying relative priorities for a given set of alternatives under multiple criteria on a ratio scale and stresses the importance of the consistency of the comparisons of alternatives (Teknomo 2006, Tarigan et al. 2018).

Ten open drains are selected in Shantiniketan layout, located within the Kasavanahalli village of Marathahalli, in Bengaluru. There is frequent flooding and waterlogging in the village and its vicinity during heavy rain. The primary data in this study is obtained from interview and questionnaire, which is designed for the AHP method. Six of the residents and three labourers participated in the survey who are considered to be aware of the issues faced. The questionnaire is prepared to assess the existing situation in the context of each level in the AHP Structure and pairwise comparisons. For instance, for the assessment of sub-criteria 'traffic congestion', questions are asked about the influence of inundation near a concerned drain on traffic, frequency of traffic disturbance. From these comparisons, priorities for

S. Saxena (✉) · Aakash · G. A. Kumar · B. S.B. Raj · S. I. Peeran
CMR Institute of Technology, Bangalore, India

each drain, for rehabilitation purpose, are found out using eigenvector method followed by sensitivity analysis for consistency check.

3 Results

3.1 Levels in the AHP Structure

As shown in Fig. 1, the AHP structure consists of criteria for drainage condition with physical characteristics like order (relative importance of location in the network), damage level (blocked or damaged) as well as flooding status (spread of waterlogging). Region condition criteria take care of the disturbance and affected population, while societal condition criteria take care of residents and workers' status (literacy and awareness), situation (standard of living) and flexibility to change.

3.2 Pairwise Comparisons

Pairwise comparison rating from a chosen scale (Saaty 2008) yields to comparison matrices at each level in the hierarchy structure. Eigenvector method involves computation of maximum eigen value and principal eigen vector from the comparison matrix. The normalized principal eigen vector is priority vector. Consistency for each comparison is checked by calculating consistency ratio which should be less than 0.1. This method is explained in more detail in Teknomo (2006). One such process is demonstrated for Level 1 in Table 1, followed by a consistency check.

Maximum eigen value, $L = 3.106$, $C_i = (L - n)/n - 1$, n is order of matrix. Consistency Ratio (Cr) = $C_i/R_i < 0.1$ OK, R_i is random index obtained from Table 2.

Since Cr less than 0.1, we can conclude that the comparisons are consistent and thus acceptable. The same procedures are conducted for the comparisons of the sub-criteria

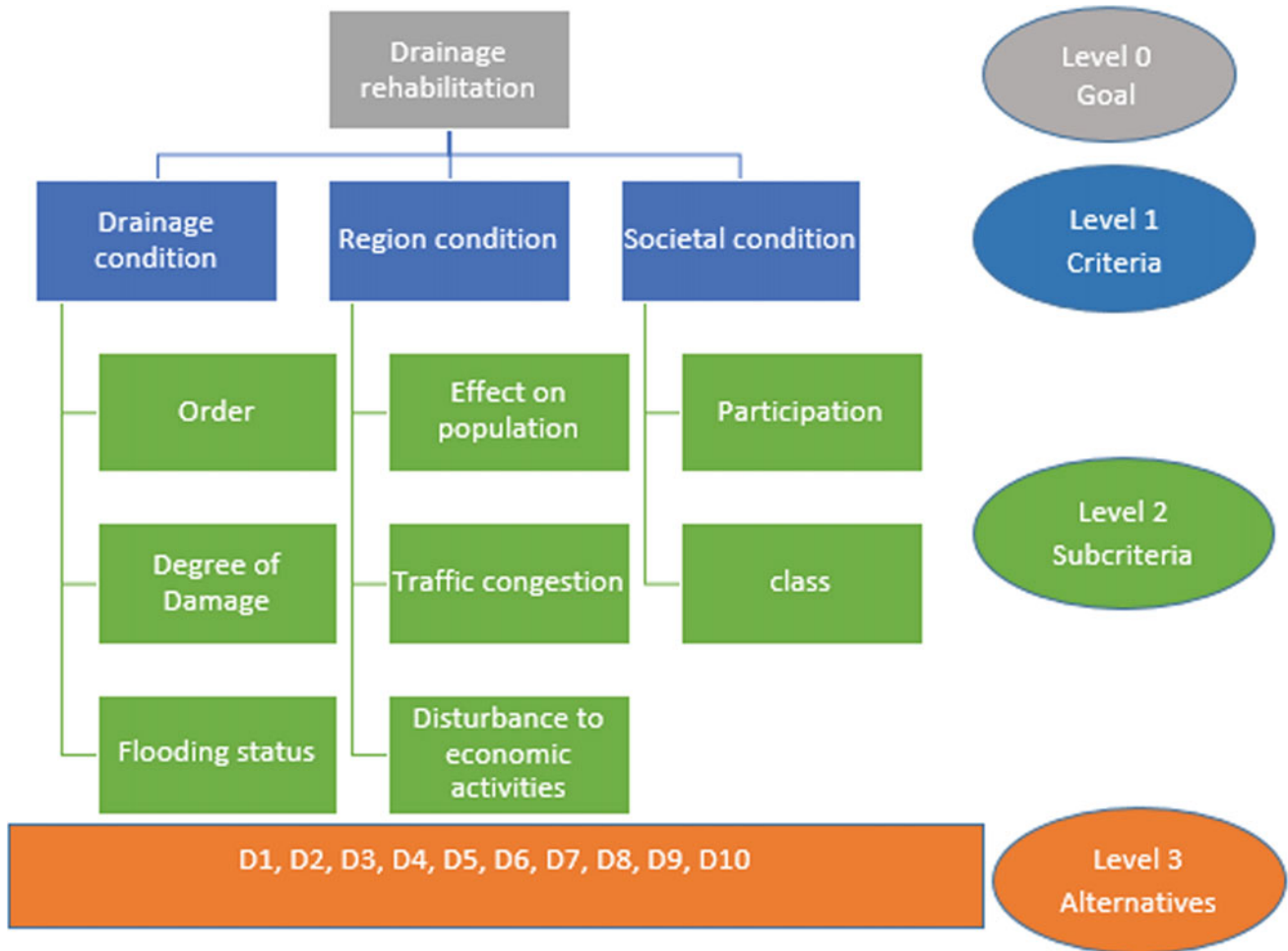


Fig. 1 Proposed AHP structure

Table 1 Comparison matrix for level 1

	DC	RC	SC	Priority vector
DC	1	3	1/5	0.330
RC	1/3	1	1/5	0.141
SC	5	1/3	1	0.526

Table 2 Average random consistency (Tarigan et al. 2018)

Matrix order n	1	2	3	4	5	6	7	8	9	10
RI	0	0	0.58	0.9	1.12	1.24	1.32	1.41	1.45	1.49

(level 2), and the alternative drains for each sub-criteria (level 3). Consistency ratio for all comparisons is found to be < 0.1. For large matrices, Matlab is used for ease in the computation.

3.3 Priority Scores

We can calculate the score of priority for each drain by formulating a summary table for all priority vectors level-wise (Tarigan et al. 2018). For example, overall priority score for D1 = $(0.330 \times 0.468 \times 0.0572) + (0.330 \times 0.146 \times 0.1149) + (0.330 \times 0.3834 \times 0.0712) + (0.141 \times 0.529 \times 0.0815) + (0.141 \times 0.301 \times 0.1708) + (0.141 \times 0.170 \times 0.0495) + (0.526 \times 0.75 \times 0.0757) + (0.526 \times 0.2495 \times 0.0757) = 0.0832$.

4 Discussion

The present work shows that water issues need to be prioritized according to their severity, effect on the population, resource health and available finances. In the study area, ten open drains are selected through a site survey for repair and maintenance to address the prevailing waterlogging nuisance. The resulting priority through this method is checked for ground truth by checking various factors like gradient, lithology, proximity to roads and nearby water-body to check the significance of the subject drain in the entire drainage system. The resultant priorities are found to be complaisant with ground truth. Extension of this work to surrounding areas in the Bengaluru city where a similar problem is encountered can have an integrated approach of AHP within a GIS environment to handle extensive data from a larger study area. This approach has gained widespread applications in environmental earth sciences such as assessment of natural hazard, land suitability, and site selection. (Bathrellos et al. 2017). The coupling of AHP with GIS to assess socio-economic and geomorphological factors as well as the presentation of the results in a spatial environment can ease the handling of larger areas and their

problem statement as demonstrated in Panagopoulos et al. 2012. Further, uncertainty analysis for each factor in the criteria chosen in the AHP method can also be included to determine the uncertainty which may happen from selection, comparison and ranking of multiple criteria (Bathrellos et al. 2017). Further, a method of risk analysis can also be added to the AHP structure as one of the sub-criteria (higher risk, higher priority) in future studies (Pietrucha-Urbanik 2015), to make the approach more reliable and robust.

5 Conclusion

We have shown that AHP can be used in a densely populated water-stressed city such as Bengaluru, as a potential decision-making tool in water resource management. As a study case, we are able to rank ten urban drains for rehabilitation. We find that drains D2, D5, D6, D8 are the top priorities consecutively. In other words, the selected drains are the most favourable to have rehabilitation.

References

Bathrellos, G.D., Skilodimou, H.D., Chousianitis, K., Youssef, A.M., Pradhan, B.: Suitability estimation for urban development using multi-hazard assessment map. *Sci. Total Environ.* **575**, 119–134 (2017). <https://doi.org/10.1016/j.scitotenv.2016.10.025>

Panagopoulos, G.P., Bathrellos, G.D., Skilodimou, H.D., Martsouka, F. A.: Mapping Urban water demands using multi-criteria analysis and GIS. *Water Resour. Manag.* **26**(5), 1347–1363 (2012). <https://doi.org/10.1007/s11269-011-9962-3>

Pietrucha-Urbanik, K.: Failure prediction in water supply system—current issues. *Adv. Intell. Syst. Comput.* **365**, 351–358 (2015)

Saaty, T.L.: Decision making with the analytic hierarchy process, *Int. J. Ser. Sci.* **1**(1), 2008

Seema, M., Manjunath, B., Nagendra, H.: Effects of urbanisation on the use of lakes as commons in the peri-urban interface of Bengaluru, India. *Int. J. Urban Sustain. Dev.* **7**(1), 89–108 (2015). <https://doi.org/10.1080/19463138.2014.982124>

Tarigan, A.P.M., Rahmad, D., Sembiring, R.A., Iskandar, R.: An application of the AHP in water resources management: a case study on urban drainage rehabilitation in Medan City. In: *IOP Conference Series: Materials Science and Engineering*, vol. 309, p. 012096 (2018)

-
- Teknomo K.: Analytical Hierarchy Process (AHP) Tutorial (2006). Retrieved from <https://people.revoledu.com/kardi/tutorial/AHP/AHP-Example.htm>
- Vanitha, P., Nagaraju, R.: Role of urban planning as a tool to mitigate the environmental repercussions due to peri-urbanisation. *J. Civil Eng. Environ. Technol.* **1**(3), 96–102 (2015)



Comparison Between Two Samples Granulates Differences of Thermal Activated Biochar from Date Palm Fiber

Djehad Bentarfa, Mohamed Lamine Sekirifa, Youcef Touil, and Mahfoud Hadj-Mahammed

Abstract

This study aims to evaluate the N₂ adsorption capacities of activated carbons prepared by physical activation of date Palm fiber on two sample of granulates and then to compare the differences between them. Adsorption isotherms were obtained from the adsorption of nitrogen at 77 K. The BET specific surface area (SBET) and the diameter of the pore was calculated based on the Brunauer-Emmett Teller (BET) equation. The microporous surface (Smicro) and external surface (Sext), as well as the micropore volume (Vmic) was evaluated by the t-plot method. The Single point adsorption determined the total pore volume. The obtained results show that each of the specific surface area, the volume microspores, volume total, and the pore diameter of the sample A15 (325.65 m²/g, 0.128 cm³/g, 0.15 cm³/g, 1.93 nm) more significant than the sample A16 (175.07 m²/g, 0.0715 cm³/g, 0.079 cm³/g, 1.88 nm) respectively due to the change only in samples granulates, The burn-off for A15 and A16 is 95.73%, 93.54% respectively, the burn-off increased with the increase of the samples granulates. The shape of the N₂ adsorption isotherms displayed H-type isotherms according to the classification of Giles.

Keywords

Activated carbon • Thermal activation • N₂ Adsorption • Date palm fiber • Microporosity

1 Introduction

Adsorption separation technology is now one of the most critical separation technologies. It is widely used for the separation and purification of gases and liquids in a wide variety of fields, ranging from petroleum, petrochemical, and chemical industries to environmental and pharmaceutical applications. A significant amount of date palm fibers are a significant source of agricultural waste likely to be of economic interest (Lazhar and Mohammed Assem 2017; Abd El Hakim and Moulay Rachid 2017). In this context, the laboratory aims, among other things, to exploit and valorize this type of natural by-products of our country. The peculiarity of this waste lies in the possibility of recycling it into industrially exploitable finished products. For some considerable time, activated carbons have been used as adsorbents in applications where impurities, in low concentrations, have to be removed. Activated carbon must possess a large volume of micropores, with appropriate pore-size distribution, in order to adsorb molecules of different sizes (Marsh 2006). The adsorption properties of activated carbons related to their porosities and their specific surfaces are exploited in many applications in the liquid or gaseous phase. The object of this work is to exploit the residues of the agriculture of date palm fiber variety Ghars in preparation of activated carbon with physical activation.

2 Materials and Methods

Preparation of raw materials: Palm waste, namely date palm fiber of Ghars, was obtained from an oasis of date palms in Ouargla, Algeria. The fibers were washed with distilled water to remove dust and other hydrophilic impurities and then dried at room temperature. After drying, they were crushed and sieved. The fractions between two sets (250 μm < d < 500 μm) and (45 μm < d < 125 μm) are activated thereafter.

D. Bentarfa (✉) · M. L. Sekirifa · Y. Touil · M. Hadj-Mahammed
Laboratoire de Biogéochimie en Milieux Désertiques, Faculté des
Mathématiques et des Sciences de la Matière, Université Kasdi
Merbah Ouargla, BP 511 30000 Ouargla, Algeria

Table 1 The yield of pyrolysis and Burn-off of date palm fibers (variety G hars)

Sample	Yield of pyrolysis (%)	Burn-off (%)
A15 (250 μm < d < 500 μm)	32.03	95.73
A16 (45 μm < d < 125 μm)	39.61	93.54

The pyrolysis procedure: A vertical furnace (Ref. BGVA12-300B, CARBOLITE) was connected to the inlet and the outlet devices allowing an upward gaseous flow through the sample. 75 g of crushed date palm fiber is introduced in a cylindrical quartz cell with an internal diameter of 40 mm including a frit disc at half-height (Sekirifa et al. 2013; Sekirifa 2013). The pyrolysis was performed at 500 °C for 2 h under a nitrogen flow of 250 mL/min and a heating rate of 5 °C/min (Table 1).

The activation procedure: the resulting pyrolyzed date stones were activated at 600 °C for 2 h using the same montage (Sekirifa et al. 2013; Sekirifa 2013). The carbon dioxide flow rate was maintained at 250 mL/min and a heating rate of 5 °C/min.

Adsorption isotherms were obtained from the adsorption of nitrogen at 77 K. The BET specific surface area (SBET) and the diameter of the pore was calculated based on the Brunauer-Emmett Teller (BET) equation. The microporous surface (S_{micro}) and external surface (S_{ext}), as well as the micropore volume (V_{mic}) was evaluated by the t-plot method. The Single point adsorption determined the total pore volume.

3 Results

3.1 Textural Proprieties of the Activated Carbons

N₂ adsorption-desorption isotherms obtained of the two samples of activated carbons at 77 K are presented in Fig. 1.

Textural characteristics obtained from N₂ and BJH adsorption isotherms; single point and t-plot method are shown in Table 2. It is clear that the shape of the adsorption isotherm and the adsorbed volume depend on the activation conditions. (Sekirifa et al. 2013; Belhachemi et al. 2014).

Table 2 shows the characteristics of both samples of activated carbon prepared from date palm fiber, type Ghars.

3.2 Characterization of Carbon Surface Chemistry

Figure 2 represents the relation between pore volume (cm³/g) and pore diameter (nm).

Pore size distribution curves Fig. 2 suggest that both the activated carbons are micro-porous materials due to the

sharp increase of pore size distribution curves for pore diameters less than 1.93 nm (Belhachemi et al. 2014).

4 Discussion

In light of the results, during the process of preparing activated carbon, many conditions affect many characteristics.

The burn-off for A15 and A16 was 95.73% and 93.54%, respectively, the burn-off increased with the increase in the sample granulates, showing that the increase in sample granulates facilitates the thermal decomposition during the carbonization process. The increase in burn-off suggested the removal of more volatile organic matters which eventually enhanced the pore development in the AC. The enhancement of the porosity could increase the ACF surface area and thus affect the adsorption capacity.

According to the figures and table, we note the following points:

- The shape of the isotherms is the first experimental tool to diagnose the nature of the specific adsorption phenomenon. The isotherms have been classified according to the classification of Giles et al. (Giles et al. 1974). According to the above classification, the adsorption isotherms of N₂ Fig. 1 compound displayed an H curve pattern.
- H-type isotherms: This case corresponds to non-porous or entirely microporous solids, that is to say having pore diameters of less than 20 Å. They are typical of adsorption in monolayers or corresponding to the filling of micropores with saturation when the available volume is filled (Nabila 2013).

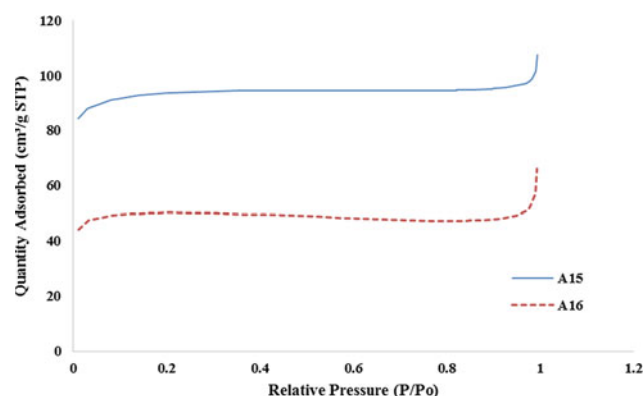
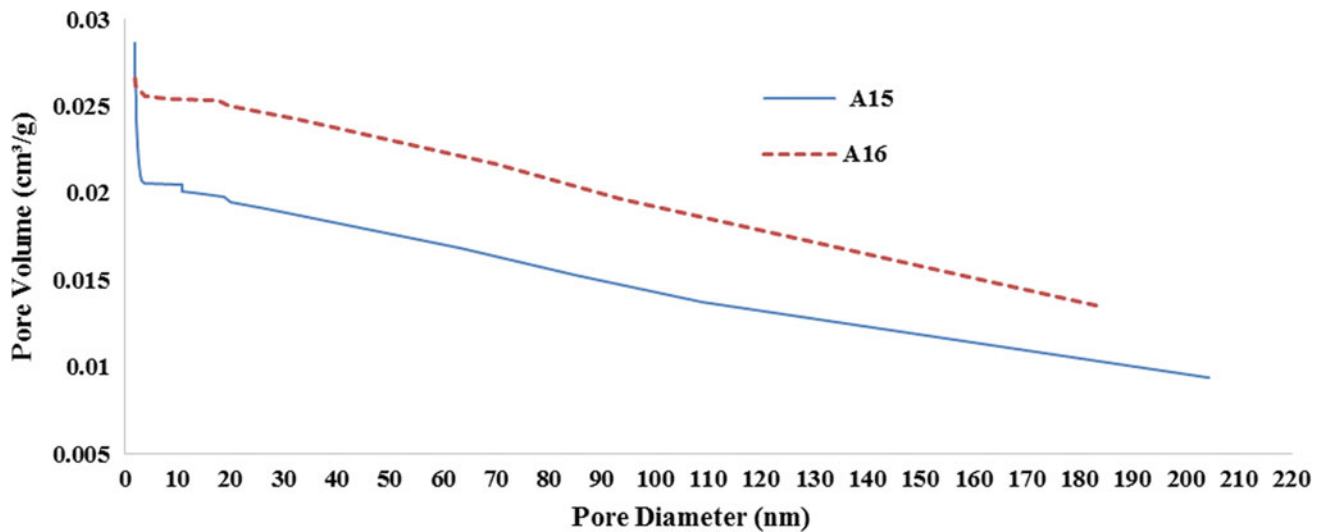
**Fig. 1** Adsorption isotherm of N₂ on activated carbon

Table 2 Characteristics of activated carbon

Activated carbons	Characteristics of activated carbon										
	Burn-off (%)	The specific surface area (m ² /g)			t-plot (cm ³ /g)			Single point (cm ³ /g)	S _{micro} /S _{BET}	V _{micro} /V _t	D _p (nm)
		Single point	BET	Langmire	S _{micro}	S _{EXT}	V _{micro}	V _t			
A 15	95.73	325.65	313.40	414.75	275.47	37.94	0.128	0.15	0.88	0.85	1.93
A 16	93.54	175.07	168.13	222.40	154.25	13.88	0.0715	0.079	0.92	0.90	1.88

**Fig. 2** Pore size distribution of activated carbons

- Through what is mentioned above in Table 2, we found that each of the specific surface area, the volume micropores, total volume, and the pore diameter of the sample A15 (325.65 m²/g, 0.128 cm³/g, 0.15 cm³/g, 1.93 nm) more significant than the sample A16 (175.07 m²/g, 0.0715 cm³/g, 0.079 cm³/g, 1.88 nm) respectively due to the change only in samples granulates.

5 Conclusions

The separation technologies are very versatile and very important, we must study it in order to develop it in all fields. In this paper, we study the absorbent material and the effect of granulomata on the process of separation. As a result, we found that the larger samples granulate, the higher the area and porosity. The sample A15 (250 μm < d < 500 μm) has a specific surface area, a volume of micropores, a total volume, and a pore diameter that are larger than the sample A16 (45 μm < d < 125 μm). The burn-off for A15 and A16 is 95.73%, 93.54% respectively; it increased with the increase

of the sample granulate. The shape of the N₂ adsorption isotherms displayed an H-type isotherm according to the classification of Giles.

References

- Abd El Hakim, B, Moulay Rachid, K.: Préparation et caractérisation d'un charbon actif à partir de coquilles d'oeufs. Master dissertation, Univ. Ouargla (2017)
- Belhachemi, M., Jeguirim, M., Limousy, L., Addoun, F.: Comparison of NO₂ removal using date pits activated carbon and modified commercialized activated carbon via different preparation methods: Effect of porosity and surface chemistry. *Chem. Eng. J.* **253**, 121–129 (2014)
- Ferguene, N.: Modélisation des phénomènes de transfert de matière/adsorption dans les particules poreuses. Magister, Génie des procédés, Génie chimique., Bejaia University, (2013)
- Giles, C.H., D'gílva, A.P., Easton, Y.A.: *J Colloid Interf Sci.* 47–766, (1974)
- Lazhar, S., Mohammed Assem, S.: Étude comparative de la capacité adsorbant de deux types de charbon actif à partir des fibres de palmier dattier. Master Dissertation, Univ. Ouargla (2017)
- Marsh, H.: Francisco rodriguez-reinoso activated carbon. (Elsevier, 08/2006)

- Sekirifa, M.L., Pallier, S., Hadj-Mahammed, M., Richard, D., Lotfi, B., Al-Dujaili, A.H.: Measurement of the performance of an agricultural residue-based activated carbon aiming at the removal of 4-chlophenol from aqueous solutions. *Energy Procedia* **36**, 49–103 (2013)
- Sekirifa, M.L.: Étude des propriétés adsorbantes des charbons activés issus des noyaux de dattes: Application au traitement d'effluent aqueux. Doctoral thesis, Univ. Annaba (2013)



Study of Rheological Behavior of “Gafsa” Clay

Safa Mkaouar, Walid Maherzi, Patrick Pizette, and Mourad Benzina

Abstract

Developing ecofriendly bricks using natural material such as clay represents an essential step toward making building sector low cost and energy efficient. This study aims to describe the physicochemical characterization and rheological property of clay taken from Gafsa, Tunisia. The rheology of clay–water mixtures was determined to understand the viscosity and plasticity behavior of the paste. In this paper, lime served as a binder at different rates to improve the quality of CEB. Lime addition effects at various percentage 20, 30, and 40% were investigated. Casson model confirmed the clay studied referring to its rheological properties. Besides, lime with ecological character ameliorates mix properties.

Keywords

Clay • Viscosity • Rheological model

S. Mkaouar (✉) · M. Benzina
Laboratory Water, Energy and Environment (LR3E),
code: AD-10-02, National Engineering School of Sfax,
Department of Materials, University of Sfax,
B.P.W.3038 Sfax, Tunisia

M. Benzina
e-mail: mourad.benzina@enis.tn

S. Mkaouar · W. Maherzi · P. Pizette
Laboratory Civil and Environmental Engineering (GCE),
Department of Civil and Environmental Engineering,
Institut Mines Télécom Lille-Douai, 941, rue Charles Bourseul,
B.P. 838, 59508 Douai, France
e-mail: walid.maherzi@imt-lille-douai.fr

P. Pizette
e-mail: patrick.pizette@imt-lille-douai.fr

1 Introduction

To preserve the environment, reducing harmful impacts and energy consumption are among a few of the concerns (Belhouchet et al. 2019). The construction field is a sector characterized by a massive amount of carbon emission. In this context, searching for new methods of building using low-cost energies becomes crucial. Clay, a well-used material in compacted earth blocks (CEB) preparation, is abundant.

Rheological property is fundamental to understand the clay behavior and obtain the optimal formulation to achieve CEB with better mechanical properties.

2 Materials and Methods

Clay collected from Gafsa (CG), Djbel Bouamrane, located in southwest of Tunisia is shown in Fig. 1. The chemical and mineralogical analysis was determined. The rheology study of clay was tested using a rheometer Antom Par MCR301 and controlled with software. A plan-type configuration was used with a diameter of 25 mm. The gap was set at 1.5 mm after a long series of performance tests.

The first step consists of preparing raw materials: clay dried in the oven and sieved to obtain the fraction 80 μm grain size. The clay/water was stirred in order to have a homogeneous paste, and then, the mixture was kept constant for a few minutes.

3 Results and Discussion

3.1 Clay Characteristics

The chemical composition indicates that CG was composed of major elements namely 57.97% of SiO_2 and 18.71% of Al_2O_3 . The percentage of K_2O (6.38%) confirms the presence of kaolinitic phases.

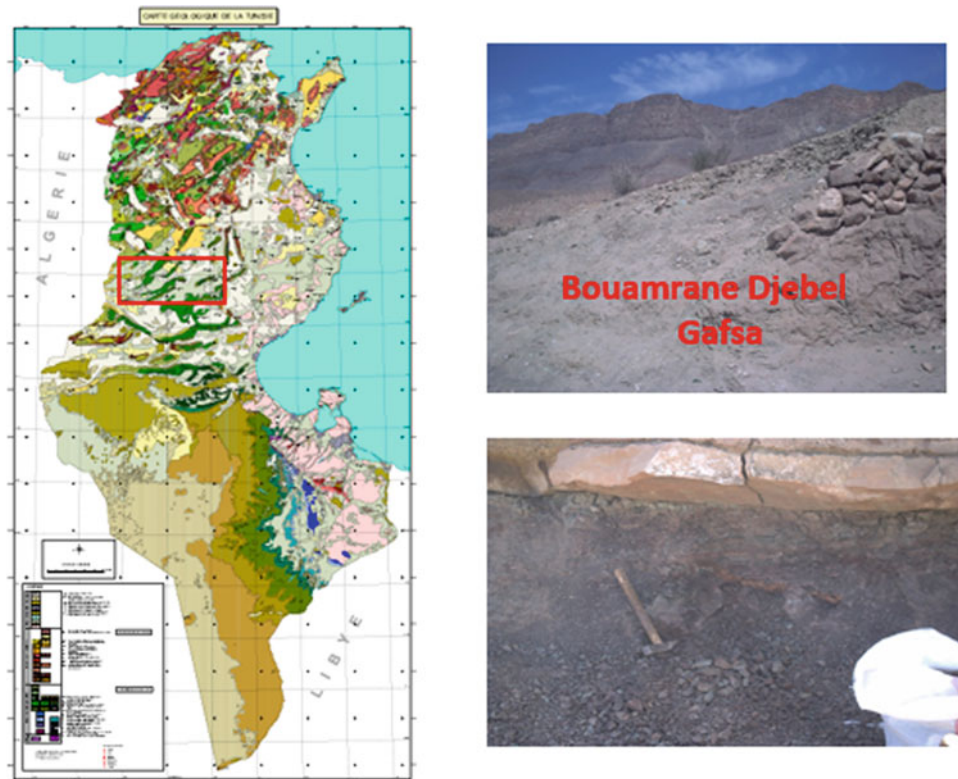


Fig. 1 Map of the sample location

3.2 Rheological Behavior

Over the years, several paste mixtures were developed. We studied water content and lime supplementation. Shear stress and paste viscosity, based on shear rate, were presented in Figs. 2 and 3. The water and lime supplementation increase

the shear stress based on the shear gradient (Fig. 2). Rheological behavior paste showed a decrease in the shear stress compared with mixture clay/water/lime, and it increased with a high percentage of lime. Therefore, this phenomenon reflects a better cohesion of paste incorporated with lime (Dewu et al. 2016; Ghailane et al. 2019).

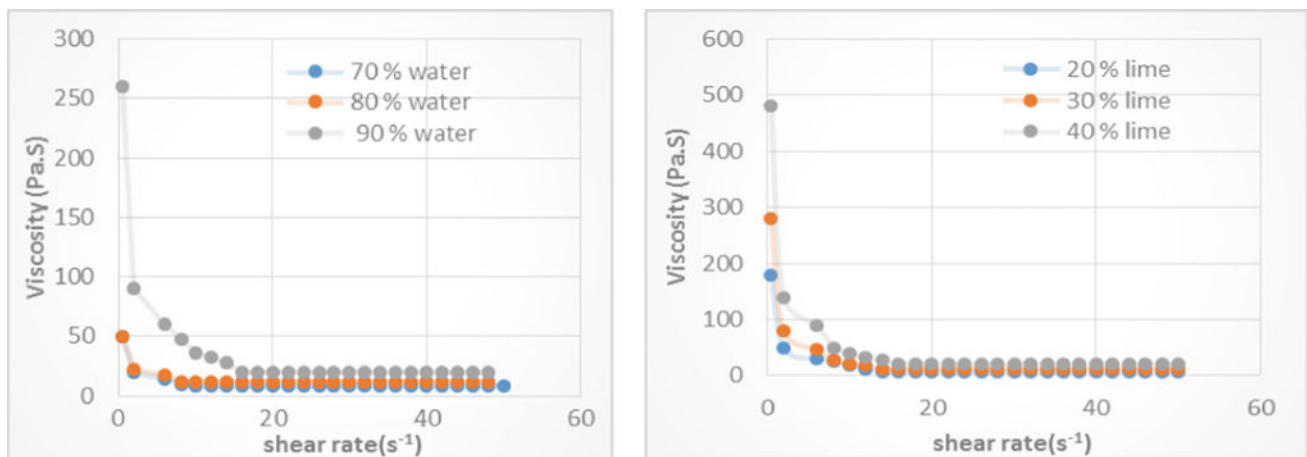


Fig. 2 Viscosity as function of shear rate

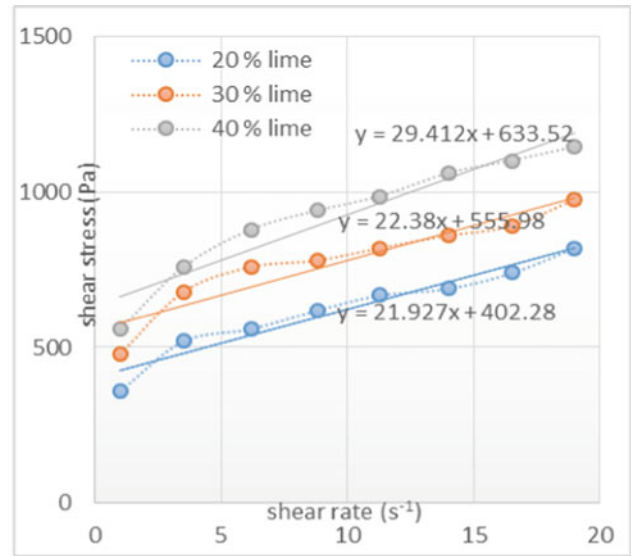
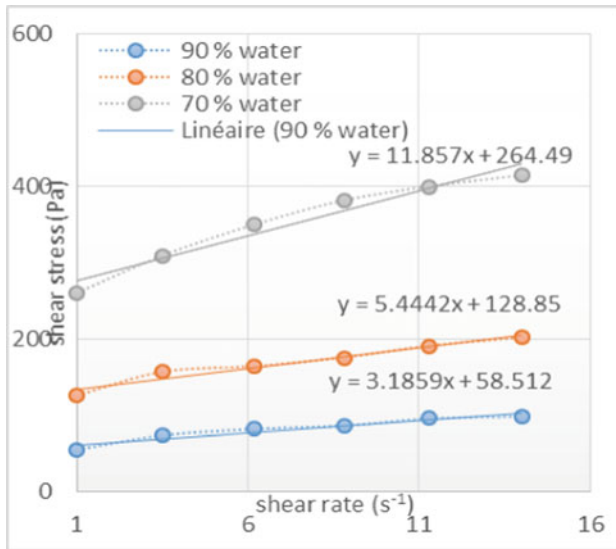


Fig. 3 Shear stress in function of shear rate

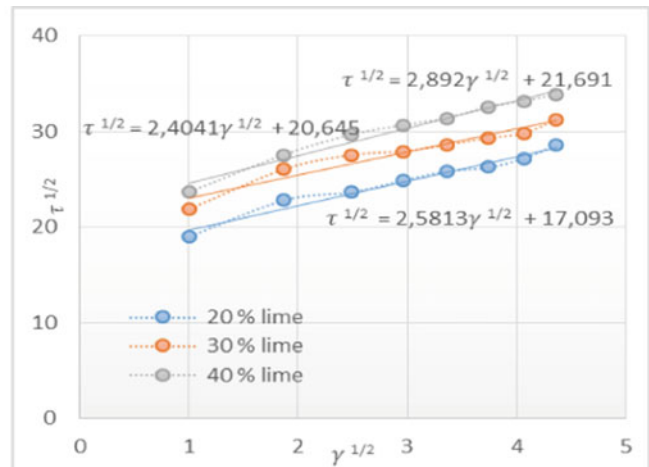
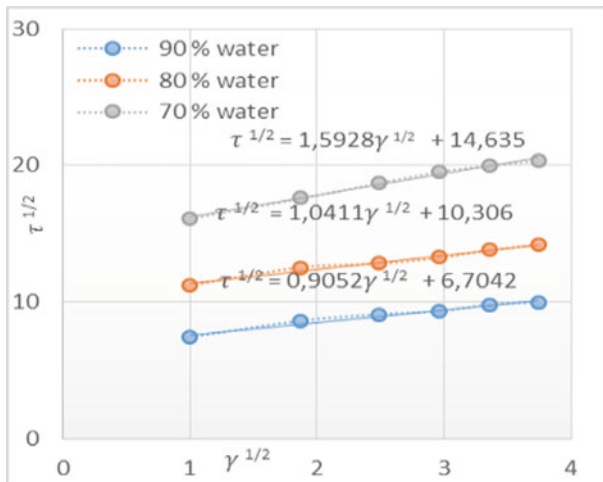


Fig. 4 Rheological behavior models for clay CG (casson model)

Nevertheless, the viscosity decreased in line with the shear gradient applied (Fig. 3). For different percentages of lime, the viscosity increased with lime addition. However, for content, the paste with lime had a higher viscosity, compared to a natural paste with water only. The addition of lime did not have any effects on the rheological property of the paste (Ghailane et al. 2019; Gomes et al. 2015).

Figure 3 presents the shear stress as a function of the velocity gradient. Newton model ($\tau = \eta\dot{\gamma}$) cannot describe the rheological behavior of obtained paste.

The rheological behavior of the Bingham type cannot be defined. As presented in Fig. 3, all points are not presented by an affine line.

The Casson model is represented by: $\sqrt{\tau} = b\sqrt{\dot{\gamma}} + \sqrt{\tau_0}$. τ : The shear stress (Pa), τ_0 : The flow threshold stress (Pa), $\dot{\gamma}$: The velocity gradient (s⁻¹).

Thus, the viscoplastic model of Casson described well the rheological behavior of the paste (Gomes et al. 2015), since the presentation $\tau^{1/2}$ as a function of $\dot{\gamma}^{1/2}$ is linear (as shown in Fig. 4).

4 Conclusion

The GC was composed of kaolinite and illite minerals and quartz as accessory minerals. Varying water and lime rate affects the rheological behavior of paste. Based on rheological

analysis, the Casson model confirmed the cost-effectiveness of the clay studied.

References

- Belhouchet, N., Hamdi, B., Chenchouni, H., Bessekhoad, Y.: Photocatalytic degradation of tetracycline antibiotic using new calcite/titania nanocomposites. *J. Photochem. Photobiol. A: Chem.* **372**, 196–205 (2019). <https://doi.org/10.1016/j.jphotochem.2018.12.016>
- Dewu B.B.M., Oladipo, M., Oladipo, A., Arabi Suleiman, A., Sabiu, B.: Iron removal from local bentonitic clay and its effect on clay rheology. *Petroleum Technol. Dev. J.* **6**(1), 66–77 (2016)
- Ghailane, H., El Boukili, G., Khaldoun, A.: Rheology of clay and clay housing in Bensmim. In: Conference: IRSEC At: Rabat (2019)
- Gomes, R., Verônica da, L., José, A., Martini, M., Valquíria de Fátima, J., Valenzuela, S., Das Graças, M., Diaz Francisco Rolando, V.: Characterization, modification and rheology of green clay. *Mater. Sci. Forum.* **820**, 60–64 (2015)



Thermal Energy Use in Hammam Righa spa, Algeria

Salima Ouali, Mohammed Moundji Hadjiat, Khaled Imessad, Khelifa Salhi, and Abdelkader Ait-Ouali

Abstract

This work aims at improving energy efficiency by using geothermal energy for heating and air-conditioning of the spa premises at Hammam Righa spa in northern Algeria. For this purpose, we chose a bungalow from the thermal station as a reference case to implement our application. The first step involves reducing the heating and cooling requirements by insulating the bungalow envelope. The second step focuses on heating the same bungalow by using geothermal energy from local geothermal resources. By applying wall insulation and double-glazing, we reduced energy consumption for heating and cooling by 59%, and as a result, we improved thermal comfort inside the bungalows.

Keywords

Energy • Hammam Righa • Geothermal • Resource • Heating • Cooling

1 Introduction

The Hammam Righa spa is located in the Ain Defla Province (Algeria), 100 km west of the capital Algiers. It is a tourist region best known for its beautiful landscapes Fig. 1, and an integral place for health, adapted to various therapeutic orientations (Guigue 1947; Ministère du Tourisme et de l'Artisanat 2010). The study site, which is 530 m above sea level, over a surface area of 16 hectares, is characterized by a Mediterranean climate, moderate in the hot summers, and cold winters.

During our audit mission, we found that old bungalows used for spa activities had large energy consumption due to

the use of gas heating and electric air conditioning. Our research project focused on integrating bioclimatic design and local geothermal energy to achieve energy efficiency and obtain the desired range of climatic comfort in the experimental bungalow (Fig. 2).

2 Resource Characterization

Hammam Righa thermal waters dominated with sulfate calcium, rise from springs at a temperature varying between 67 and 69 °C, a flow rate of 2.5 L/s, and mineralization rate of 2500 mg/L (Bouchareb et al. 2012). For the most part, these sources have disappeared because of the wells pumping. The capture is now done utilizing three wells. The first one was carried out in 1969; its main characteristics are given in Table 1.

The drilling characteristics are sufficient for a geothermal heating system (Ouali 2015). In order to limit the deposits and to control the corrosion processes, which can be caused by the relatively high mineralization of the pumped waters, we recommended:

- to maintain the operating pressure above 2.5 bar, to avoid any degassing, which favors the deposits and corrosion phenomena;
- to carry out a chemical treatment employing a regular and continuous corrosion inhibitor which can control the processes of corrosion.

3 Methodology

To make the system low cost and efficient, we choose the centralized system. Figure 3 shows the heating system; a plate heat exchanger is used to heat the stored water tank with geothermal energy. Built-in fan convectors perform the

S. Ouali (✉) · M. M. Hadjiat · K. Imessad · K. Salhi · A. Ait-Ouali
Centre de Développement des Energies Renouvelables (CDER),
B.P. 62 Route de l'Observatoire, 16340 Algiers, Algeria
e-mail: s.ouali@cderr.dz



Fig. 1 Hammam Righa spa and bungalows, Algeria



Fig. 2 Experimental bungalow, Hammam Righa spa, Algeria

Table 1 Characteristics of the well N°1

Well N°1	Results
Depth (m)	66
Flow (L/s)	3.7
Water temperature (°C)	68
Pressure (Bar)	1.9
pH	7
Electrical conductivity (mS/cm)	3.13
Dry residue (mg/L)	2121
Iron content (mg/L)	0.8

distribution of heat inside the bungalows; the ventilation ducts that existed in the original construction were exploited in our system. The water-cooling machine is adapted for cooling purpose.

Such a system is efficient only if the bungalows are built according to the bioclimatic standard. In order to minimize the heat loss inside the bungalow, the walls were internally insulated, using polystyrene boards and plasterboard type BA13 (Fig. 4a).

We also decided to replace the standard windows with double-glazed windows and introduce a ventilation system.

The studied building is reproduced as a virtual model using TRNSYS 17 software, which is a validated program for the simulation of buildings energy performance (Klein et al. 2009). A TMY2 (Typical Meteorological Year) hourly weather data file was generated by using the program Meteororm 7. Heating and cooling energy demand are calculated for a design indoor air temperature of, respectively, 21 °C and 24 °C, as recommended by the Algerian Building Energy Code. Thermal properties of the building elements before and after renovation are given in Table 2.

4 Results and Discussion

Figure 4 shows the method used to renovate the bungalow according to bioclimatic standard. In Fig. 4(a), the wall insulation was applied. In line with calculations based on the site's thermal balance, the bungalow energy requirement, and architectural data, an optimal 5 cm of polystyrene was obtained. In Fig. 4(b), the double glass was mounted instead of standard windows. The fan coil is shown in Fig. 5.

The simulation results show that the heating energy requirements decrease from 100 to 35 kWh/m² and the cooling energy demand decreases from 125 to 60 kWh/m² after renovation.

By applying wall insulation and double-glazing, we reduced energy consumption for heating and cooling by 59%, and as a result, we improved the thermal comfort inside the bungalows. Knowing that the average electricity consumption for a group of five bungalows is 54,000 kWh per year, the use of geothermal energy for heating rather than electricity allowed us to reduce the energy bill by 80%, and also CO₂ emissions by 22.5 tons of carbon per year. Applying this renovation plan to the remaining 16 bungalows group can reduce CO₂ emissions by 360 tons per year.

5 Conclusion

The combination of bioclimatic techniques in the construction and exploitation of local geothermal energy for air-conditioning are complementary and necessary for efficient and economical consumption of energy, which could reduce the environmental impact. Through this pilot experience, we have achieved remarkable results in terms of aesthetics, thermal comfort, and energy consumption.

Fig. 3 Heating system

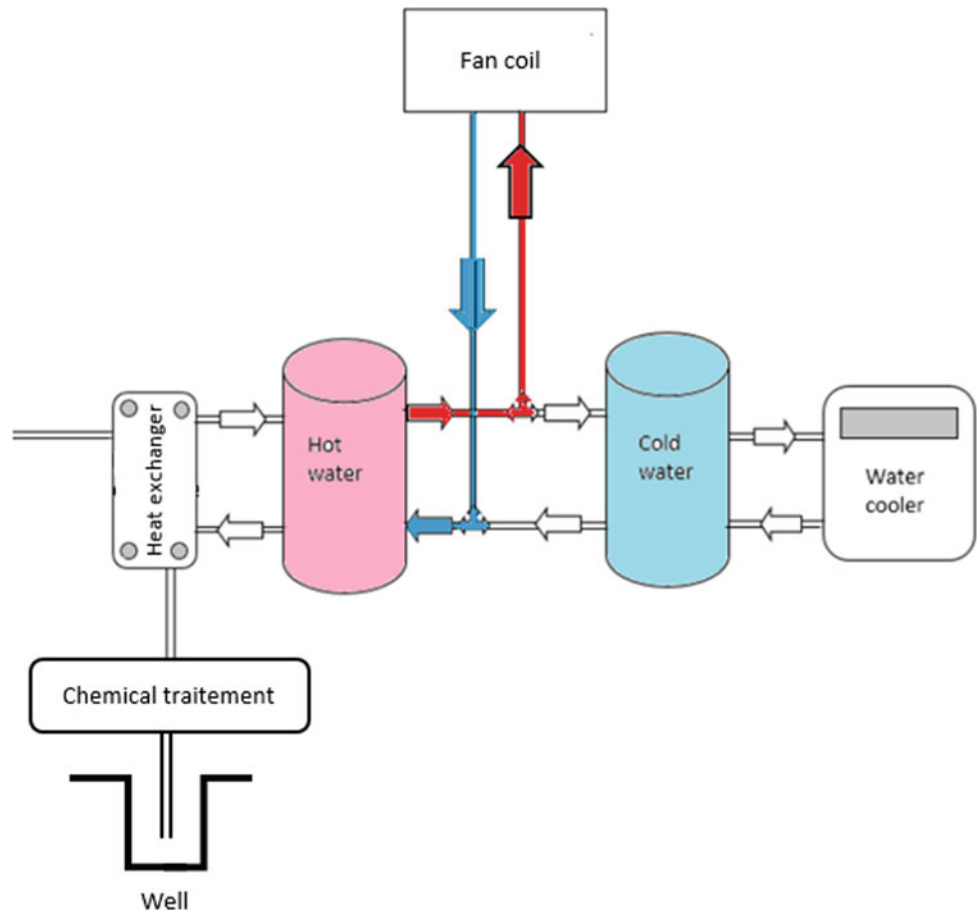


Fig. 4 Internal insulation of walls (a), Double-glazed window doors (b)



Table 2 Thermal properties of the building elements before and after renovation

	Before renovation		After renovation	
	Composition	U value W/m ² .K	Composition	U value W/m ² .K
External walls	Mortar (2 cm) Cinderblock (20 cm) Plaster (2 cm)	2.2	Mortar (2 cm) Insulation (5 cm) Cinderblock (20 cm) Plaster (2 cm)	0.58
Roof	Waterproofing Concrete (10 cm) Solid brick (5 cm)	2.7	Waterproofing Concrete (10 cm) Insulation 5 Solid brick (5 cm)	0.62
Windows	Simple glass	5	Double glass	1.4



Fig. 5 Fan convector built-in, bungalow of Hammam Righa spa, Algeria

Acknowledgements We would like to sincerely thank all of those who have helped bring this work to light. Warm thanks go to the Algerian Renewable Energy Development Center (CDER) and the Tourist Management Company, Spa—Hammam Righa, for all the facilities granted during the realization of this project. Our thanks go as well to Mrs Akila Khoudja for the efforts she provided during field

works. We would like to express our deepest gratitude to all reviewers and particularly for Mz Dhouha Mabrouk, for having reviewed our paper and contributed to improving its linguistic quality.

References

- Bouchareb, F.Z., Boudoukha, A., Haouchine, A.: Hydrogéochimie et géothermométrie : apports à l'identification du réservoir thermal des sources de Hammam Righa, Algérie. *Hydrol. Sci. J.* (2012)
- Guigue, S.: Les sources thermominérales de l'Algérie - Étude géochimique. *Bull. Serv. Carte Géol. Algér. 3ème Sér., Fasc. 9*, 112 (1947)
- Klein, S.A., Beckman, W.A., Mitchell, J., Duffie, J.A., Duffie, N.: TRNSYS 17: A transient system simulation program. University of Wisconsin, Madison USA, Solar Energy Laboratory (2009)
- Ouali, S.: Contribution à l'étude de quelques réservoirs géothermiques en Algérie. Doctoral thesis. USTHB University, Algiers- Algeria, (2015)
- Ministère du Tourisme et de l'Artisanat-Algérie. Etude intégrale de dix sources thermales d'importance nationale et international. Rapport n°2 - 174 1087 (2010)

**Hydrology, Hydrogeology, Hydrochemistry,
Water Resources (T10): Hydrology, Land Use
and Climatology—Rainfall and Evaporation**



Statistical Prediction of Sri Lankan Rainfall from October to December

Pabodini Karunapala

Abstract

Sri Lanka receives large amounts of rainfall from October to December (OND). In this study, multiple linear regression models for the prediction of OND Sri Lankan rainfall are proposed for lead times of 1 and 2 months. Correlation analysis and partial least square regression method were used to identify predictors that included the sea surface temperature anomaly tendencies over southern Atlantic, southern Pacific and western Pacific, and Maritime Continent at lead times of 1 and 2 months. Except for the extreme years, these models showed high forecasting capability with significant three-year-out cross-validated correlation coefficient skill of 0.69 and 0.68 for 1979–2012 at the 1- and 2-month lead times, respectively.

Keywords

OND Sri Lankan rainfall • Multiple regression models • Seasonal forecast

1 Introduction

Sri Lanka receives the highest amount of its annual rainfall from October to December (OND), and this season is associated with the main agricultural season known as “Maha” in Sri Lanka. Rainfall during this season significantly affects agricultural activities and hydropower productivity of Sri Lanka. During OND, the rainfall rate is approximately $150\text{--}300\text{ mm month}^{-1}$, while the other months receive $50\text{--}120\text{ mm month}^{-1}$. This considerably intense OND rainfall often causes severe flooding and landslides. Therefore, prediction of the seasonal rainfall during OND is important.

P. Karunapala (✉)
Department of Meteorology, Colombo, Sri Lanka

Most of the Asian seasonal rainfall forecast models are based on predictability of sea surface temperature (SST). For example, empirical prediction models for “Meiyu” (May–June) rainfall in Taiwan were developed by (Yim et al. 2015) using three predictors based on the 2-m air temperature and SST. Lee and Seo (2013) constructed an SST-based statistical prediction model to forecast Changma (mid-June to end of July) precipitation over South Korea for a lead time of one month. For South Asia, Sahai et al. (2003) used SST to build multiple regression models for the prediction of Indian summer monsoon rainfall. Motivated by these studies, the relationship between Sri Lankan OND rainfall and SST anomalies was examined and multiple regression models were constructed to predict the OND rainfall.

2 Data and Methodology

The monthly Global Precipitation Climatology Project (GPCP) Version 2.2 (Huffman et al. 1997) was used. The monthly SST dataset used was obtained from the Version 1.1 of Hadley Centre Global Ice and Sea Surface Temperature dataset (HadISST1) provided by the United Kingdom Meteorological Office (UKMO) (Rayner 2003).

Sri Lanka rainfall index (SLRI) is defined as the normalized time series of OND rainfall anomaly averaged over Sri Lanka region ($79^{\circ}\text{E}\text{--}82^{\circ}\text{E}$ and $5^{\circ}\text{N}\text{--}10^{\circ}\text{N}$) for the period of 1979–2012. The correlation coefficients between the SLRI and sea surface temperature anomaly (SSTA) tendency were calculated at 1- and 2-month lead times. The 1-month lead time is defined as the August minus June and then the 2-month lead time is defined as July minus May. Statistically significant areas at 95% confidence level were selected as the predictors. To avoid multi-collinearity, the partial least square regression (PLSR) method, e.g. Black et al. (2017), has been employed. The regression models were computed using training period (1979–1999) and used for independent predictions during the years 2000–2012.

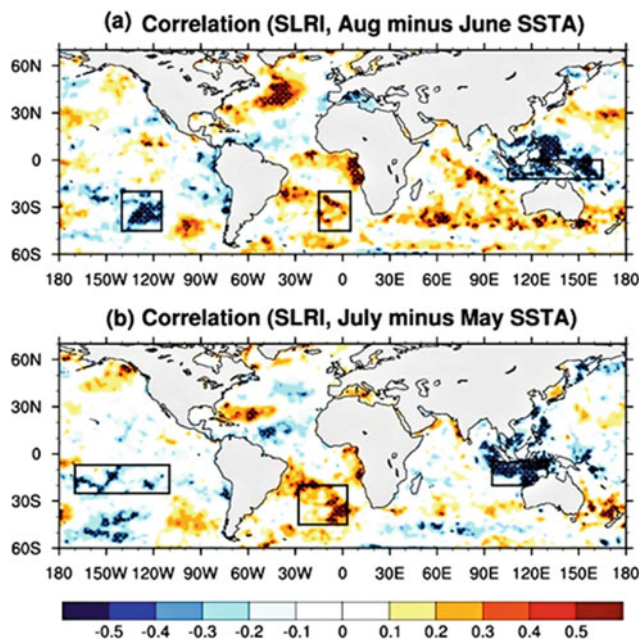


Fig. 1 Correlation coefficient maps between the SSTA and SLRI are shown at **a** 1- and **b** 2-month lead times, respectively. The boxes indicate the regions of the three predictors. Black crosses mark the areas that are statistically significant at the 95% confidence level

3 Results and Discussion

The correlation coefficients between the SLRI and SSTA tendencies were calculated to select the predictors for 1- and 2-month lead times. (Fig. 1 and Table 1). The correlation coefficients between SLRI and the predictors are shown in Table 2.

The predictor variable which has 95% significant correlation coefficient with the minimum root mean square error

(RMSE) is selected as the first predictor field (Sahai et al. 2003). Based on these conditions, southern Atlantic SSTA tendency (SA) is selected as the first predictor field. Area averaged SA is normalized and regressed against the SLRI to obtain the first partial regression coefficient. To obtain the second predictor field, the correlation coefficients between the SLRI and the residual SSTA field were calculated, where the residual SSTA field is defined by linearly removing the SA from the SSTA field. The southern Pacific SSTA tendency (SP) field is selected as the second predictor field. The same process is repeated to obtain the third predictor, western Pacific and Maritime Continent SSTA tendency (WP & MC). By repeating the same procedure, the predictors for the 2-month lead time are obtained (Fig. 1b). The following Eqs. (1) and (2) represent the multiple regression models for the 1- and 2-month lead times, respectively.

$$\text{SLRI} = 0.292(\text{SA}) - 0.357(\text{SP}) - 0.411(\text{WP \& MC}) \quad (1)$$

$$\text{SLRI} = 0.446(\text{SA}) - 0.302(\text{SP}) - 0.409(\text{WP \& MC}) \quad (2)$$

At the 1-month lead time, the correlation coefficient reaches 0.69 for the training period, and it is 0.65 for the validation period. At the 2-month lead time, the correlation coefficient is 0.68 for the training period and 0.71 for the validation period. To verify the prediction skill, the three years out cross-validation method (Yim et al. 2015) is used for all 34 years as shown by the blue lines in Fig. 2. The correlation coefficients between the SLRI and three-year-out cross-validated rainfall values were 0.69 and 0.68 at the 1- and 2-month lead times, respectively. The 60-year average rainfall in Sri Lanka during OND is 810.3 mm; however, during 1993, the country received 1249 mm but the models

Table 1 Definitions and the domains of the predictors selected for the prediction of Sri Lankan OND rainfall at 1-, and 2-month lead times, respectively

Predictor	Meaning	Aug minus June (1-month lead)	July minus May (2-month lead)
WP & MC	Western Pacific and maritime continent SST tendency	0–12S 105E–165E	05S–20S 95E–130E
SP	Southern Pacific SST tendency	20S–45S 115W–140W	07S–25S 110W–170W
SA	Southern Atlantic SST tendency	20S–45S 05E–15W	20S–45S 03E–28W

Table 2 Correlation coefficients between the SLRI and predictors at 1- and 2-month lead times, respectively

Predictor	Aug minus June (1-month lead)	July minus May (2-month lead)
WP & MC	−0.40*	−0.40*
SP	−0.47**	−0.40*
SA	0.32	0.37*

*Significant correlation at 95% confidence level

**Significant correlation at 99% confidence level

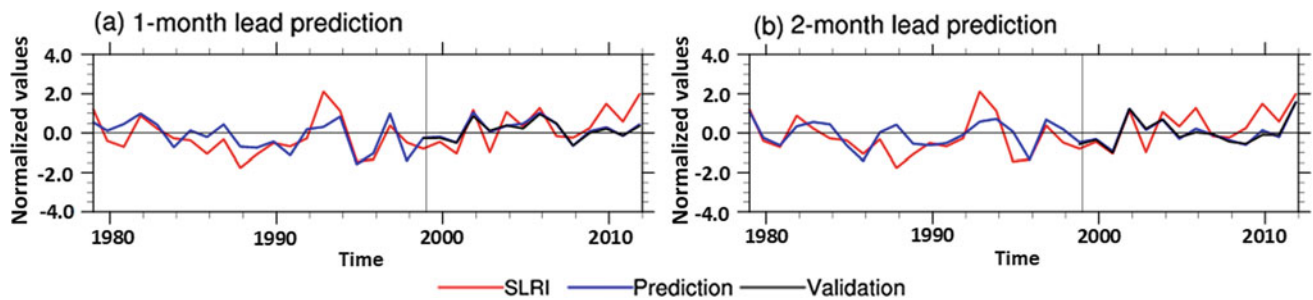


Fig. 2. Multiple regression models at **a** 1-month and **b** 2-month lead times. The observation, i.e. SLRI, is shown in red. The three-year-out cross-validated prediction is shown in blue. Independent prediction for the validation period (2000–2012) is shown in black

do not show that much rainfall. The reason for the high amount of rainfall is the formation of weather systems such as depressions and tropical cyclones in the Bay of Bengal.

4 Conclusion

Three independent predictors are selected through the partial least square regression method to build empirical models to predict the Sri Lankan OND rainfall. The first predictor is SA, the second predictor is SP and the third predictor is WP & MC. Using the three predictors, two multiple linear regression models were constructed to predict Sri Lankan OND rainfall at 1- and 2-month lead times. The three-year-out cross-validated prediction skill for 34 years (1979–2012) reaches 0.69 and 0.68 at the 1- and 2-month lead times, respectively.

Acknowledgements The author thanks Dr. Changhyun Yoo, Assistant Professor, Department of Climate and Energy Systems Engineering, Ewha Womans University, Seoul, South Korea, for providing his expert advice on this study.

References

- Black, J., Johnson, N.C., Baxter, S., Feldstein, S.B., Harnos, D.S., L'Heureux, M.L.: The predictors and forecast skill of northern hemisphere teleconnection patterns for lead times of 3–4 weeks. *Mon. Weather Rev.* **145**, 2855–2877 (2017)
- Lee, S.-E., Seo, K.-H.: The development of a statistical forecast model for changma. *Weather Forecast.* **28**, 1304–1321 (2013)
- Huffman, G.J., Adler, R.F., Arkin, P., Chang, A., Ferraro, R., Gruber, A., Janowiak, J., McNab, A., Rudolf, B., Schneider, U.: The global precipitation climatology project (GPCP) combined precipitation dataset. *Bull. Am. Meteorol. Soc.* **78**, 5–20 (1997)
- Sahai, A.K., Grimm, A.M., Satyan, V., Pant, G.B.: Long-lead prediction of Indian summer monsoon rainfall from global SST evolution. *Clim. Dyn.* **20**, 855–863 (2003)
- Rayner, N.A.: Global analyses of sea surface temperature, sea ice, and night marine air temperature since the late nineteenth century. *J. Geophys. Res.* **108**, 4407 (2003)
- Yim, S.Y., Wang, B., Xing, W., Lu, M.M.: Prediction of Meiyu rainfall in Taiwan by multi-lead physical–empirical models. *Clim. Dyn.* **44**, 3033–3042 (2015)



Spatiotemporal Rainfall Variations: Case Study of Wadi Koutine Watershed (South Tunisia)

Mongji Ben Zaied, Mohamed Ouessar, and Messaoud Guied

Abstract

An accurate representation of the spatiotemporal precipitation distribution is very important, mainly because of the erosion risk and flooding. To study the spatiotemporal rainfall variability in the Wadi Koutine watershed (southern Tunisia), rainfall collected data were analyzed over a period of fifty years (1969–2018). The trend analysis and evaluation have been based on the inter-annual variation coefficient. The rainfall index variation shows a deficit period that starts from the 1990s and follows a long period surplus between 1969 and 1990. The study of the rain distribution at the spatial scale is based on the existing rain gauges network, the collected data is interpolated by an adequate method in the objective to obtain the isohyets map. However, there are large numbers of spatial interpolation methods and the choice of one of them must be done based on many criteria. Four spatial interpolation methods were evaluated by a cross-validation method on the Koutine watershed. Between the four interpolation methods used, the method giving the optimal result is the radial networks of the basic function (RBF) method, which is the most appropriate for our case. Besides, the spatial coefficient of variation shows significant variability (mean CV > 30%) with a positive trend.

Keywords

Spatiotemporal variability • Geostatistical analyses • Rainfall trends • Watershed • Dry areas

1 Introduction

Knowledge of the spatiotemporal variability of precipitation is an important and strategic issue. Water scarcity is becoming more and more important. Indeed, with the almost

Present Address:

M. Ben Zaied (✉) · M. Ouessar · M. Guied
Institut des Régions Arides IRA de Médenine, Médenine, Tunisia

universal trend toward the reduction of annual rainfall, the study of the distribution of rainfall at the spatial and temporal scales is very significant, especially in arid zones subjected to a low annual rainfall. Understanding of the anticipated climate-change-driven multi-scale spatiotemporal shifts in precipitation and attendant river flows is crucial to the development of water resources management approaches (Nema et al. 2018). At the scale of Tunisia, the climate change scenarios show a decrease in precipitation between -5 and -10% by 2020 (GIZ and MARE 2012). The situation will be more pronounced by 2050, with a decrease ranging from -10 to -29%. In this context, the object of this paper is to study rainfall distribution at spatial and temporal scales.

2 Materials and Methods

In this framework, this work aims to analyze the spatiotemporal variability of precipitation. Therefore, appropriate interpolation and analysis methods for the elaboration of isohyet maps are used in order to help in the construction and validation of climate change scenarios. It constitutes a spatiotemporal analysis of data to identify major trends at the scale of an arid catchment.

2.1 Study Site

The study site (SS) is located in the Jeffara area, northeast of Medenine city which is part of the Tunisian southeastern region (Fig. 1). This SS, which covers an area of 279 km², drained by Wadi Koutine, flows from the mountain range of Béni Kheddache and arrives at the county of Medenine Nord. The highest point of the watershed with an altitude of 650 m is at Jbel Moggar (Ouessar et al. 2009).

2.2 Rainfall Data

Having an arid climate, the rainfall in the study site is characterized by low averages, high irregularity (both in time and in space) and torrential characteristics. The annual average during the observed years (1969–2018) is between 234 mm in the mountains and 173 mm in the downstream area.

The study area has been equipped with climatic and weather stations for several years. These data acquired in situ are being updated, depending on the availability of existing data at different time steps: daily, monthly or annual. An initial quality analysis of rainfall series focused on their duration and quantity in mm. Rainfall data were collected for about forty years (1968–2018) with a variable time interval from eight stations located in the study region. The analysis and evaluation of the rainfall data trend were done based on the spatial and inter-annual variation coefficients.

2.3 Interpolation Methods

In order to study the spatial variability of the annual rainfall, we have developed, based on interpolation methods, maps of the spatial distribution of rainfall at the scale of the watershed. In fact, spatial interpolation techniques are divided into two categories: deterministic methods and stochastic methods that take into account the concept of chance while relying on a random function (Baillargeon 2002). Rainfall stations in the study area have a poor spatial distribution, so geostatistical interpolation methods will not be applied. Indeed, these methods based on kriging techniques require a good geometric distribution of data. Four interpolation techniques based on deterministic methods (radial basis function: RBF, inverse distance weight: IDW, global and local polynomial interpolations: GPI and LPI) have been retained to cover all the theoretical foundations of spatial interpolation techniques.

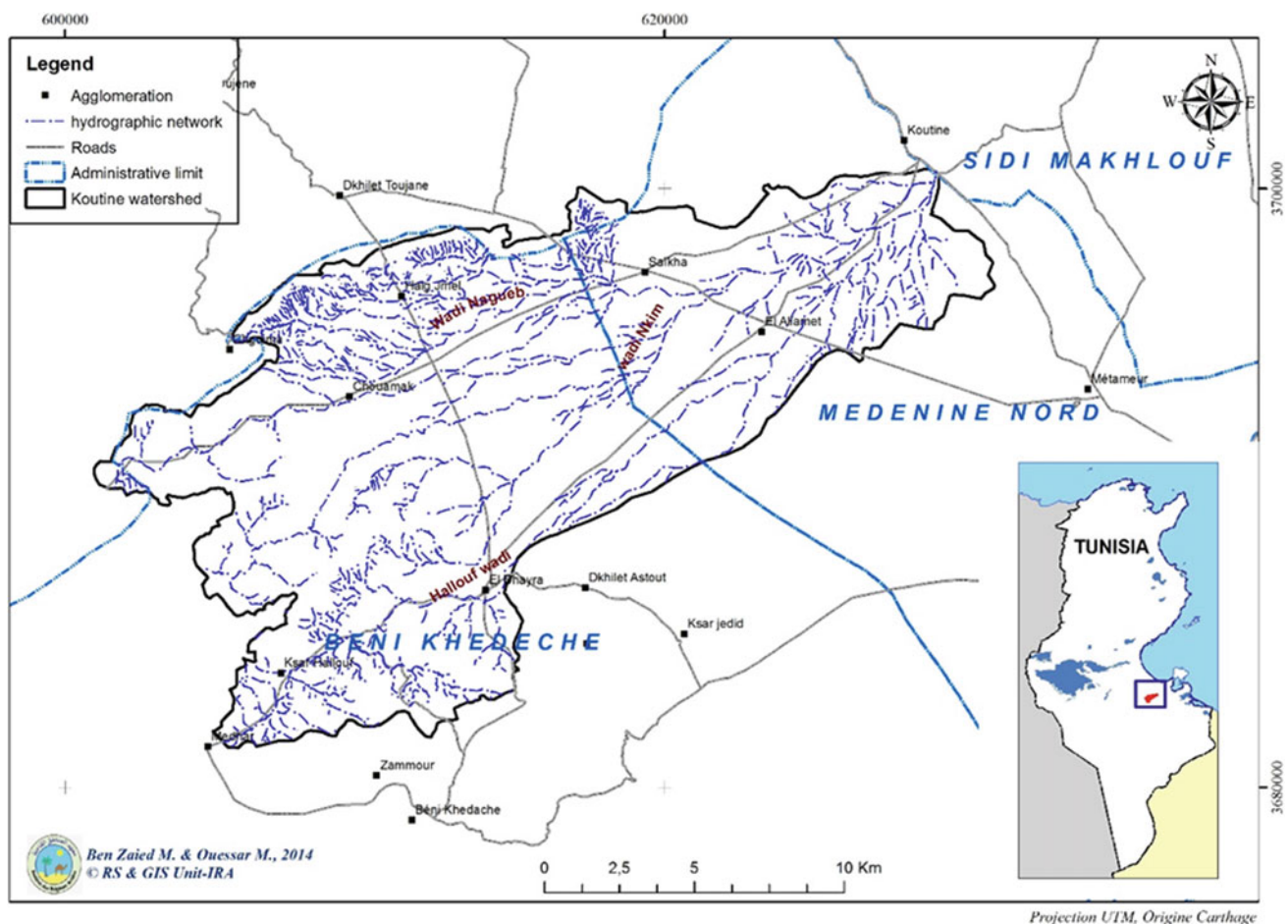


Fig. 1 Study site location map

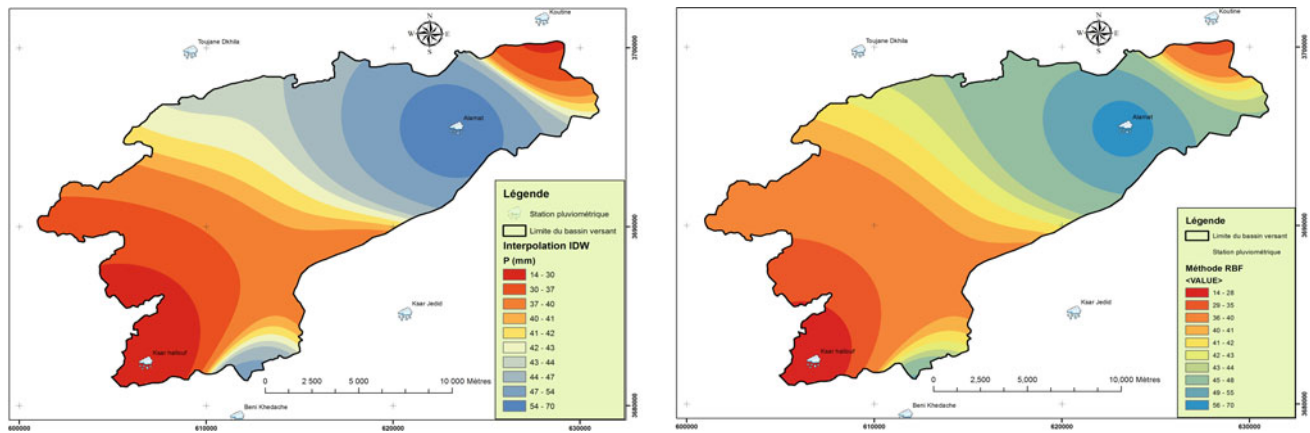


Fig. 2 Rainfall interpolations using IDW (left) and RBF (right) methods (year 2005)

3 Results

3.1 Rainfall Spatial Variation

Figure 2 shows an example of interpolation in the year 2005, using RBF (on the right) and IDW methods (on the left).

The statistics estimation error (Fig. 4) shows that the RBF method was more accurate and less biased because the mean of errors was closer to zero (0.9) and the standard deviation was lower with a decrease of about 11% compared to the LPI, 4% compared to the IDW and 1% compared to the GPI method.

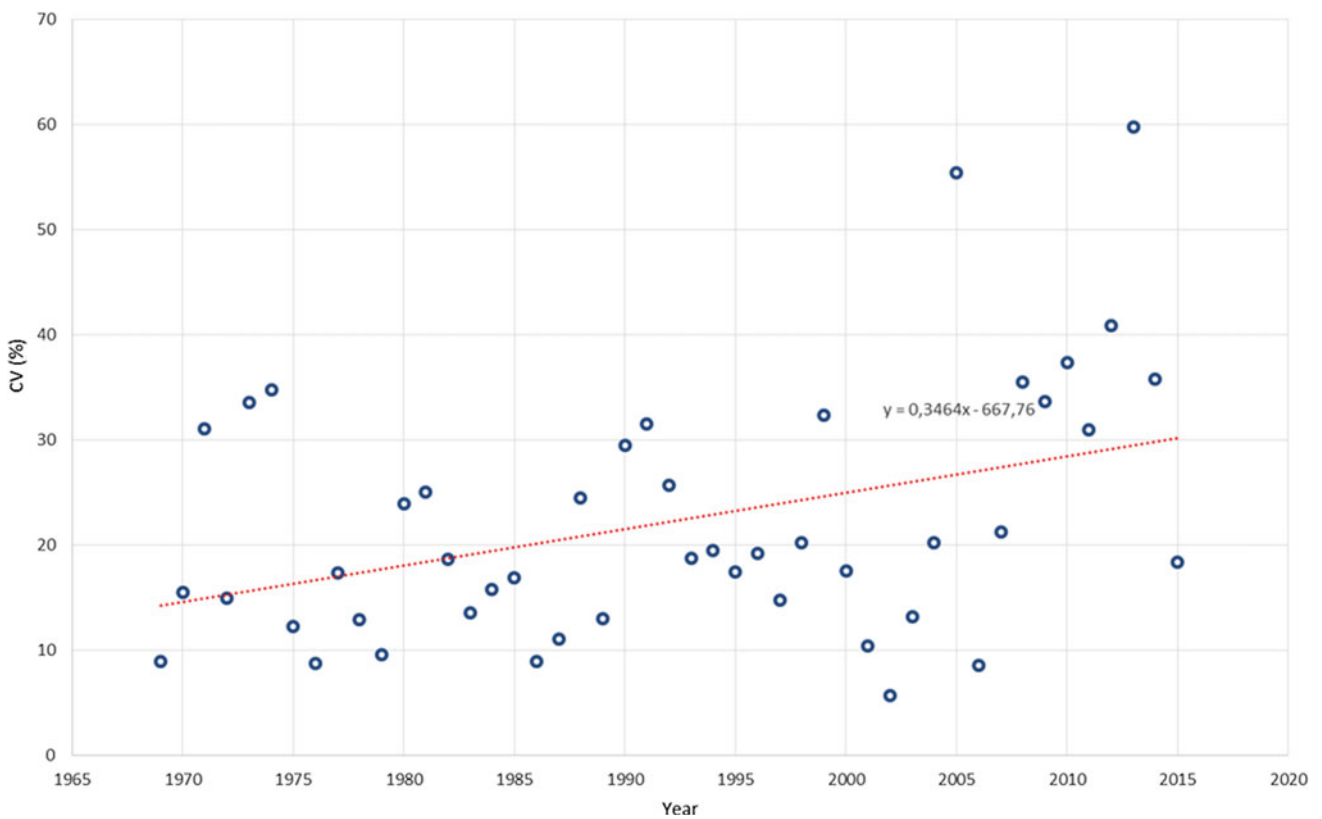


Fig. 3 Inter-annual variation of rainfall spatial coefficient in Wadi Koutine watershed

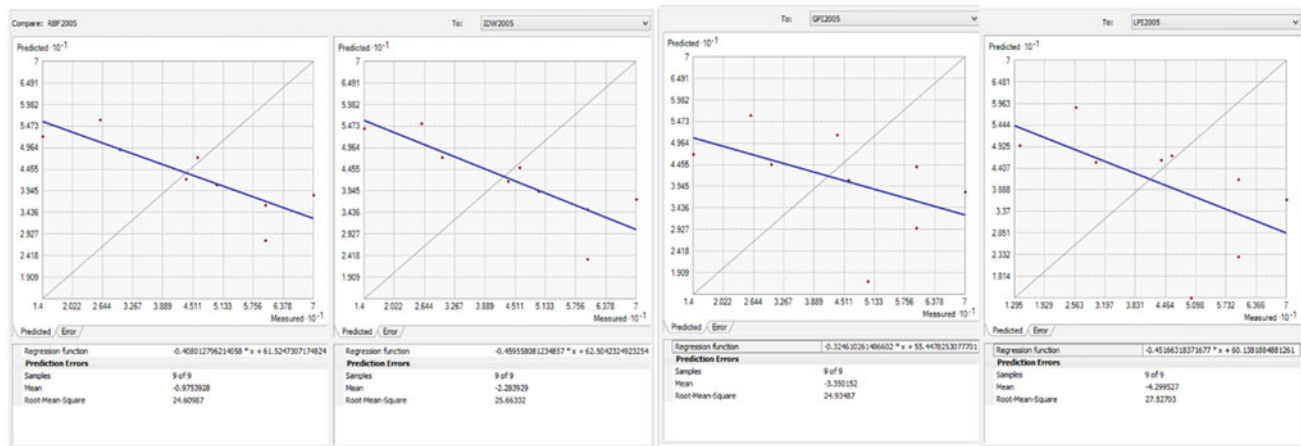


Fig. 4 Comparison between interpolation methods using cross-validation tools

3.2 Inter-annual and Spatial Variabilities of Rainfall

Under the current climate variability, the region was characterized by arid conditions and a very strong inter-annual variability in total rainfall, ranging from 24 to 587 mm. The study area experienced a relatively wet period that declined during the 1980s. However, the linear trend characterizes the 1969–2018 period. Therefore, the spatial coefficient of variation ($CV = (\text{Rainfall standard deviation})/(\text{mean rainfall})$) showed significant spatial variability (mean $CV > 30\%$) with a positive trend. The inter-annual variation was also important; the variation coefficient for mean annual values was 40% (Fig. 3).

4 Discussion

The comparative study of the correlation, which compares the measured values and the estimated values, allowed us to select between the four interpolation methods the most adapted to our case. The method giving the optimal result is RBF (Fig. 4).

The difference between the rainfall of a year P_i and the average annual precipitation P (drought index) makes it possible to estimate the annual rainfall deficit. The values of this index were negative in most cases (succession of dry years).

Interpolation of annual data from different stations shows that the spatial variation of precipitation is more significant

upstream than it is downstream. The rainfall variation coefficients are less than 60% during the studied period.

5 Conclusion

Under the current climate variability, the study site is characterized by arid conditions and a very strong inter-annual and spatial variability in total rainfall. The spatial coefficient of variation shows significant spatial variability (mean $CV > 30\%$) with a positive trend. The study of rainfall spatiotemporal variability is very important to the development of water resources management approaches at local and regional scales.

References

- Nema, M.K., Khare, D., Adamowski, J., Chandniha, S.K.: Spatio-temporal analysis of rainfall trends in Chhattisgarh State, Central India over the last 115 years. *J. Water Land Dev.* **36**, 117–128 (2018). <https://doi.org/10.2478/jwld-2018-0012>
- GIZ and MARE: Stratégie Nationale sur le Changement Climatique. Rapport de la stratégie, 165p (2012)
- Ouessar, M., Bruggeman, A., Abdelli, F., Mohtar, R.H., Gabriels, D., Cornelis, W.M.: Modelling water-harvesting systems in the arid south of Tunisia using SWAT. *Hydrol. Earth Syst. Sci.* **13**, (2009). <https://doi.org/10.5194/hess-13-2003-2009>
- Baillargeon, C.: Le Krigeage: revue de la théorie et application à l'interpolation spatiale de données de précipitations. M.Sc, Université Laval, Québec (2002)



Rainwater Quality in Some Urban and Rural Sites of Cameroon (Central Africa)

Aicha Foupouagnigni, Andrew Ako, Jude Mengnjo, Gloria Eneke, Josephine Ndjama, Bertil Nlend, George Nkeng, and Takeshi Ohba

Abstract

Seventy-two rainwater samples were investigated in some rural and urban sites across Cameroon for their chemical content. The objectives were to assess the potability of rainwater and the possible source of atmospheric inputs and to understand the biogeochemical cycles of the major ionic species. Rainwater in most of the sites was acidic (pH ranging from 4.92 to 6.41). A significant contribution of Ca^{2+} was observed in all sites, due mainly to the incorporation of soil dust in the precipitation. The K^+ and NO_3^- contributions to the ionic load of rainwater in rural sites are a reflection of the dominant agricultural activities across Cameroon. High Ca^{2+} , Mg^{2+} , SO_4^{2-} , and K^+ to Na^+ enrichment ratios relative to seawater ratios indicated the significant terrigenous influence on water chemistry, mainly from the Sahara dusts. About 62.5% of the samples were $\text{Ca}^{2+}\text{-Mg}^{2+}\text{-Cl}^-\text{-SO}_4^{2-}$ water type. Based on TDS, major ion, and trace metal contents, rainwater is considered suitable for human consumption.

Keywords

Atmospheric pollution • Rainwater chemistry • Rural • Urban • Cameroon • Water quality

1 Introduction

Rainfall signature integrates both the long-range transport of chemical species by clouds and the local scavenging of atmospheric aerosols during the rain event. These vary strongly both from event to event and within a single event because rainout and washout proportions strongly depend on the environment of the sampling site (urbanized, rural, or remote) (Bertrand et al. 2009). Understanding the main constituent of rainwater chemistry, what affects them, and their ecotoxicology is very important since rainwater plays a great role in earth water storage replenishment and ecosystems' life and equilibrium.

In spite of difficulties in collecting and preserving rain samples in tropic zones, precipitation chemistry in both rural and urban areas has been the subject of interesting research in the last few decades (Freydier et al. 2002; Sigha-Nkamdjou et al. 2003). However, in Cameroon, only few studies have been conducted on rainwater chemistry (Sigha-Nkamdjou et al. 2003; Galy-Lacaux et al. 2009; Wirmvem et al. 2014).

This study presents the chemical composition of rainwater determined at some urban and rural sites in Cameroon. This study is valuable in understanding the possible origin of atmospheric pollutants and the biogeochemical cycles of the major ionic species which are essential to determine deposition trends and improve modeling of atmospheric processes, as well as developing suitable emission control strategies.

2 Materials and Methods

Monthly rainfall samples were collected in Douala (January–November 2018), Yaoundé (January to September 2018), Dang (September to December 2018), and Ndop and Ndwara (June to October 2017). Douala and Yaoundé represent the urban sites, while Dang, Ndop, and Ndwara are located in the rural areas of Cameroon. Samples were collected

A. Foupouagnigni · A. Ako (✉) · J. Mengnjo · G. Eneke · J. Ndjama · B. Nlend
Hydrological Research Centre Yaoundé, P.O Box 4110 Yaoundé, Cameroon

G. Nkeng
National Advanced School of Public Works, P.O. Box 510
Yaoundé, Cameroon

T. Ohba
Department of Chemistry, School of Science, Tokai University,
4-1-1 Kitakaname, Hiratsuka, 259-2311, Kanagawa, Japan

monthly using artisanal bulk collectors. On the last day of the month, water from the container was properly shaken to mix and filter directly (through a 0.2 μm mesh) into a 100-mL bottle (previously rinsed with distilled water and dried in the laboratory to avoid contamination). The collected samples were stored in a refrigerator at 4 °C and analyzed for Na^+ , NH_4^+ , K^+ , Mg^{2+} , Ca^{2+} , Cl^- , NO_3^- , and SO_4^{2-} using standard methods. Alkalinity (HCO_3^-) was determined by titration. The trace metal content of rainwater samples from the urban sites was also analyzed.

3 Results

3.1 Rainwater Chemistry and Sources of Major Ionic Species

Figure 1 presents the Piper diagram for the mean rainwater chemistry in the rural and urban sites (Table 1).

4 Discussion

From the Piper diagram (Fig. 1), it is apparent that samples collected in the rural sites (Ndop, Ndawara, and Dang) are of the $\text{Ca}^{2+}\text{-Mg}^{2+}\text{-Cl}^-\text{-SO}_4^{2-}$ water type, demonstrating the dominance of alkaline earths over alkali and strong acidic anions over weak acidic anions. In the urban sites (Douala and Yaoundé), the rains are of the $\text{Ca}^{2+}\text{-Mg}^{2+}\text{-HCO}_3^-$ water

type. This is corroborated by the slightly acidic character of rainwater sampled (see Table 2) resulting from the dissolution of NO_3 and CO_2 forming nitric and carbonic acids, respectively, whose effects have been neutralized by ionic species coming from soil dust particles.

Summary statistics of trace metal concentrations in rainwater sampled at Douala and Yaoundé (urban sites) are presented in Table 1. The most abundant trace metal in rainwater is Zn (145.11 ppb) followed by Fe (84.95 ppb). The high values of metals in rainwater samples may be due to local point sources of atmospheric pollution, long-range atmospheric transport of anthropogenic activities (like mining) from other parts of the country, and the soil dust which affects the composition of wet atmospheric deposition. The monthly concentration of some of the trace metals in rainfall at urban sites of Douala and Yaoundé was within the WHO guideline values for drinking water.

In order to determine the marine contribution in the composition of rainwater, the ratio of sea salts in rainwater was calculated considering Na^+ as sea salt tracer and assuming that all Na^+ was of marine origin. As shown in Table 3, the SO_4^{2-} , K^+ , Ca^{2+} , and Mg^{2+} to Na^+ ratios of rainfall in both the urban and rural sites are higher than those in seawater basically suggesting a terrigenous origin of the ions. The dominance of Ca^{2+} , SO_4^{2-} , and K^+ relative to Na^+ and Cl^- confirms the inference that precipitation in Sub-Saharan Africa is highly influenced by terrigenous dust mostly from the Sahara Desert soils (Goni et al. 2001; Freyrier et al. 2002; Galy-Lacaux et al. 2009).

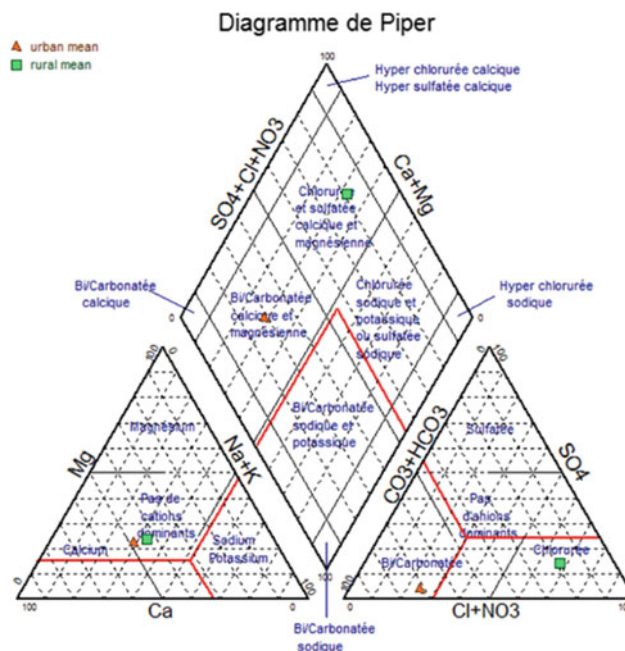


Fig. 1 Piper diagram of rainwater in urban and rural sites

Table 1 Summary statistics of trace metal concentration in rainfall at urban sites (ppb)

Element	Min	Max	Mean	Standard deviation
Mn	1.07	12.00	5.49	3
Fe	45.34	264.88	84.95	48
Be	0.01	0.02	0.01	0
Cr	0.11	13.07	1.81	3
Co	0.01	0.25	0.08	0
Ni	0.22	11.23	3.38	4
Cu	0.71	9.76	2.44	3
Zn	6.46	493.57	145.11	155
Ga	0.06	2.75	0.25	1
As	0.07	2.93	0.37	1
Rb	0.29	9.20	2.25	3
Sr	1.20	59.02	8.95	12
Ag	0.32	12.88	2.45	3
Cd	0.01	0.19	0.07	0
Cs	0.01	0.18	0.02	0
Hg	0.36	36.30	2.66	8
Tl	0.01	0.09	0.02	0
Pb	0.14	2.15	0.99	1
Th	0.10	47.71	2.96	11
U	0.04	0.77	0.09	0

Table 2 Mean pH values of rainwater sample collected

	Douala	Yaoundé	Ndop	Ndawara	Dang
pH	5.61	5.59	5.05	4.82	6.41

Table 3 Seawater, and urban and rural sites' rainwater ratio

	Cl ⁻ /Na ⁺	SO ₄ ²⁻ /Na ⁺	K ⁺ /Na ⁺	Ca ²⁺ /Na ⁺	Mg ²⁺ /Na ⁺
Seawater	1.16	0.12	0.02	0.04	0.23
Urban sites	4.29	1.42	0.46	1.84	0.51
Rural sites	1.13	2.24	3.03	3.25	1.07

5 Conclusions

The results obtained reveal that the major source of chemical enrichment in rains in both rural and urban sites across Cameroon is terrigenous dust mainly from the Sahara Desert soils, and anthropogenic and agricultural activities. Concentrations of trace metals that were determined in the rainwater samples of urban sites are relatively low. Major ions and trace element concentrations in rainwater of all the sites were within the WHO guideline values for drinking water. Based on the chemical characteristics of rainwater in the studied sites, domestic harvesting of rainwater could be taken as an alternative to pipe-borne water supply.

References

- Bertrand, G., Celle-Jeanton, H., Laj, P., Rangognio J., Chazot, G.: rainfall chemistry: long range transport versus below cloud scavenging. A two-year study at an inland station (Opme, France). *J. Atmos. Chem.* **60**(3), 253–271 (2009)
- Freydier, R., Dupré, B., Dandurand, J.L., Fortune, J.P., Sigha-Nkamdjou, L.: Trace elements and major species in precipitation at African stations: Concentrations and sources. *Bull. Soc. Geo. Fr.* **173**(2), 129–146 (2002)
- Galy-Lacaux, C., Laouali, D., Descroix, L., Gobron, N., Liousse, C.: Long term precipitation chemistry and wet deposition in a remote dry Savanna site in Africa (Niger). *Atmos. Chem. Phys.* **9**(5), 1579–1595 (2009)

- Goni, I.B., Fellman, E., Edmunds, W.M.: Rainfall geochemistry in the Sahel region of northern Nigeria. *Atmosp. Environ.* **35**(25), 4331–4339 (2001)
- Sigha-Nkamdjou, L., Galy-Lacaux, C., Pont, V., Richard, S., Sighomnou, D., Lacaux, J.P.: Rainwater chemistry and wet deposition over the Equatorial forested ecosystem of Zoétélé (Cameroon). *J. Atmos. Chem.* **46**(2), 173–198 (2003). <https://doi.org/10.1023/A:1026057413640>
- Wirnvmem, M.J., Ohba, T., Fantong, W.Y., Ayonghe, S.N., Hogarh, J.N., Suila, J.Y., Asaah, A.N.E., Ooki, S., Tanyileke, G., Hell, J.V.: Origin of major ions in monthly rainfall events at the Bamenda Highlands, NorthWest Cameroon. *J. Environ. Sci.* **26**, 801–809 (2014)



Probabilistic Analysis Using Physically Based and Hydrogeological Models for Rainfall-Induced Shallow Landslide Susceptibility (Northern of Morocco)

Hassane Rahali and Houda Loukili

Abstract

The most destructive landslides are triggered by extreme rainfall events. In this paper, a probabilistic method for assessing shallow landslide susceptibility is proposed based on critical rainfall threshold (CRT) and the integration of a hydrogeological model (the topographic wetness index (TWI)) with a physically based model using the infinite slope stability (ISS) method. Both inputs are combined within a stochastic framework to get a spatially and temporally variable definition of landslide hazards. While CRT is used to accomplish temporal forecasting, the integration of TWI and ISS using a stochastic modification of their inputs using Monte Carlo (MC) simulation provides an uncertainty-based and, thereby, more reliable assessment of the probability of landslide occurrence. The probabilistic approach demonstrates a fair predictive performance with an AUC (area under the ROC curve) of 73.2%. These results emphasize the importance of integrating the CRT within the stochastic dynamic framework for a more accurate and reliable assessment of the landslide hazard.

Keywords

Landslide susceptibility • Critical rainfall • Stochastic

1 Introduction

The Rif mountains in northern Morocco are highly vulnerable to landslides which cause damage to infrastructure and human losses. The majority of these slope instabilities are a result of rainfall. In 2009, the Al Hoceima area was hit by a

H. Rahali (✉) · H. Loukili
University Mohammed V in Rabat, Institut Scientifique, GEOPAC
Research Center, Geophysics and Natural Hazards Laboratory,
Rabat, Morocco
e-mail: hassane.rahali@um5.ac.ma

very heavy rainstorm, which resulted in several landslides and considerable casualties.

Susceptibility to landslide assessment is performed mostly using statistical models (Cervi et al. 2010) and physically based models (Montgomery and Dietrich 1994). Physically based models analyze the mechanical condition of slopes using mathematical equations and give slope stability variation in response to varying hydrological conditions by coupling a physically based model with a hydrological model. Furthermore, they can most accurately predict the terrain stability under various climatic and hydrological scenarios.

In this study, we used a probabilistic analysis method to assess shallow landslide susceptibility based on critical rainfall analysis and the combination of the ISS model (Duncan and Wright 2005) with a hydrogeological model (TWI), where both geotechnical and hydrological parameters were considered as random variables using normal distributions in a stochastic framework. Model's predictive performance evaluation was performed using the landslide inventory and the area under the ROC curve.

2 Materials and Methods

The Al Hoceima area (Fig. 1) is highly vulnerable to landslides, especially shallow translational slides. It is characterized by various lithological types, but the marl and shale series predominate and are the most vulnerable zones to landslides in this region (Rahali 2017). The climatic regime in this area is characterized by dry summers and cold winters. The rainfall, often torrential, is the main triggering factor. Most landslides occurred with rainfall rates above or equal to 60 mm (Lacroix 1968).

The proposed approach (Fig. 2) requires knowledge of several input parameters such as topographical, lithological, geotechnical, and hydrogeological data, and the results strongly depend on the quality and detail of the input data.

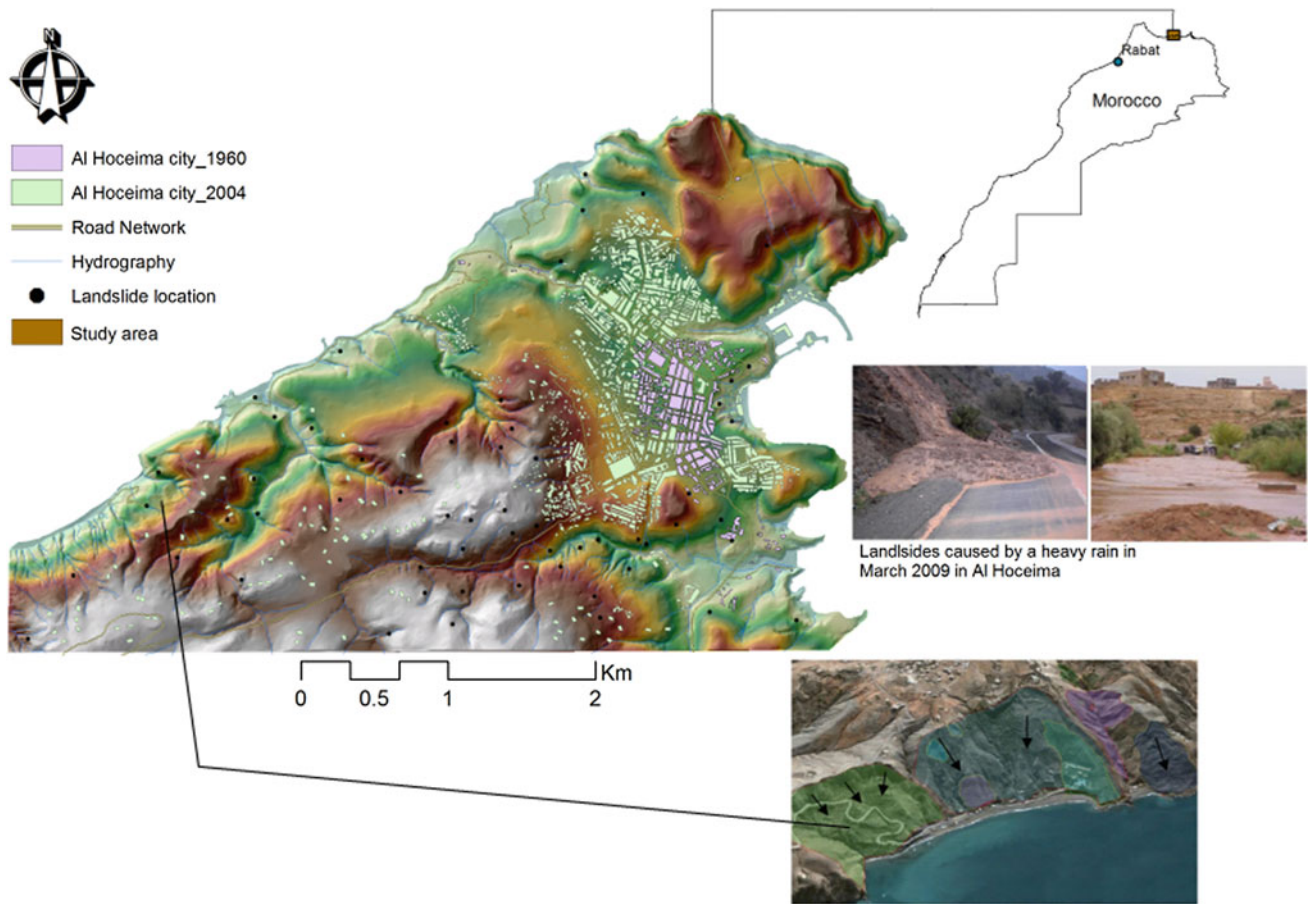


Fig. 1 Localization of the study area

Shallow landslides in Al Hoceima region are initiated by loss of shear strength, resulting from the increase in pore water pressure, caused by rainfall events (Lacroix 1968). The fundamental assumption is that critical water content is required to initiate failure. This critical water content is the threshold which, when reached or exceeded, is likely to trigger landslides.

We used a minimum steady-state rainfall needed to trigger shallow landslides under existing topographic conditions, referred to by Montgomery et al. (1998) (Montgomery et al. 1998) as the critical rainfall (CR) which is calculated as follows:

$$CR = \frac{T \sin \beta}{a} + \left[\frac{c}{\gamma_w z \cos^2 \beta \tan \phi} + \frac{\gamma}{\gamma_w} \left(1 - \frac{\tan \beta}{\tan \phi} \right) \right] \quad (1)$$

where

- CR critical rainfall (mm/h)
- T soil transmissivity (m^2/h)
- β slope surface inclination (degrees)
- a specific catchment area (m)
- c effective cohesion (Pa)

- γ_w unit weight of water (10 N/m^3)
- z soil depth from the ground surface (m)
- ϕ effective angle of shearing resistance (degrees)
- γ unit weight of soil (N/m^3)

The ISS model assumes a planar slip surface on an infinitely extended planar slope and is generally used with shallow landslides having a small depth in comparison with the length and width of landslides and slopes.

Based on the linear Mohr–Coulomb failure criterion, the factor of safety used here, as soil Stability Index (SI) is defined (Park et al. 2013) as:

$$SI = \frac{c + (\gamma - m\gamma_w)z \cos^2 \beta \tan \phi}{\gamma z \sin \beta \cos \beta} \quad (2)$$

with z_w representing the saturated soil thickness above the slip surface, $m = z_w/z$ (dimensionless) is the ratio of the groundwater level to the soil depth; which is the proportion of the saturated soil column at instability conditions. To model the hydrologic control on m , Montgomery and Dietrich (1994) adopted a steady-state shallow subsurface flow

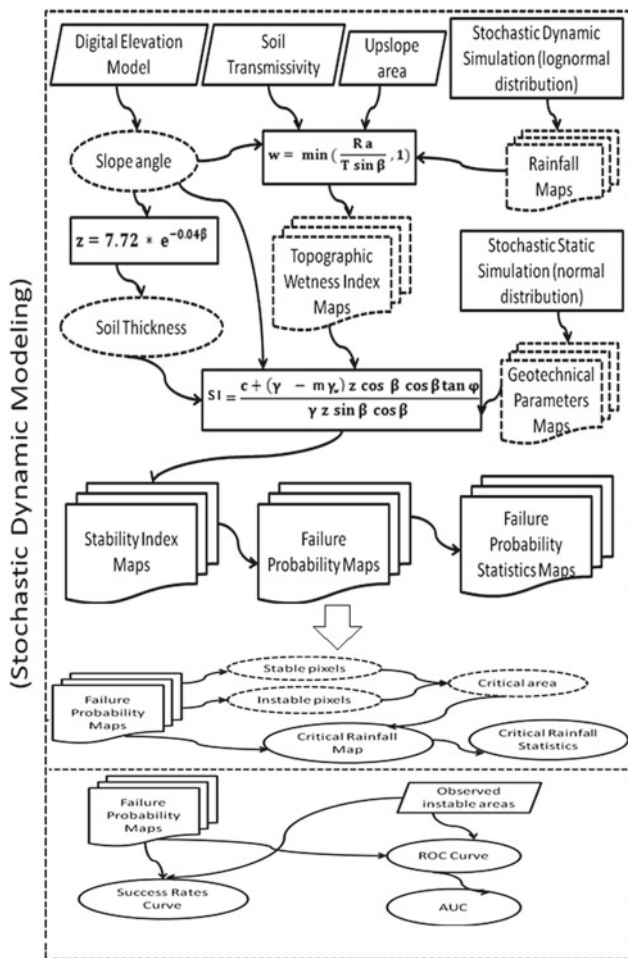


Fig. 2 Methodological flowchart for the stochastic dynamic modeling

based on TOPMODEL (Beven et al. 1995). The steady-state representation of subsurface flow, namely TWI (w), is derived from the local subsurface lateral flow and coupled with ISS to evaluate the pore water pressure as a function of rainfall intensity (R) and soil transmissivity (T) across the upslope specific contributing area (a):

$$w = \frac{z_w}{z} = \min\left(\frac{Ra}{T \sin \beta}, 1\right) \quad (3)$$

The R/T ratio combines both climate and hydrogeological factors. The transmissivity T represents the water flow within the soil. The parameter R , the steady-state recharge rate, is influenced by many factors such as rainfall intensity. The recharge assumed to be a function of the rainfall intensity is derived from the critical rainfall analysis and the soil saturates when $w = 1$.

3 Results and Discussion

3.1 Critical Rainfall Threshold

Using a steady-state rainfall rate of 10 mm/h, the CR is variable on a scale of values (Fig. 3a), where lower values indicate a greater propensity for instability while higher values indicate stability. This scale also encompasses areas identified as unconditionally stable (stable even with a maximum of rainfall rates i.e. areas of a relatively gentle slope ($\tan \theta \geq \tan \theta$) and unconditionally unstable (instability will occur even under dry conditions $\tan \theta \leq \tan \theta$). Inspection of the structure of Eq. (1) reveals that CR increases with a decrease in the local slope and decreases with an increase of the specific catchment area. Areas, thus, with the same value of CR have equal topographic control on shallow landslide initiation.

Inspection of Fig. 3 reveals that topographic elements in the steep areas close to the river are characterized as unconditionally unstable, judging from the fact that the convergent hollow areas i.e., zero-order valley are susceptible to shallow landsliding, and that the shallow subsurface flow or the saturated through flow seems to be the dominant factor for the occurrence of shallow landsliding in those zones of topographic convergence as reported by Iida (1999). CR increases downslope and higher values are found close to the topographic divide, corresponding mostly to gentle slope areas. Based on the results of the critical rainfall map, 40% of the study area requires rainfall between 0 and 60 mm/h to cause instability from which 50% with a critical rainfall between (0–40 mm/h) and 30% between (0–20 mm/h). The value of 7 mm/h of rainfall was considered as the threshold that starts a global initiation of failure in our study area.

3.2 Probabilistic Slope Stability Analysis

To build a probabilistic analysis, we incorporated our model in a stochastic framework. First, the pore water pressure is computed within the hydrogeological model (Eq. 3) using a variable amount of rainfall intensity and a stochastic soil transmissivity map. After that, the factor of safety map was calculated using stochastic parameters (cohesion, friction angles, and unit weight of soil) and the other parameters (z , slope, etc.) as deterministic within the ISS model (Eq. 2). This process was repeated 500 times (500 MC samples) to generate the failure probability (FP) maps (Fig. 3b) defined as the probability that the factor of safety is less than one.

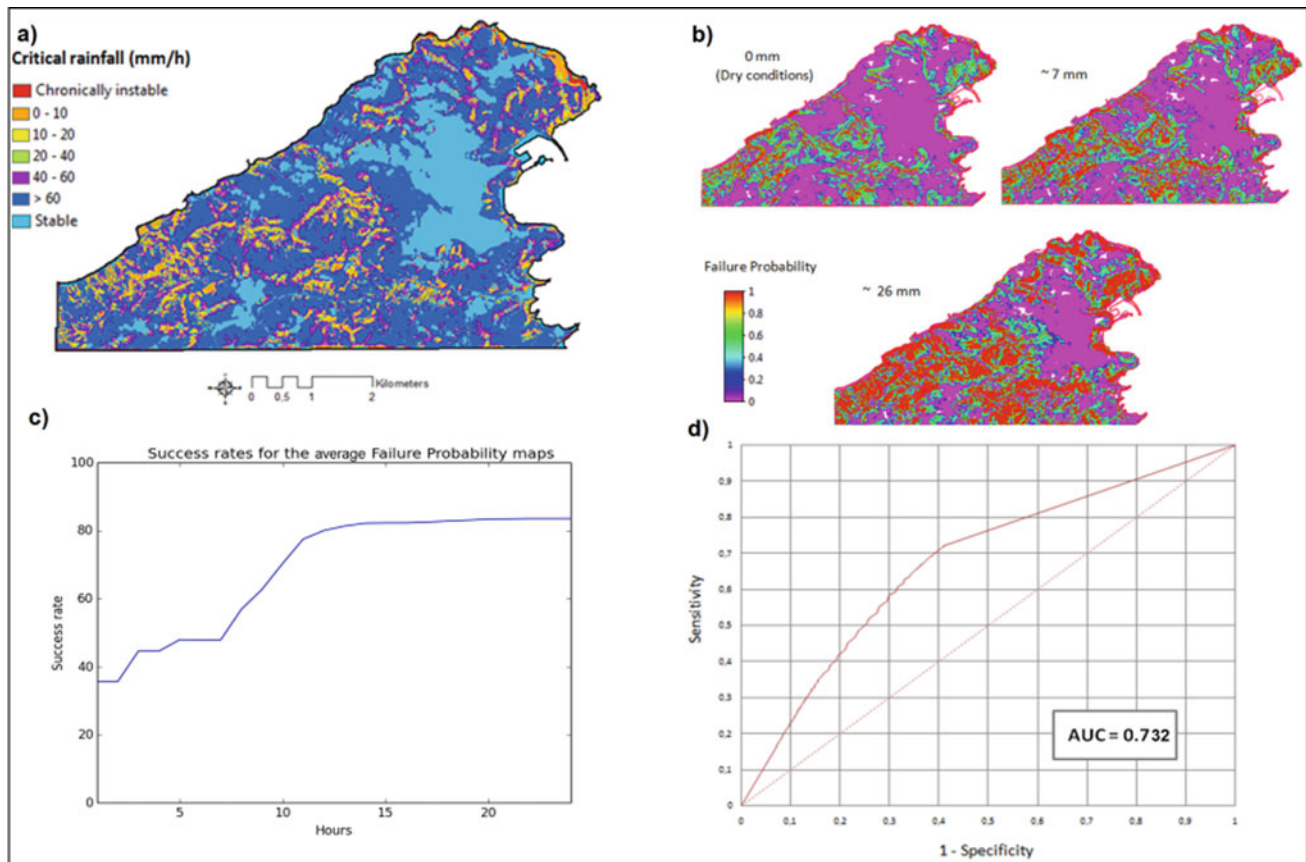


Fig. 3 a Critical rainfall map, b mean FP maps for different amounts of rainfall, c success rates of the average FP maps, d ROC curve and AUC metric

We used the observed unstable areas and the FP maps to get the success rate variation of the FP model (Fig. 3c). The success rate for our model improved over time from dry 34.48% to 85.1% under moist conditions (26 mm rainfall). For the threshold-independent ROC analysis (Fig. 3d), the stochastic model under dynamic moisture conditions achieved fairly good performance with an AUC of 73.2%. In general, the high concentration of the high FP values occurred on areas with steep slopes and low shear strengths and, especially, in zones with shales, marl-dolomite, and flysch. The integration of different rainfall amount scenarios emphasizes clearly the influence of the pore water pressure in landslide slope stability.

4 Conclusions

Predicting landslide susceptible locations is a complex task that will always need more and more studies. This research presents a probabilistic analysis based on the combination of the ISS model and the topographic wetness index using the results of the critical rainfall analysis. A case study is

presented in order to show the full capability of the probabilistic modeling.

For this case study, we did geotechnical measurements and also collected some test data values regarding the range of the strengths of various geologic units that are present in the area. Shear strength values were, therefore, summarized and spatialized based on values from different surveys in the area and the relative strength description of the underlying simplified geology from the literature. These values were then adjusted, if necessary, to preserve the static stability of slopes under dry conditions. In addition, some adjustments were made in cohesion and friction angle values to reflect the current spatial density of landslides and, thereby, improve the fit of the model.

Though the geology of this region is extremely complex, the formations that characterize it, range from the Palaeozoic to lower secondary, but are generally limited in lithofacies to limestones and shales. Shales underlying limestone are highly folded, faulted, and fractured losing their 'indurated' hardness and becoming friable. This highlights, in general, the systematic involvement of a schistose weathered material in the slope failure. Limestones contain gypsum inclusions

which are specific material for gullying, ravine, and slope movement.

The practical advantages in using both modeling methods for investigating rainfall as a potential trigger, arise from the size of the study area (14 km²) and the intended output map scale of 1:10 000. The challenge would be its transferability toward a regional scale (1:25,000 and 1:50,000). However, extending the size of the study area will bring along some limitations regarding the availability of data sources that offer full spatial coverage and a reasonable map scale and introduce a number of parametric uncertainties into the modeling.

From the above, we can conclude that it would be more difficult to transfer physically based or even the stochastic model's results, obtained with spatialized parameters at the scale 1: 10,000 but acquired at an even larger measurement scale to a larger geographic scale. We do acknowledge, however, that up-scaling is more beneficial in terms of decision-making as many environmental managers and policymakers, require the environmental assessments at a regional scale.

The main interest of this work was to evaluate the performance of the stochastic modeling based on the critical rainfall threshold. We demonstrated that the inclusion of the probabilistic framework in the deterministic modeling can improve the accuracy of the model, and we pointed out the importance of the inclusion of a critical rainfall analysis.

References

- Beven, K.J., Lamb, R., Quinn, P.F., Romanowicz, R., Freer, J.: Topmodel. In: Singh, V.P., (ed.), *Computer Models of Watershed Hydrology*. Water Resources Publications, pp. 627–668 (1995)
- Cervi, F., Berti, M., Borgatti, L., Ronchetti, F., Manenti, F., Corsini, A.: Comparing predictive capability of statistical and deterministic methods for landslide susceptibility mapping: a case study in the northern Apennines (Reggio Emilia Province, Italy). *Landslides* **7**, 433–444 (2010)
- Duncan, J.M., Wright, S.G.: *Soil Strength and Slope Stability*. John Wiley and Sons, New York (2005)
- Iida, T.: A stochastic hydro-geomorphological model for shallow landsliding due to rainstorm. *CATENA*, **34**, 293–313 (1999)
- Lacroix, A.M.: Les glissements de terrain, présentation d'une carte prévisionnelle des mouvements de terrain dans le Rif. Service des mines et géologie [Landslides, presentation of a preliminary map of slope movements in the Rif]. *Maroc Rapport* **27**, 45–54 (1968)
- Montgomery, D.R., Sullivan, K., Greenberg, M.H.: Regional test of a model for shallow landsliding. *Hydrol. Process.* **12**, 943–955 (1998)
- Montgomery, D.R., Dietrich, W.E.: A physically based model for the topographic control of shallow landsliding. *Water Resour. Res.* **30** (4), 1153–1171 (1994)
- Park, H.J., Lee, J.H., Woo, I.: Assessment of rainfall-induced shallow landslide susceptibility using a GIS-based probabilistic approach. *Eng Geol.* **161**, 1–15 (2013)
- Rahali, H.: Improving the reliability of landslide susceptibility mapping through spatial uncertainty analysis: a case study of Al Hoceima, Northern Morocco. *Geocarto Int.* **34**(1), 43–77 (2019). <https://doi.org/10.1080/10106049.2017.1357767>



Assessment of Climate Variability and Its Impact on the Environment and Water Resources in the Mount Cameroon Area

Andrew Ako Ako, Monjoa Monono Zita, and Enoh Jeanot Fongoh

Abstract

Climate variability has been a global issue in recent time due to its environmental and socio-economic impact. This study evaluates climate variability and its impact on the environment and water resources in the Mount Cameroon area. Temperature and rainfall data were obtained from three Cameroon Development Corporation (CDC) Weather Stations (Idenau, Tole and Debundscha). Field data were also collected through interviews using open participatory approach with the residents of the study area to give their views on, and perceptions about, the impact of climate change and variability in the region. Analyses of rainfall and temperature records from 1985 to 2016 were carried out to understand the patterns and trends over Mount Cameroon area and also assess future projections in climate. Rainfall and temperature trends show that, by 2030, rainfall averages in the study area will fluctuate by 40% per annum with an average temperature of 27 °C. This variability could lead to an increase in the frequency of floods and droughts, thereby affecting water availability and increasing environmental degradation.

Keywords

Climate variability • Environment • Water resources • Mt. Cameroon

1 Introduction

Climatic change is an emerging issue in the recent decades, particularly with its adverse impacts on life on earth. Climate is variable over space and time, triggered by natural as well as anthropogenic forcing factors (IPCC 2001). According to Graedel and Crutzen (1993), climate is defined as “average statistics of meteorological conditions over a period of time ranging from months to thousands or millions of years”. Change and variability of these climatic conditions induce an increase in extreme hydrological events, such as flood and drought, with both environmental and socio-economic consequences (Ayoade 1998; Ayonghe 1930). The evaluation of climate variability is, therefore, significant to guide policy-makers and stakeholders to appropriate adaptation strategies for sustainable growth and development (Negm et al. 2020a, b).

Cameroon, located in central Africa, has also been affected and is vulnerable to climate change and variability in recent years. Molua and Lambi (2006) outlined six major floods from 1983 to 2008 that occurred in Yaoundé, the capital city of Cameroon. These events caused significant material damage and losses in human life with many persons left homeless. In Cameroon, it is generally observed that the annual rainfall has decreased with an increasing variability in the amounts of rainfall (Mathias 2014). During the period 1968–2006, the surface water resources in the northern part of Cameroon were reduced by about 30%, while the reduction was about 14% in the southern parts of Cameroon. It is estimated that, between 2035 and 2100, the annual average temperature will rise from 0.7 to 4.6 °C in the northern part of Cameroon and from 0.5 to 3.5 °C in the bimodal forest zone (Mathias 2014).

Being the pride of south-western Cameroon, the Mount Cameroon area with a humid climate has been characterised by changes in the spatial and temporal distribution of temperature and precipitation due to climate change, which in turn will increase both the intensity and frequency of extreme events like droughts and floods. The Mount

A. A. Ako (✉) · E. J. Fongoh
Hydrological Research Centre, P.O. Box 4110 Yaoundé,
Cameroon

M. M. Zita
National Advanced School of Public Works Yaoundé,
P.O. 510 Yaoundé, Cameroon

Cameroon area is commonly noted for its rich volcanic soil fertility and substantial water availability that has resulted in intense settlement and agricultural exploitation of the lower flanks for livelihood (Ako et al. 2012).

Within this context, this study seeks to analyse rainfall and temperature variability in the Mount Cameroon area from 1985 to 2016 using data collected from three weather stations. The local observed trends are discussed and compared with global trends in temperature and rainfall.

2 Materials and Methods

2.1 The Study Area and Climatic Setting

Mount Cameroon is an isolated ancient volcano in proximity of the Atlantic coast in Equatorial Africa. It is located at 4°8'13"N, 9°8'10"E. The mountain rises steeply in as little as 18 m from sea level to 4095 m at the summit.

The Mount Cameroon area falls within the tropical climate with a decrease in mean annual temperatures from 26 to 29 °C, at sea level, and to 0 °C at the top. This large temperature gradient is associated with a decrease in rainfall. The rainy season lasts from April to October and is characterised by heavy downpour. The maximum rainfall occurs from July to August. The dry season extends from November to March.

2.2 Data Collection and Sampling

The climatic data from three meteorological stations covering different areas of Mount Cameroon were collected from

the CDC meteorological service. Data were analysed through the area-weighted average from which regression lines were generated for rainfall, air temperature and number of rainfall days.

Shot direct interviews with the aid of self-administered questionnaires were held with 250 local residents (large commercial and small-scale farmers included) to assess out their perceptions about the impact of climate change on water resources for livestock and crop production and their environment at large.

3 Results

3.1 Rainfall Pattern and Trend

The average monthly rainfall calculated from 1985 to 2016 is presented in Fig. 1. The rainfall pattern indicated that rainfall is highly variable in the municipality, and the variability has been intensified in the last three decades.

Using regression lines, the rainfall trend was envisaged and it shows that in the next 12 years (by 2030) rainfall averages in the study area will fluctuate between 610 and 852 mm per annum, with high incidences of floods and droughts.

3.2 Temperature Patterns and Trends

Figure 2 shows the patterns and trends of average annual temperature in Tole, Debundscha and Idenau from 1985 to 2016. Similar to rainfall, temperature has been highly variable over the years of the study period, but with an upward trend in recent years.

Fig. 1 Rainfall patterns and trends in **a** Tole, **b** Debundscha and **c** Idenau

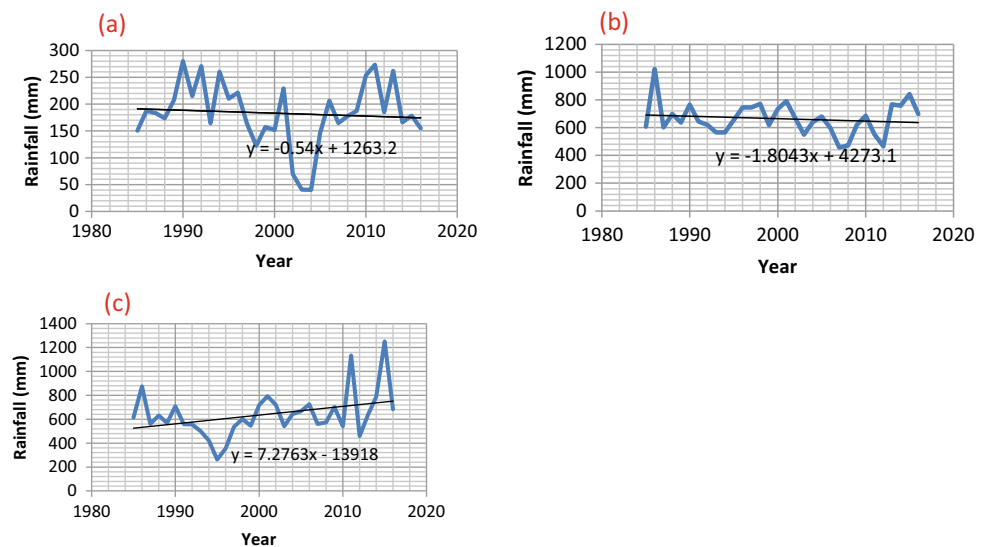
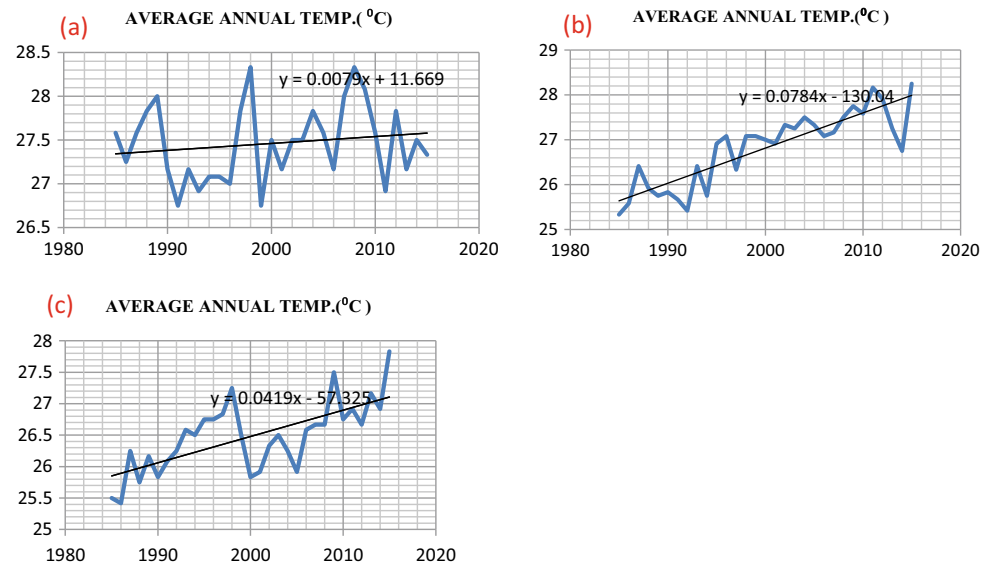


Fig. 2 Temperature patterns and trends for **a** Tole, **b** Debundscha and **c** Idenau



4 Discussion

The rainfall pattern is highly variable with a generally decreasing trend in rainfall in the area. Rainfall data analysis has shown that rainfall patterns and trends in the Mount Cameroon area are not changing but have become highly variable in recent years. The frequency of floods and drought has increased in recent years affecting water availability and, to a lesser extent, water quality. Results from interviews showed that, there are heavy rainfall events within a short period, leading to drastic floods.

The increasing temperatures could also result in increasing evapotranspiration that triggers high intensity rains causing floods, as well as a decrease in water availability. Ayonghe (1930) showed a net rate of temperature increase of 0.95 °C between 1930 and 1995 over Cameroon. Individual global and regional climate models (GCMs and RCMs) for the West Africa region indicate that in future, there will be mostly drier conditions over the western Sahel and wetter conditions in the northern regions of the Gulf of Guinea. The RCMs predict consistent drying in conjunction with more warming over the western regions of the interest area but show no significant rainfall changes in the southern regions (Diallo et al. 2012). Human activities are estimated to have caused approximately 1.0 °C of global warming above pre-industrial levels, with a likely range of 0.8–1.2 °C. Global warming is likely to reach 1.5 °C between 2030 and 2052 if it continues to increase at the current rate (IPCC 2018).

5 Conclusion

Rainfall and temperature data analyses show that rainfall and temperature patterns in the Mount Cameroon area are not changing but have become highly variable in recent years which has had effect on the environment and water resources.

References

- Ayoade, J.O.: Introduction to climatology for the tropics. Spectrum, Ibadan (1998)
- Ayonghe, SN.: A quantitative evaluation of global warming and precipitation in Cameroon from 1930 to 1995 and projections to 2060. pp. 142–155, Unique Printers, Bamenda (2001)
- Ako, A.A., Jun, S., Takahiro, H., Makoto, K., Akoachere, R.A., Nkeng, G.E., Takem, G.E: Spring water quality and usability in the Mount Cameroon area revealed by hydrogeochemistry. Environ. Geochem. Health (34) 615–639 (2012)
- Diallo, I., Sylla, M.B., Giorgi, F., Gaye, A.T., Camara, M.: Multimodel GCM-RCM ensemble-based projections of temperature and precipitation over west africa for the early 21st Century. Int. J. Geophysics. 19 pages (2012)
- Graedel T.E., Crutzen Paul, J.: Atmospheric change: earth system perspective (1993)
- IPCC (Intergovernmental Panel on Climate Change): Mitigation. Cambridge University Press, Cambridge, U.K., and New York, U. S.A. (2001)
- IPCC: Global warming of 1.5°C: summary for policymakers. IPCC, Switzerland. www.ipcc.ch (2018)
- Mathias, F.F.: An assessment of impacts of climate change on available Water resources and security in Cameroon. University of Dschang, Cameroon (2014)

-
- Molua, E.L., Lambi, C.M.: Climate, Water resources in cameroon. <https://www.researchgate.net/publication/266448446> (2006)
- Negm, A., Bouderbala, A., Chenchouni, H., Barcelo, D.: Water resources in Algeria - Part I: assessment of surface and groundwater. Cham, Springer (2020a)
- Negm, A., Bouderbala, A., Chenchouni, H., Barcelo, D.: Water resources in Algeria - Part II: water quality, treatment, protection and development. Cham, Springer (2020b)



Mapping and Assessment of Evapotranspiration Over an Oasis in Arid Ecosystem Using Remote Sensing and Biophysical Modeling

Khalid Turk, Faisal Zeineldin, and Abdullah S. Aljughaiman

Abstract

This study was conducted in Al-Ahsa Oasis located in the eastern region of Saudi Arabia, aiming to estimate the annual actual evapotranspiration (ETA) for different land use systems based on Landsat-8 satellite data during 2017/2018. Initially, six land use and land cover (LULC) types were identified, namely: date palm, cropland, bare land, urban land, aquatic vegetation, and open water bodies. The surface energy balance algorithm for land (SEBAL) supported by climate data was used to compute the ETA. The SEBAL model outputs were validated using the FAO Penman–Monteith method coupled with field observation and measurements. The annual ETA was varied between 800 and 1400 mm.year⁻¹ for date palm, while it was 2000 mm.year⁻¹ for open water. An average of 800 mm.year⁻¹ was observed in croplands. The study concludes that the ETA produced from the satellite data and the SEBAL model is useful for water resource management at the Oasis scale.

Keywords

Actual evapotranspiration (ETA) • Landsat-8 data • SEBAL model • FAO Penman–Monteith • Al-Ahsa Oasis

1 Introduction

Evapotranspiration (ET) is an essential process for defining the mass and energy relationship between soil, crop, and atmosphere (Allen et al. 2007). The measurement of ET is necessary for water management in arid ecosystems, and it has significant impacts on irrigation water requirement (Bastiaanssen et al. 2000; Anderson et al. 2012; Haj-Amor et al. 2018). Remote sensing and biophysical modeling were used in recent studies to estimate ET in different regions of Saudi Arabia (Madugundu et al. 2017; Elhag and Bahrawi 2017; Mahmoud and Alazba 2016). Al-Ahsa Oasis is one of the major agricultural areas in Saudi Arabia. The hyper-arid climate with an annual rainfall of less than 100 mm.year⁻¹ makes groundwater the main source of irrigation in the Oasis. Precise information of the actual evapotranspiration (ETA) is crucial for policymakers and water planners to develop and formulate strategies for agricultural water resources management in Al-Ahsa Oasis. The objective of the study is to assess the potential of Landsat-8 data for estimating the annual ETA under different ecosystems in Al-Ahsa Oasis, Saudi Arabia.

2 Methodology

Landsat-8 satellite data were collected over the study area during Apr. 2017–Mar. 2018 to cover the summer and winter seasons. Also, a global digital elevation model (DEM) was used for topographic and atmospheric corrections (Malbêteau et al. 2017). Climate data were collected from two meteorological stations located in Al-Ahsa Oasis. These data include air temperature, relative humidity, wind speed, and net radiation. Field measurement and observations were collected from three different sampling sites located within the Oasis. LULC were classified using the supervised classification method.

K. Turk (✉) · F. Zeineldin · A. S. Aljughaiman
Water Studies Center, King Faisal University, P. O. Box 400,
Al-Ahsa, 31982, Saudi Arabia

K. Turk
Faculty of Agricultural and Environmental Sciences,
University of Gadarif, P. O. Box 449 Gadarif, Sudan

A. S. Aljughaiman
College of Agricultural and Food Sciences, King Faisal
University, P. O. Box 420, Al-Ahsa, 31982, Saudi Arabia

The surface energy balance algorithm for land (SEBAL) developed by Bastiaanssen et al. (Bastiaanssen et al. 2005) was used to calculate the ETa from satellite images. The SEBAL key input data consist of satellite measurement of surface albedo, leaf area index (LAI), normalized difference vegetation index (NDVI), and surface temperature. The produced ETa by Landsat-8 and SEBAL model was validated using the FAO Penman–Monteith method (Allen et al. 1998).

3 Results and Discussion

3.1 LULC Mapping

The results of LULC are represented in Fig. 1. They show the major LULC classes identified by the acquired 2017/2018 Landsat-8 images, namely date palm, cropland, bare land, urban land, aquatic vegetation, and water. The area occupied by each LULC type within the Oasis boundaries is described in Table 1. The date palm covers about 40% of Al-Ahsa Oasis area since it is the most important land use class for the local and national

economy. Croplands used only 19% of the Oasis area; they are dominated by rice and vegetables. The bare land class occupies around 39% of the Oasis area. The overall classification accuracy was 89%, with a Kappa index of 87%, while the user's and producer's accuracies differed with LULC types (Table 1).

3.2 The Annual Actual Evapotranspiration

The annual ETa produced by SEBAL model for the different LULC types in Al-Ahsa Oasis is shown in Fig. 2. The ETa rates of date palm trees ranged from 800 to 1400 mm.year⁻¹ during the period Apr. 2017 to Mar. 2018. The annual water consumption for date palm is highly variable, and this might be attributed to the type of irrigation system and the age variations of date palm trees along the Oasis.

The open water evaporation lost was around 2000 mm.year⁻¹, while an average of 1,600 mm.year⁻¹ was evaporated from aquatic vegetation. Nevertheless, croplands showed the lower annual ETa of 800 mm.year⁻¹ compared to the date palm. The annual ETa of urban lands is affected

Fig. 1 LULC map of the study area

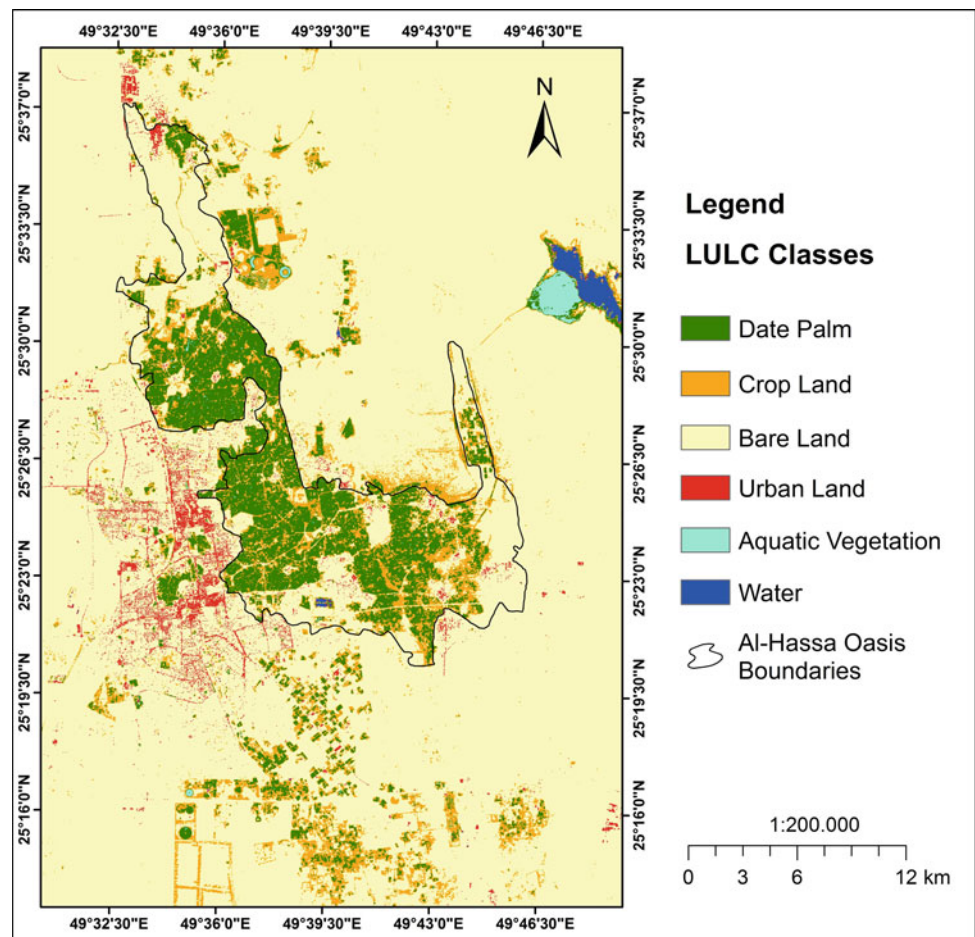
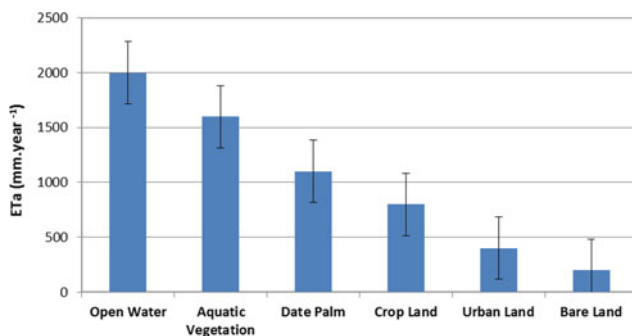


Table 1 Areas and accuracy assessment of LULC within Al-Ahsa Oasis boundary

LULC	Area		Classification accuracy (%)	
	hectare	%	User's	Producer's
Date palm	8820	40.1	95	94
Cropland	4199	19.1	83	81
Bare land	8636	39.2	95	93
Urban land	278	1.3	82	86
Aquatic vegetation	37	0.2	75	92
Water	30	0.1	100	100
Overall			89	
Kappa statistic			87	

**Fig. 2** Annual ETa values produced by SEBAL for the different LULC types in Al-Ahsa Oasis during Apr. 2017 to Mar. 2018. Bars denoted standard error

by the irrigation of trees, lanes, and parks. It is also likely that some more rooted vegetation withdraws groundwater (Mihi et al. 2019).

4 Conclusions

The current water resources situation in Al-Ahsa Oasis is critical because the groundwater used for irrigation is non-renewable. This study demonstrates the power of spatially distributed remote sensing data and the biophysical modeling to quantify the critical processes of the soil-crop-atmosphere continuum. The spatial data produced by Landsat-8 data and SEBAL model will allow a thorough analysis of the irrigation practices for the different growing seasons in Al-Ahsa Oasis and also in regions of similar conditions. However, validation measures for soil moisture are required.

References

- Allen, R.G., Tasumi, M., Trezza, R.: Satellite-based energy balance for mapping evapotranspiration with internalized calibration (METRIC) —Model. *American Society of Civil Engineers. J. Irrig. Drain. Eng.* **133**, 380–394 (2007)
- Anderson, M.C., Allen, R.G., Morse, A., Kustas, W.P.: Use of Landsat thermal imagery in monitoring evapotranspiration and managing water resources. *Remote Sens. Environ.* **122**, 50–65 (2012)
- Allen, R., Pereira, L. A., Raes, D., Smith, M.: *Crop Evapotranspiration*. FAO Irrigation and Drainage Paper 56, Rome (1998). ISBN: 92-5-104219-5
- Bastiaanssen, W.G.M., Noordman, E.J.M., Pelgrum, H., Davids, G., Allen, R.G.: SEBAL for spatially distributed ET under actual management and growing conditions. *J. Irrig. Drain. Eng.* **131**(1), 85–93 (2005)
- Bastiaanssen, W.G.M., Molden, D.J., Makin, I.W.: Remote sensing for irrigated agriculture: examples from research and possible applications. *Agr. Water Manag.* **46**, 137–155 (2000)
- Elhag, M., Bahrawi, J.A.: Realization of daily evapotranspiration in arid ecosystems based on remote sensing techniques. *Geosci. Instrum. Method. Data Syst.* (2017)
- Haj-Amor, Z., Ritzema, H., Hashemi, H., Bouri, S.: Surface irrigation performance of date palms under water scarcity in arid irrigated lands. *Arab. J. Geosci.* **11**, 27 (2018)
- Madugundu, R., Al-Gaadi, K.A., Tola, E., Hassaballa, A.A., Patil, V. C.: Performance of the METRIC model in estimating evapotranspiration fluxes over an irrigated field in Saudi Arabia using Landsat-8 images. *Hydrol. Earth Syst. Sci.* **21**, 6135–6151 (2017)
- Mahmoud, S.H., Alazba, A.A.: A coupled remote sensing and the surface energy balance based algorithms to estimate actual evapotranspiration over the western and southern regions of Saudi Arabia. *J. Asian Earth Sci.* **124**, 269–283 (2016)
- Malbêteau, Y., Merlin, O., Gascoin, S., Gastellu, J.P., Mattar, C.: Correcting land surface temperature data for elevation and illumination effects in mountainous areas: a case study using ASTER data over a steep-sided valley in Morocco. *Remote Sens Environ.* **189**, 25–39 (2017)
- Mihi, A., Tarai, N., & Chenchouni, H.: Can palm date plantations and oasisification be used as a proxy to fight sustainably against desertification and sand encroachment in hot drylands?. *Ecol. Indic.* **105**, 365–375 (2019)



Interception Loss from the Sprinkler-Irrigated Coffee Plantation

Pandu Narayana and K. Varija

Abstract

Evaporation losses for two sets of experiments were carried out during a hot summer day. To measure the evaporation losses, pairs of funnel-type rain gauges were used in the interspace between plants and below the canopy to measure rainfall and through-fall, respectively, at an equal distance from the jet. Water depths under two types of sprinkler irrigation jets with varying discharge rates were measured. The experiment has been done close to the same operating conditions. The results showed that evaporation losses were 29.6 and 21.1 per cent, respectively, for the two sets of experiments. The losses are comparable to the air temperature and vapour pressure deficit. Water loss due to drift has not been considered in the present study due to negligible wind speed on the day of the experiment and windbreaks from the shading trees. During strong winds, the actual losses will be higher than the measured experimental values.

Keywords

Evaporation loss • Through-fall • Sprinkler irrigation • Agrarian forest

1 Introduction

Evaporation losses during crop irrigation are the major water losses in agrarian forests due to their high vegetative growth. When the water is sprayed by the sprinkler jets, certain part of the water is evaporated directly into the atmosphere in the course of trajectory, and another part is intercepted by the vegetation (Yazar 1984). Evaporation of the water from the broad leaves, and thicker canopies are generally high due to

the bigger surface area of the vegetation (Maidment et al. 1993). In agrarian watersheds, irrigation of the crops by withdrawing water from nearby groundwater sources from unconfined or confined aquifers may be considered as a local water recycling with evaporation loss to the atmosphere as the loss to the water budget (Fellah et al. 2018). However, water loss due to drift forms the major part of the evaporation loss (Molle et al. 2012). It is neglected in the study due to negligible wind speed on the day of the experiment and windbreaks from the forest trees. The water other than evaporation and drift falls back to the catchment and remains in the catchment. Only the water evaporating and transpiration from the plants are the forms of water loss from the watershed.

Coffee plantation in southern India is one such example. The majority of the irrigation requirements are met with tube wells, open wells and farm ponds. The plants are cultivated under the shade of forest trees which form two different canopies. Irrigation is required before the monsoon season for the blossoming of the flowers to get a better yield. Coffee plantations form thick canopies which intercept large amounts of water during irrigation and rainfall. The intercepted water evaporates into the atmosphere to meet the atmospheric demand. Measuring the magnitudes of interception in the irrigational practices is of prime importance to make irrigation-based decisions.

The present experiment shows the representative intercepted evaporation losses in the sprinkler irrigation practices and helps in understanding the water budget in the small watersheds.

2 Study Area and Experimental Setup

The experimental setup described in this paper was conducted in the Central Coffee Research Institute, Balehonuru, in the state of Karnataka of southern India. The study area is located at 13°22'N, 75°28'E at an elevation of 900 m

P. Narayana (✉) · K. Varija
Department of Applied Mechanics and Hydraulics, National Institute of Technology, Surathkal, Karnataka, India

from mean sea level. The area of the watershed is 120 hectares. The average annual rainfall of the region is 2589 mm. Most of the rainfall occurs during the monsoon season from June to September and reduces during post-monsoon, from October to November. Few spells of convective rainfall occur other than the monsoon season. Winter occurs from December to February followed by summer or pre-monsoon, from March to May. The mean maximum and minimum temperatures were 27.5 °C and 16.5 °C. The catchment consists of sandy clay loam soil with infiltration rates close to 10 cm/hr. Coffee, black pepper (*Piper nigrum*) and Arecanut (*Areca catechu*) are the major crops in the region.

The experiment was conducted on 21st of March, 2019. To measure evaporation losses, three pairs of funnel-type rain gauges were used in the free space and below the bushes at different radii of the sprinkler jets to measure water depths at different radii. In this study, the difference between the water depths measured in the free space and below the vegetation of strictly the same radial distance is taken as evaporation loss. It is assumed that an equal amount of water is delivered at all the points of equal radius even though the depths vary along different radii of the reach of the sprinkler jet. The rain gauges were placed at 3 m (10ft), 7.6 m (25ft), 10.6 m (35ft) and 15.2 m (50ft) distance from the jet. The maximum coverage area of the jet is 18.2 m (60ft). The study area and field setup are shown in Figs. 1 and 2, respectively. Mean radial distance is used to calculate the average area of cover for a particular rain gauge at a distance. Meteorological conditions and calculations are shown

in Tables 1 and 2, respectively. A telemetric rain gauge was used to verify the even distribution of water with constant intensity, and it was used only in the free space. Water depths were measured under two conditions. One with the rain gauges under a single jet from 12:00 to 16:00 h and the other with the two jets overlapping from 16:00 to 20:00 h. Two types of sprinkler jets, namely a jumbo jet with a higher discharge rate, and a rain gun with a comparatively low discharge rate, were used for the study. Both jets were covering a maximum radius of 18.2 m (60ft). The evaporation losses are compared with vapour pressure deficit and air temperature.

The evaporation loss from the canopy is calculated from the relationship;

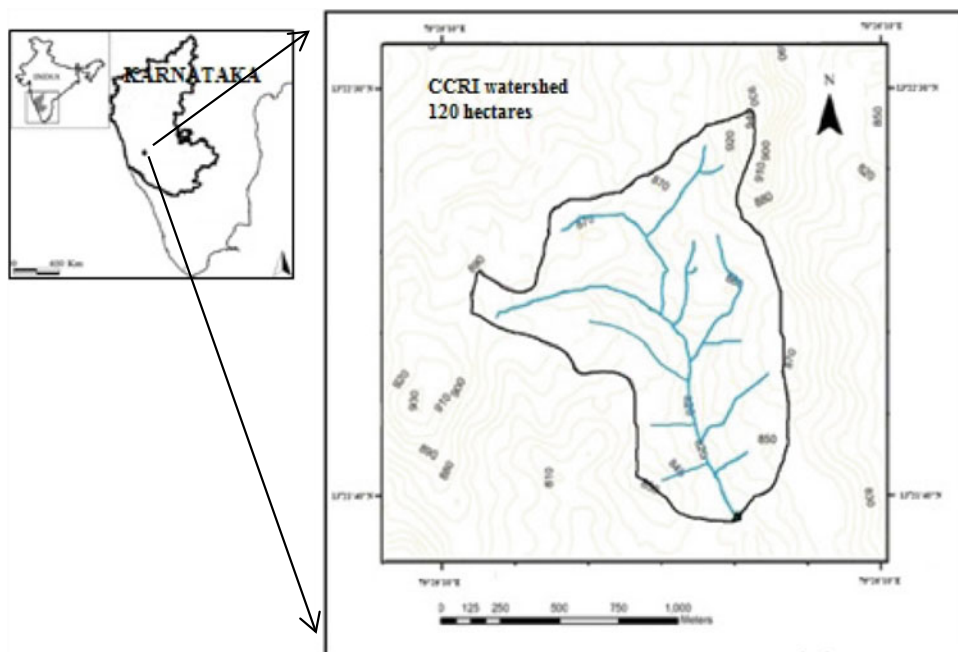
$$E(\%) = 100 * (RF - TF) / RF$$

where E is the evaporation loss (%); and RF is the applied water; and TF is the water passing through the vegetation

3 Results and Discussion

For the two tests conducted, the observations are given in Table 2. The average evaporation loss from three pairs of rain gauges was 29.6 and 21.1 per cent, respectively. The evaporation losses ranged from 4 to 49%. The first test, conducted in the mid-noon between 12:00 and 16:00 h, had an average temperature of 34.8 °C and the second test during the evening hours between 16:00 and 20:00 h had an average of 26.7 °C. Table 1 shows that the evaporation

Fig. 1 Location map of the study area



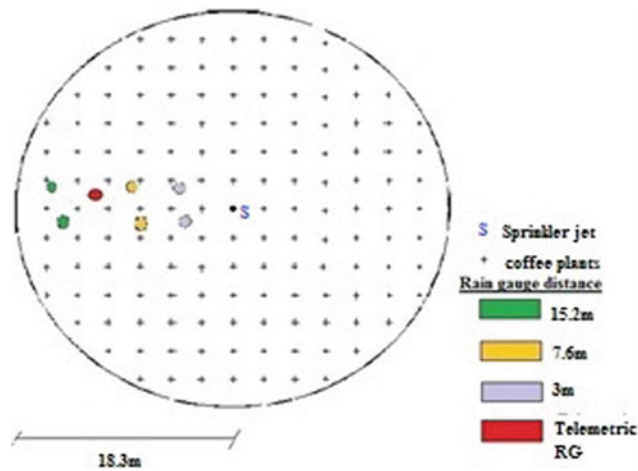


Fig. 2 Layout of the experimental setup

Table 1 Meteorological parameters and corresponding evaporation loss

Date Time	Wind speed (km/h)	VPD (kPa)	Air temperature (*C)	Average evaporation loss (%)
21-03-2019 07:00	0	0.152	18.2	29.6
21-03-2019 08:00	0	0.173	19.4	
21-03-2019 09:00	0	0.697	25.5	
21-03-2019 10:00	0	1.391	28.8	
21-03-2019 11:00	0	2.852	33.3	
21-03-2019 12:00	0	4.318	35.7	
21-03-2019 13:00	0	4.372	35.3	
21-03-2019 14:00	0	4.166	35.5	21.1
21-03-2019 15:00	1	4.047	35.1	
21-03-2019 16:00	1	3.275	33.4	
Avg			34.8	
21-03-2019 17:00	1	2.512	30.8	
21-03-2019 18:00	0	1.939	27.9	
21-03-2019 19:00	0	1.495	25.1	
21-03-2019 20:00	0	1.336	23.0	26.7
Avg			26.7	

losses are proportional to the average temperature and vapour pressure deficit. No correlation was established between the evaporation loss and average temperature or vapour pressure deficit as the number of tests conducted are only two and the values are just representative.

4 Conclusion

From the present study, measured evaporation losses prove to be a major water loss in irrigation. Additional experiments can be carried out to find out the rates of

evaporation losses for better results. For any crop-water requirement, the duration of pumping can be altered according to the measured evaporation rates, thus saving the water and operating costs of irrigation. This method can be applied to measure the evaporation loss from the sprinkler-irrigated short (height) crops by placing the rain gauge under the canopy (below the ground for the crops nearly touching the ground) and corresponding open space rain gauge by clearing the small area of crops at equal radial distances if no free space is available. The author recommends measuring evaporation at different seasons and growth stages of the crop.

Table 2 Evaporation losses, rain gauge distances and the measured depth of RF and TF

	RG Dist (m)	Mean Rad (m)	Coverage Area (sqm)	RF (mm)	Vol (m ³)	TF (mm)	TF/RF	Evp (%)
Shift 1 (12:00 to 16:00 h) (Rain gun)	3.0	5.3	89	19.0	1.7	12.1	0.64	36
	7.6	9.1	173	14.0	2.4	13.5	0.96	4
	10.7*	13.0	264	13.6	3.6	-	-	-
	15.2	18.3	523	20.9	10.9	10.7	0.51	49
					18.7		Avg	29.6
			Discharge (L/s)		1.3			
Shift 2 (16:00 to 20:00 h) (Jumbo jet and rain gun)	3.0	5.3	89	70.4	6.3	49.5	0.70	30
	7.6*	8.4	131	55.0	7.2	-	-	-
	9.1	10.7	137	79.6	10.9	39.9	0.72	28
	12.2	18.3	693	55.0	38.1	51.7	0.94	6
*Telemetric rain gauge					62.5			
			Discharge (L/s)		4.3		Avg	21.1

Acknowledgements The meteorological data was procured and experiment was conducted in Central Coffee Research Institute (CCRI), Balehonnuru, India. The authors gratefully acknowledge Dr.Y.Raghu-ramulu, D' Souza George Felix and Patil Somashekhargouda for their kind support in carrying out this study.

References

- Fellah, S., Khiari, A., Kribaa, M., Arar, A., Chenchouni, H.: Effect of water regime on growth performance of Durum Wheat (*Triticum durum* Desf.) during different vegetative phases. *Irrig. Drain.* **67**(5), 762–778 (2018). <https://doi.org/10.1002/ird.2289>
- Maidment, D.R.: Handbook of hydrology, vol. 9780070. McGraw-Hill, New York (1993)
- Molle, B., Tomas, S., Hendawi, M., Granier, J.: Evaporation and wind drift losses during sprinkler irrigation influenced by droplet size distribution. *Irrig. Drain.* **61**(2), 240–250 (2012). <https://doi.org/10.1002/ird.648>
- Yazar, A.: Evaporation and drift losses from sprinkler irrigation systems under various operating conditions. *Agric. Water Manag.* **8**(4), 439–449 (1984). [https://doi.org/10.1016/0378-3774\(84\)90070-2](https://doi.org/10.1016/0378-3774(84)90070-2)

**Hydrology, Hydrogeology, Hydrochemistry, Water
Resources (T10): Hydrology, Land Use and
Climatology—Runoff and Catchment Studies**



Predicting Vertical Distribution of Sediment Concentrations in Uniform Open Channel Flows

Abdelali Terfous, Mira Sabat, and Abdellah Ghenaim

Abstract

This work presents a theoretical model for predicting the vertical distribution of suspended sediment concentrations in open channel flows. The model developed uses a new sediment diffusivity coefficient obtained by the application of the Itakura and Kishi correction method to the Kerssens sediment diffusivity profile. Based on this diffusivity coefficient, a theoretical formulation for computing sediment concentration is derived analytically, using the well-known convection–diffusion equation. We compare results from the proposed model with experimental measurements and existing theoretical models, obtained by previous researchers, in order to evaluate the applicability of the present model to predict particle concentration profiles in open channel flows. The computed values of sediment concentrations are in good agreement with the experimental data reported in the bibliography.

Keywords

Open channel flows • Suspended sediment • Vertical concentration • Diffusivity coefficient

1 Introduction

Prediction of suspended sediment concentration continues to be one of the major challenges in river dynamics. Various numerical and analytical formulas of different orders of complexity are used to represent suspended sediment

concentrations. Many theoretical models are proposed for steady flows. Rouse (1937) suggested a formula for vertical distribution using the settling velocity of suspended sediment and the turbulent diffusion coefficient. Itakura and Kishi (1980) established a theoretical model based on the Monin–Obukhov length theory. Umeyama (1992) studied the vertical distribution of suspended sediment in open channels theoretically using a new mixing length concept. A wide range of models (Ghoshal et al. 2013), mentioned above, uses the diffusivity coefficient established by Rouse (1937) or that proposed by Kerssens et al. (1979) and Van Rijn (1984).

In the present work, we are formulating a model for predicting suspended sediment concentrations in open channel flows. We will develop a new sediment diffusivity model by combining the properties of the sediment diffusivity profiles presented in the work of Kerssens et al. (1979) and Van Rijn (1984), and the properties of the sediment diffusivity model presented by Itakura and Kishi (1980). The obtained coefficient is used for the resolution of the convection–diffusion equation, in order to obtain an appropriate theoretical model to calculate sediment concentration distribution.

2 Methods

We consider the vertical distribution of a suspended sediment concentration in a steady and uniform flow under equilibrium conditions. For low concentrations, the convection–diffusion equation giving the transport of suspended sediment concentration in the vertical direction can be obtained by equating the downward fluxes caused by gravity and the upward fluxes caused by turbulence:

$$\varepsilon_s \frac{dc}{dz} + w_s c = 0 \quad (1)$$

where ε_s is the sediment diffusivity coefficient (m^2/s), c is the volumetric concentration ($0 \leq c \leq 1$), w_s is the particle settling velocity (m/s), and z is the vertical coordinate (m).

A. Terfous (✉) · A. Ghenaim
INSA Strasbourg, Icube Laboratory, Strasbourg, France
e-mail: abdelali.terfous@insa-strasbourg.fr

M. Sabat
University of Balamand, Faculty of Sciences, Department of
Mathematics, El-Koura, Lebanon

In previous researches, different forms of sediment diffusivity profiles were developed. These different forms have been associated with various concepts regarding the mixing in the near-bed boundary layer (Rouse 1937; Itakura and Kishi 1980; Kerssens et al. 1979; Van Rijn 1984).

Rouse (1937) considered the diffusion coefficient as a parabolic function of the water depth that takes null values at the channel bottom and at the free surface, which reaches its maximum value at the mid-depth:

$$\varepsilon_s = \beta \varepsilon_m = \beta \kappa u_* z / h (h - z) \quad (2)$$

where κ is the von Karman constant, u_* is the shear velocity, h is the water depth, ε_m is the momentum diffusivity coefficient, and β is the ratio of sediment diffusivity to momentum diffusivity.

In the present study, we apply the Itakura and Kishi (1980) correction method to the profile of Van Rijn (1984) to obtain a representation of the suspended sediment distribution, particularly near the free surface. We keep the same conditions used by Itakura and Kishi (1980):

$$\varepsilon_s = \kappa u_* z (1 - z/h) (1 + \varphi_2 z/h)^{-1} \quad (3)$$

where $(1 + \varphi_2 z/h)^{-1} = R$ is the correction factor introduced by Itakura and Kishi (1980). The correction method is applied to Kerssens et al. and Van Rijn's model.

$$\varepsilon_m = \begin{cases} \varepsilon_{m,\max} = 0.25 \kappa u_* h & \text{for } z/h > 0.5 \\ 4z/h (1 - z/h) \varepsilon_{s,\max} & \text{for } z/h \leq 0.5 \end{cases} \quad (4)$$

3 Results

3.1 Sediment Diffusivity Profiles

To obtain the sediment diffusivity profile 1, the parabolic constant profile (Van Rijn 1984) is multiplied by the correction factor of Itakura and Kishi (1980). The result is given by:

$$\varepsilon_s = \begin{cases} 0.25 \kappa u_* h (1 + \varphi_2 z/h)^{-1} & \text{for } z/h > 0.5 \\ \kappa u_* h z / h (1 - z/h) (1 + \varphi_2 z/h)^{-1} & \text{for } z/h > 0.5 \end{cases} \quad (5)$$

3.2 Sediment Concentration Profiles

We applied the modifications of Itakura and Kishi to the parabolic constant profile of Kerssens et al. and developed the vertical suspended sediment concentration profiles using Eq. (5). Two domains of study are used: $z/h \leq 0.5$ and

$z/h > 0.5$. The vertical distribution of the sediment concentration over the whole water depth is given by:

$$\frac{c}{c_a} = \begin{cases} \left[\frac{a}{z} \left(\frac{h-z}{h-a} \right)^{(1+\varphi_2)} \right]^{Z_1} & \text{for } z/h \leq 0.5 \\ \left[\frac{a(h/2)^{\varphi_2}}{(h-a)^{(1+\varphi_2)}} \right]^{Z_1} \exp\{-4Z_1(z/h - 1/2)[1 + \frac{\varphi_2}{2}(z/h + 1/2)]\} & \text{for } z/h > 0.5 \end{cases} \quad (6)$$

4 Discussion

The concentration model obtained by Eq. (6) was tested against the experimental data of Itakura and Kishi, Vanoni and Brooks (1957), Einstein and Chien (1955), Coleman (1986), and Lyn (1988). It was also compared with the existing theoretical models of Rouse (1937), Kerssens et al. (1979), and Itakura and Kishi (1325). Figure 1 shows the comparison between the present model and the parabolic profile (Rouse 1937), the parabolic constant profile (Kerssens et al. 1979; Rijn 1984), and the Itakura and Kishi (1980) profile and data.

5 Conclusions

In the present study, we present a model to compute the vertical distribution for suspended sediment concentration in open channel flows when the mean concentration is known. The study then focused on the corrections introduced to the classical Rouse profiles, mainly the ones that led to the parabolic constant profile and the Itakura and Kishi profile. The results of these corrections permit to establish a model to compute a new sediment diffusivity coefficient. The diffusivity profile is introduced in a simplified version of the

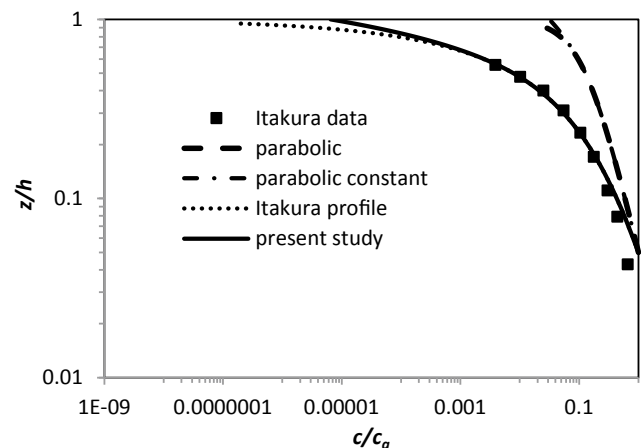


Fig. 1 Concentration profiles compared to the data of Itakura and Kishi (1980)

convection–diffusion equation that was then integrated to generate a concentration profile. This profile is validated with experiments from the bibliography.

References

- Coleman, N.L.: Effects of suspended sediment on the open channel velocity distribution. *Water. Resou. Res.* **22**(10), 1377–1384 (1986)
- Einstein, H.A., Chen, N.: Effects of heavy sediment concentration near the bed on velocity and sediment distribution. *MRD Sedim. Ser.* **8**, (1955)
- Ghoshal, K., Mazumder, B., Chakraborty, C.: Velocity and concentration profiles in uniform sediment-laden flow. *Int. J. Sed. Res.* **28**(2), 194–209 (2013)
- Itakura, T., Kishi, T.: Open channel flow with suspended sediments. *J. Hydraulics Div. ASCE* **106**(HY8), 1325–1343 (1980)
- Kerssens, P., Prins, A., Van Rijn, L.C.: Model for suspended sediment transport. *J. Hydraulic Eng.* **105**(HY5), 461–476 (1979)
- Lyn, D.A.: A similarity approach to turbulent sediment-laden flows in open channels. *J. Fluid. Mech.* **193**, 1–26 (1988)
- Rouse, H.: Modern conception of the mechanics of fluid turbulence. *Trans ASCE* **102**, 463–543 (1937)
- Umeyama, M.: Vertical distribution of suspended sediment in uniform open channel flow. *J. Hydraulic Eng.* **118**(6), 936–941 (1992)
- Van Rijn, L.C.: Sediment transport part II: suspended load transport. *J. Hydraulic Eng.* **110**(11), 1613–1641 (1984)
- Vanoni, V.A., Brooks, N.H.: Laboratory studies of the roughness and suspended load of alluvial streams. Final Report to Corps of Engineers, U.S. Army Missouri River Division, Pasadena, USA (1957)



Contribution to the Study of Flood Risks in the North West of Algeria (Case of Oued Khemis in Tlemcen)

Sarra Bouraoui and Abderrahmane Medjerab

Abstract

After a drought in the 1990s, Tlemcen (Algeria) experienced heavy rains. The rains of recent years have caused several floods. They have become frequent and usually cause significant damage. Urbanism, climate change and floods: Case of Tlemcen city in Algeria. The examination of our results concerning the impacts of flood risks on the agglomeration of the Province of Tlemcen for different periods $T = 5$ years and $T = 100$ years, as well as the visualization of Khemis wadi in 3D, shows that, for the return periods examined, there is always overflow of the minor bed, which is required to make adjustments. This study presents a method of flood risk studying in Oued Khemis, Tlemcen region.

Keywords

Flood risk • Wadi overflow • Wadi flood • Watershed of Wadi Khemis • Flood return-periods

1 Introduction

For some time now, the city of Tlemcen has been experiencing repeated floodings, the last ones still in memory took place on 19 October 2007, 24 October 2008 and 13 November 2012. The floods caused extensive damage, flooded roads, blocked hoppers, isolated neighbourhoods and a paralysed city (Tanavud et al. 2004; Kellenberg and Mobarak 2008). A relief organization has also been set up to deal with possible disasters; therefore, it is a rapid or slow submergence of an area that can be inhabited. It corresponds to overflows water; it is a natural phenomenon linked to the geomorphological and meteorological characteristics of a

watershed. It only becomes a risk when it causes the damage of any kind.

2 Geographical Location of Oued Khemis

Its length is 117 km, with a sub-basin of 340 km² (Fig. 1), drains a valley in the Tlemcen Mountains and joins the Tafna at the Beni Bahdel dam level (Boussaid 2013).

3 Methods

The different characteristics of the Oued Khemis watersheds are determined using the Global Mapper and Arc-GIS software. For this study, we have chosen to use the mathematical model (HEC-RAS 5.0.5) (Hydrologic Engineering Center-River Analysis System) which is a hydraulic analysis software designed to model free surface flows in natural and artificial channels, taking into account crossing structures. It allows to simulate progressively variable flows in steady state and transient mode and to perform water line calculations in dynamic mode by simulating the different obstacles. The modelling of the wadi is based on cross profiles and roughness coefficients for each section.

4 Results and Discussion

The morphological characteristics of the Oued Khemis Catchment Areas are reported in Fig. 1; Table 1.

The empirical formulas for flood determination, flood hydrograph of Wadi Khemis and geometry of the cross-sectional profiles and long profile of the Khemis Wadi overflow are shown in Figs. 2, 3 and Table 2.

$$Q_{Tp\%} = 2K \log(1 + a \cdot P_{\text{moy}}) \cdot \frac{A}{\sqrt{L}} \sqrt{1 + 4 \log T - \log A}$$

S. Bouraoui (✉) · A. Medjerab
University of Science and Technologies Houari Boumediene,
Bab Ezzouar, Algeria

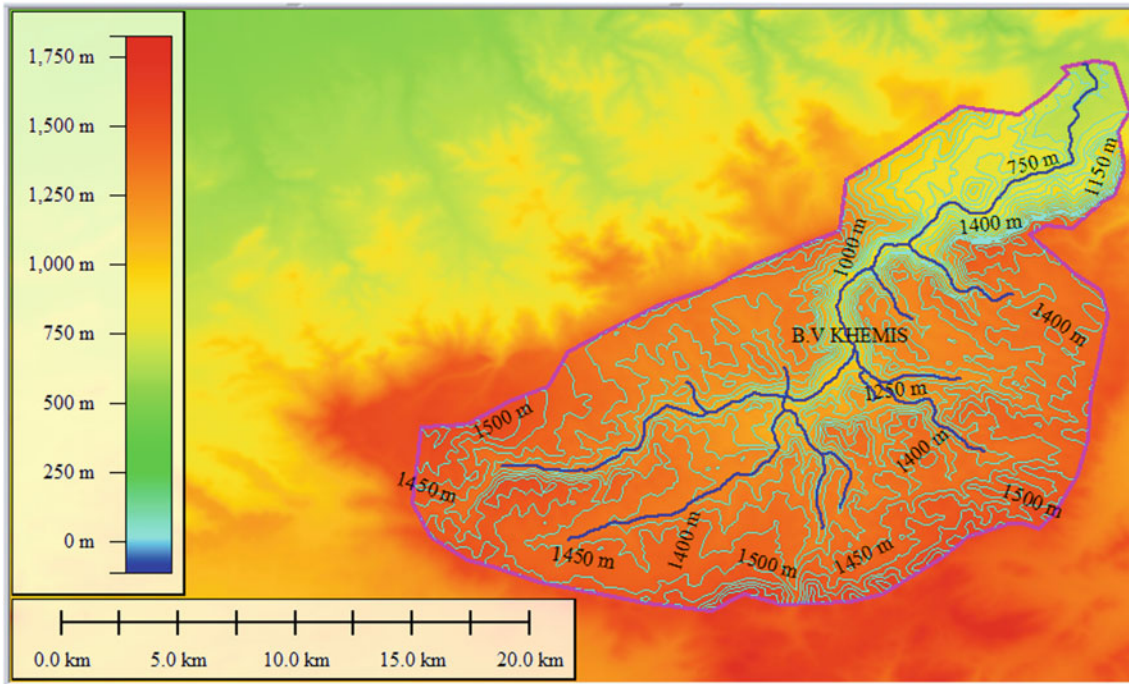
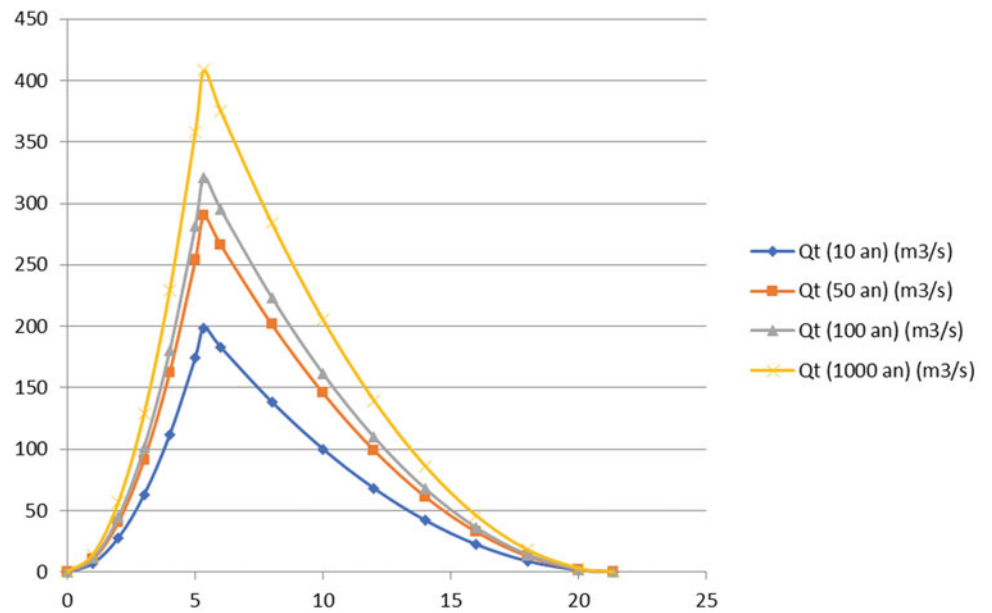


Fig. 1 Delimitation of the catchment areas Oued Khemis (created using Global mapper 18)

Table 1 Characteristics of the Khemis Wadi watershed

	Surface (km ²)	Scope of consolidation (km)	Lw (km)
BV	327	83.32	24.258

Fig. 2 Flood hydrograph (Wadi Khemis)



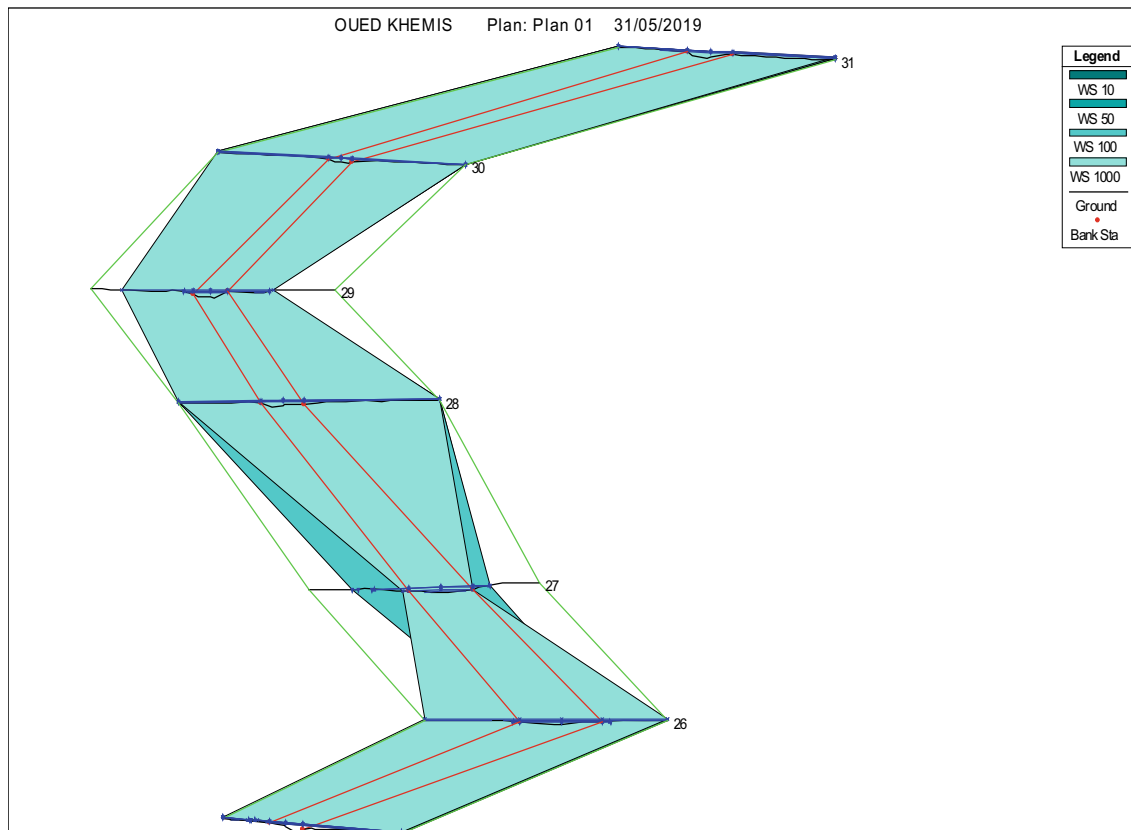


Fig. 3 Geometry of the cross profiles and long profile of the Khemis wadi overflow ($T = 5$ and $T = 1000$ years)

Table 2 Flood flow calculations

Frequency (%)	Return period (ans)	Ce	A (km ²)	Tc	Pjmax	Ptc (mm)	I (mm/h)	Annual P (m)	Lp (km)	Q max (m ³ /s)
0.1	10	0.4	327	5.34	87.49	49.42	9.26	0.395	24.2	198.81
0.02	50	0.4	327	5.34	121.07	68.39	12.81	0.395	24.2	289.80
0.01	100	0.4	327	5.34	135.26	76.41	14.31	0.395	24.2	321.14
0.001	1000	0.4	327	5.34	182.16	102.9	19.27	0.395	24.2	408.34

The examination of the cross profiles carried out for different periods $T = 5$ years and $T = 100$ years, as well as the visualization of Wadi Khemis in 3D, shows that, for the return periods examined, there is always overflow of the minor bed, which is necessary to do with the development of the watercourse.

5 Conclusion

The Province of Tlemcen has been confronted with floods and has tried to mitigate this phenomenon through development schemes aimed at eliminating or at least controlling

river floods that periodically endangered human lives and hindered its economic development.

This work consists in carrying out a hydrological study of the Khemis wadi catchment area, as well as a modelling of the hydraulic behaviour of the flow of this wadi. The results showed that there is a risk of flooding because of the topography of the wadi worsened by the scattered dwellings and the different anthropogenic activities that do not respect of its nature.

The hydraulic modelling carried out using HEC-RAS of the watercourse sections of the Khemis wadi, the subject of the study made it possible to observe the areas that can be overrun by floodwater.

References

- Adjim, H., Djedid, A., Hamma, W.: Urbanism, climate change and floods: case of Tlemcen city in Algeria. *Urbanism Arhitectura Constructii* **9**(1), 71–80 (2018)
- Boussaid, F: Dynamics of aquatic fauna in the source zone: case of Oued Tafna, p. 21 (2013)
- Kellenberg, D.K., Mobarak, A.M.: Does rising income increase or decrease damage risk from natural disasters?. *J. Urban Econ.* **63**(3), 788–802 (2008). <https://doi.org/10.1016/j.jue.2007.05.003>
- Tanavud, C., Yongchalemchai, C., Bennui, A., Densreesekul, O.: Assessment of flood risk in Hat Yai municipality, Southern Thailand, using GIS. *J. Natural Disaster Sci.* **26**(1), 1–14 (2004). <https://doi.org/10.2328/jnds.26.1>



Risk Assessment of Flash Floods in Eastern Egyptian Desert

Ahmed Mohamed Helmi[✉], Omar Zohny, and Ashraf El Mustafa

Abstract

Flash floods are natural phenomena characterized by their short duration and big volume within a limited available response time. As a natural phenomenon, flash floods depend on climatic conditions, geological nature, and prevailing terrain. The floods often occur in Egypt at the beginning of the fall season as of mid-October. In Egypt, the highest population density is centralized around the Nile banks, and high-density touristic compounds and scattered big cities with connecting roads are distributed along the whole Red Sea coast. The wadies in the Egyptian Eastern Desert drain either to the west side toward the Nile or to the east toward the Red Sea. The existing and high rates of urban expansion without proper consideration of wadi paths led to considerable wadi encroachments and catastrophic incidents. Due to the huge amount and cost of work required to assess the encroachments and the implementation of proper flood mitigation measures, a prioritization for the wadies according to their peak flow standardized risk factor (PFSRF) is a critical task since most of the encroachments are located at wadies' outlets. Stormwater harvesting can provide a share in reducing freshwater stress associated with a reduction in the required drainage structures, accordingly another catchment prioritization is provided based on runoff volume standardized risk factor (RVSRF). The provided RVSRF can guide the designer

to give a priority for artificial lakes and dams as a recommended flood mitigation measure for such catchments.

Keywords

Peak flow • Runoff volume • Standardized risk factor • Stormwater harvesting • Freshwater stress

1 Introduction

The water resources in Egypt, as in all Middle East and North Africa (MENA) Region, are subjected to high stresses due to the population increase; therefore, the flood mitigation measures are not only for protection purposes but also for the proper use of this freshwater resource. “Water is a resource before being a threat. That is why it would be of little use to consider flood risk assessment (FRA) by itself without casting it in the framework of flood risk management and water management at large” (Rudari 2017).

The previous studies (El-Moustafa 2012; Mohamed 2013; MWRI 2018) considered only the catchments' morphological parameters or considered equal weight for morphological parameters while adding the volume of runoff as an additional parameter with the same weight. All the studies considered parts of the eastern desert and no regional study was provided.

2 Materials and Methods

The SRTM 90m DEM Version 4.0 files are utilized in catchment delineation and morphological parameters' calculations. The streamlines were verified against Egyptian topo maps (Scale 1:250,000). The weighted average soil conservation services–curve number (SCS-CN) for each catchment was extracted using the GIS tool from the

A. M. Helmi (✉)

Faculty of Engineering, Irrigation and Hydraulics Department,
Cairo University, Cairo, Egypt
e-mail: Ahmed.helmi@eng.cu.edu.eg

O. Zohny

Aiecon Consultants, Cairo, Egypt

A. El Mustafa

Faculty of Engineering, Irrigation and Hydraulics Department,
Ain Shams University, Cairo, Egypt

regional Egyptian CN map (Awadallah et al. 2016). The GIS was utilized to produce an isohyetal map for the study area to obtain weighted 1-in-100 weighted average maximum daily precipitation for each catchment using the rainfall analysis for meteorological station obtained from several official reports. Finally, each catchment peak 1-in-100 discharge and storm volume can be calculated.

Many thresholds have been tested for catchment delineation in order to obtain a reasonable number of catchments for this proposed regional scale. The selected threshold was set to 50 sq km; accordingly 165 catchments were obtained. The catchments' boundaries and the longest flow paths on DEM and Topo maps are shown in Fig. 1. The weighted average catchment 1-in-100 rainfall maximum daily precipitation and curve numbers are extracted from regional rainfall isohyetal maps generated according to the available rainfall station frequency analysis. Similarly, the catchments' weighted average curve number is obtained from the regional curve number map (Awadallah et al. 2016) by the application of GIS analysis tools as shown in Fig. 2. HEC-HMS software was utilized to calculate the catchments' peak discharge based on SCS type II six hours' storm distribution. The lag time is calculated based on the following formula:

$$T_L = 0.6 \times T_c$$

$$= 0.6 \times \left[0.019472 \frac{L^{0.77}}{S_1^{0.385}} \right] (1 + (80 - CN) * 0.04) \quad (1)$$

where: T_L = lag time in minutes, T_c = time of concentration in minutes, L = longest flow path, and S_1 = slope of the longest flow path.

In this research, as long as the collected data are sufficient to calculate the runoff peak discharge, it will be used in its standardized value as the evaluating risk factor for the catchments. The peak flow standardized risk factor (PFSRF) internally contains the morphological, geological, and meteorological parameters in their weighted form. PFSRF will be used to categorize the catchments based on their risk. The runoff volume standardized risk factor (RVSRF) will be utilized as additional catchment risk categorization which will show the stormwater harvesting potential in addition to the risk generated if no proper flood mitigation measures are provided.

Peak Flow Standardized Risk Factor (PFSRF)

$$= \frac{PF - PF_{\min}}{PF_{\max} - PF_{\min}} \quad (2)$$

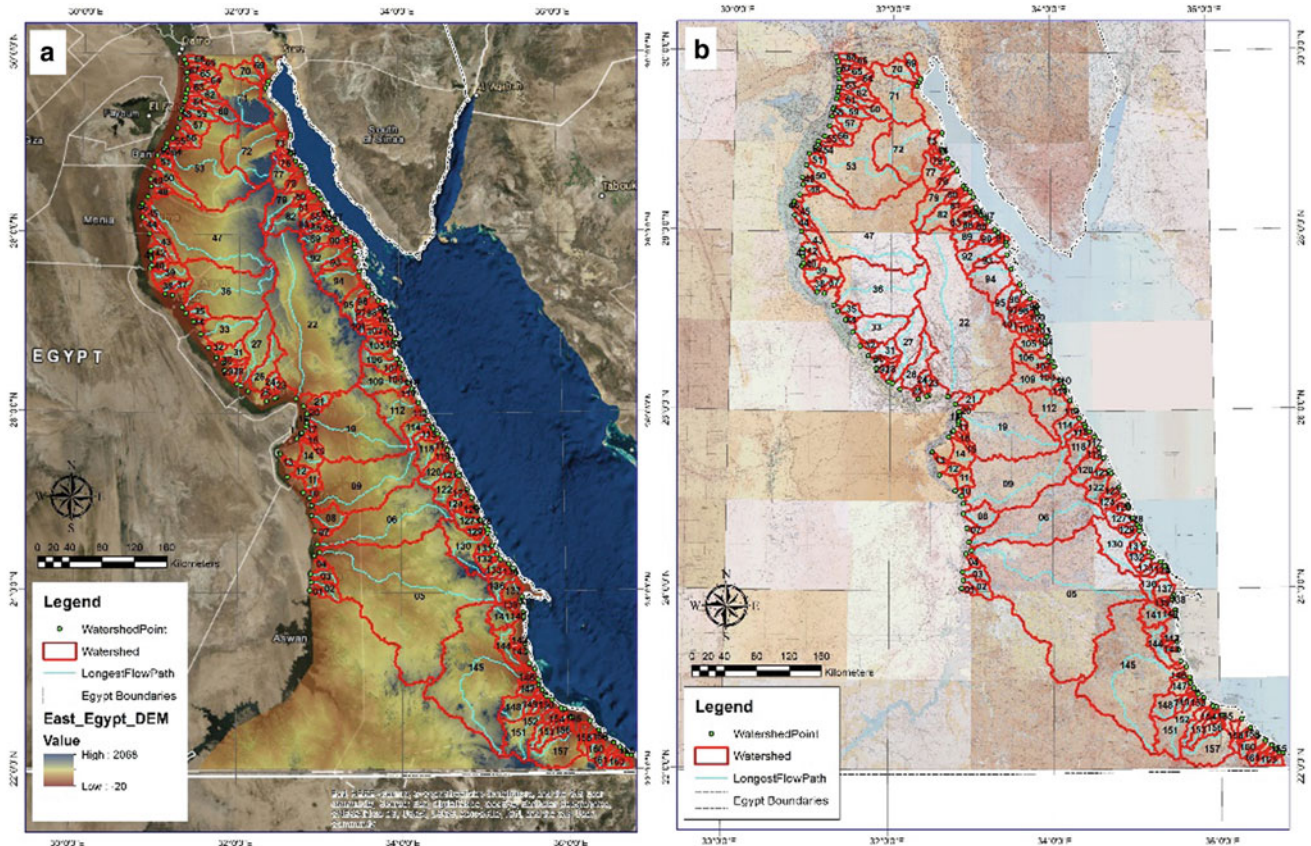


Fig. 1 Delineated main catchments a on DEM raster and b on topographic maps

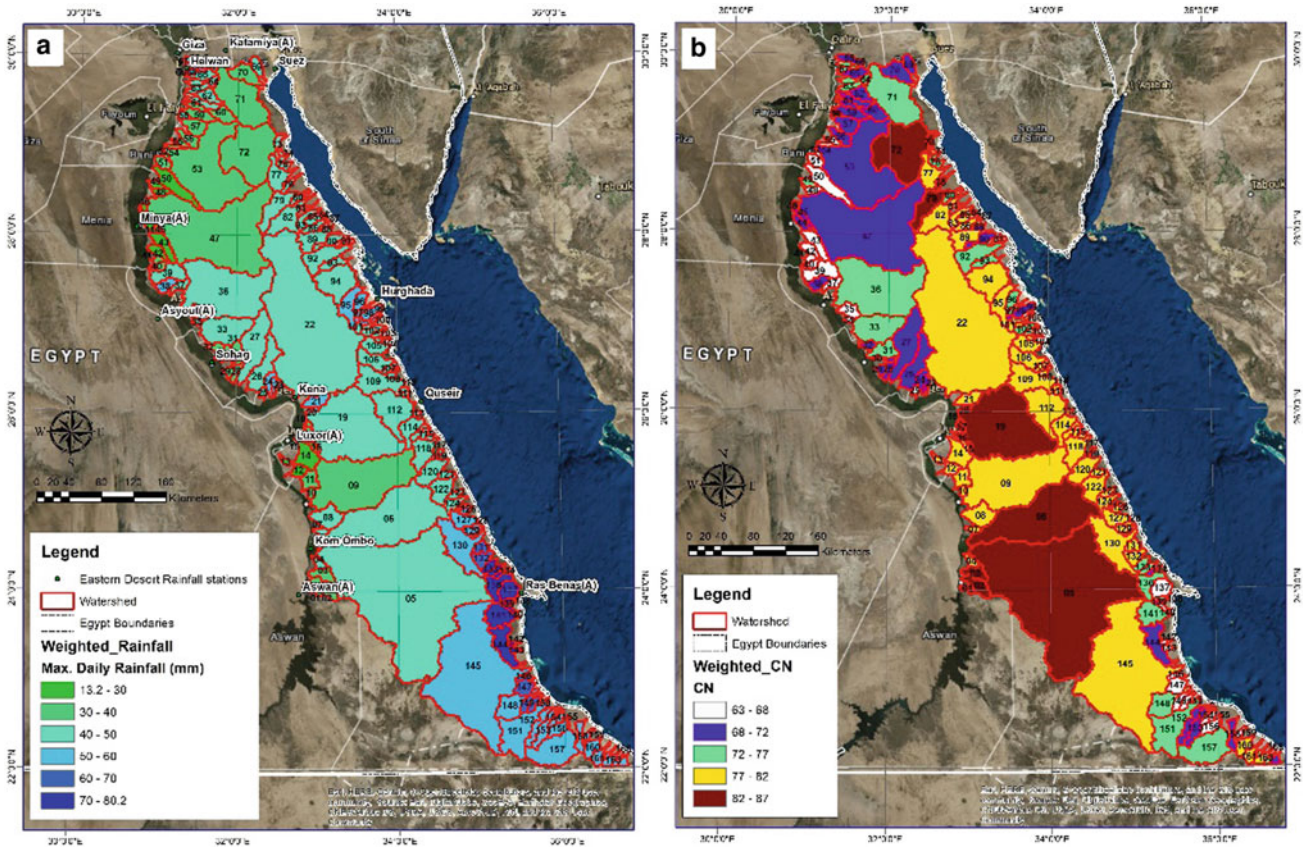


Fig. 2 Catchments' weighted average a 1-in-100 maximum daily precipitation and b curve number (CN)

Table 1 Quartile data ranges

Limits	Runoff volume (1000 m ³)	Discharge (m ³ /sec)
Q1	1216	36
Q2	2239	91
Q3	7014	204
IQR	5798	167
Upper limit	15711	455

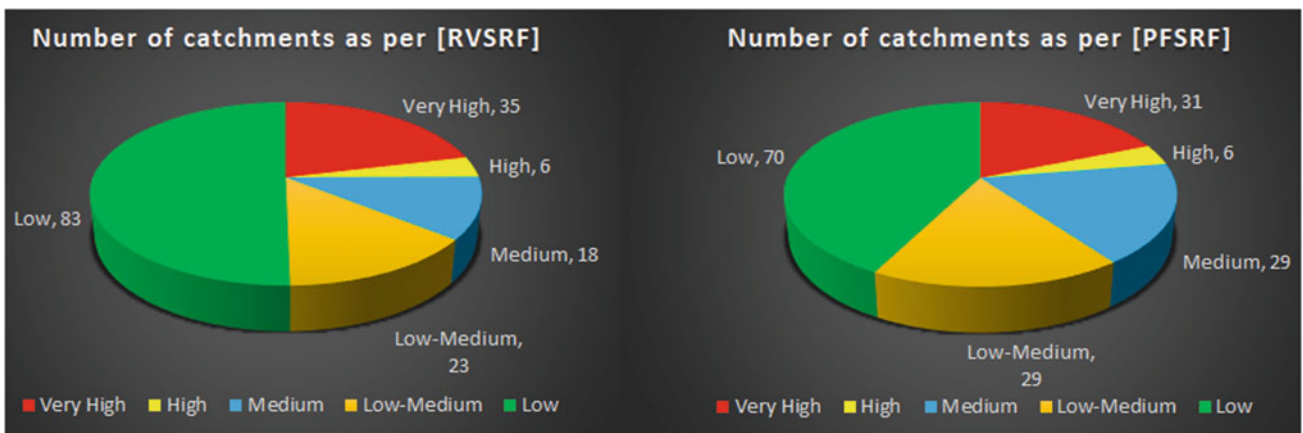


Fig. 3 Catchments' number in each risk category for PFSRF and RVSFRF

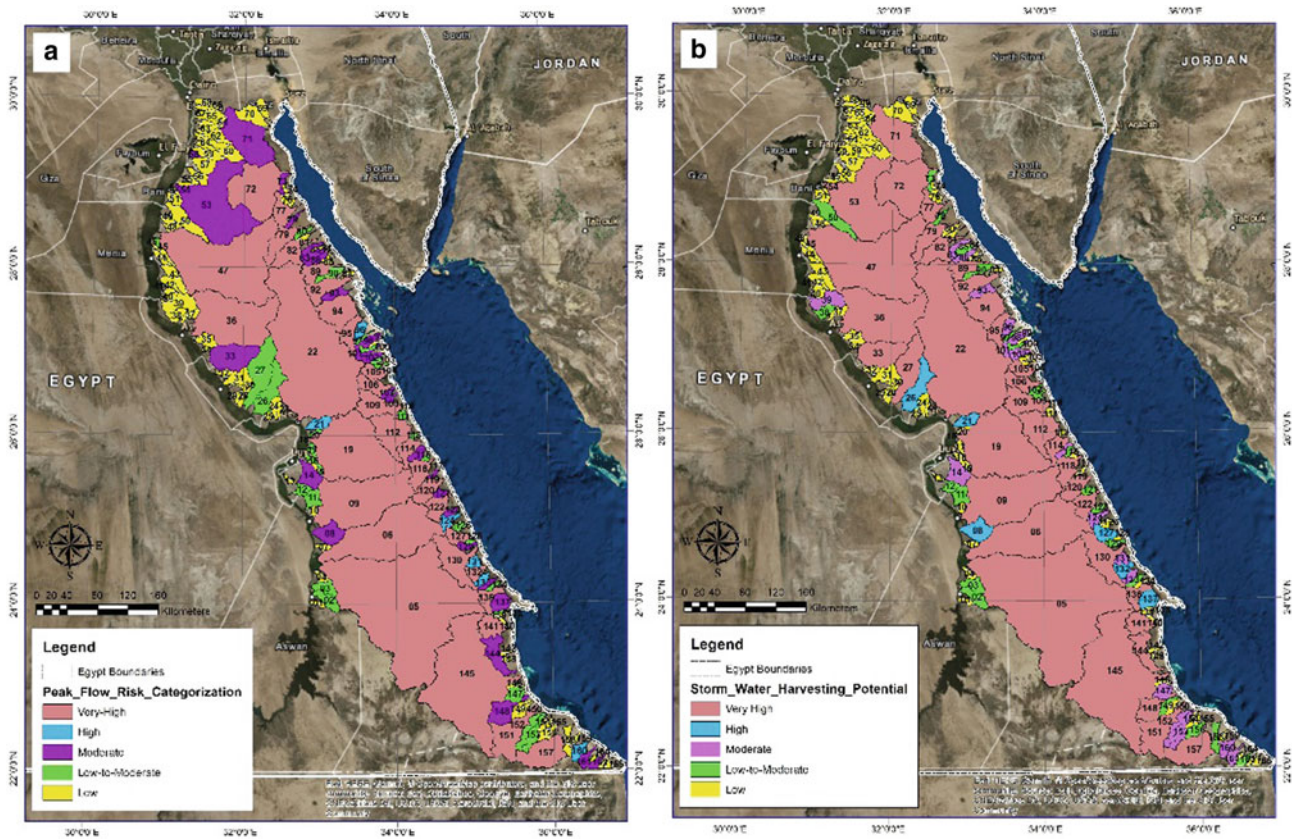


Fig. 4 Detailed catchment categorization according to PFSRF and RVSFR

$$\text{Runoff Volume Standardized Risk Factor (RVSFR)} = \frac{RV - RV_{\min}}{RV_{\max} - RV_{\min}} \quad (3)$$

3 Results and Discussion

According to the obtained HEC-HMS hydrologic modeling output results, a wide range of total runoff volume and peak discharges was obtained due to the sheer size of the catchments' areas. This wide range should be carefully assessed prior to proceeding with the calculation of the standardized risk factors. The quartile technique was utilized to eliminate the very high values (statistical outliers) that affect the results. The data limits for calculations based on quartile assessment of the model output are given in Table 1; accordingly, the catchments with discharge values greater than 455 m³/sec will be excluded from the calculation of the PFSRF. Similarly, the catchments with total runoff volume greater than 15,711 E03 m³ will be excluded from the RVSFR. The proposed risk categorization based on the

value of the standardized risk factor (SRF) was low risk for $SRF < 0.15$, low to moderate risk for $0.15 < SRF < 0.3$, moderate risk for $0.3 < SRF < 0.5$, high risk for $0.5 < SRF < 0.7$, and very high risk for $SRF > 0.7$. Following the proposed categorization limits, Fig. 3 shows the catchments' number in each risk category for PFSRF and RVSFR. The details of catchment categorization are given in Fig. 4 where the risk categorization for each catchment is shown to be used in flood mitigation projects prioritization.

4 Conclusion

The Egyptian Eastern Desert has been categorized according to the flash flood peak flow standardized risk factor which gives priority to flood mitigation measures assessment. A second catchment categorization based on the runoff volume standardized risk factor, which guides the authorities to think about rainfall harvesting projects (artificial lakes and dams) as a flood mitigation measure to increase the rate of investment return from both flood mitigation and reduction in freshwater stress.

References

- Awadallah, A.G., Saad, H., Elmoustafa, A., Hassan, A.: Reliability assessment of water structures subject to data scarcity using the SCS-CN model. *Hydrol. Sci. J.* **61**(4), 696–710 (2016)
- El-Moustafa, A.M.: Weighted normalized risk factor for floods risk assessment. *Ain Shams Eng. J.* **3**(4), 327–332 (2012)
- Mohamed, M.: Flash flood risk assessment in the Eastern desert. M.Sc. thesis, Irrigation, and Hydraulics Department. Ain Shams University (2013)
- MWRI: Assiut Governorate Wadies Atlas (2018)
- Rudari, R.: Flood hazard and risk assessment, hazard-specific risk assess. Modul. United Nations Off. Disaster Risk Reduction, pp. 1–16 (2017)



Flood Hazards Mapping in Arid Region by Integrating Hydrologic and Hydraulic Modeling: Case Study of Wadi Qows, Jeddah, Saudi Arabia

Kuswanto Marko, Amro Elfeki, Nassir Alamri, and Hatem Ewea

Abstract

This research presents an integrated approach of hydrologic and hydraulic modeling in estimating flood discharges and mapping flood inundation during flood hazards in an urban arid region (Jeddah city, Saudi Arabia). A low resolution DEM 90m, as a basis of the model, was used to identify the watershed characteristics. The SCS method was applied to estimate the peak discharges at different return periods by using the coupled WMS and HEC-HMS software. Geometric data and cross sections for flow area and flood plain were based on DEM 90m as a basis of the hydraulic model by using the coupled WMS and HEC-RAS software. The hydrological model showed that the peak discharge could range between 34.8 (dry condition at 10 years return period) and 462.4 m³/s (wet condition at 200 years return period) of the 25th of November 2009 event. While, the expected value is 116.2 m³/s at 10 years return period under normal condition. The modeled flood inundation area has a high similarity with the flood map based on the field measurements at 10 years return period with normal condition. The model showed a 78% similarity of the inundation area, however, the estimated depth has relatively high uncertainty. The results provide an overview of the November 25th, 2009 event from a hydraulic point of view. The results are relatively good, despite the high uncertainty due to a lack of accurate data.

K. Marko (✉)

Department of Geography, Faculty of Mathematics and Natural Sciences, Universitas Indonesia, Depok, 16424, Indonesia
e-mail: kuswanto@sci.ui.ac.id

A. Elfeki (✉) · N. Alamri · H. Ewea

Department of Hydrology and Water Resource Management, Faculty of Meteorology, Environment, and Arid Land Agriculture, King Abdulaziz University, Jeddah, 21589, Kingdom of Saudi Arabia

A. Elfeki

Irrigation and Hydraulics Department, Faculty of Engineering, Mansoura University, Mansoura, Egypt

Keywords

Flood hazards · Hydrologic · Hydraulic · WMS · HEC-HMS · HEC-RAS

1 Introduction

The flood that happened on November 25th, 2009, in Jeddah, was one of the most severe flood hazards in Saudi Arabia. The severity of the flood depends on the amount of excess rainfall on the catchment and the intensities. In arid zones, such as Wadi Qows, Jeddah, where the annual rainfall is less than 200 mm (IHP-V 1999), it is common to find extremely high rainfall rates that can lead to infiltration excess overland flow and rapid flood events (Davie 2008). Besides extreme weather factors, the surface conditions of the cover which are dominated by rock outcrops can accelerate surface runoff. As evidence, since 1964 until 2010, flash hazards had happened in Saudi Arabia at least seven times causing the death of many people, thousands of people were affected, and the average economic damage value may exceed USD 19 million/year (Al-Saud 2010).

The integrated approach of GIS, WMS, HEC-HMS, and HEC-RAS in estimating flood hydrograph and flood inundation in an arid region becomes very important and useful for flood risk management. Several studies dealing with this approach have been conducted such as (Abdulrazzak et al. 2018, 2019; Elfeki et al. 2018; Marko et al. 2019; Darabi et al. 2019; Choubin et al. 2019; Mosavi et al. 2018). Therefore, the aim of this study is to simulate the severe flood hazard in Jeddah, particularly in Wadi Qows where the King Abdulaziz University is located (at the lower of the basin), using a quasi-2D model (HEC-RAS 1-D with flood plain) for inundation linked with hydrological model HEC-HMS and WMS for catchment delineation and estimated flood hydrograph. The results of these models are linked together in a GIS environment to present the

inundation zone. The presented methodology can be applied to any city in Saudi Arabia.

2 Materials and Methods

The case study area is precisely located in Wadi Qows and its downstream area that consists of an upper catchment and a low land flood plain, situated in the east of Jeddah city as shown in Fig. 1. It is in latitudes 21.5° North and longitude 39.3° East. The watershed spans across an area of approximately 63 km^2 in the upstream area are used for the hydrologic modeling computation using HEC-HMS models. The downstream part has an area of 33 km^2 which is an urbanized area for hydraulic modeling computation using HEC-RAS models. The elevations range from 27 m (asl) in the lower land area and 265 m above the mean sea level (asl) in the upland area.

There are two major steps in this research: (i) estimating the expected peak discharge in November 25th, 2009 and (ii) mapping the flood inundation due to such event. Hydrologic modeling was applied to derive the peak discharge by utilizing a coupled watershed modeling system (WMS) and HEC-HMS models. Watershed boundary and its characteristics are determined based on DEM 90 m from SRTM data. Soil conservation services (SCS) method was applied to calculate the runoff volume and direct runoff. Curve number (CN) is required to identify the watershed surface characteristic based on land use and hydrologic soil group. Rainfall data was required to build the hydrograph obtained from the observation station combining with satellite data of PERSIANN-CCS. A hyetograph method was used as a time-series data in HEC-HMS for a flood hydrograph design.

Due to the limited data of high temporal resolution of observed rainfall from rain gage station (i.e., in minute-duration), the development of rainfall temporal distribution has been conducted by Elfeki et al. (2014). The hyetograph pattern was constructed referring to the Huff distribution which is developed for the severe storm with durations less than 6 h (Elfeki et al. 2014). Assisted by statistical software, the hyetograph pattern was developed for a 5-min incremental time interval. The maximum daily rainfall at King Abdulaziz Airport in the period from 1970 to 2012 is used to test the probability distribution of the rainfall depth. Log Person Type III was found to be the best to represent the data (Elfeki and Bahrawi 2017). Finally, the peak discharge was derived for different return periods.

The second major step is mapping the flood inundation by applying hydraulic modeling using a coupled WMS and HEC-RAS. Data required is triangulated irregular network (TIN) converted from DEM; geometric data such as main channel, banks, and cross-sectional lines; manning's roughness coefficient based on land use and the peak discharges. The simulation in this study used a steady, gradually varied flow analysis which is available in HEC-RAS. Water surface profiles are computed from one cross section to another by using the energy equation with an iterative procedure that is called a standard step method (Brunner 2010).

3 Results

Table 1 shows the morphometric parameters of the upstream area of Wadi Qows based on DEM using WMS. These characteristics affect the direct runoff and include time lag, and CN is shown in Table 2.

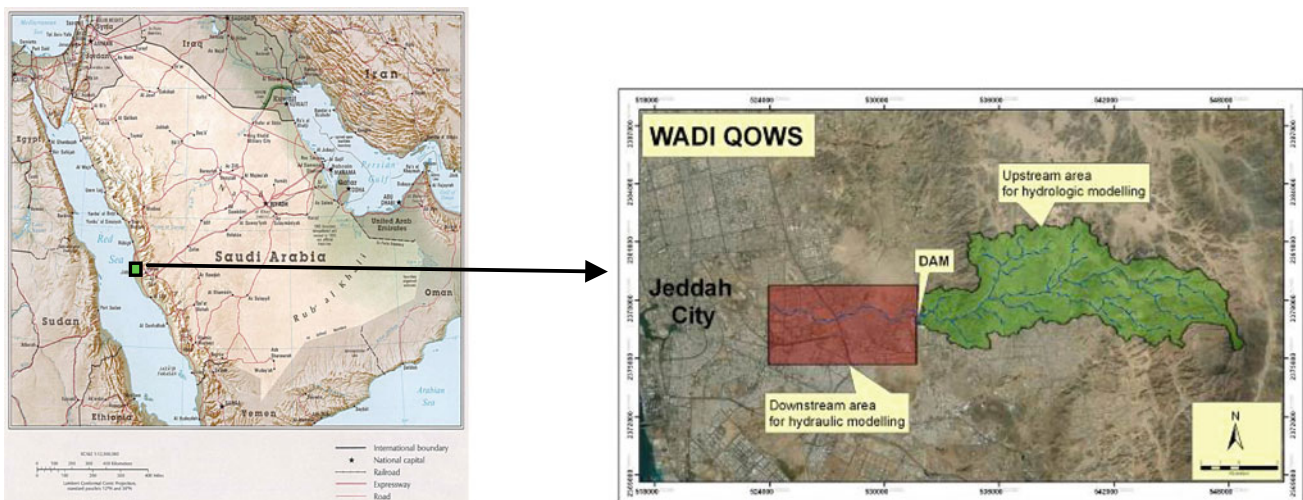


Fig. 1 The study area in Wadi Qows

Table 1 Morphometric parameters of the upstream area of Wadi Qows

Basin name	Area (km ²)	Basin length (m)	Basin slope (m/m)	Mean basin elevation (m)
Wadi Qows	63.36	16.839	0.0518	143.64

Table 2 Hydrologic parameters of the upstream area of Wadi Qows

Model	Parameter	Dry	Normal	Wet
Runoff volume (SCS Loss)	CN	70.7	85.1	93.0
	S_{max} (mm)	105.5	44.3	19.3
	I_a (mm)	21.1	8.9	3.9
	Impervious (%)	57.5	57.5	57.5
Direct runoff (SCS UH)	Lag (h)	5.7	3.6	2.7

Table 3 Peak discharge values in different conditions and scenarios

Precipitation		Peak discharge (m ³ /s)		
Return period (year)	Rainfall depth (mm)	Dry	Normal	Wet
10	70	34.8	116.2	215.2
20	83	51.4	152.0	267.2
100	116.2	101.0	248.8	402.5
200	130.7	125.0	292.4	462.4

According to the results of the design storm, the peak discharge values are classified into four different return periods and different moisture conditions as shown in Table 3. The peak discharge in dry conditions is lower than the discharge at normal conditions. The peak discharge in the wet condition is the highest. The precipitation during flooding in Jeddah was measured to be 70 mm which corresponds to a 10-year return period (Choubin et al. 2019), while the precipitation based on estimation using PER-SIANN satellite was 83 mm which corresponds to a 20-year return period. These values will be used as a basis for flood inundation mapping.

4 Discussion

Figure 2 left is the output for flood depth (from HEC-RAS) and water elevation including the extension of flood inundation area. This result is based on a peak discharge value of 116.2 m³/s in normal moisture conditions. The modeled result seems to be similar to the flood map based on the field measurement. The similarity is about 78% as shown in Fig. 1 right. However, the comparison of flood depth between modeled and observed flood areas yielded considerably different results (the maximum depth of the modeled

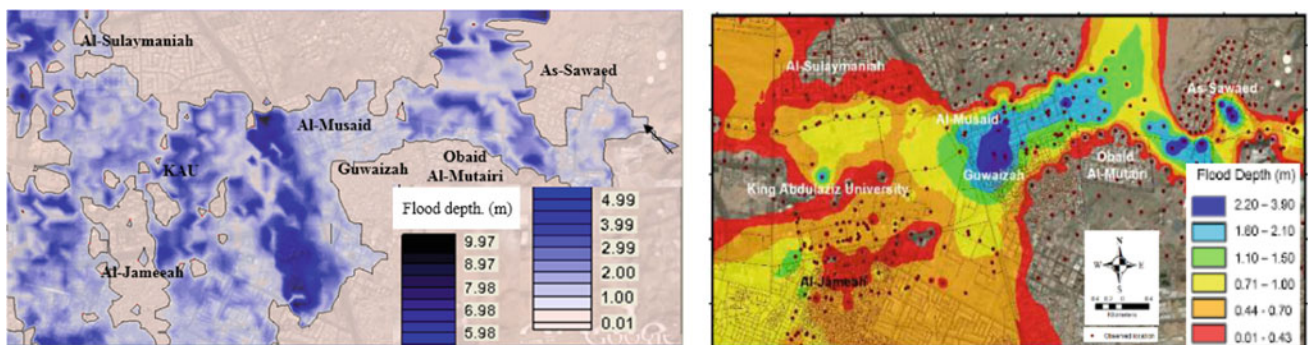


Fig. 2 Left figure: flood inundation based on hydraulic modeling using coupled WMS and HEC-RAS. Right figure: flood inundation based on field measurement

is about 8 m, while for the observed is about 4 m). This can be attributed to the low resolution of the DEM used.

5 Conclusions

Various scenarios have been conducted to simulate flood events under the available data in the area. Under the scarcity of data, the analysis provides a general overview of the November 25th, 2009 event from the hydrological and hydraulic point of view. The hydrological model estimated the peak discharge to range between 34.8 m³/s (a 10-year return period at the dry condition) and 462.4 m³/s (at 200 years return period with the wet condition). The integration of WMS and HEC-RAS can simulate the flood inundation in a quasi-2D model. Based on the hydraulic model, the maximum flood depth is 8 m, while the average flood depth is 1.72 m. The comparison between modeled and observed flood area is quite similar (at a peak discharge value of 116.2 m³/s in normal moisture condition); however, the flood depth varies considerably. The presented methodology can be applied to any city in Saudi Arabia for studying flood hazards. More accurate data should be used in the future to improve model predictions.

References

- Abdulrazzak, M., Elfeki, A., Kamis, A.S., Kassab, M., Alamri, N., Noor, K., Chaabani, A.: The impact of rainfall distribution patterns on hydrological and hydraulic response in arid regions: case study Medina Saudi Arabia. *Arab. J. Geosci.* **11**(21), 679 (2018)
- Abdulrazzak, M., Elfeki, A., Kamis, A., Kassab, M., Alamri, N., Chaabani, A., Noor, K.: Flash flood risk assessment in urban arid environment: case study of Taibah and Islamic universities' campuses, Medina, Kingdom of Saudi Arabia. *Geomat. Nat. Haz. Risk* **10**(1), 780–796 (2019)
- Al-Saud, M.: Assessment of flood hazard of Jeddah area 2009, Saudi Arabia. *J. Water Resour. Prot.* **2**(9), 839–847 (2010)
- Brunner, G.W.: HEC-RAS, River Analysis System Hydraulic Reference Manual, USACE-HEC, Davis (2010)
- Choubin, B., Moradi, E., Golshan, M., Adamowski, J., Sajedi-Hosseini, F., Mosavi, A.: An ensemble prediction of flood susceptibility using multivariate discriminant analysis, classification and regression trees, and support vector machines. *Sci. Total Environ.* **651**, 2087–2096 (2019)
- Darabi, H., Choubin, B., Rahmati, O., Haghghi, A.T., Pradhan, B., Kløve, B.: Urban flood risk mapping using the GARP and QUEST models: a comparative study of machine learning techniques. *J. Hydrol.* **569**, 142–154 (2019)
- Davie, T.: *Fundamentals of hydrology*, 2nd edn. Taylor & Francis e-Library (2008)
- Elfeki, A., Bahrawi, J.: Application of the random walk theory for simulation of flood hazards: Jeddah flood 25 November 2009. *Int. J. Emergency Manage.* **13**(2), 169–182 (2017)
- Elfeki, A.M., Ewea, H.A., Al-Amri, N.S.: Development of storm hyetographs for flood forecasting in the Kingdom of Saudi Arabia. *Arab. J. Geosci.* **7**(10), 4387–4398 (2014)
- Elfeki, A., Al-Shabani, A., Bahrawi, J., Alzahrani, S.: Quick urban flood risk assessment in arid environment using HECRAS and dam break theory: case study of Daghbag Dam in Jeddah, Saudi Arabia. In: Kallel, A., Ksibi, M., Ben Dhia, H., Khélifi, N. (eds.) *Recent Advances in Environmental Science from the Euro-Mediterranean and Surrounding Regions*, pp. 1917–1919. Springer International Publishing, Cham (2018)
- International Hydrological Programme (IHP-V): *Technical Documents in Hydrology: Flash Floods in Arid and Semi-Arid Zones*, No. 23. UNESCO, Paris (1999)
- Marko, K., Elfeki, A., Alamri, N., Chaabani, A.: Two dimensional flood inundation modelling in urban areas using WMS, HEC-RAS and GIS (Case Study in Jeddah City, Saudi Arabia). In: El-Askary, H.M., Lee, S., Heggy, E., Pradhan, B. (eds.) *Advances in Remote Sensing and Geo Informatics Applications*, pp. 265–267. Springer International Publishing, Cham (2019)
- Mosavi, A., Ozturk, P., Chau, K.-W.: Flood prediction using machine learning models: literature review. *Water* **10**(11), 1536 (2018)



What About the Erosion in the Coastal Algiers Watershed (Algeria)?

Abdelhadi Ammari and Boualem Remini

Abstract

Sediment transport and land erosion have specific impacts in Algeria, especially if we know that Algerian lands record the highest soil erosion levels in North Africa. Also, the direct impact of the moving sediments on storage capacities greatly reduces the regularized volumes of the latter. Thus, we studied the erosion phenomena over the coastal watershed of Algiers, which is one of the most important watersheds in Algeria due to its demographic aspect (more than 8 million inhabitants over a small area representing 0.5% of the whole area of the country) and to the important agricultural and industrial activities. The study concerns the sediment transport evaluation with a simple approach using the sediment concentration data of several hydrometric sites within and outside of the watershed in order to estimate the specific erosion or soil degradation and to map it in order to have a global idea about the zones which are most sensitive to erosion and which must have a priority in the watershed management programs. We deduce that the prone zones are in the upstream of Wadi Chiffa and Bouroumi, and along Wadi El Hachem where Boukerdane Dam is located.

Keywords

Coastal Algiers • Sediment transport • Erosion

1 Introduction

Algeria is a water-scarce country, mobilizing less than 600 m³ per citizen per year, despite important water mobilization efforts which allowed the construction of more than 80 dams with 7000 million cubic meters of storage capacity (Ammari and Remini 2012). The majority of the dams is localized in the north of Algeria given its climatic and topographic conditions, and seven dams are located within the coastal watershed of Algiers which is a relatively small watershed with respect to the area (12,000 km²) compared to others, but it is an important one due to the economic and demographic importance of the region. In fact, more than 8 million citizens are living in this watershed. The risks of soil degradation and dam silting are real and need a thorough investigation in order to localize the concerned zones and to estimate the erosion and sediment yield levels. Global estimation of the annual silting rate in Algeria is about 0.65% of the total storage capacity (Remini et al. 2009), which represents a financial impact of 25 million dollars according to the international standards and to the financial estimation of the Dams National Agency (ANBT).

For the present study, we have investigated the global rainfall over a period of more than 35 years using 46 rainfall recording stations. The same method is applied to explore the sediments and flows using 20 hydrometric stations within the catchment area, and 9 outside, in order to get a good spatial information distribution. The resulting map can help decisionmakers to focus on the most erodible zones when elaborating the watershed strategy management plan, especially concerning the increase the of forest cover.

A. Ammari (✉)
Ecole Nationale Supérieure d'Hydraulique, LGEE, 09029 Blida,
Algeria
e-mail: a.ammari@ensh.dz

B. Remini
Blida1 University, 09015 Blida, Algeria

2 Materials and Methods

The Coastal Algiers watershed is a hydrologic connection of some basins located in the central part of the Algerian Coast. It covers a total area of 12,000 km², with an average length of 500 km and width of 25 km Fig. 1.

After studying the entirety of the available rainfall data, we deduce that it varies from 1100 mm/year in the Sebaou basin in the eastern part, to 500 mm of rainfall expected in the Coastal Tenes basin in the west, (Fig. 2), with a mean rainfall of 700 mm over the whole watershed. The watershed is bordered and essentially consisting of mountains, Djurdjura in Sebaou basin in the east, Blida Atlas and Ganntas Mountain in the central part, and Hannougouf, Sidi Bamous, and Rokba Mountains in the west. Most of the topography is represented by mountains varying from 2300 m in altitude (Lala Khadidja, Djurdjura Mountain) in the east, to 1550 m (Le refuge, Chr ea mountain, south of Blida), 905 m (Chenoua mountain near Tipaza), and 400 m in the extreme west of the watershed. The largest plain is the Mitidja, which represents 12% of the global area, where the average of altitudes is around 100 m. We have seven dams in the watershed, from the oldest one, which was constructed during the nineteenth century (Meurad) to the most recent one (Keff Eddir). According to the National Dams Agency, the silting phenomena is not very important except in Mostakbal Dam on Bouroumi Wadi with a mean of 0.8 million m³/year, but we have to be careful, as it can

increase with the drought and also with the reduction of the forest cover.

2.1 Results

The ANRH has 75 rainfall record stations over the whole watershed, but not all are in function. The data were collected from 46 record stations, from which only 42 were retained since they have complete and homogeneous data over a period of 35 years (1975–2010). We reconstructed the rainfall data using PCA analysis (principal component analysis) and we obtained mean rainfall over the subwatersheds of the study zone. Figure 2 shows the mean rainfall of subwatersheds of Coastal Algiers arranged from the west to the east. We can observe the rise of the rainfall in the eastern part of the country.

The flow estimation is very important to see the storage possibilities and water inputs of different dam sites. We used the data of twenty hydrometric stations distributed over the whole hydrographic network of the hydrographic basin for a mean period of twenty years, Fig. 3.

We obtained the following results at each hydrometric station, Fig. 4. It is clear that the most important part of the annual flow is yielded by the Sebaou basin (from Baghlia to Tifezouine station), and Barghlia is the main station Fig. 4.

The estimation of the specific erosion, which is the ratio between the sediment yield and the area, is the first step for

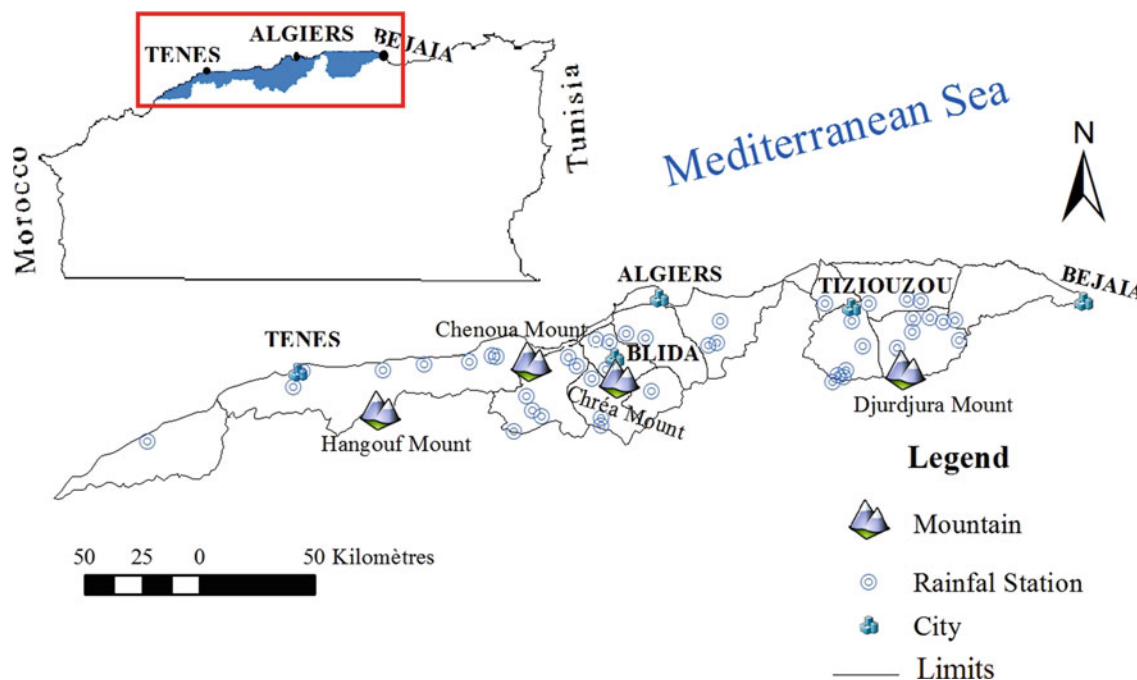


Fig. 1 Geographic situation of the watershed and rainfall stations repartition

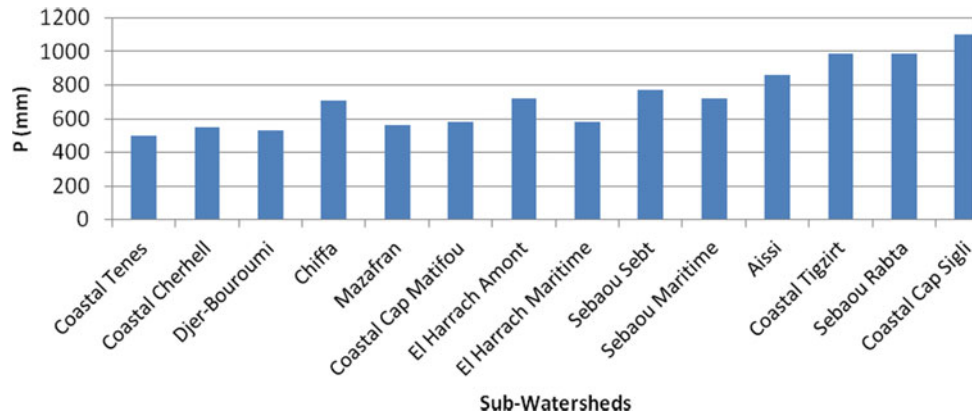


Fig. 2 Mean annual rainfall

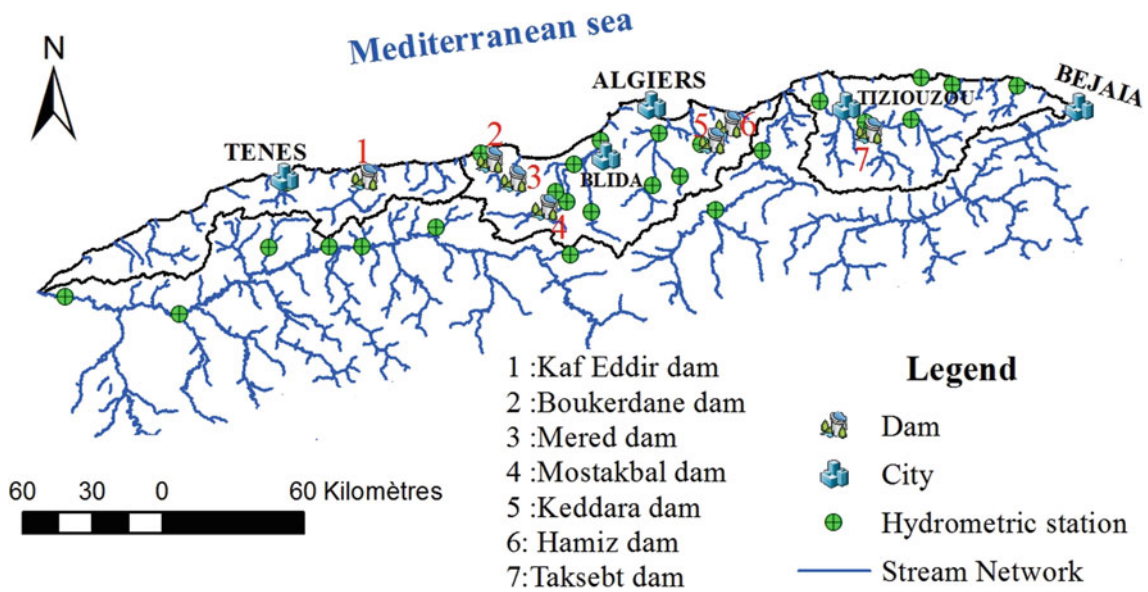


Fig. 3 Hydrometric stations and dams' localization map

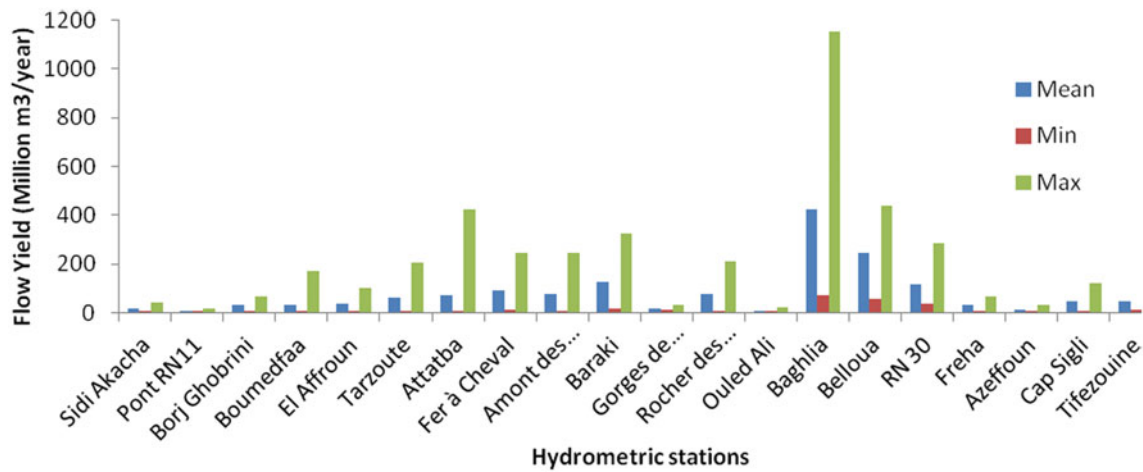


Fig. 4 Interannual flow

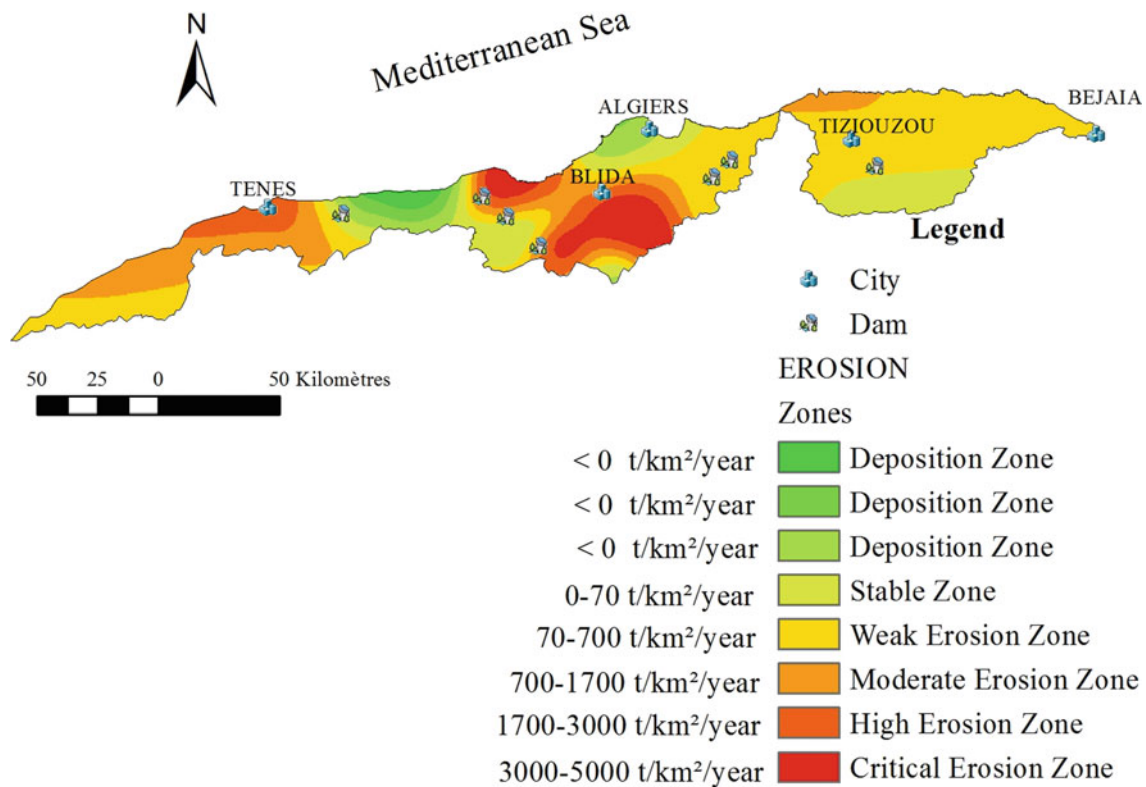


Fig. 5 Soil erosion map

the mapping of this parameter over the watershed, and we used the data of sediment concentration of the twenty hydrometric stations within the watershed but also nine other stations from Isser and Cheliff neighboring basins in order to get a better estimation along the contour limits, using statistical approach to obtain the best relationships between liquid and sediment yields. We obtained the map of Fig. 5 using the spline interpolation method which is widely used in such cases, and it allows us to localize deposition zones which are difficult to obtain by other interpolation techniques used before on the same region.

3 Discussion

We can see on the map a vulnerable erosion zone upstream Bouroumi, Chiffa and Wadi Djer Basins, south of Bliba city, which can be described as weak geological formation constituted essentially by Demmak (1982). Another vulnerable zone is observed in the Oued El Hachem Basin in the Coastal Chechell basin west of Algiers where two dams, Boukerdane and Meurad, are located. This zone is formed by weak lithology in most parts: limestones and sandstones of Miocene and Cretaceous shales representing 69% of the basin. The erodible formations are also marls and upper Cretaceous clay which form 16% of the basin (Ammari and

Remini 2012). We also observe a deposition zone (negative specific erosion) over the Mitidja plain, which is an alluvial plain, and also in the east of Damous where there is a low drainage network. Also, we consider that zones where the erosion is less than 70 t/km²/year as very low erosion zones, and, therefore, they are almost stable, because in Algeria a region with less than that value is not considered as an erosion-concerned zone.

4 Conclusions

The study allows us to localize the most important erosion zones with more than 1700 t/km²/year, in order to focus on the watershed management strategy to preserve root zone of soils and dams from the silting phenomena. We recommend the development of the forest areas and other tools to reduce the erosion and still to compare these results with remote sensing approach and land-use data in order to get more details on the dynamics and evolution of the erosion phenomenon over the Coastal Algiers watershed.

Acknowledgements Thanks to the National Water Resources Agency (ANRH) for the hydrological and geological data provided. This work was done in the framework of Young Teams, at the ENSH Blida, associated with the IRD (Jeunes Équipes Associées à l'IRD).

References

- Ammari, A., Remini, B.: Vulnérabilité à l'envasement des Barrages. Cas du bassin Hydrographique Côtiers Algérois. Phd Thesis. Biskra University. Algeria (2012)
- Demmak, A.: Contribution à l'étude de l'érosion et des transports solides en Algérie Septentrionale. Thèse de Docteur-Ingénieur. Université Paris 6. France (1982)
- Remini, B., Hallouche, W., Achour, B.: L'Algérie: Plus d'un siècle de désenvasement des barrages. L'état des ressources en eau du Maghreb. UNESCO, pp. 123–142 (2009)



Climate Change and Its Impact on Runoff and Sediment Yield (Case Study: Dez River Dam, Iran)

Mohammad Reza Eini, Kourosh Mohammadi, Reza Najib, Saman Javadi, and Golmar Golmohammadi

Abstract

Climate change is one of the leading topics in today's research because of its large-scale impact on hydrological processes. Simulation models like SWAT can be used to investigate the impact of climate change if they are calibrated and validated properly. In this research, a watershed in southwestern Iran was used as a case study and runoff and sediment calibrated with good performances for duration of 1990–2010 and validated from 2010 to 2017. The results showed that precipitation and temperature have a major upward trend. In addition, climate change increases the runoff and sediment yields in the watershed. Moreover, garden crops would be increased while cereal yields would be decreased.

Keywords

Erosion • Water security • Rainfall runoff • Sediment yield • SWAT model

1 Introduction

Universal climate change is one of the leading factors that directly affect hydrological processes (Zhang et al. 2018). In this regard, global warming is recognized as a significant issue resulting from climate change during the coming century

M. R. Eini · S. Javadi
College of Aburaihan, University of Tehran, Tehran, Iran

K. Mohammadi (✉)
HLV2K Engineering, Mississauga, ON L5L 1X2, Canada
e-mail: kourosh.mohammadi@HLV2K.com

R. Najib
Food and Agriculture Organization of the United Nations, Rome, Italy

G. Golmohammadi
University of Guelph, Guelph, ON, Canada

(Pirnia et al. 2019). Possible impacts of changes in climate including temperature and rainfall have caused variations in hydrological processes such as evapotranspiration, surface runoff, timing and magnitude of streamflow, and flood events (Arar and Chenchouni 2014; Neupane and Kumar 2015). Since the impacts are expected to have diverse influences across a region, different spatial and temporal distributions are created for water resources components. Moreover, temperature variation and wind speed affect evaporation and transpiration sub-processes, which have direct influence on the surface and subsurface water budgets. Also, semi- and fully distributed models could improve the results of estimation of future conditions (Choubin 2019; Eini 2018).

There have been several investigations of climate change and runoff or sediment in different watersheds. The climate change effect on runoff and sediment variation using SWAT model in the Purna river basin in India, considering two scenarios of RCP4.5 and RCP8.5, showed an increase from 7 to 17% for runoff, and from 2 to 16% for sediments. These changes are similar to those of the present study (Nilawar and Waikar 2019). Moreover, Tan et al. (2017) estimated that surface runoff in all tropical regions of Malaysia would increase under all RCP scenarios in future periods between 14 and 27%. On the other hand, in a basin in Alberta, Canada, it was found that sediment under the effect of climate change will face an increase of 5–25% in different regions (Shrestha and Wang 2018).

The aim of this study is to assess the effects of climate change on sediments and runoff in the upper basin of an important dam in Iran. This dam is the source of water for agriculture, electricity, industry, and drinking purposes.

2 Materials and Methods

2.1 Case Study

The Dez River watershed is a sub-basin of the Karoon Watershed (Fig. 1). The watershed has long-term annual

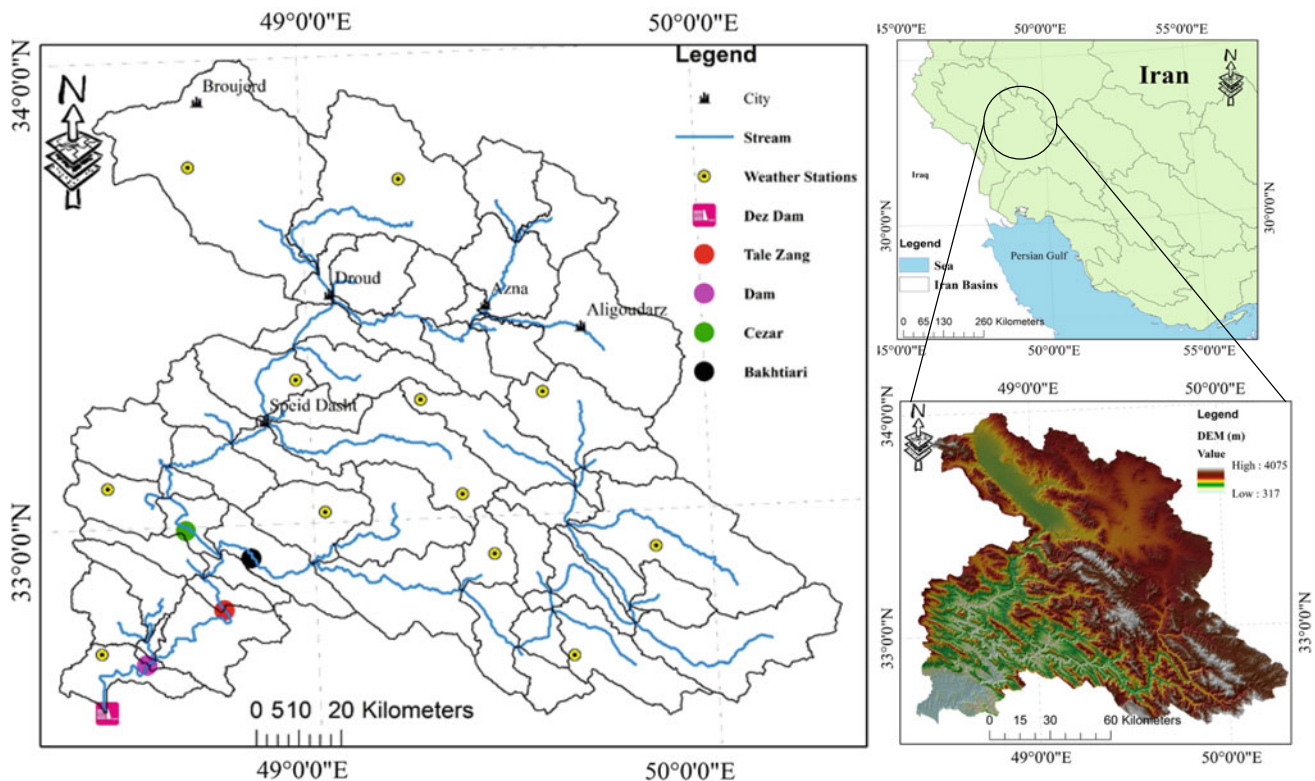


Fig. 1 Location of the study area, streams, Dez dam, and digital elevation map (DEM)

average rainfall of 700 mm with maximum and minimum temperatures of 27 °C and 12 °C, respectively. This watershed is situated in the highlands of the western and south-eastern Zagros Mountains, and it is considered as one of the most densely populated areas of the country. The dominant atmospheric precipitation in this region is snowy in the autumn and winter seasons (October to March). A large portion of annual runoff from the watershed originates from the melting of the snow from late winter to late spring (March to May).

2.2 Developing the SWAT Model

SWAT is a long-term, continuous, physically distributed model developed for predicting the effect of land management practices on the hydrology, sediment yield, and water quality in agricultural watersheds (Arnold et al. 2012; Eini et al. 2019).

In this study, ArcSWAT2012 was used, as a visual interface to prepare a SWAT model (version 2012) within ESRI ArcMap 10.2. The model was set up using a 10 m digital elevation map, the global soil map provided by the FAO (Fischer et al. 2008) with a resolution of 10 km and the

GLCC (https://lta.cr.usgs.gov/glcc/globe_int) land use map with a resolution of 1 km were used.

2.3 Downscaling of AOGCMs

In this research, five Atmosphere–Ocean General Circulation Models (AOGCM) considering two Representative Concentration Pathway (RCP) scenarios, RCP 4.5 and RCP 8.5, were applied for the near period (2021–2040). These two scenarios illustrate the optimistic and pessimistic situations in the future.

3 Results and Discussion

3.1 Runoff and Sediment Simulation

In this research, the SWAT model showed reasonable performance in runoff, as well as sediment calibration and validation in monthly time steps in the discharge stations. Table 1 shows Nash Sutcliffe Efficiency (NSE) and coefficient of determination (R^2) values in the calibration (1990–2010) and validation (2010–2017) periods.

Table 1 Simulation results in calibration (1990–2010) and validation (2010–2017) periods

Discharge station	Runoff				Sediment			
	Calibration		Validation		Calibration		Validation	
	R ²	NS	R ²	NS*	R ²	NS	R ²	NS*
Cezar	0.77	0.75	0.62	0.61	0.73	0.75	0.59	0.72
Bakhtiari	0.71	0.62	0.60	0.55	0.65	0.69	0.68	0.70
Tale Zang	0.81	0.74	0.61	0.69	0.68	0.69	0.62	0.61
Dam	0.84	0.77	0.70	0.70	0.67	0.71	0.61	0.66

The results showed that SWAT had relatively better performance in the calibration period in comparison with the validation period, both for runoff and sediments. This is usually expected for validation. The Bakhtiari sub-watershed had the lowest performances possibly due to the lower quality and more errors in field data. More investigation is required to assess the quality of data in the watershed.

3.2 Impact of Climate Change on Runoff and Sediment Yield

Monthly changes of precipitation and max–min temperatures were also applied to the developed SWAT model after the calibration and validation processes. Runoff variations in the RCP4.5 scenario did not show any unreasonable changes in the runoff amount, and changes will take place as time displacement. In addition, in spring, there is an increase in runoff in all scenarios. For instance, in June, 154 cubic meters per second (m³/s) in the base period will change, for RCP 4.5 and RCP 8.5, to 205 m³/s and 199 m³/s, respectively. Runoff variations in the RCP8.5 scenario indicated an increase in runoff magnitude during the spring and summer seasons. However, with an increase of about 3.5° of melting temperature, it will happen earlier with more intense evapotranspiration.

In general, the average runoff in the coming period will rise from 208 m³/s in the baseline period to about 228 m³/s in both scenarios (about 9% increase in each scenario). The results also showed that runoff variations in each scenario would be similar to each other, with a slight increase in the RCP8.5 scenario. Similar to these variations, sediment yield has also increased by approximately 6% in each scenario, from 13 to 19%.

4 Conclusions

In this study, the SWAT model was applied to simulate Dez River watershed. In general, climate change scenarios (RCP 4.5, RCP 8.5) showed favorable conditions in terms of temperature and rainfall in the future for a semi-arid region.

The model showed a good capability in simulating the runoff and sediment yield with an average accuracy of $R^2 = 75\%$. The results of the climate change scenarios showed that climate change increases the runoff rates. For example, an increase from 154 m³/s to 205 and 199 m³/s was predicted for runoff in both scenarios. An increase from 13 to 19% was projected for sediment yield.

References

- Arar, A., Chenchouni, H.: A “simple” geomatics-based approach for assessing water erosion hazard at montane areas. *Arab. J. Geosci.* **7** (1), 1–12 (2014)
- Arnold, J.G., et al.: SWAT: model use, calibration, and validation. *Trans. ASABE* **55**, 1491–1508 (2012)
- Choubin, B.: Streamflow regionalization using a similarity approach in ungauged basins: application of the geo-environmental signatures in the Karkheh River Basin, Iran. *Catena* **182**, 2182 (2019)
- Eini, M.R.: Discussion of ‘Intra- and interannual streamflow variations of Wardha watershed under changing climate (2018) by Naga Sowjanya P., Venkata Reddy K. & Shashi M. (*ISH Journal of Hydraulic Engineering*, <https://doi.org/10.1080/09715010.2018.1473057>) *ISH J. Hydraul. Eng.* **27**(4), 474–475 (2021). <https://doi.org/10.1080/09715010.2018.1564376>
- Eini, M.R., Javadi, S., Delavar, M., Monteiro, J.A.F., Darand, M.: High accuracy of precipitation reanalyses resulted in good river discharge simulations in a semi-arid basin. *Ecol. Eng.* **131**, 107–119 (2019)
- Fischer, G., et al.: Global agro-ecological zones assessment for agriculture (GAEZ 2008). *Camb* (2008)
- Neupane, R.P., Kumar, S.: Estimating the effects of potential climate and land use changes on hydrologic processes of a large agriculture dominated watershed. *J. Hydrol.* **529**, 418–429 (2015)
- Nilawar, A.P., Waikar, M.L.: Impacts of climate change on streamflow and sediment concentration under RCP 4.5 and 8.5: a case study in Purna river basin, India. *Sci. Total Environ.* **650**, 2685–2696 (2019)
- Pirmia, A., et al.: Contribution of climatic variability and human activities to stream flow changes in the Haraz River basin, northern Iran. *J. Hydro-Environ. Res.* **25**, 12–24 (2019)
- Shrestha, N.K., Wang, J.: Predicting sediment yield and transport dynamics of a cold climate region watershed in changing climate. *Sci. Total Environ.* **625**, 1030–1045 (2018)
- Tan, M.L., Ibrahim, A.L., Yusop, Z., Chua, V.P., Chan, N.W.: Climate change impacts under CMIP5 RCP scenarios on water resources of the Kelantan River Basin Malaysia. *Atmos. Res.* **189**, 1–10 (2017)
- Zhang, L., Cheng, L., Chiew, F., Fu, B.: Understanding the impacts of climate and landuse change on water yield. *Curr. Opin. Environ. Sustain.* **33**, 167–174 (2018)



Investigation of Hydrological Variability in Medjerda Watershed (NW Tunisia)

Hamida Cherni, Imen Turki, Zeineddine Nouaceur, Nicolas Iecoq, Walid Oueslati, Mohsen Ben Alaya, Valérie Mesnages, and Radhia Souissi

Abstract

Climate change is one of the major global issues of our time with a direct impact on the hydrological system. It increases the frequency of extreme weather events, especially droughts and floods. Ten rainfall and hydrological stations, with continuous monthly precipitation and streamflow records over the period 1965–2017, were considered in the analysis to understand the hydrological variability (precipitation and streamflow) in Medjerda's basin (Northern Tunisia), one of the main rivers of Tunisia. This study also aimed to examine the influence of the dominant climatic patterns in the hydrological system [North Atlantic Oscillation (NAO), the Sea Surface Temperature (SST), Southern Oscillation Index (SOI), El Niño Southern Oscillation (ENSO), and Mediterranean Oscillation Indices (MOI)]. A “Bertin matrix” chronological graphical method and wavelet coherence analysis were also used to determine the different periods of dry and wet cycle changes and to identify and describe the variability in Medjerda stream-

flows. The statistical analyses show that the rainfall in the basin of Medjerda varies widely on the temporal scale, but it follows the same variation in all the stations. This analysis also shows that the streamflow variation in rivers changes over time and from upstream to downstream, with a fairly fast and strong hydrological response upstream, and a medium to low downstream disturbance. This phenomenon is affected by several conditional factors of the flow (lithology, vegetation, morphology, ...). The wavelet coherence analysis did not show a coherence between NAO/streamflow and precipitation/NAO identified at the inter-annual scale in the basin of Medjerda. Therefore, we can conclude that the phenomenon is not the same as the one in Algeria and Morocco.

Keywords

Medjerda • Hydrological variability • Precipitation • Streamflow • Climatic patterns (NAO MOI • AMO)

H. Cherni (✉) · M. Ben Alaya · R. Souissi
Laboratory of Useful Materials, National Institute of Research and Physico-Chemical Analysis Technopole, 2020 Sidi Thabet, Ariana, Tunisia

I. Turki · N. Iecoq · V. Mesnages
Morphodynamic Continentale and Coastal Laboratories (UMR CNRS M2C), University of Rouen, 76130 Mont-Saint-Aignan, France

Z. Nouaceur
Laboratory UMR CNRS 6266 IDEES, Department of Geography, Planning, Environment, The University of Rouen, 76130 Mont-Saint-Aignan, France

W. Oueslati
Laboratory of Mineral Resources and Environment, Department of Geology Faculty of Sciences of Tunis, University of Tunis El Manar, Tunis El Manar, Tunisia

1 Introduction

Climate change has major impacts on water quality, flooding, runoff, and many other environmental factors (Scavia et al. 2002). Indeed, global change is a great challenge for the hydrological scientific community to improve our understanding of the impacts of climate fluctuations on water resources (Massei et al. 2017; Cloke and Hannah 2011; Negm et al. 2020).

The climate in Tunisia is mostly semi-arid with a strong Mediterranean influence which leads to a high variability of the river discharges, and the rainfall follows a high spatial and temporal variability. That is why, ten rainfall and hydrological stations, with continuous monthly precipitation and streamflow records over the period 1965–2017, were considered in the analysis to understand the hydrological

variability (precipitation and streamflow) in Medjerdah's basin ($23,700 \text{ km}^2$) (Fig. 1), one of the main rivers in Tunisia, as much by its length, the surface of its watershed as by the volume of water which it carries.

2 Data and Methods

The Medjerda basin is a very fragile environment. Due to its location in the humid part of the country, the basin is the setting for an intense agricultural activity, and its water resources are highly exploited. It is characterized by a sub-humid to semi-arid climate, with a mean annual rainfall on the watershed of 480 mm year^{-1} (1950–1979) (Rodier et al. 1981). The rainfall pattern is irregular in time and in space, from 1965/1966 to 2016/2017. Ghardimaou shows an annual rainfall of 460 mm; SidiSalem Barrage, 417 mm; and Oued Mallegue 300 mm.

Monthly rainfall and streamflow data, extracted between 1965 and 2017 and without missing values, are considered in the analysis to understand the hydrological variability (precipitation and streamflow) and to define the wet and dry periods in Medjerdah's basin. A statistical analysis was carried out such as the cross-correlation (ccf) which is a function used to determine the lag at which the correlation between two time series is strongest to measure the hydrological response. The method of CWT was applied in this study for a time–frequency, spectral decomposition. It aims to examine the influence of the dominant climatic patterns in the hydrological system [North Atlantic Oscillation (NAO), the Atlantic Multidecadal Oscillation (AMO), and Mediterranean Oscillation Indices (MOI)]. The “Bertin matrix” chronological graphical method and wavelet coherence analysis are also used to determine the evolution of dryness and wetness periods and to identify and describe variability in Medjerda streamflows.

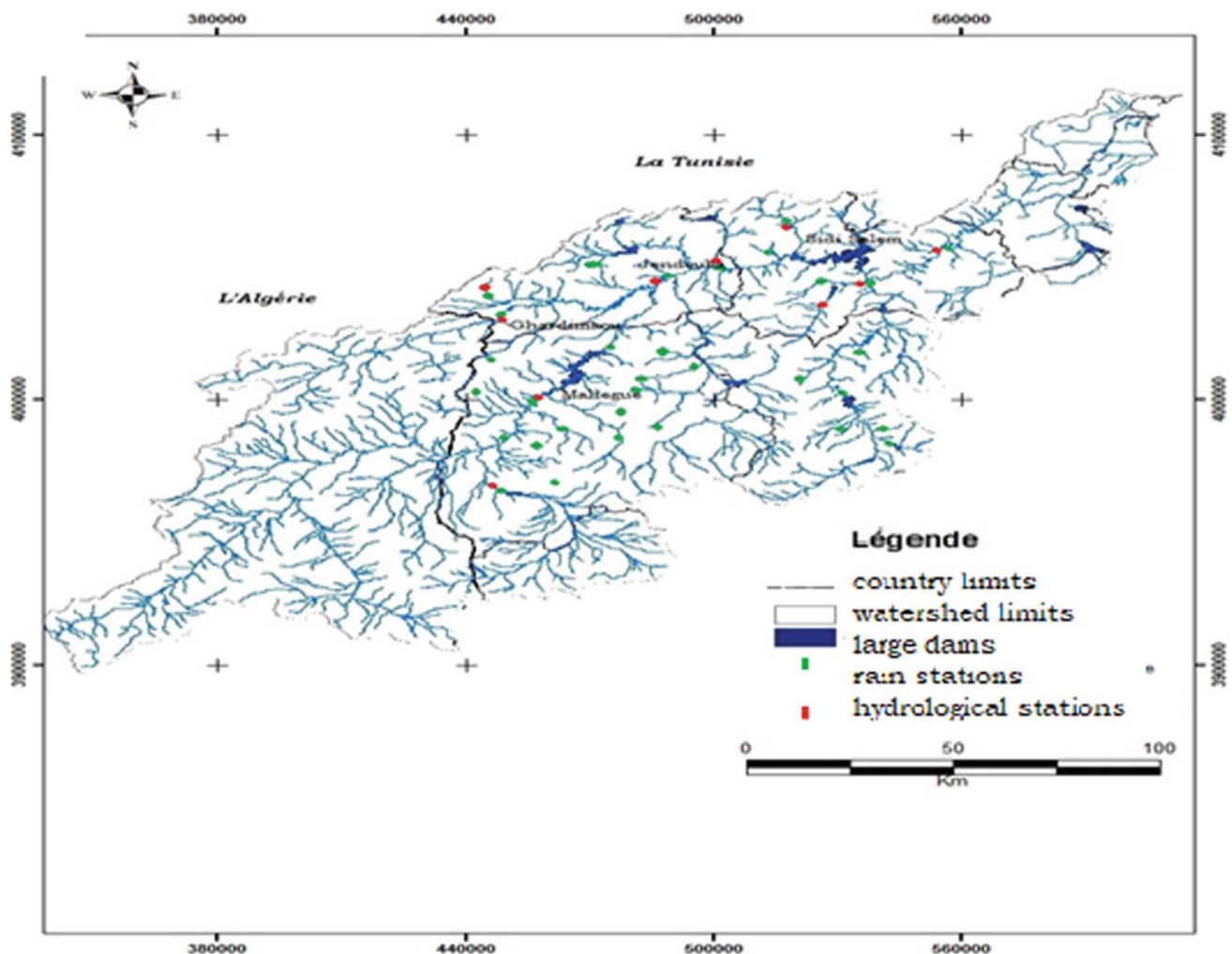


Fig. 1 Study area: the watershed of Medjerdah

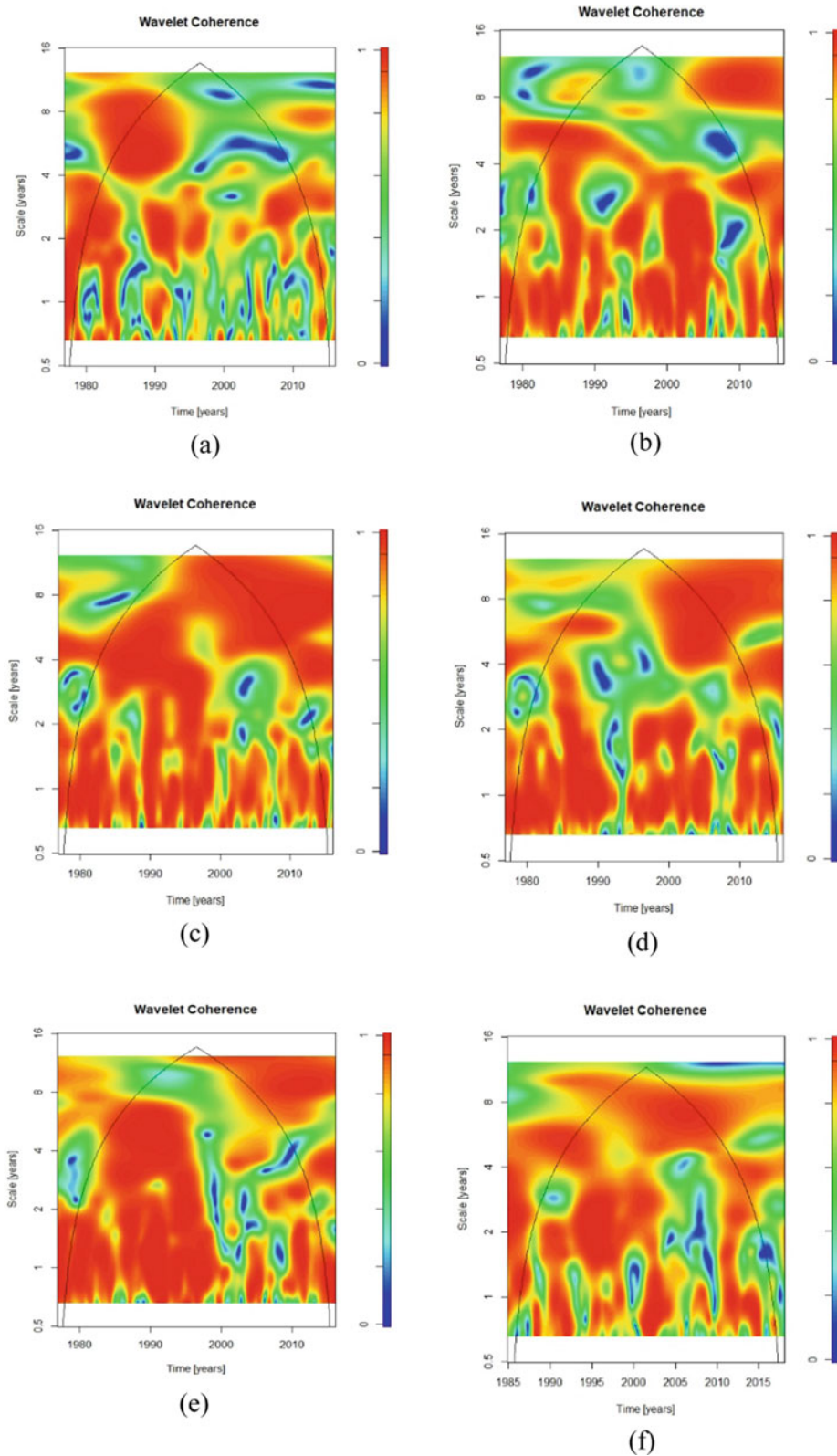


Fig. 2 Continuous wavelet transformation of the coherence between monthly precipitation time series and streamflow in Medjerda basin. **a** Bou Salem station, **b** Ghardimaou basin, **c** Jendouba station, **d** Raghai station, **e** Sarath station, and **f** Slouguia station

3 Results and Discussion

The rainfall variability in Medjerda's basin was analyzed using simple statistical methods. These statistical analyses showed that the rainfall in the basin of Medjerda was very variable on the temporal scale, but it followed the same variation in all the stations. This analysis also showed that the streamflow variation in rivers changed over time and from upstream to downstream with a fairly fast and strong hydrological response upstream and medium to low downstream disturbance. This phenomenon was affected by several conditional factors of the flow (lithology, vegetation, morphology, etc.). Bertin's matrix allowed us to determine three different cycles between 1965 and 2016: A variable cycle from 1965 to 1973, a second cycle that had a long dry period between 1974 and 1995, and the last had a long wet period between 1996 and 2015.

The continuous wavelet spectrum of the coherence between the monthly precipitation and the streamflow of Medjerda basin is presented in Fig. 2; where three principal energy bands can be extracted: 1y band, observed during the study period, 2–4y and 4–8y bands, which were discontinuous in time (Fig. 2). The wavelet coherence analysis identified the percentage coherence between precipitation, streamflow, and climate partners. The NAO contribution in Medjerda's precipitation varies for the different modes of variability at the inter-annual scale in the basin of Mejadra. Therefore, we can conclude that we have the same phenomenon as in Algeria, Morocco, and France. In Marrakech and Algeria (Turki et al. 2016a; b), the coherence of the NAO and rainfall was between 40 and 60%, and it was demonstrated in the Seine (river in France) precipitation studied by Massei et al. (2007).

4 Conclusion

The hydrological variability in the Medjerda basin and the possible links with the climate fluctuations were studied in this paper. The climate in Tunisia is mostly semi-arid with a strong

Mediterranean influence, which leads to a high variability of the river discharges, and the rainfall follows a high spatial and temporal variability. The wavelet coherence analysis did not show a coherence between NAO/streamflow and precipitation/NAO identified at the inter-annual scale in the basin of Medjerda. Therefore, we can conclude that the phenomenon is not the same as the one in Algeria and Morocco.

References

- Cloke, H.L., Hannah, D.M.: Large-scale hydrology: advances in understanding processes, dynamics and models from beyond river basin to global scale. *Hydrol. Process.* **25**(7), 991–995 (2011). <https://doi.org/10.1002/hyp.8059>
- Massei, N., Dieppois, B., Hannah, D.M., Lavers, D.A., Fossa, M., Laignel, B., Debret, M.: Multi-time-scale hydroclimate dynamics of a regional watershed and links to large-scale atmospheric circulation: Application to the Seine river catchment, France. *J. Hydrol.* **262–275** (2017). <https://doi.org/10.1016/j.jhydrol.2017.01.008>
- Massei, N., Durand, A., Deloffre, J., Dupont, J.P., Valdes, D., Laignel, B.: Investigating possible links between the North Atlantic Oscillation and rainfall variability in Northwestern France over the past 35 years. *J. Geophys. Res.* **112**, D09121 (2007). <https://doi.org/10.1029/2005JD007000>
- Negm, A., Bouderbala, A., Chenchouni, H., Barcelo, D.: *Water Resources in Algeria - Part I: Assessment of Surface and Groundwater*. Springer, Cham (2020). <https://doi.org/10.1007/978-3-030-57895-4>
- Rodier, J.A., Colombani, J., Claude, J., Kallel, R.: *Le bassin de la Medjerda*. Monographies hydrologiques de l'ORSTOM, 451p (1981)
- Scavia, D., Field, J.C., Boesch, D.F., Buddemeier, R.W., Burkett, V., Cayan, D.R., Fogarty, M., Harwell, M.A., Howarth, R.W., Mason, C., Reed, D.J., Royer, T.C., Sallenger, A.C., Titus, J.G.: Climate change impacts on U.S. Coast. Mar. Ecosyst Estuaries **25**(2), 149–164 (2002). <https://doi.org/10.1007/bf02691304>
- Turki, I., Laignel, B., Laftouhi, N., Nouaceur, Z., Zamrane, Z.: Investigating possible links between the North Atlantic Oscillation and rainfall variability in Marrakech (Morocco). *Arab. J. Geosci.* **9**, 243 (2016a). <https://doi.org/10.1007/s12517-015-2174-z>
- Turki, I., Laignel, B., Massei, N., Nouaceur, Z., Benhamiche, N., Madani, K.: Hydrological variability of the Soummam watershed (Northeastern Algeria) and the possible links to climate fluctuations. *Arab. J. Geosci.* **9**, 477 (2016b). <https://doi.org/10.1007/s12517-016-2448-0>



Water Quality Variation Along the Tigris River

Ali Chabuk, Nadhir Al-Ansari, Ali Almaliki, Jan Laue,
and Hussain M. Hussain

Abstract

The Tigris and Euphrates Rivers are the main water resources for Iraq. Recently, Iraq has experienced water shortage problems due to the climate change and the construction of dams within the upper parts of the catchment. In this work, the total dissolved salts (TDSs) along the Tigris River were measured in eleven stations during wet and dry seasons. The interpolation method (IDW) in ArcGIS was used to generate the interpolation for TDS in the wet and dry seasons in the Tigris River. The regression prediction was used between the three measured and the observed values in the other three stations. The results showed that the quality of TDS becomes more unsuitable for human use beyond Baghdad toward the south.

Keywords

Total dissolved salts • Water quality • IDW •
Interpolation method • Tigris River • Iraq

1 Introduction

The water resources in the Middle East are scarce. Iraq was considered as an exception due to the presence of the Tigris and Euphrates Rivers. The area of Iraq covers 438,103 km², and its population exceeds 32 million. The total water

consumption in Iraq reaches 42.3 billion m³/year. This is used for agriculture (90%), industry (6%), and human use (4%). Recently, the flow of the Tigris and Euphrates Rivers started to decrease, and Iraq is now facing water shortage problems (Al-Ansari and Adamo 2018; Al-Ansari et al. 2018a, 2018b). This is due mainly to climate change and to the construction of dams in the upper parts of the catchment in neighboring countries.

The Tigris River rises from the southeastern part of Turkey. It is 1718 km long. It drains an area of 472,606 km² (17%, 2%, 29%, and 52% in Turkey, Syria, Iran, and Iraq, respectively). The average flow of the Tigris River was about 21 billion m³ until 1973, when dams started to be built. At that period, the discharge of the river at Baghdad was 1207 m³/s. Now, the discharge is 522 m³/s (ESCWA (Economic and Social Commission for Western Asia) 2013; Al-Ansari 2016).

It has been noticed that, with the decrease of the flow in the Tigris River, the quality of its water is deteriorating (ESCWA (Economic and Social Commission for Western Asia) 2013; Al-Ansari et al. 2018c). In this research, the total soluble salt (TDS) along the Tigris River was studied in 11 locations during the year 2016 to observe the variations in wet and dry seasons.

2 Predicting the TDS Concentration Along the Tigris River Using the Interpolation Method (IDW)

Eleven locations were selected on the Tigris River from the northern part near the Turkish–Iraqi border to the southern part near the confluence of the Tigris and Euphrates Rivers (Fig. 1). The total dissolved salts (TDSs) from all these stations were measured in the year 2016 during the wet season (October to March) and the dry season (April to September). Three stations (Al-Shraqat, Al-Tarmiyah, and Ali Al-Garbi) were used for prediction after implementing

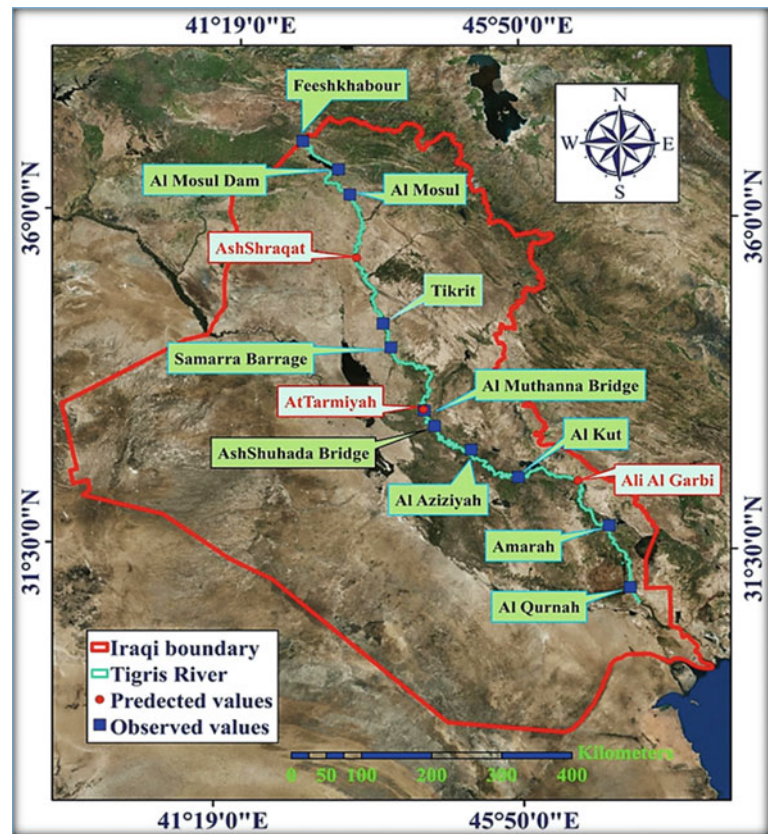
A. Chabuk
University of Babylon, Al Hilla, 51001, Iraq

N. Al-Ansari (✉) · J. Laue
Lulea University of Technology, 971 87 Lulea, Sweden
e-mail: nadhir.alansari@ltu.se

A. Almaliki
Ministry of Science and Technology, Baghdad, 10001, Iraq

H. M. Hussain
University of Kufa, Kufa, 54003, Iraq

Fig. 1 Tigris River map and the stations that were used for measuring the different parameters



the interpolation between the eleven points using the inverse distance weighted (IDW) method in ArcGIS (10.5). This method was used to generate the interpolation for each map of a parameter in the wet and dry seasons in the Tigris River. The IDW technique is principally reflected in the first law of Waldo Tobler in geography (Tomislav 2009). The IDW method depends on a technique of accurate local deterministic interpolation (Watson and Philip 1985). According to Panhalkar and Jarag (2015), the IDW method is considered more suitable than other methods (e.g. kriging and Topo to Raster), because these methods generate an interpolation for the selected points with more deviation.

3 Results and Discussion

Figure 2 shows the predicted maps for the TDS concentrations along the Tigris River for wet and dry seasons through measuring the TDSs at eleven locations from the north toward the south. The results evidently showed that the TDS values were increasing toward the south (Fig. 3). This increase is related to several reasons. These are:

- Construction of dams and related irrigation projects: This is where evaporation increases to reach about 8 billion m^3 (Al-Ansari and Adamo 2018; Hillel 1994; Abbas et al. 2018). In addition, the backwater to the river from irrigation projects is another factor which contributes to increasing the salinity of the water.
- Wastewater and waste of war: About 83% of wastewater is directly discharged into the rivers (Geopolicy 2010). Waste from the two Gulf wars is another source of contamination.
- Population growth rates: This rate is considered very high, particularly in Iraq. Besides, most of the population in riparian countries resides on the banks of the rivers (Worldmeters 2018).

For the wet and dry seasons, the regression prediction between three observed values and predicted values (resulted from predicting maps) was used (Fig. 4). These three stations are: Al-Shraquat, Al-Tarmiyah, and Ali Al-Garbi. The results showed that the coefficient of determination (R^2) between the observed and the predicted values was high.

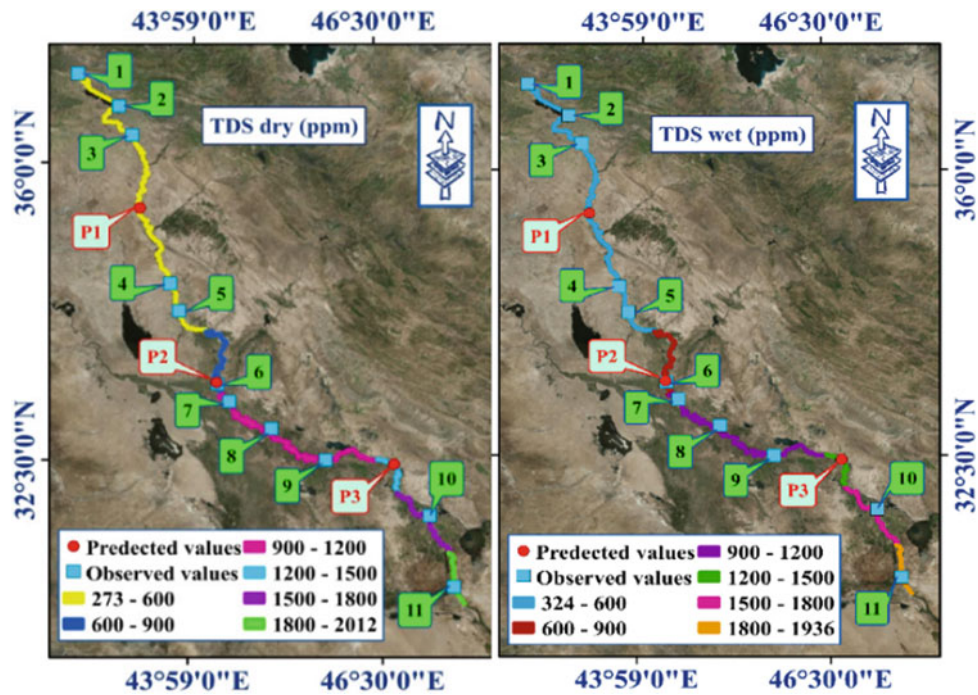


Fig. 2 TDS variation along the Tigris River in wet and dry seasons

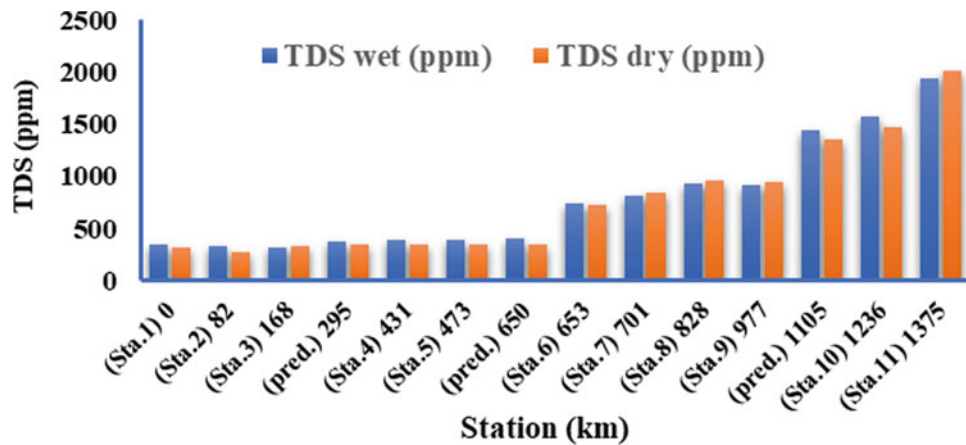


Fig. 3 TDS variation at the selected stations with their respective distance along the Tigris River

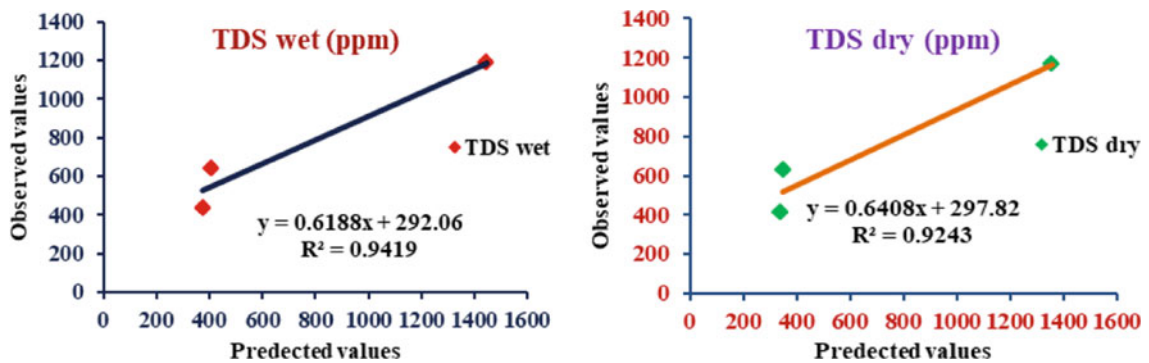


Fig. 4 Relationship between observed and predicted values for TDS in the Tigris River for the wet and dry season

4 Conclusions

The current study was conducted to measure the TDS concentrations in the Tigris River in 2016. The IDW interpolation method in ArcGIS was used to generate the TDS values along the Tigris River, where eleven stations were selected on the River for predilection purposes. Three stations were then used to confirm the values that resulted from the predicting maps using the IDW method within GIS. Generally, the flow of the Tigris River is decreasing with time while the salinity of water and soil is increasing. The water becomes improper for human consumption in the south of Baghdad. This is due to several factors such as the extensive backwater flow from irrigation projects as well as industrial activities.

References

- Abbas, N., Wsaimi, S., Al-Ansari, N., Sultana, N.: Water resources problems of Iraq: climate change adaptation and mitigation. *J. Environ. Hydrol.* **26**(6), 1–11 (2018)
- Al-Ansari, N.A.: Hydropolitics of the Tigris and Euphrates Basins. *Engineering* **8**, 140–172 (2016)
- Al-Ansari, N.A., Adamo, N.: Present water crises in Iraq and its human and environmental implications. *Engineering* **10**(6), 305–319 (2018)
- Al-Ansari, N., Adamo, N., Sissakian, V., Knutsson, S., Laue, J.: Water resources of the Tigris River catchment. *J. Earth Sci. Geotechn. Eng.* **8**, 21–42 (2018a)
- Al-Ansari, N., Adamo, N., Sissakian, V., Knutsson, S., Laue, J.: Geopolitics of the Tigris and Euphrates Basins. *J. Earth Sci. Geotechn. Eng.* **8**, 187–222 (2018b)
- Al-Ansari, N., AlJawad, S., Adamo, N., Sissakian, V., Laue, J., Knutsson, S.: Water quality within the Tigris and Euphrates catchments. *J. Earth Sci. Geotechn. Eng.* **8**(3), 95–121 (2018c)
- ESCWA (Economic and Social Commission for Western Asia): Inventory of shared water resources in western Asia. Salim Dabbous Printing Co., Beirut, pp. 626 (2013)
- Geopolicity: Managing the Tigris-Euphrates watershed: the challenge facing Iraq, part III structural drivers of change. 24 (2010)
- Hillel, D.: *Rivers of Eden: the struggle for water and the quest for peace in the Middle East*. Oxford University Press, New York (1994)
- Panhalkar, S.S., Jarag, A.P.: Assessment of spatial interpolation techniques for river bathymetry generation of Panchganga River basin using geoinformatic techniques. *Asian J Geoinformatics* **15**, 9–15 (2015)
- Tomislav, H.: *Practical guide to geostatistical mapping*, 2nd edn. EUR 22904 EN (2009)
- Watson, D.F., Philip, G.M.: A refinement of inverse distance weighted interpolation. *Geoprocessing* **2**, 315–327 (1985)
- Worldmeters: Countries in the world by population (2018). <http://www.worldometers.info/world-population/population-by-country/>



Physicochemical Quality of Surface Water in the Jijel Region (Northeast Algeria)

Abdelmalek Drouiche, Faouzi Zahi, Taha Hocine Debieche, Hocine Sakta, and Souhil Mahdid

Abstract

The present study aimed to evaluate the physicochemical quality of surface water in the Jijel region. It also aims at identifying the effects of the water pollution in the region and its origin. A total of 31 samples of water were collected from the eastern and western parts of the region and analyzed for different physicochemical parameters. The results obtained showed an organic pollution of river waters from the eastern part, especially downstream of the later with 1.46–5 mg L⁻¹ of ammonium and from 0.12 to 3.67 mg L⁻¹ of nitrites. For the major elements, higher values of the electrical conductivity (approximately 3460 µS/cm) and high concentrations of some chemical elements (e.g., sulfate 509.43 mg L⁻¹) were recorded in the affluent of the Bourchaid River. The rivers of the western part revealed an acceptable physicochemical quality, as the concentration of chemical elements complies with the standards of surface water (system for evaluating the water quality of rivers, version 2).

Keywords

Jijel region • Major elements • Organic pollution • Physicochemical quality • Surface water

1 Introduction

In Algeria, the question of water quality is one of the main environmental issues, because of the sanitary and economic consequences of water pollution. Population growth and

A. Drouiche (✉) · F. Zahi · T. H. Debieche · S. Mahdid
Research Team Water and Environment, Geological Engineering Laboratory, University of Mohamed Seddik Benyahia Jijel, B. P. 98 Ouled Aissa, 18000 Jijel, Algeria

H. Sakta
Department of Earth Sciences and Universe, University of Mohamed Seddik Benyahia, Jijel, Algeria

industrial activities have contributed to pollution and deterioration of the quality of water resources and compromised receiving environment disequilibrium (Negm et al. 2020a, 2020b). Earlier studies in different parts of the world (Derwich et al. 2010; Ghachtoul et al. 2005; Ouhmidou et al. 2015; Gaury et al. 2018; Kumar et al. 2019a, 2019b) and Algeria (Marouf and Remini 2014; Derradji et al. 2007; Belabed et al. 2017; Gaagai et al. 2017) have indicated the influence of anthropogenic activities on the surface water quality and its changing scenario. The Wilaya of Jijel is located in northeastern Algeria (Fig. 1). Its orographic system is mainly mountainous (82%). The geology of the Jijel region (Fig. 1) is composed of (1) metamorphic formations essentially forming the mountains, (2) sedimentary formations, generally forming alluvial plains of wadis, sand dunes, limestone and sandstone formations and (3) magmatic formations.

This study aimed to determine the physicochemical characteristics of surface water and the type and impact of pollution on water quality.

2 Materials and Methods

The concentration of different physicochemical parameters was studied using 20 water samples collected from the eastern part and 11 from the western part of the region during April 2017. An upstream and downstream sample for the wadis of the eastern part and a downstream sample for the wadis of the western part were collected because there is not any anthropogenic activity in the upstream part. Treatment and preservation of water samples were done according to the general guidelines (Grondin 1982; Brittany Water Agency 2006; WHO 2008).

The choice of sampling stations (Fig. 2) was made according to the level of human and industrial activities.

Parameters like temperature, electrical conductivity, redox potential and pH were determined in situ using portable multi-350i meter. The concentrations of Ca²⁺, Mg²⁺,

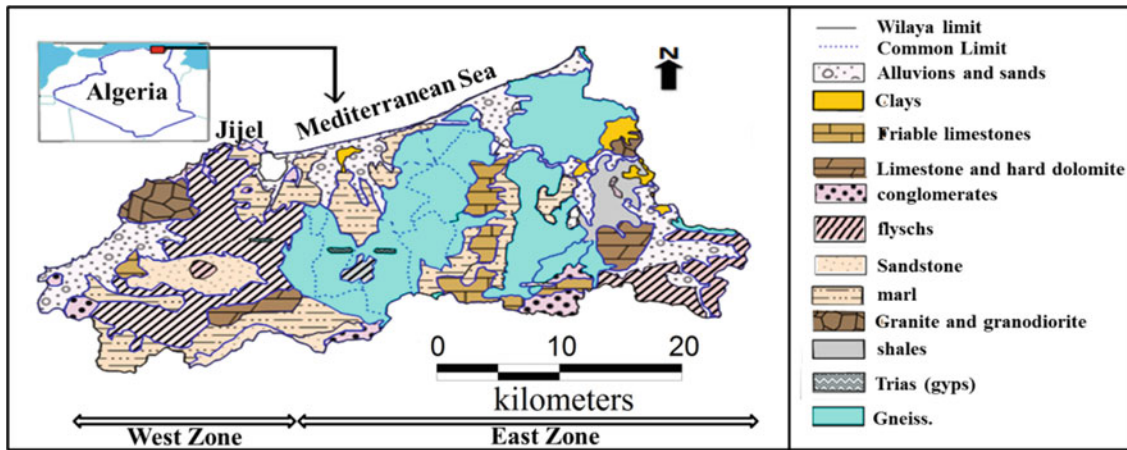


Fig. 1 Location map and lithology of Jijel region

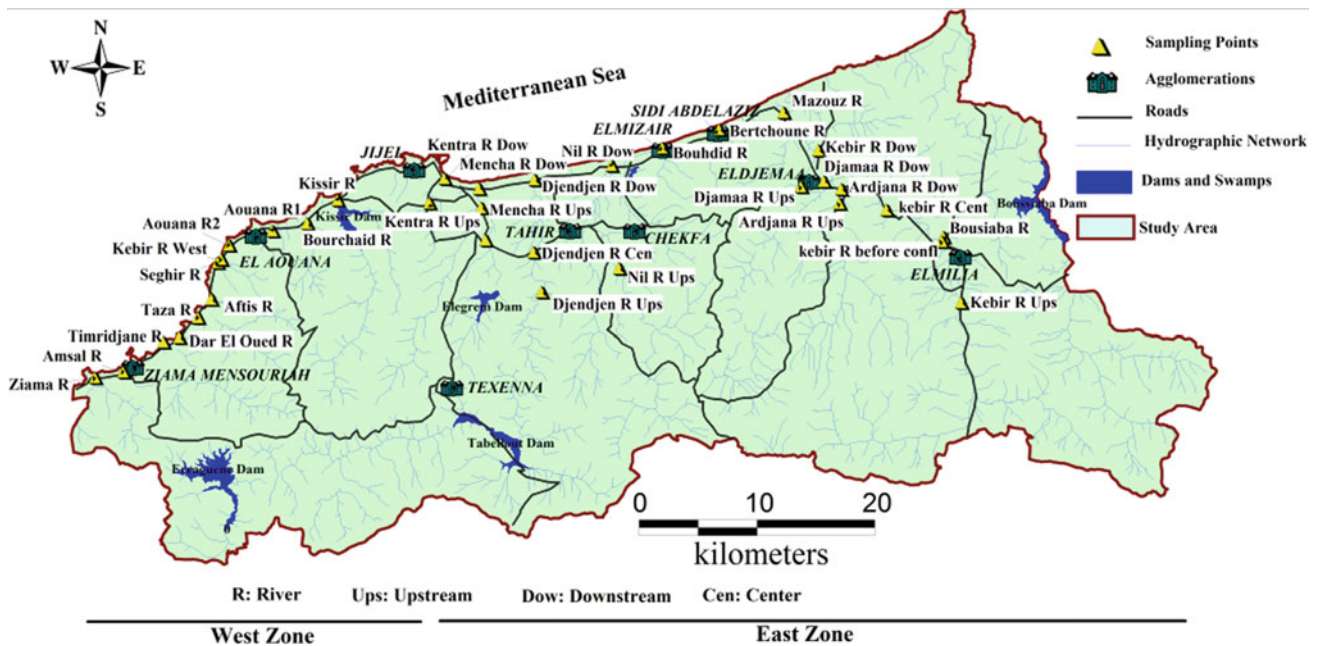


Fig. 2 Inventory map of sampling points

Na^+ , K^+ , Cl^- , HCO_3^- , NO_3^- , NO_2^- , NH_4^+ and PO_4^{3-} were determined according to standard methods as suggested by Rodier (1996). The ionic balance is generally around 5%.

3 Results and Discussion

From east to west of the Jijel region, water parameters revealed considerable modifications.

The temperature of the different wadis showed considerable variations from one station to another (7.2–22.2 °C). This was due to the time of temperature measurement and variation of air temperature. The pH is related to the buffer

system developed by carbonate, bicarbonate and carbonic acid, etc. (Ghachtoul et al. 2005). The water of all wadis was found to be alkaline (7.88–9.05). This could be explained by the geological nature (limestone, dolomite, marls and flysch), the land crossed and the domestic sewage discharges from the different agglomerations (Bouaroudj et al. 2019).

The upstream waters of the Ardjana, Djamaa and Nil wadis had similar physicochemical characteristics. An oxidizing medium with an Eh varied between 204 and 269 mV, whereas the electrical conductivity varied from 351 to 479 $\mu\text{S}/\text{cm}$, which indicated low mineralization. The concentrations of nitrates (0.57–4.39 mg L^{-1}), nitrites (0.005–0.02 mg L^{-1}) and ammonium (0.16–0.29 mg L^{-1}) were

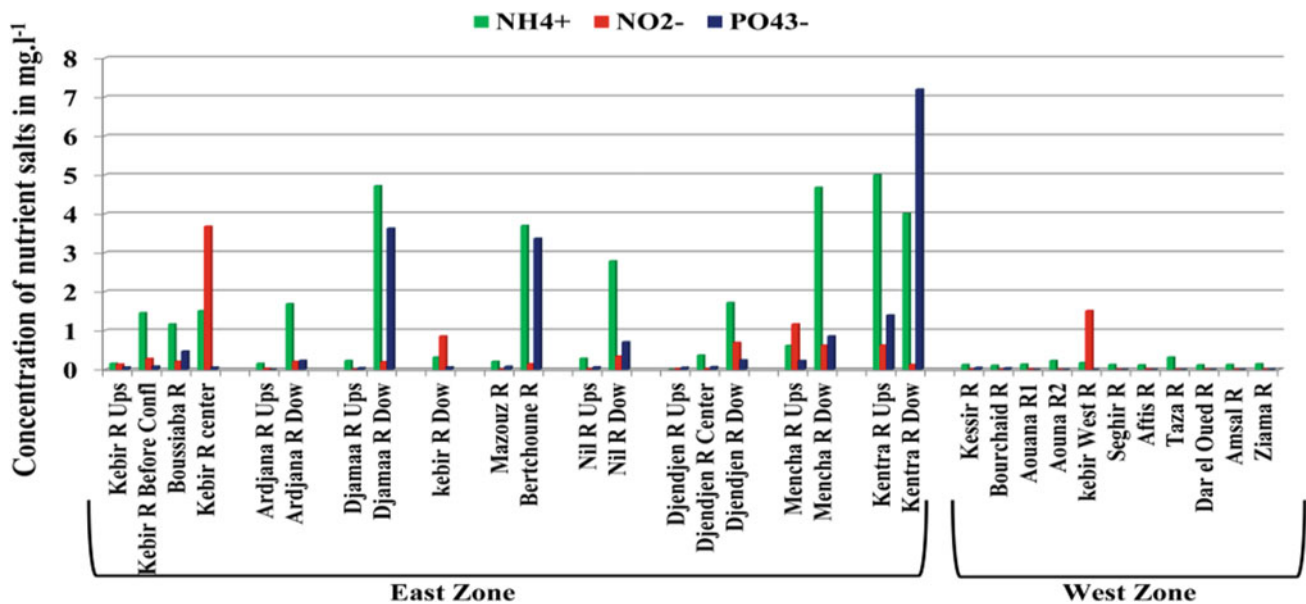


Fig.3 Variation of fertilizing elements in the Jijel region

low. These nitrogenous compounds are related to the degradation of organic matter (vegetation cover that covers the mountains of its sub-watersheds). The phosphate ($0\text{--}0.06\text{ mg L}^{-1}$) and sulfates ($26\text{--}33\text{ mg L}^{-1}$) were also determined within permissible limit (Fig. 3) and impact of anthropogenic activities and mineral dissolution (Gaury et al. 2018; Kumar et al. 2019b).

For the water of the Oued Kebir and the downstream rivers of the eastern part of the region, high electrical conductivity values ($666\text{--}5300\text{ }\mu\text{S/cm}$) were noted indicating the charged water. The redox potential varies between -32 and 414 mV and indicated an oxidizing reducing medium. High values of ammonium ($0.16\text{--}5\text{ mg L}^{-1}$), phosphate ($0.06\text{--}7.2\text{ mg L}^{-1}$), nitrite ($0.01\text{--}3.67\text{ mg L}^{-1}$) and bicarbonates ($156.16\text{--}395.28\text{ mg L}^{-1}$) were linked to urban discharges that flow directly into these wadis during their passage by the main agglomerations of the region (Derradji et al. 2007) and to the rejections of the El-Milia tannery (1.46 mg L^{-1} in ammonium and 0.83 mg L^{-1} of nitrite) at the Oued Kebir station before confluence. The river waters of the western part showed almost no organic pollution, with the exception of the Kebir West river, which had a high nitrite value (1.52 mg L^{-1}) explained by the presence of a public dump next to the river. The water electrical conductivity of these wadis oscillated between 473 and $1909\text{ }\mu\text{S/cm}$, indicating charged water. This variation depends essentially on the geochemical nature of the rocks encountered in the sub-watersheds of these wadis, in particular substances resulting from the alteration of carbonate rocks (Ouhmidou et al. 2015; Gaagai et al. 2017).

4 Conclusion

Upstream of the discharges issued from principal agglomerations, upstream of the confluence, surface water of different rivers present some favorable abiotic factors particularly pH, nitrate, phosphate and nitrite. In the downstream, water environment conditions are more unfavorable because of domestic and industrial effluents coming from agglomerations through the water stream. The important concentrations in orthophosphate, nitrite and ammonium in the downstream stations have their origin in the industrial and domestic discharges.

References

- Belabed, B.E., Meddour, A., Samraoui, B., Chenchouni, H.: Modeling seasonal and spatial contamination of surface waters and upper sediments with trace metal elements across industrialized urban areas of the Seybouse watershed in North Africa. *Environ. Monit. Assess.* **189**(6), 265 (2017). <https://doi.org/10.1007/s10661-017-5968-5>
- Bouaroudj, S., Menad, A., Bounamous, A., Ali-Khodja, H., Gherib, A., Weigel, D.E., Chenchouni, H.: Assessment of water quality at the largest dam in Algeria (Beni Haroun Dam) and effects of irrigation on soil characteristics of agricultural lands. *Chemosphere* **219**, 76–88 (2019). <https://doi.org/10.1016/j.chemosphere.2018.11.193>
- Brittany Water Agency: Sampling of Samples in the River; Sampling Technique for Physicochemical Analysis; Technical Guide 134p (2006)
- Derradji, F., et al.: Impact of organic pollution on the quality of surface waters in northeastern Algeria. *Sécheresse* **18**(1), 7–23 (2007)

- Derwich, E., Benziane, Z., Benaabidate, L.: Diagnostic of physico-chemical and bacteriological quality of fez wastewaters rejected in sebou River: Morocco. <https://doi.org/10.1007/s12665-010-0745-5>
- El Ghachtoul, Y., Alaoui Mhamidi, M., Gabi, H.: Eutrophication of reservoirs at Smir and Sehla dams (Morocco): causes, consequences and management instructions. *J. Water Sci.* **18**, 75–89 (2005)
- Gaagai, A., Boudoukha, A., Boumezbeur, A., Benaabidate, L.: Hydrochemical characterization of surface water in the Babar watershed (Algeria) using environmetric techniques and time series analysis. *Int. J. River Basin Manag.* **15**(3), 361–372 (2017). <https://doi.org/10.1080/15715124.2017.1299157>
- Gaury, P.K., Meena, N.K., Mahajan, A.K.: Hydrochemistry and water quality of Rewalsar Lake of Lesser Himalaya, Himachal Pradesh, India. *Environ. Monit. Assess.* **190**(2), 84 (2018). <https://doi.org/10.1007/s10661-017-6451-z>
- Grondin, J.L.: Methods of sampling and conditioning surface water, Technical Note No. 3, Overseas Scientific and Technical Research Office (1982)
- Kumar, P., Mahajan, A.K., Meena, N.K.: Evaluation of trophic status and its limiting factors in the Renuka Lake of Lesser Himalaya, India. *Environ. Monit. Assess.* **191**(2), 105 (2019a). <https://doi.org/10.1007/s10661-019-7247-0>
- Kumar, P., Meena, N.K., Mahajan, A.K.: Major ion chemistry, catchment weathering and water quality of Renuka Lake, north-west Himalaya, India. *Environ. Earth Sci.* **78**(10), 319 (2019b). <https://doi.org/10.1007/s12665-019-8315-z>
- Marouf, N., Remini, B.: Study of Beni Haroun dam pollution (Algeria). *Desalin. Water Treat.* (2014) <https://doi.org/10.1080/19443994.2014.982192>
- Negm, A., Bouderbala, A., Chenchouni, H., Barcelo, D.: Water Resources in Algeria - Part I: Assessment of Surface and Groundwater. Springer, Cham (2020a). <https://doi.org/10.1007/978-3-030-57895-4>
- Negm, A., Bouderbala, A., Chenchouni, H., Barcelo, D.: Water Resources in Algeria - Part II: Water Quality, Treatment, Protection and Development. Springer, Cham (2020b). <https://doi.org/10.1007/978-3-030-57887-9>
- Ouhmidou, M., Chahlaoui, A., Kharroubi, A., Chahboune, M.: Study of the physico-chemical and bacteriological quality of the barrage Hassan Addakhil of Errachidia (Morocco). *J. Mater. Environ. Sci.* **6**(6), 1663–1671 (2015)
- Rodier, J.: Analysis of water, natural waters, wastewater, seawater, p. 1383, 8th edn. Dunod, Paris, France (1996)
- WHO (World Health Organization): Guidelines for drinking water quality, recommendation, vol. 1, 3rd edn. Geneva (2008)

**Hydrology, Hydrogeology, Hydrochemistry, Water
Resources (T10): Hydrology, Land Use and
Climatology—Hydraulic Modeling**



Pairing GIS and Distributed Hydrological Models Using MATLAB

Sleimane Hariri, Sylvain Weill, Jens Gustedt, and Isabelle Charpentier

Abstract

Observed data are required to carry out hydrological simulations in a watershed for use by policy-makers. Hydrological simulations, thus, require extensive interdisciplinary knowledge about modelling, computer sciences, databases and GIS. A MATLAB pre-process prior to the hydrological modelling is presented for educational purposes and for an easy uptake by non-GIS users. Moreover, this allows for parallel computing. This pre-process builds on two renowned and freely available MATLAB toolboxes providing GIS and mesh functionalities. Additional functionalities allow for a decomposition of watersheds with respect to parameterized constraints, including the meshing of the subdomains and the construction of an oriented flow graph. The method is exemplified by a study on a sub-basin of the Saar River.

Keywords

Hydrology • Domain decomposition method • GIS modelling

1 Introduction

Data—topography, climate, land cover and soil properties—are required to carry out hydrological simulations in a watershed for use by policy-makers. These data are of

S. Hariri (✉) · J. Gustedt · I. Charpentier
ICube UMR 7357, Université de Strasbourg and CNRS,
67412 Illkirch, France
e-mail: shariri@unistra.fr

S. Weill
LHyGeS UMR 7517, Université de Strasbourg and CNRS,
67000 Strasbourg, France

J. Gustedt
INRIA, Rocquencourt, France

different nature and are usually provided according to their own standard data formats. Topography and land cover data are freely available from national agencies or transnational projects like Copernicus or CORINE Land Cover. Climate data are scarcer in both time and resolution. Fortunately, simulations can be performed using re-analyses (Caillouet et al. 2019). Soil and geology parameters are usually unknown, but calibrated using climate data, discharge data and hydrological models.

Digital elevation models (DEMs) store projected topographic information in a gridded format and constitute fundamental data to hydrological studies (McDonnell 1996). Spatial heterogeneities can be accounted by means of a decomposition of the watershed into smaller geographical units. Conceptual models deal with sub-watersheds to facilitate routing. River analyses are carried out using a one- or two-dimensional partial differential model discretized by meshing the major bed and splitting it longitudinally. Watershed simulations, along with surface and underground flows, involve more complex meshes and numerical methods. Domain decomposition has another major advantage since it offers the opportunity to run simulations on a parallel platform.

Only basic interdisciplinary knowledge in GIS, hydrology or computer sciences is usually insufficient to carry out numerical simulations because pairing GIS tools, database and computer models is not an easy task. QGIS and GMSH are loosely interfaced by means of Python and read/write shapefiles. The Python-based open-source framework PIHMgis (Bhatt et al. 2014) goes one step further by managing the coupling of GIS tools, data and distributed hydrological modelling through pre- and post-processes. Although a user interface exists and the program code is available, further developments require a good knowledge of GIS tools, Python and the programming language of the hydrological model under study.

To overcome this shortfall, MATLAB is chosen as a framework for pairing GIS and parallel/distributed

hydrological models. Thereby, it enables to take advantage of the existing toolboxes (Schwanghart and Kuhn 2010; Kourakos and Harter 2014). This short paper presents a pre-processor written in MATLAB that allows the management of DEMs with regard to hydrological structures, hydrological modelling and parallel computing.

2 Methods

The approach is to propose a user-friendly upgradeable open-source interface implemented in a classical language in science and educational communities. MATLAB meets these requirements. Additionally, it provides visualization functionalities. Several free toolboxes, namely TopoToolbox (Schwanghart and Kuhn 2010) and mSim (Kourakos and Harter 2014), offer particular GIS operations and mesh generation (through GMSH), respectively. Working in a non-GIS scientific computing framework rather than in a GIS or Python environment may facilitate the uptake by engineering students.

The pre-process workflow ranges from the DEM reading to the watershed decomposition and sub-mesh generation, carried out with respect to user's constraints.

2.1 Domain Decomposition

The watershed decomposition can be organized such that it fulfils parameterized, user-defined constraints:

1. The account for important hydrological structures (dams/ponds/discharge stations) or bridges that can create logjams; these are "primary checkpoints";
2. The partition of the domain into more sub-watersheds by placing "secondary checkpoints" on the stream;
3. The design of sub-watersheds with similar areas, typically a few km². The interest is threefold: (i) assigning homogeneous data (soil and climate) at the sub-watershed level to account for the spatio-temporal variability, (ii) dealing with hydrological sub-models of a similar size and (iii) balancing the computational load on a parallel platform.

All these checkpoints are inlets or outlets of the sub-watershed they delineate. At a surface level, these flow interfaces are located on the stream. Domain decomposition functionalities are implemented by building on (Schwanghart and Kuhn 2010; Kourakos and Harter 2014) and on MATLAB.

2.2 Pre-Process Workflow

A graphical user interface (not shown here) articulates GIS and meshing operations as follows: (1) read the DEM (Schwanghart and Kuhn 2010), (2a) define user outlets as suggested by the first constraint, (2b) automatically insert additional outlets to satisfy the third constraint, (3) partition the watershed by delineating drainage basins with respect to these outlets (Schwanghart and Kuhn 2010), (4) format the partition as a shapefile for plotting purposes (*shapewrite* and *shaperead* of the "mapping MATLAB toolbox"), (5) mesh the subdomains (Kourakos and Harter 2014), (6) determine inlet and outlet faces and (7) order subdomains to build an upstream to downstream graph. The files generated (sub-domain mesh and oriented flow graph) are used as input files for the hydrological model.

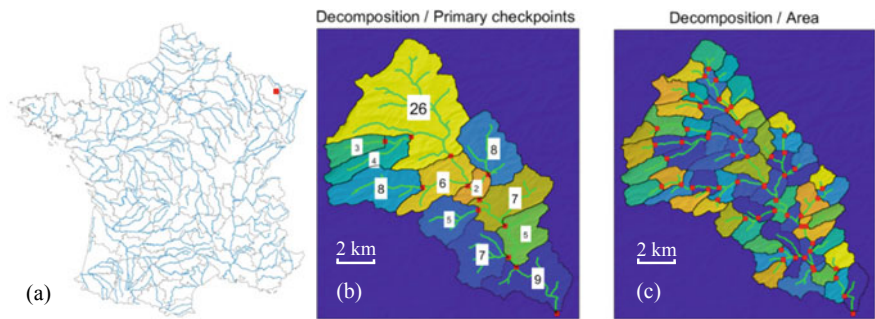
3 Results

For the sake of clarity in the figures, the small watershed (89 km²) of the Mutterbach stream near to the city of Sarralbe (Région Grand-Est, France) is used. To serve as a defence waterline in 1940, six ponds and five dams were built to supply water and to control the floods in the valley. These constitute a set of 11 primary checkpoints allowing for water management. In Fig. 1b, the decomposition is carried out with respect to these hydrological structures (marked with red squares). To anticipate parallel computing, secondary checkpoints have been added to fulfil the third constraint. Figure 1c displays a decomposition into 58 subdomains, the areas which range from 1 km² to 2.5 km² with an average value of 1.54 km². The numbers of nodes/elements in the sub-meshes are equal to 1260/2200 on average, respectively.

4 Discussion

Hydrological simulations require a large interdisciplinary knowledge about modelling, computer sciences, databases, GIS, etc. For educational purposes and an easy uptake by non-GIS users, our interdisciplinary team (hydrologists, computer scientists and mathematicians) have worked on MATLAB pre- and post-processes to the hydrological modelling. These build on two renowned and freely available MATLAB toolboxes (Schwanghart and Kuhn 2010; Kourakos and Harter 2014) providing GIS and mesh functionalities, respectively. Note that both were designed in a hydrological context and come with user guides.

Fig. 1 **a** Location in France (red point); **b** decomposition/checkpoints; **c** load-balanced refined decomposition



For the sake of reproducibility, the proposed domain decomposition functionalities (parameterized constraints, watershed decomposition and oriented flow graph) will be exhaustively described and documented in a future work. Then, MATLAB codes will be made freely available to serve as a basis to implement other decomposition constraints. Complementary tests were performed on the Saar watershed, partly located in France and Germany.

This hydrology-targeted MATLAB–GIS framework is intended to be useful not only for educational purposes or for a first contact with GIS tools for hydrology modelling, but also as a common basis for interdisciplinary studies with non-GIS users. Moreover, it benefits from the numerous toolboxes already developed in and for MATLAB.

5 Conclusion

The MATLAB–GIS interface builds on two renowned and freely available MATLAB toolboxes providing GIS and mesh functionalities. It has been designed for an easy uptake by non-GIS users and modellers in hydrology. The resulting

watershed decomposition can be interfaced with a conceptual model or with a parallelized finite element model for watershed simulations by using the oriented flow graph for routing.

References

- Bhatt, G., Kumar, M., Duffy, C.J.: A tightly coupled GIS and distributed hydrologic modeling framework. *Environ. Model. Softw.* **62**, 70–84 (2014)
- Caillouet, L., Vidal, J.-P., Sauquet, E., Graff, B., Soubeyroux, J.-M.: SCOPE Climate: a 142-year daily high-resolution ensemble meteorological reconstruction dataset over France. *Earth Syst. Sci. Data* **11**(1), 241–260 (2019)
- Kourakos, G., Harter, T.: Vectorized simulation of groundwater flow and streamline transport. *Environ. Model. Softw.* **52**, 207–221 (2014)
- McDonnell, R.A.: Including the spatial dimension: using geographical information systems in hydrology. *Prog. Phys.* **20**(2), 159–177 (1996)
- Schwanghart, W., Kuhn, N.J.: TopoToolbox: a set of Matlab functions for topographic analysis. *Environ. Model. Softw.* **25**(6), 770–781 (2010)



Use of Hydrological Modeling as a Tool for Climate Model Evaluation at Oued el Abid Catchment [Tunisia]

Khalil Djebbi and Hamouda Dakhlaoui

Abstract

Hydrological impacts of climate change result from the combined effect of climate variables simulated by climate models. However, these variables are generally evaluated independently. We propose to evaluate climate model simulations in a process-oriented framework using hydrological modeling. We evaluate eleven GCM-RCMs climate variables (precipitation and temperature) issued from EURO-CORDEX, over a 30-year reference period (1970–2000) for Oued El Abid catchment situated in northern Tunisia, by using HBV-light rainfall-runoff model. Six discharge metrics were used to explore the representation of the hydrological processes. Due to the climate system complexity, there is no model that can reproduce this system perfectly. This implies applying bias correction before using their outputs in impact studies. In this study, we use Quantile Delta mapping to bias correct climate variables. Our results confirm the importance of bias correction. Additionally, we present a ranking of climate models according to their hydrological performance. GCM-RCM IPSL-IPSL-CM5A-MR-SMHI-RCA4 is the best in the reference period (metrics are met), whereas GCM-RCM IC-EC-EA- KNMI-RACMO22E is the worst for the study catchment area.

Keywords

GCM • RCM • HBV-light • Rainfall-Runoff model • Bias correction • EURO-CORDEX

1 Introduction

Tunisia is situated in a hot spot of climate change. Recent climate change scenarios project an important decrease in precipitation and an increase in mean annual temperature (Dakhlaoui et al. 2017). This could result in critical water stress in the future. However, only a few studies have considered the hydrological impacts of climate change in Tunisia (Dakhlaoui et al. 2019). Rainfall-runoff models forced with regional climate change scenarios are commonly used to evaluate the impact of climate change at catchment scale (Bastola et al. 2011). Regional climate change scenarios are based on global climate model downscaling techniques to fix the issue of inconsistent resolutions. The reduction is based either on regional climate models (RCMs) (Rummukainen 2001) or statistical techniques (Maraun et al. 2010), or on a mixture of both. Temperature and precipitation primarily control the runoff. The realism of hydrological simulations might represent how well climate models (including intervariable interactions) represent these variables (Hakala et al. 2018). We suggest using hydrological modeling to assess the atmospheric forcing supplied by the latest GCM-RCM (general model of circulation forcing regional climate model). We aim to rank GCM-RCMs based on how well they enable us to capture hydrological variables.

2 Data and Methods

2.1 Study Catchment

Oued El Abid catchment in Northern Tunisia was selected for this study. The study catchment is situated within a semi-arid climate with a warm and dry season which extends from June to August (Dakhlaoui et al. 2017) (Fig. 1).

K. Djebbi (✉) · H. Dakhlaoui
LMHE, Ecole Nationale d'Ingénieurs de Tunis, Université Tunis
El Manar, BP37, 1002 Tunis Le Belvédère, Tunisia

H. Dakhlaoui
Ecole Nationale d'Architecture et d'Urbanisme, Université de
Carthage, Sidi Bou Said, Tunisia

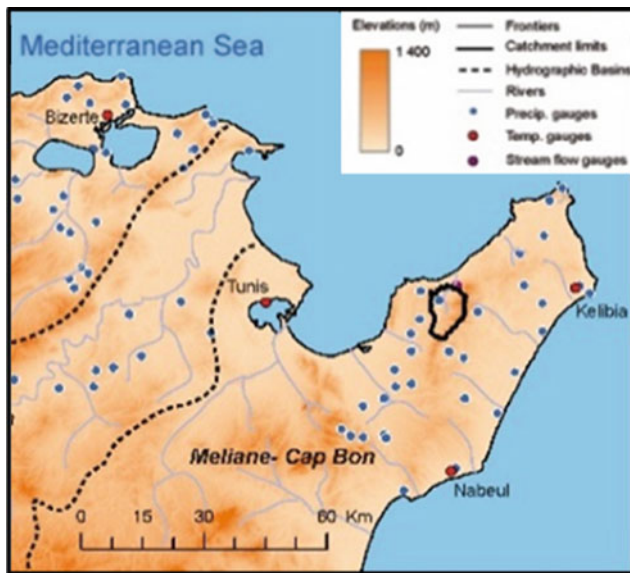


Fig. 1 Study catchment

2.2 High-Resolution Climate Simulations and Bias Correction of Climate Variables

Daily temperature and precipitation time series, simulated by 11 GCM-RCMs (general circulation model forcing regional climate model), were obtained from CORDEX (Coordinated Regional Downscaling Experiment, www.cordex.org). Given the location of the catchments, the European domain was selected (EURO-CORDEX, <http://www.euro-cordex.net/>; Table 1). EURO-CORDEX simulations are the most recent high-resolution climate projections for the European domain with a 0.11° resolution ($\sim 12 \times 12$ km).

Table 1 GCM-RCM used in this paper

N°	GCM	RCM
1	CNRM-CERFACS-CNRM-CM5	CLMcom-CCLM4-8-17
2	CNRM-CERFACS-CNRM-CM5	SMHI-RCA4
3	ICHEC-EC-EARTH	CLMcom-CCLM4-8-17
4	ICHEC-EC-EARTH	DMI-HIRHAM5
5	ICHEC-EC-EARTH	KNMI-RACMO22E
6	ICHEC-EC-EARTH	SMHI-RCA4
7	IPSL-IPSL-CM5A-MR	IPSL-INERIS-WRF331F
8	IPSL-IPSL-CM5A-MR	SMHI-RCA4
9	MOHC-HadGEM2-ES	CLMcom-CCLM4-8-17
10	MPI-M-MPI-ESM-LR	CLMcom-CCLM4-8-17
11	MPI-M-MPI-ESM-LR	SMHI-RCA4

2.3 Bias Correction

Quantile Delta mapping (QDM, Canon et al. 2015) multiplies observed values at the same quantiles by the ratio of model values (interest period divided by calibration period). It was utilized as a bias correction method to correct the daily precipitation and temperature of the GCM-RCMs. The aim of QDM is to correct the distribution of the climate model data so that it matches the distribution of the observational data. It consists of estimating quantiles for both observation and modeled climate variable within a control period. A transfer function is then created by interpolation between corresponding quantile values. Here, the cumulative distribution functions (CDFs) of observed and modeled climate variables were estimated using empirical percentiles. Values in between the percentiles were approximated using linear interpolation. The transfer function of the QDM was based on a 30-year control period (1970–2000), which is the recommended time length for climate applications.

2.4 Hydrological Model

Daily stream flow values for the catchment were simulated using the Hydrologiska Byråns Vattenbalansavdelning (HBV) light model (Seibert and Vis 2012). As input, HBV-light requires daily temperature, precipitation and potential evapotranspiration. The hydrological models were run at a daily time step, but their efficiency evaluation was performed on 10-day averages, since this study is focused more on water resources than on the day-to-day variability and the averaged discharge values were more reliable than the daily values.

2.5 Evaluation of Performance of GCM-RCMs Over the Reference Historical Period

The hydrological metrics adopted here include: Low flow (Q5), high flow (Q95), annual mean maximum, mean flow, long-term mean monthly discharge for the dry-warm season: June, July, August (JJA) and the wet-cold season: December, January and February (DJF).

3 Results and Discussion

3.1 Evaluating Individual Effects of Quantile Mapping

We compared monthly long-term mean precipitation and temperature biases to check the downscaled model's output efficiency against observational data (Figs. 2 and 3). The raw GCM-RCM overestimates the precipitation during warm seasons (by 5.7–44 mm per month), but underestimates it during cold seasons by about 40 mm per month. Regarding temperature, climate models reproduced well the reality with an obvious seasonality.

The QDM demonstrates a notable ability to reduce rainfall bias and reproduce the seasonality (Fig. 4). It was also capable of reducing the original simulated model's temperature to become identical with the observed values (Fig. 5), which highlights QDM's outstanding capacity to decrease the initial designs' bias over the research region. QDM-downscaled models underestimate extreme precipitation values exceeding 70 mm/month and overestimate them for precipitation less than 7 mm/month.

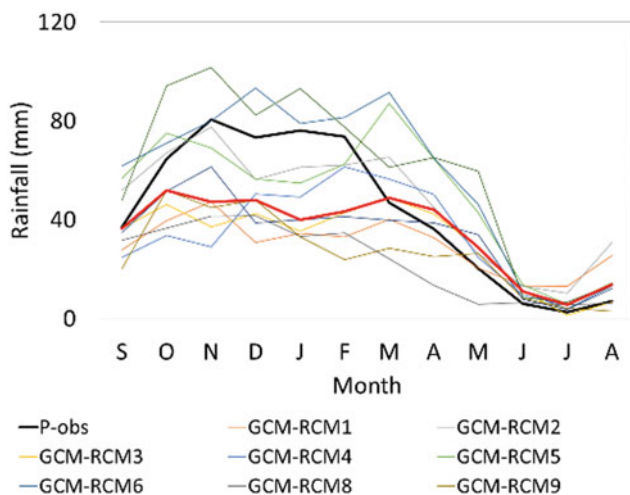


Fig. 2 Raw simulated rainfall

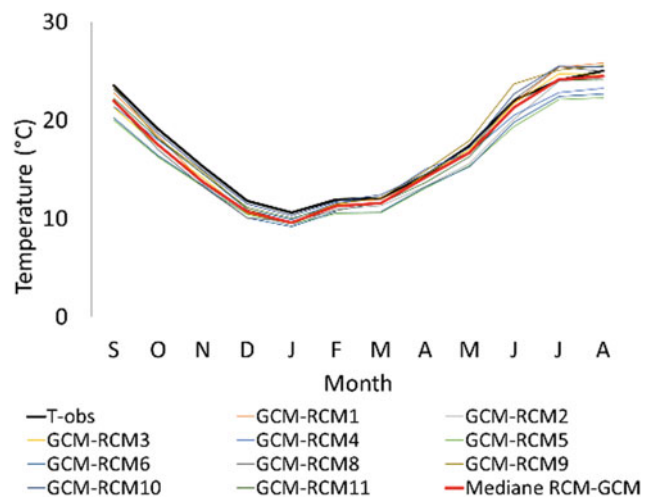


Fig. 3 Raw simulated temperature

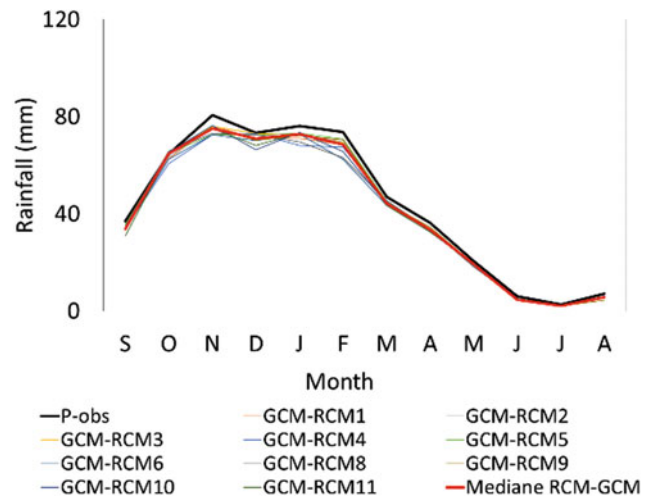


Fig. 4 Bias-corrected rainfall

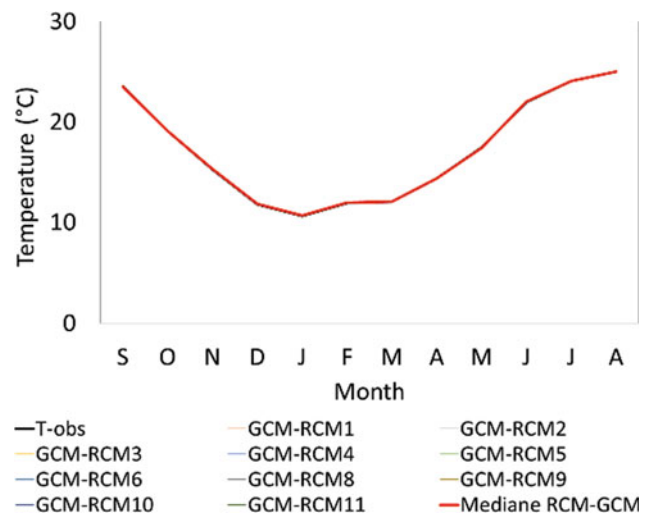
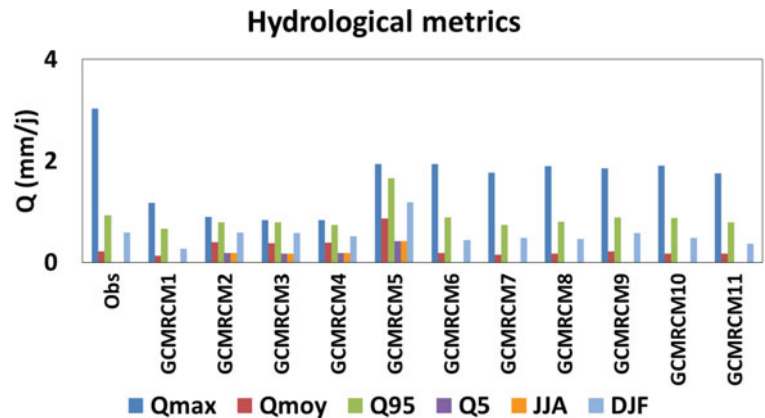


Fig. 5 Bias-corrected temperature

Fig. 6 Hydrological metrics

3.2 Hydrological Modeling

Metrics of streamflow resulting from HBV-light model forced by bias-corrected RCM-GCM simulations came very close to those resulting from measured seasonal streamflow values, over the 1970–2000 reference period. QDM has a usually positive effect on the metrics of discharge with a 90% enhancement rate for all the cases. As Fig. 6 shows, GCM-RCMs 8, 7 and 6 perform the best in the reference period, while GCM-RCM 5 is the worst, while the others can be used but carefully.

References

- Bastola, S., Murphy, C., Sweeney, J.: The role of hydrological modelling uncertainties in climate change impact assessments of Irish river catchments. *Adv. Water Res.* **34**, 562–576 (2011). <https://doi.org/10.1016/j.advwatres.2011.01.008>
- Cannon, A., Sobie, S., Murdock, T.: Bias correction of GCM precipitation by quantile mapping: How well do methods preserve changes in quantiles and extremes? *J. Climate.* **28**(17), 6938–6959 (2015). <https://doi.org/10.1175/JCLI-D-14-00754.1>
- Dakhlaoui, H., Ruelland, D., Trambaly, Y., Bargaoui, Z.: Evaluating robustness of conceptual rainfall-runoff models under climate variability in Northern Tunisia. *J. Hydrol.* **550**(2017), 201–217 (2017). <https://doi.org/10.1016/j.jhydrol.2017.04.032>
- Dakhlaoui, H., Ruelland, D., Trambaly, Y.: A bootstrap-based differential split-sample test to assess the transferability of conceptual rainfall-runoff models under past and future climate variability. *J. Hydrol.* **575**, 470–486 (2019). <https://doi.org/10.1016/j.jhydrol.2019.05.056>
- Hakala, K., Addor, N., Seibert, J.: Hydrological modeling to evaluate climate model simulations and their bias correction. *J. Hydrometeor.* **19**(8), 1321–1337 (2018). <https://doi.org/10.1175/JHM-D-17-0189.1>
- Maraun, D., Wetterhall, F., Chandler, R.E., et al.: Precipitation downscaling under climate change: Recent developments to bridge the gap between dynamical models and the end user. *Rev. Geophys.* **48**, 1–38 (2010). <https://doi.org/10.1029/2009RG000314>
- Rummukainen, M.: Climate change impacts on runoff in Sweden assessments by global climate models, dynamical downscaling and hydrological modelling. *Clim. Res.* **16**, 101–112 (2001). <https://doi.org/10.3354/cr016101>
- Seibert, Vis, M.J.P.: Teaching hydrological modeling with a user-friendly catchment-runoff-model software package. *Hydrol. Earth Syst. Sci.* **16**, 3315–3325 (2012). <https://doi.org/10.5194/hess-16-3315-2012>



Hydraulic Modeling with HEC-RAS 2D in the Urban Area of Casimcea (Romania) Catchment

Constantin Cerneaga, Gabriel Dobrica, and Carmen Maftai

Abstract

Flood simulation models have a wide variety of approaches that are available to compute the water surface elevations associated with a flood event. Two-dimensional (2D) numerical simulation proved to be an important tool for understanding flood events. The present study aims to analyze the 2002 flood event in the Casimcea catchment, Casimcea village sector, using the 2D capabilities of the HEC-RAS hydraulic model. The Casimcea catchment is located in the southeast of Romania in the Dobrogea region. Hydraulic modeling was performed to provide important information from the flood event including the depth of inundation, flow velocity and water surface elevations within the study area. The results that have been obtained from the simulation show a flood map that can be beneficial to local and infrastructure planners, risk managers and emergency services during extreme and intense rainfall events.

Keywords

Flood • Hydraulic modeling • Casimcea catchment

1 Introduction

Flood is a natural hazard that results from a combination of hydrological and meteorological factors. Floods can be considered as the most important natural disasters with an occurrence higher than any other natural hazard and affecting more people than the other entire natural hazards together (Sonmez et al. 2017).

In recent years, floods have caused large material losses in Europe, including Romania. OFDA/CRED international data bases and the Prevention Web projects show that the number of floods increased in the last decades with 50 and 96.4% of the population affected by floods (PreventionWeb 2019). In Romania, Galati and Tulcea counties are among the areas most affected by floods, but Constanta, Bacau, Vrancea, Vaslui, Teleorman, Olt and Dolj may also be in a similar situation, according to ISU (Inspectorate for Emergency Situation) (Asiguropedia 2019).

The aim of the present paper is to investigate the potential of HEC-RAS 2D tools to locate flood-prone areas according to the Flood Directive (2007). The study area is the Casimcea catchment1—Casimcea village sector, which is located in the southeastern part of Romania, in the Dobrogea region.

2 Materials and Methods

2.1 Study Area

The Casimcea catchment is located in the Dobrogea-Littoral basin of southeastern Romania, as shown in Fig. 1, and covers parts of two counties, Tulcea and Constanta.

The basin drains an area of approximately 742.33 km², with a main river, Casimcea, which flows into the Taşaul Lake. The Casimcea River is the most important river in Dobrogea and has a length of 76.13 km. Its annual average flow is 0.083m³/s, with variations between 0.03 and 0.180m³/s (Pena and Nardi 2018). The annual rainfall for the

C. Cerneaga (✉) · G. Dobrica · C. Maftai
Doctoral School of Applied Sciences, Ovidius University of
Constanta, Constanta, Romania

C. Maftai
Civil Engineering Faculty, Transilvania University of Brasov,
Brasov, Romania

C. Cerneaga · G. Dobrica
Dobrogea Branch, Romanian Water Agency, Constanta, Romania

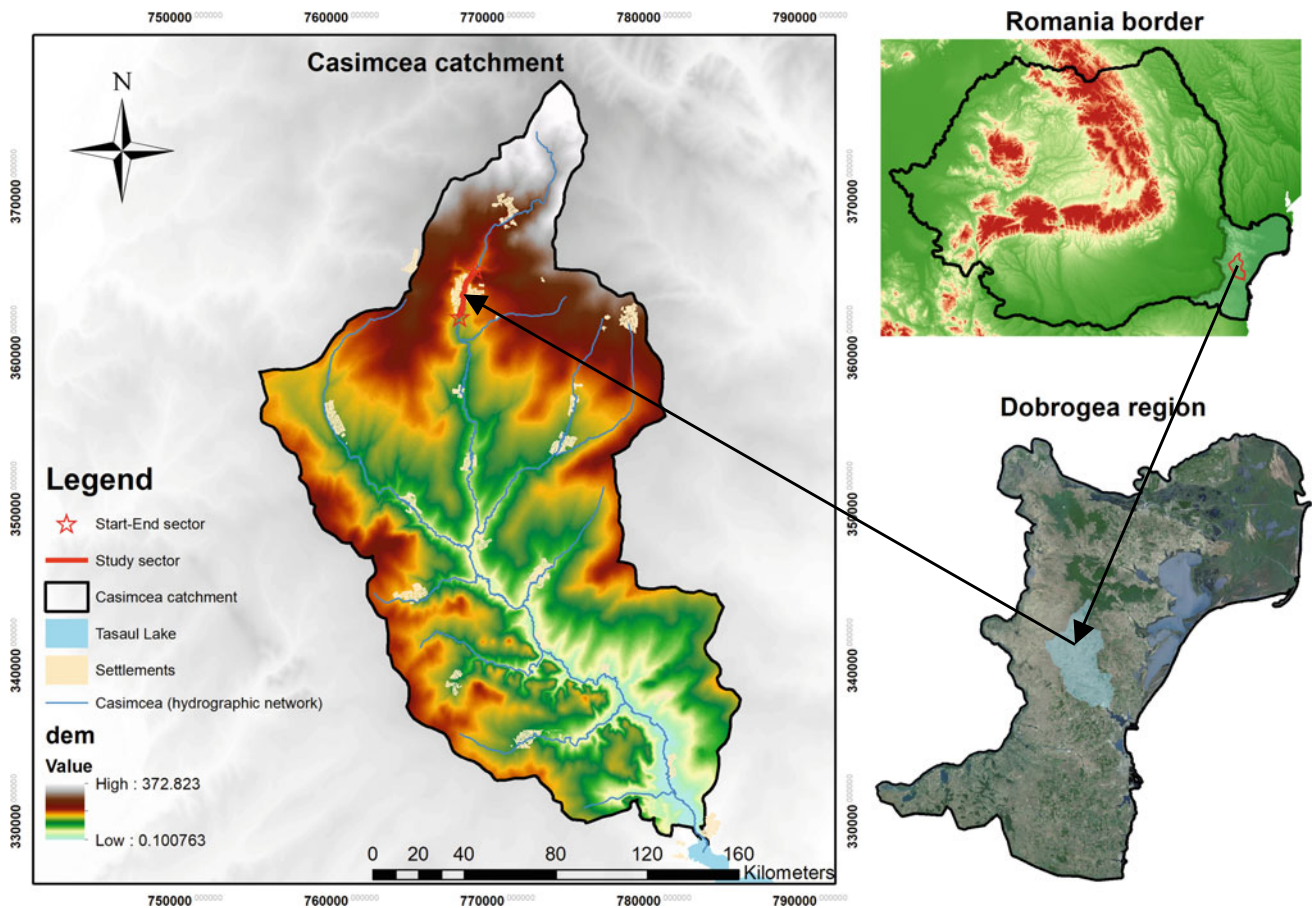


Fig. 1 Map of the study basin, southeast of Romania, in the Dobrogea region

Casimcea basin is 452 mm, and the average temperature is 10.8 °C (Climate data for cities worldwide 2019).

2.2 Materials

For this study, we used a hydrological and cartographical data set. The hydrological data sets and the digital elevation model with 2 m vertical accuracy used for the flood modeling were obtained from “Romanian Waters” National Administration—Dobrogea Water Branch (RWNA-DWB).

The watershed delineation was carried out by using ArcGIS software.

Basic hydrological data consist of maximum actual flow rates resulting from the corresponding flowchart (Fig. 2). The maximum value recorded corresponds to the exceedance probability of occurrence of 0.1%.

2.3 Methods

One-dimensional hydraulic model was successfully used during years for flood simulation in rivers. However, over the last 20 years, the extensive development in computational capacity has increased the research and practical use of two-dimensional modeling (Moreta and Lopez 2017).

For the present study, the flood event was simulated using the HEC-RAS model developed by the USACE (US Army Corps of Engineers). In HEC-RAS, both 1D and 2D can use the fully dynamic Saint Venant equations of Conservation of Mass and Conservation of Momentum (Moya Quiroga et al. 2016).

Manning’s n value was estimated from Chow (1959), considering the physical characteristics of the river’s channel. The value that we chose for our type of channel (clean, winding, some pools, shoals, weeds and stones) is 0.045.

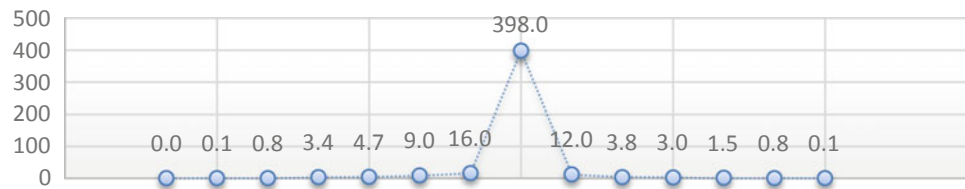


Fig. 2 Flow hydrograph, 30–31 May, 2002

3 Results

This study highlights the value of floodplain terrain analysis for processing high resolution DTMs to produce upscaled geometry for 2D inundation mapping.

The results obtained for 1000 return period are presented in Fig. 3. For scenarios presented in these figures, the villages situated in the lowland (e.g., Casimcea) are flooded.

4 Discussion

The proposed floodplain terrain analysis procedure for creating 2D inundation models is able to consistently simulate the inundation. The flood limits resulted from HEC-RAS are between 20 and 219 m, the depth of inundation has a maximum of 7.38 m and the maximum flow velocity is 3.38 m/s, and in this case it is necessary to find the optimum

flood defense solutions for our study area. By comparing the results obtained using the 2D hydraulic model with the ones obtained by RWNA-DWB (Fig. 3 left—the red lines), it is obvious that the HEC-RAS 2D hydraulic model can describe the flood-prone area.

5 Conclusion

The study is associated with the analysis of flood occurrences of 0.1% which can help evaluate the flood risk for extreme hydrological events. The results of this study support the probabilistic flood hazard mapping and provide water resources managers with valuable information for planning and implementing flood risk mitigation strategies. However, the results will be verified and compared with different Manning values that will be calculated according to land use.

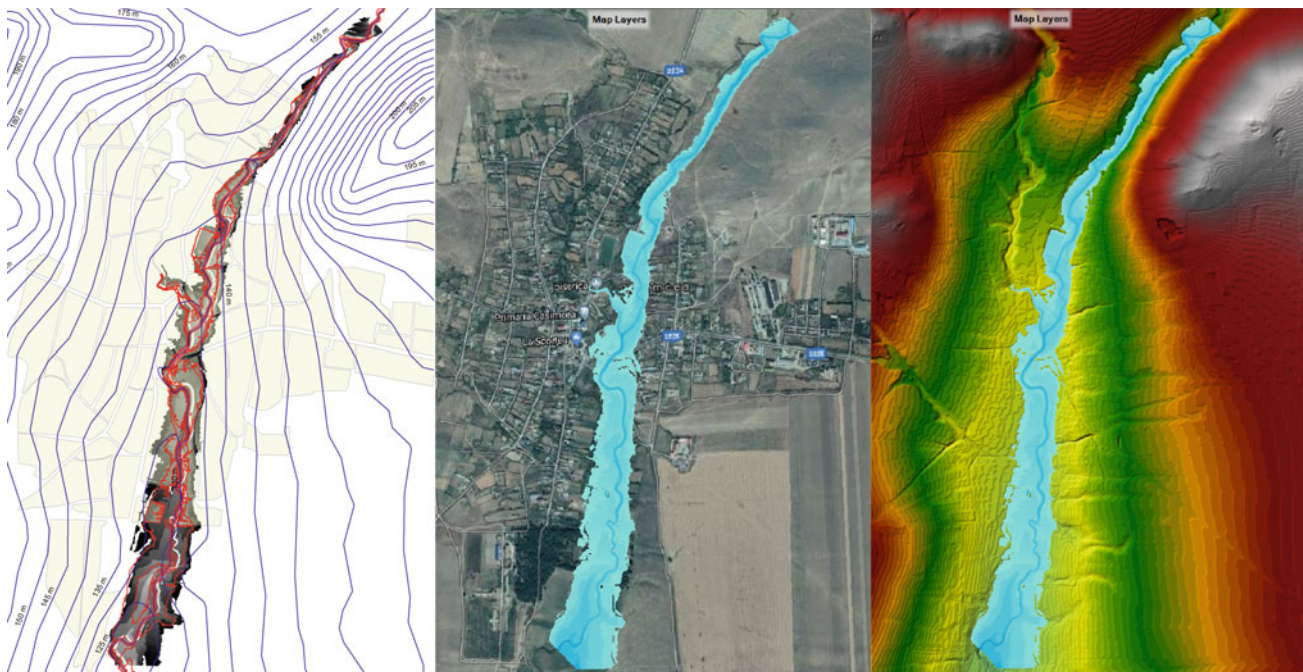


Fig. 3 Floodplain mapping of the Casimcea River simulated by HEC-RAS 2D

Acknowledgements This work is supported by the project ANTRE-PRENORDOC, in the framework of Human Resources Development Operational Programme 2014–2020, financed from the European Social Fund under the contract number 36355/23.05.2019 HRD OP /380/6/13—SMIS Code: 123847.

References

- Asiguropedia. <http://asiguropedia.ro>. Last accessed 06 June 2019
- Chow, V.T.: Open-channel hydraulics. McGraw-Hill, New York (1959)
- Climate data for cities worldwide. <https://en.climate-data.org>. Last accessed 08 June 2019
- Directive 2007/60/EC on the assessment and management of flood risks
- Moreta P.M., Lopez Querol S.: Numerical modeling in flood risk assessment: UK case study. *Civ. Eng. Res. J.* **3**(1), 555601 (2017). <https://doi.org/10.19080/CERJ.2017.03.555601>
- Moya Quiroga, V., Kure, S., Udo, K., Mano, A.: Application of 2D numerical simulation for the analysis of the February 2014 Bolivian Amazonia flood: Application of the new HEC-RAS version 5. Ribagua—*Revista Iberoamericana del Agua* **3**, (2016)
- Pena, F., Nardi, F.: Floodplain terrain analysis for coarse resolution 2D flood modeling. *Hydrol.* **5**(4), 52 (2018). <https://doi.org/10.3390/hydrology5040052>
- PreventionWeb. <http://www.preventionweb.net/english/>. Last accessed 06 June 2019
- Sonmez, O., Demir, I.H., Demir, F., Dobrucali, E.: Determination of flood inundation areas and assessment of flood hazard costs in urban settlements: a case study of AGVA. *J. Environ. Prot. Ecol.* **18**(2), 509–523 (2017)



Sensitivity Analysis of the SAFSAF River Catchment Model Using Two Objective Functions

Fares Laouacheria, Leila Djellit, Said Kechida, Moncef Chabi, and Faiza Balla

Abstract

Understanding the complex relationships between rainfall and runoff processes is necessary to accurately estimate the amount of runoff generated in a catchment. Surface runoff was simulated using the Hydrologic Modeling System (HEC-HMS). The meteorological model was developed within HEC-HMS from rainfall data. To account for infiltration loss and runoff estimation, the methods of the number of soil conservation service curves (SCS-CN) and the unit hydrograph of SCS were used. The assessment of the behavior and performance of the hydrological model is usually performed and reported through simulated and observed variability comparisons. In this work, we used two objective functions (root mean square error (RMSE) and percent error peak discharge (PEPD)) with the observed flood hydrograph for the case of the sub-catchment “W220” for the period of January 1–2, 2019, to examine the sensitivity of these parameters, which can be used to determine preliminary estimation ranges of their values for future modeling.

Keywords

Rainfall-runoff • RMSE • PEPD • Catchment • HEC-HMS

1 Introduction

Knowing the volume of runoff in a catchment is important for the sustainable planning and management of water resource projects. Rainfall-runoff models are often used as tools for

F. Laouacheria (✉) · S. Kechida · M. Chabi
Laboratory of Soils and Hydraulic, Badji-Mokhtar Annaba University, P.O.Box 12, 23000 Annaba, Algeria

L. Djellit · F. Balla
Department of Hydraulic, Badji-Mokhtar Annaba University, P.O.Box 12, 23000 Annaba, Algeria

flow modeling, monitoring of water levels under different water conditions, and flood forecasting (Alfy 2016). Modeling uses a variety of techniques to predict flow, such as physically based distributed models (Ghumman et al. 2017), stochastic models, and global conceptual models (Pham et al. 2018; Anshuman et al. 2018). The uncertainties associated with the results of these models and the identities of their parameters must be examined (Ahmadalipour and Moradkhani 2017). In this study, this task is carried out by performing a sensitivity analysis using the hydrological modeling system of the Hydrological Engineering Center (HEC-HMS). The process of evaluating the performance of a hydrological model requires the hydrologist to make subjective and/or objective estimates of the simulated model behavior to the observed model. Generally, many performance criteria contain an amount of the error term (the difference between the simulated variable and variable observed at each time step) standardized by a measure of variability in the observations. Many researchers have used statistical indicators to evaluate model performance (Gupta et al. 2009; Wang and Solomatine 2018). The objective of this study was to develop a rainfall-runoff model, to assess the runoff volume of the SASAF river catchment and the assessment of catchment behavior from the comparison of two performance indicators for the objective functions namely root mean square error (RMSE) and percent error peak discharge (PEPD) in order to know the parameters that have a high sensitivity on the model output during comparison on the simulated and observed flow hydrograph. In this work, the storm event of 1 and 2 January, 2019, recorded in the period of 1990–2019, was selected for the calibration purpose.

2 Materials and Methods

The analyses were performed in the SAFSAF river catchment (Fig. 1), located in the Northern-East part of Algeria. The area of the catchment is 1165.82 km².

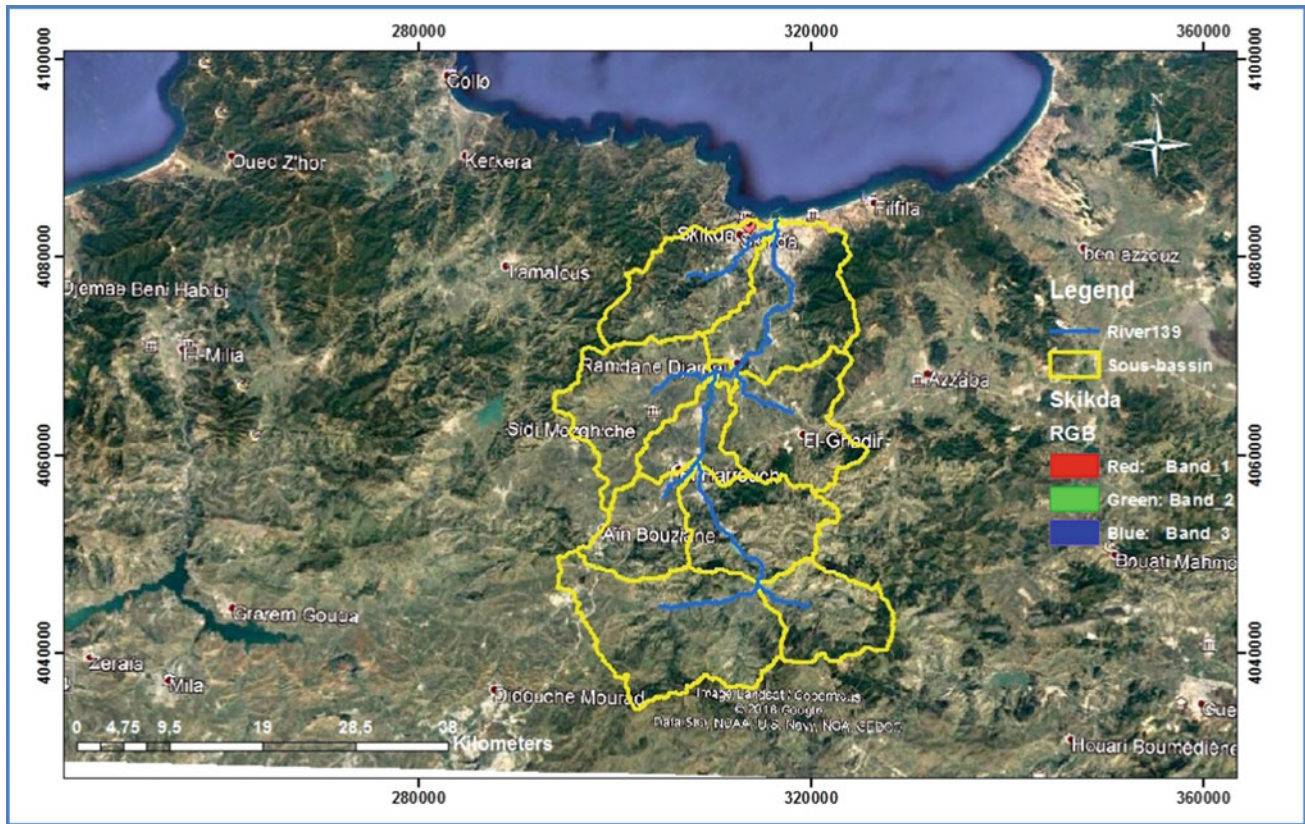


Fig. 1 Location of the study area

In this work, the HEC-HMS model was chosen as the flow prediction model and univariate gradient algorithm was used to calibrate the model. In the first time, the analysis was based on the highest daily precipitation recorded at the Skikda precipitation station for 20 years daily data for the period between 1990 to 2019. Effective precipitation, which describes direct runoff, was determined by SCS-CN method. The SCS model based on synthetic unit hydrographs was subjected to the calibration process. In the other hand, the performance calculations of the parameters of the model were carried out at the level of the sub-catchment “W220”, which is the only sub-catchment equipped with a gauging station of KHMAKHAM and automatically calibrated based on the univariate gradient model and two objective functions: PEPD and RMSE. Sensitivity analysis of the parameters was then selected based on their effect on peak flow and total volume.

$$PEPD = 100 \left| \frac{Q_o - Q_s}{Q_o} \right| \quad (1)$$

where Q_o and Q_s are the observed and simulated peak flow.

$$RMSE = \left(\frac{\sum_{i=1}^N (Q_{i,Obs} - Q_{i,Sim})^2}{N} \right)^{\frac{1}{2}} \quad (2)$$

where $Q_{i, Obs}$ and $Q_{i, Sim}$ are the observed and simulated flow in time step i . N is the number of time steps considered.

3 Results of the Model Performance

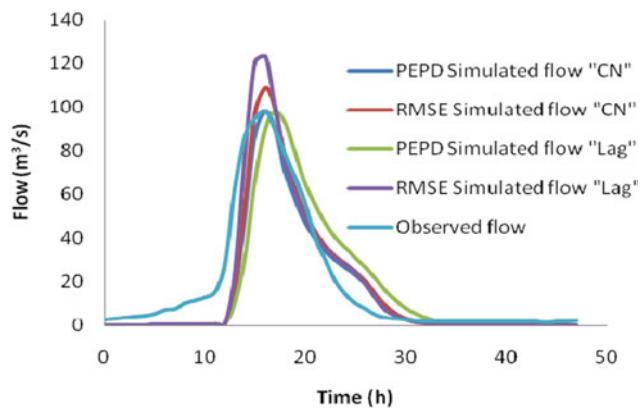
Two objective functions were used for the optimization of the parameters of the hydrological model (CN and lag time), namely the root mean square error (RMSE) and the percentage of peak flow error (PEPD). In this part, the optimization was applied to the sub-catchment “W220” which is equipped with a KHMAKHAM gauging station. From this station, we were able to construct the observed flood hydrograph during the period of January 1 and 2, 2019.

4 Discussion

It can be seen from Table 1 and Fig. 2 that there are wide differences among the calibrated performance indicators for the two objective functions. It is clear that the objective functions, RMSE and PEPD, have the best relative error value of volume with -8.82% in the case of the input parameter “Lag time” (Table 1), whereas the objective

Table 1 Simulated and observed peak flow and total volume during calibration

Objective function	Parameter	Peak flow (m ³ /s)			Total volume (mm)		
		Simulated	Observed	RE (%)	Simulated	Observed	RE (%)
RSME	CN	108	98	10.20	29	34	-14.71
	Lag	123	98	25.50	31	34	-8.82
PEPD	CN	98	98	0.00	27	34	-20.59
	Lag	98	98	0.00	31	34	-8.82

**Fig. 2** Simulated and observed flow hydrographs during calibration

function RMSE represents the worst relative error value of peak flow with 25.50% in the case of the input parameter “Lag time” (Table 1). The optimization of the CN and lag time parameters by the two objective functions RMSE and PEPD showed that the CN is less sensitive than lag time with regard to the volume. In the case of the objective function RMSE, the CN is more sensitive than lag time with regard to the peak flow. The sensitivity of the CN and lag time in the case of the objective function PEPD is the same with regard to the peak flow (Table 1 and Fig. 2). However, there is change in the time of peak estimated at 1 h when using the PEPD in the case of the input parameter, lag time.

5 Conclusion

In this work, HEC-HMS model and univariate algorithm were applied on the SafSaf River catchment in northeastern Algeria with the aim to assess the effects of different

objective functions. Two objective functions and their combinations were chosen to calibrate the model, and their performances were assessed and compared. The smallest differences between the simulated and observed peak flows were obtained using PEPD, and the biggest differences between the simulated and observed volume were obtained using RMSE. A sensitivity analysis was carried out where the parameters of the SCS model have wide variability for both objective functions.

References

- Ahmadalipour, A., Moradkhani, H.: Analyzing the uncertainty of ensemble-based gridded observations inland surface simulations and drought assessment. *J. Hydrol.* **555**, 557–568 (2017)
- Anshuman, A., Eldho, T.I., Poovakka, A.K.: Performance Evaluation of SWAT with a Conceptual Rainfall Runoff Model GR4J for a Catchment in Upper Godavari River Basin. Indian Institute of Technology Bombay, Powai, India (2018)
- El Alfy, M.: Assessing the impact of arid area urbanization on flash floods using GIS, remote sensing, and HEC-HMS rainfall-runoff modelling. *Hydrol. Res.* **47**, 1142–1160 (2016)
- Ghumman, A.R., Al-Salamah, I.S., AlSaleem, S.S., Haider, H.: Evaluating the impact of lower resolutions of digital elevation model on rainfall-runoff modelling for ungauged catchments. *Environ. Monit. Assess* **189**, 54 (2017)
- Gupta, H.V., Kling, H., Yilmaz, K.K., Martinez, G.F.: Decomposition of the mean squared error and NSE performance criteria: implications for improving hydrological modelling. *J. Hydrol.* **377**, 80–91 (2009)
- Pham, M.T., Vernieuwe, H., Baets, B.D., Verhoest, N.E.C.: A coupled stochastic rainfall–evapotranspiration model for hydrological impact analysis. *Hydrol. Earth Syst. Sci.* **22**, 1263–1283 (2018)
- Wang, A., Solomatine, D.P.: Practical experience and framework for sensitivity analysis of hydrological models: six methods, three models, three criteria. *Hydrol. Earth Syst. Sci. Discuss.* (2018) [preprint]. <https://doi.org/10.5194/hess-2018-78>



Optimized Agricultural Scenarios of Proposed Kalabagh Dam Under Conjunctive Operation of Tarbela and Kalabagh Reservoirs Using Agro-Economic Model

Muhammad Sanaullah, Abdur Rehman, Muhammad Kamran, Ejaz Ahmed Abbasi, Muhammad Qasim Mahmood, and Muhammad Imran

Abstract

Kalabagh Dam (KD) is one of the proposed dams on the river Indus in Pakistan. The modeling approach was used for the estimation of agricultural benefits in prospect of conjunctive use of Tarbela and Kalabagh reservoirs. The agriculture parameters have been projected from 2001–2016 for growth rates of resources. Results of an agro-economic model (Indus Basin Model Revised) has established that canal diversions increased up to 5 MAF (42% annually) for the Upper Indus River Canals (UIRC), including the Chashma Right Bank Canal (CRBC), while for Lower Indus River Canals (LIRC), 7 MAF (58%) was observed. The future area under various crops has been predicted with an increase in annual cropping intensity to 19%, resulting in an additional demand for water for watercourse head by 27%. About 17% predicted rise in canal supplies will be helpful in fulfilling the water shortages through increasing groundwater pumpage by 23%. Model analysis indicates that annual river flows below Kotri will decline from 37.336 to 26.88 MAF due to

utilization of the Indus river water by the upstream Kalabagh canal commands. The comparison of value added per household yielded a rise of 13% for Punjab, 14% for Sindh, and about 200% for the Baluchistan province.

Keywords

Cropping intensity • Indus Basin Model Revised (IBMR) • Value added per house Hold • Storage reservoir • River flows • Agro-economic model

1 Introduction

With increasing population and depleting water resources, Pakistan is quickly heading toward a situation of water deficit and a threat of famine (Ahmad and Kutcher 1992; Ahmad et al. 1995; Kamal 2009). On the other hand, the gross capacity of Tarbela, Mangla and Chashma reservoirs in Pakistan has been depleted to 4.58 MAF by the year 2007 and the gross storage loss would reach 6.27 MAF by the year 2013 (World Bank Report 1987, 1990). About 59 million acre feet of water were recorded through Kotri barrage during the 2010-flood, and it is obvious that large dams like KD can play a role in flood prevention. However, it should not be considered as the only way of preventing floods in the Khyber Pakhtunkhwa (KPK) province and other measures should also be adopted after the completion of regional studies (Jehangir et al. 2002; Butt et al. 2015). Along with other benefits, the Kalabagh dam would be an economical source of power generation and irrigation (Butt et al. 2015).

Development of technology has triggered the vulnerability of water, energy and agricultural sectors of the Indus River System of Pakistan (Wescoat Jr et al. 2000; Mustafa

M. Sanaullah (✉) · M. Imran
Institute of Geology, University of the Punjab, Lahore, Pakistan
e-mail: sana.ullah.geo@pu.edu.pk

A. Rehman
Water and Power Development Authority (WAPDA), Lahore, Pakistan

M. Kamran
Southwest Jiatong University, Chengdu, China

Present Address:
E. A. Abbasi
Institute of Geology, University of Azad Jammu and Kashmir, Muzaffarabad, AJK, Pakistan

M. Q. Mahmood
College of Earth and Environmental Sciences, University of the Punjab, Lahore, Pakistan

2007). Therefore, at the moment, two storage reservoirs, including Diamer Basha upstream of Tarbela, and the Kalabagh dam downstream, are a necessity to regulate the abnormal flows which are foreseen during next decade in the Indus river to save the Indus Basin Irrigation System (IBIS) (Islam et al. 2008; Piracha and Majeed 2011; Anjum et al. 2016). To isolate the irrigation benefits from Kalabagh, this study has been conducted exclusively for KD without including any other new storage reservoir in the system, such as Bhasha-Diamer, Raised Mangla, and many others (Fig. 1). This work addresses the issue of agricultural water use, as well as domestic water use, and the effect of dam operations on future water demand.

2 Materials and Methods

This study has been conducted through the application of the Indus Basin Model Revised (IBMR) which is an agro-economic and irrigation optimization model, developed by the World Bank for the evaluation of water resources projects for IBIS. The structure of IBMR has been modified by increasing the Agro-Climatic Zones (ACZ) from 9 to 12 for distinct-ACZ delineation and the model has been updated for 2000–01 datasets. The IBMR has been validated against these datasets to

ensure that it simulates the actual variables with respect to the critical variables, for example; cropping pattern, fertilizer inputs, river flows, and canal diversions at canal head. The agricultural parameters have been projected from 2001 base year to the year 2016 for the growth rates of resources.

The future demand for crop and livestock commodity is determined through growth rates and has been estimated in line with the growing population rate of 2.8% per annum. This is not a forecasting exercise but simply recognition that change will occur in the system to the extent that some of them can be projected for the realistic assessment of Kalabagh benefits. The growth rate of the crop yields has been computed based on the crop yields data from 1981 to 2001 for different crops.

3 Results and Discussion

The suggested Rule Curves (RCs) for the monthly operation of the Kalabagh reservoir and the Tarbela reservoir under the conjunctive operation of Tarbela with Kalabagh (Kalabagh Dam Project Feasibility Report, 1987) demonstrates that the releases from the reservoirs or storage in the reservoirs are based on the storage capacity, reservoir operation Rule Curves (upper and lower) and the canal water allocations

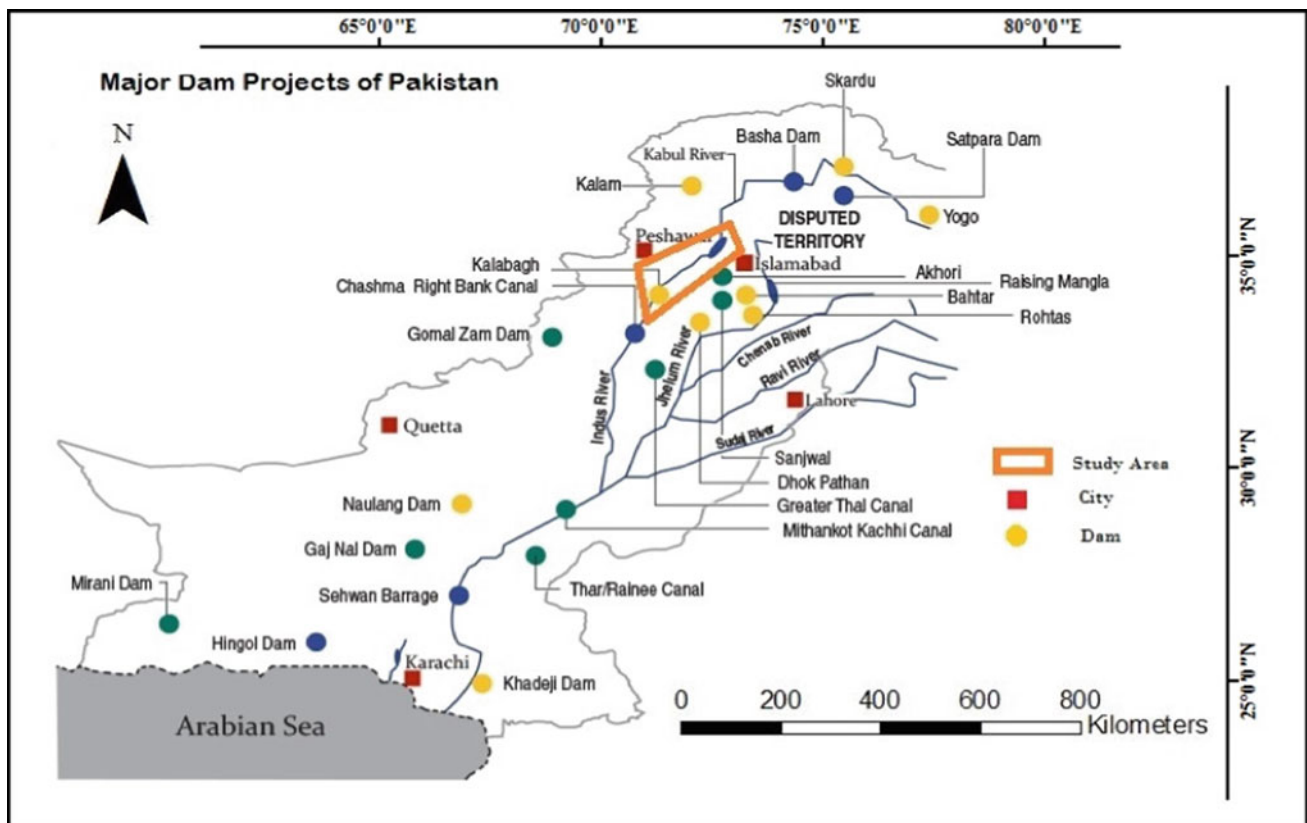


Fig. 1 Location map of Terbela and purposed Kalabagh dams along with other major dam projects in Pakistan

assumed for a particular scenario. The comparison shows that during Rabi (the Winter crop season), river flows at the Kalabagh upstream increase by 6.7%, at Chashma upstream by 12%, and at Guddu (above) by 32%. Whereas, during Kharif (the Summer crop season), the flows may decrease by 1.4% at Kalabagh (above), by 2% at Chashma (above) and by 9% at Guddu (above) which is due to water storage in upstream reservoirs during Kharif. The water from the Indus River is diverted to various canal commands including; Chashma Right Bank Canal (CRBC), Northwest Frontier Province (NWFP), Punjab canals off-taking from Chashma, Trimu, Sidhnai, and Taunsa Barrages, and all the canals irrigating Sindh and Baluchistan provinces.

This increase in annual cropping intensity is due to the addition of Kalabagh Reservoir in the system which can be further increased by adding more reservoirs including, Bhasha-Diamer, among others. This comparison shows that during Rabi, Punjab has fallow land by 15%; Sind, 38%; and Baluchistan, 24%. During Kharif, more slack land is available than during Rabi which is 29% in Punjab, 53% in Sind, and more than 75% in Baluchistan (Figs. 2 and 3).

The simulated changes in crop production with the Kalabagh Dam as compared to base year show an increase in major crops including, basmati rice, 116%; Irri rice (a type of rice), 139%; cotton, 156%; sugarcane, 117%; and wheat, 170%—with an overall increase in production of crops by 124%. The water shortages were computed through comparison of water requirements and water availability at crop root zone and watercourse head (canal outlet).

Based on the proposed Kalabagh reservoir operation rule curves and canal water allocations, it has been calculated that during Rabi, releases from Tarbela reaching Kalabagh (above) would increase by 8.5% and the Indus river flows at Chashma (above) would increase by 12%. Whereas, during Kharif, the river flows may decrease by 1.8% at Kalabagh (above) and by 2% at Chashma (above) due to upstream storage. According to the adopted water allocation scenario, the annual canal diversions at canal head of the Kalabagh command are expected to increase by 12 MAF (from 70 to 82 MAF) with 5 MAF (42%) for Upper Indus Canals of Punjab, including CRBC and 7 MAF (58%) for Lower Indus Canals of Sind and Balochistan Provinces. This increase is more in the Rabi season up to 29% than in the Kharif season (21%).

Based on the demand growth rate, projected crop yields and canal water allocation scenario, it has been estimated that the cropping intensity during the Rabi season may increase by 13%, and in Kharif by 6%, resulting in an annual cropping intensity of 135% in comparison with the base year cropping intensity of 115.9%. The increase in the cropping intensity has resulted in an increase in water requirements at watercourse head by 27%, whereas, the canal supplies increased by 15% and the resulting water shortage which will be fulfilled through groundwater pumping (Fig. 4). Overall, results at the Indus Basin level show that in spite of increased canal diversions during Rabi and Kharif, the gap between annual water requirements and canal water supplies at the watercourse level have not been reduced but rather, widened further, which indicates the need for more storage

Fig. 2 Monthly operational rule curves of Kalabagh reservoir

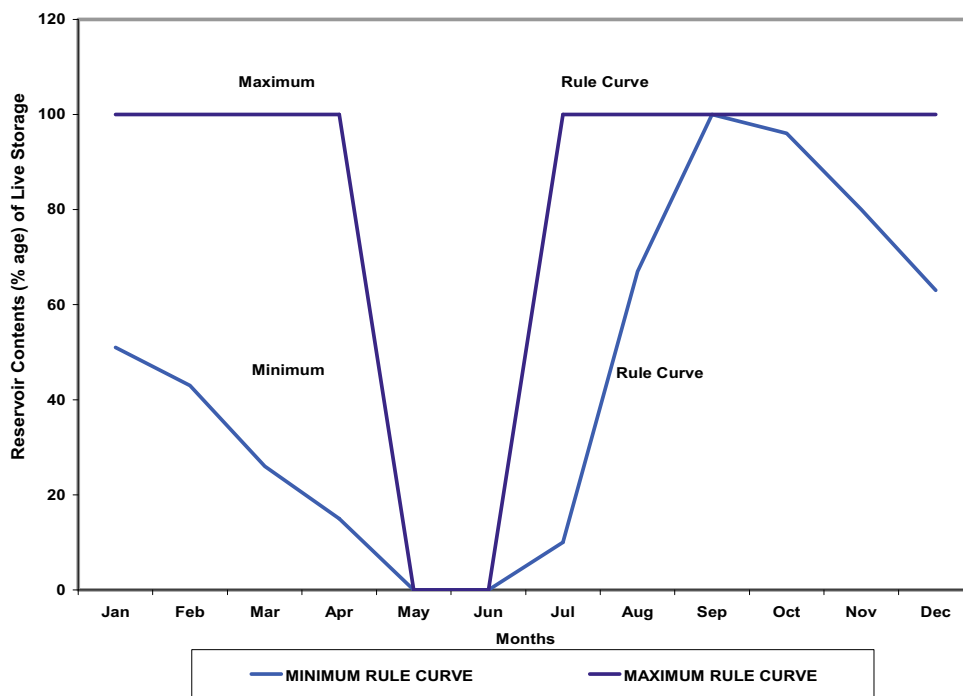


Fig. 3 Monthly rule curve for Tarbela reservoir by year 2016 (under conjunctive operation of Tarbela and Kalabagh reservoirs)

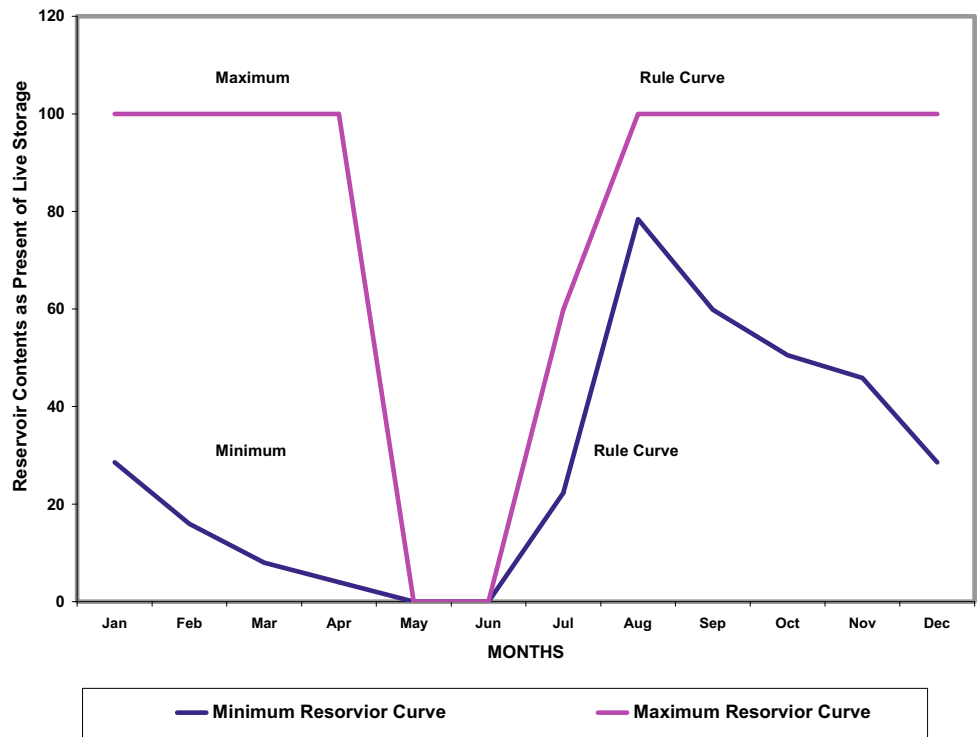
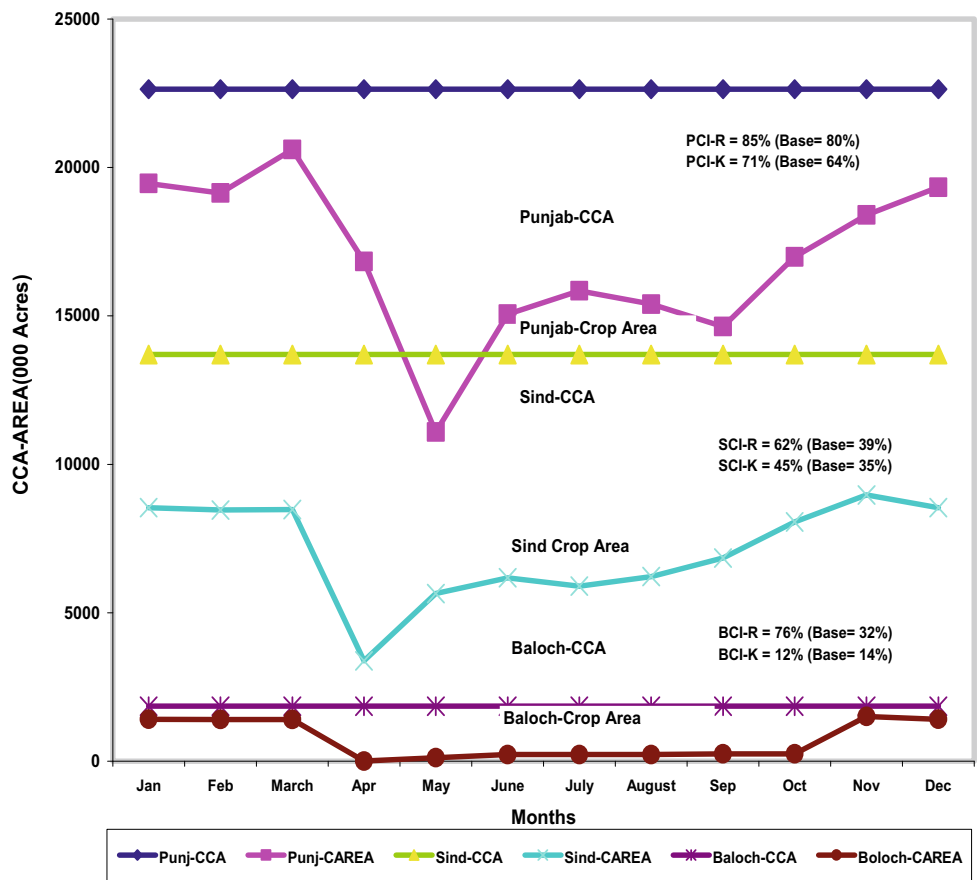


Fig. 4 Monthly comparison of crop area and CCA (with Kalabagh Dam Project-2016)



reservoirs in the system because the Kalabagh storage alone cannot meet future requirements.

4 Conclusions

The estimated mass balance indicates an increase in pumping from the areas of fresh groundwater as compared to the recharge. An increase has been observed in recharge to groundwater aquifer due to increased canal supplies during Rabi, which is proposed to be balanced by groundwater pumping, as well as the implementation of water conservation projects. The expected increase in value added per household is more than 100% with an annual growth rate of 6%, which is the incremental benefit at the farm level. Similarly, for the Baluchistan province, an increase of more than 200% in value addition is estimated, resulting in less population and farm household for canal irrigated areas. The construction of the Kalabagh Dam Project needs to be started immediately to avoid scarcity of fresh water which is approaching to the critical stage. Along with Kalabagh, other mega reservoirs on the Indus river have to be considered to fulfill the required future irrigation water needs even with the critical exploitation of groundwater.

References

- Ahmad, M., G.P. Kutcher.: Irrigation planning with environmental considerations: A case study of Pakistan's Indus basin. In: World Bank Tech. Paper No. 166. World Bank, Washington D. C (1992)
- Ahmad, M.U.D., Bastiaanssen, W.G.M., Feddes, R.A.: Sustainable use of groundwater for irrigation: a numerical analysis of the sub-soil water fluxes. *Irrig. And Drain* **51**, 227–241 (1995)
- Anjum, W.A., Ahmad, S.R., Sanaullah, M., Majid, Z., Mirza, K.: Geographic information system and modelling approach for groundwater systems of rechna doab Pakistan. *Pak. J. Sci.* **68**(4), 470–476 (2016)
- Butt, A., Khan, A., Ahmad, S.S.: Evaluation of increasing susceptibility of areas surrounding Kala Bagh Dam, Pakistan to flood risk: a review. *Middle East J. Bus.* **10**(2), 27–32 (2015)
- Islam, A., Raghuwanshi, N.S., Singh, R.: Development and application of hydraulic simulation model for irrigation canal network. *Irr. Drainage Eng.* **134**(1), 49–59 (2008)
- Jehangir, W.A., Ali, N., Salik, K.M.: Trade-offs between gross farm income, groundwater and salinity at sub-division level in the Rechna Doab. In: *Proceeding International Workshop on Conjunctive Water Management for Sustainable Irrigated Agriculture in South Asia; April 16–17, 2002*. International Water Management Institute Lahore, Pakistan (2002)
- Kamal, S.: Pakistan's water challenges: Running on empty. Kugelman and Hathway (eds), Woodrow Wilson International Center. Washington (2009)
- Mustafa, D.: Social construction of hydro-politics: the geographical scales of water and security in the Indus basin. *Geogr. Rev.* **97**(4), 484–501 (2007)
- Piracha, A., Majeed, Z.: Water use in pakistan's agricultural sector: water conservation under the changed climatic conditions. *Int. J. Water Res. and Arid Env* **1**(3), 170–179 (2011)
- Wescoat, J.L., Halvorson, S.J., Mustafa, D.: Water management in the Indus Basin of Pakistan: a half-century perspective. *Int. J. Water Res. Dev* **16**(3), 391–406 (2000)
- World Bank Report: 1987 The Agricultural Impact of Kalabagh Dam, Report, 1, The World Bank Washington, DC (1987)
- World Bank Report: Water Sector Investment Planning Study: guide to the Indus Basin model Revised. The World Bank, Washington, D. C. <http://documents.worldbank.org/curated/en/946011468154460456/Water-sector-investment-planning-study-guide-to-the-Indus-Basin-model-revised> (1990)

Hydrology, Hydrogeology, Hydrochemistry, Water Resources (T10): Hydrology, Land Use and Climatology—Surface Water Management



Pressure Change Control to Avoid Pipes Burst Disaster: An Exploratory Study

Wahiba Mokrane

Abstract

Several cases of water supply pipe bursts occur as a high, vertical jet of water and cause important flooding damages. This may be related to the type of material used in the equipment or to the negligence of pressure tests which are recommended to be done before the system's operating. In this work, we focused our idea on the pressure field as the influencing parameter. However, we presented at first the manner to follow for pressure tests; then, we studied the impact of the material type on the wave speed and, consequently, on the maximum of overpressure evaluation. On the other hand, we inspected the critical overpressure under the effect of the buckling load for the four pipe material types considered. The lower celerity calculated was for the concrete with elastic joints pipe. Thus, the maximum service pressure was also for this type of material. However, the ductile iron type presented the minimum value of the critical overpressure in buckling condition.

Keywords

Water supply • Pipe bursts • Pressure test • Buckling • Celerity

1 Introduction

Throughout all the continents of the world, pipe bursts occur as a consequence of bad water management. About ten years ago, an overpressure of 80 m was seen in Melbourne, Australia, as shown in Fig. 1. A piece from the pipe was snatched and ejected causing serious damages. Another incident occurred two years ago, in Kiev, Ukraine, which

caused the destruction of a road (see Fig. 2). In Algeria, a discharge pipe burst happened at the pumping station of Djebahia; an overpressure of 40 m high was seen then (see Fig. 3). Hence, the pressure behaviour studies seem to be very important and related tests must be done carefully and seriously during the water supply project realizations. Therefore, we present some important steps to follow. In this study, we compared the celerity aiming to have an idea about the maximum service pressure for four different types of material. When an empty pipe is subject to a buckling charge, it is considerably damaged. So, in the last part we compare the critical overpressure of the four types of pipe materials with the same diameter.

2 Methods

Before the water supply network pipes built become operational, pressure tests must be carried out in order to ensure the equipment's waterproofing properties. These tests must be carried out as follows: firstly, all foreign bodies must be expelled from the pipes; then, using a temporary device, the pipe is progressively filled from the lower points. After pressurizing the pipe for 5 mn, the purges situated at the other extremity are opened. The test is executed with the maximum service pressure for 30 mn. Then, pressure must be decreased (using the purge) and pressure values must be registered for specified times. Also, risk analysis based on the probability approach may be added (Eksplatacja 2017; Pietrucha and Zelazko 2017).

We considered four types of pipe materials which were, respectively, the polyethylene high density 'PEHD', fibre-glass reinforced polyester 'PRV', concrete with elastic joints 'BETON' and the ductile iron 'FONTE'. The maximum service pressure was defined by means of the water hammer value (www.groupe-chiali.com) and was estimated by Ghidaoui (2005):

$$\Delta P = \rho a \Delta v \text{ or } \Delta H = \pm a \Delta v / g \quad (1)$$

W. Mokrane (✉)

MVRE Research Laboratory, Higher National School of Hydraulics, Blida, Algeria



Fig. 1 Pipe burst in Melbourne (<https://www.planet.fr/international-video-lexplosion-spectaculaire-dune-conduite-deau-en-australie.262572.29335.html?page=0%2C1>)



Fig. 2 Pipe burst in Kiev (https://www.youtube.com/watch?v=Agb_pboPhBs)



Fig. 3 Pipe burst in Djebahia (<https://www.express-dz.com/2018/11/27/bouira-explosion-spectaculaire-dune-conduite-deau-a-la-station-de-pompage-de-djebahia/>)

where ‘ ρ ’ is the water density, ‘ Δv ’ the flow velocity, ‘ g ’ the gravity acceleration and change ‘ a ’ the wave celerity calculated by:

$$a = \sqrt{1/\rho[1/\varepsilon + d/(E.e)]}$$

The wave speed is in m/s; it includes in its evaluation the water elasticity in N/m^2 , the material elasticity coefficient ‘ E ’ in N/m^2 , and the pipe thickness ‘ e ’ in m.

The maximum service pressure ‘PMS’ was given by simple addition of the maximum pressure change to the pressure service ‘PS’ as follows: $PMS = PS \pm \Delta p$

When a groundwater level exceeds the water pipe kidney axe (Jacob 2006), the effect of the buckling charge must be taken into account (Pietrucha and Zelazko 2017). The critical pressure for the four pipe materials was calculated using the following formula, where ‘ μ ’ is Poisson coefficient:

$$P_c = [2E/(1 - \mu^2)][e/d]^3$$

3 Results

3.1 Results Related to the Wave Celerity

Results of the wave celerity for each type of the pipe material are shown in Fig. 4.

3.2 Results Related to the Buckling Charge Effect

The critical overpressure values which in this case are illustrated as follows (see Fig. 5).

4 Discussion

From Fig. 4, we observed maximum wave celerity of 1430 m/s for the ‘PRV’ as the pipe material for a diameter of 0.4 m. With the same diameter, the ‘PEHD’ took the second place with 1420 m/s of velocity value. ‘FONTE’ with 1410 m/s was in the third place and the ‘BETON’ with 1310 m/s came last. We deduce that the ‘PRV’ presents the maximum service pressure value, while the ‘BETON’

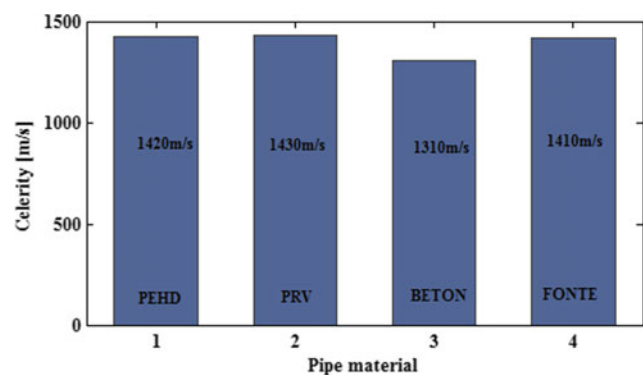


Fig. 4 Wave celerity for the four types of pipe materials (1: high-density polyethylene, 2: fibreglass reinforced polyester, 3: concrete with elastic joints, 4: ductile iron)

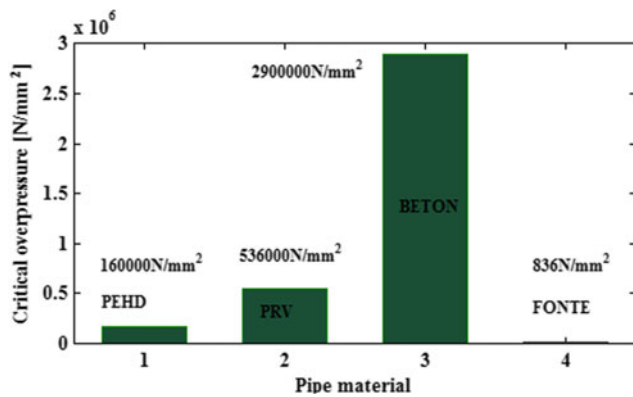


Fig. 5 Critical pressure under the bucking charge effect for different pipe materials (1: high-density polyethylene, 2: fibreglass reinforced polyester, 3: concrete with elastic joints, 4: ductile iron)

presents the minimum one. On the other hand, the inspection of the critical value of the overpressure under an external charge influence is shown as results in Fig. 5. Our conclusion was that the ductile iron 'FONTE' gives the minimum critical overpressure of 836 N/m²; 'PEHD' has a value of 160 000 N/mm²; 'PRV', 536 000 N/mm²; and, finally, the higher value was observed for concrete with elastic joints 'BETON' with 2 900 000 N/mm², in the case of an empty pipe.

5 Conclusions

Choosing the most adequate material for water supply network pipes is an important element to ensure people's safety over long periods of time. So, giving careful attention to the

pressure change may help avoid disasters similar to those we cited in different regions of the world. This work aims to sensitize decision-makers about the importance of overpressures in the case of filled and empty pipes related to four materials. We deduced from the celerity wave values that the 'PRV' gives the highest maximum service pressure while the 'BETON' gives the highest critical overpressure under a bucking charge. Finally, we recommend more security measures be taken by paying more attention to the type of pipe material and to pressure changes. In addition, and in order to predict burst events, a probability risk analysis must be considered.

References

- Eksplatacja, N.: Case study of failure simulation of pipelines conducted in chosen water supply system. *Maintenance Reliab.* **19**(3), 317–323 (2017)
- Ghidaoui, S.: A review of water hammer theory and practice. *Appl. Mech. Rev.* **58**, 49–75 (2005)
- <https://www.express-dz.com/2018/11/27/bouira-explosion-spectaculaire-dune-conduite-deau-a-la-station-de-pompage-de-djebahia/>
- <https://www.planet.fr/international-video-lexplosion-spectaculaire-dune-conduite-deau-en-australie.262572.29335.html?page=0%2C1>
- https://www.youtube.com/watch?v=Agb_pboPhBs
- Jacob, S.: *Le dimensionnement mecanique des tuyaux d'assainissement*. Cerib, Produits-ouvrages (2006)
- Pietrucha, K., Zelazko, A.: Approaches to Assess distribution water failure **61**(3), 632–639 (2017)
- www.groupe-chiali.com



A Review on the Reuse of Treated Wastewater in Algeria: Scenario and Sustainability Issues

Sabri Dairi, Dounia Mrad, Ali Bouamrane, Yassine Djebbar, and Habib Abida

Abstract

This study aims to examine and analyze water resources data in Algeria, related to wastewater treatment and reuse. Data were collected based on a survey of the concerned organizations, including the Ministry of Water Resources (MWR), the National Office of Sanitation (ONA), Wastewater Treatment plants (WWTP), and Pond Stations (PS). Complications related to sewer connection rates, unification of effluents, and wastewater treatment are the main quantification constraints in space and time. Currently, Algeria indirectly reuses 484 Hm³ of wastewater, among which only 425 Hm³ are subjected to treatment. The rest simply undergoes dilution in the natural environment. For a better use of this specific resource, an approach based on prioritization criteria of WWTP programming is adopted in order to prepare a construction plan for WWTPs implementation over a planning period reaching the horizon 2030. Reuse through inter-seasonal storage shall also be considered. This planning aims to define the potential and the agricultural opportunities of this non-conventional water resource, to meet the ever-increasing demands for water.

Keywords

Wastewater reuse • Sustainability • Treated wastewater • Algeria

1 Introduction

In Algeria, the reuse of wastewater for agricultural purposes is on the rise because of the scarcity of water resources, especially in arid and semi-arid areas where conventional waters are decreasing due to climate change impact (Hamoda 2004; Boye 2008; Hannachi et al. 2016; Negm et al. 2020a). Moreover, water resources are affected by different factors, including an ever-increasing demand, the lack of water resources mobilization works, and the contamination of both surface and groundwater resources by various anthropogenic activities (Nichane and Khelil 2014; Negm et al. 2020b). To overcome this water stress situation, considering non-conventional water resources, such as wastewater reclamation and reuse, becomes a necessity. According to Ceneapa (2003), the country has implemented, since 2000, an agricultural strategy through the National Plan for Agricultural Development for the valorization of treated wastewater in the agricultural sector (Stratégies 2007).

Wastewater reuse has become unavoidable in order to meet the challenge of water stress (Bahri 2003; Mebarki 2008; Guemmaz et al. 2020). It represents a strategic choice in Algeria. The question is no longer whether to reuse or not. The question is rather how and at which rate should we reuse, taking into account the institutional, cultural, financial, and technological constraints.

The annual volume of wastewater generated by the Algerian population is 927 million m³/year, among which 700 million m³/year are treated and reused by industrial activities (3.1 million m³/year) and irrigation (3.4 Hm³/year) (Bouchaala et al. 2017). In 2014, 108 WWTPs were in operation, including 60 lagoon stations (Bouchaala et al. 2017). The irrigated area in Algeria is currently about 950000 ha on an irrigable potential of 2.2 million ha (Hannachi 2018). As a reminder, the useful agricultural area is of the order of more than 8.5 million hectares (Bessaoud 2019). The needs corresponding to agricultural, urban, and industrial uses are currently higher than the mobilized water

S. Dairi (✉) · D. Mrad · Y. Djebbar
Laboratory of Research Infra-Res, University Mohamed Cherif
Mesaadia, Souk Ahras, Algeria

A. Bouamrane
Kasdi Merbah University, Ourgla, Algeria

H. Abida
Laboratory GEOMODELE, University of Sfax, 3029 Sfax,
Tunisia

resources, which requires trade-offs, sometimes difficult especially in drought periods (Negm et al. 2020a, b).

To reserve a satisfactory volume for irrigation, the state considered an ambitious program for the construction of major water infrastructures for the horizon 2030, to reduce water losses in water supply networks, agricultural irrigation systems and other industrial and public water use facilities. Strategies to fight water pollution were also implemented. According to key figures for the month of January 2019, drawn up by the National Office of Sanitation, Algeria has 153 wastewater treatment plants in operation of which: 75 activated sludge plants, 75 stations per natural or aerated lagoons, and three planted filters using macrophytes. The treatment capacity of these stations is estimated to be 12 million Eq/H, which is equivalent to 800 Hm³/year on a volume of rejected water estimated at 1.4 billion m³/year.

The objective of this study was to: (a) analyze the present situation of water resources in Algeria, particularly in the field of wastewater treatment and reuse, based on data from a survey of the various organizations active in this field; (b) present a strategy to ensure the sustainability of resources and good water governance in a context of sustainable development (Bouchedja 2012); (c) propose a reuse program for the horizon 2030, resulting in a systematic approach to review and update the wastewater reclamation and reuse plan.

2 Material and Methods

The adopted methodology consists of conducting a field survey, targeting organizations active in the field of water resources in Algeria. These are the Ministry of Water Resources (MRE), the National Office of Sanitation (ONA), Wastewater Treatment Plants (WWTP), and Pond Stations (PS) of Algeria. Field campaigns were conducted by the InfraRes Laboratory research team on water resources to gather information from relevant agencies. In addition, field investigations, interviews with officials and stakeholders in the field of water resources, bibliographic research and web graphics on the internet and on the official websites of national and international organizations were carried out. Data were also collected and selected from press articles, written documents, data sheets, official reports related to the national water plan, and statistics produced by relevant bodies at the ministry level (texts and guidelines) based on the method described by Bouchaala (2017).

3 Results and Discussion

The reuse of wastewater is a practice that dates back to ancient times. According to the Ministry of Water Resources (MRE), as of the 2010s, programs for the construction and

modernization of wastewater treatment plants for the reuse of wastewater in irrigation have been implemented. The ratio of wastewater reuse to resource allocation estimates the contribution of wastewater reuse to irrigation. According to Bouchaala (2017), this contribution represents 13.37% in Chelif Zahrez Hydrographic Region, 21.4% in the Constantine-Seybousse-Mellegue Basin, and 34.92% in the Oranie-Chott-Chergui Hydrographic Region. The latter is clearly deficient in rainfall compared to other regions of Northern Algeria (about 400 mm/year). The reuse component of wastewater for irrigation becomes even predominant with a ratio of 45%, or even 100% in the case of the Mléta irrigation perimeter in the region of Oran (Western Algeria).

Mok and Hamilton (2014) reported that there are health risks associated with wastewater irrigation for human food crops, particularly with surface irrigation techniques common in the developing world. Many farmers in water-scarce regions of developing countries, for instance, use wastewater to irrigate vegetables and other agricultural crops, a practice that will expand with climate change.

Reuse can be done directly or indirectly. It is also done by one of two methods: (i) reuse through a small regulating tank; (ii) reuse through inter-seasonal storage. Data related to wastewater reuse in the context of irrigation development illustrate the future challenges of water in Algeria. Besides direct reuse of treated wastewater, this latter may be intercepted after passage into the natural environment in a hydraulic system, such as a dam, to be reused with or without treatment. The volume of wastewater reused in an indirect way was shown to reach 48% of the wastewater produced at the national level. This confirms the sewage treatment program that flows into the watersheds of dams and hillside reservoirs. This is in line with the priorities of the Ministry in the field of WWTP construction, especially related to the preservation of surface and groundwater resources. Based on these results, the reuse policy could be reformulated under different scenarios to undertake the following: (i) Improving the quality of treated wastewater and distributing it as it is processed by accelerating treatment inside dams' watersheds; (ii) Mixing of wastewater with runoff water stored in surface reservoirs.

4 Conclusion

This study showed that despite a connection rate to the sewerage system close to 87% in Algeria, the volumes treated are low, which implies impacts on the surrounding physical, biological, and human systems. Indeed, a significant amount of wastewater continues to spill into the natural environment without treatment, while they can be treated by the existing wastewater treatment plants. This may be explained by the fact that nominal capacities are guideline

values based on parameters that are very often amplified through safety factors for design reasons. Therefore, a systematic effort through case-by-case studies must be undertaken to determine the actual capacities of WWTPs, which may result in huge savings in investment.

We then looked at the ambitious planning program of WWTPs through a priority system on the basis of which future WWTPs are identified and programmed by 2030, taking into account both voluntary and trend-based options. The results obtained show that treated wastewater in relation to the volume produced within watersheds is expected to increase to 73% in 2030. This programming must be taken with care where it is technically and economically feasible to group several agglomerations around a single WWTP. It allowed us—based on the calculations of the production of wastewater and the projection of new WWTPs—to estimate the total volume of wastewater that can be treated for all agglomerations in the hydrographic regions of the country. Finally, it is important to note that the integrated management of treated wastewater in Algeria, now institutionally recognized as a public–private partnership model, is the best approach for the efficient and sustainable management of treated wastewater to meet the ever-increasing water demands.

References

- Bahri, A.: Water reuse in the Middle East, North Africa and Mediterranean Countries. In: National Research Institute for Agricultural Engineering, Water and Forestry, Tunisia, Kyoto Water Forum (2003)
- Bessaoud, O., Pellissier, J.P., Rolland, J.P., et al.: Rapport de synthèse sur l'agriculture en Algérie (2019)
- Bouaroudj, S., Menad, A., Bounamous, A., Ali-Khodja, H., Gherib, A., Weigel, D.E., Chenchouni, H.: Assessment of water quality at the largest dam in Algeria (Beni Haroun Dam) and effects of irrigation on soil characteristics of agricultural lands. *Chemosphere* **219**, 76–88 (2019). <https://doi.org/10.1016/j.chemosphere.2018.11.193>
- Bouchaala, L., Charchar, N., Gherib, A.E.: Ressources hydriques: traitement et réutilisation des eaux usées en Algérie. *Algerian J. Arid Environ.* **12**, 84–95 (2017). <https://www.asjp.cerist.dz/en/article/40098>
- Bouchedja, A.: La politique nationale de l'eau en Algérie, 10ème Conférence Internationale Euro-RIOB, Istanbul-Turkey (2012)
- Boye, H.: Water, energy, desalination and climate change in the Mediterranean. Sophia Antipolis: Plan Bleu (2008)
- Ceneapa: Problématique du développement rural. Analyse et prospective, collection les mutations du monde rural, **28**, 116 (2003)
- Dairi S.: La simulation dynamique comme un outil d'aide à la décision pour la gestion des stations d'épuration à boues activées. Doctoral thesis, Université, Annaba, Algeria (2018)
- Driss, L., Soulaymane, I., Lahcen, M., et al.: Diagnostic socio-économique et environnemental de l'irrigation des cultures maraichères avec les eaux usées non traitées: cas de la zone urbaine et périurbaine de la ville de Meknès au Maroc. *ScienceLib Editions Mersenne* **5**, 130212 (2013)
- Guemmaz, F., Neffar, S., Chenchouni, H.: Physicochemical and bacteriological quality of surface water re-sources receiving common wastewater effluents in drylands of Algeria. In: Negm, A., Bouderbala, A., Chenchouni, H., Barcelo, D. (eds.) *Water Resources in Algeria—Part II: Water Quality, Treatment, Protection and Development*. Springer Nature Switzerland, 117–148 (2020). <https://doi.org/10.1007/978-3-030-57887-9>
- Hamoda, M.F.: Water strategies and potential of water reuse in the south Mediterranean countries. *Desalination* **165**, 31–41 (2004). <https://doi.org/10.1016/j.desal.2004.06.004>
- Hannachi, A., Gharzouli, R., Tabet, Y.D., et al.: Wastewater reuse in agriculture in the outskirts of the city Batna (Algeria). *J. Fund. Appl. Sci.* **8**(3), 919–944 (2016). <https://doi.org/10.4314/jfas.v8i3.15>
- Hannachi, A.: Les politiques publiques du recyclage des eaux usées traitées en agriculture périurbaine: enquête auprès des acteurs de la filière à Batna. Doctoral thesis (2018)
- Khiati, M.: Stratégies, politiques et systèmes de connaissances agronomiques, Cfva de Médéa, 10–13 Juin 2007, p. 6
- Mok, H.F., Hamilton, A.J.: Exposure factors for wastewater-irrigated Asian vegetables and a probabilistic rotavirus disease burden model for their consumption. *Risk Anal.* **34**(4), 602–613 (2014)
- Mebarki, A.: Le défi de l'eau en Algérie : ressources, aménagements et gestion durable (31ème Congrès International de Géographie UGI, Tunis, Tunisie, 12–15 Août 2008)
- Nichane, M., Khelil, M.A.: Changements Climatiques et Ressources en Eau en Algérie: Vulnérabilité, Impact et Stratégie d'Adaptation. *Revue Des Bioressources* **257**(3242), 1–7 (2014)
- Negm, A., Bouderbala, A., Chenchouni, H., Barcelo, D. (Eds.): *Water Resources in Algeria—Part II: Water Quality, Treatment, Protection and Development*. The Handbook of Environmental Chemistry Series. Cham (2020a). <https://doi.org/10.1007/978-3-030-57887-9>
- Negm, A., Bouderbala, A., Chenchouni, H., Barcelo, D. (Eds.): *Water Resources in Algeria—Part I: Assessment of Surface and Groundwater*. The Handbook of Environmental Chemistry Series, Springer Nature Switzerland (2020b). <https://doi.org/10.1007/978-3-030-57895-4>
- PNE (le plan national de l'eau), 2010. Réalisation de l'étude d'actualisation du plan national de l'eau. Mission 2: ressources en eau non conventionnelles. MRE/DEAH/SOFRECO. Août (2010)



Infiltration Boxes as a Part of Urban Storm-Water Management. A Case Study: Port of Pancevo, Serbia

Denisa Djordjevic, Mladen Milanovic, Dragan Milicevic, and Zeljka Ostojic

Abstract

Urban storm-water in common practice flows directly to the sewage networks which increases the pipe diameters and consequently leads to very high pipeline investment costs. The construction of infiltration boxes can improve that situation. In this study, infiltration boxes-based approach was compared to the standard collector storm-water drainage system in the Port of Pancevo in Serbia (Southeast Europe). This concept allows up to a 50% cheaper and more efficient drainage system. Usage of infiltration boxes can help to avoid over-dimensioning of storm-water drainage systems with almost 2.5 times reduction of the collector diameter and increase four times the efficiency of water treatment plants. Overall results strongly support using the infiltration boxes in the urban storm-water management.

Keywords

Infiltration basins • Urban storm-water management • Port of Pancevo

1 Introduction

Extreme events such as heavy precipitation (Gocic et al. 2016), high evaporation (Trajkovic and Kolakovic 2010), large temperature fluctuations (Kisi and Yildirim 2005), or droughts (Gocic and Trajkovic 2013) have often occurred in

D. Djordjevic
Faculty of Civil Engineering, Brno University of Technology,
Brno, Czech Republic

M. Milanovic (✉) · D. Milicevic
Faculty of Civil Engineering and Architecture, University of Nis,
18000 Nis, Serbia

Z. Ostojic
Hidroprojekat Saobraćaj, 11000 Belgrade, Serbia

recent years. Because of that, urban storm-water management has become a very important part of integral water management. Urban storm-water usually flows directly to sewage networks (Khodashenas and Azizi 2019; Helmi et al. 2019). This approach increases the pipe diameters, pipeline investment costs, and treatment costs and decreases treatment efficiency (Brown et al. 2009).

The construction of infiltration boxes can improve urban storm-water management. A new storm-water approach includes decreasing and slowing down the outflow from hard, impervious surfaces (Marlow et al. 2013; Rodríguez-Sinobas et al. 2018). The main objective of this paper is to analyse using infiltration boxes as part of an urban storm-water management system.

2 Materials and Methods

In this paper, the drainage system of the Port of Pancevo was used as a case study. The port of Danube Pancevo is located on the left bank of the Danube at km 1 + 153 of the river, at the mouth of the river Tamiš into the Danube. The subject area covers an area of about 120 ha. The temperature extremes varied between -21 and 38 °C, and maximum daily precipitation of 94 mm is recorded in this area.

A unique collector for both storm-water from the roof and the roads was adopted by the preliminary design (Fig. 1a). A section of rain sewage system (DN/ID1500) (length of 1000 m), which passes through a roadway between the planned warehouses, was analysed. This section has the maximum water flow of $Q = 3.38 \text{ m}^3 \text{ s}^{-1}$ at a flow velocity of $v = 1.9 \text{ m s}^{-1}$ with a charge of 95.2% and minimal channel drop loss of 0.15%. The complete volume of water goes to the treatment plant, which consists of sedimentation tanks, oil separator, and pump station.

In this research of the rainfall on the location of Port of Pančevo, infiltration boxes were used to receive conditionally clean water from their warehouse roofs, and a designed

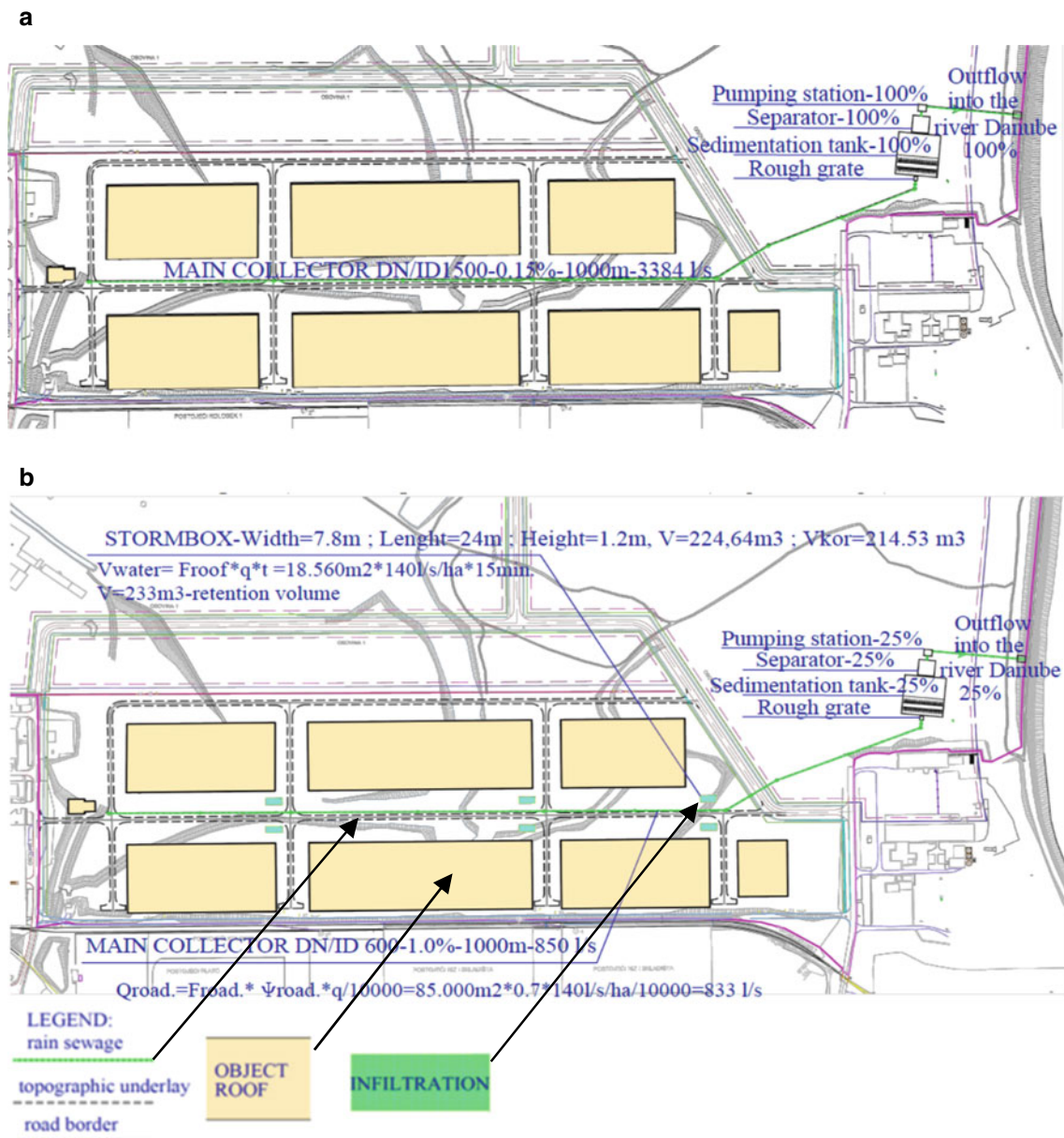


Fig. 1 a The unique collector DN/ID 1500 (original design). b Six infiltrations + Collector DN/ID 600 (redesign)

collector on that location was provided for the reception of water from roads and streets. The condition for the application of the system of boxes is that the ground water level is below the bottom level of infiltration surface storage. The disposition of the infiltrations is shown in Fig. 1b (six rectangles).

The infiltration boxes used in this study are made of polypropylene, each having a volume of 0.21 m³ and reinforced pillars with an effective capacity of 95.5%. Infiltration volume and number of infiltration boxes, and the static verification of the lifting capacity for heavy traffic loads, with the calculation of associated earthworks, were done with a certified software package from the manufacturer.

3 Results and Discussion

Rainwater calculations were done in the EPA Storm Water Management Model (SWMM) program. The following rainfall data were calculated by rational method: 15 min intensity rainfall of 140 L/s/ha with a return period of 2 years for all sub-basins, mean runoff coefficient 0.66. The coefficient of filtration is $k = 10^{-4} \text{ m s}^{-1}$ and green cover is 0.3. According to those data, the collector maximum flow of 0.83 m³ s⁻¹ was estimated, and the new redesign collector DN/ID600 (only for storm-water from roads and streets) was adopted. It has the maximum water flow of $Q = 0.85 \text{ m}^3 \text{ s}^{-1}$

at a flow velocity of $v = 2.9 \text{ m s}^{-1}$ with a charge of 92% and minimal channel drop loss of 1.0%. It can be concluded that the collector's maximum flow was decreased from 3.38 to $0.85 \text{ m}^3 \text{ s}^{-1}$. This is important for a water treatment plant because 75% less water will come to the plant.

According to computational rainfall and roof area, the infiltration volume of 233 m^3 was estimated and dimensions were adopted (width = 7.8 m; length = 24 m; height = 1.2 m; $V = 225 \text{ m}^3$; No. of boxes = 1.040; discharge time: 2.7 h).

The new approach provides a 75% reduction in the volume of atmospheric water to be collected by the pipeline and transported to the pump and separator, which results in the reduction of the dimensions of the pipeline, pump station, and separator. The cost of the pipeline is reduced by 50% in comparison with the classical approach, and the cost of the separator and pump station by around 65%. The total reduction of the investment cost of the new variant in comparison with the classical one, including the construction cost of storm-boxes, is reduced by 56%.

It can be concluded that the advantages of the concept with infiltration boxes help avoid the over-dimensioning of storm-water drainage systems, increase the efficiency of water treatment plants, lower outflow rate, flatten flow peaks, regulate groundwater levels, and lower the influence of the sewage flow on the water receiver.

4 Conclusions

The main advantage of this study is the use of the infiltration boxes for the mitigation of atmospheric runoff peaks, as well as the implementation of an infiltration concept into the sewage system as elements for the reduction of the collector installation. Storm-water can be collected in the area where it falls. This new approach does not require any additional fees as opposed to the traditional approach. Water from retention can be used to process water in factories, irrigate parks, or for cleaning purposes.

In this paper, the infiltration boxes-based concept was applied to the Port of Pancevo (Serbia) instead of the classic drainage system. According to the comparative economic indicators for both concepts, it can be concluded that the

infiltration boxes-based approach allows to make great cost savings and has many other advantages. Those facts strongly support the use of infiltration boxes as part of an urban storm-water management system.

Acknowledgements The authors wish to express appreciation to the reviewers for their valuable comments and suggestions concerning this manuscript. The presented research is a part of the project of Serbian Academy of Sciences and Arts Branch in Nis (O-15-18) and is also funded by the Ministry of Education, Science and Technological Development of the Republic of Serbia (TR37018).

References

- Brown, R.R., Keath, N., Wong, T.H.F.: Urban water management in cities: historical, current and future regimes. *Water Sci. Technol.* **59** (5), 847–855 (2009)
- Gocic, M., Shamshirband, S., Razak, Z., Petkovic, D., Sudheer, Ch., Trajkovic, S.: Long-term precipitation analysis and estimation of precipitation concentration index using three support vector machine methods. *Adv. Meteorol.* 7912357 (2016)
- Gocic, M., Trajkovic, S.: Drought characterisation based on Water Surplus Variability Index. *Water Resour. Manage.* **28**(10), 3179–3191 (2013)
- Helmi, A.M., Mahrous, A., Mustafa, A.E.: Urbanization growth effect on hydrological parameters in mega cities. case study: 5th Settlement-Cairo-Egypt. In: Chamine et al. (eds.) *Advances in Sustainable and Environmental Hydrology, Hydrogeology, Hydrochemistry and Water Resources, Advances in Science, Technology and Innovation*, pp. 409–412, Springer Nature (2019)
- Khodashenas, S.R., Azizi, J.: The effect of urban development on urban flood runoff (Case Study: Mashhad, Iran). In: Chamine et al. (eds.) *Advances in Sustainable and Environmental Hydrology, Hydrogeology, Hydrochemistry and Water Resources, Advances in Science, Technology and Innovation*, pp. 409–412, Springer Nature (2019)
- Kisi, O., Yildirim, G.: Discussion of “Forecasting of Reference Evapotranspiration by Artificial Neural Networks” by Slavisa Trajkovic, Branimir Todorovic, and Miomir Stankovic. *J. Irrig. Drain. Eng.* **131**(4), 390 (2005)
- Marlow, D.R., Moglia, M., Cook, S., Beale, D.J.: Towards sustainable urban water management: a critical reassessment. *Water Res.* **47** (20), 7150–7161 (2013)
- Rodríguez-Sinobas, L., Zubezu, S., Perales-Momparler, S., Canogar, S.: Techniques and criteria for sustainable urban storm-water management. The case study of Valdebebas (Madrid, Spain). *J. Cleaner Prod.* **172**(20), 402–416 (2018)
- Trajkovic, S., Kolakovic, S.: Comparison of simplified pan-based equations for estimating reference evapotranspiration. *J. Irrig. Drain. Eng.* **136**(2), 137–140 (2010)



Application of Different LID Technologies for the Drainage of Urban Areas: A Case Study—Pek Settlement, Serbia

Slavisa Trajkovic, Dragan Milicevic, Mladen Milanovic, and Milan Gocic

Abstract

There are big issues in the drainage of storm-water in urban areas. The key issue is frequent floods during intensive rain, because the sewage system was constructed using the classical approach (wastewater—domestic/industrial and storm-water are collected together, and go to the nearest recipient through pipes). In order to improve this state, a new approach for storm-water management was made based on the decentralized systems. The paper presents the application of Low Impact Development (LID) techniques on urban areas, i.e. on the Pek settlement in Kucevo (Serbia). In order to have a more purposeful analysis of applied techniques, three variant solutions were made.

Keywords

Storm-water • Sewage system • LID techniques • Serbia

1 Introduction

The impermeable urban areas have rapidly increased, mainly owing to rapid urbanization. The consequences of this trend in urban areas are the increased runoff production and velocity (which directly causes flooding), and low level of water quality (Khodashenas and Azizi 2019). In brief, the entire hydrologic cycle has changed in rapidly developed urban areas (Gocic et al. 2016; Jacobson 2011). On the other hand, practical knowledge has shown that classical systems of storm-water management are not capable of draining storm-water in rapidly developed urban areas. As a measure that supports using the decentralized systems and a more

careful urban planning, Low Impact Development (LID) technology was presented. One of the main characteristics of LID technology is to keep the runoff volume in urban zones at the level of the pre-urban runoff volume (Dietz 2007; Ibrahim et al. 2019).

There are several studies where LID techniques were analysed (Eckart et al. 2018; Matos et al. 2019; Wang et al. 2018). The analysis of the hydrological impact of LID's technology on the campus of the University of Trás-os-Montes e Alto Douro in Portugal was made (Matos et al. 2019). The authors showed that the reduction of discharges using the LID solutions (versus classical solutions) was between 68 and 95% of total discharge. What is more, the effectiveness of urban storm-water infrastructure was investigated at four urban catchments in Singapore, using the modelling of future scenarios (Wang et al. 2018).

The paper presents the application of different LID techniques with a classical sewage system, through three variant solutions for the Pek settlement in Serbia.

2 Materials and Methods

The study area in this paper is the settlement of Pek in Kucevo, located in the north-eastern part of Serbia. The terrain is mostly mountainous (Homolje mountains are the highest with 940 m) and the river Pek is the greatest river in Kucevo municipality, with a flow of 48.5 m³/s. The settlement of Pek has a temperate continental climate with daily T extremes from −27 to 40°C and extreme daily precipitation of 113 mm. The settlement of Pek covers the area of 2.54 ha with almost 800 inhabitants.

The Pek settlement does not have a storm-water sewage system. The main reasons for this state can be classified into two groups, as natural and cost conditions. The terrain of the Pek settlement is very unfavourable, i.e. the streets are raised in relation to the surrounding terrain, so the building of curbs for surface drainage of storm-water is not possible. This

S. Trajkovic (✉) · D. Milicevic · M. Milanovic · M. Gocic
Faculty of Civil Engineering and Architecture, University of Nis,
18000 Nis, Serbia
e-mail: slavisa@gaf.ni.ac.rs

causes frequent floods (caused by storm-water), because all the storm-water from the impermeable areas represents a potential cause of floods. Furthermore, the river Pek represents the only place where collected storm-water can go. Thus, this river is prone to flash flooding, and with additional amounts of water, the bank areas can be easily flooded. An economic analysis showed that building a sewage system for the drainage of storm-water would be very expensive for the following reason: The pipe diameter would be large and a lot of pump stations would have to be built for storm-water pumping (based on the topographic conditions).

Based on the terrain configuration, a plan of detail regulations for surface areas, water quantity, and conditions for storm-water drainage, three LID techniques were used: vegetative swales, infiltration trenches, and porous asphalt. The primary goal of the proposed techniques is to remove (drain) storm-water, as a measure of flood prevention, from streets, pavements and parking lots.

EPA SWMM (EPA Storm-water Management Model) software was used to create a model for the examination of different solutions for storm-water sewage management. SWMM is the software used for the design and analysis of sewers and drainage systems.

Three variant solutions for storm-water drainage were made. The first variant solution represents only the classical sewage system. The second variant solution consists of vegetated swales, infiltration trenches and the storm-water sewage system in order to cover all the potential causes of floods. The third variant solution is based on porous asphalt (which covers 50% of the impervious areas in Pek) and storm-water sewage. The sewage systems used in the second and third solutions involve a much smaller diameter of pipes than in the first variant solution.

3 Results and Discussion

The SWMM model covers the area of the total catchment of 2.36 ha. The catchment is divided into nine sections. For calculation, the Hazen-Williams method was used for the

storm-water simulation as well as precipitation with a 10-year return period.

According to simulation results, Variant 2 had the greatest values of total storm-water infiltration at the entire catchment. The values of Variant 1 are almost 1/3 lower than the values of Variant 2, and Variant 3 values are twice less than the ones of Variant 2, for all sub-catchments. Furthermore, the results showed that the procedure where storm-water is drained from impervious areas into vegetated swales and infiltration trenches leads to an almost complete annulment of runoff from impermeable surfaces. In addition, replacing impermeable asphalt with porous asphalt leads to a significant reduction in surface runoff. The results for the total runoff from the observed Pek settlement showed that Variant 1 had the greatest value of 162.23 mm for the total catchment, i.e. the values of Variant 1 for all the sections are almost twice greater than the values of Variant 2, Fig. 1. The values for Variants 2 and 3 are similar.

The results of the total storm-water inflow into the recipient are shown in Fig. 2. The hydrograph shows a peak of 221.63 l/s in Variant 1, and of 145.96 l/s in Variant 2, i.e. there is a peak reduction of 34% when porous asphalt is used for storm-water management. The peak is almost completely annulled in Variant 2, i.e. when swales and infiltration trenches are used.

4 Conclusions

A comprehensive analysis of three variant solutions, based on the classical sewage system and LID techniques was made for the Pek settlement. The effects of the applied LID techniques are clearly highlighted throughout the paper. What is more, the best results were obtained by the second solution (vegetated swales, infiltration trenches and storm-water sewage system), where the total inflow into the recipient was annulled. The third solution, based on the porous asphalt and storm-water sewage, is the most practical solution, which also yields good results. It can be concluded

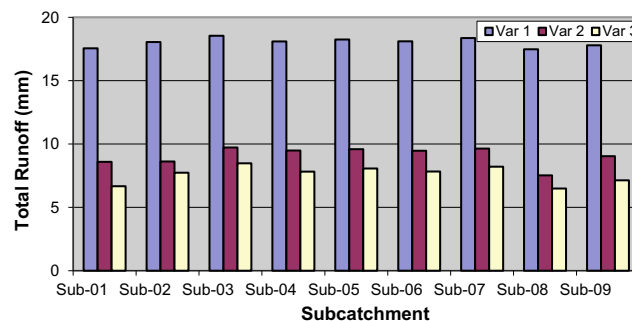
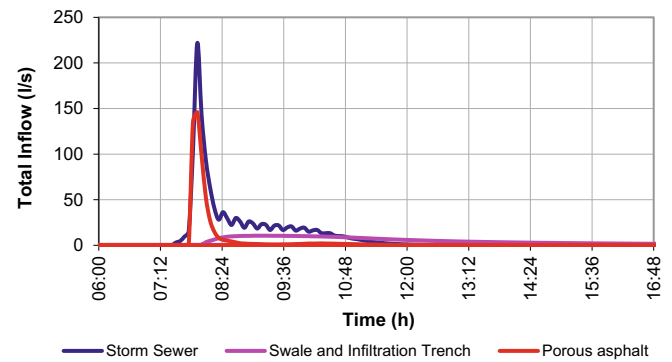


Fig. 1 Total runoff for the Pek settlement

Fig. 2 Total inflow into the recipient



that LID technology based on decentralized systems represents the most useful solution for the drainage of storm-water in the Pek settlement.

Acknowledgements The presented research is a part of the project of the Serbian Academy of Sciences and Arts, Branch in Niš (0-15-18), and is also funded by the Ministry of Education, Science and Technological Development of the Republic of Serbia (TR37018,37003).

References

- Dietz, M.E.: Low impact development practices: a review of current research and recommendations for future directions. *Water Air Soil Pollut.* **186**, 351–363 (2007)
- Eckart, K., McPhee, Z., Bolisetti, T.: Multiobjective optimization of low impact development stormwater controls. *J. Hydrol.* **562**, 564–576 (2018)
- Gocic, M., Shamshirband, S., Razak, Z., Petkovic, D., Sudheer, Ch., Trajkovic, S.: Long-term precipitation analysis and estimation of precipitation concentration index using three support vector machine methods. *Adv. Meteorol.* 7912357 (2016)
- Ibrahim, M.G., Elboshy, B., Mahmod, W.E.: Integrated Approach to Assess the Urban Green Infrastructure Priorities (Alexandria, Egypt). In: Chamine et al. (eds.) *Advances in Sustainable and Environmental Hydrology, Hydrogeology, Hydrochemistry and Water Resources, Advances in Science, Technology and Innovation*, pp. 413–415. Springer Nature (2019)
- Jacobson, C.R.: Identification and quantification of the hydrological impacts of imperviousness in urban catchments: a review. *J. Environ. Manage.* **92**(6), 1438–1448 (2011)
- Khodashenas, S.R., Azizi, J.: The Effect of Urban Development on Urban Flood Runoff (Case Study: Mashhad, Iran). In: Chamine et al. (eds.) *Advances in Sustainable and Environmental Hydrology, Hydrogeology, Hydrochemistry and Water Resources, Advances in Science, Technology and Innovation*, pp. 409–412. Springer Nature (2019)
- Matos, C., Briga Sa, A., Bentes, I., Pereira, S., Bento, R.: An Approach to the implementation of low impact development measures towards an ecocampus classification. *J. Environ. Manage.* **232**, 654–659 (2019)
- Wang, M., Qing Zhang, D., Su, J., Wen Dong, J., Keat Tan, S.: Assessing hydrological effects and performance of low impact development practices based on future scenarios modeling. *J. Clean. Prod.* **179**, 12–23 (2018)



An Overview of Vadose Zone Characterization for the Assessment of the Impact of Burial on Groundwater in South-Western Nigeria

Charles A. Oyelami, Olabanji A. Ojo, Mutiu A. Fakunle, Oluwole E. Ajayi, and Uche E. Tochukwu

Abstract

Improper siting of cemeteries may sometimes be responsible for groundwater pollution which affects surface and groundwater quality. The environmental impact of cemeteries close to residential area was assessed in this research with the aim of establishing their safety or otherwise in terms of water quality and proper selection of soil materials for cemetery siting. An integrated approach involving geotechnical characterization, vertical electrical sounding and groundwater quality assessment was adopted. The topography reflects a wetland that slopes into a gaining stream located about <10 m from the cemetery. The soil within the cemetery consists of coarse-grained porous lateritic soil, clay and silt (0.22–3.88%) with a high percentage of gravel/sand (73.50–83.96%). Water analysis revealed high total coliform content, 14–89, except in the control well and a total hardness between 86 and 380 mg/L. Most cation values were higher than MPL as compared with WHO drinking water standard and the Nigeria drinking water standard. Geophysical investigation revealed that the depth to contamination corresponds with the depth to the aquifer in the study area. The study concluded that the location of the cemetery has a high risk potential of environmental impact on its immediate vicinity, arising from the thin unsaturated zone.

vicinity. Little attention has been given to cemeteries as a potential source of contamination because cemeteries are believed to be sacred places where investigations are seldom carried out in Africa. Secondly, the spirit of the dead is assumed to be resting and there should be no disturbance around them. And lastly, the dead have nothing to do with the living; therefore, there could be no interaction (based on religious beliefs) or impact from the dead on the living. All these are myths and they are not scientifically proven. Research reveals that incessant siting of cemeteries may be responsible for groundwater pollution, not necessarily because of toxicity of human corpses, but through an increment in the concentrations of naturally occurring organic/inorganic substances up to a level sufficient to render groundwater unusable or unpotable (Spongberg and Becks 2000; Dippenaar 2014). Decomposition of human body has been found to be directly dependent on the environmental factors like climate, weather, rate and intensity of precipitation, topography, conditions of the soil and above-ground temperature (Rodriguez and Bass 1985; Mann et al. 1990; Spongberg and Becks 2000; Sorlini et al. 2013; Dippenaar 2014). Soil selection and thickness of the vadose, or unsaturated zone, have equally been found to be important factors in determining the impact of cemeteries on its immediate environment. Therefore, the present study is aimed at investigating the soil–water interaction within the vicinity of selected cemeteries in order to establish the potential risk associated with the already existing cemeteries in the area. Cemeteries have contributed negatively to groundwater quality around the world, and these have been reported in several studies. Inadequate potable water supply remains one of the major challenges in developing countries. Rodrigues and Pacheco (2010) demonstrated that cemeteries contributed to ground water contamination. They recommended site-specific risk assessments for cemetery sites, taking into consideration the geological and hydrogeological conditions, as well as the proximity of receptors, such as boreholes, hand dug wells and springs. A safe cemetery siting distance

1 Introduction

Cemeteries in some parts of Africa are sited within or very close to residential communities with no regard to their potential impact on the groundwater pollution within the

C. A. Oyelami (✉) · O. A. Ojo · M. A. Fakunle · O. E. Ajayi · U. E. Tochukwu
Department of Geological Sciences, Osun State University,
Osogbo, Oke-Baale, Osogbo, PMB 4494, Nigeria
e-mail: adebayo.oyelami@unosun.edu.ng

of about 250 m from any source of potable water was recommended by the WHO (1998). As a result, large numbers of inhabitants depend on unsafe water for consumption as well as domestic use. The little water present within the subsurface may not equally be safe due to contamination from quite a number of sources. Some of these are dumpsites, effluents from industries, waste disposals and sewages from conveniences as well as from cemeteries.

2 Methodology

An integrated approach was employed in this research work. This involves geophysical investigation to establish the possibility of contamination within the study area; followed by water sampling to assess the extent of the contamination and finally the geotechnical test to ascertain the vulnerability of the soils. Six vertical electrical soundings (VES) using Schlumberger array were carried out to study the depth to the contamination. The obtained data were interpreted using the partial curve matching techniques prior to iteration applying the iterative software. Ten water samples were collected from wells and rivers within the vicinity of the cemetery at random and analysed for the physical, chemical and biological constituents. Cations and heavy metals analyses were carried out using atomic absorption spectrophotometer, while anion analysis was done using the iron chromatographic method and the titrimetric method was used for SO_4 and HCO_3 . The biological constituents (total coliforms, faecal Streptococci and *Escherichia coli*) were analysed by using the enzymatic substrate method (Colilert) (Stevens et al. 2003). A control well was also sampled far away from the cemetery. The results from the analyses were compared with the World Health Organization's (2016) standard as well as the Nigeria Water Standard (NWS) in order to determine the significance of the contamination. The geotechnical aspect of the study consisted in taking six bulk soil samples from two hand dug pits, one from the upper section of the cemetery (Pit 1) and the other from a waterlogged area in the lower part of the cemetery. The soil samples were taken to the laboratory where index, engineering and mineralogical tests were carried out. The index and engineering properties tests were carried out at the soil laboratory of the Osun State University, Osogbo, Nigeria. These include natural moisture content, specific gravity grain size analysis, Atterberg limit (liquid limit, plastic limit, plasticity index and linear shrinkage), compaction test and porosity estimation from the tests. All the tests were carried out according to the British Standard BS 1377(1990) procedures (BSI 1990; Oyelami and Van Rooy 2016) where small modifications were necessary.

3 Results and Discussions

3.1 Climate, Vegetation, Relief and Drainage

The climate of the study sites can be described as humid to sub-humid tropical with distinct dry and wet seasons (Talabi 2013). The total annual rainfall ranges between 1500 and 2500 mm with peaks in June and October. The mean annual temperature is about 28 °C with a 3 °C annual variability, and the relative humidity average is 90% throughout the year (Oyelami and Van Rooy 2016; Gbadegehin and Nwagwu 1990). Relative humidity is high with daily values at 1600 h ranging between 60 and 90%. The Osun River is perennial and its volume fluctuates with the seasons. The river flows throughout its course across the basement complex with a trellis drainage pattern (Fig. 1).

3.2 Geophysical Investigation

From the study, the lithology within the cemetery exhibited a thin layer of clayey sand to sandy topsoil that ranged in thickness from as low as 0.25 m in VES 7 to as high as 1.56 m in VES 4 with resistivities from 46.6 Ωm in VES 4–97.72 Ωm in VES 2 (Fig. 2). This was directly underlain by a clayey sand/clay interval in certain areas. The weathered layers showed very low resistivity values that ranged from 3.18 in VES 3 to 37.6 in VES 5 which indicated the presence of a high conductivity anomaly within the saturated zone (Fig. 2). The high conductive anomaly was suspected to be a result of contamination. This depth varied between 2.1 m, around the stream, and about 3.9 m in other locations; a depth which corresponded to the depth to the aquifer in the study area. Possibly, leachate from the decaying cadavers may have penetrated into the saturated layer within the subsurface, thereby contaminating the subsurface water.

3.3 Hydrogeology

Generally, the relative abundance of the anions was observed to be in the order of $\text{NO}_3^- > \text{HCO}_3^{1-} > \text{Cl}^-$. NO_3^- seems to predominate with an average concentration of 59.17 mg/L, a value above the acceptable WHO water quality standard and Nigeria drinking water standard of 50 mg/L. This is followed by HCO_3^{--} (52.8 mg/L) and Cl^- (28.3 mg/L). NH_4^+ concentration value was observed to be greater than the permissible limit, with an average value of 2.04 mg/L, a value far above the 1.5 mg/L of the WHO quality standard. The following concentrations were also recorded: Mg^{2+} (23.5 mg/L), Ca^{2+} (84 mg/L) and Na^+ (144 mg/L). Few other cations and anions were observed to be higher than the

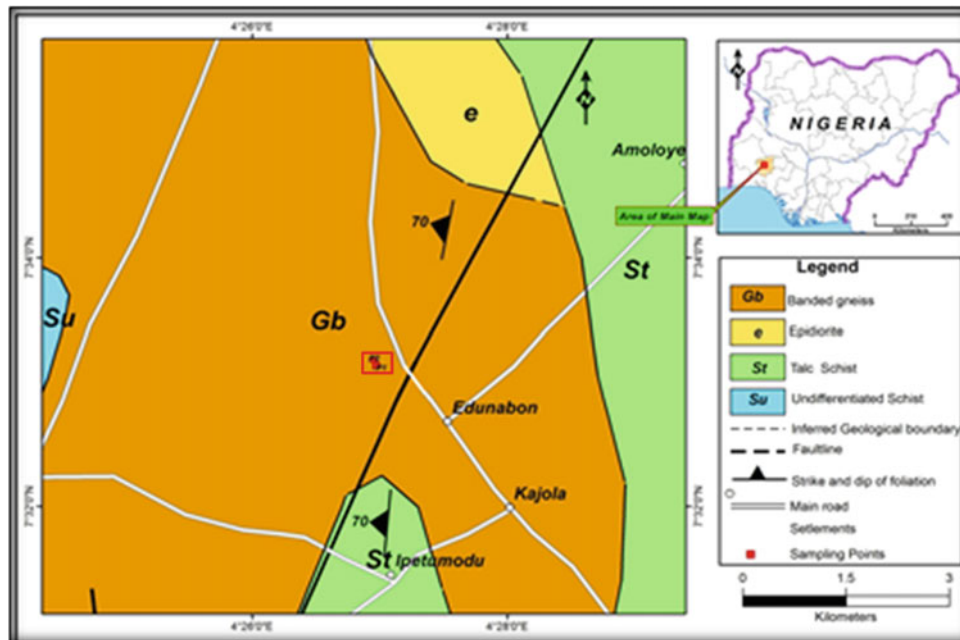


Fig. 1 Map shows rock types in the study area

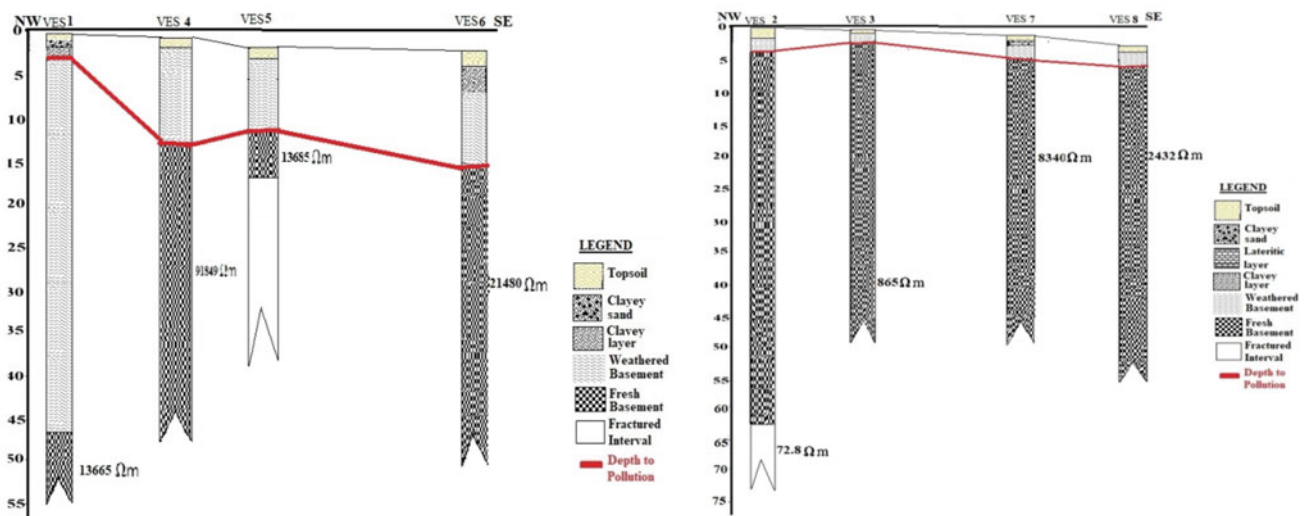


Fig. 2 Geo-electric sections show various depths to contamination based on their resistivity

acceptable WHO limit. Potable groundwater should contain less than 75 mg/L of Ca^{2+} . The values determined in the study area (Ca^{2+} 84 mg/L) were higher than the WHO's limit and, as such, were not suitable for human and domestic consumption. The high concentration is likely attributed to the presence of leachate from the cemetery in the surrounding area which finds its way into the saturated layers. The depth to water varied according to the slope of the study area. The depth to water at Pit 1 was >3 m, while at Pit 2, it was <1 m.

Most organisms in the soil are known to survive better in a pH range of 6–7, and die off more quickly under more acidic soil conditions. The pH value within the study area ranged between 6.5 and 8.5, an indication of the likelihood that the alkalinity condition in the area would favour the retention of bacteria and viruses. The electrical conductivity (EC) measured ranged from 10 to 230 $\mu\text{S}/\text{cm}$. The conductivity around the cemetery was higher compared to those away from the cemetery. The result indicated a certain level of

contamination from the effect of cemetery on the groundwater. The total coliform content was between 14 and 89 mg/L except in the control well where it was lesser than the permissible limit of 10 mg/L.

3.4 Soil Studies

Index properties of soil from the study area revealed that the percentage of coarse material, which corresponds to sand and gravel particles, ranged between 73.50 and 83.96% with an average of 79% while the percentage of fine-grained material ranged between 4.28 and 14.48% with an average of 7.71%. The soil from the study area reflected the mineralogy and textural characteristics of the parent rock (Oyelami and Van Rooy 2018). The slope of the study area showed that fluids were expected to move from Pit 1 (containing higher amounts of coarse grain materials) to Pit 2, thus giving way for contaminants to diffuse into the surrounding. This was evident in the increased moisture content of soils in Pit 2. Generally, the results of the soil index properties in the study area showed that serious pollution can be caused to the environment and, thereby, it was not suitable for a safe siting of a cemetery. For example, in Pit 2 which has a shallow water level depth, additional minerals such as actinolite, smectite, sepiolite and plagioclase were present; however, they were absent in Pit 1. The absence of some mineral species in each of the locations with respect to the other may be explained by the topographical gradient in the study area. In an aerobic environment, it was expected that oxides of Fe^{3+} will be abundant as compared to those where the water level is close to the surface. Thus, in Pit 1, we had Fe_2O_3 of 11.2%, whereas in Pit 2, it is 9.6%. The kaolinite content was reduced from 49.5 to 12.9% and muscovite from 11.2 to 0%. Similarly, it was also expected for regions with shallow water levels that oxides of Ca and Mg should be of significant quantity in solution. Thus, in Pit 2, where the water level was close to the surface, CaO and MgO contents were 3.73 and 2.37%, respectively, compared to Pit 1 where respective contents of CaO and MgO are 0.65 and 0.89%. In terms of safe siting of the cemetery, these results tended to be a negative influence rather than a positive one. The only advantage it offered is in the presence of smectite (from the

mineralogical analysis), a swelling clay which has the potential of preventing leachates from getting into the groundwater. This potential is grossly outweighed by the near surface water levels which in turn acts as a transport medium for leachates in solution and hasten the interaction between the leachates and groundwater. Nevertheless, it may be argued that water neutralizes a moving leachate, but that would depend on the load and type of the leachate.

4 Conclusions

This study has demonstrated that the unsaturated zone is one of the most important factors which protect the environment. The thickness of the vadose zone dictates to a large extent the rate and influence of contaminants and leachates on its immediate environment. Index soil properties within the vicinity of cemeteries control the rate of percolation and movement of leachates from the decomposing bodies. Coarse soil fractions are naturally porous and permeable (except in a few cases). Soil stabilization by way of introducing soils rich in clay content is recommended for a safe siting of cemeteries.

References

- British Standard Institution (BSI) **BS 1377**: Parts 1–9 London (1990)
- Dippenaar, M.A.: *Bull. Eng. Geol. Env.* **73**, 1105–1115 (2014)
- Gbadegesin, A., Nwagwu, U.: *Agric. Ecosyst. Environ.* **31**, 99–113 (1990)
- Mann, R.W., Bass, W.M., Meadows, L.J.: *J. Forensic Sci. JFSCA* **35** (1), 103–111 (1990)
- Oyelami, C.A., Van Rooy, J.L.: *Environ. Earth Sci.* **75**, 1475 (2016)
- Oyelami, C.A., VanRooy, J.L.: *Environ. Earth Sci.* **77**, 178 (2018)
- Rodrigues, L., Pachecho, A.: *Environmental 2010: Situation and Perspectives for the European Union* (2003)
- Rodriguez, Bass: *J. Forensic Sci. JFSCA* **30**(3), 836–852 (1985)
- Sorlini, S., Palazzini, D., Sieliechi, J.M.: *Martin B. Ngassoum Sustainab.* **5**, 3060–3076 (2013)
- Spongberg, A.L., Becks, P.M.: *J. Soil Contam.* **9**, 87–97 (2000)
- Stevens, M., Ashbolt, N., Cunliffe, D.: *National Health and Medical Council Act. Canberra* (2003)
- Talabi, A. O.: *Mineraloške in kemične značilnosti glavnih kamnin podlage v državi Ekiti v JZ Nigeriji* (2013)
- WHO, Regional Office for Europe. *World Health Organization. EUR/ICP/EHNA 01 04 01 (A). 1–11* (1998)



Water Quality Indicators in River Basins—A Portuguese Case Study (Northern Portugal)

Margarida Antunes, Ana Brás, and Paula Marinho

Abstract

The objective of this work is the identification of the main contamination sources in the Vizela river watershed and the potential effects on water quality. The physico-chemical parameters temperature, pH, Total Dissolved Solids (TDS), electrical conductivity (EC), redox potential (Eh), chloride, fluoride, bromide, nitrite, nitrate, sulphate, and phosphate water contents were analysed. The microbiological parameters *Escherichia coli* and intestinal *enterococci* were monitored over the time. The obtained results indicate that the water located downstream the Vizela river is the most contaminated, although there has been an improvement in the water quality over the time. The microbiological contents are higher than parametric Portuguese values defined for human consumption, and often also for the parametric values defined for recreation water activities. As a preventive and monitoring measure, it is recommended to monitor the various physico-chemical and microbiological parameters in water points, with a spatial and temporal regular and constant monitoring.

Keywords

Surface water • Industrial activity • Nitrites • Contamination • Monitoring

1 Introduction

Water quality in a watershed is one of the most relevant issue. Meeting water quality goals to sustain environmental quality in a large scale, multi-state water system is a challenge

M. Antunes (✉) · A. Brás · P. Marinho
ICT, University of Minho, Campus de Gualtar,
4710 - 057 Braga, Portugal
e-mail: imantunes@dct.uminho.pt

(Fernandez and McGarvey 2019). The increase in population over the last decades, as well as the occurrence of water stress areas, constitutes an important source of contamination for surface and groundwater (Negm et al. 2020). Water quality in a watershed is mainly controlled by anthropogenic activities and natural processes, which may be directly or indirectly influenced by the surface activities (Pratt and Chang 2012; Ai et al. 2015; Vasconcelos 2015; Belabed et al. 2017).

The industrial activities concentrated in the Valley of Ave river and the proliferation of energy production units have intensified the sources of contamination, mainly industrial and domestic ones. To recover the natural conditions of the Ave River, in 1999, a regional programme “Vale de Ave’s depollution system” was implemented. However, after the application of this project, the ecological status of the river did not go beyond the classification of “poor quality”, according to the Portuguese Environment Agency (Rong et al. 2019). The objective of this work is the identification of local and diffuse contamination sources located in the Vizela River, aiming to improve the river water quality.

2 Study Area

The Ave river is in the North of Portugal, inserted in the Portuguese Hydrographic Region (RH2)—River Cávado, Ave and Leça (Agência Portuguesa do Ambiente 2015). It is about 98 km long. Along with its main tributaries, East River (right bank) and Vizela River on the left bank, it occupies an area of about 240 km² (Soares et al. 1999).

The textile industry and agricultural activities are the principal activities. In the study area, the total annual rainfall is over 1400 mm, with the highest temperature in June (19.9 °C) and the lowest one in November (11.5 °C) (Brás 2018).

Five water points were selected and analysed, between July and October 2018, in the Vizela river watershed. The water points are spatially distributed from the Vizela river source (point V5) to the confluence with Ave river (point

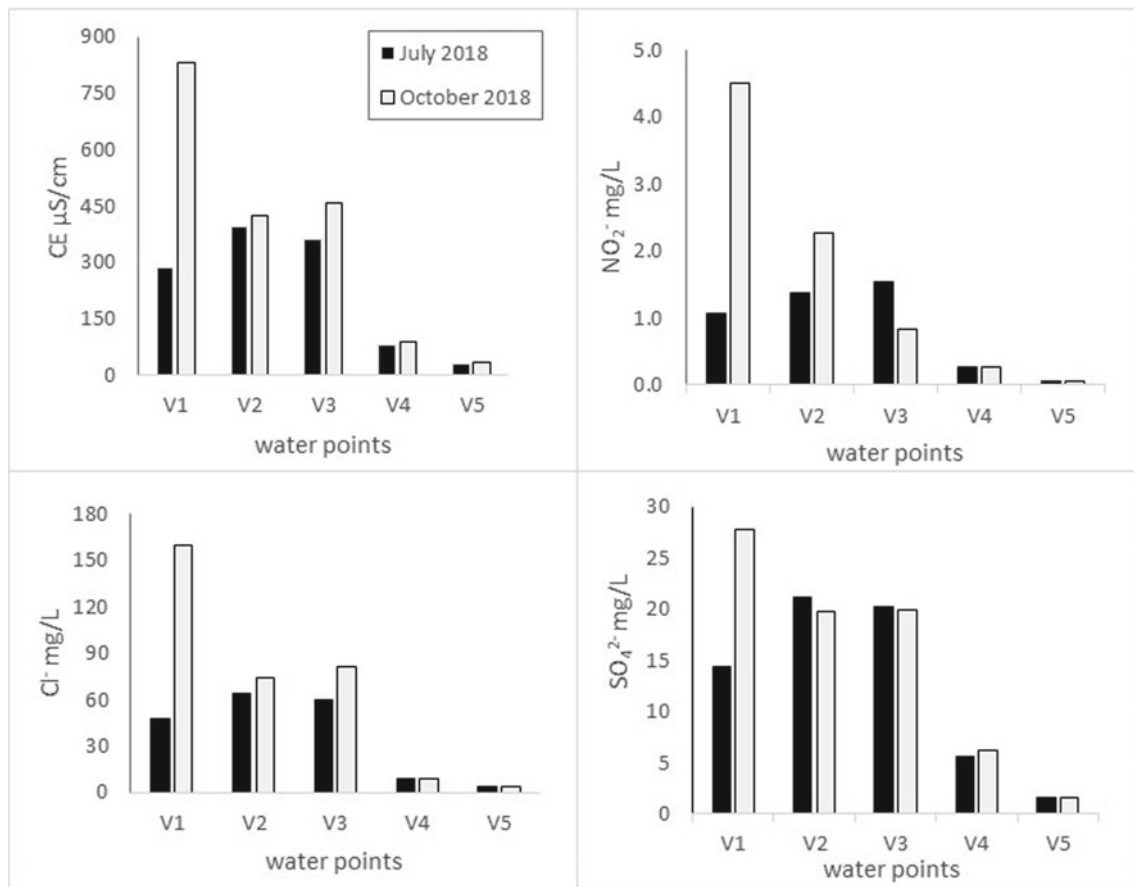


Fig. 1 Seasonal variation of water from the Vizela river

V1). The physico-chemical parameters: electrical conductivity (EC), temperature, pH, Eh, and Total Dissolved Solids (TDS) were determined in situ, and selected anions were determined by ion chromatography at the University of Minho (Braga, Portugal). The microbiological parameters (*Escherichia coli* and intestinal Enterococci) were determined between 2012–2017 (Câmara Municipal de Vizela 2018).

3 Results and Discussion

Water temperature is an indicator of water quality and will affect dissolved oxygen and pH values. The highest temperature value was obtained in September (V1 = 22° C), while the lowest one in October 2018 (V5 = 18.2° C). The pH value ranged between 6.9–7.9, without a significant temporal variation. Total dissolved solids (TDS) varied between 423 mg/L (point V1) and 18 mg/L (point V5), with a similar variation in electrical conductivity (EC; Fig. 1). In October, the highest TDS and EC values were obtained. The highest chloride water content was detected in October, although in the water points V4 and V5, no significant

temporal variation was observed. The water sample V1 had a maximum content of 160.1 mg/L Cl⁻, with a significant temporal variation (Fig. 1).

Nitrite water content was higher in October than in July, except for water point V3. The water content showed a maximum of 4.5 mg/L NO₂⁻ (point V1) and a minimum of 0.050 mg/L NO₂⁻ (point V5). The water from V1, V2, and V3 were unsuitable for human consumption because NO₂⁻ content was above the Portuguese parametric value (0.5 mg/L) (Brás 2018). The highest SO₄²⁻ water content was observed in October (points V1 and V4) and the lowest one in water from V5 (Fig. 1). The microbiological parameters showed the occurrence of *Escherichia coli* above the parametric value for recreation activities (Diário da República: 2007).

4 Conclusions

The obtained results show that water downstream the Vizela river is the most contaminated, although there has been an improvement in water quality in the river watershed over time, mainly since the creation of the regional programme, in

1999. Otherwise, upstream water presents the lowest contents in most of the analysed parameters, because it is closer to the natural spring of the Vizela river. Water contamination increases with distance from the source of the Vizela River. The microbiological parameters, represented by *E. coli* and intestinal Enterococci water content, were higher than parametric Portuguese legislated values indicated for human consumption and is also above the parametric value defined for recreation activities. The monitoring of water physico-chemical and microbiological parameters is strongly recommended in the Vizela river watershed including a spatial and temporal water network.

References

- Agência Portuguesa do Ambiente: Plano de Gestão da Região Hidrográfica do Cávado, Ave e Leça (RH2), Parte 2—Caracterização e diagnóstico da região hidrográfica, p. 273 (2015)
- Ai, L., Shi, Z.H., Yin, W., Huang, X.: Spatial and seasonal patterns in stream water contamination across mountainous watersheds: linkage with landscape characteristics. *J. Hydrol.* **523**, 398–408 (2015)
- Belabed, B.E., Meddour, A., Samraoui, B., Chenchouni, H.: Modeling seasonal and spatial contamination of surface waters and upper sediments with trace metal elements across industrialized urban areas of the Seybouse watershed in North Africa. *Environ. Monit. Assess.* **189**(6), 265 (2017)
- Brás, A.F.S.: Avaliação dos riscos ambientais e qualidade da água numa bacia hidrográfica—caso de estudo no rio Vizela (Norte de Portugal). Unpublished Mstthesis, University of Minho, p. 62 (2018)
- Câmara Municipal de Vizela: Análises microbiológicas de 2012 a 2017 de *Escherichia coli* e *Enterococos intestinais*. Unpublish reports (2018)
- Diário da República: Dec-Lei n.º 306/2007. Ministério do Ambiente, do Ordenamento do Território e do Desenvolvimento Regional, Série I, 5747 - 57652007 (2007)
- Fernandez, L., McGarvey, D.: Water quality decisions and policy for an interstate watershed. *Water Res. Econ.* **27**(100130), 1–13 (2019)
- Negm, A., Bouderbala, A., Chenchouni, H., Barcelo, D.: *Water Resources in Algeria - Part II: Water Quality, Treatment, Protection and Development*. Springer, Cham (2020)
- Pratt, B., Chang, H.: Effects of land cover, topography, and built structure on seasonal water quality at multiple spatial scales. *J. Haz. Mat.* **209–210**, 48–58 (2012)
- Rong, Q., Cai, Y., Su, M., Yue, W., Yang, Z., Dang, Z.: A simulation-based bi-level multi-objective programming model for watershed water quality management under interval and stochastic uncertainties. *J. Environ. Manag.* **245**, 418–431 (2019)
- Soares, H., Boaventura, R., Machado, A., Esteves da Silva, J.: Sediments as monitors of heavy metal contamination on the Ave river basin (Portugal): multivariate analysis of data. *Environm. Pol.* **105**, 311–323 (1999)
- Vasconcelos, A.S.: Estudo da qualidade da água do Rio Ave: relevância da relação entre indicadores microbiológicos, macroinvertebrados e parâmetros físico-químicos. P 162. Unpublished Mstthesis, University of Porto (2015)

**Hydrology, Hydrogeology, Hydrochemistry,
Water Resources (T10): Hydrogeology and
Hydrochemistry—Hydrodynamics Aspects**



Transient Drain Spacing Equations for Different Initial Water Table Conditions

Ammar Yousfi and Mohammed Mechergui

Abstract

With respect to the drainage problem, an attempt was made to derive transient drain spacing equations using the linearized Boussinesq equation. An alternative technique of linearization has been applied to suit for initially flat and steady-state (elliptical) water shapes. In deriving these formulas, the average depth of the flow region was also assumed to be dependent on the initial water table conditions. Compared to existing transient drainage theories, the newly derived drain spacing equations give comparable spacing. As an initial condition, the steady-state (elliptical) water table profile is shown to be more appropriate for designing subsurface drainage systems under transient conditions.

Keywords

Boussinesq equation • Drainage system • Transient conditions • Drains spacing • Linearization

1 Introduction

The classical Boussinesq equation has been used and subsequently linearized to derive transient drainage equations under various initial water table profiles. Glover–Dumm (1954,1964) obtained analytical solutions assuming an initially flat and four-degree parabolic water table shape, respectively. In deriving these equations, the used linearization technique consists in assuming that the depth of the impervious layer below the drain is very large compared to the water table's height above the drains. In this study, we employed an alternative method of linearization to obtain

new transient drain spacing equations for two limiting cases of initial water table conditions: flat and steady-state water table shapes.

2 Materials and Methods

We consider a two-dimensional problem (Fig. 1) with the following assumptions: (1) the soil is homogeneous, isotropic and incompressible; (2) the fluid is homogeneous and incompressible. Before proceeding with the analysis of this problem, the following boundary conditions are considered: (i) a zero-horizontal flux is assumed at drain mid-spacings and drain locations, (ii) a zero-vertical flux is assumed at the barrier depth and at the soil surface; (iii) the tile drains are assumed to run partially full.

The Boussinesq equation (1904) based on the principle of continuity and Dupuit–Forchheimer (DF) assumptions is taken to be the governing equation describing the fall of the water table and expressed as (Yeh and Singh 1970):

$$\mu \frac{\partial h_0}{\partial t} = K_s \frac{\partial}{\partial x} \left\{ (h_0 + d) \frac{\partial h_0}{\partial x} \right\} \quad (1)$$

Subject to the following initial and boundary conditions:

$$\begin{aligned} t = 0 \quad h_0(x, 0) &= h_i(x) \quad \text{for } 0 \leq x \leq L \\ t > 0 \quad h_0(L, t) &= 0 \quad \text{for } x = L \\ t > 0 \quad \frac{\partial h_0}{\partial x} \Big|_{x=L} &= 0 \quad \text{for } x = 0 \end{aligned} \quad (2)$$

where K_s —the saturated hydraulic conductivity [LT^{-1}], μ —the drainable porosity [–], d the depth of the impervious layer below the drain level [L], x —the abscissa [L], t —stands for time [T], L —the half drain spacing [L], $h_i(x)$ —is a defined function describing water table height initially [L] and $h_0(x, t)$ —the height of the water table above the drain level [L]. Before starting the mathematical development, it should be noted that Eq. (1) based on DF

A. Yousfi (✉) · M. Mechergui
Institut National Agronomique de Tunis, 43 Rue Charles Nicole
El Mahrajène, 1082 Tunnis, Tunisia
e-mail: mechergui.med@inat.agrinet.tn

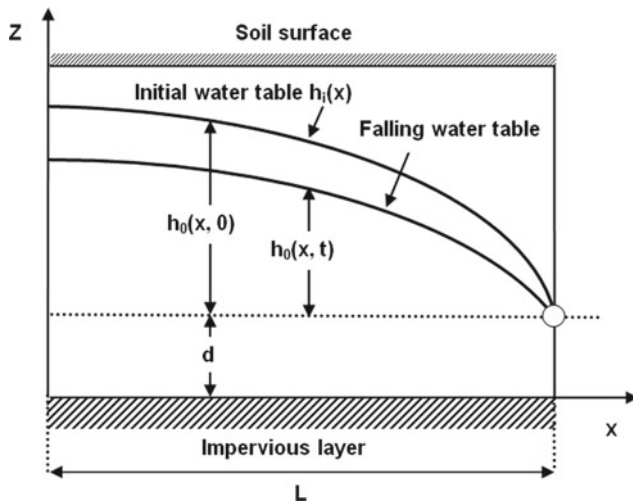


Fig. 1 Sketch of falling water table in tile-drained soils

assumptions does not consider the radial resistance of flow towards drains not reaching the impervious layer. To account for the extra resistance caused by the radial flow in the vicinity of the drains, we used Hooghoudt (1940)'s concept of the equivalent depth. So, we simply replace the actual depth to the impervious layer (d) with a smaller equivalent depth (d_e). To obtain analytical solutions, two initial water table shape conditions are considered as limiting cases for drainage design:

- Case 1: A constant water table height h_{m0} , exists everywhere between the drains except at the drains where the water table suddenly drops to zero (flat profile):

$$h_i(x) = h_{m0} \text{ for } 0 < x < L \text{ at } t = 0 \quad (3)$$

- Case 2: A steady-state water table shape (elliptical profile) (Kao 2002):

$$\frac{h_i^2(x) + 2d_e h_i(x)}{h_{m0}^2 + 2d_e h_{m0}} = \frac{L^2 - x^2}{L^2} \quad (4)$$

where h_{m0} the initial water table height at mid-spacing ($h_i(0)$) [L]. Flat and steady-state water table shapes represent the extreme conditions which would be met in practice. So, their uses as initial conditions are of interest in modelling the falling water table profile as well as in designing subsurface drainage. These conditions will be implemented for obtaining the analytical solution of the Boussinesq equation (Eq. 1). This equation is nonlinear so that a linearization method is used to obtain analytical solutions. By setting $\frac{\partial h_0}{\partial t} = \frac{1}{2\bar{D}} \frac{\partial(h_0^2 + 2d_e h_0)}{\partial t}$ to suit for the assumed initial water table conditions and combining with Eq. (1) yields:

$$\mu \frac{\partial}{\partial t} (h_0^2 + 2d_e h_0) = K_s \bar{D} \frac{\partial^2}{\partial x^2} (h_0^2 + 2d_e h_0) \quad (5)$$

where \bar{D} —the average depth of flow region such $\bar{D} = h_{av} + d_e[L]$ and h_{av} —the average water table height [L] which can be calculated as $h_{av} = \frac{\int_0^L h_i(x) dx}{L}$.

The resulting equation is in linear form and can be easily solved to describe falling water tables.

3 Results and Discussion

By separation of variables and following Ozisik (1980)'s approach, analytical solutions using the linearized Boussinesq equation (5) with the initial and boundary conditions given by Eqs. (2), (3) and (4) can be obtained as follows:

- Case 1: A constant water table height h_{m0} (flat profile)

$$\frac{h_0^2(x, t) + 2d_e h_0(x, t)}{h_{m0}^2 + 2d_e h_{m0}} = 2 \sum_{k=0}^{\infty} \frac{(-1)^k}{\beta_k} \cos\left(\beta_k \frac{x}{L}\right) \exp\left(-\beta_k^2 \frac{K_s \bar{D}}{\mu L^2} t\right) \quad (6)$$

- Case 2: A steady-state water table shape (elliptical profile)

$$\frac{h_0^2(x, t) + 2d_e h_0(x, t)}{h_{m0}^2 + 2d_e h_{m0}} = 4 \sum_{k=0}^{\infty} \frac{(-1)^k}{\beta_k^3} \cos\left(\beta_k \frac{x}{L}\right) \exp\left(-\beta_k^2 \frac{K_s \bar{D}}{\mu L^2} t\right) \quad (7)$$

where $\beta_k = (2k + 1) \frac{\pi}{2}$. Evaluating $h_0(x, t)$ at $x = 0$ in Eqs. (6) and (7) to obtain height of the water table at the midpoint between the drains, h_{mt} , and taking only the first term of the series (the remaining terms can be neglected), new transient drainage equations for computing drain spacing ($E = 2L$) can be expressed as follows:

- Case 1: A constant water table height (flat profile)

$$\frac{\pi^2 K_s \bar{D} t}{\mu E^2} = \text{Log} \left\{ \frac{4}{\pi} \left(\frac{h_{m0}^2 + 2d_e h_{m0}}{h_{mt}^2 + 2d_e h_{mt}} \right) \right\} \text{ where } \bar{D} = h_{m0} + d_e \quad (8)$$

- Case 2: A steady-state water table shape (elliptical profile)

$$\frac{\pi^2 K_s \bar{D} t}{\mu E^2} = \text{Log} \left\{ \frac{32}{\pi^3} \left(\frac{h_{m0}^2 + 2d_e h_{m0}}{h_{mt}^2 + 2d_e h_{mt}} \right) \right\} \left(\frac{32}{\pi^3} \cong 1.03 \right) \quad (9)$$

$$\text{where } \bar{D} = \frac{1}{2} \left\{ d_e + \frac{(h_{m0} + d_e)^2}{\sqrt{h_{m0}^2 + 2d_e h_{m0}}} \arcsin \left(\frac{\sqrt{h_{m0}^2 + 2d_e h_{m0}}}{(h_{m0} + d_e)} \right) \right\}.$$

Finally, it may be interesting to compare the drain spacings obtained from Eqs. (8) and (9) to those obtained from the common transient drainage equations used for design, namely the solutions proposed by Glover (Dumm, 1964) and Van Schilfgaarde (1964), respectively reproduced as follows:

$$E^2 = \frac{\pi^2 K_s (d_e + h_{m0}/2) t}{\mu \text{Log} \left(\frac{3.7}{\pi} \left(\frac{h_{m0}}{h_{mt}} \right) \right)} \tag{10}$$

$$E^2 = \frac{9K_s d_e t}{\mu \text{Log} \left(\left(\frac{h_{m0}}{h_{mt}} \right) \left(\frac{h_{mt} + 2d_e}{h_{m0} + 2d_e} \right) \right)} \tag{11}$$

Van Schilfgaarde’s solution was derived for an initially elliptical water table shape without linearizing the Boussinesq equation. However, Glover–Dumm’s formula was obtained from the linearized Boussinesq equation using an initially flattened parabola of the fourth degree to represent the initial water table condition. To compare, the followings arbitrary data have been used: the drainable porosity μ is 0.1, the saturated hydraulic conductivity K_s is 1.0 m/d and the time t required for water table drop is 7 days. The remaining data and results are given in Table 1.

The water table fall is kept constant at 0.4 m. The calculations are done for a tile drain with a radius r_0 of 0.05 m, and the equivalent depth d_e is calculated using the series solution developed by Van der Molen and Wesseling (1991) expressed as follows Eqs. (12):

$$d_e = \frac{\frac{\pi E}{8}}{\text{Log} \left(\frac{E}{\pi r_0} \right) + 2 \sum_{n=1}^{\infty} \text{Log} \{ \coth(n\delta) \}}, \text{ where } \delta = \frac{2\pi D}{E} \tag{12}$$

Numerical results show that the newly derived transient equations generally give comparable spacings in comparison with Van Schilfgaarde and Glover–Dumm’s formulae. But one can notice that if the depth of the impervious layer below the drains increases the difference in computed drain spacings increases. Particularly, it is shown that for a ratio of $h_{m0}/h_{mt} \leq 1.5$ and for a deep impervious layer (e.g. D 3.0 m), the newly developed formula given by Eq. (9) as well as Van Schilfgaarde’s formula, based on the same initial water table conditions (elliptical profiles), gives higher drain spacings compared with the new developed formula given by Eq. (8) and Glover–Dumm’s formula. The maximum difference is about 26%. In all cases, the two latter formulae yield approximately the same results.

4 Conclusions

New transient drainage equations have been derived based on the Boussinesq equation using an alternative linearization technique. Initial water table conditions have been assumed

Table 1 Computed drain spacings (E (m)) for different depths D and water table heights

Water table heights (m)	$h_{m0} = 0.8$ m and $h_{mt} = 0.4$ m				$h_{m0} = 1.2$ m and $h_{mt} = 0.8$ m				$h_{m0} = 1.6$ m and $h_{mt} = 1.2$ m			
	Equation (8)	Equation (9)	Equation (10)	Equation (11)	Equation (8)	Equation (9)	Equation (10)	Equation (11)	Equation (8)	Equation (9)	Equation (10)	Equation (11)
0.0	19.6	18.8	19.1	17.3	29.2	29.0	28.2	28.9	37.8	39.0	36.2	40.3
1.0	32.4	33.4	32.2	32.5	42.9	45.9	42.9	46.7	51.6	57.1	51.5	59.6
3.0	44.2	48.0	45.0	46.8	57.3	65.2	58.9	65.8	67.2	79.4	69.4	82.3
5.0	51.1	56.5	52.5	55.1	65.9	77.1	68.7	77.6	76.9	93.2	80.7	96.8

to be flat with steady-state (elliptical) shape, as extreme conditions to be occurred in practice. A comparison with existing transient drainage theories shows that the derived drain spacing formulas give comparable results. More generally, the analysis indicates that the initial steady-state water table (elliptical shape) condition is shown to be more appropriate for drain spacing design under transient conditions. Further work should be carried out to evaluate the reliability of the proposed solutions under field conditions.

References

- Boussinesq, J.: Recherches théoriques sur l'écoulement des nappes d'eau infiltrées dans le sol; compléments. *Journal De Mathématiques Pures Et Appliquées* **10**(1 & 4), 5–78 (1904)
- Dumm, L.D.: New formula for determining depth and spacing of subsurface drains in irrigated lands. *Agric. Eng.* **35**, 726–730 (1954)
- Dumm, L.D., Transient-flow concept in subsurface drainage: Its validity and use, pp. 142–145. *Trans. ASAE* (1964)
- Hooghoudt, S.B.: Algemeenebeschouwing van het probleem van de detailontwateringen de infiltratie door middel van parallel loopende drains, greppels, slootenenkanalen. *Versl Landbouwk Onderz* **14**, 46 (1940)
- Kao, C., Fonctionnement hydraulique des nappes superficielles de fonds de vallées en interaction avec le réseau hydrographique. Dissertation, p. 266. ENGREF, Paris (2002)
- Ozsisik, M.N., *Heat Conduction*, pp. 71–72, 201–203. Wiley, New York (1980)
- Van der Molen, W.H., Wesseling, J.: A solution in closed form and a series solution to replace the tables for the thickness of the equivalent layer in Hooghoudt drain spacing formula. *J. Agric. Water Manag.* **19**, 1–16 (1991)
- Van Schilfgaard, J.: Closure, Design of tile drainage for falling water tables. *J. Irrig. Drainage Div Amer. Soc. Civil Eng.* **90**, 71–73 (1964)
- Yeh, W.W., Singh, R.: Transient flow between parallel drains. *J. Hydrology.* **11**, 301–312 (1970)



Goelectrical Studies for Groundwater Exploration in Fractured Rock Terrane (Ambaji Basin, India)

Rudra Mohan Pradhan, Ramesh Deshmukh,
Enamundram Chandrasekhar, Guru Balamurugan,
and Tapas Kumar Biswal

Abstract

Goelectrical studies have been widely used for characterization of the subsurface features for groundwater exploration, environmental aspects, etc. The present study involves the application of multi-electrode resistivity imaging (MERI) to demarcate potential zones for groundwater exploration. The Wenner-Schlumberger (WS) array has been deployed for the mapping of weathered and fractured zones. Previously, in the study area (Ambaji basin, Gujarat), a number of drill wells failed and dried up due to a lack of understanding of the local fracture systems. Hence, this goelectrical investigation has been conducted in fractured basement rocks for sitting borewells for sustainable groundwater use in the Ambaji basin (Aravalli terrane), Gujarat, India.

Keywords

Fractured rock • Groundwater • Ambaji Basin • Aravalli • Gujarat

1 Introduction

For domestic and irrigation needs, rural communities depend on groundwater as the main source of water supply. The study area (Ambaji basin) is a rural area and underlain by Precambrian basement rocks viz. granites, basic granulites, and calc-granulites. A number of drill wells (hand pump,

dug wells, bore wells) failed and dried up due to improper scientific investigation of the local fracture systems. The development of these crystalline basement aquifers is highly variables, and the productivity are very low due to the poor porosity and permeability. These basement aquifers are confined to weathered and fractured zones. The electrical resistivity survey is cost-effective and extensively used for mapping subsurface structures, and groundwater exploration purposes (Acworth 2019, 2001; Cardarelli and Donno 2019; Carruthers and Smith 1992). The resistivity values mostly depend on the geological formations. As compared to traditional four-electrode systems (1D), multi-electrode resistivity imaging (2D and 3D imaging) produces more realistic models to understand a complex aquifer system. Thus, the multi-electrode resistivity imaging (MERI) technique was used to characterize both fractured and weathered zones. A combined inversion Wenner-Schlumberger (WS) configuration has been used for the present study because it provides a very good resolution (signal to noise ratio) of the vertical and horizontal variations of the subsurface resistivity (Cardarelli and Donno 2019; Chandrasekhar et al. 2014; Loke 2004). Previously, no such scientific investigation has been carried out related to groundwater potential zone mapping, management, and development in spite of being a highly populated zone. Increasing demand for water resources puts stress on the exploration of groundwater from less reliable sources of basement rock aquifers and, hence, it is important to delineate groundwater potential zones. So, the aim of the present study is to demarcate potential sites for bore wells/dug wells for sustainable groundwater use in the Ambaji basin.

2 Study Area

The Ambaji basin (Aravalli terrane) is located in the Banaskantha district of Gujarat, India, and lies in between latitude 24° 13' N to 24° 21' N and longitude 72° 30' E to

R. M. Pradhan (✉) · R. Deshmukh · E. Chandrasekhar ·
T. K. Biswal
Indian Institute of Technology Bombay,
Maharashtra, 400076, India

R. M. Pradhan
University of Nebraska-Lincoln, Lincoln, NE 68588, USA

G. Balamurugan
Tata Institute of Social Sciences, Deonar, Mumbai, 400088, India

72° 50'E. The study area extends over 260 km², encompassing 18 villages. The density of the population is about 165 per sq. km. The area falls under the semiarid type of climate and marked by extremely hot and dry (April to July), and rainy (August to September) seasons. The average temperature ranges between 30–42 °C, and the average annual rainfall is 578.88 mm. The drainage network in the Ambaji basin is constituted mainly by the Balaran River, a tributary of the Banas River. The aquifer systems consisted of two hydrogeological units in the study area, i.e., shallow unconfined or weathered zones, ranging from 1–15 m, and fractured bearing zones. The general groundwater flow direction is from the northeast to southwest direction. The groundwater level (bgl) varies from 2.5 to 20.65 m in the pre-monsoon and 0.65 to 17.85 m in the post-monsoon season (Pradhan and Biswal 2018). Geologically, the study area belongs to the Aravalli mobile belt and is underlain by Precambrian basement rocks. The major rock types are three types of granites (G1: gneissic, G2: coarse-grained, and G3: fine-grained), calc-schists and basic granulites (Fig. 1). The rocks are highly fractured along the faults and shear zones (Pradhan and Biswal 2018).

3 Methodology

A total of twenty-five multi-electrode resistivity imaging were conducted (December 2017) in the study area using SYSCAL Pro 48 electrode channel (IRIS Instruments) multi-electrode resistivity system. However, a total of six traverses have been used for this study (Fig. 1). Wenner-Schlumberger (WS) array has been used for this survey with an electrode spacing of 5.0 and 235.0 m spreading lengths for each traverse. Proper contact between electrodes and ground surface was ensured by fixing electrodes and connecting jumpers for keeping good conductivity. After the survey, the obtained datasets were processed through RES2DINV inversion software to determine the distribution of true resistivity from apparent resistivity values (Griffiths and Barker 1993). To improve the matching with field data, the data sets were inverted using multiple iterations to derive a model distribution which produces a section with a root mean square (RMS) value less than or equal to 5% (Acworth 2001). The absolute error has been minimized to less than 5% for better accuracy and interpretation of the results.

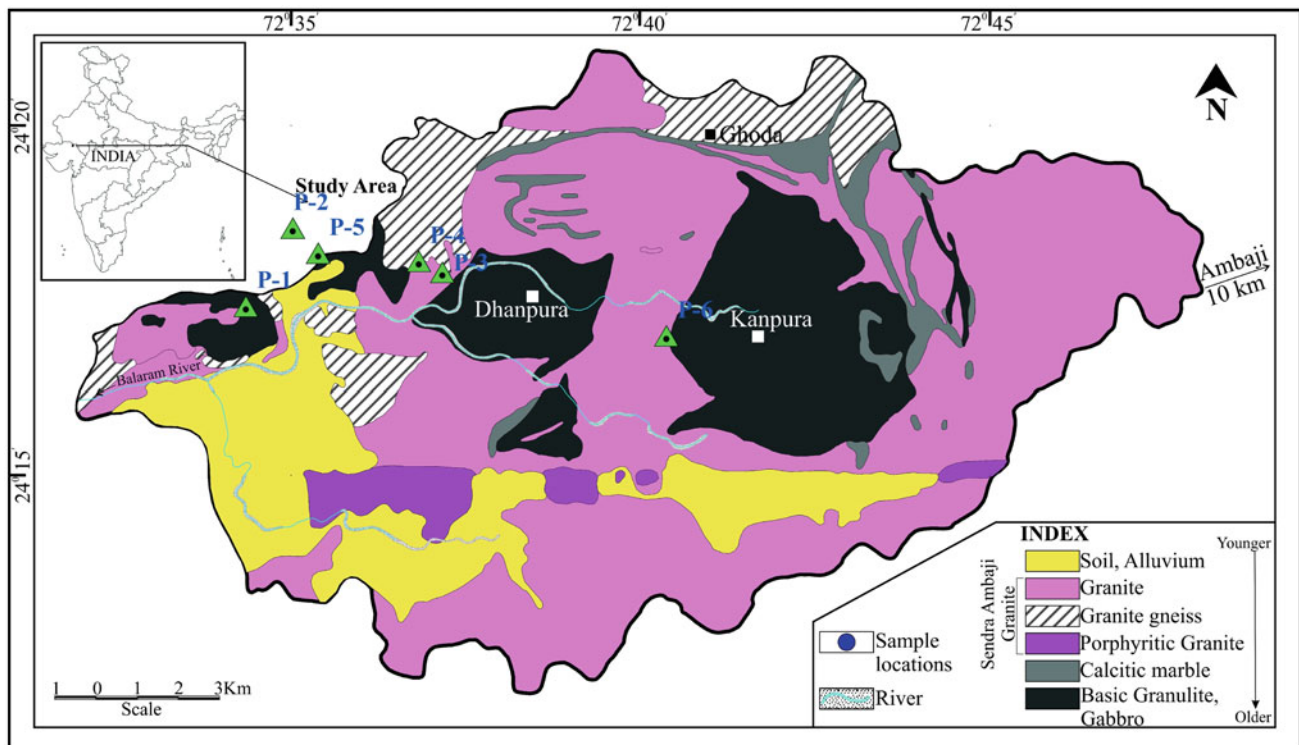


Fig. 1 Geological map of the Ambaji basin and resistivity survey locations (after Pradhan and Biswal 2018)

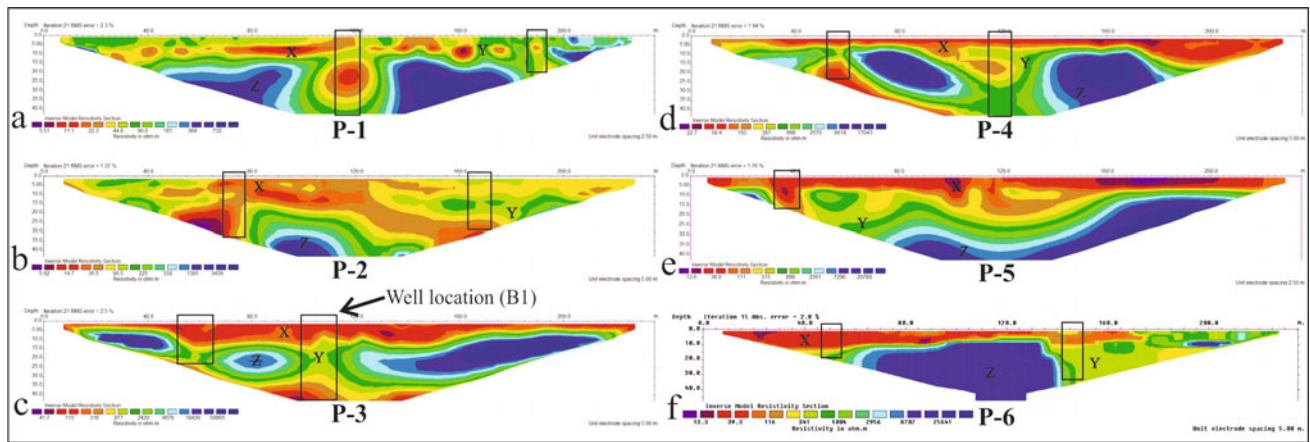


Fig. 2 Subsurface profile in the Dhanpura area (B1; Refer in Fig. 2c)

4 Results

The results show that the study area consists of saprolites/ weathered zones, fractured-, and fresh basements. The soil or saprolite may be divided into upper and lower units as is shown by the variation in resistivity values due to the mineral composition and the degree of weathering of rocks. The 2D inverted resistivity models of profiles P-1 to P-6 are shown in Fig. 2. All the resistivity models show approximately 1–15-m-thick layer weathered zones in the top and followed by fractured zones and basement rocks. The ERT sections (Fig. 2a–f) show the geoelectrical resistivity with three different zones (labeled with X: Soil and weathered granites, Y: fractured zones, and Z: massive hard rock). The upper zone has low resistivity which ranges from 5 to 120 Ω. m and a thickness of 20 to 30 m, indicating a water-bearing fractured and weathered zone. The lower zone (labeled as Z) has higher resistivities, indicating a massive basement and granitic body (Fig. 2a–f). Vertical or steeply fractured zones (Fig. 2a, c, and f) are identified in the Ajapur Mota-1, Dhanpura, and Ghoda areas (marked in a black rectangle). These zones can be targeted for pinpointing borehole sites. Generally, groundwater storativity in basement rocks increases with an increase in overburden weathered zones and fractured zones. The weathered zones and fractured zones have a higher yield capacity than the basement rocks. The weathered zones represent basement rocks which have relatively high porosity and permeability and can be used for sitting large-diameter dug wells. Further, the interpreted 2D resistivity model is validated with one existing borehole data (Fig. 3) in Dhanpura area (P-3). A borehole drilled up to a depth of 65-m encountered soil layer, weathered granite, fractured zone and fresh granite basement as incurred from the lithology of the well (Fig. 3). This shows a good pact

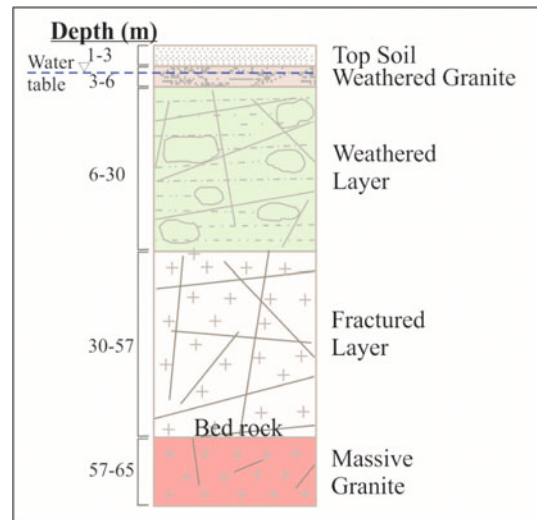


Fig. 3 Inverse model Resistivity sections. a Ajapur Mota-1 (P-1). b Surela-1 (P-2). c Dhanpura (P-3). d Surela-2 (P-4). e Ajapur Mota-2 (P-5). f Ghoda (P-6)

between resistivity values and interpretation. This succession is clearly visible in the existing bore well (B1) in the Dhanpura area.

5 Conclusions

The electrical resistivity imaging based on multi-electrode Wenner-Schlumberger (WS) configuration has been used to characterize the variations in the near-surface structures in Precambrian basement rocks of the Ambaji basin. In semi-arid regions like the Ambaji basin, the geoelectrical survey (MERI) has a valuable contribution for demarcating groundwater potential zones and sitting boreholes as it

satisfactorily incorporates horizontal-lateral variations in bulk resistivity. The basement feature has been delineated through WS configuration that involves saprolites, weathered-, fractured-, steep contact zones and fresh basements. These indicate that the WS configuration for resistivity imaging is sensitive to vertical features such as faults and fractured zones and steep contacts which have a significant role for sitting boreholes/dug wells for sustainable groundwater use.

Acknowledgements TK Biswal acknowledged the Ministry of Earth Sciences (MoES), Govt. of India for the sponsored project (MoES/P.O. (Geosci)/50/2015). RM Pradhan is thankful to the Department of Earth Sciences, IIT Bombay, for giving the necessary facilities to carry out the present work and IUSSTF for WARI Fellowship (at the University of Nebraska-Lincoln, USA). We are thankful to the editor and anonymous reviewers for their constructive comments and suggestions which improved the manuscript.

References

- Acworth, I.: The electrical image method compared with resistivity sounding and electromagnetic profiling for investigation in areas of complex geology: a case study from groundwater investigation in a weathered crystalline rock environment. *Explor. Geophys.* **32**, 119–128 (2001)
- Acworth, I.: *Investigating Groundwater*. CRC Press (2019)
- Cardarelli, E., De Donno, G.: Advances in electric resistivity tomography: Theory and case studies. In: *Innovation in Near-Surface Geophysics*, pp. 23–57. Elsevier (2019)
- Carruthers, R.M., Smith, I.F.: The use of ground electrical survey methods for siting water-supply boreholes in shallow crystalline basement terrains. *Geol. Soc., London, Spec. Publ.* **66**, 203–220 (1992)
- Chandrasekhar, E., Ramesh, D., Gurav, T., Biswal, T.K.: Assessment of groundwater salinity in Nellore district using multi-electrode resistivity imaging technique. *J. Earth Syst. Sci.* **123**, 1809–1817 (2014)
- Griffiths, D.H., Barker, R.D.: Two-dimensional resistivity imaging and modelling in areas of complex geology. *J. Appl. Geophys.* **29**, 211–226 (1993)
- Loke, M.H.: Tutorial: 2-D and 3-D Electrical Imaging Surveys, pp. 1–136. GeotomoSoftware, Malaysia (2004)
- Pradhan, R.M., Biswal, T.K.: Fluoride in groundwater: a case study in Precambrian terranes of Ambaji region, North Gujarat, India. *Proc. Int. Assoc. Hydrol. Sci.* **379**, 351–356 (2018)
- Acworth, I.: The electrical image method compared with resistivity sounding and electromagnetic profiling for investigation in areas of



Hydrodynamic Functioning of Rhythmic Springs—Case of the M’chaki Spring (Jijel, NE Algeria)

Taha-Hocine Debieche, Azzedine Bouzenoune, Faouzi Zahi, Abdelmalek Drouiche, Souhil Mahdid, Youcef Rouikha, Boualem Mayache, Amal Chine, Asma Gherib, and Fatima Aidli

Abstract

Rhythmic springs have always attracted the curiosity of people and scientists about how they work. The M’chaki spring in Jijel is the only one in Algeria with a permanent rhythmic flow. In order to determine its hydrodynamic functioning, this research work was conducted. A total of three hydrodynamic measurements and water sampling campaigns were carried out: during two high water periods (April 2016 and May 2019) and during one low water period (September 2017). The results show that the hydrodynamic functioning of the spring is linked to a tri-siphon system, located in Liasic carbonate rocks (dolomites and limestones) and Triassic breccia formations. Finally, a conceptual schema of the hydrodynamic functioning of this spring has been proposed.

Keywords

Karst • Siphon • Flow • Gauging • Hydrogeochemistry

1 Introduction

A rhythmic spring is a discontinuous flow spring whose flow is periodically interrupted at more or less regular intervals, even in an uninfluenced state. Its flow is rhythmic (intermittent), ranging from a few minutes to several hours. These springs are quite rare, we find 50 to 100 in the world

T.-H. Debieche (✉) · A. Bouzenoune · F. Zahi · A. Drouiche · S. Mahdid · Y. Rouikha · A. Chine · A. Gherib · F. Aidli
Geological Engineering Laboratory (LGG), Faculty of Nature and Life Sciences, University of Mohamed Seddik Benyahia—Jijel, B.P. 98 Ouled Aissa, 18000 Jijel, Algeria

B. Mayache
Laboratory of Biotechnology, Environment and Health, Faculty of Nature and Life Sciences, University of Mohamed Seddik Benyahia—Jijel, B.P. 98 Ouled Aissa, 18000 Jijel, Algeria

(Bonacci and Bojanic 1991; Igracev 2014). In Algeria, the rhythmic spring has not been described according to literature search. Only the M’chaki spring in Jijel has a rhythmic character. This spring has been reported in a few rare cartographic documents (Abu Obeid El Bekri 1965; Ehrmann 1946). Until now, no scientific study has been carried out on this spring; hence, the interest of this article which aims to determine its hydrodynamic functioning.

2 Study Area

The M’chaki spring is located in the northeast of Algeria in the province of Jijel and exactly in the municipality of Selma Benziada (Fig. 1) at an altitude of 545 m.

The point of resurgence of the spring is localized on the rockslide plane of the Triassic breccia (Fig. 2) and near the Liasic limestones and dolomites.

The rhythmic spring of M’chaki is characterized by several cycles per day. The two photographs in Fig. 3 illustrate the flow difference between the minimum flow (permanent flow) and the maximum flow (permanent and temporary flow) of a cycle.

3 Materials and Methods

Three campaigns were carried out to study the functioning of this spring:

- The first two campaigns, 23/4/2016 (high water period) and 30/9/2017 (low water period), were focused on float gauging of the water flow and water sampling.
- The third campaign, 13/5/2019 (high water period), was focused on the study of the variation of the cycle time (stop and run time) of the spring, during a period of 8 hours. In total, ten cycles were followed.

Fig. 1 Administrative situation of the rhythmic spring of M'chaki

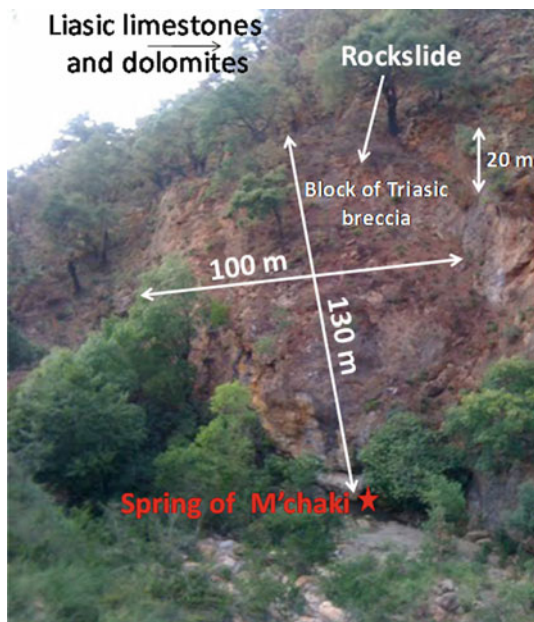


Fig. 2 Rockslide over the M'chaki spring within the study area



Fig. 3 Minimum and maximum flows of a cycle of the rhythmic spring of M'chaki (May 2019)

The chemical analysis of the major elements was made by the titrimetric and spectrometric methods.

The rainfall data are available only for the years 2017 and 2018. The average precipitation for the months of April and May is 117 and 54 mm, respectively, while the precipitation of September 2017 is 29 mm.

4 Results

The results obtained show that: (i) the minimum flow of the spring is 100 L s^{-1} during the period of high water and 24 L s^{-1} during the period of low water, and (ii) the maximum flow during the high water period is 282.2 L s^{-1} for the first cycle and 224.5 L s^{-1} for the second cycle. On the other hand, during the low water period, there is a decrease in maximum flow, it is only 132.9 L s^{-1} for the first cycle and 69.2 L s^{-1} for the second cycle.

The flow variation between high and low water is related to the water inflow from precipitations. Also, the variation in the maximum flow between two successive cycles of the spring could be explained by additional water supplies probably related to the existence of a second siphon. To confirm this hypothesis, the time variation of ten cycles (flow and stop time of the source) of the spring was

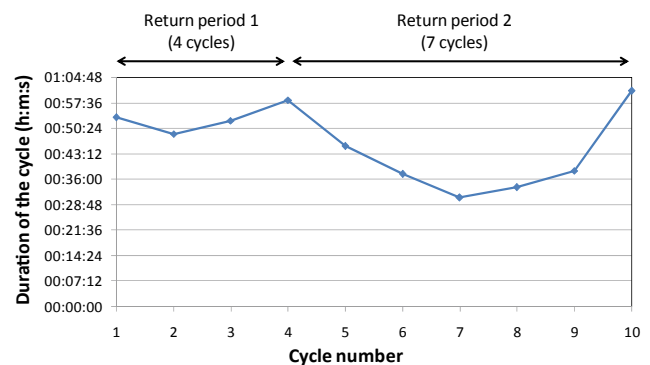
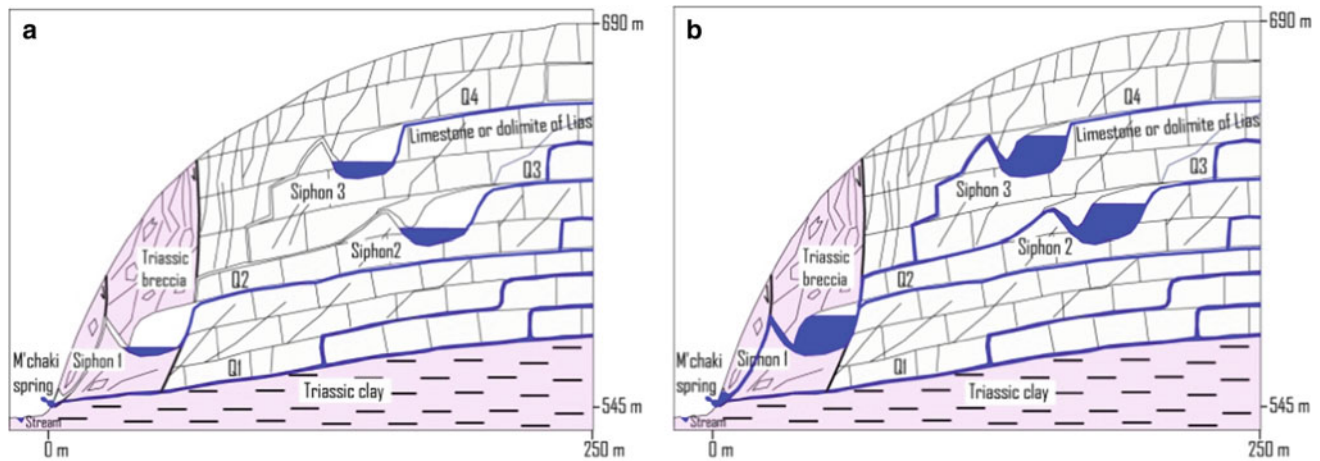


Fig. 4 Time variation of the ten cycles of the spring (May 2019)



Legend: A: Permanent flow; B: Permanent and temporary flow.

Q1: water supply flow of the permanent flow; Q2, Q3 and Q4: water supply flow of siphons 2, 3 and 4.

Fig. 5 Conceptual schema of the hydrodynamic functioning of the M'chaki spring

followed. The results obtained are shown in Fig. 4. This figure shows two return periods for the cycle time: the first concerns four cycles and the second concerns seven cycles. The first return period can be interpreted as the functioning of two siphons. On the other hand, the second return period indicates additional water supplies and, therefore, the existence of a third siphon.

The chemical analysis carried out on the waters of the spring showed high concentrations in sulphates (240 mg L^{-1}) and in hydrogen carbonate (240 mg L^{-1}), indicating two origins of the water, one is the Liasic carbonates rocks and the other is the Triassic gypsiferous formations.

The conceptual schema that can be proposed for the hydrodynamic functioning of the spring is presented in Fig. 5.

5 Conclusion

This study shows the usefulness of hydrodynamic and hydrochemical responses to understand the functioning system of rhythmic springs. On the local level, it allows to

draw up a first schema illustrating the functioning of the M'chaki spring.

This study, however, remains incomplete and requires more precision on the functioning system of the spring. These complements of precision can be brought by a fine geological study, and hydrodynamic and hydrogeochemical monitoring of the spring for a long period and by scientific works in geophysics, isotope geochemistry, tracer test and hydrogeological modelling.

References

- Abu Obeid El Bekri: Description of North Africa. Bi-lingual edition. Mac Guckin de Slane translation. Ed. Adrien—Maisonneuve. Paris, 193 (1965)
- Bonacci, O., Bojanic, D.: Rhythmic karst springs. *Hydrolog. Sci. J.* **36** (1), 35–47 (1991)
- Ehrmann F.: Geological map of Tamesguida, scal 1/50.000, with notice (1946)
- Igracev, N.: Comparative analysis of the flow activity of the Homoljska Potajnica Intermittent spring. *J. Geogr. Inst. Cvijic.* **64**(1), 1–12 (2014)

**Hydrology, Hydrogeology, Hydrochemistry,
Water Resources (T10): Hydrogeology and
Hydrochemistry—Chemical and Quality Aspects**



Assessment and Mapping of the Pollution Risk of Springs Water: The Case Study of Taher Region (Jijel, Northeast Algeria)

Amal Chine, Taha-Hocine Debieche, and Boualem Mayache

Abstract

The region of Taher (Jijel, N-E Algeria) is characterized by the presence of several springs emerging naturally on the surface that are frequently used by the citizens for drinking. However, these springs are exposed to several forms of pollution, particularly from agricultural and urban sources, which can change their physicochemical quality and cause a harm to human health. The objective of this study is to evaluate and map the physicochemical quality of spring water in the study area using the water quality evaluation system (WQES-Groundwater). To achieve this goal, a sampling campaign was carried out during July 2017. The results obtained revealed that some springs have a very bad quality in terms of chloride and nitrate concentrations.

Keywords

Spring water • WQES—groundwater • Chlorides • Nitrates • Pollution

1 Introduction

Springs water are often considered to be of good physicochemical quality and are widely used by the population for drinking water supply (DWS). Bacteriological and physicochemical contamination of these waters can endanger human health. In this study, the Quality Evaluation System (WQES-Groundwater) is a mathematical tool (Hamlat and

A. Chine (✉) · T.-H. Debieche
Water and Environment Research Team, Geological Engineering Laboratory (LGG), Faculty of Nature and Life Sciences, University of Mohamed Seddik Benyahia, Jijel, Algeria

B. Mayache
Laboratory of Biotechnology, Environment and Health, Faculty of Nature and Life Sciences, University of Mohamed Seddik Benyahia, Jijel, Algeria

Guidoum 2018) used to assess level degradation chemistry water quality of the springs of the Taher region (Jijel, N-E Algeria). Various water quality index (WQI) has been formulated, also developed and applied in several studies such as Olowe et al. 2016; Packialakshmi et al. 2015.

2 Study Area

The Taher Region is located in N-E Algeria at 250 km from the Algiers (capital). The geology of the region is composed essentially of three formations: (a) sand dunes (coarse and fine sands), permeable, of quaternary age; (b) detrital deposits (pebbles and clays of continental origin), permeable to semi-permeable, of Pontian (upper Miocene) age; and (c) gray marl, impermeable, of Burdigalian age (lower Miocene). Several springs emerge at the permeable/impermeable or semi-permeable contact.

3 Materials and Methods

In order to give a good assessment of the spring waters' quality, a sampling campaign was carried out during the summer period (July 2017), when the demand for spring water is high and the risk of pollution is of major concern. A total of 13 representative springs from the study area were sampled. The physical parameters (pH and EC) were measured in situ, using the WTW 350i field multi-parameters kit. The chemical elements were analyzed in the Laboratory of Geological Engineering (LGG) using two methods (Rodier et al. 2009): titrimetric for Ca^{2+} and Cl^- and spectrometry for NO_3^- and SO_4^{2-} with the aid of VWR UV-1600PC spectrophotometer.

The evolution of the chemical quality of the springs was assessed according to the water quality evaluation system (WQES—Groundwater) which is based on the notion of alteration. WQES serves to identify level and to assess the

status of water quality degradation of springs. It may be defined by the thresholds of each parameter into five classes with respective colors and each class representing of an index. This index is calculated by means of the equations determined by BRGM, but the final index is obtained by the difference to the value 100 (BRGM 1997; Water Agencies 2003).

4 Results

The mapping of the spatial distribution of the water quality evaluation index (Fig. 1) and projecting the results of physicochemical analysis on the diagram of WQEI (Fig. 2), showed an alteration index as follows:

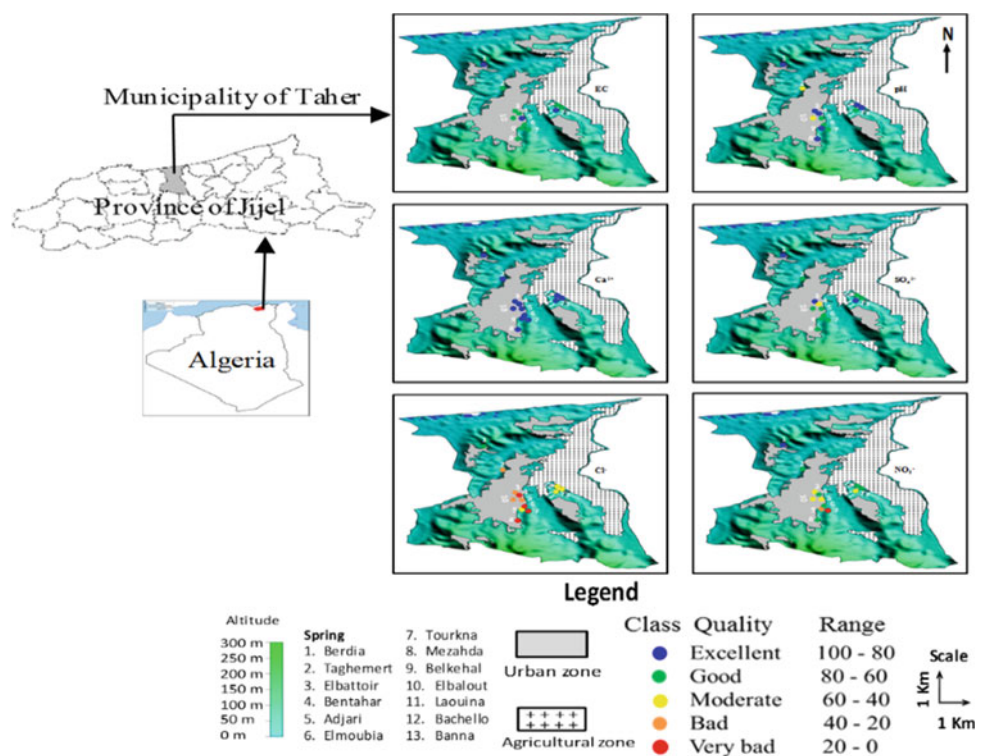
- **EC** (electrical conductivity) values ranged from 255 to 1238 $\mu\text{s cm}^{-1}$. Overall, 15.4% of the springs had a excellent, while 84.6% was good.
- **pH** value fluctuated from 6.0 to 7.1 also 53.9% of springs characterized excellent quality; therefore, 30.8% of springs categorized good quality and 15.3% of springs were moderate quality. The latter quality was observed at two springs, namely Taghemert and Elballoute.
- **Ca²⁺** concentration varied between 17.6 and 56.1 mg L⁻¹; also, all the springs (100%) were of excellent water quality (WQEI equal 89.2).

- **SO₄²⁻** content recorded from 11 to 112 mg L⁻¹ and 23.07% of springs of the study area marked excellent quality, after 69.23% of springs observed good quality. The Bentahar spring (7.7%) was moderate quality (WQEI is 56.7).
- **Cl⁻** concentration remarked between 71 and 300 mg L⁻¹. It had four quality classes: good at the Berdia spring (7.69%), moderate (30.77%), bad (30.77%) and very bad (30.77%). Their water quality evaluation indices values were successively as follows: (64.22); (49.00); (33.50); (9.40).
- **NO₃⁻** concentration observed between 6.5 and 114.2 mg L⁻¹. It recorded five quality classes: excellent at the Berdia spring (7.69%), good (38.46%), moderate (38.46%), bad at the Belkehal spring (7.69%) and very bad at the Tourkna spring (7.69%). The values of their water quality evaluation indices were successively as follows: (87.06); (68.42); (47.14); (37.54); (13.06).

5 Discussion

Some pH values of springs were lower than the Algerian standards of 6.5–8.5. EC values do not exceed the Algerian standards of 2800 $\mu\text{s cm}^{-1}$.

Fig. 1 Quality maps for the alteration of physicochemical parameters (pH and EC) and chemical elements (Cl⁻, Ca²⁺, SO₄²⁻ and NO₃⁻)



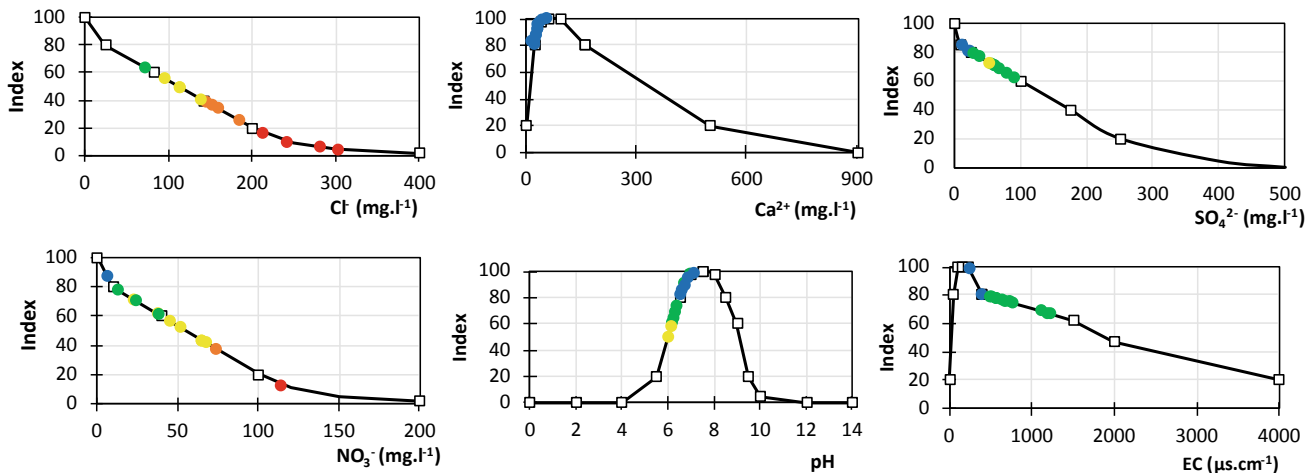


Fig.2 Diagram of the spring water quality evaluation index by altering physicochemical parameters (pH and CE) and chemical elements (Cl^- , Ca^{2+} , SO_4^{2-} and NO_3^-)

The concentrations of calcium, sulfate and chloride in the springs were in accordance with the Algerian standards, respectively: 200, 400, and 500 mg L^{-1} (OJAR 2006). However, according to the quality index by the alteration of the chloride, it had two quality classes: bad with chloride concentration ranged of 125–200 mg L^{-1} and very bad with chloride concentration varied of 213–301.75 mg L^{-1} because this last is higher than the WQE system standard of 200 mg L^{-1} .

Some springs showed a nitrate concentration higher than the Algerian standard 50 mg L^{-1} , and according to WQES, the quality of these springs classified between moderate and very bad. Its origin is inorganic (artificial or synthetic fertilizer) and/or organic (animal waste—manure spreading or urban wastewater) (Katz et al. 1999). These high amounts of nitrate can cause diseases such as the “baby-blue” syndrome, stomach cancer, leukemia, decreased body growth, slow reflexes and increased size of the thyroid (Batool et al. 2018).

The study recommends that administrative officials prohibit the use of these polluted springs for DWS and establish a protection perimeter for other springs.

6 Conclusions

This study demonstrates the effectiveness of the Water Quality Evaluation System (WQES), and this method consists in producing a detailed water quality assessment, but it remains limited to give an overall assessment of physico-chemical quality, preferably to create and apply a single index for a total determination of water quality.

Finally, the overall estimate of the proportion of the spring water quality index of six alterations in this study according to WQES is defined in five quality classes: excellent (33.33%), good (38.46%), moderate (15.39%), bad (6.41%) and very bad (6.41%).

References

- Batool, A., Samad, N., Kazmi, S., Ghufraan, M.A., Imad, S., Shafqat, M., Mahmood, T.: Spring water quality and human health: an assessment of natural springs of Margalla hills Islamabad zone- III. *Int. J. Hydrol.* **2**(1), 14–46 (2018)
- BRGM. Development of a water quality evaluation system, Document 1: Characterization of the functions of their states, Report BRGM R39166, p 44 (1997). (In French)
- Hamlat, A., Guidoum, A.: Assessment of groundwater quality in a semiarid region of Northwestern Algeria using water quality index (WQI). *Appl. Water Sci. J.* **8**(220), 1–13 (2018)
- Katz, B.G. Hornsby, H.D. Bohlke, J.F. Mokrayer, M.F.: Sources and Chronology of Nitrate Contamination in Spring Waters, Suwannee River Basin, Florida. Water-Resource Investigations Report 99-4252, pp. 1–51. Tallahassee, Florida (1999)
- Official Journal of the Algerian Republic (OJAR): Interministerial order fixing the proportions of elements contained in natural mineral waters and spring waters and their treatment or authorized additions. The law n°27, 9–12 (2006) (In French)
- Olowe, B.M., Oluyegbe, J.O., Famurewa, O.: An assessment of drinking water quality using water quality index in ado-ekiti and environs, Nigeria. *Am. Chem. Sci. J.* **12**(2), 1–7 (2016)
- Packialakshmi, S., Deb, M., Chakraborty, H.: Assessment of groundwater quality index in and around Sholinganallur Area, Tamil Nadu. *Sci. Technol. Indian J.* **8**(36), 1–7 (2015)
- Rodier, J., Legube, B., Merlet, N.: Water analysis, 9^{ed}. Dunod, Paris (2009)
- Water Agencies, MEDD. Groundwater Quality Evaluation System: WQES—Groundwater, Presentation Report Version 0.1, pp. 3–50 (2003). (In French)



Seasonal Variation of Water Quality/Jericho Spring Group (Palestine)

Amer Marei, Saed Khayat, and Husam Uteir

Abstract

5.1 MCM/year of treated and raw wastewater flow in the western part of Wadi Al Quit catchment area partially contributes to the groundwater recharge. Al Sultan, Al Dyuk, and Al Nuwemeh springs in the Jericho area/Jordan Valley are considered as the main domestic water sources for Jericho City. A rise in the concentrations of electrical conductivity, dissolved organic carbon (DOC), total nitrogen (TN), chloride and bromide concentration, and Na/Cl ratio was recorded during the winter and spring seasons. This indicates that a mixture process between the freshwater recharge and wastewater pollutants stored in the unsaturated zone takes place during the early winter season; thus, fresh recharge mobilizes the pollutant within the fractured/karstified aquifer and causes an impulse of a relatively high concentration in spring water. Pollutants in Al Sultan and Al Dyuk springs have the same trend, while Al Nuwemeh spring behaves differently; this indicates that the latter has different groundwater flow systems.

Keywords

Jericho springs group • Carbonate aquifer • Wastewater

1 Introduction

Spring discharges are considered as the main source of drinking water besides being partially used for agriculture in the Jericho area. Jericho springs drain about 14 MCM/year

from the upper part of the Mountain Aquifer system (MERC 1999). Wadi Quilt is one of the main natural surface and subsurface drainage systems in the study area, with a watershed of about 176 km² (PWA 2009). Palestinian urban areas and Israeli settlements are located within the Wadi Quilt watershed, in the West (Fig. 1). One hundred and nineteen thousand Palestinians (Jericho Municipality 2010) and about 29 thousand Israeli settlers are living within the Wadi Quilt watershed (Palestinian Statistical Office 2016; Shraideh 2014). The total annual domestic water consumption is about 6.3 MCM, whereas the generated wastewater is about 5.1 MCM. Only 2.2 MCM is treated in Al-Bireh Wastewater Treatment Plant (Oded Fixler 2011). In general, surface runoff ranges between 0.5 and 12 MCM/annually (Asaf et al. 2007). Asaf et al. (2007) estimated the annual amount of untreated and surface runoff at about 12 MCM/annually of fresh, treated, and raw wastewater eastward to the Jordan Valley (Samhan et al. 2011). Previous studies show that biological oxygen demand (BOD) concentrations of surface water mixed with wastewater range between 20 and 136 mg/L (Daghrach 2005). The aquifer system is fed through two recharge sources: direct recharge from rainfall and through the infiltration of surface water, including wastewater through the highly fractured, deeply eroded Wadi floor (Guttman 1998).

The objective of this study is to determine some seasonal water quality parameters, such as EC, Cl⁻, Br⁻, DOC, TN, and Na⁺, as indicators of the impact of wastewater infiltration in the recharge zones.

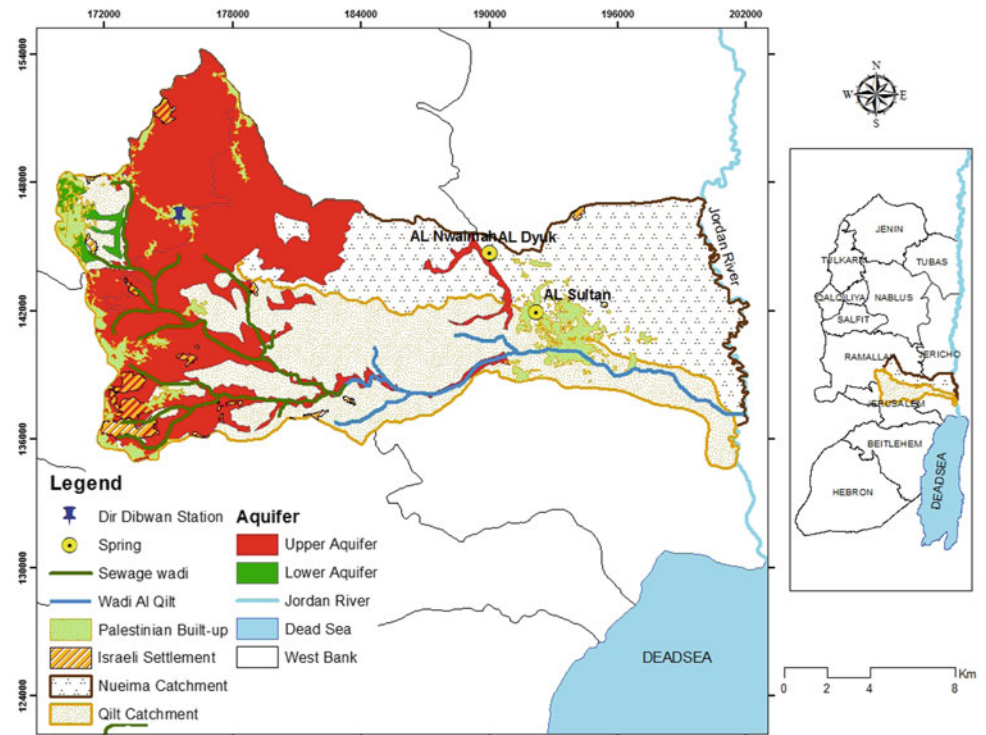
2 Materials and Methods

Thirteen groundwater samples were collected in three sampling campaigns between August 2015 and April 2016. The samples were handled according to the standard method (Begin 1974) (Table 1). Rainfall data were collected from Dir Dibwan meteorological station to recharge with water

A. Marei (✉) · H. Uteir
Environmental Research Lab, Al Quds University, East Jerusalem,
Israel
e-mail: marei@staff.alquds.edu

S. Khayat
Palestine Technical University Kadoorie, Tulkarm, Israel

Fig. 1 Springs location, geological map, and Wadi Al Qilt drainage system (Hoetzi et al. 2008)



quality (Ministry of Transportation 2010). Electrical conductivity (EC), pH, and temperature were measured in the field using a WTW multi-electrode instrument. Ion-selective electrode methods were used to measure chloride and bromide concentrations. AAS method was used to determine major cations including sodium concentration. Spectrophotometer methods were used to determine sulfate and nitrate. Titration method was used to measure the bicarbonate (Begin 1974). Analytical Jena instrument 2000 was used to measure dissolved organic carbon (DOC) and total nitrogen (TN). Charge balance of equivalent contents for observed ions shows that inorganic charge balance error is less than 5%. Groundwater contents of conservative ions (Cl and Br), in addition to DOC and TN, are used in this paper to evaluate the seasonal variation of water quality. The Na/Cl molar ratio is a common method used by several types of research to trace the additional sources of salts (Rofe and Raffety 1963; Marei et al. 2010; Khayat et al. 2009).

3 Results

The upper aquifer system consists mainly of highly fractured, karstified limestone, and dolomite of Upper Cretaceous age. Wastewater infiltrates through the Wadi floor to the unsaturated zone in the western part of the watershed (Fig. 1). The total rainfall at Dir Dibwan station was 477.6 mm during the hydrological year 2015–2016 (Ministry of Transportation 2010). August–October samples

present water quality at the end of summer and the beginning of autumn season, respectively, whereas January and April samples present winter and spring seasons, respectively. Table 1 shows a cumulative rainfall at Dir Dibwan station and selected physical and chemical properties of three water springs, namely Al Sultan, Al Dyuk, and Al Nuwemeh.

4 Discussion

Variation of pH values is not significant and reflects the characteristics of fresh groundwater of highly fractured, karstified aquifer. The highest EC values were recorded during January after 44% of the annual rainfall, and the lowest values in August. The highest chloride values were recorded during April for Al Sultan and Al Dyuk springs, and in January for Al Nuwemeh spring, while the lowest values were recorded during August, and this trend shows the impact of groundwater replenishment during the recharge seasons. Na/Cl ratio (>1) was found during the winter and spring seasons, at Al Sultan spring more often than at the other springs, which indicates a contribution of wastewater in the recharge rate (Khayat et al. 2009). The highest bromide values were measured during April, compared to January for chloride when the accumulative annual rainfall reaches 99%. The highest DOC and TN values were measured in Al Sultan and Al Dyuk springs during January, whereas the lowest concentrations were measured in Al Nuwemeh spring (MERC 1999).

Table 1 Accumulated rainfall and selected physical and chemical properties of water springs

Spring	Date	Rainfall mm	pH	T °C	EC μ S/cm	Cl ⁻ mg/L	Na ⁺ mg/L	Na ⁺ /Cl ⁻ mmol/L	Br ⁻ mg/L	DOC mg/L	TN mg/L
Al Sultan	1.08.2015	0.0	7.0	24	661	55.0	56.0	1.5	0.5	1.5	4.8
	1.10.2015	0.0	7.3	21	693	32.0	27.0	1.2	0.5	2.2	6.4
	1.01.2016	211.4	7.4	21	786	70.0	69.0	1.3	0.6	18.4	7.2
	1.04.2016	265.1	7.5	22	776	83.0	26.0	0.4	2.1	3.3	5.3
Al Dyuk	1.08.2015	0.0	7.3	21	684	54.0	54.0	1.5	0.6	2.3	4.3
	1.10.2015	0.0	7.4	22	685	53.0	24.0	0.6	0.6	4.9	5.3
	1.01.2016	211.4	7.3	21	754	68.0	75.0	1.6	0.6	14.4	7.1
	1.04.2016	265.1	7.4	22	724	72.0	24.0	0.4	2.0	1.3	5.7
Al Nuwemeh	1.08.2015	0.0	7.4	23	687	56.0	60.0	1.6	0.5	2.4	4.9
	1.10.2015	0.0	7.5	22	688	35.0	26.0	1.1	0.6	3.5	5.4
	1.01.2016	211.4	7.4	21	747	68.0	69.0	1.6	0.6	2.9	6.8
	1.04.2016	265.1	7.3	21	716	59.0	25.0	0.6	2.3	2.1	5.5

5 Conclusions

Discharge of wastewater in the natural drainage system of the upper Wadi Al Qilt catchment area has a negative impact on the water quality of the three springs (Al Sultan, Al Dyuk, and Al Nuwemeh) that are considered as the main domestic sources of water for Jericho City. The degradation of the water quality depends on the recharge mechanism during the winter season. Transfer of wastewater from the western part of the catchment in a closed pipeline downstream to the Jordan valley is important to prevent additional future deterioration of this spring water. Wastewater could help solve the water shortage problem in the agricultural sector.

References

- Asaf, L., Negaoker, N., Tal, A., Laronne, J., Al Khateeb, N.: Transboundary stream restoration in Israel and the Palestinian authority. In: Lipchin, C., Pallant, E., Saranga, D., Amsterdam, A. (eds.) *Integrated Water Resources Management and Security in the Middle East*, pp. 285–296 (2007)
- Begin, Z. B.: *Geological Map of Israel, Jericho Sheet 9-III, 1:50,000, with explanatory notes*. Geological Survey, Jerusalem, Israel (1974)
- Daghrah, G.: *Pollution and water quality assessment of Wadi Al Qilt*. Master thesis, Birziet University/Palestine (2005)
- Guttmann, Y.: *Hydrogeology of the Eastern Aquifer in the Judea Hills and Jordan Valley*. Technical Report, Tahal Consulting Engineers Ltd, Tel Aviv, Israel, (1998).
- Hoetzel, H., Flexer, A., Guttman, J., Bensabat, J., Ali, W., Yelin-Dror, A.: Flow pattern of low permeability zones in a fissured karst aquifer—3-D flow model of the Marsaba-Feshkah area, Dead Sea. In: *EUG Conference April 2008, Vienna, Austria* (2007)
- Jericho Municipality: Water Department Personal communication, Jericho/Palestine (2010)
- Khayat, S., Moller, P., Geyer, S., Marai, A., Siebert, C., Abu, H.F.: Hydrochemical variation in the springs water between Jerusalem-Ramallah Mountains and Jericho Fault. *Palestine. Environ. Geol.* **57**, 1739–2175 (2009)
- Marei, A., Khayat, S., Weise, S., Ghannam, S., Sbaih, M., Geyer, S.: Estimating groundwater recharge using the chloride mass-balance method in the West Bank. *Palestine. Hydrol. Sci. J.* **55**(5), 780–792 (2010)
- Middle East Regional Cooperation Program (MERC): *Water Quality along the Jordan River “A geochemical Perspective on the Sources of Salts” Final Report* (1999)
- Ministry of Transportation, *Rainfall Data Base, Ramallah/Palestine*, (2010)
- Oded Fixler: *Master plan for the national water and sewage sector—The policy paper—Israel Water Authority* (2011)
- Palestinian Statistical Office (2016)
- Palestinian Water Authority (PWA): *Data Base, Ramallah—Palestine* (2009)
- Rofe and Raffety, West Bank. *The Hashemite Kingdom of Jordan. Central Water Authority*. Westminster, London. Rofe and Raffety Consulting Engineers (1963)
- Samhan, S., Freise, K., Von Tuempling, W., Poellmann, H., Ghanem, M.: Anthropogenic trace metals and their enrichment factors in Wadi Al Qilt sediment. *Palestine. Int. J. Environ. Stud.* **68**(4), 495–507 (2011)
- Shraideh, H.A.: *Water Quality Modeling of Al-Qilt Stream*, Master of Water and Environmental Engineering, An Najah University (2014)



Estimating Natural Backgrounds and Threshold Values of Hydrochemical Parameters in a Desert Area (India)

Abdur Rahman, Kamal Tiwari, and Nepal Mondal

Abstract

Hydrochemical background and threshold values have been estimated to assess groundwater quality using cumulative probability distribution of the major ions for 36 groundwater samples collected during two climatic conditions in a desert area from Western India. The results indicated that the different segments on the probability plots are to be used as an indicator of the different processes of groundwater pollution. Broadly, we have found 2–3 segments on the probability distributions. The first segment having the inflection values of Na^+ , Cl^- and SO_4^{2-} is 161, 121 and 28 mg/L, respectively. It may have been treated as the natural backgrounds. Their threshold values have also been estimated as 181, 186 and 139 mg/L for the Na^+ , Cl^- and SO_4^{2-} ions, respectively, considering their reference values as per the BIS norms. Furthermore, the second threshold values of chloride and sulfate ions were found to be 218 and 195 mg/L, respectively. It leads to the inference that there are two different hydrochemical processes involved in the deterioration of the groundwater quality w.r.t. the background levels. But the concentrations of EC in the groundwater samples vary from 680 to 5000 $\mu\text{S}/\text{cm}$ during the sampling periods, whereas the concentrations of Na^+ , Cl^- , SO_4^{2-} , HCO_3^- , NO_3^- and F^- varied from 34 to 1000, 43 to 1212, 5 to 279, 207 to 1098, 2 to 85 and 0.1 to 2.6 mg/L, respectively. It shows that the groundwater quality has been deteriorated by the industrial effluents

and irrigation practices in the west and southwest parts of the study area.

Keywords

Hydrochemistry • Natural backgrounds • Threshold values • Desert area • Western India

1 Introduction

About 0.6% of freshwater is available for use in the world (Gleick and Iwra 1996). Freshwater quality is continuously changing due to human activity and climatic changes (Mattia et al. 2017). Groundwater flow, climate, rainfall, human activities, geology and overexploitation trigger the mobilization of naturally occurring contaminants and facilitate injection of anthropogenic pollutants into the subsurface (Rajesh et al. 2015; Dermatas 2017; Negm et al. 2020a, 2020b). The natural background level, or baseline, is defined as “the range of concentration of a given element, isotope or chemical compound in solution derived entirely from natural, geological, biological or atmospheric sources under condition not perturbed by anthropogenic activity” (Edmunds and Shand 2009). The threshold value is the environmental water quality standards (Scheidleder 2012; Mondal 2018) which is used to decide whether some given groundwater is suitable for human use or not. Therefore, the establishment of a threshold value is imperative for all pollutants. Indeed, this threshold value acts as indicator of pollution that could be identified in groundwater bodies which fail to achieve good groundwater chemical status in accordance with the Water Framework Directive (WFD) (2000). So, the quality of water resources has been a serious day-to-day concern (Alley et al. 1999) particularly in the desert areas. On the basis of knowledge, there is no document for the determination of groundwater pollution in a desert area, namely the Sanganer Block in the Jaipur

A. Rahman (✉) · N. Mondal
Earth Process Modeling Group, CSIR-National Geophysical
Research Institute, Hyderabad, Telangana, India
e-mail: alrahman@ngri.res.in

Present Address:

A. Rahman · N. Mondal
Academy of Scientific & Innovative Research (AcSIR),
Ghaziabad, Uttar Pradesh, India

K. Tiwari
National Institute of Technology (NIT), Garhwal, Uttarakhand,
India

district, Rajasthan, located in the western part of India. The main objectives of this study are to establish background and threshold values in the groundwater of the area.

2 Methodology

2.1 Study Area

The study area is situated in the western part of India and lies between longitudes: 75.45°E–75.90°E and latitudes: 26.70°N–26.92°N (Fig. 1a) with an area of about 636 km² and covers about 45.5% of urban clusters. Topographically, it varies from 330 to 438 m above mean sea level (m, amsl). In terms of geology, the area falls under Quaternary alluvium sediment, gneiss and schist of the Delhi Super Group and the Bhilwara Super Group. The main water bearing formation is weathered and fractured quartz–biotite schist (Central Ground Water Board (CGWB) 2000).

2.2 Groundwater Samplings and Analysis

A total of 36 groundwater samples were collected from wells (Fig. 1a) covering dry and wet seasons in the months of May and October 2014. The samples were collected in 100 mL polythene bottles and used for the analysis of major ions. The ions were analyzed by the standard methods as

described by APHA (1985). The background level or baseline of groundwater bodies was estimated by cumulative frequency plot (Panno et al. 2006), and the threshold value (TV) was calculated according to the BRIDGE methodology (Müller et al. 2006).

3 Results and Discussion

3.1 Groundwater Chemistry

The EC values of groundwater ranged between 790 and 5000 $\mu\text{S}/\text{cm}$ with an average value of 1916 $\mu\text{S}/\text{cm}$ during the dry season, and from 680 to 4600 $\mu\text{S}/\text{cm}$ with a mean value of 1936 $\mu\text{S}/\text{cm}$ during the wet season. The results indicated poor groundwater quality in the southern part compared to the northern part. The average TDS value was 1088 mg/L in the dry season and 1098 mg/L in the wet season. The study showed that about 83 and 89% of the samples exceeded the BIS standard (BIS 2012) with respect to TDS, respectively, in the wet and dry season. The concentrations of Na^+ , Cl^- , SO_4^{2-} , HCO_3^- , NO_3^- and F^- ranged from 34 to 100, 43 to 1212, 5 to 279, 220 to 1098, 2 to 85 and 0.02 to 2.6 mg/L, respectively, for the two sampling periods. The hydrochemical data for the dry season indicated that 38.8, 33.3, 33.3 and 22.2% of TDS, Cl^- , NO_3^- and F^- exceeded the Indian Drinking Water Standard, while 44.4, 33.3, 44.4 and 16.6% exceeded these standards in the wet season.

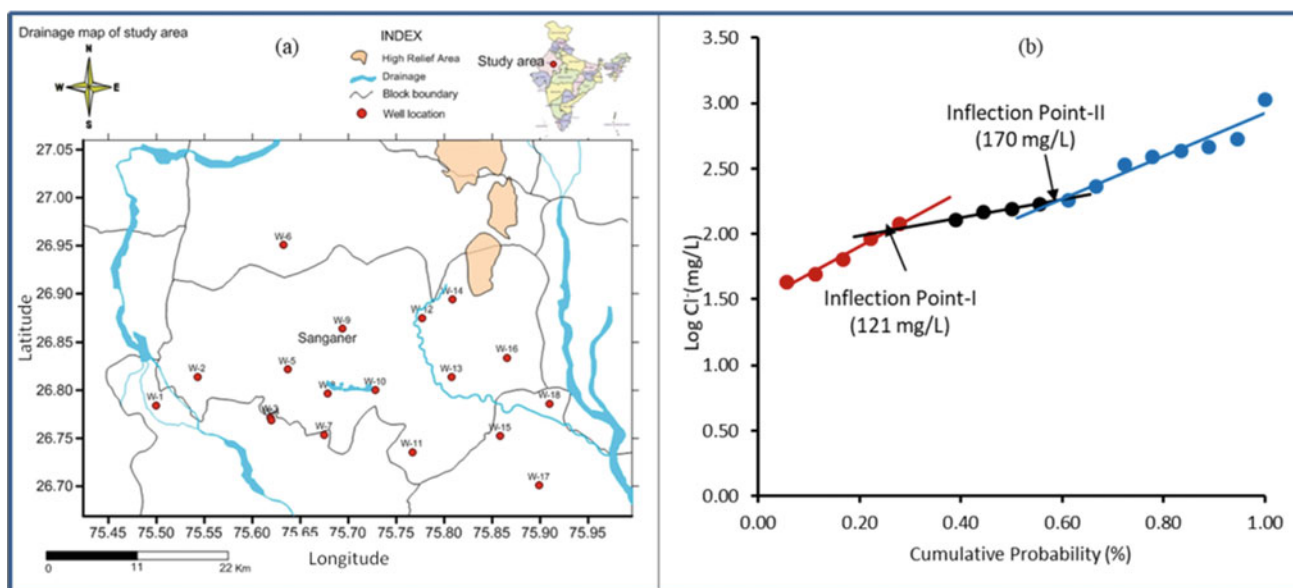


Fig. 1 a The location of study area along with drainage patterns and sampling points. b The cumulative probability distribution of chloride concentration in groundwater

3.2 Hydrochemical Backgrounds and Threshold Values

Cumulative probability distributions of Cl^- , SO_4^{2-} , Na^+ and NO_3^- were plotted for both the dry and wet seasons. The first inflection points obtained were 161, 121 and 28 mg/L, respectively, for Na^+ , Cl^- and SO_4^{2-} . These inflection points were considered as natural backgrounds of the respective ions. In the wet season, the Cl^- concentrations showed two inflection points on the cumulative plots (Fig. 1b), which indicated several factors which are responsible for groundwater pollution. These natural backgrounds had been contoured, corresponding to the total concentrations of the ions. As an example, the contours of natural background and total concentration of chloride and other hydrochemical constituents are plotted and the difference between both may be utilized for the identification of groundwater pollution, and the degrees of pollution loads could also be identified based on the difference between the two.

Background values (BVs) are applied to know the deviation of groundwater quality within the threshold value (TV). Further the threshold value (TV) for sodium, chloride, sulfate and nitrate were calculated according to the BRIDGE methodology (Müller et al. 2006). According to this method, the TVs were derived as the ratio between the estimated background level (BL) and reference value (REF). If $\text{BL} < \text{REF}$, an average of both was used for the estimation of first threshold value (TV), and if $\text{BL} > \text{REF}$, then simply $\text{TV}_2 = \text{BL}$ for the second threshold value. It is applied to know the anthropogenic processes responsible for groundwater quality deviation from its background. Therefore, the first threshold values were calculated as 181, 186, 139 and 37 mg/L for the Na^+ , Cl^- , SO_4^{2-} and NO_3^- ions, respectively. The second threshold values of Cl^- and SO_4^{2-} were calculated as 218 and 195 mg/L, respectively. Two thresholds indicate two different hydrochemical processes involved in the deterioration the groundwater quality in the west and southwest parts of the study area.

4 Conclusions

Natural backgrounds and threshold values of hydrochemical parameters have been estimated using cumulative probability distribution in a desert area of Western India. This area has a long industrial history and that industrial activity is responsible for unbalancing the chemistry of the groundwater resource. As an example, the background value of chloride concentrations in groundwater samples of the study area is estimated at 121 mg/L, whereas the first threshold value was calculated as 186 mg/L and as 218 mg/L for the second. This indicates that there are two hydrochemical processes involved in the deterioration of the groundwater quality.

Acknowledgements Dr. V.M. Tiwari, Director of CSIR-NGRI, Hyderabad, has given permission to present this article (Ref. No.: NGR/Lib/2019/Pre101). First author has contributed this research work under his Junior Research Fellowship [Ref. No.: 31/023(0240)/2018-ERR-I, dated; 13-07-2018]. The anonymous reviewers have given their constructive comments to improve the article. The authors are thankful to them.

References

- Alley, W.M., Reilly, T.E., Franke, O.L.: Sustainability of Groundwater Resources: US Geological Survey Circular, vol. 1186, p. 79 (1999)
- American Public Health Association (APHA): Standard Methods for the Examination of Water and Waste, 16th edn, pp. 100. Am public health Association Washington DC (1985)
- BIS 2012 Indian Standards Specification for drinking water; IS: 10500: 2012, 2nd Rev., BIS, New Delhi (2012)
- Central Ground Water Board (CGWB): 2000 Project on beneficiation of ground water quality with reference to fluoride problems. CGWB Report, Western Region, Jaipur, p. 14 (2000)
- Dermatas, D.: Waste management and research and the sustainable development goals: focus on soil and groundwater pollution. *Waste Manag. Res.* **35**(5), 453–455 (2017)
- Edmunds, W.M., Shand P.: Groundwater baseline quality. *Natural groundwater Quality*, pp. 1–21. Blackwell Publishing (2009)
- Gleick, H.P., Iwra, M.: Basic water requirements for human activities: meeting basic needs. *Water Int.* **21**, 83–92 (1996)
- Mattia D.C., Crosta G.B., Frattini P., Perico, R., Volpi, G.: Hydrofacies reconstruction of glaciofluvial aquifers and groundwater flow modelling in a densely urbanized area under changing climatic conditions. *Hydrol. Earth Syst. Sci. Discuss* (2017). <https://doi.org/10.5194/hess-2017-555>
- Mondal, N.C.: Reconnoitering hydrochemical background using log-probability distribution in a Channel Island, Andhra Pradesh. In: Giridhar, M.V.S.S. (ed.) Proceedings of 5th National Conference on Water, Environment & Society (NCWES-2018, held on 4–6th June, 2018, JNTU, Hyderabad), pp.271–277. Publisher: BSP Books Pvt. Ltd., Hyderabad (2018)
- Müller, D., Blum, A., Hart, A., Hookey, J., Kunkel, R., Scheidleder, A., Tomlin, C., Wendland, F.: Final proposal for a methodology to set up groundwater threshold values in Europe, Deliverable D18, BRIDGE project (2006)
- Negm, A., Bouderbala, A., Chenchouni, H., Barcelo, D.: Water resources in Algeria - Part I: assessment of surface and groundwater. In: *The Handbook of Environmental Chemistry Series*. Cham, Springer (2020a)
- Negm, A., Bouderbala, A., Chenchouni, H., Barcelo, D.: Water resources in Algeria - Part II: water quality, treatment, protection and development. *The Handbook of Environmental Chemistry Series*. Cham, Springer (2020b)
- Panno, S.V., Kelly, W.R., Martinsek, A.T., Hackley, K.C.: Estimating background and threshold nitrate concentrations using probability graphs. *Ground Water* **44**, 697–709 (2006)
- Rajesh, R., Brindha, K., Elango, L.: Groundwater quality and its hydrochemical characteristics in a shallow weathered rock aquifer of southern India. *Water Qual. Expo. Health* **7**(4), 515–524 (2015)
- Scheidleder, A.: Groundwater threshold values, In-Depth Assessment of the Differences in Groundwater Threshold Values Established by Member States. *Environment Agency Austria, Austria* (2012)
- Water Framework Directive (WFD): Directive 2000/60/EC of the European parliament and of the Council Establishing a Framework for Community Action in the Field of Water Policy (2000)



Influence of Water-Rock Interaction on the Fluoride Contamination of Groundwaters from Bhokar, (Nanded District, Maharashtra, India)

Dipak Panaskar, Vasant Wagh, and Ranjeet Pawar

Abstract

In India, fluoride is the major pollutant of natural origin in groundwater. Fluoride in drinking water may be either beneficial or detrimental depending on its concentration and total amount ingested. The high amount of fluoride contained in water causes dental and skeletal fluorosis when it enters the body. The concentration of the fluoride in the groundwaters and the lithology provide the important signatures to identify the sources of contamination. The geochemical characterization of 89 groundwater samples from the Bhokar area has been carried out. In the study area, the fluoride contents in groundwater range from 0.01 to 6.95 mg L⁻¹ and are seen to be high above the safe limit of 1.5 mg L⁻¹ given by WHO. A higher content of fluoride was observed in the areas underlain by granitic gneisses. It can be concluded that water-rock interaction is the main process responsible for the high concentration of fluoride. The fluoride rich minerals from the aquifer rock must have been dissolved in groundwater by dissolution. The higher content of fluoride in the groundwater found in wells which are close to lineaments indicates a possibly higher rate of dissolution process. The increase and decrease in the lateral extent of the fluoride contamination zone in pre- and post-monsoon seasons, respectively, corroborate the dissolution and dilution processes. These indicate the rock-water interaction as the main process responsible for the high concentration of fluoride.

Keywords

Fluoride • Geochemistry • Groundwater • Bhokar

1 Introduction

Environmental fluorine enrichment has both natural and anthropogenic sources. The chemical weathering of some fluoride (F) containing minerals—like fluorite, apatite, crinoline, topaz, biotite, etc.—leads to fluorine enrichment of soils and groundwater (Totsche et al. 2000). The discharge of fluoride from some industries—e.g. semiconductors, steel, aluminium, glass, ceramic factories, phosphate fertilizers and electroplating—is among the main anthropogenic sources of F pollution (Arnesen and Krogstad 1998). Extensive application of phosphate fertilizers (containing 1.5–4% F) in agriculture is another important source of F input to soils (Loganathan et al. 2001). Groundwater is the most important source of F. The secondary sources are related to pollution from industries (ceramic factories, coal burning) and agricultural activities, particularly the use of phosphatic fertilizers. According to Perel'man, fluorite is the most widely distributed fluorine-bearing mineral in nature, while fluorapatite is a very common member of the immiscible phase generated during early differentiation of mafic and ultramafic magmas, forming apatite-magnetite rocks (Perel'man 1977). Under supergene environment conditions, due to the high reactivity coefficient, the element occurs as highly mobile fluoride ion but its mobility is severely restricted across a calcium barrier due to CaF₂ precipitation (Perel'man 1977). It is for this reason that, under supergene environment conditions, the average fluorine content of calcium-rich sedimentary rocks—like calcareous shale, limestones, dolomite, calcareous sandstone, etc.—is high (Deshmukh et al. 1995). In arid and semi-arid regions, the fluoride content of groundwater is higher than that of groundwater in humid areas (Deshmukh and Chakravarti 1995).

D. Panaskar (✉) · V. Wagh
School of Earth Sciences, S. R. T. M. University, Nanded,
Maharashtra, India

R. Pawar
Department of Civil Engineering, SVERIs College of
Engineering, Pandharpur, Solapur, Maharashtra, India

A concentration of F in drinking water in the range of 0.5–1.0 mg L⁻¹ is beneficial for the production and maintenance of healthy bone and teeth. The acceptable maximum concentration of F in drinking water is 1.5 mg L⁻¹ (ICMR 1987; ISI 1983; Loganathan et al. 2001; Panaskar et al. 2006; Fan et al. 2003; WHO 1993). Fluoride is essential for the development of tooth enamel, dentin, and the bones. As several studies have shown, low doses of F are useful for the prophylaxis of caries and for the treatment of osteoporosis (Chandra et al. 1981). Fluoride is especially beneficial to young children below eight years of age when present within permissible limits of 1.0–1.5 mg L⁻¹ for calcification of dental enamel. The excess of fluoride in drinking water causes dental fluorosis and skeletal fluorosis (Sorg 1978).

2 Methodology

For the present study, the Sita Nadi Watershed area of Bhokar Taluka, Nanded District, has been selected (402 sq. km). A total of 89 representative groundwater samples from dug/bore wells (depth 50–450 ft) have been collected during

the pre- and post-monsoon seasons of 2012 (Fig. 1). Fluoride was determined using an Ion Analyser by adopting the standard methods given by APHA (2005). Surfer 9.0 software was used for the preparation of spatial F distribution maps.

3 Results

The Fluoride content of groundwater samples in the pre-monsoon season of 2012 ranged from 0.01 to 6.6 mg L⁻¹ (Table 1). The minimum content was recorded for sample number 69, while the maximum content was recorded for sample number 39. The average Fluoride and Standard Deviation (SD) values of the groundwater are 0.82 mg L⁻¹ and 0.99, respectively. In the post-monsoon season of 2012, the F of groundwater samples ranged from 0 to 6.95 mg L⁻¹ (Table 1). The minimum F was recorded for sample number 30, while the maximum F was recorded for sample number 39. The average F and SD values of the groundwater are 0.66 mg L⁻¹ and 0.96, respectively. The highest desirable limit of F is 1 mg L⁻¹ and the maximum permissible limit is 1.5 mg L⁻¹ given by WHO (1997). In 2012, the majority of groundwater samples in the pre- and post-monsoon seasons

Fig. 1 Study area map with groundwater sample locations

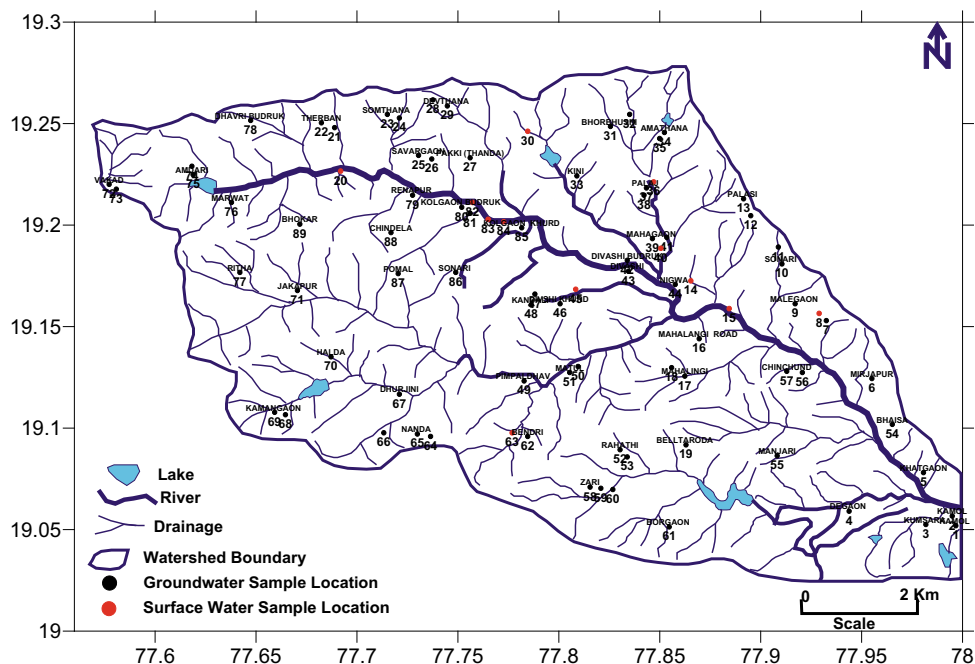


Table 1 Fluoride content in groundwater of pre- and post-monsoon seasons 2012

Fluoride (mg L ⁻¹)	Pre-monsoon	Post-monsoon
Minimum	0.01	0
Maximum	6.6	6.95
Average	0.82	0.66
Standard deviation	0.99	0.96

(75.3% and 91%, respectively) showed less F content than the highest desirable limit; the F content in 11.2% and 1.1% of the groundwater samples in the pre- and post-monsoon seasons, respectively, fell above the highest desirable limit, but below the maximum permissible limit. However, 13.5% and 7.9% of the groundwater samples in the pre- and post-monsoon seasons of 2012, respectively, showed an F content that exceeds the maximum permissible limit given by WHO (1997).

4 Discussion

It is evident that areas with a high F concentration (above Maximum Permissible Limit (MPL)) are located at the centre of the Sita river watershed, while areas with an F concentration above the Highest Desirable limit (HDL) but below MPL are located at the centre, and at five different locations in the southern part of the Sita river watershed in the pre-monsoon season of 2012. In the pre-monsoon season, the increase of the area extent with a high fluoride concentration (above MPL), as well as the five additional locations showing a fluoride concentration above HDL as compared to the post-monsoon season, corroborate the dissolution of fluoride from the basement rocks, i.e., granitic rocks, through the wall-rock interaction process (Fig. 2a, b). On the contrary, the decrease in the area extent with a high fluoride concentration (above MPL) in the post-monsoon season is an indication of a dilution process caused by precipitation.

The groundwater samples from Mahagaon, Divshi khurd, Divshi budruk, Kolgaon khurd, Kolgaon budruk, and Matul mainly contain high F amounts. Most of the study area is covered by basalt and is underlain by granitic rocks. Granite is one of the important sources of fluoride contamination. Most of the groundwater samples from the study area show F concentrations below the permissible limit. On the other

hand, people from such areas are also affected by dental fluorosis. This indicates that water is not only the source of fluoride contamination; other factors like nutrition and environmental conditions are also responsible.

The major trends of the lineaments are seen in NW–SE and NE–SW. The major lineaments trend in the NW–SE direction, whereas the minor lineaments trend is in the NE–SW direction. The major lineament, i.e. the Sita lineament, trend is in the NW–SE direction, which follows the Sita River course and passes from Renapur, Kolgaon Budruk, Kolgaon Khurd, Divshi Budruk, and Divshi Khurd villages (Panaskar et al. 2016). It is interesting to note that the groundwater samples which are near the Sita lineament showed higher concentrations of F. This can be attributed to the granitic rocks as a source of fluoride which is overlain by basalt in this area. Since the lineament is a weak zone, the fluoride from the granitic rock is getting leached out by the process of dissolution, thus contaminating the groundwater in this region.

5 Conclusions

In the study area, the high F concentration in the pre-monsoon season as compared to the post-monsoon season corroborates the dissolution of fluoride from the basement rocks, i.e. granitic rocks, through the wall-rock interaction process. On the contrary, the F content decreases in the post-monsoon season due to dilution and precipitation. The F content is unevenly distributed in groundwater and its concentration keeps on changing from time to time, both vertically and horizontally. Hence, every drinking water source has to be tested individually, and regular monitoring needs to be done. The usage of wells with high fluoride concentrations for drinking and irrigation purposes should be banned.

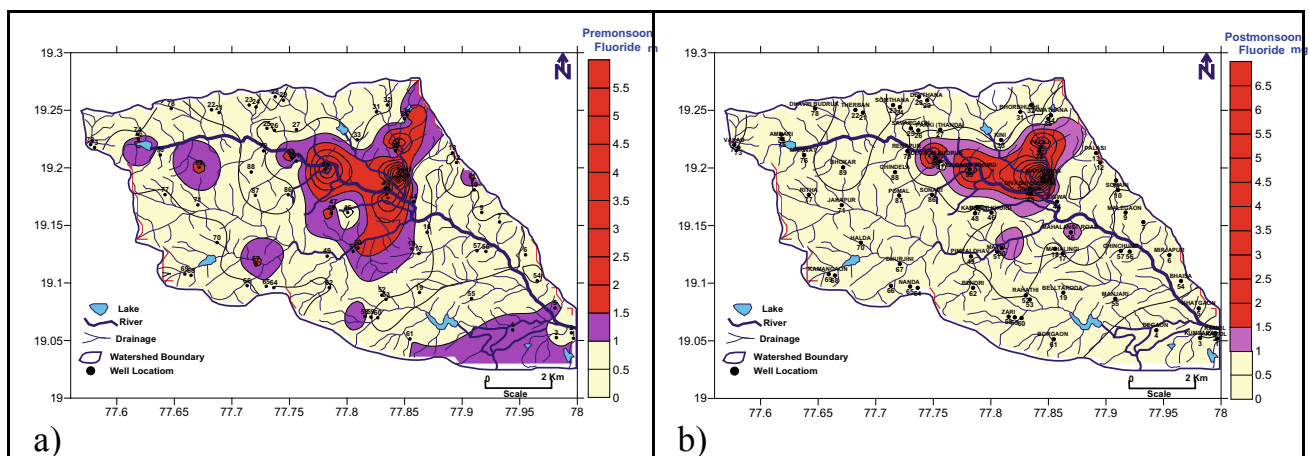


Fig. 2 Spatial distribution of Fluoride in groundwater of the study area

References

- APHA, A.: Standard methods for the examination of water and wastewater, 21st edn. American Public Health Association, New York (2005)
- Arnesen, A.K.M., Krogstad, T.: Sorption and desorption of fluoride in soil polluted from the aluminum smelter at Ardal in Western Norway. *Water Air Soil Poll.* **103**, 357–373 (1998)
- Chandra, S.J., Thergaonkar, V.P., Sharma, R.: Water quality and dental fluorosis. *Ind. J. Pub. Hlth.* **25**, 47–51 (1981)
- Deshmukh, A.N., Chakravarti, P.K.: Hydrogeochemical and hydrological impact of natural recharge on aquifers of fluorosis endemic areas—A case study of Chandrapur district, (M.S.). *Gondwana Geol. Mag.*, 169–185 (1995)
- Deshmukh, A.N., Valadaskar, P.M., Malpe, D.B.: Fluoride in environment: a review. *Gondwana Geol. Mag.* **9**, 1–20 (1995)
- Fan, X., Parker, D.J., Smith, M.D.: Adsorption kinetics of fluoride on low cost materials. *Water Res.* **37**, 4929–4937 (2003)
- ICMR: Indian Council of Medical Research. Manual of standards of quality for drinking water supplies (1987)
- ISI: (Indian Standard Institute) Indian Standard Specifications for drinking water, IS 10500 (1983)
- Loganathan, P., Hedley, M.J., Wallace, G.C., Roberts, A.H.C.: Fluoride accumulation in pasture forages and soils following long-term applications of phosphorus fertilizers. *Environ. Poll.* **115**, 275–282 (2001)
- Panaskar, D.B., Wagh, V.M., Pawar, R.S.: Hydrochemical characterization of groundwater in bhokar taluka of Nanded district, Maharashtra, India. In: *Proceeding of Environmental Science and technology*, Vol. 1, pp. 32–38. American Science Press, USA (2016)
- Perel'man, A.I.: *Geochemistry of elements in the supergene zone*, p. 266. Keter Publishing House, Jerusalem Ltd. (1977)
- Sorg, T.J.: Treatment technology to meet the interim primary drinking water regulations for inorganics. *J. Am. Water Work. Assoc.* **70**(2), 105–111 (1978)
- Totsche, K.U., Wilcke, W., Korbus, M., Kobza, J., Zech, W.: Evaluation of fluoride-induced metal mobilization in soil columns. *J. Environ. Qual.* **29**, 454–459 (2000)
- WHO (World Health Organization): *Guidelines for drinking water quality, health criteria and other supporting information*, Vol. 2, 2nd edn. WHO, Geneva (1997)
- WHO (World Health Organization): *Guidelines for drinking water quality, recommendations*, Vol. 1, P. 130, 2nd edn. Geneva (1993)



Signatures of Dryas Groundwater in Stratified Aquifers of Kuwait-Paleoclimatic Significance

Chidambaram Sabarathinam and Tariq Rashid

Abstract

Kuwait group Aquifers (KGA) and Dammam formation (DFm) are the two major aquifers from which groundwater is being extracted in Kuwait. KGA is chiefly sandy, calcareous, and gypsiferous, and the DFm is predominantly of Limestone. Twenty-two groundwater samples were collected from KGA and 17 from DFm; the age of these samples vary from 32 Ka to 636 years. The younger samples were predominantly distributed along the coast. Groundwater samples collected showed representations of Dryas (14–10 Ka). This was reflected by the fluctuations in $\delta^{18}\text{O}$ and d -excess values responding to the varying climatic conditions. Progressive enrichment of isotope values was observed from Pleistocene to the recent/Holocene samples. The oldest groundwater of Dammam formation (32–12 Ka) does not play a significant role in the groundwater chemistry of this aquifer. It was inferred that the groundwater samples of warmer periods have higher ionic strength.

Keywords

Paleowater • D-excess • Stable isotope • Geochemistry

1 Introduction

Dryas period in the geological time scale has been studied by different authors to interpret the climatic variation with ice cores (Fairbanks 1989), sediment (Starkel et al. 1996), and biota (Carlson et al. 2007). Dryas is subdivided into oldest (14–13.2 Ka), older (12.2–11.8 Ka), and younger (10.8–10 Ka) (Pirrus and Raukas 1996). Studies on the radiometric dates of groundwater and the stable isotope

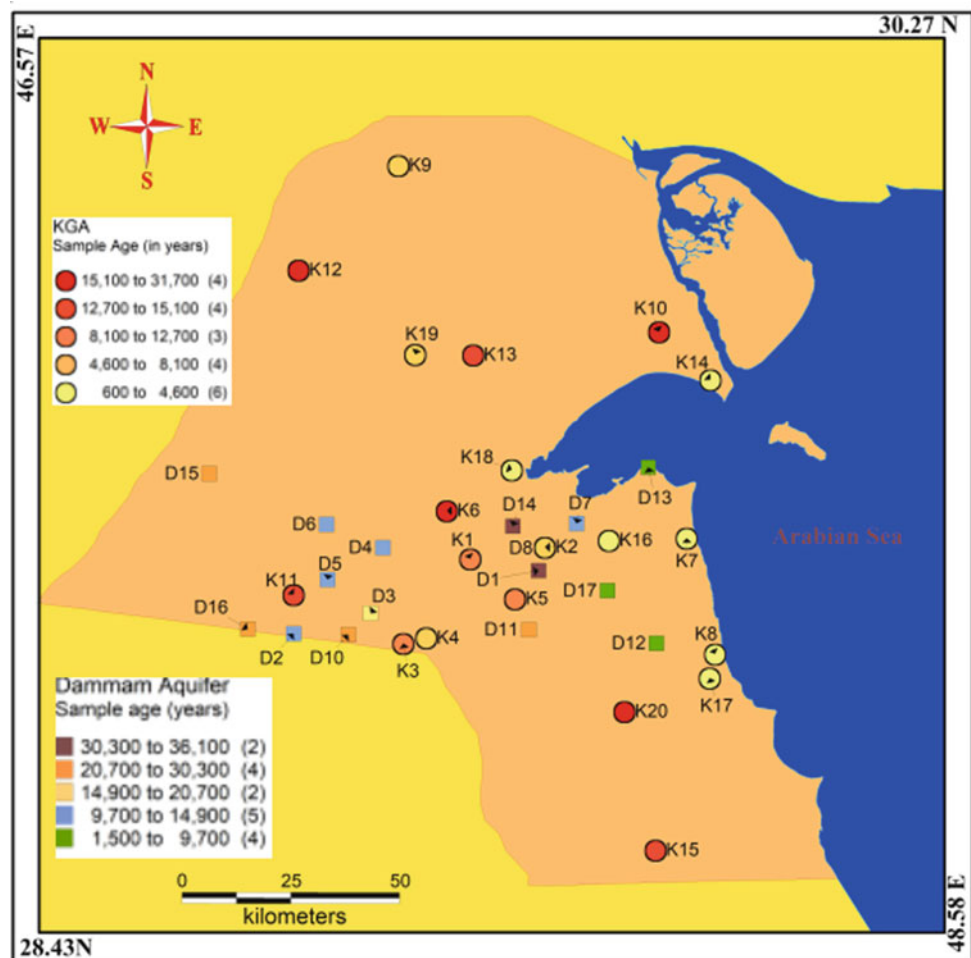
signature had acted as one of the paleoclimate proxies. Since the $\delta^{18}\text{O}$ and δD help to identify the environment of recharge, d -excess the extent of evaporation, and ^{14}C the age of the water, isotopes were used as paleoclimate proxies (Li et al. 2015). This study focuses on, the identification of the Dryas and other paleowaters, its relationship to paleoclimate and their geochemical signatures.

2 Study Area and Methodology

The selected locations fall within $28^{\circ} 32' 11.590''$ – $29^{\circ} 45' 18.493''$ N, and $47^{\circ} 40' 8.47''$ – $48^{\circ} 44' 5.584''$ E (Fig. 1). The Kuwait group of Aquifers (KGA) represented by Dibdibba and Ghar, followed by Dammam Formation (DFm) of the Hasa Group are the two potential aquifers of the region. The KGA has two aquifers, namely the northern Dibdibba formations and the central and southern Ghar formations. The KGA is saturated along the shoreline KGA is saturated along the shore and dry in the southwest part and near the Ahmadi ridge. The water level in the aquifer of the KGA ranges from about 90 m above sea level along the southwest and almost equal to the sea level along the coast. Dammam Formation's thickness ranges from approximately 150 m, in the southwest, to approximately 280 m in the northeast. The piezometric distribution in the Dammam Formation ranges from about 90 m north to a few meters above the sea level (Abusada 1988). The KGA and DFm aquifers are interconnected in many places. Groundwater samples were collected from both aquifers based on the spatial availability of operating wells, 22 from KGA and 17 from DFm (Fig. 1) during January 2019. They were collected from the monitoring wells through a submersible pump. The collected samples were filtered and analyzed for, electrical conductivity (EC) and pH, total dissolved solids (TDSs) by evaporation method, major cations, and anions using ion chromatograph. The samples were analyzed for stable isotopes of oxygen and hydrogen using laser spectroscopic

C. Sabarathinam (✉) · T. Rashid
WRC, Kuwait Institute for Scientific Research, Safat, Kuwait
e-mail: csabarathinam@kisir.edu.kw

Fig. 1 The distribution of sample locations and spatial variation of groundwater ages



analyzer with a precision ($\pm 0.3\%$ for $\delta^{18}\text{O}$, $\pm 3.0\%$ for $\delta^2\text{H}$). Stable carbon isotope was measured using isotope ratio mass spectrometer, and ^{14}C content was determined by accelerated mass spectrometry (AMS) with a precision of 3%. Samples were analyzed for $\delta^{18}\text{O}$, δD , $\delta^{13}\text{C}$, and ^{14}C in IAEA and BioFocus lab, Germany. ^{14}C age corrections were made by using the Pearson and Hanshaw (1970) method.

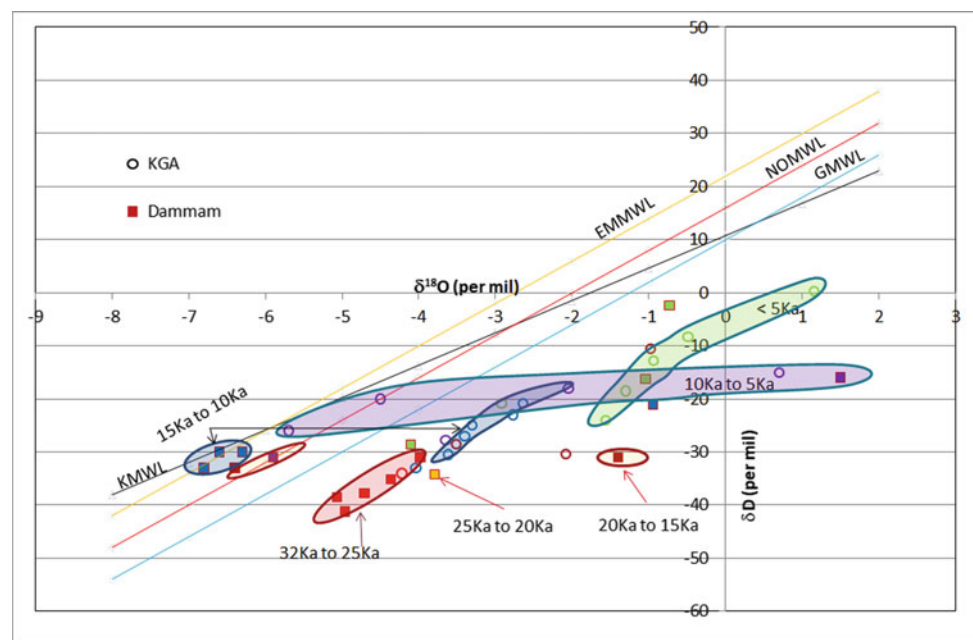
3 Results and Discussion

The mean value of $\delta^{18}\text{O}$ in DFm was -3.85% (ranged from -6.8 to 1.5%), and that of KGA is -2.46% (ranged from -5.7 to 1.16%). On average, the groundwater of DFm (ranged from 1.5 to 36 Ka) was older than KGA (ranged from 636 to 31Ka) (Table 1). The spatial variation of the samples with respect to age (Fig. 1) showed that the younger groundwater falls along the coast, irrespective of the formation. The older groundwater of KGA is represented diagonally along NW to SE of the study area, but in DFm, it is represented in the central and western margin of the country. The $\delta^{18}\text{O}$ and δD values of the samples were compared with Eastern

Mediterranean Meteoric Water Line (EMMWL) (Gat et al. 2003), North Oman Meteoric Water Line (NOMWL) (Gat and Carmi 1970), Kuwait Meteoric Water Line (KMWL) (Hadi et al. 2016) and Global Meteoric Water Line (GMWL) (Craig 1961) (Fig. 2). Few water samples of Dammam Formation representing Dryas period were observed to fall along the EMMWL and near to KMWL. Samples of 10–5 Ka collected from Dammam Formation are also observed to fall parallel to NOMWL. It is inferred that the groundwater representing Dryas of Dammam formation were depleted, while that of KGA were enriched and plot parallel to GMWL. Figure 2 also shows that there has been a subsequent enrichment of stable isotopes since 36 Ka. There is a wide variation of $\delta^{18}\text{O}$ values in the samples of 10–5 Ka indicating vast variations in climate, as this period is represented by the 8.2 Ka cooling event. The *d-excess* values were studied to infer the variation of *d-excess* with age. This parameter has a significance with respect to climate and to determine the source of precipitation as it reflects the fractionation and, thus, evaporation and humidity conditions during the time of recharge (Bhattacharya et al. 2003; Hadi et al. 2016). Variations in *d-excess* are predominantly noted

Table 1 Summary of the geochemical analysis of the groundwater samples collected in both the aquifers

	KGA (<i>n</i> = 22)				Dammam (<i>n</i> = 17)			
	Min	Max	Avg	Std Dev	Min	Max	Avg	Std Dev
$\delta^{18}\text{O}$ (‰)	-5.70	1.16	-2.47	1.73	-6.80	1.50	-3.86	2.47
$\delta^2\text{H}$ (‰)	-34.06	0.27	-21.61	8.71	-41.26	-2.37	-28.84	9.79
<i>d-excess</i>	-20.60	19.60	-2.03	8.96	-28.00	22.80	1.58	15.16
^{14}C (‰)	2.17	75.00	31.42	23.01	1.28	83.40	19.44	24.94
^{13}C (‰)	-13.60	10.15	-8.61	4.84	-19.05	-3.95	-9.30	3.38
Age (years)	636.00	31,675.46	10,095.85	7021.28	1500.99	36,010.70	17,189.16	10,464.25
Temp (°C)	27.30	30.20	28.95	0.79	28.40	34.00	31.40	1.81
pH	6.82	8.06	7.34	0.32	6.49	7.70	7.31	0.26
EC ($\mu\text{S}/\text{cm}$)	4720.00	92,000.00	14,423.24	18,636.51	3200.00	49,300.00	7457.65	10,981.21
TDS (mg/L)	2870.00	74,914.00	10,493.24	15,341.84	2570.00	33,077.00	5248.06	7229.91
Ca (mg/L)	200.00	1855.00	681.05	348.60	260.00	2080.00	499.25	424.02
Mg (mg/L)	38.30	2547.00	286.50	524.90	92.80	745.00	180.73	154.19
Na (mg/L)	568.00	22,856.00	2666.19	4824.06	327.00	9116.00	1057.35	2081.90
K (mg/L)	9.80	515.00	65.76	109.78	8.20	267.00	31.49	60.86
SO_4 (mg/L)	609.60	6097.30	1955.63	1222.11	870.00	2435.80	1338.71	430.55
Cl (mg/L)	6.80	44,121.00	4637.43	9296.11	351.50	20,359.00	1927.66	4764.31
HCO_3 (mg/L)	38.30	170.00	98.58	34.46	21.20	173.00	112.78	37.02
NO_3 (mg/L)	0.00	329.00	59.02	69.87	0.88	88.00	17.64	22.75
SiO_2 (mg/L)	16.00	170.00	55.76	37.12	5.60	21.30	13.07	4.27

Fig. 2 Relationship between stable isotopes of oxygen and hydrogen. A comparison of these samples with different Meteoric water lines and groundwater ages

in the DFm than KGA. The *d-excess* variations (Fig. 3) in the DFm, during 14–10 Ka, correspond to the Dryas period (glacial conditions). The influence of Early Dryas is noted in the DFm and not in KGA. Subsequent climatic variations

after 10 Ka are recorded more in KGA. The ionic strength of the samples were correlated with the age (Fig. 4), and it was inferred that there are no major variations except for periods of glaciation (Siegel 1989). There is an increase of

Fig. 3 Variation of *d-excess* with respect to the ages, indicating the influence of climate

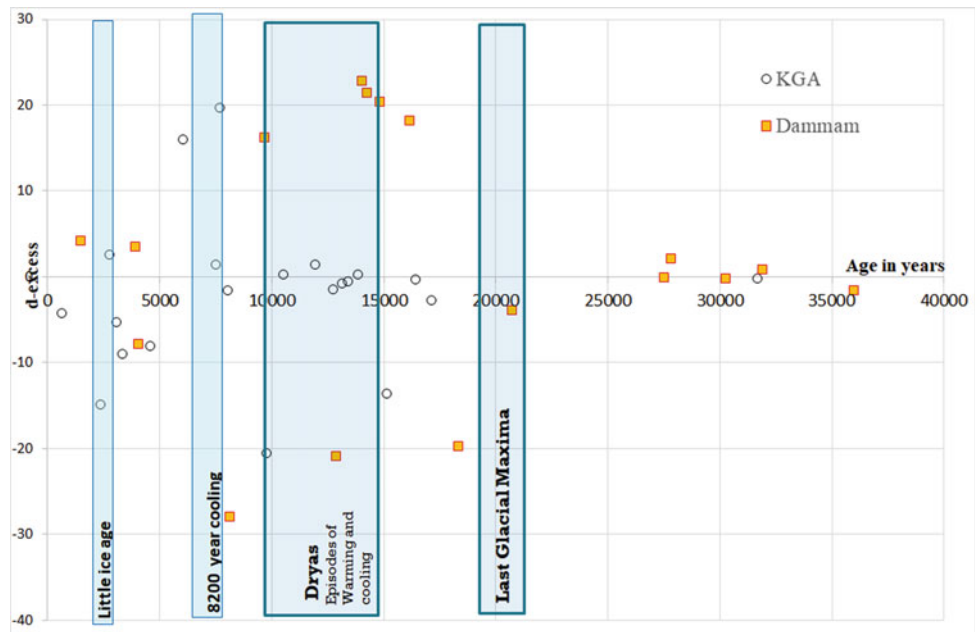
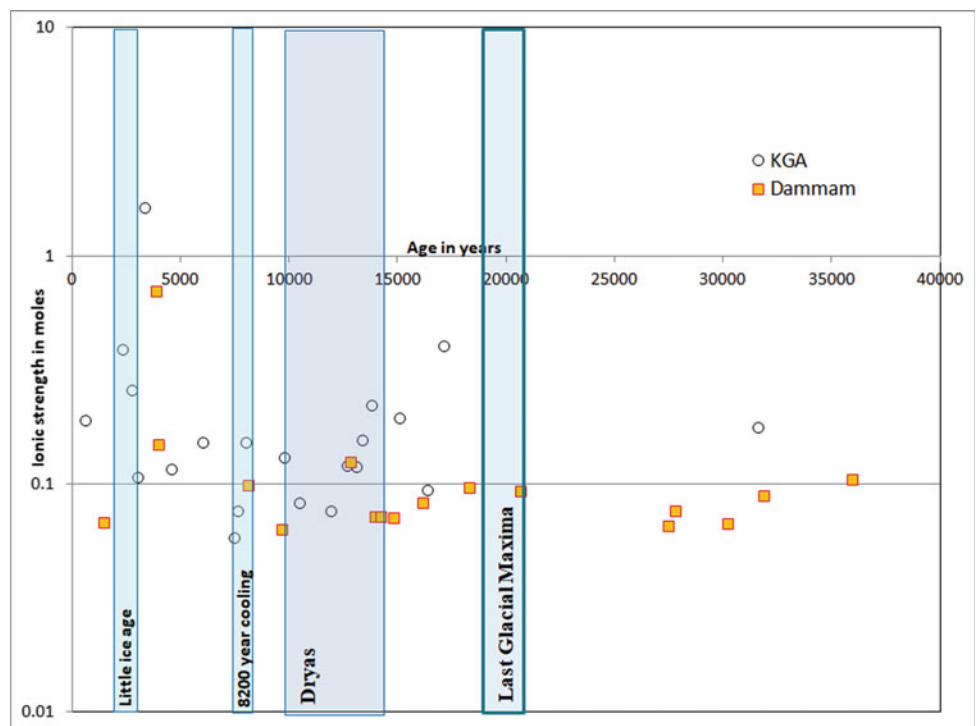


Fig. 4 Fluctuations of ionic strength in the groundwater samples with respect to the age



ionic strength in groundwater after the glaciation period, and it is more predominant in the KGA which lies above the DFm. The correlation analysis, principal component analysis, and factor score analysis were carried out for the geochemical data of both KGA and DFm. The statistical analysis of the chemical data shows no significant geochemical process during the Oldest Dryas in DFm.

4 Conclusions

The groundwater samples were observed to range in age from Pleistocene to recent Holocene irrespective of the formations considered for the study. The older groundwater was observed along the central and western margin of the

study area. Progressive enrichment of stable isotopes in the samples were noted from Pleistocene to recent years. The climatic changes were reflected in the *d-excess* values predominantly in DFm. The post glaciation periods were inferred to be geochemically significant. Samples representing the oldest Dryas were observed in the DFm, and no major process contributed to the geochemistry of groundwater during this period.

References

- Abusada, S.M.: The essentials of groundwater resources of Kuwait. Kuwait Institute for Scientific Research, Report No. KISR, p. 2665 (1988)
- Bhattacharya, S.K., Froehlich, K., Aggarwal, P.K., Kulkarni, K.M.: Isotopic variation in Indian monsoon precipitation: records from Bombay and New Delhi. *Geophys. Res. Lett.* **30**(24) (2003)
- Carlson, A.E., Clark, P.U., Haley, B.A., et al.: Geochemical proxies of North American freshwater routing during the Younger Dryas cold event. *Proc. Natl. Acad. Sci.* **104**, 6556–6561 (2007). <https://doi.org/10.1073/pnas.0611313104>
- Craig, H.: Isotopic variations in Meteoric waters. *Science* **133**, 1702–1703 (1961). <https://doi.org/10.1126/science.133.3465.1702>
- Fairbanks, R.G.: A 17,000-year glacio-eustatic sea level record: influence of glacial melting rates on the Younger Dryas event and deep-ocean circulation. *Nature* **342**, 637–642 (1989). <https://doi.org/10.1038/342637a0>
- Gat, J.R., Carmi, I.: Evolution of the isotopic composition of atmospheric waters in the Mediterranean Sea area. *J. Geophys. Res.* **75**, 3039–3048 (1970). <https://doi.org/10.1029/jc075i015p03039>
- Gat, J.R., Klein, B., Kushnir, Y., et al.: Isotope composition of air moisture over the Mediterranean Sea: an index of the air-sea interaction pattern. *Tellus B* **55**, 953–965 (2003). <https://doi.org/10.1034/j.1600-0889.2003.00081.x>
- Hadi, K., Kumar, U.S., Al-Senafy, M., Bhandary, H.: Environmental isotope systematics of the groundwater system of southern Kuwait. *Environ. Earth Sci.* (2016). <https://doi.org/10.1007/s12665-016-5886-9>
- Li, J., Pang, Z., Froehlich, K., Huang, T., Kong, Y., Song, W., Yun, H.: Paleo-environment from isotopes and hydrochemistry of groundwater in East Junggar Basin, Northwest China. *J. Hydrol.* **529**, 650–661 (2015)
- Pearson, F.J., Hanshaw, B.B.: Sources of dissolved carbonate species in groundwater and their effects on carbon-14 dating. In: *Isotope Hydrology 1970*. IAEA, Vienna, pp. 271–286 (1970)
- Pirrus, R., Raukas, A.: Late-Glacial stratigraphy in Estonia. In: *Proceedings of the Estonian Academy of Sciences*. *Geology* **45**, 34–45 (1996)
- Siegel, D.I.: *Geochemistry of the Cambrian-Ordovician aquifer system in the northern Midwest, United States*. United States Government Printing Office, Washington (1989)
- Starkel, L., Pazdur, A., Pazdur, M.F., et al.: Lake-level and groundwater-level changes in the Lake Gosciąg area, Poland: palaeoclimatic implications. *The Holocene* **6**, 213–224 (1996). <https://doi.org/10.1177/095968369600600207>



The Role of Hydraulic Turnover Time in the Assessment of Water Quality in Portuguese Aquifer Systems

Lisa Martins¹, Alcino Oliveira¹, Luís Sanches Fernandes¹, and Fernando Pacheco¹

Abstract

In general, this study was developed to assess the hydraulic turnover time in several representative watersheds of the Portuguese territory using a low-cost innovative method. This method combines the average streamflows, flow regimes, and shows to be effective when applied in water quality management. The results may hold back the fulfillment of sustainable development goals related to water and sanitation until 2030 and, hence, deserve reflection by water planners and policy-makers to ensure a better water quality for human consumption. The validation exercise provided further evidence that this innovative method functions as a suitable tool for predicting and safeguarding water quality. Furthermore, the application of this innovative method is the keystone of groundwater quality protection in the watersheds of the Portuguese territory.

Keywords

Groundwater quality • Flux velocity • Hydraulic conductivity • Travel time

1 Introduction

The storage and transport of groundwater in the Earth's crust is crucial for geohazards planning. By 2030, the sustainable development goals are to achieve equitable access to safe drinking water, improve the water quality by reducing pollution from anthropogenic sources, and minimize the release of hazardous nitrates. Knowledge of how the groundwater transport in aquifer systems works can facilitate the application of accurate models, which, in turn, may lead to a new strategic tool for water resources planning. At a time of disinvestment in Portugal, and with increasingly expensive isotopic methods to obtain the hydraulic turnover time, it is essential to apply other efficient and low-cost innovative methods that promote efficient management of the water resources quality. This innovative method can unleash a strategic approach in water resources protection, contributing to an overview of larger-scale hydraulic turnover time, covering the Portuguese aquifer systems. The development of studies on hydraulic turnover time is critical for policy-makers to ensure the qualitative status of aquifers and sustainable groundwater management (Pacheco 2015; Pacheco et al. 2018). The main purpose of this study is to understand the relationship between hydraulic turnover time and the nitrate concentration in representative watersheds of the Portuguese territory. For future perspective, it is crucial to ascertain when effective nitrate decontamination will occur in aquifer systems, eliminating the pollution source, following the sustainable development goals. This goal 6 of Agenda 2030 alert for time limits, which in the case of travel time in groundwater, may still be within the pre-established deadline. It is, therefore, essential to comprehend if it is possible to fulfill this goal of water security to ensure better-integrated water resources management.

L. Martins (✉) · L. S. Fernandes
Center for Research and Technology of Agro-Environment and Biological Science, University of Trás-os-Montes e Alto Douro, 5001-801 Vila Real, Portugal
e-mail: lmartins@utad.pt

A. Oliveira
Geosciences Center, University of Coimbra, University of Trás-os-Montes e Alto Douro, 5001-801 Vila Real, Portugal

F. Pacheco
Chemistry Research Center, University of Trás-os-Montes e Alto Douro, 5001-801 Vila Real, Portugal

2 Materials and Methods

To understand the importance of hydraulic turnover time in water quality assessment and management, eleven hydrogeological basins were strategically studied (Fig. 1a).

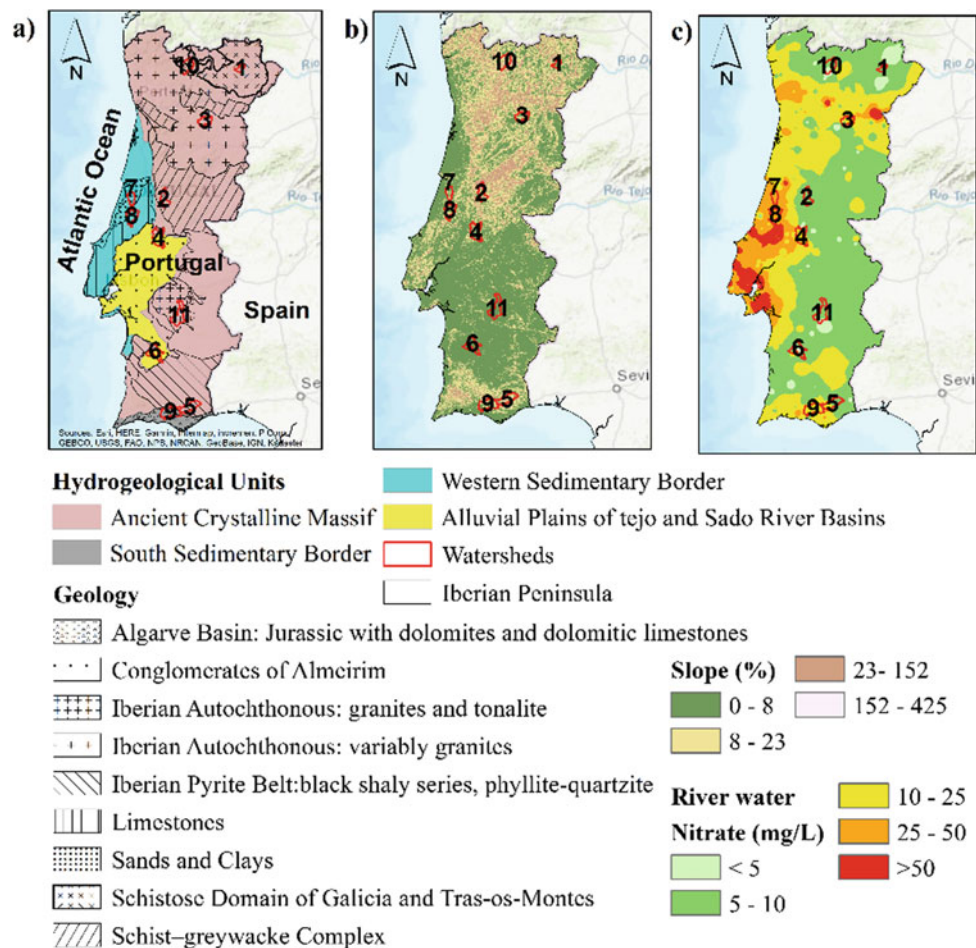
Despite being a small country, Portugal presents, in all its extension, varied lithologies from granites, schists, limestones, sands, clays, conglomerates, etc. (Fig. 1b). The slope for the entire country contrasts with a topography composed essentially by lowlands and craggy reliefs (Fig. 1c). In an aquifer system, the hydraulic turnover time is the travel time of water from the point of recharge to the catchment point, being conditioned by the permeability of geological formations and climatic conditions (recharge) (Kendall and McDonnell 1998). Groundwater turnover time was estimated using a simplified expression, solely dependent on average stream flows and flow regimes (Pacheco 2015):

$$t = \frac{1.98}{Q \sqrt{a_1 a_3}} \quad (1)$$

The Q (m^3/s) is the streamflow discharge rate, and the a_1 a_3 values are retrieved from a scatter plot $\ln(\Delta Q/\Delta t)$ versus $\ln(Q)$. Using the Brutsaert method (Brutsaert and Nieber 1977), the lower envelope of the scatter points is represented by two straight lines, one with a slope $b = 1$, and the other with a slope $b = 3$. The y-values where these lines intercept $\ln(Q) = 0$ are the parameters a_1 and a_3 . To validate the model, it is important to understand the relationship between flux velocity (v) and the hydraulic turnover time. For this, Darcy's Law was used to calculate the flow velocity, being obtained through the product of the hydraulic conductivity (K , m/s) and the hydraulic gradient (i) represented by the slope. It should be noted that the vast majority of hydraulic conductivity data were obtained from Domenico and Schwartz (1990). However, for basin No. 7, the hydraulic conductivity data were taken from Almeida et al. (2000).

$$v = Ki \quad (2)$$

Fig. 1 Hydrogeological, topography, and nitrate contamination represented in the studied region: **a** hydrogeological units adapted from Pacheco and Sanches Fernandes (2016); **b** hillside slopes obtained from the analysis of a digital elevation model (DEM) (Ministério do Ambiente e Transição Energética Direcção Geral do Território); **c** maximum nitrate concentrations in river waters. In **c** the plotted concentrations was adapted from (Nacional and de Informação de Recursos Hídricos). The classification of the IDs was depicted in Table 1



3 Results

In general, the results of calculated hydraulic turnover time by a new formula using the Brutsaert method are depicted in Fig. 2a, and Table 1. These results show quite variable values of transport time ($t = 6.78\text{--}52.98$ yr).

At the regional level of rocks outcropping with greater cartographic representation, the hydraulic conductivity presents some disparities ($K = 7.005\text{E-}09$ to 0.02615 m/s), mainly due to the wide range of current igneous, sedimentary, and metamorphic lithologies. The nitrate concentrations for the several studied watersheds vary from 6.83 to 49.37 mg/L. The validation of this new hydraulic turnover time method is portrayed in Fig. 2b, showing an inverse relationship between flow velocity and turnover time, and a significant coefficient of determination ($R^2 = 0.47$).

4 Discussion

The nitrate concentrations in the studied watersheds fulfill the Nitrates Directive (2006/118/EC) threshold considered to be acceptable for drinking water, which is 50 mg/L. However, it is worth recalling that the US Environmental Protection Agency (EPA) determines a maximum contaminant level for nitrates to protect against the blue-baby syndrome of 10 mg/L (EPA 2019). In seven watersheds with maximum values of nitrates above 10 mg/L (Max. = 11.50–49.37 mg/L), four of them present higher hydraulic turnover times ($t = 12.97$ to 26.55 yr), making it impossible to fulfill the clean water of sustainable development goals within the pre-established deadline (2030), eliminating the cause. It should also be noted that in this work, we are only assuming a transport flow without any chemical debugging or denitrification

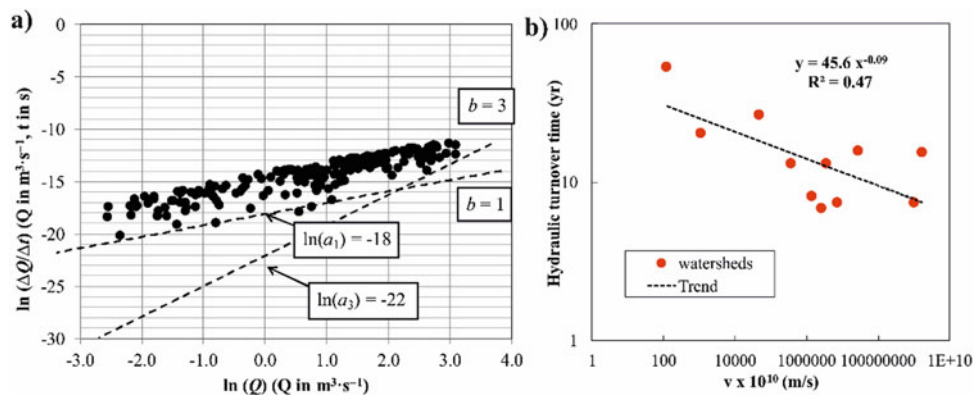


Fig. 2 Application of the Brutsaert method in the calculated hydraulic turnover time and the validation method using the flux velocity of Darcy’s Law: **a** Brutsaert method diagram of watershed No. 3; **b** validation with hydraulic turnover time versus flux velocity

Table 1 Geology, drainage area, flow discharge (Q), hydraulic turnover time (t), hydraulic conductivity (K), slope, flux velocity (v), and maximum values of nitrates for each watershed

ID	Geology	Drained area (km ²)	Q (m ³ /s)	t (yr)	K (m/s)	Slope (%)	$v \times 10^{10}$ (m/s)	NO ³ (Max.; mg/L)
1	SQ	189.60	2.58	52.98	1E-09	12.63	126.31	6.91
2	T	185.41	45.76	8.11	1E-05	14.39	1,439,071.95	9.30
3	TM, BG	185.00	4.49	6.78	2.765E-05	9.39	2,596,335.00	21.99
4	CG	322.43	294.38	15.36	0.02615	6.53	1,707,595,000.00	40.24
5	SSG	284.29	3.19	20.20	7.005E-09	16.25	1138.31	15.36
6	SPC	261.81	6.60	26.55	3E-06	1.63	48,902.45	11.50
7	SCL	247.14	1.96	7.36	0.000112	6.49	7,269,265.23	38.70
8	LM	238.62	2.51	7.35	0.0100005	10.18	1,018,050,900.00	49.37
9	DDL	324.59	1.11	12.97	3.001E-06	12.21	366,361.05	19.65
10	GPS	259.57	8.72	15.66	0.00015	18.98	28,470,759.20	9.41
11	BGT	328.04	2.34	13.04	0.00015	2.35	3,525,094.00	6.83

SQ schists and quartzites, T turbidites; TM, BG two mica and biotite granites, CG conglomerates, SSG shale, siltstones, and greywackes, SPC sand, pelitic rocks and conglomerates, CL sands and clays, LM limestones, DDL dolomites, and dolomitic limestones, GPS granites and parautochthonous schists, BGT biotite granites, granodiorites, and tonalites. Q discharge rate, t hydraulic turnover time, K hydraulic conductivity, v flux velocity, Max. maximum

phenomenon. These purifying phenomena, by reducing nitrates, may lead to levels below the threshold imposed earlier than expected. On the other hand, the flow velocity validated this new method for calculating the hydraulic turnover time, because it helps to determine the relationship between them. When calculated by this original method, this time of contaminant transport must be inversely proportional to the flow velocity, and this inverse relationship exists ($R^2 = 0.47$, Fig. 2b). However, this coefficient of determination could be higher if we used local hydraulic conductivity data. Nonetheless, if there is a relationship, slower flows will be associated with longer hydraulic turnover time, so they will be more difficult to decontaminate the aquifer system. It is also recognized that geology and topography control the circulation of groundwater.

5 Conclusions

The nitrate concentrations fulfill the Nitrates Directive (2006/118/EC) threshold for drinking water (50 mg/L) but exceed in seven watersheds, as US EPA limits to protect against blue-baby syndrome (10 mg/L). In these particular cases, it is impossible to fulfill the sustainable development goal within the pre-established term. In the limit, accepting that nitrates do not undergo through a process of denitrification, among other chemical purifying phenomena, it can be assumed in the first analysis of water quality that in watersheds with low hydraulic turnover time, the decontamination will be useful, eliminating the source. In the short term, the implementation of this low-cost and innovative hydraulic turnover time method guarantees greater efficiency in the management of water quality.

Acknowledgements This research was sponsored by the INTERACT project, “Integrated Research in Environment, Agro-Chain and

Technology,” no. NORTE-01- 0145-FEDER-000017, in its line of research entitled BEST, cofinanced by the European Regional Development Fund (ERDF) through NORTE 2020 (North Regional Operational Program 2014/2020). The authors are integrated into CITAB research center, financed by the FEDER/COMPETE/POCI—Operational Competitiveness and Internationalization Program, under Project POCI-01-0145-FEDER-006958, and National Funds of FCT—Portuguese Foundation for Science and Technology, through the project UID/AGR/04033/2021. For the author integrated into the CQVR, the research was additionally supported by National Funds of FCT—Portuguese Foundation for Science and Technology, under the project UID/QUI/00616/2021.

References

- Almeida, C., Mendonça, J.J.L., Jesus, M.R., Gomes, A.J.: *Sistemas Aquíferos de Portugal Continental*. Water Institute, Portugal (2000)
- Brutsaert, W., Nieber, J.L.: Regionalized drought flow hydrographs from a mature glaciated plateau. *Water Resour. Res.* **13**, 637–643 (1977)
- Domenico, P.A., Schwartz, F.W.: *Physical and chemical hydrology*. Wiley, New York (1990)
- EPA Homepage, US Environmental Protection Agency, <https://www.epa.gov/nutrientpolicy-data>. Last Accessed 06 May 2019
- Kendall, C., McDonnell, J.J.: *Isotope tracers in catchment hydrology* (1998). ISBN 044450155X
- Ministério do Ambiente e Transição Energética Direcção Geral do Território Available online: www.dgterritorio.gov.pt. Accessed on 12 May 2019
- Pacheco, F.A.L.: Regional groundwater flow in hard rocks. *Sci. Total Environ.* **506–507**, 182–195 (2015)
- Pacheco, F.A.L., Sanches Fernandes, L.F.: Environmental land use conflicts in catchments: a major cause of amplified nitrate in river water. *Sci. Total Environ.* **548–549**, 173–188 (2016)
- Pacheco, F.A.L., Martins, L.M.O., Quininha, M., Oliveira, A.S., Sanches Fernandes, L.F.: Modification to the DRASTIC framework to assess groundwater contaminant risk in rural mountainous catchments. *J. Hydrol.* **566**, 175–191 (2018)
- Sistema Nacional de Informação de Recursos Hídricos <http://snirh.apambiente.pt/>



Hydrogeological and Hydrochemical Characterization of Mejel Bel Abbas Aquifer (West-Central Tunisia)

Mouez Gouasmia, Abdelkader Mhamdi, Ferid Dhahri, and Mohamed Soussi

Abstract

The Mejel Bel Abbas region (west-central Tunisia) constitutes a subsiding lowland filled with Plio-Quaternary deposits. These deposits contain shallow aquifer exploited for agricultural and drinking water purposes. A good management of these groundwater resources requires recognizing their hydrodynamics and their chemical processes. The piezometric map shows that groundwater flows from north to south toward the Gafsa North plain. The piezometric profile demonstrates that the piezometric level is related to the topography of the terrain. Miocene sands and Plio-Quaternary aquifers form together a single free hydrogeological unit. Chemical analyses revealed that groundwater within this hydrogeological unit is rich in sulphates and chlorides. The total mineralization of analysed samples highlights a good chemical quality that remains almost uniform over the entire Mejel Bel Abbas region. The Plio-Quaternary aquifer, however, yields groundwater supersaturated with carbonate minerals and saturated with halite and gypsum.

Keywords

Hydrogeology • Hydrochemistry • Aquifer • Mejel Bel Abbas

M. Gouasmia (✉) · A. Mhamdi · F. Dhahri
Faculty of Sciences of Gafsa, University of Gafsa,
Sidi Ahmed Zarroug, 2112 Gafsa, Tunisia

M. Gouasmia · A. Mhamdi · M. Soussi
Faculty of Sciences of Tunis, LB18ES07: Sedimentary Basins and
Petroleum Geology, University of Tunis El Manar, El Manar II,
2092 Tunis, Tunisia

F. Dhahri
Faculty of Sciences of Tunis, Laboratory 3G (Geodynamics,
Geo-Digital and Geomaterials), University of Tunis El Manar,
El Manar II, 2092 Tunis, Tunisia

1 Introduction

The region of Mejel Bel Abbas, located in west-central Tunisia, is characterized by a semi-arid climate and an annual rainfall of 200 mm. This context, which is characterized by the great spatial and temporal variability of its water potential, makes Mejel Bel Abbas (Fig. 1) a region with relatively variable and limited renewable water resources, which requires a better evaluation of the aquifer's potential.

The most important aquifer in this region is the Plio-Quaternary, whose water resources are intensively exploited. The second, the aquifer of Miocene sandstone, which is characterized by a high porosity and a very large thickness, is operated only by a single borehole.

In order to better recognize these hydrogeological potentialities, a hydrogeochemical study was carried out in the region to identify the hydrodynamism of the Plio-Quaternary aquifer as well as the chemical characteristics of these waters.

2 Materials and Methods

The piezometric data used in this study were obtained from the measurements of 12 available monitoring wells in 2016, using a manual piezometric probe. Water samples were collected from nine wells abstracting the Plio-Quaternary and Miocene aquifers. The laboratory of the Regional Commissariat for Agricultural Development of Kasserine performed the analyses of anions and cations using a Dionex ion chromatography system. The results of the content assessments of major elements within groundwater samples are used to draw a Piper diagram and some correlation plots between major elements. These have been used to investigate the hydrochemical properties of this aquifer and the origin of its mineralization (Shouakar-Stash et al. 2007).

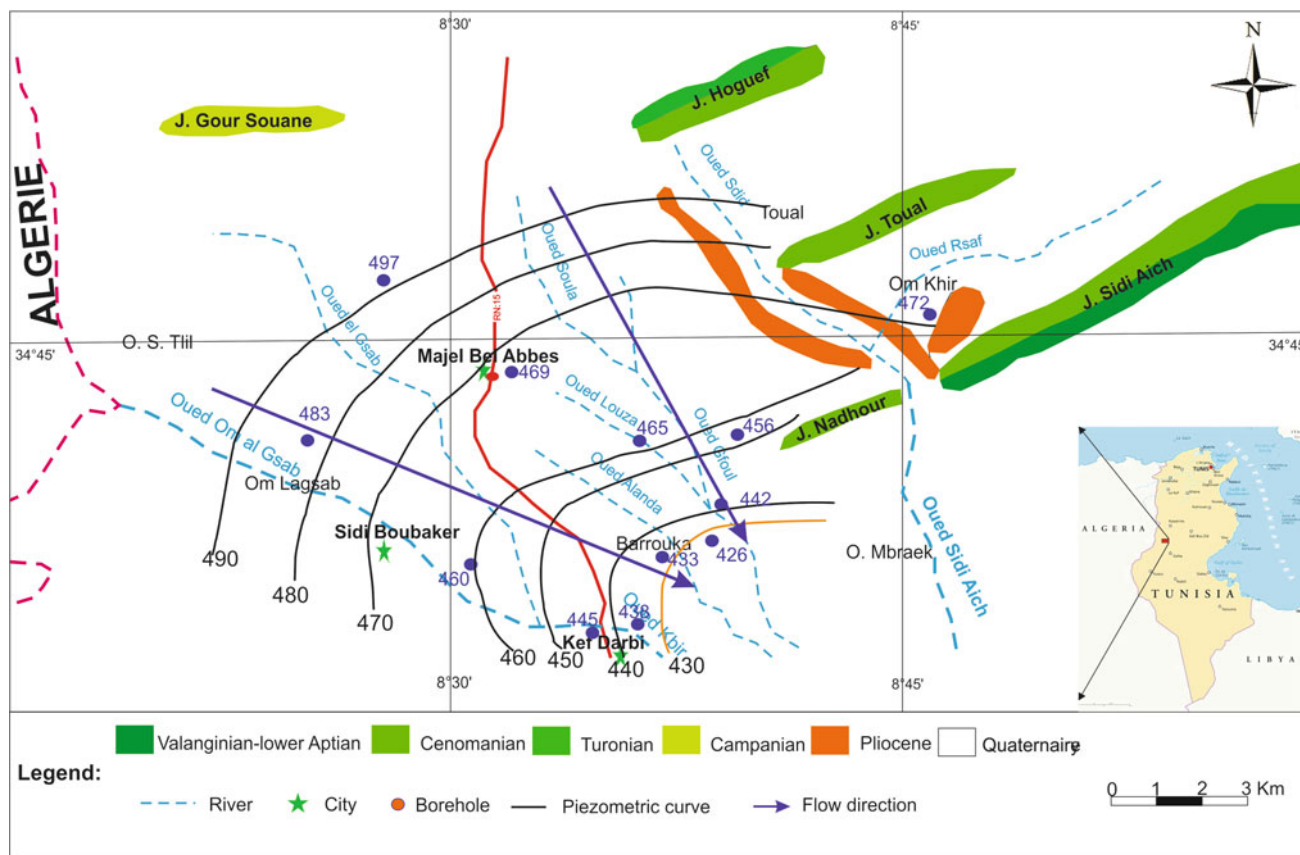


Fig. 1 Piezometric contour map and groundwater flow (2016)

3 Results and Discussion

3.1 Hydrodynamics of the Plio-Quaternary Aquifer

The piezometric map established in 2016 (Fig. 1) shows a general flow from *N* to *S* with a spill of water from the basin of Mejel Bel Abbas to the North Gafsa basin. The depression profile drawn from the piezometric map, from Mejel Bel Abbas to the plain of North Gafsa, shows that the piezometric altitude is related to the surface topography. The thickness of the unsaturated zone reaches its maximum at Mejel Bel Abbas (140 m) and gradually decreases to 50 m upstream of the plain of North Gafsa. It appears that the underground flow coming from the basin of Mejel Bel Abbas has for outlet the region of the threshold of North Gafsa.

In the south, the piezometric curves are tightening and showing a relatively stronger hydraulic gradient, drawing a hydraulic slope more inclined towards the south, then varying laterally. This variation is explained by the fact that the Plio-Quaternary filling captured is entirely in the form of a free aquifer.

3.2 Hydrochemistry

The salinity values of the Mejel Bel Abbas range from 0.83 to 0.97 g L⁻¹. These values are obtained indirectly from measured conductivity. The plotted Piper diagram (Simler 2000) shows that the water stored within the Plio-Quaternary aquifer have SO₄-Cl facies (Fig. 2). The graphical representation of the hydrochemical analyses of the Schoeler Berkaloff diagram (Fig. 2) shows more or less parallel curves. The variations observed reflect the changes in the lithological nature and local environmental conditions, as well as geochemical leaching processes and dissolutions that contribute to the change in the local water composition. The majority of water samples from the Mejel Bel Abbas aquifer system have a good hydrochemical quality and indicate that the origin of the water is the same.

Determining the mechanism of salinization of aquifer waters involves determining the origin of each chemical element according to its behaviour with respect to salinity and other elements.

With the exception of Ca and SO₄, all the curves have a good correlation between the major elements and the sums of the anions and cations. Indeed, they show their contribution to the acquisition of the salt load of water from the

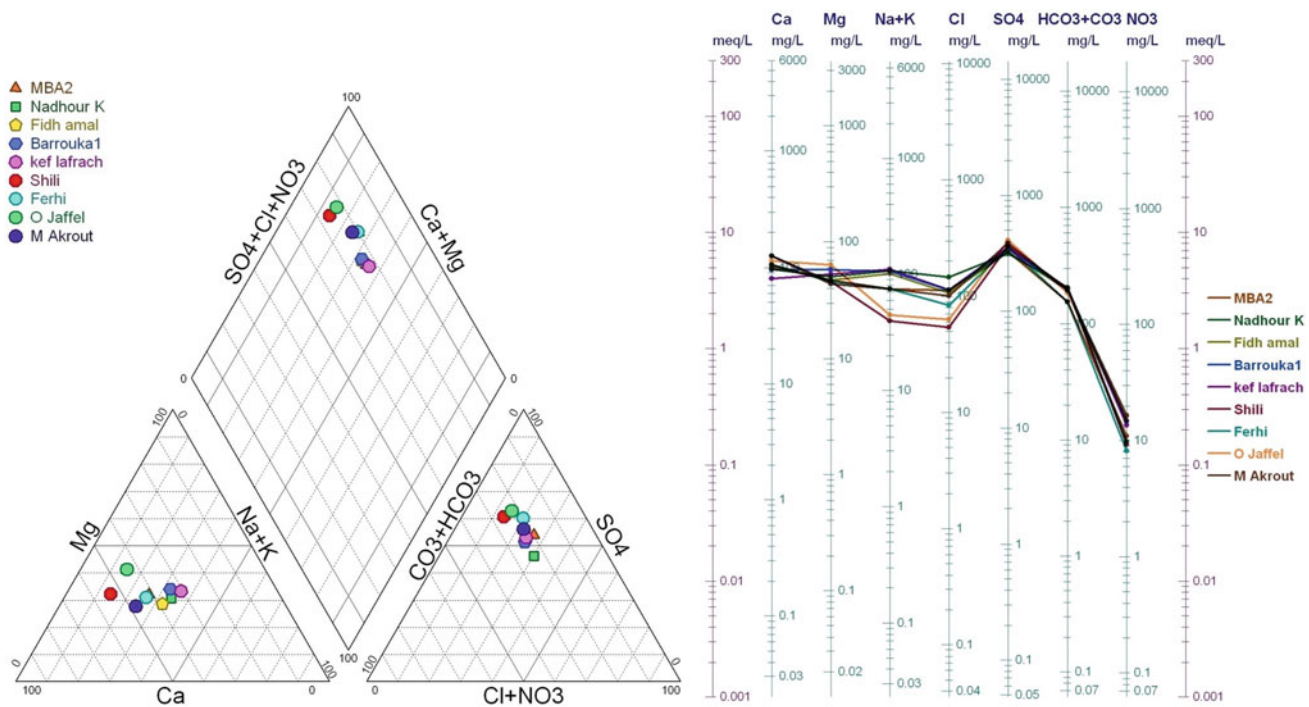


Fig. 2 Piper and Schoeller-Berkaloff diagrams

Plio-Quaternary aquifer. The Na/Cl and Ca/SO₄ ratios show that all of the samples are correlated. This explains the unique origin of these major elements, which is probably related to the dissolution of halite and gypsum. For the Ca/HCO₃ and Ca/Mg ratios (respectively, $R^2 = 0.41$ and $R^2 = 0.1$), the correlations indicate a different origin for these two elements and do not prove a dissolution of the dolomites in the reservoir.

The study of the saturation index values shows that the waters of the Plio-Quaternary aquifer are generally supersaturated with respect to the carbonate and undersaturated in minerals or in equilibrium state for the evaporitic minerals (Gouasmia et al. 2018).

4 Conclusions

The Majel Bel Abbes basin, a depression with high subsidence especially in the central part, is filled with continental heterogeneous detrital sediments ranging from Miocene to Plio-Quaternary. These series rest unconformably on the limestones of the Upper Cretaceous. The Plio-Quaternary is formed by clay sands and sandy clays whose thickness is variable in places with great power in the centre of the bowl.

The piezometric map showed a general N-S flow towards the plain of North Gafsa. Based on the piezometric curves

and the hydrodynamic characteristics, we estimated the exploitable resources to 373 L/s.

The geochemical study concluded that the waters are of excellent chemical quality since the dry residue is less than 1 g L⁻¹. It has also shown that the waters of the Plio-Quaternary and those of the Miocene are SO₄-Cl facies.

The Miocene sands and the Plio-Quaternary unit collected from different depths of the aquifer indicate that it functions hydrogeologically as a single unconfined aquifer system.

References

- Gouasmia, M., Khorchani, H., Mhamdi, A., Dhahri, F., Soussi, M.: Hydrogeological characterization of a carbonate aquifer using geophysical and geochemical approach: case of the Krachoua Formation in Tataouine area, Southern Tunisia. *Arab J. Geosci.* **11**, 786 (2018). <https://doi.org/10.1007/s12517-018-4150-x>
- Shouakar-Stash, O., Alexeev, S.V., Frapce, S.K., Alexeeva, L.P., Drimmie, R.J.: Geochemistry and stable isotopic signatures, including chlorine and bromine isotopes, of the deep groundwaters of the Siberian Platform Russia. *Appl. Geochem.* **22**, 589–605 (2007)
- Simler, R.: Logiciel d'hydrochimie. Diagrammes (v5.0). Laboratoire d'Hydrogéologie d'Avignon (2000)



Spatial Distribution of Nitrate Level in a Deep Aquifer Located in an Agricultural Region (North Tunisia)

Nizar Troudi, Fadoua Hamzaoui-Azaza, Ourania Tzoraki, and Mounira Zammouri

Abstract

The Guenniche deep aquifer (from 75 to 300 m), located in the Bizerte governorate (North Tunisia), is used to supply water for drinking, irrigation, and other needs. It is underlying three small-scale industrial zones and an agricultural area that uses chemical fertilizers and animal manure to improve soil fertility. The present research deals with the physicochemical properties of the groundwater in Guenniche deep aquifer by analyzing ten (10) boreholes in both the wet season (October 2015) and the dry season (May 2016). The results showed that the levels of nitrate were between 8 and 111 mg/L for the wet season and the dry season, respectively. The World Health Organization sets the nitrate limit at 50 mg/L, and 45 mg/L is the national standard. Three boreholes located in the region of El Alia in the south east of the study area exceeded the standards in the dry and wet seasons. Human activities on the surface, in addition to the non-existence or poor condition of sewer channels, are the major factors behind the degradation of Guenniche deep groundwater. This research suggests an urgent need for continuous monitoring of groundwater, particularly those water bodies intended for drinking purposes. Recommendations to the officials and policymakers of the government are given to move toward finding permanent solutions in this matter for the future protection of Guenniche deep aquifer.

Keywords

Deep aquifer • Nitrate • Pollution • Guenniche plain • North Tunisia

1 Introduction

The signs of urban progress, accelerating population growth, and the growing demand of consumption and production have put greater pressures on the natural resources, including the climate, natural ecosystems, and the aquatic environment (Li et al. 2019; Walha et al. 2007; Zammouri et al. 2013; Zereg et al. 2018; Troudi et al. 2019). Groundwater quality control is crucial to ensure long-term durability and to protect them from all forms of pollution, because it is a life-supporting resource for mankind and has the aim to protect both of the human health and the environment (Li et al. 2019; Wu et al. 2019; Yin et al. 2019). In Mediterranean countries, groundwater is mostly used as a source of potable water, and it is being more and more affected by human activity because of urban, industrial, and agricultural waste, which could cause serious implications for the future food security and downgrade the potable water quantity of acceptable quality (Zereg et al. 2018; Biddau et al. 2019; Negm et al. 2020a, 2020b). Nitrate is a problem in several regions worldwide, originating from the overuse of fertilizers, plus the organic manures, human wastewater, and industrial effluents that reinforce its presence in high levels in groundwater (Wu et al. 2019; Yin et al. 2019; Biddau et al. 2019; Negm et al. 2020b). The World Health Organization (WHO 2006) determined the nitrate limit in drinking water at 50 mg/L (WHO), and 45 mg/L is the Tunisian norm (NT) (NT 2013). If these limits are to be surpassed, human health may be threatened by diseases; including spontaneous abortions, birth malformations, blue baby syndrome, increase in the risks of methemoglobinemia and gastric cancer, damage to stomach lining, mouth ulceration,

N. Troudi (✉) · F. Hamzaoui-Azaza · M. Zammouri
Laboratory of Sedimentary Basins and Petroleum Geology (SBPG), LR18 ES07, Geology Department, Faculty of Sciences of Tunis, University of Tunis El Manar, Tunis 1060, Tunisia
e-mail: nizar.troudi@fst.utm.tn

O. Tzoraki
Department of Marine Sciences, University of the Aegean, Mytilene 81100, Greece

non-Hodgkin's lymphoma, hypertension, and reproductive toxicity (Wu et al. 2019; Rivett et al. 2008; Paladino et al. 2018). The Guenniche plain is located in the far north of Tunisia, over an area of approximately 130 km². The importance of agricultural production makes the Guenniche plain one of the most active farming areas in Bizerte governorate (CRDA 1998). Not all municipalities are connected to the drainage canals (Troudi et al. 2019), and the number of residents in these municipalities rose by more than 15,000 inhabitants over three decades to reach more than 74,000 people in 2014 (INS 2014). There are three multi-industrial zones (textile, oil refinery, etc.) in the Guenniche plain area. The objective of the current study is to explore the nitrate levels, to compare them to national and international standards and to investigate the potential nitrate sources. The results of this study will advance the knowledge of the nitrate threat in the Mediterranean environment and may help regional and national authorities to take measures that lead toward protecting groundwater resources in areas of intense agricultural activity.

2 Materials and Methods

2.1 Study Area

The plain of Guenniche is located between latitudes 35° 10' N, 37° 15' N and longitudes 9° 66' E, 10° E, and it belongs to the southeastern part of Bizerte governorate (far north of Tunisia) (Fig. 1). The research area is made up of three municipalities El Alia, Menzel Bourguiba, and Menzel Djemil, and small rural localities: Hariza, Khétmine, Maghraoua, El Jouaouda, and El Azib. Wadi Guenniche is the most important stream in the study area which consists of

many other ephemeral streams (tributaries), such as Wadi El Malah, Wadi Nechrine, Wadi Hela, Wadi El Jaddara, Wadi Echrichira, and Wadi El Galaa (Fig. 1a).

The climate in the Guenniche plain is defined as semi-humid climate with a mean rainfall of 600 mm/year, and the annual average temperature is 18.6 °C (INM 2016). The Guenniche plain is a region with important irrigated land, involving the use of a significant amount of nutrients (Troudi et al. 2019) (e.g., chemical fertilizers, organic fertilizers) and pesticides to ensure an important and good quality production. Regarding the geology and hydrogeology of the area, the Guenniche plain is a large basin created and filled after the great post-villafranchian tectonic phase by the Tyrrhenian Sea with Quaternary sediments, (Haj Ltaief 1995) represented by sands, alluviums, screes, sandstones, silts, clays, limestones, which are permeable and contain two aquifers more or less separated by clay intercalations (Haj Ltaief 1995; Ennabli 1966). The shallow aquifer of Quaternary age which is exploited by low-depth wells that are between 3 and 30 m deep (Haj Ltaief 1995), and the deep aquifer which dates back to the Mio-Pliocene age is between 75 and 300 m deep (Haj Ltaief 1995). It reaches Eocene levels in some places (Haj Ltaief 1995). The aquifers communicate with each other based on the conducted data made in this region, either by the weakly permeable bases (sandy clays, clay sands, etc.) which separate them or by structural accidents in certain places (Haj Ltaief 1995). The deep groundwater flow direction is from the east to the west (Fig. 1b). Bizerte Lake is the main natural outlet of the Guenniche deep groundwater. The groundwater of this plain provides supplies for the potable water, all daily and industrial activities, and most importantly, it is the main source of irrigation water.

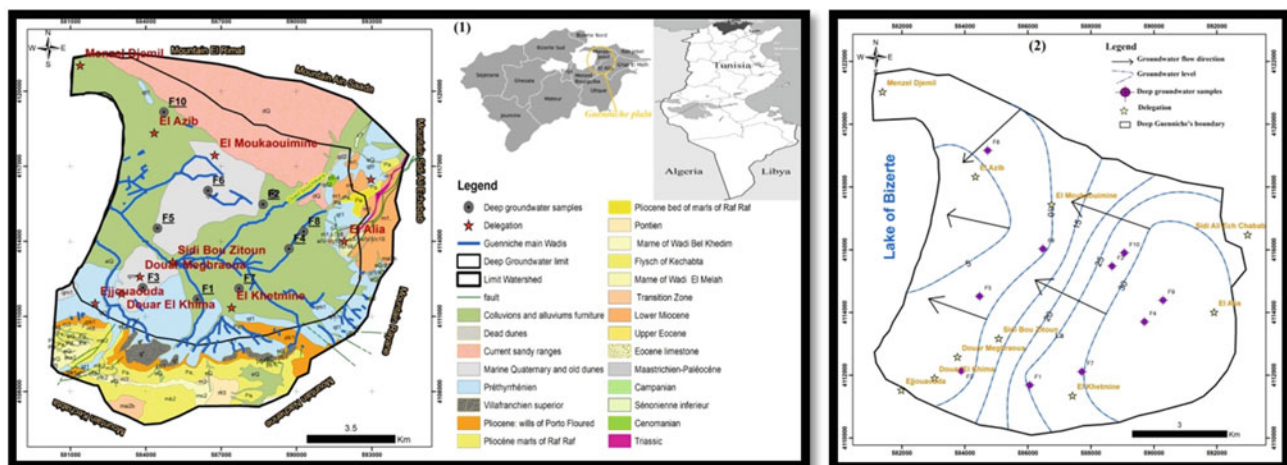


Fig. 1 a Location of the study area, geological map, and the borehole sampling points; b Groundwater deep Guenniche's level map

2.2 Materials and Methods

Ten (10) groundwater-monitoring borehole samples were collected in polyethylene bottles from active pumping wells belonging to the Guenniche deep aquifer at the end of the dry season (October 2015) and the wet season (May 2016). Before collecting each sample, groundwater is pumped for over 10 min to guarantee the presence of fresh water in each sample. Subsequently, and by the use of a portable field kit in situ, the temperature (T°), hydrogen potential (pH), and electrical conductivity (EC) are analyzed. All the samples are stored at 4 °C in an icebox until transported to the laboratory. Groundwater samples were filtered with 0.45 μ m millipore filter paper, acidified with nitric acid and stored at 4 °C into a freezer until the moment of the analysis at the Gdir El Golla laboratory of the National Company of Exploitation and Distribution of Drinking Water (SONEDE) in Tunis. The total dissolved solids (TDS) is determined by evaporation to determine the salinity of the borehole samples. The nitrate analysis is conducted by the use of the salicylate of sodium by molecular absorption (spectrophotometric method). The nitrite analysis was made by “the method of reactive Zambelli” (spectrophotometric method). The analysis is successful if the calculated ionic balance error of each groundwater sample is within the limits of 5%.

3 Results and Discussion

Table 1 summarizes the statistics of physicochemical parameters at the Guenniche deep groundwater in the dry season (October 2015) and the wet season (May 2016).

The pH gives a rough idea of spatial and temporal variations of water by the quality and the infiltration rate of recharge water and of water–rock interaction in the aquifer (Abboud 2018). Results suggest that the groundwater samples were neutral to mildly alkaline in the Guenniche deep aquifer in both seasons, where the pH values ranged from 6.97 to 7.72 during the dry season and between 6.9 and 7.72 during the wet season, which makes them all in desirable

interval set by national (NT) and international (WHO) standards (Table 1). The results of the temperature in the Guenniche deep aquifer were convergent in both seasons and varied from 19.3 to 21.5 °C during the wet season, and from 19.1 to 22.3 °C during the dry season (Table 1), this indicates that there is no effect caused by the atmospheric climate. The electrical conductivity (EC) values ranged from 0.73 to 6.14 mS/cm for the dry season and from 0.89 to 5.84 mS/cm for the wet season with an average value of 2.6 mS/cm of the two periods (Table 1). EC and TDS are typically closely correlated in water (Hiscock 2005). TDS mainly indicated the various kinds of minerals present in the groundwater, and the Guenniche deep aquifer water samples exceeded the WHO standard limits at 1000 mg/L in eight boreholes analyzed and in two boreholes compared to 2000 mg/L limit set by the Tunisian standard (NT); they varied from 414 to 3842 mg/L for the dry season and from 510 to 3650 mg/L for the wet season with a mean value of 1580 mg/L for both periods (Table 1). The water saturation of major cations and anion salts, in combination with the water–rock dissolution phenomena initialization during the water flow from the surface to the lower depths, may explain the presence of high TDS values in all the water samples (Abboud 2018). The results of nitrite in each borehole sample and in the dry and wet seasons felt within the limit value of national (NT) and international (WHO) standards set at 0.2 mg/L (Table 1). Nitrate concentrations varied from 8.1 to 111.9 mg/L, in the dry season with a mean value of 42.9 mg/L and between 8.2 to 109.2 mg/L, with mean at 39.7 mg/L in the wet season (Table 1). Average nitrate concentration is the highest in F1, F2, and F7 to the west of El Alia region in both seasons compared (Fig. 2) to WHO and NT standards, with a slight level change in the three boreholes from season to season. The concentration of nitrate in P7 borehole exceeded the standards’ limit by 15 mg/L in both seasons. F1 and F2 exceed the WHO and NT limits to beyond 100 mg/L in both sampling periods (October 2015 and May 2016).

A total of 90% of the plain of Guenniche land is farmland, of which 70% is an irrigated land (CRDA 1998). The livestock numbers reached 31,565 sheep and 5526 cattle in

Table 1 Average values and range of physicochemical results of the Guenniche deep groundwater

Parameters	Dry season (October)			Wet season (May)			Standards	
	Min	Max	Mean	Min	Max	Mean	WHO	NT
T (°C)	19.1	22.3	20.8	19.3	21.5	20.53	–	–
pH	6.97	7.72	7.26	6.9	7.72	7.17	6.5–9.5	6.5–8.5
EC (mS/cm)	0.73	6.14	2.6	0.89	5.84	2.632	2.5	1.5
TDS (mg/L)	414	3842	1598.8	510	3650	1564.2	2000	1000
NO ₃ ⁻ (mg/L)	8.08	111.9	42.88	8.2	109.2	39.68	50	45
NO ₂ ⁻ (mg/L)	0.003	0.049	0.023	0.01	0.046	0.024	0.2	0.2

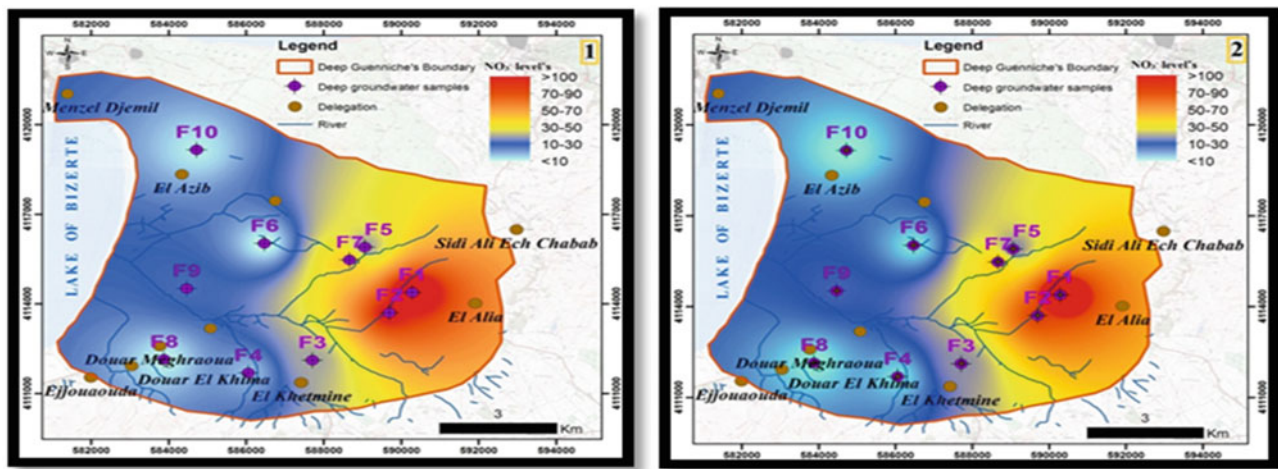


Fig. 2 Spatial distribution of nitrate levels (mg/L) in 1 the dry season and 2 Wet season in the deep aquifer of the plain of Guenniche

2015 in the study area with an estimation of 100 kg/ha/year of nitrogen from farm fluxes (CTV 2015). During the sampling, an accumulation of high quantities of animal manure was noted, even close to the studied boreholes, strengthening the hypothesis of nitrate migration to the groundwater. Nitrate levels in groundwater increase with the application of chemical fertilizers. The most frequently used fertilizers in the area are the DAP N-P₂O₃ and Ammonium and super 45, with an application rate of over 450 kg/ha/year (CTV 2015) and 300 kg/ha/year, respectively, in the leguminous activity farms. The drainage from fertilized fields and contaminated water bodies can also serve as a source of nitrate. Previous studies by (Zereg et al. 2018; Wu et al., 2019; Yin et al. 2019; Biddau et al. 2019) indicated that the main source of the presence of the nitrate elements in the water is associated with the different human activities in the surface which are reflected by groundwater pollution. The west of El Alia region is a rural area lacking adequate infrastructure like sewer systems, so the wastewater discharges in the surface enters the streams of Wadi Guenniche and El Mellah. It is the main reason which explains the presence of high nitrate levels found near these ephemeral streams. The study of Hamza et al. (2010) stated that the shallow aquifer has been classified as vulnerable to pollution by nitrate elements due to its low depth and the type of soil (permeable in most of the area's surface) which facilitates the transport of those elements by surface water and the infiltration of irrigation water; consequently, the transport of NO₃⁻ from the surface to the shallow aquifer. The shallow and deep aquifers are separated by semi-permeable layers in some areas (Haj Ltaief 1995), and the presence of a fault in El Alia region to NE-SW direction, of 25 km long and 4–5 km deep (Kacem 2004), could explain the presence of nitrate in the vicinity of

the boreholes. To the west (toward the lake of Bizerte), the yellow and blue colors in the map (Fig. 2) indicate very low nitrate levels, which can be explained by the impermeable rocks that separate the shallow from the deep aquifer (Haj Ltaief 1995), thus, protecting the deep aquifer from all surface anthropogenic pollution.

4 Conclusions

The results of the samples taken from the Guenniche deep groundwater during the dry and wet seasons showed high levels of NO₃⁻ up to 100 mg/L in two boreholes, and in one, the level was 60 mg/L. Three boreholes located in El Alia region exceeded the national and international standards (Fig. 2). The chemical and organic manure are the principal sources of NO₃⁻, in addition to the discharges of wastewater in the rural areas which are not connected to the sanitation channels. The permeability of the soil is one of the reasons behind NO₃⁻ elements' transport from the surface to the shallow aquifer and may, thus, be transmitted to the deep aquifer through the semi-permeable bottom (in some places) and through the fault located in El Alia region. Pinpointing pollution and natural causes as being at the origin of water contamination is of huge importance to address the problem efficiently and to apply the best policies regarding the groundwater resources' management. It is really important in the future work to increase the number of borehole samples and study the hydrogeochemical and stable isotopic in the Guenniche groundwater system which would provide the best approximation of the link between the different aquifers, as well as the hydrogeochemical modeling study of the Guenniche groundwater in order to help protect these vital resources.

References

- Abboud, I.A.: Geochemistry and quality of groundwater of the Yarmouk basin aquifer, north Jordan. *Environ. Geochem. Health* **40**, 1405–1435 (2018). <https://doi.org/10.1007/s10653-017-0064-x>
- Biddau, R., Cidu, R., Da Pelo, S., Carletti, A., Ghiglieri, G., Pittalis, D.: Source and fate of nitrate in contaminated groundwater systems: assessing spatial and temporal variations by hydrogeochemistry and multiple stable isotope tools. *Sci. Total Environ.* **647**, 1121–1136 (2019). <https://doi.org/10.1016/j.scitotenv.2018.08.007>
- CRDA: *Annuaire de surveillance piézométrique des nappes de 1998 à 2013*. Publ. CRDA, Bizerte, Tunisie (1998)
- CTV: *Cellule Territoriale de Vulgarisation (Commissariat Régional de Développement Agricole) El Alia Bizerte* (2015)
- Ennabli, M.: *Etude hydrogéologique de la plaine de l'Oued Guénniche*. Rapport interne BIRH, p 77 (1966)
- Haj Ltaief, Z.: *Nappe de l'oued Guénniche: Evaluation des ressources et impact de la surexploitation*. DEA, FS Tunis, Univ. Tunis II, p 94 (1995)
- Hamza, M.H., Maâlej, A., Ajmi, M., Added, A.: Validity of the vulnerability methods DRASTIC and SI applied by GIS technique to the study of diffuse agricultural pollution in two phreatic aquifers of a semi-arid region (Northeast of Tunisia). *Aquamundi-Am* **01009**, 57–64 (2010)
- Hiscock, K.M.: *Hydrogeology: principles and practice*. Wiley, New York, p 389. ISBN 978019857634 (2005)
- INM: "Institut National de la météorologie" *Données climatologique de la plaine de Guénniche* (2010–2016), (2016)
- INS: *Institut National de la Statistique, Recensement général de la population et du logement* (2014)
- Kacem, J.: *Etude sismotectonique et évaluation de l'Alia sismique régional du nord-est de la Tunisie: apport de la sismique réflexion dans l'identification des sources sismogéniques*. Thèse Doct, FST, Univ. Tunis2 (2004)
- Li, P., He, X., Guo, W.: Spatial groundwater quality and potential health risks due to nitrate ingestion through drinking water: a case study in Yan'an City on the loess plateau of northwest China. *Human Ecol. Risk Assess.* **25**(1-2), 11–31, (2019). <https://doi.org/10.1080/10807039.2018.1553612>
- Negm, A., Bouderbala, A., Chenchouni, H., Barcelo, D.: *Water Resources in Algeria - Part I: Assessment of Surface and Groundwater*. The Handbook of Environmental Chemistry Series. Springer, Cham (2020a). <https://doi.org/10.1007/978-3-030-57895-4>
- Negm, A., Bouderbala, A., Chenchouni, H., Barcelo, D.: *Water Resources in Algeria - Part II: Water Quality, Treatment, Protection and Development*. The Handbook of Environmental Chemistry Series. Springer, Cham (2020b). <https://doi.org/10.1007/978-3-030-57887-9>
- NT: *Norme tunisienne NT 09-14, relative a la qualite des eaux de boisson* (2013)
- Paladino, O., Seyedsalehi, M., Massabò, M.: Probabilistic risk assessment of nitrate groundwater contamination from greenhouses in Albenga plain (Liguria, Italy) using lysimeters. *Sci. Total Environ.* **634**, 427–438 (2018). <https://doi.org/10.1016/j.scitotenv.2018.03.320>
- Rivett, M.O., Buss, S.R., Morgan, P., Smith, J.W.N., Bemment, C.D.: Nitrate attenuation in groundwater: a review of biogeochemical controlling processes. *Water. Res.* **42**(16), 4215–4232 (2008). <https://doi.org/10.1016/j.watres.2008.07.020>
- Troudi N., Hamzaoui F., Zammouri M., Tzoraki O.: Distribution of Trace Elements in the Shallow Aquifer of Guénniche (North Tunisia). In: Chaminé H., et al. (eds) *Advances in Sustainable and Environmental Hydrology, Hydrogeology, Hydrochemistry and Water Resources*. CAJG 2018. *Advances in Science, Technology & Innovation*. Springer, Cham (2019). https://doi.org/10.1007/978-3-030-01572-5_28
- Walha, K., Amar, R.B., Quemeneur, F., Jaoued, P.: Déminéralisation des eaux saumâtres du sud tunisien par électrodialyse ou par osmose inverse (Demineralization of brackish water of southern Tunisia by electro dialysis or by reverse osmosis). *J. Soc. Chim. Tunis.* **9**, 133–142 (2007)
- WHO: *Guidelines for drinking-water quality*, vol. 1, *Recommendations*, 3rd ed. World Health Organization, Geneva. www.who.int/water_sanitation_health. ISBN 978 92 4 154761 1 (2006)
- Wu, J., Lu, J., Wen, X., Zhang, Z., Lin, Y.: Severe nitrate pollution and health risks of coastal aquifer simultaneously influenced by saltwater intrusion and intensive anthropogenic activities. *Arch. Environ. Contam. Toxicol.* **77**, 79–87 (2019). <https://doi.org/10.1007/s00244-019-00636-7>
- Yin, S., Xiao, Y., Gu, X., Hao, Q., Liu, H., Hao, Z., Meng, G., Pan, X., Pei, Q.: Geostatistical analysis of hydrochemical variations and nitrate pollution causes of groundwater in an alluvial fan plain. *Acta Geophys.* **67**, 1191–1203 (2019). <https://doi.org/10.1007/s11600-019-00302-5>
- Zammouri, M., Jarraya-Horriche, F., Odo, B.O., Benabdallah, S.: Assessment of the effect of a planned marina on groundwater quality in Enfida plain (Tunisia). *Arab. J. Geosci.* **7**(3), 1187–1203 (2013). <https://doi.org/10.1007/s12517-012-0814-0>
- Zereg, S., Boudoukha, A., Benaabidate, L.: Impacts of natural conditions and anthropogenic activities on groundwater quality in Tebessa plain, Algeria. *Sustain. Environ. Res.* **28**(6), 340–349 (2018). <https://doi.org/10.1016/j.serj.2018.05.003>



Evaluation of Groundwater Quality in Rural Part of Central India with Special Emphasis on Fluoride Concentration

Rajshree Yenkie, Deepak Malpe, Deepali Marghade, Dhananjay Meshram, and Biswajit Hazarika

Abstract

Groundwater in many parts of the world has been contaminated with high concentrations of elements like fluoride (F^-). Hydrogeological investigations have been carried out in rural parts of Wani area of central India in an attempt to assess the quality of groundwater vis-à-vis its suitability for drinking and irrigation purposes. These were accomplished by evaluating the physicochemical parameters obtained from the analysis of 114 groundwater samples collected during the November 2018 period using standard methods. Groundwater in the area is generally hard-to-very-hard type and alkaline in nature. A wide disparity has been shown by total hardness, conductivity, NO_3^- and HCO_3^- in majority of the samples. The concentration of F^- (0.05–2.36 mg/L) is quite alarming in many locations of the area. The groundwater of the area is mainly of $CaHCO_3$ and mixed $CaMgCl$ types. The US salinity laboratory (USSL) diagram shows that the groundwater is free from sodium hazards, but the salinity hazard varies from low to very high throughout the area. Sodium percentage revealed that 70% of the samples are under a good-to-permissible category. High concentration of NO_3^- observed in the samples is mostly due to poor sanitary conditions around the water sources and other anthropogenic activities. Cases of dental fluorosis have been observed in areas where F^- concentrations exceed 1 mg/L. High F^- concentrations can be attributed to the alkaline nature, semiarid conditions and rock–water interaction process.

Keywords

Groundwater • Drinking water quality • Fluoride • Central India

1 Introduction

Most countries, including India, utilize groundwater sources for taking care of local demand and advancement. Groundwater quality is as important as its quantity owing to its suitability for different purposes (Negm et al. 2020a, 2020b). The presence of low or high concentrations of certain ions is a major issue as they may make the groundwater inadequate for many purposes, and fluoride (F^-) is one such an ion that causes health issues. In India, more than 66 million individuals, including 6 million children, are affected by fluoride poisoning (Susheela 2007). A lot of work has been carried out on the presence of F^- in groundwater and its health implications (Li et al. 2019; Raj and Shaji 2017). The present study reports the presence of F^- in the groundwater and also intends to identify the hydrochemical and anthropogenic contamination factors responsible for the deterioration of the water quality using different physicochemical parameters.

2 Study Area

The study area (longitude 78°40'19" to 79°08'58" E and latitude of 19°51'42" to 20°09'15" N) is the part of Penganga sub-basin of Godavari Basin, which covers the rural part of Wani area of Central India (Fig. 1a). The area is characterized by semiarid to tropical climate with annual average rainfall of 1038.8 mm.

Geologically, the area is occupied by Penganga limestones of Neoproterozoic age overlain by Gondwana Supergroup rocks, which are further overlain by basaltic lava flows of

R. Yenkie · D. Malpe (✉) · B. Hazarika
Department of Geology, RTM Nagpur University,
Nagpur, 440001, India

D. Marghade
Department of Chemistry, Priyadarshini Institute of Engineering
and Technology, Nagpur, India

D. Meshram
Department of Geology, Sawitribai Phule Pune University,
Pune, 411007, India

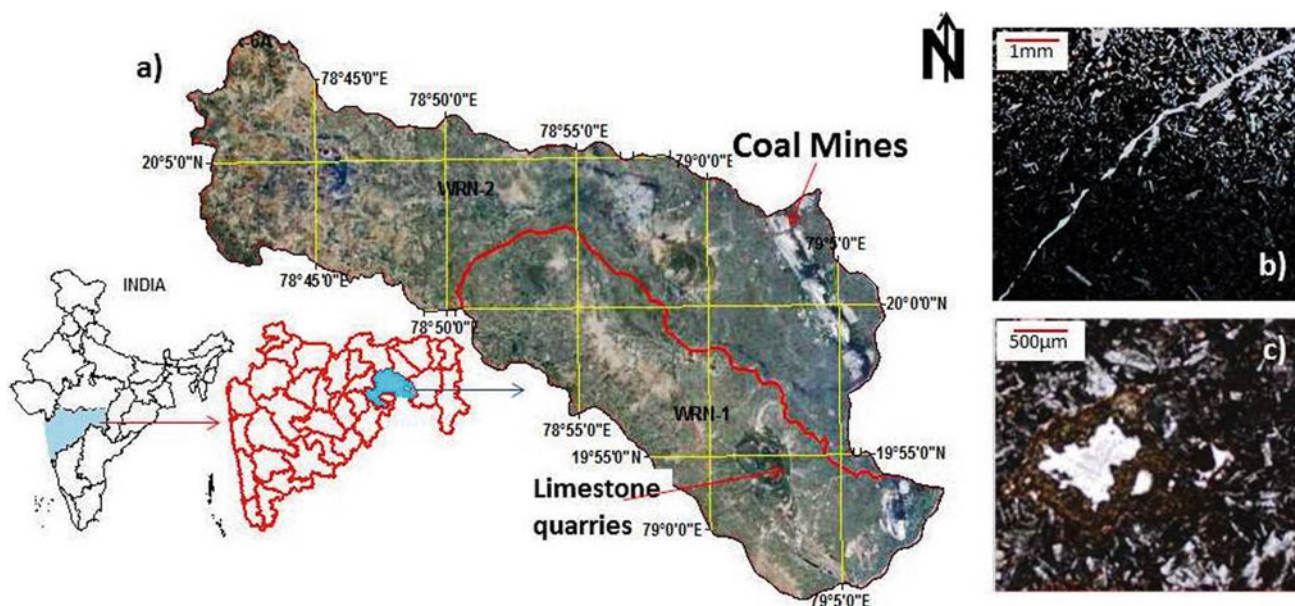


Fig. 1 a Location map of study area, b vein and c grains of fluorite in basalt

Deccan Volcanic Province. Quaternary alluvium and black soil overlie all the older formations (GSI 2001). Petrological studies of the host rocks of groundwater sources showed the occurrence of fluorite veins and grains (Shareef et al. 2010; Fig. 1b, c). In general, groundwater occurs under phreatic conditions in shallow aquifers and under semi-confined to confined conditions in the deeper aquifers. Rain-fall is the main source of groundwater recharge in the area.

3 Results and Discussion

A set of 114 groundwater samples was collected from deeper aquifers (45–50 m depth) during November 2018 and analyzed for physicochemical parameters at the chemical laboratory of the department. The standard procedures recommended by the American Public Health Association were followed during sample collection, preservation and analysis (APHA 1997) (Table 1). The ionic balance error for studied ions is within $\pm 5\%$.

The order of abundance of major ions observed in the area was $\text{Ca}^{2+} > \text{Na}^+ > \text{Mg}^{2+} > \text{K}^+ = \text{HCO}_3^- > \text{Cl}^- > \text{SO}_4^{2-} > \text{NO}_3^- > \text{F}^-$. The groundwater of the area is slightly acidic to alkaline in nature. A wide variation has been observed in various ions (Table 1). In some areas, their concentration exceeds the permissible limit for drinking (WHO 2011; BIS 2012).

In the present case, both natural processes—like chemical weathering and leaching from aquifer rocks—and

anthropogenic activities—such as the application of nitrogenous fertilizers in farming practices, poor sanitary conditions around the water sources, human and animal waste and sewage—could be responsible for the deterioration in the groundwater quality.

In 26.32% of the samples, the F^- concentration is more than 1.0 mg/L. In the absence of any anthropogenic source, the F^- in groundwater is derived from the leaching from F^- bearing minerals like fluorite (Fig. 1b, c). In addition to this semiarid climate, the high pH of the groundwater could have also contributed to the F^- concentration.

The piper's plot (Fig. 2) (Piper 1944) demonstrates that the vast majority of the samples fall under CaHCO_3 and mixed CaMgCl types with minor NaCl and mixed CaNaHCO_3 type, where alkaline earth ($\text{Ca}^{2+} + \text{Mg}^{2+}$) exceeds the alkali ($\text{K}^+ + \text{Na}^+$) and weak acid (HCO_3^-) exceeds strong acid (Cl^- and SO_4^{2-}).

The plot of samples on the US salinity diagram (Fig. 3) (US Salinity Laboratory Staff 1973) delineates that water samples of the study area mostly fall over C3-S1 field with minor C4-S1 and C4-S2. Most of the samples show water of high salinity low sodium type, which can be utilized for irrigation in all types of soils with little peril of replaceable sodium.

Classification based on Wilcox (Wilcox 1955) suggests that 70.2% of the samples are of good-to-permissible water type which can be used for the irrigation over salt-tolerant and semi-tolerant soils under favorable drainage conditions, whereas 6.2% (doubtful) and 23.6% are unsuitable for irrigation.

Table 1 Physicochemical parameters of groundwater samples (n = 114)

Parameter	Min	Max	Mean	Std deviation	WHO (2011)	BIS (2012)
pH	6.30	8.50	7.39	0.42	6.5–8.5	6.5–8.5
EC (µS/cm)	650.00	9130.00	2058.66	1421.48	1400	-
TDS (mg/L)	353.60	5347.63	1172.75	924.97	1000	500
TH (mg/L)	160.00	2202.50	707.35	383.65	500	300
TA (mg/L)	60.00	960.00	463.02	128.18	–	200
Ca ²⁺ (mg/L)	24.00	540.00	123.81	73.56	200	75
Mg ²⁺ (mg/L)	2.19	362.07	96.67	65.79	50	30
Na ⁺ (mg/L)	7.00	953.00	119.60	165.82	200	–
K ⁺ (mg/L)	0.25	581.00	39.98	96.01	12	–
CO ₃ ²⁻ (mg/L)	0.00	48.00	0.87	5.75	–	–
HCO ₃ ⁻ (mg/L)	73.20	1171.20	563.12	157.47	–	–
Cl ⁻ (mg/L)	21.30	2421.10	200.46	309.72	250	250
SO ₄ ²⁻ (mg/L)	8.36	858.30	158.18	199.07	250	200
NO ₃ ⁻ (mg/L)	1.00	1096.34	150.84	241.45	50	45
F ⁻ (mg/L)	0.05	2.36	0.78	0.51	1.5	1

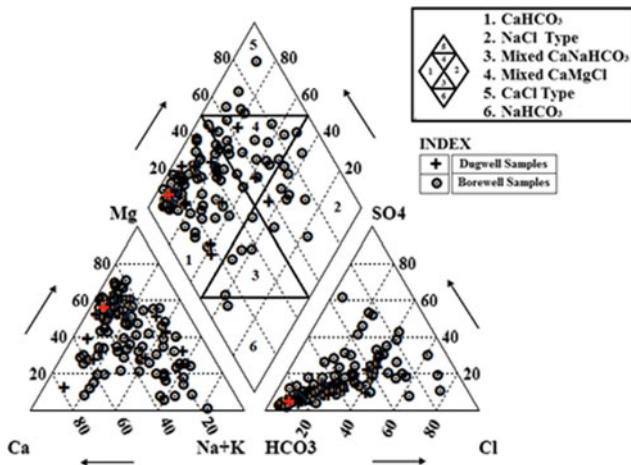


Fig. 2 Piper plot for samples of study area

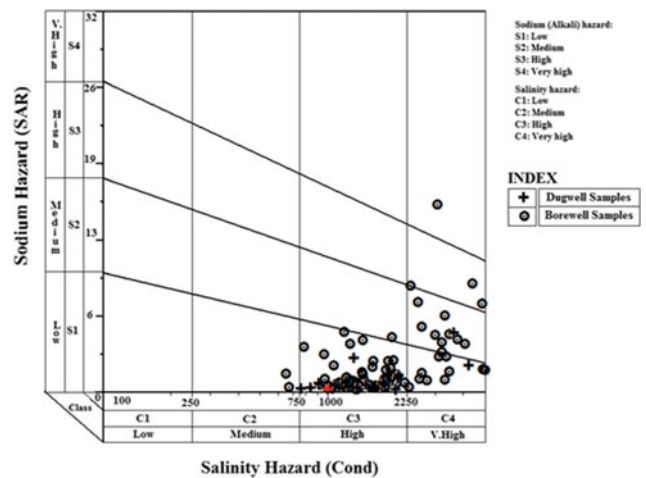


Fig. 3 US salinity laboratory diagram

4 Conclusions

- Elucidation of hydrochemical examination uncovers that the groundwater in the study area is hard and alkaline in nature.
- The comparison of analyzed data with WHO and BIS indicates higher concentrations of TH, Cl⁻, TDS, NO₃⁻ and F⁻. High TDS, Cl⁻ and NO₃⁻ are the results of anthropogenic activity, while F⁻ contamination is mainly due to the natural geogenic process like leaching of F⁻ bearing minerals, alkaline nature of groundwater and semiarid climatic conditions.

- Piper trilinear diagram suggests that the water of study area is mostly of CaHCO₃ and mixed CaMgCl types, with alkaline earth exceeding alkalis and weak acids exceeding strong acids.
- The US salinity diagram shows the dominance of C3-S1 and C4-S2 water types, reflecting that almost 79% of the groundwater samples of the study area show a high-to-very-high salinity hazard which is beyond the allowable limit for irrigation despite the fact that it has low alkalinity danger. Based on Na %, about 18% of the groundwater sources are doubtful-to-unsuitable for irrigational purposes. Such areas require adequate drainage and salt-tolerance cropping pattern to overcome suitability problems.

References

- APHA: Standard Method for the examination of water and wastewater. 18th edn. American Public Health Association, New York (1997)
- BIS: Drinking water specifications. Bureau of Indian Standards, IS, 105002012 (2012)
- GSI: District resource map of Yavatmal district, Maharashtra. Geological Survey of India, central Region, Nagpur (2001)
- Li, P., He, X., Li, Y., Xiang, G.: Occurrence and health implication of fluoride in groundwater of loess aquifer in the Chinese loess plateau: a case study of Tongchuan, Northwest China. *Exposure and Health* **11**(2), 95–107 (2019)
- Negm, A., Bouderbala, A., Chenchouni, H., Barcelo, D.: Water Resources in Algeria - Part I: Assessment of Surface and Groundwater. Springer, Cham (2020a). <https://doi.org/10.1007/978-3-030-57895-4>
- Negm, A., Bouderbala, A., Chenchouni, H., Barcelo, D.: Water Resources in Algeria - Part II: Water Quality, Treatment, Protection and Development. Springer, Cham (2020b). <https://doi.org/10.1007/978-3-030-57887-9>
- Piper, A.M.: A graphic procedure in the geochemical interpretation of water analyses. *Trans. Am. Geophys. Union* **25**, 914–928 (1944)
- Raj, D., Shaji, E.: Fluoride contamination in groundwater resources of Alleppey, southern India. *Geosci Front* **8**(1), 117–124 (2017)
- Shareef, M., Gohain, B., Mahajan, M.: Petrographic and geochemical studies of borehole core samples for fluoride determination in Dharna village, Pandharkawada Taluka, Yavatmal District, Maharashtra. Unpub. Report Geological Survey of India, Central Region, Nagpur (2010)
- Susheela, A.K.: A treatise on fluorosis. 3rd edn. Fluorosis Research and Rural Development Foundation, Delhi (2007)
- US Salinity Laboratory Staff: Diagnosis and improvement of saline and alkali soils. 2nd edn. US Department of Agriculture Handbook No. 60, Washington (1973)
- WHO: Guidelines for drinking-water quality. 4th edn. World Health Organization, Geneva (2011)
- Wilcox, L.: Classification and use of irrigation waters. US Department of Agriculture, Circular 969, Washington, DC, USA (1955)



Groundwater Arsenic and Iron Contamination in the Gangetic Plains of India: Safe Drinking Water Option on Quaternary Stratigraphy

Babar Ali Shah

Abstract

Late Quaternary stratigraphy, geomorphology, and sedimentation in the entrenched channels and floodplains of the upper, middle, and lower Ganga plains in the states of Uttar Pradesh, Bihar, Jharkhand, and West Bengal have control on groundwater arsenic contamination. Arsenic analysis was done through atomic absorption spectrometry, and Iron was analyzed by the use of UV spectro-photometer. Arsenic contamination in groundwater above 50 µg/L is reported in Unnao and Allahabad districts in the upper Ganga plain. In the middle Ganga plain, 66% of tubewells from Buxar, Ghazipur, Varanasi, and Mirzapur districts and 89% of tubewells from Vaishali, Patna, Bhojpur, and Ballia districts have arsenic > 10 µg/L (WHO guideline). Most of the arsenic-affected villages are located close to abandoned or present meander channels of the Ganga River. In contrast, tubewells located in Kanpur, Allahabad, Mirzapur, Chunar, Varanasi, Saidpur, Ghazipur, Muhammadabad, Ballia, Buxar, Ara, Chhapra, Patna, and Hazipur towns are arsenic-safe in groundwater because of their positions on the Pleistocene Older Alluvium upland surfaces. In the middle Ganga plain, 77% of tubewells are located in shallow depth (21–40 m). About 40% of tubewells have arsenic > 50 µg/L within the depth of 17–50 m. The iron content in tubewell water samples varies from 0.1 to 13 mg/L. In the lower Ganga plain, arsenic contaminated aquifers (arsenic >10 µg/L) are confined in the Holocene entrenched channels and floodplains of the Bhagirathi River.

Keywords

Arsenic • Tubewell water • Newer alluvium • Older alluvium • Fluvial geomorphology

B. A. Shah (✉)

Department of Geological Sciences, Jadavpur University, Kolkata, India

1 Introduction

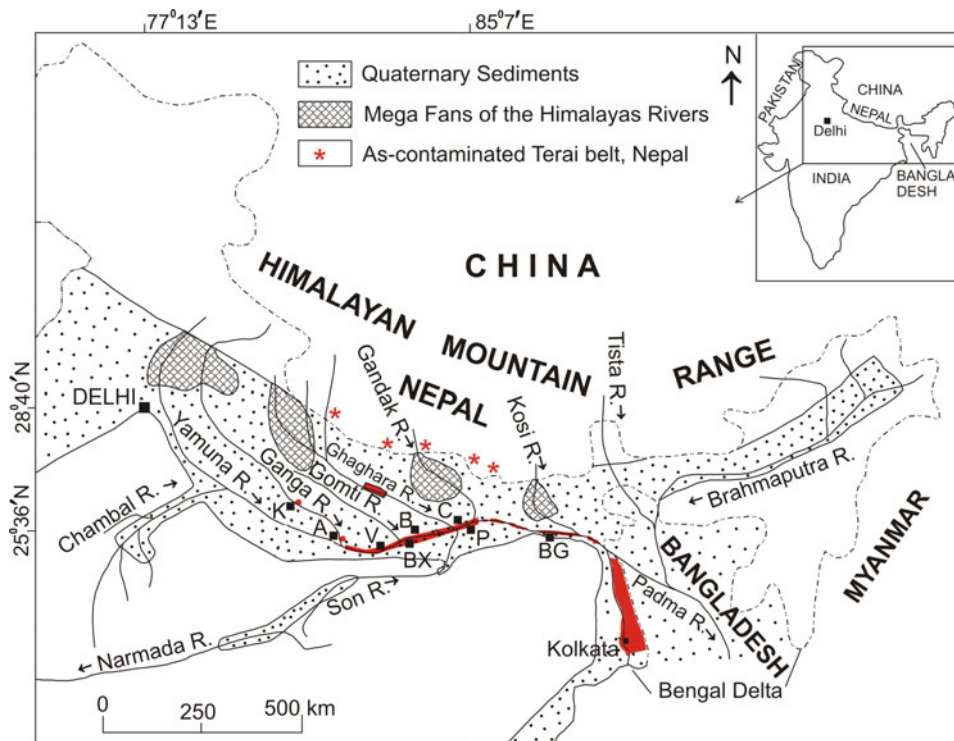
Groundwater arsenic (As) pollution incidents were reported in different parts of the world such as Bangladesh, India, Pakistan, Nepal, China, Hungary, Vietnam, Thailand, Cambodia, Tiwan, Inner Mongolia, Ghana, Egypt, Japan, Argentina, Mexico, USA, and Chile (Mandal and Suzuki 2002; Ravenscroft et al. 2009). Drinking As-contaminated groundwater above 50 µg/L causes skin diseases, cardiovascular, renal, and respiratory diseases, as well as lung, bladder, liver, kidney, and prostate cancers (Smith et al. 1992). The upper permissible limit of As in drinking water is 10 µg/L (WHO 1993) which has been endorsed by the Bureau of Indian Standards (Bureau of Indian Standards 2003). Groundwater As contamination in the Gangetic plains in India (lower, middle and upper) has been reported by various workers (Chakraborti et al. 2003; Acharyya and Shah 2007; Central Ground Water Board 2010; Shah 2014).

Groundwater As in tubewells was tested from the Holocene Newer Alluvium aquifers and the Pleistocene Older Alluvium aquifers (Fig. 1). The main objective of the study is to investigate the distribution of groundwater As in entrenched channels and floodplains of the lower, middle, and upper Ganga plains and role of Quaternary stratigraphy for a safe drinking water option.

2 Geological Settings

The study areas in the lower, middle, and upper Ganga plains in the states of Uttar Pradesh, Bihar, and Jharkhand and West Bengal are shown in Fig. 1. The Varanasi Older Alluvium constitutes upland surfaces, which are occupying major parts of the Ganga plains. The Varanasi Older Alluvium consists of multiple sequence of sand, silt, and clay. The Pleistocene Older Alluvium sediments are recognized by yellow–brown colored sediments with profuse calcareous and ferruginous concretions (Kumar et al. 1996). The Ganga River Basin has

Fig. 1 Quaternary sediments in the Indo-Ganga foredeep and Bengal Basin. The study areas in the upper and middle Ganga plains, Ghaghara River plain and West Bengal delta plain. Abbreviations: K—Kanpur, A—Allahabad, V—Varanasi, BX—Buxar, B—Ballia, C—Chhapra, P—Patna and BG—Bhagalpur



low-lying floodplain areas which are constituted by the Newer Alluvium sediments. The Bengal delta covers most of Bangladesh and parts of the West Bengal, India.

3 Materials and Methods

Tubewell water samples (214) were stabilized in 10 ml pre-washed plastic bottles with 1 drop of dilute nitric acid (1:1) of analytical grade. The information of tubewell depth was acquired from the owner of the tubewell. Arsenic and iron were analyzed at the laboratory of the School of Environmental Studies, Jadavpur University. Arsenic analysis was done through flow injection hydride generation atomic absorption spectrometry (FI-HG-AAS) system of Perkin-Elmer Model 3100 (Samanta et al. 1999). Iron was analyzed by 1, 10 phenanthroline method by the use of UV spectro-photometer.

4 Results and Discussion

4.1 Groundwater Arsenic and Iron in the Gangetic Plains

Arsenic contamination in groundwater above 50 $\mu\text{g/L}$ in the upper Ganga plain has been reported from the Unnao district

of UP in the Suklaganj-Kanpur urban areas and Allahabad district in Uttar Pradesh (Chakraborti et al. 2009).

Tubewell water samples were analyzed from Buxar, Ghazipur, Varanasi, and Mirzapur districts the middle Ganga plain. It may be noted that 66% of tubewells have As concentrations above 10 $\mu\text{g/L}$ (WHO guidelines), and 36% of tubewells have As above 50 $\mu\text{g/L}$. Maximum concentrations of As and Fe in tubewell water samples are 550 and 9.3 mg/L, respectively. About 77% of tubewells are installed in shallow depth, ranging from 21 to 40 m. Tubewells located on Buxar, Muhammadabad, Ghazipur, Saidpur, Varanasi, Chunar, and Mirzapur towns are As-safe in groundwater (<10 $\mu\text{g/L}$), because of their positions on the Older Alluvium upland surfaces (Shah 2014).

Tubewell water samples were analyzed from Vaishali, Patna, Bhojpur, and Ballia districts in the middle Ganga plain (Fig. 2). It was noted that 89% of tubewells have As concentrations above 10 $\mu\text{g/L}$, and 50% of tubewells have As above 50 $\mu\text{g/L}$. Maximum concentrations of As in tubewell water is 1300 $\mu\text{g/L}$ at the Semariya Ojjhapatti village. Iron content in tubewell water varies from 0.1 to as much as 13 mg/L (Shah 2014). There is no good correlation between As and Fe, where the lower value of As corresponds with a higher value of Fe and vice versa. Tubewells in Ballia, Ara, Chhapra, Patna, and Hazipur towns are located on the Older Alluvium upland surfaces and are As-safe in groundwater.



Fig. 2 Google satellite imagery shows spatial distribution of As-contaminated tubewells in entrenched channels and floodplains of the Ganga-Ghaghara River system

Apart from the above studies, groundwater As contamination has been reported from different parts of the middle Ganga plain. Currently, 57 blocks in 15 districts of Bihar are As-affected ($>10 \mu\text{g/L}$). The As-affected districts in Bihar are Buxar, Bhojpur, Patna, Saran, Vaishali, Begusarai, Samastipur, Lakhisarai, Purnea, Kathitar, Khagaria, Darbhanga, Bhagalpur, Kishanganj, and Munger (Chakraborti et al. 2003; Nickson et al. 2007; Central Ground Water Board 2010; Shah 2014).

The Bengal delta plain is extensively affected by groundwater As pollution, which affects mainly lower grounds comprising the Holocene deltaic sediments, whereas the Older Alluvial uplands and inter-fluve areas are generally unaffected. Currently, the groundwater of nine districts of West Bengal is As-contaminated. Arsenic contaminated aquifers are mainly confined in the Holocene entrenched channels and floodplains of the Bhagirathi River in the six districts (Malda, Murshidabad, Nadia, North 24-parganas, Kolkata, South 24-parganas) of West Bengal and mostly in the eastern parts of the Bhagirathi River (Chakraborti et al. 2003).

4.2 Sources and Release Mechanism of Arsenic

Groundwater arsenic mobilization in the Gangetic plains has similarity with the Bengal delta. Biomediated reductive dissolution of hydrated iron oxide (HFeO) that occurs mainly as coatings on sediment grains and corresponding oxidation of sedimentary organic matter is regarded as the main mechanism, which mobilizes As to groundwater from

aquifer sediments (Kinniburgh and Smedley 2001). The anaerobic heterotrophic Fe^{3+} reducing bacteria (IRB) dissolve discrete phases of HFeO, with a consequent release of its sorbed As to groundwater (Islam et al. 2004).

5 Conclusions

The major parts of the Ganga plains consist of inter-fluve upland surfaces of the Pleistocene Older Alluvium. Shallow level As-contaminated aquifers of the Holocene age are extensive in the upper and middle Ganga plains and Bengal delta. The Pleistocene sediments capped by aquitardic paleosol and oxidized zone, and sediments beneath them are free of arsenic contamination. The Pleistocene uplands were dissected and entrenched by paleochannels, which were filled by organic rich Holocene sediments, and became prone to As pollution. The environment of the Pleistocene aquifers is not favorable to release sorbed As into groundwater and aquifers' groundwater is generally arsenic-safe. In As-contaminated areas, deeper tubewells in the Pleistocene Older Alluvium aquifers would be a better option for As-safe drinking water in the upper, middle, and lower Ganga plains.

References

- Acharyya, S.K., Shah, B.A.: Groundwater arsenic contamination affecting different geologic domains in India—a review: influence of geological setting, fluvial geomorphology and Quaternary stratigraphy. *Environ. Sci. Health Part A* **42**, 1795–1805 (2007)

- Bureau of Indian Standards: Indian standard: drinking water. Specification (first revision), Amendment vol. 2. New Delhi (2003)
- Central Ground Water Board: Ground water quality in shallow aquifers of India, pp.117. Faridabad (2010)
- Chakraborti, D., Mukherjee, S.C., Pati, S., Sengupta, M.K., Rahman, M.M., Chowdhury, U.K., Lodh, D., Chanda, C.R., Chakraborty, A. K.: Arsenic groundwater contamination in Middle Ganga Plain, Bihar, India: a future Danger? *Environ. Health Perspective* **111**, 1194–1200 (2003)
- Chakraborti, D., Ghorai, S., Das, B., Pal, A., Nayak, B., Shah, B.A.: Arsenic exposure through groundwater to the rural and urban Population in the Allahabad-Kanpur track in the Upper Ganga Plain. *J. Environ. Monit.* **11**, 1455–1459 (2009)
- Islam, F.S., Gault, A.G., Boothman, C., Polya, D.A., Charnock, J.M., Chatterjee, D., Lloyd, J.R.: Role of metal-reducing bacteria in arsenic release from Bengal delta sediments. *Nature* **430**, 68–71 (2004)
- Kinniburgh, D.G., Smedley, P.L.: Arsenic contamination of groundwater in Bangladesh. British Geological Survey Report, WC/00/19. Dhaka (2001)
- Kumar, G., Khanna, P.C., Prasad, S.: Sequence stratigraphy of the foredeep and evolution of the Indo-Gangetic plain, Uttar Pradesh. *Geol. Surv. India Spec. Publ.* **21**, 173–207 (1996)
- Mandal, B.K., Suzuki, K.T.: Arsenic round the world: a review. *Talanta* **58**, 201–235 (2002)
- Nickson, R., Sengupta, C., Mitra, P., Dave, S.N., Banerjee, A.K., Bhattacharya, A., Basu, S., Kakoti, N., Moorthy, N.S., Wasuja, M., Kuma, M., Mishra, D.S., Ghosh, A., Vaish, D.P., Srivastava, A.K., Tripathi, R.M., Singh, S.N., Prasad, R., Bhattacharya, S., Deverill, P.: Current knowledge on the distribution of arsenic in groundwater in five states of India. *Environ. Sci. Health Part A* **42**, 1707–1718 (2007)
- Ravenscroft, P., Brammer, H., Richards, K.: *Arsenic Pollution: a Global Synthesis*. Wiley-Blackwell, Chichester (2009)
- Samanta, G., Roy Chowdhury, T., Mandal, B., Biswas, B., Chowdhury, U., Basu, G., Chanda, C., Lodh, D., Chakraborti, D.: Flow Injection Hydride Generation Atomic Absorption Spectrometry for determination of arsenic in water and biological samples from arsenic-affected districts of West Bengal, India, and Bangladesh. *Microchem. J.* **62**, 174–191 (1999)
- Shah, B.A.: Arsenic in groundwater, Quaternary sediments, and suspended river sediments from the Middle Gangetic Plain, India: distribution, field relations, and geomorphological setting. *Arab. J. Geosci.* **7**, 3525–3536 (2014)
- Smith, A.H., Hopenhayn, C., Bates, M.N., Goeden, H.M., Hertz, I., Duggan, H.M., Wood, R., Kosnett, M.J., Smith, M.T.: Cancer risks from arsenic in drinking water. *Environ. Health Prospective* **97**, 259–267 (1992)
- WHO: *Guideline for drinking water quality. Recommendations*, vol. 1, 2nd edn. Geneva (1993)



Hydrochemical Characteristics and Assessment of the Impact of Mining Activities on Groundwater Quality in Enyigba-Ameri, Southeastern Nigeria

Olufemi Victor Omonona[✉], Amobi Chigozie Ekwe, and George-Best Azuoko

Abstract

Mine water laden with trace elements from mining pits around the Enyigba-Ameri area (EAA), Nigeria, is constantly being discharged into nearby streams without any pre-treatment. Since the entire population of EAA depends on groundwater for their domestic and agricultural uses, it is imperative to assess the impact of mining activities on the groundwater, which is being recharged by streams and precipitation. Water samples were collected during pre-mining (PRM) and post-mining periods (POM) and analyzed for their physicochemical characteristics and trace element concentrations using the standard field and laboratory methods. Gibbs diagrams revealed that rock weathering constitutes the only process that determines the groundwater chemistry during the PRM and POM periods. Groundwater quality assessment using HPI showed that during the PRM, pollution of the groundwater was low and below critical limits, whereas high and above critical limits were found in the POM samples. The observed pollution levels during the POM period can be safely attributed to the release of heavy metals into the environment from mining activities in the area. Management of existing aquifers in the mining area can be enhanced through legislation against indiscriminate mine wastewater disposal. Groundwater planning and development should be concentrated in areas outside the metallogenic nucleus as the cost of remediating contaminated aquifers may not be cost-effective.

Keywords

Enyigba-Ameri area • Post-mining (POM) • Pre-mining (PRM) • Water class • Water quality

1 Introduction

Heavy metal pollution in groundwater is a serious global environmental issue because of its effects on human health and ecosystems due to its high toxicity even at low concentrations (Singh and Kamal 2016; Ouali et al. 2018). Heavy metals could be released into groundwater through geogenic and anthropogenic sources (Reza and Singh 2010). Anthropogenic contamination usually results in very high metal concentrations in groundwater and in the environment (Karbassi et al. 2008) and is derived from sources such as mining and industrial effluents (Nouri et al. 2008). Mining in the Enyigba-Ameri area (EAA) is thought to have some adverse environmental impacts, especially on groundwater and the ecosystem. EAA is entirely underlain by Albian carbonaceous shale, and the area is drained by the Ebonyi River. The aquifers in the area are shallow, less than 40 m, and unconfined. Onwuka et al. (2019) in their study observed the heavy metal distribution at the Central Benue Trough Barite-Saline Field, Nigeria, and confirmed that the groundwater is contaminated with heavy metals, and that there is a high correlation between all the metals and barite. Rwiza et al. (2016) in their study of the gold mining area of Tanzania observed that the groundwater is contaminated by the heavy metals like Fe, Al, As, and Pb. They also observed a strong correlation between metal concentrations in water sampling site and the distance from the mine tailings dam. Heavy metals emanating from mining activities are potential pollutants in groundwater resources. The present study is aimed at evaluating the groundwater quality status of Enyigba-Ameri with respect to physicochemical parameters, major ions, and heavy metal concentrations. The need of assessment of major ions and heavy metal contaminants in water samples is vital in groundwater studies (Kumar et al. 2019a, 2019b; Kumar and Kumar 2019; Gaury et al. 2018).

O. V. Omonona (✉) · A. C. Ekwe · G.-B. Azuoko
Department of Physics/Geology/Geophysics, Alex Ekwueme
Federal University, Ndufu Alike, Nigeria
e-mail: victor.omonona@funai.edu.ng

2 Materials and Methods

A total of 16 groundwater samples (8 samples during the pre-mining period (2009) and 8 samples during post-mining period, 2016)) were collected from the same localities in pre-washed high-density polyethylene bottles from the shallow wells and deep boreholes and analyzed for their physicochemical characteristics and heavy metal contents. Transient parameters (temperature; electrical conductivity (EC); total dissolved solids (TDS) and pH) were measured in situ at the time of sample collection using HachSension2 portable meters. The chemical analyses were carried out at the Chemical Laboratory, UNICEF Assisted Laboratory, Ibadan, Nigeria. Atomic absorption spectrophotometer was used in analyzing the cations, while the anions were analyzed using titration methods in accordance with the APHA (American Public Health Association) standard methods (APHA 2005). Reagent blank determinations were used to correct the instrument readings.

The comparative study of the water quality of the pre-mining (PRM) and post-mining (POM) was carried out using the HPI method described by Edet AE, Offiong OE (2002) (Edet and Offiong 2002).

$$TEPI = \sum_{i=0}^n \frac{H_c}{H_{mac}} \quad (1)$$

where H_c is the monitored concentration of the i th parameter and H_{mac} is the maximum allowable concentration of the i th parameter.

HPI has been effectively employed to characterize groundwater pollution and model groundwater quality of an

area (Tiwari et al. 2017). All the statistical analyses were carried out using Statgraphic Centurion XI.

3 Results and Discussion

3.1 Hydrochemical characteristics

The summary statistics of physicochemical parameters, major ions, and heavy metals is presented in Table 1. The pH values ranged from 7.0 to 7.91 at the PRM period and from 6.02 to 6.21 at the POM period. Groundwater during the PRM was found to be largely neutral, while during POM, the groundwater became acidic in nature. The low pH values during POM may be attributed to the effect of acid mine drainage, emanating from mining activities. The major ion concentrations during PRM and POM periods are in the order of abundance of $Ca^{2+} > HCO_3^- > NO_3^- > K^+ > Mg^{2+} > Na^+ > Cl^- > SO_4^{2-}$ and $HCO_3^- > Ca^{2+} > Mg^{2+} > Cl^- > Na^+ > SO_4^{2-} > K^+ > NO_3^-$, respectively. Pearson's correlation model gives a relationship between two or more variables (Adams et al. 2001). A strong correlation ($r > 0.7$) was observed between pH, K, and NO_3^- which indicates that pH may have played a significant role in the release of the K and NO_3^- ions. TDS was related to the major elements, HCO_3^- , Cl, Na, Ca, and Mg, with a high correlation coefficient ($r > 0.7$). These relationships imply that the major elements contribute to the dissolved solids. A strong correlation ($r > 0.7$) was also observed between K and NO_3^- . The fact that NO_3^- has a strong positive correlation ($r = 0.732$) with K and weak negative correlation coefficient values with other ions (SO_4^{2-} , $r = -0.16$; HCO_3^- , $r = -0.44$; Cl, $r = -0.41$; Na, $r = -0.25$;

Table 1 Summary statistics of the hydrochemical data

	pH	TDS	TH	NO_3^-	SO_4^{2-}	HCO_3^-	Cl	K	Na	Ca	Mg	Fe	Pb	Zn	HPI
PRM															
Min	7.00	52.00	21.00	35.20	0.00	20.00	2.00	10.22	8.20	8.00	0.24	0.01	0.01	0.90	3.83
Max	7.91	494.00	228.00	85.67	58.00	110.00	34.00	31.08	13.78	49.60	13.67	0.98	0.01	1.40	8.16
Mean	7.45	350.18	109.87	54.96	17.00	69.75	17.25	22.23	10.78	30.42	6.37	0.41	0.01	1.10	5.97
CV	0.07	2237.80	390.81	285.25	318.28	106.22	95.92	41.69	3.45	167.36	23.51	0.16	0.00	0.04	26.01
SD	0.28	149.65	19.77	16.88	17.84	32.59	9.79	6.45	1.85	12.93	4.84	0.40	0.00	0.02	1.55
POM															
Min	6.02	18.00	48	0.19	3.00	52.00	6.17	1.00	3.11	16.00	3.91	0.11	0.08	0.11	15.36
Max	6.21	116.00	630	2.41	93.00	630.00	121.08	18.00	76.98	192.00	46.88	1.75	1.82	7.36	200.66
Mean	6.08	317.25	208.25	0.95	23.37	210.75	40.63	7.87	20.27	62.60	15.28	0.95	0.66	2.74	78.33
CV	0.00	153.00	411.00	0.53	889.12	386.73	1216.23	28.12	556.61	3528.55	210.35	0.28	0.14	5.98	94.08
SD	0.06	391.76	64.12	0.73	29.81	196.65	34.87	5.30	23.59	59.40	14.50	0.53	0.06	2.44	73.69

TH—total hardness; HPI—heavy metal pollution index; SD—standard deviation; Min—minimum; max—maximum; CV—coefficient of variation (%)

Ca, $r = -0.35$; Mg, $r = -0.38$) suggests that both K and NO_3 released from the same sources and by the same processes. Gibbs diagram (Fig. 1b) revealed that rock-water interactions (rock dominance) constitute the main physico-chemical controlling process of groundwater chemistry.

3.2 Groundwater water quality

The qualities of groundwater during the two time periods were evaluated using the following quality assessment parameters: pH, TH, TDS, NO_3 , Cl, and SO_4 . The concentrations of these indices were compared with the (WHO 2011) guideline to ascertain their suitability for drinking purposes. During the PRM, the groundwater quality was grossly affected by NO_3 , and 75% of the water samples during the period have a concentration greater than the maximum allowable limit (MAL) of 40 mg/L (it is required that NO_3 contaminated water should be treated before use by pregnant women and infants to avoid methemoglobinemia or “blue-baby” syndrome). However, during the POM, all the water samples have concentrations below the MDL. Hardness tests, such as calcium carbonate, classified the water of the area as soft (37.5%), moderately hard (25%), hard (25%), and very hard (12.5%) during the PRM period and as soft (12.5%), moderately hard (37.5%), hard (12.5%), and very hard (37.5%) during the POM period. This index showed an increase in the deterioration of the water quality during the POM caused by more dissolution of carbonate minerals that is enhanced by an increase in water acidity (lower pH) during the period. The values of pH and TDS and

concentrations of Cl and SO_4^{2-} of all the groundwater samples are far below their maximum allowable limits for both time periods.

3.3 Heavy metals contents and contaminations

The results of the HPI values of groundwater from the area are presented in Table 1 for the two time periods. The table shows that the HPI values during the POM is far greater than those of PRM, and this may be attributed to anthropogenic contributions resulting from the mining activities in the area. HPI values can be classified into three categories, namely low pollution (HPI < 15), medium pollution (HPI = 16–30), and high pollution (HPI > 30) (Edet and Offiong 2002). Thus, there was low pollution of the groundwater during the PRM, with the highest value of HPI at 8.16. After the commencement of mining, the pollution of the groundwater became high, with the least value of HPI at 15.36.

A critical pollution index value of 100 is set (Prasad and Kumari 2008) above which the overall pollution level should be considered unacceptable for drinking water, thus, indicating that groundwater samples are critically polluted with respect to heavy metals. Looking at the results, all the groundwater samples have HPI below the critical pollution index at the PRM period, while all the groundwater samples at the POM period have HPI values above the critical pollution index. This showed a serious deterioration in the quality of the groundwater of the area as a result of mining activities.

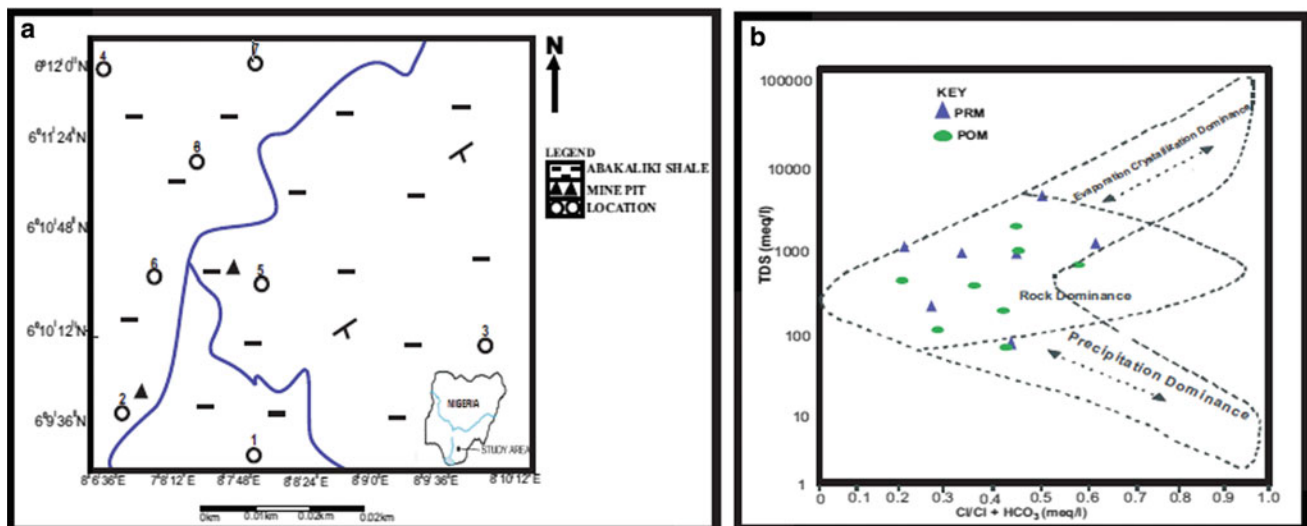


Fig. 1 a: Geological map of the Enyigba-Ameri area; b: Gibbs hydrochemical diagram

4 Conclusion

The present study has revealed that the quality of the groundwater from the Enyigba-Ameri area has been seriously impacted by the release of trace elements emanating from the mining activities going on in the area. Groundwater usage in the area for any intended purpose should be used only after adequate treatment, such as the in situ chelate flushing that has been carried out on the aquifer.

References

- Adams, S., Titus, R., Pietersen, K., Tredoux, G., Harris, C.: Hydrochemical characteristics of aquifers near Sutherland in the Western Karoo. *South Africa J. Hydrol.* **241**(1–2), 91–103 (2001)
- APHA: Standard methods for the examination of water and wastewater. 21st edn American Public Health Association/American Water Works Association/Water Environment Federation, Washington DC (2005)
- Edet, A.E., Offiong, O.E.: Evaluation of water quality pollution indices for heavy metal contamination monitoring. A study case from Akpabuyo-Odukpani area, Lower Cross River Basin (southeastern Nigeria). *GeoJournal* **57**, 295–304 (2002). <https://doi.org/10.1023/B:GEJO.0000007250.92458.de>
- Gaury, P.K., Meena, N.K., Mahajan, A.K.: Hydrochemistry and water quality of Rewalsar Lake of Lesser Himalaya, Himachal Pradesh, India. *Environ. Monit. Assess.* **190**, 84 (2018). <https://doi.org/10.1007/s10661-017-6451-z>
- Karbassi, A.R., Monavari, S.M., Nabi Bidhendi, G.R., Nouri, J., Nematpour, K.: Metal pollution assessment of sediment and water in the Shur River. *Environ. Monit. Assess.* **147**(13), 107–116 (2008). <https://doi.org/10.1007/s10661-007-0102-8>
- Kumar, P., Mahajan, A.K., Meena, N.K.: Evaluation of trophic status and its limiting factors in the Renuka Lake of Lesser Himalaya, India. *Environ. Monit. Assess.* **191**, 105 (2019a). <https://doi.org/10.1007/s10661-019-7247-0>
- Kumar, P., Kumar, P.: Removal of cadmium (Cd-II) from aqueous solution using gas industry-based adsorbent. *SN Appl. Sci.* **1**(4), 365 (2019). <https://doi.org/10.1007/s42452-019-0377-8>
- Kumar, P., Meena, N.K., Mahajan, A.K.: Major ion chemistry, catchment weathering and water quality of Renuka Lake, north-west Himalaya, India. *Environ. Earth. Sci.* **78**, 319 (2019b). <https://doi.org/10.1007/s12665-019-8315-z>
- Negm, A., Bouderbala, A., Chenchouni, H., Barcelo, D.: Water resources in Algeria - Part I: Assessment of Surface and Groundwater. Cham, Springer (2020a). <https://doi.org/10.1007/978-3-030-57895-4>
- Negm, A., Bouderbala, A., Chenchouni, H., Barcelo, D.: Water Resources in Algeria - Part II: Water Quality, Treatment, Protection and Development. Cham, Springer (2020b). <https://doi.org/10.1007/978-3-030-57887-9>
- Nouri, J., Mahvi, A.H., Jahed, G.R., Babaei, A.A.: Regional distribution pattern of groundwater heavy metals resulting from agricultural activities. *Environ. Geol.* **55**(6), 1337–1343 (2008). <https://doi.org/10.1007/s00254-007-1081-3>
- Onwuka, O.S., Umar, N.D., Omonona, O.V., Idris, I.G.: Heavy metals and rare elements distribution in the brine fields of Awe, Keana and Giza, central Benue trough Nigeria. *J. Afr. Earth Sc.* **135**, 103514 (2019). <https://doi.org/10.1016/j.jafrearsci.2019.103514>
- Prasad, B., Kumari, S.: Heavy metal pollution index of ground water of an abandoned open cast mine filled with fly ash: a case study. *Mine Water Environ.* **27**(4), 265–267 (2008)
- Reza, R., Singh, G.: Assessment of heavy metal contamination and its indexing approach for river water. *Int. J. Environ. Sci. Tech.* **7**(4), 785–792 (2010)
- Rwiza, M.J., Kim, K.W., Kim, S.: Geochemical distribution of trace elements in groundwater from North Mara large-scale gold mining area of Tanzania. *Groundwater Monitoring and Remediation* **36**(2), 83–93 (2016). <https://doi.org/10.1111/gwmmr.12152>
- Singh, G., Kamal, R.K.: Heavy metal contamination and its indexing approach for groundwater of Goa mining region. *Appl. Water Sci.* **7**, 1479–1485 (2017). <https://doi.org/10.1007/s13201-016-0430-3>
- Tiwari, A.K., Maio, M., Amanzio, G.: Evaluation of metal contamination in the groundwater of the Aosta valley Region, Italy. *Int. J. Environ. Res.* **11**, 291–300 (2017). <https://doi.org/10.1007/s41742-017-0027-1>
- WHO: Guidelines for Drinking Water Quality. World Health Organization, Geneva (2011)
- Ouali, N., Belabed, B.E., Chenchouni, H.: Modelling environment contamination with heavy metals in flathead grey mullet *Mugil cephalus* and upper sediments from north African coasts of the Mediterranean Sea. *Sci. Total Environ.* **639**, 156–174 (2018). <https://doi.org/10.1016/j.scitotenv.2018.04.377>



Groundwater Hydrochemistry in a Coalmine and Source Analyses of Major Ions (Qingdong Coalmine, China)

Kai Chen, Linhua Sun, and Jiying Xu

Abstract

In this study, forty-six groundwater samples have been collected in the Qingdong coalmine, Northern Anhui Province of China, and their major ion hydrochemistry has been analyzed by multivariate statistical methods in order to get information about the source of major ions, which can help to better understand the water–rock interactions and the identification of the source of inrush water. The results show that the hydrochemical compositions of the groundwater samples from three aquifer systems are different, which imply that they have undergone different types and degrees of water–rock interactions and can be used for the construction of a water source identification model. Weathering of silicate minerals (Source 1) and dissolution of evaporate minerals (Source 2) have been identified to be responsible for the chemical variations of the groundwater, and their contribution ratios have been quantified by the Unmix model.

Keywords

Groundwater • Hydrochemistry • Water–rock interaction • Water inrush

1 Introduction

Due to the high production of coal, a series of disasters occurred during the mining process. Previous studies have shown that water inrush, as one of the five main coalmine

K. Chen · L. Sun (✉) · J. Xu
Key Laboratory of Mine Water Resource Utilization of Anhui
Higher Education Institutes, Suzhou University, Anhui, 234000,
China
e-mail: sunlinh@126.com

K. Chen · L. Sun
School of Earth and Environment, Anhui University of Science
and Technology, Anhui, 232001, China

disasters (water, fire, gas, dust, roof), has brought huge economic losses and/or death to human beings (Wu et al. 2013; Xu and Bu 2015).

A series of natural factors are responsible for the occurrence of water inrush accidents in coalmines: e.g., the quantity of water in the aquifers, the channel for water flow, the hydro-connection between aquifers and the thickness of the water-resisting layer (Gui and Chen 2006). Therefore, understanding the hydrological condition of the coalmine before the water inrush is the most fundamental work for the prevention of water inrush-related accidents in coalmines, and finding out the source of water inrush is the most important one after any water inrush incident (Gui et al. 2016). Therefore, several methods have been proposed (Jiang and Liang 2006; Sun et al. 2007; Chen et al. 2009; Zhang et al. 2009; Zhou et al. 2010; Huang and Chen 2011).

In this study, forty-six groundwater samples have been collected from the three aquifer systems in the Qingdong coalmine, and multivariate statistical methods have been applied to their major ion concentrations in order to get information about: (1) identifying the major ion sources of groundwater in the three aquifer systems and (2) quantifying the contributions of each source.

2 Materials and Methods

The aquifer in the Qingdong coalmine can be divided into four systems, from shallow to deep: loose layer (LA), coal-bearing sandstone (CA), Taiyuan formation limestone (TA), and Ordovician limestone (OA). The main rock types in the LA include clay, sandy clay, and calcareous clay. Permian is the main coal-bearing strata in the area and the main constituent in CA including mudstone, siltstone, sandstone (mainly feldspathic quartz sandstone), and coal seams. Comparatively, the major surrounding rock type in the TA and OA are limestone, followed by mudstone and sandstone.

In this study, forty-six groundwater samples were collected from roadway and borehole in the coalmine in July 2017 (see Table 1). The concentrations of eight kinds of major ions were measured at Key Laboratory of Mine Water Resource Utilization of Anhui Higher Education Institute. The analytical methods are as follows: Na^+ , K^+ , Ca^{2+} , Mg^{2+} , Cl^- , and SO_4^{2-} , which were tested by ion chromatography (ICS-600–900), whereas the HCO_3^- and CO_3^{2-} were tested by traditional acid–base titration. Moreover, Na^+ and K^+ were expressed as $\text{Na}^+ + \text{K}^+$ in the article because of the low concentrations of K^+ and the similarity of chemical properties between them. The qualitative information about the source of the major ions were obtained by factor analysis (Maiz et al. 2000), whereas the US Environmental Protection Agency Unmix model was employed for getting the quantitative information (Reghunath et al. 2002).

3 Results and Discussion

3.1 Major Ion Concentrations

Among these three aquifer systems, the CA samples have the highest mean concentrations of $\text{Na}^+ + \text{K}^+$ (647 mg/L), whereas the TA samples have the highest mean concentrations of Ca^{2+} (321 mg/L), Mg^{2+} (133 mg/L), Cl^- (225 mg/L), and SO_4^{2-} (1556 mg/L) and the LA samples have the highest mean concentrations of HCO_3^- (370 mg/L). For the physical parameters, the LA and CA samples have higher pH values; however, they have relatively lower TDS contents (Table 1). Na- SO_4 type is the most popular one, which occupies 71% of the LA, 100% of the CA, and 42% of the TA samples, respectively (Fig. 1). Comparatively, the UN1 and UN2 samples are divided into Na- SO_4 types, whereas the UN3 and UN4 groundwater samples are classified into Mg- SO_4 and Na- SO_4 types. It can

also be noticed from Fig. 2 that the UN1 and 2 samples are similar to the CA samples, whereas the UN3 and 4 samples are similar to the TA samples.

3.2 Mechanism Controlling Groundwater Chemistry

The Gibbs diagram (Gibbs 1970) has been applied for getting the relationship between groundwater chemistry and the surrounding rock types of the aquifer. The formulas for the calculation are as follows: Gibbs I = $\text{Cl}^- / (\text{Cl}^- + \text{HCO}_3^-)$ and Gibbs II = $(\text{Na}^+ + \text{K}^+) / (\text{Na}^+ + \text{K}^+ + \text{Ca}^{2+})$ (unit in meq/L). After the calculation, the range of the Gibbs I values and Gibbs II values was 0.05–0.97 and 0.38–0.99, respectively. In combination with their TDS contents, such a result indicated that water–rock interaction and evaporation (or dissolution of evaporates) have played important roles in controlling the groundwater chemistry.

Two factors are extracted based on the criterion of eigenvalue >1, and the results were shown in the Table 2. Factor 1, accounting for 46.4% of the total variance explanation, positively corresponded to Ca^{2+} , Mg^{2+} , Cl^- and SO_4^{2-} , but negatively corresponded to HCO_3^- , whereas Factor 2, accounting for 29.8% of the total variance explanation, with positive loadings of $\text{Na}^+ + \text{K}^+$ and negative loadings of Ca^{2+} and Mg^{2+} . Hence, Factor 2 can be explained to be the weathering of silicate minerals, which can release $\text{Na}^+ + \text{K}^+$ and HCO_3^- simultaneously, whereas Factor 1 is associated with the dissolution of chlorides and sulfate minerals, because they can release Ca^{2+} , Mg^{2+} , Cl^- , and SO_4^{2-} into the water.

It is also observed in the plots of factor scores (Fig. 2) that the groundwater samples from different aquifer systems have undergone different types and degrees of water rock interactions: CA—dominated by the weathering of silicate; TA—dominated by the dissolution of chloride and sulfate;

Table 1 Statistical results of parameters of the groundwater samples in three aquifers (mg/L)

Aquifer	$\text{Na}^+ + \text{K}^+$	Ca^{2+}	Mg^{2+}	Cl^-	SO_4^{2-}	HCO_3^-	CO_3^{2-}	pH	TDS
LA (n = 7)	157–265 (223)	3–72 (39)	11–65 (38)	24–161 (97)	100–427 (275)	7–729 (370)	0–76 (21)	7.2–9.1 (8.1)	689–1106 (884)
CA (n = 16)	326–799 (647)	11–119 (46)	5–61 (23)	83–233 (184)	381–1333 (1000)	191–525 (334)	0–98 (17)	7.7–8.9 (8.3)	1105–2649 (2081)
TA (n = 19)	281–566 (384)	196–553 (321)	77–193 (133)	108–283 (225)	1255–2064 (1556)	188–317 (258)	0–14 (1)	7.1–8.5 (7.7)	2322–3524 (2751)
UN (n = 4)	386–697 (534)	56–433 (208)	26–337 (144)	89–205 (145)	1115–3123 (1809)	151–293 (232)	0–14 (5)	7.7–8.3 (7.9)	2077–4557 (2948)

Note—The LA, CA, TA, and UN are the loose layer aquifer, the coal-bearing sandstone aquifer, Taiyuan formation limestone aquifer, and unknown aquifer, respectively

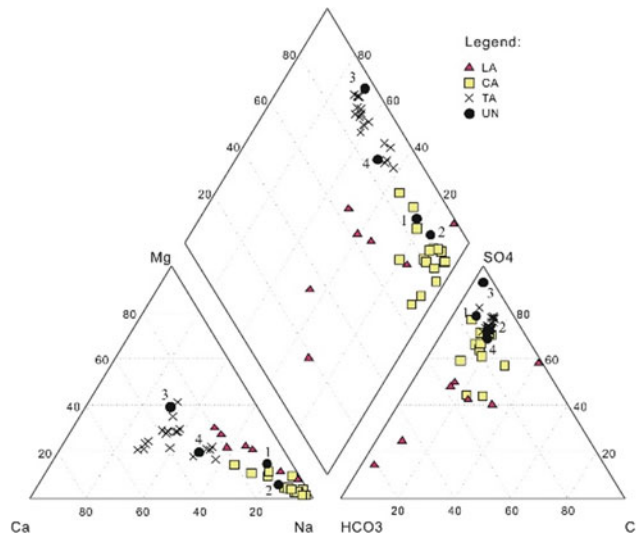


Fig. 1 Piper diagram

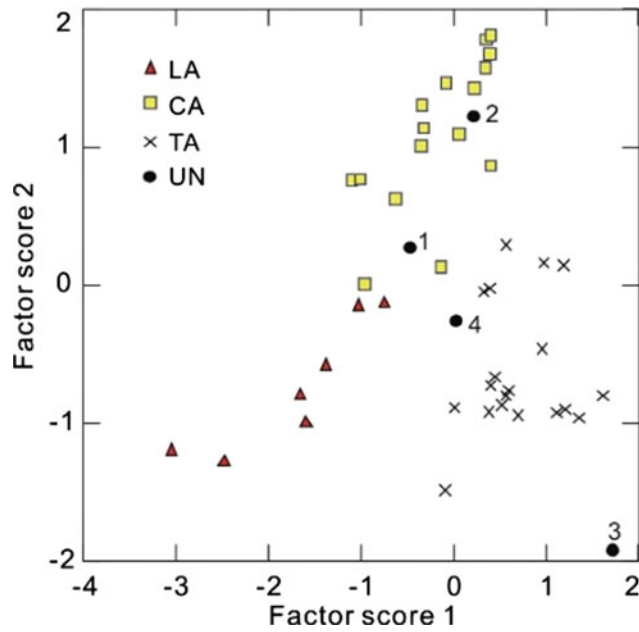
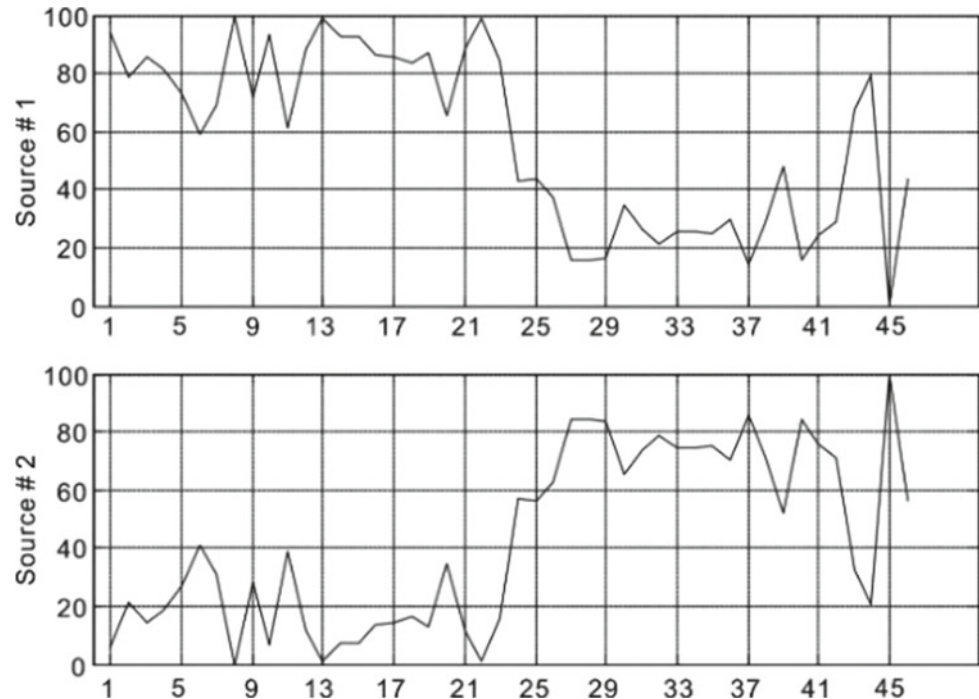


Fig. 2 Plots of factor scores

Table 2 Results of factor analysis

Species	Factor 1	Factor 2
Na ⁺ + K ⁺	0.250	0.894
Ca ²⁺	0.725	-0.615
Mg ²⁺	0.571	-0.745
Cl ⁻	0.784	0.155
SO ₄ ²⁻	0.902	-0.161
HCO ₃ ⁻	-0.667	0.059
Eigen value	2.787	1.787
Variance explained	46.4%	29.8%

Fig. 3 Variations of source contributions. Samples 1–7, 8–23, and 24–42 are the LA, CA, and TA samples, respectively, whereas 43–46 are UN samples



LA—low degrees of water rock interaction relative to the CA and TA.

Two sources were determined by the Unmix model (Fig. 3). Source 1, dominated by $\text{Na}^+ + \text{K}^+$, HCO_3^- , and Cl^- , should be explained by the weathering of silicate minerals and dissolution of chloride, and Source 2, dominated by Ca^{2+} , Mg^{2+} , and SO_4^{2-} , can be explained as the result of the dissolution of evaporate minerals (sulfates). Such considerations can be demonstrated by the contributions of these sources, as the samples from the LA and CA have the highest contributions from Source 1 (>60%), consistent with the truth that this aquifer system is richer in clastic rocks relative to the TA, which was mainly contributed by Source 2 (>50%). As for the samples with unknown sources, Source 1 has high contributions to the UN1 and UN2 (similar to the LA and CA samples), whereas Source 2 has high contributions to UN3 and UN4 (similar to the TA samples).

4 Concluding Remarks

The hydrochemical compositions of the groundwater samples from three aquifer systems are significantly different, which show that the types and degrees of water–rock interactions in these three aquifer systems are different from one another. Two sources were obtained and can be responsible for the chemical variations of the groundwater by factor analysis: weathering of silicate minerals and

dissolution of evaporates, and their contribution ratios to each groundwater sample have been quantified by Unmix model. Such results can be applied for the understanding of water–rock interaction in a coalmine, in order to provide theoretical information for the identification of an inrush water source at a coalmine.

Acknowledgements This work was financially supported by the Academic Funding for Top-talents in Disciplines of Universities in Anhui Province (gxbjZD48), the Foundation of Scholarship Leaders (Reserve) in Suzhou University (2018XJHB08).

References

- Chen, H., Li, X., Liu, A.: Studies of water source determination method of mine water inrush based on Bayes' multi-group stepwise discriminant analysis theory. *Rock Soil Mech.* **30**(12), 3655–3659 (2009)
- Gibbs, R.: Mechanisms controlling world water chemistry. *Science* **170** (3962), 1088–1090 (1970)
- Gui, H., Chen, L.: Hydrogeochemistic evolution and discrimination of groundwater in mining district. Geological Publishing House, Beijing (2006)
- Gui, H., Lin, M., Song, X.: Research on pore water and disaster prevention in China coalmines. *Water Prac. Technol.* **11**(3), 531–539 (2016)
- Huang, P., Chen, J.: Fisher identify and mixing model based on multivariate statistical analysis of mine water inrush sources. *J. China Coal Soc.* **36**(supp1), 131–136 (2011)
- Jiang, A., Liang, B.: The particle swarm optimization support vectors machine method of identifying standard components of ions of groundwater. *J. China Coal Soc.* **31**(3), 310–313 (2006)

- Lewis, C., Norris, G., Conner, T., Henry, R.: Source apportionment of Phoenix PM_{2.5} aerosol with the Unmix receptor model. *J. Air Waste Manag. Assoc.* **53**(3), 325–338 (2003)
- Maiz, I., Arambarri, I., Garcia, R., Millan, E.: Evaluation of heavy metal availability in polluted soils by two sequential extraction procedures using factor analysis. *Environ. Pollut.* **110**(1), 3–9 (2000)
- Reghunath, R., Murthy, T., Raghavan, B.: The utility of multivariate statistical techniques in hydrogeochemical studies: an example from Karnataka, India. *Water Res.* **36**(10), 2437–2442 (2002)
- Sun, L.: Hydrochemical variation during groundwater mixing: a case study with multivariate statistical approach. *Water Prac. Technol.* **8**(3), 399–408 (2013)
- Sun, L., Gui, H.: Establishment of water source discrimination model in coal mine by using hydrogeochemistry and statistical analysis: a case study from Renlou Coal Mine in northern Anhui Province, China. *J. Coal Sci. Eng. (China)* **18**(4), 385–389 (2012)
- Sun, Y., Yang, G., Zheng, L.: Distinguishing system study on resource of mine water inrush based on GIS. *Coal Geol. Explor.* **35**(2), 34–37 (2007)
- Wu, Q., Zhao, S., Sun, W., Cui, F., Wu, C.: Classification of the hydrogeological type of coal mine and analysis of its characteristics in China. *J. China Coal Soc.* **38**(6), 901–905 (2013)
- Xu, H., Bu, W.: Analysis of water-inrush for deep coal floor in a coal mine. *Electron. J. Geotech. Eng.* **20**(10), 4189–4196 (2015)
- Zhang, R., Qian, J., Ma, L., Qin, H.: Application of extension identification method in mine water-bursting source discrimination. *J. China Coal Soc.* **34**(1), 33–38 (2009)
- Zhou, J., Shi, X., Wang, H.: Water-bursting source determination of mine based on distance discriminant analysis model. *J. China Coal Soc.* **35**(2), 278–282 (2010)



Chemical and Organic Contamination Degree of Waters in the Lacustrine Complex of El Kala (Northeastern Algeria)

Badreddine Saadali, El Fadel Derradji, Hicham Zerrouki, Nabil Bougherira, Sofia Bahroun, and Abdelkader Khiari

Abstract

The lacustrine complex of El Kala (LCEK) is recognized for its biodiversity richness and its perennial water resources, which have allowed it to be included in the Ramsar List thanks to the ecological and scientific importance of its wetlands. The lacustrine complex has, therefore, been under protection against all harmful human activities for its preservation. However, the vicinity of the wetlands has been encroached in the last decades, as exemplified by increased socioeconomic activities at the expense of the lacustrine ecosystem. The objective of this work is to identify the degree of chemical contamination of waters and of pollution by organic bodies in relation to the resulting domestic discharges and to the use of fertilizers in agriculture. Therefore, four superficial and six groundwater samples were collected and analyzed in the laboratory for some major chemical and organic parameters, namely sodium, sulfates, chlorides, nitrates, biological oxygen demand, chemical oxygen demand, phosphates, total phosphorus, ammonium, and dissolved oxygen. The contamination index (CI) and the organic pollution index were determined. The CIs' values for the majority of the samples were lower than 7, indicating a low chemical contamination of waters. The organic pollution index ranged from high (2.3) to very high (1.5–1.8), suggesting the waters are polluted by organic substances. Also, the waters in the

LCEK are likely charged with organic bodies in high concentrations, which may cause a risk of pollution of an anthropogenic origin that will have a negative impact on the maintenance of the ecosystem.

Keywords

Ramsar site • Anthropogenic pollution • IHE • Organic substances • Water quality

1 Introduction

Water is life (Cleland and CF 2002) because it guarantees the survival and the maintenance of the living species (Carl 1937), especially the perpetuity of the human being (Gleick 1996). Man needs a good water quality for drinking, irrigating crops, and stimulating the industry growth. He looks for the best places to get water in big quantities, including freshwater ecosystems (rivers, wetlands) (Postel and Richter 2003). Man enters his environment aggressively by destroying the flora, throwing his garbage which contains harmful substances, leading to the degradation of the water quality and biodiversity (Aras et al 2018). Many studies have approached the problem of water contamination by chemical, organic, and metallic bodies (Alfy 2012; Saadali et al 2015; Belabed et al. 2017; Boujghad et al 2019; Haouti et al 2018; Loucif et al. 2020) through the discharge of solid and liquid products depending on the increase in water demand due to population growth and accompanied socioeconomic activities.

The lacustrine complex of El Kala (LCEK) is located in the extreme northeast of Algeria, on the Algerian-Tunisian boundaries. The study area is formed by wetlands classified in the Ramsar List as Waterfowl Habitats: the lacustrine sites (Tonga, Oubeira, Mellah, and Blue Lake), the integral reserve of the Noir Lake peat bog, and the alder stands of Ain-Khiar. The LCEK is approximately within latitude 36°46'–36°55' N and longitude 08°11'–08°38' E (see Fig. 1).

B. Saadali (✉) · H. Zerrouki
Larbi Ben M'hidi University, 04000 Oum El Bouaghi, Algeria
e-mail: saadali.badreddine@univ-ueb.dz

E. F. Derradji · N. Bougherira
Badji Mokhtar University, 23000 Annaba, Algeria

S. Bahroun
Chadli Bendjedid University, 36000 El Tarf, Algeria

A. Khiari
Natural Resources and Management in Sensitive Environments
Laboratory, Larbi Ben M'hidi University, 04000 Oum El Bouaghi,
Algeria

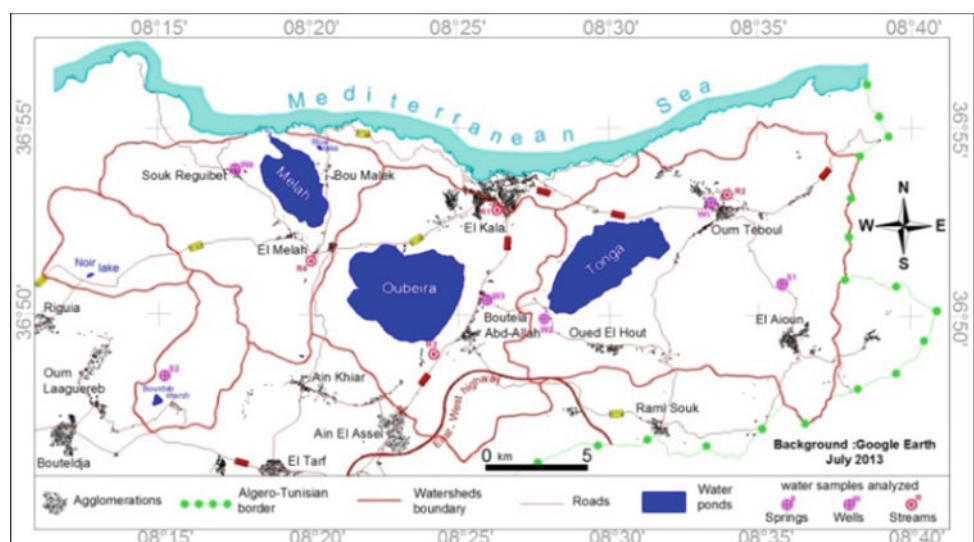
Fig. 1 Location of the study area

According to the aridity index I_{DM} (Martonne 1926), the study area is positioned in the semi-humid climate range, with an I_{DM} equal to 27.29, from the data of El Kala climatic station (1971–2010), an average annual rainfall of 770.1 mm, and an average annual temperature of 18.22 °C. Inside the LCEK, hitherto devoid of any human implantation threatening its biodiversity, there were human infrastructures spreading in parallel with a continued demographic growth (see Fig. 2).

This has led to the degradation of wetlands by socioeconomic activities. In this work, we focused on the interpretation of the chemical and organic parameters of the water samples collected and analyzed in the laboratory to determine the appropriate pollution indices and assess the levels of water contamination in the LCEK waters.

2 Methods

A total of six (06) groundwater samples from hand-dug wells (W) and springs (S) and a total of four (04) superficial water samples from the watercourses (R) were collected during the month of July 2011 (see Fig. 2). The water samples were transferred to Fertial's central laboratory for the determination of sodium (Na^+), sulfates (SO_4^{2-}), chlorides (Cl^-), phosphates (PO_4^{3-}), and total phosphorus (P_2O_5) concentrations. Biological oxygen demand for five days (BOD_5), chemical oxygen demand (COD), nitrates (NO_3^-), and ammonium (NH_4^+) were determined at Horizon laboratory. The dissolved oxygen (O_2) concentrations were determined at the laboratory of the Water and Sanitation Society of Annaba and El Tarf (SEATA).

Fig. 2 Delineation of watersheds and distribution of agglomerations inside the LCEK

The CI is calculated by attributing a number from 1 to 9 (classes) where the obtained concentrations of each of the four chemical parameters (Na^+ , SO_4^{2-} , Cl^- , and NO_3^-) are positioned (see Table 1); the sum of the obtained numbers corresponds to the value of CI. The highest value of CI exceeding the value 7 indicates that the water is very contaminated, and so, very polluted. The following equation is used to calculate the CI (Rouabhia et al 2004):

$$\text{CI} = \Sigma([\text{Na}^+] + [\text{SO}_4^{2-}] + [\text{Cl}^-] + [\text{NO}_3^-])$$

The method of the Institute of Hygiene and Epidemiology (IHE) is feasible by the availability of concentrations of BOD_5 , COD, NH_4^+ , O_2 , PO_4^{3-} , and P_2O_5 . The principle is to position the obtained values of the six organic parameters according to the five classes (see Table 2). The average of the class numbers, obtained by the six parameters, gives the value of the IHE index which is represented according to

five color classes (see Table 3) corresponding to the organic pollution levels (Saadali et al 2019).

3 Results and Discussion

3.1 Contamination Index (CI)

The CI values ranged between 3 and 14 with the majority of the samples (9 out of 10) having low CI (≤ 7). Only one sample of the well (W2), located at Oued El Hout, presents a high CI value of 14 (see Table 4). The high concentrations of chemical elements could be attributed to the presence of salt crystals in the subsoil and the nature of uncultivated soils rich in organic matter (Saadali 2016).

The waters are slightly contaminated and slightly polluted by these chemical elements ($\text{CI} \leq 7$), whereas the water of

Table 1 Interval of classes for chemical parameters (Rouabhia et al 2004)

Class concentration (mg/L)	1	2	3	4	5	6	7	8	9
Na^+	<250	250–500	500–750	750–1000	>1000	–	–	–	–
SO_4^{2-}	<250	250–500	500–750	750–1000	>1000	–	–	–	–
Cl^-	<250	250–500	500–750	750–1000	>1000	–	–	–	–
NO_3^-	<15	15–25	25–35	35–45	45–55	55–65	65–75	75–85	85–95

Table 2 Class interval of organic parameters

Parameter class	BOD_5 (mg- O_2 /L)	COD (mg- O_2 /L)	NH_4^+ (mg-N/L)	Dissolved O_2 (%)	PO_4^{3-} ($\mu\text{g-P/L}$)	P_2O_5 ($\mu\text{g-P/L}$)
5	≤ 1	≤ 5	≤ 0.05	90–110	≤ 50	≤ 50
4	1.1–3	5.1–10	0.06–0.5	70–89	51–100	51–100
3	3.1–5	10.1–20	0.51–1	50–69	101–200	101–200
2	5.1–10	20.1–50	1.01–2	30–49	201–400	201–400
1	>10	>50	>2	<30	>400	>400

Table 3 Water pollution grid according to IHE

Pollution degree	No	Low	Moderate	High	Very high
IHE index	5 - 4.6	4.5 - 4	3.9 - 3	2.9 - 2	1.9 - 1

Table 4 Contamination indexes of analyzed waters

Sample	W1	W2	W3	W4	S1	S2	R1	R2	R3	R4
CI	3	14	7	5	3	3	5	4	3	4

Table 5 Average classes and water pollution degree according to the IHE

Sample	W2	W3	W4	R1	R2	R4
IHE	2.3	2.3	2.3	1.8	1.5	1.8
Pollution degree	High	High	High	V. High	V. High	V. High

the well (W2) is highly contaminated and highly polluted by these elements ($CI > 7$).

3.2 Organic Pollution Degree

The averages calculated of IHE indices are all below 2.9 (see Table 5). The IHE indices have a constant value of 2.3 for groundwater represented by the orange color, but vary between 1.5 and 1.8 for surface water represented by red color.

This indicates that the groundwater has high levels of organic pollutants, while the surface waters contain very high levels of organic pollutants, suggesting that the waters in LCEK are polluted by certain organic elements of anthropogenic source.

4 Conclusions

The purity of the LCEK has been affected by the irrational human intervention on the physical environment normally protected by the state considering its ecological importance. This is exemplified by the computed CI from the results of the chemical analysis conducted on both groundwater and superficial water samples collected from the area. The organic pollution index also indicated a high degree of pollution by organic substances resulting from anthropogenic activities. The consequences of the water quality deterioration could cause dysfunction in the lifestyle of living species. Our main aim of this study was to indicate the water pollution, from human origins, which is one of the main factors of environmental degradation. The findings may provide, to local and scientific communities, an overview of a possible deterioration of aquatic environments and a disruption of the ecological balance that can, in future, affect this sensitive and presumably protected area, by increasing anthropogenic activities and water pollution.

References

- Aras, K., Omed, M., Broder, M.: Geochemical and environmental investigation of the water resources of the Tanjero area, Kurdistan region, Iraq. *Arab. J. Geosci.* **11**, 461 (2018). <https://doi.org/10.1007/s12517-018-3825-7>
- Belabed, B.E., Meddour, A., Samraoui, B., Chenchouni, H.: Modeling seasonal and spatial contamination of surface waters and upper sediments with trace metal elements across industrialized urban areas of the Seybouse watershed in North Africa. *Environ. Monit. Assess.* **189**(6), 265 (2017). <https://doi.org/10.1007/s10661-017-5968-5>
- Boujghad, A., Bouabdli, A., Baghdad, B.: Groundwater quality evaluation in the vicinity of the Draa Sfar Mine in Marrakesh, Morocco. *Euro-Mediterr. J. Environ. Integr.* **4**, 12 (2019). <https://doi.org/10.1007/s41207-018-0096-3>
- Carl, G.C.: Flora and fauna of brackish water. *Ecol* **18**(3), 446–453 (1937). <https://doi.org/10.2307/1930619>
- Cleland, C.E., Chyba, C.F.: Defining 'Life'. *Orig. Life Evol. Biosph.* **32**, 387–393 (2002). <https://doi.org/10.1023/A:1020503324273>
- El Alfy, M.: Integrated geostatistics and GIS techniques for assessing groundwater contamination in Al Arish area, Sinai, Egypt. *Arab. J. Geosci.* **5**(2), 197–215 (2012). <https://doi.org/10.1007/s12517-010-0153-y>
- El Haouti, R., Anfar, Z., Et-Taleb, S., Benafqir, M., Lhanafi, S.E., Alem, N.: Removal of heavy metals and organic pollutants by a sand rich in iron oxide. *Euro-Mediterr. J. Environ. Integr.* **3**, 17 (2018). <https://doi.org/10.1007/s41207-018-0058-9>
- Gleick, P.H.: Basic water requirements for human activities: meeting basic needs. *Water Int* **21**(2), 83–92 (1996). <https://doi.org/10.1080/02508069608686494>
- De Martonne, E.: L'indice d'aridité. *Bulletin de l'Association de géographes français* (9), pp. 3–8, Paris (1926)
- Loucif, K., Neffar, S., Menasria, T., Maazi, M.C., Houhamdi, M., Chenchouni, H.: Physico-chemical and bacteriological quality assessment of surface water at Lake Tonga in Algeria. *Environ. Nanotechnol. Monit. Manag.* **13**, 100284 (2020). <https://doi.org/10.1016/j.enmm.2020.100284>
- Postel, S., Richter, B.: *Rivers for Life: Managing Water for People and Nature*. Island Press, Washington, DC (2003)
- Rouabhia, A., Baali, F., Kherici, N., Djabri, L.: Vulnérabilité et risque de pollution des eaux souterraines de la nappe des sables miocènes de la plaine d'El MA EL Abiod (Algérie). *Sécheresse* **15**(4), 347–352 (2004)
- Saadali, B.: Impact de l'activité anthropique sur la dégradation de la qualité des eaux et de l'environnement : Cas du Parc National d'El Kala (Nord-Est algérien). Doctoral thesis. Annaba University (2016)
- Saadali, B., Derradji, E.F., Saboua, T., Remita, R., Zahi, F.: Impact of the anthropogenic activity on the degradation of the environment and water's quality: El Kala National Park (North East of Algeria). *Rev. Sci. Technol. Synthèse* **30**, 66–75 (2015)
- Saadali, B., Mihoubi, N., Ouddah, A., Bouroubi, B.: Organic pollutants evolution and degrees of contamination of Hammam Grouz dam waters, North-East of Algeria. In: Chaminé, H.I., Barbieri, M., Kisi, O., Chen, M., Merkel, B.J. (eds.) *Advances in Sustainable and Environmental Hydrology, Hydrogeology, Hydrochemistry and Water Resources 2018, Advances in Science, Technology & Innovation*, vol. 1, pp. 145–148. Springer Nature, Switzerland (2019). https://doi.org/10.1007/978-3-030-01572-5_36



Identification of Groundwater Quality and Hydrogeochemical Processes in the Shallow Aquifer of El-Oued (Algerian Sahara)

Boualem Bouselsal and Kamel Zouari

Abstract

The shallow aquifer of El-Oued (South East Algeria) consists of sand, sandstone, clay sand and gypsum of Quaternary-age. It has long been a main source of supply for drinking and agricultural uses. The mechanism of the acquisition of saline load of waters and evaluation of water quality are determined by analyzing the hydrochemical data. This study showed that water quality does not conform with the drinking water and irrigation standards. Currently the surface water is characterized by high salinity ($3.2\text{--}46.1 \text{ mg L}^{-1}$) and, therefore, is less used for domestic purposes. The mineralization of water mainly depends on the dissolution of evaporates (gypsum and halite in particular), the mixing with deep aquifers (the Continental Intercalaire and the Complex Terminal), cationic exchange and anthropogenic activities.

Keywords

Agricultural use • El-Oued • Shallow aquifer • Water quality

1 Introduction

For a long time, water from the shallow aquifer of El-Oued has been used by the population for drinking and irrigation purposes. Due to the increasing demand for water in the region, people use water from deep sources (the Continental Intercalaire aquifer and the Complex Terminal aquifer). The shallow aquifer, without treatment, may be

polluted and thus can affect the regions of the lower Sahara (Saibi et al. 2009; Bouselsal and Kherici 2014). The objective of this study is to evaluate the water quality of the shallow aquifer for different uses and to understand its mineralization process.

2 Study Site

The study area is located in southeastern Algeria. It includes the most important urban centers of the Wilaya which extends from Ogla in the South to Kouinine in the North, with agricultural zones on the East and West borders of the urban centers. It lies between $290000 \text{ E}/315000 \text{ E}$, and $3680000 \text{ N}/3700000 \text{ N}$, spread over an area of 500 km^2 , with a population of about 250,000.

The El-Oued aquifer system is characterized by the superposition of three aquifer layers (UNESCO 1972; OSS 2003). These are from bottom to top, the Continental Intercalaire aquifer (CI), the Complex Terminal aquifer (CT) and the shallow aquifer. The latter consists of Quaternary-age detrital formations represented by sands, sandstones, clay sands and gypsum, with a substratum made of clay. The average depth of the substratum is 60 m. The piezometric map (Fig. 1) shows that the flow of the aquifer is generally from SW to NE. Urban centers and agricultural areas are irrigated from deep aquifers form piezometric domes, resulting in the rapid infiltration of urban water and the return of pumped irrigation water from boreholes that capture deep aquifers (CT and CI).

3 Materials and Methods

For the realization of this study, a sampling campaign and hydrochemical measurements were carried out using twenty-five (25) water samples collected from the boreholes

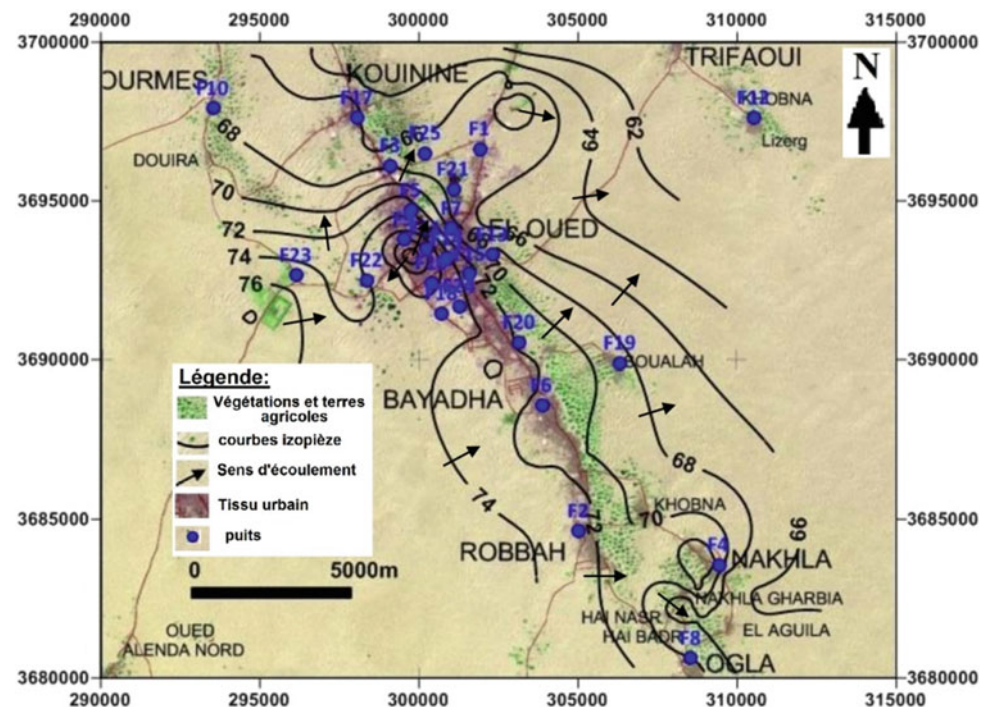
B. Bouselsal (✉)

Laboratoire des Réservoirs Souterrains Pétroliers Gaziers et Aquifères, Kasdi Merbah University, Ouargla, Algeria

K. Zouari

Laboratoire de Radio-Analyse et Environnement, Ecole Nationale des Ingénieurs de Sfax, Sfax, Tunisia

Fig. 1 Piezometric map of June 2017 and positioning of sampled wells



of the free shallow aquifer of El-Oued (Fig. 1), in June 2017. The physico-chemical parameters (pH, temperature and electrical conductivity) were determined in situ, using a portable multimeter. Water samples were collected in polyethylene sampling bottles following the Rodier (Rodier 1383) sampling protocol for laboratory analysis.

The statistical analysis was done using XLSTAT 2015 for Windows. In order to assess the chemical quality of water against the World Health Organization (WHO) drinking water standards and to identify the most important factors controlling the groundwater geochemistry, the principal component analysis (PCA) was conducted. Twelve (12) hydrochemical variables and twenty-five (25) samples were processed using multivariate statistical techniques.

4 Results and Discussions

4.1 Ability of Water for Human Consumption

Based on the results in Table 1, the waters of the shallow aquifer were found to be non-potable. The salinity observed was very high, in the range of 3.25–46.10 (mg L^{-1}), whereas the total hardness ranged from 104.2 to 1513.6 French degrees. According to WHO (WHO 2011; Kumar et al. 2019a), water is classified as hard to very hard. The nitrate value exceeds the limit of 50 mg L^{-1} .

4.2 Suitability of Water for Agricultural Use

The curve of the American salinity diagram (Fig. 2), according to Richards (Richards 1954; Kumar et al. 2019b; Gaury et al. 2018), in which the electrical conductivity is considered as salinity hazard and SAR as sodium risk (alkalinity), showed that a sample (F_{17}) fell within the C_4S_1 class indicating that the sampled water had a very high salinity and a low sodium adsorption ratio. Seventeen samples belonged to the C_4S_2 class indicating a very high salinity and an average adsorption rate of sodium. Four water samples (F_1 , F_7 , F_{13} and F_{23}) fell into class C_4S_3 indicating water that is unsuitable for irrigation but can be used under certain conditions; very permeable soils, good leaching and salt-tolerant plants. Finally, three samples (F_{21} , F_{22} and F_{25}) had a very high electrical conductivity ($EC > 10,000 \mu\text{S/cm}$) and $SAR > 30$, which indicated that the water is unsuitable for irrigation (Bouaroudj et al. 2019). The high salinity is due to very arid climatic conditions, causing strong evaporation which concentrates the soil solution (Chevry and Robert 1998).

4.3 Origins of Mineralization of Waters

The principal component analysis performed on the basis of the previous 12 parameters was limited to two factors (F_1 and F_2), which accounted for 85.79% of the total

Table 1 Basic statistics of the physicochemical parameters of the shallow aquifer

Parameter	WHO Standards	Min	Max	Mean
Ca ²⁺ (mg L ⁻¹)	200	200	5625	719.3
Mg ²⁺ (mg L ⁻¹)	150	81.9	1408	269.3
Na ⁺ (mg L ⁻¹)	200	130	9562.5	946.2
K ⁺ (mg L ⁻¹)	12	18.5	540	79.2
Cl ⁻ (mg L ⁻¹)	500	240	13,650	1556.7
SO ₄ ²⁻ (mg L ⁻¹)	400	960	15,125	2390.9
HCO ₃ ⁻ (mg L ⁻¹)	240	58	741.2	315.1
NO ₃ ⁻ (mg L ⁻¹)	50	0	247.5	119.6
Temperature (°C)	18–25	22.1	30.4	25.1
pH	6.5–8.5	6.8	8.8	7.5
Dissolved matter (mg L ⁻¹)	1500	3256	46,100	7427.1
EC (µS/cm)	1000	3334	47,200	7832.6

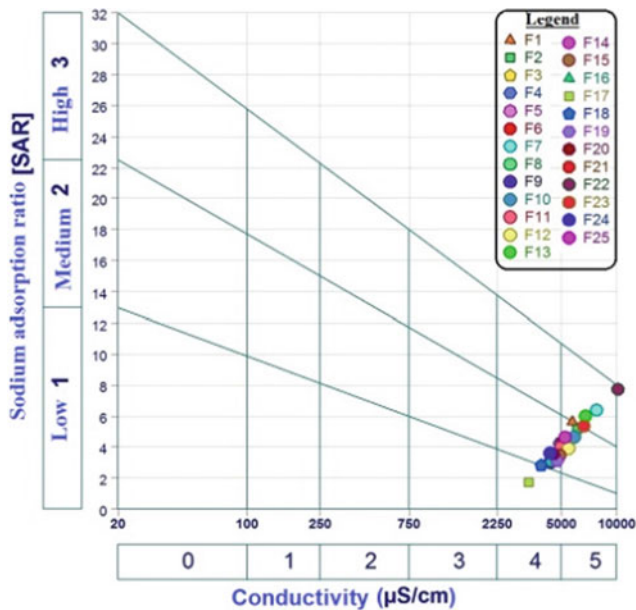


Fig. 2 Evolution of SAR as a function of water conductivity

variance. The projection of the variables on the F₁-F₂ plot (Fig. 3) showed that the factor F₁ represented 71.23% of the total variance. It was considered a major factor in water mineralization since it was strongly correlated with most major elements (Ca²⁺, Na⁺, K⁺, SO₄²⁻, Cl⁻). This indicates that the interaction of the waters with the host rock, in particular the evaporites (NaCl, CaCl₂, KCl, CaSO₄·2H₂O and Na₂SO₄), played an important role in the acquisition of water salinity (Slimani et al. 2017). On the other hand, the F₁ axis opposing nitrate to the rest of the major elements reflected the result of anthropogenic processes, including nitrate contamination related to the application of chemical fertilizers in agricultural areas and the infiltration of

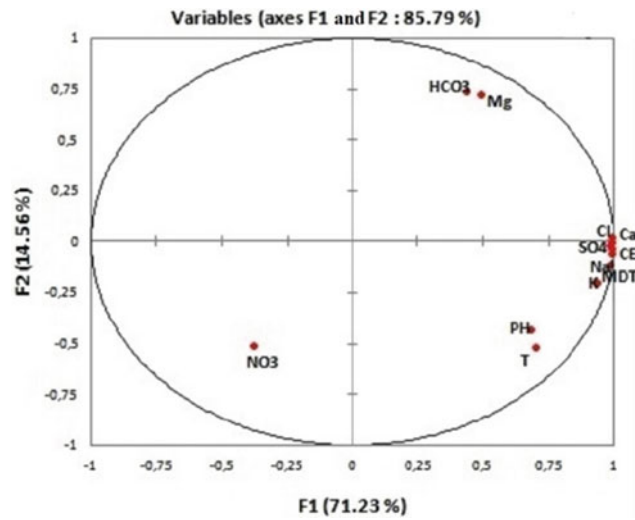


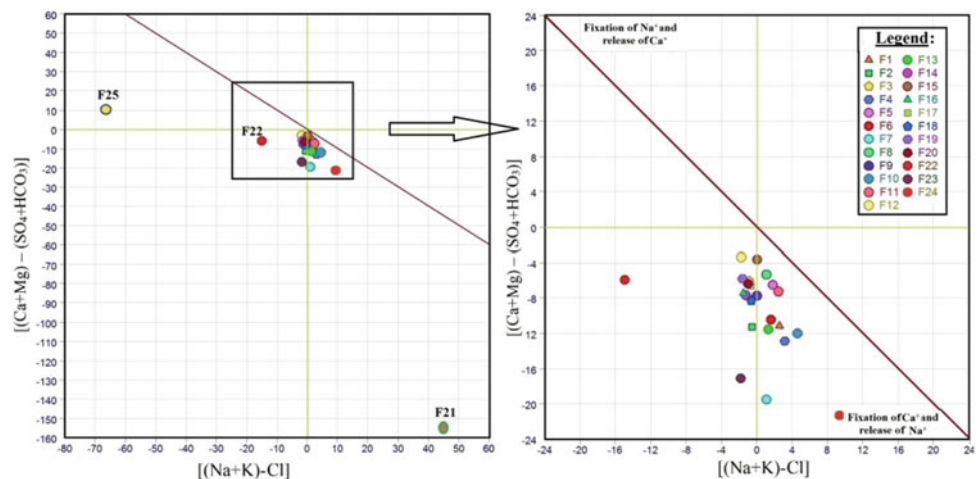
Fig. 3 Principal component analysis of the variables

domestic wastewater (Rahmati et al. 2019; Sajedi-Hosseini et al. 2018) because of the virtual absence of the sanitation network.

The factor F₂, which represented 14.56% of the total variance, opposed the magnesium (Mg) and the bicarbonate (HCO₃) against the rest of the major elements, testifying for the effect of the mixing of the waters of deep layers (CT and CI) on the chemistry of the waters of the shallow aquifer (Guendouz et al. 2006).

Calculation of saturation indices of calcite and dolomite by the FREEQC (Parkhurst and Appelo 2013) software showed different degrees of saturation. In fact, the calcite varies from -0.27 to +2.49; the dolomite, -0.46 to +4.04. Therefore, it could be inferred that the majority of the water taken is saturated, due to the contribution of these minerals. Evaporitic minerals had lower degrees of saturation than

Fig. 4 Correlation diagram of $[(Mg + Ca) - (SO_4 + HCO_3)]$ and $(Na + K - Cl)$ of the water shallow aquifer of El-Oued



carbonate minerals. Gypsum had indexes ranging from -0.65 to $+1.05$ (where 8% of the water samples did not reach the saturation point), followed by anhydrite, whose index varied from -0.87 to $+0.87$ (92% of the wells were under-saturated). Finally, the halite whose indices varied from -6.16 to -2.74 and thus was considered as under-saturated.

The baseline exchange between groundwater and the sandy-clayey and sandy-clay formations of the aquifer was evidenced by the relation $[(Mg^{+2} + Ca^{+2}) - (SO_4^{-2} + HCO_3^{-})]$ as a function of $(Na^+ + K^+ - Cl^-)$ (Fig. 4) (Garcia et al. 2001), which showed an increase in $(Na^+ + K^+)$ levels in relation to the decrease in $(Mg^{+2} + Ca^{+2})$ level for the majority of the sampled points. However, a group consisting of three points (F₂₁, F₂₂ and F₂₅) was distinguished in the DIAGRAM software with a ratio of SO_4^{-2}/Cl^- less than 1. These samples were supersaturated in gypsum and anhydrite, a consequence of the strong evaporation of water, located at a very shallow depth (<0.40 m).

5 Conclusion

The geochemical study of the shallow aquifer of El-Oued made it possible to evaluate the quality of the water supply intended for drinking and irrigation purposes. The water quality does not comply with WHO drinking water standards as it is highly mineralized with nitrate contents exceeding the recommended values. The water quality is also unsuitable for irrigation purposes because it is very saline and of poor-to-bad quality by Riverside standards.

Multivariate and geochemical statistical analysis showed that the mineralization of the waters of the shallow aquifer is related to the dissolution of evaporites (gypsum and halite in particular), mixing with the waters of deep aquifers (CT and CI), cation exchange and anthropogenic inputs.

References

- Bouaroudj, S., Menad, A., Bounamous, A., Ali-Khodja, H., Gherib, A., Weigel, D.E., Chenchouni, H.: Assessment of water quality at the largest dam in Algeria (Beni Haroun Dam) and effects of irrigation on soil characteristics of agricultural lands. *Chemosphere* **219**, 76–88 (2019). <https://doi.org/10.1016/j.chemosphere.2018.11.193>
- Bouselsal, B., Kherici N.: Effets de la remontée des eaux de la nappe phréatique sur l'homme et l'environnement : cas de la région d'El-Oued (Sud-Est Algérie). *Afr. Sci.* **10**(3) (2014)
- Chevry, C.L., Robert, M.: La dégradation des sols irrigués et de la ressource en eau : une menace pour l'avenir de l'agriculture et pour l'environnement des pays au sud de la méditerranée. *Etude Et Gestion Des Sols* **5**(4), 217–226 (1998)
- Garcia, M.G., Hidalgo, M.D.V., Blesa, M.A.: Geochemistry of groundwater in the alluvial plain of Tucuman province Argentina. *J. Hydrol.* **9**, 597–610 (2001). <https://doi.org/10.1007/s10040-001-0166-4>
- Gaury, P.K., Meena, N.K., Mahajan, A.K.: Hydrochemistry and water quality of Rewalsar Lake of Lesser Himalaya, Himachal Pradesh India. *Environ. Monit. Assess.* **190**(2), 84 (2018). <https://doi.org/10.1007/s10661-017-6451-z>
- Guendouz, A.H., Moulla, A.S., Remini, B., Michelot, J.L.: Hydrochemical and isotopic behaviour of a Saharan phreatic aquifer suffering severe natural and anthropic constraints (case of Oued-Souf region, Algeria). *Hydrol. J.* **14**, 955–968 (2006). <https://doi.org/10.1007/s10040-005-0020-1>
- Kumar, P., Mahajan, A.K., Meena, N.K.: Evaluation of trophic status and its limiting factors in the Renuka Lake of Lesser Himalaya India. *Environ. Monit. Assess.* **191**(2), 105 (2019a). <https://doi.org/10.1007/s10661-019-7247-0>
- Kumar, P., Meena, N.K., Mahajan, A.K.: Major ion chemistry, catchment weathering and water quality of Renuka Lake, north-west Himalaya India. *Environ. Earth Sci.* **78**(10), 319 (2019b). <https://doi.org/10.1007/s12665-019-8315-z>
- OSS (Observatoire Sahara et Sahel): Système aquifère du Sahara septentrional: gestion commune d'un bassin transfrontière. Rapport de synthèse. OSS, Tunisie, pp. 322 (2003)
- Parkhurst, D.L., Appelo, C.A.J.: Description of input and examples for PHREEQC version 3 -A computer program for speciation, batch-reaction, one-dimensional transport, and inverse geochemical calculations: U.S. Geological Survey Techniques and Methods, book 6, chap A43, pp. 497 (2013)
- Rahmati, O., Choubin, B., Fathabadi, A., Coulon, F., Soltani, E., Shahabi, H., Bui, D.T.: Predicting uncertainty of machine learning

- models for modelling nitrate pollution of groundwater using quantile regression and UNEEC methods. *Sci. Total Environ.* **688**, 855–866 (2019). <https://doi.org/10.1016/j.scitotenv.2019.06.320>
- Richards, L.A.: Diagnosis and improvement of saline alkali soils. US Department of Agriculture, Handbook no. 60. Washington, DC (1954)
- Rodier, L.: Analyse de l'eau: eaux naturelles, eaux résiduaire, eau de mer. 8th edn. Dunot, Paris, pp. 1383 (1984)
- Saibi, H., Semmar, A., Mesbah, M., Ehara, S.: Variographic analysis of water table data from the Oued-Souf phreatic aquifer, North Eastern part of the Algerian Sahara. *Arabian J. Geosci.* **2**, 83–93 (2009). <https://doi.org/10.1007/s12517-008-0021-1>
- Sajedi-Hosseini, F., Malekian, A., Choubin, B., Rahmati, O., Cipullo, S., Coulon, F., Pradhan, B.: A novel machine learning-based approach for the risk assessment of nitrate groundwater contamination. *Sci. Total Environ.* **644**, 954–962 (2018). <https://doi.org/10.1016/j.scitotenv.2018.07.054>
- Slimani, R., Guendouz, A.H., Trolard, F., Moulla, A.S., Hamdi-haïssa, B., Bourrié, G.: Identification of dominant hydrogeochemical processes for groundwaters in the Algerian Sahara supported by inverse modeling of chemical and isotopic data. *Hydrol. Earth Syst. Sci.* **21**, 1669–1691 (2017). <https://doi.org/10.5194/hess-21-1669-2017>
- UNESCO.: Etude des Ressources en Eau de Sahara Septentrional. UNESCO, Paris, France (1972)
- WHO.: Guidelines for drinking-water quality, 4th edn, pp. 564 (2011)



Stable Isotope Evidences on Mechanisms and Sources of Groundwater Recharge in Quaternary Aquifers of Kelantan, Malaysia

Mohammad Muqtada Ali Khan, Kishan Raj, Aweng A./L. Eh Rak, Hafzan Eva Mansor, Roslanzairi Mostapa, Kamarudin Samuding, and Zameer Ahmad Shah

Abstract

It is vital to outline the mechanisms of recharge of aquifers as far as water resources management is concerned. Monitoring variations in isotopic signatures ($\delta^{18}\text{O}$ and $\delta^2\text{H}$) can provide us with valuable inputs on groundwater recharge processes. In the present study, the stable isotope ($\delta^{18}\text{O}$ and $\delta^2\text{H}$) contents of groundwater, rainwater, and surface waters from the Northern parts of Kelantan, Malaysia, were employed to trace the recharge processes. In the Kelantan area, the recharge of shallow groundwater is mainly due to precipitation from northeast monsoon. The recharge mechanisms for shallow groundwater, especially in low-lying areas, are the infiltration of surface water. The primordial isotopic signatures (pre-evaporation) of post-season groundwater samples fall well within the isotopic range of post-season rainwater, signifying direct recharge from precipitation without any major fractionation. The narrow isotopic range for post-season implies that groundwater recharge for post-season occurs during a limited interval compared to pre-season. The aquifer in the area is isotopically heterogeneous and shows enrichment towards north-west during post-season and south-east during pre-season.

Keywords

Mechanism • Groundwater recharge • Environmental isotopes • Malaysia

M. M. A. Khan (✉) · K. Raj · A. A./L.E. Rak · H. E. Mansor
Faculty of Earth Science, Universiti Malaysia Kelantan,
Campus Jeli, 17600 Jeli, Kelantan, Malaysia
e-mail: muqtada@umk.edu.my

R. Mostapa · K. Samuding
Malaysia Nuclear Agency, 43000 Kajang, Bangi, Malaysia

Z. A. Shah
Geological Survey of India, Northern Region, Jammu,
UT: Jammu & Kashmir 180006, India

1 Introduction

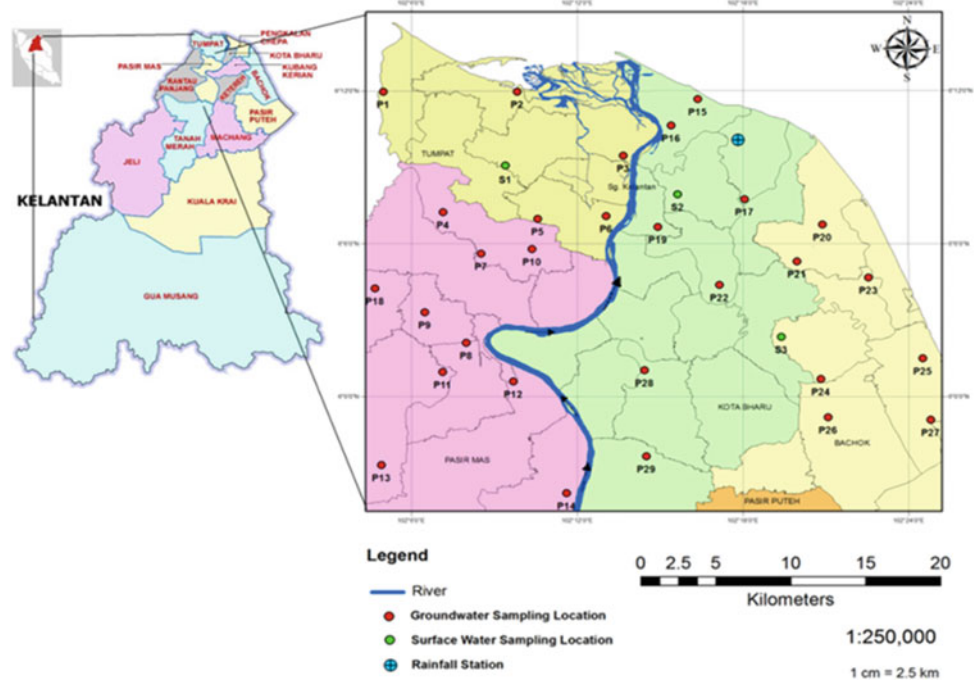
Population increase in Kelantan is putting a consistent and ever-increasing pressure on fresh groundwater resources. Groundwater is the main source of water supply in Kelantan as far as the drinking water supply is concerned. It is essential to assess and monitor the recharge in Kelantan area under any water resource management programme. Any variation in hydrogen (^2H) and oxygen (^{18}O) in precipitation forms the main primary data required for groundwater recharge investigations (Ingraham et al. 1998; Gupta and Deshpande 2003; Kortelainen 2009; Gat 2010; Voss et al. 2018). These include the sources and timing of recharge, retention time and circulation of groundwater (Kortelainen 2009). Such a study will require long-term data of stable isotopes in rainfall (IAEA/WMO. 2015). Regrettably, stable isotope data of precipitation in Kelantan are not available, nor has any detailed groundwater stable isotopic investigation been carried out yet. The meteoric water line, which is important in groundwater recharge evaluation, has not been established in the Kelantan. For a comprehensive groundwater recharge assessment, there is a need for additional isotopic data of rainfall in Kelantan meteoric line.

The main aim of the investigation is to understand the differences and relationships in isotopic compositions within various water types and to assess the source and mechanism of groundwater recharge.

2 Materials and Methods

The present study is confined to the northern part of Kelantan state in Malaysia which covers an area of approximately 1400 km². The area lies between latitudes 5° 55" and 6° 15" north, and between longitudes of 102° 4" and 102° 25" east (Fig. 1). Geologically, the area is covered by Quaternary sediments with granitic bedrock. The sediments from the quaternary comprise marine, fluvial and other

Fig. 1 Sampling locations in parts of Kelantan. (Source: Modified by JUPEM)



deposits observed in main rivers and coastal region. The study area experiences a humid tropical climate controlled by two monsoon seasons (i.e. northeast and southwest monsoon) and characterized by wet and dry seasons throughout the year.

Twenty-nine groundwater samples were collected uniformly over the entire study area during pre-seasons (January 2016) and post-seasons (June 2016), respectively. All the groundwater samples were collected from first aquifer in which groundwater depth is very shallow (< 8 m). Three surface water samples were also collected from river waters and other small tributaries from locations S1, S2 and S3. Apart from that, rain water samples were collected on monthly basis for a period of a year from July 2015 to June 2016 to create a local meteoric water line. Analysis of isotopic compositions of $\delta^{18}\text{O}$ and $\delta^2\text{H}$ is conducted at Malaysia Nuclear Agency using IRMS instrument.

3 Results

3.1 Isotopic Composition of Groundwater and Surface Water Samples

The average values of $\delta^{18}\text{O}$ in groundwater during both pre-season and post-season are -5.30‰ and -6.40‰ , respectively. From the calculated pre-season data, the regression line that best fit the equation is generated as follows:

$$\delta^2\text{H} = 6.7355\delta^{18}\text{O} + 7.1617$$

The best fit regression line equations for groundwater samples collected during the post-season is expressed as:

$$\delta^2\text{H} = 4.936\delta^{18}\text{O} - 7.3869$$

From the analysis, the surface water has $\delta^2\text{H}$ values in the range of -37.41 to -26.88‰ , and $\delta^{18}\text{O}$ values ranging from -6.9 to -5.9‰ during the pre-season. The average values of $\delta^2\text{H}$ and $\delta^{18}\text{O}$ during the pre-season are -33.78‰ and -6.47‰ , respectively. For the post-season, the $\delta^2\text{H}$ values are recorded between -38.45 and -33.17 , while for $\delta^{18}\text{O}$, the value ranges from -5.7 to -5.63‰ . The average value of $\delta^2\text{H}$ calculated during the post-season is -35.52‰ , whereas for $\delta^{18}\text{O}$ values is -5.65‰ , respectively.

3.2 Groundwater Relationships of $\Delta 2\text{H}$ and $\Delta 18\text{O}$ During the Pre-Season

The groundwater trend line equations slope reveals a less steep slope compared to LMWL trend lines as shown in (Fig. 2). An effort is made to identify the possible genesis of isotope sources in groundwater prior to process, such as evaporation, by evaluating the change in slope of both stable isotopic compositions of $\delta^2\text{H}$ and $\delta^{18}\text{O}$ as the trend line deviates from the local meteoric water line. Based on the plot, it can be understood that natural processes, such as evaporation, influence the water movements in the study area as it explains the scattering of the samples' plots.

Fig. 2 Plot of $\delta^2\text{H}$ versus $\delta^{18}\text{O}$ during pre-season January 2016

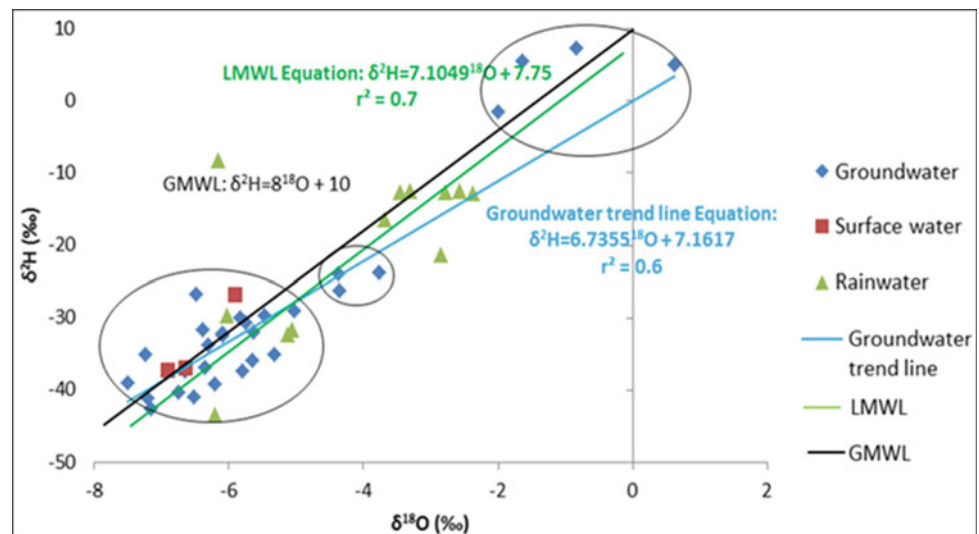
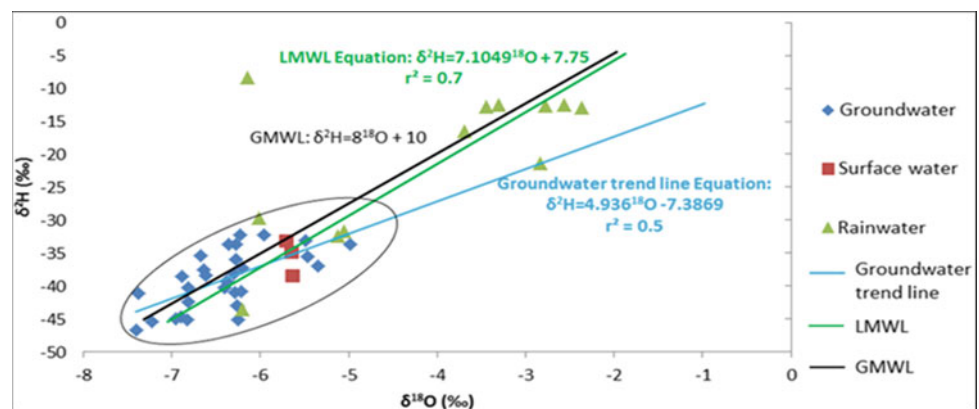


Fig. 3 Plot of $\delta^2\text{H}$ versus $\delta^{18}\text{O}$ during post-season June 2016



From the plots, three significant clusters are observed in terms of $\delta^{18}\text{O}$ configurations in groundwater. The first cluster exhibits low $\delta^{18}\text{O}$, ranging from -8 to -5‰ , with major groundwater plots. The second cluster ranges plots at around -4‰ , with three groundwater plots, while the third cluster ranges from -2 to 1‰ , with four groundwater plots. These different clusters may denote recharge of groundwater via rainfall activities, possibly from different monsoons, including north-east monsoons and south-west monsoons which transport precipitates with varying isotopic compositions. The cluster depicts varying recharging conditions which portray to similar depths. A closer observation of $\delta^2\text{H}$ - $\delta^{18}\text{O}$ composition during the seasonal changes depicts minor variations. These can be attributed to low residence periods of the water bodies.

3.3 Groundwater Relationships of $\Delta 2\text{H}$ and $\Delta 18\text{O}$ During the Post-Season

For the post-season, the groundwater trend line equation reflects a less steep slope compared to slopes of pre-season

trend line as depicted in (Fig. 3). Yet, the pre-season trend line slopes are lower than the local meteoric water line. Few groundwater samples are observed to be plotted below the local meteoric water line denoting enrichment of isotope which occurs as a result of evaporation processes taking place directly upon the soil surfaces exposed during the recharge phase. For the post-season, most of the sample plots fall near the local meteoric water line which denotes processes such as evaporation that appear to impact the shallow groundwater system. Based on the plot of the trend line, it can be inferred that surface water samples from post-seasons are more prone to evaporation state compared to samples from the pre-season as surface water samples plotted during these period lie close and below the groundwater trend line as shown in (Fig. 3).

4 Discussion

A comparison of the stable isotopic signatures of groundwater and precipitation of both pre- and post-seasons indicates that the precipitations are the main source of

groundwater recharge in the area. The recharge mechanisms for shallow aquifers, especially in low-lying areas are the infiltration of surface water. The primordial isotopic signatures (pre-evaporation) of post-season groundwater samples fall well within the isotopic range of post-season rainwater signifying direct recharge from precipitation without any major fractionation. The narrow isotopic range for the post-season implies that groundwater recharge for post-seasons occurs during a limited interval compared to the pre-season. A closer observation of $\delta^2\text{H}$ - $\delta^{18}\text{O}$ composition during the seasonal changes depicts minor variations. These can be attributed to low residence periods of the water bodies owing to the shallow nature of the aquifer. In addition, there is no clear indication of elevated values or abnormality in $\delta^2\text{H}$ and $\delta^{18}\text{O}$ values suggesting a single (or identical) input source(s) in the course of recharge period. The aquifer in the area is isotopically heterogeneous and shows enrichment towards the north-west during the post-season, and the south-east during the pre-season.

5 Conclusions

The application of stable isotopes has presented significant contributions and clarifications on groundwater systems. Based on the explanation, it can be inferred that most groundwater regimes are being recharged by the local precipitates or rainwater. Besides, the isotopic signature shows certain processes which influence groundwater and surface water, such as evaporation processes. To conclude, the groundwater resources in the study area commonly comprise sources from recent origins. Keeping the shallow nature of the aquifer in the area under consideration, all human activities which can directly or indirectly affect the aquifer

must be monitored regularly. The findings of this study enable and quantify an enhanced understanding regarding groundwater resources in the northern parts of Kelantan, thus aiding and benefiting related governance on developing systematic utilization methods to better manage these precious resources.

Acknowledgments The authors are highly thankful to the faculty of Earth Science, Universiti Malaysia Kelantan, Campus Jeli, for basic facilities to carry out this research work. Dr. Wan Zakaria from Nuclear Agency Malaysia is warmly thanked for providing vital inputs throughout this study.

Funding: The financial assistance is received from Fundamental Research Grants (R/FRGS/A08.00/00644A/002/2015/000228 and R/FRGS/ A0800/00644A/003/2018/00556) is highly acknowledged.

References

- Gat, J.R.: Isotope hydrology: a study of the water cycle. In: Series on Environmental Science and Management, vol. 6. Imperial College Press, London (2010)
- Gupta, S.K., Deshpande, R.D.: Synoptic hydrology of India from the data of isotopes in precipitation. *Curr. Sci.* **85**, 1591–1595 (2003)
- IAEA/WMO.: Global network of isotopes in precipitation. The GNIP database. Accessible at <http://www.iaea.org/water> (2015)
- Ingraham, N.L.: Isotopic variations in precipitation. In: Kendall, C., McDonnell, J.J. (eds.) *Isotope Tracers in Catchment Hydrology*, pp. 87–118. Elsevier, Amsterdam (1998)
- Kortelainen, N.: Isotopic composition of atmospheric precipitation and shallow groundwater in Olkiluoto: O-18, H-2 and H-3. Working report 2009–06, Posiva (2009)
- Voss, K.A., Bookhagen, B., Sachse, D., Chadwick, O.A.: Variation of deuterium excess in surface waters across a 5000-m elevation gradient in the east-central Himalaya. *Hydrol. Earth Syst. Sci.* (2018). <https://doi.org/10.5194/hess-2018-534>



Identification of Contamination Sources Through the Application of Nitrogen, Oxygen and Deuterium Isotopes in Estarreja Shallow Aquifer, Aveiro (Portugal)

Ana Carolina Pires Marques, Maria do Rosário Carvalho, and Eduardo Anselmo Ferreira da Silva

Abstract

Agriculture and the chemical industry are the most important activities in the Estarreja municipality and have put at risk the quality of surface water and groundwater, leading to a great vulnerability of the Estarreja shallow aquifer. In this respect, the main goal of the present study is the identification of contamination sources through the application of nitrogen and oxygen isotopes, beside the deuterium and oxygen isotopes in the Estarreja shallow aquifer. Results of $\delta^{15}\text{N}$ and $\delta^{18}\text{O}$ indicate isotopic signatures for ammoniacal fertilizers, wastewater and animal manure, clearly showing the influence of industrial and agricultural activities. The $\delta^2\text{H}$ and $\delta^{18}\text{O}$ enrichment of some samples could suggest a salinization phenomenon.

Keywords

Estarreja • Groundwater • Nitrate • N origin • Stable isotopes

1 Introduction

Nitrate Directive (91/676/EEC) concerns the protection of the water quality against pollution caused by nitrate from agricultural sources. It aims to reduce the quantities of nitrate in water and prevent its continued rise. Additionally, the Urban Wastewater Directive (91/271/EEC) aims to protect the environment from the harmful effects caused by wastewater discharges. The implementation of Nitrate

Directive and the Water Framework Directive (2000/60/EC) led to the designation of large areas vulnerable to nitrate pollution, designated as Nitrate Vulnerable Zones (NVZs). NVZs are areas at risk from agricultural nitrate pollution in which groundwater contains or could contain (if no action is taken to reverse trend) more than 50 mg/L of NO_3 . The objectives are to ensure that the nitrate concentration in surface water and groundwater does not exceed the limit of 50 mg/L, as well as to control the incidence of the eutrophication phenomenon.

In the Estarreja region, the groundwater shows a nitrate concentration of up to 140 mg/L. Agriculture and the chemical industry are the most important activities in the Estarreja municipality with a perfect symbiosis between them since the 1930s. Around the 1950s, the installation of the Estarreja Chemical Complex (EQC) took place with a huge investment mainly in the production of ammonia for the manufacture of nitro-ammoniacal fertilizers used in agriculture.

The literature has described some approaches in order to distinguish between the different sources of nitrate in groundwater, generally with $\delta^{15}\text{N}$ and $\delta^{18}\text{O}$ in the NO_3 . The $\delta^2\text{H}$ and $\delta^{18}\text{O}$ in the water are useful to understand the hydrological cycle as well as the salinization phenomenon. The present study aimed to discriminate the contamination sources through the application of these two isotope couples in waters from the Estarreja shallow aquifer.

2 Materials and Methods

The study area is characterized by Holocene and Pleistocene detrital sedimentary deposits (Teixeira 1962). This area has two important aquifer systems (Marques da Silva 1990): (a) the Aveiro Cretaceous Multi-Aquifer System (ACMAS) and (b) the Aveiro Quaternary Aquifer System (AQAS), which is essentially made up of three main aquifer units with different hydrogeological and hydraulic characteristics

A. C. P. Marques (✉) · E. A. F. da Silva
Department of Geosciences, University of Aveiro, Campus
Universitário de Santiago, 3810-193 Aveiro, Portugal

M. do Rosário Carvalho
Department of Geology, Faculty of Sciences, IDL University of
Lisbon, Campo Grande 016, 1749-016 Lisboa, Portugal

between them (Ordens 2007). The upper aquifer is laid in modern deposits (Holocene) that comprise dune formations or dune sands and alluvial deposits (Almeida et al. 2000). The second aquifer unit, a semi-confined aquifer, is laid in Pleistocene deposits, at the Quaternary base aquifer (Ordens 2007). The third aquifer unit is made up of Cretaceous Sandstones and Clays (Layer 1) and Schists from Precambrian Xisto-Grauváquico Complex (XGC), before 540 Ma (Fig. 1).

One field campaign was carried out in Estarreja (4 and 5 May 2018) for water sampling at wet season. A total of 37 wells or small diameter holes were sampled with a maximum depth of 7 m at the Estarreja shallow aquifer. The $\delta^2\text{H}$ and $\delta^{18}\text{O}$ measurements (vs. V-SMOW—Vienna-Standard Mean Ocean Water) were performed by mass spectrometry, at the SIAF—Stable Isotopes and Instrumental Analysis Facility (Portugal). Nitrate extraction and $\delta^{18}\text{O}$ and $\delta^{15}\text{N}$ determination were carried out in frozen samples shipped to the Environmental Isotope Laboratory in the University of Waterloo (Canada) and analyzed with a continuous flow isotope-ratio mass spectrometer, with a precision of 0.5‰.

3 Results and Discussion

3.1 $\delta^2\text{H}$ and $\delta^{18}\text{O}$ in Water

The sampled groundwater has a meteoric origin considering the Global Meteoric Water Line (GMWL, (Craig 1961)) represented by the equation $\delta^2\text{H} = 8 \delta^{18}\text{O} + 10$ or the Meteoric Water Line in Portugal (RMWL, (Carreira et al. 2006))

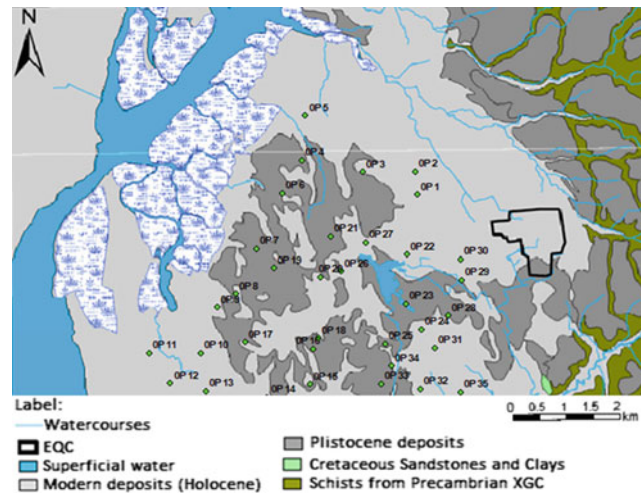


Fig. 1 Geologic framework

with isotopes relation following the equation $\delta^2\text{H} = (6.78 \pm 0.10) \delta^{18}\text{O} + (4.45 \pm 4.65)$, $R = 0.95$, because all the samples are plotted around the lines (Carreira et al. 2006) and all the deviations can be explained by physical processes as the slope of the evaporation line is 5.57, a value between 3 and 6. The samples show excess of deuterium (d) values that can reach $-15.1\text{z}\%$. In Fig. 2, it is possible to identify different groups of water: $\delta^2\text{H}$ enriched samples probably associated with a great humidity at the recharge area (black dots); samples enriched in heavy isotopes showing a shift to the right of the water lines that could be affected by evaporation or mixed with seawater (blue and green dots); and samples depleted in $\delta^2\text{H}$

Fig. 2 Isotopic composition of $\delta^2\text{H}$ and $\delta^{18}\text{O}$ from the Estarreja shallow aquifer and its location in relation to GMWL (Craig 1961) and RMWL (Carreira et al. 2006)

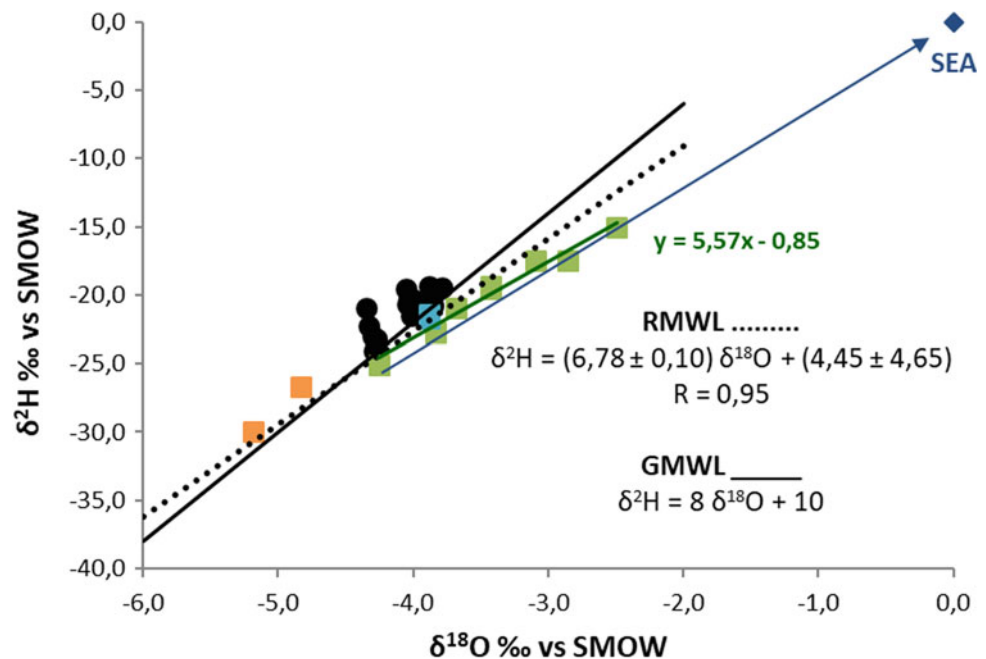
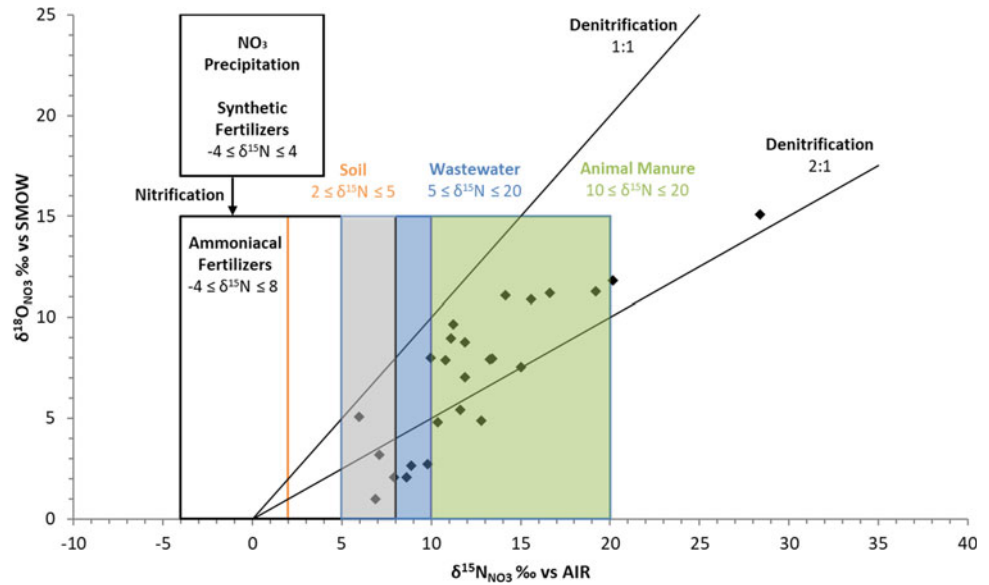


Fig. 3 Stable isotope composition of dissolved nitrate in groundwater: $\delta^{15}\text{N}$ and $\delta^{18}\text{O}$; fields are according to bibliography (see 5. Discussion and Conclusions); the trends resulting from nitrate transformation processes, nitrification and denitrification (Kendall et al. 2007)



and $\delta^{18}\text{O}$ that can be related to far way recharge, representing condensation phenomena (orange dots).

3.2 $\delta^{15}\text{N}$ and $\delta^{18}\text{O}$ in NO_3

The dissolved nitrates in groundwater have three different types of $\delta^{15}\text{N}$ isotopic signature: overlap between wastewater and animal manure (Fig. 3, $10 \leq \delta^{15}\text{N} \leq 20$ (Kendall et al. 2007) (Fernandes et al. 2019)), overlap between ammoniacal fertilizers and wastewater ($5 \leq \delta^{15}\text{N} \leq 8$, (Fernandes et al. 2019)) and a typical signature of wastewater ($8 \leq \delta^{15}\text{N} \leq 10$, (Fernandes et al. 2019) (Aravena et al. 2010)).

4 Conclusions

In terms of $\delta^2\text{H}$ and $\delta^{18}\text{O}$ in water, the samples represented by the blue and green dots can suggest a salinization phenomenon as they can be mixed with seawater, assuming that the $\delta^2\text{H}$ and $\delta^{18}\text{O}$ values for seawater are close to zero. In relation to $\delta^{15}\text{N}$ and $\delta^{18}\text{O}$ in NO_3 , it is possible to conclude that the samples with an isotopic signature of overlap between wastewater and animal manure could indicate clearly an agriculture component, in contrast to the samples with an isotopic signature of overlap between ammoniacal fertilizers and wastewater which can suggest an industrial and/or an agriculture component. The isotopic signature of ammoniacal fertilizers can have its origin as industrial products or as fertilizers applied in soils.

References

- Almeida, C., Mendonça, J.J.L., Jesus, M.R., Gomes, A.J.: Sistemas Aquíferos de Portugal Continental. INAG, Lisboa (2000)
- Aravena, R., Mayer, B., Aelion, C.M.: Isotopes and processes in the nitrogen and sulfur cycles. In: Höhener, P., Hunkeler, D., Aravena, R. (eds.) *Environmental Isotopes in Biodegradation and Bioremediation*, pp. 203–246. CRC Press, Boca Raton (2010)
- Carreira, P.M., Valério, P., Nunes, D., Araújo, M.F.: Temporal and seasonal variations of stable isotopes (d^2H and d^{18}O) and tritium in precipitation over Portugal. IAEA. In: *Conference and Symposium Papers 26/P. Isotopes in Environmental Studies—Aquatic Forum 2004*, pp. 370–373 (2006)
- Craig, H.: Isotopic variations in meteoric waters. *Science* **3465**, 1702–1703 (1961). <https://doi.org/10.1126/science.133.3465.1702>
- Fernandes, P., Carvalho, M.R., Silva, M.C., Rebelo, A., Zeferino, J.: Application of nitrogen and boron isotopes for tracing sources of anthropogenic contamination in Monforte—Alter do Chão Aquifer System. *Portugal. Sustain. Water Resour. Manag.* **5**(1), 249–266 (2019). <https://doi.org/10.1007/s40899-018-0265-1>
- Kendall, C., Elliott, E.M., Wankel, S.D.: Tracing anthropogenic inputs of nitrogen in ecosystems. In: Michener, R., Lajtha, K. (eds.) *Stable Isotopes in Ecology and Environmental Science*, 2nd edn., pp. 375–449. Blackwell Publishing Inc., Oxford (2007)
- Marques da Silva, M.A.: Hidrogeologia del sistema multiacuífero Cretácico del Bajo Vouga—Aveiro (Portugal). Dissertação de doutoramento. Universidade de Barcelona, Barcelona (1990)
- Ordens, C.M.: Estudo da contaminação do aquífero superior na região de Estarreja. Coimbra, Universidade de Coimbra. Faculdade de Ciências e Tecnologia. Departamento de Ciências da Terra, 150 p. Dissertação apresentada à Universidade de Coimbra para cumprimento dos requisitos necessários à obtenção do grau de Mestre em Geociências, ramo Ambiente e Ordenamento do Território (2007)
- Teixeira, C.: Carta Geológica de Portugal 1/50000. Notícia explicativa da Folha 13-C (Ovar). Serviços Geológicos de Portugal, Lisboa (1962)

Hydrogeological Conceptual Modelling of Geothermal Waters in Urganlı, Western Anatolia, Turkey

Nevzat Özgür and Seher Büyükşahin

Abstract

The study area is located in the western part of the continental rift zone of the Gediz within the Menderes Massif and consists of Paleozoic schists, intercalation of carbonate schists, mica schists, phyllites, marbles, Mesozoic carbonate rocks and ophiolites, and Cenozoic sediments such as travertine deposits and alluvium. The impermeable mica schists form the basement rocks in the area. The Paleozoic marbles constitute a reservoir for geothermal waters and, especially, an aquifer for groundwater. In the area, Pliocene to recent sedimentary rocks are of cap rocks for the formation of geothermal waters. The geothermal waters in Urganlı, with surface temperatures of 75 °C and reservoir temperatures of 180 °C, can be considered as Na-HCO₃ type geothermal waters rather than Ca-Mg-HCO₃ type groundwaters. The geothermal waters in the area were represented in a hydrogeological conceptual model. The Kula volcano located in the rift zone of Gediz within the Menderes Massif, with a last-eruption age of up to 18,000 years, might be considered as a heat source for the geothermal waters.

Keywords

Turkey • Western Anatolia • Menderes Massif • Gediz • Urganlı • Geothermal waters • Modelling

1 Introduction

The geothermal field of Urganlı located in the western part of the continental rift zone of the Gediz, in the northern part of the Menderes Massif was selected for our investigations

N. Özgür (✉) · S. Büyükşahin
Faculty of Engineering, Department of Geological Engineering,
Suleyman Demirel University, Isparta, Turkey
e-mail: nevzatozgur@sdu.edu.tr

(Fig. 1; Özgür 1998). The area offers at least three production wells of geothermal waters and groundwaters in a depth ranging from 22 to 80 m used in greenhouses and for irrigations. The aim of this paper is (i) to describe geothermal waters from the hydrogeological, hydrogeochemical and isotope-geochemical points of view and (ii) to represent a hydrogeological conceptual model of geothermal waters in the study area.

2 Results

2.1 Geological Setting

In Urganlı, the Paleozoic metamorphic rocks form the basement rocks consisting of calcschists, micaschists, quartzschists, quartz-muscoviteschists, and quartz-muscovite-biotite schists (Vural et al. 2009; Büyükşahin et al. 2016). In the study area, beige- and brown-coloured intercalations of marbles occur in the eastern part of SarıçTepe. In the N and E of the area, Paleozoic marbles overlie the metamorphic rocks. Marbles are dolomitic in some cases, and they show a dark grey colour at the bottom and are light grey and moderate-to-bulky crystallized at the top (Vural et al. 2009; Büyükşahin et al. 2016). The Paleozoic metamorphic rocks are overlain by Mesozoic limestones, dolomitic limestones and allochthonous ophiolites located in the NW of the study area (Vural et al. 2009). The limestones are more dolomitic in composition at the bottom. Dolomites contain secondary calcite fillings and do not show any distinct layering. The Paleozoic and Mesozoic rocks in the area are overlain by Pliocene sediments and Quaternary travertine, alluvium, and talus deposits discordantly. At the bottom of Pliocene deposits, there are conglomerates, sandstones, siltstones and claystones overlain by clayey limestones and claystones concordantly. Detritic sediments such as conglomerates, sandstones, siltstones and claystones are widespread in the area. In general, conglomerates

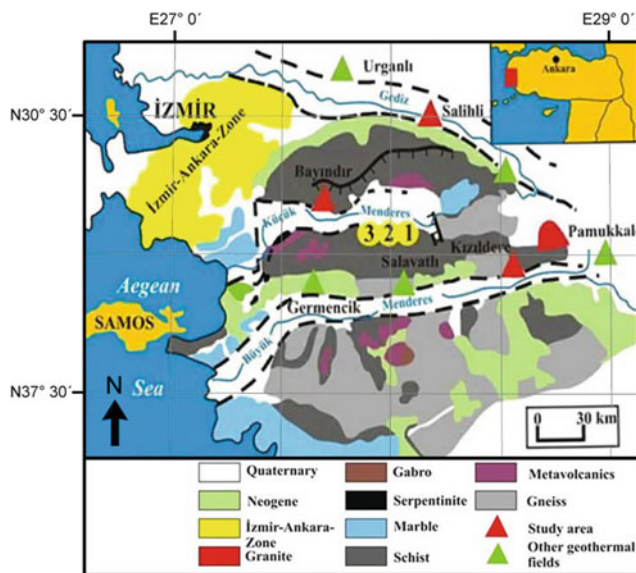


Fig. 1 Geological map of the Menderes Massif and the location of the study area of Urganlı. 1: Mercury deposit of Haliköy, 2: Antimony deposit of Emirli, 3: Arsenopyrite and gold deposit of Küre (Özgür 1998)

rounded from moderate to coarse are adhered by carbonates and clay cements loosely. Sandstones in grey and greenish grey colours are intercalated with fine layered claystones and siltstones here and there. In the study area, the Quaternary travertine deposits and alluvium represent the youngest rock formations.

2.2 Hydrogeology, Hydro Geochemistry and Isotope Geochemistry

In the study area, the Paleozoic metamorphic rocks form the impermeable basement and play an important role in the formation of the geothermal reservoir due to their impermeable features. Marbles in Paleozoic metamorphic rocks are suitable for the formation of reservoir rocks of the geothermal waters due to their intense fragments and karst formation. The Paleozoic marbles as reservoir rocks are overlain by the Pliocene Vişneli formation as a cap rock discordantly. The Vişneli formation is overlain by the impermeable Yaka formation in the Pliocene age as a second cap rock concordantly. The last two formations are overlain by recent travertine deposits and alluvium discordantly, which are widespread in the area and can be considered as cap rocks. The area is characterized by semiarid climate conditions with an annual rainfall of 500 mm and an annual temperature of 17 °C.

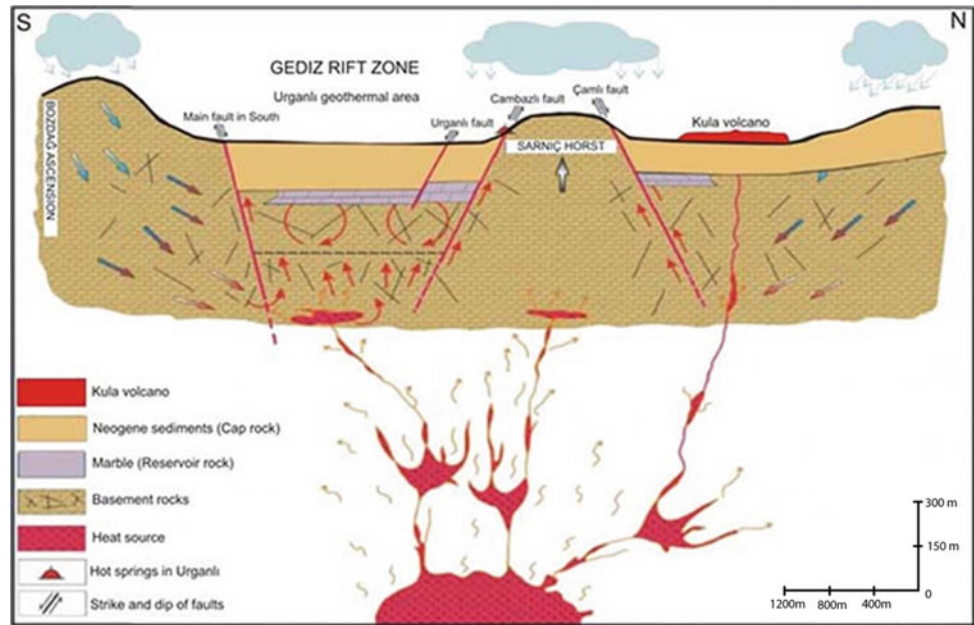
Three samples of geothermal waters and mixed groundwaters of Urganlı, collected in the year of 2016, are considered as Na-HCO₃ and Ca-Mg-HCO₃ type waters, respectively (Özgür 1998; Büyükşahin et al. 2016). Hydro-geochemically, the geothermal waters in the area display a dominant cations order of Na + K > Ca > Mg and a dominant anions order of HCO₃ > SO₄ > Cl. The geothermal waters in Urganlı are immature waters according to the ternary diagram of Na1/1000-K1/100-√Mg (Giggenbach 1988). Moreover, geochemical thermometers of Na-K and Na-K-Ca show reservoir temperatures ranging from 130 to 210 °C in the study area, which correspond to measured temperatures in production wells (Büyükşahin et al. 2016).

In the study area of Urganlı, the stable isotope compositions (δ¹⁸O and δ²H) in the geothermal waters might be found in Özgür (1998); Büyükşahin et al. 2016). The δ²H values in geothermal waters vary between -56.0 and -45.9‰, whereas the δ¹⁸O values range from -8.88 to -6.72‰ (Özgür 1998; Büyükşahin et al. 2016; Özgür 2017). The tritium contents measured in these waters vary between 0.7 and 8.4 TU. One sample of geothermal waters lies along the meteoric water line, whereas four samples of high-temperature geothermal waters deviate from the meteoric water line, indicating an intense water-fluid interaction under high-temperature conditions (Özgür 1998; Büyükşahin, et al. 2016; Özgür 2017). In one sample, the ³H value of 8.8 TU shows an atmospheric or anthropogenic origin. Therefore, a mixing process between groundwaters and geothermal waters occurs in the area of Urganlı and environs. In comparison, the other samples with ³H contents ranging from < 0.7 to < 1.2 TU indicate that there is no mixing between fresh waters and geothermal waters, as proved by the δ¹⁸O versus δ²H diagram (Büyükşahin et al. 2016; Özgür 2017).

3 Discussion and Conclusion

In Urganlı and environs, the evolution of geothermal waters can be represented by a hydrogeological conceptual model as shown in (Fig. 2). In the system, the meteoric waters percolate through zones and permeable clastic sediments into the reaction zone of the roof area of a magma chamber located at a probable depth of 4–5 km, where meteoric fluids are heated by the cooling magmatic melt for that Middle Miocene to recent volcanic rocks, i.e. Kula volcanics, might be taken into account and ascend to the surface due to their lower density caused by convection cells. The volatile components of CO₂, SO₂, HCl, H₂S, HB, HF and the out of the magma reach the geothermal water reservoir, where an

Fig. 2 Hydrogeological conceptual modelling of geothermal waters of Urganlı and environs. [Modified from Vural et al. (2009); Büyüksahin et al. (2016); Özgür (2017)]



equilibrium is formed between altered rocks, gas components, and fluids (Özgür 1998). Thus, the geothermal waters ascend into the tectonic zones of weakness at the continental rift zones in form of hot springs, gases, and steams. These fluids are characterized by high-to-medium CO_2 , H_2S and NaCl contents. It is very important that the fluids indicate a reduced, pH-neutral environment after equilibrium adjustment with rocks in the reaction zone. The Kula volcano, located in the rift zone of Gediz with a last-eruption age of up to 18,000 years, might be considered as a heat source for the formation of geothermal waters in the study area. The geothermal waters in the study area are used for balneological aims and in greenhouses.

Acknowledgements This study was funded by the Scientific Research Coordination Office of the Suleyman Demirel University, under contract numbers 4140-YL1-14 and 4730-YL1-16.

References

- Büyüksahin, S.: Urganlı (Turgutlu, Manisa) veyakınçevresijeotermal-sularınınhidrojeolojikmodellemesi, M.Sc. thesis, Graduate School of Applied and Natural Sciences, Süleyman Demirel Üniversitesi (2016)
- Giggenbach, W. F.: Geothermal solute equilibria. Derivation of Na-K-Ca-Mg geoindicators. *Geochim. Cosmochim. Acta* **52**, 2749–2765 (1988)
- Özgür, N.: Aktive und fossile Geothermalsysteme in den kontinentalen Riftzonen des Menderes-Massives, Westanatolien. Freie Universität Berlin, Türkei. Habilitationsschrift (1998)
- Özgür, N., Büyüksahin, S., Yıldırım, B., Aydemir, E.: Hydrogeological, hydrogeochemical and isotope geochemical features of the geothermal waters in Urganlı and environs, Western Anatolia, Turkey. *J. Eur. Feder. Geol.* **1**(1), 1-10 (2017)
- Vural, S.: Urganlı (Turgutlu, Manisa) jeotermal alanının jeolojisi ve hidrojeokimyasal özellikleri, M.Sc. thesis, Graduate School of Applied and Natural Sciences, Kocaeli Üniversitesi (2009)



Hydrogeological Modeling of Geothermal Waters in Balçova, İzmir, Turkey

Nevzat Özgür and Mine Alacalı

Abstract

The study area, showing a rift structure resulting from the N-S extensional forces due to effects of West Anatolian neotectonical features, is located within the boundary 15 of İzmir City. The geothermal waters of Balçova can be considered as Na-(Cl)-HCO₃ type. The geochemical thermometers in the area show reservoir temperatures of up to 180 °C. The alteration mineral assemblages consist of quartz, illite, siderite, ankerite, clinocllore and albite. Stable isotopic parameters of $\delta^{18}\text{O}$ versus δD show that there is an intensive water–rock interaction. The ^3H values of the samples range from 2.50 TU to less than 1.0 TU, indicating a mixing of geothermal waters with fresh groundwaters. Saturation indexes of minerals show that the water samples collected from the geothermal field of Balçova are oversaturated with respect to calcite, dolomite and quartz minerals. Thus, these minerals have a high ability to precipitate into the production wells causing a scaling problem.

Keywords

Turkey • Western Anatolia • İzmir • Balçova • Geothermal Waters • Hydrogeological Modeling

1 Introduction

The geothermal field of Balçova, located within the province capital of İzmir City, is a very famous study area with a high potential of geothermal waters (Fig. 1), (Alacalı 2012). In the area, geothermal waters are used for space heating, green house heating and balneological purposes. There are up to

30 shallow and deep wells with depths ranging from 48 to 250 m, and from 430 to 110 m and average measured temperatures ranging from 102 to 131 °C, respectively. The aim of this study is (i) to describe the geothermal waters from the hydrogeological, hydrogeochemical and isotope geochemical points of view and (ii) to represent a hydrogeological conceptual model of geothermal waters in the study area.

2 Results

2.1 Geological Setting

The geothermal field of Balçovais is located within the province capital of İzmir and consists of the Upper Cretaceous İzmir-flysch, the Yeniköy formation in Miocene age, the Pliocene Cumaovası volcanics, and Quaternary talus and alluvium (Alacalı 2012). The İzmir-flysch—which is composed of metasandstones, phyllittes, diabases, serpentinites and limestones—forms the basement rock overlain by the Miocene Yeniköy formation discordantly.

2.2 Hydrogeology, Hydrogeochemistry and Isotope Geochemistry

The İzmir-flysch as a basement rock is slightly metamorphosed and can be considered as an impermeable rock. In metasandstones within the İzmir-flysch, there are very intense fractures and fissures due to tectonical situation in the area. Moreover, the limestones in the İzmir-flysch show fractures and fissures. Therefore, the metasandstones and limestones as intercalations in the İzmir-flysch can be considered as reservoir rocks. Primarily, the impermeable İzmir-Flysch allows geothermal waters to ascend throughout the secondary permeable zones of the Agamemnon-1 fault,

N. Özgür (✉) · M. Alacalı
Faculty of Engineering, Department of Geological Engineering,
Suleyman Demirel University, Isparta, Turkey
e-mail: nevzatozgur@sdu.edu.tr

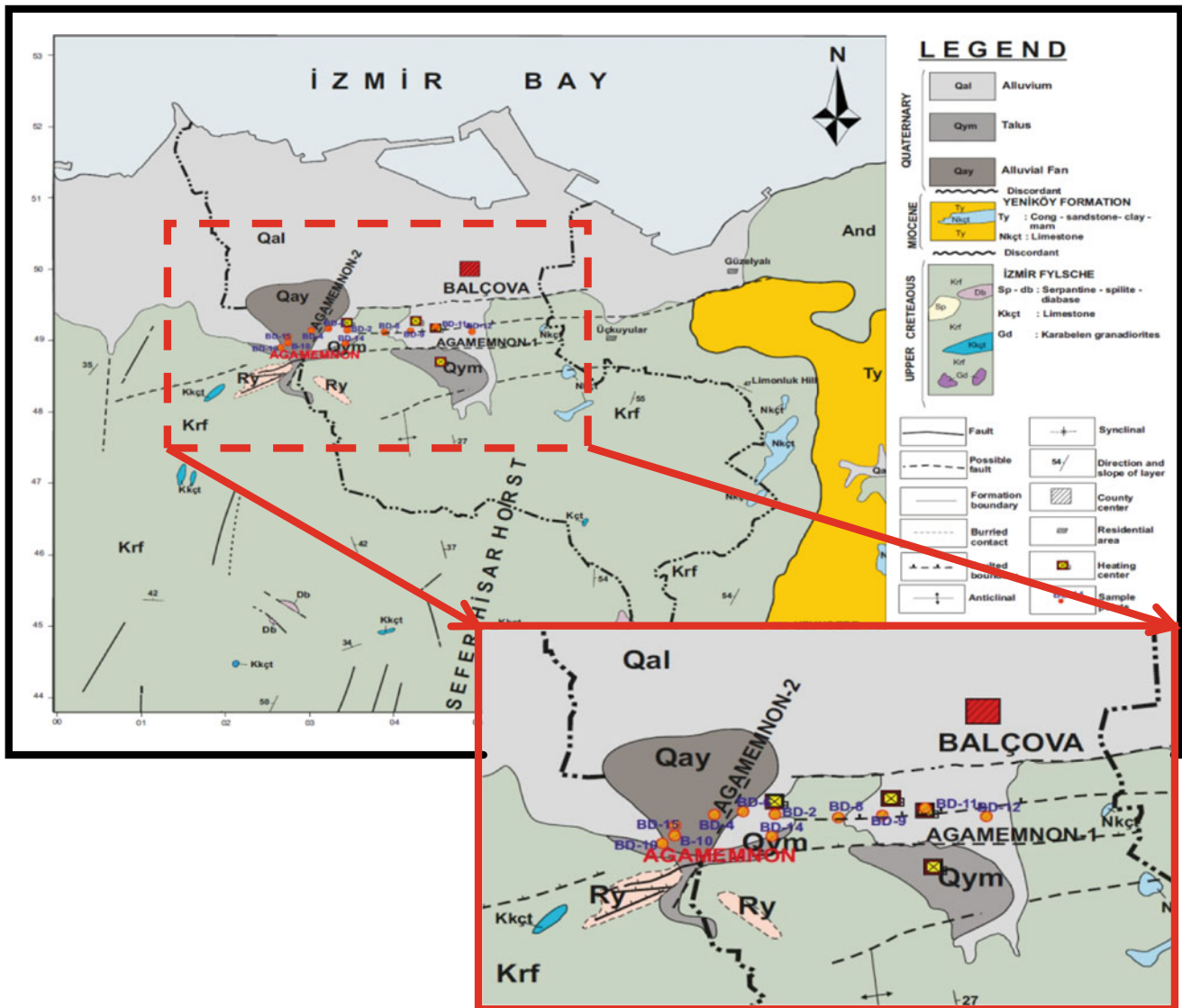


Fig. 1 Location and geologic map of Balçova in province capital of Izmir (Alacalı 2012)

accepted as the main channel for geothermal waters with a high flow rate.

For hydrogeological, hydrogeochemical and isotope geochemical laboratory works, we have collected 13 samples with in-situ measurements such as temperatures, pH, Eh, conductivity values, dissolved oxygen values and alkalinity (Alacalı 2012). The cations such as Na^+ , K^+ , Ca^{2+} , Mg^{2+} , Si^{4+} , Al^{3+} , B^{3+} , Li^+ , As^{3+} were analyzed by ICP-OES, while the anions such as SO_4^{2-} , NO_3^- , Cl^- and F^- were analyzed by IC. The data were evaluated using the software program AquaChem 3.7 (Calmbach 1999). The geothermal waters of Balçova can be considered as an Na-(Cl)- HCO_3 type water (Alacalı 2012; Calmbach 1999). Geothermal waters are distinguished by the dominant cations $\text{Na} + \text{K} < \text{Ca} < \text{Mg}$ and the dominant anions $\text{HCO}_3 < \text{Cl} < \text{SO}_4$.

In the diagram of $\text{Na1/1000-K1/100}-\sqrt{\text{Mg}}$, the geothermal waters of Balçova and environs are immature waters (Alacalı 2012; Giggenbach 1988). Regarding the isotope geochemical analyses of the samples, the $\delta^{18}\text{O}$ and δD ratios show that the origin of the geothermal waters in the field is meteoric. The ^3H values of the samples range between 0.00 and 2.5 TU. The isotope ratios for $\delta^{18}\text{O}$ and δD for the geothermal waters from the study area range from 5.29 to 5.79‰ and -33.3 to -38.3‰, respectively. The deviation of the $\delta^{18}\text{O}$ values of the geothermal waters and cold water from the continental meteoric water line indicates an intense water-rock interaction in depth, under high temperature conditions and isotopic enrichment of δD due to the transition phase of water into vapor, such as during the evaporation process. There is a mixing of geothermal waters with fresh waters.

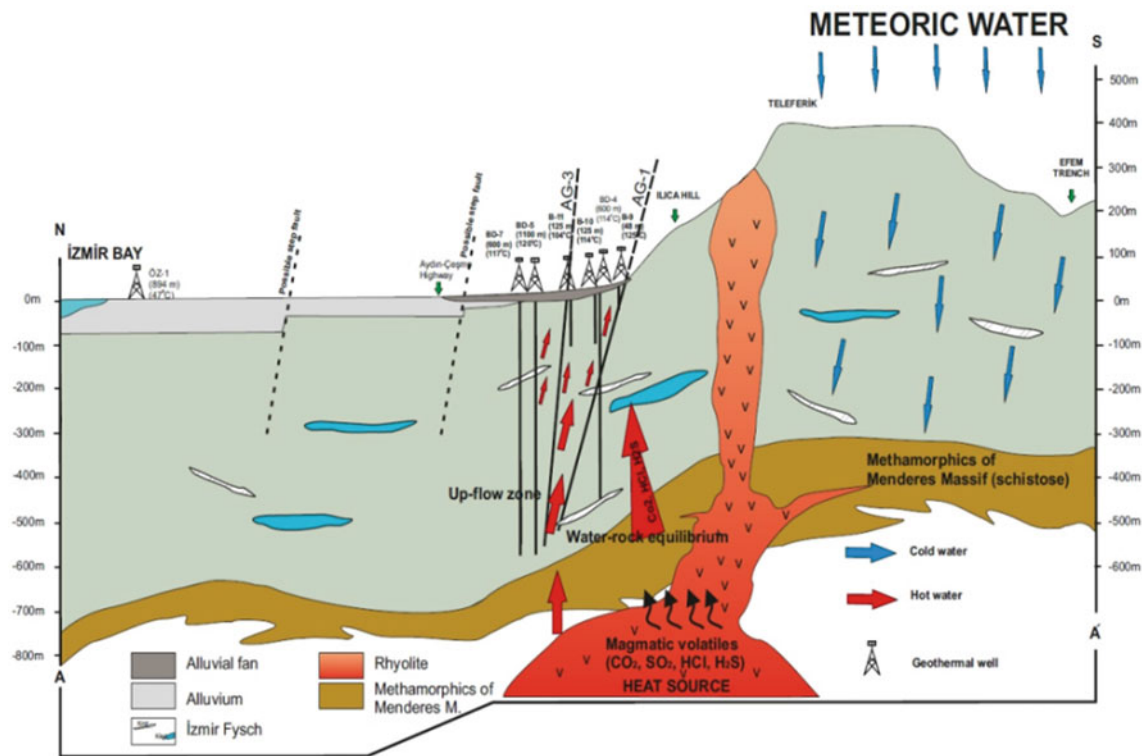


Fig. 2 Hydrogeological modeling of the geothermal waters of Balçova and environs. [Modified from Alacalı (2012)]

Regarding the isotope geochemical analyses, the waters circulating are young in age. The low values of $3H$ indicate that the waters in the field are recharged by precipitations before nuclear bomb tests.

3 Discussion

The stable isotope chemical analyses of the geothermal water samples indicate that the geothermal waters circulating in the field of Balçova are of a meteoric origin. The geothermal waters obtained by the deep drilling of wells in the Quaternary alluvium and alluvial fan on the downthrown block of the Agamemnon-I Fault are fed by the meteoric waters fallen onto the rising block of the fault (Fig. 2).

The meteoric waters falling upon the rising block infiltrate deeply through the fractures of the İzmir Flysch and are heated by the magma due to the thinning of continental crust caused by the rifting system. The heated waters ascend along the faults, fractures and crack systems in the region. In the course of this circulation, since some water–rock interactions take place between the geothermal water and the heated rocks, the geothermal water and rocks undergo some hydrogeochemical reactions. Magma-induced volatiles such as CO_2 , SO_2 , HCl , H_2S , HB , HF and He ascend in gaseous

phases and reach the reservoir (Özgür 1998). During this ascension, an equilibrium calibration between the rocks, gases and water occurs. The fluids ascending following this calibration comprise more CO_2 , H_2S , and HCl . The hydrothermal convection (heat convection) allows the hot waters of lower density to ascend. Thus, the pH neutral-characterized hot water points with gaseous and vapor components reach the surface through the tectonic weakness zones (Fig. 2). The character of waters ascending after the water–rock calibration in BGS is similar to bicarbonate solutions. Volatiles such as CO_2 and H_2S ascending from the magma compose a neutral medium along the long contacts due to the water–rock interactions (Özgür 1998). Hydrogen carbonate and bicarbonate-sulfate solutions form. In this case, Na is the major cation since $CaCO_3$ is slightly soluble in hot waters and K and Mg are absorbed by clays (here minerals) such as illite, clinocllore. The bicarbonate waters forming near the surface ascend through weakness zones such as faults and fractures. The geothermal waters in the study area are used for district heating and in green houses.

Acknowledgements This study was funded by the Scientific Research Coordination Office of the Suleyman Demirel University, under contract numbers 1863-D-09.

References

- Alacalı, M.: Hydrogeological modeling of the geothermal system in Balçova. SuleymanDemirel University, Graduate School of Natural and Applied Sciences (2012)
- Calmbach, L.: "AquaChem Computer code-Version 3.7: Aqueous geochemical analyses, plotting and modelling", Waterloo Hydrogeologic: Waterloo, Canada (1999)
- Giggenbach, W. F.: Geothermal solute equilibria. Derivation of Na-K-Ca-Mg geothermometers. *Geochim. Cosmochim. Acta* 52. 2749–2765 (1988).
- Özgür, N.: Aktive und fossile Geothermalsysteme in den kontinentalen Riftzonen des Menderes-Massives, Westanatolien. Freie Universität Berlin, Türkei. Habilitationsschrift (1998)



Assessment of Seawater Intrusion in a Coastline City Using GIS (Tripoli Lebanon)

Marianne Saba, Amal Iaaly, and Najib Gerges

Abstract

This paper evaluates the impact of seawater intrusion on the Miocene aquifer that covers the area of Tripoli. The existing aquifer, located under the city of Tripoli, spanning from Abou Samra hill toward the Mina shoreline, suffered a severe reduction of the stored water volume due to the unplanned urban expansion, the increase in water demand, the random drilling of wells and the untreated wastewater that spills exactly in front of Tripoli coastline. All these factors combined led to the saline water intrusion due to the reverse injection flow from the sea toward lower emptied cavities onshore. This has in turn led to a severe deterioration in the water quality of Tripoli city. To assess the current situation, a field survey was conducted to collect and gather underground water samples from various sites across the city and its surroundings in an attempt to analyze the Miocene aquifer of the North Governorate. The Geographic Information System was used as the main tool to both investigate and visualize the hydrophysical, hydrochemical, microbial onshore and water levels of the collected samples in the studied region. The maps generated using GIS constituted visual aids to support decisions regarding the sustainable development and management of groundwater.

Keywords

GIS • Seawater intrusion • Hydrochemical • Hydrophysical • Pumping

M. Saba · A. Iaaly (✉) · N. Gerges
Civil Engineering Department, University of Balamand, Koura,
Lebanon
e-mail: amal.iaaly@balamand.edu.lb

M. Saba
e-mail: marianne.saba@balamand.edu.lb

1 Introduction

Lebanon is known for the availability of abundant surface and groundwater resources. However, the Lebanese citizens are suffering from a severe shortage of water within their households. The lack of good management makes the exploitation of water less feasible due to the shortage of public water networks and wells. The shortage in water is due, primarily, to the lack of appropriate legislation regarding the management of water resources, and, secondly, to physical and geological factors, such as overexploitation, climate change and the acute geologic setting (Metni et al. 2004). This resulted in a number of problems in groundwater, namely: quality deterioration, alteration of springs and groundwater runways, variation of water level, flushing of groundwater into the sea, and saltwater intrusion.

Hence, the aim of this research is to assess the groundwater quality, i.e., the hydrochemical, hydrophysical, and microbial parameters of Tripoli over a period of two years. Results were assessed using the Geographic Information System (GIS) due to its visual capabilities in presenting the extent of pollution in the studied region (Shaaban 2010; Nafyad and Shankar 2018; Muzenda et al. 2019).

2 Method

The study is based on four sampling campaigns that gathered samples from 46 locations during various wet and dry seasons. Several criteria were taken into account to ensure the proper collection of the samples, such as the conformity to rigid quality control standards; the lookup for the appropriate casing for the piezometric study; the identification of all the parameters that need to be analyzed and associated logistics (number and type of containers, coolers, etc.); the selection of sampling sites using aerial photos, maps, and geographical locations; and last but not least the setting of sampling

cycles both static and dynamic for water leveling (Nafyad and Shankar 2018; Muzenda et al. 2019).

Thirty-one wells were selected as shown in Fig. 1 in both public and private locations. The depth of these wells varies from 5 to 500 m, according to the North Lebanese Water Establishment (NLWE). The studied groundwatershed covers the miocene aquifer, the depth of the wells varies quite considerably according to the location. The studied wells that are close to the seashore have a depth between 5 and 7 m below the sea level, whereas the wells located further up in the hills of Abou Samra and the upper areas near Sir Al Daniye have a groundwater level as deep as 300–550 m below mean sea level. The physical parameters were tested on-site by the use of HORIBA apparatus. The test collected the following parameters: pH, temperature, conductivity, total dissolved solids (TDS), and dissolved oxygen (DO). On the other hand, the hydrochemical analysis required carrying the sampled water in 250–500 mL plastic polyethylene bottles, while sterilized cups were used for the microbial study.

The Microbiological Tests: *E. coli*, Coliforms, and *Salmonella* were measured using the membrane-filter method. As for the chemical parameters, the water quality was tested in the environmental laboratory using an ion chromatography (IC). It is commonly used for the analysis of common

anions and cations. In our case, anions such as fluoride, phosphate, bromide, chloride, nitrite, nitrate, and sulfate were detected. As for cations, the IC covered sodium, potassium, calcium, magnesium, ammonium, sodium, and lithium. The samples were injected into the ion chromatograph (Dionex ICS-2000 Ion Chromatography System (ICS-2000)) where samples underwent ion analyses using suppressed conductivity detection. The water samples were injected to the IC with the help of disposable syringes (1 cc) and syringe filters (0.45 μ m).

All the data collected were then entered into GIS, and a spatial interpolation using Kriging was performed. The Universal Kriging interpolation is a spatial interpolation method that forecasts the values of data in areas that are not sampled.

3 Results and Discussion

The analyses of the collective hydrochemical, physical and microbial water testing and water leveling parameters were schemed using GIS. The conception of these maps allowed the visualization of the sampling campaign results and aimed at verifying the interrelation between water depths and saline water intrusion. For physical testing, a paramount amount of



Fig. 1 Public (blue) and private wells (yellow) sampled in Tripoli (Color figure online)

salinization was detected in the seashore area of Tripoli. In Tripoli, the aquifer extends from the area surrounding Tripoli, Koura, and Zgharta until it reaches the offshore of Tripoli. Its thickness ranges between 100 and 200 m. The aquifer consists of reef limestone, marly limestone, limestone, and horizons of marl and sandy marl. Depending on the nature of lithology, the intensity of the fracturing and karst development and dissolution activity (Bakalowicz 2015), the values of transmissivity varied from 5 to 5460 m²/day with a geometric mean of 55 m²/day. With the overgrowth of the population, excessive pumping of groundwater has been one of the major issues that are aggravating this situation in the North of Lebanon, with an obvious reduction of the weight of the overlying freshwater which, in turn, will decrease or even reverse the seaward flow so that seawater moves landward into the aquifer. This process is known as seawater intrusion.

Regarding, the hydrochemical and microbial analysis, some parameters exceeded the WHO drinking standards as well as the Lebanese standards. Many factors could be behind the current situation. To begin, the Northern Lebanese region is famous for its agricultural activities, such as

olive culture and orange plantations. Taking into consideration the hard geological sedimentary formation that is quite dominant in this area, in addition to factors such as irrigation and uncontrolled continuous use of fertilizers and pesticides, the salinity of the soil keeps on increasing with time, thereby explaining the high salinity concentrations seen in the 31 studied wells, with TDS values ranging from 500 to 1500 ppm.

The hydrochemical parameters highlighted high values when compared to the standards. One of the most prominent parameters was chloride, stressing the extent of seawater intrusion. Chloride concentrations in groundwater are associated with the presence of salts originating from many sources. Chloride is one of the major constituents of seawater. It is chemically stable and moves at about the same rate as intruding seawater, thus alerting to one of the most important indicators of seawater intrusion into an aquifer. In this aquifer, chloride concentrations are studied in Fig. 2. According to the World Health Organization (WHO) and Lebanese Standards, the Maximum Contaminant Level (MCL) of Chloride is 25 mg/L. In the case of the Tripoli aquifer, as seen in Fig. 2, the values exceeded the acceptable

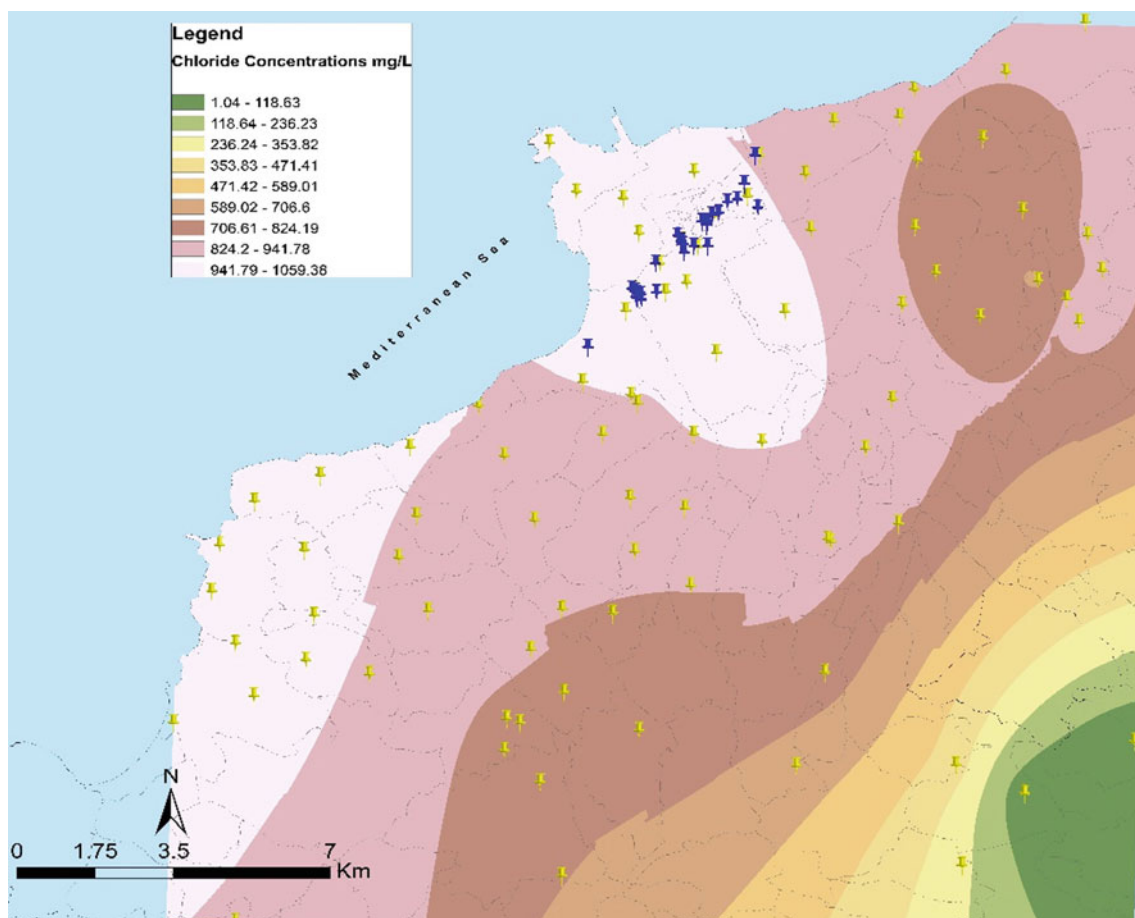


Fig. 2 Chloride concentration in Tripoli

standard and reached values higher than 100 mg per liter (mg/L); thereby, the higher Cl content in the areas that are remote from the sea (Bakalowicz 2015) indicates seawater intrusion.

As for the microbial testing realized during the four different sampling campaigns, the groundwater contained a wide range of microbial groups available in surface water and soils. These microbes include bacteria, fungi, and protozoa and are representative of the most physiological types, i.e., *E. coli*, Coliforms, and *Salmonella*. Most of the time, these pathogenic bacteria are from domestic, agricultural and other anthropogenic activities, namely untreated wastewater (Guemaz et al. 2020; Loucif et al. 2020). The lack of the working wastewater treatment plant is leading to untreated sewage being discharged into the Mediterranean Sea, thus, leading, by a reverse process, to the infiltration of this untreated water into the aquifer. This was obvious in the samples taken onshore; *E. coli*, Coliforms, and *Salmonella* were present in all the samples.

When assessing the static and dynamic levels offshore and in Tripoli, it was seen that an irrational over-pumping of the groundwater has been occurring due to overpopulation which in turn led to an increase in water demand. This implies that the rate of water abstraction is higher than the rate of recharge, leading to groundwater mining (Chami et al. 2009; Khadra et al. 2017).

Through the sampling campaigns, the statistical data resulting from the interpolation done by the GIS software also showed trends of consistently higher concentrations of minerals near the shoreline or consistent increases of concentrations with depth over time. As for the water level study, Fig. 3 displays the area with a general flow pattern

from the boundaries and areas of recharge toward the corridor of Tripoli, which is the discharge area. The head values in the Tripoli area are below sea level, and this is due to the high demand for water, and therefore, the high density of wells. These values observed below the seawater head are serious as they are indicators of seawater intrusion. This phenomenon will result in lowering the hydraulic conductivity, especially in a karstic aquifer, and thereby, lowering the productivity of the aquifer (Bakalowicz 2015). A second general trend that can be observed in this static water-level map of the aquifer is that a decrease in groundwater depth is more widely spaced in the Tripoli corridor area than in the rest of the aquifer. This movement which is seen in Fig. 3 suggests that the salinity values are higher in the Tripoli area than in the rest of the aquifer.

4 Conclusions

In the Tripoli area, the total annual recharge of the aquifer is 71 million m³, with a main natural outflow to the Mediterranean Sea and a withdrawal of groundwater from pumping wells. The actual outflow to the sea is 60.9 million m³/year, and the discharge by the present pumping wells is estimated at 13.9 million m³/year, thus leading to a total discharge from the aquifer of 74.8 million m³/year. The overall assessment of the total recharge and discharge rates revealed that the aquifer is currently being mined at an annual rate of 3.8 million m³. In addition to the permanent loss of groundwater from storage, the mining of groundwater makes the aquifer in the Tripoli area vulnerable to land subsidence and contamination by seawater intrusion. Based on the

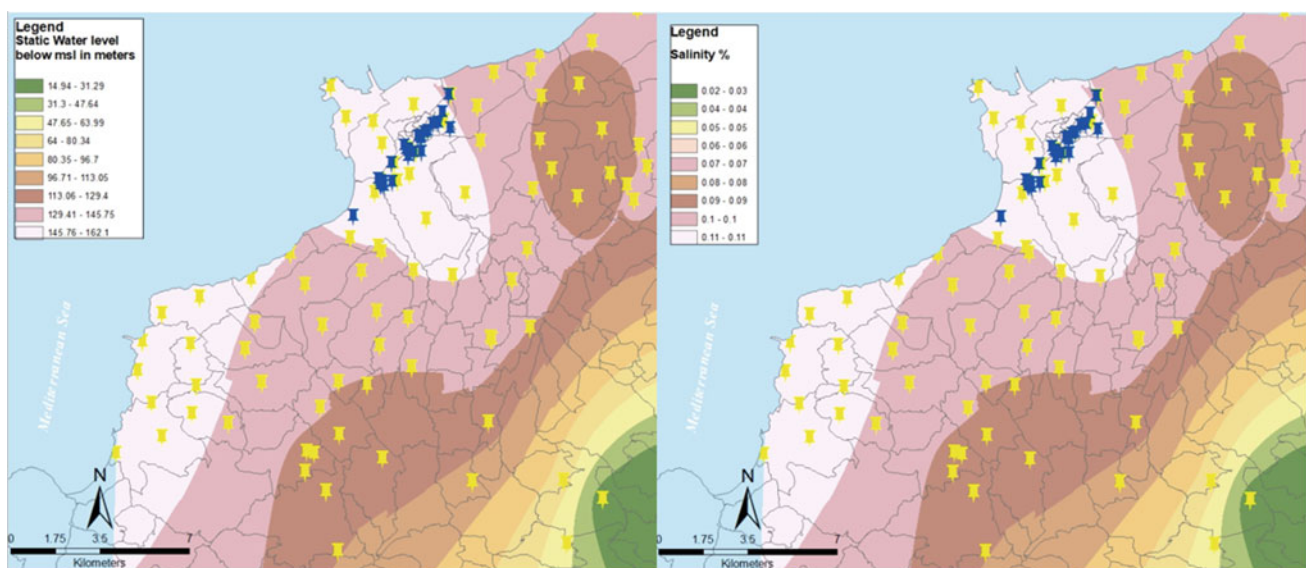


Fig. 3 Static water level versus salinity impact in Tripoli

hydrochemical, hydrophysical, and bacteriological studies accomplished for the 31 studied wells in the area, the groundwater was found to be clearly affected by pollution, mostly due to salinization and agricultural activities, thus indicating seawater intrusion which resulted from an uncontrolled pumping of wells. The integration of the numerical model by the use of GIS gave a clearer view of the condition of the aquifer.

References

- Bakalowicz, M.: Karst and karst groundwater in the Mediterranean. *Environ. Earth Sci.* **74**, 5–14 (2015). <https://doi.org/10.1007/s12665-015-4239-4>
- Chami, D., Moujabber, M., Scardigno, A.: Regional water balance and economic assessment as tools for water management in Coastal Lebanon. *Water Resour. Manage.* 2361–2378 (2009)
- Guemmaz, F., Neffar, S., Chenchouni, H.: Physicochemical and bacteriological quality of surface water re-sources receiving common wastewater effluents in drylands of Algeria. In: Negm, A. et al. (eds.). *Water Resources in Algeria - Part II: Water Quality, Treatment, Protection and Development*. Cham, Springer, pp. 117–148 (2020). https://doi.org/10.1007/978-3-319-40014-0_10
- Khadra, W., Stuyfzand, P., Breukelen, B.: Hydrochemical effects of saltwater intrusion in a limestone and dolomitic limestone aquifer in Lebanon. *Appl. Geochem.* **79**, 36–51 (2017)
- Loucif, K., Neffar, S., Menasria, T., Maazi, M.C., Houhamdi, M., Chenchouni, H.: Physico-chemical and bacteriological quality assessment of surface water at Lake Tonga in Algeria. *Environ. Nanotechnol. Monit. Manag.* **13**, 100284 (2020). <https://doi.org/10.1016/j.enmm.2020.100284>
- Metni, M., El-Fadel, M., Sadek, S., Kayal, R., Lichaa, D.: Groundwater resources in Lebanon: a vulnerability assessment. *Int. J. Water Resour. Dev.* **20**, 475–491 (2004)
- Muzenda, F., Masocha, M., & Misi, S.N.: Groundwater quality assessment using a water quality index and GIS: a case of Ushewokunze Settlement, Harare, Zimbabwe. *Phys. Chem. Earth* **112**, 134–140 (2019). <https://doi.org/10.1016/j.pce.2019.02.011>
- Nafiyad, S.K., Shankar, K.: Groundwater quality assessment using water quality index and GIS technique in Modjo River Basin, central Ethiopia. *J. Afr. Earth Sci.* **147**, 300–311 (2018)
- SJ Builders Australia: Groundwater hydrogeochemistry. <https://sjbuilders.blogspot.com/2013/11/groundwater-hydrogeochemistry.html>
- Shaaban, A.: Support of space techniques for groundwater exploitation in Lebanon. *J. Water Resour. Prot.* **2**, 469–477 (2010)

**Hydrology, Hydrogeology, Hydrochemistry, Water
Resources (T10): Water Resources Management**



Groundwater Resource Management in the Hard Rock Terrain of Upper Ponnaiyar Watershed Using Remote Sensing and GIS

Arunachalam Subramaniam, Parameswari Kaliyaperumal, and Sakthivel Rathinagiri

Abstract

Groundwater has been one of the most important natural resources for life on earth. It is a dynamic and rechargeable natural resource. In the present work, an attempt was made to identify the groundwater potential zones by taking the hard rock terrain of the upper Ponnaiyar watershed as a study area, using remote sensing and geographical information system (GIS). Different overlaying thematic layers prompting the groundwater—such as slope, geology, lineament density, soil, geomorphology, land use and drainage density—have been used to categorize the ground water potential zones. The weightage and ranking scores were assigned to each thematic layer based on its influence on the groundwater potential. The results of the study clearly show that 0.29% of the study area are high potential zones since the study location is mostly covered by hard rocks allowing less permeability, whereas 45.67% represent moderate potential zones, which are accounted for by the secondary porosity through cracks and lineament. This basic information is necessary for artificial groundwater recharge to enable sustainable water resource management.

Keywords

Groundwater potential zone • Thematic maps • Weighted overlay analysis • GIS

1 Introduction

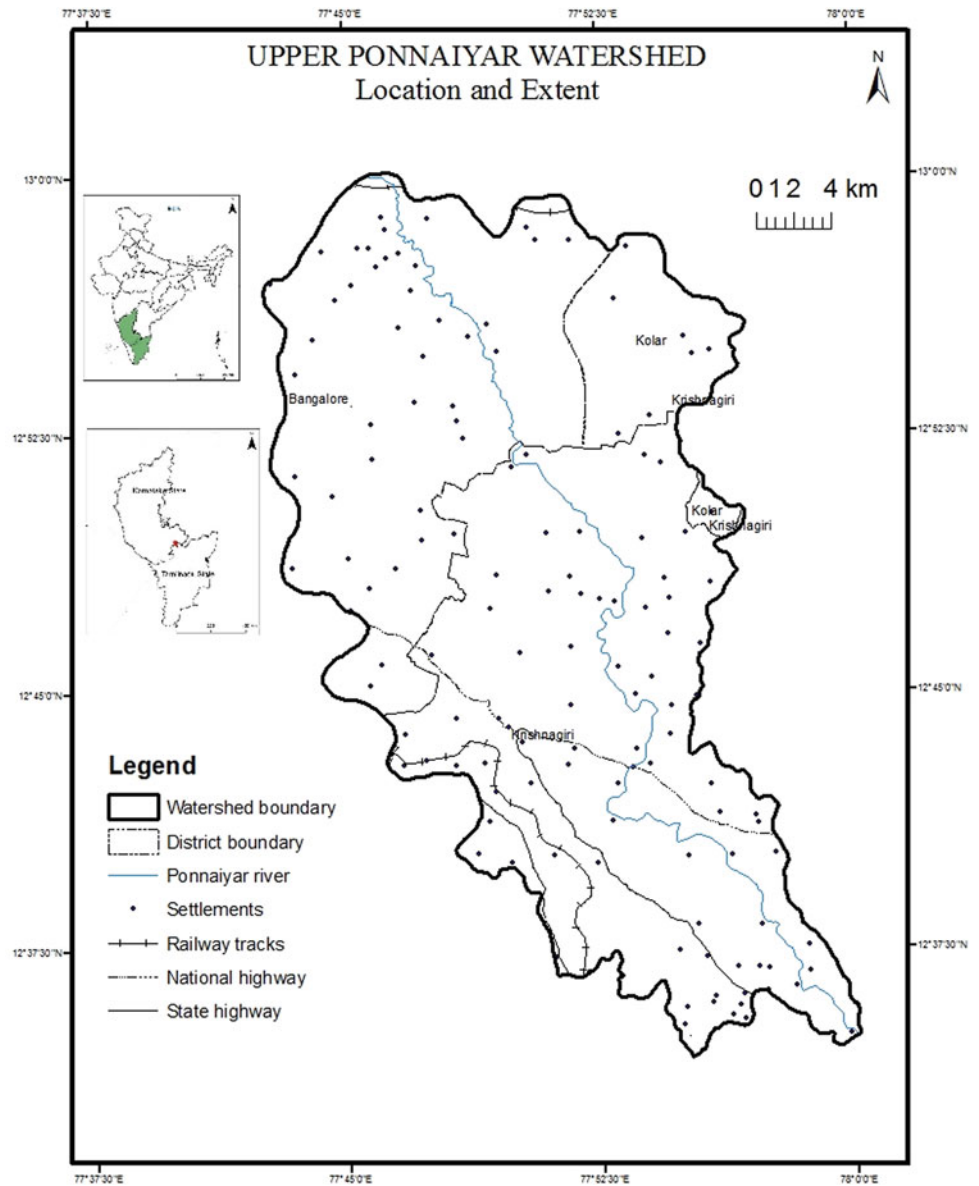
Groundwater potential zones are governed by various geoenvironmental parameters such as drainage, texture, lineament and land use (Sarkar et al. 2001; Machiwal et al., 2011; Jahan et al., 2019; Negm et al., 2020a, 2020b). Ramalingam and Santhakumar (2000) demonstrated the use of remote sensing and GIS techniques for delineating potential areas for groundwater recharge for the entire state of Tamil Nadu. The upper Ponnaiyar watershed, Krishnagiri district of Tamil Nadu, India, has been selected for this study. The study area lies between 12°30' to 13°N latitudes and 77°45'E to 78°E longitudes (Fig. 1). It covers a geographical area of 832.85 sq.km and a total length of 69.42 km. The Ponnaiyar River originates in the Chikkaballapur district of Karnataka, at an elevation of about 900 m above mean sea level, and then flows from south to east for 400 km through Karnataka and Tamil Nadu in India, finally, emptying into the Bay of Bengal at Cuddalore. The upper part of the upper Ponnaiyar basin is covered by the Archaean rocks such as Gneiss, Hornblende biotite gneiss, Pyroxene granulites, Pyroxene granulites, Quartzite, Ferruginous Quartzite, and Amphibolites.

2 Materials and Methods

The Indian satellite imagery Cartosat with a 2.5 m resolution, the survey of India Toposheet (57 H/13, 14 and 57 L/2) on a 1:50,000 scale, the geological map published by a Geological Survey of India (1985), and the soil map by NBSS were used to prepare thematic maps. The analysis was conducted using Arc GIS 10.1 to identify the ground water potential zones. Finally, weightage and rank were assigned based on the groundwater suitability index for each parameter to determine the groundwater potential zones in the study area. The groundwater suitability index is the sum of

A. Subramaniam (✉) · P. Kaliyaperumal
Higher College of Technology, Muscat, Oman

S. Rathinagiri
Bharathidasan University, Thiruchirappalli, India

Fig. 1 Study area map

the products of weightage by rank of the schemes as given below.

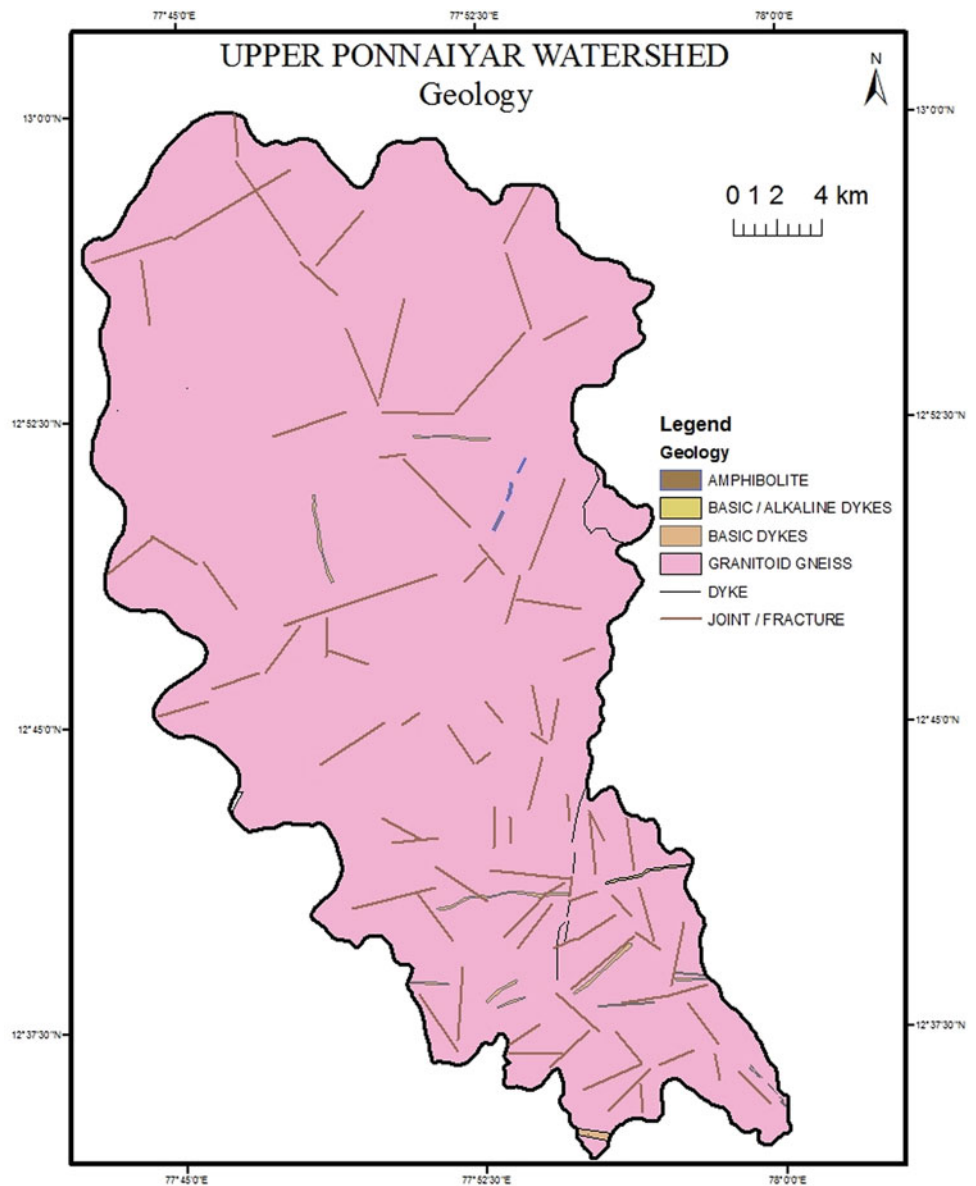
$$GWP = \sum W \times R \quad (1)$$

where GWP: Groundwater Potential, W : Weightage, R : Rank.

Groundwater potential zones are classified as having high, moderate, low, and very low potential. The zones are derived by grouping the suitability index using standard deviation measures.

3 Results

The target of the study is to identify groundwater potential zones using integrated thematic maps. The types of hard rocks that are predominant in the study area include the granitoid gneiss, basic dykes of amphibolite, and basic/alkaline dykes (Fig. 2). The granite gneiss rock has less permeability since it is a hard rock. However, the study area depends on the secondary porosity through lineament which favors groundwater movement. Therefore, more weightage

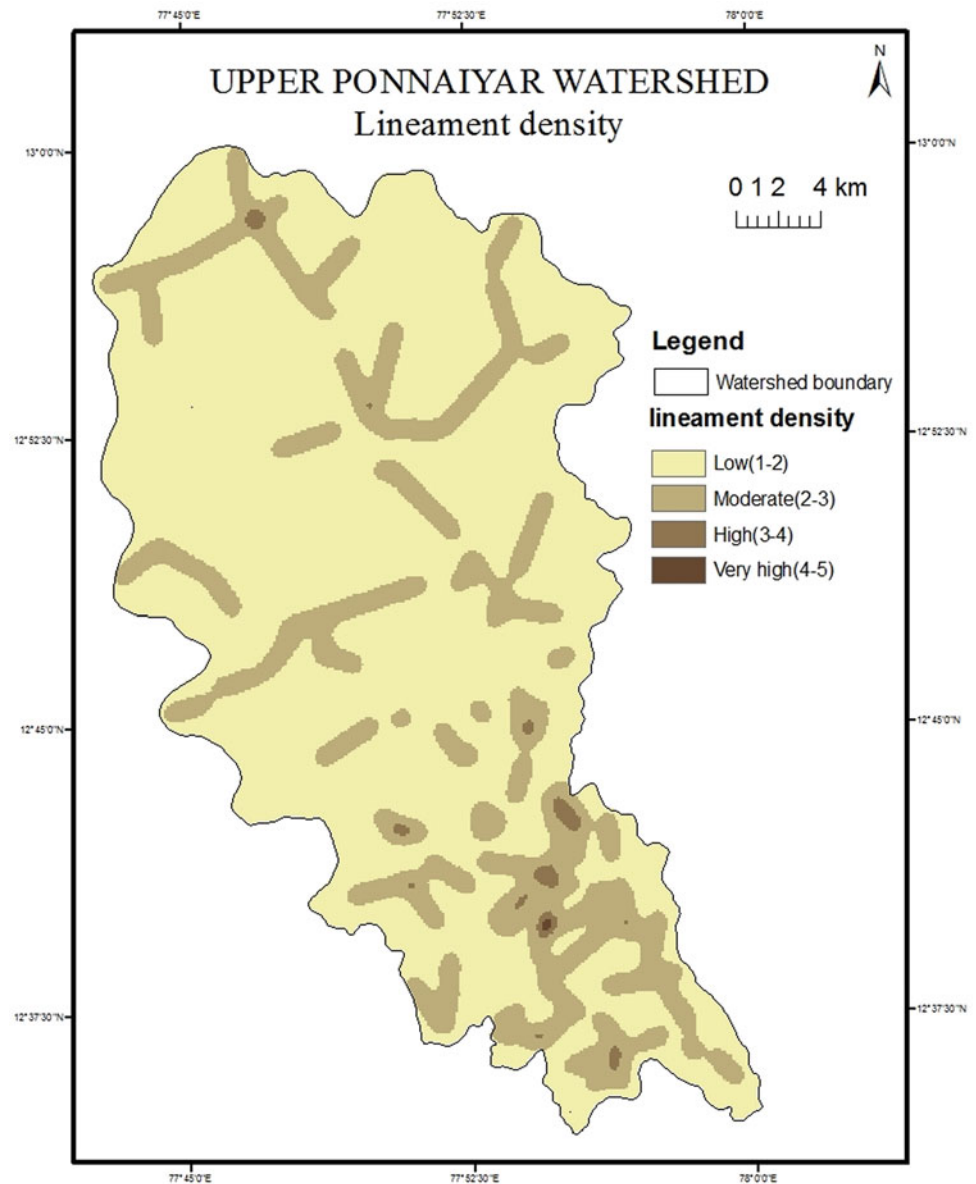
Fig. 2 Geology map

is assigned to places having a high lineament density (Fig. 3). Soil types such as clay loamy, clayey-skeletal, clayey soils, and red gravelly soil are observed in the study area (Fig. 4). Red gravelly soil has been assigned with a high rank as it allows better water infiltration when compared to clay soils. A gentle slope with a very high lineament density was considered for potential infiltration in the study area, and geomorphological landforms such as a pediplain and a valley fill with cropland have a considerable amount of water infiltration (Figs. 5 and 6). Based on the land use and land cover, the water body and crop land are assigned with more weightages considering the water infiltration (Fig. 7).

Subsequently, the maps are integrated to evaluate the groundwater potential zones into high, moderate, low, and very low by a weighted overlay analysis based on the assigned ranks and weightages (Table 1).

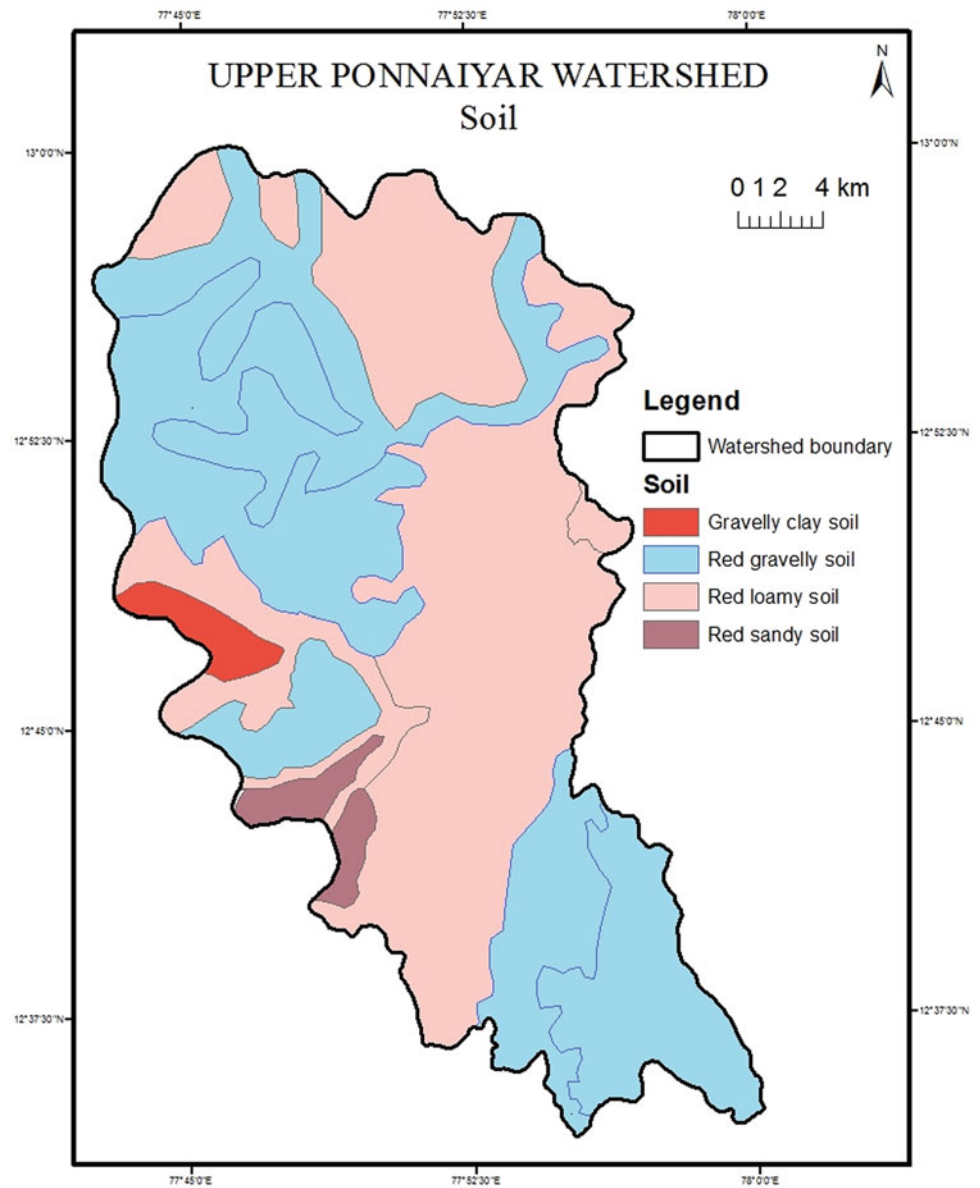
4 Discussion

Based on the analysis, the final ground water potential map was prepared, and the water potential zones were categorized into high, moderate, low, and very low as in Fig. 8. It was observed that nearly 0.29% (2.4 km²) of the area was

Fig. 3 Lineament density

categorized as high groundwater potential zones. It is due to a high-rise, undulating terrain and to the intensity of the lineament in the shear zone which is characterized by very gentle slope and geomorphological features such as pediplain and flood plains, which indicates fairly high groundwater potential zones. About 45.67% (380.38 km²) of the area was categorized as having a moderate groundwater potential, since these zones were cramped on gentle, very gentle, or moderate slopes. The high intensity of the lineament in granitoid gneiss and dykes is also responsible for

a moderate potential. Geomorphologically, the zone stretches over shallow pediments, flood plain, pediplain, and pediments. The land use shows stony waste, open forest, and dense forest, which aids to maintain a moderate groundwater potential. The low and very low groundwater potential zones which occupy 53.60% (446.47 km²) and 0.32% (3.6 km²), respectively, are found in regions which are covered with hard granite rocks, have a steep slope, and therefore, have a high runoff and a low groundwater infiltration.

Fig. 4 Soil map

5 Conclusion

The integration of GIS and remote sensing techniques provides an excellent tool for the determination of groundwater potential. The groundwater potential is computed for the relative assessment of groundwater potential zones by the

integration of all the factors that influence the occurrence and movement of groundwater in a region. This assessment can assist in the identification of artificial recharge zones to improve the groundwater level for effective and efficient groundwater management. The demand for water for human consumption can, thus, be fulfilled through appropriate planning and sustainable water management.

Fig. 5 Slope map

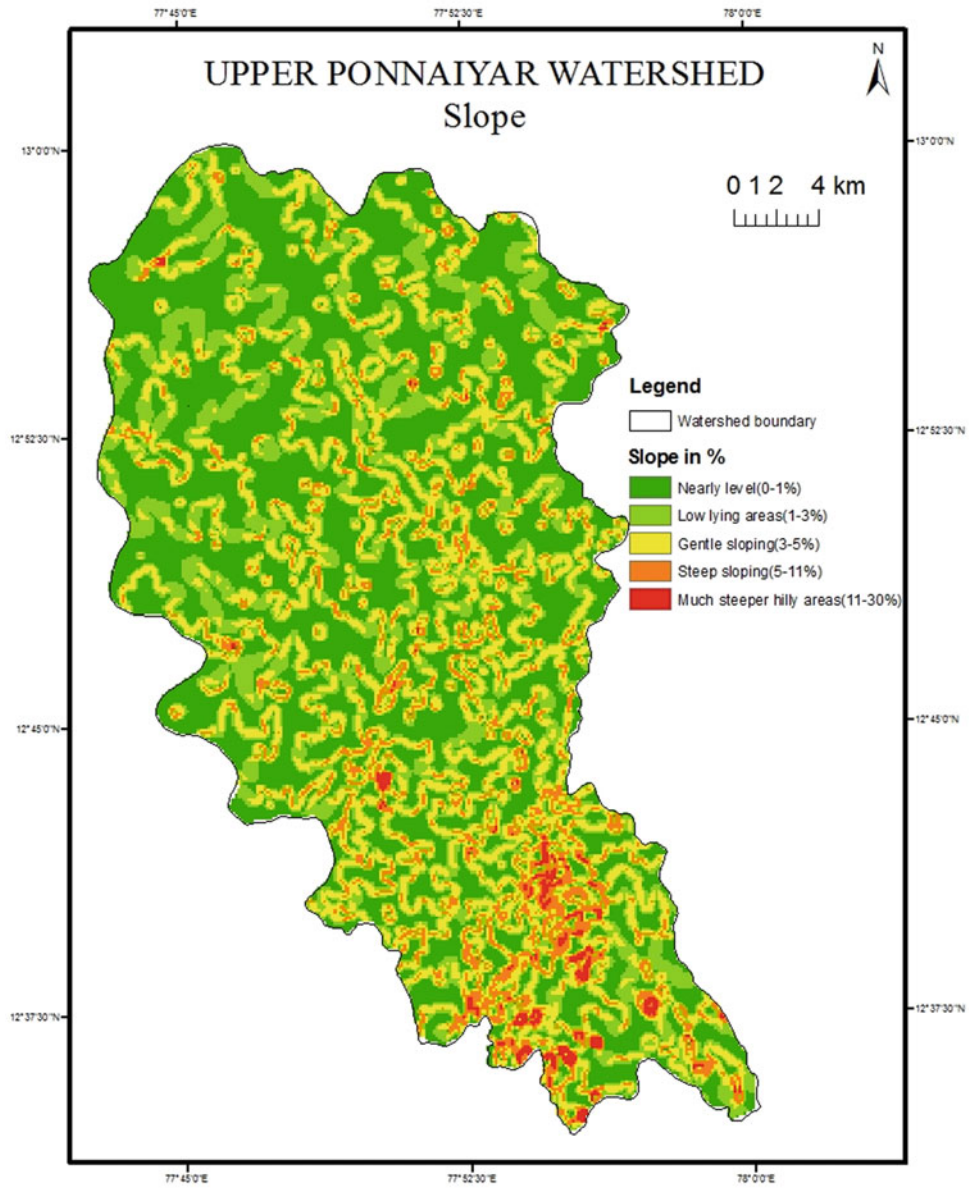


Fig. 6 Geomorphology

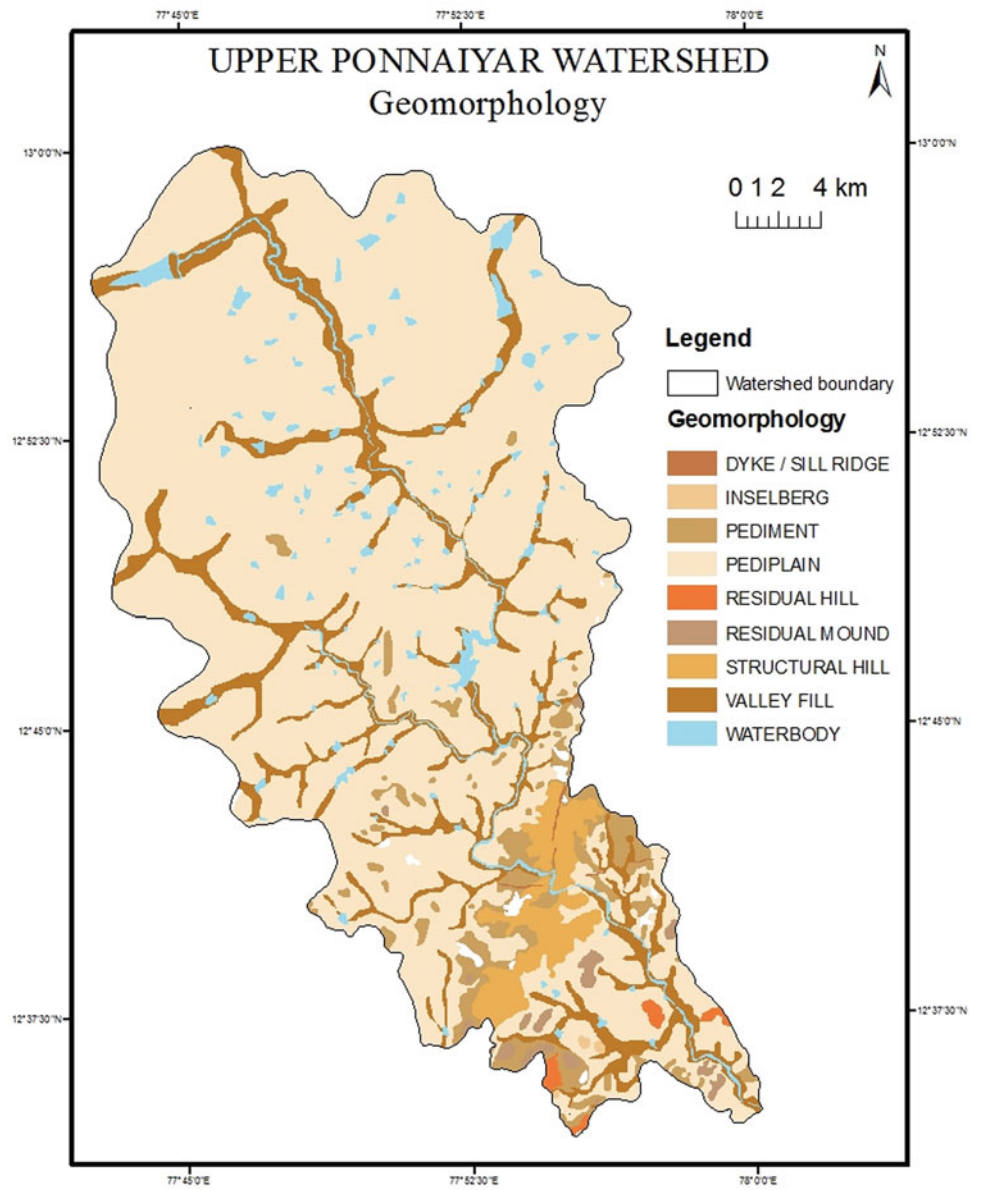


Fig. 7 Land use/Land cover

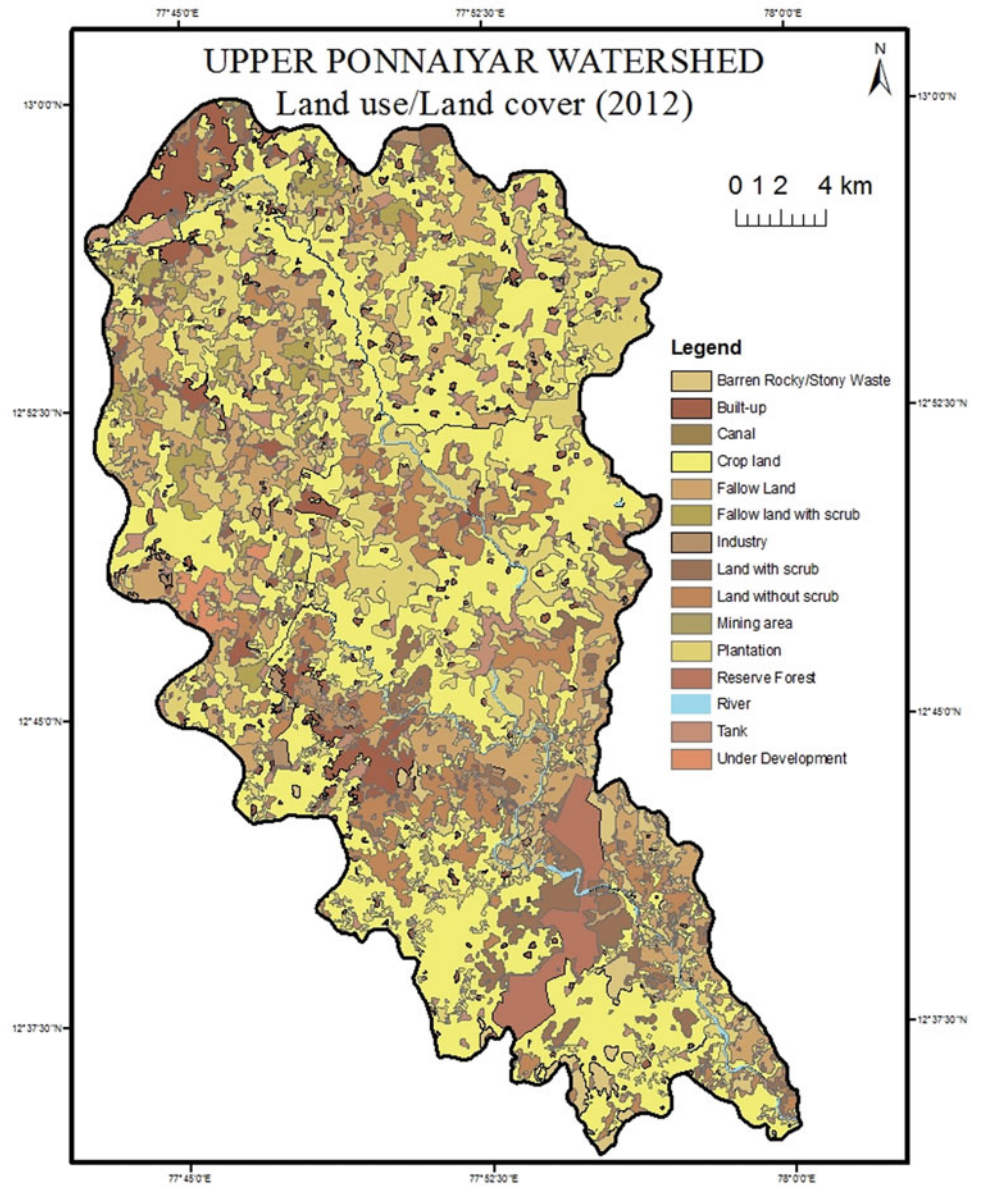
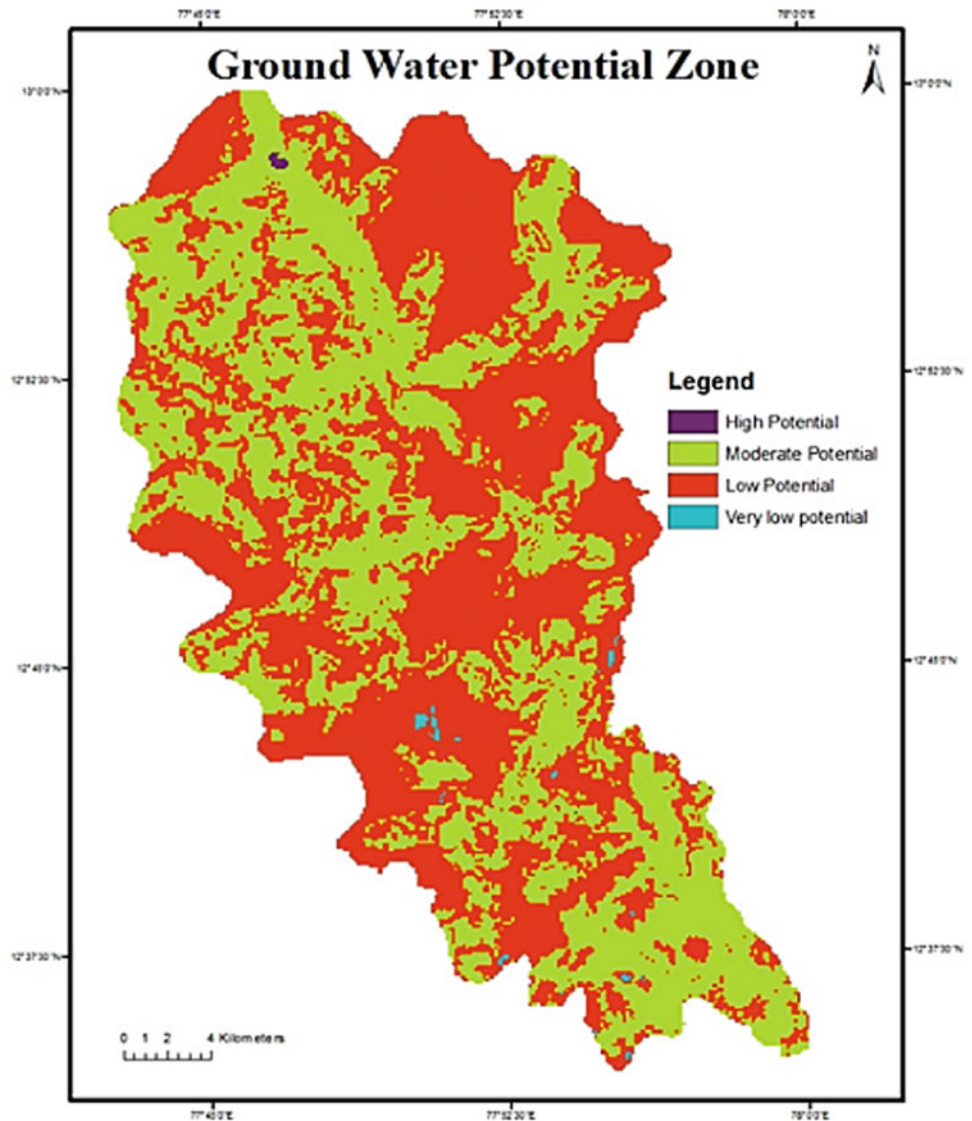


Table 1 Assigned ranks for the individual features of the themes for groundwater potential zoning

Thematic layers	Map	Related features	Ranks
	Weightage		
Geology	1	Granitoid gneiss	3
		Basic dykes	3
		Basic/Alkaline dykes	2
		Amphibolite	1
Slope	2	Low	2
		Gentle	1
		Moderate	3
		High	4
Lineament density	3	Very high	1
		High	2
		Moderate	3
		Low	4
Soil	4	Red sandy	1
		Gravelly clay	3
		Red loamy	2
		Red gravelly	1
Geomorphology	5	Structural hill	4
		Inselberg	4
		Residual mount	3
		Residual hill	3
		Dykes	3
		Pediments	2
		Pediplain	1
		Waterbody	1
Drainage density	6	Valley fill	1
		Very high	4
		High	3
		Moderate	2
Land use /land cover	7	Low	1
		Build-up land	2
		Crop land	1
		Water body	1
		Stony waste	4
		Land with scrub	3
		Reserved forest	2
		Fallow land	2

Fig. 8 Categorized groundwater potential zones in the study area



References

- Jahan, C.S., Rahaman, M.F., Arefin, R., Ali, M.S., Mazumder, Q.H.: Delineation of groundwater potential zones of Atrai–Sib river basin in north-west Bangladesh using remote sensing and GIS techniques. *Sustain. Water Resour. Manage.* **5**, 689–702 (2019). <https://doi.org/10.1007/s40899-018-0240-x>
- Machiwal, D., Jha, M.K., Mal, B.C.: Assessment of groundwater potential in a semi-arid region of India using remote sensing, GIS and MCDM techniques. *Water Res. Manage.* **25**, 1359–1386 (2011). <https://doi.org/10.1007/s11269-010-9749-y>
- Negm, A., Bouderbala, A., Chenchouni, H., Barcelo, D.: Water Resources in Algeria - Part I: Assessment of Surface and Groundwater. The Handbook of Environmental Chemistry Series. Springer, Cham (2020a). <https://doi.org/10.1007/978-3-030-57895-4>
- Negm, A., Bouderbala, A., Chenchouni, H., Barcelo, D.: Water Resources in Algeria - Part II: Water Quality, Treatment, Protection and Development. The Handbook of Environmental Chemistry Series. Springer, Cham (2020b). <https://doi.org/10.1007/978-3-030-57887-9>
- Sarkar, D.C., Deota, B.S., Raju, P.L.N., Jugran, D.K.: A geographical system approach to evaluation of groundwater potentiality of Shamri micro watershed in the Shimla Taluk, Himachal Pradesh. *J. ISRS* **29**(3), 152–164 (2001). <https://doi.org/10.1007/bf02989927>
- Ramalingam, M., Santhakumar, A.R.: Case study on artificial recharge using remote sensing and GIS. In: Map India 2000, 3rd international conference and exhibition on GIS, GPS and remote sensing, CSDMS, New Delhi, India (2000). <https://www.geospatialworld.net/article/case-study-on-artificial-recharge-using-remote-sensing-and-gis/>



Innovative Conveyancing System Techniques Implemented by Saudi Geological Survey to Ensure Minimum Hydrogeological Impact on Wadi Ibrahim Groundwater Aquifer

Ahmed El-Hames, Samer Shouman, Abdulaziz Al-Solami, and Bandar Tunsi

Abstract

Protecting the hydrogeological regime in Wadi Ibrahim is a very crucial issue due to its vital role in providing the Zamzam Well with groundwater (GW). The Zamzam Studies and Research Center at the Saudi Geological Survey endeavours to utilize the best and most creative techniques through implementing the best management practice to ensure the groundwater flow is not obstructed and/or adversely affected by the new development projects taking place in the Wadi and having their foundation laid inside the aquifer extent. This paper aims to present solutions to these complex problems through modern and innovative approaches. Some of these techniques, implemented methods, and innovative solutions are presented in this article.

Keywords

Wadi Ibrahim • Zamzam Well • Groundwater flow • Makkah City • Building foundations

1 Introduction

Makkah is a typical modern city whose importance stems from the existence of some Islamic religious landmarks and holly shrines such as the Grand Mosque (Al Haram) where the blessed Well of Zamzam is located. This well is a part of the Wadi Ibrahim aquifer that has recently been affected by intensive urbanization in the form of high towers and condenses infrastructures. The Zamzam Studies and Research Center (ZSRC) at the Saudi Geological Survey (SGS) ensure the supply of Zamzam Waters, in terms of quality and

quantity, in the face of intensified urbanization and increasing demand. The Zamzam Studies and Research Center (ZSRC) has developed and improved innovative techniques to diminish the impact of the structures on the GW regime in the Wadi Ibrahim aquifer over the years, by near real-time maps and modelling of the water table elevation based on monitoring well data and by analysing the risk assessment of the likely impact on the aquifer. The aim of this article is to highlight some of the techniques that became part of the ZSRC rules of thumb in all foundation projects taking place in the Wadi Ibrahim area.

2 Geological and Hydrogeological Setting

The Zamzam Well lies within the Wadi Ibrahim catchment, which runs through the City of Makkah, and taps the GW from wadi alluvium and, to a much lesser extent, the underlying highly weathered and fractured bedrock. It is covered with a complex sequence of Precambrian, intensely fractured, igneous, and metamorphic rocks. The southwestern sector of the catchment area is underlain by highly to moderately foliated intrusions, mainly of granodiorite, quartz diorite, and diorite intercalated with amphibolite gneiss. In contrast, the north-eastern portion of the watershed is primarily underlain by highly fractured, massive granitic intrusions with subordinate amphibolite (Al-Solami et al. 2009).

3 SGS Implemented Techniques

3.1 Reinstating Original Hydraulic Conductivity

The gravel system is an effective measure to mitigate damming effects by reinstating the hydraulic conductivity after constructing the foundation. It is essential to determine the thickness of the gravel that will be sufficient to compensate

A. El-Hames (✉) · S. Shouman · A. Al-Solami · B. Tunsi
Zamzam Studies and Research Center, Saudi Geological Survey,
P.O. Box: 54141 Jeddah, 21514, Kingdom of Saudi Arabia
e-mail: hames.as@sgs.org.sa

for the blocked flow due to concrete foundations. Three distinguished cases of gravel system are explained here.

(A) **Side Gravel Trenches:** The GW flows at the upstream (q_u) and downstream (q_d) of the foundation under the water table are equal. The flow at the upstream side consists of the flow perpendicular to the building and the flow at both sides of the buildings where gravel trenches are laid. Since the GW flow through building is zero, the flow through gravel trenches (q_g) is the only flow at the upstream area. The flow equation can be written as:

$$q_d = 2 \times q_g \quad (1)$$

Assuming the hydraulic gradient at upstream and downstream is the same, Eq. 1 can be rewritten as:

$$K_m(L + 2T_s) = K_g 2T_s \quad (2)$$

K_m is original material's hyd. Cond., K_g is the side gravel's hyd. Cond., and T_s is the minimum thickness of each side gravel trenches along the full depth of the building below the water table. Rearranging Eq. 2, gives:

$$T_s = \frac{K_m L}{2(K_g - K_m)} \quad (3)$$

(B) **Gravel blanket under the constructed foundation:** If all GW flow is to be allowed (passed) through the gravel blanket laid under the building, following the same assumption—that the hydraulic gradient at the upstream and downstream sides of the building is the same—leads to the following equation for GW flow at both sides:

$$q_d = q_{bu} + q_{gu} \quad (4)$$

q_d is the flow at the downstream side, q_{bu} and q_{gu} are the flows through the building material and the gravel blanket, respectively, at the upstream side. Assuming that GW flow through building material is zero, Eq. 4 can be rewritten as follows:

$$K_m(b_d + T_{gu}) = K_{gu} T_{gu} \quad (5)$$

K_m is the hyd. Cond. of the original material, b_d is the building depth under the water table, T_{gu} is the thickness of the gravel blanket under the building, and K_{gu} is the hyd. Cond. of the gravel blanket under the building. Rearranging Eq. 5 leads to:

$$T_{gu} = \frac{K_m b_d}{K_{gu} - K_m} \quad (6)$$

(C) **Gravel system around pile foundation:** SGS do not usually grant permission for deep foundation (piles) in Wadi Ibrahim, except in rare cases where developers can guarantee the safety of GW. If a number of piles are to be constructed in one line perpendicular to the flow direction, with a pile diameter (P_d), the following flow equation can be used to calculate the thickness of the gravel required:

$$T_G = \frac{K_m P_d}{2(K_G - K_m)} \quad (7)$$

where more complex systems of shallow or deep foundations, where multi-irregular and not inline foundation to be constructed, SGS has developed and adapted a more comprehensive 3D GW modelling technique as explained in the next section.

3.2 Integrated 3D Groundwater Modelling in Wadi Ibrahim

To study the impact of complex development on the GW regime in Wadi Ibrahim and Zamzam Well, an integrated 3D GW model was developed based on the MODFLOW (Harbaugh et al. 2000) and on the groundwater management system GMS (V.10). The model consists of seven layers, three in the alluvium material, two in the weathered rocks, and two in the fractured rocks. The model is redesigned for each particular project and regularly updated by incorporating extra data from a detailed site investigation at the



Fig. 1 Execution of GW flow system under tower *F* following GW model outputs

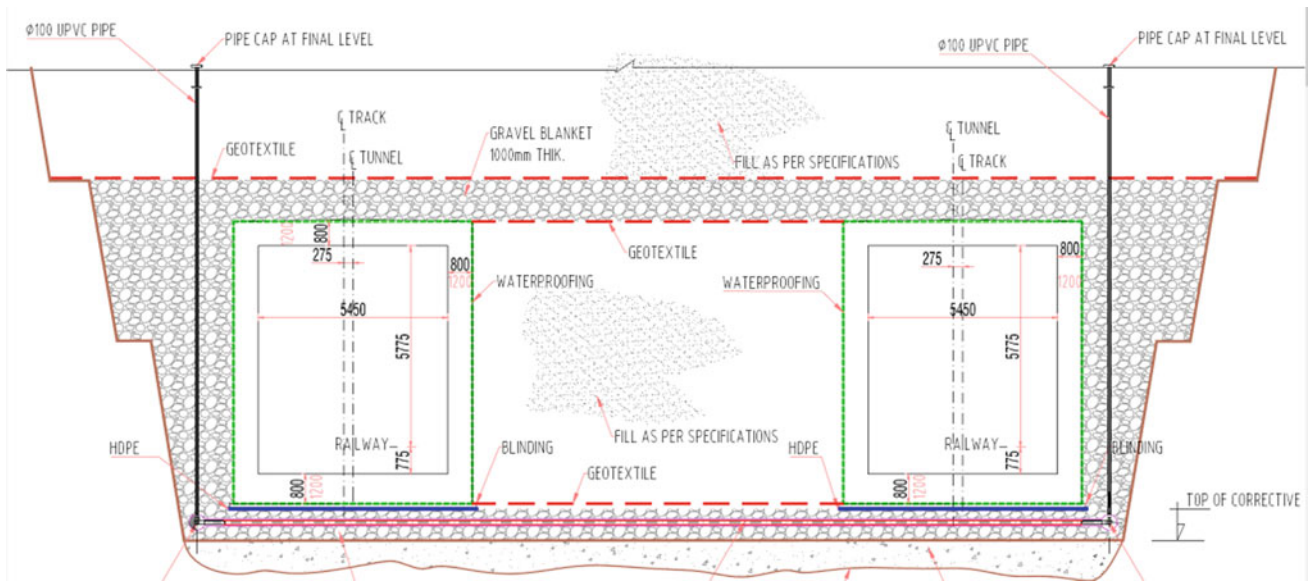


Fig. 2 Recommended gravel filter and perforated pipes system around metro tunnel

project site. The modelling output recommendations and their implementation for only two mega projects (an old project and a recent one) are shown here.

- (A) **King Abdulaziz Endowment Tower (The Clock Tower):** This project was built facing Kaaba, directly inside Wadi Ibrahim. Its foundation was accidentally located on inclined Schist Rocks, which are water-conducting rocks, too weak to handle the load of a skyscraper. It was recommended to replace this rock with stronger materials. The effect of the rock replacement on the GW system in the area was assessed by utilizing a specially designed model developed for this project. The GW flow system under Tower F was redesigned to handle the tower load and to ensure the flow is not obstructed by the newly designed tower foundation [Fig. 1].
- (B) **King Abdulaziz Road (KAAR) Project:** This project stretches to the west of the Holly Mosque between Jabal Omar Development and the Third Ring Road. It intersects three different watersheds, amongst them is Wadi Ibrahim. It was critical to ensure that no negative impact on the GW regime in the area would take place due to the construction work. A special GW model was redeveloped to study the possible impact of the project foundation on the GW regime. A backfill of gravel, gravel filter, and blanket thickness around the metro tunnels along this project were recommended from the model outputs as shown in Fig. 2.

4 Conclusion

In this paper, the development of a number of innovative techniques developed and implemented by SGS to alleviate the GW flow and diminish the impact of constructing shallow and deep foundations in Wadi Ibrahim is described. Adopting these techniques is believed to be very beneficial to maintain natural GW conditions by reducing damming effects, minimizing risk on building foundations and street flooding due to GW rise as a result of flow-blocking and hydraulic conductivity reduction. These techniques may also be adopted and utilized by other developers and contractors.

References

- Al-Solami, A., Al-Barakati, G., Sayed, S.A.S., Al-Bahloul, S., Al-Tunsi, B.: Engineering geological mapping of the holy city of Makkah Al Mukarramah, Saudi Arabia. In: Culshaw, M.G., Reeves, H.J., Jefferson, I., Spink, T.W. (eds.) Engineering geology of tomorrow's cities. Geological Society, London, Engineering Geology Special Publication 22 (2009)
- Harbaugh, A.W., Banta, E.R., Hill, M.C., McDonald, M.G.: MODFLOW-2000, the U.S. Geological Survey modular ground-water model-User guide to modularization concepts and the Ground-Water Flow Process. USGS Open-File Report 00-92. Reston, Virginia: U.S. Geological Survey (2000)



A Sustainable Water Resources Management Plan for the Kurdistan Region, Iraq

Serwan M. J. Baban and Ghazi F. Haji

Abstract

The Kurdistan region which is characterised by arid and semi-arid climate conditions will continue to suffer from critical water shortages, due to its regional hydro-geological situation and the likely impact of global climate change on rainfall quantities and patterns. Moreover, the adjacent upstream countries have aggressive plans for, and are racing towards, building large numbers of giant dams and vast irrigation projects. The area is experiencing an increase in water demand due to a growing population, improvements in life quality and development activities. This combination of conditions will require water resource managers and decision makers to balance a dwindling supply with an escalating demand. This paper will report and examine the development and implementation of a plan for Sustainably Managing Water Resource in the area. The plan was introduced during June 2012 with a framework to deliver the stated objectives during 2019/2020, which is proposed to be extended to 2025. The plan examined the main challenges and identified the priorities and various means of realising the plan which included increasing water volume and storage. The paper will also report on the outcomes to date as well as the barriers to implementation. Overall, the outcomes show an optimistic picture of tangible and conceptual achievements which include completed projects and imbedding modern management practices such as informed and participatory decision making.

Keywords

Water resources • Management • Sustainability • Kurdistan region • Iraq

1 Introduction

The Kurdistan region is rather rich in water resources with five large rivers running through it. These include the Khapoor, Great Zab, Little Zab, Awaspee and Serwan. The total annual water flow capacity stands at 30 billion cubic metres. About 60% of the water sources of the rivers are located within Kurdistan, and 40% is sourced outside of the region. The varied topography created three associated rainfall regimes, namely high rainfall (700–1100 mm), medium rainfall (400–700 mm) and low rainfall (under 400 mm) (Baban 2012, 2013a). The water resources sector in the Kurdistan region is experiencing an increase in water demand due to a growing population, improvements in life quality and development activities, whilst the adjacent upstream countries are implanting aggressive plans for, and are racing towards, building large numbers of giant dams and vast irrigation projects (Baban 2006).

Furthermore, the Intergovernmental Panel on Climate Change (IPCC) uses the tools of climate models with future scenarios of forcing agents (i.e. greenhouse gases and aerosols) as input to make projections of future climate changes, which illustrates the possibilities that could lie ahead. Based on the relevant scenario which presents the resulting projections of changes in the future climate in the area, the Kurdistan region is likely to be affected by an overall low rainfall with higher intensity and low frequency. This deduction is also indicating the presence of a critical scarcity of water in the region due to climate change (Mahmood et al. 2018), and the Fertile Crescent has been steadily drying since 1931, with a decline in vegetation since 2008 and a sharp decline in groundwater compared to the

S. M. J. Baban (✉)
Kurdistan Region Presidency, Ostrava, Iraq

G. F. Haji
Ministry of Agriculture and Water Resources, Kurdistan Region
Government, Erbil, Iraq

mean of the previous six years (Naranjo 2016). As temperatures climb and evaporation increases, the demand for water increases particularly by farmers to increase their irrigation (Baban 2005, 2013a; Lelieveld FN 2012). The Intergovernmental Panel on Climate Change (IPCC 2014). This combination of conditions will require water resource managers and decision makers to balance a dwindling supply with an escalating demand (Baban 2012, 2013b, 2014).

Reliable information about water resources is one of the most important strategic factors influencing decision making and development (Negm et al. 2020a, 2020b). However, the region suffers from a scarcity of reliable and compatible data sets. For example, the soils map for Iraq was constructed during the 1960s (Buringh 1960; Baban et al. 2004), this is not unusual as the process of collecting, analysing and verifying the information requisite to planning is expensive and requires a lot of time; hence, it can be considered as one of the barriers to sustainable development in developing countries (Baban 2005; Negm et al. 2020a, 2020b). However, there are clear indications that the information poverty obstacle can be overcome by using reputable technologies that facilitate management decisions, such as Geoinformatics to collect, handle and analyse the necessary data sets, as well as to expand our understanding of the processes involved at the appropriate scales (Baban 2006; Arar and Chenchouni 2012).

It should also be indicated that the insufficient funds allocated to obtain reliable data and information are a serious obstacle. However, it is evident that floods and draughts can raise awareness of risk and the need for management. In recent times, the region has suffered a series of high intensity rainfall events which have caused an unprecedented loss of lives and property during 2019. This fact must be used as a wake-up call to the seriousness of the situation to create pressures for increasing expenditure on water resources management. This paper will recount, examine and evaluate the implementation of a specifically developed plan during June 2012, what has been achieved to date, the expected outcomes during the proposed extended plan delivery time of 2025, and the barriers to full plan implementation. The plan aimed to provide science-based, practical steps to rehabilitate, improve and sustainably manage water resources. The plan examined the main challenges, as well as identified the priorities and various means of realising the plan. These included increasing water volume and storage, minimising demand, and using management regulatory options and education.

2 Planning for Sustainable Water Resources Management

Given the complexity of the issues, the ongoing practices and decision-making and implementation processes in the region, it was necessary to establish some practical and

principle guidelines for decision making by relevant government agencies and to agree on a code of ethics and conduct to maintain a strategic focus, whilst maintaining consistency and transparency such as making scientific- and evidence-based decisions, build effective and transparent systems, always follow process and ensure that public interest and the law are supreme and commitment to 'Collective and Representative Decision Making' (Baban 2013a, 2013b, 2014). Moreover, ongoing frequent meetings with stakeholders and experts as well as the analysis of available statistics charting the progress of the plan, which was established during 2009 (Ministry of Agriculture (MoA) 2009), led to developing a draft Plan. This plan was gradually refined and enhanced based on the consultative process involving government experts, all local universities, relevant parliamentary groups and the public (Ministry of Agriculture and Water Resources (MoAWR) 2012). It was established that the overall objective is to secure necessary water for drinking, farming, manufacturing and tourism. Hence, it is critical to sustainably manage available water resources (Baban 2012, 2006, 2013b).

Unfortunately, the planned objectives for 2018 needed to be extended to 2025 due to a lack of financing from 2014–2018 owing to budgetary difficulties between the region and the federal government, the reduction in Petrol prices which is the main source of income for the region, as well as and the disruptions and security issues caused by ISIS activities around the region (Middle East Research Institute (MERI) 2018).

Table 1 shows the region's needs for water organised by categories, the region's capacity in 2011, the completed and ongoing projects during 2019 and the expected deliverables at the end of the proposed extended period to 2025. The information has been colour-coded, so green means 100% of what is needed has been achieved, yellow represents achieving 50% or more of what is required and red shows achievements of less than 50% of the required water. Using this information and the outcomes from the consultative process with all regional experts, the following priorities have emerged:

1. Using a holistic approach and developing legislations and laws for sustainably managing water in the region.
2. Benefiting from the surface water and reserving the over-exploited groundwater.
3. Strengthening the relationship between the Ministry's research centres and relevant universities.
4. Raising awareness regarding the sustainable use of water and involving all stakeholders in the decisions making process.
5. Encouraging the private sector's involvement.
6. Planning and being prepared for climate change impacts and natural disasters.

Table 1 Kurdistan region's needs for water by categories, its capacity in 2011, the completed and ongoing projects during 2019 and the expected deliverables at the end of the proposed extended period to 2025. (1) UNAMI: Water Resource Management 2010. (2) 200 litres/person/day—estimated by the Ministry of Municipality and Tourism/General Directorate of Water and Sewerages. (3) 175 litres/person/day—estimated by the Ministry of Municipality and Tourism/General Directorate of Water and Sewerages. (4) 8 litres/small size livestock/day, 30 litres/large size livestock/day—estimated by Ministry of Agriculture and Water Resources.

Region's Water needs by sectors	Region's Water needs by volume	The Region's capacity in 2011		The region's capacity in 2019		Objective for 2025	
		Capacity	%	Capacity	%	Capacity	%
Agriculture	(1) 10 billion m ³ 767,897 hectares (50% of the land)	5.5 billion m ³ Only 2256 billion m ³ is used to irrigate 177,406 hectares of land	22.6%	5.5 billion m ³ Only 2257 billion m ³ is used to irrigate 283,375 hectares of land	22.6%	Storage of 14.247 billion m ³ and the usage of 7387 billion m ³ to irrigate 322,500 hectares of land	84%
Drinking water	(2) 365 million m ³	365 million m ³	100%	365 million m ³	100%	438 million m ³ for six million people	120%
Industry	(3) 320 million m ³	320 million m ³	100%	320 million m ³	100%	One billion m ³	312%
Livestock	(4) 20 million m ³	20 million m ³	100%	20 million m ³	100%	25 million m ³	125%
Total	10,705,000.00 m ³	6,461,000,000 m ³ 2,961,000,000 m ³ has been used		6,461,000,000 m ³ 2,962,000,000 m ³ has been used		15,710,000,000 m ³ and should benefit from 8,850,000,000 m ³	

3 Successes and Outcomes

A review of the outcomes, achievements and shortcomings showed that:

- Over all, the Ministry has a significant critical mass and believes in employing scientific concepts and evidence-based planning.
- A holistic approach for management through focusing on hydrological catchment management and carrying capacity concepts.
- Developing a draft law for preserving and protecting water resources in the Kurdistan Region, this was submitted to the Council of Ministers and had its first reading.
- Reserving the groundwater by developing and enforcing legislations in coordination with the local government agencies to switch dominantly from ground water to surface water.
- Making use of modern methods and technologies such as promoting water preservation, harvesting and carrying capacity principles to minimise floods and landslides.
- Developing meaningful collaboration between the government and the local and international Universities and Research Institutions.
- Include all stakeholders in the decisions-making process through field visits, direct meetings and communication via a specifically developed Web site.
- Encouraging the private sector involvement by attempts to build the necessary projects through 'Build Operate Transfer' (BOT) and long-term loan schemes.

9. Tangible outcomes for realising sustainable water resources management through building a number of dams, ponds and irrigation projects as follows:
10. The plan shows that, by 2025, the region will have 14.247 Billion m³ storage capacity through completing (Table 1):
 - 15 small and medium size dams (to date 9 are completed and 6 are under construction)
 - 18 large dams (to date 7 are completed, 11 under construction and 13 are planned to be implemented and completed by 2025)
 - 616 ponds (to date 91 are completed, 25 are under construction and 500 are planned to be implemented and completed by 2025)
 - 3894 small irrigation projects (3369 are completed, 25 are under construction and 500 are planned to be implemented and completed by 2025).
 - Strategic irrigation projects (to date 9 are completed, 2 are under construction and 12 are planned to be implemented and completed by 2025)

4 Conclusions

Achieving sustainable water resources management is critical for the region. However, identifying and performing the necessary reforms in the water sectors in the region is a difficult and a complex challenge. In terms of process, a clear and realistic vision for specifying the priorities in order to achieve sustainable water resources management is required. The implementation will need an effective roadmap with clear objectives and a timeframe developed based on consultations with all stakeholders. This paper reported on the progress of the implementation of a specifically developed road map in June 2012, aimed to achieve sustainable water management.

Challenges facing the full realisation of the strategic objectives and possible ways forward include the extensive efforts by neighbouring upstream countries to build numerous giant dams and massive irrigation projects, budget allocation, instability in the region, climate change, as well as the lack of local data and an inefficient use of research-driven management options. Therefore, there is an increasing need for dialogue with neighbouring countries, focusing on developing applied research aiming to improve holistic management, sustainable development and carrying capacity principles, using geoinformatics to manage climate change impacts. The outcomes are rather optimistic despite

the difficult period from 2014–2018 during which the region experienced severe financial difficulties and was subjected to disruptions and security threats caused by the ISIS activities around the region.

To date, 9 small and medium size dams and 7 large dams have been completed, in addition to 91 ponds, 3369 small irrigation projects and 9 strategic irrigation projects. Furthermore, several other projects are either under construction or planned for implementation and completion by 2025. The Ministry has also adopted participatory decision-making principles and developed a sharp focus on quality assurance processes.

References

- Arar, A., Chenchoune, H.: How could geomatics promote our knowledge for environmental management in Eastern Algeria?. *J. Environ. Sci. Technol.* **5**(5), 291–305 (2012). <https://doi.org/10.3923/jest.2012.291.305>
- Baban, S.M.J.: Accomplishing sustainable development in Southern Kurdistan using geoinformatics; an overview. *Int. J. ZANIN* **1**(1), 29–38 (2005)
- Baban, S.M.J.: Developing a geoinformatics based approach to manage water resources in Southern Kurdistan. *Int. J. ZANIN* **2**(1), 27–45 (2006)
- Baban, S.M.J.: Achieving sustainable food and water resources production and security in the Kurdistan region, Iraq; Challenges and opportunities. In: *Agriculture and Water Resources in Kurdistan Iraq; Issues and Opportunities Conference*, pp. 13–14. UK (2012)
- Baban, S.M.J.: Progress in the agricultural and water resource sectors of the Kurdistan regional government, Iraq. In: *Third World Kurdish Scientific Congress*, pp. 11–13. Stockholm, Sweden (2013a)
- Baban, S.M.J.: Building a secure future through realizing sustainable development in the Federal Region of Kurdistan, Iraq. Chapter 3, In: Heshmati et al. (eds.) *Perspectives on Kurdistan's Economy and Society in Transition*, vol. 2, pp. 32–47. Cambridge Scholars Publishing, UK (2013b)
- Baban, S.M.J., Ramlal, B., Al-Tahir, R.: Issues in information poverty and decision-making in the Caribbean region, a way forward. *West Indian J. Eng.* **27**(1), 28–37 (2004)
- Baban, S.M.J.: *Achieving food and water sufficiency and security for Kurdistan Region, Iraq*. Kurdistan Regional Government Printers. Erbil, Kurdistan Regional Government, May 2014 264 pages. Catalogue Record in the General Directorate of Public Libraries, Kurdistan Regional Government, Iraq: 1 (2014)
- Buringh, P.: *Soils and soil conditions in Iraq*. Republic of Iraq, Ministry of Agriculture, Directorate General of Agricultural Research and Projects (1960)
- Lelieveld et al.: Climate change and impacts in the Eastern Mediterranean and the Middle East. *Climate Change* **114**, 667–687, Springer (2012). <https://doi.org/10.1007/s1058-012-0418-4>
- Mahmood A., Yousuf M., Nada R, Jalal H.Y.: Sustainable water management in Iraq (Kurdistan) as a challenge for government responsibility. *Water* **10**(11), 1651 (2018). <https://doi.org/10.3390/w10111651>
- Middle East Research Institute (MERI): Visions for stabilising the Middle East. *MERI Forum* 2018, pp. 34 (2018). <http://www.merik.org/wp-content/uploads/2018/12/MERI-Forum2018.pdf>

- Ministry of Agriculture (MoA): The strategic plan for agriculture sector for Kurdistan region government. Ministry of Agriculture, pp. 176 (2009)
- Ministry of Agriculture and Water Resources (MoAWR): The road map for achieving food and water sufficiency and security in the Kurdistan region, Iraq. Ministry of Agriculture and Water Resources, pp. 31 (2012)
- Naranjo, L.: Crisis in the Crescent, Drought Turns the Fertile Crescent into a Dust Bowl (2016). <https://earthdata.nasa.gov/learn/sensing-our-planet/crisis-in-the-crescent>
- Negm, A., Bouderbala, A., Chenchouni, H., Barcelo, D.: Water resources in Algeria - Part I: assessment of surface and groundwater. Cham, Springer (2020a). <http://doi.org/10.1007/978-3-030-57895-4>
- Negm, A., Bouderbala, A., Chenchouni, H., Barcelo, D.: Water resources in Algeria - Part II: water quality, treatment, protection and development. Cham, Springer (2020b). <https://doi.org/10.1007/978-3-030-57887-9>
- The Intergovernmental Panel on Climate Change (IPCC) (2014). <https://www.ipcc.ch/organization/organization.shtml>



Aquifers Depletion and Asymmetry Access to Groundwater: A Study Across Farmers' Classes in Tunisia

Hacib El Amami, Sondes Fkiri, and Jean Robert Kompany

Abstract

Most studies undertaken on the impact of groundwater overexploitation on economic farms did not take into account the spatial distribution of groundwater withdrawal externalities across farmers. This paper seeks to analyze the distribution of externality costs among different categories of farmers using surface wells in the central part of Tunisia. The results showed that externality costs were unevenly distributed. Large farmers are much less affected compared to medium and small farmers. Small farmers experienced the higher costs. These categories are likely to be rapidly losing access to groundwater. However, if the trend of groundwater overdraft continues in the future, all categories of individual farmers will be affected, as well as the society as a whole. Therefore, sustainable policies should be implemented to prevent further degradation. The involvement of local users is suggested as one of these policies.

Keywords

Groundwater • Externalities costs • Distribution • Small farmers • Large farmers

1 Introduction

In Tunisia, groundwater use is unmetered and users face no marginal costs of extraction beyond the energy costs of pumping. As indicated by Ellen and Jessoe (2018), this means that, as long as a farmer has property rights over land which sits above an aquifer, he can extract as much

groundwater as he chooses. As a result, an individual user imposes a cost, or externality, on other users in the form of lower water table and higher pumping and investment costs. The impact of groundwater overexploitation on agricultural development and economic farms is known and well-documented (Molle et al. 2018). However, most studies do not take into account the spatial distribution of groundwater withdrawal externalities across farmers and how the access to this resource can be differentiated among different classes of farmers.

This paper is an attempt to analyze the economic access to groundwater and the distribution of externalities resulting directly from groundwater depletion among different categories of farmers using surface wells in the central part of Tunisia. It also seeks to investigate which category of farmers can continue to benefit from their share in the common pool resource and who will possibly lose their legitimate share.

2 Methodology

The study was conducted in the area of Sidi Bouzid, located in the Center of Tunisia (Fig. 1a). A sample of 45 farmers covering various farm-size categories were interviewed from April–June 2018. Strongly governed by the arid climate, the average annual rainfall in the area, calculated during the period (1936–2012), was approximately 250 mm and characterized by significant annual fluctuations. The average annual evaporation is 1470 mm, and the evaporation-to-rainfall ratio for the area is 7.5. Due to the aridity of the climate, the area has little surface water, and groundwater is the only source of irrigation water.

According to DGRE (2014), the average groundwater level has quickly declined from about 24 m below ground level, before the year 1991, to about 32 m during 2008 at the rate of about 53 cm/annum (Fig. 1b). Such a declining level not only disrupts the ecological balance, but also puts heavy

H. El Amami (✉) · S. Fkiri · J. R. Kompany
Carthage University, Carthage, Tunisia

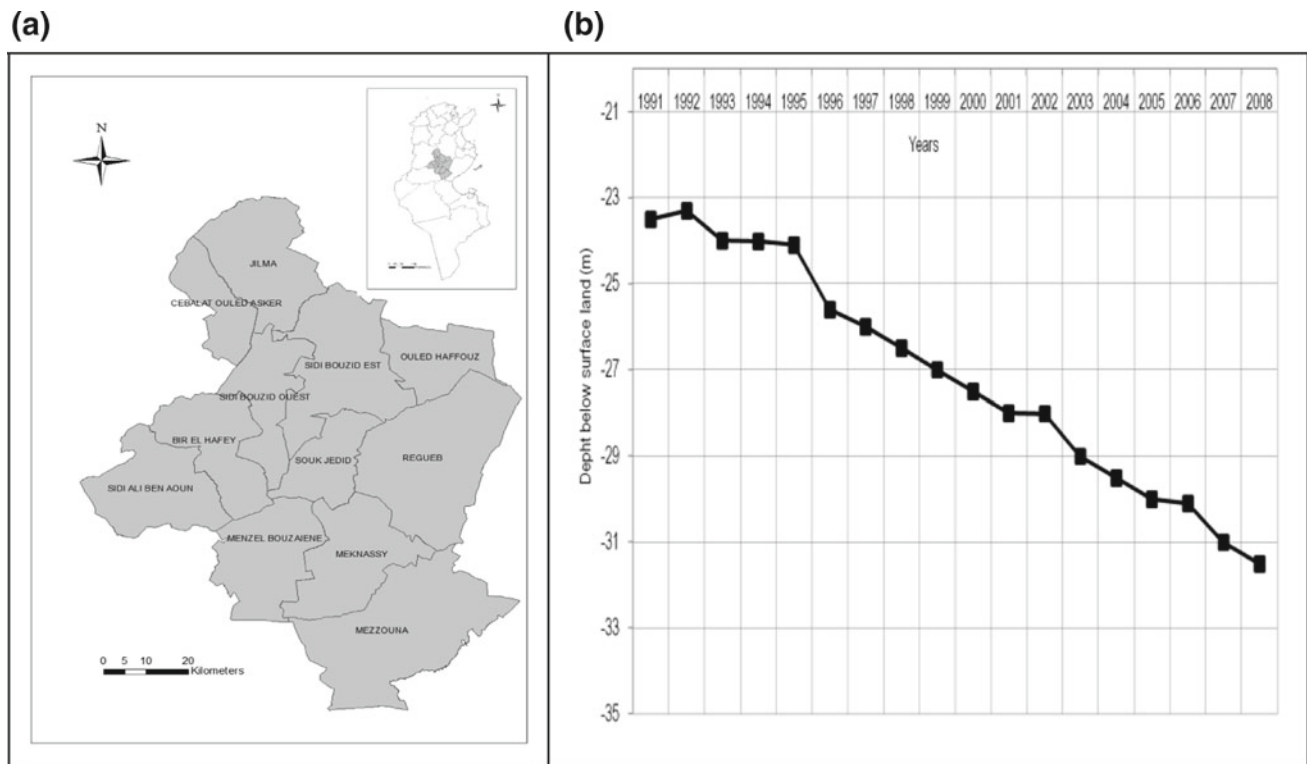


Fig. 1 a Localization of study area. b Trend in average groundwater level

financial burden on farmers, because it requires huge investments including drilling or hugging new wells, repeated deepening works of existing wells, construction of intermediate storage structures and purchasing more powerful pumps that can pump from a greater depth.

The annual cost of irrigation was estimated by amortizing the capital cost on well investment. Following Sharif and Aschok (2011), the amortized investment cost is the sum of amortized investments on new wells or deepening the existing ones, pump sets and accessories, above-ground storage structures, as well as annual repairs and maintenance costs. The capital cost of the well and the above-ground storage structure was amortized over their entire expected life span. The amortized cost per cubic meter of groundwater extracted is obtained by dividing the sum of amortized investment costs and energy costs by the total groundwater used on a farm.

3 Results

3.1 Increasing Investment Cost

The externality costs resulting from the degradation of groundwater resources are very unevenly distributed across the different categories of farmers, as shown in Table 1. The investment cost in irrigation increased with the decrease in the holding size. It was the highest for small farms with TND374/ha, followed by medium with TND107/ha. For large farms, this cost is only TND50/ha, which is 7.5 times lower than that observed for small farmers.

This is because small farmers have to bear the same amount of investment on deepening the existent wells, as that of large farmers, but large farmers have the possibility to

Table 1 Additional investment costs in irrigation per category of farmers

Components	Small farms	Medium farms	Large farms
Land holding size (ha)	3	6	20
Amortized investment cost (TND/ha)	374	107	50

Table 2 Pumping costs of groundwater by classes of farmers

Components	Small farms	Medium farms	Large farms
Pumped water (m ³ /year)	13,370	34,800	68,000
Amortized investment in irrigation (TND*/m ³)	0.056	0.011	0.006
Total cost of pumping water (investment cost + energy)	0.162	0.117	0.112

*1 TND \approx 0.35 USD in 2018

irrigate a larger area and, thus, enjoy the benefits of the economies of scale.

3.2 Increasing Pumping Cost

The cost per cubic meter of pumped water, including both the cost of energy and amortized cost of investment, increases as the irrigated area decreases. It was the highest for small farmers with TND0.162, followed by medium farmers with TND0.117, and large farmers with TND0.112 (Table 2). This inequality across different categories of farmers was due mainly to the limited irrigated areas by small farmers. Thus, the pumping cost per cubic meter increases as the irrigated area decreases, implying that economic access to groundwater becomes increasingly in favor of large farmers.

4 Discussion

In the study area, groundwater depletion adversely affects economic access to groundwater resources, and farmers with smaller land holdings are the worst affected. Higher indicators, in terms of increasing investment costs per unit of land and pumping cost per cubic meter, were observed at the level of these categories followed by medium farms. Large farmers are much less affected, implying an asymmetric access to groundwater among categories of farmers. It is expected that, in the short-medium term, large farmers would continue to enjoy their share on groundwater resources as they are able to offset the declining groundwater table by deepening the existing wells with low costs or by drilling new boreholes. Small and medium farmers, owning less than 3 and 6 ha, respectively, would be in a quite vulnerable position. As a result, these categories are likely losing access to groundwater.

However, if the trend of groundwater overdraft continues in the future, all categories of individual farmers will be

affected, as well as the society as a whole. Since groundwater depletion is resulting directly from unregulated water use and anarchic multiplication of the number of wells, a significant policy reform is, therefore, necessary if we are to prevent further degradation. Among possible sustainable policies, this study suggests, in parallel to policies and instruments currently implemented, the involvement of local users with the assistance of Regional Department of Agriculture (CRDA) to ensure effective control on groundwater withdrawal.

5 Conclusion

Results revealed that groundwater depletion adversely affects economic access to groundwater resources, and farmers with smaller land holdings are the worst affected, thus, leading to asymmetric access to groundwater. Large farmers are much less affected, and it is expected that this category should continue, at least in the short and medium terms, to enjoy their share of these resources. However, if access to groundwater continues to be managed under the “laissez-faire” mode, all the categories of farmers will be impacted, as well as the society as a whole. Practical and efficient management policies are, therefore, needed to prevent further degradation.

References

- DGRE : Annuaire piézométrique de la Tunisie. Ministère de l'Agriculture et des Ressources hydrauliques, pp. 329 (2014)
- Ellen, B., Jessoe, K.: Water markets and climate change adaptation: Micro-level evidence on agricultural water demand. Mimeo (2018)
- Molle, F., López-Gunn, E., Steenbergen, F.V.: The local and national politics of groundwater overexploitation. *Water Altern.* **11**(3), 445–457 (2018)
- Sharif, M., Ashok, K.R.: Impact of groundwater over-draft on farm income and efficiency in crop production. *Agric. Econ. Res. Rev.* **24**, 291–300 (2011)



Hydrogeological Features of Geothermal Waters and Travertine Deposits in Pamukkale, Western Anatolia, Turkey

Nevzat Özgür and Emre Uzun

Abstract

The study area is located in the northern shoulder in the eastern part of the rift zone of the Büyük Menderes, in which there are two continental rift zones of the Büyük Menderes and the Gediz converge. Geothermal waters of Pamukkale have outlet temperatures of about 36 °C and reservoir temperatures of up to 180 °C and are of Ca–Mg–SO₄–HCO₃ type as well as immature waters. Travertine deposits of Pamukkale are one of the events of world wonders, which are immediately associated with decreasing temperature and partial pressure of CO₂. Genetically, the solubility of CaCO₃ which is controlled by CO₂ partial pressure, temperature and pH values play an important role for the formation of travertine deposits basically, in which reaction equilibriums are ascribed to importance. Travertine deposits with an age of uranium series of at least 400 ka form this one of the important Pamukkale.

Keywords

Turkey • Pamukkale • Geothermal waters • Travertine deposits • World wonders

1 Introduction

The study area of Pamukkale is located 20 km NW of the province capital of Denizli in which the two rift zones of the Büyük Menderes and the Gediz with an elevation of about 360 m converge (Uzun 2017). The aim of this study is (i) to update hydrogeological, hydrogeochemical and isotope geochemical data with regard to geothermal waters of Pamukkale, (ii) to elucidate the formation of travertine

deposits and (iii) to create a hydrogeological model of geothermal waters in the area.

2 Results

2.1 Hydrogeology, Hydrogeochemistry and Isotope Geochemistry

In the area, Paleozoic mica schists are of impermeable basement rocks. The intercalation of gneisses, marbles and quartzites in mica schists is permeable and forms the deep reservoir, Mesozoic limestones, Eocene to Pliocene sedimentary rocks and Quaternary alluviums, and travertine deposits are permeable rocks and can be considered as shallow reservoirs. Paleozoic marbles as reservoir rocks are found between Karahayıt and Pamukkale (in the NE part of the Pamukkale geothermal outlets), whereas Mesozoic limestones as reservoir rocks occur to the N of Pamukkale geothermal outlets. Pliocene sedimentary rocks occur in the surrounding area of Pamukkale geothermal outlets in the upper part of Yenice horst between Pamukkale and Karahayıt.

In the area, the Kolonkaya and Tosunlar formations with a total thickness of up to 600 m form an intercalation of claystones, marls and sandstones and are to consider as good cap rocks for the shallow reservoir (Uzun 2017). In the area, geothermal waters are of Ca–Mg–(SO₄)–HCO₃ type in the Piper diagram (Uzun 2017). Hydrogeochemically, the geothermal waters display dominant cations of Ca > Mg > Na + K and dominant anions of HCO₃ > SO₄ > Cl. In addition to important hydrogeochemical features, geothermal waters have high sulfate contents, which are associated with sulfide and gypsum minerals in impermeable basement and cap rocks, i.e., Tosunlar formation. In the plot of Na/1000–K/100–√Mg, the waters are of immature waters (Uzun 2017). Finally, geochemical cation thermometers of Na–K and Na–K–Ca show reservoir temperatures between 150 and 180 °C in the study area.

N. Özgür (✉) · E. Uzun
Faculty of Engineering, Department of Geological Engineering,
Suleyman Demirel University, Isparta, Turkey
e-mail: nevzatozgun@sdu.edu.tr

2.2 Travertine Deposits

The formation of travertine deposits of Pamukkale is related to the geological, tectonical and geomorphological features in the area. In the area of Pamukkale, geological formations as carbonate rocks are found and provide essential carbonate sources for the formation of travertine deposits. Volcanic activities in age from Middle Miocene to Pliocene in the area play a very important role in the formation of travertine deposits since 400 ka by (i) affecting as a heat source for the geothermal waters, (ii) advancing decarbonatization processes in the depth and (iii) playing a part to the CO₂ contents by mantle degassing. In the area, there were compressional and extensional tectonic features. The extensional tectonic features continue and are associated with the development of the study area which cause a network of faults, joints and fissures in the area and may enhance circulation of geothermal waters intensively. In the area, there are rainfall rates of up to 600 mm and high mountains with an elevation of up to 2000 m which ensure essential meteoric waters and hydraulic conditions for geothermal waters for the formations of travertine precipitations.

Geochemically, the solubility of calcite (CaCO₃) controlled principally by CO₂ partial pressures, temperatures and pH values is very important for the formation of travertine precipitations. In this connection, the reaction equilibrium scales for this process: (1) H₂O + CO₂ ⇌ H₂CO₃ (CO₂ is dissolved in waters as H₂CO₃). (2) CaCO₃ + H₂CO₃ ⇌ Ca²⁺ + 2HCO₃⁻. In the system in which the travertine precipitations are taking place, the process that increases the CO₂ proportion enhances dissolution of calcite (CaCO₃), whereas each reduction in CO₂ proportion precludes the precipitation of calcite (CaCO₃). Under the lower pH values, in which most carbonates suffer solutions as H₂CO₃, the chemical reaction in the equation proceeds to the right side; whereas under higher pH values, the reaction proceeds to the left side due to the precipitation of CaCO₃ as travertine deposits. It is known that CO₂ is less soluble in hot waters than in cold waters. In the end of the process, the solubility of calcite decreases slightly with increasing temperatures. (3) CaCO₃ + H⁺ ⇌ Ca²⁺ + HCO₃⁻ (HCO₃⁻ ions are derived from the reaction of H⁺ with the carbonates). In Pamukkale, the temperatures and CO₂ partial pressures form two rival partners for the formation of travertine deposits. In this connection, CO₂ partial pressure decreases, when probable temperatures play a secondary role. High temperatures which decrease in ascending geothermal waters increase CaCO₃ solubility in waters. Furthermore, the pressure release due to the escape of CO₂ at the surface, encourages travertine precipitations. In areas with high volcanic activities in depth, i.e., volcanic rocks in Denizli [7], the partial pressure of CO₂ in which calcite (CaCO₃) is soluble is very high. CO₂ can be consumed

with additional carbonate dissolutions in reservoirs. Moreover, the CO₂ partial pressures decrease insignificantly.

In addition, geothermal waters are supersaturated due to CaCO₃ when geothermal waters can reach the reservoir. Carbonates components precipitate if temperature equilibrium by the fast ascending geothermal waters does not take place in the same proportion as the pressure decrease at outflow. In Pamukkale, the formation of travertine deposits can be explained in five different travertine phases: (1) In the first phase, the formation of the Çökelez fault with a strike in NW–SE direction was generated. The geothermal outflows are controlled by the faults. Nowadays, travertine precipitations are noticeable in high elevation areas. These travertine deposits have a uranium series age of 400 ka (Uzun 2017). (2) There is a modern origin of travertine deposits. This phase was developed by the Karahayıt fault. These travertine deposits are widespread in accordance with foothill slope. (3) In the area, a stairway faults exist. The travertine deposits are found in SE part of Pamukkale which were utilized in the construction of the ancient city of Hierapolis. In this phase of travertine deposits, the stairway faults were generated. And (4) nowadays, the last phase of travertine precipitations forms the landscape. Great parts of travertine deposits in higher elevation areas must have been eroded. Recent travertine deposits form modern carbonate precipitations as travertine deposits. They must be protected by the flow of geothermal waters on the travertine deposits against the oxidation processes.

3 Discussion and Conclusion

The geothermal waters of Pamukkale can be represented as a hydrogeological model schematically. In the system, the meteoric waters percolate in the drainage area at fault, fracture and fissure zones, as well as through permeable clastic sediments into the reaction zone of a magma chamber in a depth of up to 5 km. In this depth, meteoric fluids are heated by the cooling magmatic melt which is represented by Middle Miocene to recent volcanic rocks (i. e. Denizli, Kula and Kula volcanoes), and ascend to the surface because of lower density caused by plate tectonical convection cells. The formation of travertine deposits is associated with solubility of calcite (CaCO₃) controlled principally by temperatures, pH values and CO₂ partial pressures, when reaction equilibriums play an important role. For travertine deposits of the first phase, a uranium series age of 400 ka has been accepted (Dilsiz et al. 2004). Recent travertine deposits of Pamukkale form the modern carbonate precipitations consisting mainly of aragonite. In the study area, the travertine deposits can be observed in terms of terrace, ridge and channel-type travertine (Fig. 1).

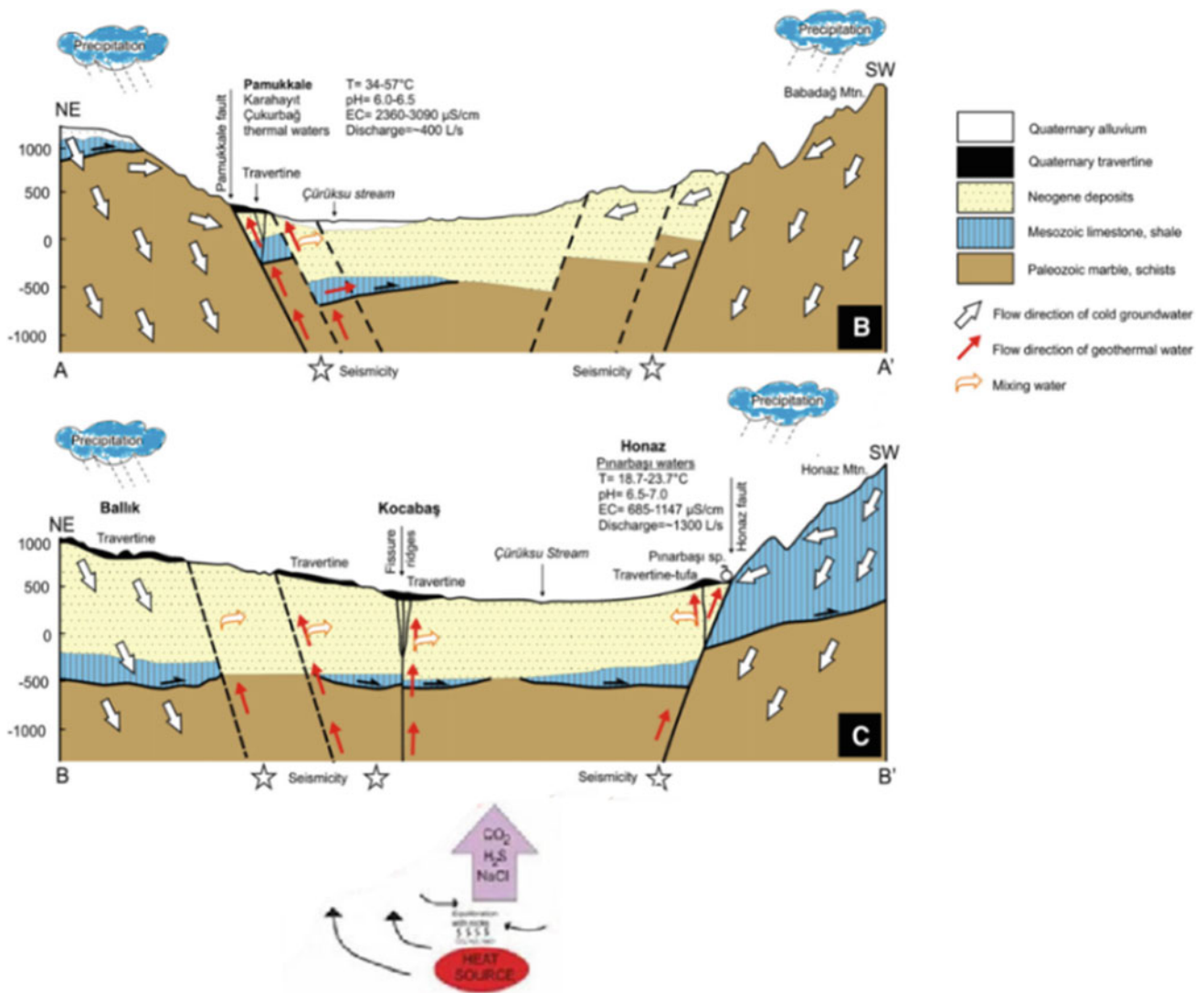


Fig. 1 Hydrogeological modeling of the geothermal waters of Pamukkale and environs [Modified from; Altunel and D'Andria (2019); Alçiçek et al. (2019); Dilsiz et al. (2004); Uzun 2017)]

Acknowledgements This study was funded by the Scientific Research Coordination Office of the Suleyman Demirel University, under contract numbers 4494-YL1-15.

References

- Alçiçek, H., Bülbül, A., Yavuzer, İ., CihatAlçiçek, M.: Origin and evolution of the thermal waters from the Pamukkale Geothermal Field (Denizli Basin, SW Anatolia, Turkey): Insights from hydro-geochemistry and geothermometry. *J. Volcan. Geother. Res.* **372**, 48-70 (2019). <https://doi.org/10.1016/j.jvolgeores.2018.09.011>
- Altunel, E., D'Andria, F.: Pamukkale Travertines: a natural and cultural monument in the world heritage list. In: *World Geomorphological Landscapes* (2019)
- Dilsiz, C., Marques, J.M., Carreria, P.M.M.: The impact of hydrological changes on travertine deposits related to thermal springs in the Pamukkale area (SW Turkey). *Envir. Geo.* **45**, 808–817 (2004). <https://doi.org/10.1007/s00254-003-0941-8>
- Uzun, E.: Formation, history and prevention of travertine deposits in Pamukkale (Denizli) (in Turkish), M.Sc. thesis, Graduate School of Applied and Natural Sciences, Süleyman Demirel Üniversitesi, Turkey (2017)